

DTIC FILE COPY



AD-A219 747

FAILURE ANALYSIS HANDBOOK

C. R. Walker, K. K. Starr

Pratt & Whitney
P.O. Box 109600
West Palm Beach, FL 33410-9600

August 1989

Final Report for Period 1 September 86 - 29 April 89

Approved for public release; distribution unlimited

Materials Laboratory
Wright Research and Development Center (WRDC)
Air Force Systems Command (AFSC)
Wright-Patterson Air Force Base, Ohio 45433-6533



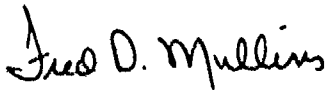
90 03 12 116

NOTICE

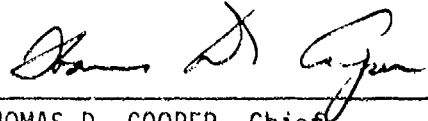
When Government drawings, specifications, or other data are used for any purpose other than in connection with a definitely Government-related procurement, the United States Government incurs no responsibility or any obligation whatsoever. The fact that the government may have formulated or in any way supplied the said drawings, specifications, or other data, is not to be regarded by implication, or otherwise in any manner construed, as licensing the holder, or any other person or corporation; or as conveying any rights or permission to manufacture, use, or sell any patented invention that may in any way be related thereto.

This report is releasable to the National Technical Information Service (NTIS). At NTIS, it will be available to the general public, including foreign nations.

This technical report has been reviewed and is approved for publication.



FRED D. MULLINS
Materials Integrity Branch
Systems Support Division
Materials Laboratory
FOR THE COMMANDER



THOMAS D. COOPER, Chief
Materials Integrity Branch
Systems Support Division
Materials Laboratory



WARREN P. JOHNSON, Chief
Systems Support Division
Materials Laboratory

If your address has changed, if you wish to be removed from our mailing list, or if the addressee is no longer employed by your organization, please notify WRDC/MLSA, WPAFB, OH, 45433-6933 to help us maintain a current mailing list.

Copies of this report should not be returned unless return is required by security considerations, contractual obligations, or notice on a specific document.

REPORT DOCUMENTATION PAGE

1a. REPORT SECURITY CLASSIFICATION Unclassified		1b. RESTRICTIVE MARKINGS None	
2a. SECURITY CLASSIFICATION AUTHORITY N/A		3. DISTRIBUTION/AVAILABILITY OF REPORT approved for public release; distribution unlimited.	
2b. DECLASSIFICATION/DOWNGRADING SCHEDULE N/A			
4. PERFORMING ORGANIZATION REPORT NUMBER(S) P&W/ED FR-20820		5. MONITORING ORGANIZATION REPORT NUMBER(S) WRDC-TR-89-4060	
6a. NAME OF PERFORMING ORGANIZATION United Technologies Corporation		7a. NAME OF MONITORING ORGANIZATION Materials Laboratory (WRDC/MLSA) Wright Research and Development Center	
6b. OFFICE SYMBOL <i>(if applicable)</i>		7b. ADDRESS (City, State and ZIP Code) Wright-Patterson Air Force Base, Ohio 45433	
6c. ADDRESS (City, State and ZIP Code) Pratt & Whitney/Materials Engineering South P.O. Box 109600 West Palm Beach, FL 33410-9600		7c. ADDRESS (City, State and ZIP Code)	
8a. NAME OF FUNDING/SPONSORING ORGANIZATION Air Force Wright Aeronautical Laboratories		9. PROCUREMENT INSTRUMENT IDENTIFICATION NUMBER F33615-86-C-5007	
8b. OFFICE SYMBOL <i>(if applicable)</i>		10. SOURCE OF FUNDING NOS.	
8c. ADDRESS (City, State and ZIP Code) Wright-Patterson Air Force Base, Ohio 45433-6533		PROGRAM ELEMENT NO. 62101F	PROJECT NO. 2418
11. TITLE (Include Security Classification) Failure Analysis Handbook		TASK NO. 04	WORK UNIT NO. 48
12. PERSONAL AUTHOR(S) C. R. Walker, K. K. Starr			
13a. TYPE OF REPORT Final	13b. TIME COVERED FROM 9-1-86 TO 4-29-89	14. DATE OF REPORT (Yr., Mo., Day) 1989 August 18	15. PAGE COUNT 760
16. SUPPLEMENTARY NOTATION			
17. ICSSATI CODES FIELD GROUP SUB GR		18. SUBJECT TERMS (Continue on reverse if necessary and identify by block number) Failure Analysis, Fatigue, Fractography, SEM and TEM	
19. ABSTRACT (Continue on reverse if necessary and identify by block number) <p>The objective of this program was to update and augment the two primary Air Force failure analysis handbooks, Electron Fractography Handbook and SEM/TEM Fractography Handbook, published in 1965 and 1975, respectively, with a new "Failure Analysis Handbook." The new handbook includes fractography of alloys and conditions not previously covered in other handbooks. The handbook also is a guide for procedures and lists other sources of information.</p>			
20. DISTRIBUTION/AVAILABILITY OF ABSTRACT UNCLASSIFIED/UNLIMITED <input checked="" type="checkbox"/> SAME AS RPT <input type="checkbox"/> DTIC USERS <input type="checkbox"/>		21. ABSTRACT SECURITY CLASSIFICATION unclassified	
22a. NAME OF RESPONSIBLE INDIVIDUAL Fred Mullins		22b. TELEPHONE NUMBER (include Area Code) 513-255-5117	22c. OFFICE SYMBOL WRDC/MLSA

FOREWORD

This technical report covers work performed under Air Force Contract F33615-86-C-5007, "Failure Analysis Handbook" from 1 September 1986 through 31 April 1989. The work reported herein was performed by the Materials Engineering and Technology Laboratories of Pratt & Whitney (P&W) Advanced Engineering Operations, West Palm Beach, Florida. The contract was administered by Mr. Fred Mullins, of the Air Force Wright Research and Development Center (WRDC).

The principal investigator was C. R. Walker. The Pratt & Whitney program manager was Dr. K. K. Starr, reporting to L. E. Hess, Supervisor, Engine Components Investigations Group. Dr. Starr is responsible for coordinating contract. Mr. C. R. Walker is responsible for technical efforts and reporting. Mr. J. R. Cobia prepared the proposal and was program manager and principal investigator for this program from 1 September 1986 through 31 August 1987.

Other individuals that made significant contributions to the program were;

Mr. D. P. Deluca for LCF testing, Mr. J. Mucci for tensile, stress rupture, and hydrogen embrittlement testing, Mr. J. W. Fischer for HCF testing, Mr. H. M. Privett III, for stress corrosion testing, Mr. J. R. Warren for TMF testing, Mr. E. Werdt for metallographic documentation, and Miss H. A. Foster for document preparation. Technical consultants to the program were Mr. L. E. Hess (Failure Analysis) and Mr. C. T. Torrey (Metallography). Mr. H. R. Nesor conducted all scanning electron microscope documentation of the specimens and assisted with fractographic analysis. Other engineers and technicians in the metallography, engine component investigation and mechanics of materials and structures groups made contributions.

Accession For	
NTIS GRA&I	<input checked="" type="checkbox"/>
DTIC TAB	<input type="checkbox"/>
Unannounced	<input type="checkbox"/>
Justification	
By _____	
Distribution/	
Availability Codes	
Dist	Avail and/or Special
A-1	

Table of Contents

<u>Section</u>	<u>Page</u>
I. INTRODUCTION	
1) Background	1
2) Objective	1
3) Program Description	1
II. FAILURE ANALYSIS TECHNIQUES AND METHODS	
1) Approaches to Failure Analysis	3
a) Common Sense Approach	3
b) Logic Networks, Fault Trees and Other Approaches to Failure Analysis	4
2) Care and Handling of Fracture Surfaces	6
a) Preservation and Handling of Fracture Surfaces	6
b) Cleaning Fracture Surfaces	6
c) Breaking Open Cracks	7
3) Visual Examination Techniques	8
a) No Magnification Examination - Field Examination Techniques.	8
b) Macroscopic Examination	8
c) Macroscopic Features	9
4) Scanning Electron Microscope (SEM) Examination	11
a) Advantages and Limitations	13
b) Sample Preparation and Cleaning	14
c) Documentation Sequence and Identification of Photographs ...	14
d) Viewing Replicas in the SEM	15
e) X-ray Energy Spectroscopy and Wavelength Dispersive Spectroscopy	16
5) Transmission Electron Microscope (TEM) Examination	16
a) Advantages and Limitations	16
b) Specimen Preparation	18
c) Fatigue Striation Counts	19
6) Chemical Analysis Techniques	20

<u>Section</u>	<u>Page</u>
7) Metallographic Examination	20
a) Sectioning Through Origins	20
b) Evidence of Plastic Deformation	20
c) Maximum Metal Temperature Analysis	22
d) Replication of Large Parts	22

III. FRACTURE MODES

1) Introduction	24
2) Ductile Overstress	24
a) Macroscopic Appearance	24
b) SEM Appearance	24
1) Dimple Size	24
2) Dimple Shape	28
3) Cleavage	30
a) Macroscopic Appearance	30
b) SEM Appearance	31
1) Cleavage Steps and River Patterns	31
2) Tilt and Twist Boundaries	31
3) Feathery Cleavage	31
4) Herringbone Structure and Wallner Lines	31
5) Cleavage Tongues	31
6) Quasi-Cleavage	32
4) Fatigue	36
a) Macroscopic Appearance	37
b) SEM Appearance	38
1) Stage I	38
2) Stage II	38
a) Striation Spacing	39
b) Striation Appearance	39
c) Fatigue Steps	40
3) Stage III	44
4) Thermal Mechanical Fatigue (TMF)	44
5) Decohesive Rupture	46
a) Microstructural Appearance	46
b) Microstructural Variables	46
c) Environmental Factors	46
1) Stress Corrosion Cracking	46
2) Liquid Metal Embrittlement	50
3) Hydrogen Embrittlement	50

IV. ATLAS OF FRACTOGRAPHS

1)	Introduction	52
2)	Test Conditions	52
3)	Material Specifications	53
4)	Test Matrix	55
5)	Mechanical Test Results, Fractography and Service Failures.....	58
	a) M-50 (Bearing and Tool Steel).....	58
	b) 15-5PH (Stainless Steel).....	95
	c) Custom 455 (Stainless Steel).....	108
	d) Type 347 (Stainless Steel).....	156
	e) A-286 (High Ni Stainless Steel).....	201
	f) Incoloy 901.....	261
	g) Incoloy 909.....	285
	h) Inconel 600.....	340
	i) Inconel X-750.....	424
	j) PWA 1480 (Cast Ni-Base Single Crystal).....	512
	k) MP-159 (Cobalt-Base Alloy).....	564
	l) Ti-6Al-2Sn-4Zr-2Mo.....	629
	m) Ti-6Al-4V.....	712

V. REFERENCE SECTION

1)	Introduction	726
2)	Failure Analysis Handbooks	726
3)	Fractograph Handbooks	728
4)	Failure Analysis Books and Articles	737
5)	Failure Analysis Source Books and Case Histories	739
6)	Special Publications	740
7)	Logic Networks and Other Approaches to Failure Analysis	744
8)	Computerized Data Bases	745
9)	Journals and Abstracts	747
10)	Technical Societies and Institutes	748

I. INTRODUCTION

1. BACKGROUND

→ Aircraft service failures of any type, from a simple rivet failure to complete engine failure, have the potential to result in loss of the aircraft and personnel. Accurate determination of the cause of the failure may yield information that will prevent similar future failures from occurring. It is helpful for the investigator to have a data base of known failure modes to draw from in forming his conclusions. → to p 1)

Several handbooks are presently available to investigators, offering scanning and transmission electron microscope (SEM and TEM) fractographs of alloys commonly employed in airframes and aircraft engines. The two primary Air Force failure analysis handbooks, "Electron Fractography Handbook" and "SEM/TEM Fractography Handbook", were published in 1965 and 1975, respectively.

2. OBJECTIVE

This program's objective was to create an updated volume of fractography of alloys that are presently, or in the near future will be, used in USAF aircraft. This volume addresses how differences in material and service conditions will affect the fracture appearance of service failures, relative to the fractography generated under controlled laboratory conditions. Additionally, the volume contains an annotated reference section of sources for failure analysis data.

3. PROGRAM DESCRIPTION

This program consisted of three tasks, requiring 24 months of technical effort. Task I involved generating and characterizing fracture surfaces under controlled laboratory conditions. Test conditions and procedures for tensile (smooth and notched), HCF (smooth and notched), LCF, TMF, high temperature fatigue, stress rupture, stress corrosion cracking and hydrogen embrittlement were defined. Material was acquired, machined into the necessary specimens and tested to produce the required fracture surfaces. Finally, the fracture surfaces were characterized by macrophotography, electron microscopy and metallographic techniques.

Task II involved the interpretation of the fracture surfaces generated in Task I. The appearance of the laboratory induced fractures were discussed, relative to expected changes in appearance resulting from differences in such variables as temperature, stress conditions, strain rate, geometry, manufacturing variables, microstructure, surface conditions, and alloy contamination. Examples of service failures are included in this area. These service failures were selected to closely

represent or compliment the pedigree failures from Task I. These failures were taken from contractor's internal data base.

Task III generated a literature survey of information of use to the failure analyst. This was used to create an annotated reference section, detailing sources for specific information. Basic information about how to perform a failure analysis and interpret fractographs are presented, resulting in a text that may serve as a starting point for any failure investigation.

II. FAILURE ANALYSIS TECHNIQUES AND METHODS

The techniques and methods used in failure analysis and fractography have been well documented in a number of books and articles. Many of these have been included in Section V, the Reference section. Reference numbers 1-4, 7, 9, 15, 20 and 22 are particularly appropriate.

1. APPROACHES TO FAILURE ANALYSIS

A. Common Sense Approach

A common sense approach to failure analysis works well in most cases. The goal is to ensure that all needed documentation and measurements are done prior to any destructive examinations. The following chronological list of possible steps or "recipe" to help to avoid leaving out an important step:

- o Collect background information, data, history, documentation and samples. This should include appropriate photographic documentation, collection and protection of fractured or failed components, and collection of specimens for chemical analysis, such as corrosion products or corrosive agents. Question people at the scene who have knowledge about or witnessed the failure.
- o Determine primary and secondary damage. This must be done by the on-site investigator, who may or may not be a failure analyst. Even in complex failures, it is usually possible to determine a primary source of the damage. Get help from those who best know and understand the hardware.
- o Examine failed components. Use a good stereo binocular microscope to carefully examine the failed parts and fracture surfaces. Serious failures often inspire a flurry of activity during which pertinent data and observations may be missed. It may be advisable to have more than one person examine the hardware independently.
- o Measure and inspect failed components. Where possible, make pertinent physical measurements of failed components. Use selected nondestructive inspection (NDI) techniques to look for additional cracks, secondary cracks or damage. Such techniques include fluorescent magnetic particle inspection (MPI), fluorescent penetrant inspection (FPI), X-ray radiography, ultrasonic inspection and eddy current inspection.
- o Examine fracture surfaces microscopically to determine modes and origins. This can be either a nondestructive or a destructive step, depending on specimen size and the type of microscope used. Smaller specimens, on the order of an inch cube, will fit directly into most modern scanning electron microscopes (SEM's). Larger specimens may need to be cut down. Remember to protect fracture

surfaces during cutting operations. Cutting is not required for transmission electron microscopes (TEM's), since replicas of fracture surfaces are examined.

- o Examine metallographic sections. This is usually a destructive step, although surface spot polishing may be nondestructive. Microstructural evaluation, grain size measurement and microhardness testing should be done at this time.
- o Determine cause of failures. Although examination of fracture surfaces will usually determine a mode of failure, such as material overstress or fatigue, the fundamental cause of the failure may not be obvious. Work with project, test, design and structural engineers as needed to determine the cause of failure.

B. Logic Networks, Fault Trees and Other Approaches to Failure Analysis

The common sense approach to failure analysis works well enough most of the time, at least for simpler failures. However, for more complicated or complex failures, or failures involving large numbers of components, a more sophisticated approach may be helpful.

George (46) developed a chart in which he divided and subdivided various causes of failure of metallic components. Failure categories included fracture and nonfracture, temperature, mechanical (stress) and corrosion (environment), and defects in design, manufacturing and assembly.

Collins, Hagan and Bratt (47) described a method they called the "failure-experience matrix." This matrix was a three-dimensional array of cells, with failure modes along one axis, component mechanical function along a second axis and corrective actions taken along the third axis. The matrix was used to help categorize failure analysis data for a large number of failed helicopter components. Even so, the matrix was sparsely populated. If more data were available, a designer could enter the matrix with a component of particular function and easily find out the known failure modes and possible corrective actions.

Louthan (48) applied Fault Tree techniques to the failure analysis of high strength low alloy (HSLA) steels, emphasizing stress corrosion cracking and hydrogen embrittlement. He defined a fault tree to be "a graphical technique that provides a systematic description of the combinations of possible occurrences in a system which can result in a fault or undesired event," in this case, a failure.

Jackson et al. (49) applied Kepner-Tregoe methodology to the failure analysis of boiler tubes. They used Kepner-Tregoe, a systematic problem-solving methodology, to help identify the root cause of failure, in addition to identifying the mode.

Raghuran and Shamala (50) reviewed the fault tree technique and the failure experience matrix as applied to failure analysis. Again, the emphasis was to go beyond determining the mode of fracture, to the root

cause of the failure, then using this information effectively to help prevent future failures.

Smith and Grove (51) applied failure analysis logic networks (FALN) to the failure analysis of composite materials. Logic networks are related to fault trees and flow charts, in that they can help guide failure analysts through the various nondestructive and destructive analysis techniques and procedures that are available.

Figure II-1 shows a modified version of Smith and Grove's sublogic network for fractography, illustrating how the technique can be applied to metals. The more sophisticated and systematic approaches to organization and analysis of metallic failures have merit, particularly for complex failures. Less complex failures may not warrant or require the additional time and effort.

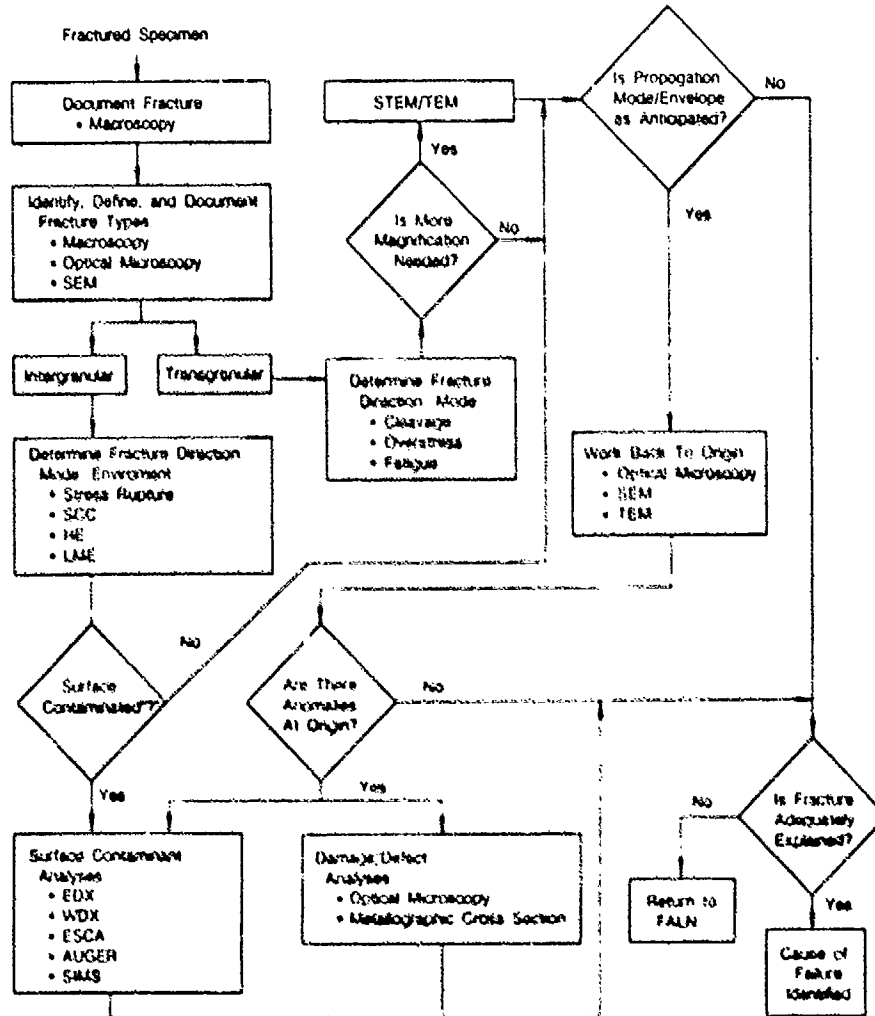


FIGURE II-1: Modified version of Smith and Grove's sublogic network for fractography. The network has been modified for application to metals.

2. CARE AND HANDLING OF FRACTURE SURFACES

A. Preservation and Handling of Fracture Surfaces

Many of the significant features on fracture surfaces are microscopic and must be protected from mechanical and environmental damage. Low alloy steels have little inherent corrosion resistance and must be protected from even atmospheric corrosion by covering with oil or grease, providing moisture-free storage or applying a protective spray coating, such as Krylon Crystal Clear (Borden, Inc.). Any coating used must be totally soluble in an organic or other mild solvent. Fortunately, most other aerospace alloys possess good atmospheric corrosion resistance.

To prevent mechanical damage, each fracture surface should be placed in a separate paper envelope or plastic bag. Fracture surfaces on larger parts may be covered with cloth or cardboard. Resist the temptation to fit the two halves of the fracture back together, as this could damage microscopic features. Do not pick at the fracture surface with tweezers or other instruments. Any unnecessary contact with the fracture surface should be avoided because acids or other contaminants on the hands could damage fine features.

B. Cleaning Fracture Surfaces

When possible, cleaning of fracture surfaces should be avoided, especially where analysis for contaminant elements or corrosion products may be required. If a fracture surface is covered by loosely adherent dust or dirt, a soft natural fiber brush may be used. Dry compressed air is also useful for removing loose contamination. Do not use stiff plastic brushes or any kind of metal brush because plastic can be embedded in the fracture and metal can mechanically damage the features. If dried mud is present on the fracture, warm soapy water and a stiffer natural fiber brush may be used. Parts should be immediately rinsed, dried with dry compressed air and reprotected.

Oils and greases may be removed by organic solvents, such as mineral spirits or a vapor degreasing agent such as trichloroethane. Final cleaning just prior to examination in the SEM is often done ultrasonically in alcohol or acetone.

An alternate method of cleaning is to repeatedly replicate the area of interest with cellulose acetate replicating tape. Each time the dried tape is removed, the fracture becomes cleaner. Carefully remove the tape, especially on rougher surfaces to avoid tearing the tape and leaving remnants behind. Leaving a final application of tape on the surface affords extra protection until it is time for examination.

A general rule is to use the gentlest and mildest cleaning procedures possible. Any corrosion or attack of the base metal by a cleaning agent, even on a microscopic scale, will probably damage the fracture surface. If the fracture surface is severely corroded or oxidized, the chances are good that any fracture features have already been destroyed, and cleaning will

not restore them. However, overall or general features, such as chevron markings or fatigue thumbnails, may remain.

C. Breaking Open Cracks.

In order to perform fractography on a crack, the crack must first be broken open to expose the surfaces. The usual approach is to estimate the length and depth of the crack, notch or cut the part to near the ends of the crack and the bottom of the crack, and to open up the crack without smearing the crack surfaces together. It is often convenient to cut a V-notch on the back side, away from the crack, then squeeze the V shut with pliers or a vise. See Figure II-2. Methods of cutting include: hack saws, abrasive cutting wheels, dremel tools, air-powered hand grinders and metallographic cut-off machines.

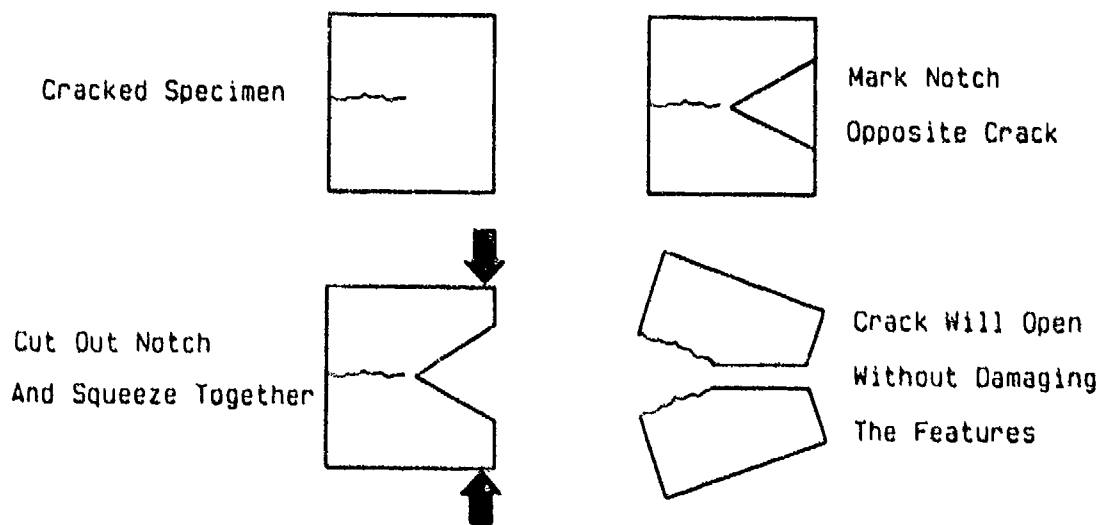


FIGURE II-2: Schematic showing technique for opening a crack without damaging surface features. The extent of the crack is estimated and a V-shaped notch is drawn on the side opposite the crack. The notch is then cut out and the two halves are squeezed together to open the crack.

3. VISUAL EXAMINATION TECHNIQUES

A. No Magnification Examination - Field Examination Techniques

Many failure analysts seldom get into the field. Parts or components are brought to them for examination. This probably is because much of the equipment needed for modern failure analysis is not portable. When field activity is required, the failure analyst must pay close attention to detail.

- o Take time to carefully look over the site and try to determine which damage is primary (occurred first) and which is secondary (occurred later or as a result of). Document the failure site with still photographs and sketches to show the layout, and record distance measurements.
- o Ask questions and talk to witnesses to learn service history and sequence of events leading up to the failure. Record this information in writing or with a tape or video recorder.
- o Collect and protect specimens for further analysis. Methods of preserving fracture surfaces were discussed in Section 2A. Specimens for chemical analysis, such as corrosion products or corrosive agents, should be placed in glass or plastic bottles, or plastic bags. Dry specimens may be placed in paper envelopes.
- o Select other parts or components for further examination. Mating or related hardware may require laboratory examination for cracks or other damage. In aerospace failures, entire engines and airframes are often recovered.

B. Macroscopic Examination

Macroscopic examination of fracture surfaces, cracks or other damage is a very important aspect of failure analysis. The instrumentation used depends on where the examination is to be done.

- o In the field or in a shop setting where a stereo microscope may not be available, a hand-held magnifying glass, perhaps with battery powered illumination, is a good alternative. Magnification is usually about 10X, although anything up to about 15X may be used. Higher magnification lenses or small microscopes are usually not helpful because they are difficult to hold steady and because illumination is difficult.
- o Stereo microscopes are the best choice for macroscopic examination of fracture surfaces. The three-dimensional effect lends depth to features and appears to improve resolution. Some microscopes have fixed magnifications, while others have "zoom" capability, which allows the analyst to identify areas of interest at lower magnification, then examine finer features at

higher magnification. Magnification ranges vary from about 5X up to as high as 100X for some instruments. Illumination is another important factor. Oblique illumination often brings out fracture surface details better than more direct lighting, but it is convenient to have both capabilities.

- o Macroscopic photography is another important tool for the failure analyst because it can permanently document failed parts and fracture surfaces and provide photographs for presentation of results. A 4 inch X 5 inch camera works much better than a 35-mm camera for this because the larger negative can record more detail. Black-and-white Polaroid film, preferably that which yields a negative (Type 55), works well, because you can immediately see if the photograph captured what you wanted to show. Color photography is sometimes advantageous, particularly to show oxidation or corrosion product hues.

Several interchangeable lenses are needed to cover a magnification range of 1/8X to 30X. Illumination is again important, with oblique lighting better in some instances and more direct lighting better in others. Fixed illumination is acceptable for many lower magnification photographs, but the technique of "painting" often works better for higher magnification photographs. Painting is a technique where the camera shutter is opened in a darkened room and light is applied to the part or fracture surface by waving or playing a concentrated light source, such as a small bulb or flood light, over areas of interest, emphasizing and highlighting desired features.

C. Macroscopic Features

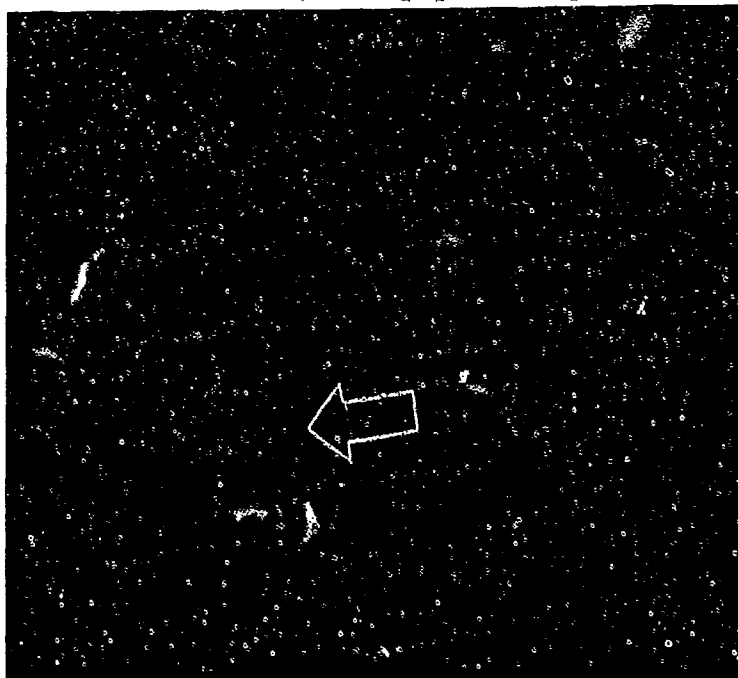
Start viewing fractured hardware at low magnifications and progress to higher magnifications. Look for evidence of plastic deformation or distortion. Ductile materials that have fractured due to material overstress (overload) usually exhibit plastic deformation, while brittle materials usually do not. Fatigue fractures of even fairly ductile materials, however, may not exhibit deformation. The presence of a significant shear lip, or angled ridge along the edge of a fracture surface, is also a measure of ductility and can indicate the area of the section that fractured last.

One of the things to look for on a fracture surface is directionality. Do the features appear to be emanating from a single area or starting point called an origin, or perhaps from multiple origins? Overstress fractures of brittle materials often exhibit a chevron pattern (Section III, Figure III-17) of nested letter V's, or herringbone pattern, that points back towards the origin. Overstress fractures of more ductile materials sometimes exhibit tear ridges or cleavage steps, lines that tend to emanate from an origin area.

Progressive fractures may exhibit arrest lines or arrest marks (Figure II-3), sometimes referred to as beach marks or clamshell marks. These are places where the crack arrested, the loading changed or the environment changed, and appear as irregular elliptical or semi-elliptical rings radiating outward from one or more origins. Fatigue fracture surfaces often exhibit a series or even many arrest lines, while stress corrosion fracture surfaces may exhibit none or only a few. Even those progressive fractures that do not show a series of arrest lines may exhibit the elliptical or semi-elliptical shape, surrounded by the final fracture at critical crack size due to material overstress.

Finally, ductile fractures often exhibit a fibrous or silky smooth texture at lower magnifications (Section III, Figure III-5) due to their transgranular nature. Some brittle fractures, particularly elevated temperature fractures, exhibit an irregular or rough granular texture because of their intergranular nature.

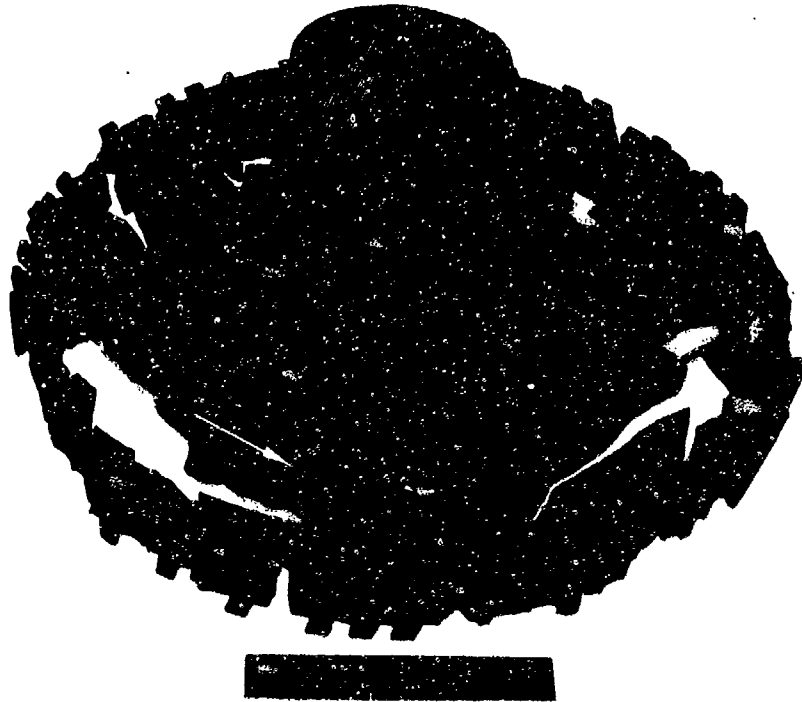
Fracture mapping is a technique often employed to help analyze complicated failures of structures like bridges, pressure vessels, aircraft airframes, composites and rocket motor cases. Chevron marks or other fracture features are used to determine macroscopic fracture directions on individual fragments and these are combined on an overall map of the fracture. This map hopefully will show the fracture emanating from a primary origin area. The usefulness of this technique is illustrated in Figure II-4, a photograph of a reconstructed titanium alloy compressor disk that burst during proof testing at cryogenic temperature.



FAL 93833

MAG: 3X

FIGURE II-3: Arrest marks on the opened surface of a fatigue crack. The spacings between arrest marks become narrower as the crack progresses through a thicker section (arrow).



FE 255662

FIGURE II-4: Reconstructed compressor disk that fractured during cryogenic proof testing. The directions of fracture propagation (black arrows) were marked on each fragment before reconstruction so a map of fracture progression could be used to identify a primary origin area (white arrow).

4. SCANNING ELECTRON MICROSCOPE (SEM) EXAMINATION

The scanning electron microscope, usually referred to as "SEM," uses an electron beam rather than light to illuminate a specimen or fracture surface. The microscope contains an electron gun that generates and accelerates electrons to energies typically between 5 and 30 keV, electromagnetic lenses and apertures that focus the electron beam to a spot typically 30-40 angstroms in diameter, electromagnetic coils that scan or raster the beam on the specimen, and an electron detector used to form an image on a cathode ray tube (CRT) (Figure II-5). Because electron beams are impeded by air molecules, the system must operate under vacuum (10^{-6} - 10^{-7} torr).

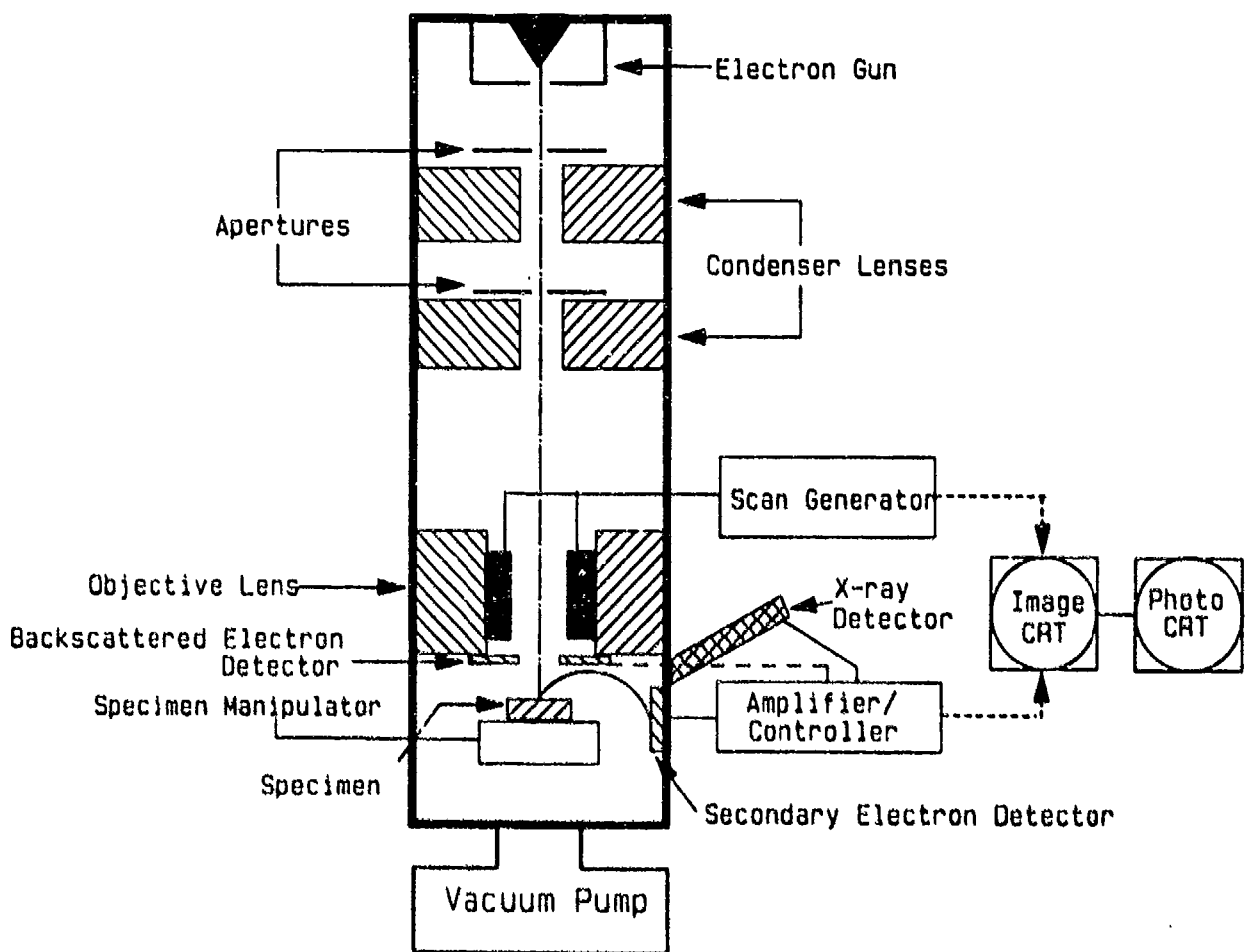


FIGURE II-5: Schematic showing typical components of a modern SEM.

When the beam of electrons strikes a specimen, several different types of electrons are generated, including secondary electrons, back-scattered electrons and Auger electrons. These electrons emanate both from the surface and from slightly subsurface, giving sampling depth. In addition, low intensity X-rays are generated. Commercial SEM instruments use secondary electrons to form images, but may also be equipped with back-scattered electron and X-ray detectors.

As a first approximation, the specimen image appears as viewed from the perspective of the electron detector, illuminated in the direction of the electron beam. Back-scattered electrons follow line-of-sight trajectories, whereas secondary electrons can follow curved trajectories. The difference can affect the generated image. Back-scattered electron images are sometimes useful because they give contrast due to variations in atomic number. This can be used to highlight chemical segregation or inclusions.

A. Advantages and Limitations

The SEM is undoubtedly the most versatile modern instrument available to failure analysts. It images electrons that are emitted back from a solid specimen, rather than imaging electrons that pass through a very thin specimen, as does a transmission electron microscope, or "TEM." As a result, the SEM possesses a number of advantages and disadvantages.

Advantages of the SEM:

- o Resolution is much better than for light microscopes, permitting magnifications of from 10X to 100,000X, although 10X to 30,000 is more attainable in practice. This resolution is possible because electrons have very short wavelengths and theoretical resolution is inversely proportional to wavelength, and because of the small spot size of the electron beam that is used to scan the surface.
- o Depth of field (depth of focus) is much better than for light microscopes, permitting irregular surfaces to be kept in focus. The depth of focus ranges from 2 mm (0.08 inch) at 10X to 1 micron (40 microinches) at 10,000X. This is possible because of the small divergence of the electron beam striking the sample.
- o Direct examination of specimens or fracture surfaces is conveniently done, with specimen chamber size being the major limitation. If a specimen will fit inside the microscope without cutting, the technique becomes essentially nondestructive. One exception to this is organic specimens which can be damaged by high energy electron beams. To avoid this, lower accelerating voltages can be used.
- o Elemental chemical analysis of a specimen can be carried out in the microscope by equipping it with an X-ray detector.

Disadvantages of the SEM:

- o Resolution is not as good as for TEM microscopes because lower electron accelerating voltages must be used and because a scanned or rastered electron beam is used in the SEM.
- o Images sometimes seem somewhat unrealistic because the electron image is derived from both surface electrons and slightly subsurface electrons, which may give a fracture surface a slightly "translucent" appearance.
- o Relating the actual angular orientation of a specimen to the microscope image may be difficult because the relative tilt of the specimen and the apparent viewing angle of the electron detector obscure geometric relationships.
- o Larger specimens may have to be cut down in size to fit into the microscope. Although modern SEM's may be able to hold a specimen several inches long and an inch or more high, not enough freedom of movement may remain to view the entire specimen. SEM's with even larger specimen chambers are becoming available.
- o Specimens must have a relatively low vapor pressure ($\leq 10^{-3}$ torr) due to vacuum requirements of the SEM.
- o Unetched metallographically polished flat surfaces usually do not present sufficient contrast for good images at lower magnifications, below 300-400X.

B. Sample Preparation and Cleaning

As was mentioned earlier, specimen size limitations depend on the size of the specimen chamber, and on the size and capabilities of the specimen handling stage in the microscope. Assuming that a specimen will fit or can be cut down to fit inside the microscope, it may still require cleaning. Because the microscope operates under vacuum, the specimen must be dry and free of volatile materials, oil and grease. Cleaning procedures were described in Section 2B. In addition, the specimen must have adequate electrical conductivity. If it does not, it can be given a thin vapor deposited coating of carbon or gold. If X-ray analysis or imaging is to be done, care must be exercised in cleaning so as not to remove, dissolve or contaminate that which is to be analyzed. Dirty specimens can lead to a dirty microscope, which can result in poor resolution, increased maintenance and down time.

C. Documentation Sequence and Identification of Photographs

Careful identification and orientation of SEM photos is essential to correctly interpret them later. Examination and documentation should begin at lower magnifications, followed by higher magnification examination of

selected areas. The SEM operator or the failure analyst must understand the orientation of the specimen in the microscope and clearly mark and identify photographs, either with a grease pencil directly on the photos or with a pen on the white margins of the photos.

D. Viewing Replicas in the SEM

When a specimen or fracture surface is too large to be placed directly into the SEM and for some reason cannot be cut down in size, the fracture can be examined through the use of cellulose acetate (plastic) replicas. The replicas must be coated (vapor deposited) with a thin layer of carbon or gold to provide electrical conductivity. Of course, no chemical analysis work can be done unless some loosely adherent material can be extracted from the surface of the specimen and incorporated into the replica. Care must be taken to avoid locally overheating and damaging the replica with the electron beam in the microscope.

E. X-ray Energy Spectroscopy (XES) and Wavelength Dispersive Spectroscopy (WDS) Analysis Techniques

One of the advantages of the SEM is that it can also be equipped with an X-ray detector. Two types of detectors are typically used. If a wavelength dispersive (WDS) type of detector is employed, analysis can be more accurate but will be much more time consuming. WDS is more typical of electron probe microanalyzer, or electron microprobe, instrumentation. If an energy dispersive type of detector is employed, analysis may be less accurate but will be much less time consuming. XES is more typical of SEM instrumentation.

The XES X-ray detector can be used in two ways in the SEM. It can be used to generate X-ray energy spectra showing characteristic X-ray peaks for the elements present in a specimen (Figure II-6). These data can be used to generate an elemental chemical analysis of the specimen. The X-ray detector can also be used to generate an elemental X-ray image or map of the surface being examined by collecting X-rays of a narrow energy range corresponding to the characteristic X-rays of a single element. Because the intensity of X-rays is relatively low, the quality and detail of the image will be relatively crude. Even so, the method can be very effective when combined with an electron image and can reveal local areas of chemical segregation.

XES analysis can be conducted on a large area yielding an average composition, on a small area or on a spot yielding local composition of a specimen. Smaller areas of analysis generally require longer X-ray collection times for good results. The electron microprobe instrument is better suited for analyzing very small areas (small spot sizes), such as might be required for fine precipitates or analysis of diffusion gradients. The latter instrument is also more capable of analyzing for elements of low atomic number.

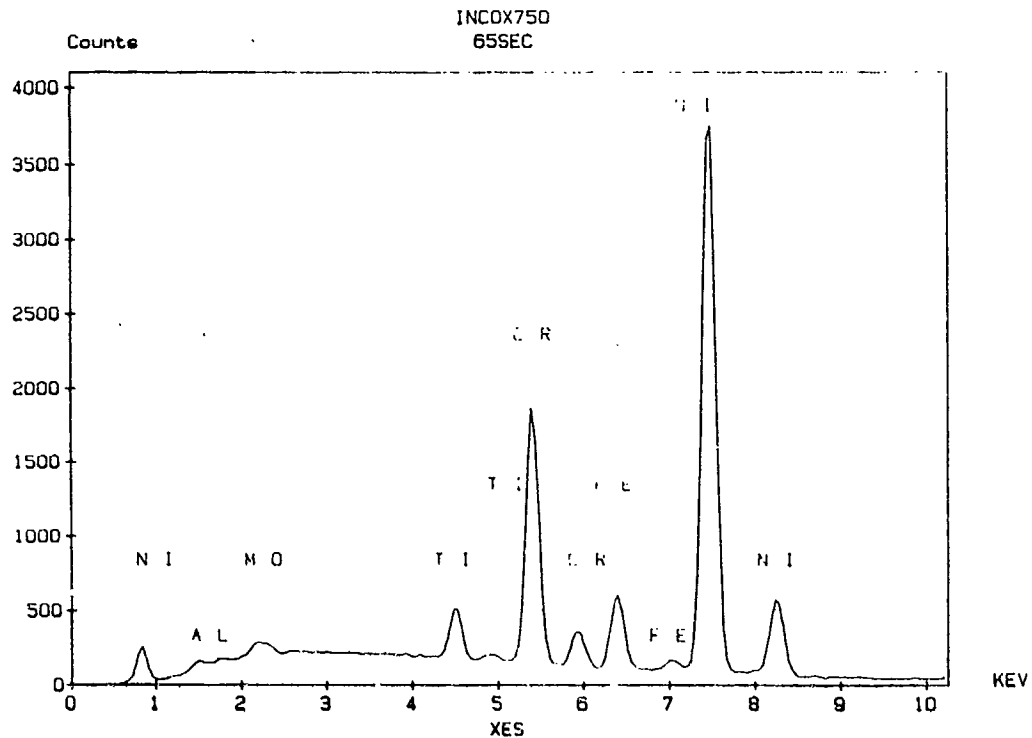


FIGURE II-6: XES spectrum showing the elements present in Inconel X-750.

5. TRANSMISSION ELECTRON MICROSCOPE (TEM) EXAMINATION

The transmission electron microscope, usually referred to as "TEM," predates the SEM. The TEM also uses electrons to illuminate a specimen, but it does not scan or raster the electron beam. Rather, the electron beam passes through the specimen producing a greatly magnified image on a phosphorus screen. Figure II-7 shows a schematic of the TEM. The specimen may be an extremely thin metal disk (foil), 3 mm in diameter and locally less than 100 angstroms in thickness, or may be a plastic or carbon replica of a surface. The latter method, where a carbon replica is made of a fracture surface and viewed in the TEM, may be used to determine the fracture mode in failure analysis.

A. Advantages and Limitations

Although the TEM is not as versatile as the SEM when applied to failure analysis, it does possess some advantages. Advantages of the TEM over the SEM are:

- o Resolution is better than for the SEM. Thus, fine fatigue striations are generally resolved much more clearly. This is possible because higher accelerating voltages can be used in the TEM and because it uses a simpler electron optical system. Magnifications of 30,000-50,000X are easily attainable with the TEM, but low magnifications are limited to about 1,000X.

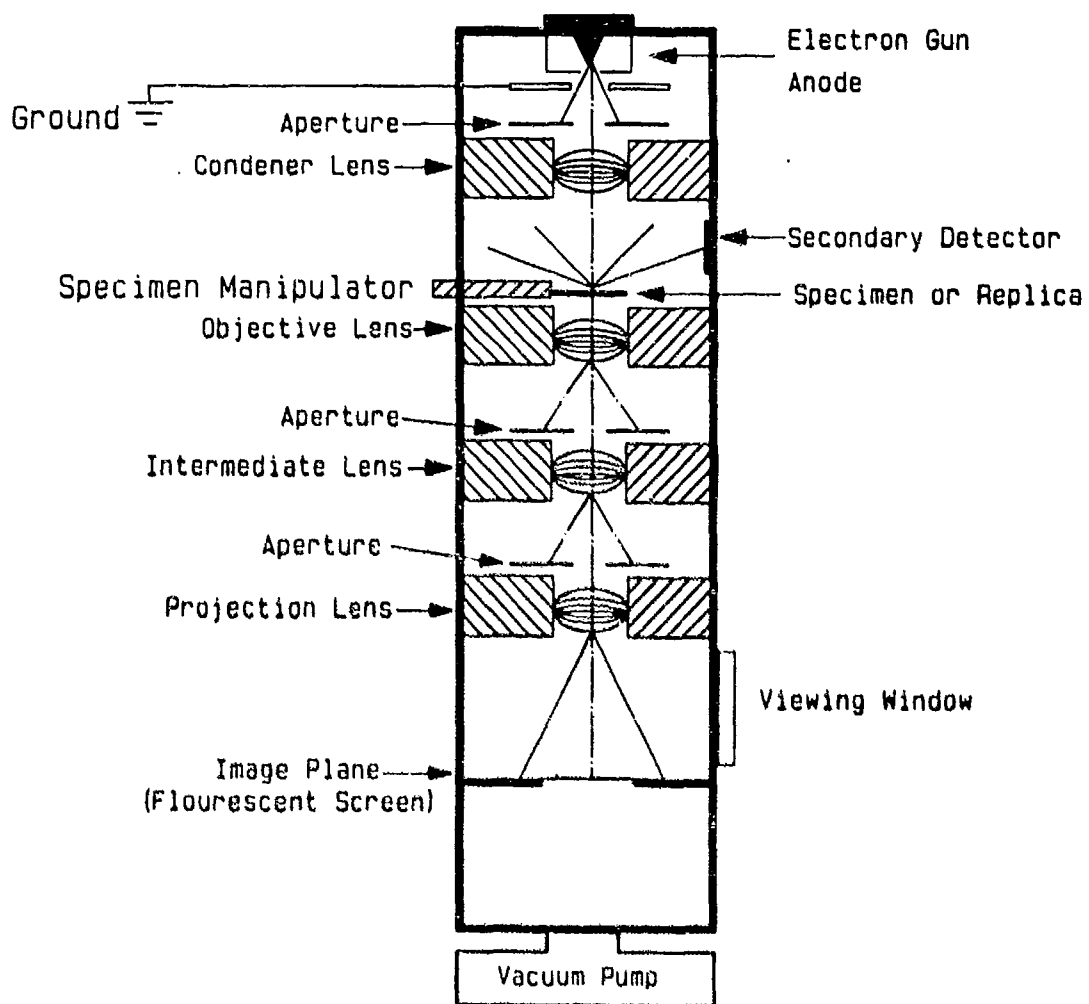


FIGURE II-7: Schematic showing the basic components of a TEM.

- o Topographical features sometimes appear more realistic in the TEM than in the SEM. This is because the replicas viewed in the TEM yield only topographical (surface) features, while SEM images are derived from both surface and slightly subsurface electrons. TEM images are also enhanced by "shadowing" the replicas, to give perspective.

Disadvantages of the TEM:

- o Direct examination of fracture surfaces is not feasible.
- o Only small specimens (replicas) can be accommodated.
- o Limited low magnification capabilities make judging specimen orientation more difficult than for the SEM.
- o Replicas may contain artifacts.
- o Specimen preparation is time-consuming and requires considerable skill.
- o Elemental chemical analysis cannot be carried out where replicas are employed.

B. Specimen Preparation - Replicas

Although there are several methods of obtaining replicas of fracture surfaces for examination in the TEM, probably the most common is the two-stage shadowed carbon replica. In this method, 0.001-0.01 inch thick cellulose acetate tape is softened with a few drops of acetone, pressed onto the fracture surface with a finger or resilient pad, allowed to dry, and peeled off or stripped. Often the first replica will contain entrapped dirt from the fracture surface. Repeated replications will clean the fracture surface and eventually yield a cleaner replica. The final "clean" replica is mounted upside down (fracture side up) on a glass slide.

To improve contrast and to give a sense of perspective, replicas are usually "shadowed" by directionally vapor depositing a heavy metal or alloy at an angle (typically 15-45 degrees) to the fracture surface (Figure II-8). Chromium, germanium and gold-palladium are commonly used. This is usually done with the replica double-sided taped to a glass slide.

After shadowing, a layer of carbon is vapor deposited on the replica surface. The replica sandwich is then cut into small squares and placed carbon-side down on small copper or nickel TEM grids. The plastic is extracted, usually by acetone or acetone vapors, leaving a shadowed carbon replica on a TEM grid.

TEM replicas are labor and technique intensive, and fragile. As a result, a number of types of artifacts may be created on the replica fracture surface, and care must be exercised in interpreting these.

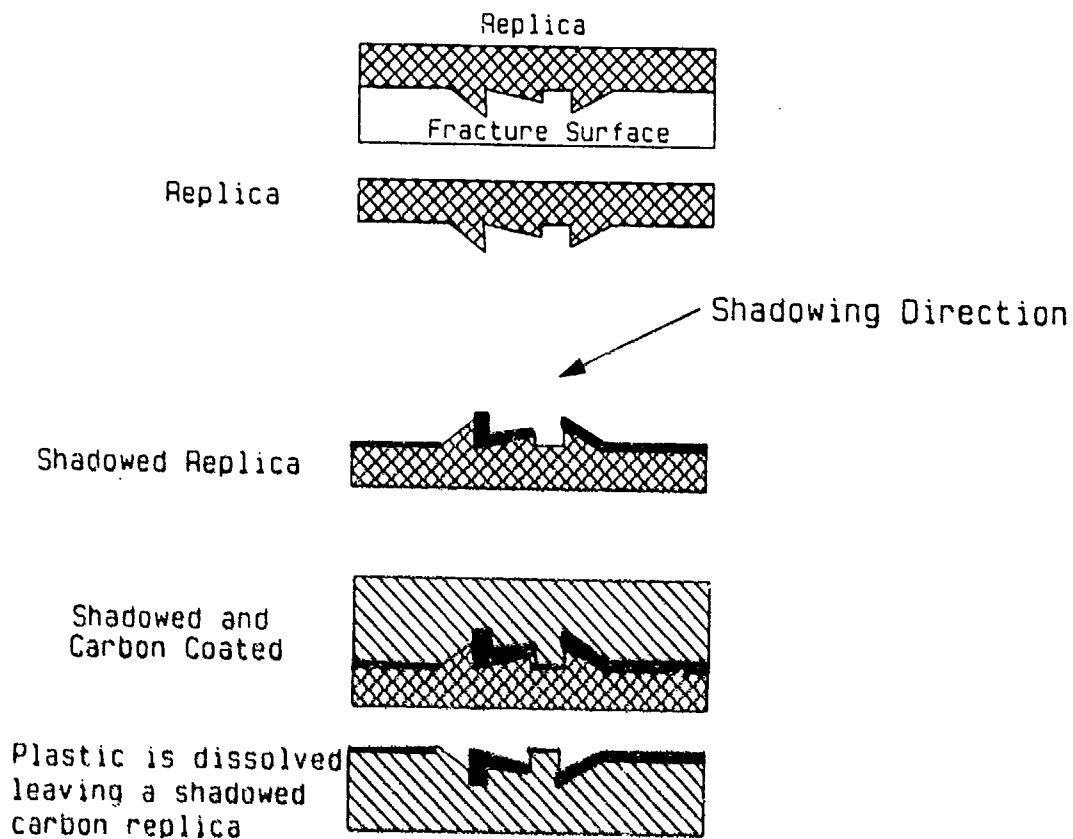


FIGURE II-8: Schematic showing the technique used to prepare TEM replicas. SEM replicas are prepared in the same way except that the replica is shadowed with metal and viewed directly without carbon coating and dissolving the plastic.

C. Fatigue Striation Counts

One of the more useful applications of TEM microscopy to failure analysis is in counting fatigue striations. Fatigue striations, particularly fine striations, are generally much more clearly resolved in the TEM than in the SEM. Striation counts are done by examining a replica or replicas at measured distances from an origin area or surface. Photographs are taken of typical striations at each location at appropriate magnifications, such as 3,000X, 10,000X and 30,000X.

The number of striations in a conveniently chosen length are physically counted on each photograph, that number divided by the measured length, and multiplied by the magnification of the photograph. This results in an estimate of the number of striations per unit length, or striation density.

A plot of striation density versus distance (from the origin area or surface) is made, containing points derived from the various photographs, and a line or curve is fit through the points. Integration of the striation density versus distance curve yields an approximate ($\pm 10\%$ to $\pm 50\%$) total number of striations on the fracture surface.

A striation count can be used to help determine the specific fatigue mode (HCF or LCF) and subsequently what may be causing the fatigue. This is done by first assuming that each significant loading cycle after crack initiation corresponds to one fatigue striation and then comparing with potential fatigue "drivers." Also, knowing the frequency of significant loading cycles would permit calculation of the time required for crack propagation.

6. CHEMICAL ANALYSIS TECHNIQUES

Most chemical analysis done as part of failure analysis is probably done by XES in the SEM or by WDS in the electron microprobe. Occasionally, more diverse or advanced analysis techniques are warranted. Table II-1, adapted from Volume 10 of the Metals Handbook (9th Ed.), is included here for reference.

7. METALLOGRAPHIC EXAMINATION

The procedures of metallographic preparation, polishing and etching are widely known and described in detail elsewhere. However, specific applications to failure analysis may require special care and diligence.

A. Sectioning Through Origins

If an origin area is identified during the course of fractographic examination, it is usually desirable to make a metallographic section through the area. Careful sectioning may be required, perhaps with a low speed diamond impregnated cutting wheel, or "diamond saw." Material defects or other anomalies are of interest, such as inclusions, prior cracks, embedded particles, microstructural anomalies, strain lines and abusive machining. Small defects may require progressive polishing, or serial sectioning. This is usually done manually by grinding off a few thousandths of an inch of material (as measured by a micrometer) at a time from a mounted metallographic specimen and examining the surface.

B. Evidence of Plastic Deformation

Strain lines (Figure II-9) are evidence of extensive plastic deformation. Severe plastic deformation resulting from abusive machining may reveal itself as severely deformed grains or even light-etching layers (Figure II-10). Abusive grinding may even locally alter the microstructure due to generated heat causing grinding burns.

Table II-1

Selected Chemical Analysis Techniques

Wet analytical chemistry, electrochemistry, ultraviolet/visible absorption spectroscopy, and molecular fluorescence spectroscopy can generally be adapted to perform many of the bulk analyses listed. ● = generally usable, N = limited number of elements or groups; G = carbon, nitrogen, hydrogen, sulfur, or oxygen; S = under special condition; D = after dissolution; Z = semiconductors only.

Method	Elem	Qual	Semi-quant	Quant	Macro/Bulk	Micro	Surface	Major	Minor	Trace	Phase ID	Structure
AAS	D	●	●	D	D	●	●	D	D	D		
AES	●	●	●			●	●	●	●	S		
COMB	G			G	G			G	G			
EPMA	●	●	●	●		●		●	●	N	S	
IA					●	●						
ICP-AES	D	D	D	D	D			D	D	D		
IR/FT-IR	Z	Z	Z	Z	Z				Z	Z		
OES	●	●	●	●	●			●	●	●		
OM						●	●					
SEM	●	●	●	S		●		●	●		S	
SIMS	●	●	●				●	●	●	S		
SSMS	●	●	●	●	●			●	●	●		
TEM	●	●	●	S		●		●	●		●	●
XPS/ESCA	●	●	●				●	●	●			
XRD		●	●	S	●			●	●		●	●
XRS	●	●	●	●	●			●	●	N		

- | | | | |
|---------|---|------|----------------------------------|
| AAS | Atomic absorption spectrometry | OM | Optical metallography |
| AES | Auger electron spectroscopy | SEM | Scanning electron microscopy |
| COMB | High-temperature combustion | SIMS | Secondary ion mass spectroscopy |
| EPMA | Electron probe x-ray microanalysis | SSME | Spark source mass spectrometry |
| ESCA | Electron spectroscopy for chemical analysis | TEM | Transmission electron microscopy |
| FT-IR | Fourier transform infrared spectroscopy | XPS | X-ray photoelectron spectroscopy |
| IA | Image analysis | XRD | X-ray diffraction |
| ICP-AES | Inductively coupled plasma atomic emission spectroscopy | XRS | X-ray spectrometry |
| OES | Optical emission spectroscopy | | |

* Adapted from Metals Handbook, 9th Ed., Vol. 10, "Materials Characterization", American Society for Metals, Metals Park, OH, 1986, pp. 3 and 4.

C. Maximum Metal Temperature Analysis

Certain alloys, particularly nickel and iron base superalloys that are strengthened by precipitation of a second phase, are amenable to temperature analysis. Some alloys can be analyzed by optical microscopy (1,000X magnification) and some require TEM microscopy (3,000-30,000X magnification). The approach is to compare microstructures of suspect engine parts or components with microstructural standards, to estimate maximum exposure temperatures. If exposure temperatures significantly exceeded heat treatment temperatures, microstructural alterations should be apparent.

Some limitations to temperature analysis occur because microstructures may be affected by factors other than temperature, including time at temperature, prior processing and applied or residual stress levels. Still, where applicable, the technique has yielded very useful data.

D. Replication of Large Parts

Microstructural review of large parts or components, or parts that are not available for destructive testing, may be accomplished by local spot grinding and polishing. This is carried out by grinding and polishing with an air powered grinder, etching, and replication of the etched surface. The replica, which can be shadowed if desired, is taped to a glass slide and examined under an appropriate (optical or electron) microscope. The affected area of the part should be chemically neutralized and polished to remove any effect of the etchant. Care must be taken so that the amount of material removed does not exceed the dimensional requirements of the part.

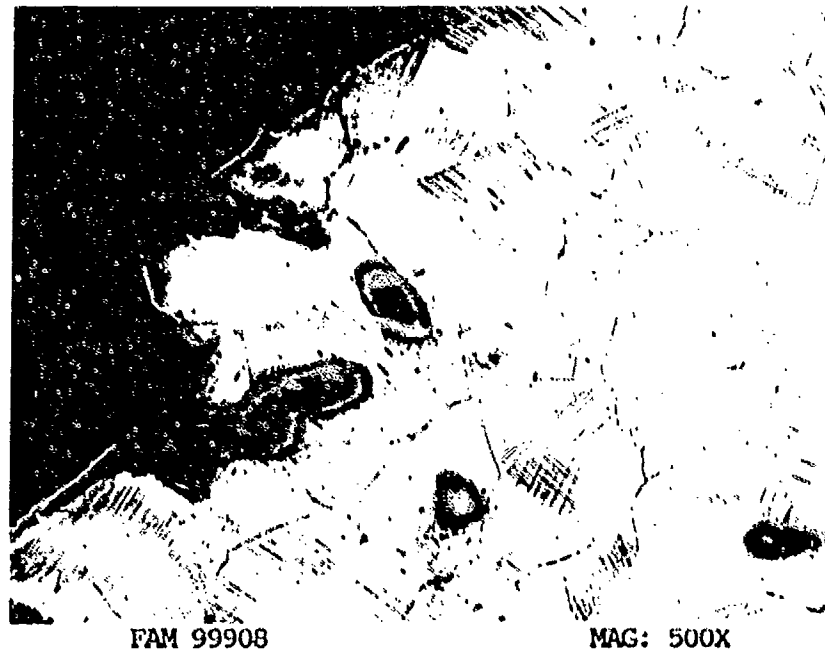
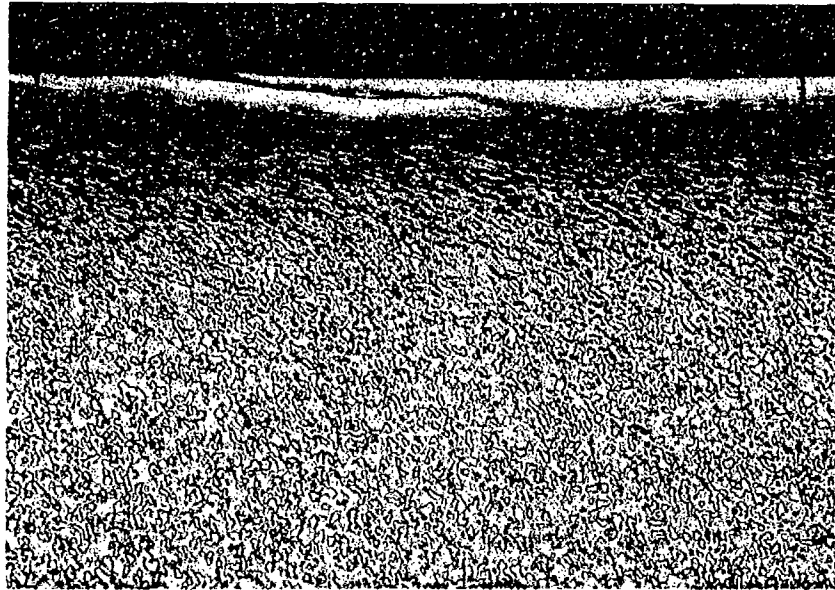


FIGURE II-9: Strain lines associated with an LCF fracture.
Etchant: Kalling's Reagent



FAM 100353

MAG: 500X

FIGURE II-10: Light-etching layer (brackets) on the surface of a gun drilled hole in a nickel-base alloy disk.

Etchant: Glyceregia

III. FRACTURE MODES

Many excellent books and articles have been written describing the fracture modes and fracture surface appearances commonly encountered in failure analysis. Many of these have been included in Section V, the Reference section. Reference numbers 1, 2, 7, and 9 are particularly appropriate.

1. INTRODUCTION

The fracture of metallic materials can occur by four basic modes. The four modes are ductile overstress (characterized by dimples), brittle overstress (low energy cleavage), fatigue, and decohesive rupture (grain boundary separation). Each of these modes has several subcategories that exhibit unique fracture features. The features commonly observed using scanning electron microscopy (SEM) and visual examination, using a stereo (binocular) optical microscopy, will be illustrated along with a brief explanation of how they are produced.

2. DUCTILE OVERSTRESS

The fracture of ductile metallic materials subjected to continuously rising stress occurs by a process known as dimple rupture. The mode gets its name from the characteristic dimpled fracture surface that is produced. As the stress is increased, dislocations move in preferred directions on preferred slip planes within the material. The motion of dislocations is impeded in regions of high strain or disorder in the matrix such as second phase particles, grain boundaries or inclusions. The dislocations tend to pile up at these sites, nucleating microvoids (Figure III-1). As these voids grow, the stress on the surrounding material increases until ductile fracture occurs (Figure III-2). The resulting fracture surface, when viewed on the SEM, exhibits cup-like depressions resulting from the elongation of the nucleated voids (Figure III-3). The nucleating particles are often visible at the bottoms of the dimples (Figure III-4).

A. Macroscopic Appearance

The macroscopic appearance of a ductile overstress fracture is generally characterized by:

- o Significant plastic deformation.
- o Primary fracture area exhibiting a fibrous appearance.
- o Final overstress area (shear lip) whose size depends on the ductility of the material, strain rate and stress concentration.

The macroscopic appearances of two ductile overstress fractures are shown in Figures III-5 and III-6.

B. SEM Appearance

1. Dimple Size

Dimpled rupture fractures can exhibit a wide range of features depending on the distribution of nucleation sites, stress orientation, temperature, ductility and strain rate. The size of the dimples is controlled by the size, number and distribution of nucleation sites. A finely dispersed second phase generally results in fine dimples because there are many sites available for nucleation and the voids do not grow large before fracture occurs (Figure III-7). Coarser dimples form when the nucleation sites are large and/or widely dispersed, allowing individual voids to grow large before final fracture (Figure III-8). Under some circumstances, voids nucleate preferentially at grain boundaries or at intersections of several grains (triple points). This results in an intergranular fracture with dimples on the grain faces and, in particular, at the grain edges. A typical intergranular ductile overstress fracture mechanism and the resulting appearance is illustrated in Figure III-9.

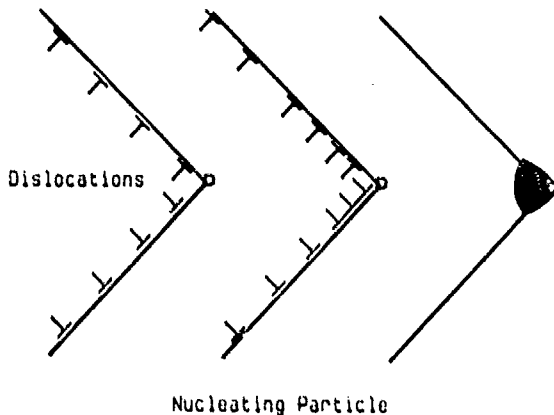


FIGURE III-1: Dislocation motion along low index close-packed planes in close-packed directions results in dislocation pile up at high strain sites in the matrix. These concentrations of dislocations eventually result in nucleation of voids.

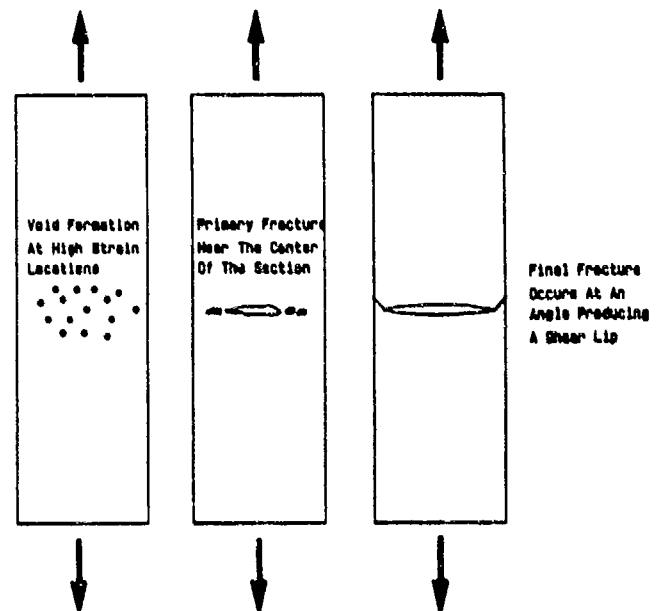
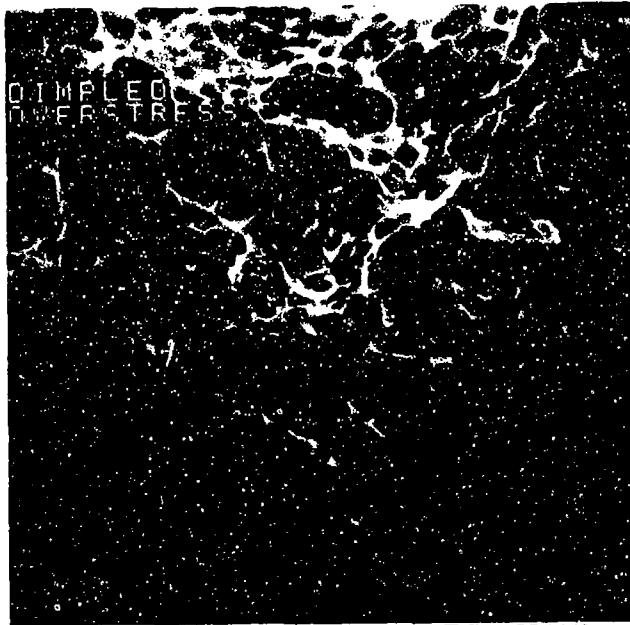
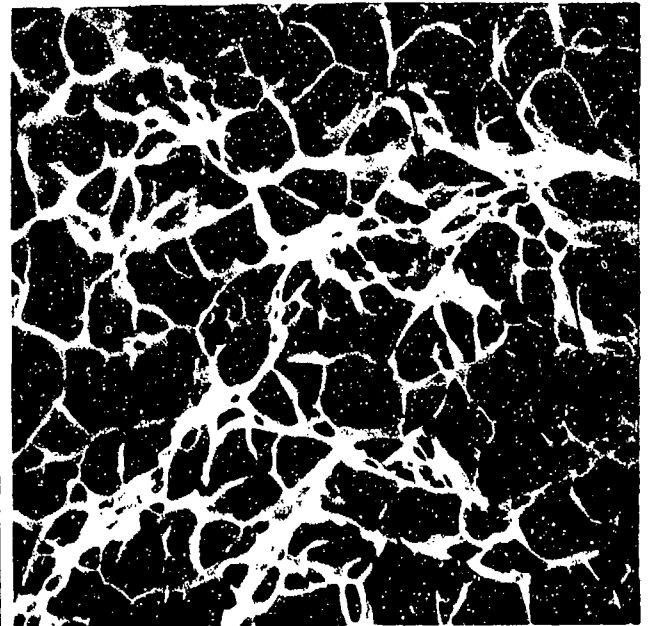


FIGURE III-2: Growth of voids at second phase particles, grain boundaries or inclusions eventually results in ductile fracture.



MAG: 6000X



MAG: 1000X

FIGURE III-3: Typical SEM appearance of a dimpled rupture fracture.

FIGURE III-4: Dimpled rupture with nucleating particles visible at the bottom of several dimples (arrows)



FAL 92556

MAG: 12X

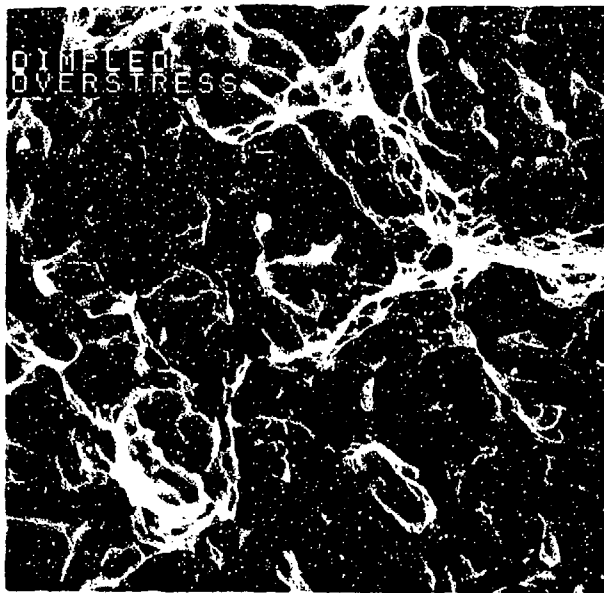
FIGURE III-5: Macroscopic appearance of a dimpled rupture fracture. Arrow indicates the origin area. The final overstress area (shear lip) is shown by a bracket.



FAL 92553

MAG: 12X

FIGURE III-6: Dimpled overstress of fracture exhibiting no clear origin area.



FAM 99399

MAG: 3000X

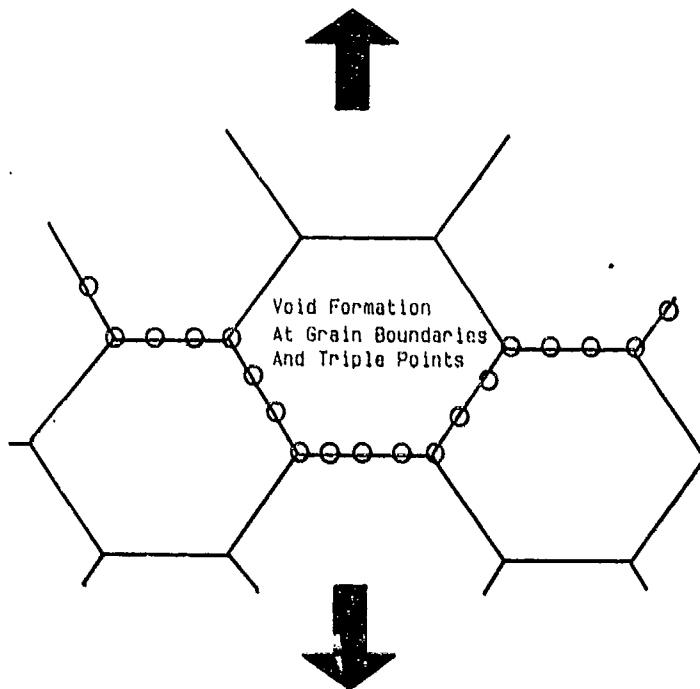


FAM 99532

MAG: 1000X

FIGURE III-7: Fine dimpled overstress resulting from finely dispersed second phase particles that act as void nucleation sites.

FIGURE III-8: Coarse dimpled overstress.



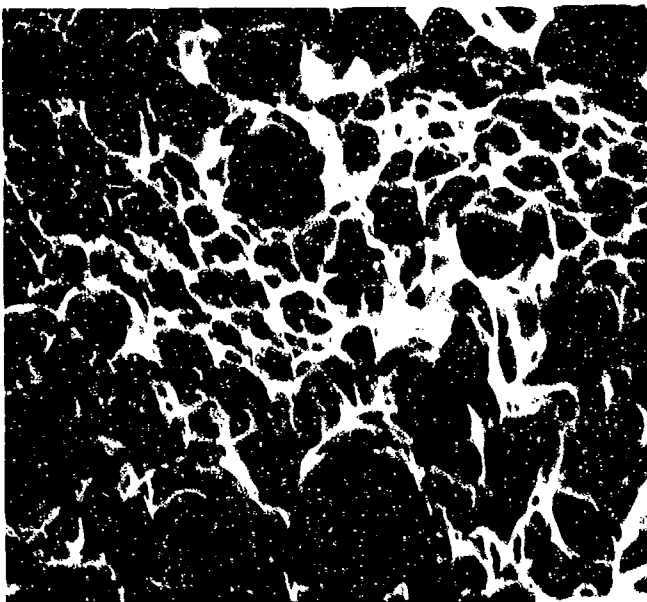
FAM 99539

MAG: 1000X

FIGURE III-9: Mechanism resulting in intergranular dimpled overstress (left) and resulting fracture surface (right).

2. Dimple Shape

The shape of dimples can be shallow equiaxed, deep conical, elongated shear, tearing or a combination of these, depending on the stress distribution. Uniaxial loading produces equiaxed dimples with a rim or lip bounding the entire cup (Figure III-10). Shear or tearing loads result in elongated dimples with a lip bounding only part of the cup, leaving an open end (Figure III-11). Tearing dimples can be distinguished from shear dimples by looking at both halves of the fracture. Tearing dimples are symmetric on mating surfaces with all dimples pointing towards the origin. Shear dimples exhibit a reversed image on mating surfaces with each dimple pointing in the direction of relative motion of its half of the fracture. Figure III-12 shows a schematic of the formation of equiaxed, shear and tensile tearing dimples (Ref 7). The depth of the dimples, whether they are equiaxed or elongated, is controlled by the plasticity of the material. A ductile material will form deeper, conical shaped dimples while a material with less ductility will exhibit very shallow dimples. Figure III-13 contrasts conical and shallow dimples. When large dimples form in a ductile material, fine features known as serpentine glide or ripples can result. These features are the result of active slip planes intersecting the surface of an existing dimple (Figure III-14) (Ref 15). The features appear as a series of roughly parallel lines on the dimple wall.



FAM 97968

MAG: 3000X

FIGURE III-10: Equiaxed dimpled over-stress with a rim or lip bounding the entire dimple.



FAM 98532

MAG: 3000X

FIGURE III-11: Elongated shear or tearing dimples exhibiting an open end. The directions of relative motion is shown by arrows.

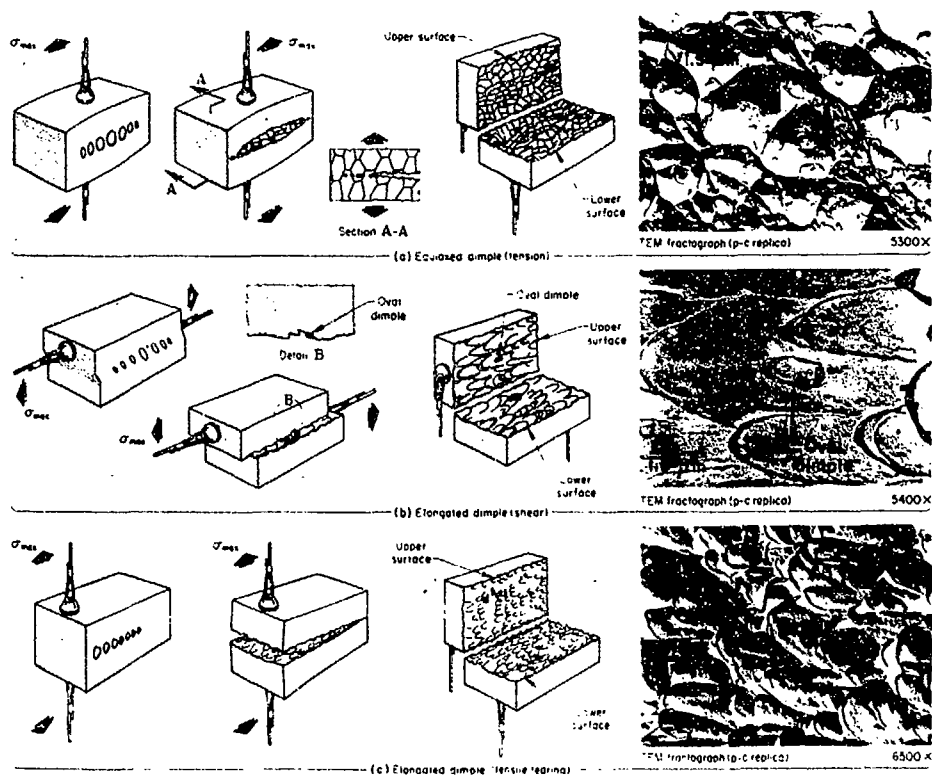
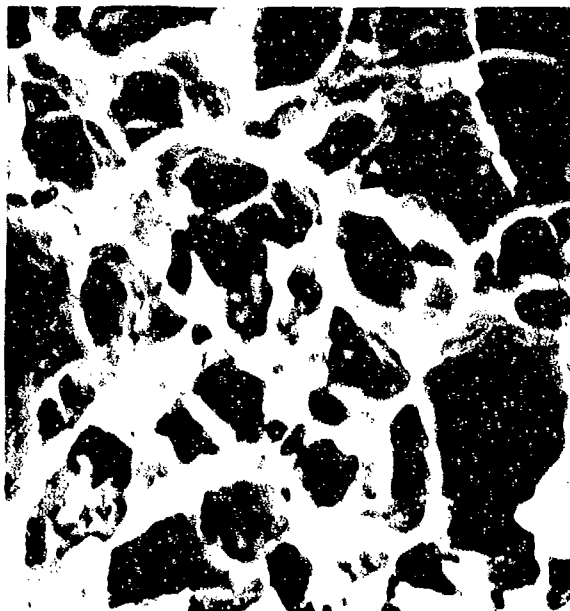
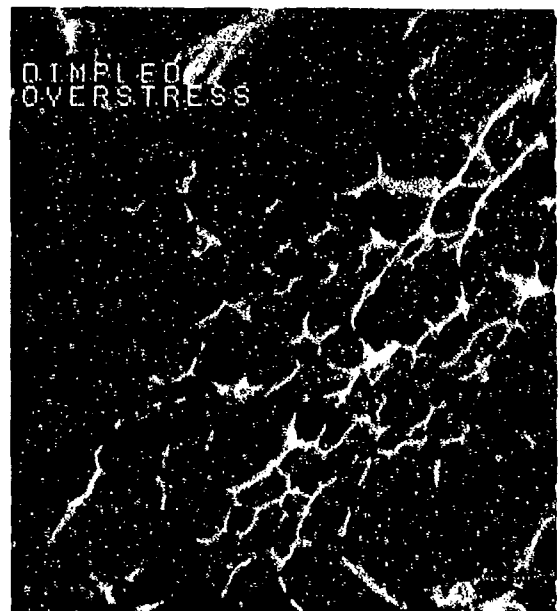


FIGURE III-12: Schematic showing the formation of equiaxed, shear and tensile tearing dimples.



FAM 97994

MAG: 3000X

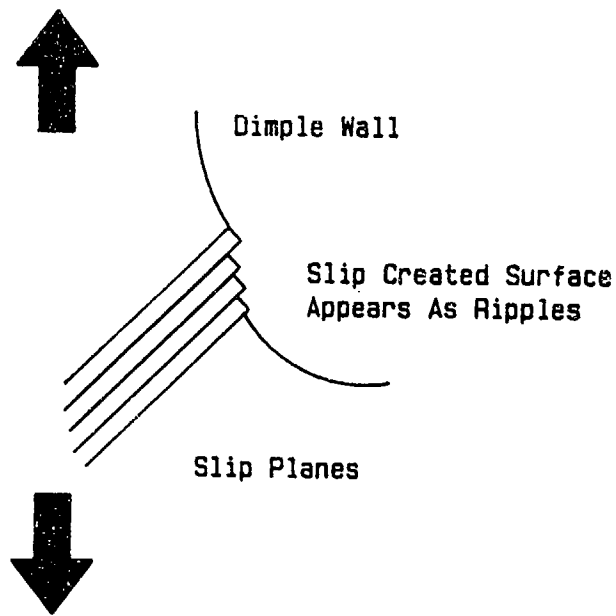


FAM 98334

MAG: 3000X

FIGURE III-13: Deep conical dimples (left) and shallow dimples (right).

Applied Tensile Stress



FAM 98395

MAG: 3000X

FIGURE III-14: Schematic showing the mechanism producing the features known as serpentine glide and ripples (left). SEM photograph illustrating the appearance of serpentine glide or ripples (arrow, right).

3. CLEAVAGE

Cleavage is the low energy fracture of a material, generally along low index planes in the crystal lattice. Cleavage fracture is favored by materials exhibiting low ductility, like ceramics, HCP metals, and metals at cryogenic temperatures. Impact loading also tends to favor low energy cleavage fracture. Theoretically, a cleavage fracture should be flat and featureless not deviating from the preferred cleavage plane. Deviations occur due to grain boundaries, low angle grain boundaries, inclusions and other lattice imperfections. These deviations from the preferred cleavage plane result in a variety of features observed at high magnification such as cleavage steps, river marks, feathery or fan-shaped cleavage, herringbone structure, and cleavage tongues.

A. Macroscopic Appearance

The macroscopic features of cleavage are characterized by:

- o Little or no plastic deformation.
- o Flat, reflective fracture surface often exhibiting a granular or faceted appearance.
- o Chevron marks which, if present, can be used to determine the direction of propagation.

Figures III-15 and III-16 show the typical macroscopic appearance of cleavage. Figure III-17 illustrates how chevron marks can be used to determine the direction of propagation.

B. SEM Appearance

1. Cleavage Steps and River Patterns

Cleavage steps are steps on a cleavage fracture surface that are formed when two or more active slip planes join. When many active planes join as the fracture progresses, a river pattern is formed (Figure III-18). The river pattern consists of a series of cleavage steps that resemble a branching river system. The direction of fracture propagation is in the downstream direction, using the river analogy (Figure III-19). Using this technique, a series of river patterns can be used to trace a complicated fracture back to its origin.

2. Tilt and Twist Boundaries

Tilt boundaries are produced when two active cleavage planes form a small angle, as if the planes were rotated around a line parallel to the boundary. Cleavage steps (river patterns) on one plane can propagate across a tilt boundary. A twist boundary results when the cleavage planes are rotated around a line perpendicular to the boundary. Cleavage steps cannot propagate across a twist boundary. Figure III-20 illustrates the formation of both tilt and twist boundaries and shows how they can be distinguished from each other (Ref 15). Figures III-21 and III-22 show a river pattern propagating across a tilt boundary. In most cases boundaries have characteristics of both tilt and twist.

3. Feathery Cleavage

Feathery or fan-shaped cleavage facets result from an array of small cleavage steps. The apex of the pattern points towards the origin. Figure III-23 shows two examples of feathery or fan-shaped cleavage. This often occurs near fatigue origins of titanium-base alloys.

4. Herringbone Structure and Wallner Lines

Herringbone structure is a unique structure thought to result from the interaction between an advancing crack front and deformation twins in the crystal lattice. Figure III-24 illustrates herringbone structure. Wallner lines consist of two groups of parallel cleavage steps intersecting to produce a criss-cross pattern (Figure III-25). Wallner lines are thought to result from the interaction of a propagating crack front with an elastic shock wave. Neither herringbone structure nor Wallner lines are typically observed using scanning electron microscopy.

5. Cleavage Tongues

Cleavage tongues are small tongue-shaped protrusions from the cleavage plane that are formed when the fracture propagates a short distance along a twin boundary intersecting the fracture surface.

6. Quasi-Cleavage

Quasi-cleavage is not a fracture mode but rather a specific fracture appearance. It is characterized by small cleavage facets on unspecified planes containing tear ridges. The quasi-cleavage fracture initiates at central cleavage facets and becomes increasingly ductile as the fracture propagates, exhibiting both dimpled overstress and tear ridges. Figure III-26 illustrates typical quasi-cleavage appearance.



FAL 92929

MAG: 12X

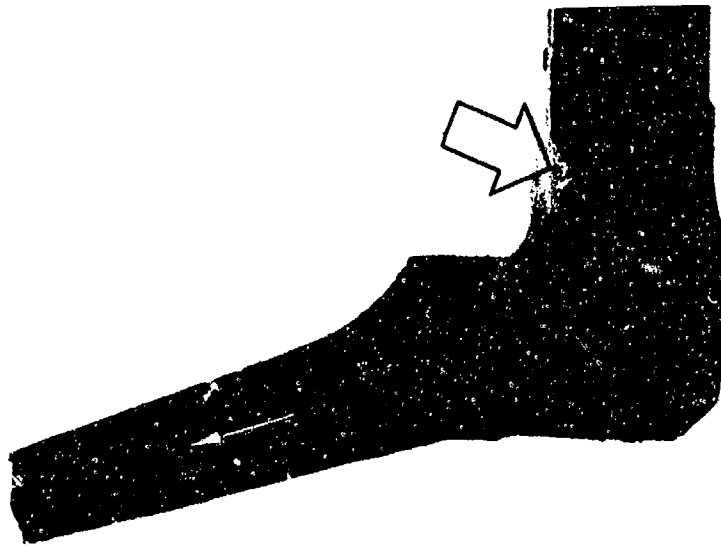
FIGURE III-15: Typical macroscopic appearance of cleavage.



FAL 92443

MAG: 10X

FIGURE III-16: Macroscopic appearance of cleavage.



FAL 92443

MAG: 3X

FIGURE III-17: Chevron marks form a herringbone pattern. The nested V's point back toward the origin. An arrow indicates the direction of propagation.



FAM 99363

MAG: 3000X

FIGURE III-18: A river pattern formed when a series of cleavage planes join. The steps separating these planes form a pattern resembling a river system.

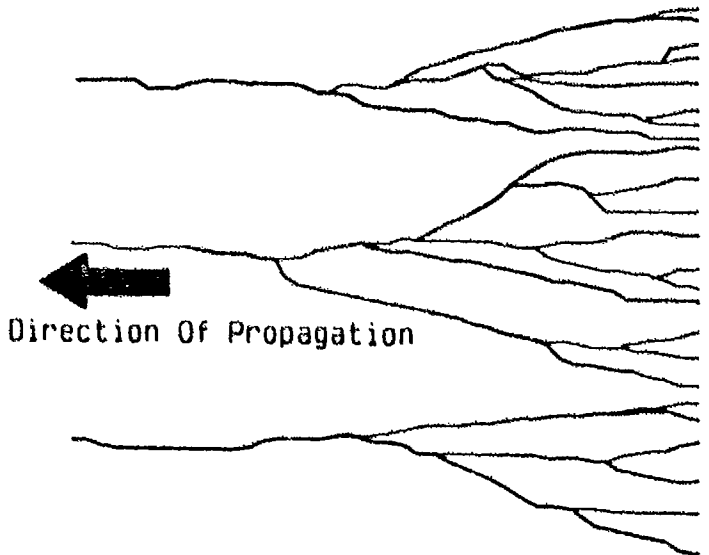
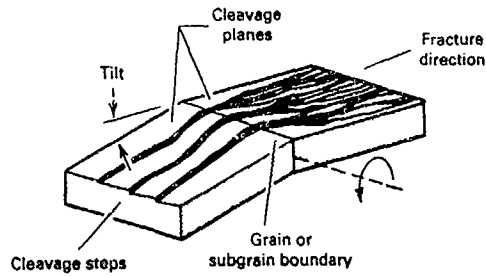


FIGURE III-19: Schematic showing how a river pattern can be used to determine the direction of propagation.



(a)

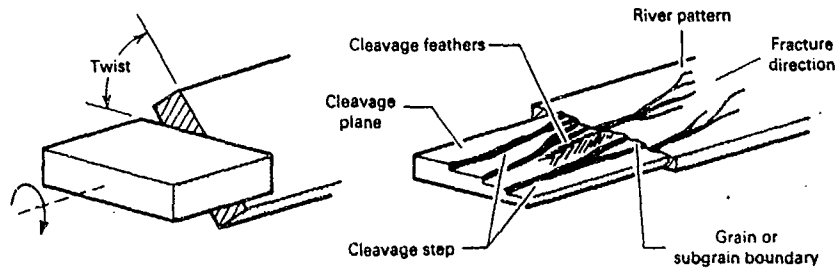
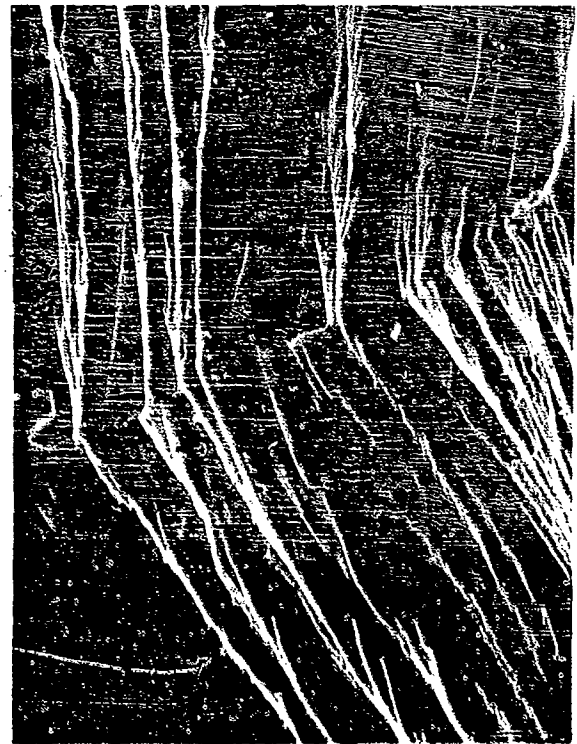


FIGURE III-20: Schematic illustrating the formation of tilt and twist boundaries and their effect on the propagation of a river pattern. The river marks can propagate across a tilt boundary but must stop and reinitiate at a twist boundary.



FAM 99943

MAG: 3000X

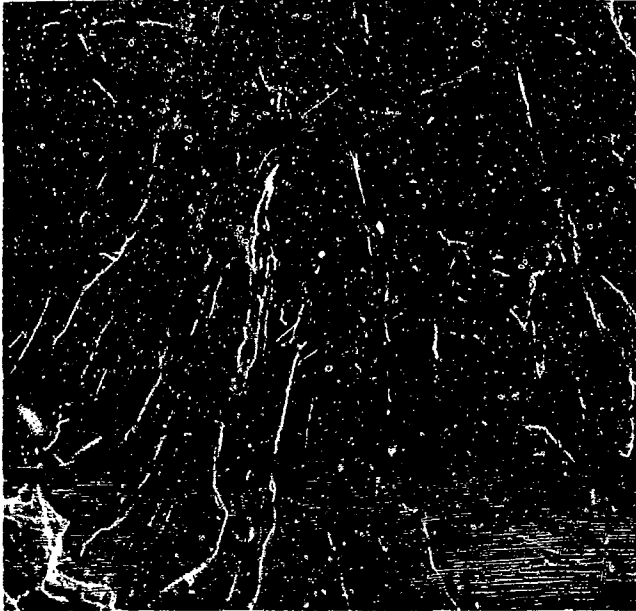


FAM 99942

MAG: 1000X

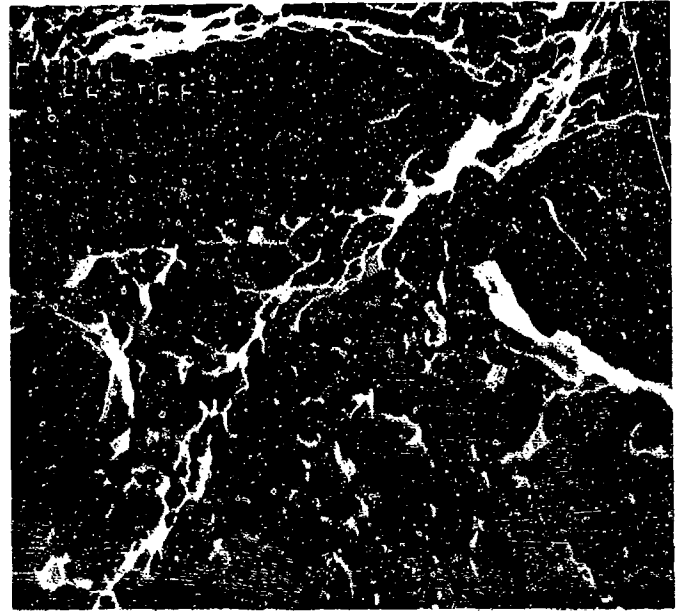
FIGURE III-21: Cleavage steps propagating across a tilt boundary (arrow).

FIGURE III-22: Tilt boundary.



FAM 98848

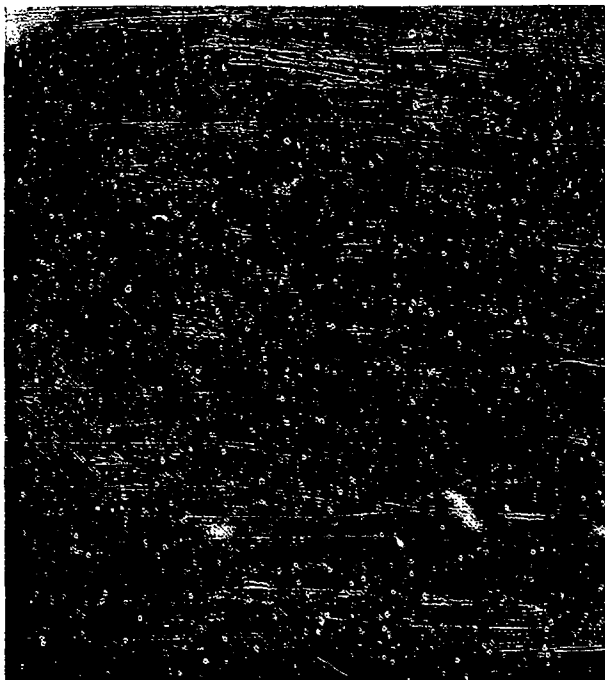
MAG: 1000X



FAM 99945

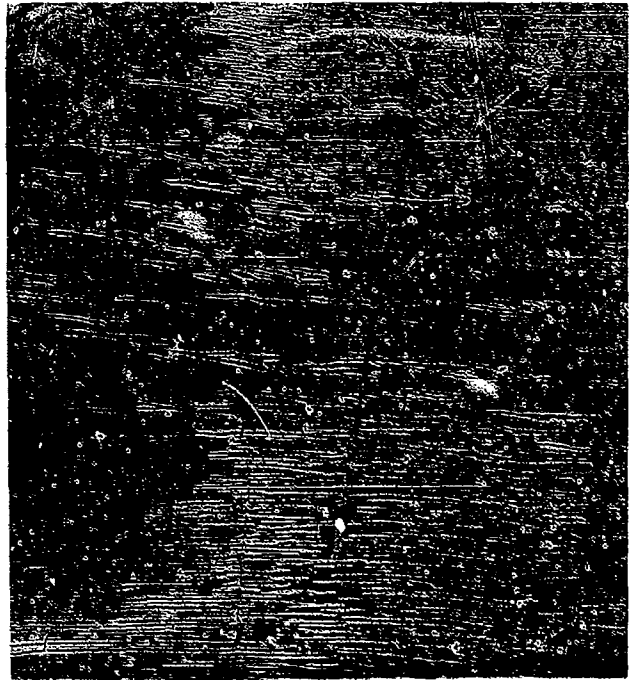
MAG: 500X

FIGURE III-23: Feathery or fan-shaped cleavage consisting of an array of fine cleavage steps, the apex of which points towards the origin.



B4000-25

MAG: 6800X



B4008-8

MAG: 6800X

FIGURE III-24: Transmission electron microscope (TEM) photograph showing a herringbone structure.

FIGURE III-25: TEM photograph illustrating Wallner lines.

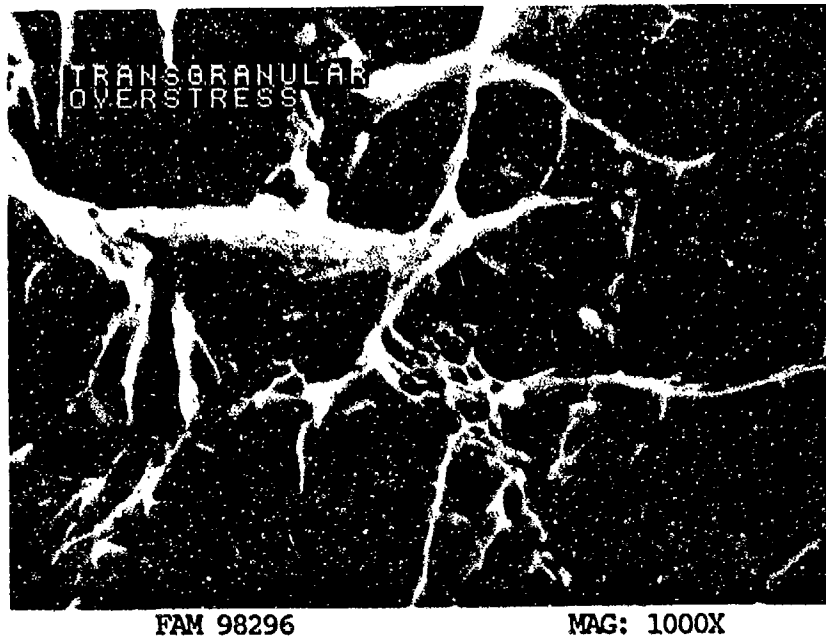


FIGURE III-26: Quasi-cleavage has both ductile and brittle features.

4. FATIGUE

Fatigue is a progressive fracture that occurs under cyclic or repetitive loading. It is generally divided into two loosely defined types: high cycle fatigue (HCF) and low cycle fatigue (LCF). HCF generally exhibits lower nominal stress, higher frequency, smaller final overstress area, and a larger number of cycles to failure than LCF. A more complete summary of the distinguishing characteristics of HCF and LCF is contained in Table III-1. In the case of aircraft engine failure analysis, HCF is considered to be caused by vibration and LCF is mission or throttle related. Somewhat arbitrary numbers like 10,000 or 100,000 cycles have been assigned by several authors as the point separating LCF and HCF. We believe that a distinction based on the source of stress (fatigue driver) provides more useful information to engineers attempting to correct a fatigue problem.

A. Macroscopic Appearance

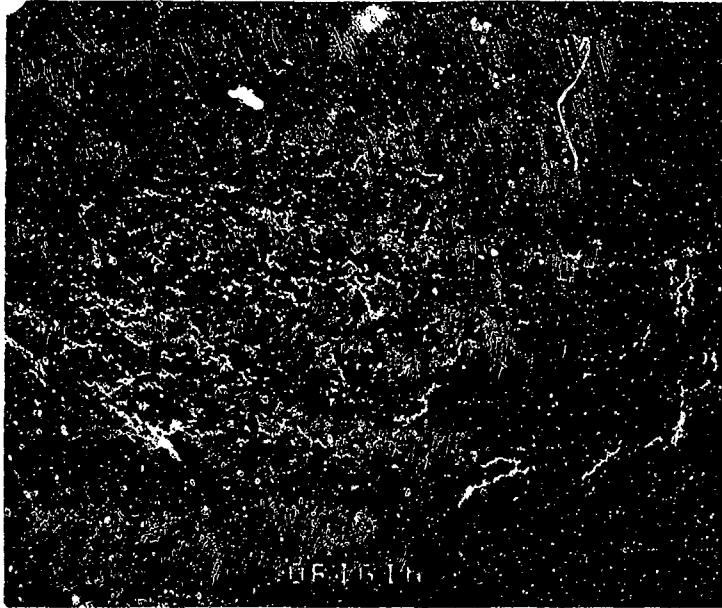
Macroscopically, fatigue is characterized by:

- o A faceted appearance at the origin (stage I).
- o Multiple fatigue origins are often separated by fatigue steps.
- o Flat transgranular propagation zone (stage II) perpendicular to the stress axis.
- o Coarse striations or arrest marks are often visible in a "clamshell" or "beachmark" pattern.
- o The overall appearance of the fatigue progression is often referred to as a thumbnail. The origin can be identified by the shape of the thumbnail.
- o The final overstress area (stage III) can occur on either the same plane or on a different plane from the fatigue progression area.
- o The size of the final overstress area can be used to help determine whether the mode was HCF or LCF.

Figures III-27 and III-28 show the typical macroscopic appearances of HCF and LCF test specimens.

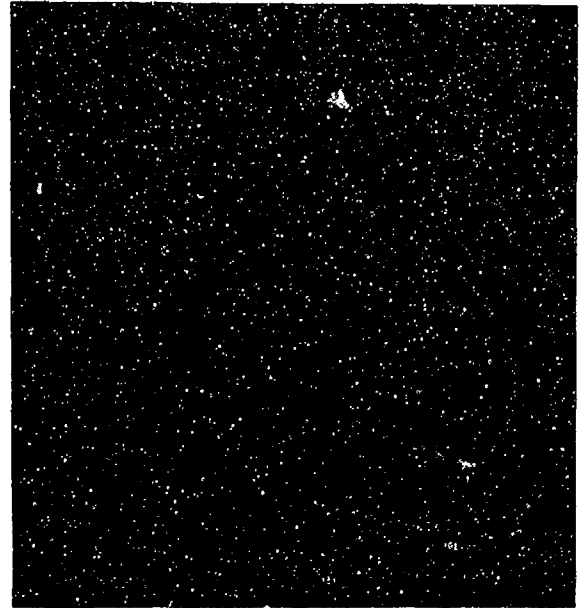
TABLE III-1: General characteristics of HCF and LCF. These are tendencies and may not be observed in all cases.

<u>High Cycle Fatigue (HCF)</u>	<u>Low Cycle Fatigue (LCF)</u>
Low cyclic stress	High cyclic stress
Driven by vibrations (high freq.) ..	Driven by mission or throttle
Striations may not be visible on SEM	Striations usually visible on SEM
Sensitive to surface condition	Relatively insensitive to surface condition
Stress less than yield	Stress may be greater than yield
Initiation controlled	Propagation controlled
Small final overstress area	Large final overstress area
Shot peening effective	Shot peening may be ineffective
Large scatter in life	Small scatter in life



FAL 93214

MAG: 9X



FAL 93832

MAG: 15X

FIGURE III-27: Macroscopic appearance of LCF.

FIGURE III-28: Macroscopic appearance of HCF.

B. SEM Appearance

1. Stage I

A fatigue crack initiates in stage I fatigue. The initiation is reported to involve slip plane separation caused by repetitive reversals on active slip plane systems. These slip systems are generally close packed planes, so the initiation and initial propagation regions often exhibit a faceted appearance. Figures III-29 and III-30 illustrate typical stage I appearances. Stage I faceting is more often found in low stress, high cycle fatigue (HCF) cracks and is often absent from high stress, low cycle fatigue (LCF) fractures. Initiation of a fatigue crack can often account for 90% of the fatigue life of a part.

2. Stage II

Stage II fatigue consists of the propagation of the crack and generally accounts for the largest portion of the fatigue crack length. Stage II often exhibits striations, although the absence of striations can occur for several reasons. The propagation is generally transgranular following the direction normal to the stress axis. Intergranular propagation can occur when a weaker grain boundary phase is present or at elevated temperatures. Figure III-31 exhibits typical transgranular

fatigue propagation. The exact mechanism for striation formation has not been determined. One proposed mechanism of striation formation is a slip plane mechanism resulting in peak-to-peak valley-to-valley matching of the mating fracture surfaces, Figure III-32 (Ref 15). Each striation is formed during one load cycle and represents the location of the crack front at that time. If the cyclic stress is decreased, the crack can arrest for one or more cycles before normal propagation resumes. This occurs due to residual compressive stress at the crack tip in the plastic zone. These arrest lines often appear as unusually large or distinct striations. If this process occurs regularly as when a fighter engine runs an accelerated mission test, banded striations are produced, Figure III-33. The depths of the striations can vary between the two halves of the fracture. One half can exhibit well developed striations while the mating surface exhibits shallow striations. This occurs when one surface experiences a higher stress than the other.

a. Striation Spacing

Striation spacing can be affected by several variables including:

- o Magnitude of the alternating stress
- o Magnitude of the mean stress
- o Frequency of the alternating stress
- o Temperature
- o Strength of the material
- o Microstructure
- o Environment

The magnitude of the alternating stress has the largest effect on the striation spacing. Increasing the alternating stress increases the striation spacing. The striation spacing often increases as the crack progresses. This occurs because the load bearing area is decreasing so the magnitudes of both the mean and alternating stresses are increasing. This effect is more pronounced in high stress LCF fractures and can be used as one feature distinguishing LCF from HCF. Figure III-34 shows the striation spacing near the origin and just before final overstress occurred in a room temperature LCF fracture. Large second phase particles or inclusions change the local stress distribution and thus can either increase or decrease striation spacing. Figure III-35 illustrates the effect of an inclusion on the local striation spacing. This usually does not affect the overall crack growth rate.

b. Striation Appearance

The striation appearance can be affected by many variables. Very soft or very hard materials often show poorly defined or no striations under conditions that would produce clear striations in other materials. Certain

material types form striations better than others. For instance, titanium-based alloys seldom exhibit striations when viewed with the SEM. Nickel-based alloys usually form clear striations. Striations with a brittle or crack-like appearances can be produced in a hydrogen environment or at high temperatures in some materials (Figure II-36). Well developed striations form slip traces on their trailing edges, and smooth leading edges. These traces can be used to determine the direction of propagation

c. Fatigue Steps

Stage I and stage II fatigue often exhibit steps similar to those observed on cleavage facets. These steps are called fatigue steps or tear ridges. Fatigue steps in an origin area often indicate multiple origins on different levels. They can be used to locate the general origin area and to separate and locate localized origins (Figure III-37). In a stage II area, fatigue steps may separate areas exhibiting locally different propagation directions (Figure III-38).



FAM 99201

MAG: 200X



FAM 98656

MAG: 200X

FIGURE III-29: Typical stage I fatigue appearance, exhibiting facets and feathery cleavage (arrow).

FIGURE III-30: Alternate stage I fatigue appearance. A facet is shown by an arrow.



FAM 99310

MAG: 6000X

FIGURE III-31: Typical stage II transgranular fatigue progression in an HCF fatigue specimen.

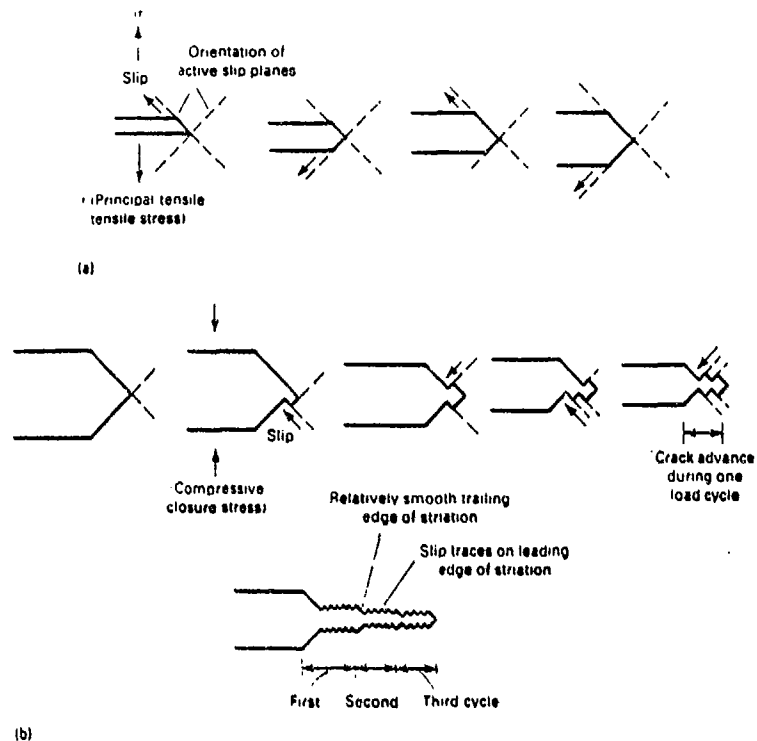
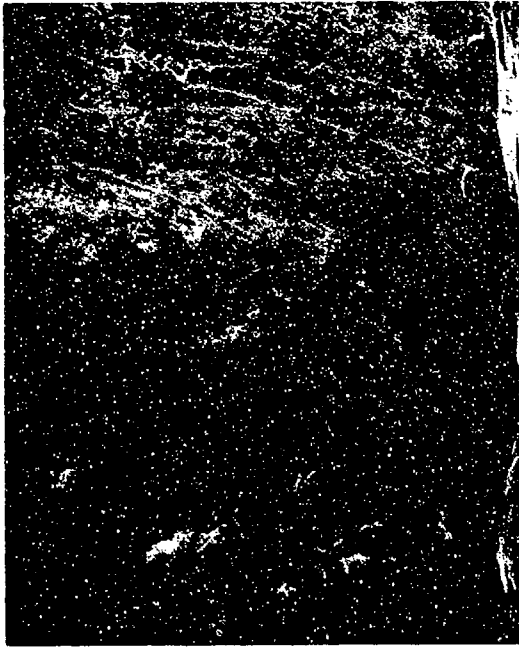
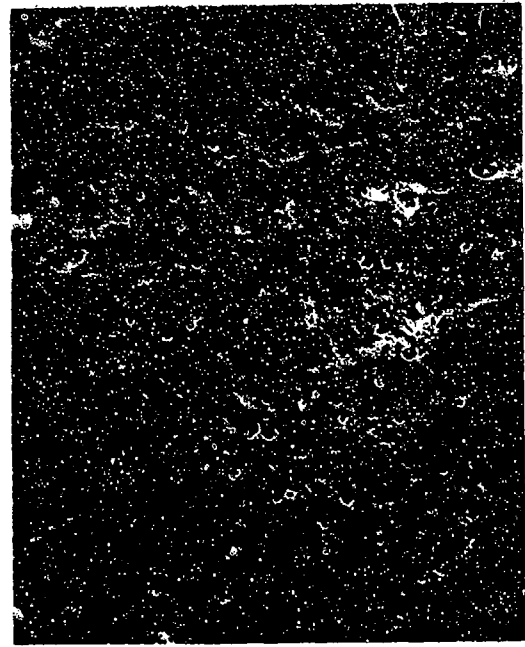


FIGURE III-32: Proposed mechanism for fatigue striation formation. The slip plane mechanism results in peak-to-peak, valley-to-valley matching on mating fracture surfaces. (a) Crack opening and crack tip blunting by slip on alternate slip planes with increasing tensile stress. (b) Crack closure and crack tip resharpening by partial slip reversal on alternate slip planes with decreasing stress.



FAL 93454

MAG: 120X



FAL 93455

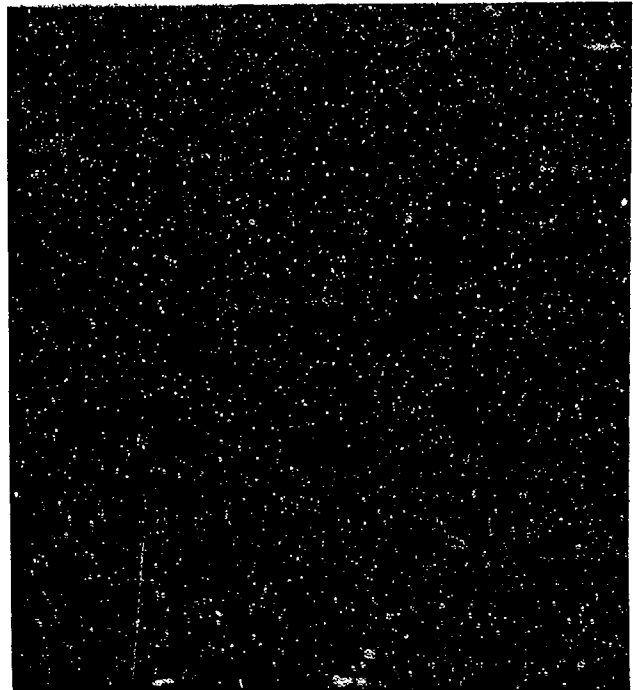
MAG: 500X

FIGURE III-33: Banded fatigue striations resulting from changes in magnitude of the alternating stresses. The part was run in an accelerated mission test. Brackets show regions of finer and coarser striations.



B4789-8

MAG: 6800X



B4789-19

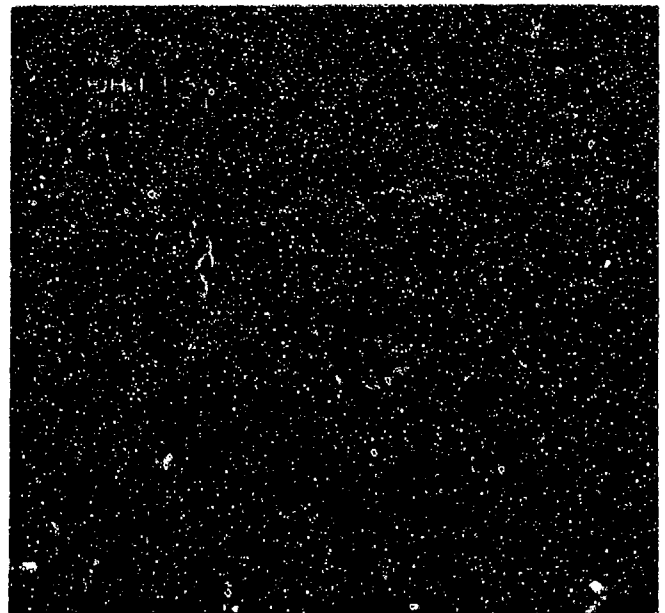
MAG: 6800X

FIGURE III-34: Striation spacing near the origin (left) and at the end of the fatigue progression area (right) in a room temperature LCF fracture. The striation spacings increase, reflecting stress increases due to reduction of the remaining load-bearing area.



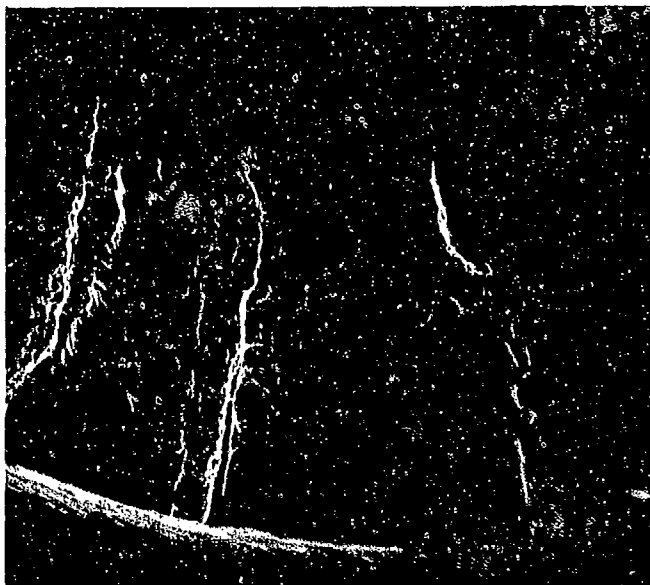
FAM 99261 MAG: 3000X

FIGURE III-35: Striation spacing changes locally when a crack front encounters an inclusion or second phase particle.



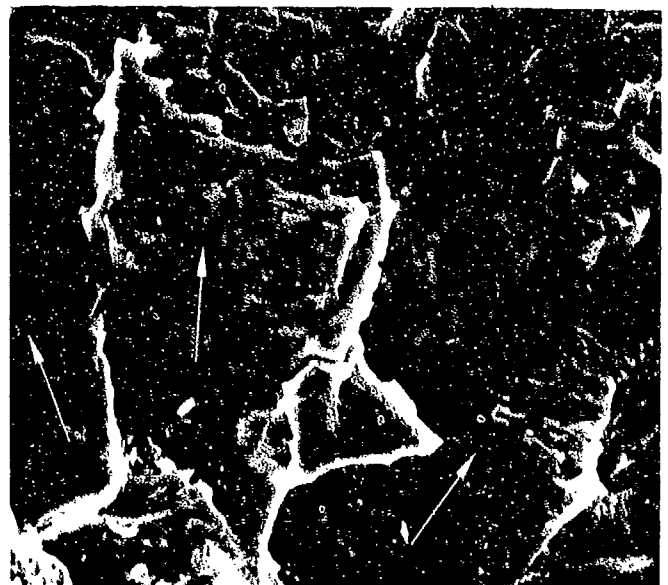
FAM 99269 MAG: 1000X

FIGURE III-36: Crack-like striations that occur in some materials in hydrogen environment or at high temperatures.



FAM 99351 MAG: 50X

FIGURE III-37: Fatigue steps or tear ridges near an origin area. These can be used to locate the origin area and to separate and locate localized origins.



FAM 99947 MAG: 1000X

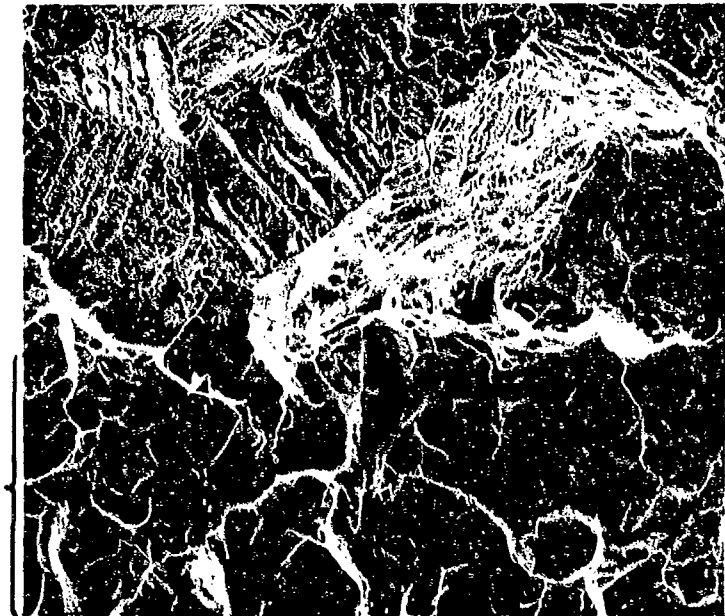
FIGURE III-38: Tear ridges (black arrows) separate areas of locally different directions of propagation. The directions of propagation are shown by white arrows.

3) Stage III

Stage III is the final overstress area. As the crack propagates in a stage II mode, the nominal stress and magnitude of the cyclic stress increase. When the crack has progressed to a critical depth or size, fatigue propagation is replaced by a fracture mode such as cleavage or dimpled overstress. The size of the final overstress area is indicative of the combined average stress and can be used to distinguish HCF from LCF. Figure III-39 shows the transition between fatigue propagation and dimpled overstress.

4) Thermal-Mechanical Fatigue (TMF)

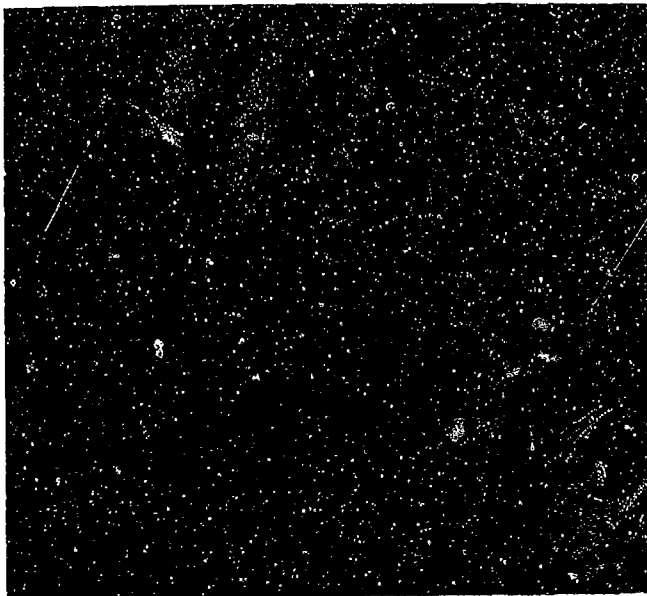
Thermal-mechanical fatigue is a special case of LCF that occurs at high temperature under combined loading generated by cyclic thermal as well as cyclic mechanical stresses. TMF often occurs in high time gas turbine hardware. The fracture surface is generally heavily oxidized, often exhibiting no striations. If striations are present, they are generally heavily oxidized (Figure III-40). Heavy oxides often exhibit what is known as mud cracking (Figure III-41). TMF is often distinguished by its appearance in metallographic cross-section. It generally presents a characteristic oxide-filled, alloy depleted V-shape caused by oxidation as the crack propagates. Figure III-42 shows the appearance of a typical TMF crack in a metallographic cross section.



FAM 99950

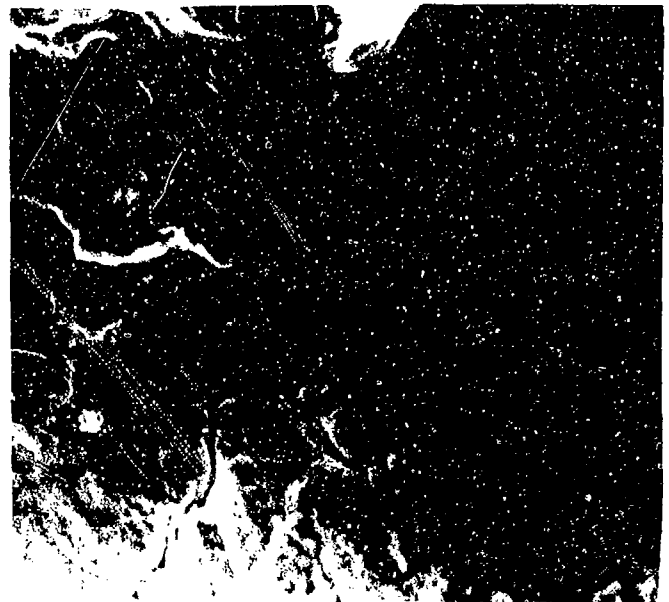
MAG: 200X

FIGURE III-39: Transition between stage II propagation (brackets) and the final overstress area.



FAM 98551 MAG: 3000X

FIGURE III-40: Heavily oxidized TMF striations.



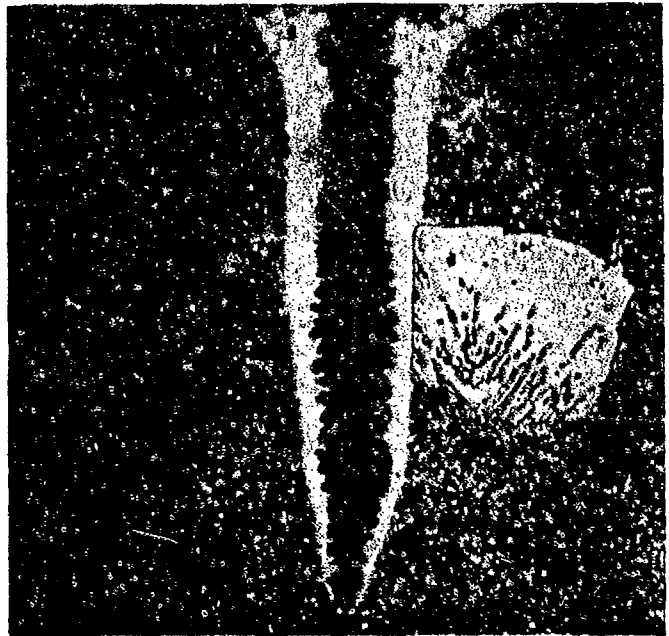
FAM 98539 MAG: 1000X

FIGURE III-41: Mud cracking occurs in TMF areas exhibiting heavy oxidation.



FAM 99936 MAG: 500X

FIGURE III-42: V-shaped TMF crack shown in a metallographic cross section. This shape is characteristic of TMF and occurs because the crack oxidizes as it progresses. Etchant: AG-21



FAM 99935 MAG: 1000X

5. DECOHESIVE RUPTURE

Decohesive rupture is a broad category of fracture modes. It is defined as fracture along a path of weakness produced by elevated temperature, microstructural variables or a reactive environment. It is usually associated with grain boundaries and often exhibits little bulk plastic deformation.

A. Macroscopic Appearance

The macroscopic appearance of a decohesive rupture fracture can vary. The fracture appearance can vary from smooth to clearly intergranular, depending on grain orientation relative to the stress axis (Figure III-43). Decohesive rupture fractures generally exhibit an intergranular appearance with either transgranular or intergranular dimpled overstress in the final fracture area (Figure III-44). Stress corrosion cracking fractures often exhibit moderate to heavy oxidation (mud-cracking) and a branching crack path (Figure III-45).

B. Microstructural Variables

Microstructural variables such as precipitation of a weak second phase at grain boundaries and segregation of lower melting point constituents to grain boundaries can contribute to grain boundary fracture at stresses below the yield stress of the material. At high temperatures and stresses, close to but not exceeding the yield stress, a process known as stress rupture occurs. Stress rupture, sometimes referred to as creep rupture, is a time-temperature-stress related fracture that occurs as a result of microvoid coalescence at grain boundaries, similar to dimpled overstress. Figure III-46 shows the two mechanisms by which this can occur: triple point cracking or grain boundary cavitation (Ref 15). Figure III-47 illustrates typical stress rupture fractures. Stress rupture is the ultimate result of creep.

C. Environmental Factors

Stress corrosion cracking (SCC), liquid metal embrittlement (LME), and hydrogen embrittlement (HE) are three of the most common decohesive rupture modes associated with environmental factors.

1) Stress Corrosion Cracking

SCC is a fracture mode that requires a specific set of factors to be present: a particular corrosive environment, susceptible material and tensile stress. The detailed mechanisms of SCC have been discussed elsewhere. The susceptibility of a material to SCC depends on variables such as microstructure, strength (hardness), grain orientation and corrosive environment. Figure III-48 shows the appearance of a stress corrosion crack surface. Figure III-49 illustrates the intergranular appearance of cracks in a metallographic cross section. Titanium-base alloys fractured by SSC often exhibit fracture features known as flutes.

Flutes are thought to be produced by the rupture of tubular voids formed by a planer slip mechanism. The presence of flutes has been used to distinguish SCC from other potential decohesive rupture mechanisms in titanium-base alloys. Figure III-50 illustrates the appearance of flutes. Flutes have also been observed under cryogenic testing conditions of Ti-based alloys.

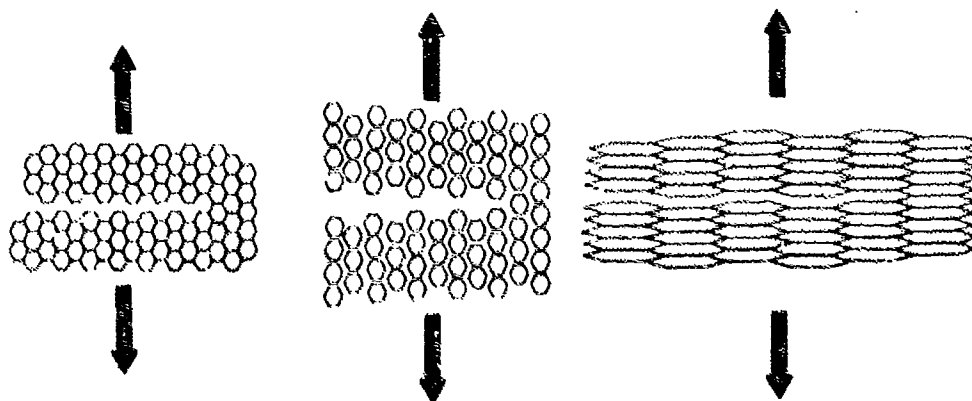
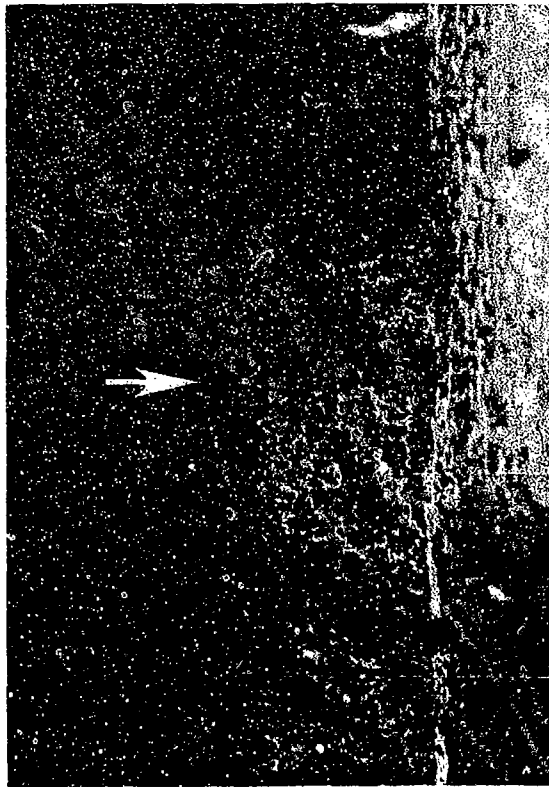
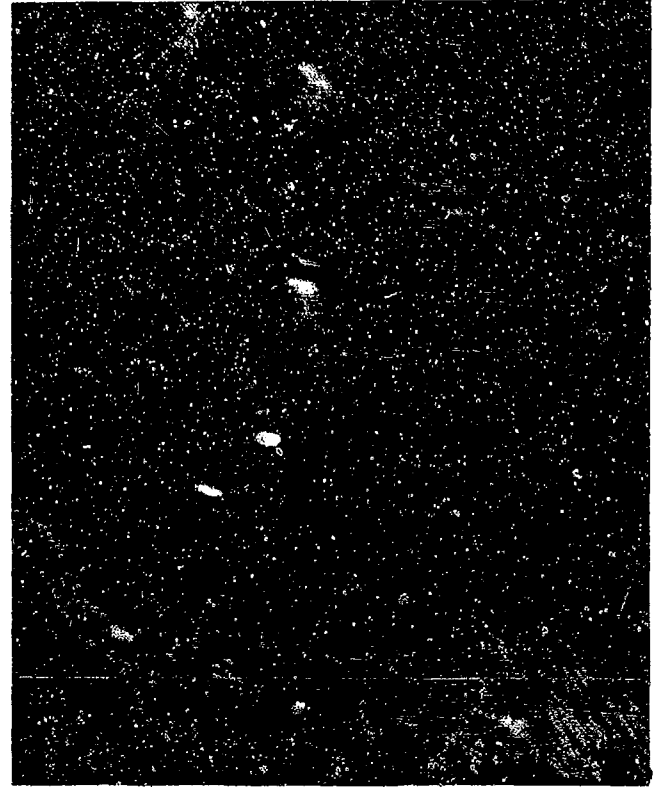


FIGURE III-43: Decohesive rupture can result in a classic intergranular fracture or a smooth appearance, depending on grain orientation relative to the stress axis.



FAM 99688

MAG: 50X



FAM 99951

MAG: 100X

FIGURE III-44: Intergranular fracture surface with transgranular dimpled overstress in the final fracture area (shear lip, arrow). This is typical of decohesive rupture.

FIGURE III-45: Optical photomicrograph of stress corrosion cracking. The branching is characteristic.

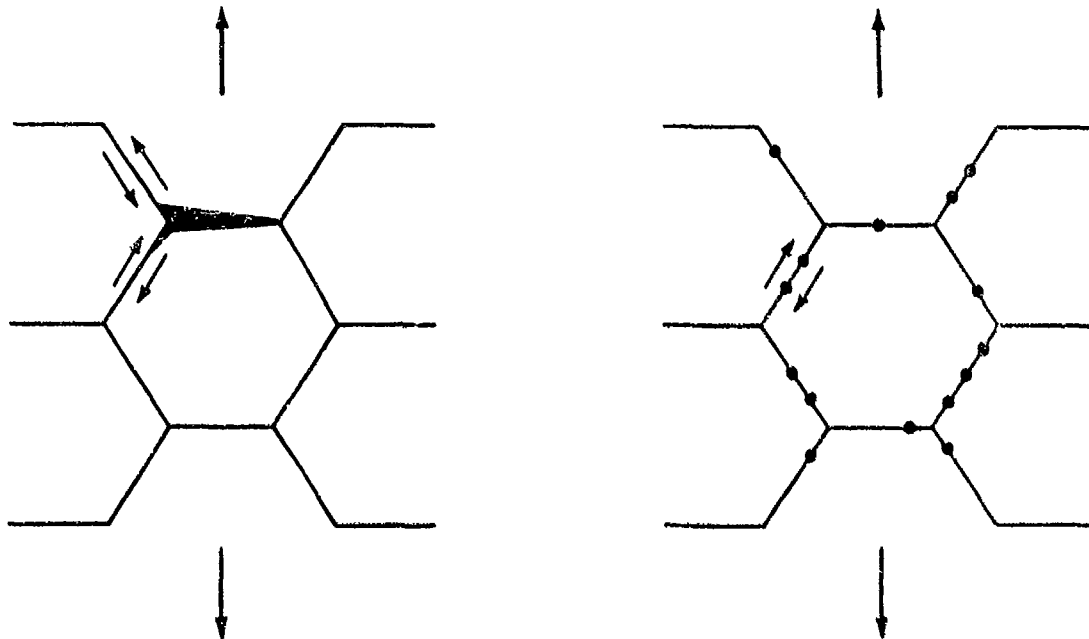
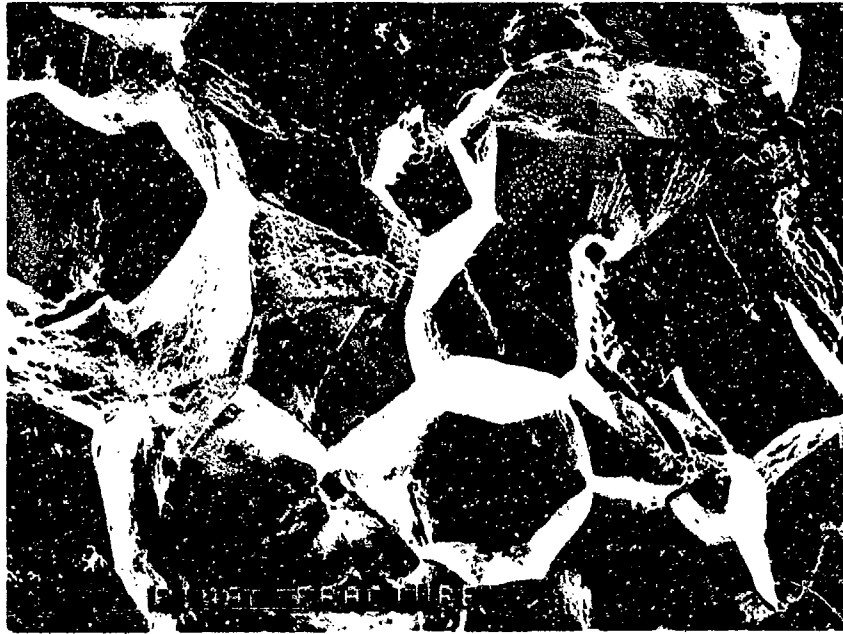


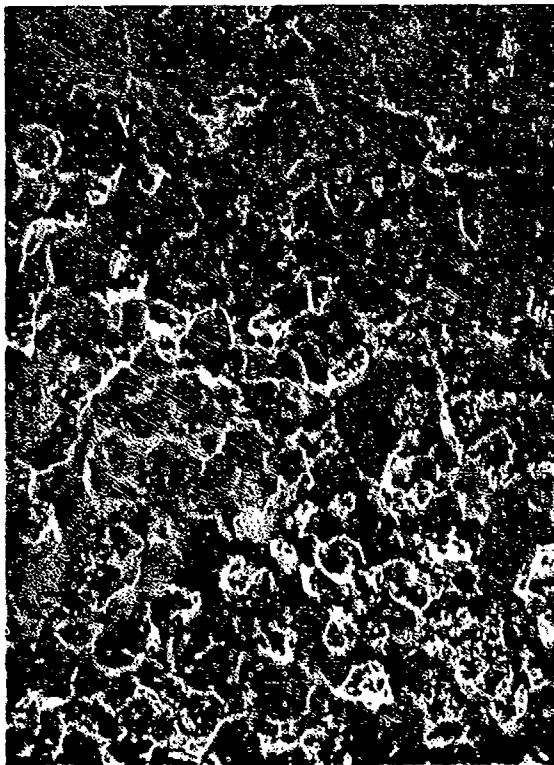
FIGURE III-46: Two mechanisms by which stress rupture can occur: triple point cracking (left) and grain boundary cavitation (right). Smaller arrows indicate the directions of grain boundary sliding.



FAM 98264

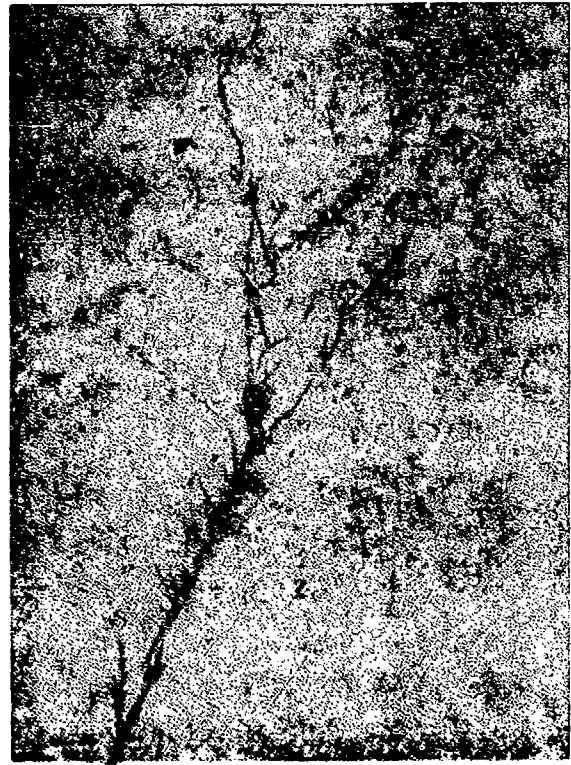
MAG: 200X

FIGURE III-47: Typical intergranular stress rupture fracture appearance.



FAM 99696

MAG: 200X

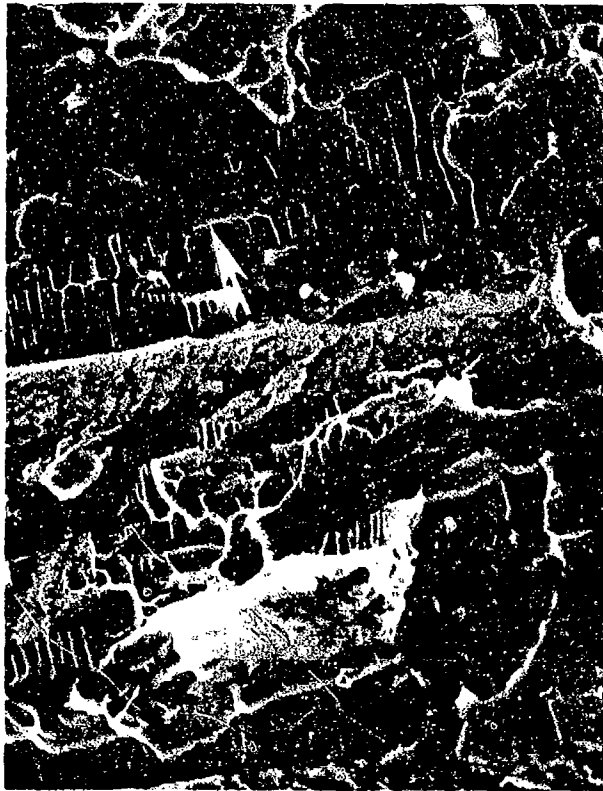


FAM 99951

MAG: 100X

FIGURE III-48: Stress corrosion cracking fracture surface exhibiting oxidized/corroded intergranular features.

FIGURE III-49: Metallographic cross section through a stress corrosion crack. The branching appearance is a distinguishing characteristic of SCC.



FAM 99954

MAG: 1000X



FAM 99955

MAG: 1500X

FIGURE III-50: Flutes (arrows) appear as ruptured tubular voids, usually oriented parallel to the stress axis. They can be well defined (left) or sporadic and hard to recognize (right).

2. Liquid Metal Embrittlement

Embrittlement by a metallic species occurs when a low-melting-point alloy penetrates the grain boundaries of a structural alloy. The alloy may then fracture intergranularly at a stress lower than its normal yield stress. Liquid metal embrittlement occurs when a metal is exposed to the low-melting-point alloy in the liquid state while under tensile stress. Certain iron-base, nickel-base, titanium, and aluminum alloys can be embrittled by lead, tin, gallium, indium, mercury, cadmium, lithium and silver in the liquid state. A more limited group of alloys are susceptible to embrittlement when the embrittling metal is in the solid state. This is known as solid metal embrittlement (SME). Stress alloying is a term occasionally applied to both LME and SME. Figures III-51 and III-52 show typical LME fracture surfaces.

3. Hydrogen Embrittlement

Certain BCC (body-centered cubic) and HCP (hexagonal close-packed) metals, such as alloys of titanium, iron and other less common alloys, experience degradation of their mechanical properties when exposed to hydrogen. The resulting fracture mode is known as hydrogen embrittlement. Although FCC (face-centered cubic) materials generally have good resistance to hydrogen embrittlement, 300-series austenitic stainless steels can be embrittled by hydrogen.



FAL 93333

MAG: 300X

FIGURE III-51: LME fracture surface exhibiting intergranular fracture through silver-base braze alloy that had penetrated the grain boundaries (arrow).



FAM 93332

MAG: 1000X

FIGURE III-52: Higher magnification view of LME fracture surface.

IV. ATLAS OF FRACTOGRAPHS

1. Introduction

The end product of Task I was a collection of fractographs of various alloys under different conditions. To accomplish this, a test matrix of alloys and types of tests necessary for each alloy was generated. The test conditions were then defined. Test materials were procured, machined into specimens and tested. Finally, the generated fracture surfaces were documented.

2. Test Conditions

The fracture specimens that were generated included tensile (smooth and notched, at low and high temperatures), high cycle fatigue (smooth and notched, at low, intermediate, and high temperatures), low cycle fatigue (low, intermediate and high temperatures), thermal-mechanical fatigue (in-phase and out-of-phase), stress rupture, stress corrosion and hydrogen embrittlement.

Tensile testing was conducted at room temperature and at temperatures at the top of the subject material's service range. Smooth specimens were tested at a strain rate of 0.005 mm/mm/min (0.005 in/in/min), per ASTM specifications. Notched specimens had a K_t of 3.0 and were tested at a crosshead speed of 1.27 mm/min (0.05 in/min).

High cycle fatigue (HCF) testing was performed at low or room temperature, a temperature at the top of the service range, and at an intermediate temperature on both smooth and notched specimens. The specimens were cycled at 1,800 cpm, with stress ratios (min/max) of -1, to simulate resonant vibration. Actual stress levels, below the yield stress, were determined at the time of testing, and were chosen to produce fracture in >100,000 cycles. Notched HCF tests used notches with K_t of 2.16, based on ASTM standards.

Low cycle fatigue (LCF) testing was performed at low or room temperature, a temperature at the top of the service range, and at an intermediate temperature. Load control testing was performed, versus strain controlled, due to cost. Our experience has shown that fracture features do not vary between the two types of tests. The specimens were cycled at 10 cpm, with a stress ratio (min/max) of 0.05. Actual stress levels, above the yield stress, were determined at the time of testing, and were chosen to produce fracture in 5,000-10,000 cycles.

Two types of thermal-mechanical fatigue testing were performed: in-phase, with temperature and stress rising and falling simultaneously, and out-of-phase, with stress rising as temperature dropped. Both types were performed at 1 cpm. A stress ratio (min/max) of -1₀ was used, based on $\pm 0.3\%$ strain. The temperatures cycled from 260 C (500 F) to the maximum service temperature. The lower limit of 260 C (500 F) was due to instrumentation limits.

Stress rupture (S/R) testing was performed at the specification S/R test temperature or, if unspecified, at the maximum service temperature. The applied stress was less than the yield stress, and was chosen to produce a fracture in a reasonable (cost effective) time period.

Stress corrosion testing was performed on bent strips of material per ASTM Section G-39 in 3.5% NaCl vapor at 95 °C (203 °F). The strips were bent to produce a stress level approximately 90% of the yield stress on the OD of the bend. The atmosphere was chosen to produce a stress corrosion fracture without causing excessive general corrosion.

Hydrogen embrittlement testing consisted of notched tensile testing of hydrogen charged specimens. Charging of the titanium and iron base specimens was accomplished by soaking in high pressure hydrogen atmosphere. The specimens were also cathodically charged in 1% HCl solution. Testing was conducted under ambient conditions. Specimen configuration and conditions were the same as the room temperature notched tensile tests.

3. Material Specifications

The alloys to be tested and the test conditions for each are listed below. Note that some specimens were provided by the Wright Research and Development Center (WRDC) Materials Laboratory.

M-50 (martensitic tool and bearing steel) was tested in the form of bar (AMS 6491A) heat treated to AMS 2759/2 at WRDC. Notched tensile tests were conducted at ambient temperature and 315 °C (600 °F). Smooth and notched HCF testing was performed at ambient temperature and 315 °C (600 °F).

15-5 PH was tested in the form of AMS 5659 bar heat treated to AMS 2759/3 in the H925 condition. The maximum specified service temperature is 316 °C (600 °F). Stress corrosion and hydrogen embrittlement were the only tests run.

Custom 455 was tested in the form of AMS 5617 bar heat treated to AMS 2759/3 in the H950 condition. The maximum specified service temperature is 427 °C (800 °F). The intermediate test temperature used was 204 °C (400 °F) and the low test temperature was ambient.

347 stainless steel was tested in the form of AMS 5646 bar. The service temperature range is 427 °C (800 °F) to 816 °C (1500 °F). These temperatures served as the intermediate and high test temperatures, respectively. Ambient temperature served for low temperature tests.

A-286 was tested in the form of AMS 5525 plate heat treated to AMS 2759/3. The maximum service temperature is 704 °C (1300 °F). The intermediate test temperature used was 204 °C (400 °F). This temperature is just below the point where a rapid drop in tensile properties occurs with increasing temperature. Ambient temperature served for the low temperature tests. The stress rupture test was conducted at 649 °C (1200 °F).

Incoloy 901 was tested in the form of FWA 1003 bar. The service temperature range is 482 C (900 F) to 704 C (1300 F). These temperatures served as the intermediate and high test temperatures, respectively.

Incoloy 909 was tested in the form of FWA 1191 bar. The maximum specified service temperature is 649 C (1200 F). The intermediate test temperature used was 204 C (400 F), corresponding to the minimum thermal expansion coefficient exhibited by this low expansion alloy. Low temperature tests were conducted at ambient temperature. The stress rupture test was conducted at 649 C (1200 F).

Inconel 600 was tested in the form of AMS 5665 bar. The maximum service temperature range is 982 C-1093 C (1800 F-2000 F). The intermediate test temperature used was 427 C (800 F). This temperature is below the point where a rapid drop in tensile properties occurs. 704 C (1300 F) was used for the high temperature tests because the material has low strength above this temperature. There is no specified stress rupture requirement. 704 C (1300 F) was used for that test.

Inconel X-750 was tested in the form of AMS 5667 (bars, forgings and rings). The specified service temperature range is 427 C-593 C (800 F-1100 F). The high temperature tests were conducted at 593 C (1100 F). The lower service limit of 427 C (800 F) served as the intermediate temperature, and ambient for the low temperature. With no specified stress rupture requirement, the maximum specified service temperature of 593 C (1100 F) was used for that test.

FWA 1480 (cast single crystal) was tested previously, and results reported in report number AFVAL-TR-84-4167. The fracture specimens resulting from that program were used to generate fractography for this program. Therefore, the conditions of the prior program were used.

MP-159 tensile, HCF and LCF testing was performed at WRDC/MLSA in the form of AMS 5843 (solutioned, worked and aged bars). Smooth and notched tensile tests were conducted at 593 C (1100 F). Smooth HCF tests were conducted at room temperature, 427 C (800 F) and 593 C (1100 F). Notched LCF tests were conducted at room temperature and 593 C (1100 F). Smooth LCF testing was limited to ambient conditions. The stress rupture specimen was tested in house at 649 C (1200 F).

Ti-6Al-2Sn-4Zr-2Mo was tested in the form of FWA 1209 (bars and forgings). The maximum specified service temperature is 538 C (1000 F). The intermediate test temperature used was 260 C (500 F). The stress rupture test was conducted at 510 C (950 F).

Ti-6Al-4V was tested in the form of AMS 4928 (bars, forgings and rings). Hydrogen embrittlement, the only test required of this alloy, was performed at room temperature.

4. Test Matrix

The matrix of tests conducted and the page numbers on which the test results, fractography and metallography can be found are listed in Tables IV-1 and IV-2.

TABLE IV-1: Materials tested and pages containing the fractography and metallography for tensile, LCF and HCF specimens. Also included are the locations of the fractography overviews.

MATERIAL	OVERVIEW	SMOOTH TENSILE	NOTCHED TENSILE	SMOOTH HCF	NOTCHED HCF	LOW TEMP LCF	HIGH TEMP LCF
M-50	58-59	NA	60-68	69-80	NA	NA	81-91
15-5 PH	95	NA	NA	NA	NA	NA	NA
CUSTOM 455	108-109	110-118	119-127	128-146	NR	NR	NR
347 SS	156-157	158-167	168-179	180-198	NR	NR	NR
A-286	201-202	203-211	212-219	225-240	NR	NR	241-250
INCOLOY 901	261	NR	NR	NR	NR	NR	262-273
INCOLOY 909	285-286	287-295	296-304	NR	NR	310-314	315-324
INCONEL 600	340-341	342-350	351-359	364-382	383-401	NR	402-414
INCO X-750	424-425	426-435	436-444	451-466	467-485	NR	486-497
FWA 1480	512-513	514-530	NR	NR	NR	NR	535-552
MP-159	564-565	566-569	570-574	580-599	NA	600-605 612-614	606-611
TI-6-2-4-2	629-630	631-640	641-648	654-669	670-686	NR	687-698
TI-6-4	712	NR	NR	NR	NR	NR	NR

NR - Not requested

NA - Not available, was to be provided by WRDC/MLSA, was dropped from the matrix

TABLE IV-2: Materials tested and pages containing the fractography and metallography for TMF, stress rupture, stress corrosion, hydrogen embrittlement and the locations of service failures.

MATERIAL	IN-PHASE TMF	OUT-OF-PHASE TMF	STRESS RUPTURE	STRESS CORROSION	HYDROGEN EMBRITTLMENT	SERVICE FAILURE
M-50	NR	NR	NR	NR	NR	92-94
15-5 PH	NA	NA	NA	96-99	100-103	104-107
CUSTOM 455	NR	NR	NR	147-151	152-155	-
347 SS	NR	NR	NR	NR	NR	199-200
A-286	NR	NR	220-224	251-253	254-258	259-260
INCOLOY 901	274-277	278-282	NR	NR	NR	283-287
INCOLOY 909	325-330	331-336	305-309	NR	NR	337-339
INCONEL 600	415-417	415-417	360-363	NR	NR	418-423
INCO X-750	498-502	503-508	445-450	NR	NR	509-511
PWA 1480	NR	553-559	531-534	NR	NR	560-563
MP-159	615-620	621-626	575-579	NR	NR	627-628
TI-6-2-4-2	699-704	705-711	649-653	NR	NR	-
TI-6-4	NR	NR	NR	NR	713-717	718-725

NR - Not requested

NA - Not available, was to be provided by WRDC/MLSA, was dropped from the matrix

M-50 (Bearing and Tool Steel)

Material Description

M-50 is a semi-high-speed steel that is used in woodworking tools, pump vanes and large gear assemblies. In the aerospace industry it is used extensively in gas turbine engine bearings and other rolling elements. M-50 can be through hardened to HRC 64 but because it is quite brittle in the fully hardened condition, it is generally tempered to HRC 55-60.

The material used in this study was AMS 6491 heat treated to AMS 2759/2. The typical room temperature mechanical properties for AMS 6491 are as follows:

Ultimate Tensile Strength:	350 ksi
0.2% Yield Strength:	250 ksi
Percent Elongation:	2.0%
Required Grain Size:	ASTM 7 or finer occa. 5 permissible
Measured Hardness:	HRC 60-62

Fractography Overview

M-50 is a relatively brittle material especially at room temperature. This is controlled, in part, by the tempering temperature. This brittle nature was evident in both the mechanical test data and in the fractography. The room temperature smooth tensile specimen fractured in the threads at a stress of 196 ksi. This is below the expected yield stress. The fracture exhibited dimpled overstress but little visual deformation or other evidence of ductility. The fracture was flat and occurred perpendicular to the stress axis. The 600 F notched tensile test specimen had a higher ultimate tensile strength, 238 ksi, and exhibited more ductile features. At low magnification the fracture surface had far more change in elevation compared to the flat room temperature specimen. At magnifications above 1000X dimpled overstress with indications of ductility such as elongated dimples, tearing and, in general, deeper features were visible. The 600 F test specimen appeared to have more cracked carbides. This may be because as the matrix becomes more ductile the carbides are relatively more brittle.

The final overstress areas of the fatigue specimens followed the same trends with temperature that were seen on the tensile specimens. Both the room temperature and 600 F smooth HCF specimens exhibited a very flat initial fatigue progression with quasi-cleavage features. The 600 F specimen had its localized origin at a carbide and the room temperature specimen originated at the surface near a carbide but it was not clear that the carbide contributed to the initiation. Neither HCF specimen exhibited fatigue striations or crack-like striations in their stage II fatigue progression areas. The 600 F specimen had a distinct shear lip in the

LCF tests were conducted at 600^oF on both smooth and notched specimens. The smooth specimen had a single origin area but no localized origin. The small fatigue propagation area exhibited feathery cleavage before the specimen fractured due to tensile overstress. The entire surface of the specimen, with the exception of the origin, had a distinct shear lip. The notched LCF specimen had a broader origin area with several localized origins and progression zones. The fatigue progressed only 0.001 inch into the specimen before final overstress occurred. Several of the local origins were associated with carbides at or near the surface. The very small fatigue zones exhibited only quasi-cleavage and feathery cleavage features.

MATERIAL

M-50

AMS 6491 Bar (Heat Treated to HRC 60-62)

TEST DATA

TEST TYPE

Notched Tensile *

TEST CONDITIONS

Strain Rate: 0.005 mm/mm/min (0.005 in/in/min) measured in gage.

Atmosphere: Air

Temperature: Room Temperature

Test Direction: Longitudinal

TEST RESULTS

Ultimate Strength: 1351.4 MPa (196 ksi)

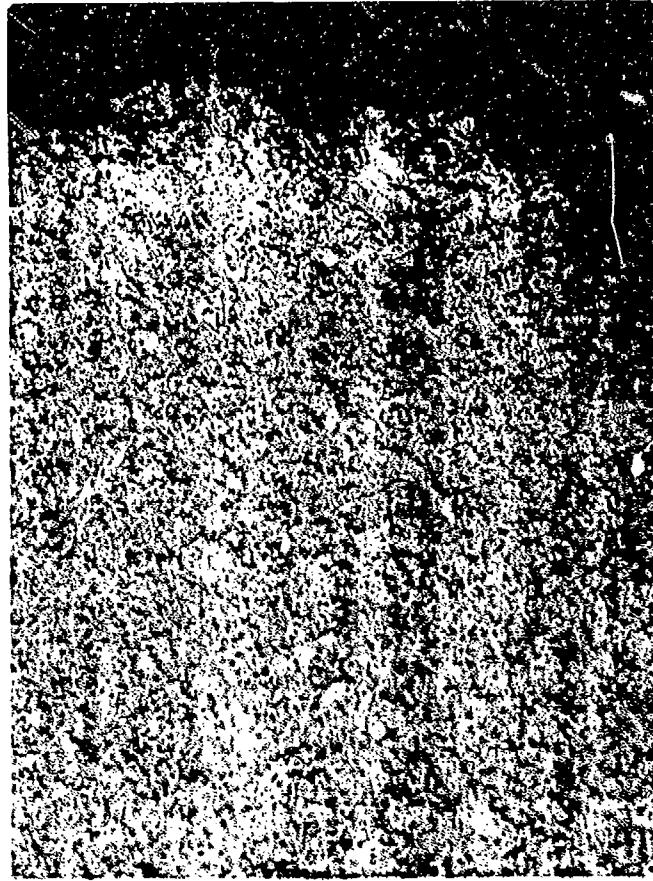
* Smooth Tensile specimen that fractured through threaded area.



FAL 94240

MAG: 10X

FIGURE 1-1: Test results and fractography of M-50 room temperature notched tensile test. The fracture surface exhibits directionality appearing to propagate from bottom left to top right of the photograph (arrow).



FAM 99741

MAG: 200X

FIGURE 1-2: Optical photomicrograph of a section through the base of the notch. Some secondary cracking is visible parallel to the primary fracture. The fracture is predominantly transgranular.

Etchant: 5% Nital

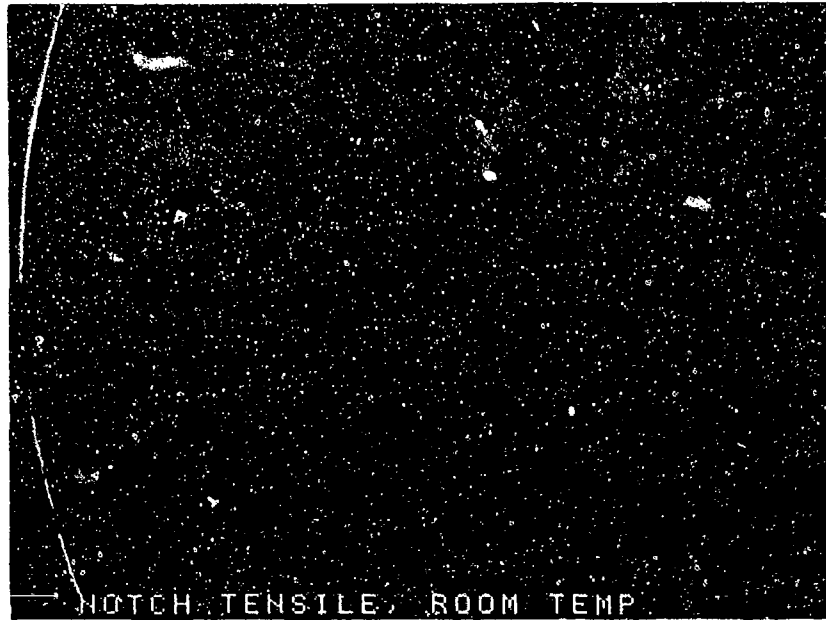


FIGURE 1-3: Low magnification photograph showing relatively flat fracture through a thread root.

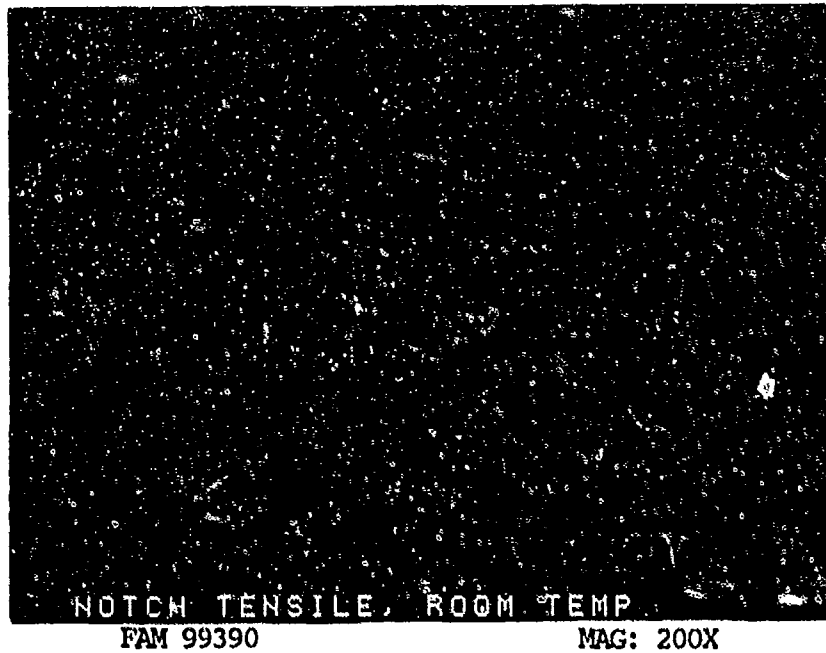


FIGURE 1-4: Higher magnification photograph of the center of the fracture surface.

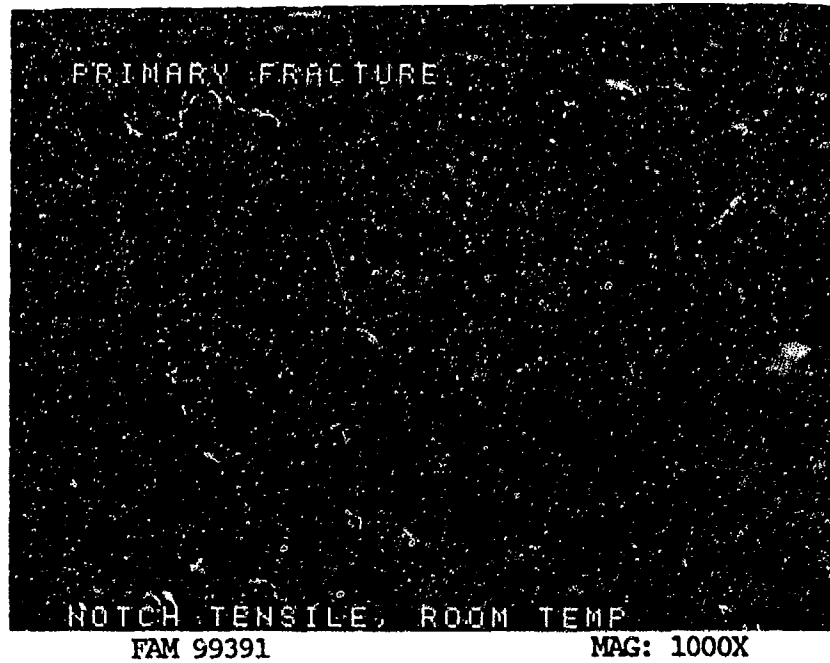


FIGURE 1-5: Higher magnification photograph of the area shown in Figure 1-3, showing dimpled overstress.

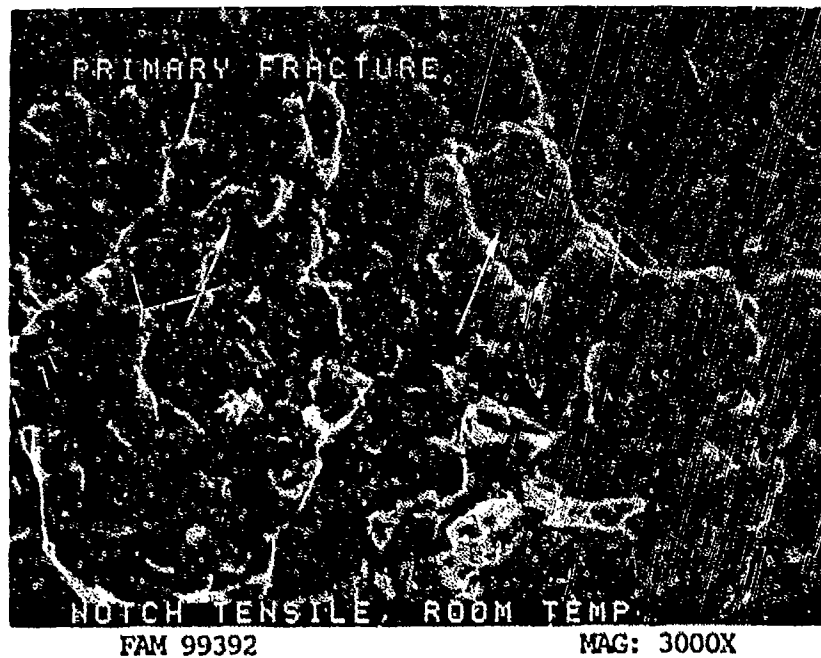


FIGURE 1-6: Fine dimpled overstress associated with carbides (arrows).

MATERIAL

M-50
AMS 6491 Bar (Heat Treated to HRC 60-62)

TEST DATA

TEST TYPE

Notched Tensile

TEST CONDITIONS

Crosshead Speed: 1.27 mm/min (0.05 in/min)

Atmosphere: Air

Temperature: 316°C (600°F)

Test Direction: Longitudinal

TEST RESULTS

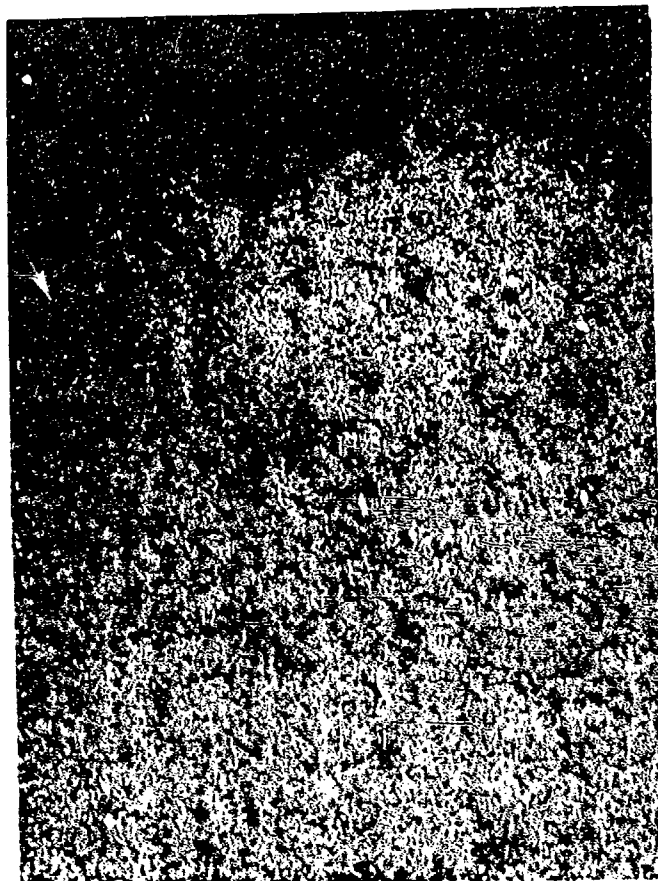
Ultimate Strength: 1640.9 MPa (238 ksi)



FAL 94238

MAG: 14X

FIGURE 1-7: Test results and fractography of M-50 316°C (600°F) notched tensile test. The fracture surface appears to exhibit deeper features than the room temperature specimen. See Figure 1-1. No clear origination area is visible.

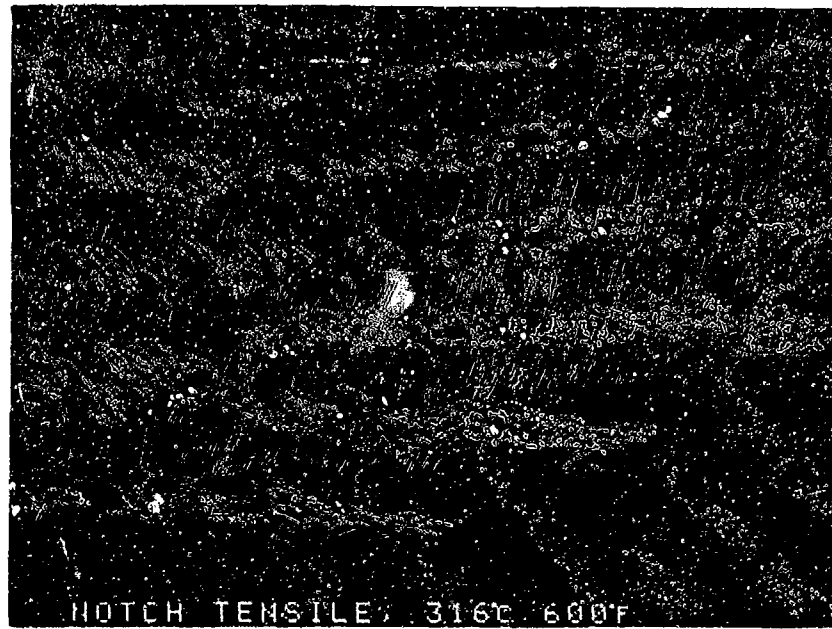


FAM 99746

MAG: 200X

FIGURE 1-8: Optical photomicrograph of metallographic cross section through the base of the notch. The fracture exhibits deep features and a secondary crack adjacent to the primary fracture (arrow). The fracture is predominantly transgranular.

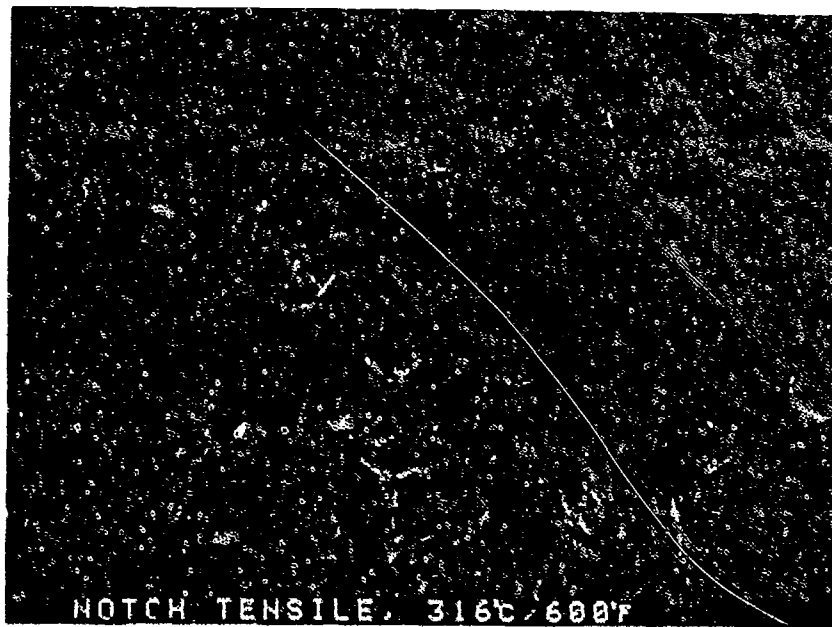
Etchant: 5% Nital



FAM 99396

MAG: 50X

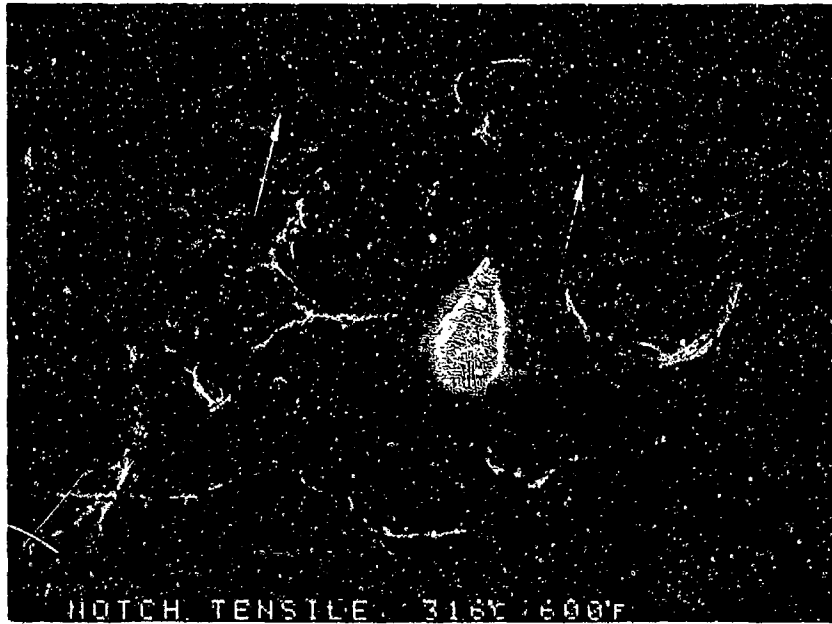
FIGURE 1-9: The fracture surface exhibits coarser features (more change in elevation) than the room temperature specimen. No shear lip is present.



FAM 99397

MAG: 200X

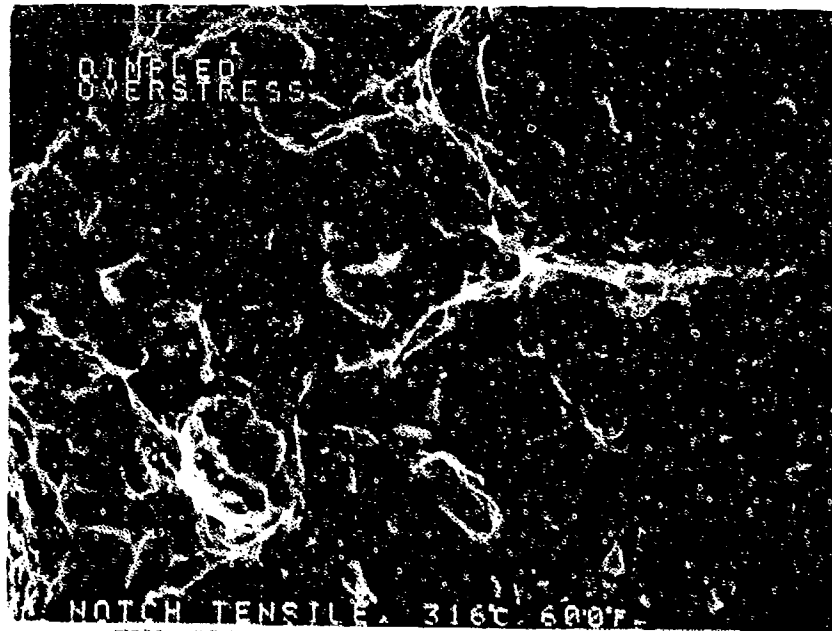
FIGURE 1-10: The fracture surface appears to exhibit dimpled overstress although no dimples are resolvable at this magnification.



FAM 99398

MAG: 1000X

FIGURE 1-11: Very fine dimpled overstress with larger fractured carbides visible in several areas (arrows). Contrast the more ductile appearance with the room temperature specimen. See Figure 1-5.



FAM 99399

MAG: 3000X

FIGURE 1-12: Fine dimpled overstress.

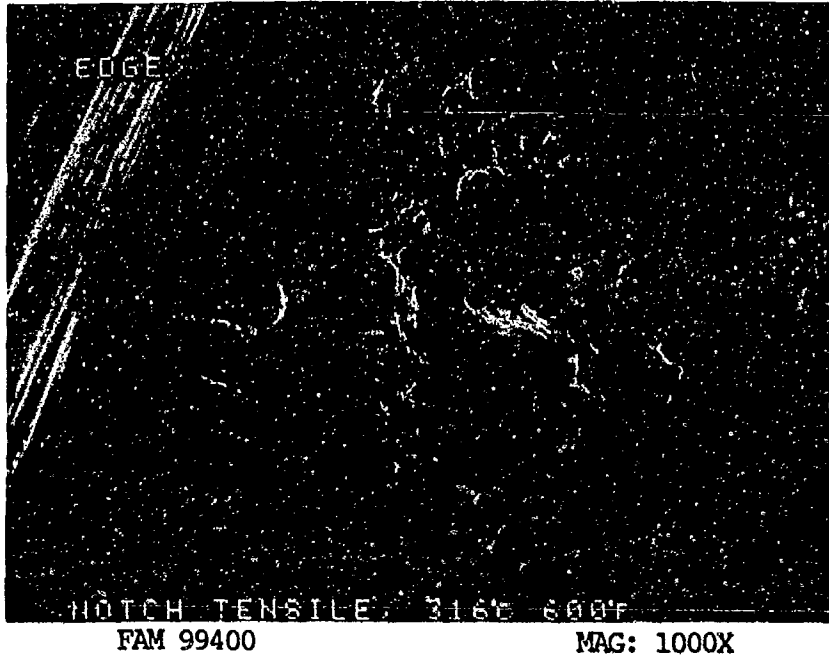


FIGURE 1-13: Flatter features and finer dimples near the edge of the specimen fracture surface.

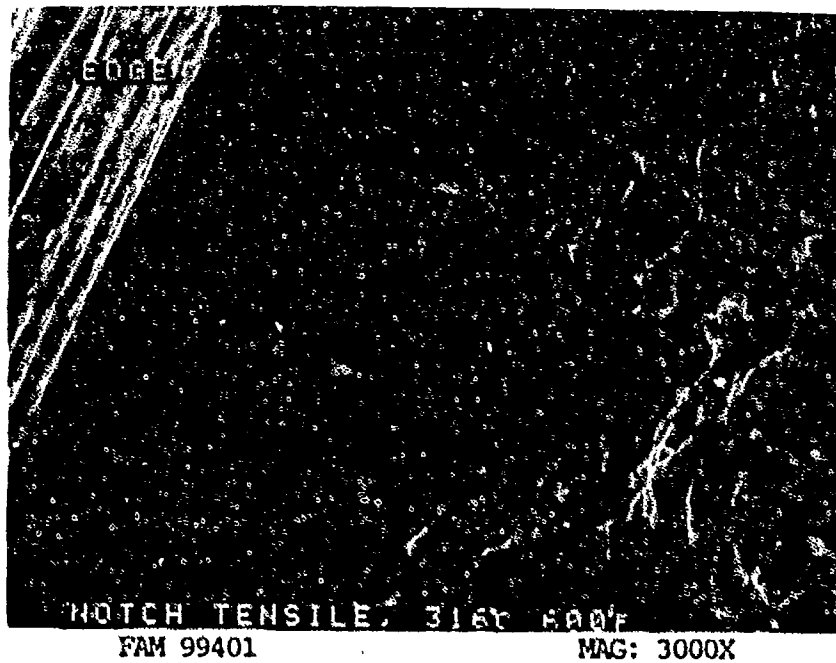


FIGURE 1-14: Higher magnification photograph of the area shown in Figure 1-13.

MATERIAL

M-50
AMS 6491 Bar (Heat Treated to HRC 60-62)

TEST DATA

TEST TYPE

Smooth HCF

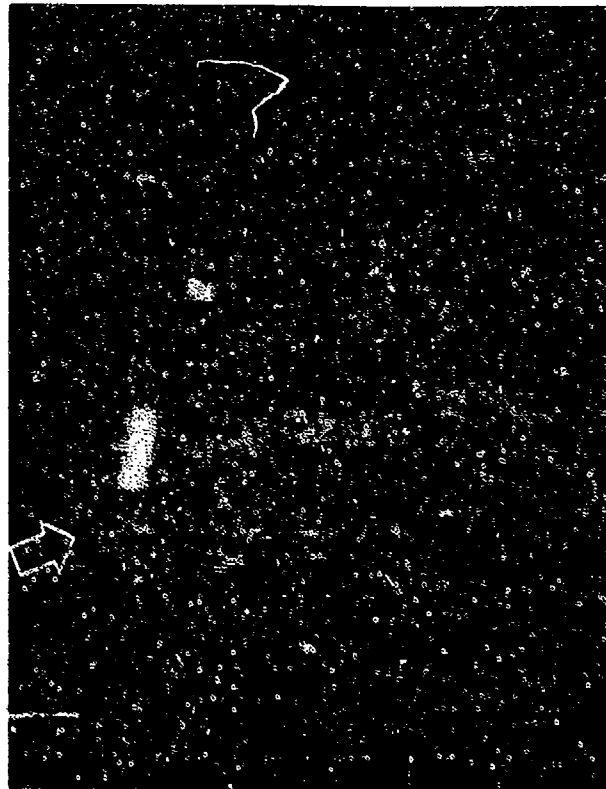
TEST CONDITIONS

Stress: 551.6 MPa (80 ksi)/27.6 MPa (4.0 ksi) DNF *
827.4 MPa (120 ksi)/41.37 MPa (6.0 ksi)
Stress Ratio: 0.05
Frequency: 1800 cpm
Atmosphere: Air
Temperature: Room Temperature
Test Direction: Longitudinal

TEST RESULTS

Cycles to Fracture: 1.0×10^6 (DNF), 27,600

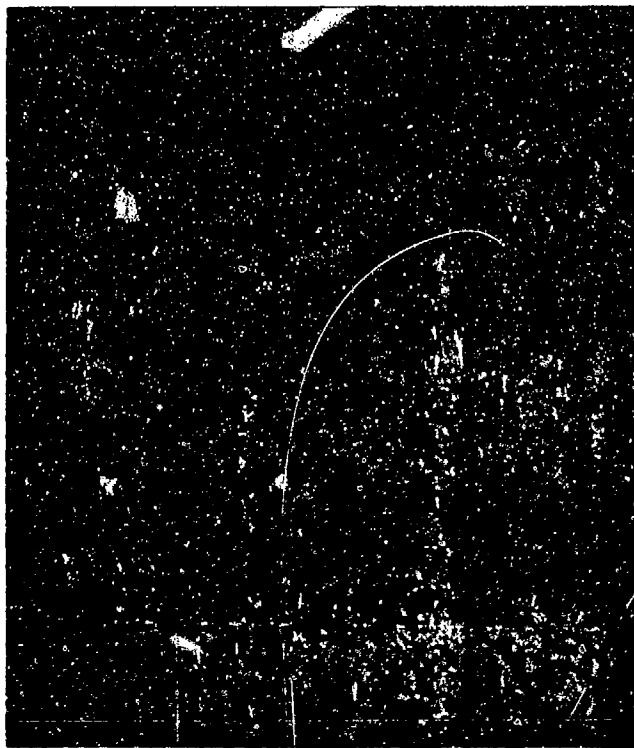
* Did Not Fracture



FAL 94290

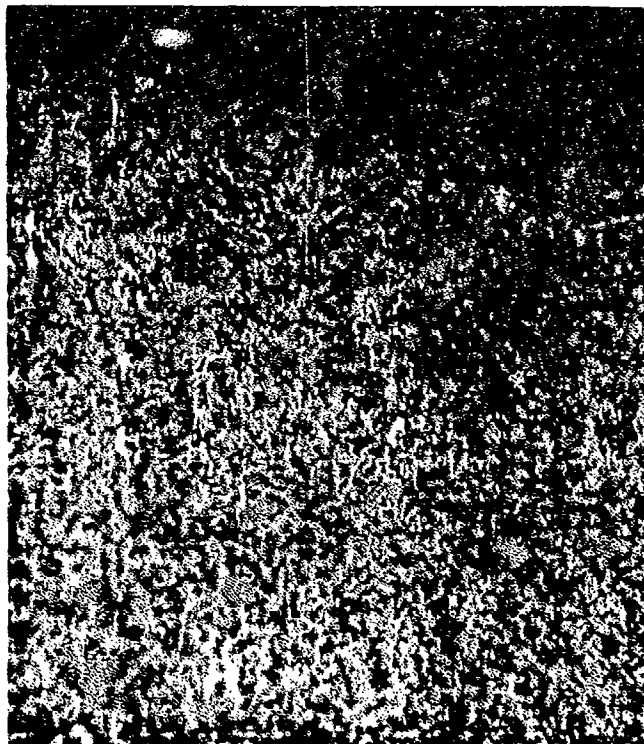
MAG: 14X

FIGURE 1-15: Test results and fractography of M-50 room temperature smooth HCF test. The entire fracture occurred on a plane perpendicular to the stress axis. Features can be seen radiating from an origin area (arrow).



FAM 100229

MAG: 200X

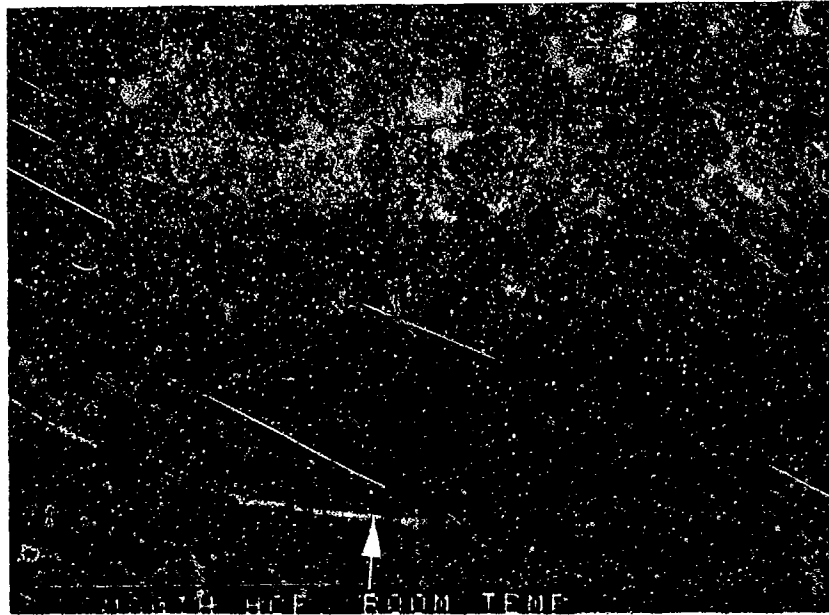


FAM 100230

MAG: 500X

FIGURE 1-16: Pair of increasing magnification optical photomicrographs showing the fatigue progression area on a plane perpendicular to the stress axis. The fracture is predominantly transgranular.

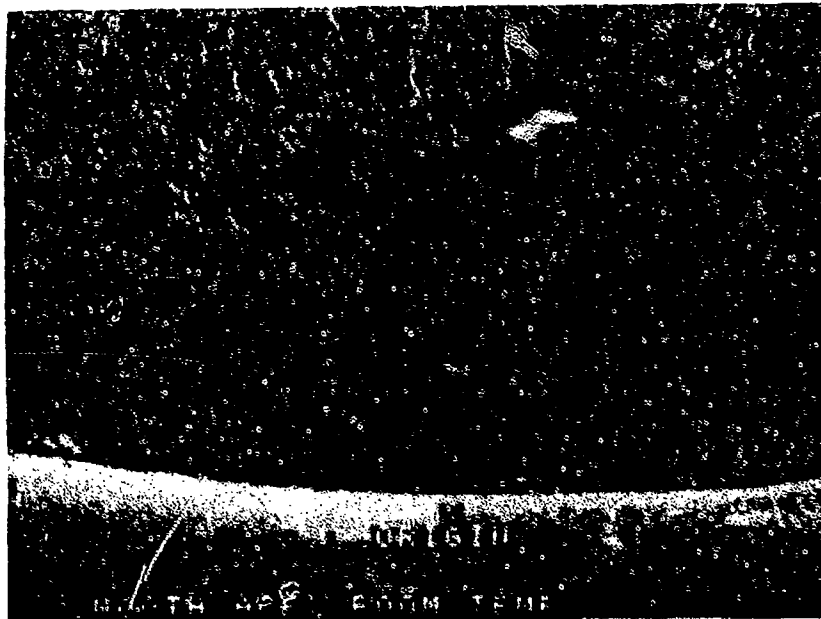
Etchant: 5% Nital



FAM 99430

MAG: 50X

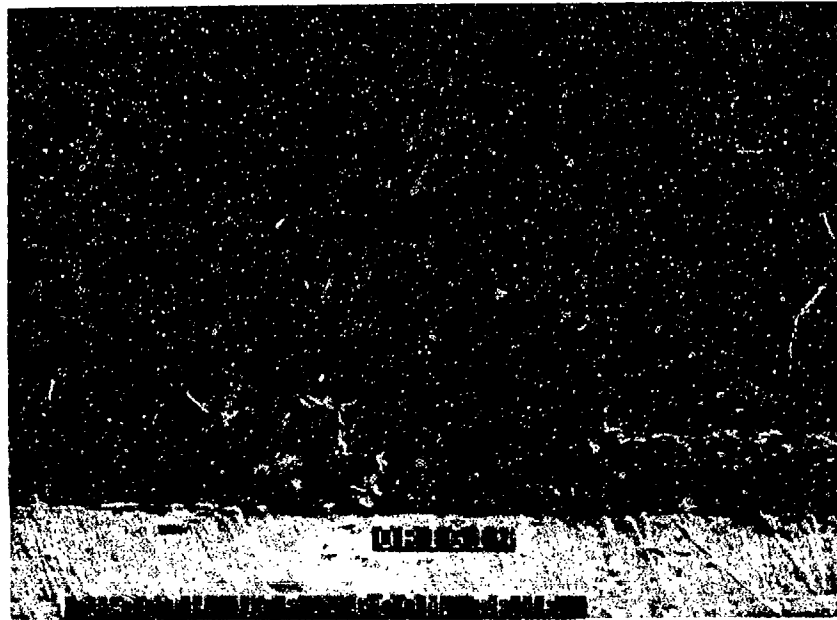
FIGURE 1-17: Low magnification photograph showing fatigue initiation and progression on a plane approximately perpendicular to the stress axis. Features can be seen radiating from the origin area (arrow).



FAM 99431

MAG: 200X

FIGURE 1-18: Higher magnification view of the origin area. The features are radiating from a localized area (arrow).



FAM 99432

MAG: 1000X

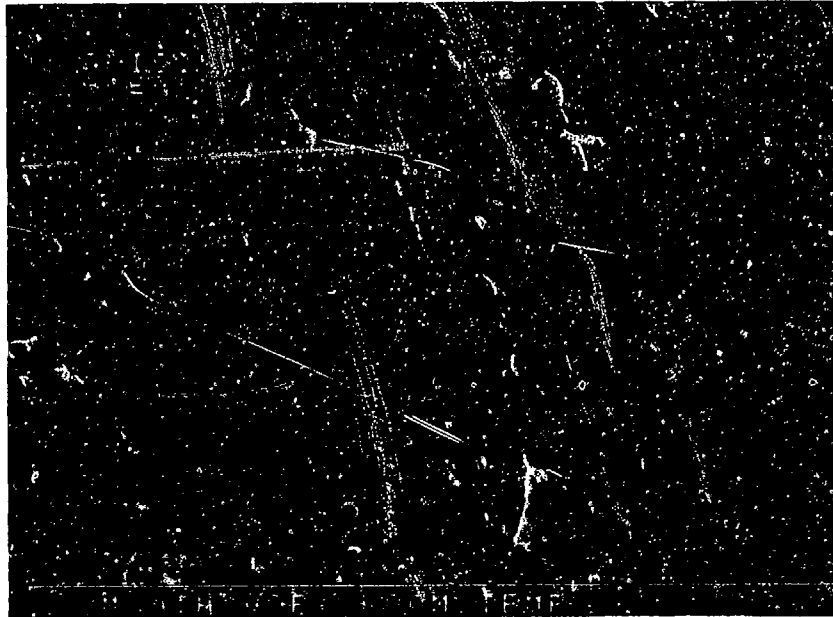
FIGURE 1-19: Higher magnification view of the origin shown in Figure 1-18. No defects are visible. A carbide (arrow) is present at the origin but it is unclear whether or not it contributed to fatigue initiation.



FAM 99433

MAG: 1000X

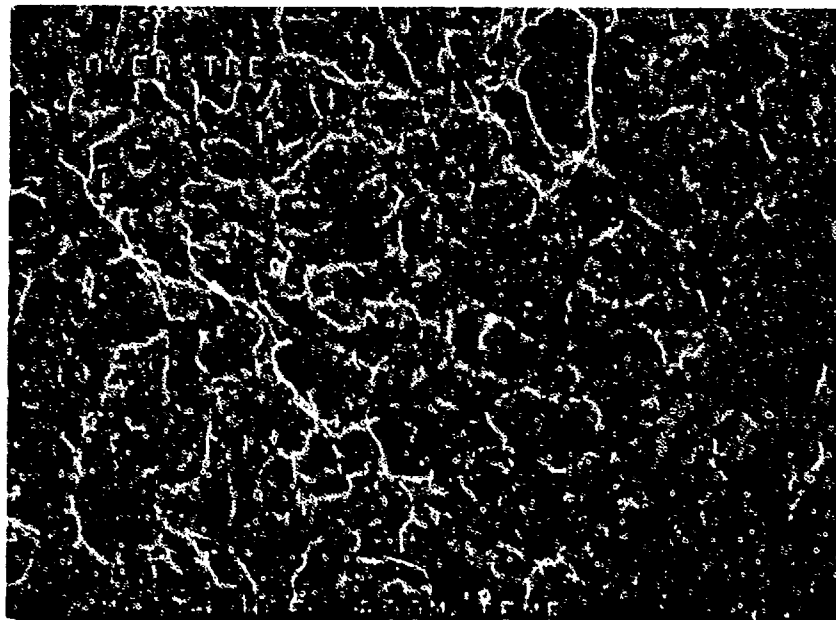
FIGURE 1-20: Area adjacent to the origin exhibiting quasi-cleavage features (mixture of fine cleavage and tearing ridges). No directionality is discernible.



FAM 99434

MAG: 3000X

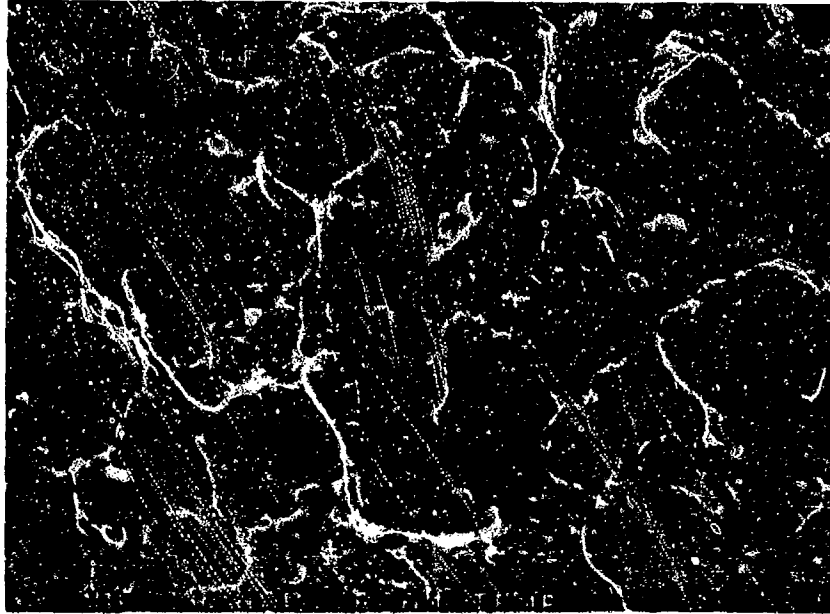
FIGURE 1-21: Higher magnification photograph of the area shown in Figure 1-20.



FAM 99435

MAG: 1000X

FIGURE 1-22: Final overstress area exhibiting features similar to the room temperature tensile specimen. See Figure 1-5.



FAM 99436

MAG: 3000X

FIGURE 1-23: Fine dimples in the final overstress area.

MATERIAL

M-50
AMS 6491 Bar (Heat Treated to HRC 60-62)

TEST DATA

TEST TYPE
Smooth HCF

TEST CONDITIONS

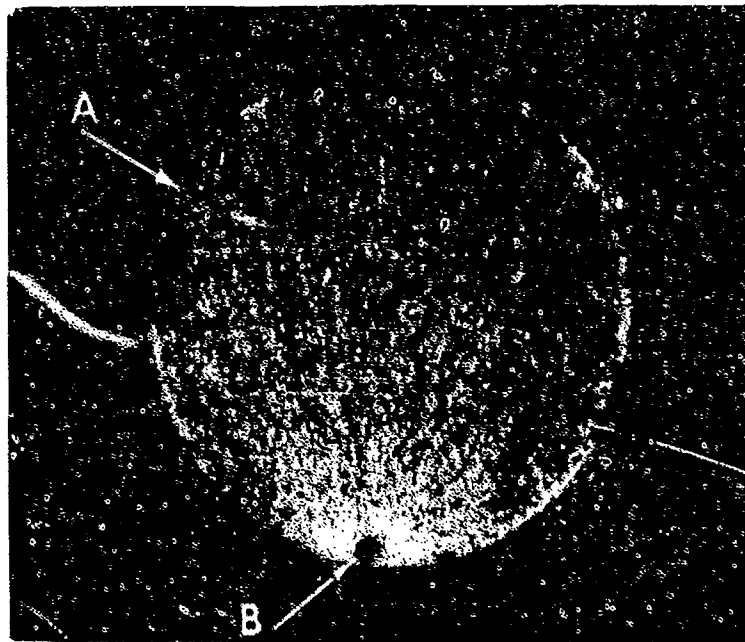
Stress: 551.6 MPa (80.0 ksi)/27.6 MPa (4.0 ksi) DNF*
689.5 MPa (100.0 ksi)/34.5 MPa (5.0 ksi) DNF
758.4 MPa (110 ksi)/37.9 MPa (5.5 ksi)

Stress Ratio: 0.05
Frequency: 1800 cpm
Atmosphere: Air
Temperature: 316°C (600°F)
Test Direction: Longitudinal

TEST RESULTS

Cycles to Fracture: 1.0×10^6 (DNF), 1.0×10^6 (DNF), 1.01×10^7

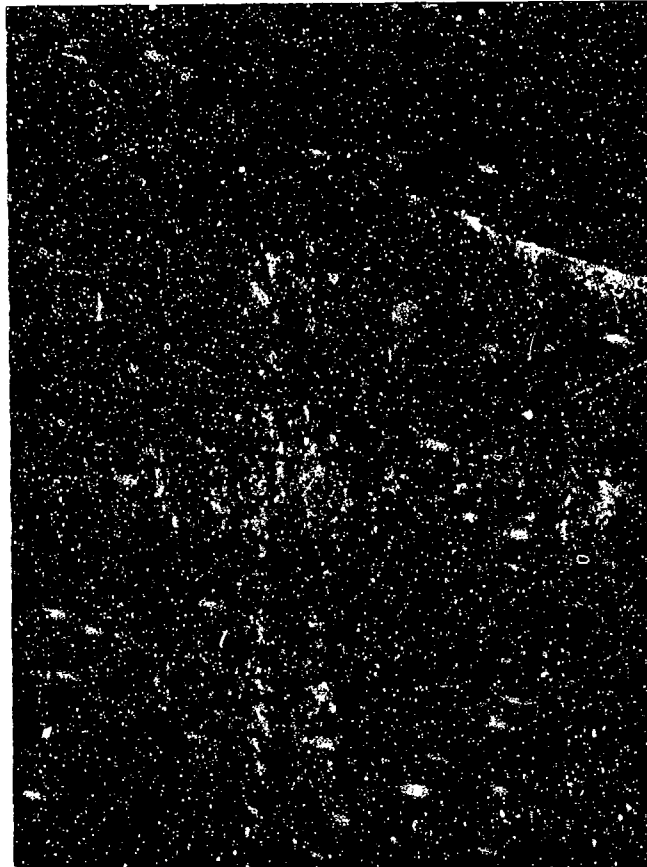
* Did Not Fracture



FAL 94291

MAG: 14X

FIGURE 1-24: Test results and fractography of M-50 316°C (600°F) smooth HCF test. The fracture is relatively flat with a small shear lip (arrow A) extending 90% of the way around the specimen. Features can be seen radiating from a subsurface origin (arrow B).



FAM 100226

MAG: 200X

FIGURE 1-25: Optical photomicrograph showing the transgranular fatigue progression area. The fracture surface is very flat, with a thin white-etching layer possibly caused by rubbing of the mating surfaces together during crack propagation.

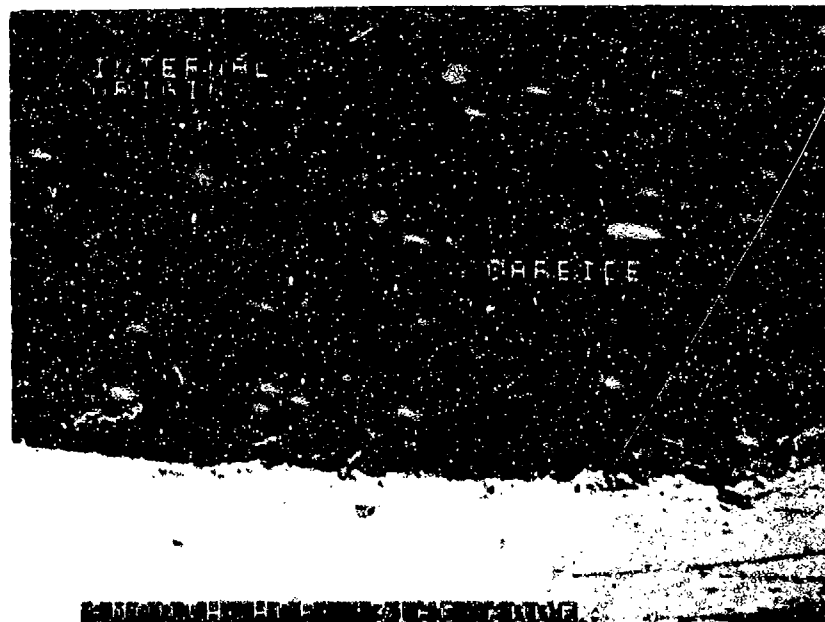
Etchant: 5% Nital



FAM 99412

MAG: 50X

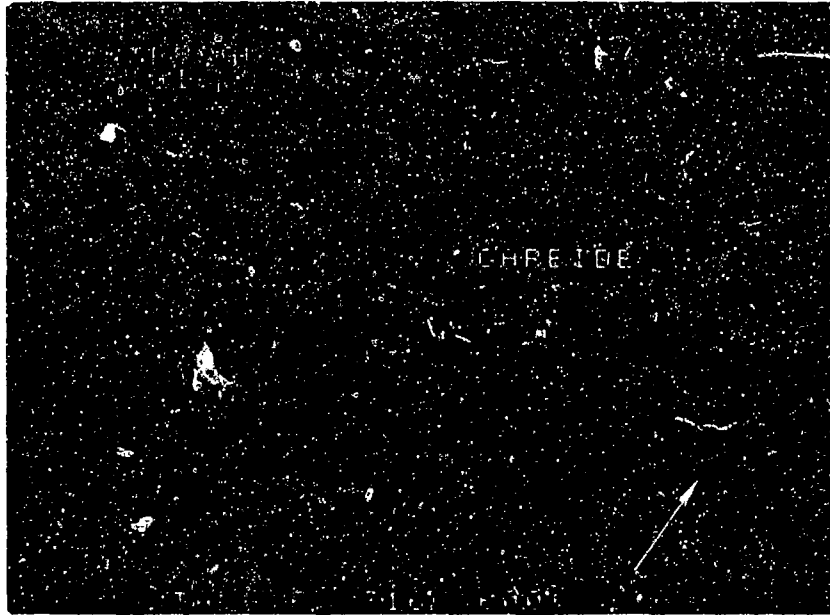
FIGURE 1-26: Low magnification photograph showing fatigue initiation and progression on a plane perpendicular to the stress axis. Features can be seen radiating from a subsurface origin. A small shear lip is visible on either side of the origin.



FAM 99413

MAG: 200X

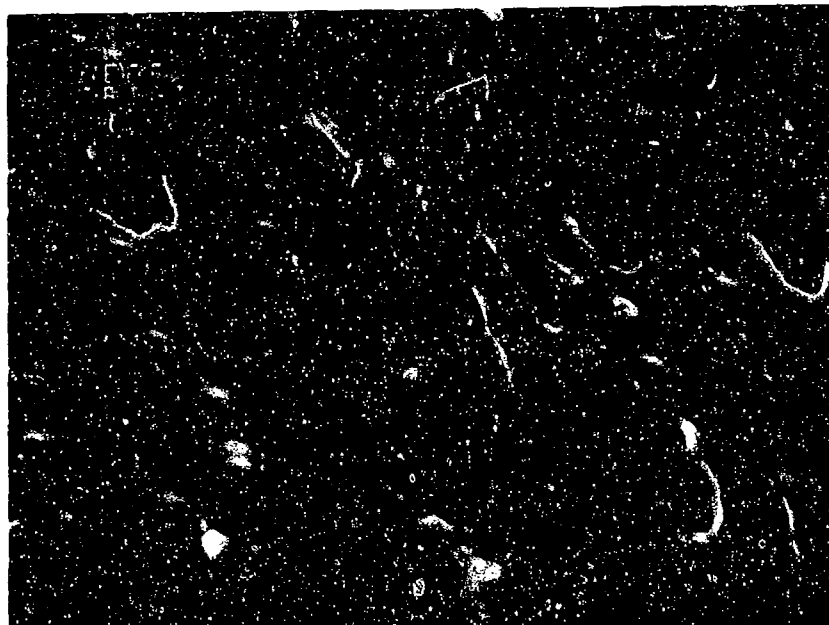
FIGURE 1-27: Higher magnification view of the origin area. A molybdenum/vanadium-rich carbide acted as a localized origin.



FAM 99414

MAG: 1000X

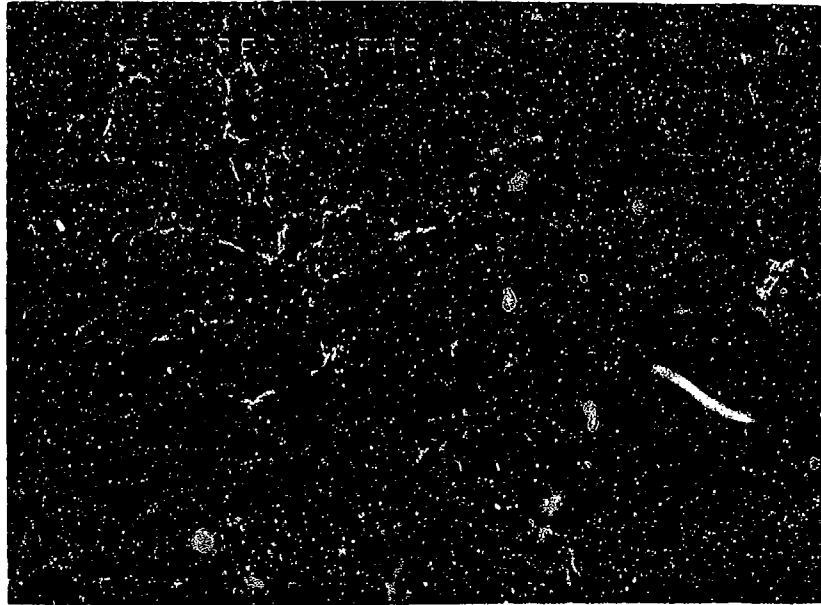
FIGURE 1-28: High magnification photograph of the origin. A second carbide (arrow) is visible adjacent to the one that initiated the fracture, but it does not appear to have contributed.



FAM 99415

MAG: 3000X

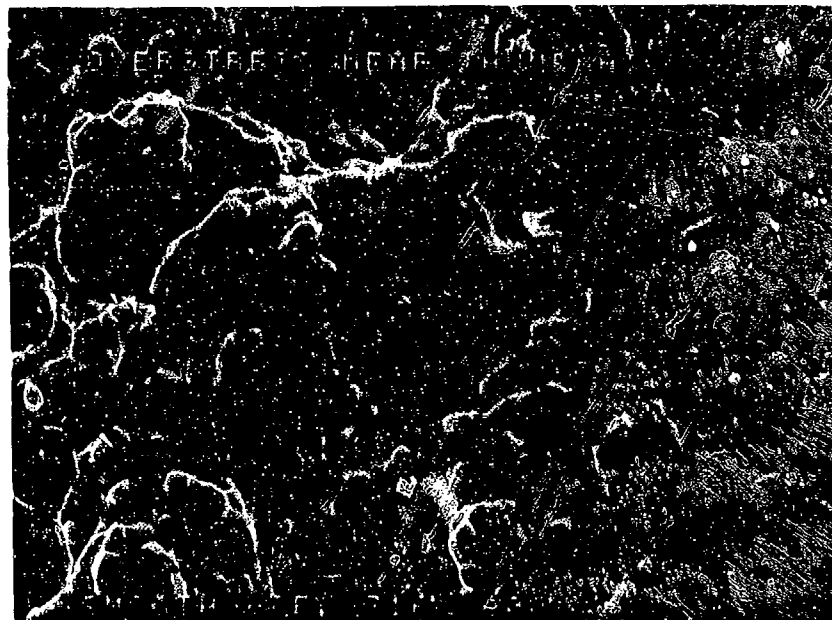
FIGURE 1-29: Smeared oxidized features near the origin. No fatigue features are visible.



FAM 99416

MAG: 1000X

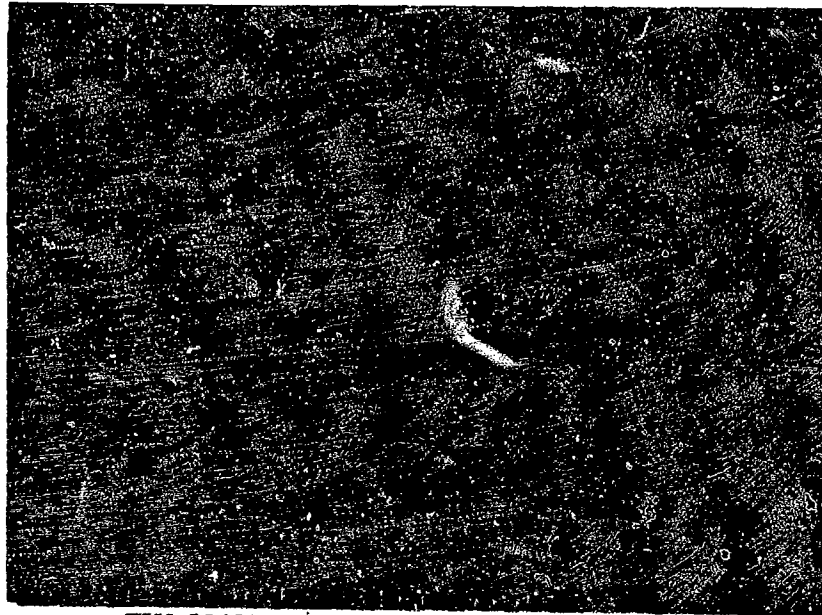
FIGURE 1-30: Overstress area adjacent to the fatigue propagation area.



FAM 99417

MAG: 3000X

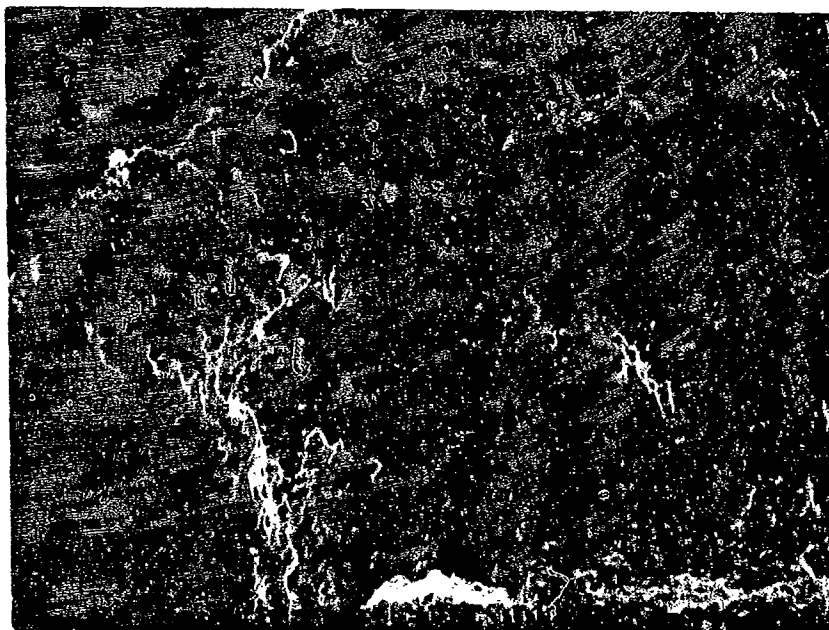
FIGURE 1-31: Higher magnification view of the area shown in Figure 1-30.



FAM 99419

MAG: 200X

FIGURE 1-32: Final overstress area (shear lip) along the edge of the specimen (bracket).



FAM 99420

MAG: 1000X

FIGURE 1-33: Higher magnification photograph of the final overstress area. Shallow shear dimples are visible.

MATERIAL

M-50
AMS 6491 Bar (Heat Treated to HRC 60-62)

TEST DATA

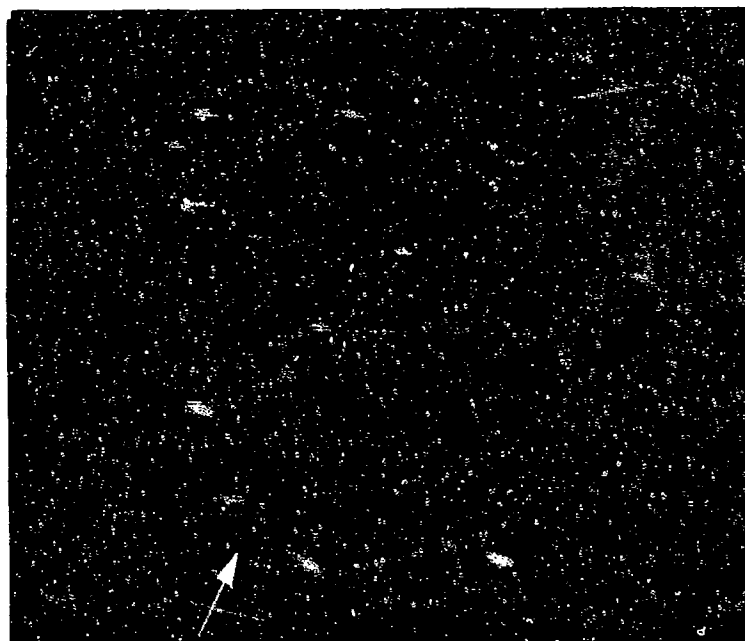
TEST TYPE
Smooth LCF

TEST CONDITIONS

Stress: 1378.9 MPa (200 ksi)/68.9 MPa (10.0 ksi)
Stress Ratio: 0.05
Frequency: 10 cpm
Atmosphere: Air
Temperature: 316°C (600°F)
Test Direction: Longitudinal

TEST RESULTS

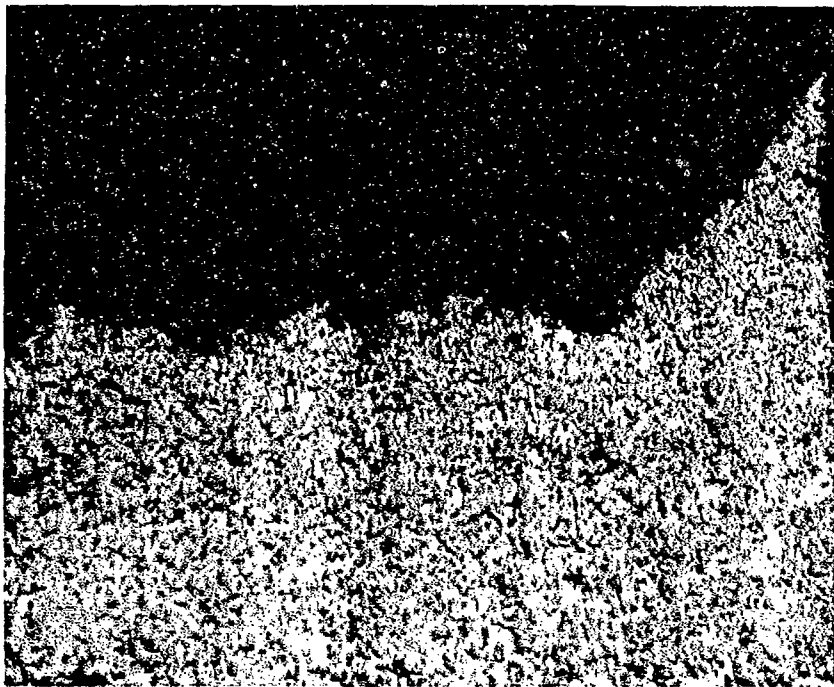
Cycles to Fracture: 1900



FAL 94289

MAG: 14X

FIGURE 1-34: Test results and fractography of M-50 316°C (600°F) smooth LCF test. The fracture exhibits a shear lip extending more than 90% of the way around the specimen. Features can be seen radiating from an origin (arrow).



FAM 100468

MAG: 200X

FIGURE 1-35: Optical photomicrograph of a metallographic cross section through the final overstress area. A shear lip is visible on the right side of the photograph.

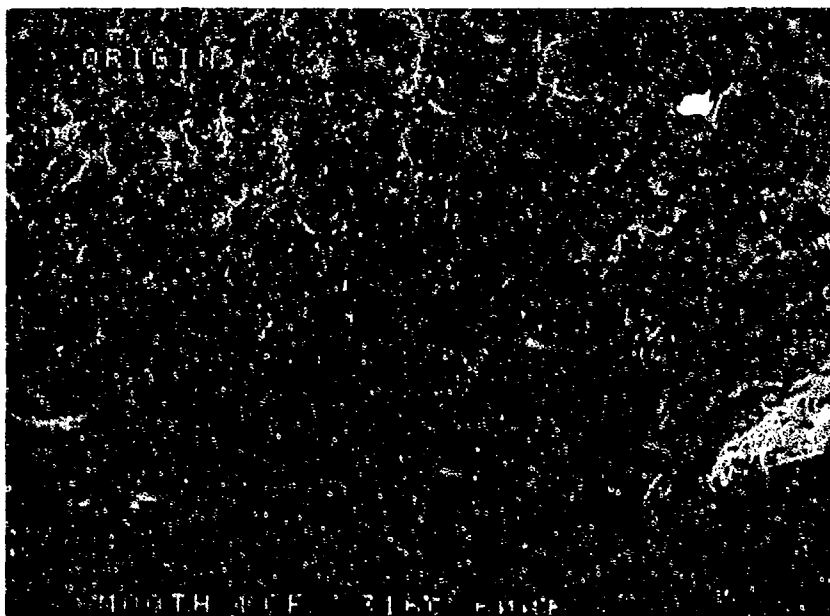
Etchant: 5% Nital



FAM 99437

MAG: 50X

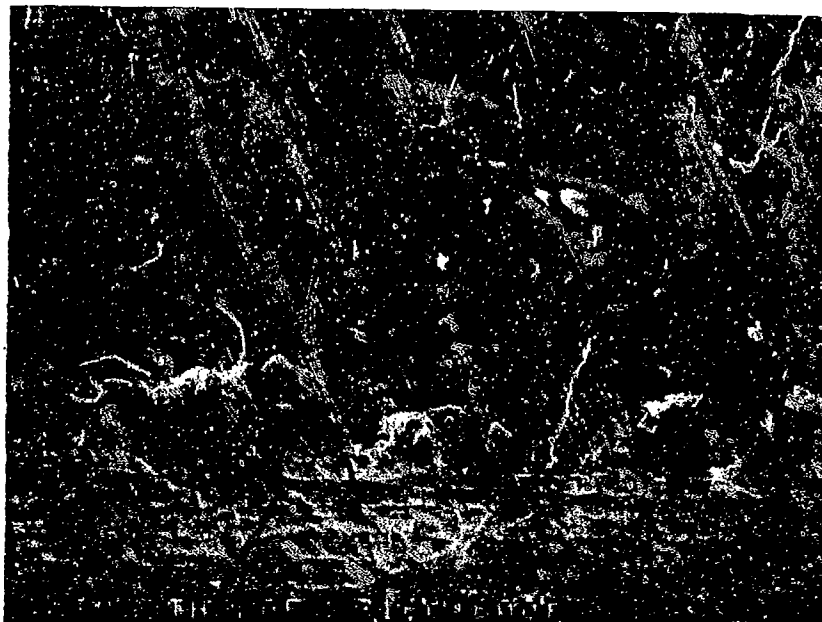
FIGURE 1-36: Low magnification photograph showing the fatigue origin area. A shear lip is visible on either side of the origin. The extent of the fatigue is shown by arrows.



FAM 99438

MAG: 200X

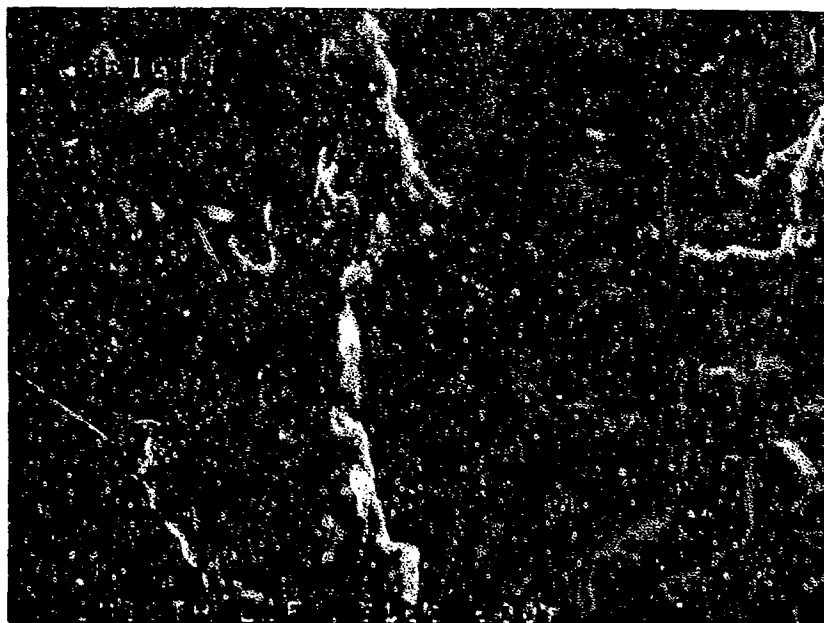
FIGURE 1-37: Higher magnification view of the origin area. Features radiate from the surface of the specimen.



FAM 99439

MAG: 1000X

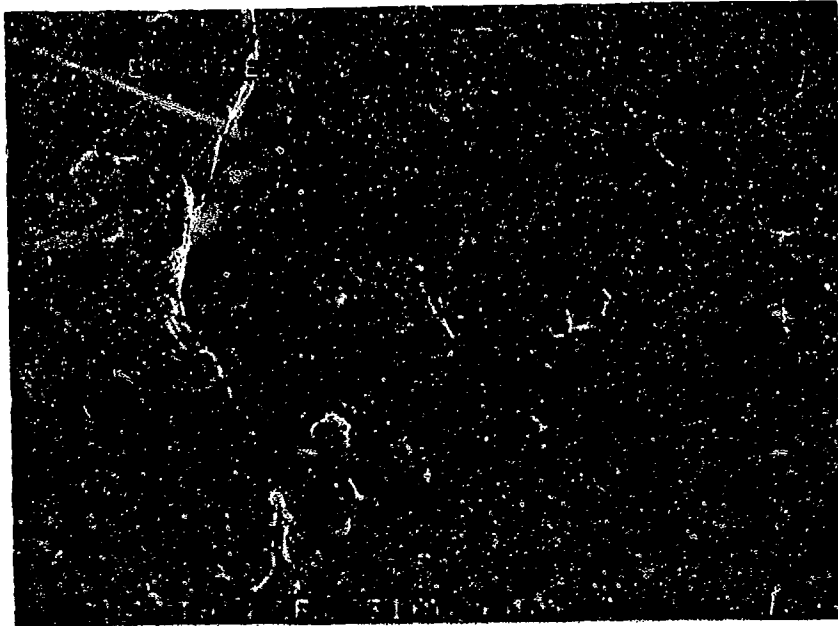
FIGURE 1-38: Higher magnification view of the origin. No defects are visible. The fracture features resemble feathery cleavage.



FAM 99440

MAG: 3000X

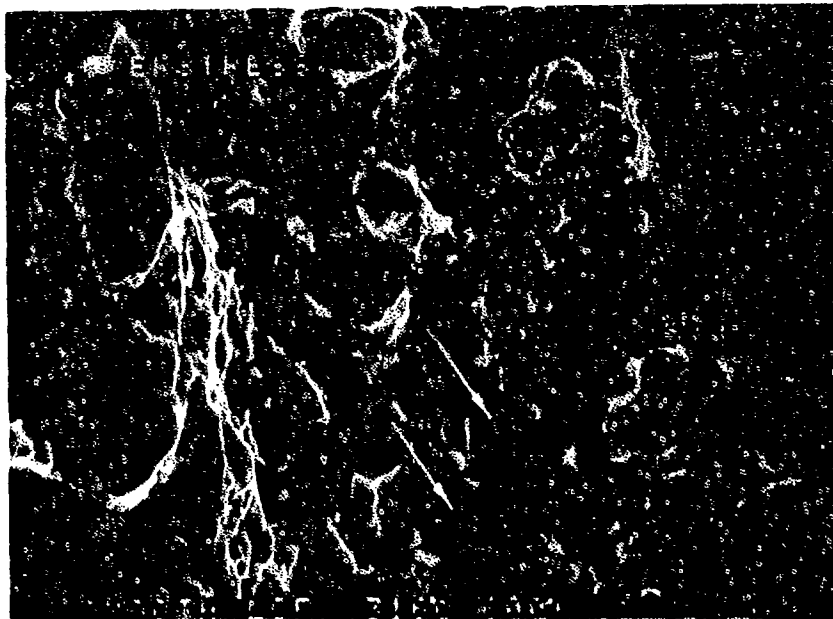
FIGURE 1-39: Fracture features in the fatigue thumbnail are oxidized.



FAM 99441

MAG: 1000X

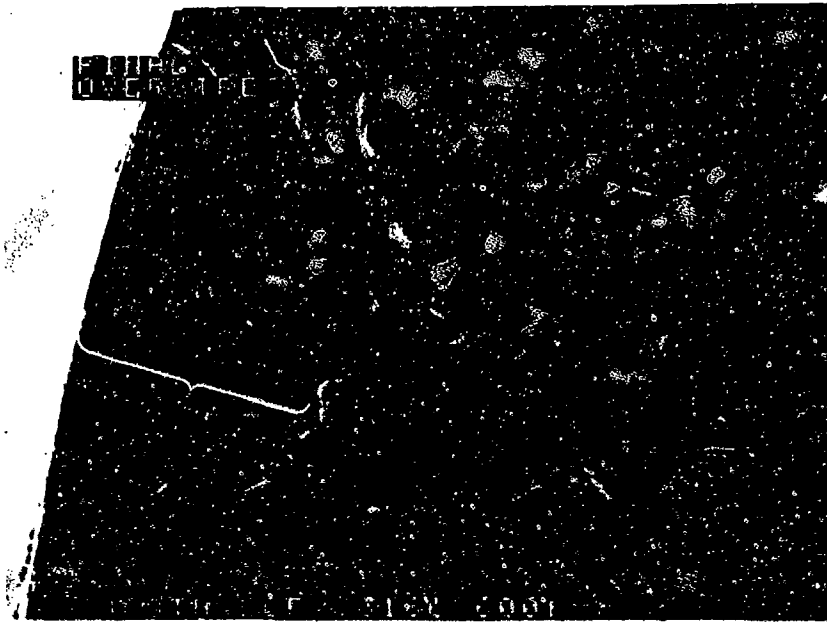
FIGURE 1-40: Dimpled overstress adjacent to the fatigue thumbnail.



FAM 99442

MAG: 3000X

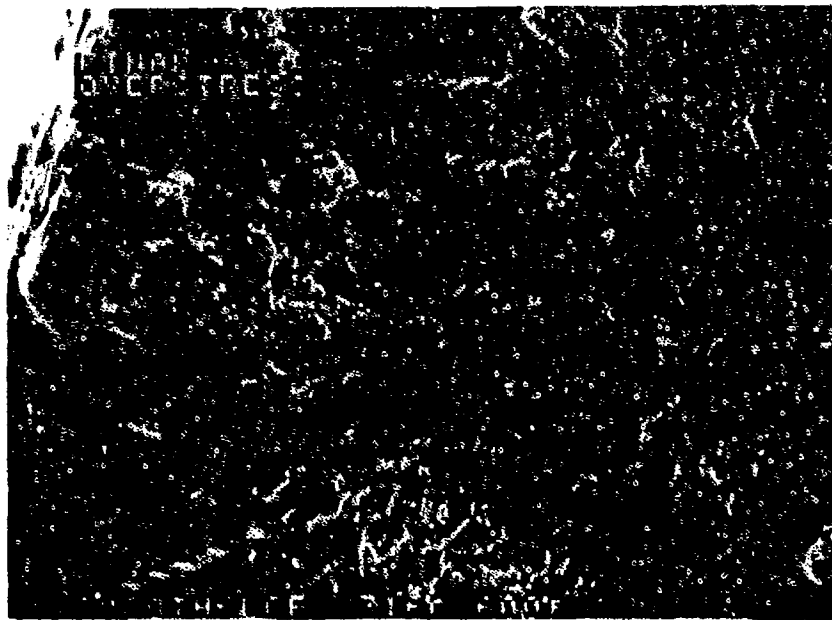
FIGURE 1-41: Higher magnification photograph of the area shown in Figure 1-40. Fine overstress dimples, carbides and fractured carbides are visible (arrows).



FAM 99443

MAG: 200X

FIGURE 1-42: Final overstress area (shear lip) along the edge of the fracture. The extent of the lip is shown by a bracket.



FAM 99444

MAG: 1000X

FIGURE 1-43: Equiaxed dimples and shallow shear dimples on the shear lip.

MATERIAL

M-50
AMS 6491 Bar (Heat Treated to HRC 60-62)

TEST DATA

TEST TYPE

Notched LCF

TEST CONDITIONS

Stress: 689.5 MPa (100.0 ksi)/34.5 MPa (5.0 ksi)
Stress Ratio: 0.05
Frequency: 10 cpm
Atmosphere: Air
Temperature: 316°C (600°F)
Test Direction: Longitudinal

TEST RESULTS

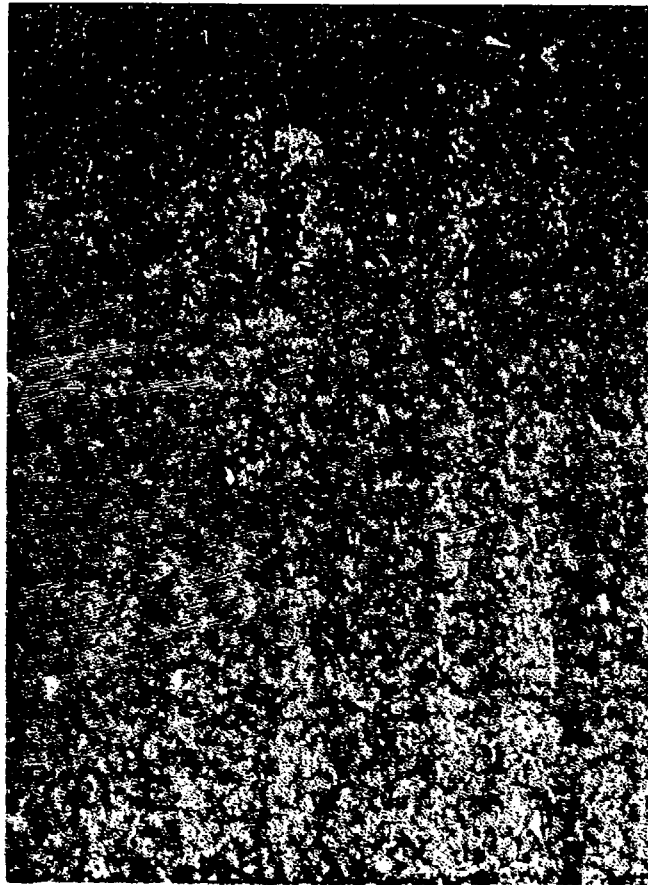
Cycles to Fracture: 500



FAL 94288

MAG: 14X

FIGURE 1-44: Test results and fractography of M-50 316°C (600°F) notched LCF test. Some directionality is visible indicating propagation from a diffuse surface origin (bracket). A narrow, discontinuous shear lip is visible (arrow).



FAM 99748

MAG: 200X

FIGURE 1-45: Optical photomicrograph of a section through the final overstress area. A small shear lip is visible (arrow). The fracture is predominantly transgranular.

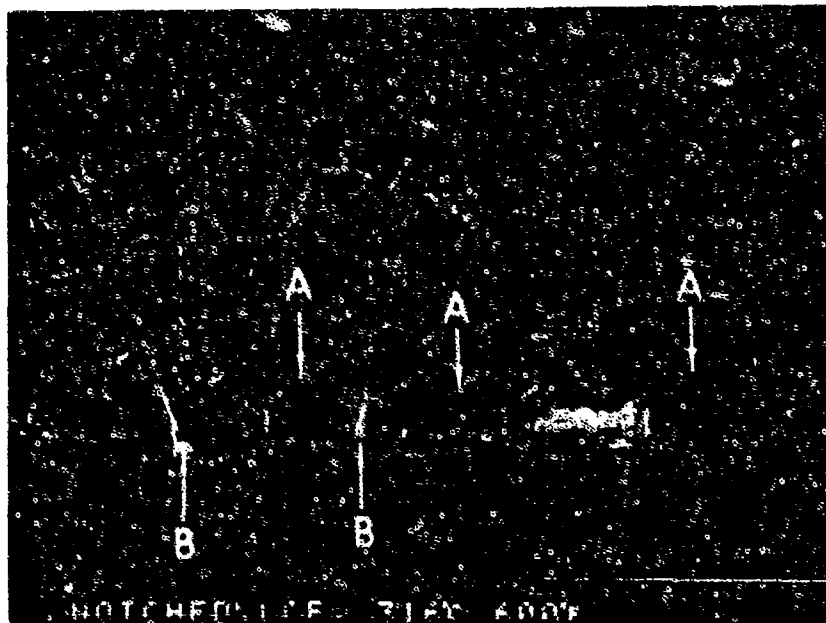
Etchant: 5% Nital



FAM 99422

MAG: 50X

FIGURE 1-46: Low magnification photograph showing fatigue initiation from multiple surface origins. The fatigue progressed to a very shallow depth before final overstress occurred.



FAM 99423

MAG: 200X

FIGURE 1-47: Multiple origins at the surface of the specimen. The depth of the fatigue progression is shown by arrows A. Steps (arrows B) can be seen separating localized origins.

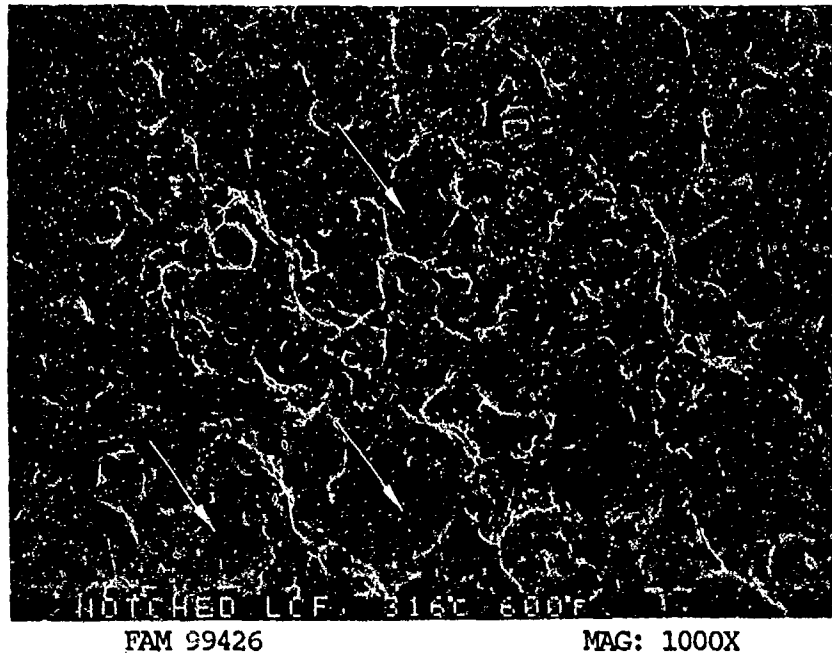


FIGURE 1-50: Final overstress area. Several carbides and cracked carbides are visible (arrows).

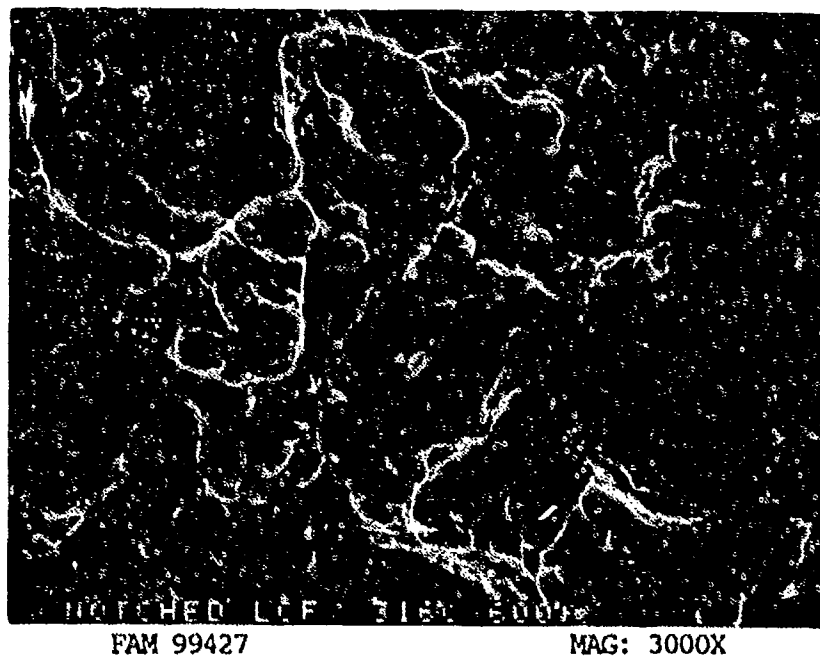


FIGURE 1-51: Higher magnification view of the area shown in Figure 1-50.

SERVICE FAILURE

FRACTURE MODE Rolling Contact Fatigue (RCF)

PART NAME Number Three Bearing Assembly

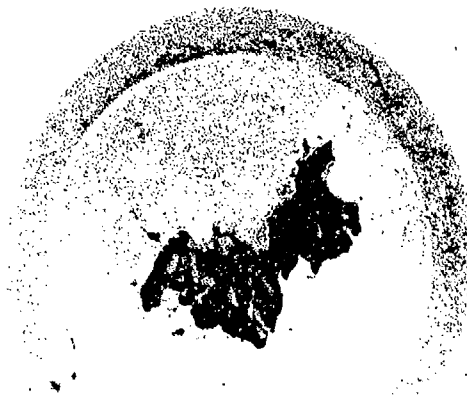
OPERATION DATA Part operated under standard gas turbine engine conditions (no oil starvation or overtemperature). No associated engine damage occurred.

PART TIME 165 hours

	<u>REQUIRED</u>	<u>ACTUAL</u>
MAT'L		
BASE	<u>M-50 steel</u>	<u>confirmed</u>
OTHER	<u>-</u>	<u>-</u>
HARDNESS	<u>HRC 60-66</u>	<u>HRC 64-65 *</u>
GRAIN SIZE	<u>ASTM 7 or finer</u>	<u>ASTM 9-10</u>
DIMENSIONAL	<u>-</u>	<u>-</u>

* Diamond pyramid hardness (DPH) conversions.

SUMMARY: Isolated number three bearing ball spall with associated raceway and cage damage was the result of rolling contact fatigue (RCF). RCF is a failure mode unique to parts such as bearings that are cyclically loaded in compression. The spall surface exhibited coarse arrest marks indicating propagation in several directions (Figure 1-53). No localized origin could be identified. Metallographic sections through the spall revealed microstructural alterations known as "butterflies" (Figures 1-56 and 1-57). Butterflies are generally associated with RCF and can occur before, during or after spalling. No other material or microstructural anomalies were found.



FAL 90708

MAG: 3X

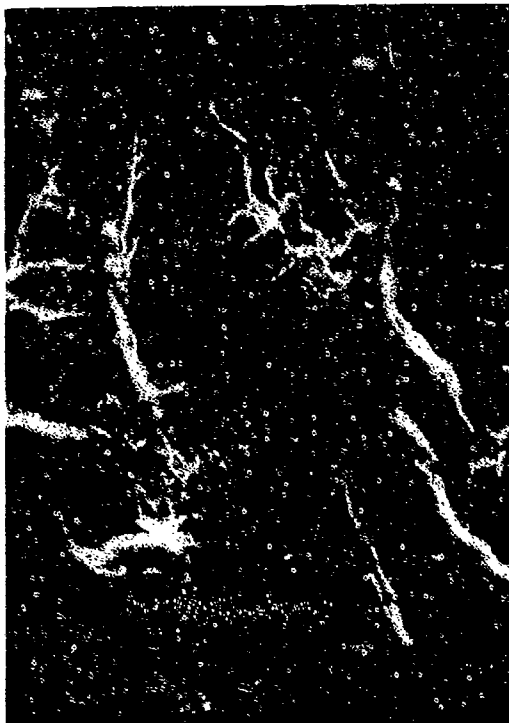


FAL 90709

MAG: 8X

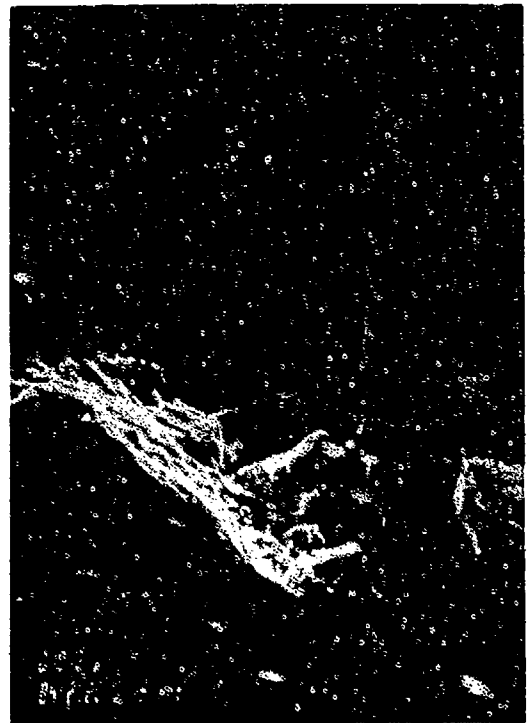
FIGURE 1-52: Overall photograph of the spall on a single ball. Adjacent balls had damage caused by the debris liberated.

FIGURE 1-53: Higher magnification photograph showing coarse arrest marks indicating propagation in several directions (arrows).



FAM 98220

MAG: 30X

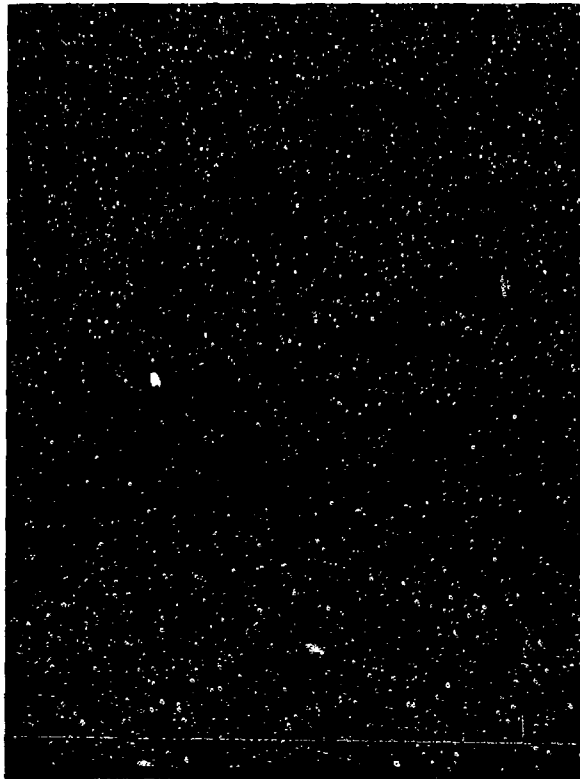


FAM 98221

MAG: 400X

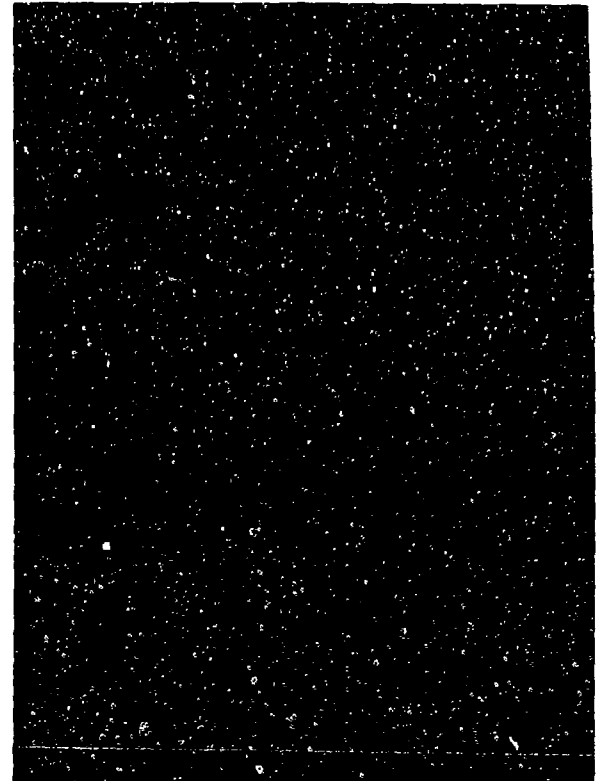
FIGURE 1-54: Coarse arrest marks in the spalled area (arrow).

FIGURE 1-55: Coarse arrest marks (arrow).



FAM 98227

MAG: 200X



FAM 98228

MAG: 500X

FIGURE 1-56: Microstructural alterations known as "butterflies" (arrows).

FIGURE 1-57: Higher magnification photograph of a butterfly on the surface of the spall (arrows).

Etchant: 5% Nital

15-5PH (Stainless Steel)

Material Description

15-5 PH is a delta ferrite free precipitation hardening martensitic stainless steel. It's composition is similar to 17-4 PH with 2% less chromium and higher nickel content. Precipitation hardening results from precipitation of a copper-rich phase at temperatures of 900 to 1150 F. The corrosion resistance of 15-5 PH is similar to Type 304 stainless steel and its oxidation resistance is reported to be better than Type 410 but inferior to Type 430 stainless steel. The alloy is produced in many forms including; plate, bar and wire.

The material used in this study was AMS 5659 heat treated to AMS 2759/3 (consumable electrode melted and solution heat treated and hardened) with a hardness of HRC 38-45 after precipitation heat treatment at 925 F for 4 hours. The typical room temperature mechanical properties for ASM 5659 are as follows:

Ultimate Tensile Strength:	170 ksi	
0.2% Yield Strength:	155 ksi	
Percent Elongation:	10% min.	
Percent Reduction in Area:	38% min.	
ASTM Grain Size:	<u>Required</u>	<u>Measured</u>
	No Requirement	14.5
Measured Hardness:	HRC 42-44 (DPH Conversions)	

Fractography Overview

Only two tests were conducted on 15-5 PH: stress corrosion and hydrogen embrittlement. The stress corrosion test was conducted on a U-bend specimen in a 3.5% NaCl vapor at 95 C (203 F). The test temperature was chosen to accelerate the fracture. The specimen fracture surface was classical intergranular, originating on the tension side. This was determined by looking at corrosion deposits both on the surface of the specimen and on the fracture surface. A thin shear lip was present along the compression surface. The metallographic section confirmed the intergranular nature of the fracture and revealed branching intergranular secondary cracks characteristic of SCC. The hydrogen embrittlement specimen was charged for 12 hours in gaseous hydrogen then tested under static tension loading conditions in air. The specimen was tested at a stress of 244 ksi for 99.3 hours at which point the stress was increased to 273 ksi. Fracture occurred after 0.7 hours at this higher stress. The fracture surface was primarily dimpled overstress with secondary cracks. A narrow shear lip possibly containing remnant cleavage features was visible at the base of the notch.

MATERIAL

15-5 PH
AMS 5659 Bar

TEST DATA

TEST TYPE

Stress Corrosion

TEST CONDITIONS

Stress: 940 MPa (136 ksi)
Environment: 3.5% NaCl (simulated sea water) vapor
Temperature: 95°C (203°F)
Test Direction: Longitudinal U-bend

TEST RESULTS

Time to Fracture: 384 hours



FAL 94625 Tension Side MAG: 3X

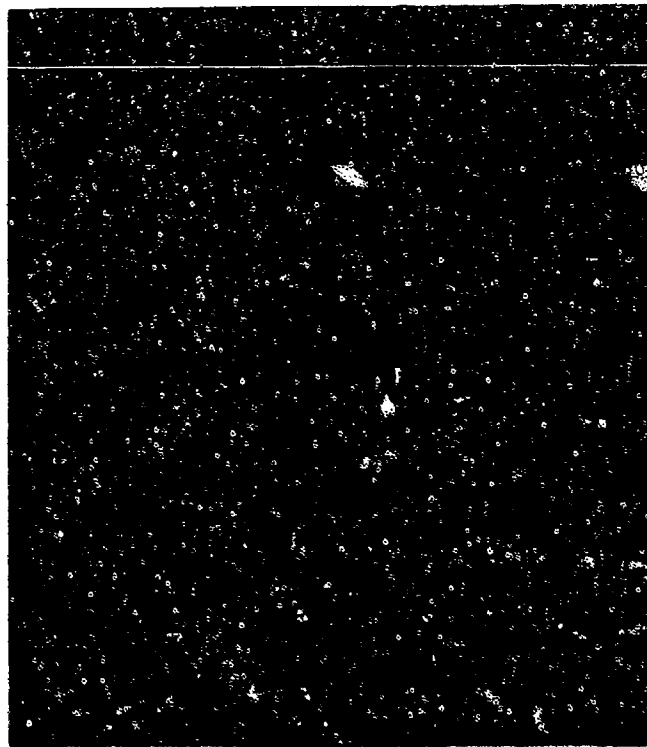
FAL 94624 Compression Side MAG: 3X

FIGURE 2-1: Test results and fractography of 15-5 PH stress corrosion test. The fracture is shown from the tension side (left) and compression side (right). The tension side exhibited corrosion attack and deposition corrosion products. The compression side was relatively free of attack.



FAM 100264

MAG: 200X



FAM 100265

MAG: 200X

FIGURE 2-2: Optical photomicrographs showing the intergranular nature of the primary fracture path (arrows, top) and typical intergranular branching secondary crack (bottom). Often these branching secondary cracks are a significant indication that the fracture mode is stress corrosion.

Etchant: Vilella's Reagent



FIGURE 2-3: Low magnification photograph of the fracture surface exhibiting intergranular features. The final overstress area is visible as a thin band at the upper edge of the specimen (arrows).

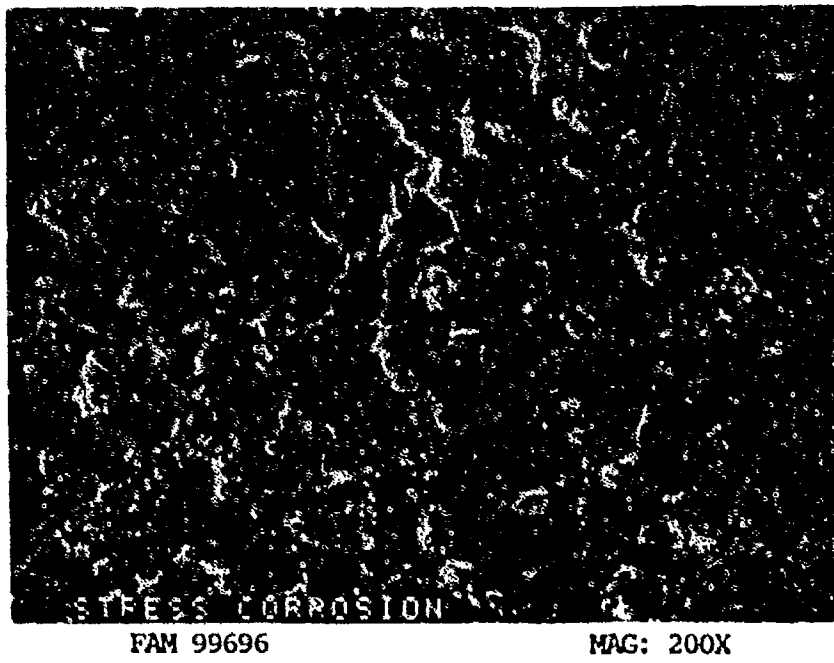


FIGURE 2-4: Oxidized intergranular fracture.

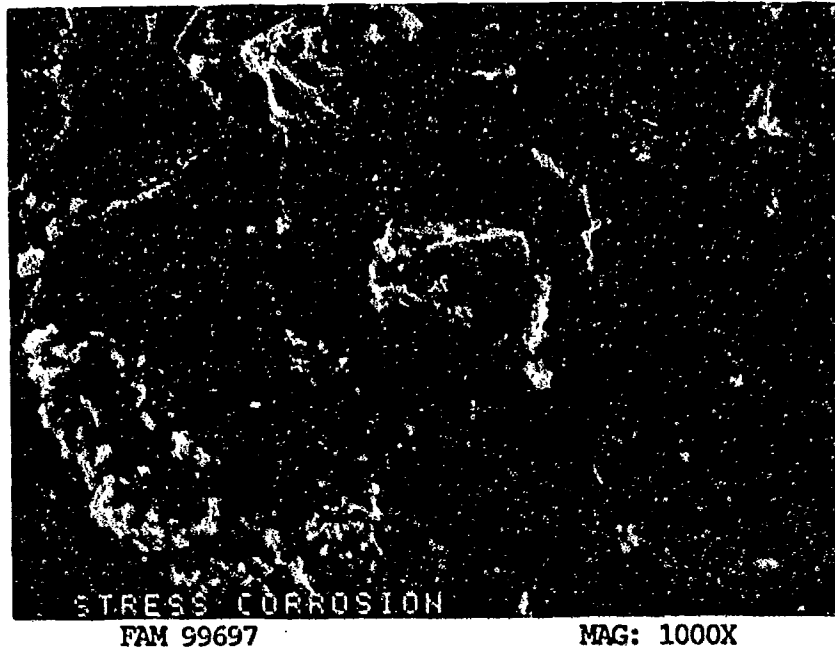


FIGURE 2-5: Higher magnification photograph of the area shown in Figure 2-4, exhibiting intergranular fracture. Corrosion products are visible on the grain faces.

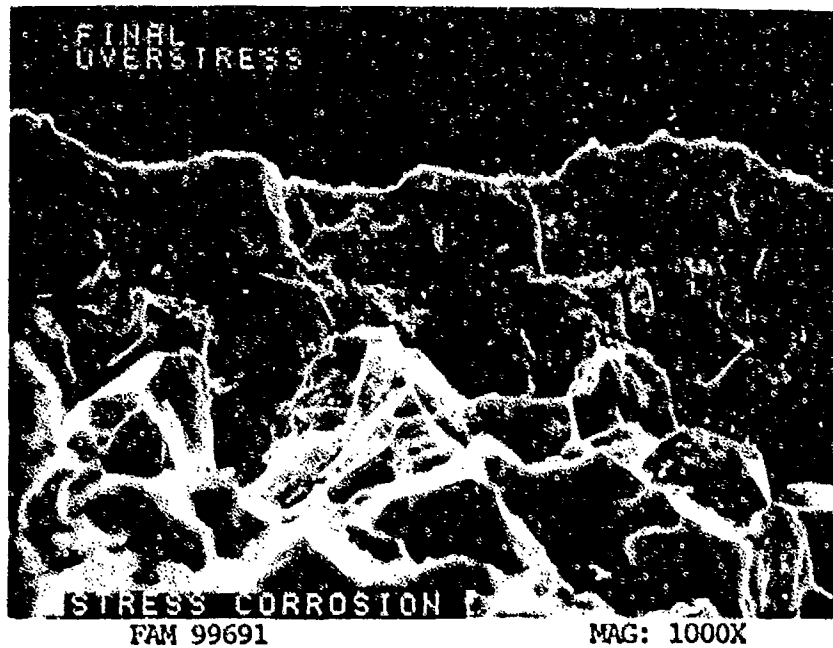


FIGURE 2-6: Final overstress area. The features have been smeared but remnant dimples appear to be present.

MATERIAL

15-5 PH
AMS 5659 Bar

TEST DATA

TEST TYPE

Hydrogen Embrittlement

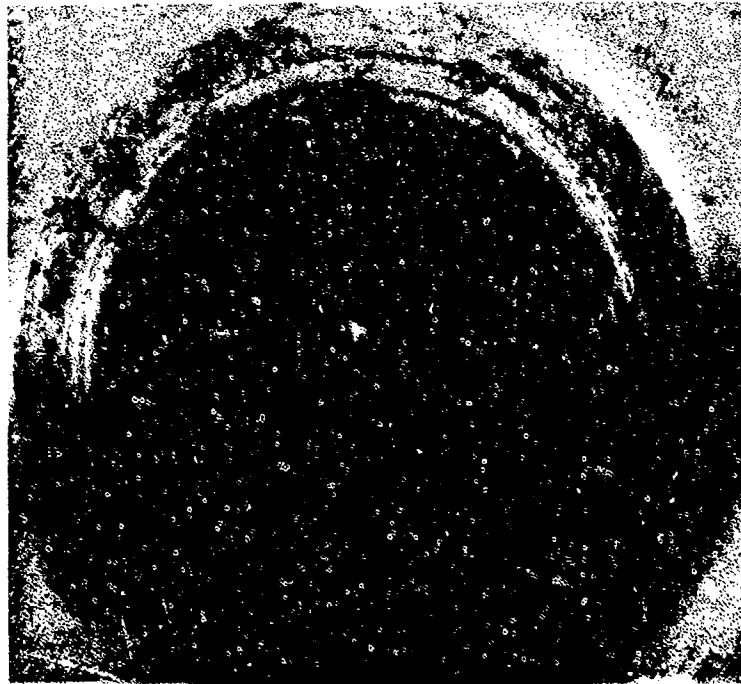
TEST CONDITIONS

Stress: 1687.3 MPa (244 ksi) DNF*
1882.3 MPa (273.0 ksi)
Atmosphere: Tested in air
Temperature: Room Temperature
Test Direction: Longitudinal
Charged for 12 hours in gaseous H₂ at 5000 psi

TEST RESULTS

Time to Fracture: 99.3 hours (DNF), 0.7 hours

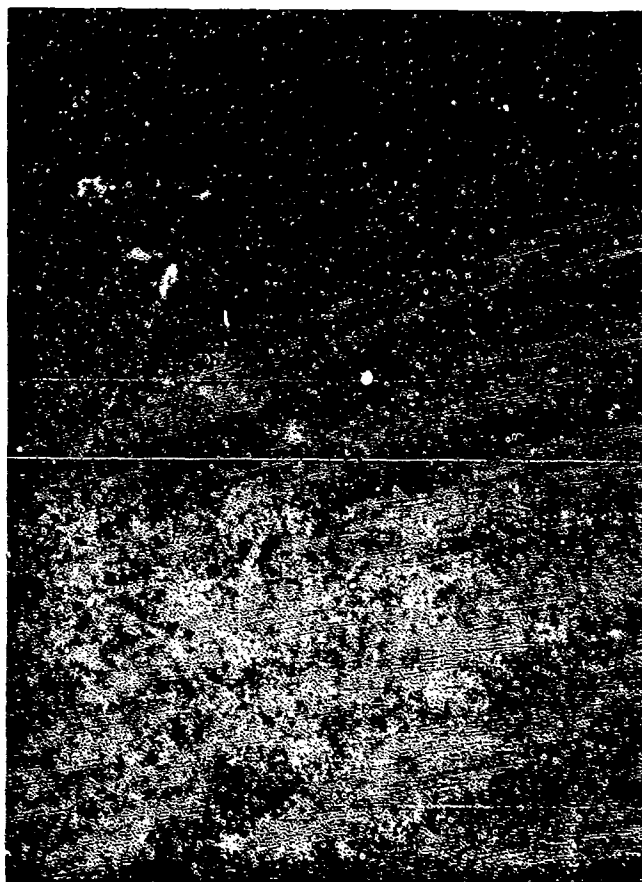
* Did Not Fracture



FAL 94527

MAG: 12X

FIGURE 2-7: Test results and fractography of 15-5 PH hydrogen embrittlement test.



FAM 100224

MAG: 200X

FIGURE 2-8: Optical photomicrograph showing a mixture of transgranular and intergranular fracture paths. Some secondary grain boundary separation is visible (arrows).

Etchant: Vilella's Reagent

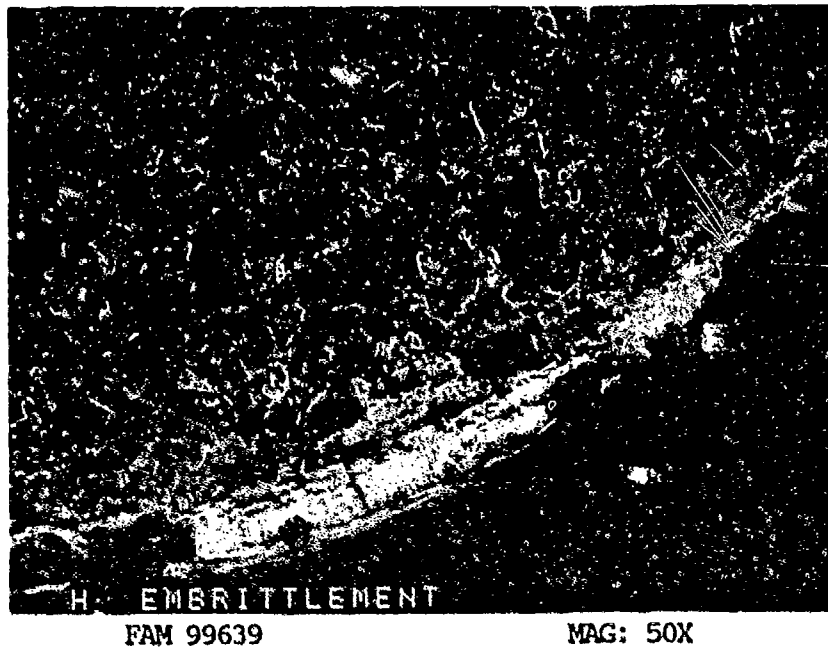


FIGURE 2-9: Low magnification photograph of the fracture surface exhibiting dimpled overstress with an intermittent shear lip (bracket) along the specimen surface. No clear evidence of embrittlement was observed.

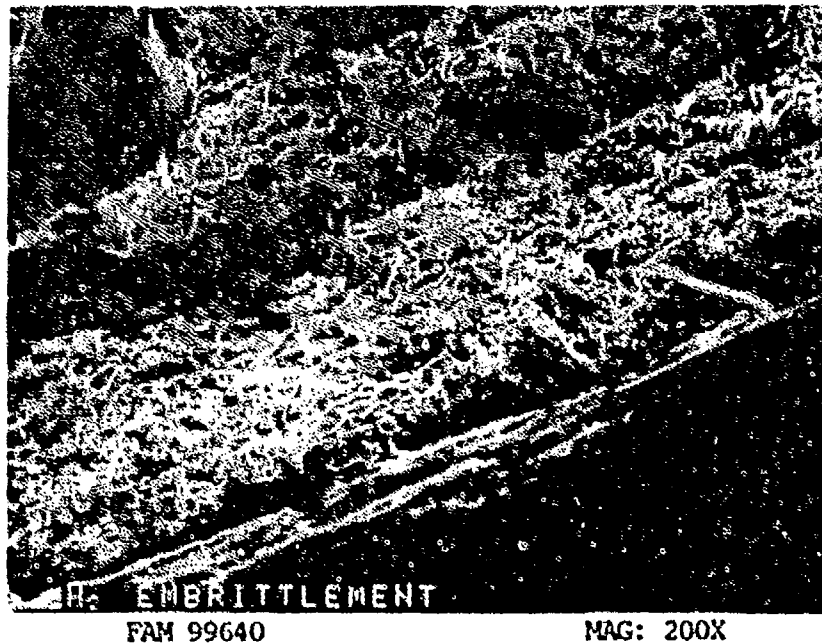


FIGURE 2-10: Higher magnification photograph of the edge of the specimen.



FAM 99641

MAG: 1000X

FIGURE 2-11: Possible remnant cleavage features at the edge of the specimen (arrows).

SERVICE FAILURE

FRACTURE MODE Overstress

PART NAME Augmentor Nozzle Control Flex Shaft

OPERATION DATA Flex shaft operates in a non-uniform low cycle stress environment.

PART TIME 488.6 hours (2235.75 operational cycles)

	<u>REQUIRED</u>	<u>ACTUAL</u>
MAT'L		
BASE	<u>17-7 PH (stainless steel)</u>	<u>confirmed</u>
OTHER	<u>-</u>	<u>-</u>
HARDNESS	<u>No Requirement</u>	<u>HRC 45-59 *</u>
GRAIN SIZE	<u>No Requirement</u>	<u>-</u>
DIMENSIONAL	<u>Required strand thickness not available.</u>	<u>O.D. strand thickness 0.030-0.031 inch</u>

* Diamond pyramid hardness (DPH) conversion.

SUMMARY: After fracture of the O.D. strands, the flex shaft drive continued to operate causing the fractured strands to rub together, smearing the fracture features. Only overstress features were found on the other strands. No material or microstructural anomalies were found.



FAL 91369

MAG: 2X

FIGURE 2-12: Overall photograph of the fractured flex shaft end. The strands are twisted and rubbed.



FAL 31370

MAG: 3X

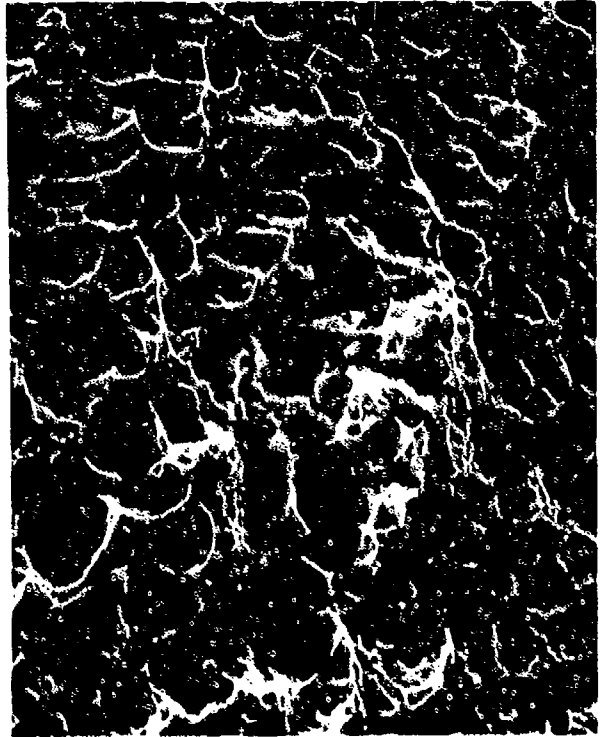
FIGURE 2-13: End view of the fractured flex shaft.



FAL 93428

MAG: 100X

FIGURE 2-14: SEM photograph of a fractured strand. The fracture appears to be the result of torsional overstress.



FAL 93425

MAG: 1000X

FIGURE 2-15: Higher magnification photograph showing a mixture of tensile and shear dimples near the center of the strand.

SERVICE FAILURE

FRACTURE MODE Fatigue (probable LCF)

PART NAME Augmentor Nozzle Control Primary Flex Shaft

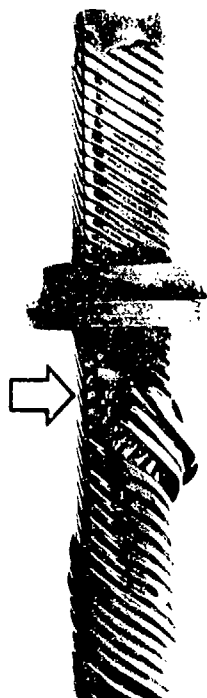
OPERATION DATA Strands were found fractured during tear-down
inspection. The shaft operated in a non-uniform low
cycle stress environment.

PART TIME 146 hours (707 operational cycles)

	<u>REQUIRED</u>	<u>ACTUAL</u>
MAT'L		
BASE	<u>17-7 PH (stainless steel)</u>	<u>confirmed</u>
OTHER	<u>-</u>	<u>-</u>
HARDNESS	<u>No Requirement</u>	<u>HRC 59-60 *</u>
GRAIN SIZE	<u>-</u>	<u>-</u>
DIMENSIONAL	<u>O.D. strand thickness not</u> <u>available.</u>	<u>0.030-0.032 inch</u>

* Diamond pyramid hardness (DPH) conversion.

SUMMARY: Five O.D. strands fractured by fatigue (probable LCF) with origins on their inside surfaces. The fatigue progressed 20-50% of the way through the strands. No material or microstructural anomalies were found.



FAL 92140

MAG: 2X

FIGURE 2-16: Overall photograph of the end of the shaft showing five fractured strands (arrow).



FAL 92141

MAG: 20X

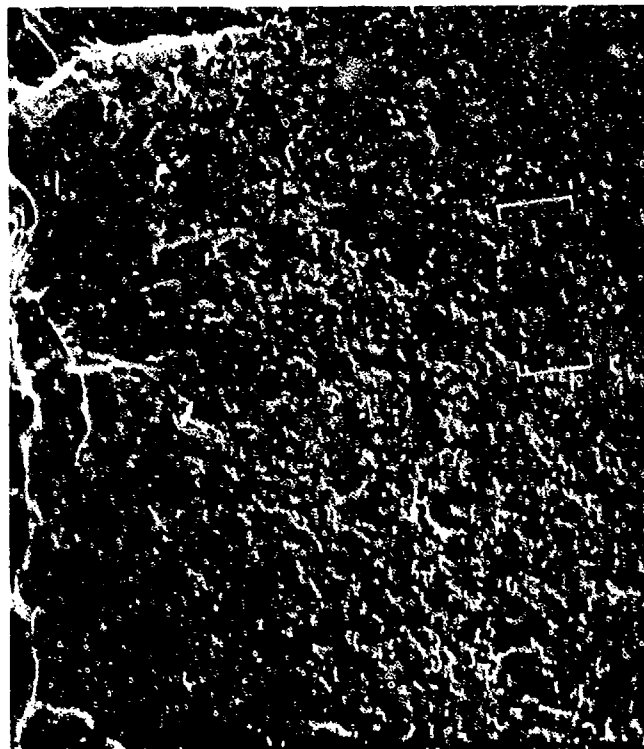
FIGURE 2-17: Close-up photograph of the five fractured strands. The smooth appearance on the I.D. side of the strands indicates fatigue.



FAL 93429

MAG: 100X

FIGURE 2-18: SEM photograph of a fractured strand. The fatigue origin area is visible at the right (arrow).



FAL 93431

MAG: 1000X

FIGURE 2-19: Fatigue progression near the origin area. Remnant striations are shown by brackets.

Custom 455 (Stainless Steel)

Material Description

Custom 455 is a low carbon Ni-Cr stainless steel with good corrosion resistance. Solution heat treating at 1500 F-1550 F followed by a water quench produces a martensitic structure that is subsequently aged for 4 hours at 900 F-1000 F followed by air cooling. Optimum mechanical properties are obtained by aging at 950 F. Custom 455 is easily fabricated and is available as billets, bars, shapes, wire, forgings, sheet, strip, plate and tubing.

The material used in this study was AMS 5617 heat treated to AMS 2759/3 (H950) with a required hardness of HRC 41.5-44.5 after precipitation treatment at 950 F for 4 hours.

	<u>H950</u>	<u>H1000</u>
Ultimate Tensile Strength:	225 ksi	200 ksi
0.2% Yield Strength:	210 ksi	185 ksi
Percent Elongation:	10% min.	10% min.
Percent Reduction in Area:	40% min.	40% min.
Measured Hardness:	HRC 47-48 (DPH Conversions)	

Fractography Overview

Smooth and notched tensile tests were conducted at room temperature and 800 F. The smooth room temperature specimen had its primary fracture originating at the center of the specimen with features radiating towards the specimen surface. The entire outside surface had a well developed 0.015 inch shear lip containing very fine shear dimpled overstress. The primary fracture exhibited a mixture of dimpled overstress and quasi-cleavage features with secondary cracking and cracked carbides. The 800 F smooth tensile specimen fracture surface was dominated by a large shear lip (0.040 inch). The primary overstress area in the center of the specimen did not show the directionality that the room temperature specimen did. This area exhibited ductile dimpled overstress with void coalescence. All of these features indicated a significant increase in ductility for the 800 F specimen. Both notched tensile specimens exhibited a narrow, poorly defined shear lip at the base of the notch (0.005 inch, RT; 0.010 inch, 800 F). The primary fracture of the room temperature specimen consisted of dimpled overstress mixed with areas of quasi-cleavage. This mixture of ductile and brittle features is called mixed mode overstress. The 800 F specimen showed only ductile dimpled overstress in the primary fracture area. Some of the larger dimples had small dimples within them. The presence of the stress concentration associated with the notch appears to have its primary affect on the features in the final overstress area. In both the smooth and notched specimens, increasing the temperature results in a more ductile appearance.

Smooth HCF specimens were tested at three temperatures: room temperature, 400 F and 800 F. Macroscopically, all three specimens had a

similar appearance. In each case fatigue initiation and propagation occurred on a plane roughly perpendicular to the stress axis. Final overstress occurred on several planes that formed an angle of approximately 45° to the stress axis. The fatigue on each of the three specimens propagated from one local origin. The room temperature and 400 F specimens had local origins at slightly subsurface defects, possibly voids. The fatigue initiation, Stage I, of all three specimens exhibited feathery cleavage features. The fatigue striation appearance changed with increasing temperature. The room temperature specimen exhibited no clearly defined striations. Possible smooth remnant striations were visible in the Stage II propagation zone. These could also be the result of smear. The 400 F specimen exhibited striations and crack-like striations (secondary cracks). The 800 F specimen had smoother, flatter striations than the 400 F specimen and a much higher percentage of large crack-like striations. The final overstress areas on all three specimens exhibited fine dimpled overstress. The dimple size appears to increase with increasing temperature. Both equiaxed and shear dimples were present.

The stress corrosion cracking U-bend specimen was exposed to 3.5% NaCl vapor at 95 C (203 F). The fracture exhibited feathery cleavage in the area that was stress corroded. The final overstress area exhibited fine dimpled overstress. The tension side of the U-bend specimen had significant attack and deposits of corrosion products. The compression side had no deposits or attack.

The hydrogen embrittlement specimen exhibited almost identical features to the room temperature notched tensile test with the exception of small patches of feathery cleavage at the specimen surface in the base of the notch.

MATERIAL

Custom 455
AMS 5617 Bar

TEST DATA

TEST TYPE

Smooth Tensile

TEST CONDITIONS

Strain Rate: 0.005 mm/mm/min (0.005 in/in/min)

Atmosphere: Air

Temperature: Room Temperature

Test Direction: Longitudinal

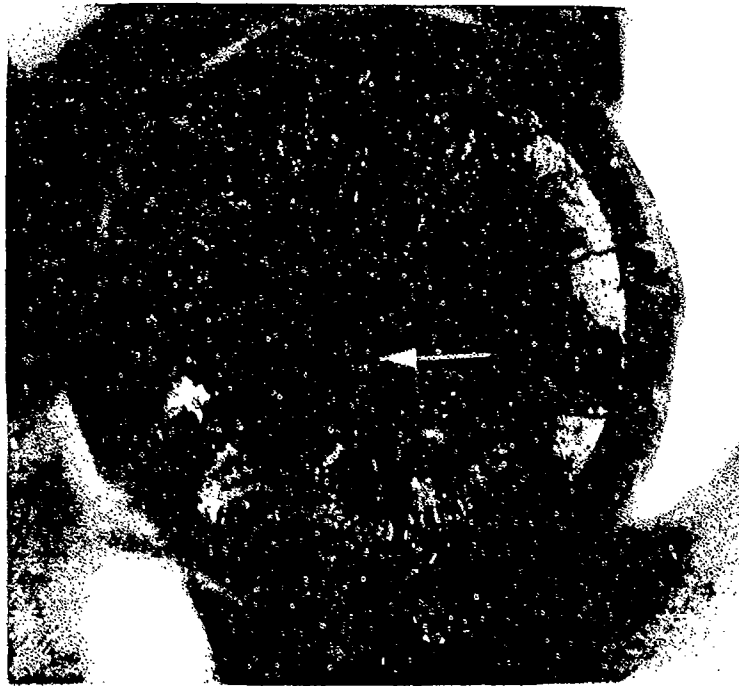
TEST RESULTS

0.2% Yield Strength: 1594.8 MPa (231.3 ksi)

Ultimate Strength: 1644.4 MPa (238.5 ksi)

Percent Elongation: 11.5

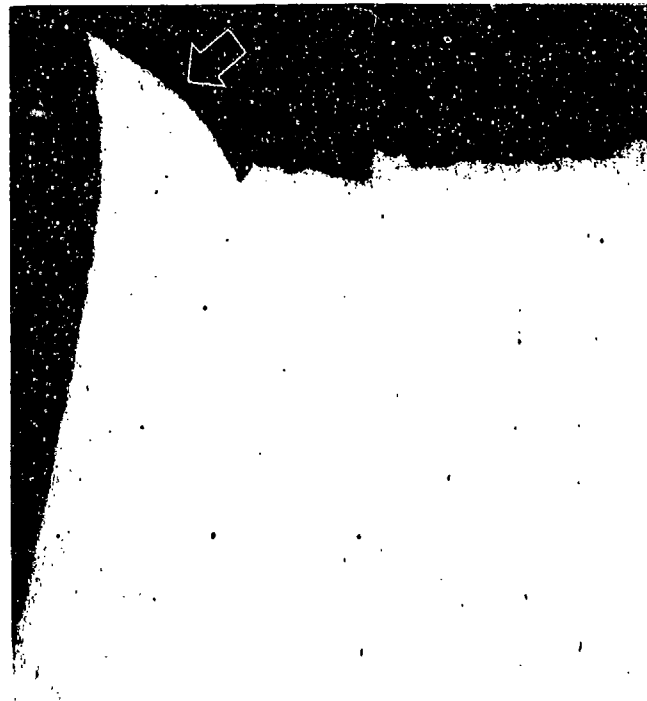
Percent Reduction of Area: 53.5



FAL 92556

MAG: 15X

Figure 3-1: Test results and fractography of Custom 455 room temperature smooth tensile test. The primary fracture area is in the center of the specimen (arrow) with features radiating outward. A well defined final fracture (shear lip) is visible along the outside surface of the specimen (bracket).



FAM 100296

MAG: 50X



FAM 100297

MAG: 100X

FIGURE 3-2: Optical photomicrographs showing the shear lip and deformation at the edge of the specimen (top). The shear lip is shown by an arrow. The center of the specimen exhibits transgranular overstress (bottom).

Etchant: Vilella's Reagent

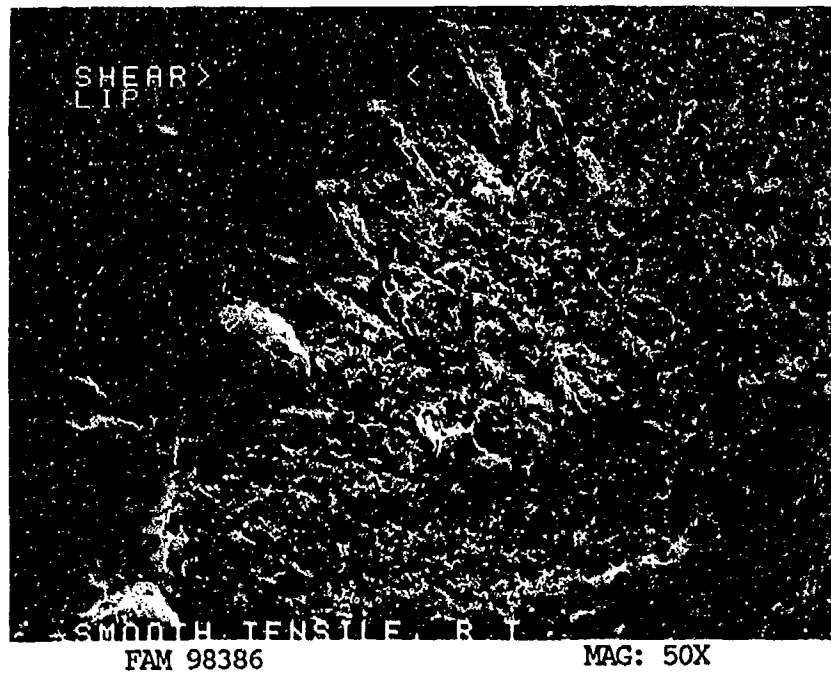


FIGURE 3-3: Low magnification view showing primary fracture area exhibiting secondary cracking and clearly defined final overstress area (shear lip).

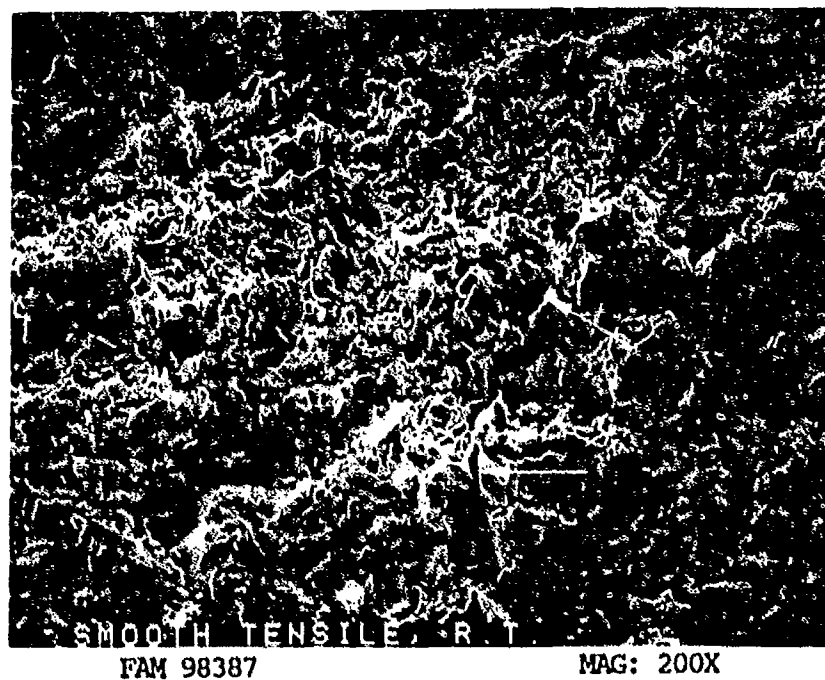


FIGURE 3-4: Dimpled overstress and secondary cracking (arrow) in the primary fracture area.

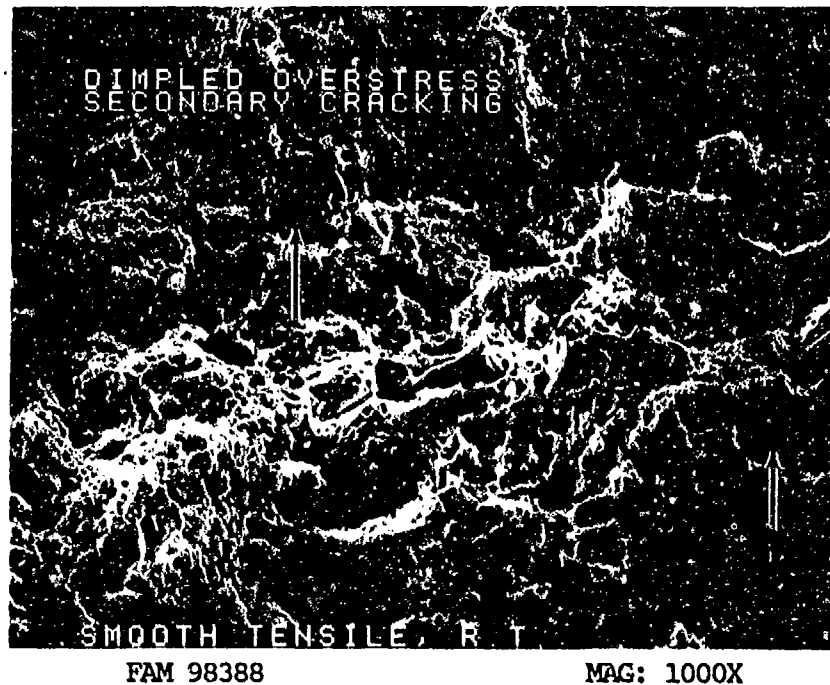


FIGURE 3-5: Dimpled overstress, secondary cracking (arrows A) and fractured carbides (arrows B) in the primary fracture area.

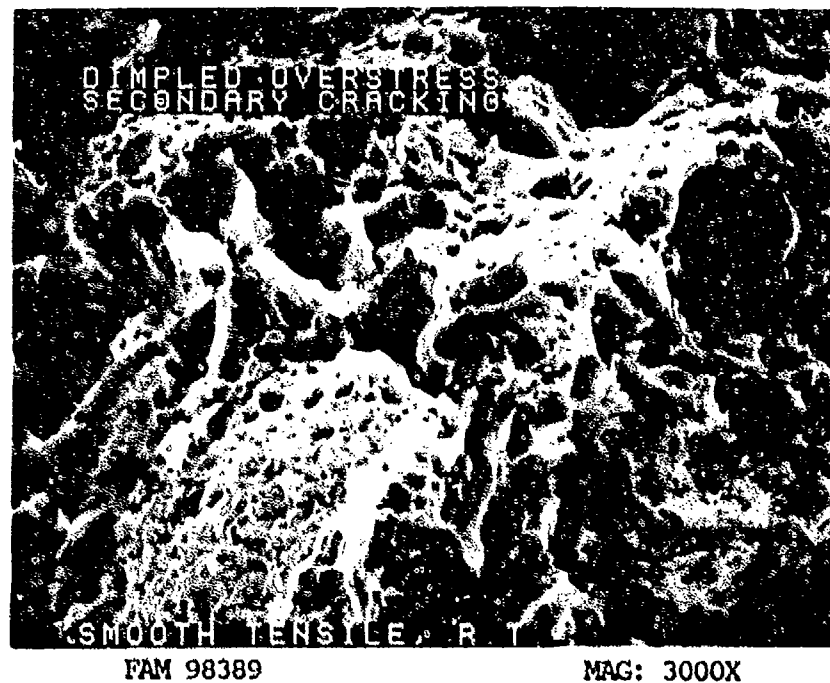


FIGURE 3-6: High magnification photograph showing fine dimpled overstress and fractured carbides in the primary overstress area.

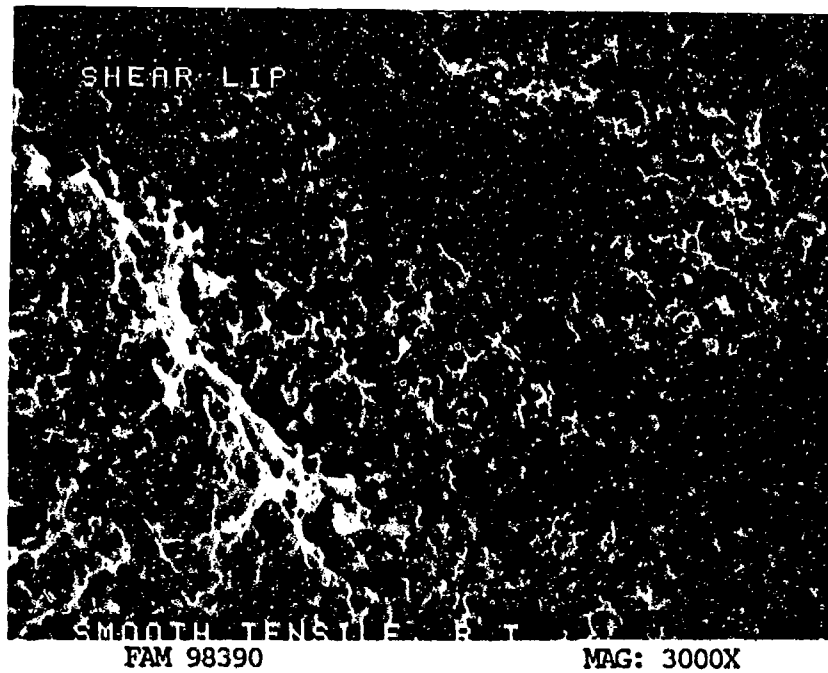


FIGURE 3-7: Fine shear dimples in the final overstress area. The directions of relative movement is shown by arrows.

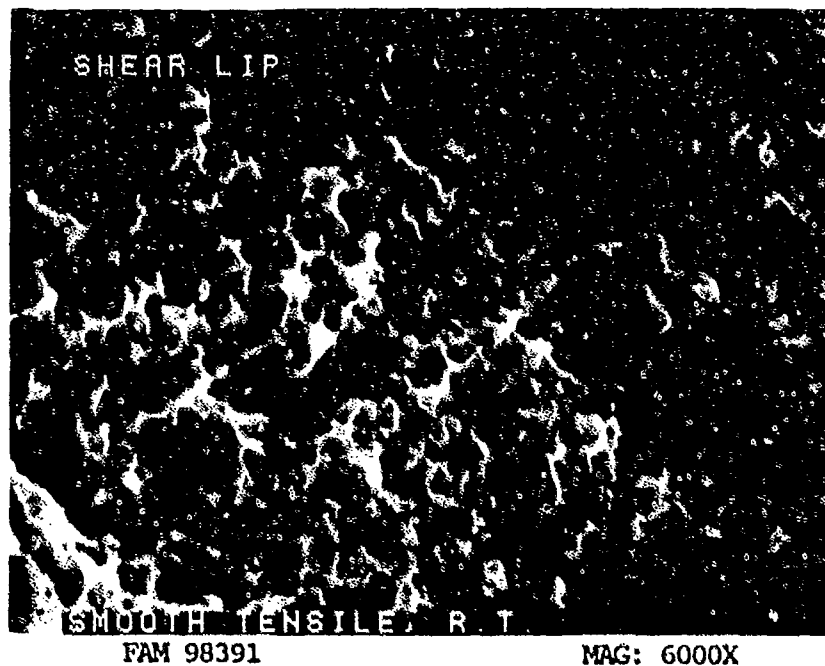


FIGURE 3-8: Fine shear dimples in the final overstress area.

MATERIAL

Custom 455
AMS 5617 Bar

TEST DATA

TEST TYPE

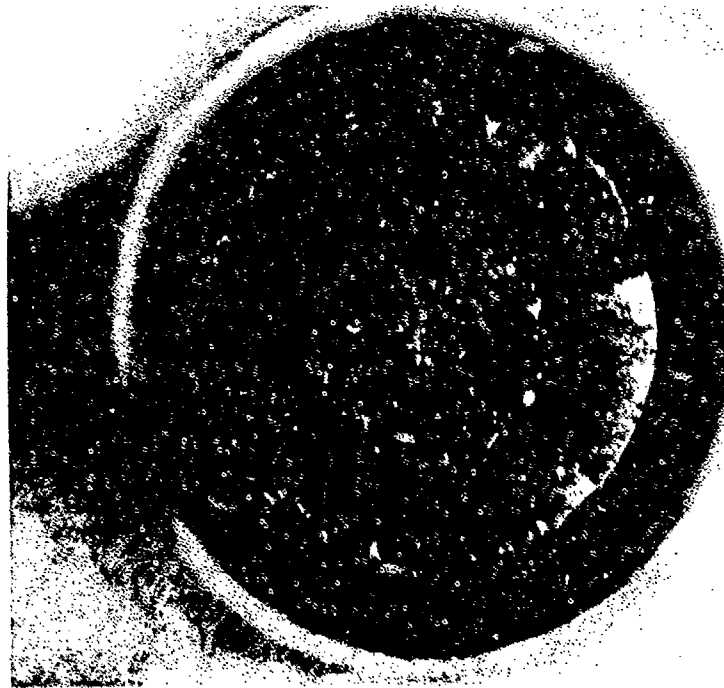
Smooth Tensile

TEST CONDITIONS

Strain Rate: 0.005 mm/mm/min (0.005 in/in/min)
Atmosphere: Air
Temperature: 427°C (800°F)
Test Direction: Longitudinal

TEST RESULTS

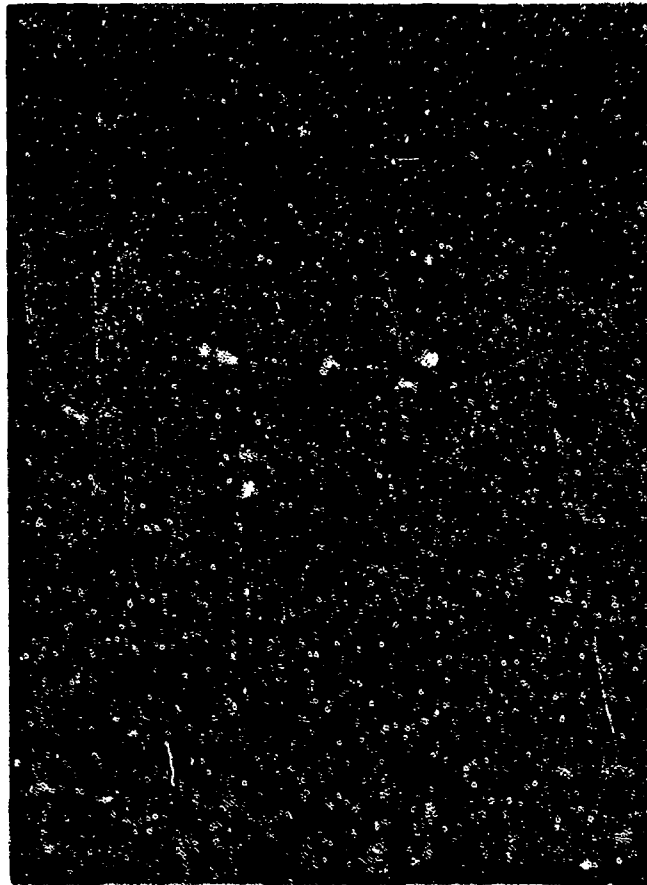
0.2% Yield Strength:	1101.1 MPa (159.7 ksi)
Ultimate Strength:	1192.1 MPa (172.9 ksi)
Percent Elongation:	15.0
Percent Reduction of Area:	66.9



FAL 92555

MAG: 15X

Figure 3-9: Test results and fractography of Custom 455 427°C (800°F) smooth tensile test. The fracture is dominated by a large final overstress area (shear lip) around the specimen. The size of the shear lip is larger than for the room temperature specimen due to increased ductility at elevated temperature.



FAM 100228

MAG: 200X

FIGURE 3-10: Optical photomicrograph showing the transgranular appearance of the entire fracture path.

Etchant: Vilella's Reagent

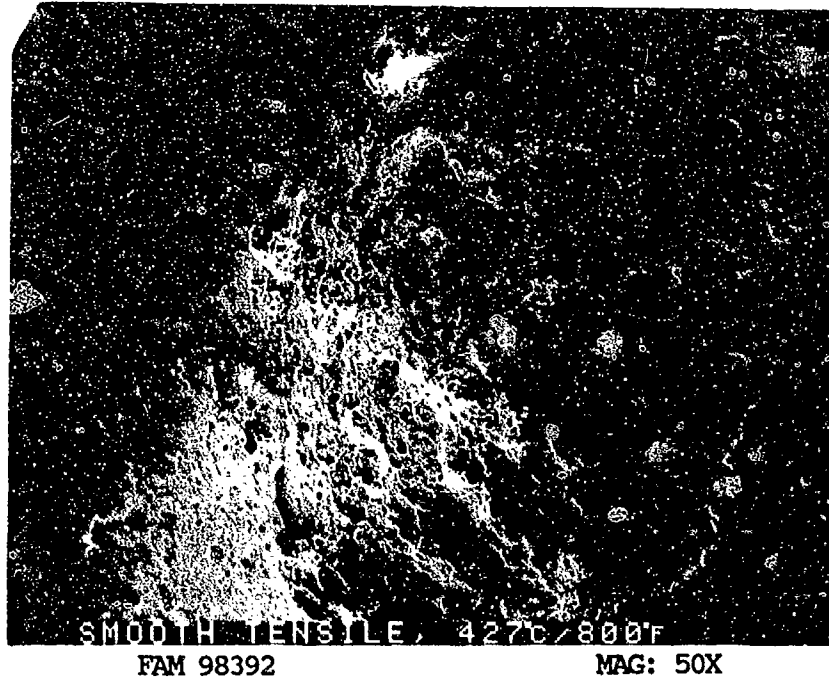


FIGURE 3-11: Low magnification view showing relatively small primary fracture area at the center of the fracture surface, with large area of final overstress (shear lip). The extent of the shear lip is shown by a bracket.

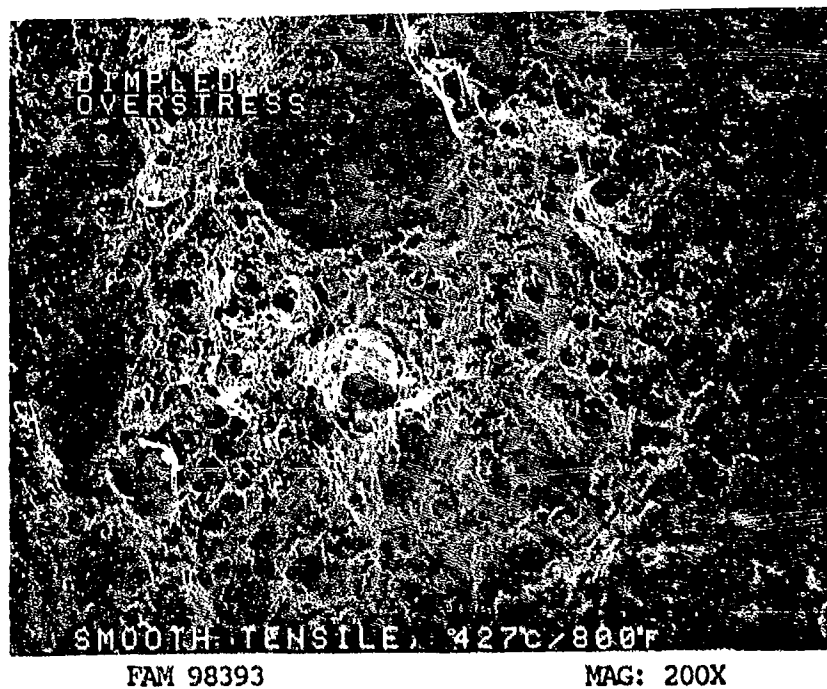


FIGURE 3-12: Dimpled overstress and void coalescence in the primary fracture area.

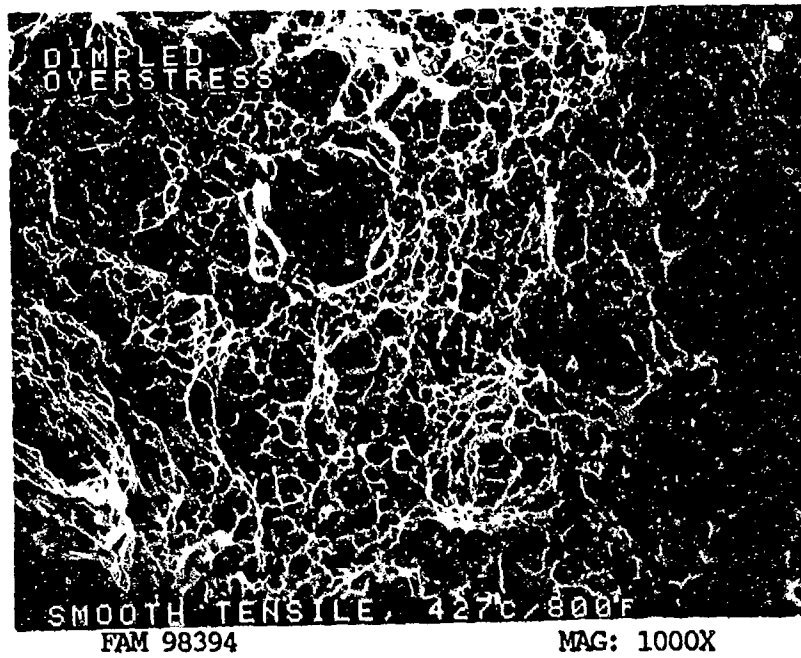


FIGURE 3-13: Fine equiaxed dimples and void coalescence (arrows) in the primary fracture area.

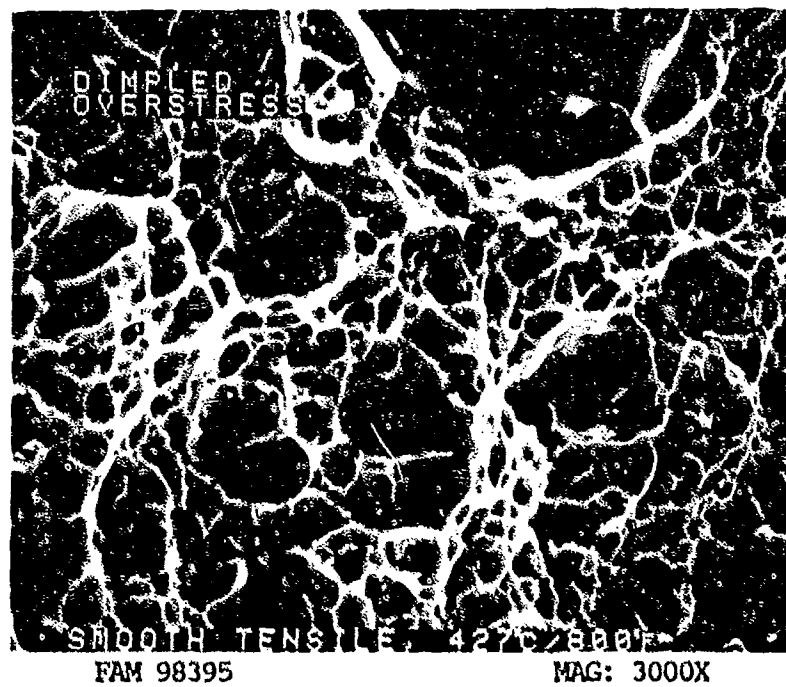


FIGURE 3-14: Fine equiaxed dimples in the primary overstress area.

MATERIAL

Custom 455
AMS 5617 Bar

TEST DATA

TEST TYPE

Notched Tensile

TEST CONDITIONS

Crosshead Speed: 1.27 mm/min (0.05 in/min)

Atmosphere: Air

Temperature: Room Temperature

Test Direction: Longitudinal

TEST RESULTS

Ultimate Strength: 2416.0 MPa (350.4 ksi)



FAL 92559

MAG: 12X

FIGURE 3-15: Test results and fractography of Custom 455 room temperature notched tensile test. The center of the specimen exhibits an uneven appearance. A narrow shear lip is visible along the outside of the specimen (arrow).



FAM 100234

MAG: 200X

FIGURE 3-16: Optical photomicrograph showing the transgranular appearance of the fracture surface path near the center of the specimen.

Etchant: Vilella's Reagent

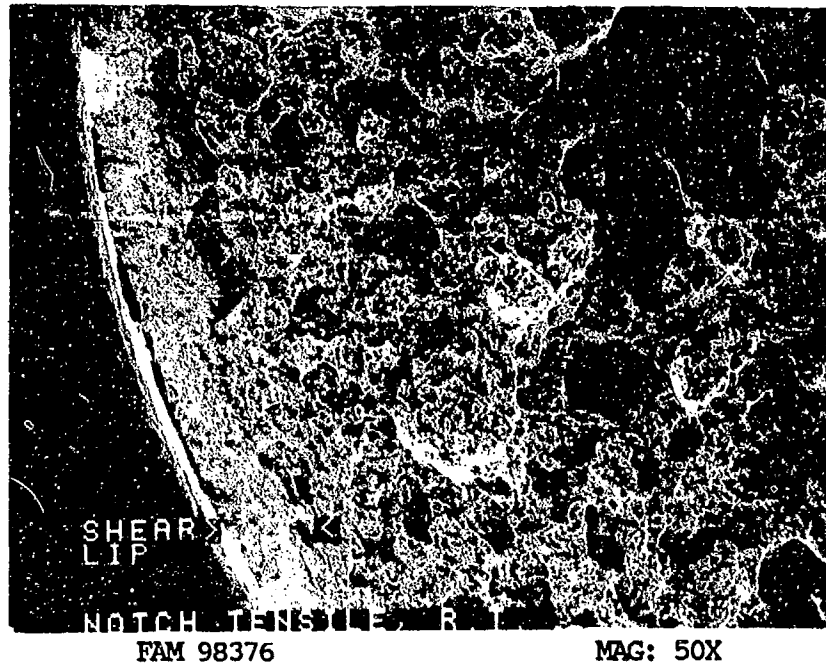


FIGURE 3-17: Low magnification photograph showing deep features in the primary overstress area and a small final overstress area (shear lip).

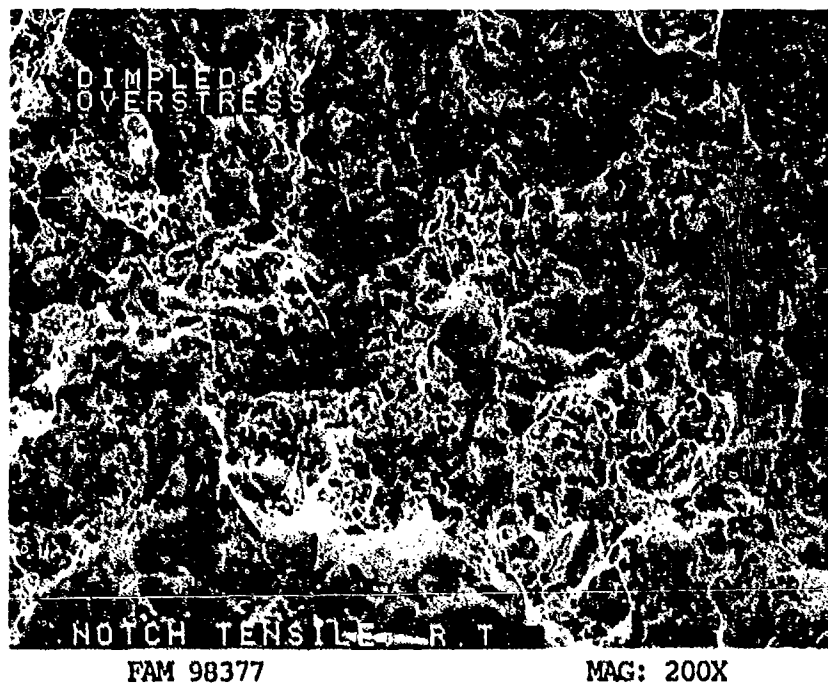


FIGURE 3-18: Shallow dimples and deep features in the primary overstress area.

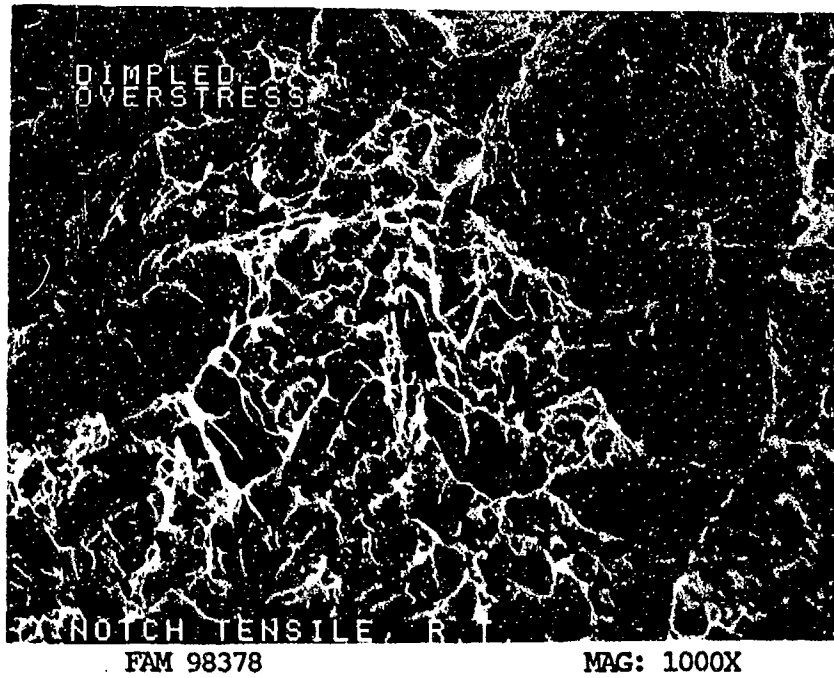


FIGURE 3-19: Very fine shallow dimples between areas of fine cleavage.

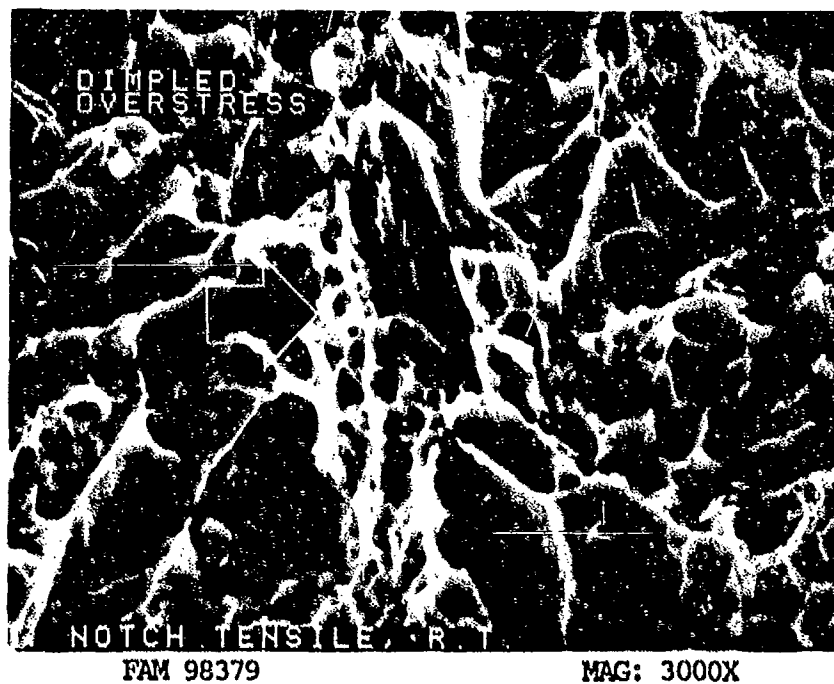


FIGURE 3-20: Fine dimples (arrow) between areas of fine cleavage (mixed mode overstress).

MATERIAL

Custom 455
AMS 5617 Bar

TEST DATA

TEST TYPE

Notched Tensile

TEST CONDITIONS

Crosshead Speed: 1.27 mm/min (0.05 in/min)

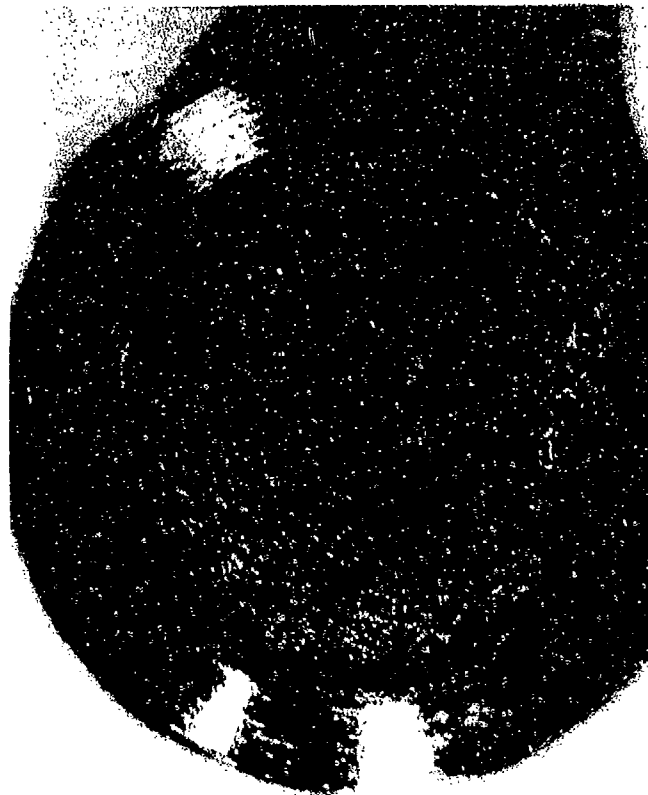
Atmosphere: Air

Temperature: 427°C (800°F)

Test Direction: Longitudinal

TEST RESULTS

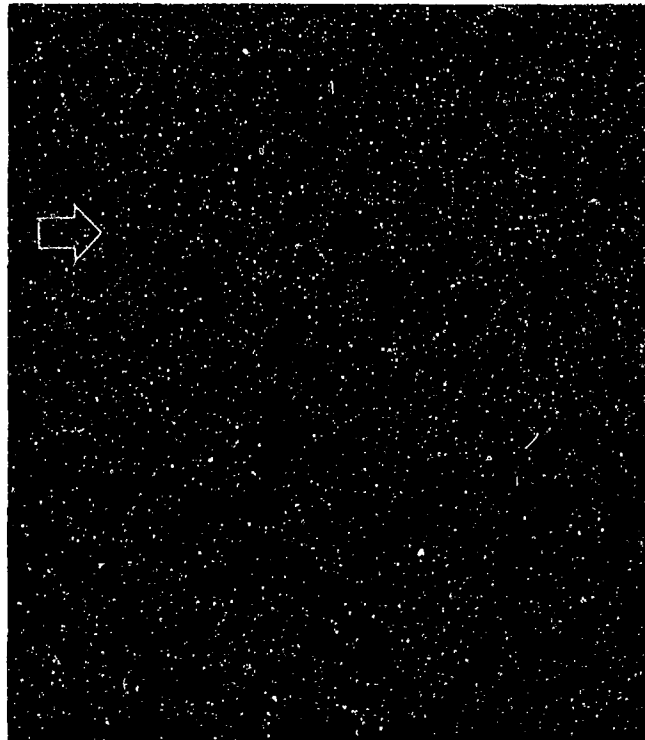
Ultimate Strength: 1777.5 MPa (257.8 ksi)



FAL 92558

MAG: 10X

FIGURE 3-21: Test results and fractography of Custom 455 427°C (800°F) notched tensile test. The primary overstress area near the center of the specimen is smoother than the room temperature specimen. The final overstress area (shear lip) is larger than that on the room temperature specimen (Figure 3-15).



FAM 100227

MAG: 100X



FAM 100233

MAG: 200X

FIGURE 3-22: Optical photomicrographs showing plastically deformed grains in the base of the notch (arrow, top). The center of the specimen exhibits a predominantly transgranular fracture path (bottom).

Etchant: Vilella's Reagent

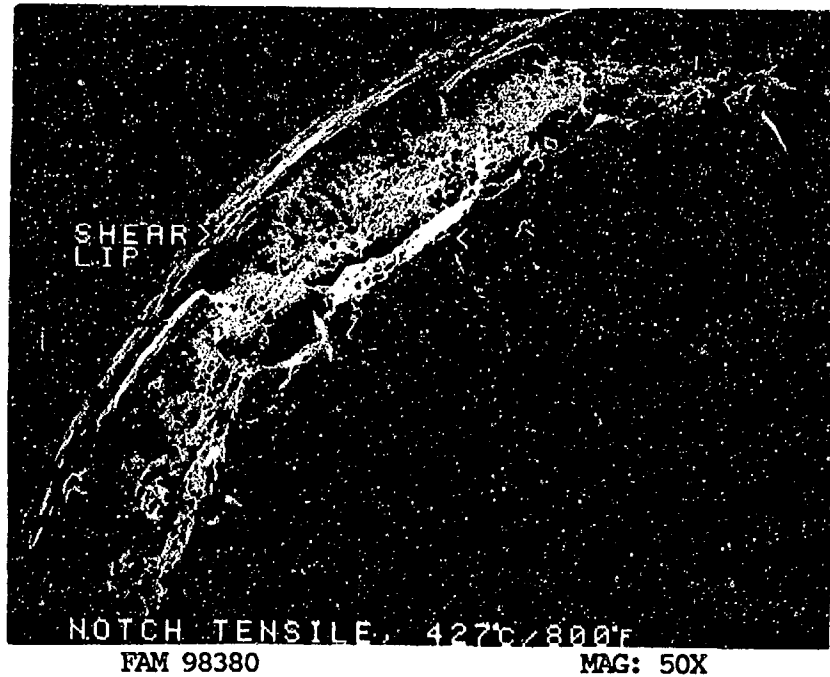


FIGURE 3-23: Low magnification view showing the primary fracture area and a clearly defined narrow final overstress area (shear lip).

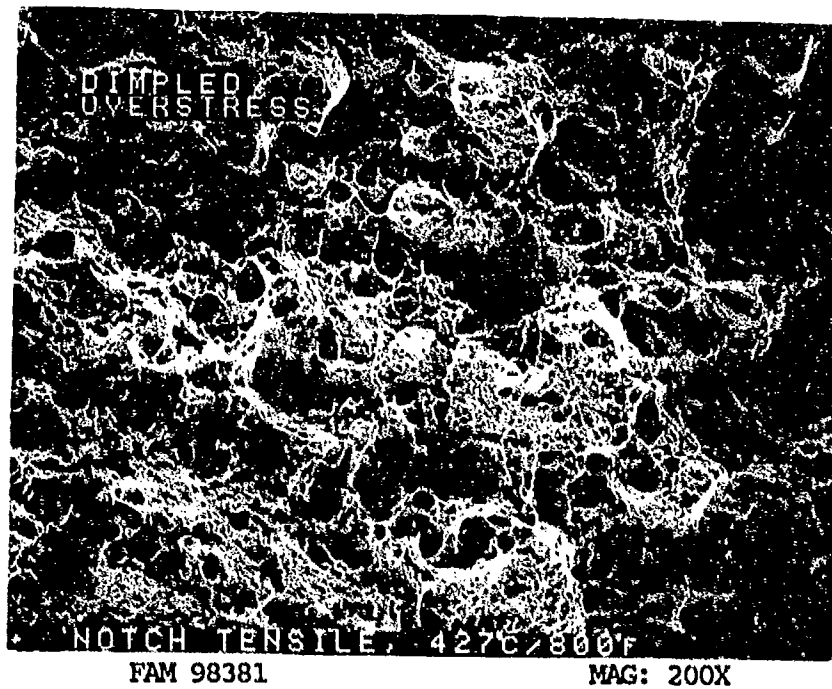


FIGURE 3-24: Primary fracture area exhibits both coarse and very fine dimples.

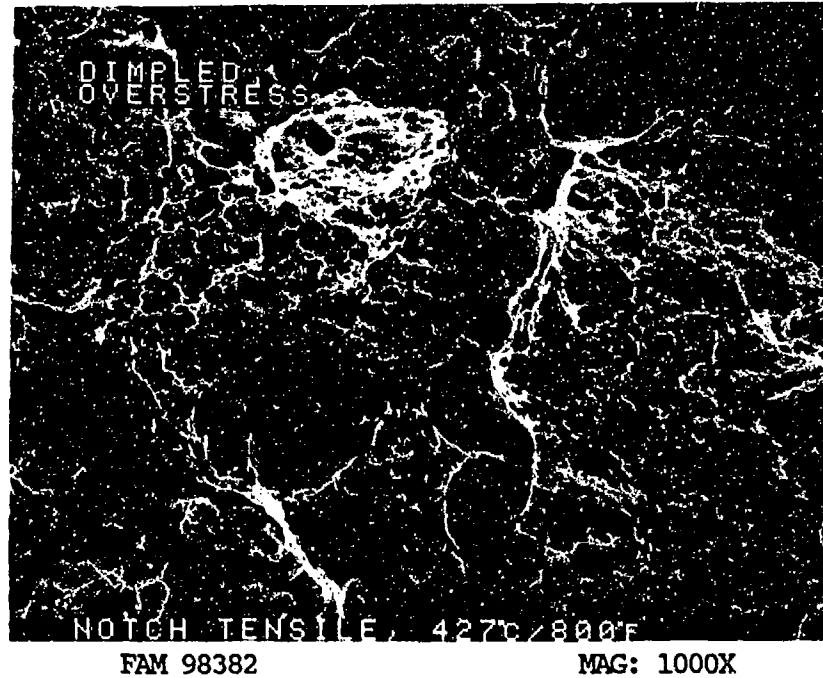


FIGURE 3-25: Mixture of coarse and very fine equiaxed dimples.

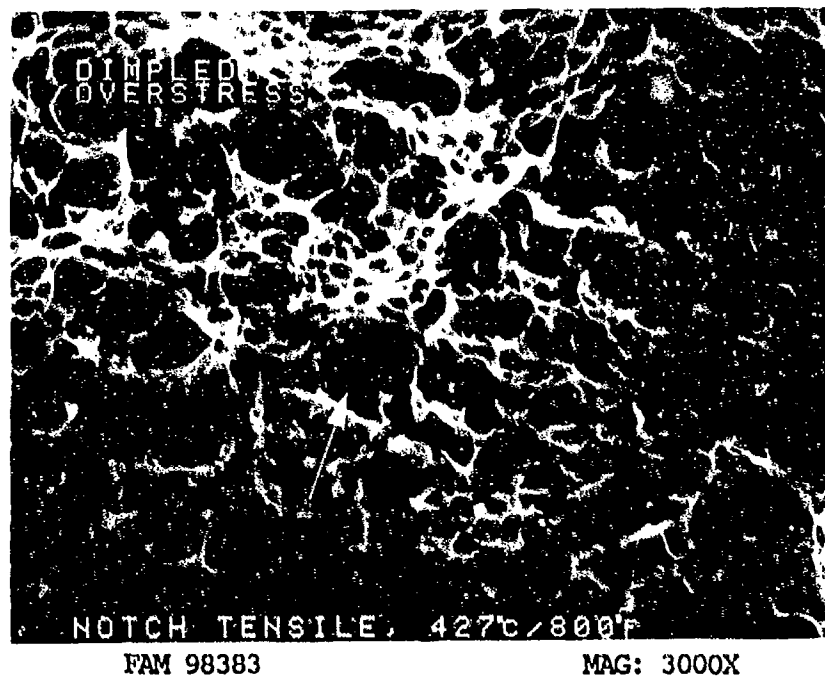


FIGURE 3-26: Higher magnification photograph of the area shown in Figure 3-25, exhibiting coarse dimples with fine dimples within them (arrow).

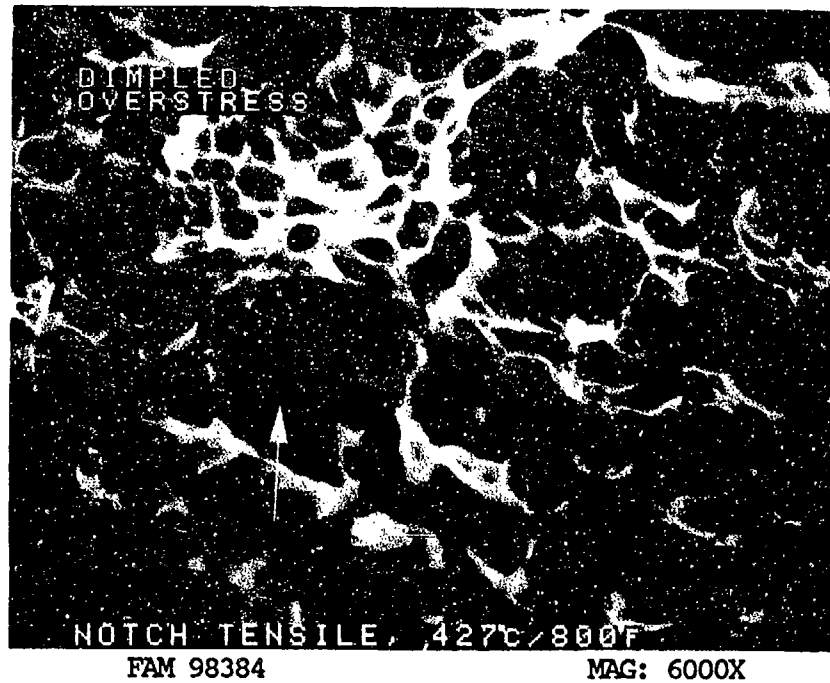


FIGURE 3-27: Very fine equiaxed dimples within coarser dimples (arrow). The surface is relatively free of oxide.

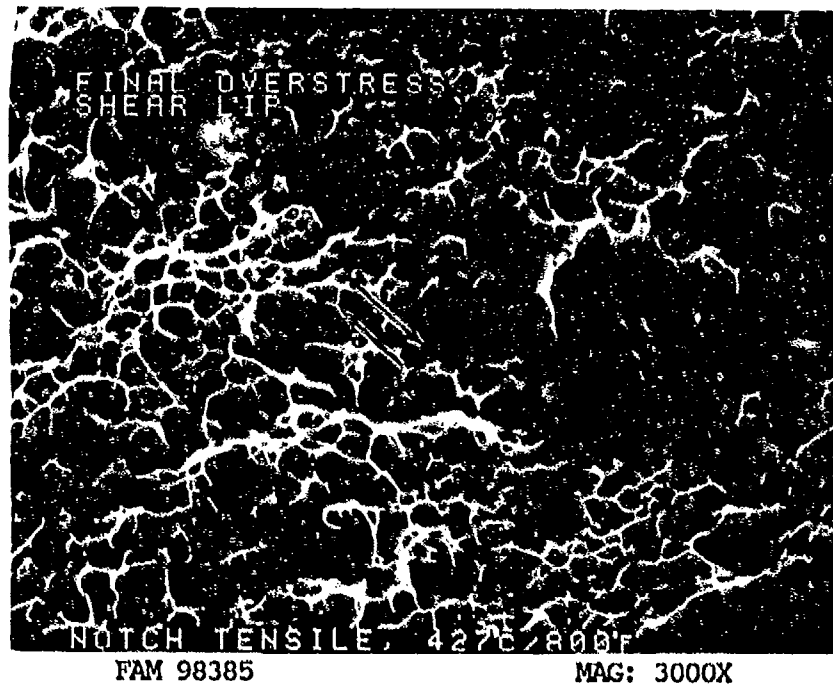


FIGURE 3-28: Mixture of fine shear dimples and equiaxed dimples in the final overstress area (shear lip). Arrows indicate the directions of relative motion.

MATERIAL

Custom 455
AMS 5617 Bar

TEST DATA

TEST TYPE
Smooth HCF

TEST CONDITIONS

Stress: 827.4 MPa (120.0 ksi)/-827.4 MPa (-120.0 ksi) DNF*
896.3 MPa (130.0 ksi)/-896.3 MPa (-130.0 ksi) DNF
965.3 MPa (140.0 ksi)/965.3 MPa (-140.0 ksi)
Stress Ratio: -1
Frequency: 1800 cpm
Atmosphere: Air
Temperature: Room Temperature
Test Direction: Longitudinal

TEST RESULTS

Cycles to Fracture: 2.97×10^5 (DNF), 2.0×10^5 (DNF), 3.06×10^4

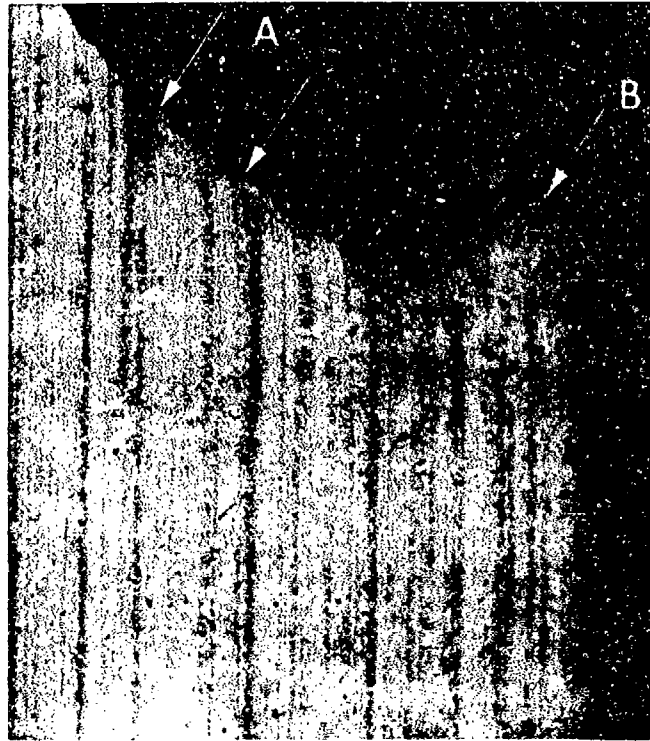
* Did Not Fracture



FAL 93828

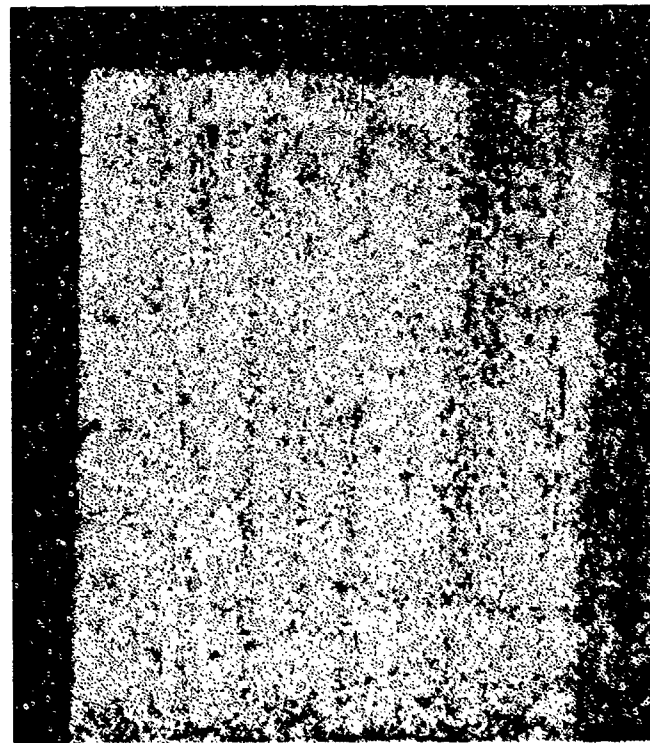
MAG: 15X

FIGURE 3-29: Test results and fractography of Custom 455 room temperature smooth HCF test. The fatigue progression zone is approximately perpendicular to the stress axis. An arrow indicates the origin area.



FAM 100263

MAG: 50X



FAM 100262

MAG: 200X

FIGURE 3-30: Optical photomicrographs showing the final overstress area (top). Grain deformation (arrows A) and a shear lip (arrow B) are visible. The fatigue progression exhibits flat transgranular fracture path perpendicular to the stress axis (bottom).

Etchant: Vilella's Reagent



FIGURE 3-31: Overall photograph of the origin area and fatigue progression area. Fatigue features can be seen radiating from the origin.

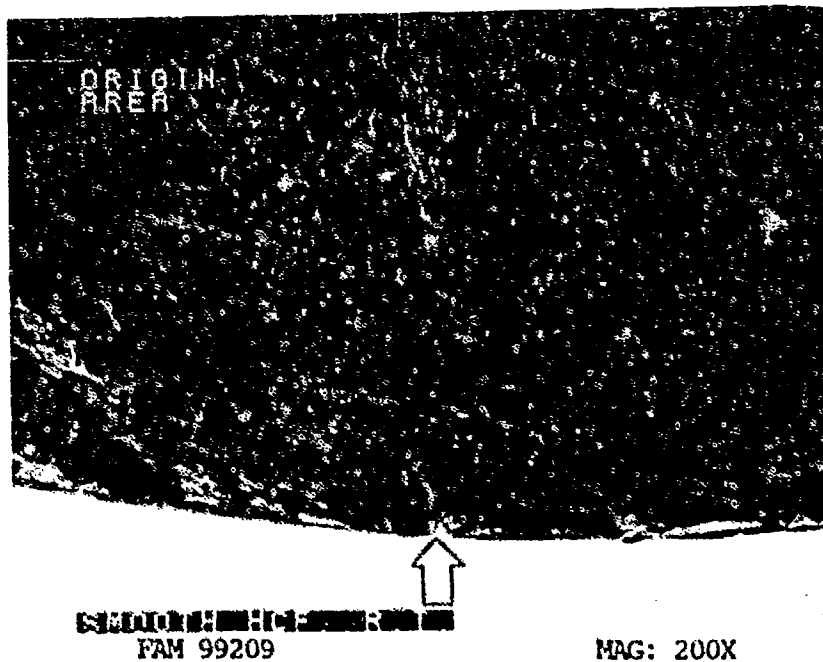


FIGURE 3-32: Higher magnification view of the origin area. The features appear to be smeared. The localized origin is shown by an arrow.

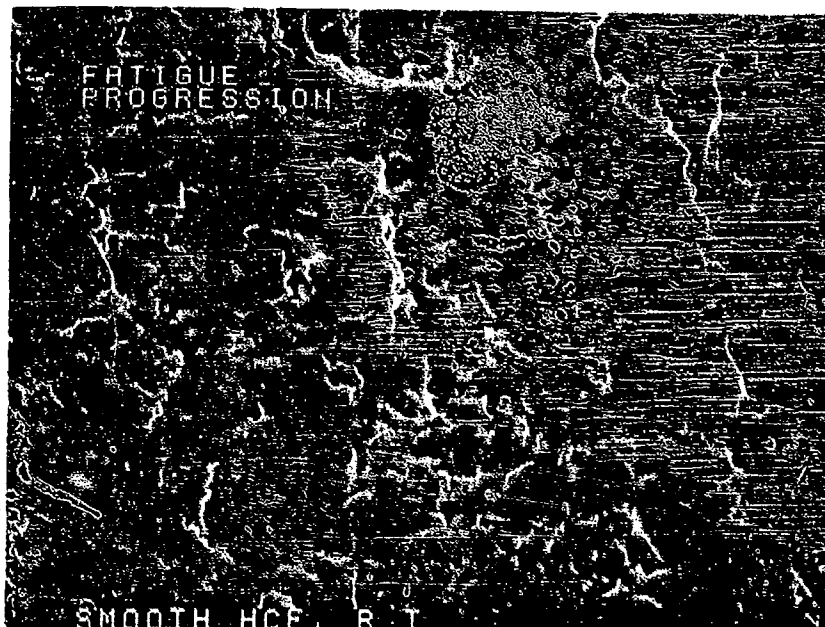


SMOOTH HOPE R. I.

FAM 99210

MAG: 1000X

FIGURE 3-33: High magnification photograph of the origin area. The localized origin is smeared, but may be at a subsurface defect (arrow).



FAM 99212

MAG: 1000X

FIGURE 3-34: Fatigue progression area showing possible remnant fatigue striations. These also could be the result of smear.

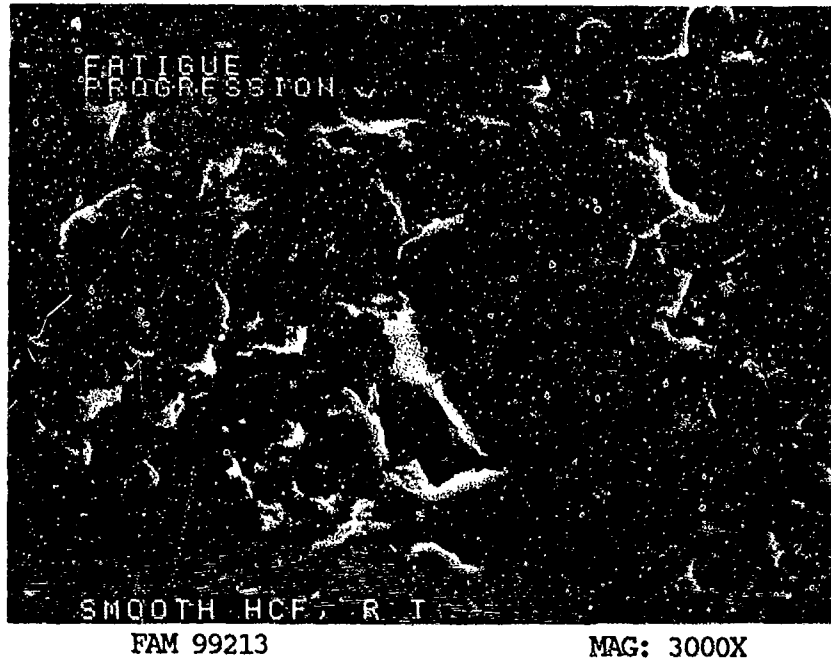


FIGURE 3-35: Higher magnification view of the area shown in Figure 3-34.

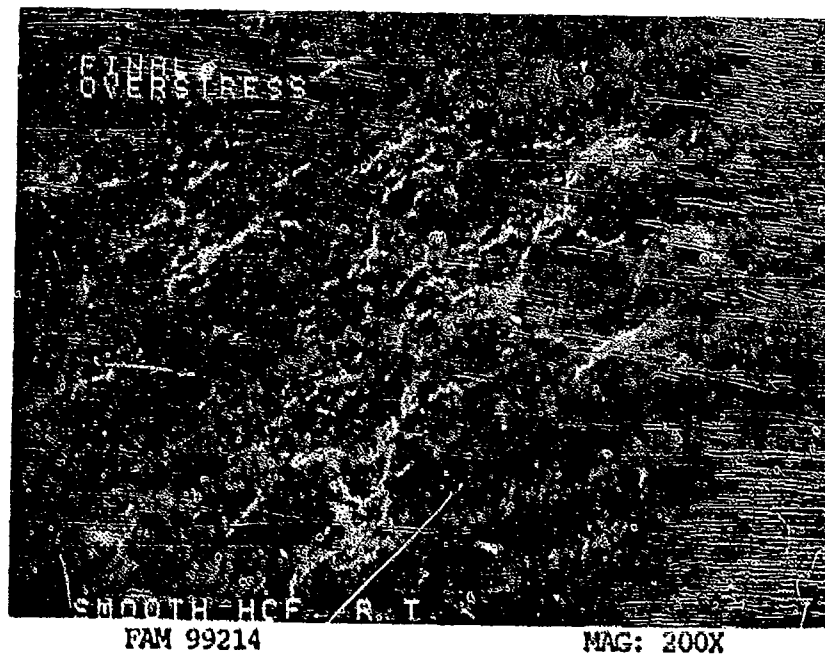


FIGURE 3-36: Final overstress exhibiting fine features.

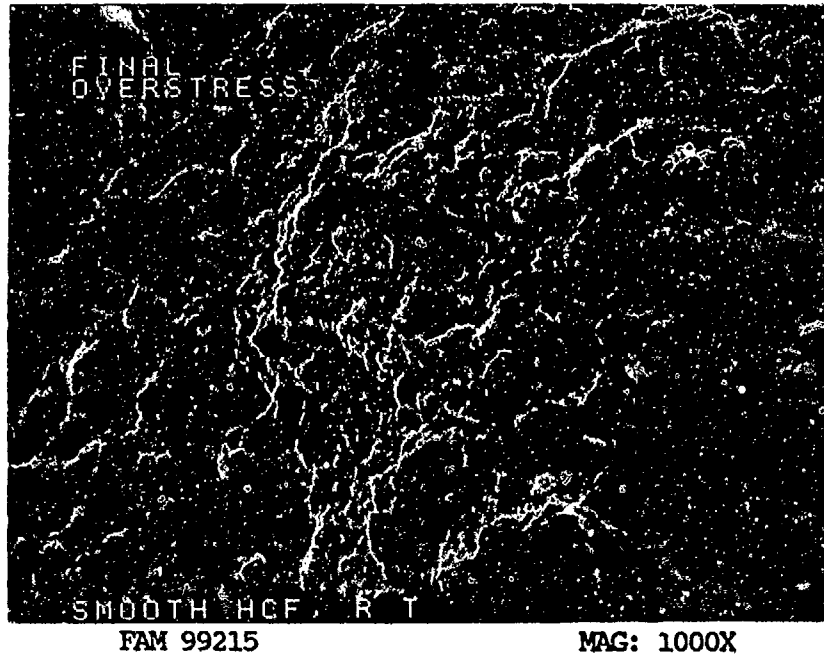


FIGURE 3-37: Fine dimpled overstress in the final overstress area.

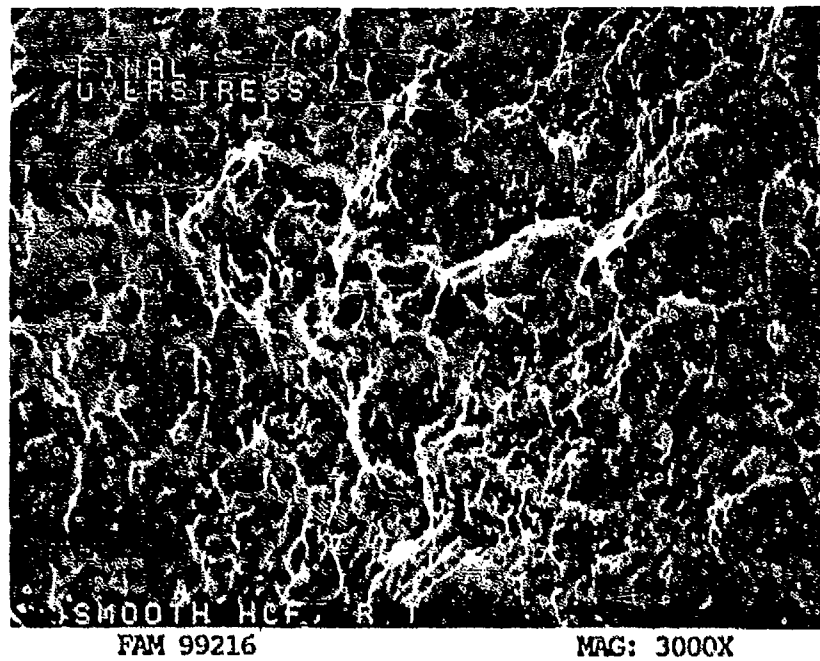


FIGURE 3-38: Very fine equiaxed dimpled overstress in the area shown in Figure 3-37.

MATERIAL

Custom 455
AMS 5617 Bar

TEST DATA

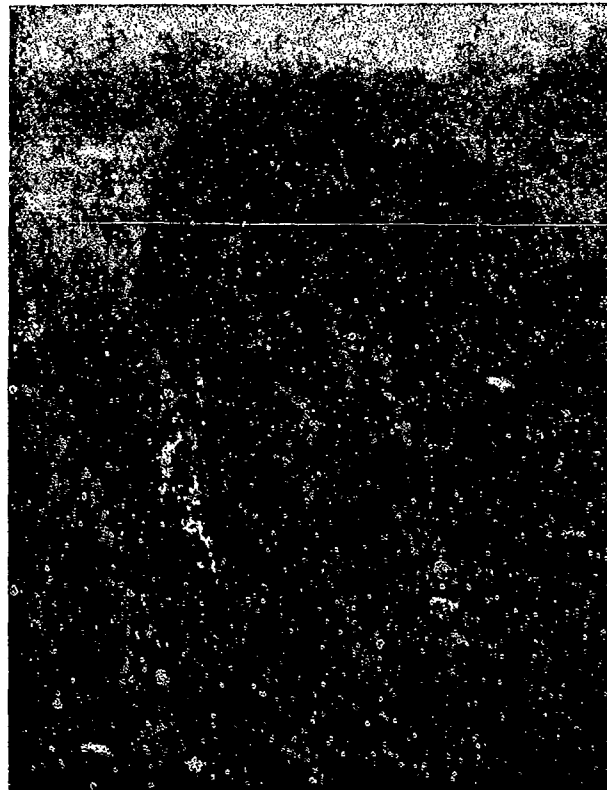
TEST TYPE
Smooth HCF

TEST CONDITIONS

Stress: 896.3 MPa (130.0 ksi)/-896.3 MPa (-130.0 ksi)
Stress Ratio: -1
Frequency: 1800 cpm
Atmosphere: Air
Temperature: 204°C (400°F)
Test Direction: Longitudinal

TEST RESULTS

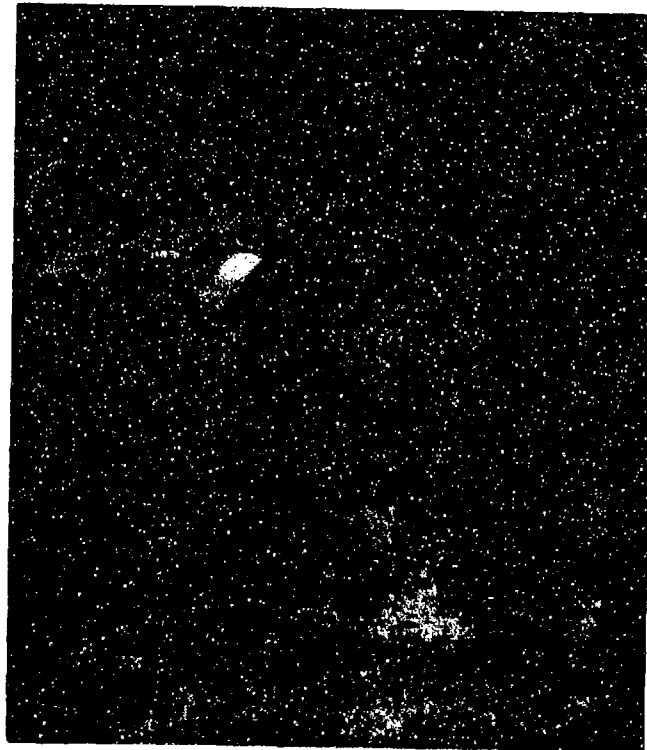
Cycles to Fracture: 181,000



FAL 93829

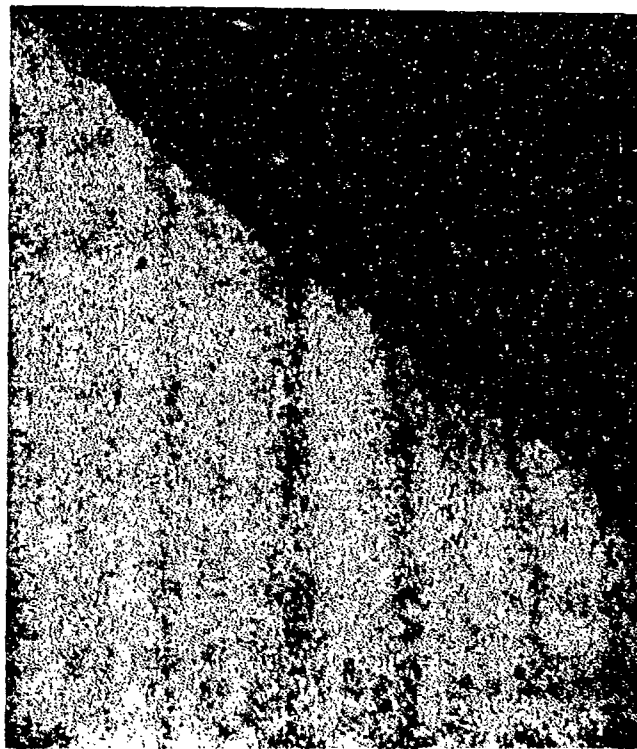
MAG: 15X

FIGURE 3-39: Test results and fractography of Custom 455 204°C (400°F) smooth HCF test. The fatigue origin and propagation areas are shown by an arrow. The fatigue occurred on a plane perpendicular to the stress axis.



FAM 100260

MAG: 200X



FAM 100261

MAG: 200X

FIGURE 3-40: Optical photomicrographs showing the fatigue progression area (top) and the final overstress area (bottom). The fatigue progressed on a plane perpendicular to the stress axis. The final overstress occurred on a plane that makes a 45° angle to the stress axis. The fracture path is predominantly transgranular.
Etchant: Vilella's Reagent

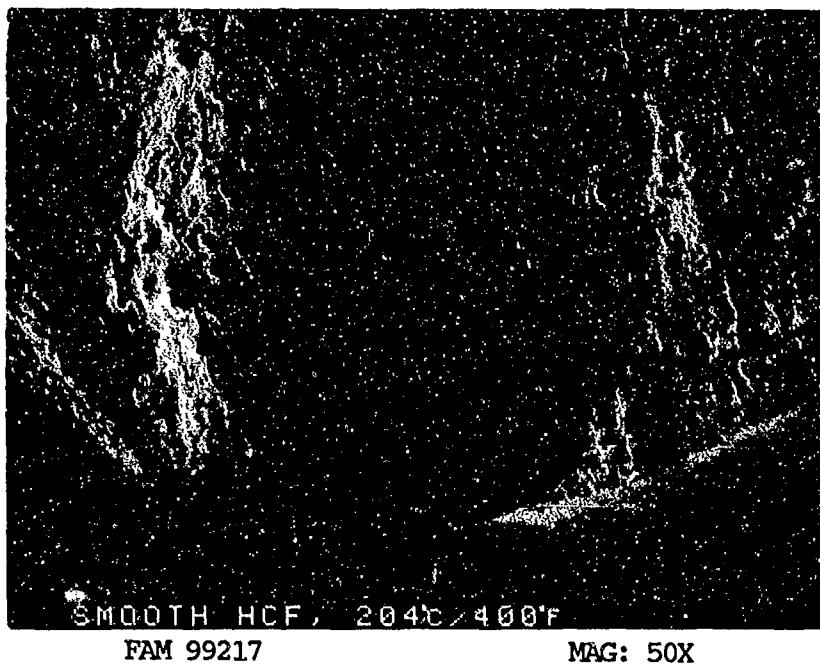


FIGURE 3-41: Overall photograph of the origin area and fatigue progression area. Fatigue features can be seen radiating from the origin (arrow).

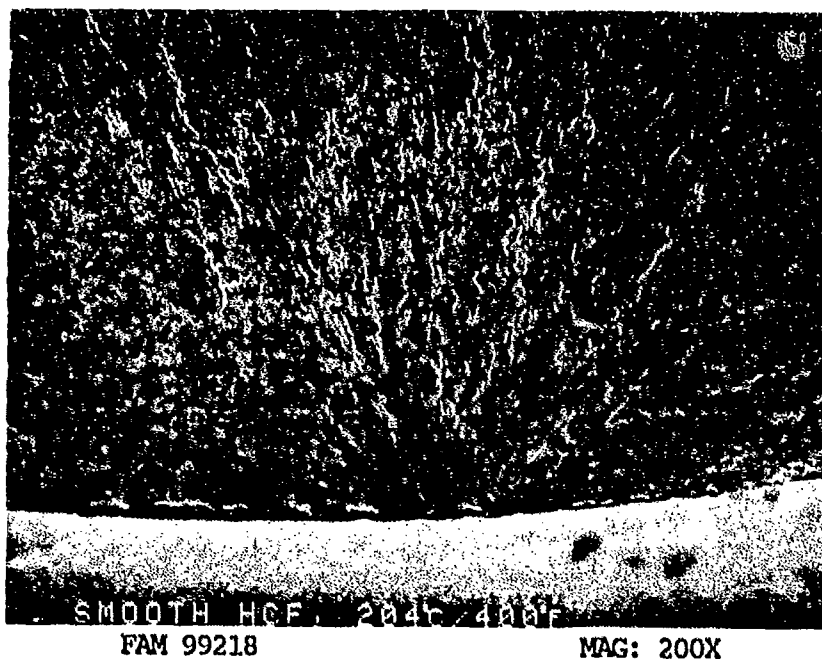


FIGURE 3-42: Higher magnification photograph of the origin area, again showing features radiating from the origin (arrow).

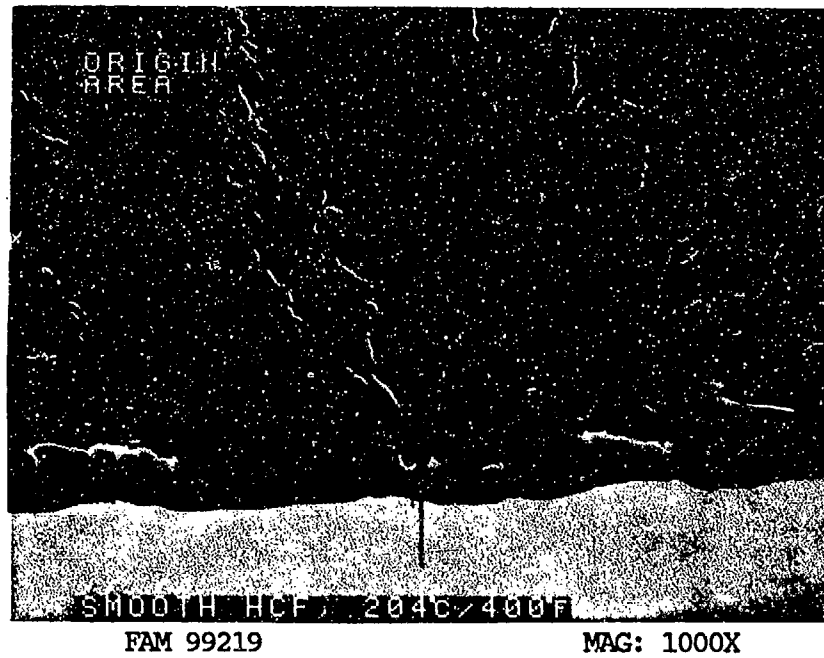


FIGURE 3-43: High magnification photograph of the origin area. The local origin is smeared, but may be at a subsurface void (arrow).

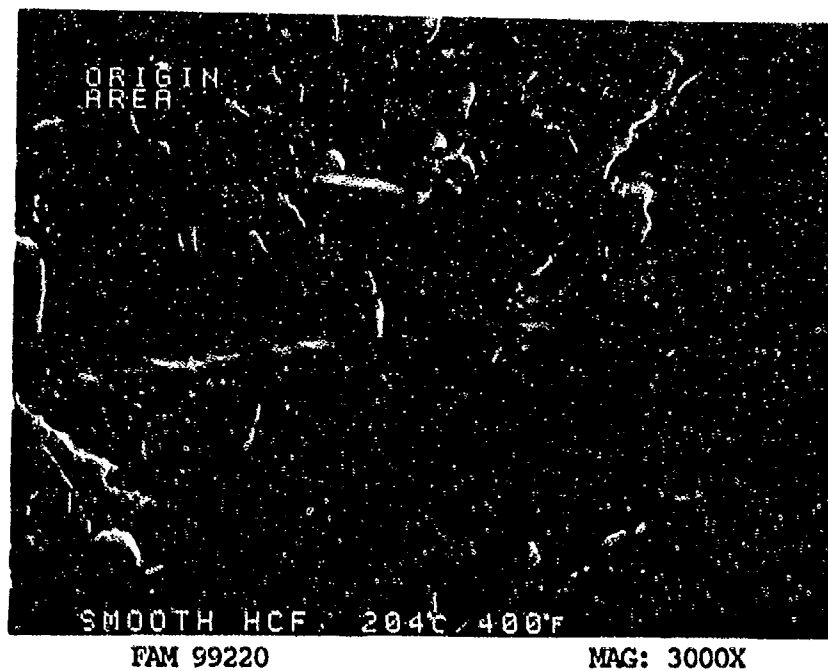


FIGURE 3-44: High magnification photograph of an area adjacent to the origin. No fatigue striations are discernible.

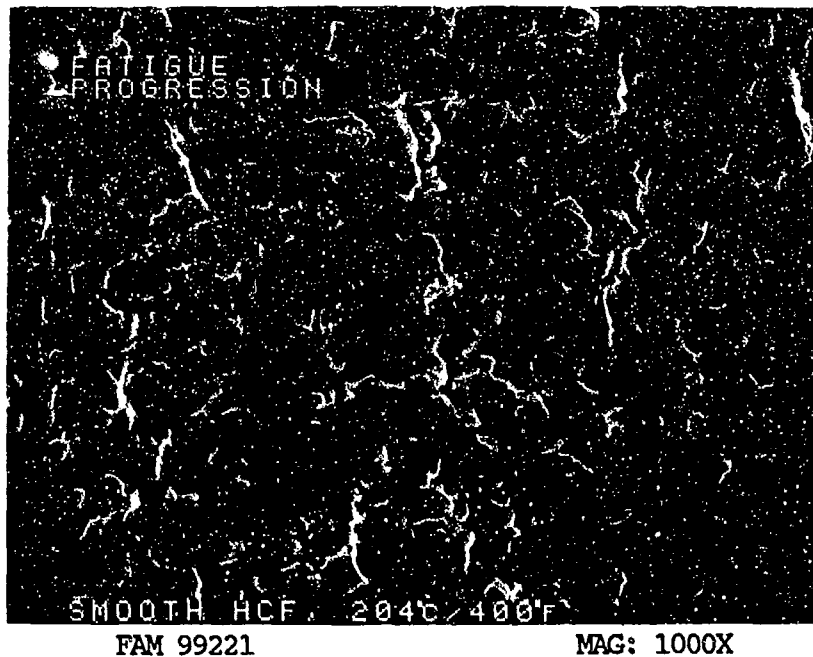


FIGURE 3-45: Fatigue progression area with no striations resolvable at this magnification.

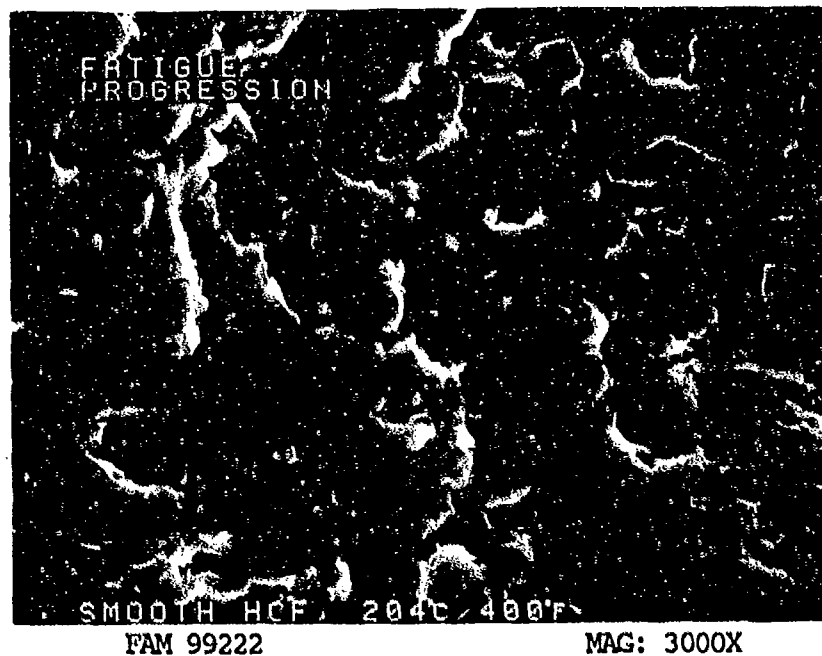


FIGURE 3-46: Higher magnification view of the area shown in Figure 3-45, showing fatigue striations, indicating propagation from bottom to top of the photograph.

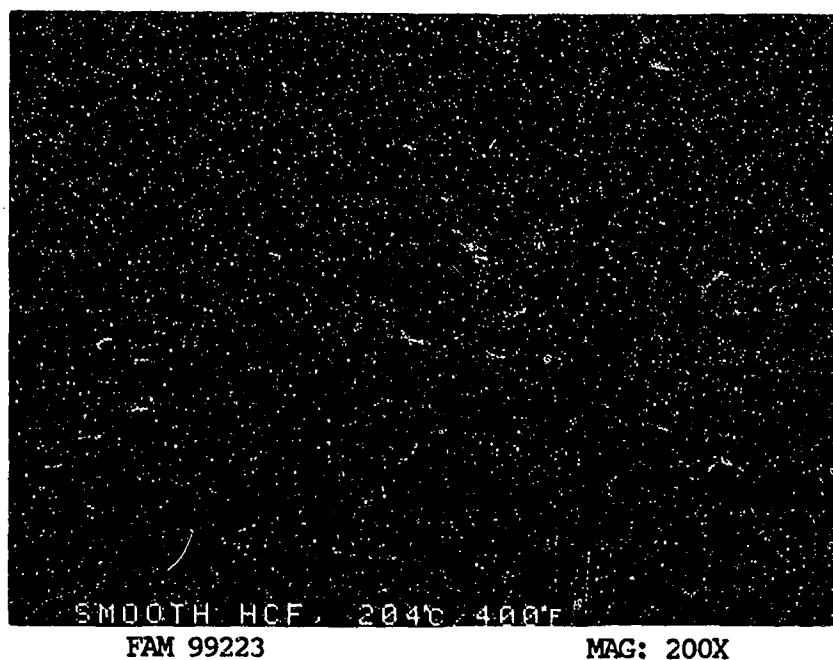


FIGURE 3-47: Final overstress showing fine features similar to the room temperature specimen.

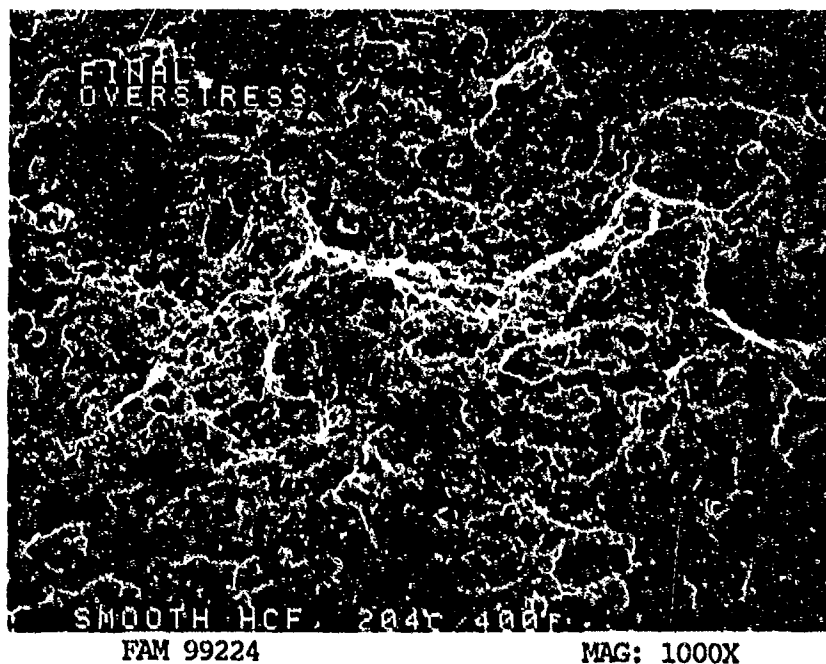


FIGURE 3-48: Fine dimpled overstress in the final overstress area.

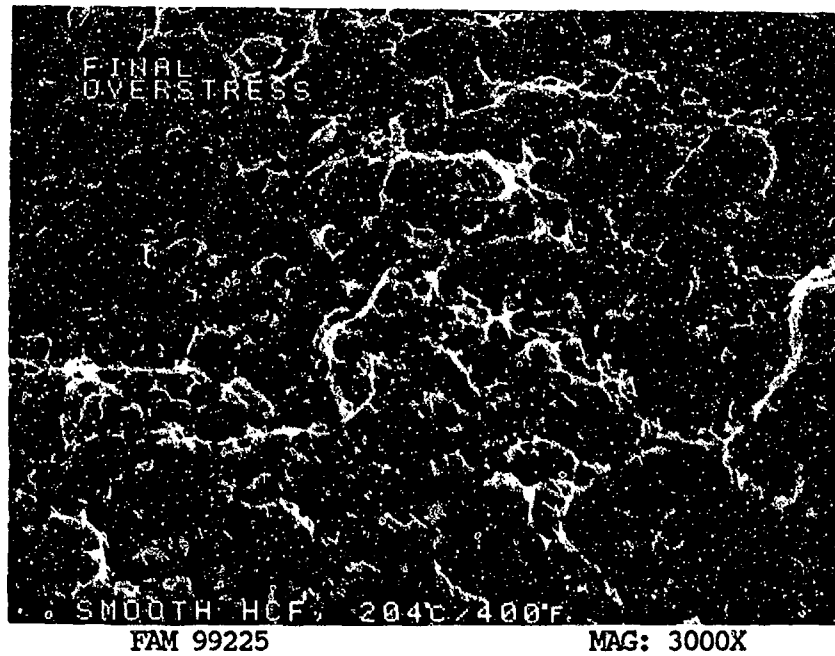


FIGURE 3-49: Very fine equiaxed dimpled overstress in the area shown in Figure 3-48.

MATERIAL

Custom 455
AMS 5617 Bar

TEST DATA

TEST TYPE
Smooth HCF

TEST CONDITIONS

Stress: 689.5 MPa (100.0 ksi)/-689.5 MPa (-100.0 ksi) DNF*
758.4 MPa (110.0 ksi)/-758.4 MPa (-110.0 ksi) DNF
827.4 MPa (120.0 ksi)/-827.4 MPa (-120.0 ksi)
Stress Ratio: -1
Frequency: 1800 cpm
Atmosphere: Air
Temperature: 427°C (800°F)
Test Direction: Longitudinal

TEST RESULTS

Cycles to Fracture: 3.74X10⁵ (DNF), 1.24X10⁵ (DNF), 1.22X10⁵

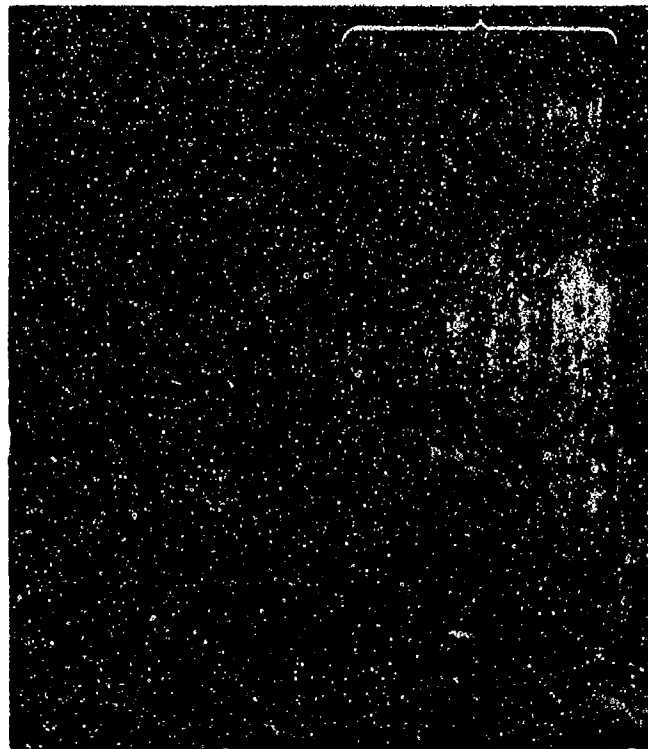
* Did Not Fracture



FAL 93950

MAG: 15X

FIGURE 3-50: Test results and fractography of Custom 455 427°C (800°F) smooth HCF test. The fatigue origin and propagation areas are shown by an arrow. The progression area appears shiny.



FAM 100267

MAG: 20X



FAM 100266

MAG: 100X

FIGURE 3-51: Optical photomicrographs showing an overall view (top) and a close-up view (bottom) of the fatigue progression area. The fatigue progression area is flat (transgranular) and occurred on a plane perpendicular to the stress axis (bracket, top). The final overstress area is rougher and deviates from the normal plane.

Etchant: Vilella's Reagent

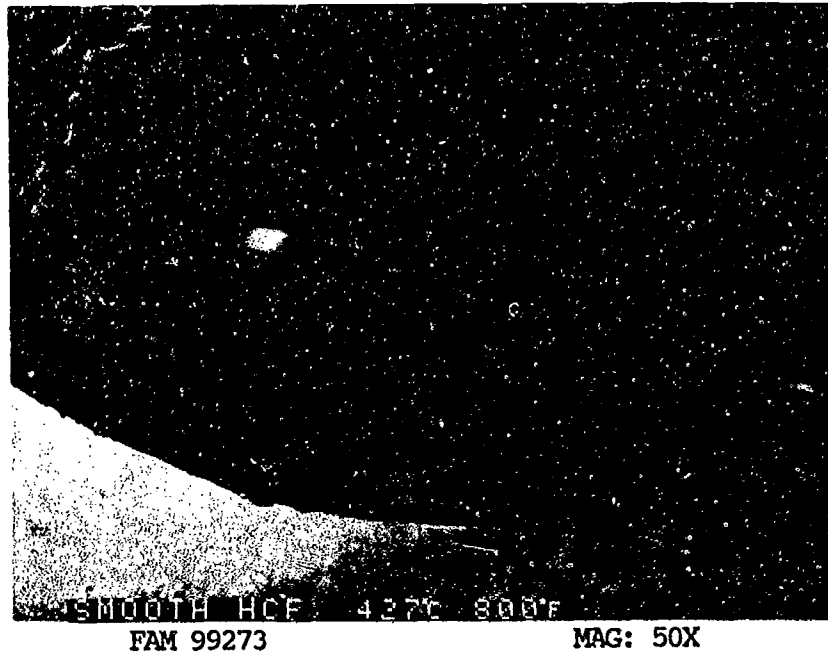


FIGURE 3-52: Overall photograph of the origin area and fatigue progression area. Fatigue features can be seen radiating from the origin (arrow).

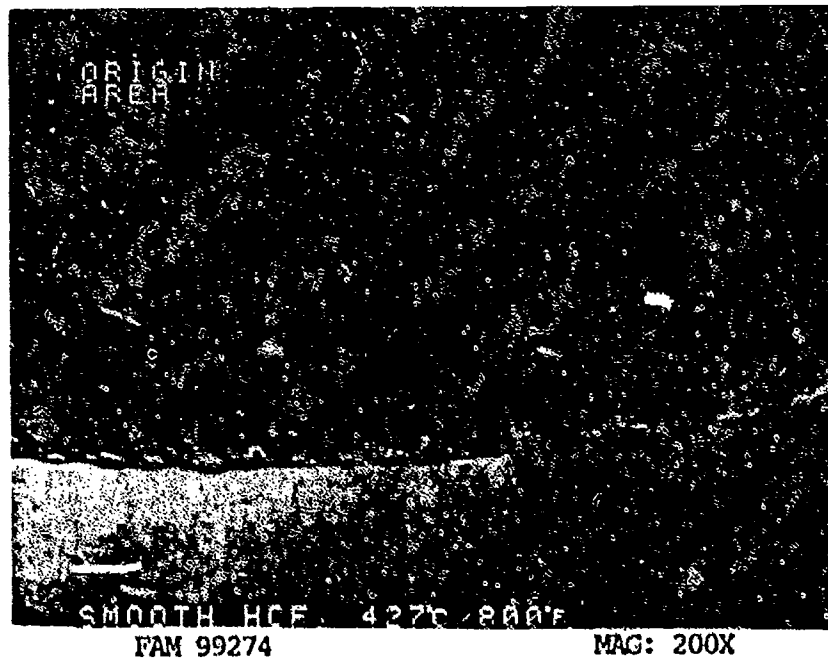


FIGURE 3-53: Higher magnification view of the diffuse origin area, again showing features radiating from the origin (arrow).

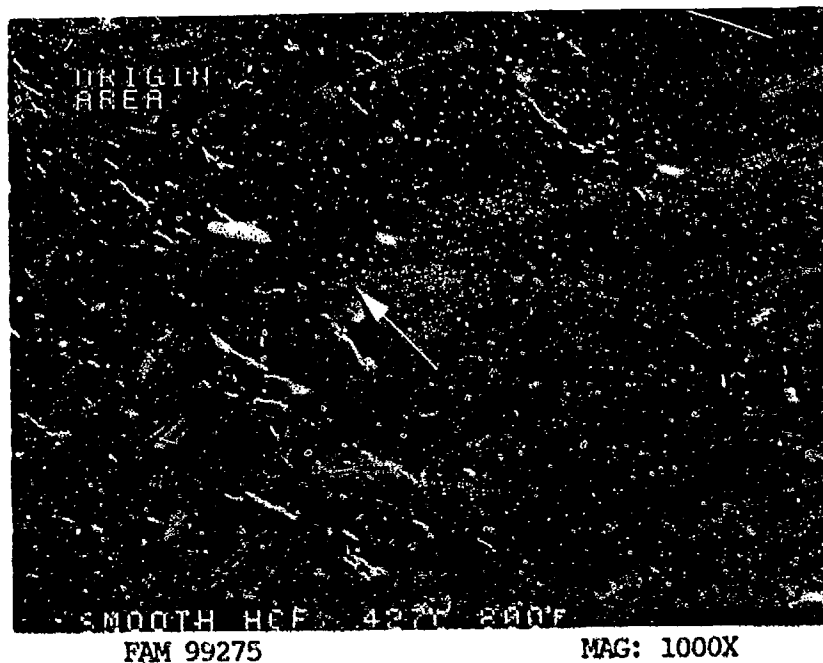


FIGURE 3-54: High magnification photograph of an area near the origin. An arrow shows the direction of propagation. No fatigue striations are discernible.

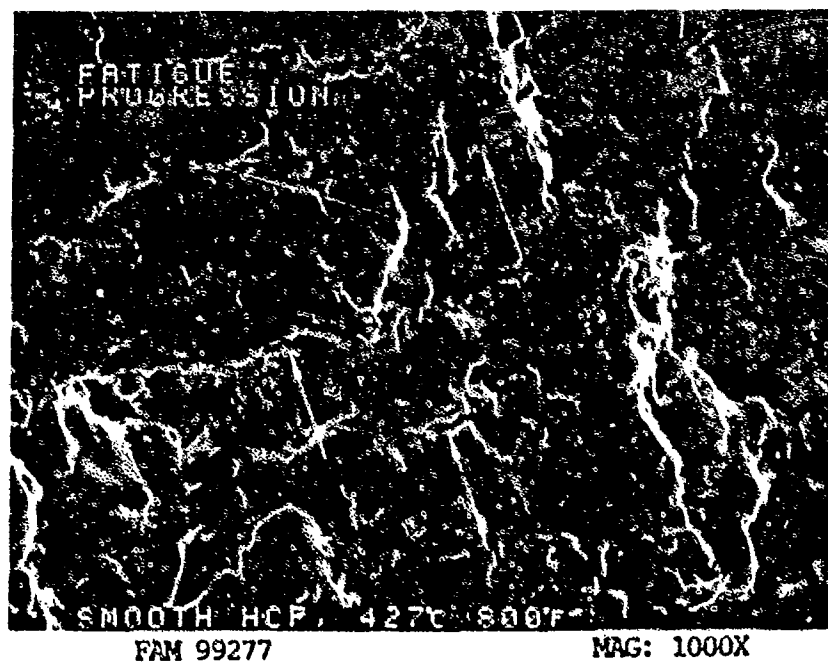
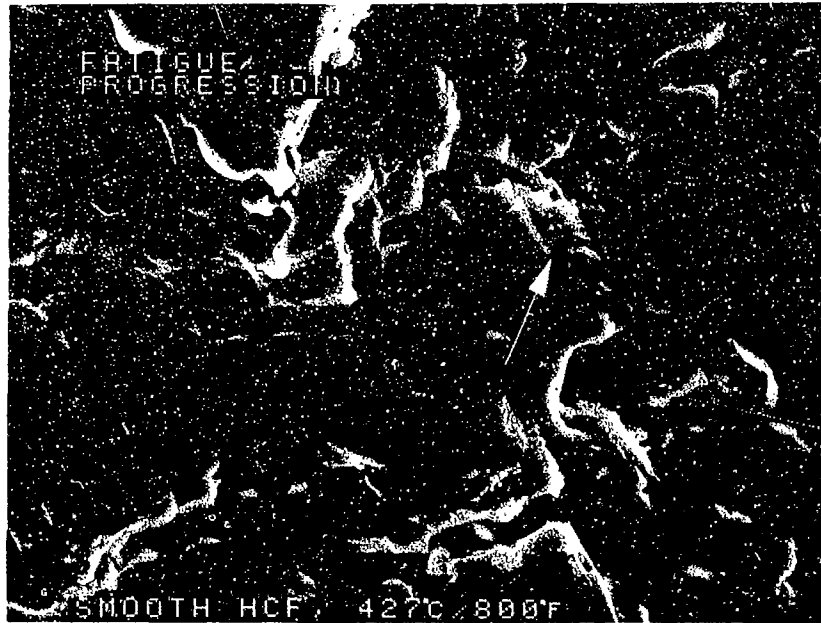


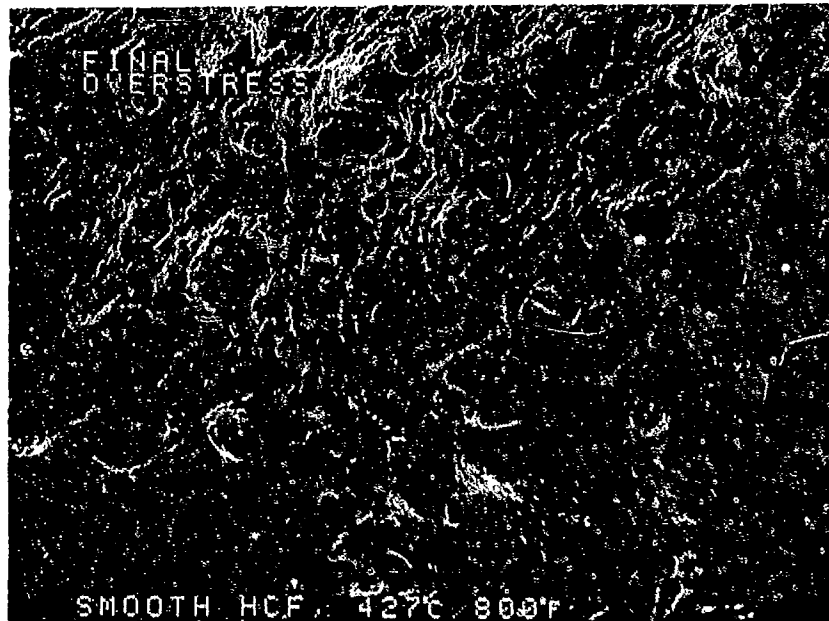
FIGURE 3-55: Fatigue progression zone exhibiting crack-like striations (arrows) with smear features perpendicular to them.



FAM 99278

MAG: 3000X

FIGURE 3-56: Higher magnification view of the area shown in Figure 3-55. Fine remnant striations are visible between the cracks (arrow).



FAM 99279

MAG: 200X

FIGURE 3-57: Dimpled overstress in the final overstress area.

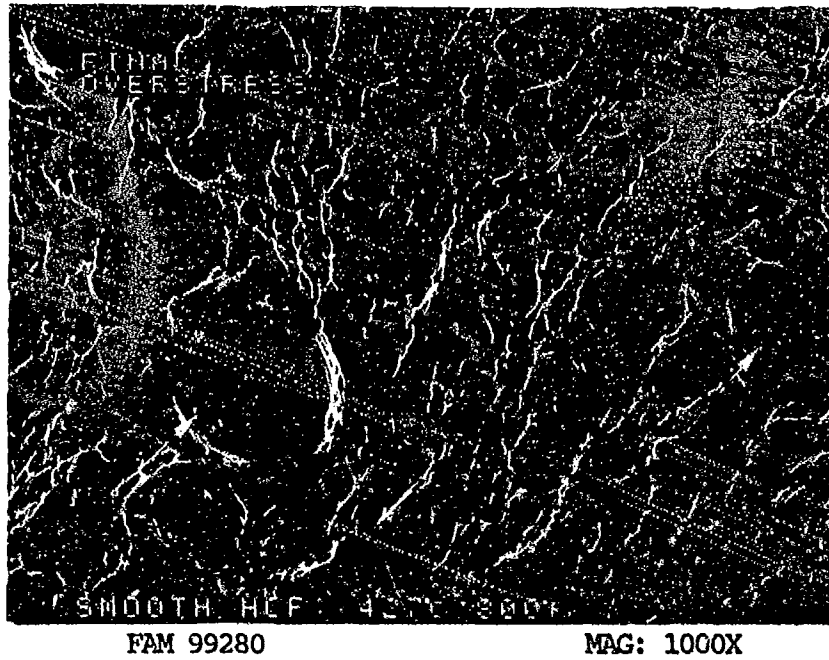


FIGURE 3-58: Dimpled overstress in the final fracture area. The dimples are coarser than on the room temperature specimen. Two voids are indicated by arrows.

MATERIAL

Custom 455
AMS 5617 Bar

TEST DATA

TEST TYPE

Stress Corrosion

TEST CONDITIONS

Stress: 1336.2 MPa (193.8 ksi)
Environment: 3.5% NaCl vapor (simulated sea water)
Temperature: 95°C (203°F)
Test Direction: Longitudinal (U-bend specimen)

TEST RESULTS

Time to Fracture: 168 hours

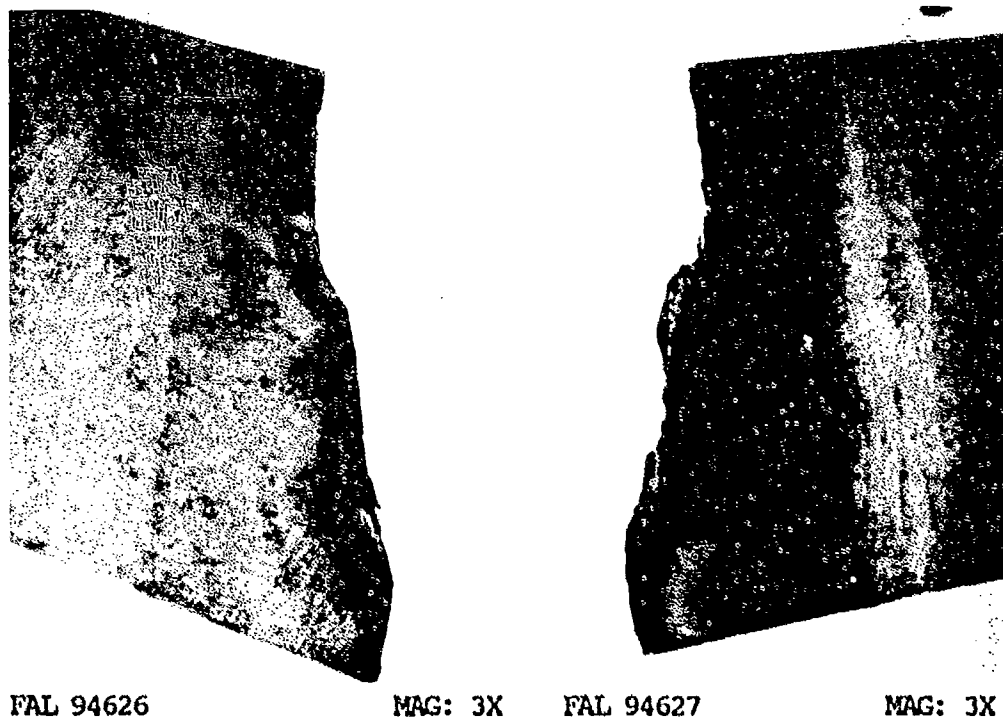
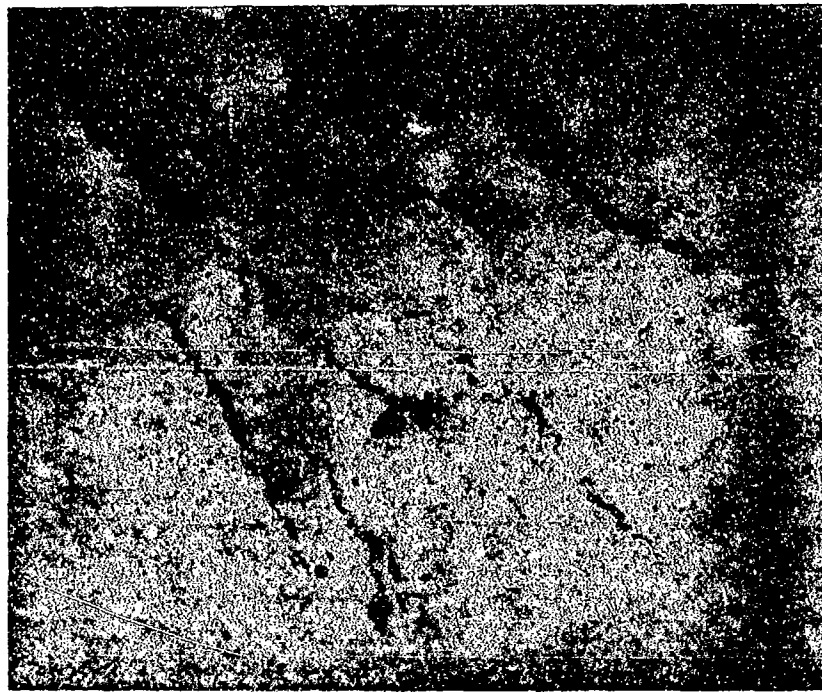
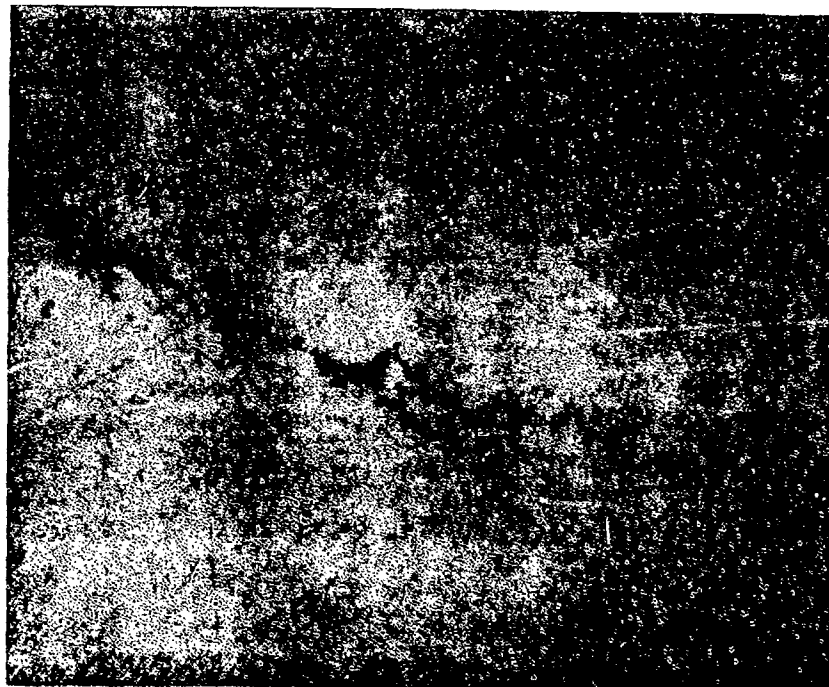


FIGURE 3-59: Test results and fractography of Custom 455 stress corrosion test flat plate specimen. The fracture is shown from the tension (left) and compression (right) sides. The tension side exhibited extensive attack and deposition of corrosion products. The compression side was relatively free of attack.



FAM 100268

MAG: 50X



FAM 100269

MAG: 100X

FIGURE 3-60: Optical photomicrographs showing the intergranular appearance of secondary cracks. These branching intergranular cracks are one of the characteristics of stress corrosion cracking. Often the mode cannot be conclusively determined by looking only at the primary fracture surface, and a metallographic section similar to this can be decisive.

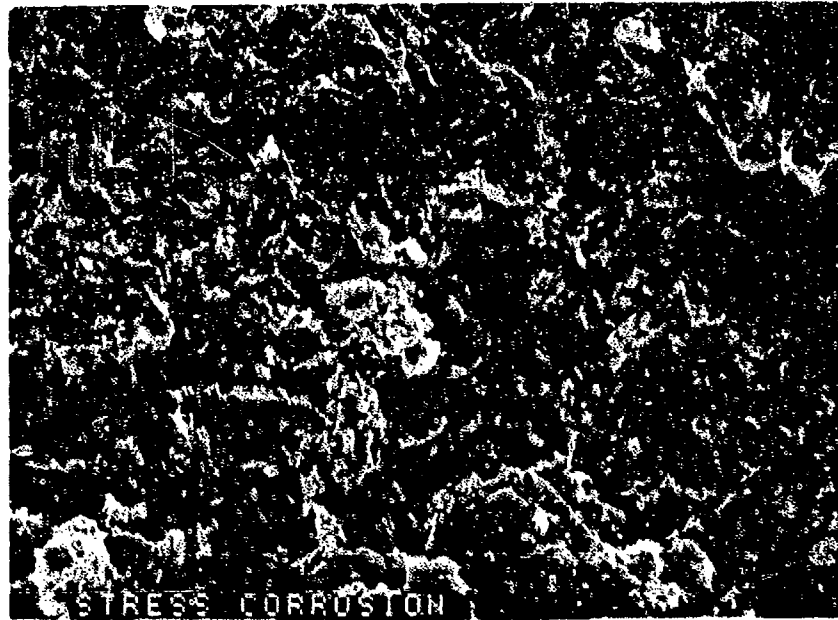
Etchant: Vilella's Reagent



FAM 99698

MAG: 200X

FIGURE 3-61: Low magnification photograph of the fracture surface exhibiting transgranular cleavage.



FAM 99699

MAG: 1000X

FIGURE 3-62: Remnant feathery transgranular cleavage.



FAM 99700

MAG: 3000X

FIGURE 3-63: Higher magnification photograph of the area shown in Figure 3-62.

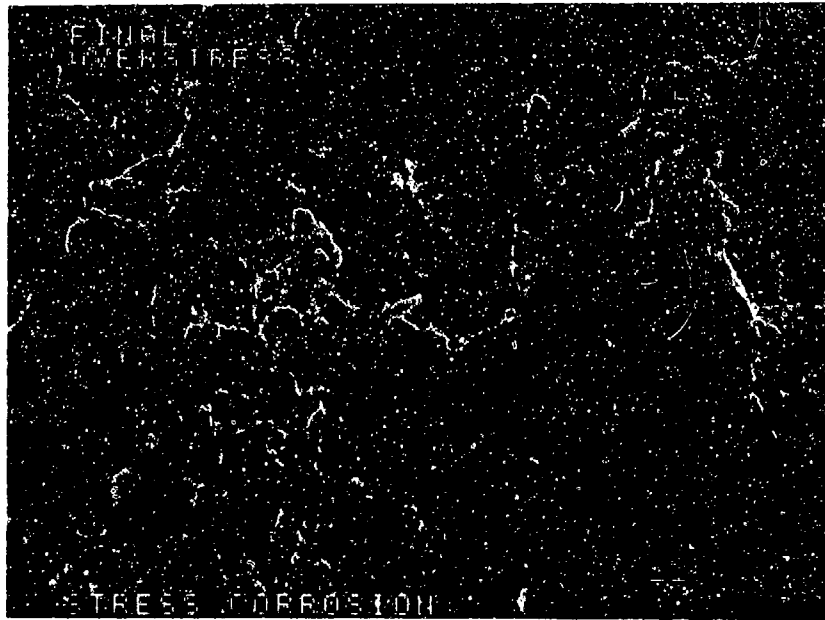


FINAL
OVERSTRESS

FAM 99693

MAG: 200X

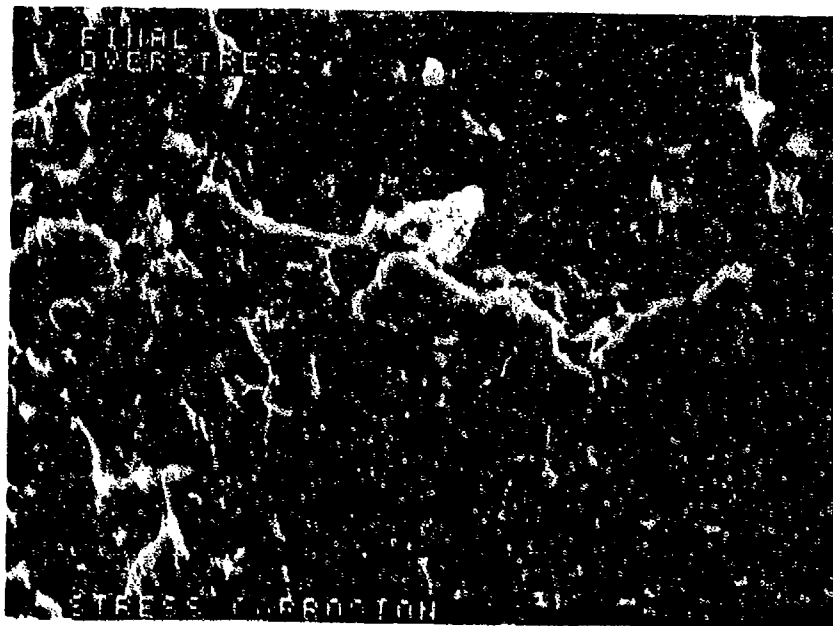
FIGURE 3-64: Final overstress area.



FAM 99694

MAG: 1000X

FIGURE 3-65: Fine dimpled overstress in the final fracture area.



FAM 99695

MAG: 3000X

FIGURE 3-66: Fine equiaxed dimpled overstress in the final fracture area.

MATERIAL

Custom 455
AMS 5617 Bar

TEST DATA

TEST TYPE

Hydrogen Embrittlement

TEST CONDITIONS

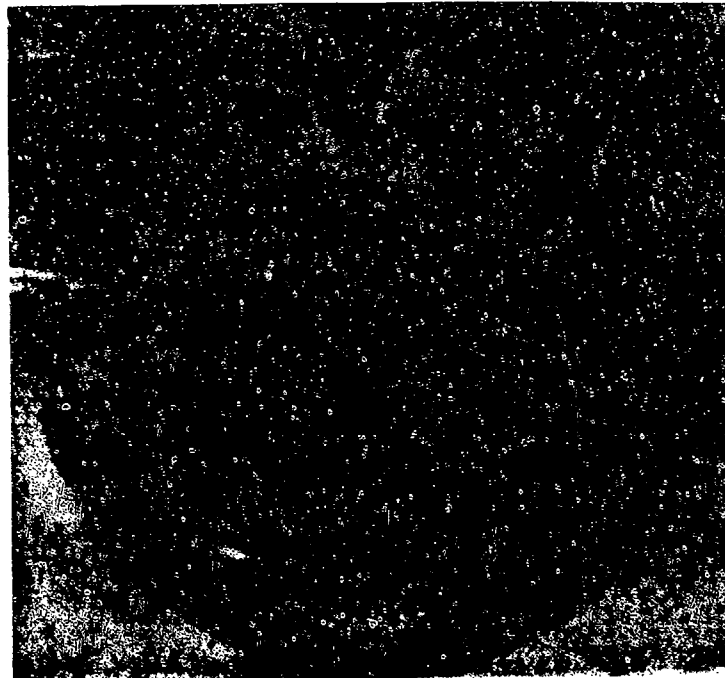
Stress: 1813.3 MPa (263 ksi) DNF*
2054.6 MPa (298.0 ksi) DNF
2345.2 MPa (333.0 ksi)

Atmosphere: Air
Temperature: Room Temperature
Test Direction: Longitudinal
Charging: Charged for 12 hours in gaseous H₂ at 5000 psi.
Cathodically charged for 2 hours in 1% aqueous
HCl, 15 Vdc, platinum anode

TEST RESULTS

Time to Fracture: 273.5 hrs. (DNF), 99.1 hrs. (DNF), Failed on Loading.

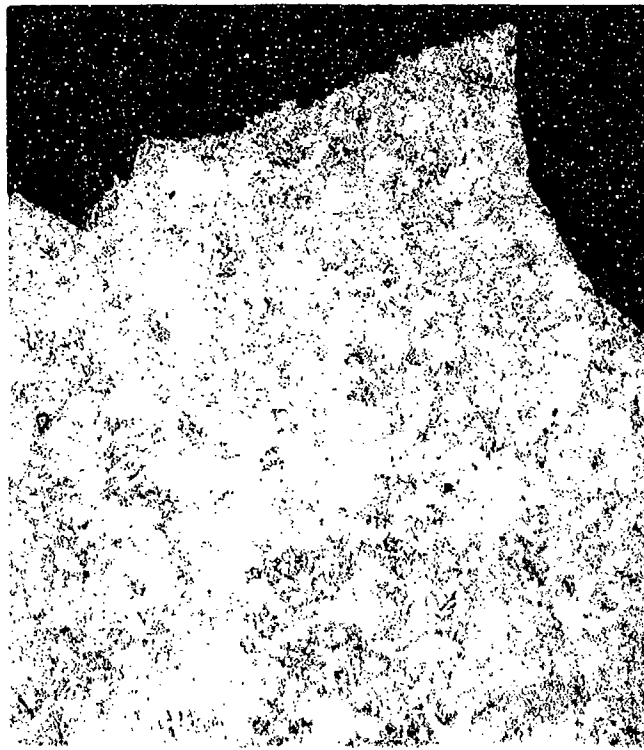
* Did Not Fracture



FAL 94528

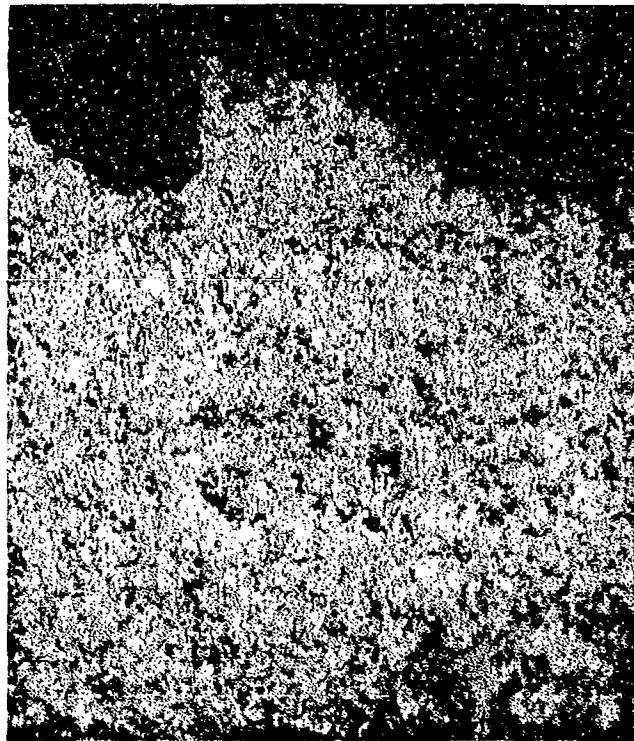
MAG: 12X

FIGURE 3-67: Test results and fractography of Custom 455 hydrogen embrittlement test.



FAM 100298

MAG: 200X



FAM 100299

MAG: 200X

FIGURE 3-68: Optical photomicrographs showing transgranular fracture paths near the edge of the specimen (top) and the center of the specimen (bottom).

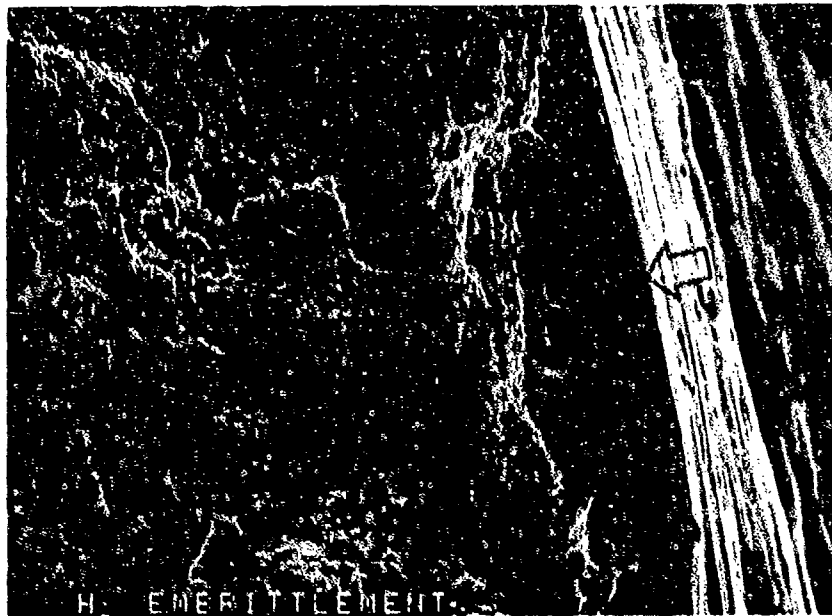
Etchant: Vilella's Reagent



FAM 99644

MAG: 200X

FIGURE 3-69: Low magnification photograph of the fracture surface exhibiting ductile overstress with patches of cleavage.



FAM 99646

MAG: 1000X

FIGURE 3-70: Remnant feathery transgranular cleavage at the surface of the specimen (arrow).

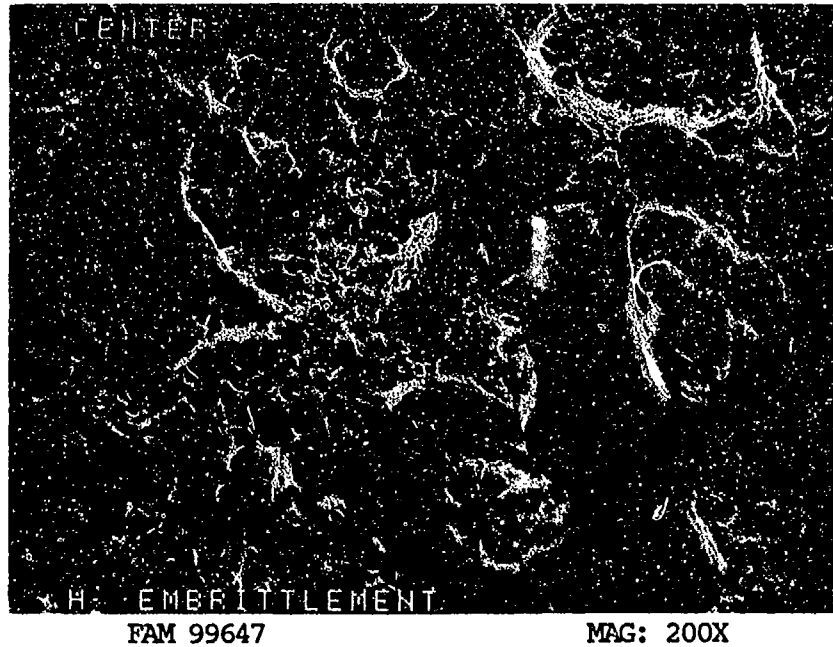


FIGURE 3-71: Fracture surface near the center of the specimen, exhibiting a mixture of dimpled overstress and patches of cleavage.

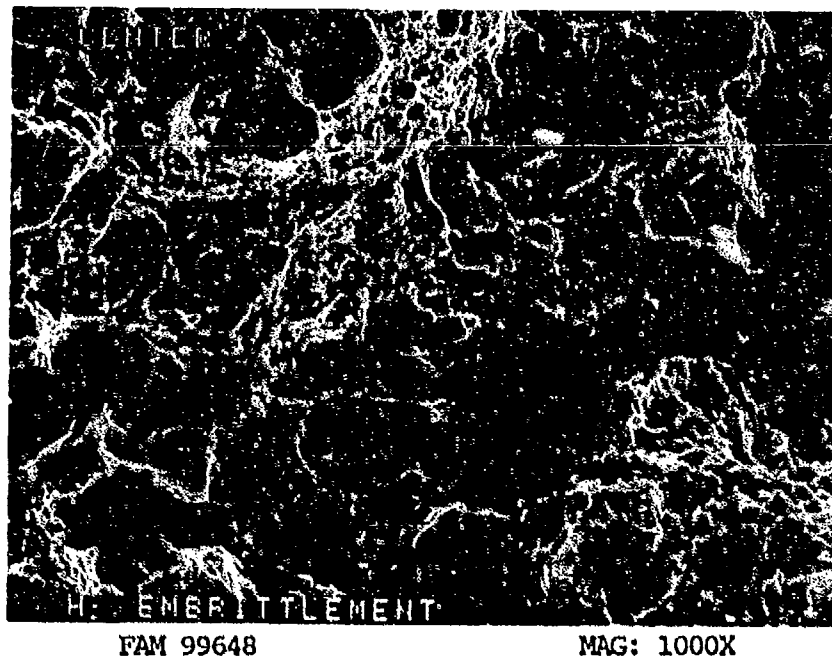


FIGURE 3-72: Higher magnification photograph of the area shown in Figure 3-71, exhibiting dimpled overstress with patches of feathery cleavage.

AISI 347 (Stainless Steel)

Material Description

Type 347 stainless steel is a stabilized austenitic stainless steel that can be hardened by cold working but not by heat treatment. Stabilization is accomplished by tying up the carbon with minor additions of columbium and tantalum. These elements form carbides throughout the microstructure which help prevent sensitization. Type 347 is less susceptible to general corrosion than Type 321. The alloy is available in the form of bar, plate, sheet, forgings, tubing, wire and castings.

The material used in this study AMS 5646 was heat treated to AMS 2759/4 with a required hardness of HRB 75-97 (BHN conversion). The typical room temperature mechanical properties for AMS 5646 (bar) are as follows:

Ultimate Tensile Strength:	90 ksi	
0.2% Yield Strength:	35 ksi	
Percent Elongation:	50% min	
Percent Reduction in Area:	65% min	
	<u>Required</u>	<u>Measured</u>
ASTM Grain Size:	-	11-12
Measured Hardness:	HRB 98-99	

Fractography Overview

Type 347 stainless steel was tested in the solution heat treated condition with no prior cold work. This resulted in very high ductility, especially in the elevated temperature specimens. Both the room temperature and 1500 F smooth tensile specimens had reduction in area of over 65%. The room temperature specimen had a very large shear lip (0.05 inch). The 1500 F specimen had no shear lip but necked to a small final overstress area before fracture. The primary fracture on the room temperature specimen showed ductile dimpled overstress with some nucleating particles visible in the bottoms of the dimples. The shear lip had a mixture of fine equiaxed and coarser shear dimples. The 1500 F specimen had very deep conical dimples covered by a light oxide. Many of the dimples had particles within them. Both the room temperature and 1500 F notched tensile specimens exhibited areas with axial faces on the fracture surfaces. The room temperature specimen exhibited a mixture of average sized and very fine dimples that occurred in patches. The dimples were deeper and coarser than those observed in the smooth room temperature specimen but not the deep conical dimples exhibited by the elevated temperature smooth specimen. The elevated temperature notched specimen had several vertical faces on the fracture that contained shear dimples and unusual shearing/tearing dimples. The equiaxed dimples were shallower and coarser than the room temperature specimen.

All three smooth HCF specimens had a similar macroscopic appearance, exhibiting flat fracture perpendicular to the stress axis. The fatigue crack propagated through greater than 90% of the cross section in each case. The room temperature and 1500 F specimens had single origins but the 800 F specimen had two localized origin areas each having a fatigue step. The origin areas (stage I) on all three specimens exhibited feathery cleavage features. No facets were observed in the origin area. Initial propagation (stage II) showed well defined striations and crack-like striations on all three specimens although the extent of oxidation increased with increasing test temperature. The 800 F and 1500 F specimens had a higher percentage of crack-like striations than were observed on the room temperature specimen. As the fatigue crack grew, the striation appearance became smoother and there were fewer crack-like striations. The striation spacing also increased noticeably. Arrest marks were visible macroscopically in the area just before final overstress occurred on all three specimens. Final overstress occurred by dimpled overstress with some quasi-cleavage features.

MATERIAL

347 Stainless Steel
AMS 5646 Bar (Solution heat treated)

TEST DATA

TEST TYPE

Smooth Tensile

TEST CONDITIONS

Strain Rate: 0.005 mm/mm/min (0.005 in/in/min)

Atmosphere: Air

Temperature: Room Temperature

Test Direction: Longitudinal

TEST RESULTS

0.2% Yield Strength: 615.0 MPa (89.2 ksi)

Ultimate Strength: 744.6 MPa (108.0 ksi)

% Elongation: 40.0

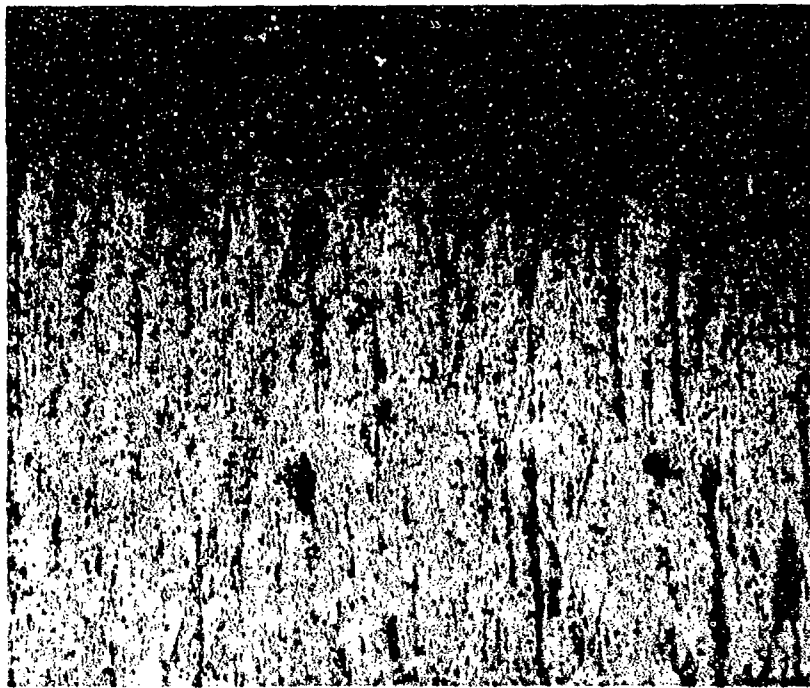
% Reduction of Area: 70.6



FAL 89835

MAG: 15X

Figure 4-1: Test results and fractography of 347 SST room temperature smooth tensile test. The entire fracture surface is dominated by a large final overstress area (shear lip, area 1). Area 2 is the primary fracture.

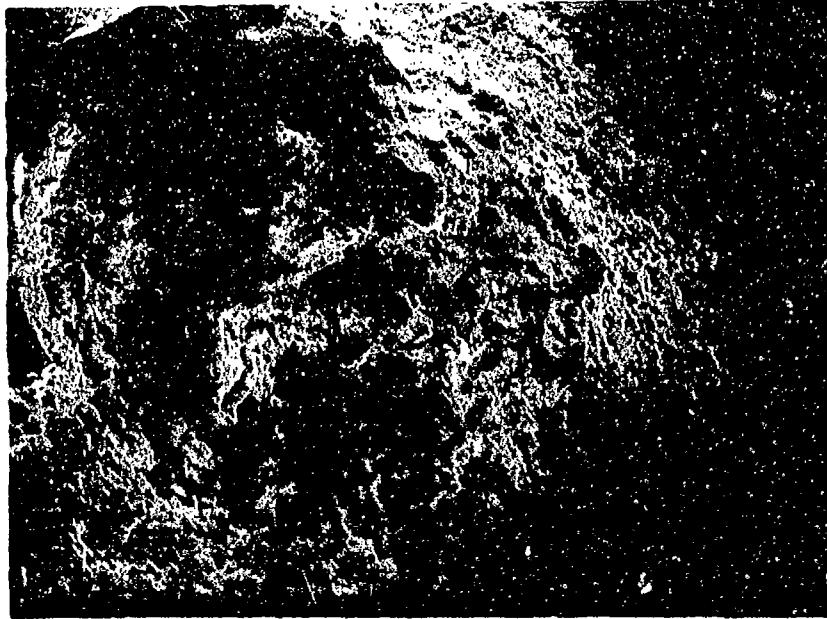


FAM 100474

MAG: 200X

FIGURE 4-2: Optical photomicrograph of a metallographic cross section through the center of the specimen. The fracture is transgranular.

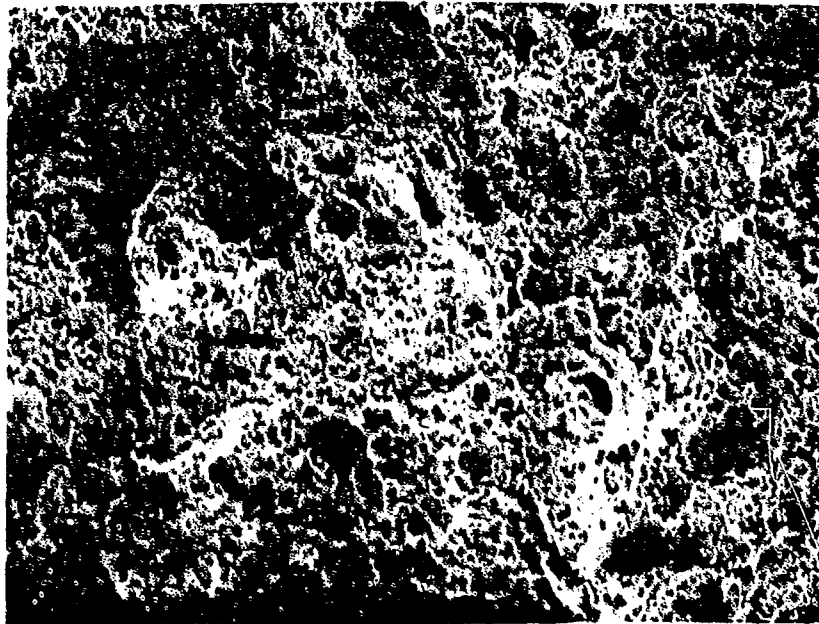
Etchant: 10% Oxalic acid electrolytic



FAM 97962

MAG: 50X

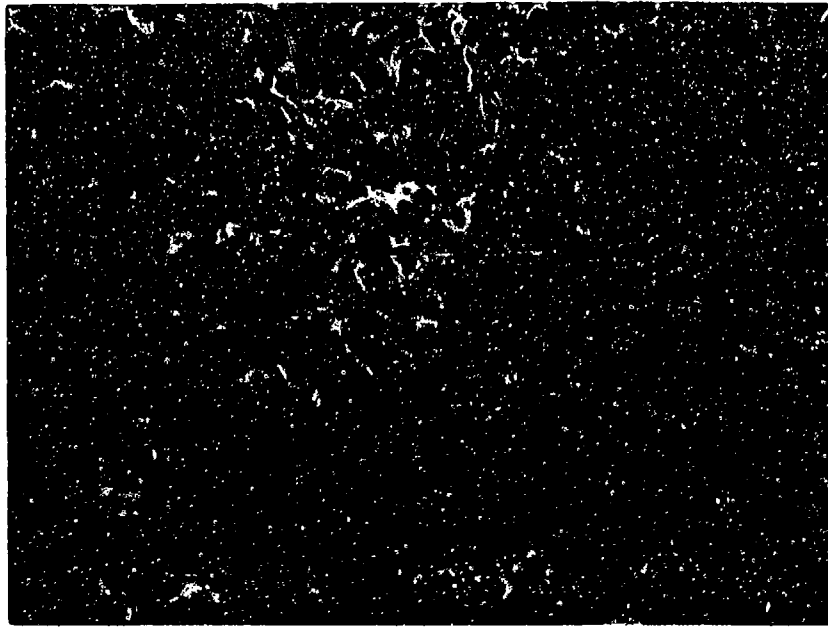
Figure 4-3: Low magnification view showing dimpled primary fracture area (area 2, Figure 4-1) and the large final overstress area (area 1, Figure 4-1).



FAM 97966

MAG: 200X

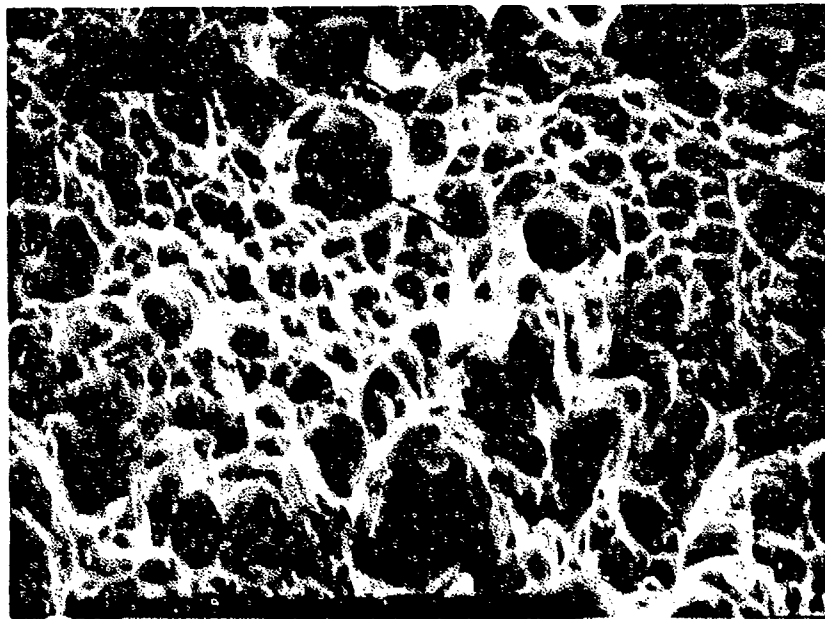
Figure 4-4: Primary fracture area exhibiting dimpled overstress.



FAM 97967

MAG: 1000X

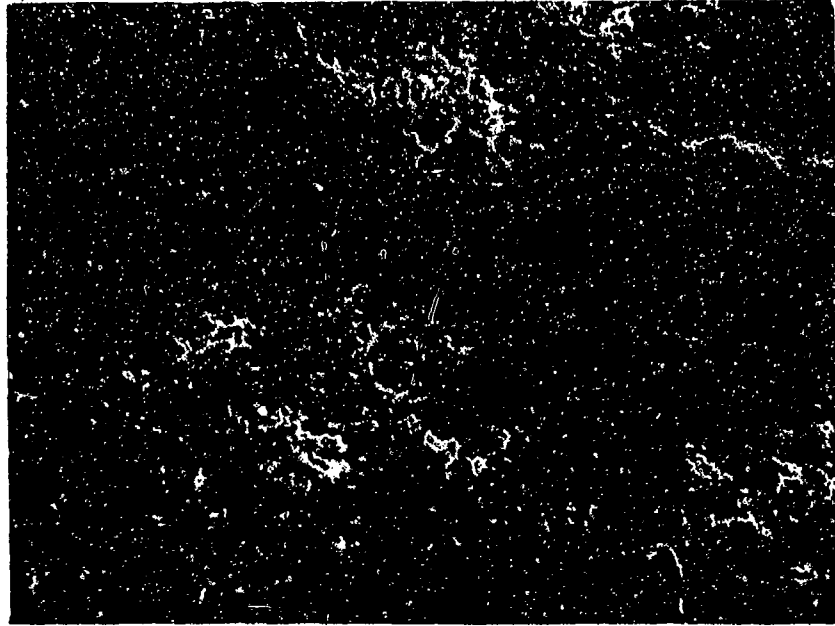
Figure 4-5: Fine equiaxed dimples in area of primary fracture shown in Figure 4-4.



FAM 97968

MAG: 3000X

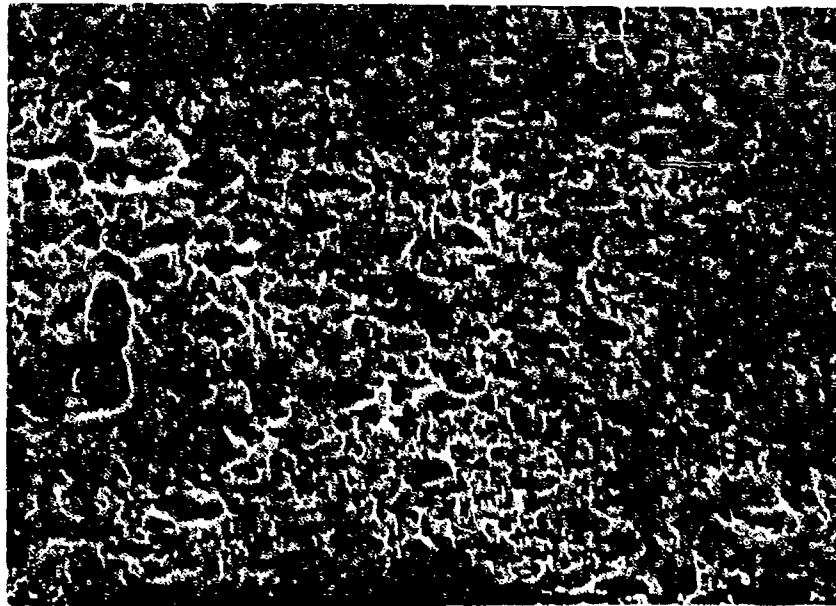
Figure 4-6: High magnification photograph of fine dimples in the primary fracture area. Nucleating particles are visible at the bottoms of several dimples (arrows).



FAM 97963

MAG: 200X

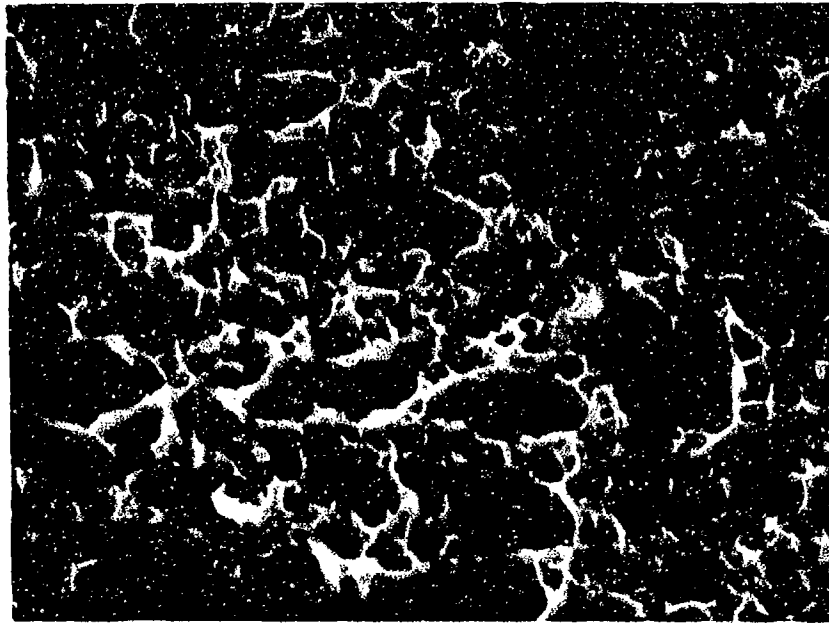
Figure 4-7: Final overstress area (shear lip).



FAM 97964

MAG: 1000X

Figure 4-8: Shear dimples in final overstress area. Arrows indicate the directions of relative motion.



FAM 97965

MAG: 3000X

Figure 4-9: High magnification photograph of shear dimples in final overstress area. Equiaxed dimples are mixed with the shear dimples.

MATERIAL

347 Stainless Steel
AMS 5646 Bar (Solution heat treated)

TEST DATA

TEST TYPE

Smooth Tensile

TEST CONDITIONS

Strain Rate: 0.005 mm/mm/min (0.005 in/in/min)
Atmosphere: Air
Temperature: 816°C (1500°F)
Test Direction: Longitudinal

TEST RESULTS

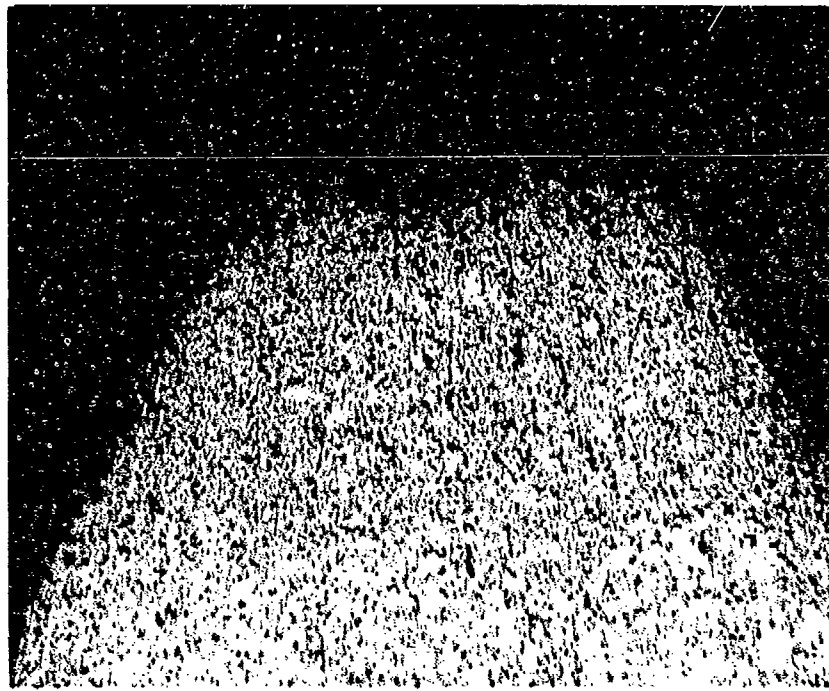
0.2% Yield Strength: 217.9 MPa (31.6 ksi)
Ultimate Strength: 241.3 MPa (35.0 ksi)
% Elongation: 65.0
% Reduction of Area: 90.0



FAL 90295

MAG: 15 X

Figure 4-10: Test results and fractography of 347 SST 816°C (1500°F) smooth tensile test. The specimen has no shear lip but experienced a large reduction of area (necking) before final overstress occurred.



FAM 100477

MAG: 50X

FIGURE 4-11: Optical photomicrograph of a metallographic cross section through the fracture surface. Extensive reduction of area is visible.

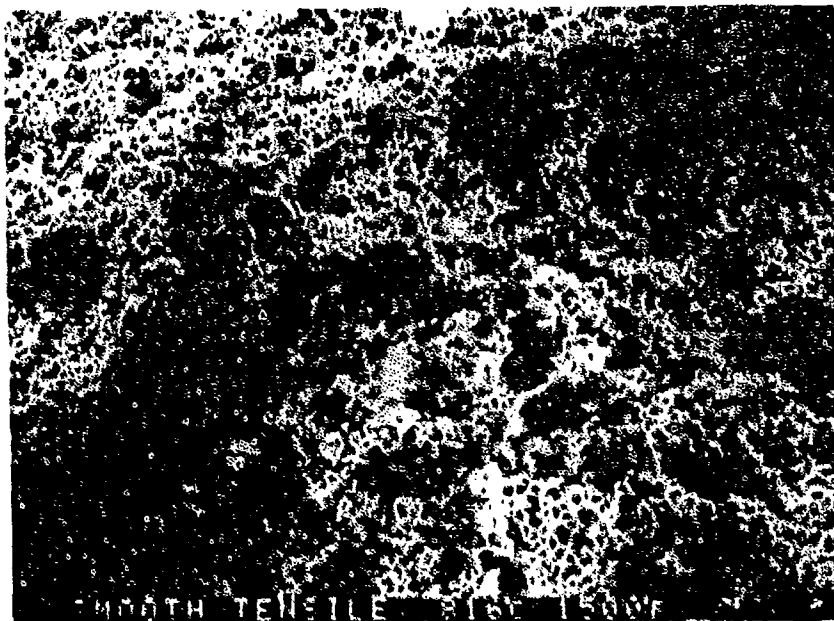
Etchant: 10% Oxalic acid electrolytic



FAM 97991

MAG: 50X

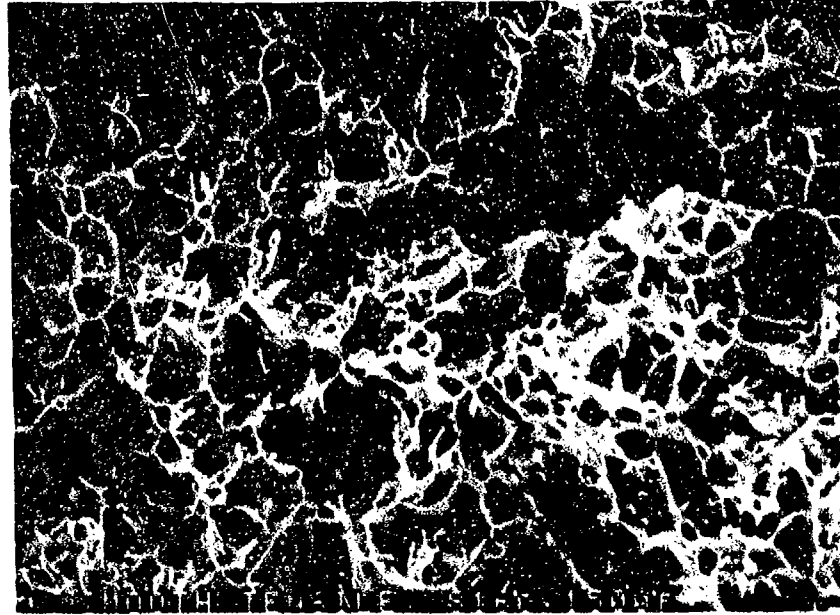
Figure 4-12: Low magnification view showing dimpled overstress covering the entire fracture surface.



FAM 97992

MAG: 200X

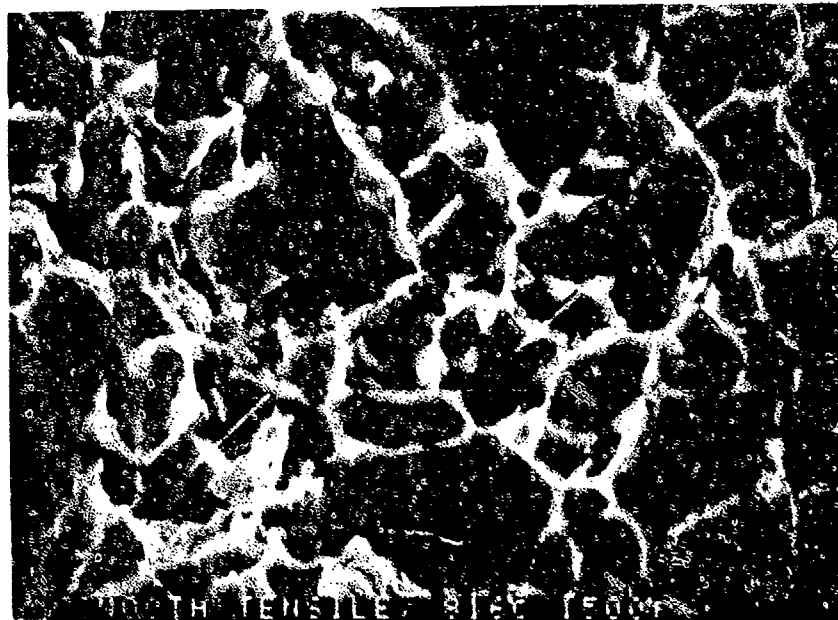
Figure 4-13: Higher magnification photograph of dimpled overstress shown in Figure 4-12.



FAM 97993

MAG: 1000X

Figure 4-14: Equiaxed dimples covered by a light oxide (charging).



FAM 97994

MAG: 3000X

Figure 4-15: High magnification view of lightly oxidized equiaxed dimples showing particles (arrows) in several of the dimples.

MATERIAL

347 Stainless Steel
AMS 5646 Bar (Solution heat treated)

TEST DATA

TEST TYPE

Notched Tensile

TEST CONDITIONS

Crosshead Speed: 1.27 mm/min (0.05 in/min)

Atmosphere: Air

Temperature: Room Temperature

Test Direction: Longitudinal

TEST RESULTS

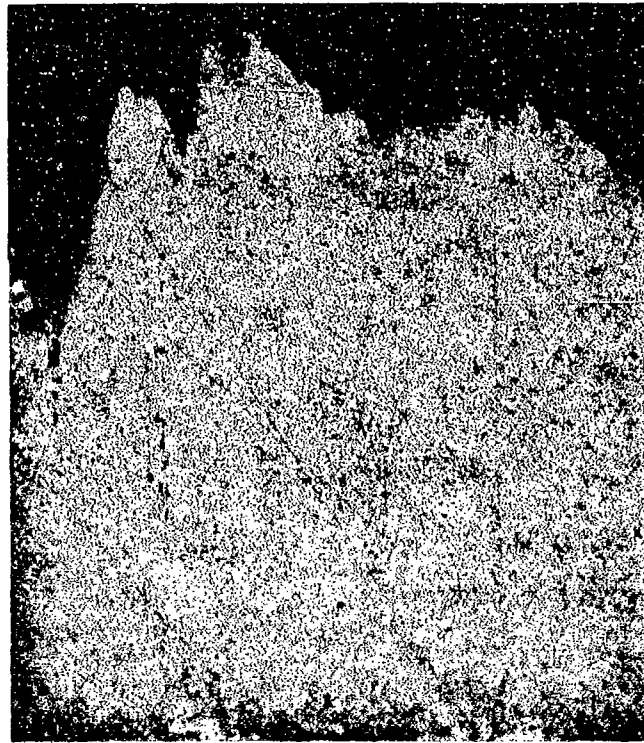
Ultimate Strength: 1078.3 MPa (156.4 ksi)



FAL 90293

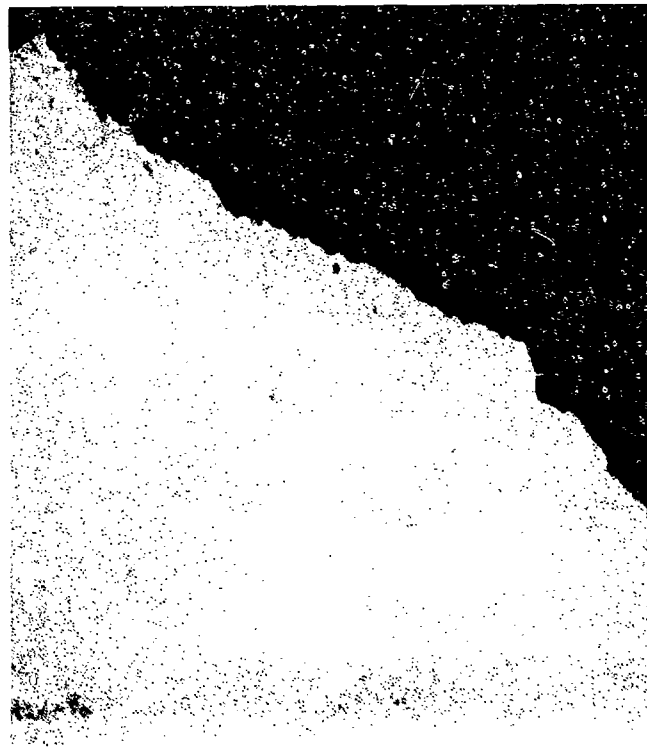
MAG: 10X

Figure 4-16: Test results and fractography of 347 SST room temperature notched tensile test. Three large secondary cracks radiate from the center of the specimen fracture surface.



FAM 100275

MAG: 200X

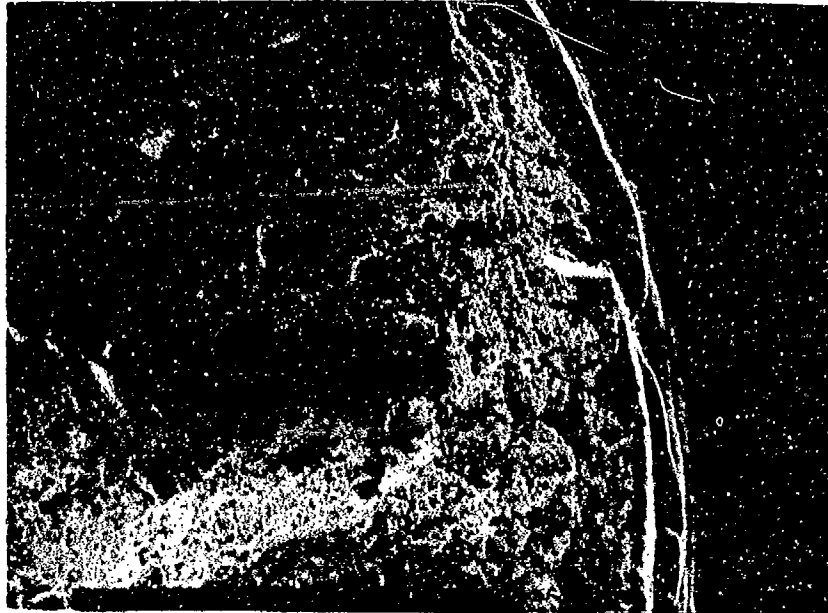


FAM 100276

MAG: 200X

FIGURE 4-17: Optical photomicrographs of the center (top) and edge (bottom) of the fracture.

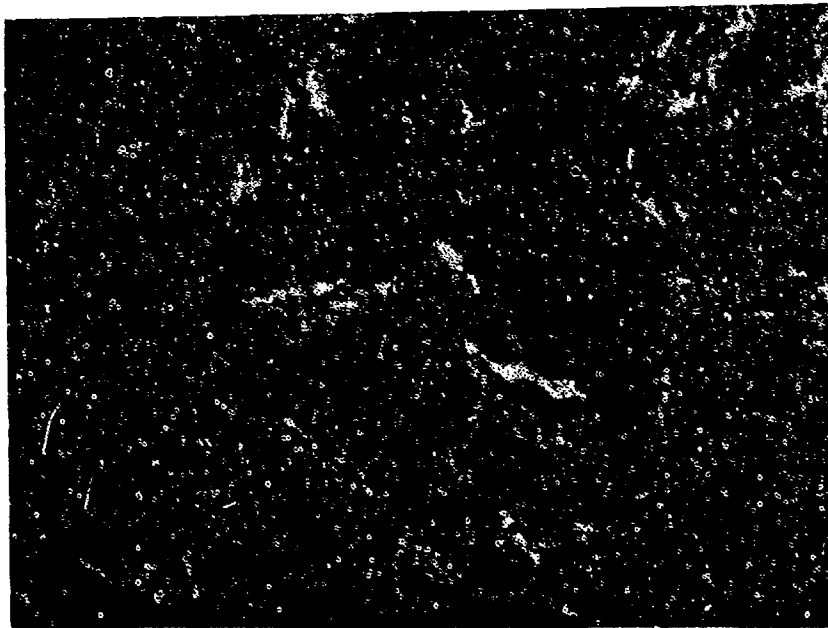
Etchant: Unetched



FAM 97984

MAG: 50X

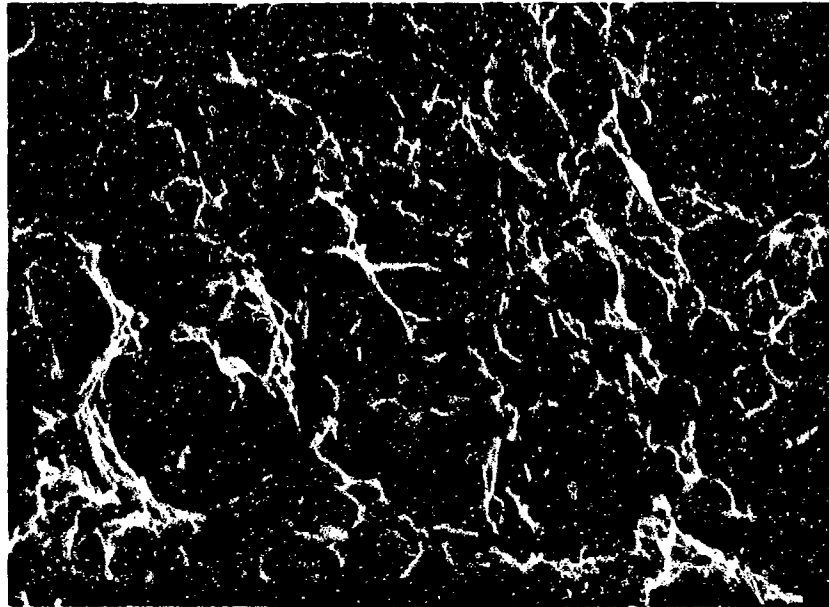
Figure 4-18: Low magnification photograph showing primary dimpled overstress area and a narrow shear lip along the surface of the specimen.



FAM 97990

MAG: 200X

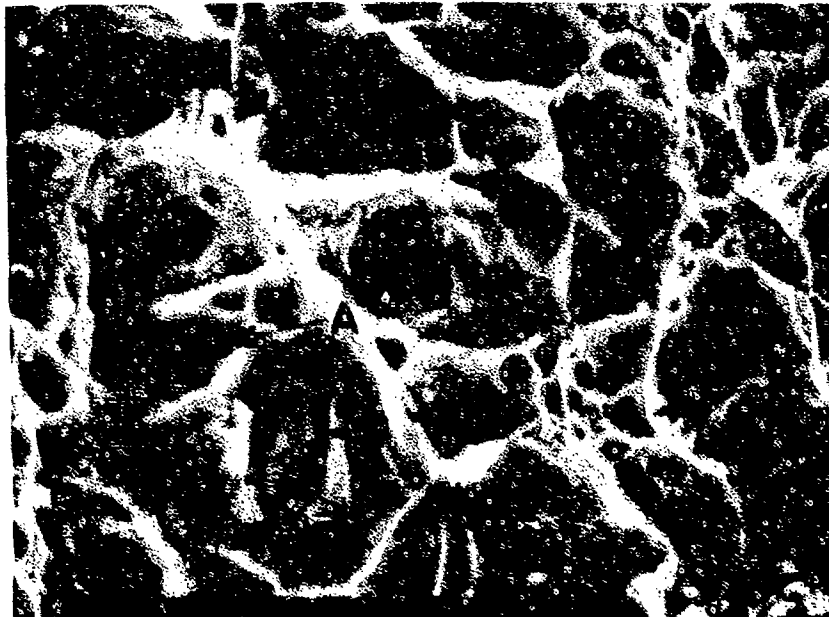
Figure 4-19: Close-up view of axial secondary crack in the primary dimpled overstress area.



FAM 97988

MAG: 1000X

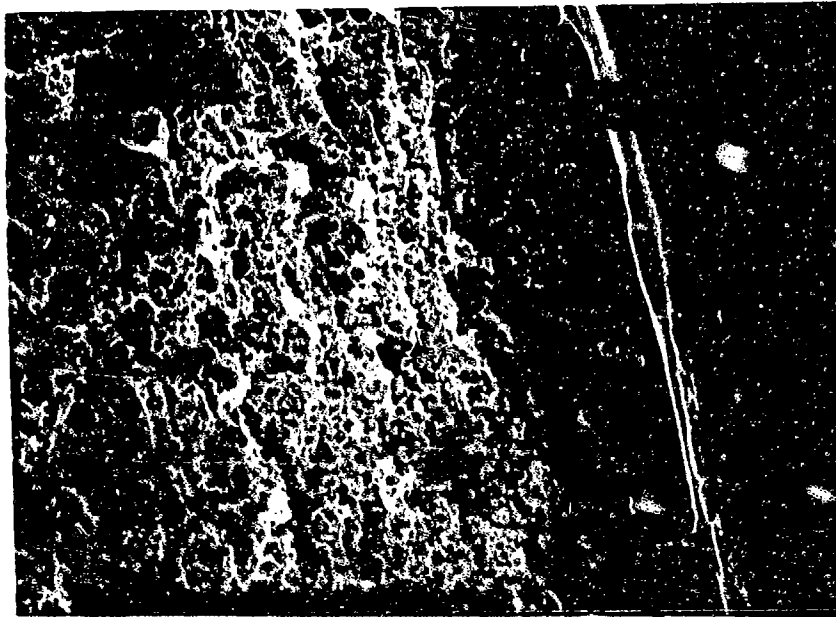
Figure 4-20: Equiaxed dimpled overstress in the primary fracture area.



FAM 97989

MAG: 3000X

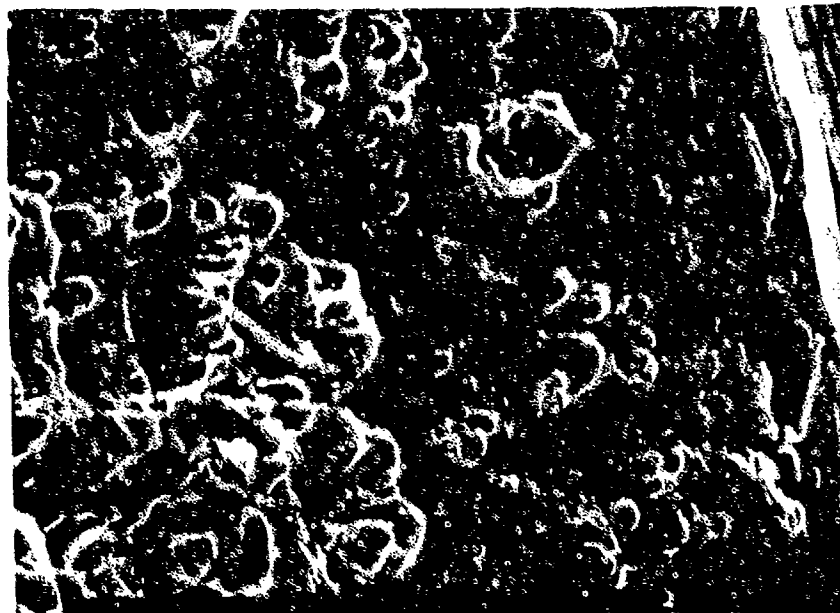
Figure 4-21: High magnification view of equiaxed dimpled overstress showing particles in the centers of the dimples (arrow A). Fine dimples are visible in patches (arrow B).



FAM 97985

MAG: 200X

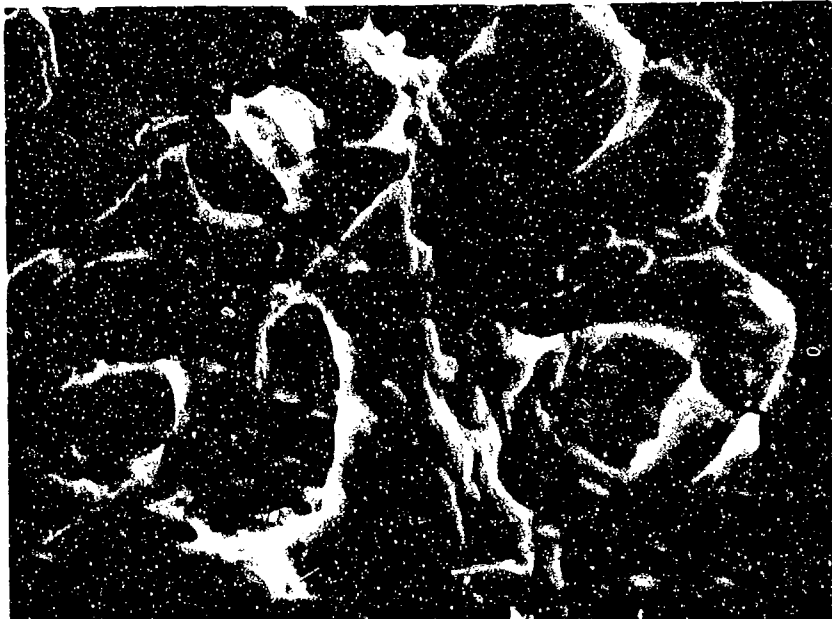
Figure 4-22: Close-up view showing the shear lip (arrow).



FAM 97986

MAG:1000X

Figure 4-23: Smeared shear dimples in the final overstress area.



FAM 97987

MAG: 3000X

Figure 4-24: High magnification photograph of the shear dimples shown in Figure 4-23.

MATERIAL

347 Stainless Steel
AMS 5646 Bar (Solution heat treated)

TEST DATA

TEST TYPE

Notched Tensile

TEST CONDITIONS

Crosshead Speed: 1.27 mm/min (0.05 in/min)

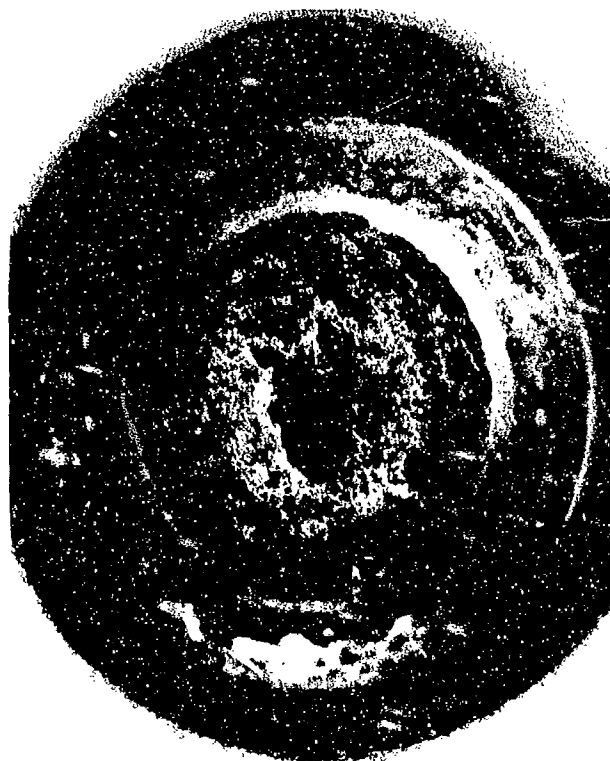
Atmosphere: Air

Temperature: 816°C (1500°F)

Test Direction: Longitudinal

TEST RESULTS

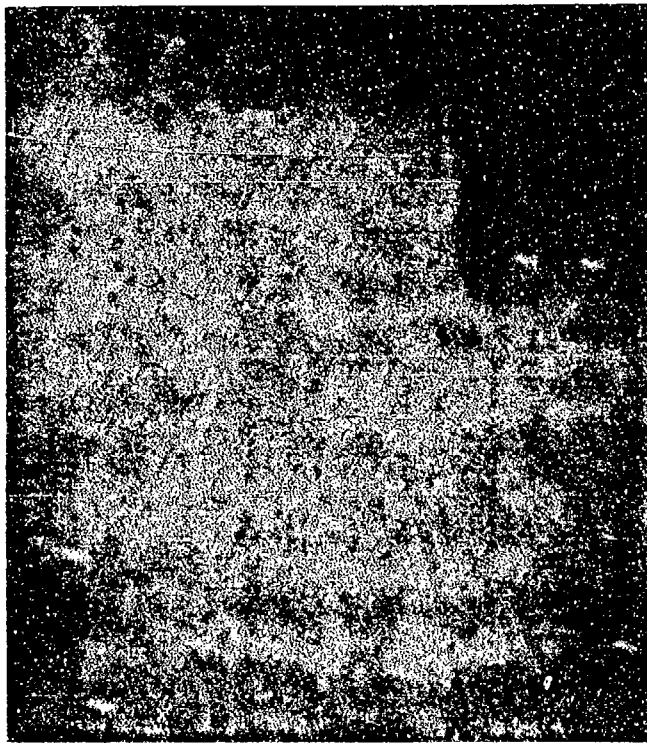
Ultimate Strength: 374.4 MPa (54.3 ksi)



FAL 90294

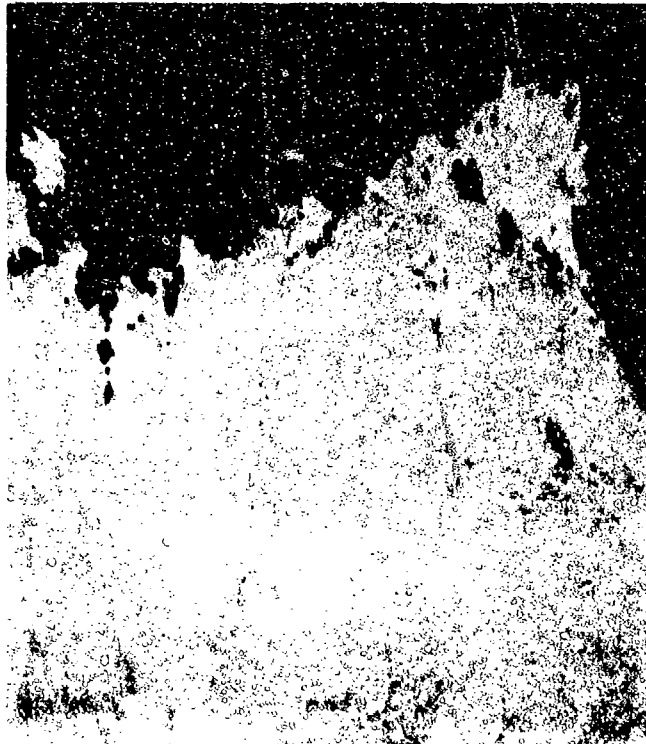
MAG: 10X

Figure 4-25: Test results and fractography of 347 SST 816°C (1500°F) notched tensile test. This specimen fracture exhibits more depth in the features than the room temperature specimen (Figure 4-16).



FAM 100273

MAG: 200X



FAM 100274

MAG: 200X

FIGURE 4-26: Optical photomicrographs of the center (top) and edge (bottom) of the fracture. This specimen exhibits more elongation and deeper voids at the fracture than the room temperature specimen. See Figure 4-17.

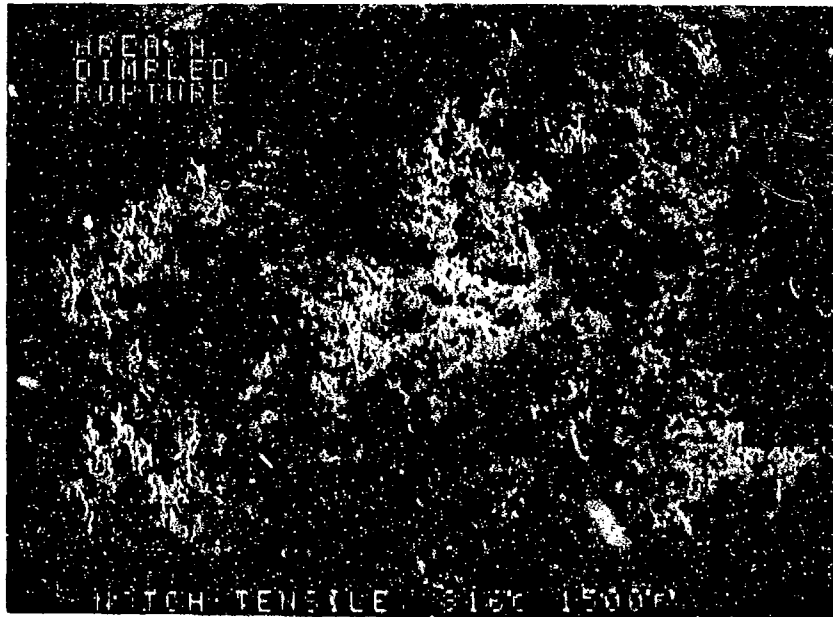
Etchant: Unetched



FAM 97995

MAG: 15X

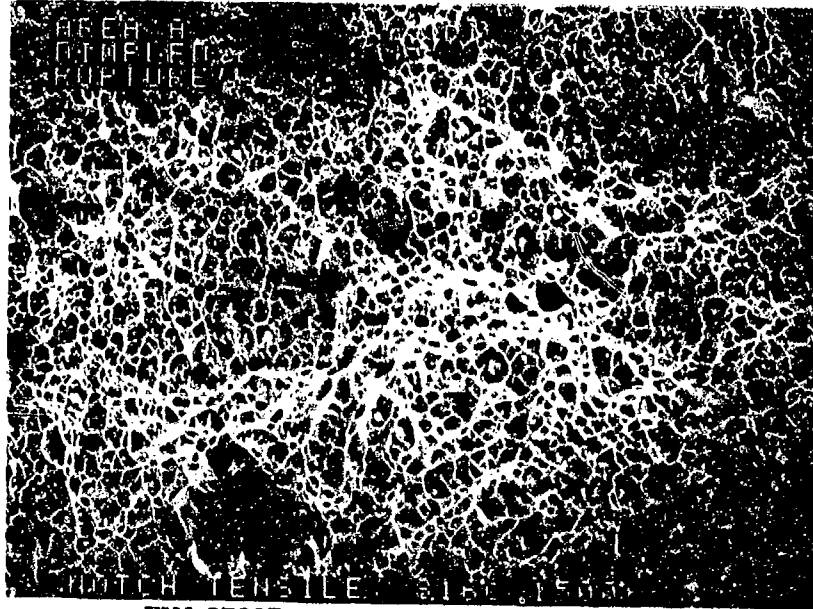
Figure 4-27: Low magnification view showing dimpled overstress (A), shear (B) and axial shear (C).



FAM 97996

MAG: 50X

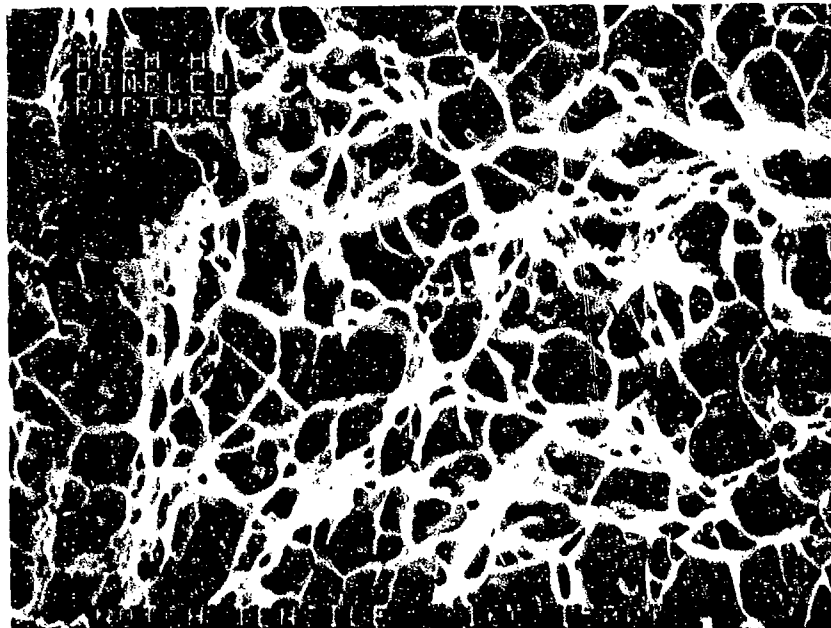
Figure 4-28: View of area A showing fine dimpled overstress.



FAM 97997

MAG: 200X

Figure 4-29: Higher magnification photograph of area A, showing fine equiaxed dimples.



FAM 97998

MAG: 1000X

Figure 4-30: High magnification view of area A showing equiaxed dimples and associated particles (arrows). The fracture surface is charging, indicating that it is lightly oxidized.

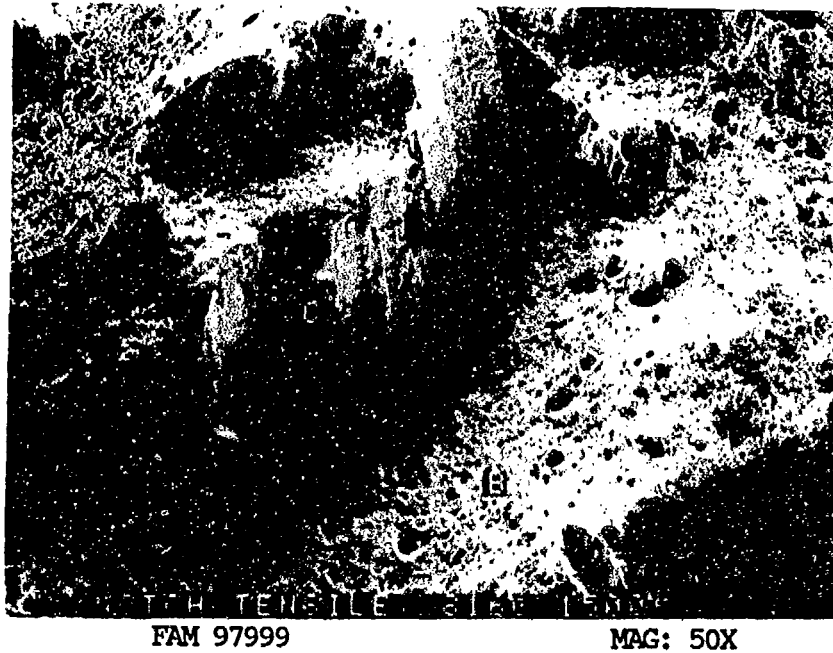


Figure 4-31: Higher magnification photograph of shear areas B and C.

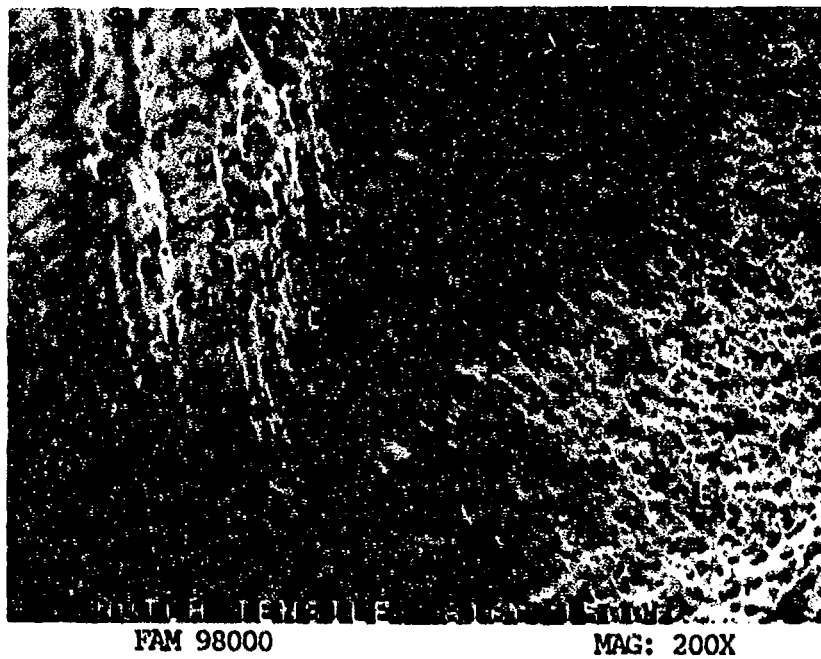
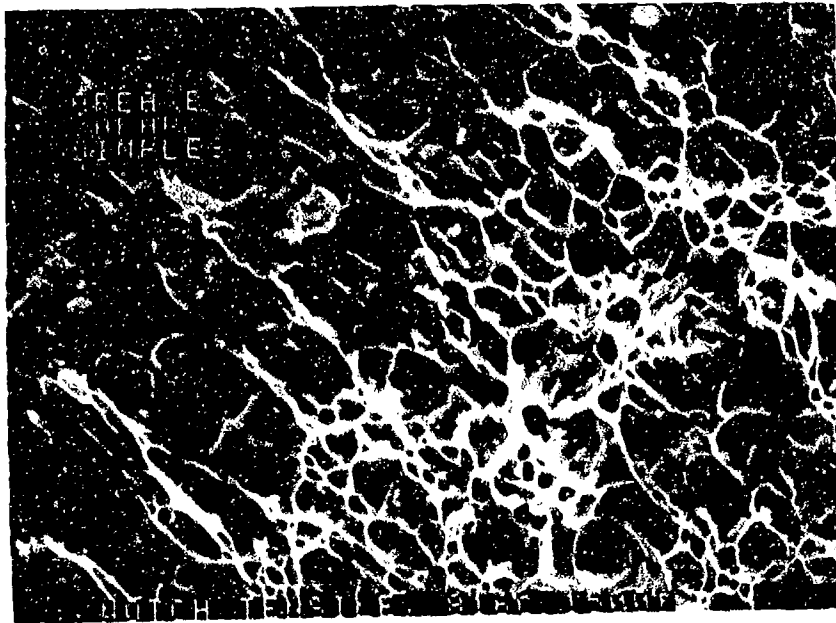


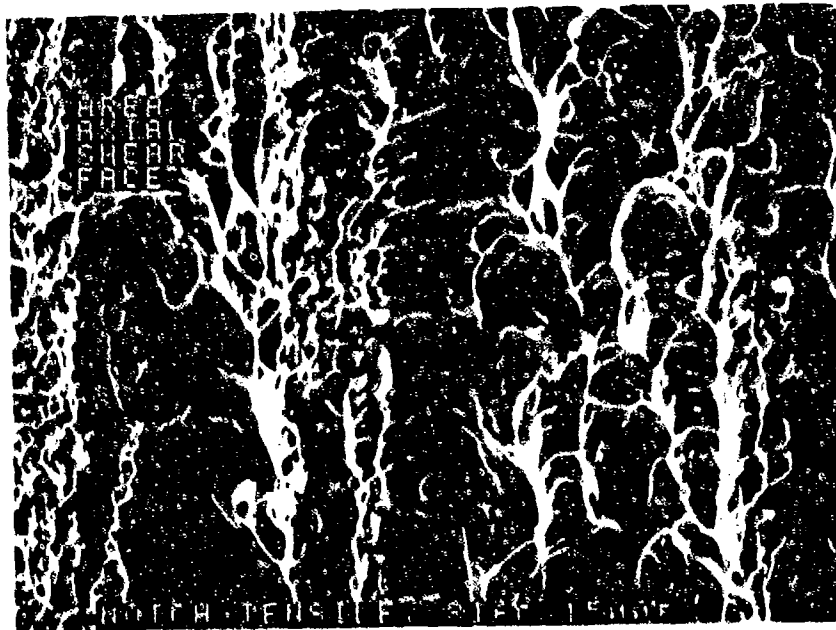
Figure 4-32: Higher magnification photograph of area shown in Figure 4-31. Shear areas B and C are visible.



FAM 98001

MAG: 1000X

Figure 4-33: High magnification view of area B showing lightly oxidized shear dimples. Arrows show the directions of relative motion.



FAM 98002

MAG: 1000X

Figure 4-34: High magnification view of area C, showing axial shear face.

MATERIAL

347 Stainless Steel
AMS 5646 Bar (Solution heat treated)

TEST DATA

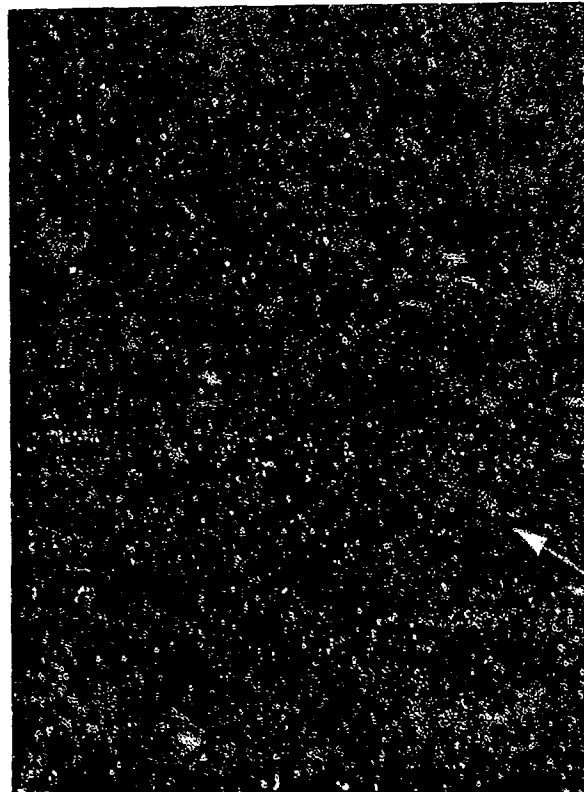
TEST TYPE
Smooth HCF

TEST CONDITIONS

Stress: 275.8 MPa (40.0 ksi)/-275.8 MPa (-40.0 ksi) DNF
344.7 MPa (50.0 ksi)/-344.7 MPa (-50.0 ksi) DNF
413.7 MPa (60.0 ksi)/-413.7 MPa (-60.0 ksi)
Stress Ratio: -1
Frequency: 1800 cpm
Atmosphere: Air
Temperature: Room Temperature
Test Direction: Longitudinal

TEST RESULTS

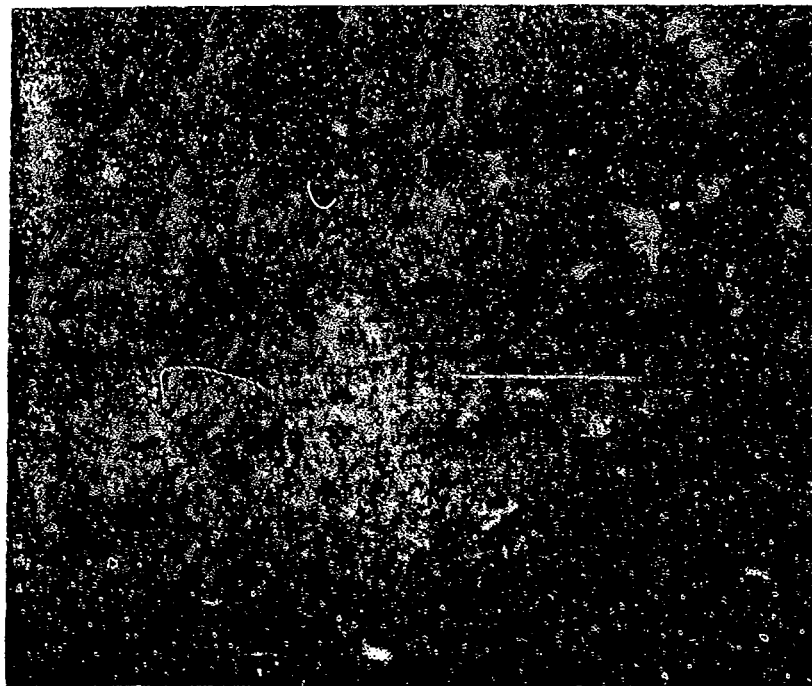
Cycles to Fracture: 1.08×10^5 (DNF), 3.55×10^5 (DNF), 3.2×10^4



FAL 93952

MAG: 15X

Figure 4-35: Test results and fractography of 347 SST room temperature smooth HCF test. The origin area is shown by an arrow.



FAM 98953

MAG: 100X

FIGURE 4-36: Optical photomicrograph of a metallographic cross section near the fracture surface. No grain elongation or strain lines are visible indicating low stress.

Etchant: 10% Oxalic acid electrolytic

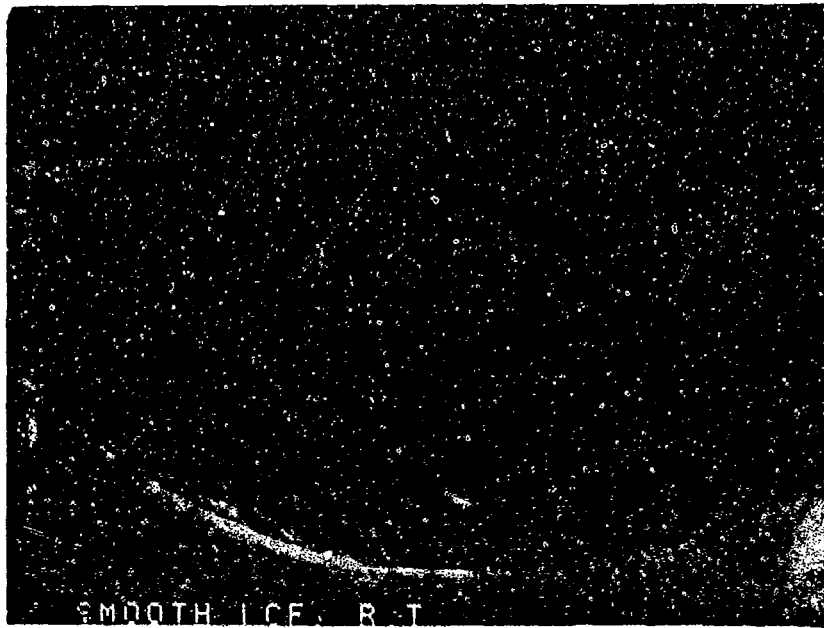


FIGURE 4-37: Low magnification photograph showing features radiating from the origin area (bracket).

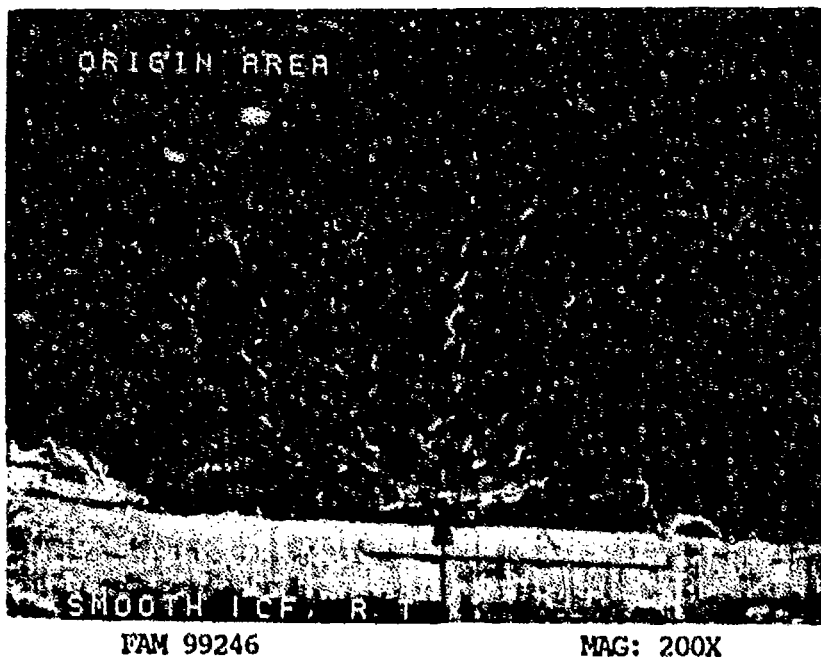
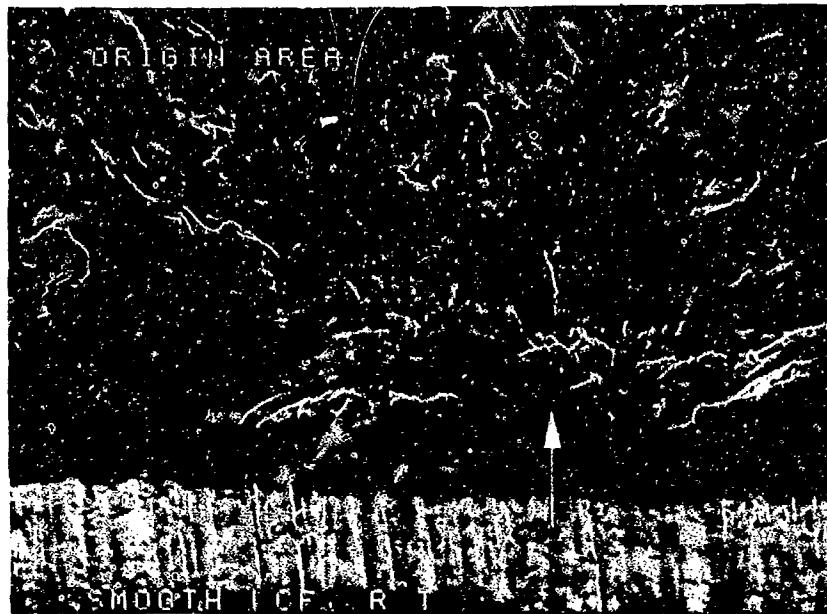


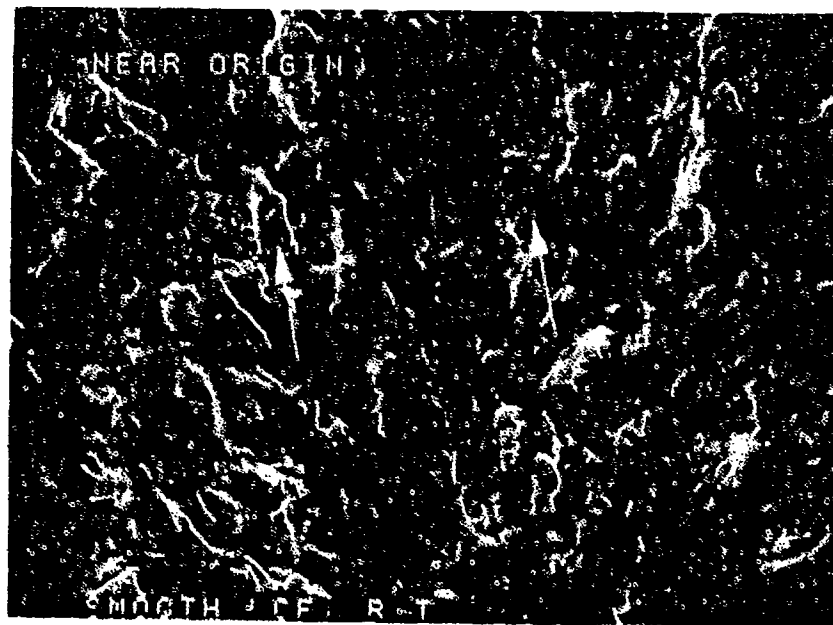
FIGURE 4-38: Fatigue features radiating from the origin (arrow). The dark patch at the surface (bracket) is a smear that occurred after the fracture.



FAM 99247

MAG: 1000X

FIGURE 4-39: Post-fracture smear at the fatigue origin. The features on the fracture were distorted when the smear occurred. Machining lines are visible on the surface adjacent to the fracture. The localized origin is indicated by an arrow.



FAM 99248

MAG: 1000X

FIGURE 4-40: Fatigue features near the origin area. Individual striations are barely resolvable (arrows).

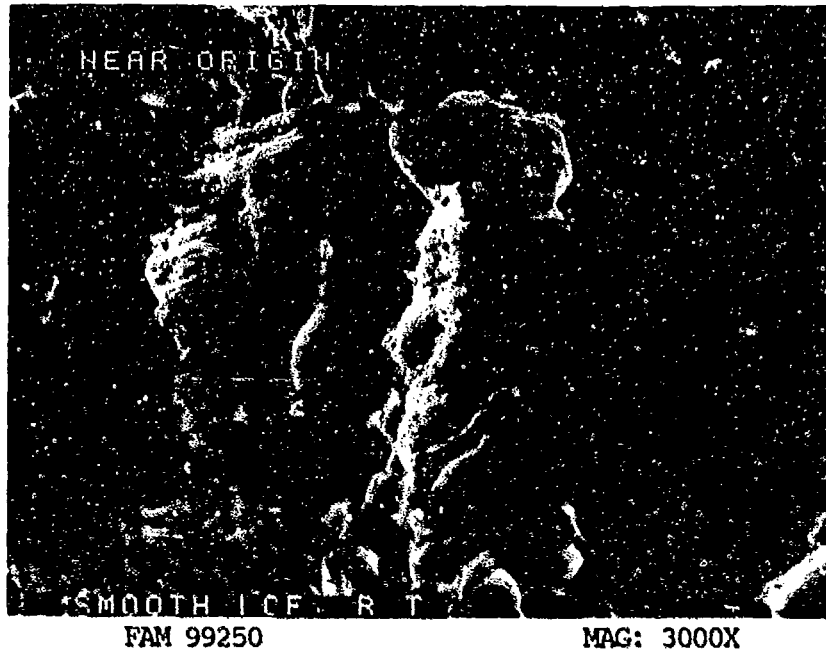


FIGURE 4-41: Fine fatigue striations and crack-like striations near the origin area. The fracture propagated from bottom to top of the photograph.

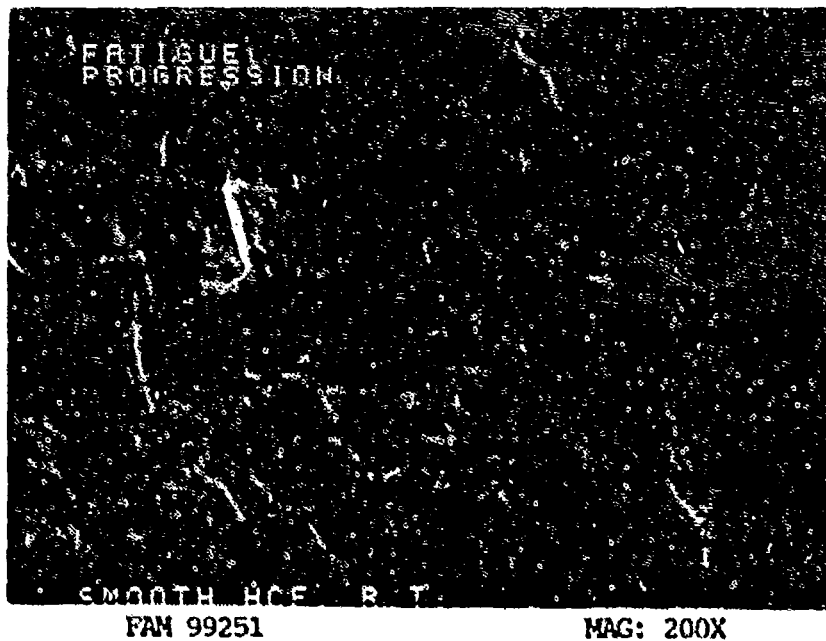


FIGURE 4-42: Flat fatigue progression area near the center of the specimen. Secondary cracking parallel to the propagation direction is also present.

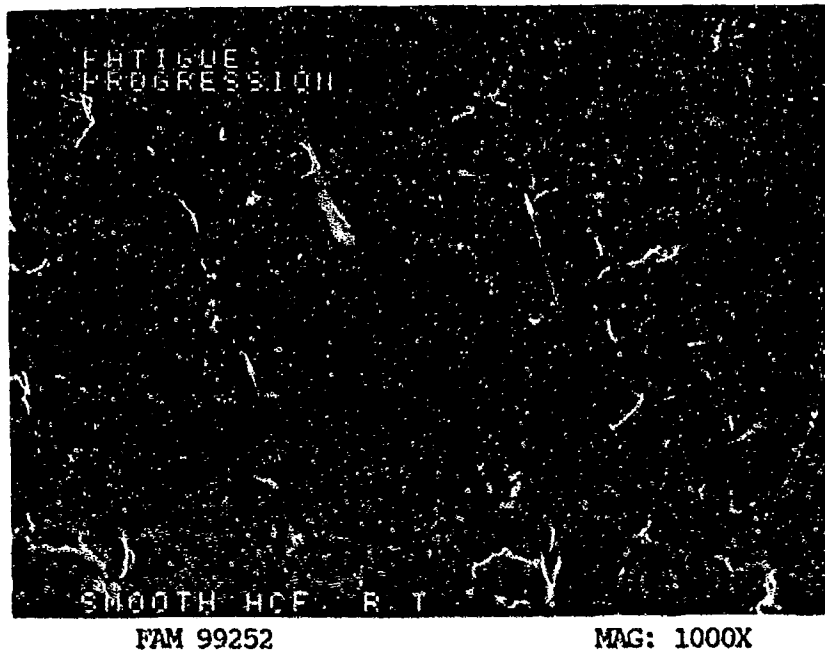


FIGURE 4-43: Coarser fatigue striations in the fatigue progression area (Figure 4-42). Small voids (arrows) (probably void coalescence) are interspersed in the fracture surface.

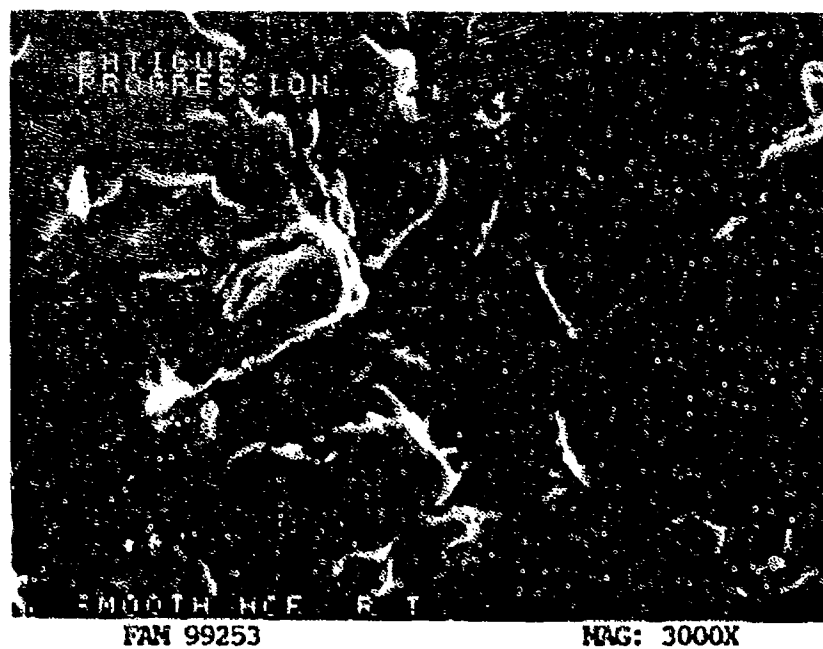


FIGURE 4-44: Higher magnification photograph of striations in the fatigue progression zone. See Figure 4-43.

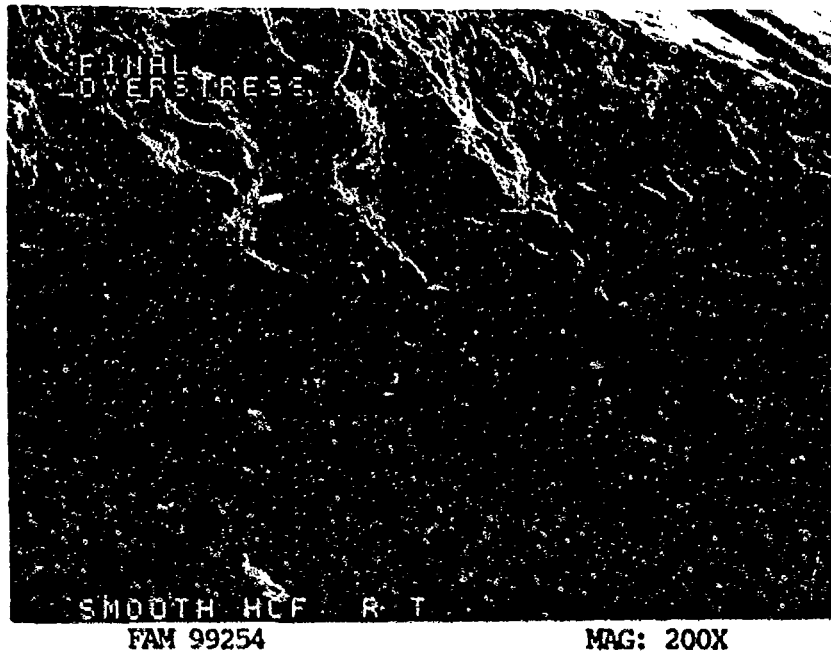


FIGURE 4-45: Final overstress area exhibiting a mixture of equiaxed dimples, shear dimples and cleavage.

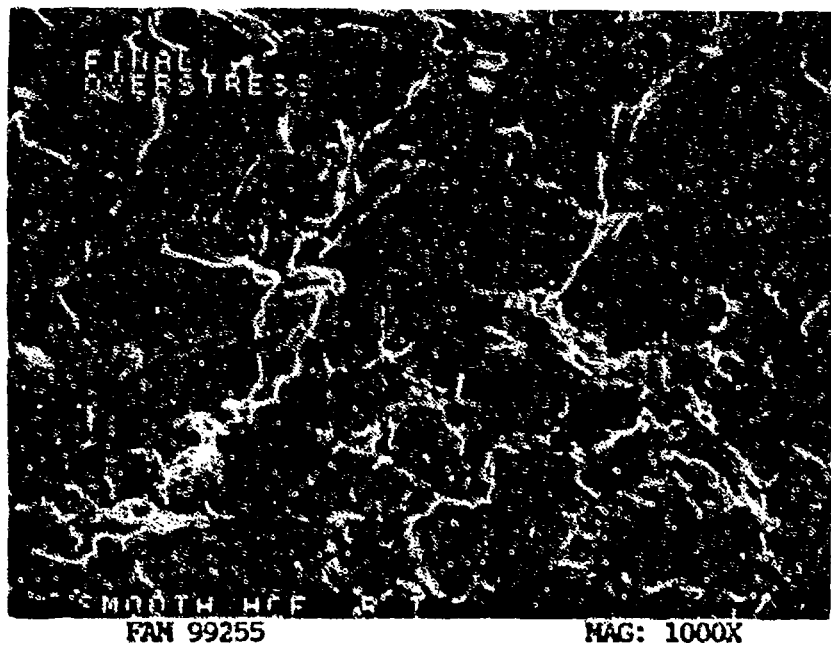


FIGURE 4-46: Dimpled overstress and tearing cleavage features (top of photograph) in the final overstress area.

MATERIAL

347 Stainless Steel
AMS 5646 Bar (Solution heat treated)

TEST DATA

TEST TYPE

Smooth HCF

TEST CONDITIONS

Stress: 344.7 MPa (50.0 ksi)/-344.7 MPa (-50.0 ksi)

Stress Ratio: -1

Frequency: 1800 cpm

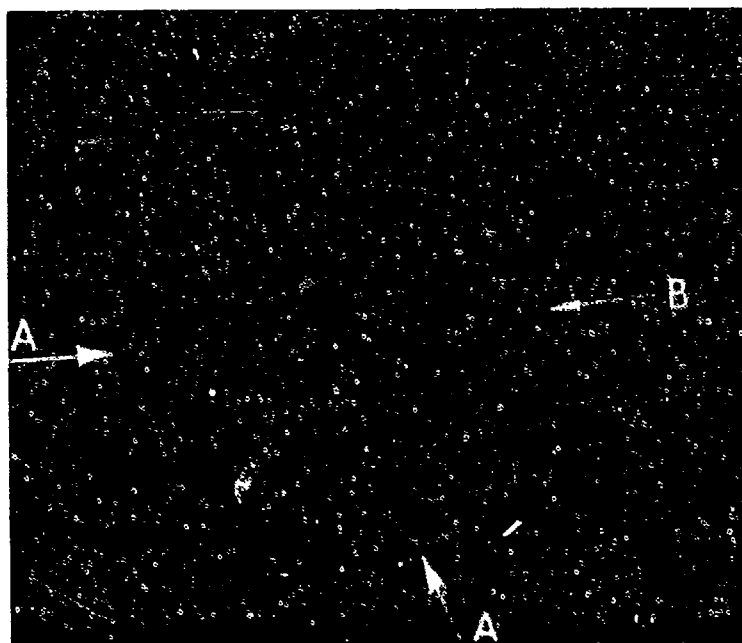
Atmosphere: Air

Temperature: 427°C (800°F)

Test Direction: Longitudinal

TEST RESULTS

Cycles to Fracture: 20,500



FAL 93951

MAG: 15X

Figure 4-47: Test results and fractography of 347 SST 427°C (800°F) smooth HCF test. The fracture propagated from two origin areas (arrows A). Arrest marks are visible near the end of the fatigue thumbnail (arrows B).

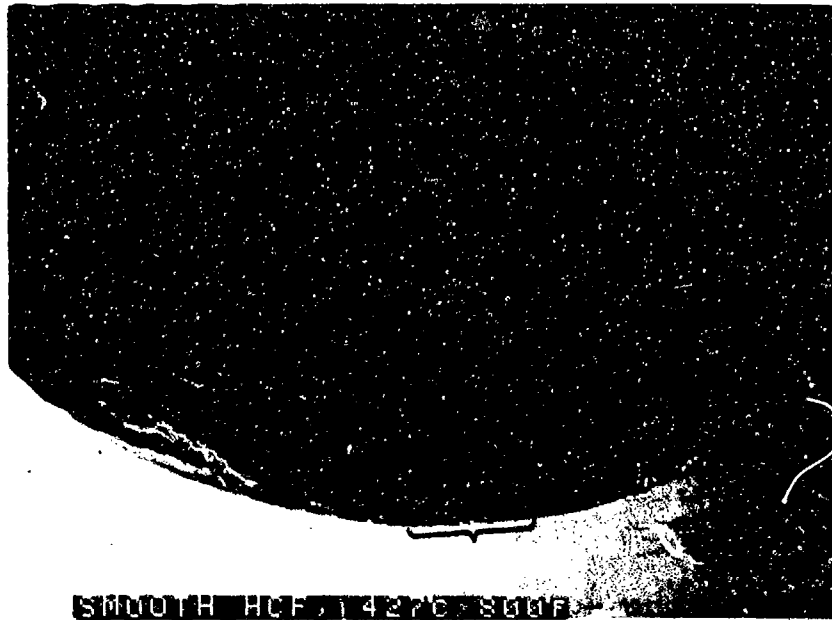


FAM 100272

MAG: 200X

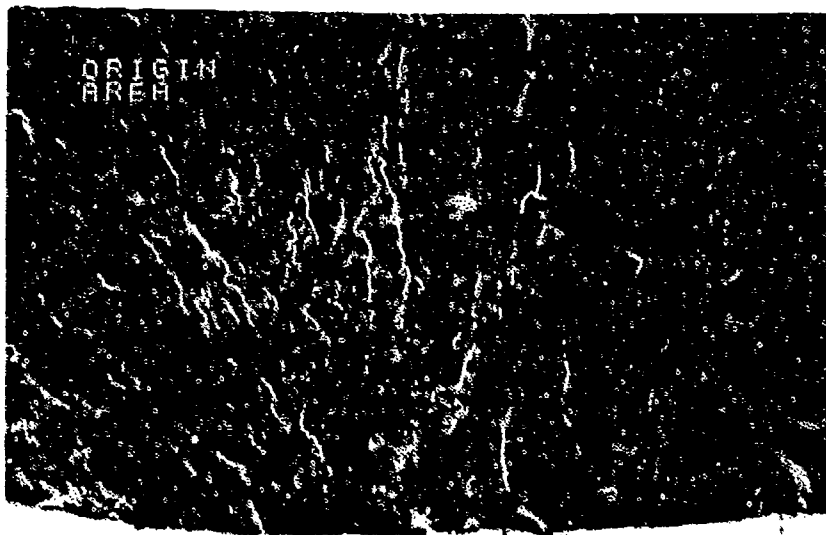
FIGURE 4-48: Optical photomicrograph showing the fatigue progression portion of the fracture on a plane perpendicular to the stress axis. The fracture path is predominantly transgranular.

Etchant: Unetched



SMOOTH HCF 4276 8100F
FAM 99256 MAG: 50X

FIGURE 4-49: Low magnification photograph showing features radiating from a diffuse origin area (bracket).



SMOOTH HCF 4276 8100F
FAM 99257 MAG: 200X

FIGURE 4-50: Fatigue features radiating from the origin. A small fatigue step, tear ridge (arrow) separates two localized origins that are close together on the surface of the specimen.

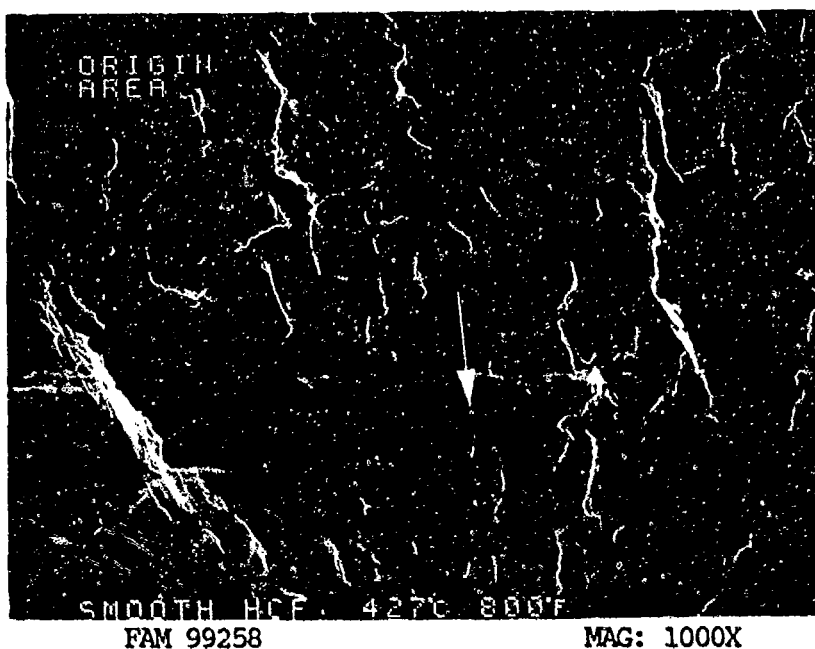


FIGURE 4-51: Striations and crack like striations near the origin area. Arrow perpendicular to the striations points back towards the origin.

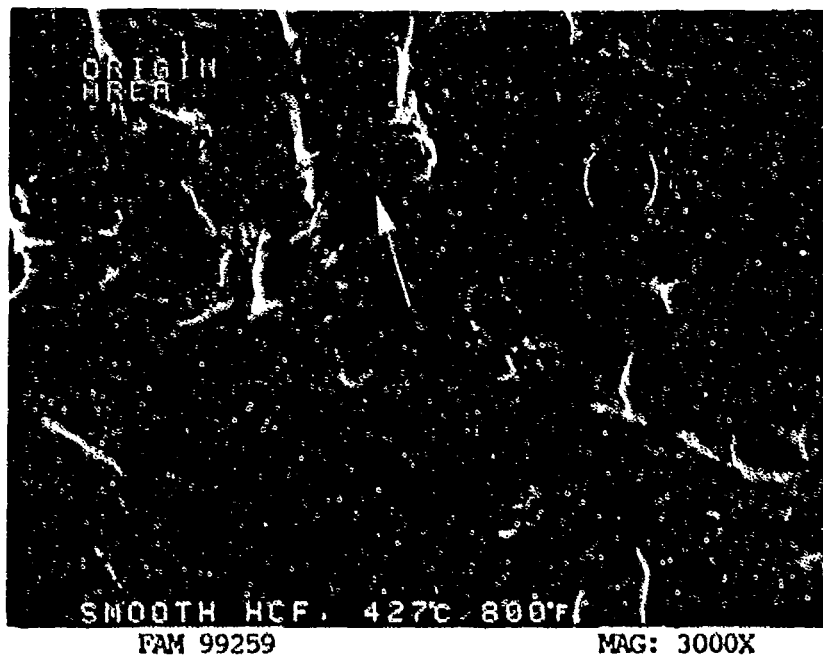


FIGURE 4-52: Fine fatigue striations and crack like striations (arrow) near the origin. Bracket contains five striations.

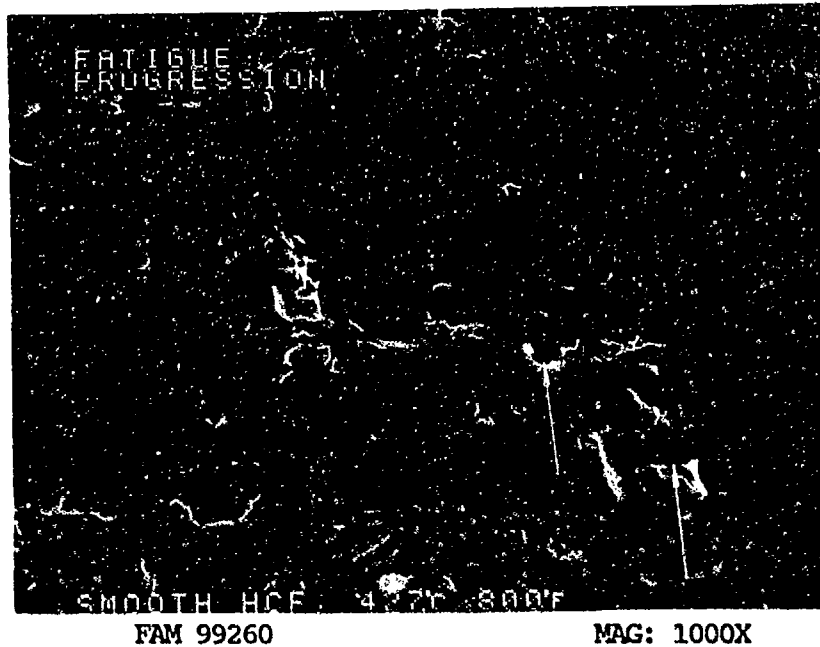


FIGURE 53: Relatively smooth fatigue striations in the fatigue progression zone near the center of the specimen. Small voids are visible (arrows).

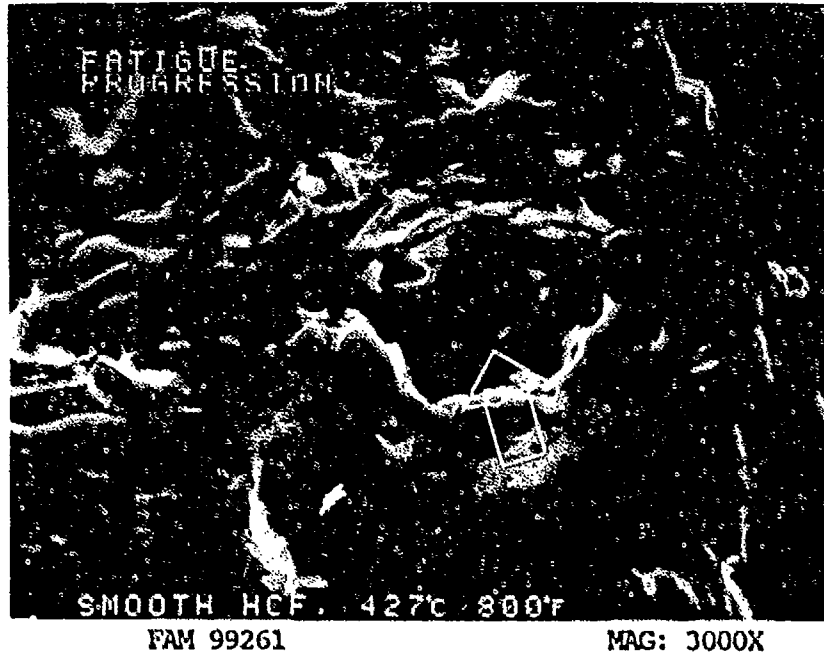


FIGURE 4-54: Higher magnification view of the flat fatigue progression area near the center of the specimen. The discontinuity in the striations (arrow) was probably caused by a carbide.

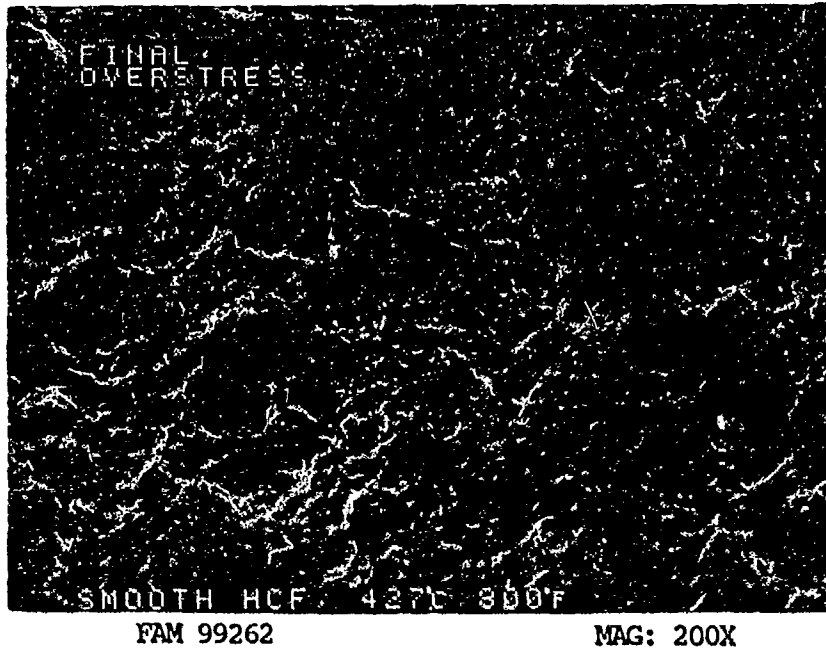


FIGURE 4-55: Final overstress area.

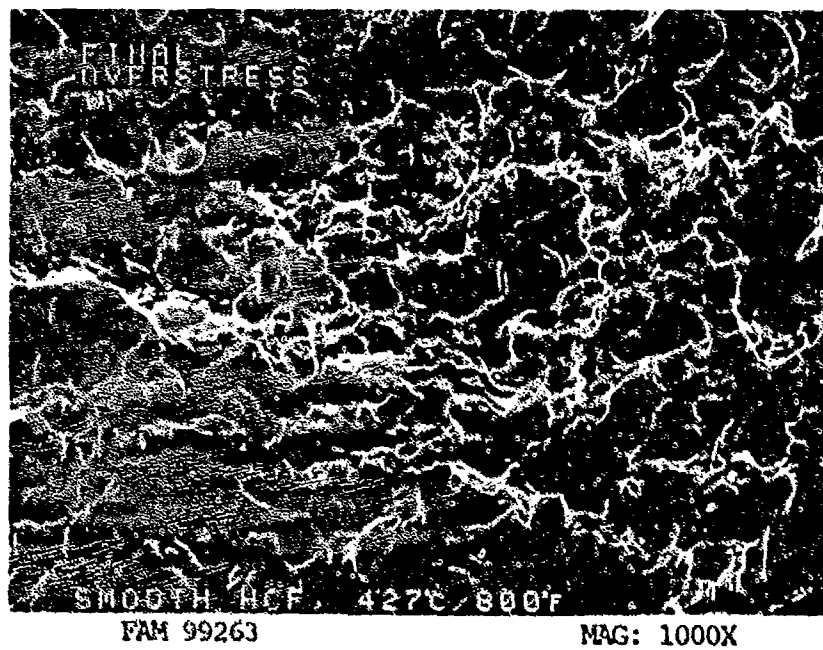


FIGURE 4-56: Dimpled overstress in the final overstress area.

MATERIAL

347 Stainless Steel
AMS 5646 Bar (Solution heat treated)

TEST DATA

TEST TYPE
Smooth HCF

TEST CONDITIONS

Stress: 137.9 MPa (20.0 ksi)/-137.9 MPa (-20.0 ksi) DNF*
172.4 MPa (25.0 ksi)/-172.4 MPa (-25.0 ksi) DNF
206.8 MPa (30.0 ksi)/-206.8 MPa (-30.0 ksi)
Stress Ratio: -1
Frequency: 1800 cpm
Atmosphere: Air
Temperature: 816°C (1500°F)
Test Direction: Longitudinal

TEST RESULTS

Cycles to Fracture: 1.09×10^5 (DNF), 1.0×10^5 (DNF), 1.07×10^5

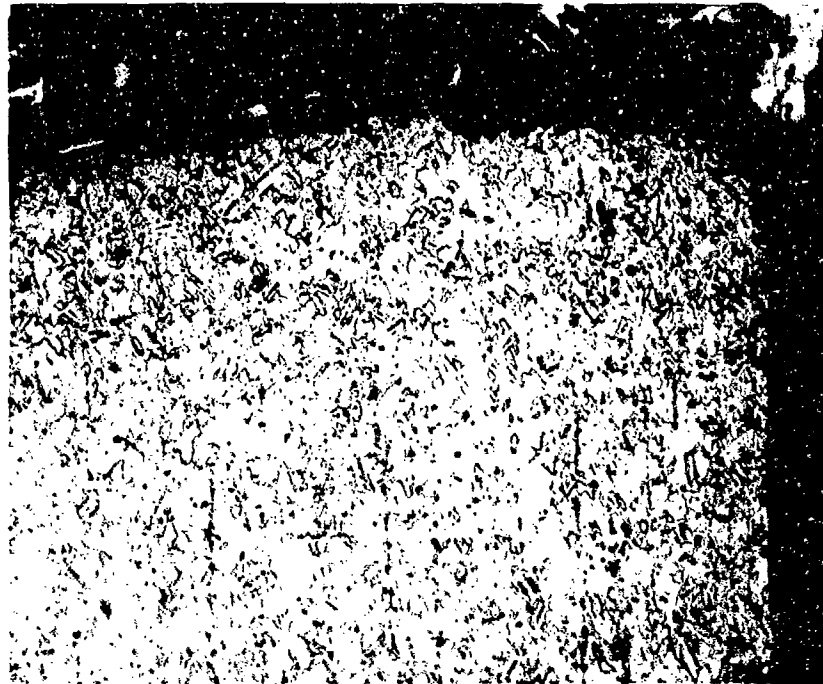
* Did Not Fracture



FAL 93953

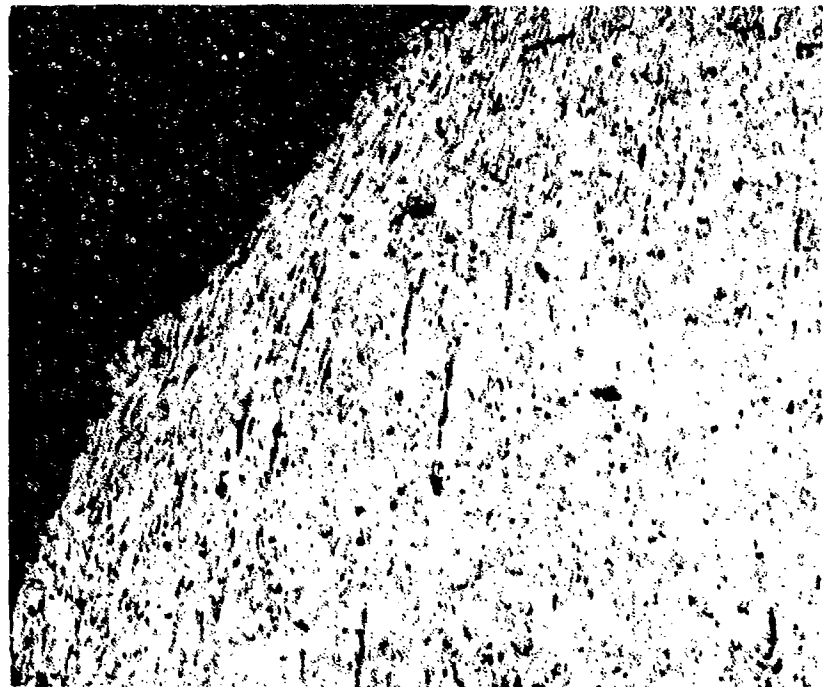
MAG: 15X

Figure 4-57: Test results and fractography of 347 SST 816°C (1500°F) smooth HCF test. Features can be seen radiating from the origin area (arrow). Arrest marks are visible near the end of the fatigue thumbnail (bracket). The fatigue extends over 80% of the fracture surface.



FAM 100475

MAG: 200X



FAM 100476

MAG: 200X

FIGURE 4-58: Optical photomicrographs of a metallographic cross section through the fracture surface. The fatigue progression is flat (transgranular) and occurred on a plane perpendicular to the stress axis (top). Grain elongation is visible in the final overstress area (bottom).

Etchant: 10% Oxalic acid electrolytic

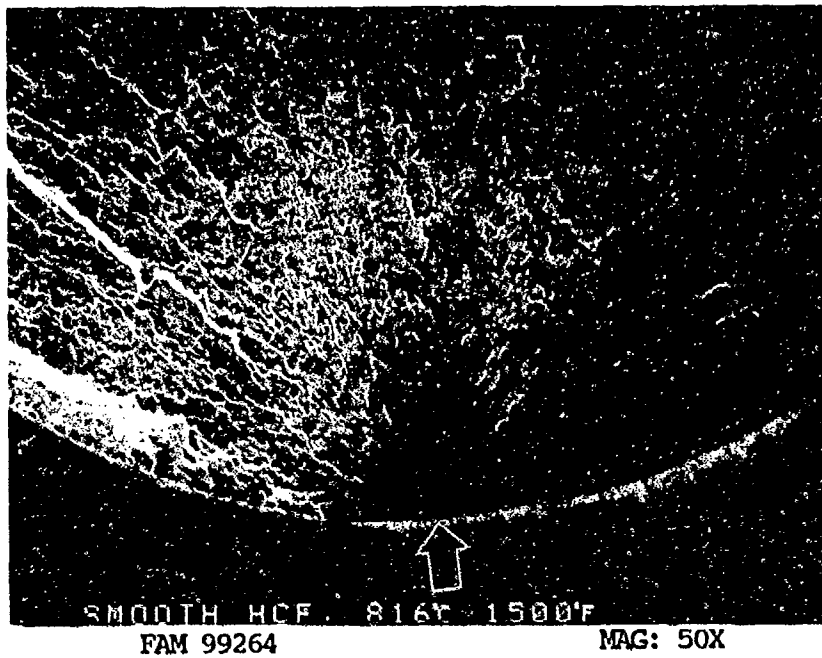


FIGURE 4-59: Low magnification photograph showing features radiating from a localized origin area (arrow, bottom center).

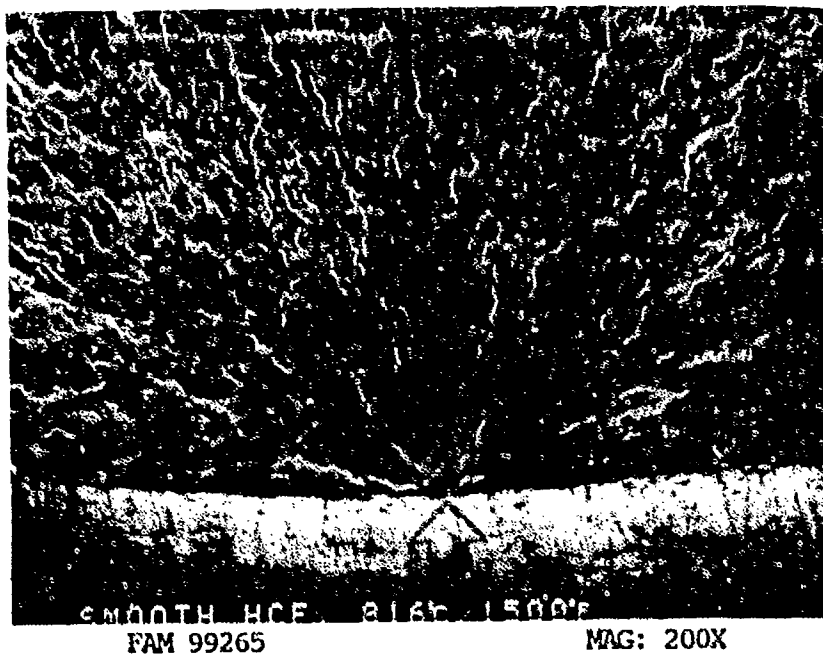


FIGURE 4-60: Fatigue features radiating from the origin (arrow).

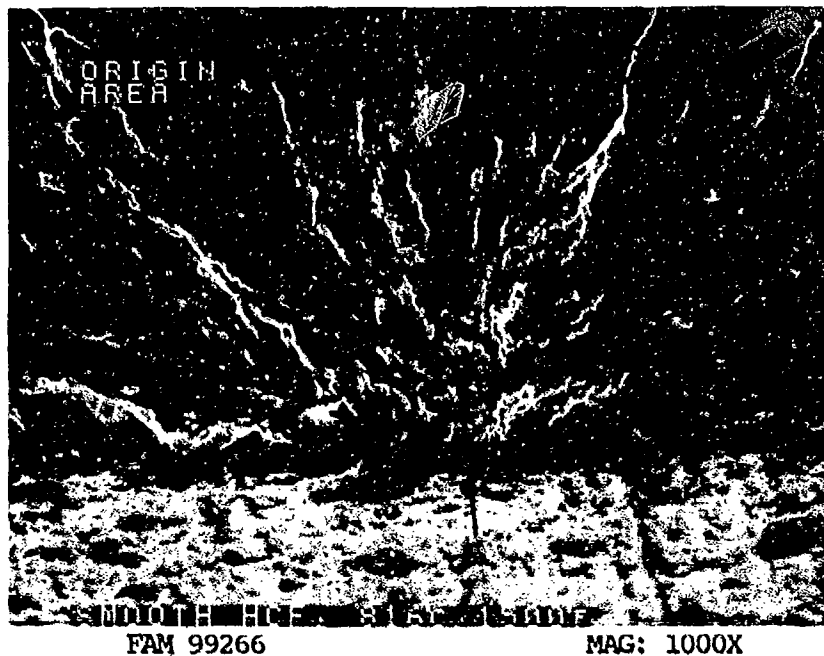


FIGURE 4-61: Higher magnification photograph of the localized origin, Figure 4-60, showing moderate oxidation and progression from a possible subsurface anomaly (arrow).

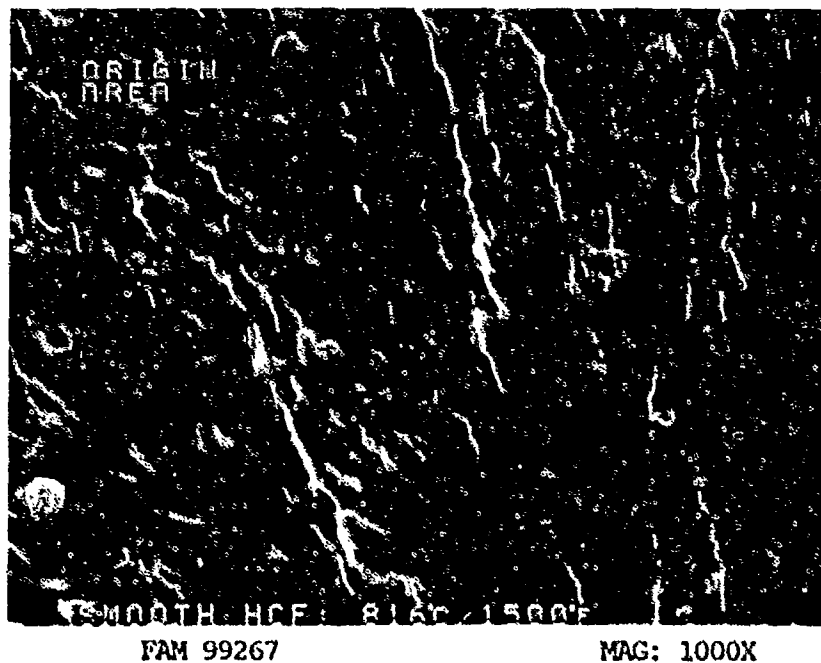


FIGURE 4-62: Flat oxidized features adjacent to the localized origin.

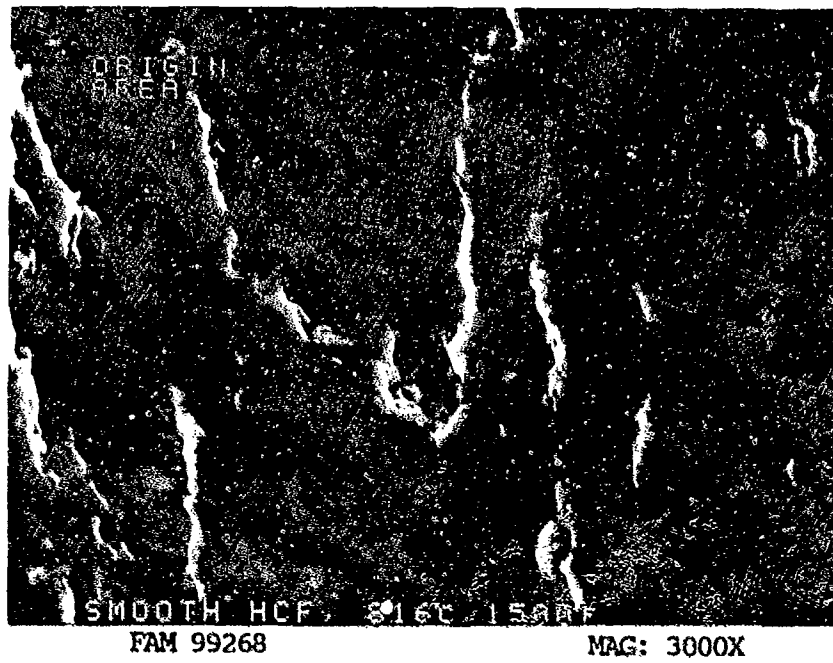


FIGURE 4-63: Heavily oxidized features near the origin area. Individual fatigue striations are not resolvable.

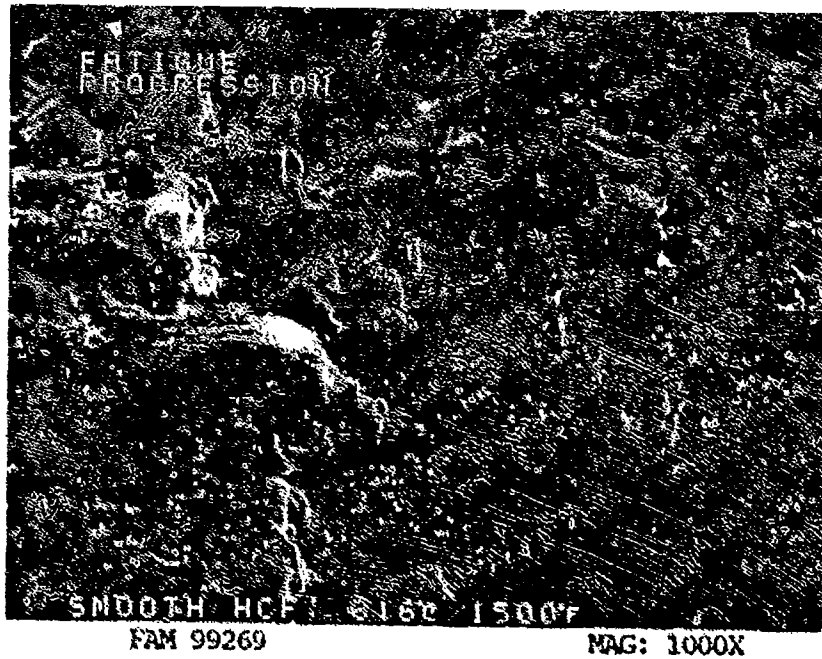


FIGURE 4-64: Relatively coarse striations and crack-like striations in the fatigue progression zone near the center of the specimen.

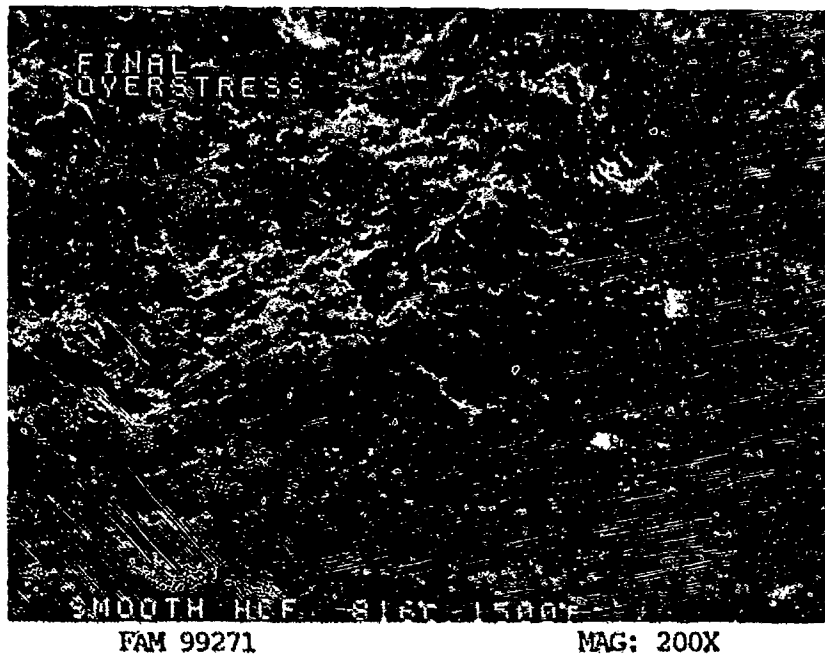


FIGURE 4-65: Dimpled overstress and void coalescence in the final overstress area.

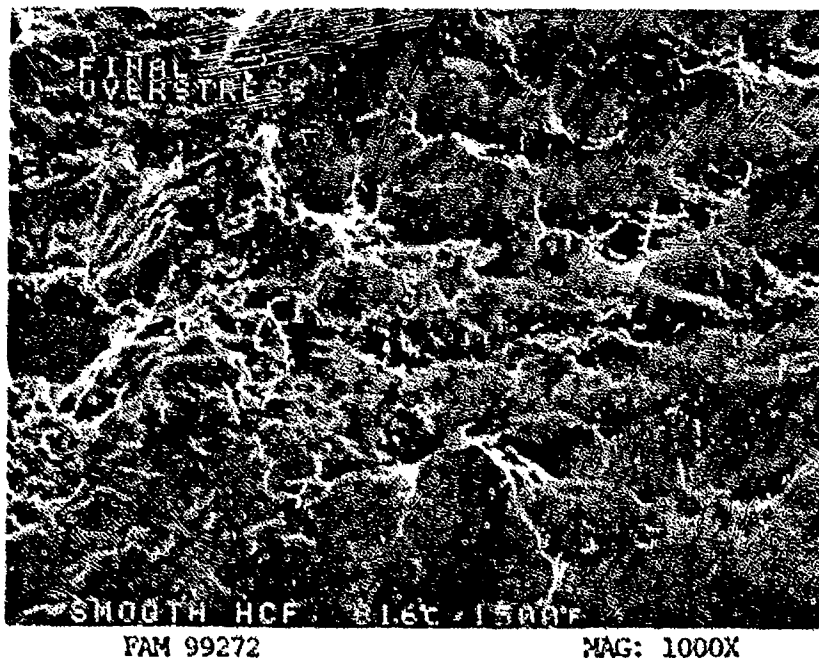


FIGURE 4-66: Oxidized, smeared and dimpled overstress in the final overstress area.

SERVICE FAILURE

FRACTURE MODE High Cycle Fatigue (reverse-bending)

PART NAME Fuel Manifold Bracket

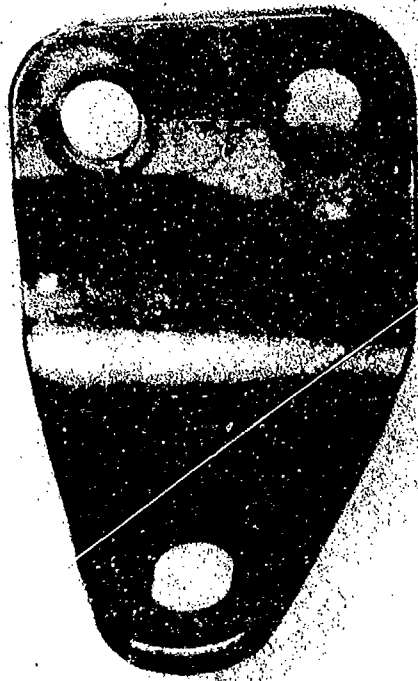
OPERATION DATA Bracket operated in accelerated mission test (AMT). It was subjected to low nominal stress with high vibratory stress.

PART TIME 282.4 hours (231 operation cycles)

	<u>REQUIRED</u>	<u>ACTUAL</u>
MAT'L		
BASE	<u>AISI 347 Stainless Steel</u>	<u>confirmed</u>
OTHER	<u>-</u>	<u>-</u>
HARDNESS	<u>No Requirement</u>	<u>HRB 89-92*</u>
GRAIN SIZE	<u>No Requirement</u>	<u>-</u>
DIMENSIONAL	<u>Thickness: 0.071-0.085 inch</u>	<u>0.077-0.078 inch</u>

* Diamond pyramid hardness (DPH) conversions.

SUMMARY: The bracket fractured by high cycle fatigue (HCF) propagating from multiple origins on both the inboard and outboard surfaces adjacent to an attachment bolt hole. The fracture surface exhibited a clearly defined shear lip near the center of the sample. This is indicative of reverse-bending loading. The lack of a large final overstress area indicates the nominal stress was low. The location of the origins was determined by the bolt head contact circle. No material or microstructural anomalies were found.



FAL 91683

MAG: 2X

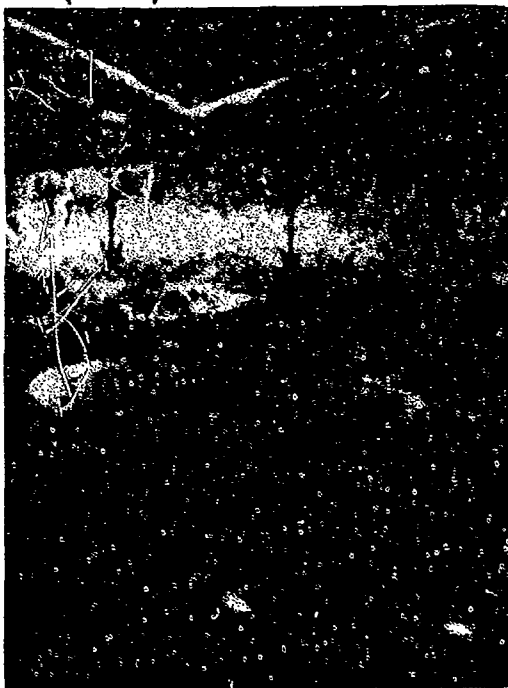


FAL 91684

MAG: 3X

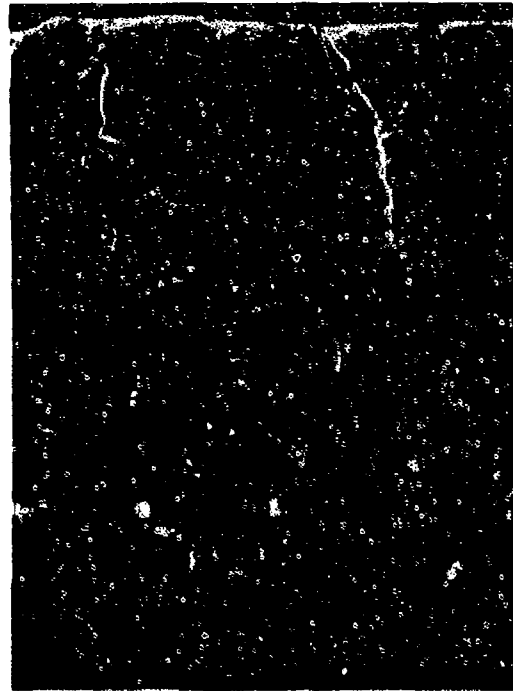
FIGURE 4-67: Overall photograph of the fractured bracket from the outboard side. The primary origins were located adjacent to one of the attachment bolt holes (arrow).

FIGURE 4-68: Overall photograph of the fracture surface showing a well defined shear lip near the center (arrows).



FAL 93320

MAG: 10X



FAL 93319

MAG: 300X

FIGURE 4-69: Low magnification SEM photograph of the primary origin area. The shear lip is shown by arrows.

FIGURE 4-70: Close-up SEM photograph of origin area on the inboard side of the bracket. Small steps indicate origin locations.

A-286 (High Ni Stainless Steel)

Material Description

A-286 is an precipitation hardened iron-base alloy with high toughness and good oxidation resistance to 1500 F (continuous) and 1800 F (intermittent). Primary applications in the aerospace industry include turbine disks, vanes, blades, shafts, cases and combustor parts. The alloy is strengthened by heat treating at 1325 F for 16 hours precipitating Ni₃(Al, Ti), gamma prime. The strength of the material can be further increased by cold working between the solution anneal and precipitation heat treatment.

The material used in this study was AMS 5525 heat treated to AMS 2759/3 with a required hardness of HRC 24-35. The typical room temperature mechanical properties for AMS 5525 are as follows. The strength increases with increasing sheet thickness and is generally higher for bar stock than sheet.

Ultimate Tensile Strength:	105-140 ksi	
0.2% Yield Strength:	85-95 ksi	
Percent Elongation:	4-15% min	
Percent Reduction in Area:	15-20% min (bars)	
	<u>Required</u>	<u>Measured</u>
ASTM Grain Size:	-	11-12
Measured Hardness:	HRC 31-33	

Fractography Overview

All four A-286 tensile specimens and the stress rupture specimen had at least a partially intergranular fracture path. The room temperature smooth tensile and stress rupture specimens were almost exclusively intergranular in the primary fracture areas. The stress rupture specimen exhibited very little evidence of ductility on the grain faces. The tensile specimens had dimples and ridges on the grain faces and patches of fine dimples at the boundaries between the grains. These features indicated ductility in the fracture. The 1300 F smooth tensile specimen had a large area of shear dimpled overstress near the surface. Both notched specimens and the elevated temperature smooth specimen exhibited varying degrees of intergranular and transgranular fracture. No clear conclusion can be made relating temperature to the fracture path based on these three specimens.

The three HCF specimens exhibited significant variation in macroscopic appearance with increasing temperature. The room temperature and 400 F specimens showed no obvious fatigue progression when viewed macroscopically. Both specimens had somewhat of a granular appearance. The 1300 F specimen exhibited a clear origin and fatigue progression area extending through greater than 50% of the cross section. The microscopic

appearance was also different for the 1300^o F specimen. Both lower temperature specimens had faceted Stage I fatigue origins and coarser well developed striations. The 1300 F specimen exhibited feathery cleavage and cleavage at the origin and a mixture of feathery cleavage and patches of fine shallower striations in the Stage II progression area. The final overstress areas on all three specimens had patches of dimpled overstress and quasi-cleavage with some intergranular character developing in the two higher temperature specimens.

The LCF specimen appearance differed considerably from the HCF specimens. Both LCF specimens propagated from multiple fatigue origins and had small isolated fatigue progression areas. The 400 F specimen had faceted Stage I fatigue at the origin and cleavage with cleavage steps in the Stage II fatigue zone. No clear striations were found. The 1300 F specimen had small fatigue initiation/propagation zones along the surface. These areas had a faceted intergranular appearance with cleavage steps and remnant striations on some of the facets. Secondary cracks were observed along the specimen surface in the gage area. The final overstress areas on both specimens occurred at an angle to the stress axis, exhibiting a mixture of cleavage, quasi-cleavage and dimpled overstress on the 400 F specimen and primarily shear dimpled overstress on the 1300 F specimen.

The stress corrosion cracking specimen exhibited feathery features and branching secondary cracks. Macroscopically, the appearance was darker due to oxidation.

The hydrogen embrittlement specimen was relatively flat except for a band approximately 0.03 inch thick at the surface that exhibited jagged steps containing dimples and patches of cleavage. The center of the specimen exhibited a mixture of dimpled rupture with quasi-cleavage. Cracked carbides were visible throughout the center of the specimen. No carbides, cracked or uncracked, were found on the other specimens. This may indicate an interaction between the carbides and the hydrogen in the lattice.

MATERIAL

A-286
AMS 5525 Plate

TEST DATA

TEST TYPE
Smooth Tensile

TEST CONDITIONS
Strain Rate: 0.005 mm/mm/min (0.005 in/in/min)
Atmosphere: Air
Temperature: Room Temperature
Test Direction: Longitudinal

TEST RESULTS
0.2% Yield Strength: 704.6 MPa (102.2 ksi)
Ultimate Strength: 1063.3 MPa (154.8 ksi)
Percent Elongation: 20.0
Percent Reduction of Area: 26.0



FAL 92496

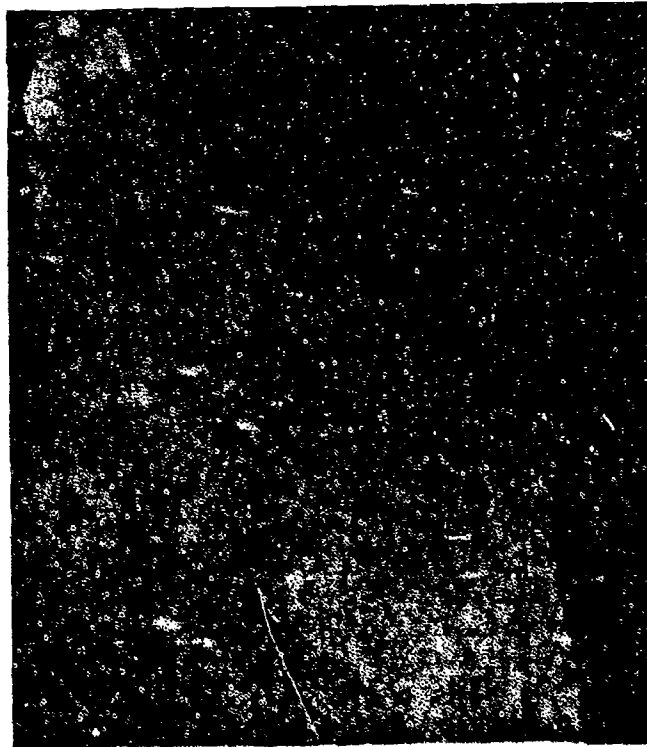
MAG: 15X

FIGURE 5-1: Test results and fractography of A-286 room temperature smooth tensile test. The fracture appears granular with no shear lip visible.



FAM 99886

MAG: 200X



FAM 99885

MAG: 200X

FIGURE 5-2: Optical photomicrographs of the center (top) and edge (bottom) of the fracture. Grain elongation in the stress direction and secondary grain boundary separation (arrows) are visible. The fracture is predominantly intergranular.

Etchant: 15ml HCl, 10ml HNO₃, 10ml acetic acid

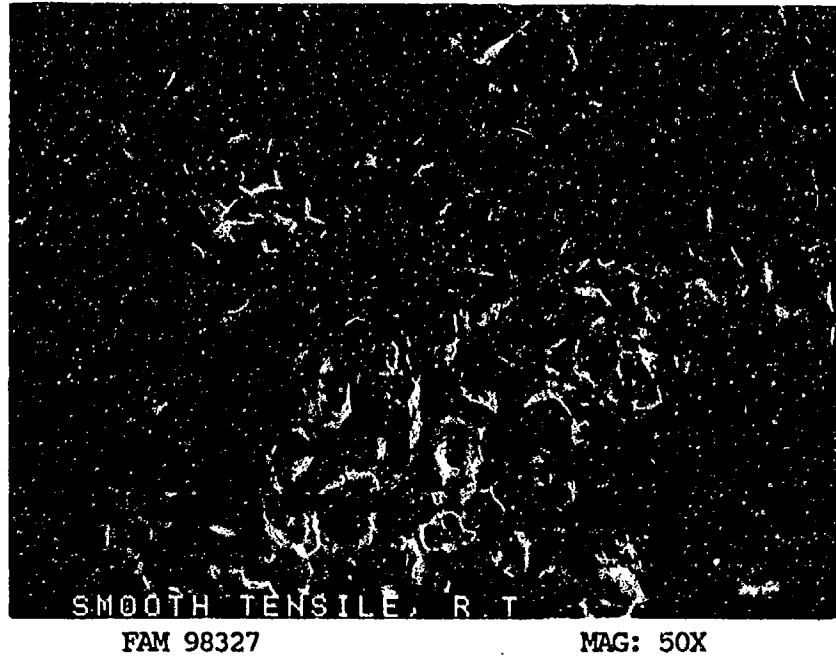


FIGURE 5-3: Low magnification photograph showing primarily intergranular overstress.



FIGURE 5-4: Intergranular overstress with some dimples at the grain boundaries (intergranular decohesion) (arrow).

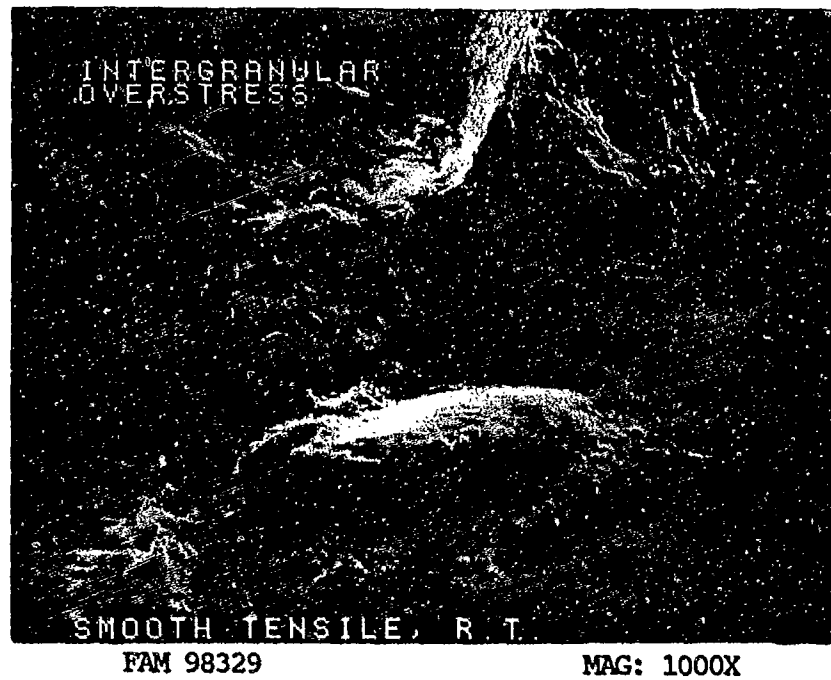


FIGURE 5-5: Intergranular overstress with slip lines present on the grain faces (arrow). These should not be confused with fatigue striations.

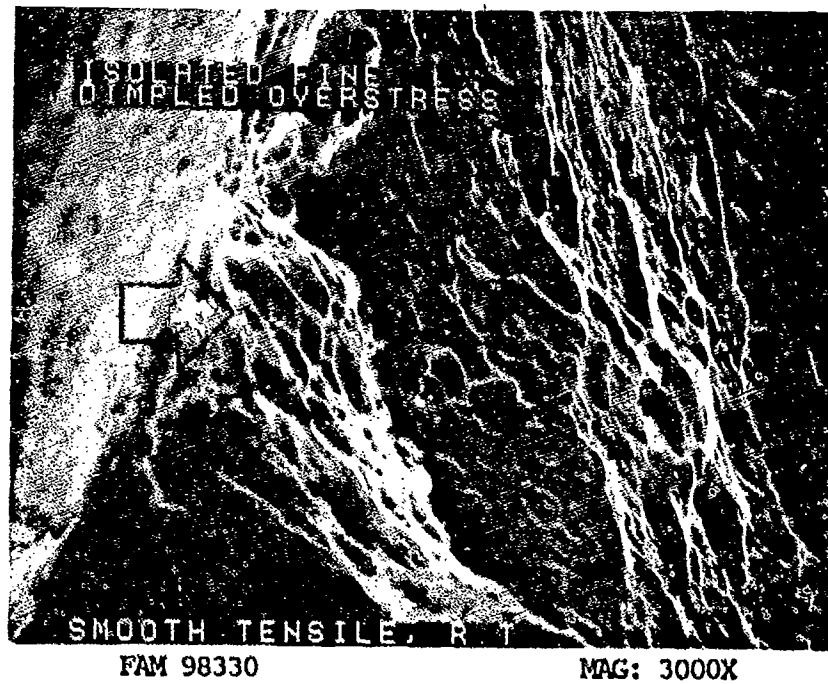


FIGURE 5-6: Isolated fine dimpled overstress at the grain boundaries (arrow).

MATERIAL

A-286
AMS 5525 Plate

TEST DATA

TEST TYPE

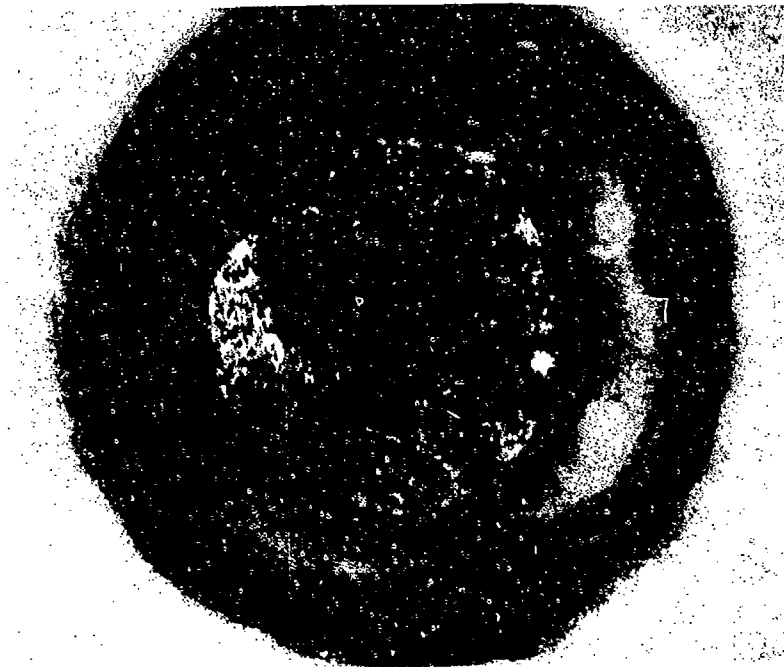
Smooth Tensile

TEST CONDITIONS

Strain Rate: 0.005 mm/mm/min (0.005 in/in/min)
Atmosphere: Air
Temperature: 704°C (1300°F)
Test Direction: Longitudinal

TEST RESULTS

0.2% Yield Strength:	623.3 MPa (90.4 ksi)
Ultimate Strength:	794.3 MPa (115.2 ksi)
Percent Elongation:	25.3
Percent Reduction of Area:	42.0



FAL 92497

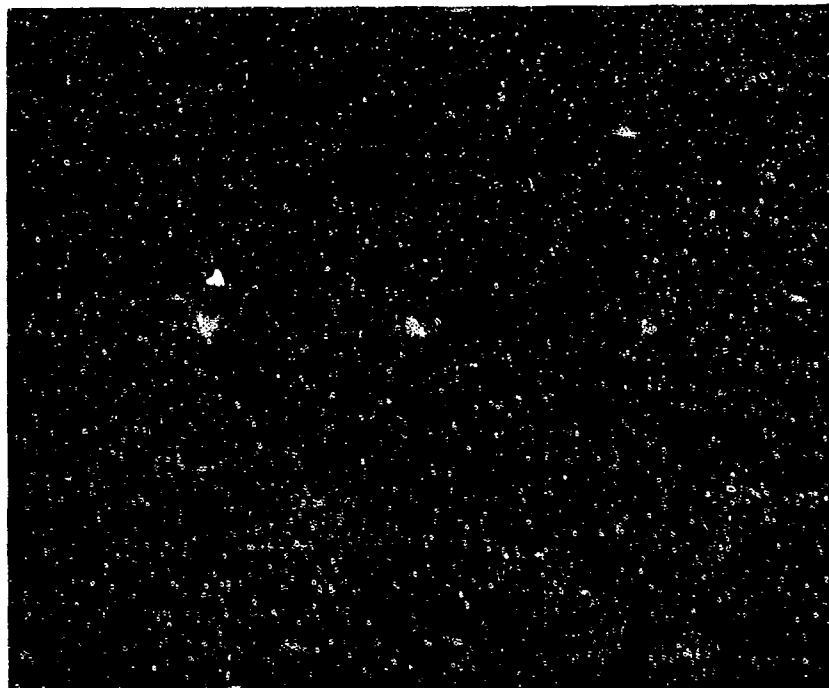
MAG: 15X

FIGURE 5-7: Test results and fractography of A-286 704°C (1300°F) smooth tensile test. The fracture appears oxidized even at low magnification.



FAM 99145

MAG: 100X



FAM 99146

MAG: 200X

FIGURE 5-8: Pair of increasing magnification optical photomicrographs of the center of the fracture. Extensive grain elongation in the stress direction and secondary grain boundary separation (arrows) are visible. Compare with the room temperature specimen, Figure 5-2.

Etchant: 15ml HCl, 10ml HNO₃, 10ml acetic acid

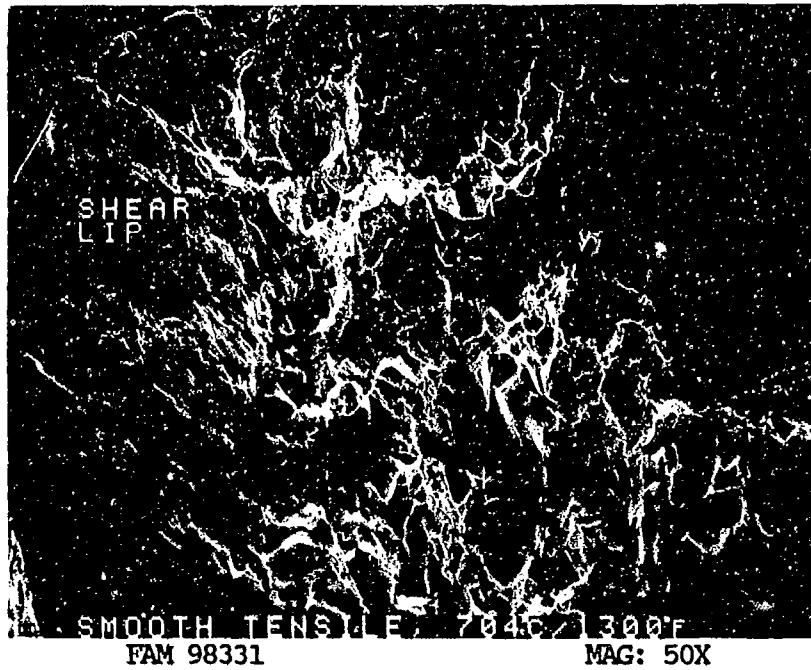


FIGURE 5-9: Low magnification photograph showing smeared shear lip area.

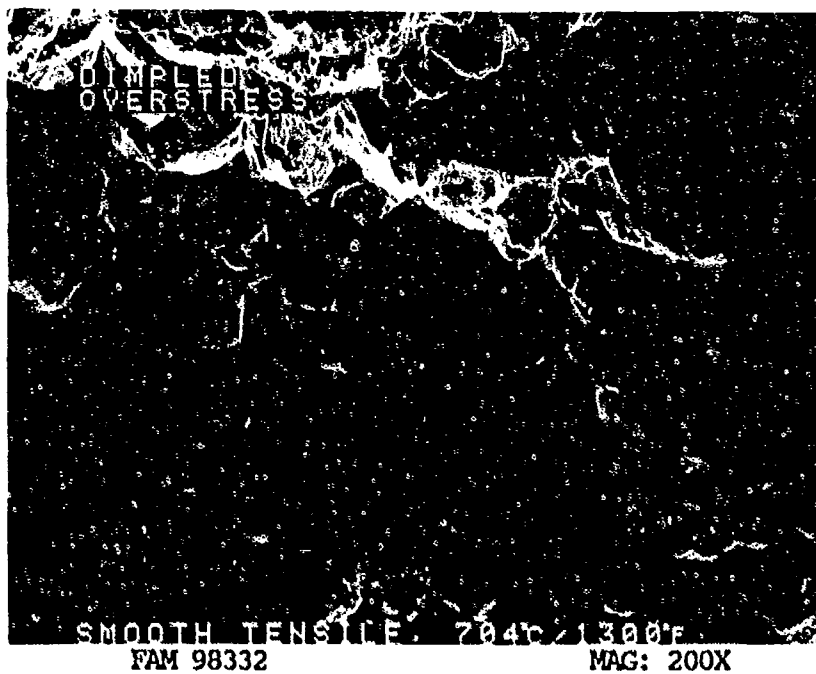


FIGURE 5-10: Mixture of fine and coarse dimpled overstress in the primary fracture area.

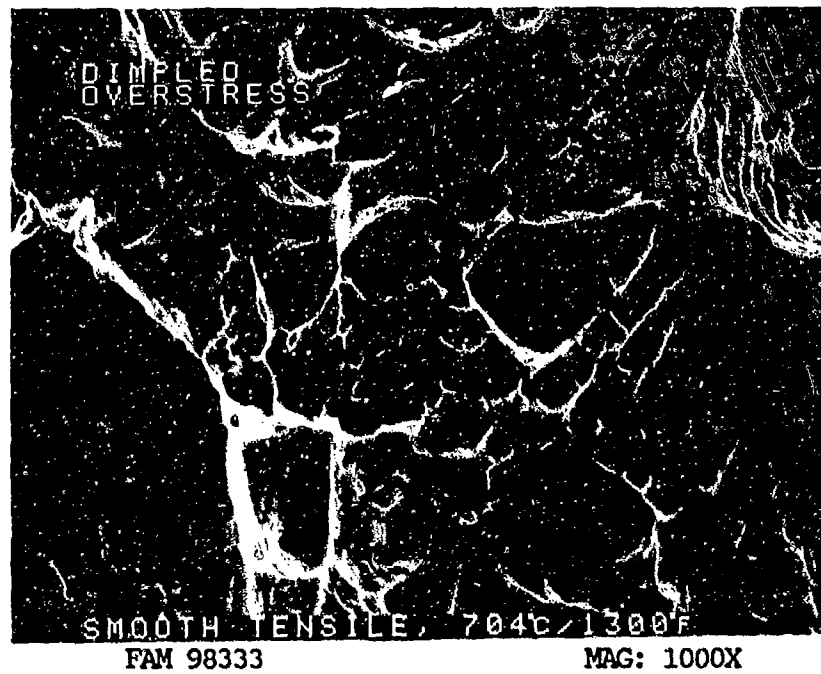


FIGURE 5-11: Mixture of coarse and fine shallow dimples in the primary fracture area. A light oxide covers the fracture surface.

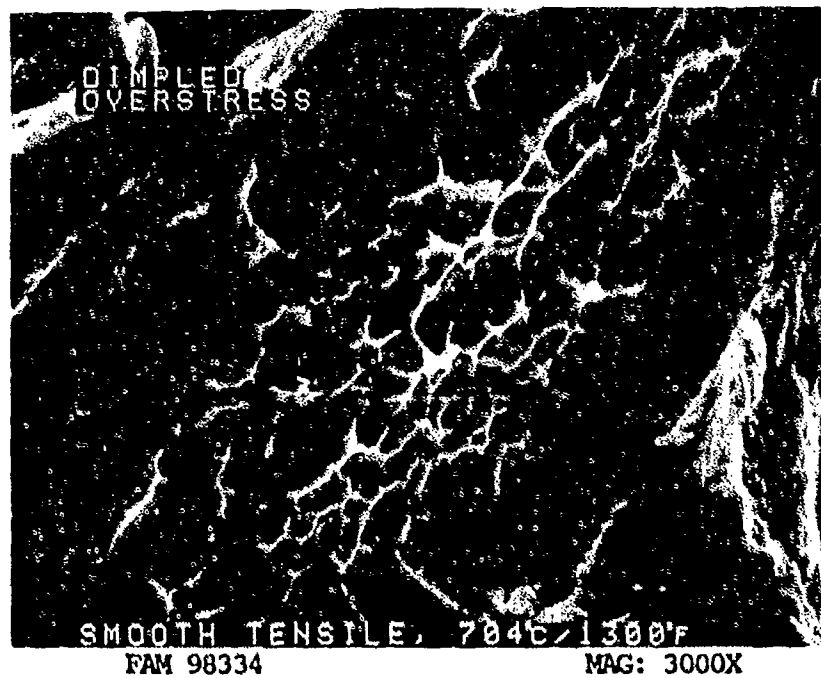


FIGURE 5-12: Patches of fine equiaxed dimples in the area shown in Figure 5-11.

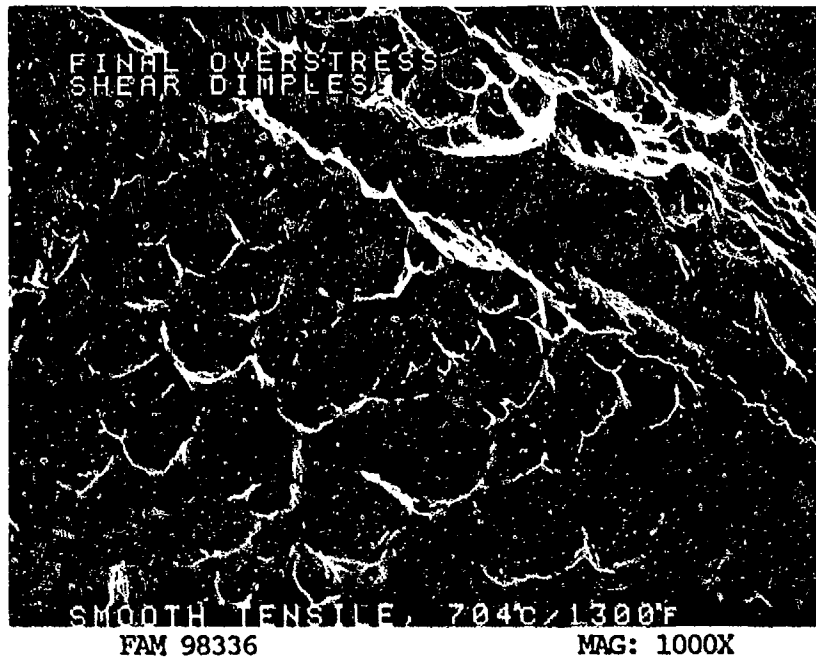


FIGURE 5-13: Oxidized shear dimples in the final overstress area. Arrows show the directions of relative motion.

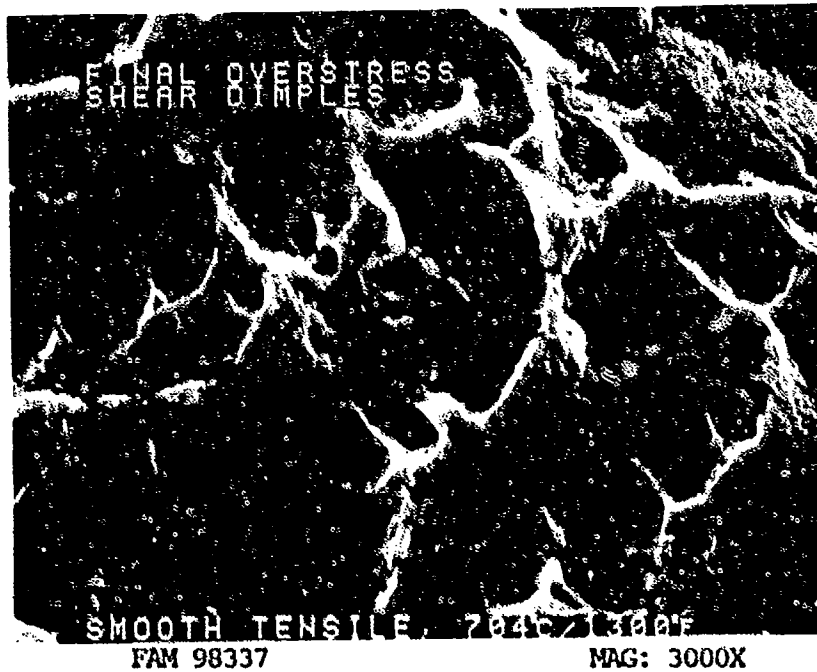


FIGURE 5-14: Oxidized shallow shear dimples in the final overstress area.

MATERIAL

A-286
AMS 5525 Plate

TEST DATA

TEST TYPE

Notched Tensile

TEST CONDITIONS

Crosshead Speed: 1.27 mm/min (0.05 in/min)

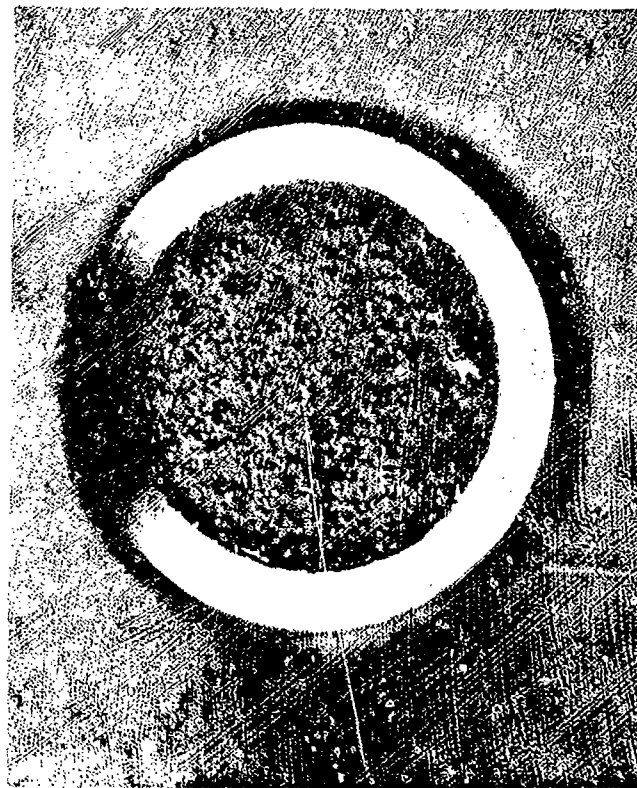
Atmosphere: Air

Temperature: Room Temperature

Test Direction: Longitudinal

TEST RESULTS

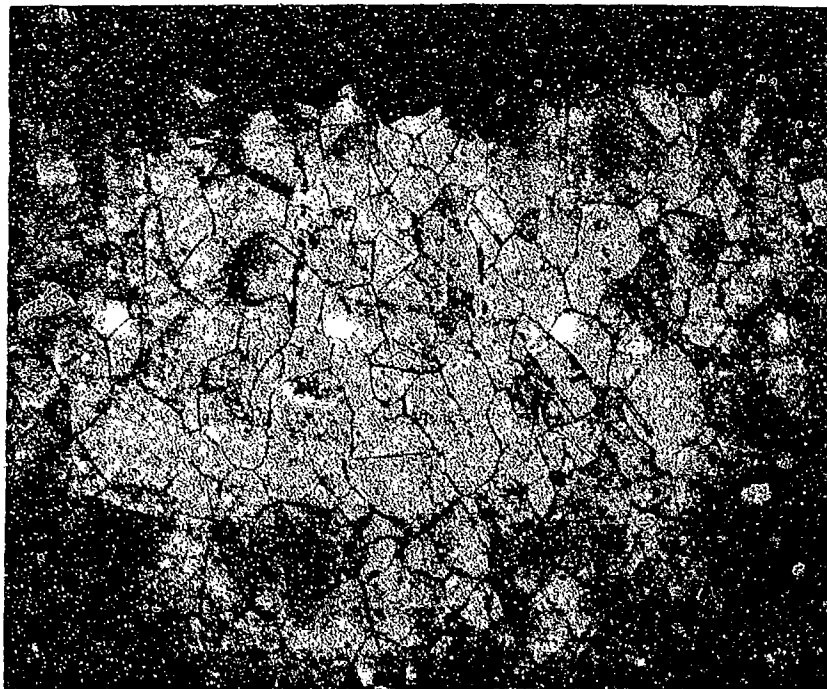
Ultimate Strength: 1347.9 MPa (195.5 ksi)



FAL 92498

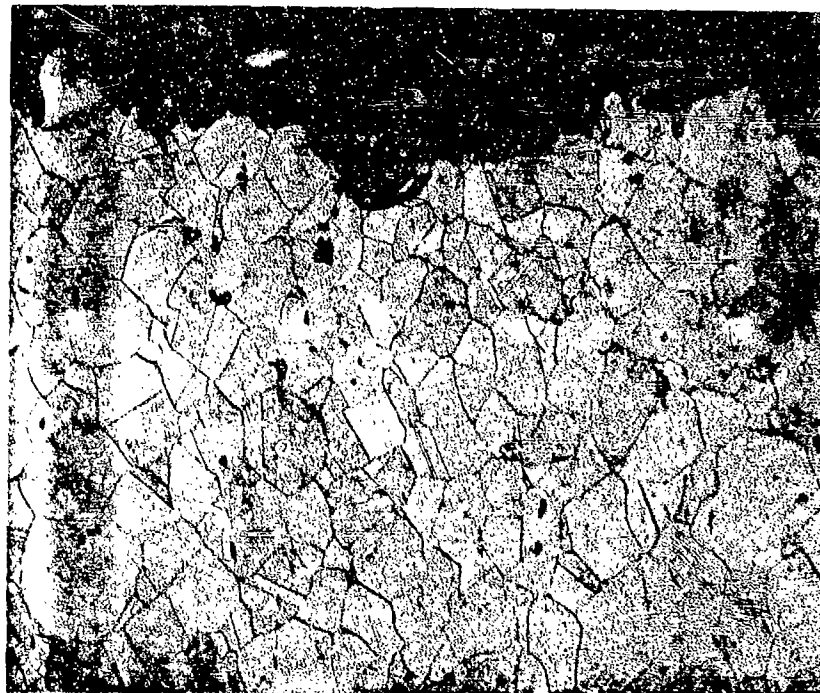
MAG: 10X

FIGURE 5-15: Test results and fractography of A-286 room temperature notched tensile test. No shear lip is visible.



FAM 99149

MAG: 100X



FAM 99151

MAG: 100X

FIGURE 5-16: Optical photomicrographs of the center of the fracture. Very little grain deformation is visible and only one area exhibits secondary grain boundary separation. Compare with the smooth tensile specimens, Figures 5-2 and 5-8.

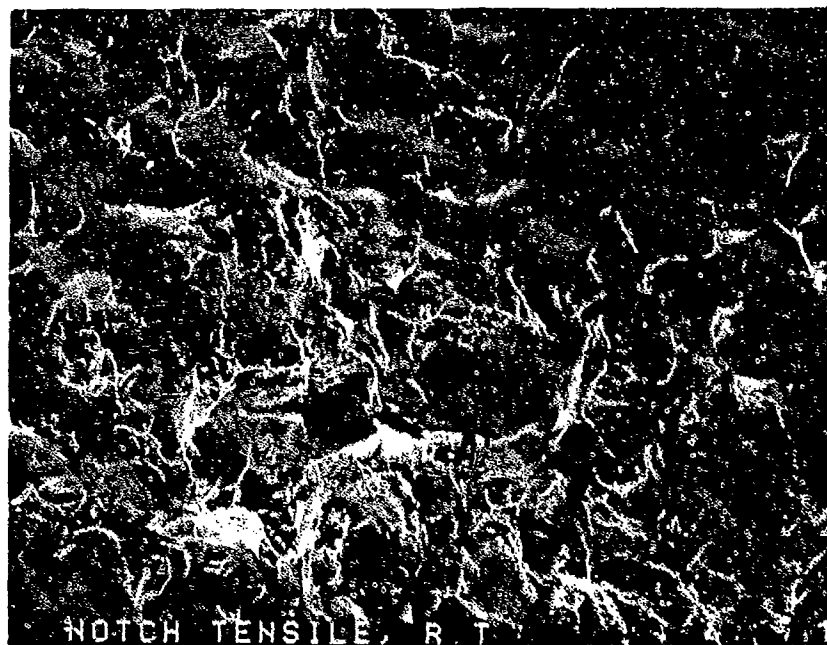
Etchant: 15ml HCl, 10ml HNO₃, 10ml acetic acid



FAM 98316

MAG: 50X

FIGURE 5-17: No shear lip is present in this low magnification photograph.



FAM 98317

MAG: 200X

FIGURE 5-18: Mixture of dimpled overstress (arrow A), cleavage (arrow B) and void formation (arrow C).

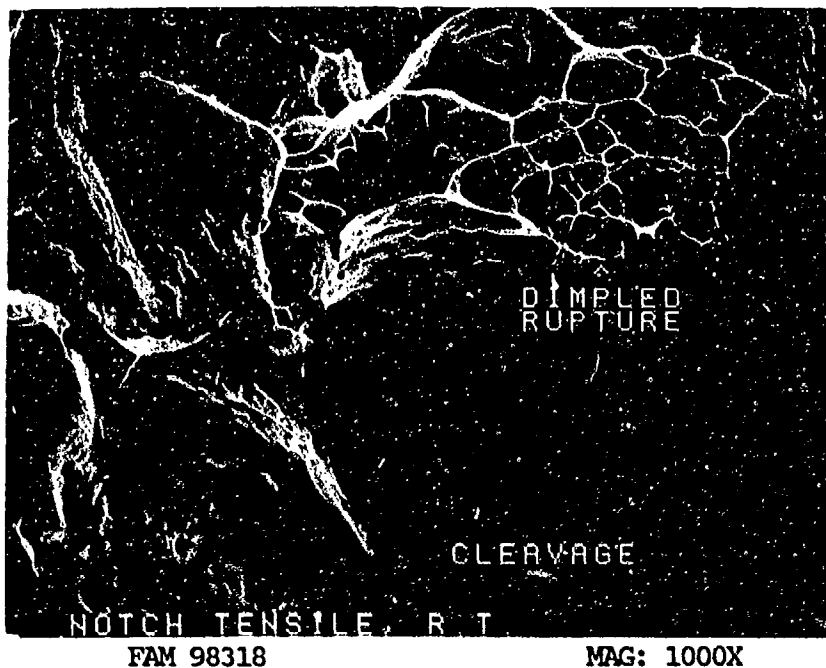


FIGURE 5-19: Mixture of dimpled overstress and quasi-cleavage (mixed mode overstress). Fine slip lines are visible on the cleavage planes (brackets). These should not be confused with fatigue striations.

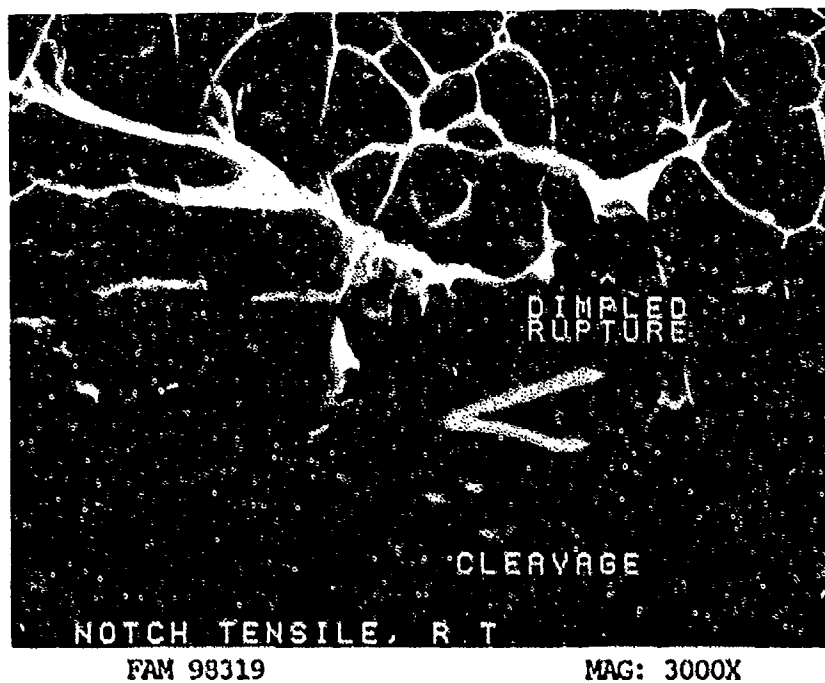


FIGURE 5-20: Boundary between dimpled overstress and a cleavage plane.

MATERIAL

A-286
AMS 5525 Plate

TEST DATA

TEST TYPE

Notched Tensile

TEST CONDITIONS

Crosshead Speed: 1.27 mm/min (0.05 in/min)

Atmosphere: Air

Temperature: 704°C (1300°F)

Test Direction: Longitudinal

TEST RESULTS

Ultimate Strength: 1130.0 MPa (163.9 ksi)



FAL 92499

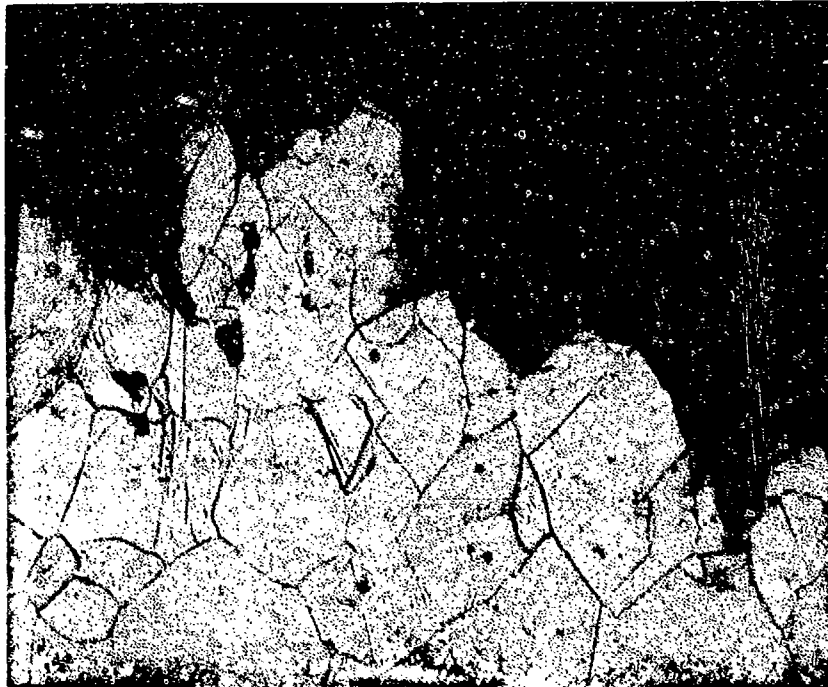
MAG: 10X

FIGURE 5-21: Test results and fractography of A-286 704°C (1300°F) notched tensile test. The fracture appears oxidized even at low magnification.



FAM 99156

MAG: 100X



FAM 99156A

MAG: 200X

FIGURE 5-22: Pair of increasing magnification optical photomicrographs of the center of the fracture. More grain deformation is visible than in the room temperature notched tensile specimen. There is still very little secondary grain boundary separation. Compare with the smooth tensile specimens, Figures 5-2 and 5-8.
Etchant: 15ml HCl, 10ml HNO₃, 10ml acetic acid

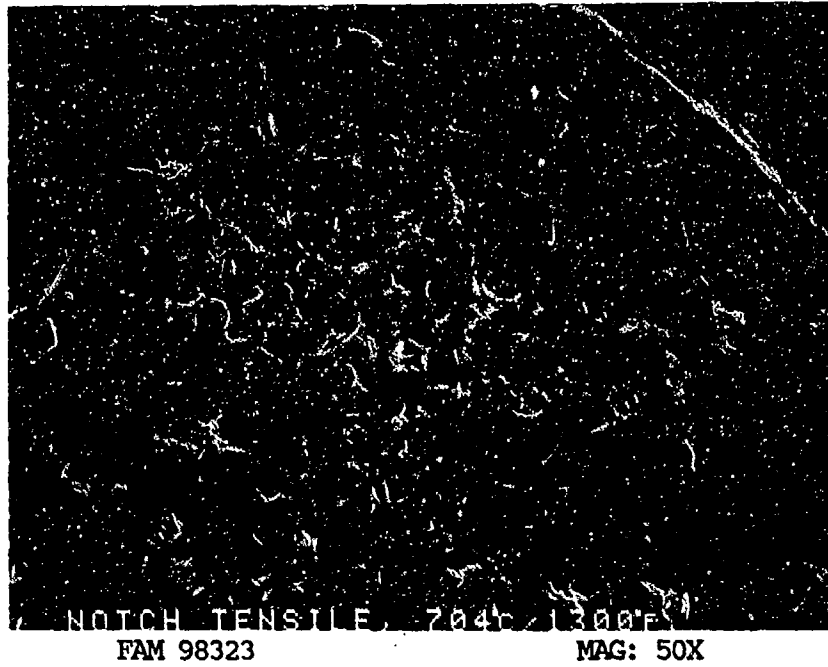


FIGURE 5-23: Low magnification photograph showing an intergranular appearance with some secondary cracking (arrow).

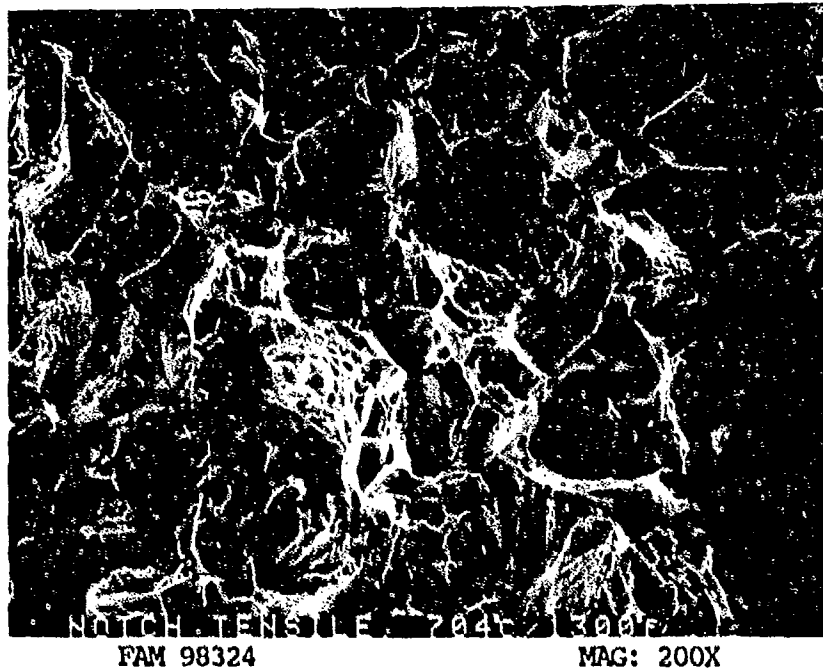


FIGURE 5-24: Mixture of transgranular and intergranular features.

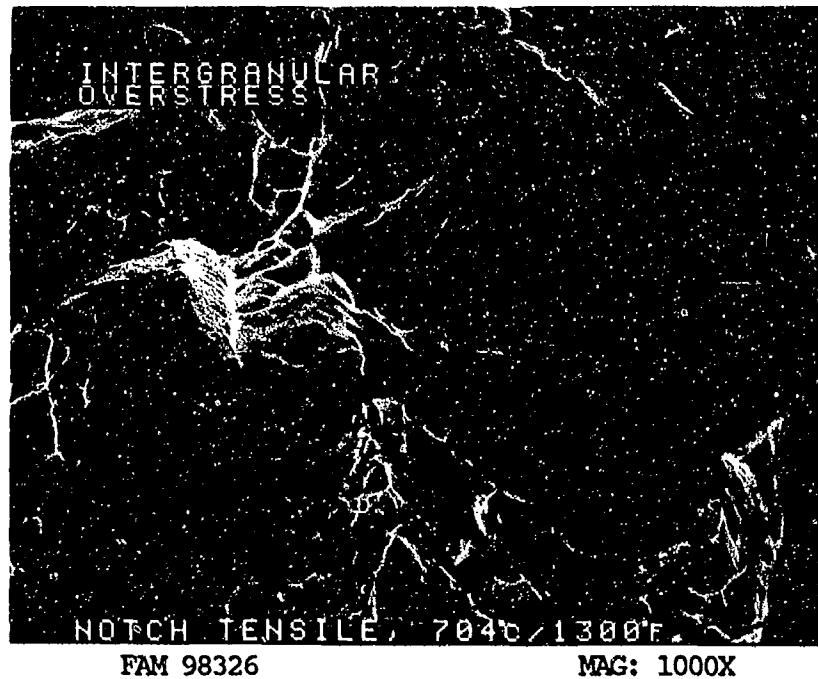


FIGURE 5-25: Mixture of cleavage and intergranular overstress with some grain boundary separation. Fine, shallow dimples are visible on some of the grain faces (arrow).

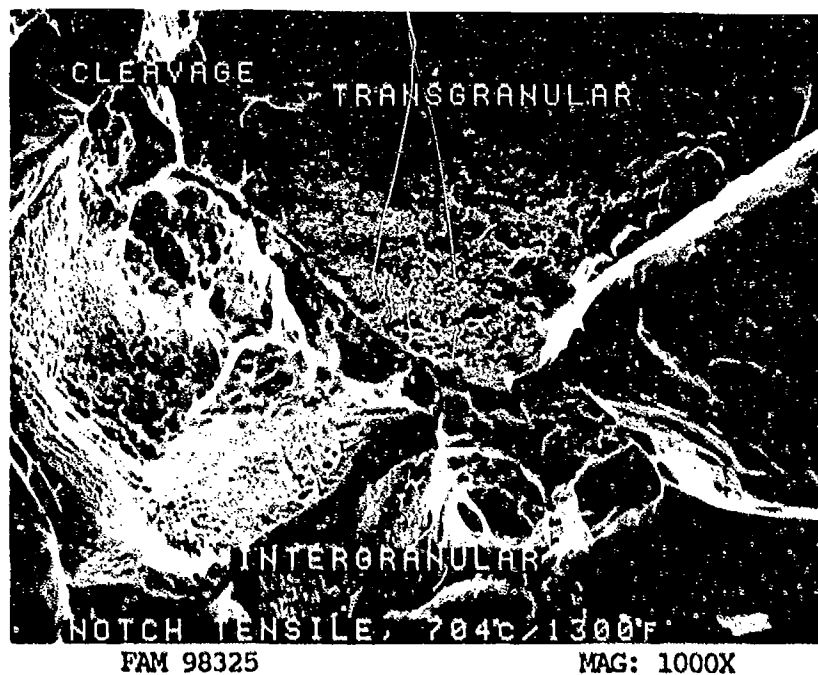


FIGURE 5-26: Higher magnification photo showing area of probable quasi-cleavage.

MATERIAL

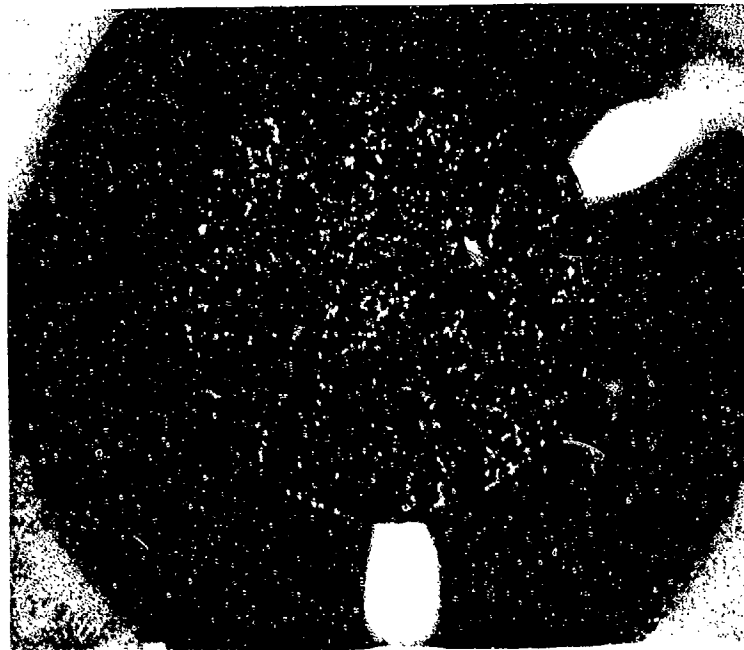
A-286
AMS 5525 Plate

TEST DATA

TEST TYPE
Stress Rupture

TEST CONDITIONS
Stress: 586.1 MPa (85.0 ksi)
Atmosphere: Air
Temperature: 649°C (1200°F)
Test Direction: Longitudinal

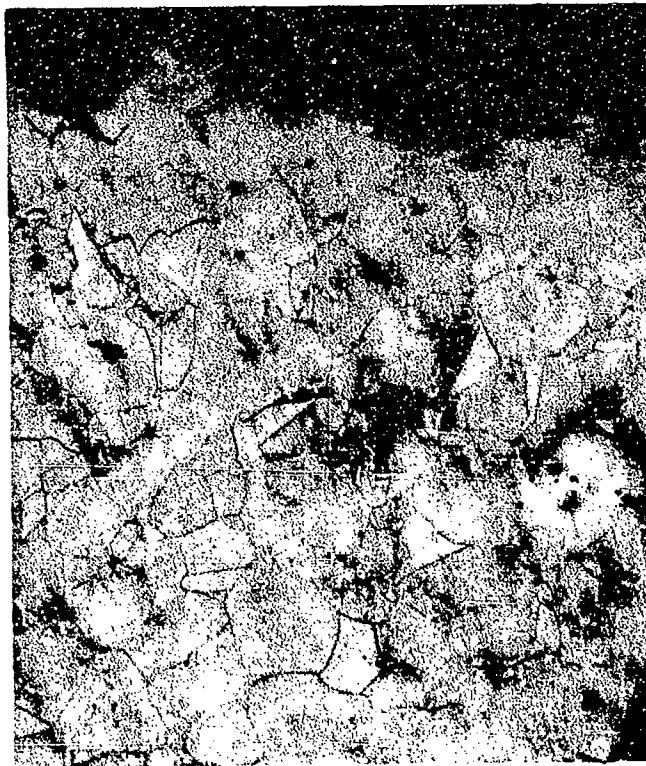
TEST RESULTS
Time to Fracture: 6.2 hours
Percent Elongation: 2.5
Percent Reduction of Area: 2.9



FAL 94374

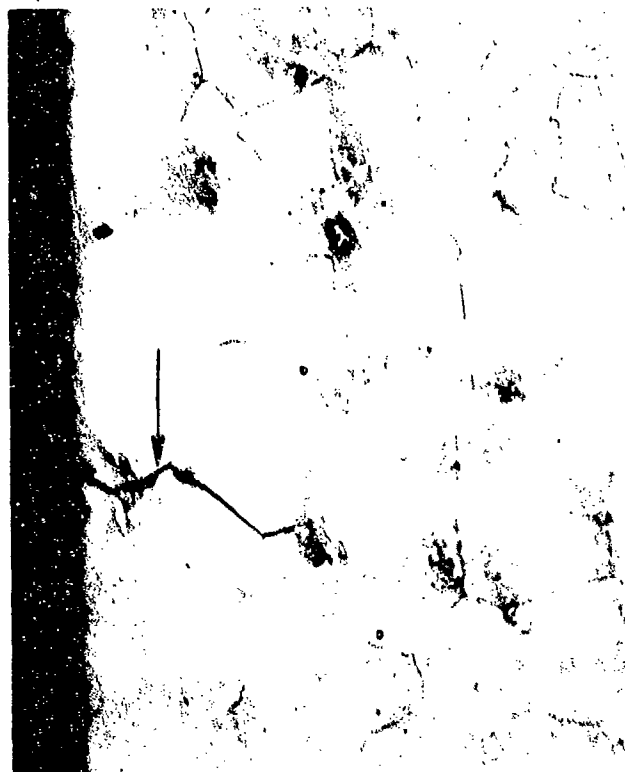
MAG: 15X

FIGURE 5-27: Test results and fractography of A-286 649°C (1200°F) stress rupture test. The fracture has a shiny intergranular appearance.



FAM 100294

MAG: 100X

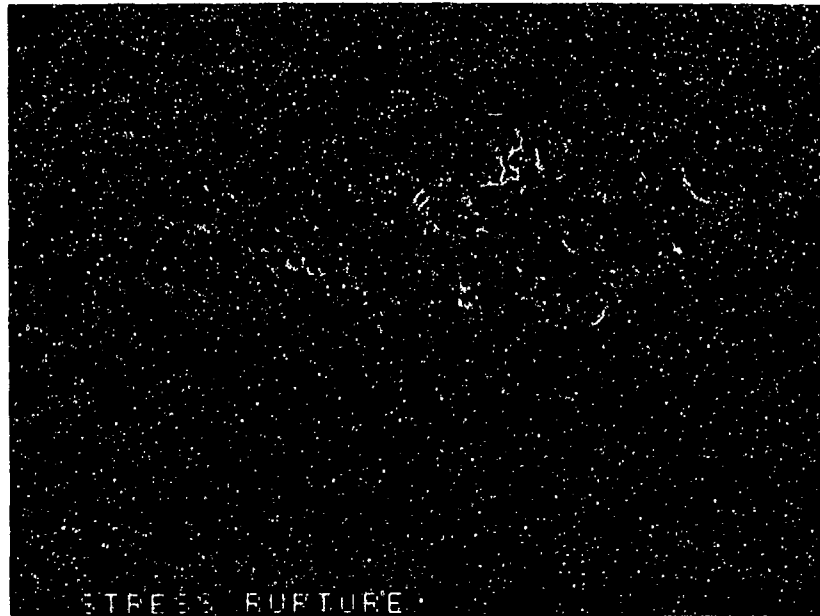


FAM 100295

MAG: 200X

FIGURE 5-28: Optical photomicrographs of the center of the fracture (top) and the gage section (bottom). Both the primary fracture path and secondary cracks along the gage section (arrow, bottom) are intergranular.

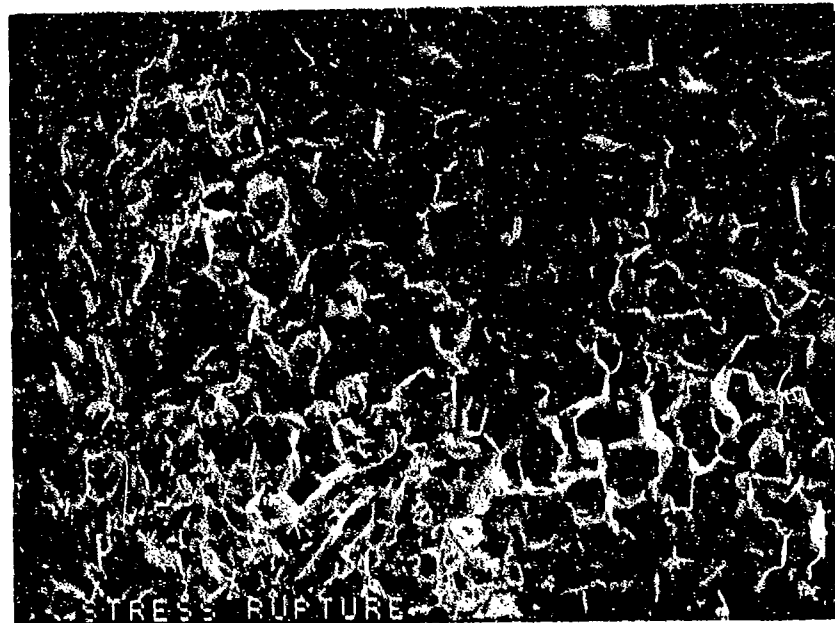
Etchant: 15ml HCl, 10ml HNO₃, 10ml acetic acid



FAM 99535

MAG: 20X

FIGURE 5-29: Low magnification photograph exhibits intergranular appearance.



FAM 99536

MAG: 50X

FIGURE 5-30: Intergranular fracture surface with some intergranular secondary cracking (arrows).



FAM 99537

MAG: 200X

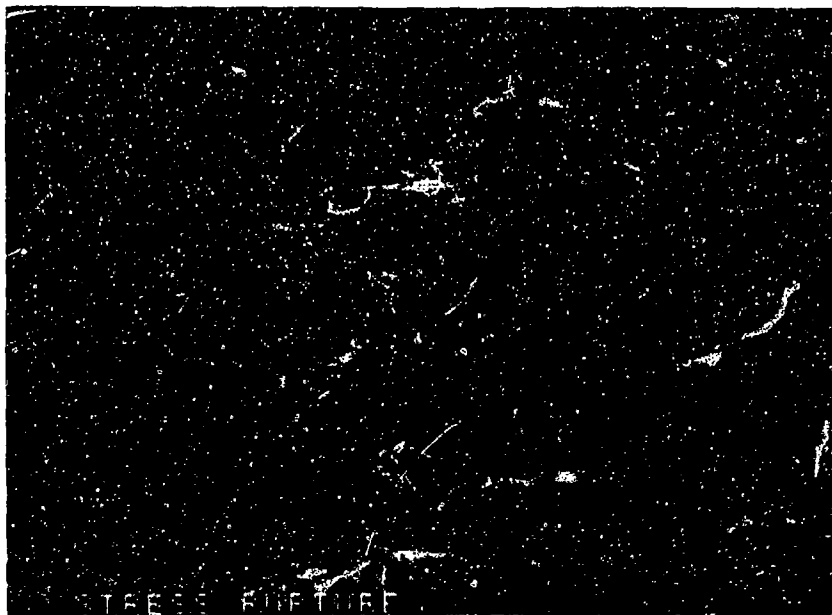
FIGURE 5-31: Intergranular rupture with intergranular secondary cracking.



FAM 99538

MAG: 1000X

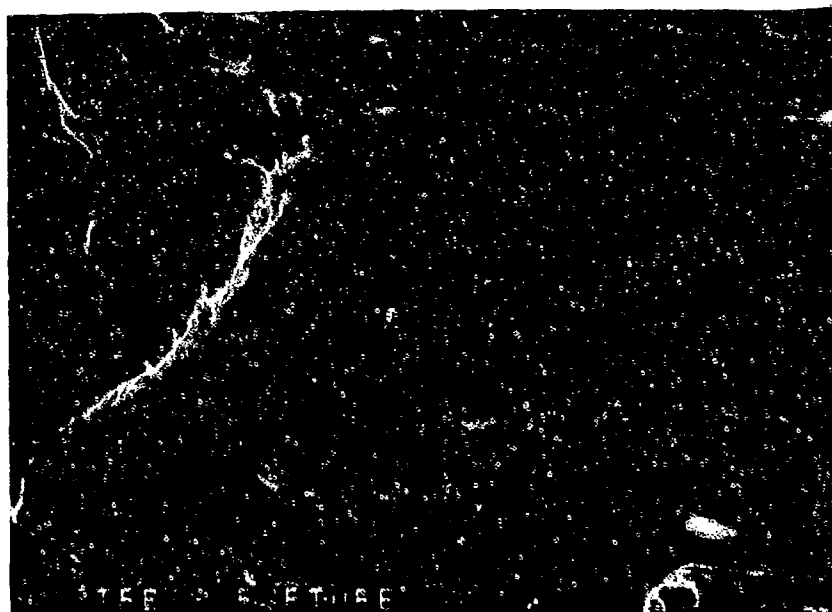
FIGURE 5-32: Higher magnification photograph of the area shown in Figure 5-31, depicting intergranular rupture.



FAM 99540

MAG: 200X

FIGURE 5-33: Mixture of transgranular overstress dimples and intergranular rupture in final overstress area.



FAM 99541

MAG: 1000X

FIGURE 5-34: Higher magnification photograph of the area shown in Figure 5-33.

MATERIAL

A-286
AMS 5525 Plate

TEST DATA

TEST TYPE
Smooth HCF

TEST CONDITIONS

Stress: 482.6 MPa (70.0 ksi)/-482.6 MPa (-70.0 ksi)
Stress Ratio: -1
Frequency: 1800 cpm
Atmosphere: Air
Temperature: Room Temperature
Test Direction: Longitudinal

TEST RESULTS

Cycles to Fracture: 10,500



FAL 93825

MAG: 15X

FIGURE 5-35: Test results and fractography of A-286 room temperature smooth HCF test.

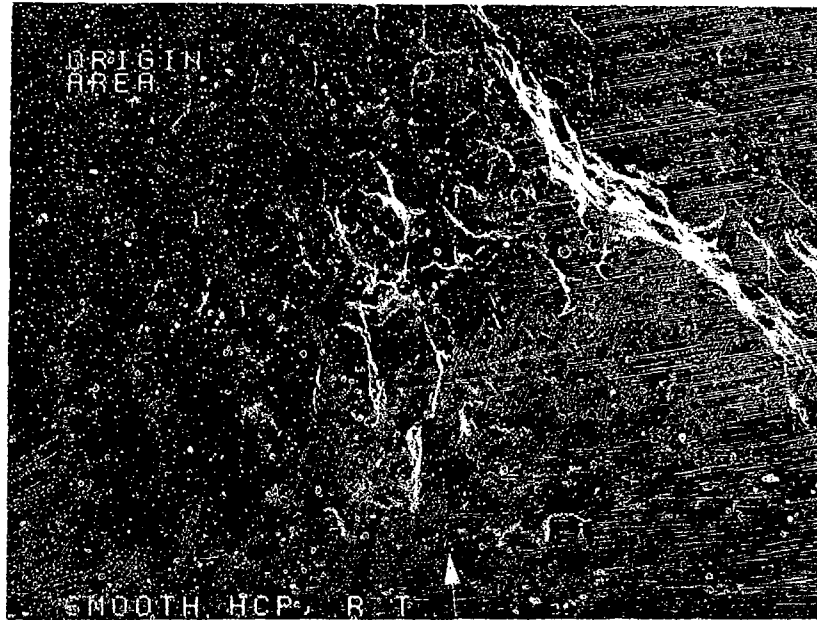


FAM 100300

MAG: 200X

FIGURE 5-36: Optical photomicrograph showing a transgranular secondary crack along the gage section. The fatigue progression is transgranular.

Etchant: 15ml HCl, 10ml HNO₃, 10ml acetic acid



FAM 99182

MAG: 50X

FIGURE 5-37: Low magnification photograph showing a stage I fatigue facet (arrow) at one of several origins.



FAM 99183

MAG: 200X

FIGURE 5-38: Higher magnification photograph of the stage I fatigue facet (arrow) shown in Figure 5-37.

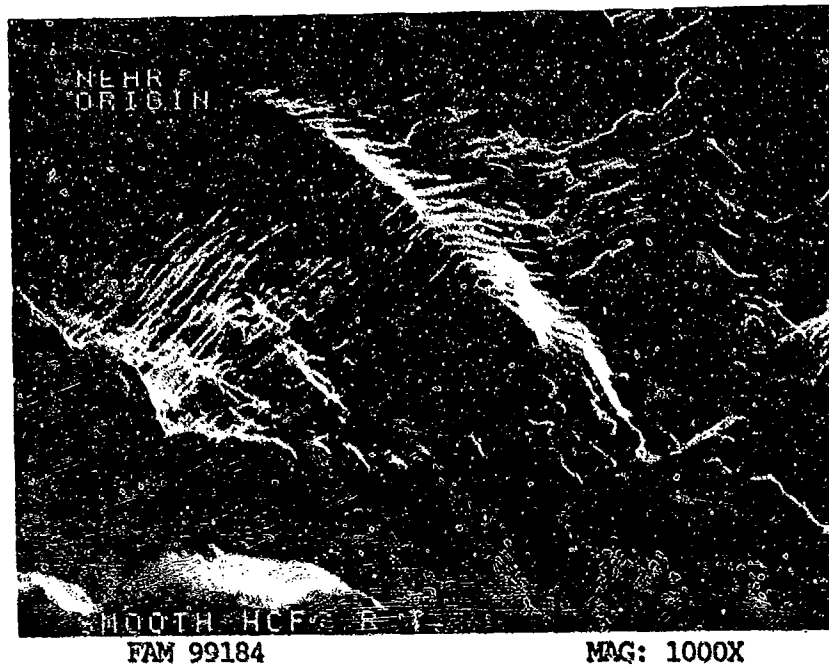


FIGURE 5-39: Fatigue striations near the origin shown in Figure 5-38. The direction of propagation is shown by an arrow.

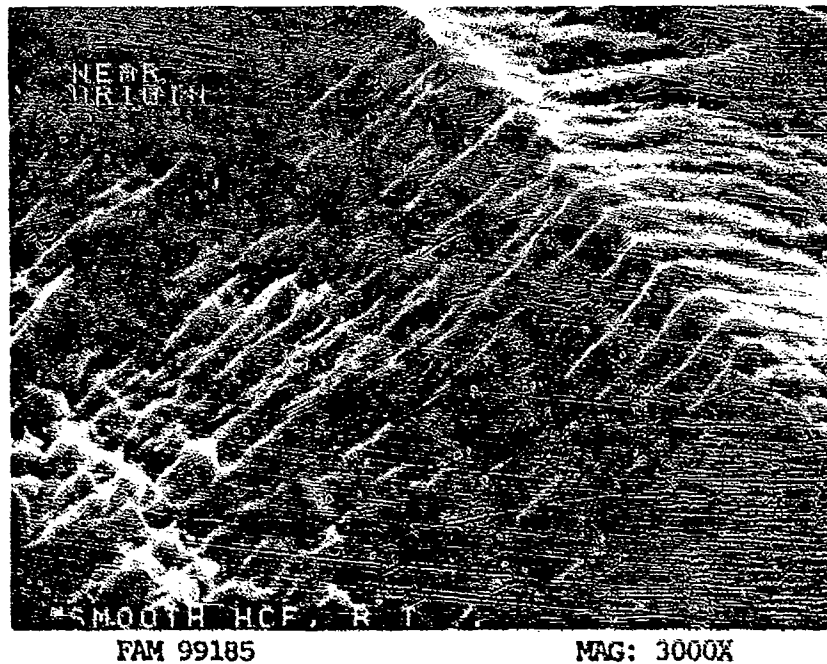


FIGURE 5-40: Higher magnification photograph of the fatigue striations shown in Figure 5-39. The fatigue propagated only a short distance into the specimen from each origin before overstress occurred.

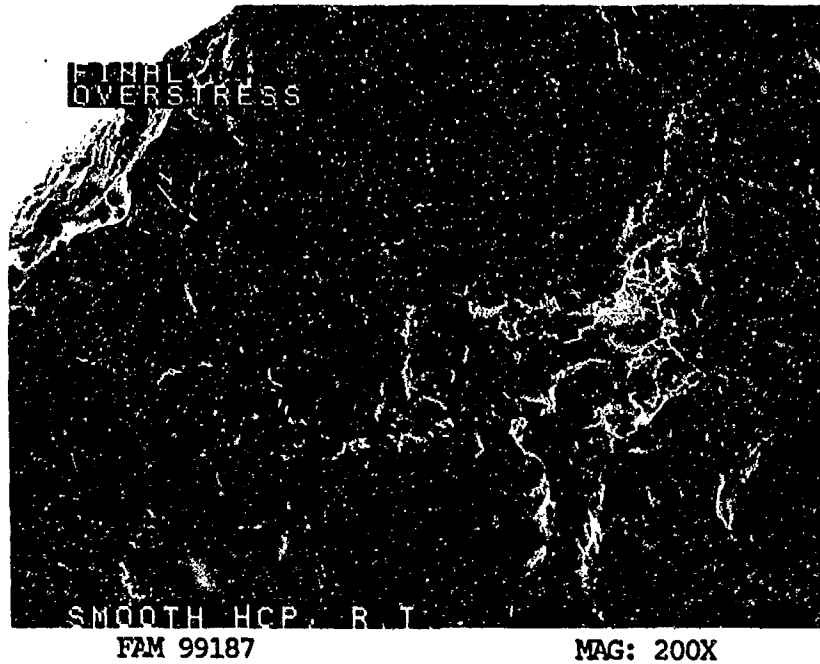


FIGURE 5-41: Mixture of cleavage type features and dimpled overstress in the final overstress area (quasi-cleavage).

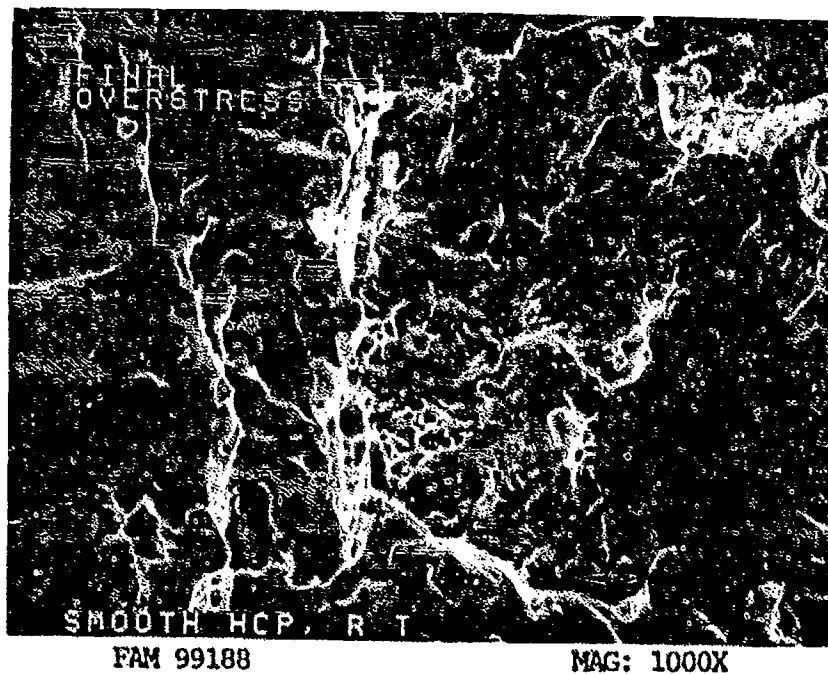


FIGURE 5-42: Higher magnification photograph showing mixture of cleavage and dimpled overstress in the final overstress area.

MATERIAL

A-286
AMS 5525 Plate

TEST DATA

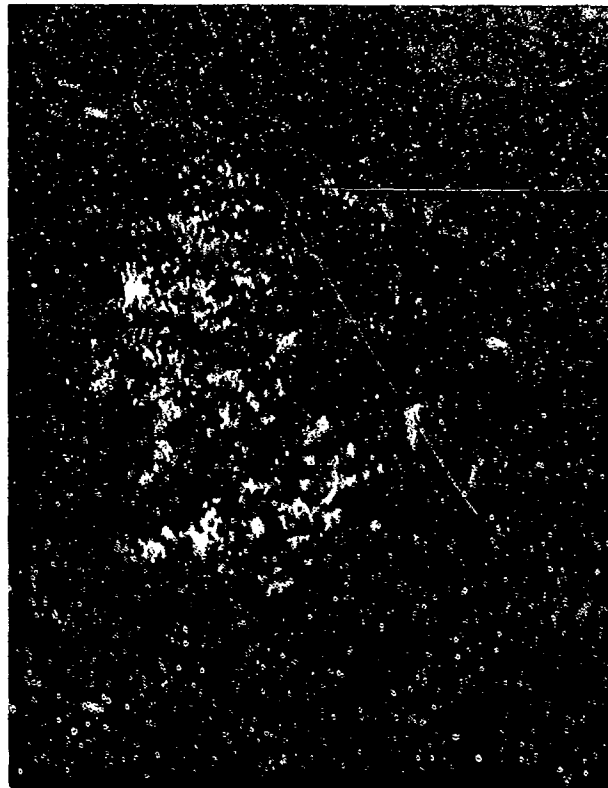
TEST TYPE
Smooth HCF

TEST CONDITIONS

Stress: 448.2 MPa (65.0 ksi)/-448.2 MPa (-65.0 ksi)
Stress Ratio: -1
Frequency: 1800 cpm
Atmosphere: Air
Temperature: 204°C (400°F)
Test Direction: Longitudinal

TEST RESULTS

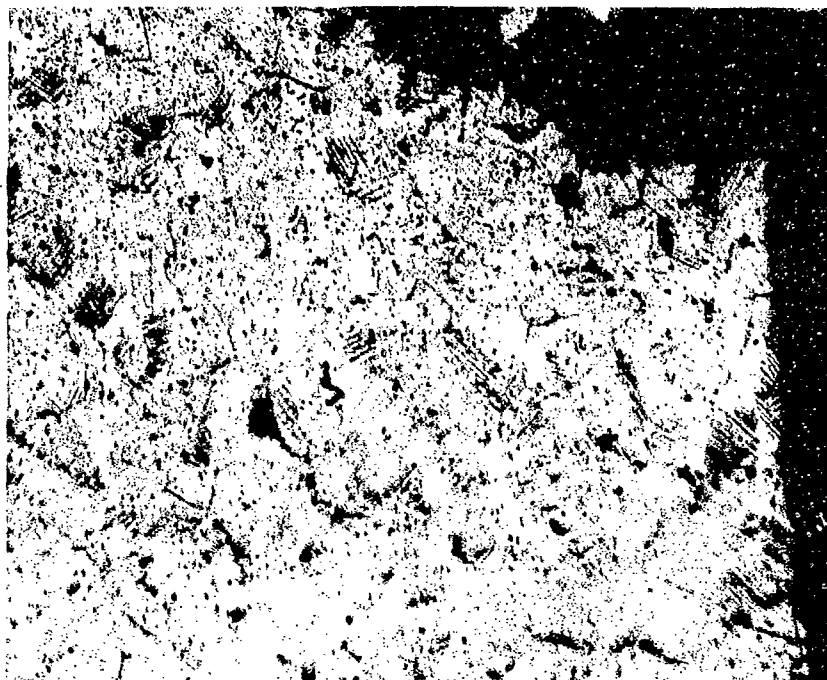
Cycles to Fracture: 11,400



FAL 93824

MAG: 15X

FIGURE 5-43: Test results and fractography of A-286 204°C (400°F) smooth HCF test. No obvious fatigue progression is discernible.



FAM 100471

MAG: 100X

FIGURE 5-44: Optical photomicrograph of a metallographic cross section through the origin area and initial fatigue progression.

Etchant: 10% Oxalic acid electrolytic

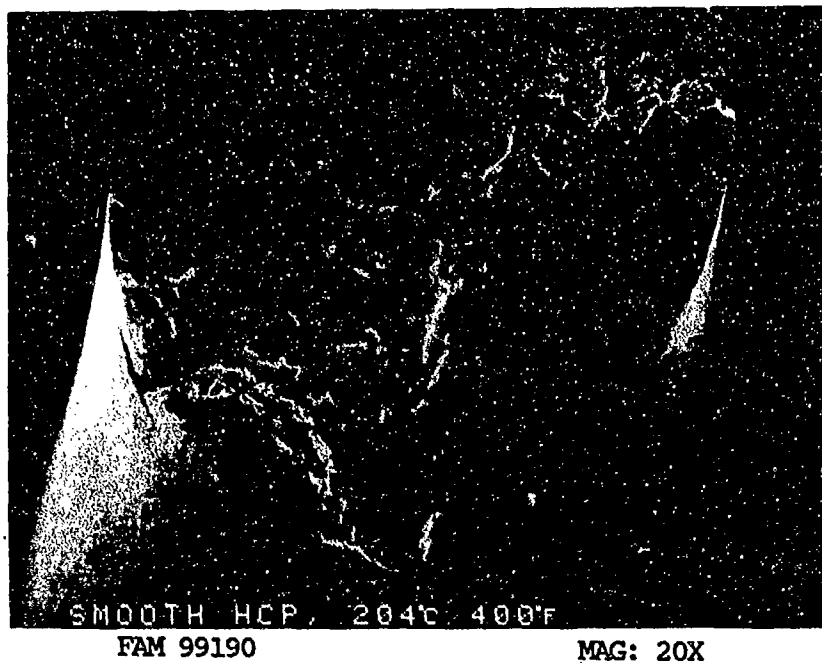


FIGURE 5-45: Overall photograph showing no obvious fatigue progression. Secondary cracking (arrow) is visible adjacent to the primary fracture (arrow).

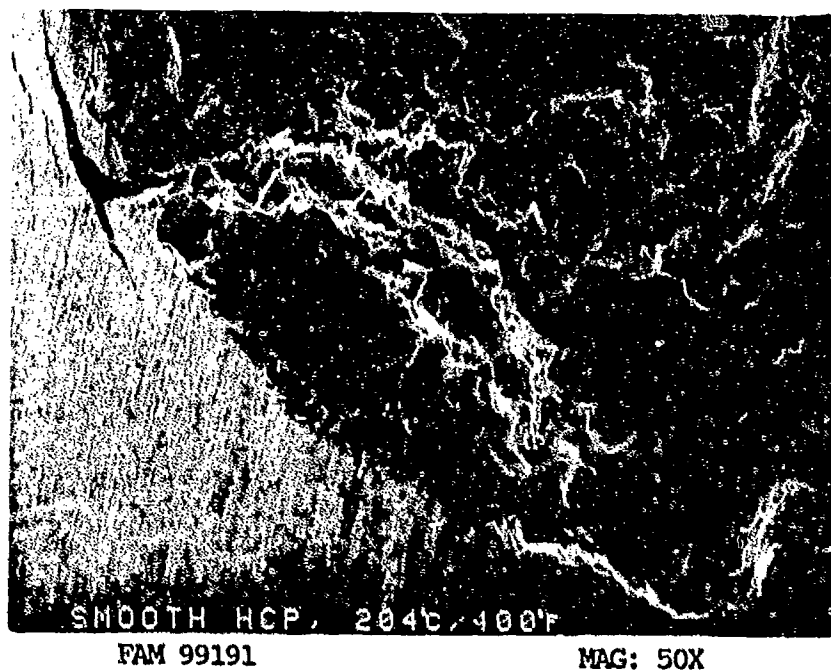


FIGURE 5-46: Photograph showing a localized origin (stage I fatigue facet, arrow).

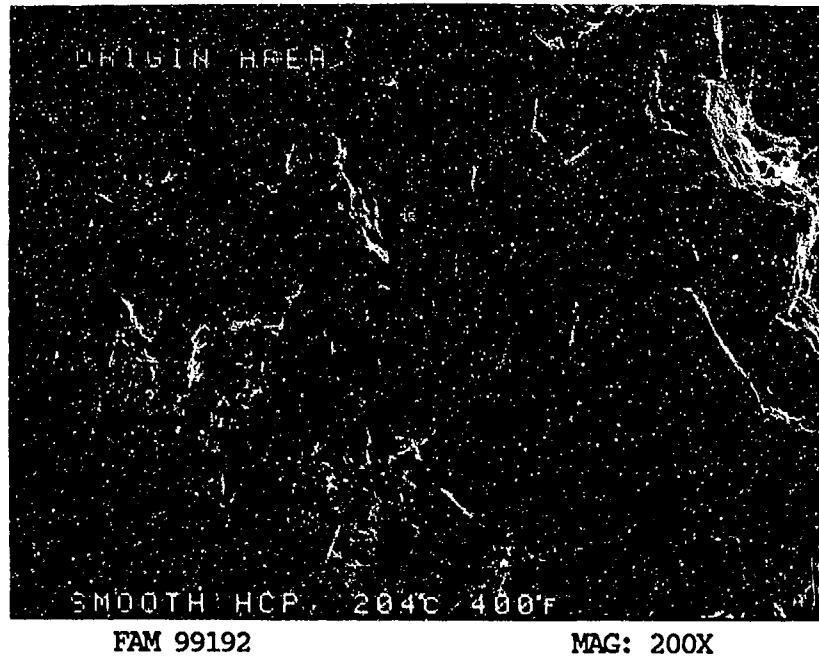


FIGURE 5-47: Stage I fatigue facet (arrow) in the origin area.

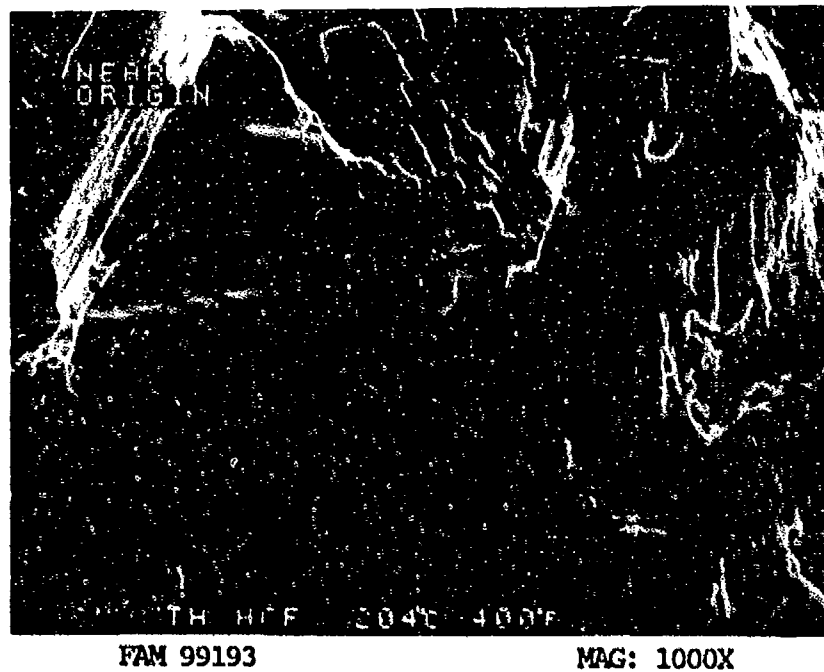


FIGURE 5-48: Remnant fatigue striations indicative of fatigue. An arrow indicates the direction of propagation.

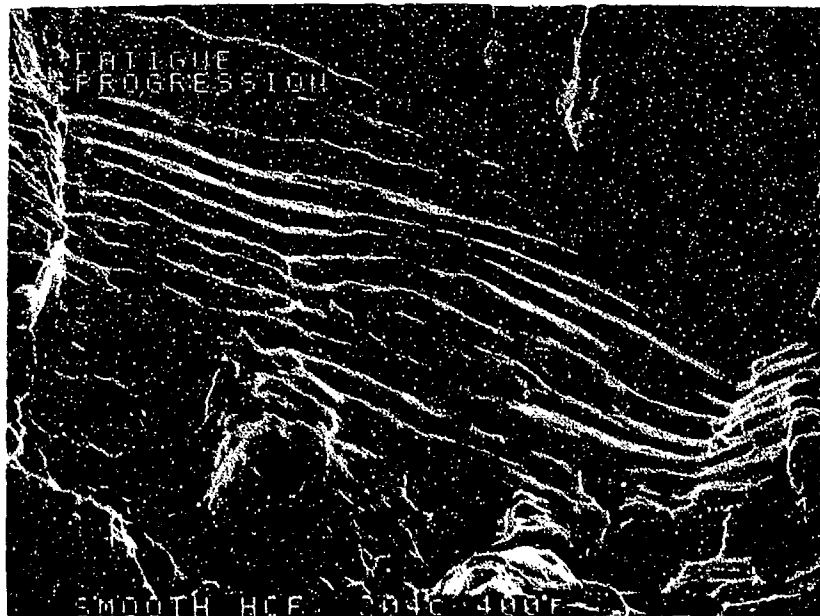


FIGURE 5-49: Fatigue striations in the fatigue progression zone.

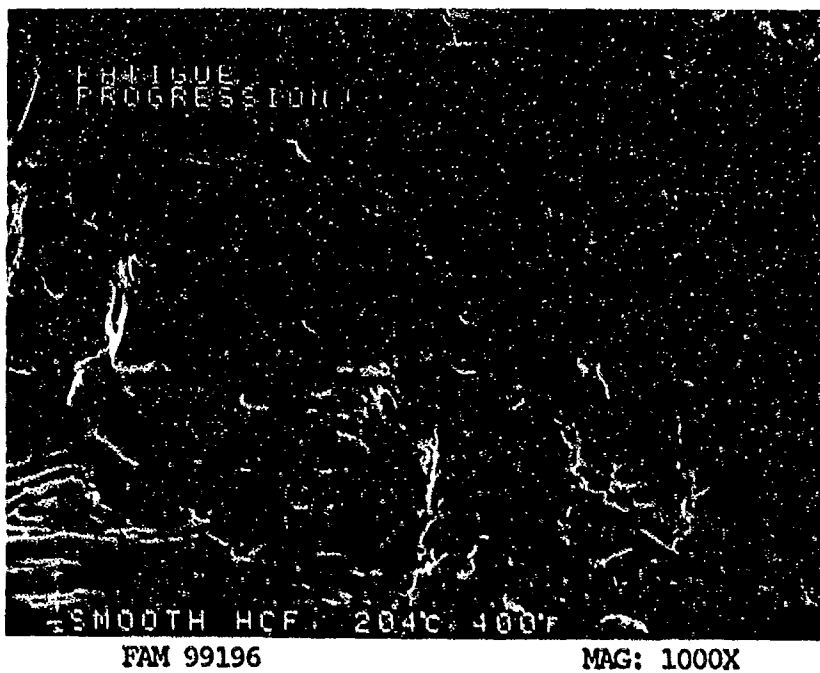


FIGURE 5-50: Crack-like striations in the fatigue progression zone. Contrast the appearance with those shown in Figure 5-49.

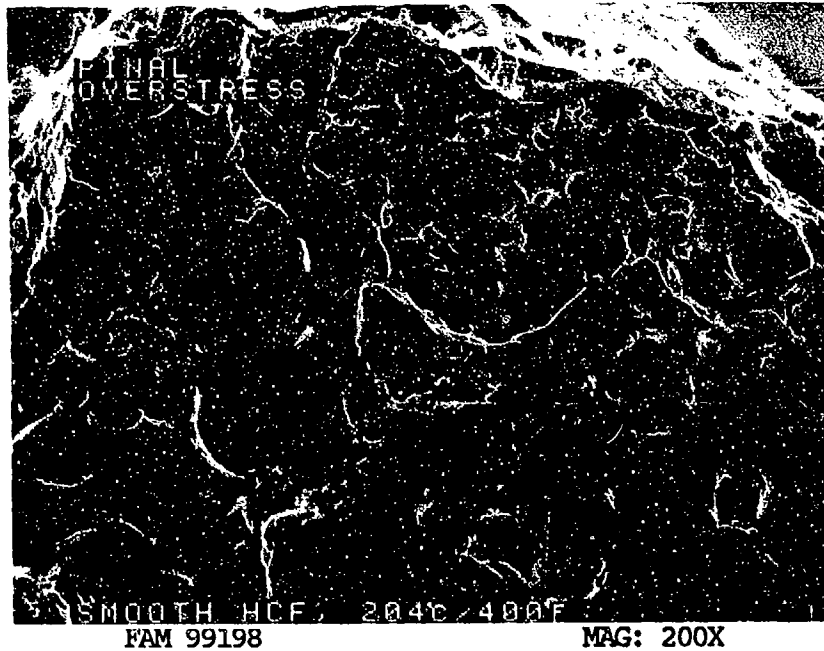


FIGURE 5-51: Mixture of dimpled overstress and cleavage features (arrows) in the final overstress area (quasi-cleavage).

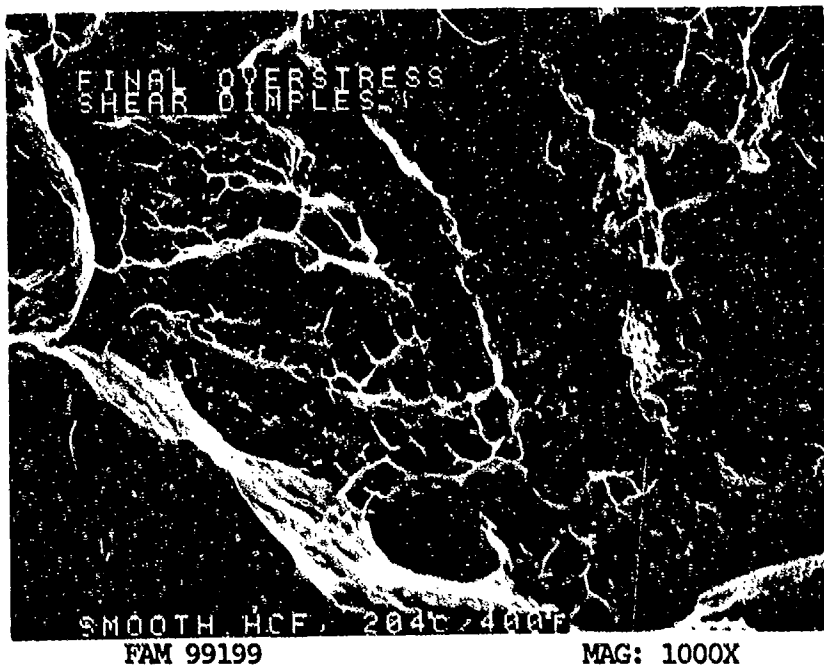


FIGURE 5-52: Dimpled overstress and cleavage in the final fracture area. Some of the dimples are very fine, some are coarser.

MATERIAL

A-286
AMS 5525 Plate

TEST DATA

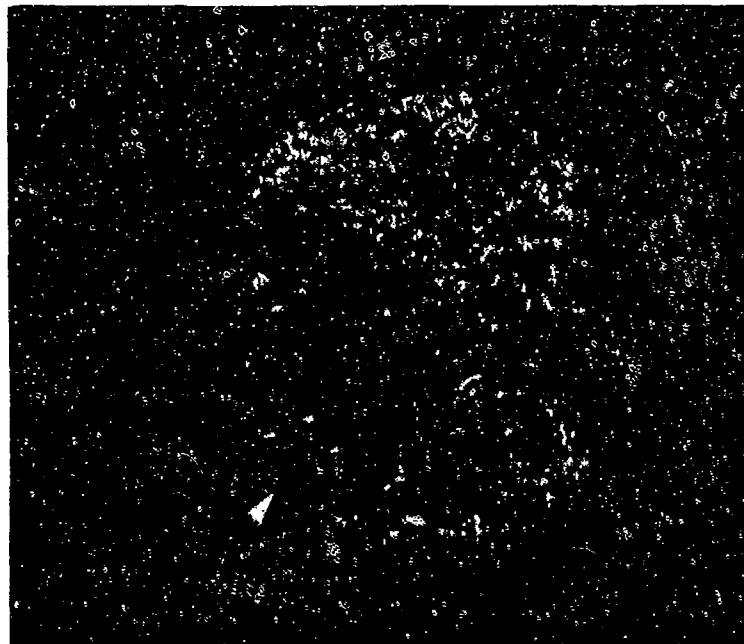
TEST TYPE
Smooth HCF

TEST CONDITIONS

Stress: 344.7 MPa (50.0 ksi)/-344.7 MPa (-50.0 ksi)
Stress Ratio: -1
Frequency: 1800 cpm
Atmosphere: Air
Temperature: 704°C (1300°F)
Test Direction: Longitudinal

TEST RESULTS

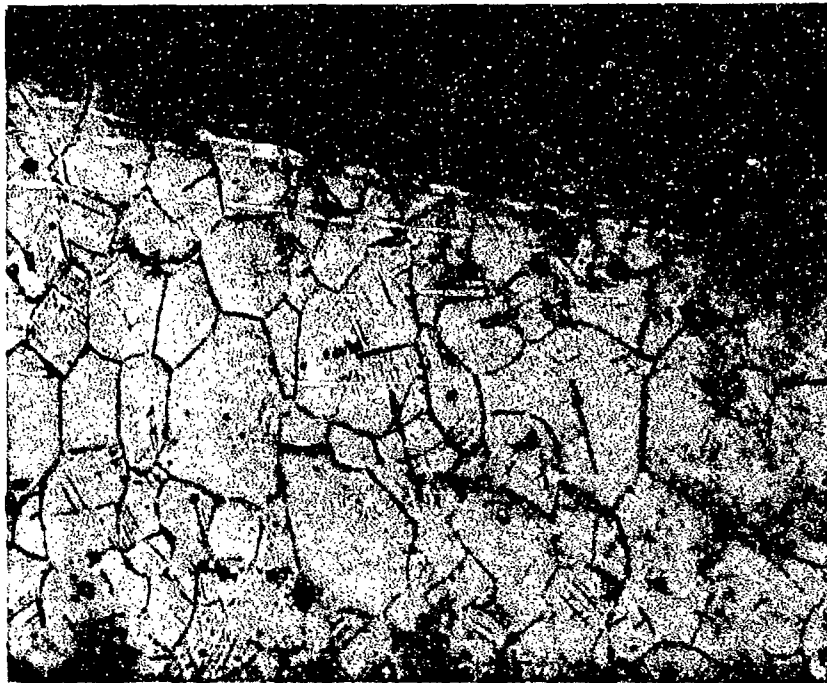
Cycles to Fracture: 249,000



FAL 93831

MAG: 15X

FIGURE 5-53: Test results and fractography of A-286 704°C (1300°F) smooth HCF test. The origin area is shown by an arrow and the extent of fatigue is shown by brackets.

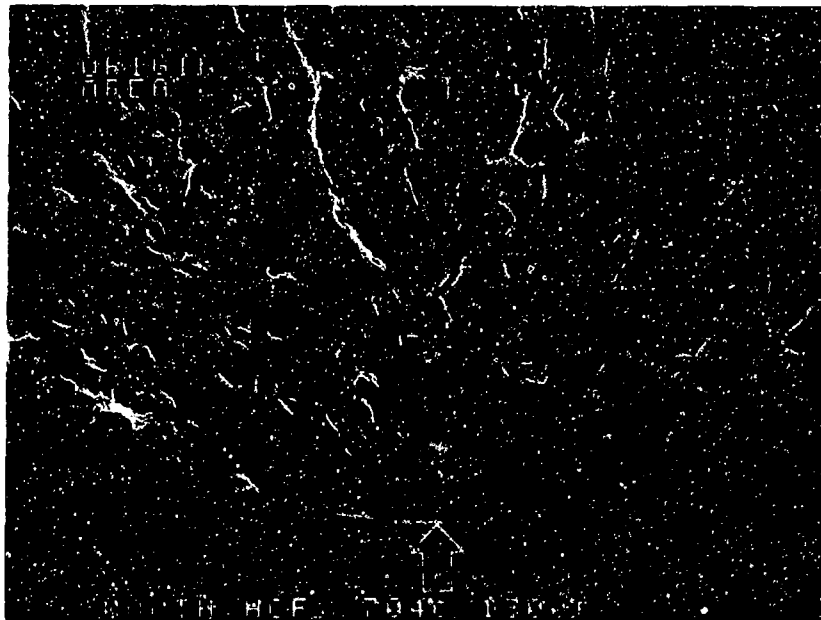


FAM 100177

MAG: 100X

FIGURE 5-54: Optical photomicrograph showing transgranular fatigue progression. Strain lines are visible in the grains near the fracture (arrows). The fracture appears to be oxidized.

Etchant: 15ml HCl, 10ml HNO₃, 10ml acetic acid



FAM 99200

MAG: 50X

FIGURE 5-55: Low magnification photograph of the origin area showing surface origin (arrow).



FAM 99201

MAG: 200X

FIGURE 5-56: Localized origin with stage I faceting. Feathery cleavage (arrows) is visible just back from the origin.

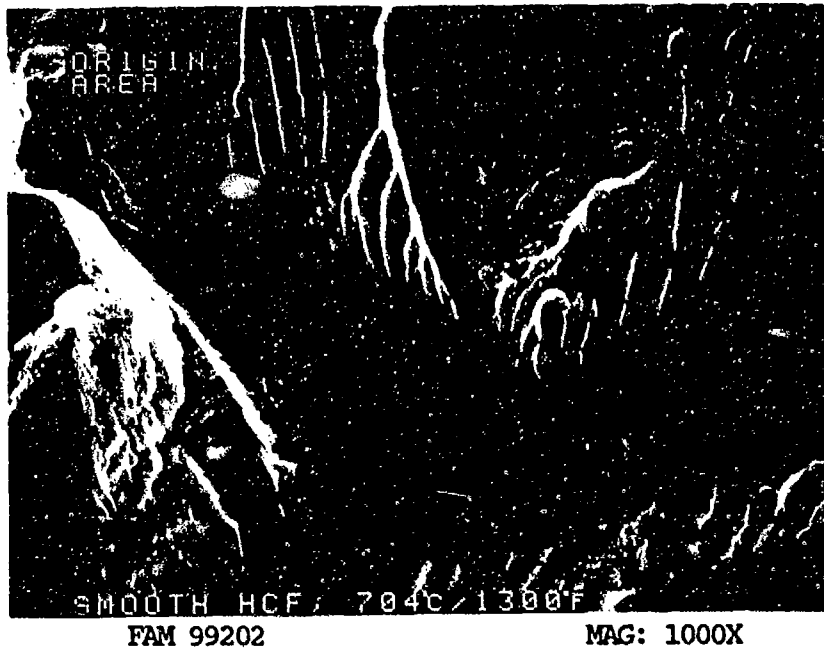


FIGURE 5-57: Possible fatigue striations on a stage I fatigue facet in the origin area. These also could be cleavage steps.

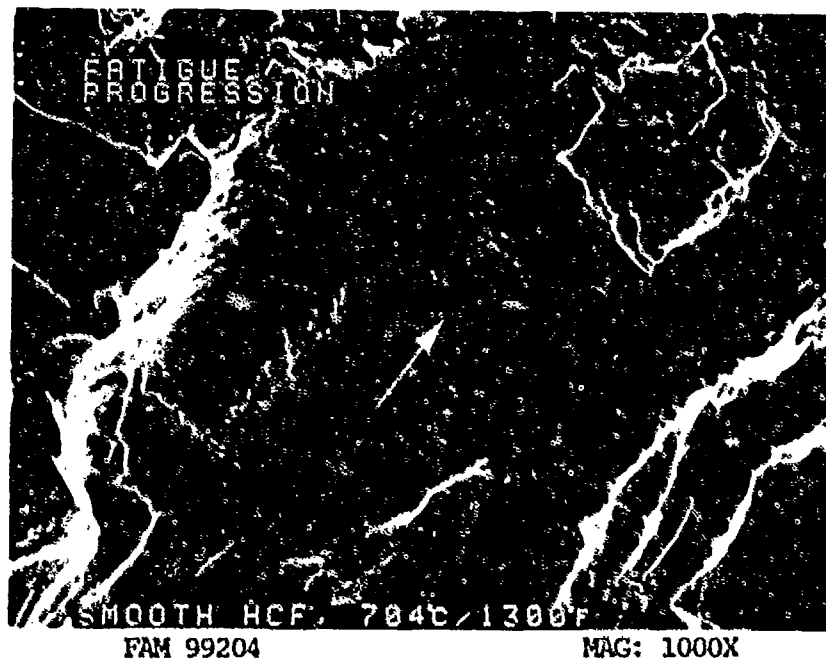


FIGURE 5-58: Fatigue striations in the fatigue progression zone near the center of the specimen. An arrow indicates the direction of propagation.

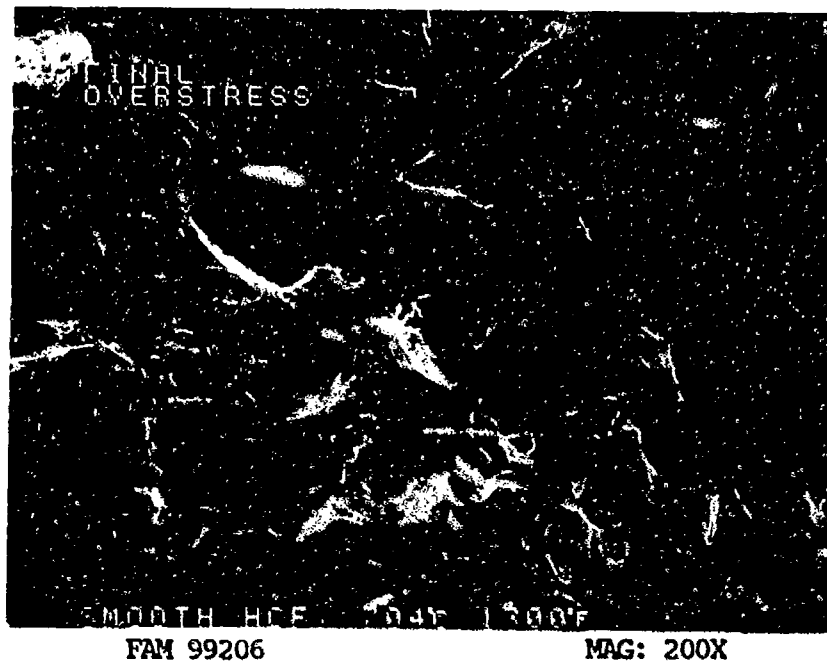


FIGURE 5-59: Dimpled overstress with some intergranular features in the final overstress area.

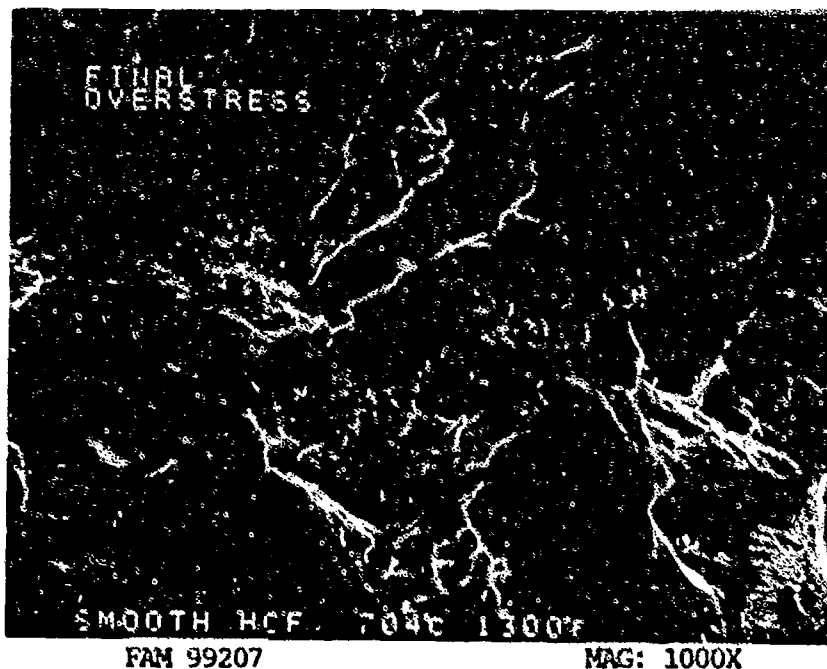


FIGURE 5-60: Higher magnification photograph showing dimpled overstress in the grain edges with fine, shallow dimples on the grain faces.

MATERIAL

A-286
AMS 5525 Plate

TEST DATA

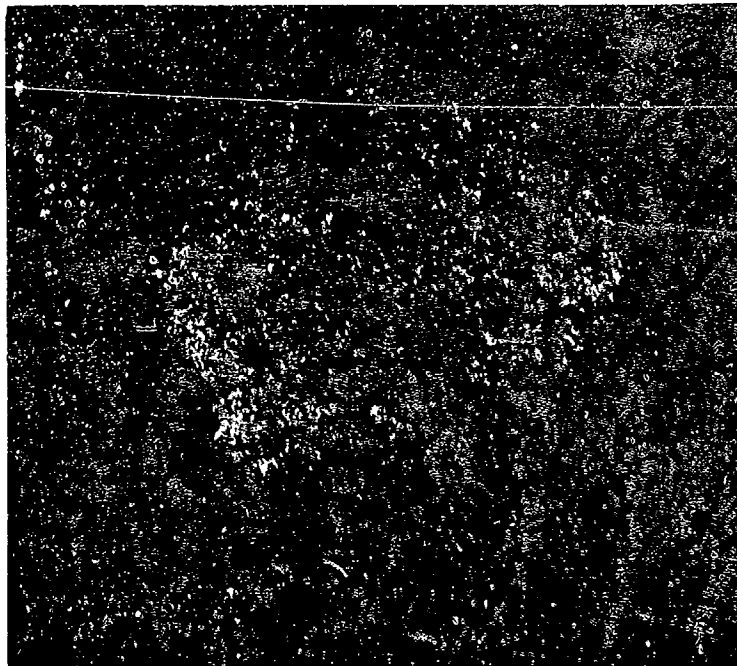
TEST TYPE
Smooth LCF

TEST CONDITIONS

Stress: 758.4 MPa (110 ksi)/ 38.0 MPa (5.5 ksi)
Stress Ratio: 0.05
Frequency: 10 cpm
Atmosphere: Air
Temperature: 204°C (400°F)
Test Direction: Longitudinal

TEST RESULTS

Cycles to Fracture: 23,410



FAL 93212

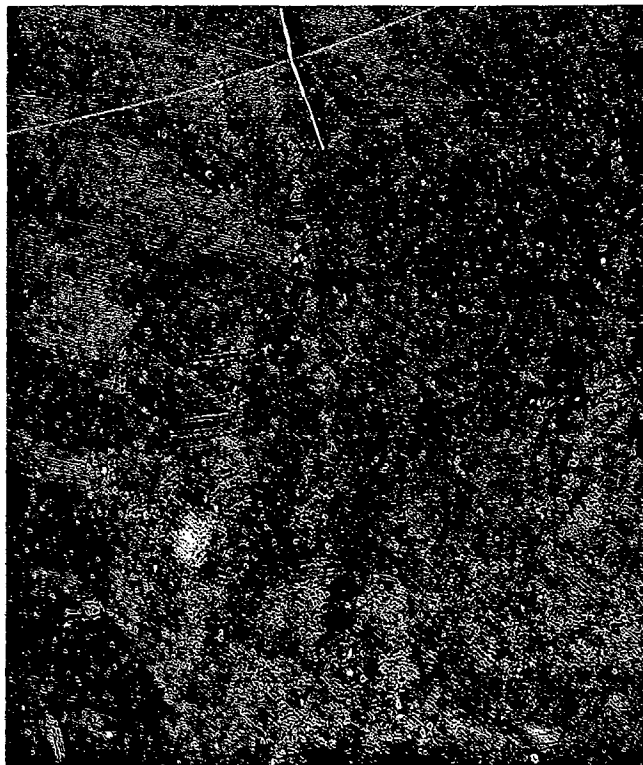
MAG: 10X

FIGURE 5-61: Test results and fractography of A-286 204°C (400°F) smooth LCF test. No fatigue progression is visible at this magnification.



FAM 100292

MAG: 100X



FAM 100221

MAG: 50X

FIGURE 5-62: Optical photomicrographs showing the transgranular fatigue progression and secondary cracks (top) and the final overstress (bottom). The final overstress area exhibits numerous subsurface secondary cracks (arrows). No strain lines are visible.

Etchant: 15ml HCl, 10ml HNO₃, 10ml acetic acid

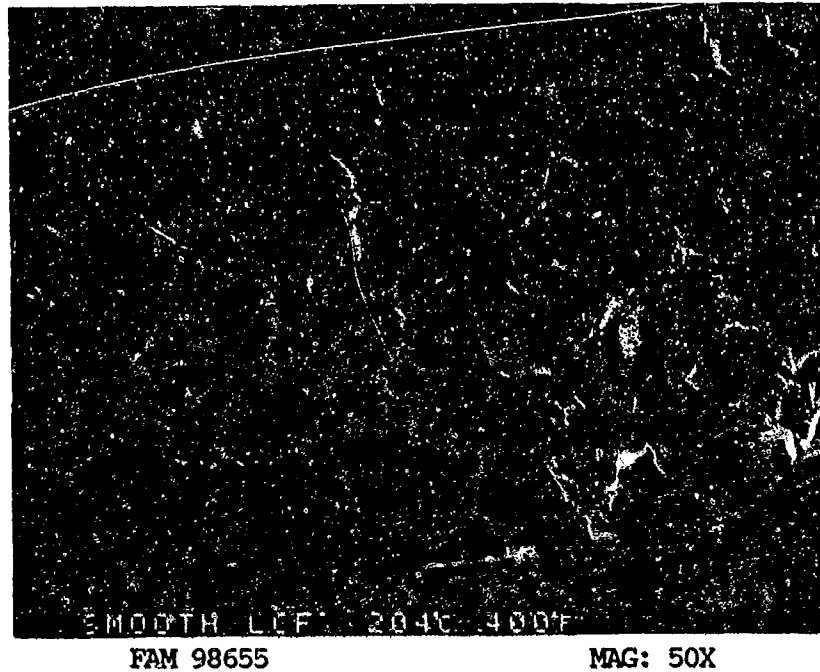


FIGURE 5-63: Low magnification photograph showing several small fatigue origin areas.

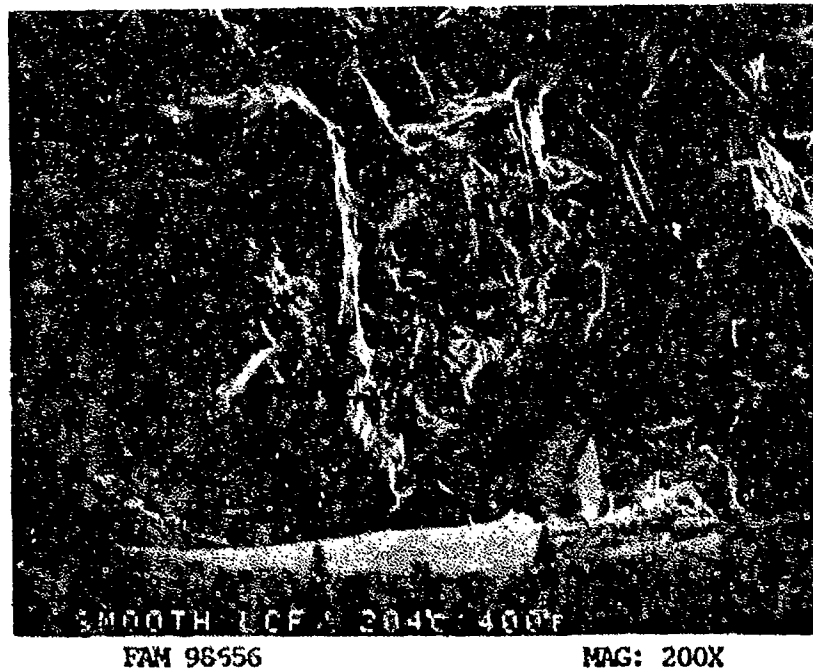


FIGURE 5-64: Several stage I fatigue facets (arrows) at the surface in the area shown in Figure 5-63.

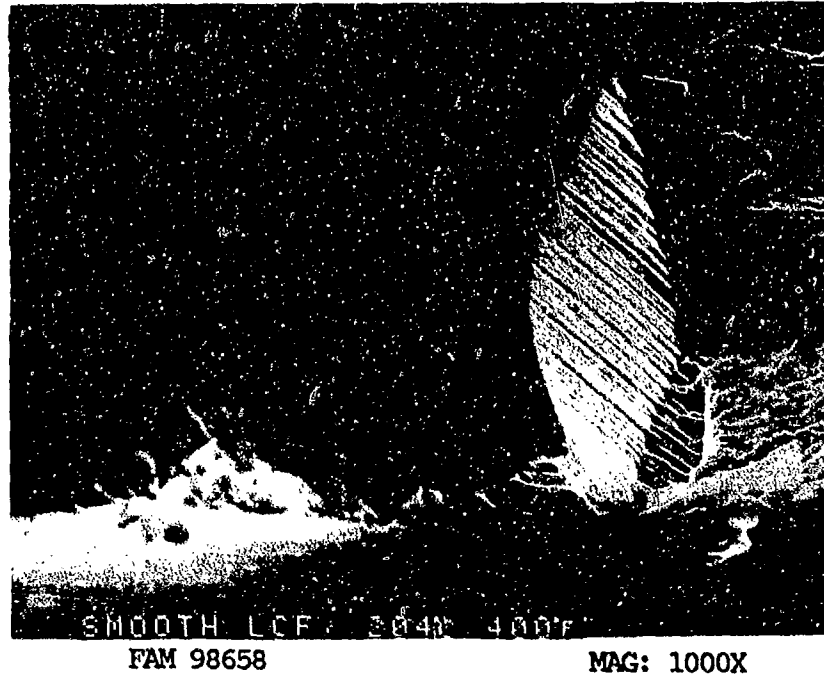


FIGURE 5-65: Higher magnification photograph of a stage I fatigue facet. The striation-like lines (brackets) on the adjacent facet are slip lines.

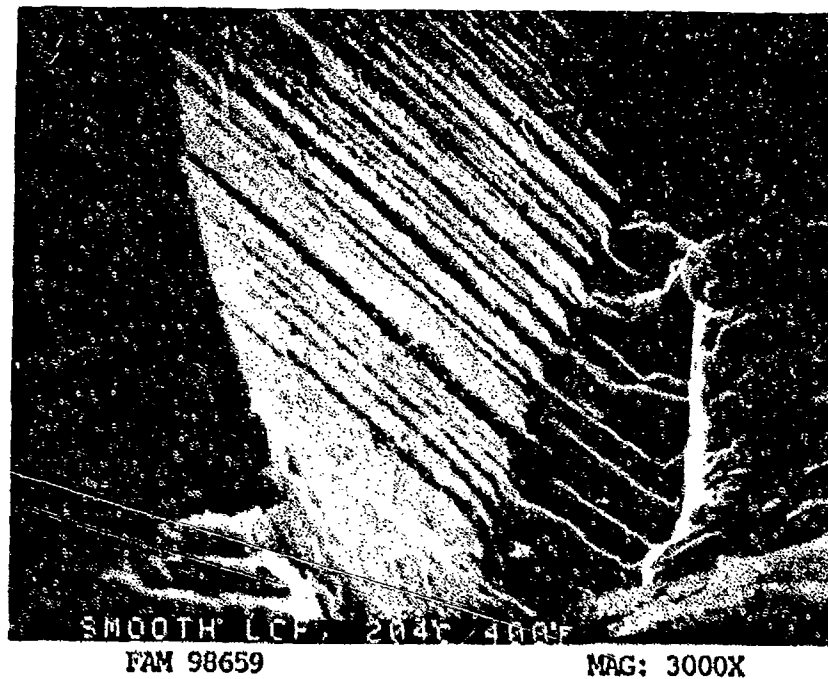


FIGURE 5-66: High magnification photograph of the slip lines shown in Figure 5-65.

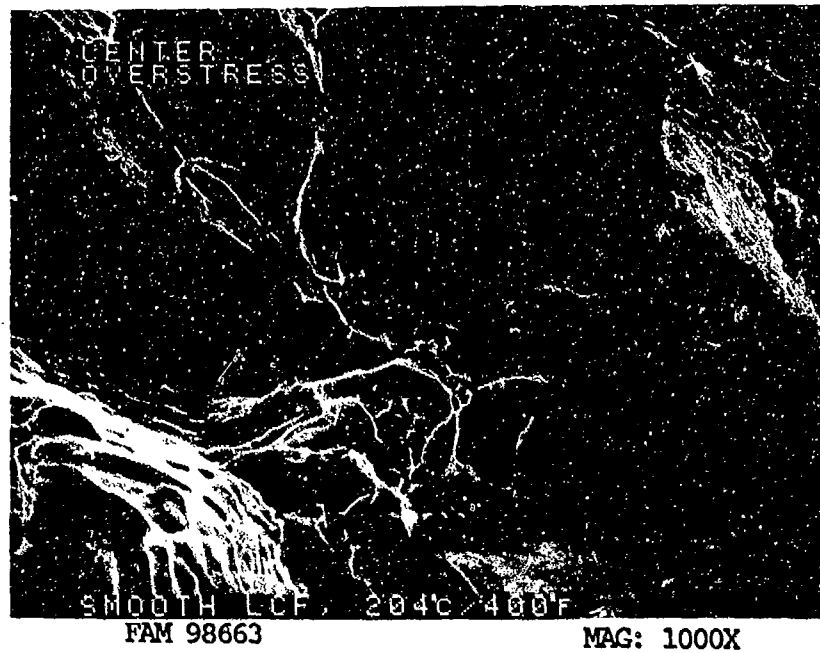


FIGURE 5-67: Overstress features near the center of the specimen are a mixture of intergranular rupture and dimpled overstress.

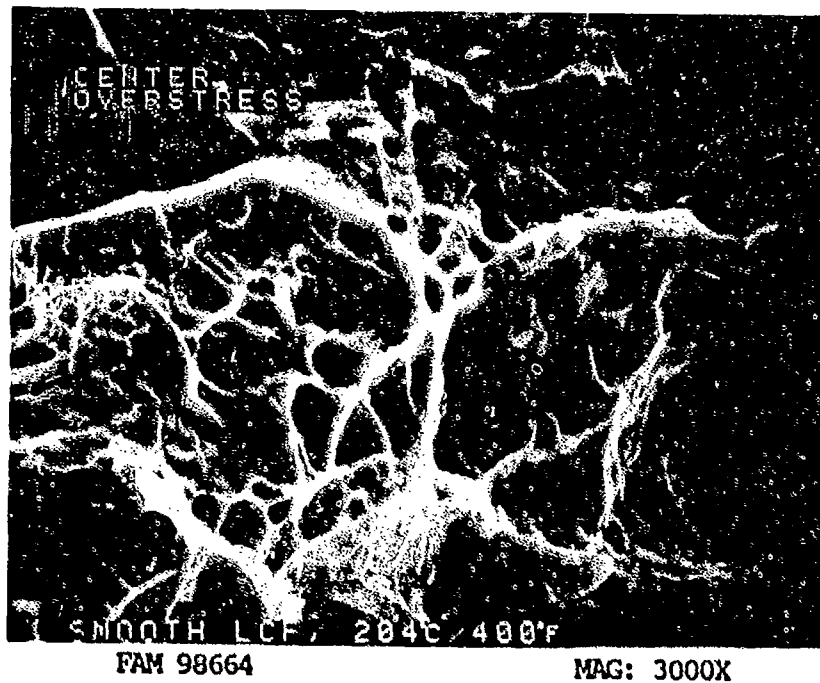


FIGURE 5-68: Dimpled overstress near the center of the specimen. A carbide is visible at the bottom of a dimple (arrow).

MATERIAL

A-286
AMS 5525 Plate

TEST DATA

TEST TYPE
Smooth LCF

TEST CONDITIONS

Stress: 689.5 MPa (100 ksi)/ 34.5 MPa (5 ksi)
Stress Ratio: 0.05
Frequency: 10 cpm
Atmosphere: Air
Temperature: 704°C (1300°F)
Test Direction: Longitudinal

TEST RESULTS

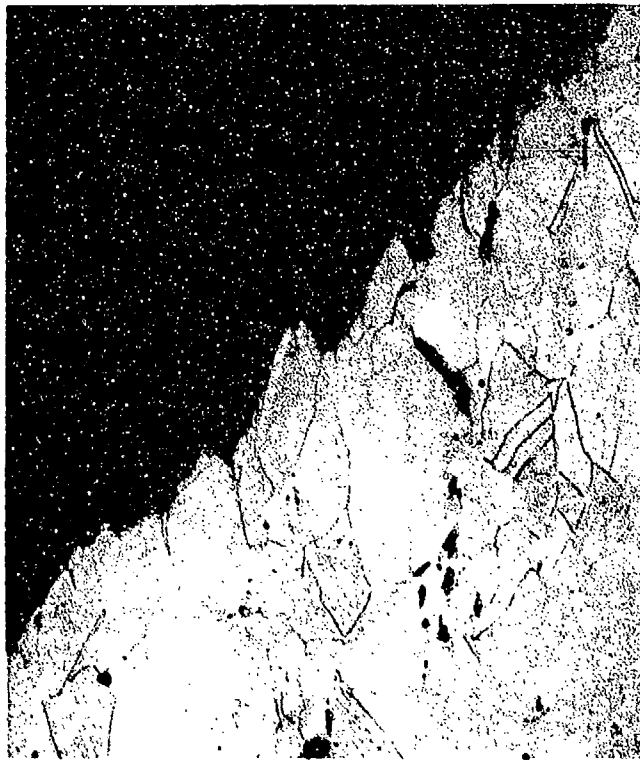
Cycles to Fracture: 364



FAL 92921

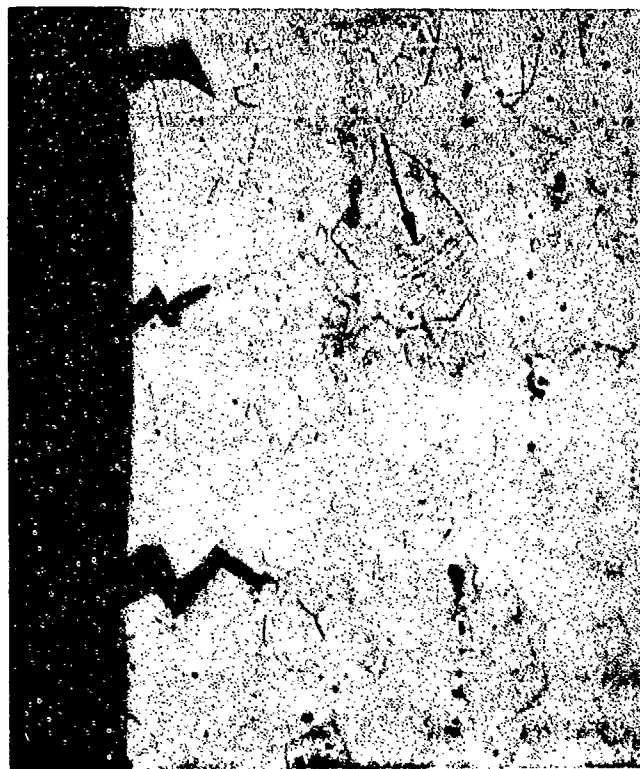
MAG: 12X

FIGURE 5-69: Test results and fractography of A-286 704°C (1300°F) smooth LCF test. No fatigue is discernible at this magnification.



FAM 100179

MAG: 200X



FAM 100178

MAG: 200X

FIGURE 5-70: Optical photomicrographs showing the final overstress area (top) and intergranular secondary cracks (bottom). The final overstress area exhibits grain elongation and some strain lines. Compare with the 400° F specimen (Figure 5-63). Strain lines are also visible in isolated grains along the gage section (arrow).

Etchant: 15ml HCl, 10ml HNO₃, 10ml acetic acid

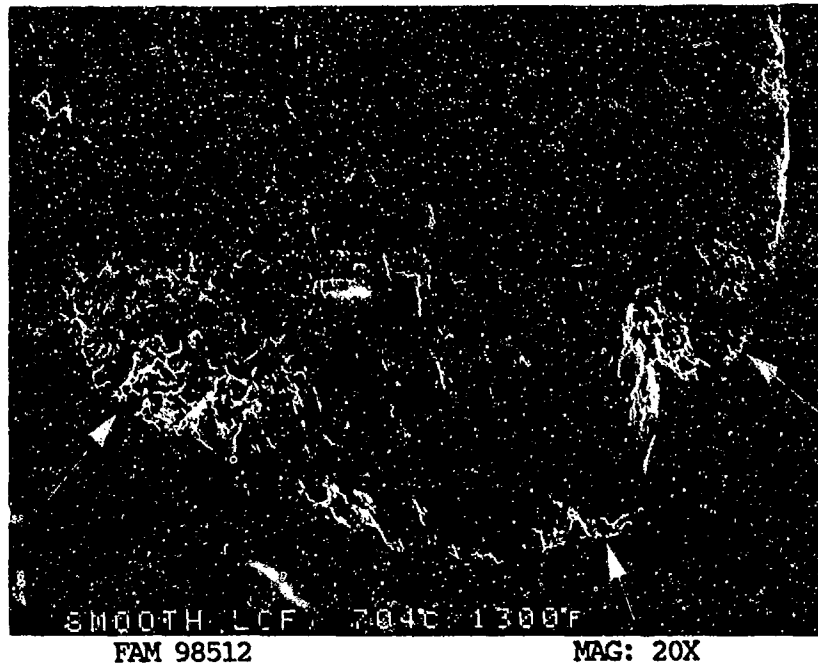


FIGURE 5-71: Overall photograph showing several fatigue origins that exhibit a granular appearance (arrows). Some secondary cracking is also visible on the specimen surface.

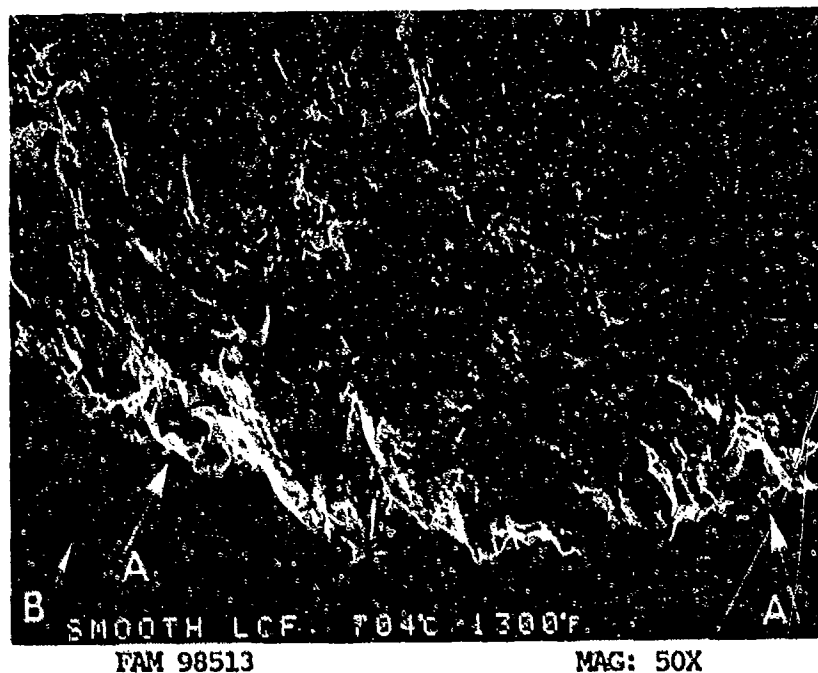


FIGURE 5-72: Photograph showing two small fatigue zones (arrows A). Secondary cracking (arrow B) is visible adjacent to the primary fracture.

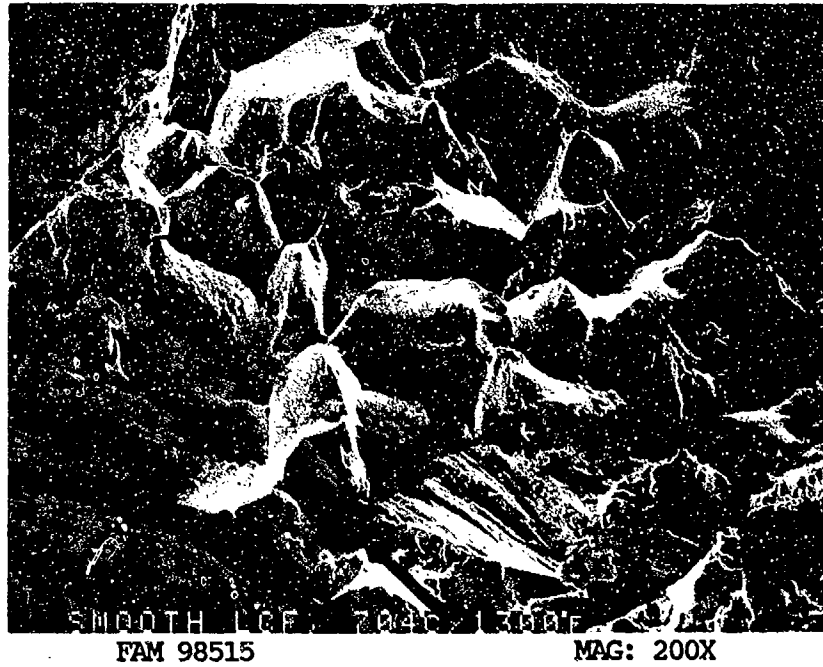


FIGURE 5-73: Intergranular appearance of the initial fatigue progression.

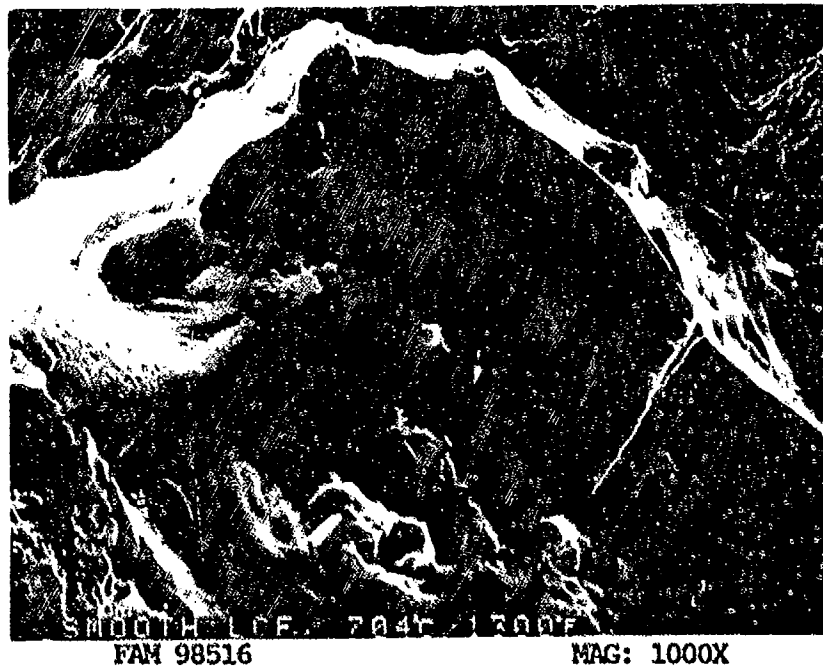


FIGURE 5-74: Remnant features indicative of fatigue. An arrow indicates the direction of propagation.

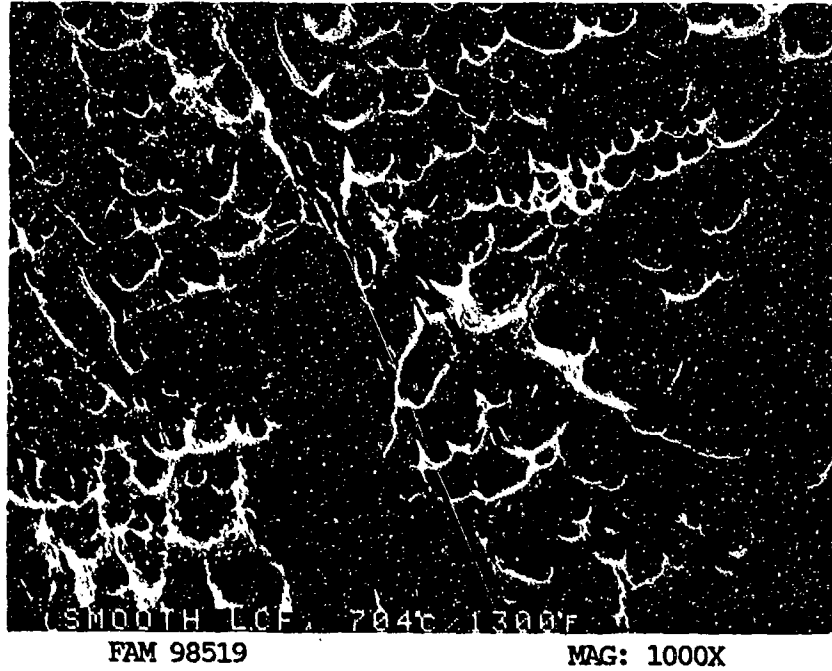


FIGURE 5-75: Shear dimples in the final overstress area. Arrows indicate the directions of relative motion.

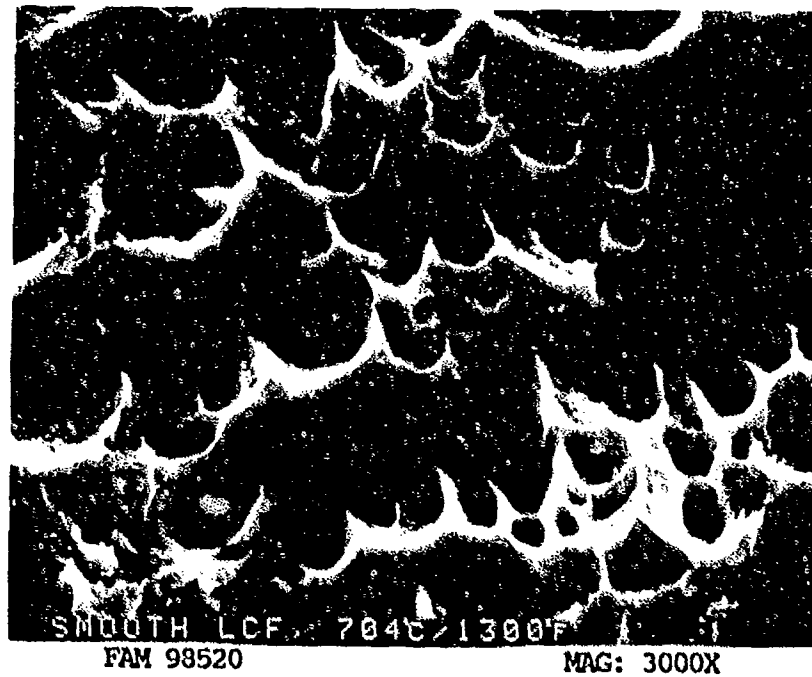


FIGURE 5-76: High magnification photo of the shear dimples shown in Figure 5-75.

MATERIAL

A-286
AMS 5525 Plate

TEST DATA

TEST TYPE

Stress Corrosion

TEST CONDITIONS

Stress: 1378.9 MPa (200.0 ksi)
Atmosphere: 3% NaCl (simulated sea water) vapor
Temperature: 93°C (200°F)
Test Direction: Longitudinal U-Bend Specimen

Test Results

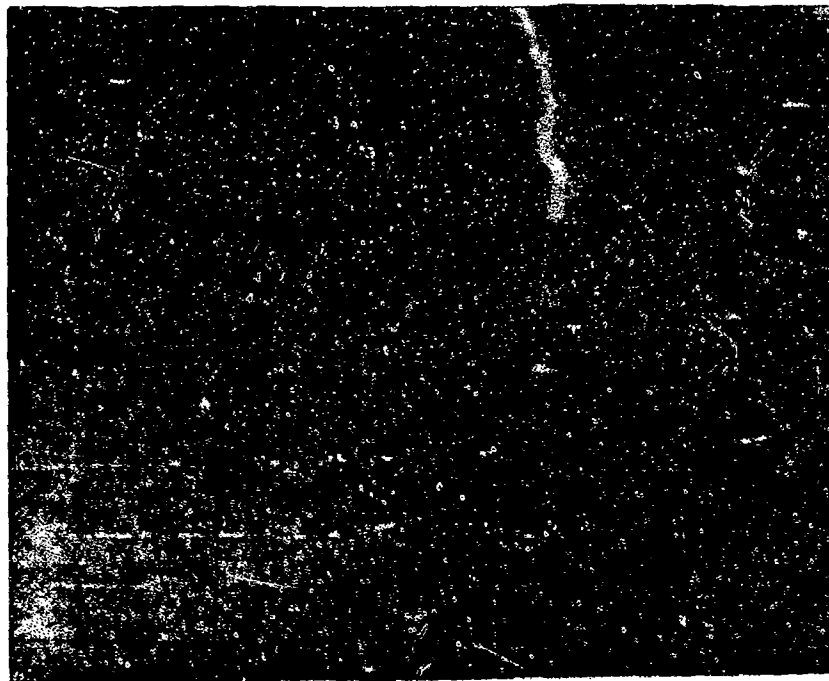
Test Time: 864 hours



FAL 97149

MAG: 8 1/2X

FIGURE 5-77: Test results and fractography of A-286 stress corrosion test. The stress corrosion area appears dark due to oxidation.

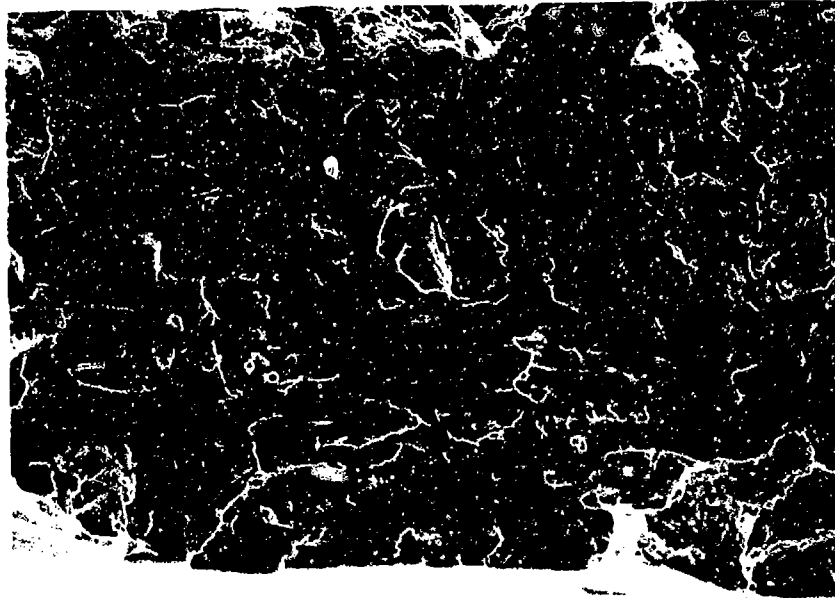


FAM 100171

MAG: 200X

FIGURE 5-78: Optical photomicrograph showing the branching cracks characteristic of stress corrosion. Often this appearance in the microstructure is the primary indication of stress corrosion.

Etchant: Unetched

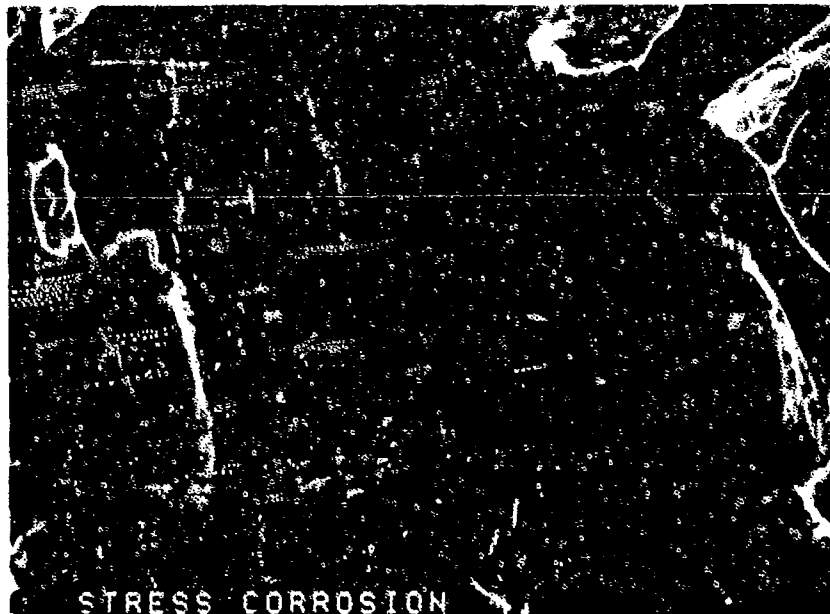


STRESS CORROSION

FAM 100450

MAG: 200X

FIGURE 5-79: Low magnification photograph of the stress corrosion area showing feathery features.



STRESS CORROSION

FAM 100451

MAG: 1000X

FIGURE 5-80: Higher magnification photograph showing steps and transverse secondary cracks along with feathery features.

MATERIAL

A-286
AMS 5525 Plate

TEST DATA

TEST TYPE

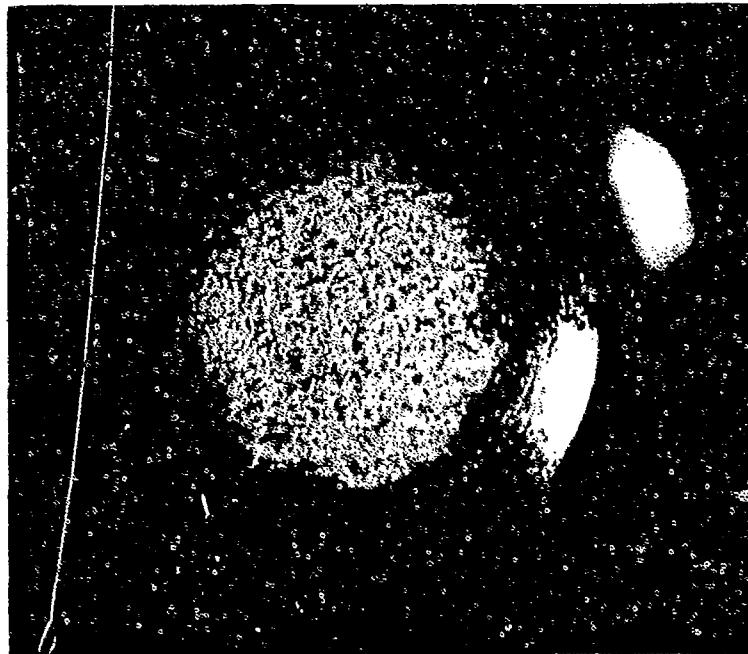
Hydrogen embrittlement

TEST CONDITIONS

Stress: 1013.8 MPa (147 ksi)
Atmosphere: Air
Temperature: Room Temperature
Test Direction: Longitudinal
Charging: Cathodically polarized 30 min. at 15Vdc in 1% aqueous HCl using a platinum anode.

Test Results

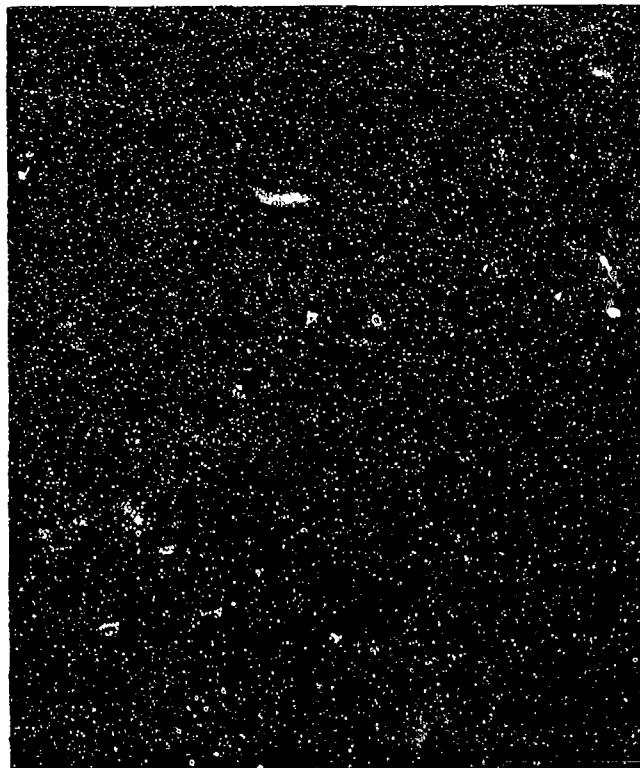
Failed during loading



FAL 93217

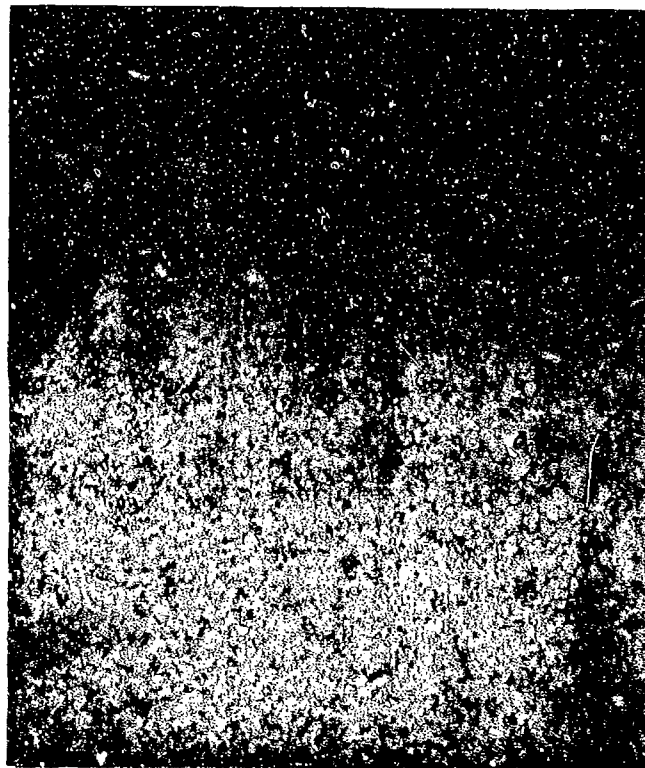
MAG: 10X

FIGURE 5-81: Test results and fractography of A-286 hydrogen embrittlement test. No shear lip is visible but the O.D. of the fracture has a jagged appearance.



FAM 100223

MAG: 200X



FAM 100222

MAG: 100X

FIGURE 5-82: Optical photomicrograph showing the center (top) and edge (bottom) of the primary fracture. The grain size is finer in this specimen than in the other A-286 specimens because this specimen was taken from a different plate of material.

Etchant: 15ml HCl, 10ml HNO₃, 10ml acetic acid

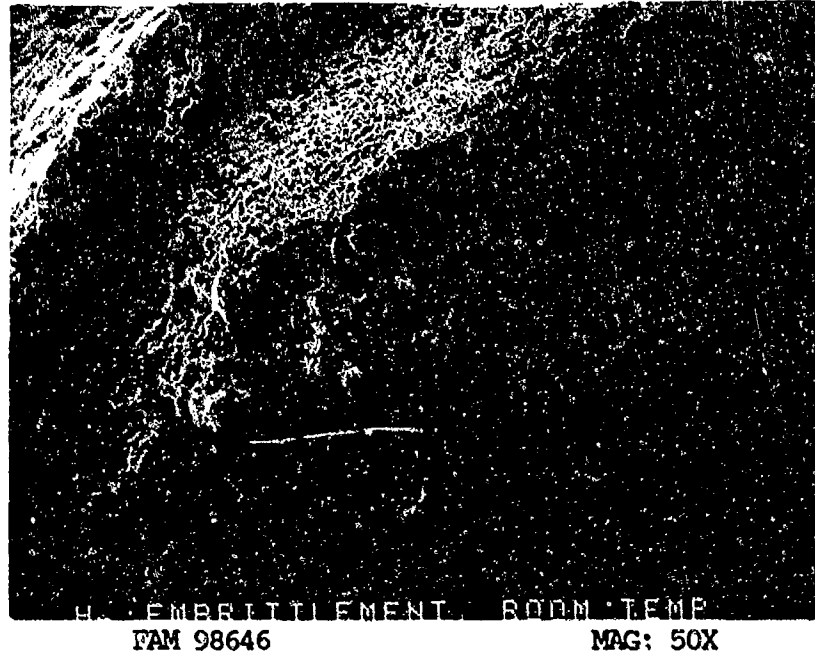


FIGURE 5-83: Low magnification photograph near the edge of the specimen.

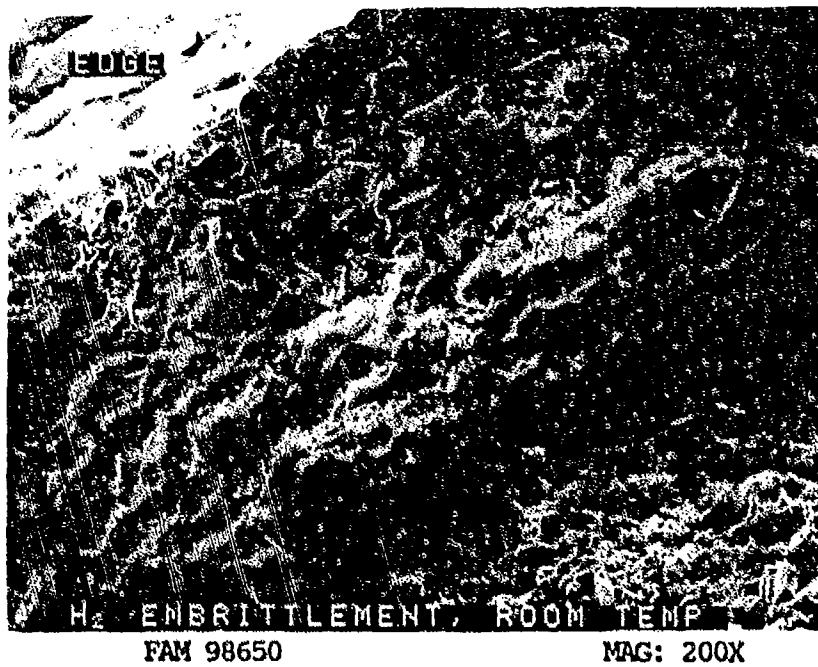


FIGURE 5-84: Lip at the outside edge of the specimen, exhibiting jagged steps.

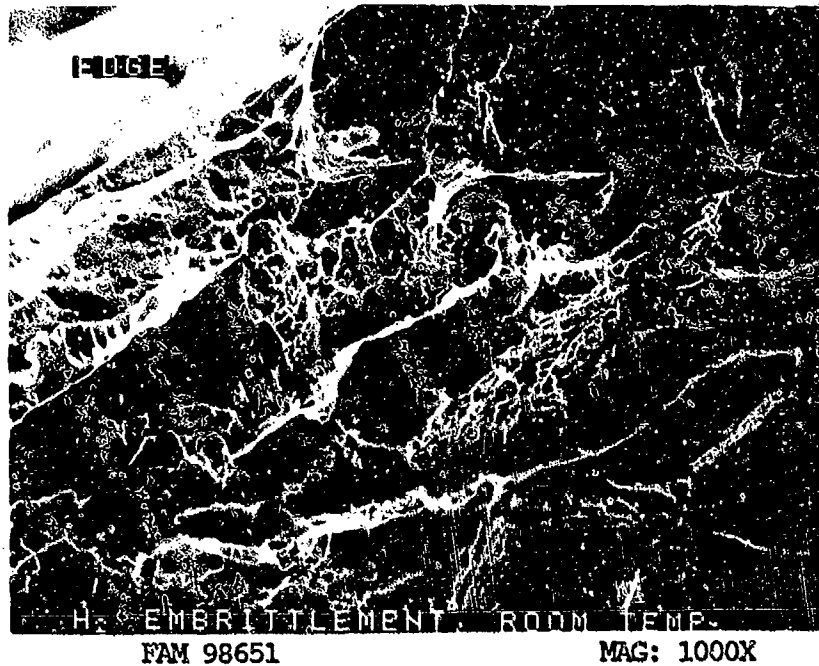


FIGURE 5-85: Jagged steps near the edge of the specimen. The steps contain small dimples and patches of cleavage.

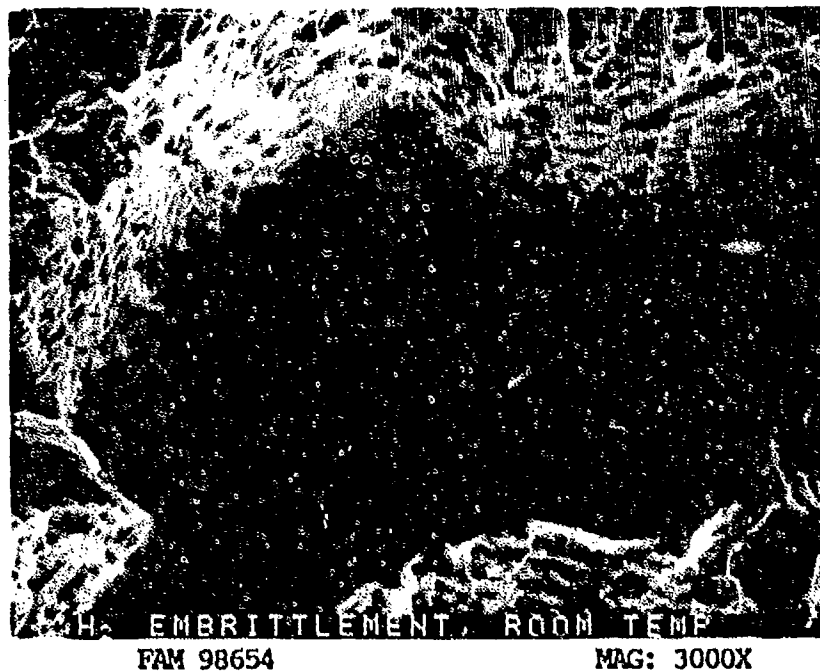


FIGURE 5-86: Higher magnification photograph of the area shown in Figure 5-85, showing steps near the edge containing dimples.

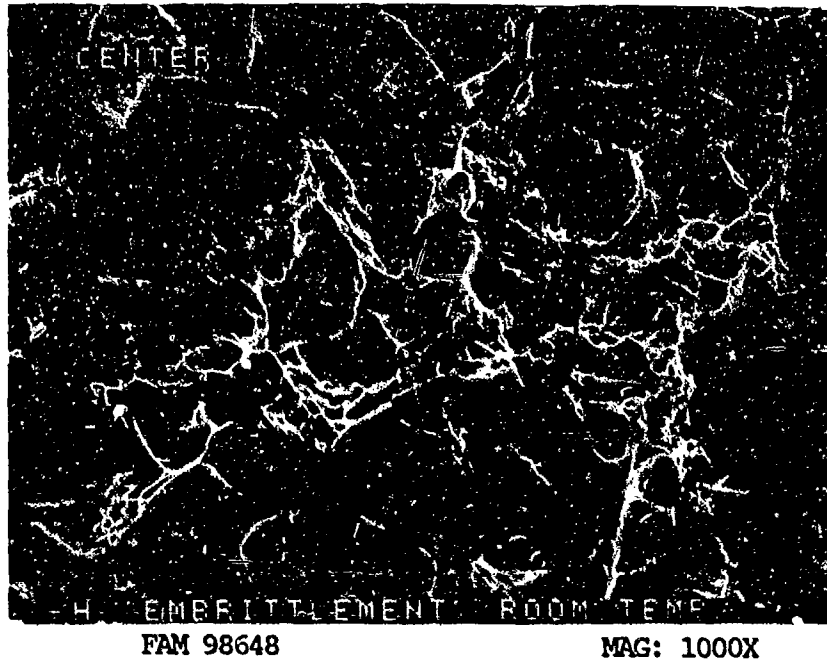


FIGURE 5-87: Final overstress area near the center of the fracture surface. Several cracked carbides are visible (arrows).

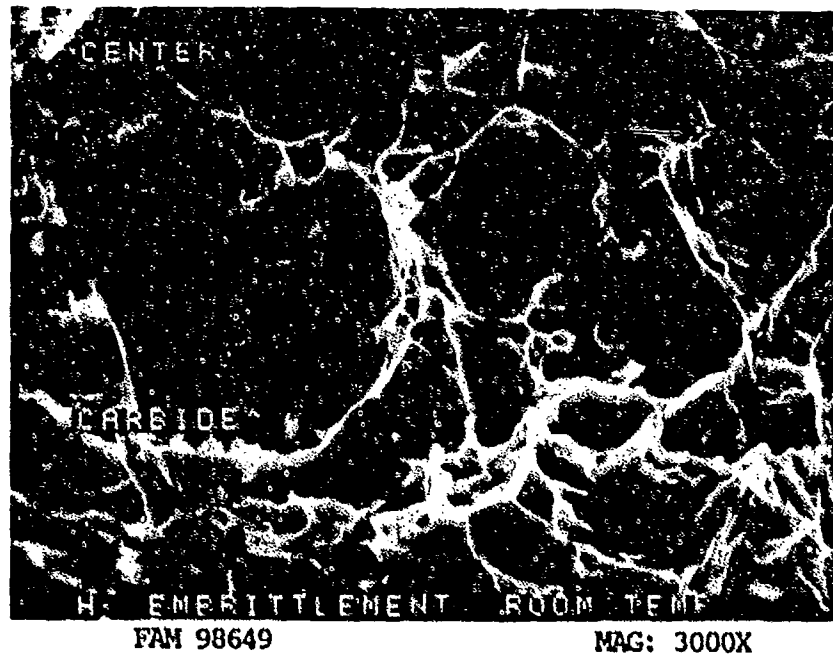


FIGURE 5-88: Dimpled overstress features in the center of the fracture. A cracked carbide is visible.

SERVICE FAILURE

FRACTURE MODE Shear Overstress (Torsion)

PART NAME Tail Cone Bolts

OPERATION DATA Fracture occurred either during tightening or loosening during assembly. Neither bolt is thought to have seen engine operation.

PART TIME New Part

	<u>REQUIRED</u>	<u>ACTUAL</u>
MAT'L		
BASE	<u>A-286 (Iron-base superalloy)</u>	<u>confirmed</u>
OTHER	<u>-</u>	<u>-</u>
HARDNESS	<u>HB 248-341</u>	<u>HB 270-275 *</u>
GRAIN SIZE	<u>No Requirement</u>	<u>-</u>
DIMENSIONAL	<u>-</u>	<u>-</u>

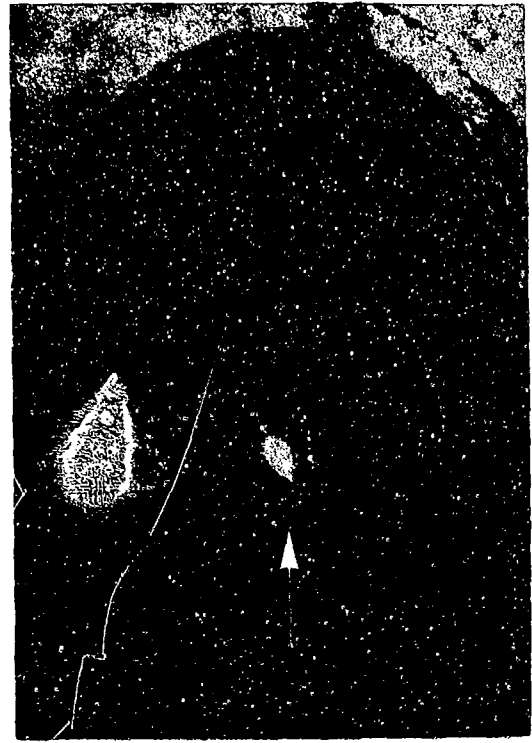
* Diamond pyramid hardness (DPH) conversions.

SUMMARY: The fracture of bolts A1 and A2 (Figure 5-89) was attributed to torsional overstress of the material. Both of the bolts were being loosened when the fracture occurred. This was determined by examination of the elongated shear dimples at the periphery of the mating fracture surfaces (Figures 5-91 and 5-92). No material or microstructural defects were found.



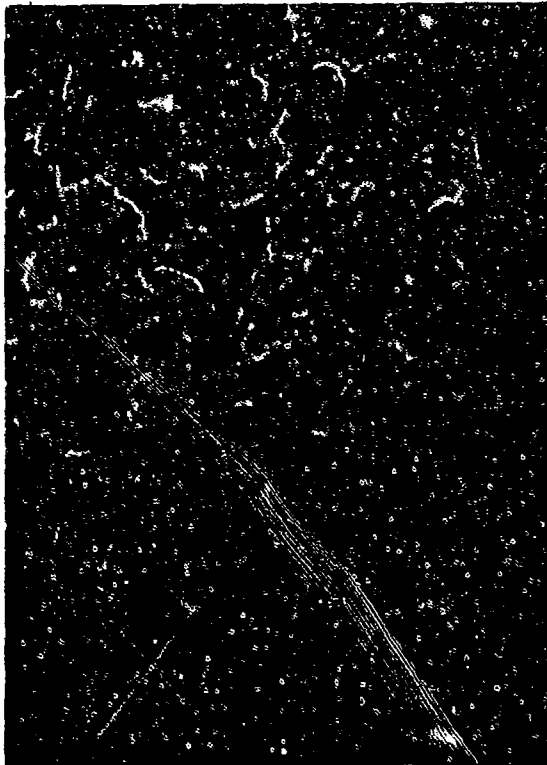
FAL 87136 MAG: 6X

FIGURE 5-89: Overall photographs of bolts A1 and A2. The torsional nature of the fractures is clearly visible.



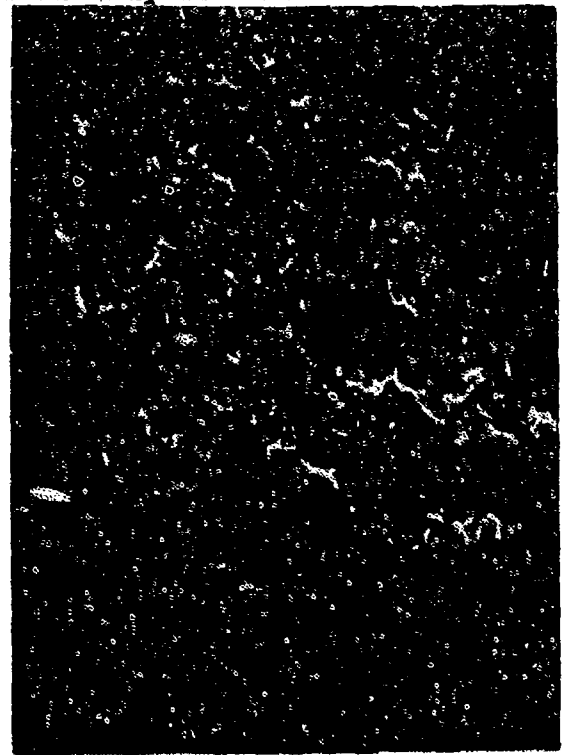
FAL 93389 MAG: 20X

FIGURE 5-90: Overall photograph of the fracture surface on tail cone bolt A1. The final overstress area is shown by an arrow.



FAL 93390 MAG: 1000X

FIGURE 5-91: Shear dimples near the edge of the fracture (location 102).



FAL 93388 MAG: 1000X

FIGURE 5-92: Shear dimples near the edge of the fracture (location 104).

Incoloy 901

Material Description

Incoloy 901 is a corrosion and oxidation resistance high nickel iron-base alloy used in the aerospace industry primarily for rotor parts operating at temperatures up to 1300 F. Incoloy 901 is available in the form of bars and forgings.

The material used in this study was heat treated to PWA 1003 (bar) with a required hardness of HB 302-388. The typical room temperature mechanical properties for PWA 1003 are as follows:

Ultimate Tensile Strength:	165 ksi min
0.2% Yield Strength:	120 ksi min
Percent Elongation:	12% min
Percent Reduction in Area:	15% min
Measured Hardness:	HB 363-432 (DPH conversion)

Fractography Overview

Both the 900^oF and 1300^oF LCF specimens had multiple faceted Stage I origins. Macroscopically, the fatigue initiation/propagation areas appeared as oxidized areas with more facets than the final overstress. Both specimens exhibited smooth oxidized fatigue striations in the Stage II fatigue propagation area, intermixed with transgranular and intergranular cleavage and quasi-cleavage. Many of the cleavage facets had slip lines. These appear as straight parallel lines that should not be confused with the generally curved, smoother striations. The final overstress areas on both specimens were a mixture of cleavage and transgranular dimpled overstress. The cleavage facets in this area often contained slip lines as were observed in the Stage II area.

The thermal-mechanical fatigue (TMF) specimens both had heavily oxidized fatigue progression areas. The in-phase specimen had one area propagating from multiple origins on the O.D. surface. The fatigue progressed through 60% of the cross section before final overstress occurred. The in-phase specimen had no well developed striations. The out-of-phase specimen had three I.D. origins and four O.D. origins, each with a discrete oxidized thumbnail area. The progression area (Stage II) contained quasi-cleavage with small patches of remnant striations. The out-of-phase specimen had heavily oxidized well developed striations in the Stage II area. The fatigue was less faceted than the in-phase specimen. The final overstress areas on both specimens exhibited a mixture of dimpled overstress and quasi-cleavage.

MATERIAL

Incoloy 901
FWA 1003 Bar

TEST DATA

TEST TYPE

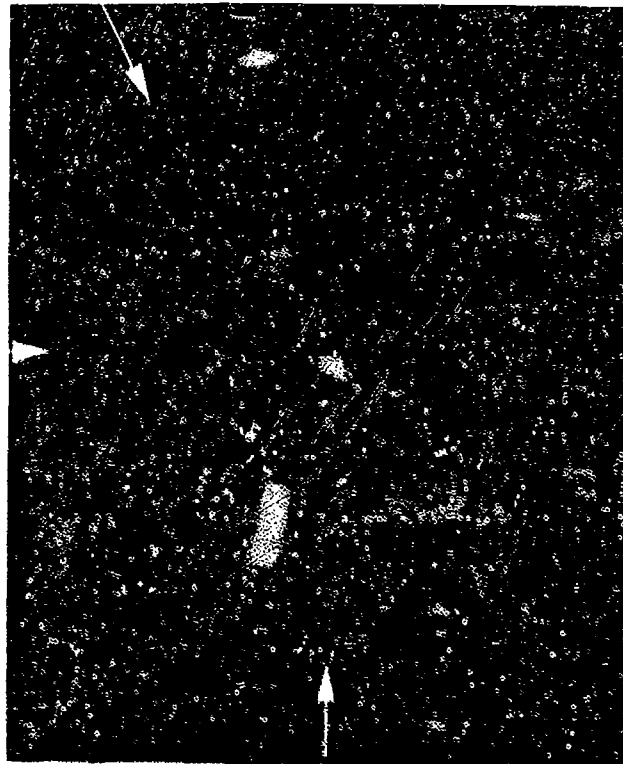
Smooth LCF

TEST CONDITIONS

Stress: 861.8 MPa (125 ksi)/ 42.7 MPa (6.3 ksi)
Stress Ratio: 0.05
Frequency: 10 cpm
Atmosphere: Air
Temperature: 482°C (900°F)
Test Direction: Longitudinal

TEST RESULTS

Cycles to Fracture: 7668



FAL 92922

MAG: 12X

FIGURE 6-1: Test results and fractography of Incoloy 901 482°C (900°F) smooth LCF test. The fatigue areas are characterized by oxidized thumbnails (arrows) at the outside surface of the specimen. The remainder of the specimen has a granular appearance.

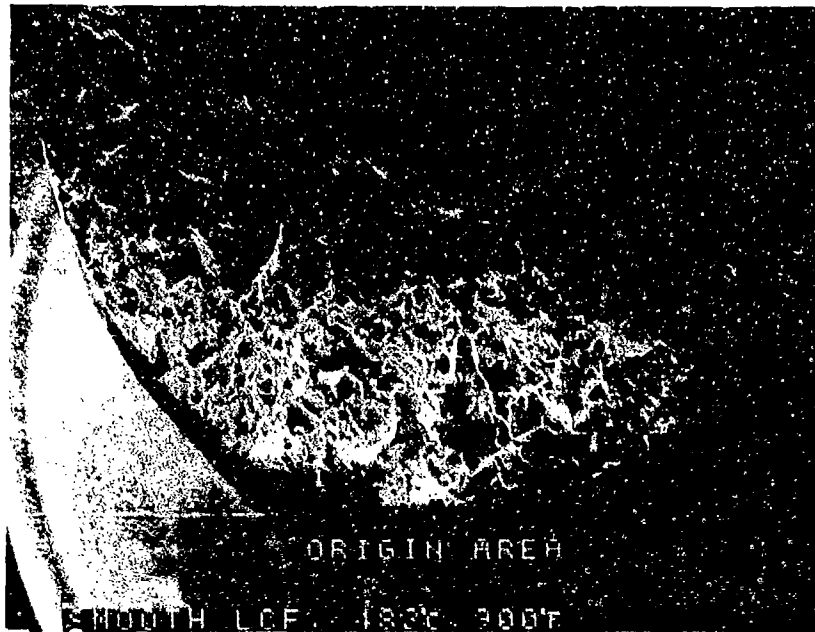


FAM 99792

MAG: 200X

FIGURE 6-2: Optical photomicrograph showing the faceted, transgranular fracture path at the fatigue origin (arrow).

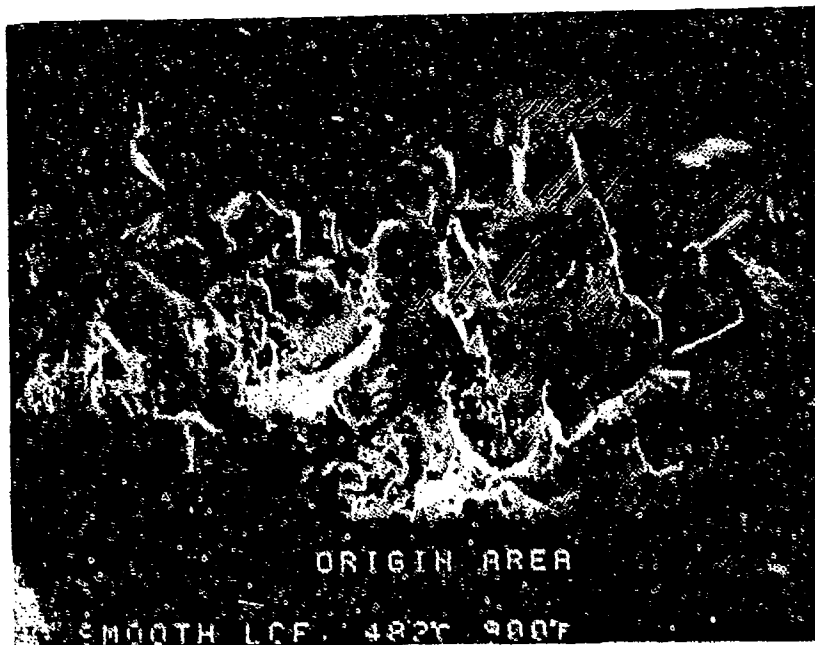
Etchant: Glyceregia



FAM 98500

MAG: 20X

FIGURE 6-3: Low magnification photograph showing a faceted fatigue progression area at the surface of the specimen.



FAM 98501

MAG: 50X

FIGURE 6-4: Higher magnification photograph of the fatigue progression area shown in Figure 6-3.

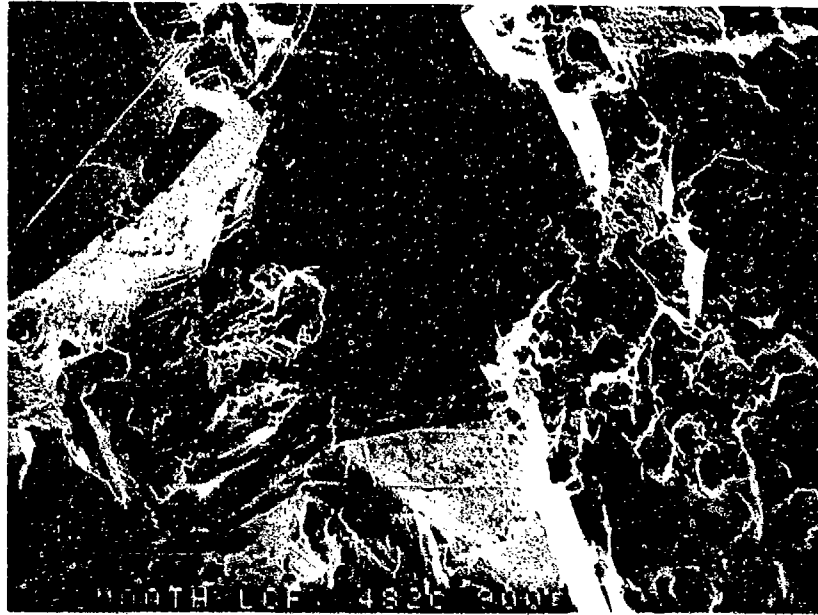


FIGURE 6-5: Higher magnification photograph of the fatigue thumbnail showing a faceted granular appearance. Slip lines are visible on the larger facets. These should not be confused with fatigue striations.

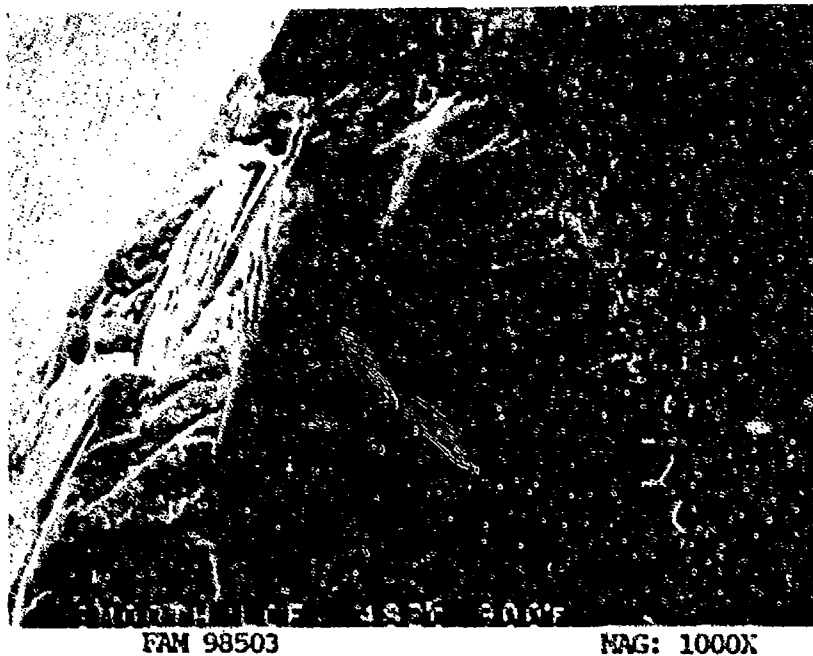


FIGURE 6-6: A small patch of fatigue striations is visible between facets. The direction of progression is shown by an arrow.

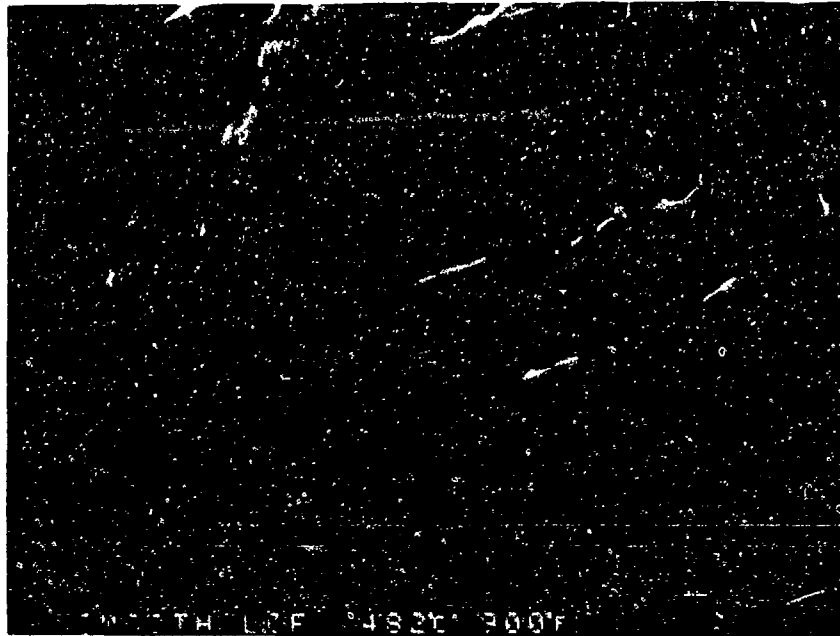


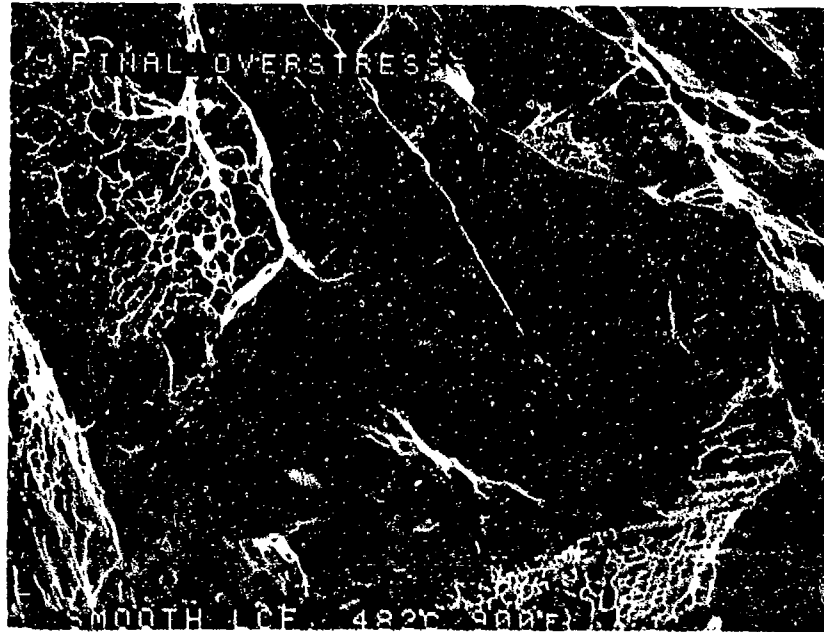
FIGURE 6-7: Higher magnification photograph of the striations shown in Figure 6-6.



FAM 98507

MAG: 200X

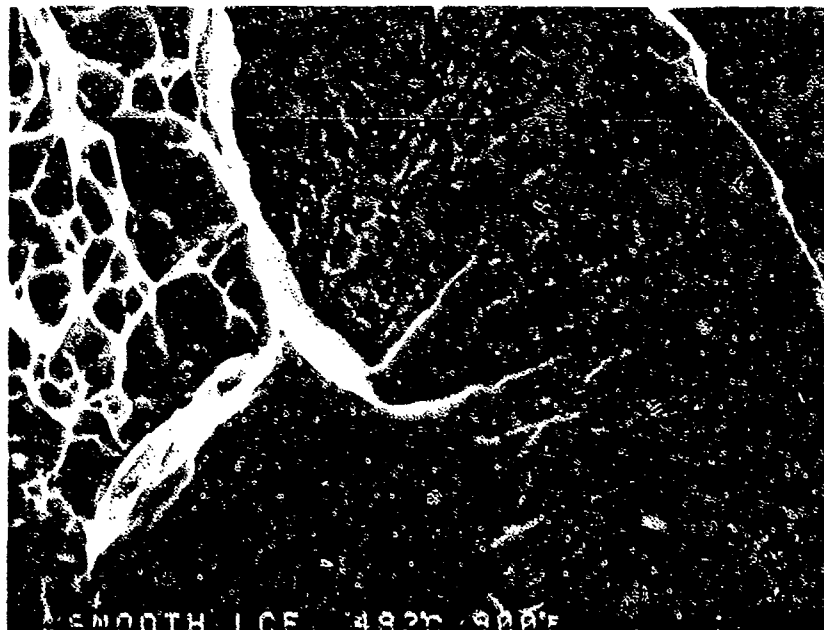
FIGURE 6-8: Final overstress area exhibiting a mixture of intergranular cleavage and transgranular dimpled overstress (mixed mode overstress).



FAM 98509

MAG: 1000X

FIGURE 6-9: Mixture of dimpled overstress and cleavage in the final overstress area.



FAM 98510

MAG: 3000X

FIGURE 6-10: Higher magnification photograph of the area shown in Figure 6-9. The striation-like lines are the result of slip and have very fine dimples between them. A possible isolated patch of fatigue striations is visible at the bottom center of the photograph (arrow).

MATERIAL

Incoloy 901
FWA 1003 Bar

TEST DATA

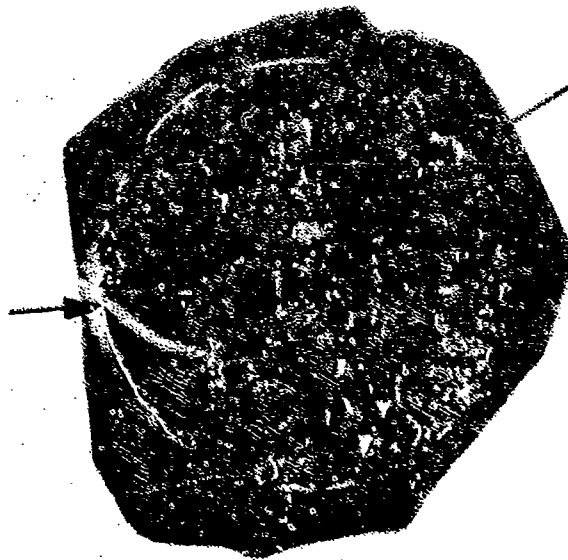
TEST TYPE
Smooth LCF

TEST CONDITIONS

Stress: 723.9 MPa (105 ksi)/ 35.9 MPa (5.2 ksi)
Stress Ratio: 0.05
Frequency: 10 cpm
Atmosphere: Air
Temperature: 704°C (1300°F)
Test Direction: Longitudinal

TEST RESULTS

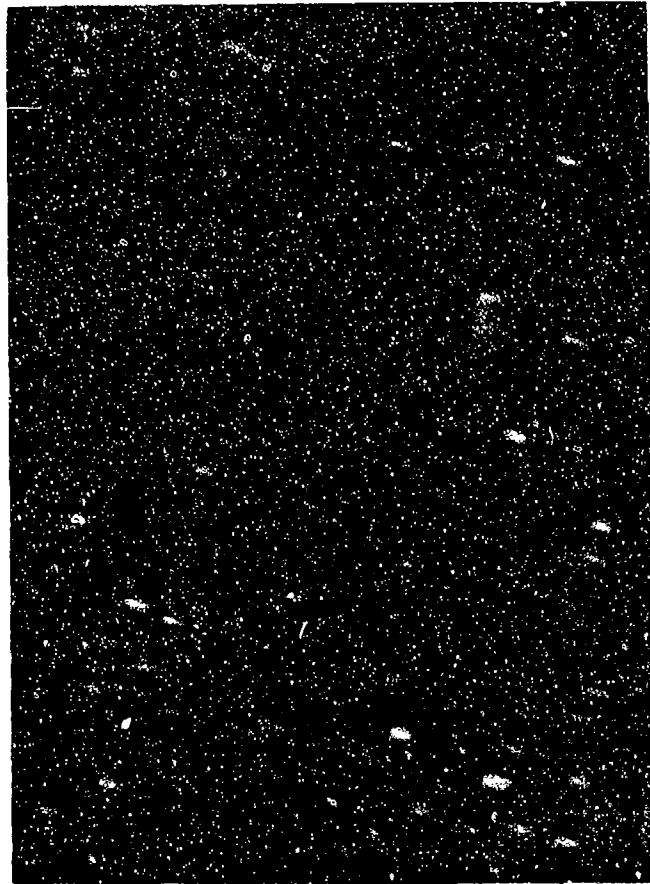
Cycles to Fracture: 2205



FAL 93209

MAG: 10X

FIGURE 6-11: Test results and fractography of Incoloy 901 704°C (1300°F) smooth LCF test. The fracture surface has a faceted appearance. The origins appear as dark areas (arrows) at the surface of the specimen.

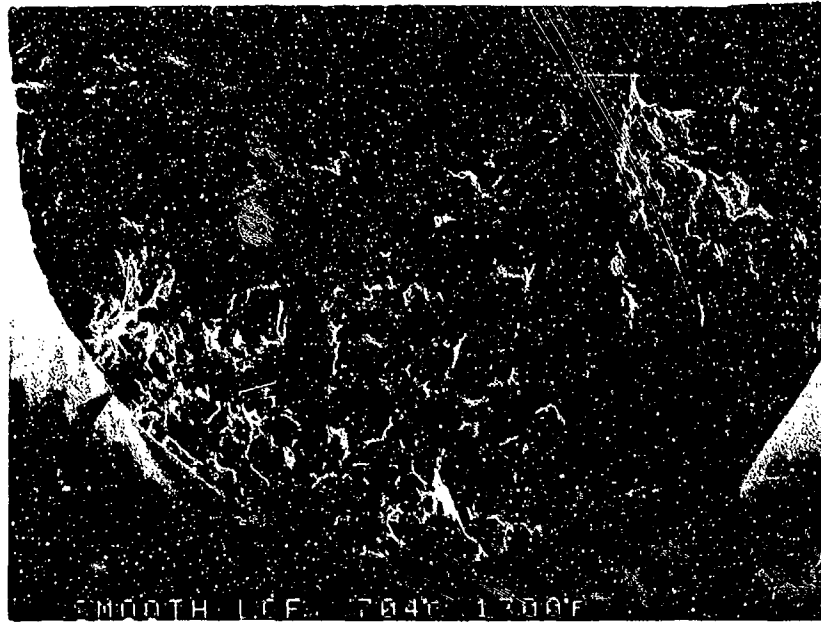


FAM 99799

MAG: 200X

FIGURE 6-12: Optical photomicrograph showing a faceted intergranular fracture path near the center of the specimen. The grain boundaries are weaker at high temperatures. Compare with Figure 6-2.

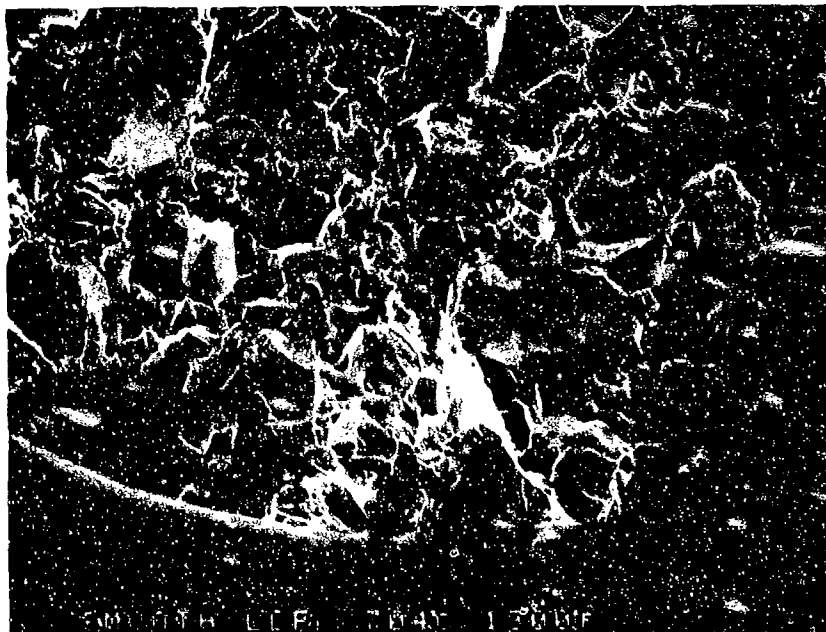
Etchant: Glycoeregia



FAM 98732

MAG: 20X

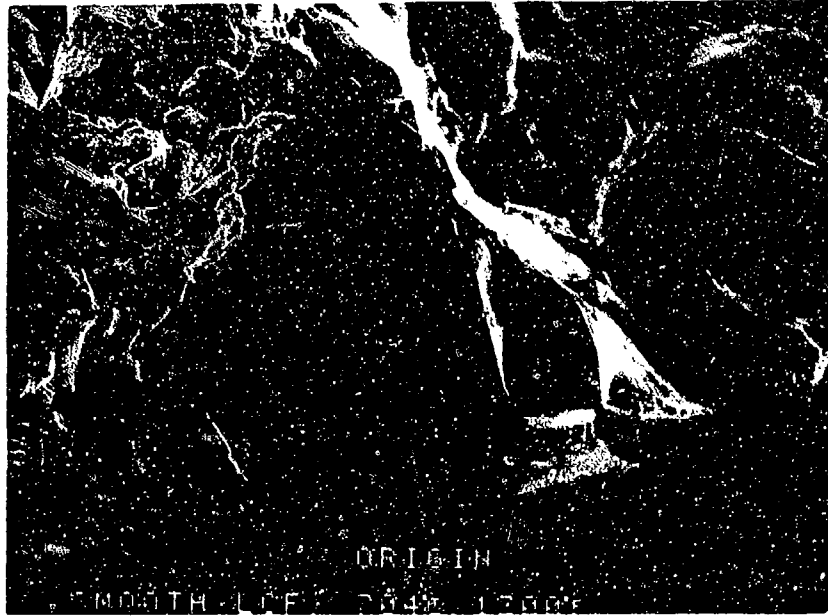
FIGURE 6-13: Low magnification photograph showing several stage I fatigue facets at origin sites (arrows).



FAM 98733

MAG: 50X

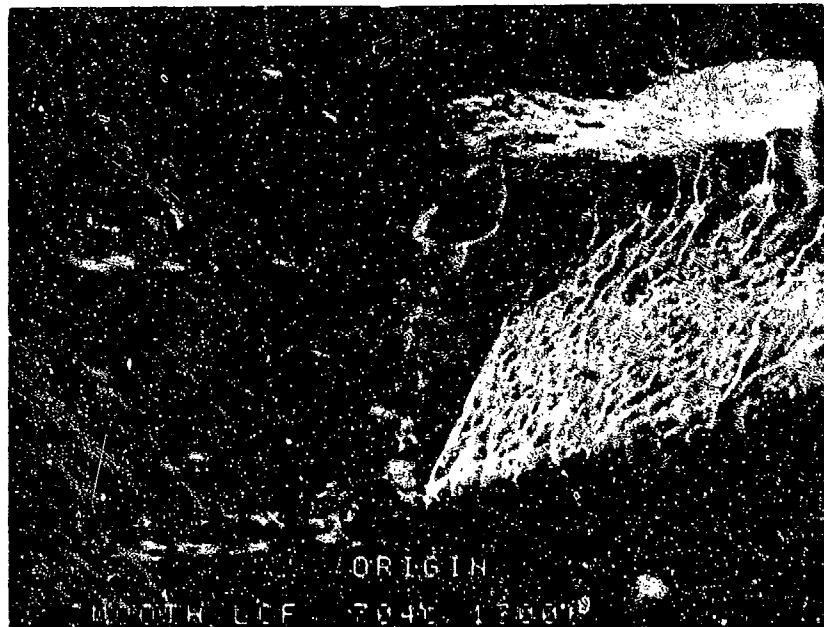
FIGURE 6-14: Higher magnification photograph of a fatigue thumbnail area. The fracture surface is a collection of fatigue facets.



FAM 98734

MAG: 200X

FIGURE 6-15: Higher magnification photograph of the origin area (stage I fatigue facet) shown in Figure 6-14.



FAM 98735

MAG: 1000X

FIGURE 6-16: High magnification photograph of the origin area shown in Figure 6-15, revealing moderately oxidized surfaces.

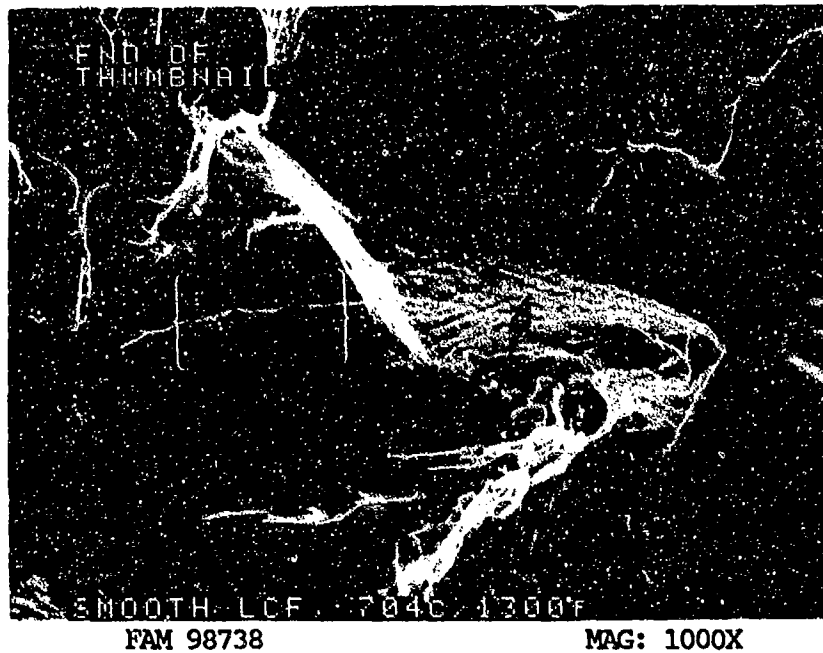


FIGURE 6-17: Remnant fatigue striations near the end of the thumbnail (brackets contain 5 striations). These should not be confused with slip lines on the adjacent facet (arrow).

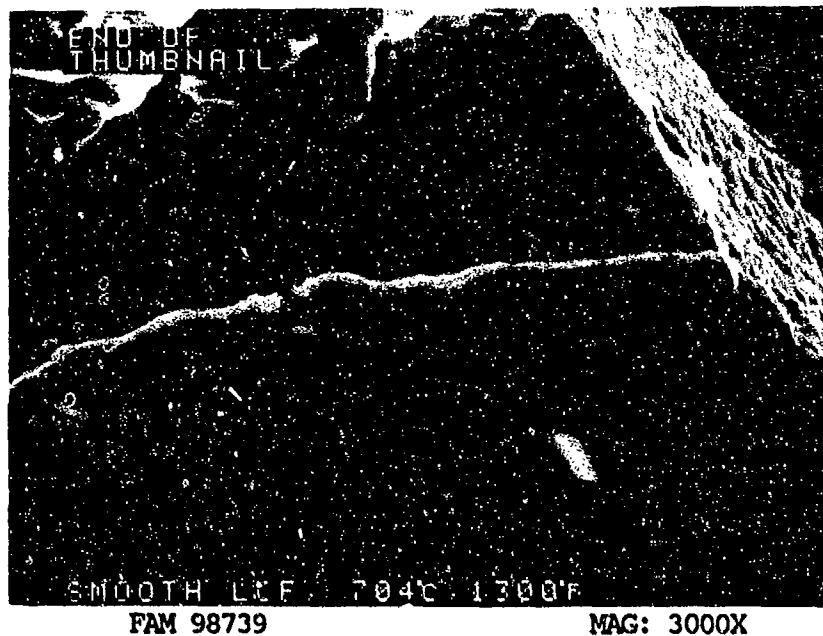


FIGURE 6-18: High magnification photograph of the remnant fatigue striations shown in Figure 6-17.

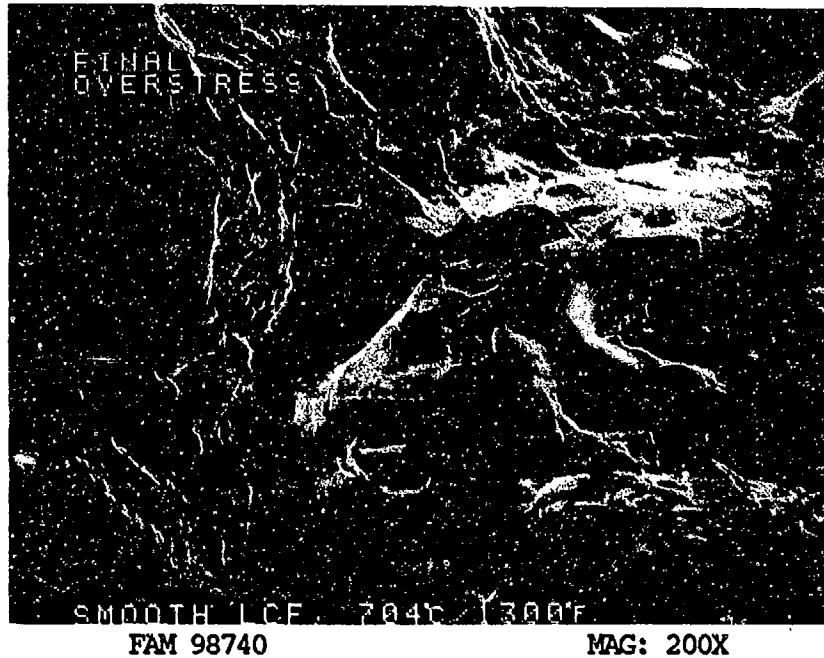


FIGURE 6-19; Final overstress area exhibiting a mixture of transgranular cleavage and dimpled overstress.

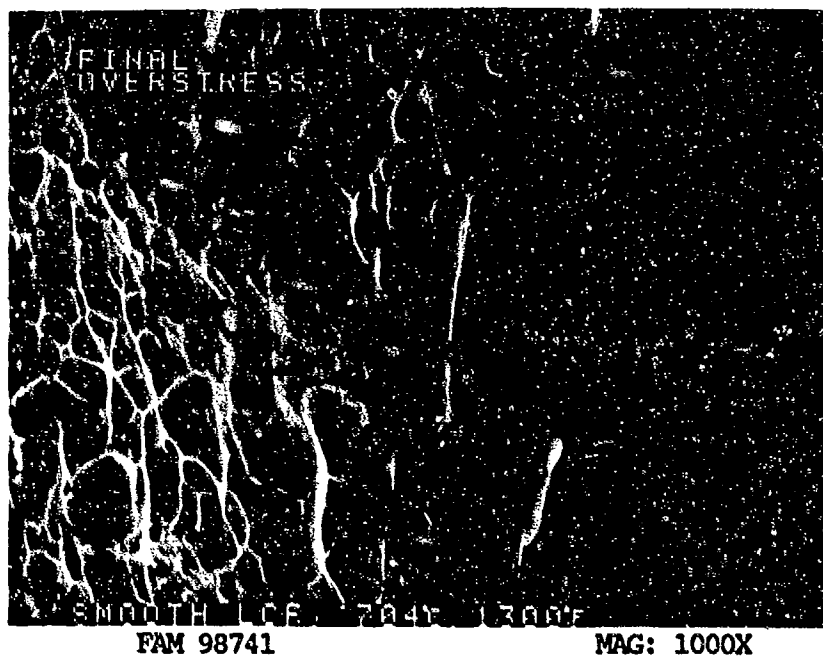


FIGURE 6-20: Boundary between dimpled overstress (left) and a cleavage facet (right). Slip lines running vertically on the facet should not be confused with fatigue striations.

MATERIAL

Incoloy 901
FWA 1003 Bar

TEST DATA

TEST TYPE

In-Phase TMF

TEST CONDITIONS

Stress: 461.9 MPa (67.0 ksi)/-551.6 MPa (-80.0 ksi)
Stress Ratio: -1.19
Frequency: 1 cpm
Atmosphere: Air
Temperature: 260°C (500°F)/ 704°C (1300°F)
Test Direction: Longitudinal

TEST RESULTS

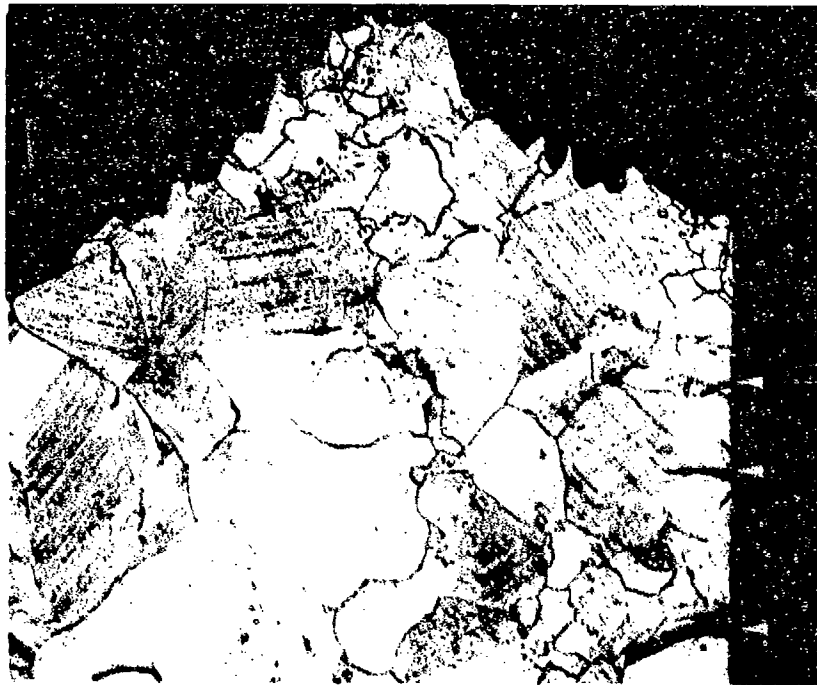
Cycles to Fracture: 2129



FAL 93216

MAG: 8X

FIGURE 6-21: Test results and fractography of Incoloy 901 in-phase TMF test. The fatigue area is heavily oxidized, (brackets) with multiple origins along the outside surface of the specimen. The final overstress area appears shiny.

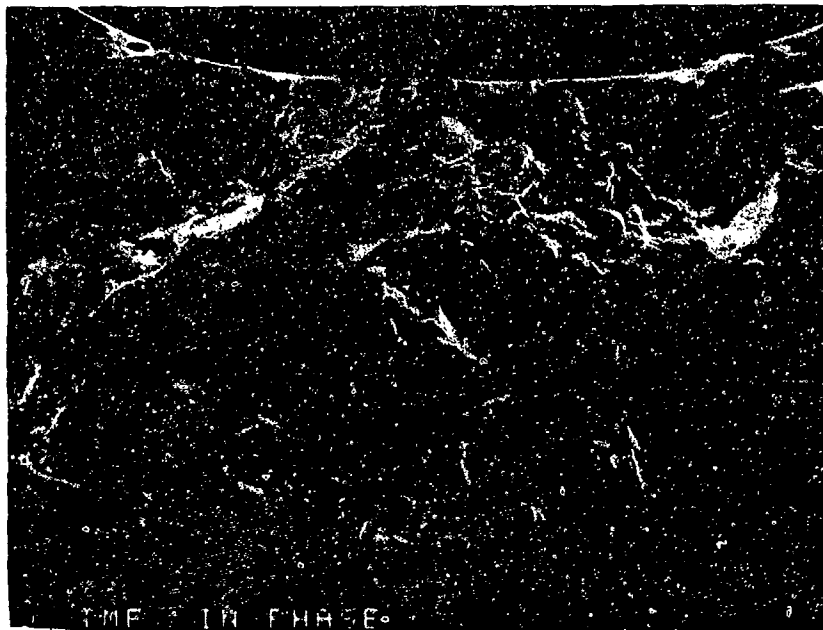


FAM 98896

MAG: 100X

FIGURE 6-22: Optical photomicrograph showing a portion of the final overstress region. Three secondary TMF cracks are visible at the surface (arrows). Slip bands are visible in most of the grains, appearing as fine parallel lines.

Etchant: Glyceregia



FAM 98743

MAG: 50X

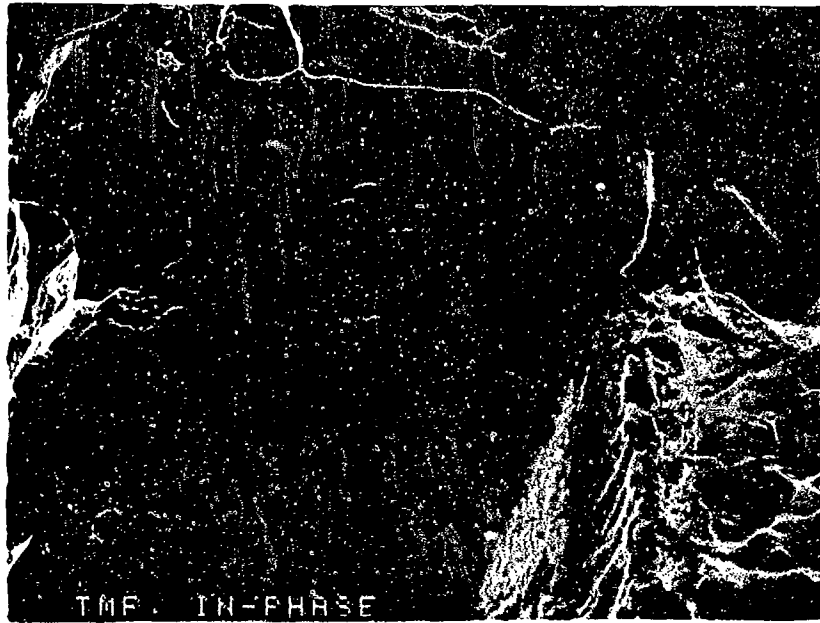
FIGURE 6-23: Low magnification photograph of the fatigue area. The origins appear to be on the O.D. surface (bottom) of the specimen.



FAM 98744

MAG: 200X

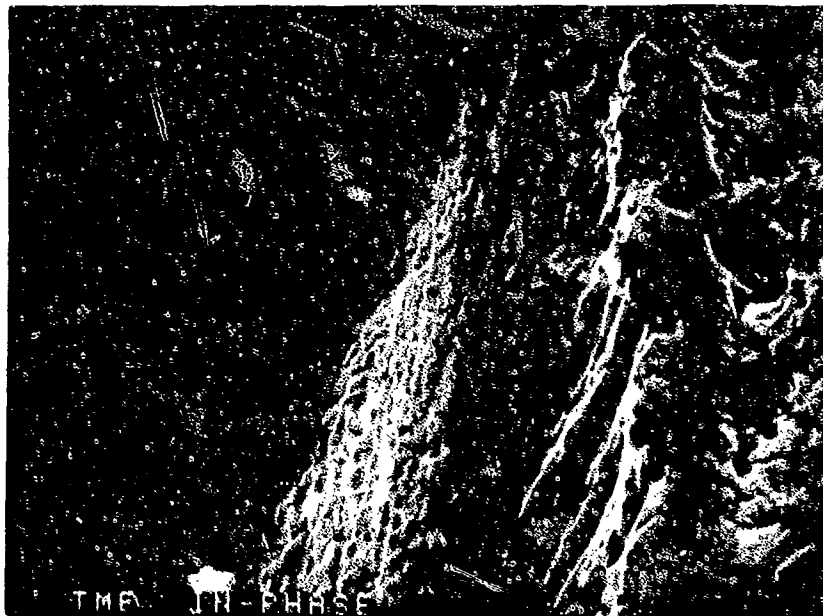
FIGURE 6-24: High magnification view of stage I fatigue at an origin area. No striations are visible.



FAM 98745

MAG: 1000X

FIGURE 6-25: Mixture of dimpled overstress and remnant fatigue features in the fatigue area. The large fatigue facet contains slip lines, with remnant fatigue striations (arrow) adjacent.



FAM 98746

MAG: 3000X

FIGURE 6-26: Higher magnification photograph of the area shown in Figure 6-25. The direction of fatigue progression is shown by an arrow.

MATERIAL

Incoloy 901
PWA 1003 Bar

TEST DATA

TEST TYPE

Out-of-Phase TMF

TEST CONDITIONS

Stress: 551.6 MPa (80.0 ksi)/-461.9 MPa (-67.0 ksi)

Stress Ratio: -0.84

Frequency: 1 cpm

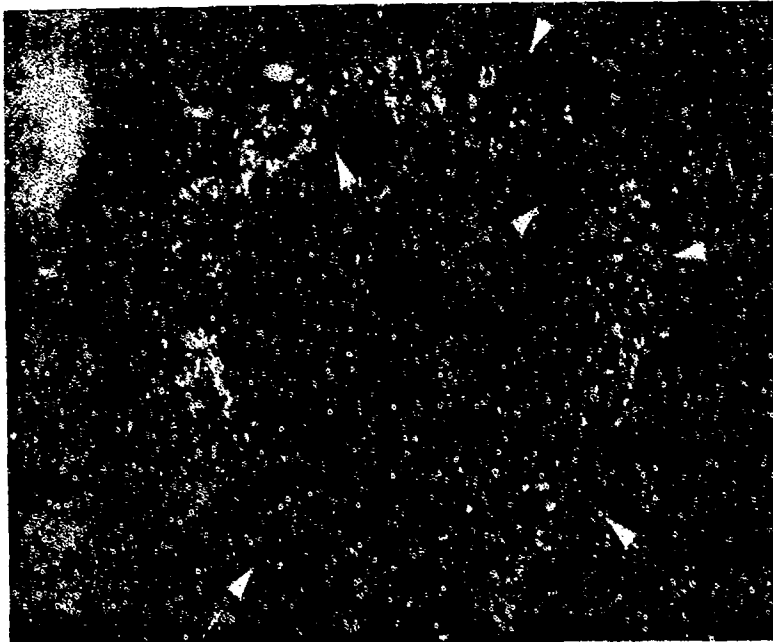
Atmosphere: Air

Temperature: 260°C (500°F) / 704°C (1300°F)

Test Direction: Longitudinal

TEST RESULTS

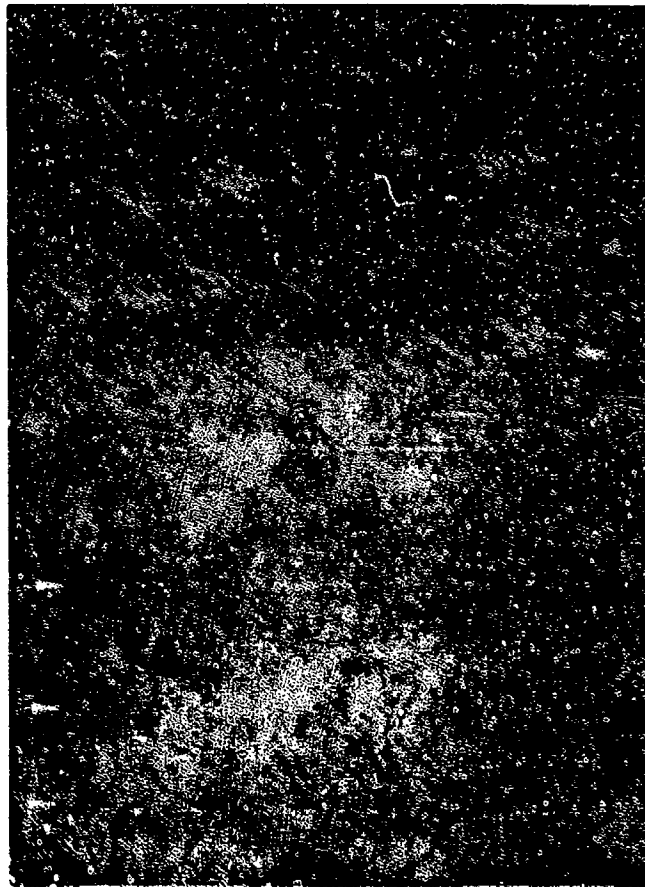
Cycles to Fracture: 5876



FAL 92926

MAG: 9X

FIGURE 6-27: Test results and fractography of Incoloy 901 out-of-phase TMF test. Several fatigue progression areas (arrows) appear as dark (oxidized) areas on both O.D. and I.D. surfaces of the specimen.



FAM 100225

MAG: 100X

FIGURE 6-28: Optical photomicrograph showing a primary fracture area and three secondary cracks (arrows). Some light strain lines are visible in the grains adjacent to the fracture (black arrow).

Etchant: Glyceregia

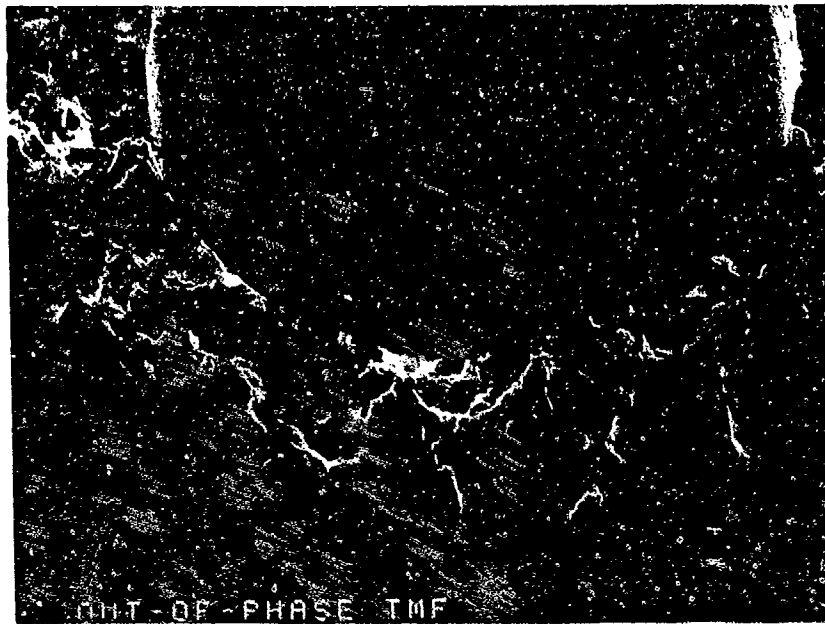


FIGURE 6-29: Low magnification view of a fatigue thumbnail area.



FIGURE 6-30: Oxidized fatigue thumbnail area. The flat oxidized appearance indicates O.D. origins (bottom). No localized origins are discernible.

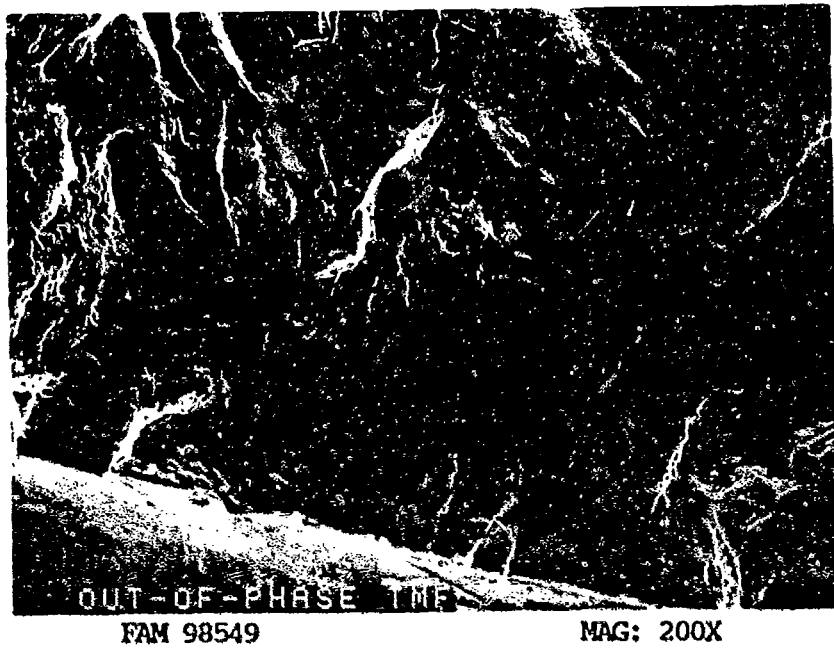


FIGURE 6-31: Fatigue thumbnail region showing remnant fatigue features (arrow).

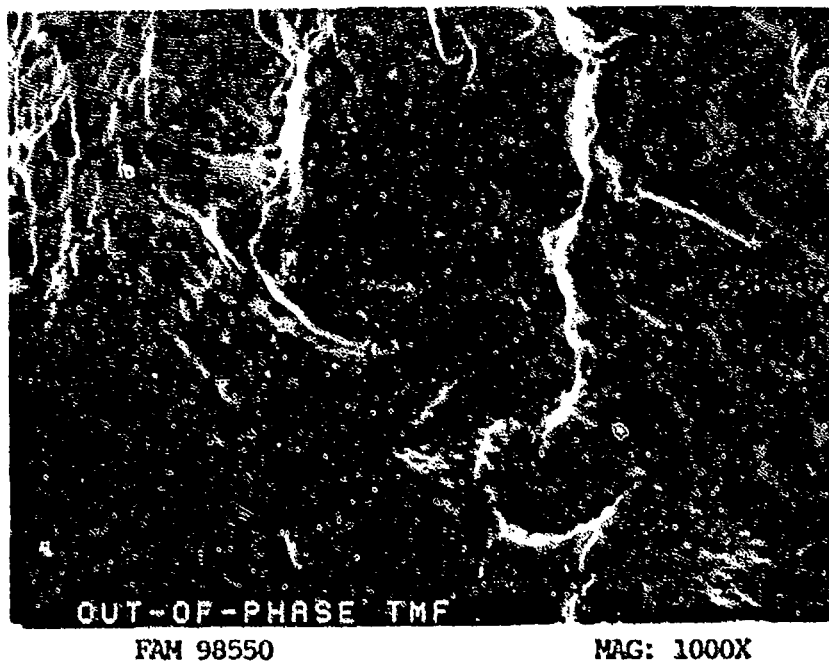


FIGURE 6-32: Heavily oxidized fatigue striations. Bracket contains five striations.

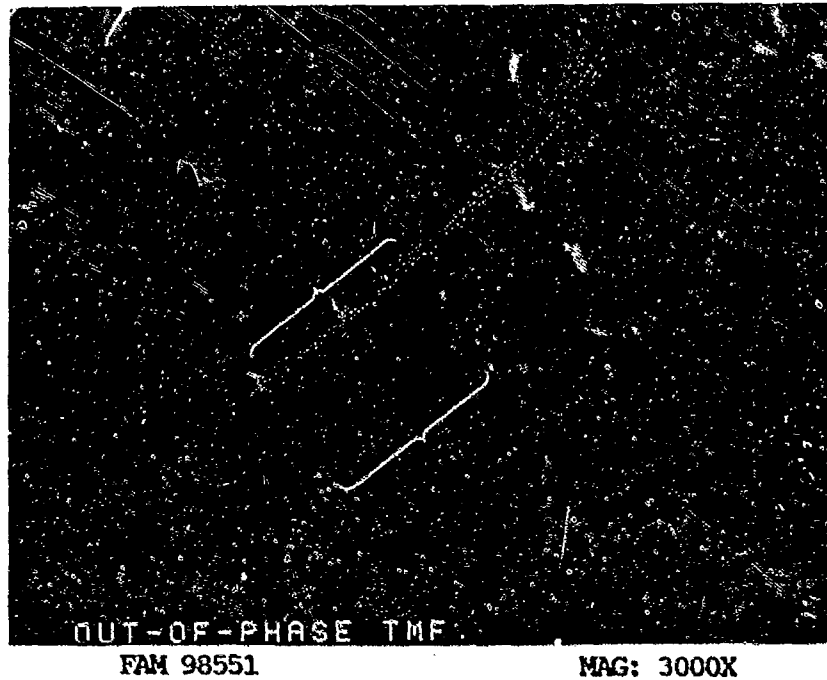


FIGURE 6-33: High magnification photograph of heavily oxidized fatigue striations. Brackets contain four striations.

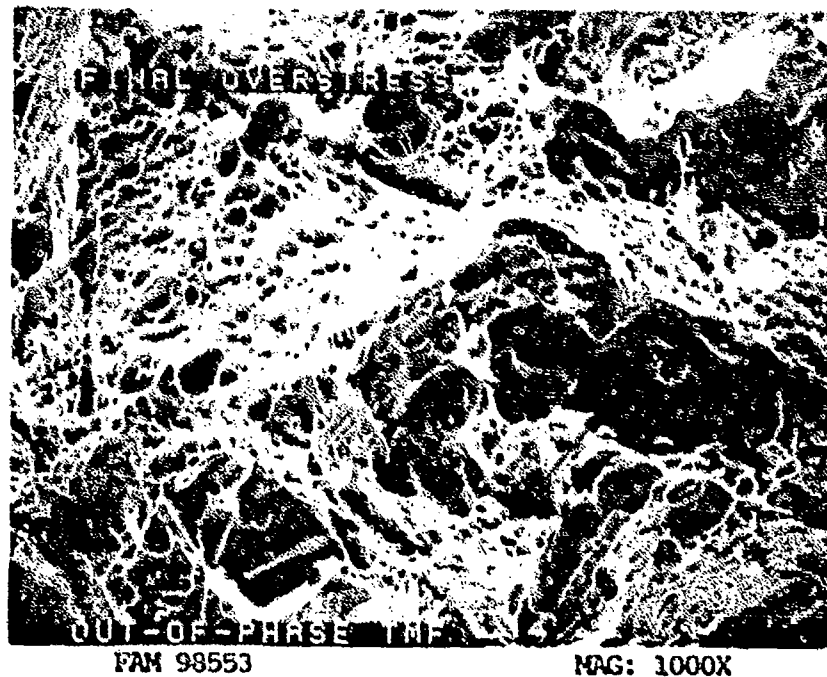


FIGURE 6-34: Dimpled overstress with small areas of cleavage (arrow) in the final overstress area.

SERVICE FAILURE

FRACTURE MODE High Cycle Fatigue (HCF)

PART NAME Eighth Stage Compressor Rotor Blade

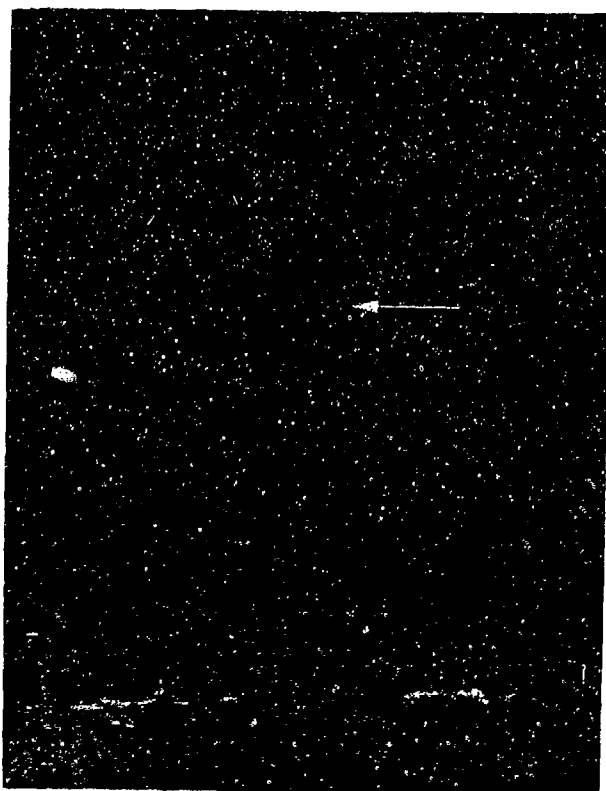
OPERATION DATA Blades cracked during green run proof test. Cracks were discovered during stress enhanced ("wink") fluorescent penetrant inspection.

PART TIME Short operation time (green run)

	<u>REQUIRED</u>	<u>ACTUAL</u>
MAT'L		
BASE	<u>Incoloy 901</u>	<u>confirmed</u>
OTHER	<u>-</u>	<u>-</u>
HARDNESS	<u>BHN 341-415</u>	<u>BHN 352-371*</u>
GRAIN SIZE	<u>ASTM 4 or finer</u>	<u>ASTM 4 or finer</u>
DIMENSIONAL	<u>-</u>	<u>-</u>

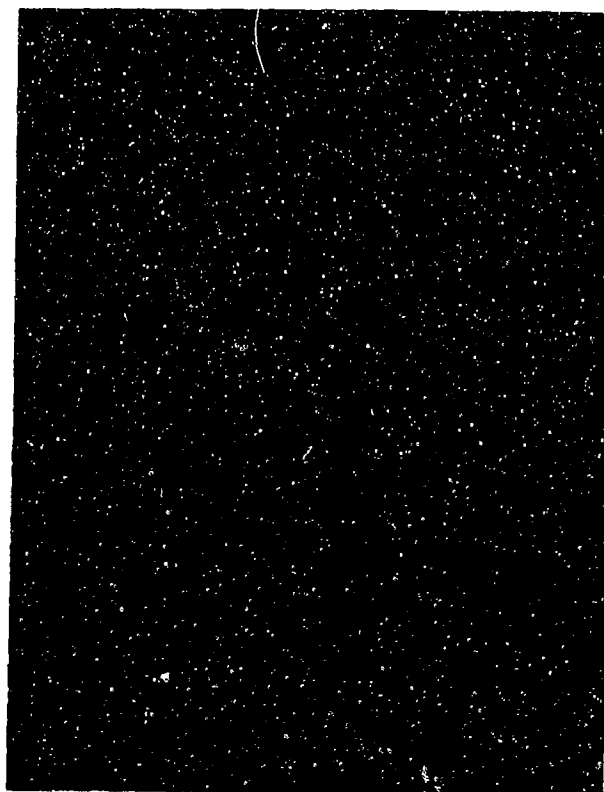
* Diamond pyramid hardness (DPH) conversions.

SUMMARY: Blade airfoils cracked transversely at the maximum root thickness (MRT) due to high cycle fatigue (HCF). The fatigue propagated from multiple origins on the convex airfoil surface at the MRT and the concave airfoil surface aft of the leading edge (Figures 6-35 and 6-36). Transmission electron microscope (TEM) examination of a replica revealed very fine fatigue striations confirming the mode to be HCF (Figure 6-38). The airfoil tip exhibited 0.010 inch of rub. Scanning electron microscope (SEM) and metallographic examination revealed no material or microstructural anomalies to account for the cracking. Examination of metallographic sections through the airfoil tip revealed no evidence of any microstructural changes due to rub.



FAL 42560

MAG: 10X



FAL 42448

MAG: 4X

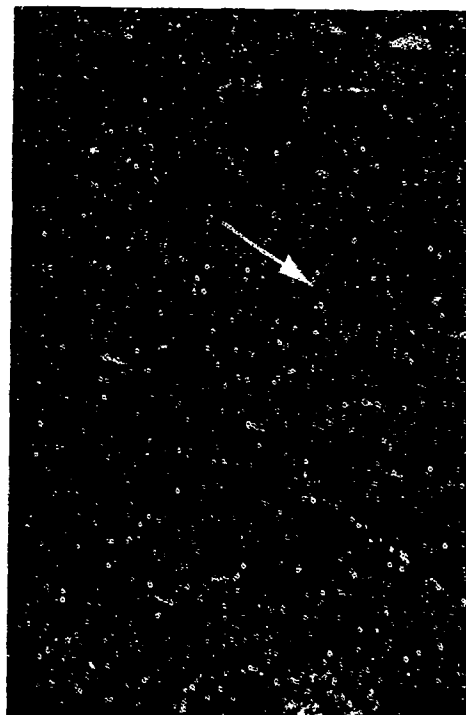
FIGURE 6-35: Airfoil section showing the profile of the fracture surface and additional cracking at the MRT location (arrow).

FIGURE 6-36: Opened crack surface showing fatigue progression at the L.E. and MRT convex side.



FAL 93491

MAG: 1000X



FAL 93493

MAG: 20,000X

FIGURE 6-37: SEM photograph showing fine fatigue striations in the fatigue progression zone.

FIGURE 6-38: TEM photograph showing very fine fatigue striations. The direction of propagation is shown by an arrow.

Incoloy 909

Material Description

Incoloy 909 is an oxidation and corrosion resistant high nickel iron-base alloy. It is used primarily for parts operating at temperatures to 1200 °F requiring moderate strength and low thermal expansion. The alloy is used in the solution treated and precipitation hardened condition. The material used in this study was heat treated to FWA 1191 with a required minimum hardness of BHN 298. The typical mechanical properties for FWA 1191 are as follows:

	<u>Room Temperature</u>	<u>1200 °F</u>
Ultimate Tensile Strength (min):	150 ksi	115 ksi
0.2% Yield Strength (min):	110 ksi	80 ksi
Percent Elongation (min):	6%	10%
Percent Reduction in Area (min):	10%	15%
	<u>Required</u>	<u>Measured</u>
ASTM Grain Size:	-	12.5 occas. 11
Measured Hardness:	BHN 287-310 (HRC conversions)	

Fractography Overview

The fractography and mechanical test data from the four tensile tests and the stress rupture test showed significant variations in ductility and fracture path. The room temperature specimens, both smooth and notched, had intergranular fractures with fine randomly shaped dimples on the grain faces. Both specimens also exhibited secondary grain boundary separation. The smooth specimen fractured perpendicular to the stress axis and had only a very small shear lip containing shallow smeared shear dimples. The notched specimen had no shear lip and was more intergranular than the smooth specimen. The 1200 °F smooth and notched specimens both fractured primarily by transgranular dimpled overstress. The smooth specimen exhibited deep conical voids covered by a uniform oxide. The fracture surface was at several angles to the stress axis and the percent elongation and reduction of area were greater than double that measured for the room temperature specimen. The 1200 °F notched tensile specimen had a 0.005 inch discontinuous shear lip at the base of the notch. Some areas on the surface had intergranular features. The features observed and mechanical data measured indicate that the alloy had weak grain boundaries with respect to the lattice at room temperature but at 1200 °F the bulk of the grain lost enough strength so that transgranular fracture occurred at the strain rates used. The stress rupture specimen, although it was tested at 1200 °F, had an intergranular fracture path. This can be explained because the stress rupture specimen was statically loaded at 90% of the 1200 °F 0.2 percent yield strength. Under this loading condition the grain boundaries again became the weakest fracture path.

Three LCF specimens were tested. One each at room temperature, 400° F and 1200 F. The room temperature and 400° F specimens had smooth Stage I fatigue facets at their origins. The room temperature specimen had four surface origin areas and the 400° F specimen had only one local origin area. Although both specimens had facets at the origins their appearances were significantly different. The 400° F specimen had smooth flat relatively featureless facets where the room temperature facets had cleavage steps, tear ridges and feathery features. The fatigue progression (Stage II) on the room temperature specimen had parallel transgranular features perpendicular to the direction of propagation. The 400° F specimen had a mixture of intergranular fracture with transgranular patches of fatigue striations. The final overstress areas were a mixture of intergranular and transgranular fracture with shallow randomly shaped dimples. The 1200° F specimen exhibited multiple surface origins. Most of the origins were at the surface but one was at a subsurface void. Both the origins and fatigue progression were heavily oxidized obscuring the fine features. No striations or other evidence of fatigue was visible. The progression did appear to have an intergranular character similar to the 400° F specimen. Secondary cracks were visible on the specimen surface in the gage section.

Both TMF specimens had multiple origins and fatigue progression zones. The in-phase specimen had both I.D. and O.D. origins with a granular appearance. High magnification examination revealed oxidized striations on a facet. Areas of very heavy oxide with mud cracking were found near the origin. The out-of-phase specimen had only O.D. origins with heavy oxide in the origin area. In the fatigue progression areas, possible remnant cyclic features were found. The final overstress area exhibited a mixture of transgranular and intergranular fine dimpled overstress.

MATERIAL

Incoloy 909
FWA 1191 Bar

TEST DATA

TEST TYPE

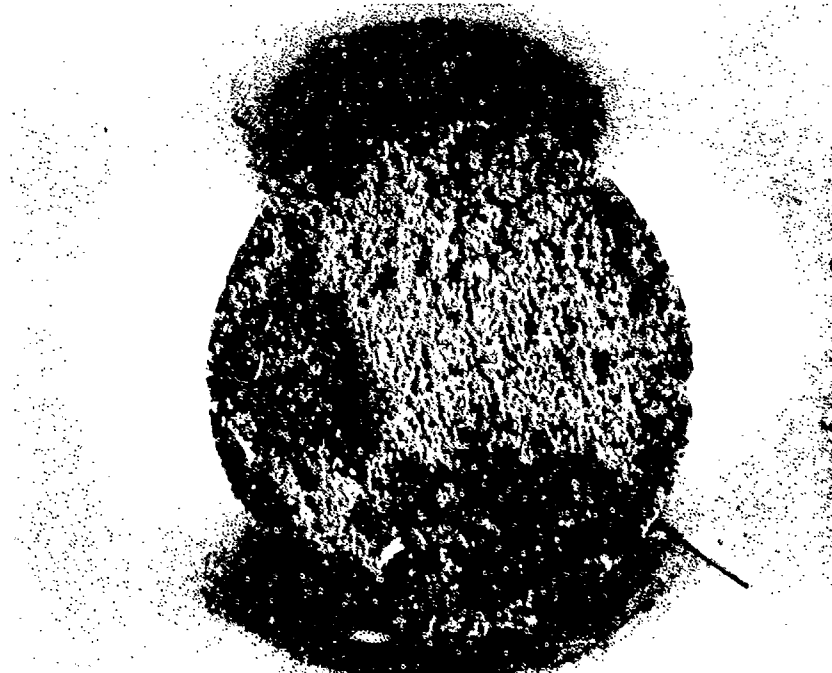
Smooth Tensile

TEST CONDITIONS

Strain Rate: 0.005 mm/mm/min (0.005 in/in/min)
Atmosphere: Air
Temperature: Room Temperature
Test Direction: Longitudinal

TEST RESULTS

0.2% Yield Strength:	812.2 MPa (117,800 PSI)
Ultimate Strength:	1183.8 MPa (171,700 PSI)
Percent Elongation:	16.0
Percent Reduction of Area:	20.1



FAL 92387

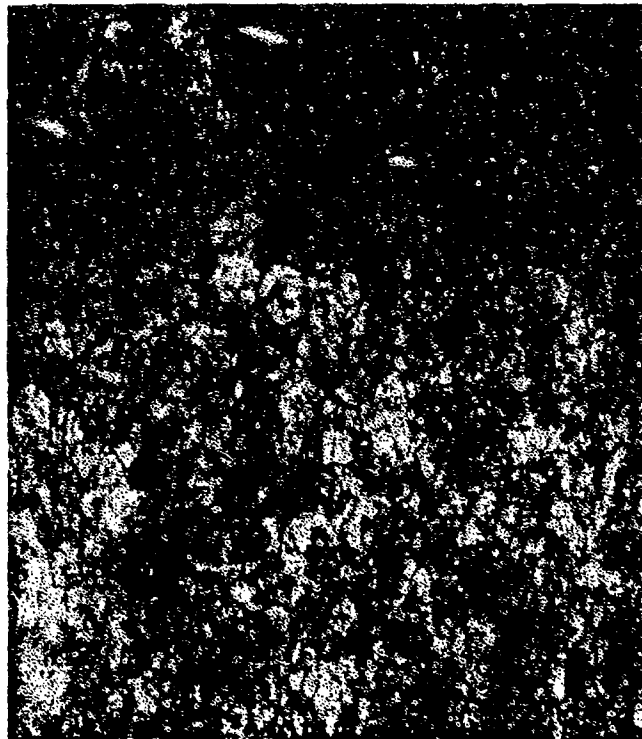
MAG: 15X

Figure 7-1: Test results and fractography of Incoloy 909 room temperature smooth tensile test. The majority of the fracture surface exhibits a granular appearance. A very narrow discontinuous shear lip is present along the surface of the specimen (arrow).



FAM 99796

MAG: 200X



FAM 99797

MAG: 200X

FIGURE 7-2: Optical photomicrographs showing the intergranular appearance of the entire fracture surface. Slip lines are visible in the grains. Some plastic deformation is visible appearing as elongated grains near the fracture.

Etchant: Glyceregia

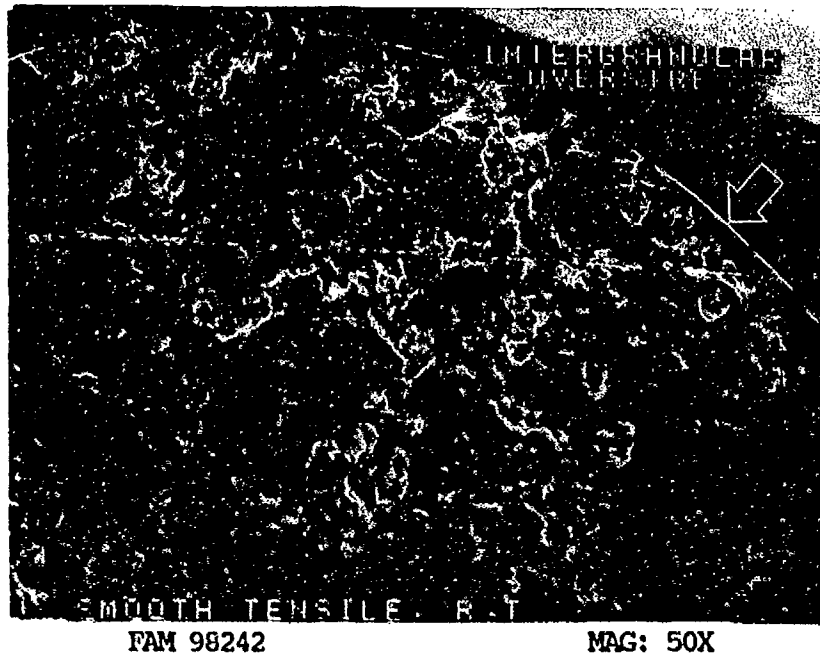


FIGURE 7-3: Low magnification photograph showing intergranular overstress in the primary fracture area and a narrow, discontinuous band of final overstress (shear lip) along the surface of the specimen (arrow).

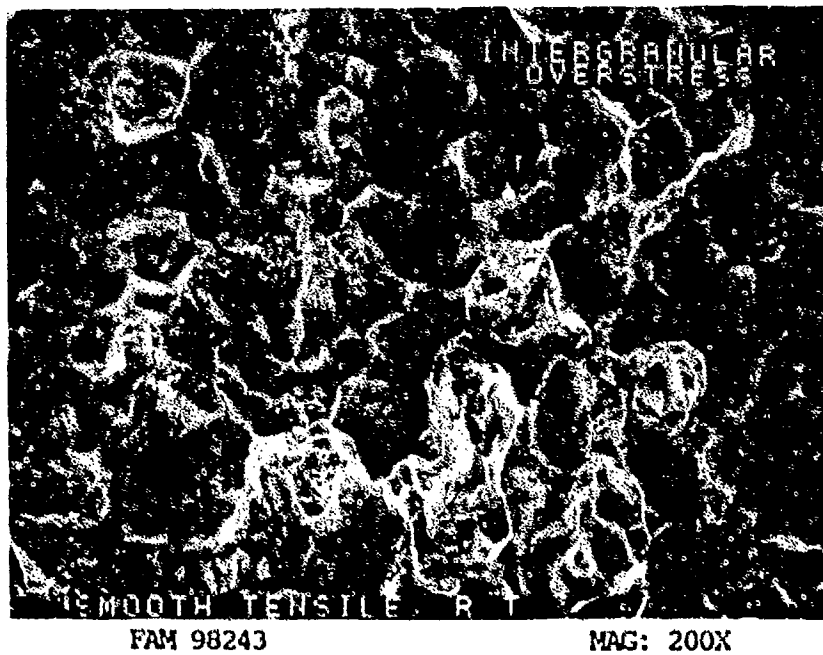


FIGURE 7-4: Intergranular overstress in the primary fracture area.

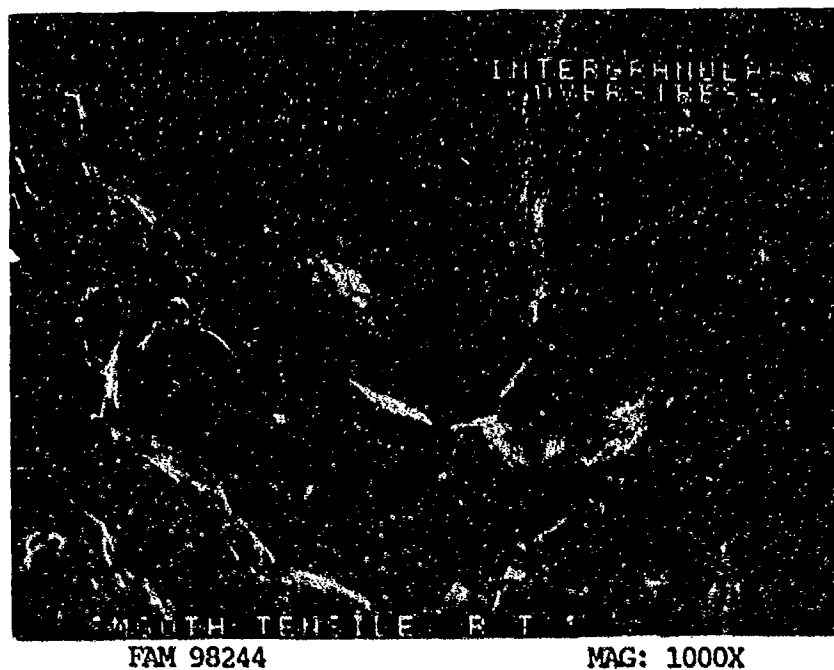


FIGURE 7-5: Intergranular overstress exhibiting fine shallow dimples on the grain faces and at the grain edges.

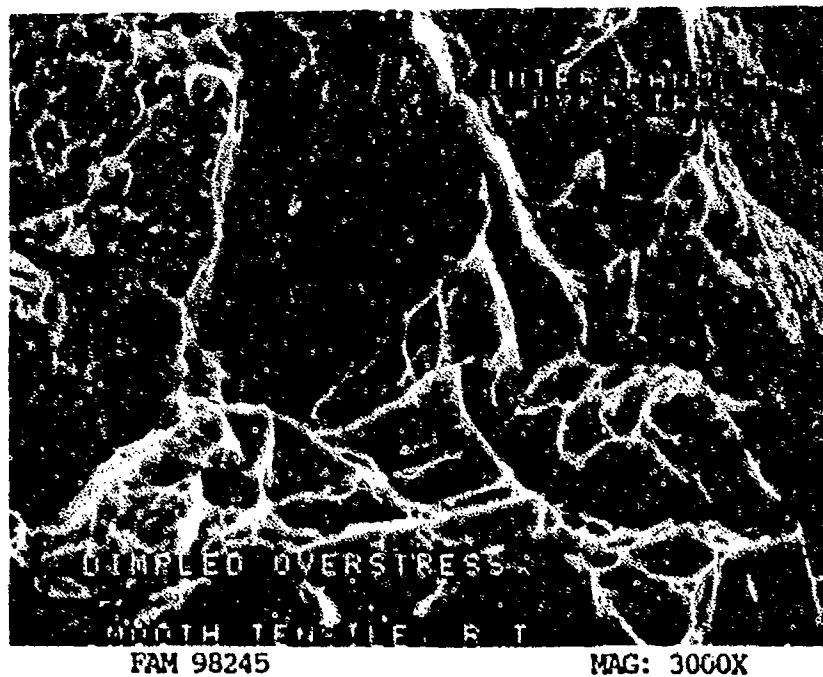


FIGURE 7-6: Higher magnification photograph of the area shown in Figure 7-5, exhibiting shallow dimples on the grain faces (arrow A) and coarser dimples at the grain edges (arrow B).

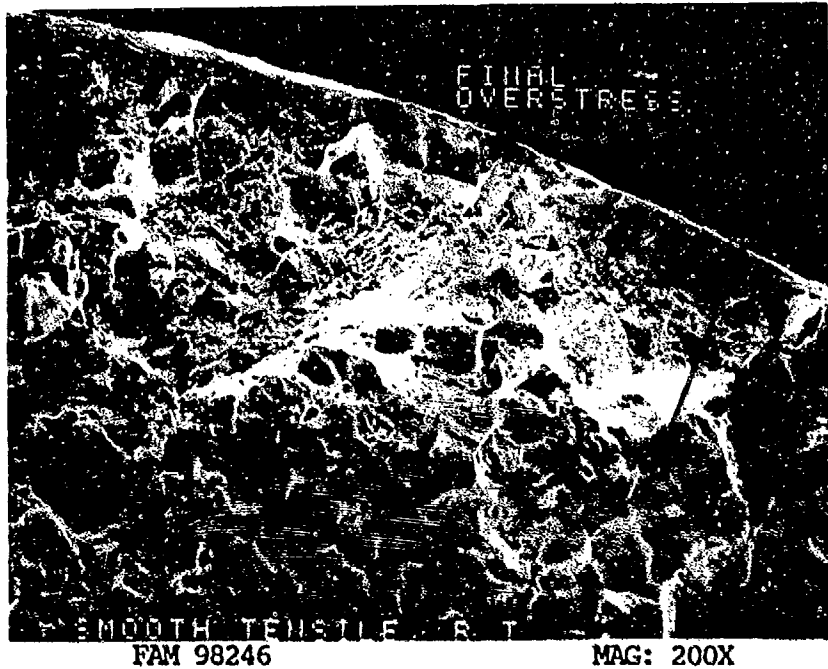


FIGURE 7-7: Final overstress area (shear lip) along the edge of the specimen. Bracket indicates the extent of the shear lip.

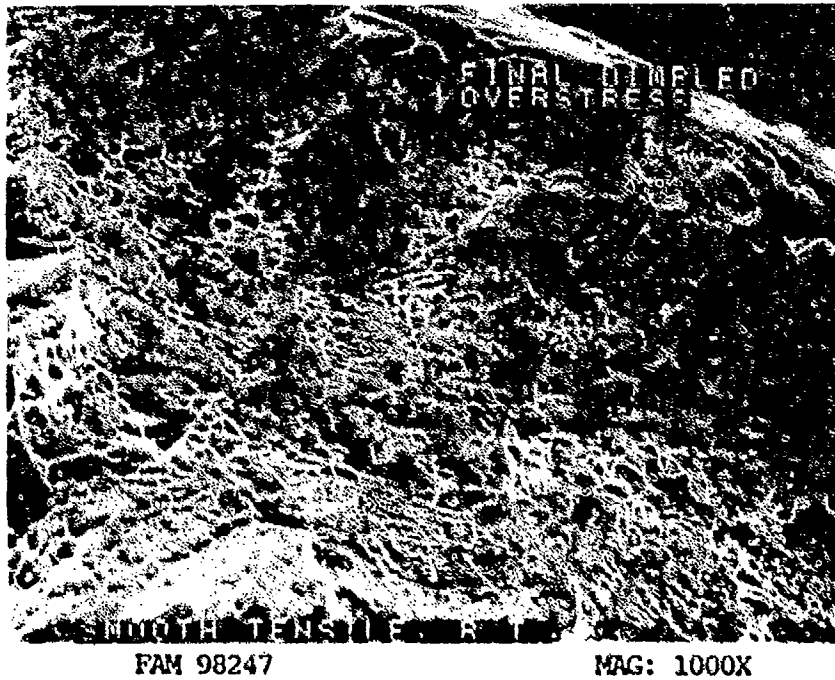


FIGURE 7-8: Sheared shallow shear dimples in the final overstress area (shear lip).

MATERIAL

Incoloy 909
FWA 1191 Bar

TEST DATA

TEST TYPE

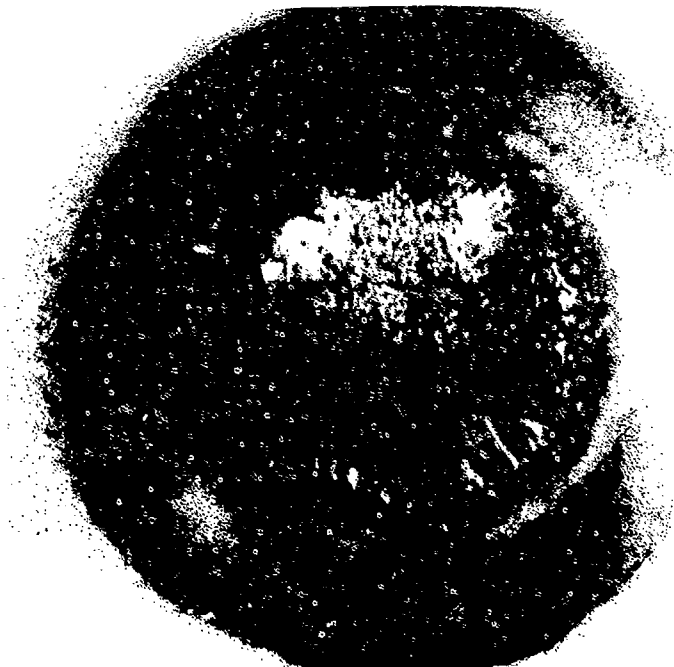
Smooth Tensile

TEST CONDITIONS

Strain Rate: 0.005 mm/mm/min (0.005 in/in/min)
Atmosphere: Air
Temperature: 649°C (1200°F)
Test Direction: Longitudinal

TEST RESULTS

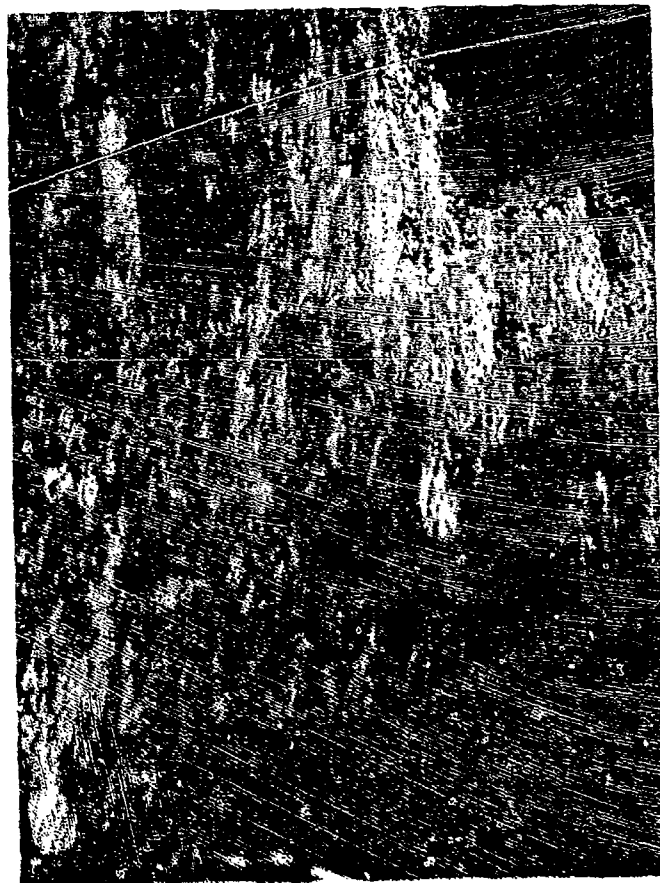
0.2% Yield Strength:	604.0 MPa (87,600 PSI)
Ultimate Strength:	899.1 MPa (130,400 PSI)
Percent Elongation:	32.7
Percent Reduction of Area:	69.6



FAL 92386

MAG: 15X

FIGURE 7-9: Test results and fractography of Incoloy 909 649°C (1200°F) smooth tensile test. The fracture surface appears completely different from the room temperature specimen, Figure 7-1, not having an intergranular appearance. While the room temperature fracture was roughly perpendicular to the stress axis, this fracture occurred on several planes.



FAM 99791

MAG: 200X

FIGURE 7-10: Optical photomicrographs of a metallographic cross section through the fracture surface. Extensive grain deformation is visible

Etchant: Glycoeregia

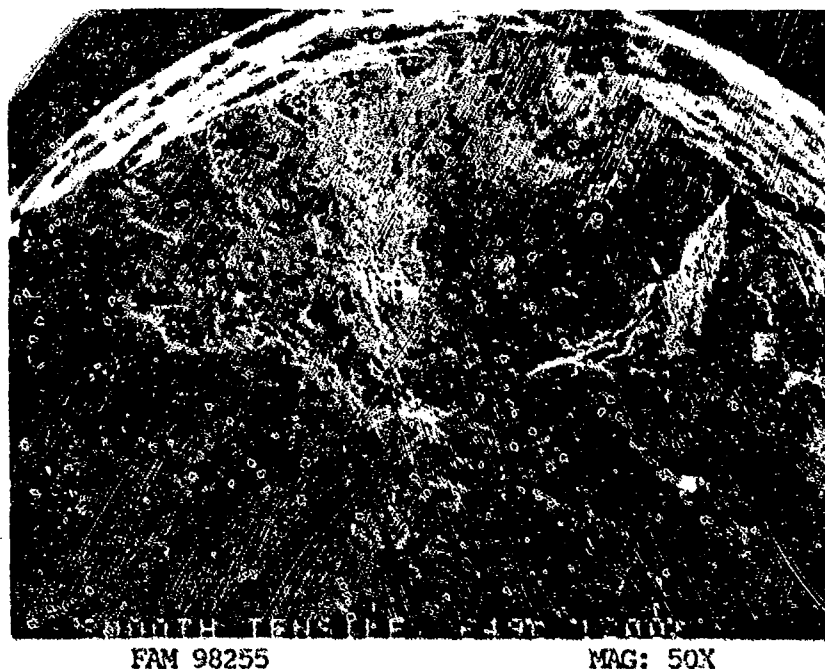


FIGURE 7-11: Low magnification view showing the depth and angularity of the fracture surface. No shear lip is present.

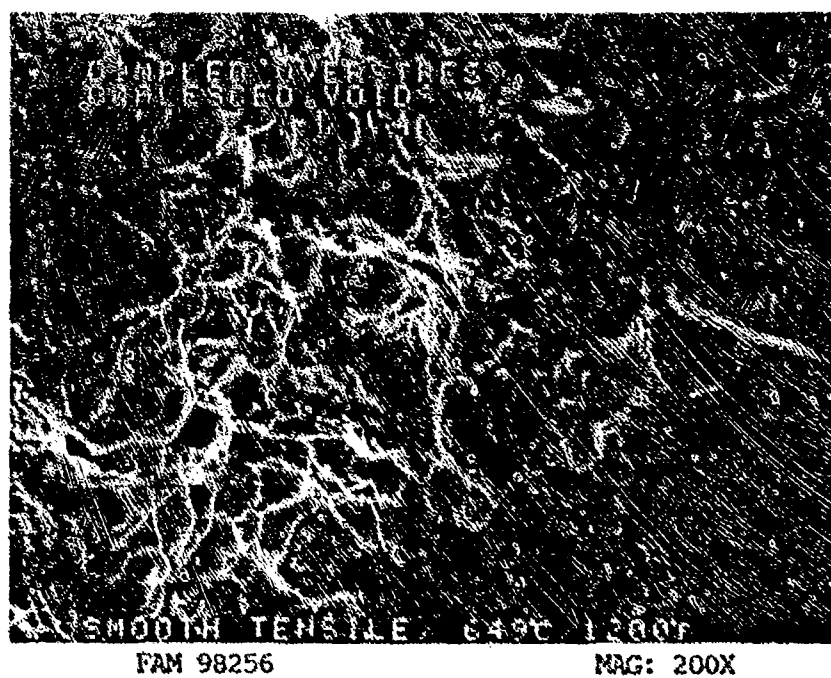
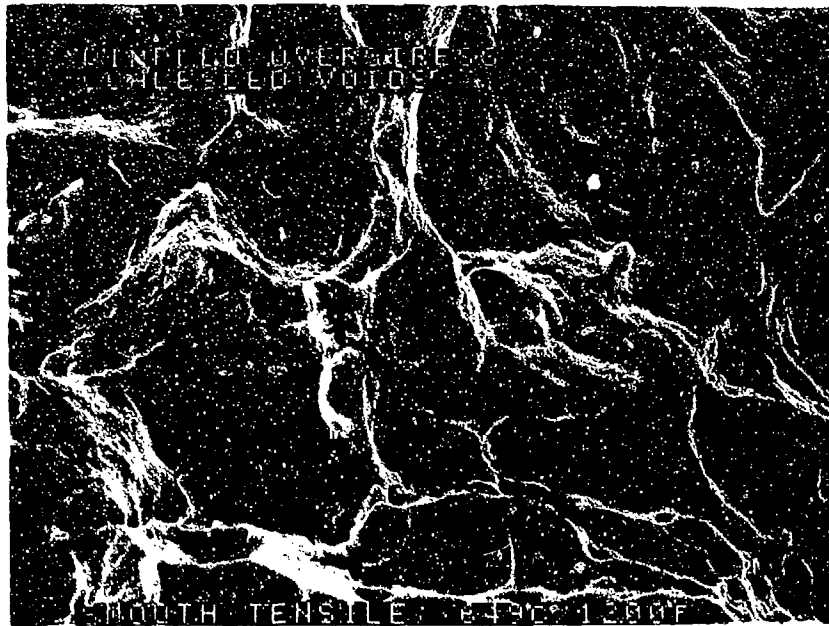


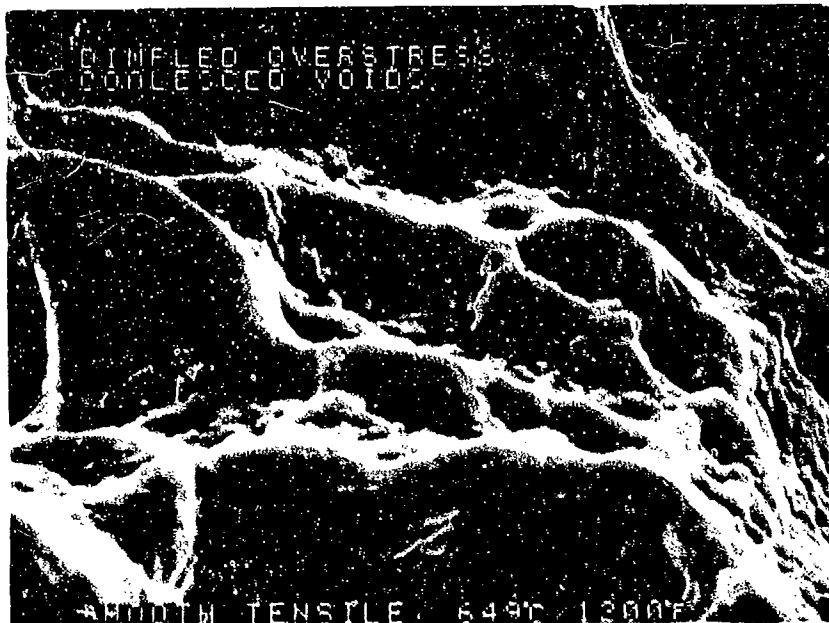
FIGURE 7-12: Dimpled overstress with void coalescence (arrows).



FAM 98257

MAG: 1000X

FIGURE 7-13: Dimpled overstress and void coalescence (arrows) covered with a uniform oxide.



FAM 98258

MAG: 3000X

FIGURE 7-14: Shallow, moderately oxidized dimples.

MATERIAL

Incoloy 909
PWA 1191 Bar

TEST DATA

TEST TYPE

Notched Tensile

TEST CONDITIONS

Crosshead Speed: 1.27 mm/min (0.05 in/min)

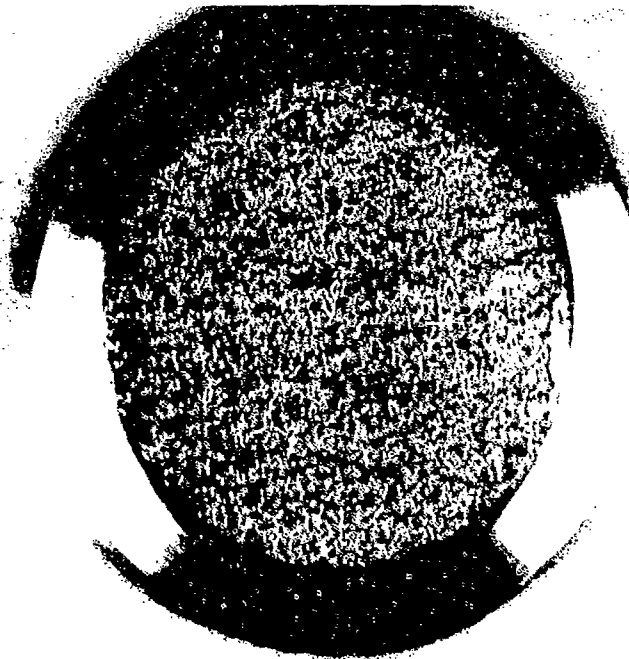
Atmosphere: Air

Temperature: Room Temperature

Test Direction: Longitudinal

TEST RESULTS

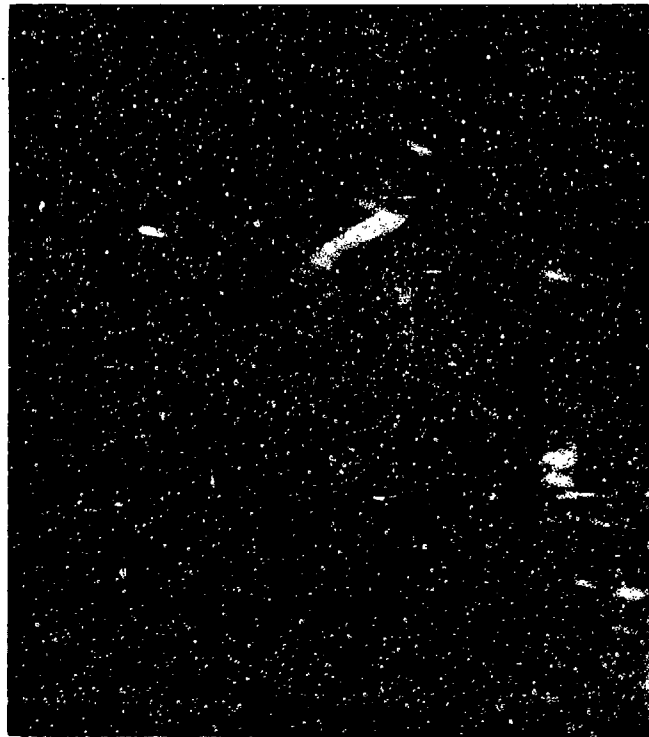
Ultimate Strength: 1250.0 MPa (181,300 PSI)



FAL 92389

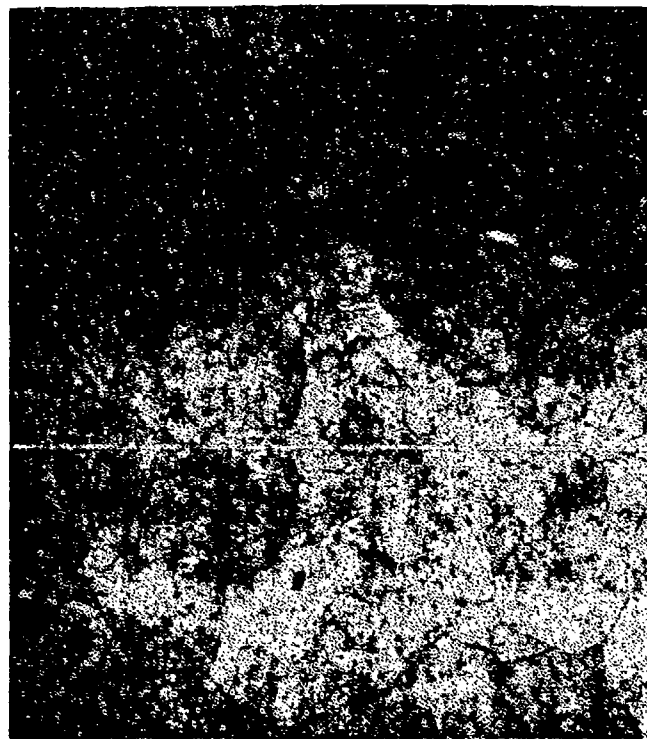
MAG: 10X

FIGURE 7-15: Test results and fractography of Incoloy 909 room temperature notched tensile test. The fracture has a fine intergranular appearance with no shear lip.



FAM 99808

MAG: 200X



FAM 99809

MAG: 200X

FIGURE 7-16: Optical photomicrographs showing the intergranular fracture path of the entire fracture surface. Slip lines are visible in the grains. Little or no plastic deformation is visible. Grain boundary separation is visible at several locations (arrows). This can also be seen in the SEM photographs.

Etchant: Glyceregia

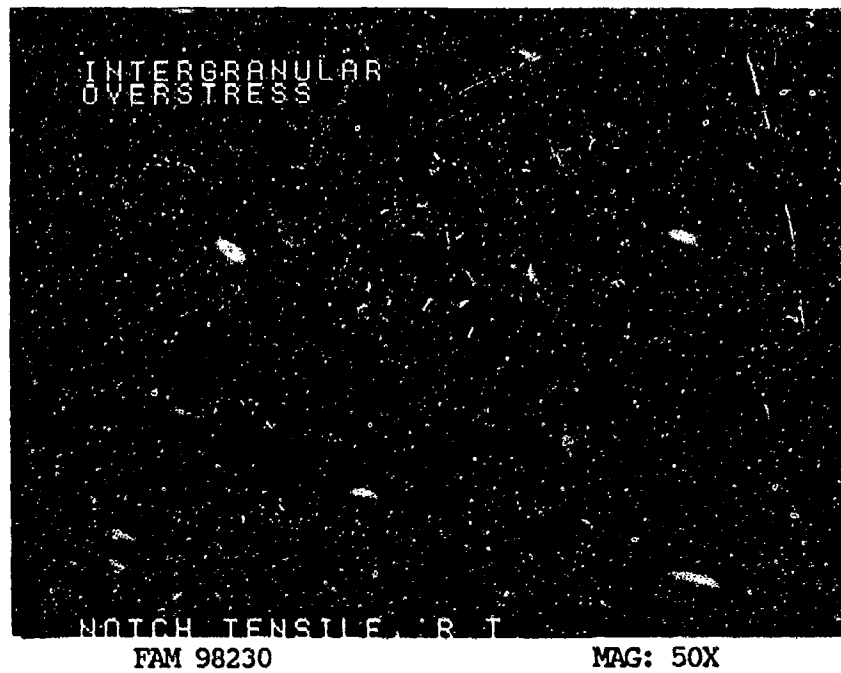


FIGURE 7-17: Low magnification photograph exhibiting intergranular overstress. Grain boundary separation is well defined and widespread.

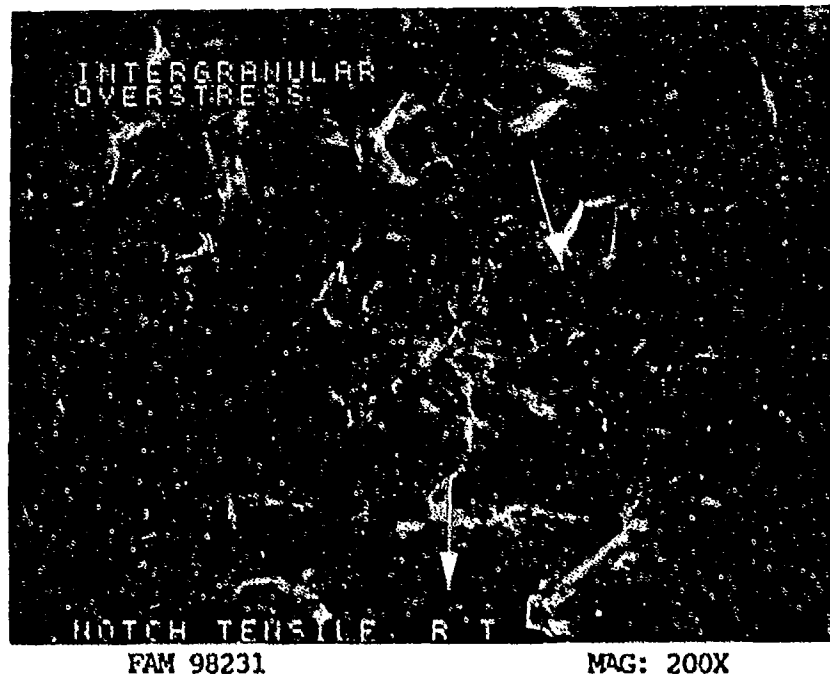


FIGURE 7-18: Intergranular overstress with grain boundary separation (arrows) in the area shown in Figure 7-17.

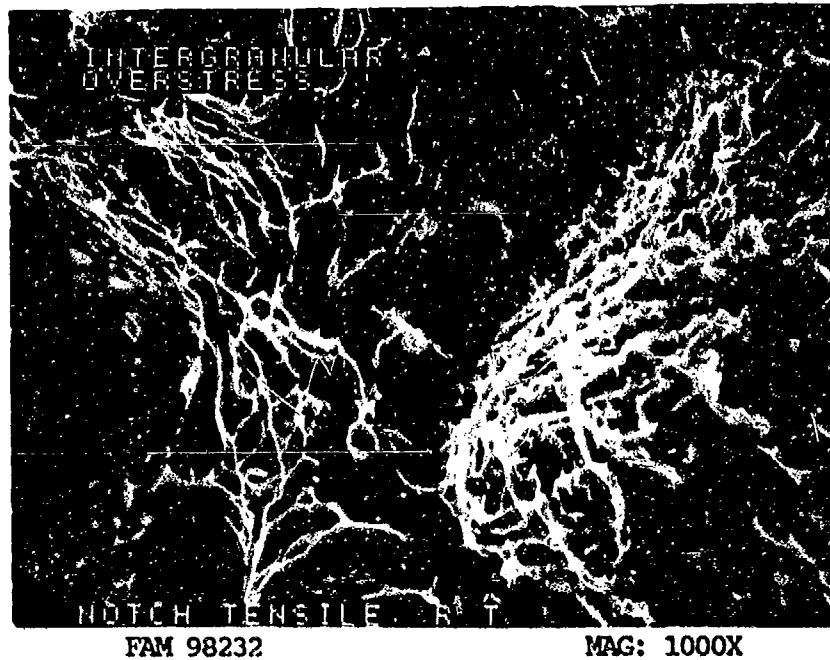


FIGURE 7-19: Intergranular overstress with both fractured and non-fractured carbides visible (arrows).

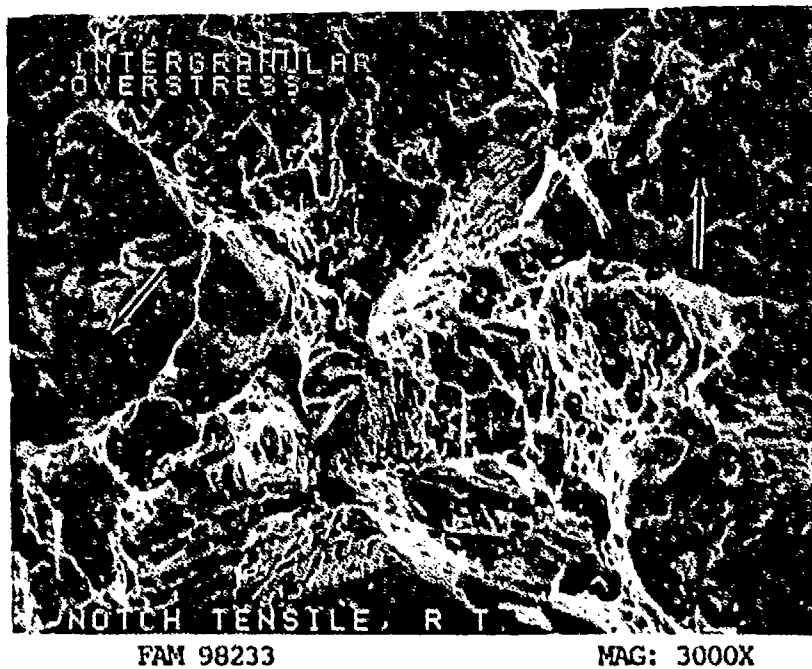


FIGURE 7-20: Fine randomly shaped dimples on the grain faces.

MATERIAL

Incoloy 909
PWA 1191 Bar

TEST DATA

TEST TYPE

Notched Tensile

TEST CONDITIONS

Crosshead Speed: 1.27 mm/min (0.05 in/min)

Atmosphere: Air

Temperature: 649°C (1200°F)

Test Direction: Longitudinal

TEST RESULTS

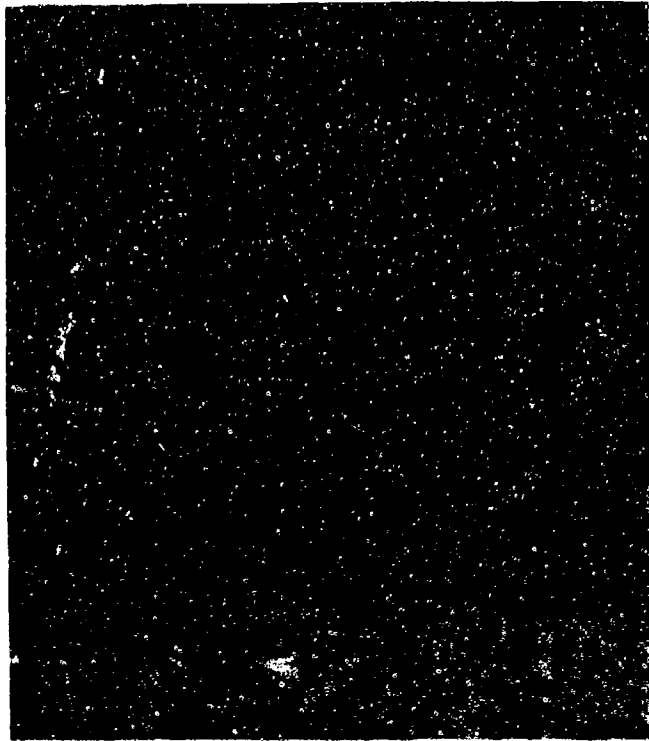
Ultimate Strength: 1332.1 MPa (193,200 PSI)



FAL 92588

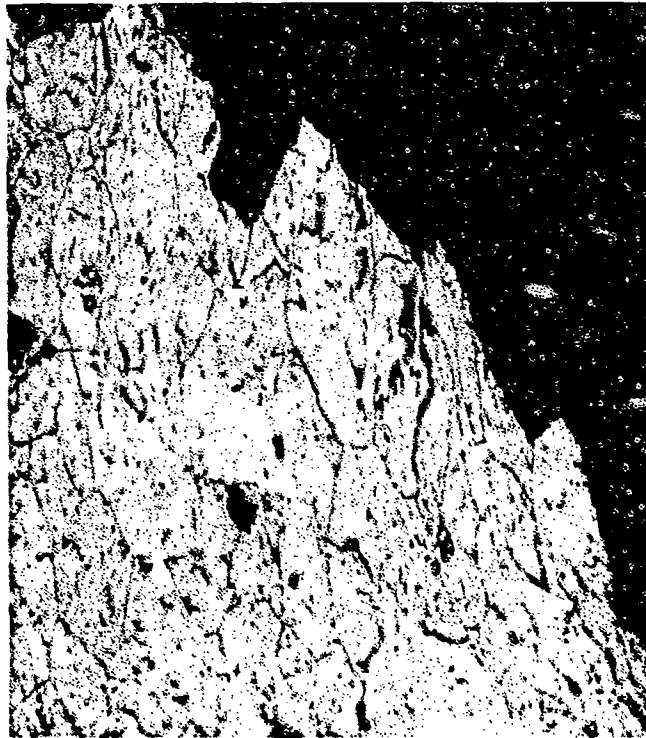
MAG: 10X

FIGURE 7-21: Test results and fractography of Incoloy 909 649°C (1200°F) notched tensile test. The fracture shows more depth than the room temperature specimen (Figure 7-15). A light oxide and a narrow discontinuous final overstress area (shear lip) are present.



FAM 99794

MAG: 200X



FAM 99795

MAG: 200X

FIGURE 7-22: Optical photomicrographs showing a predominantly transgranular fracture path (top). Compare with the room temperature specimen. Unlike the room temperature specimen, significant plastic deformation is visible at the base of the notch (bottom).

Etchant: Glyceregia

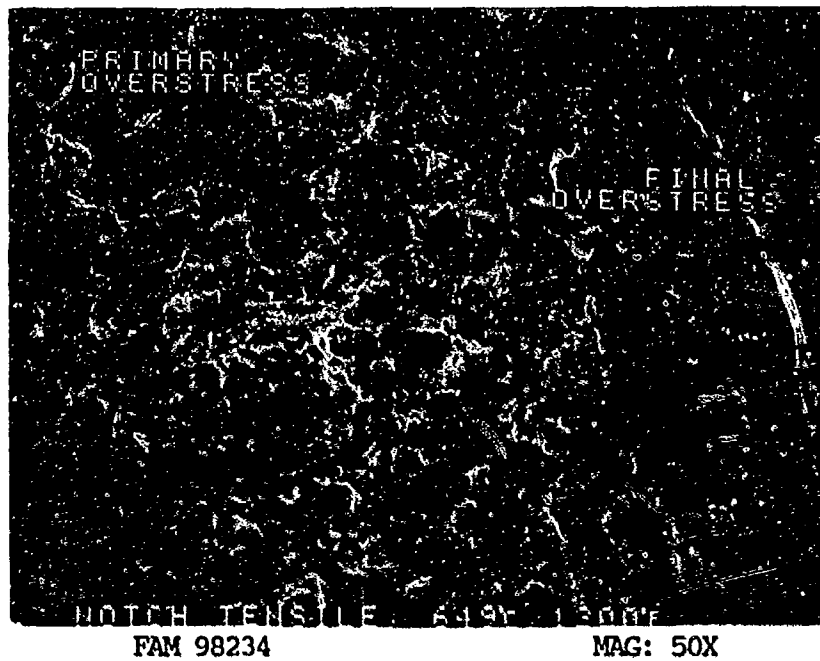


FIGURE 7-23 : Low magnification view showing primary and final overstress (shear lip) areas. The primary overstress area does not have the intergranular appearance of the room temperature specimen (Figure 7-1').

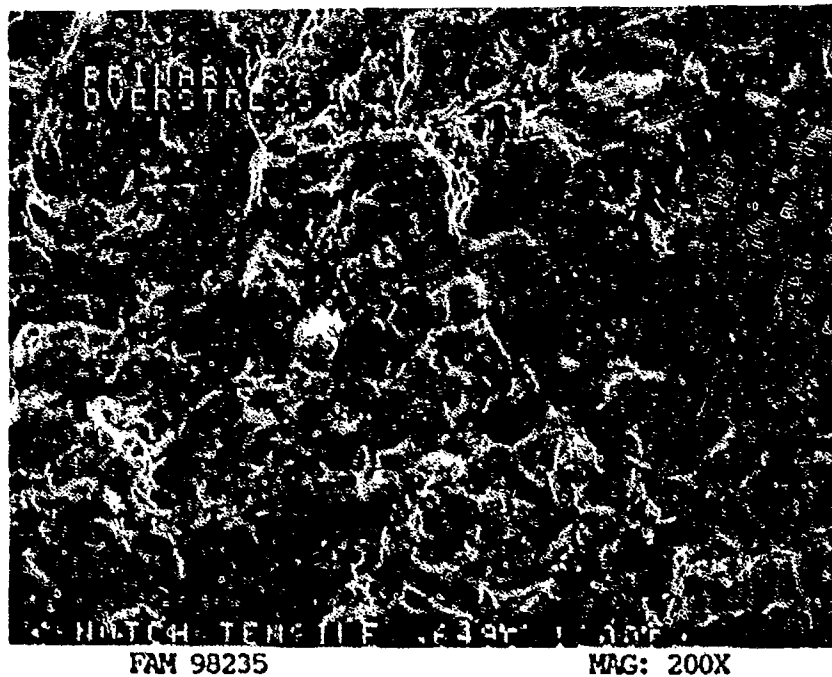


FIGURE 7-24: Primary overstress area exhibits light oxidation covering a mixture of transgranular and intergranular dimpled overstress.

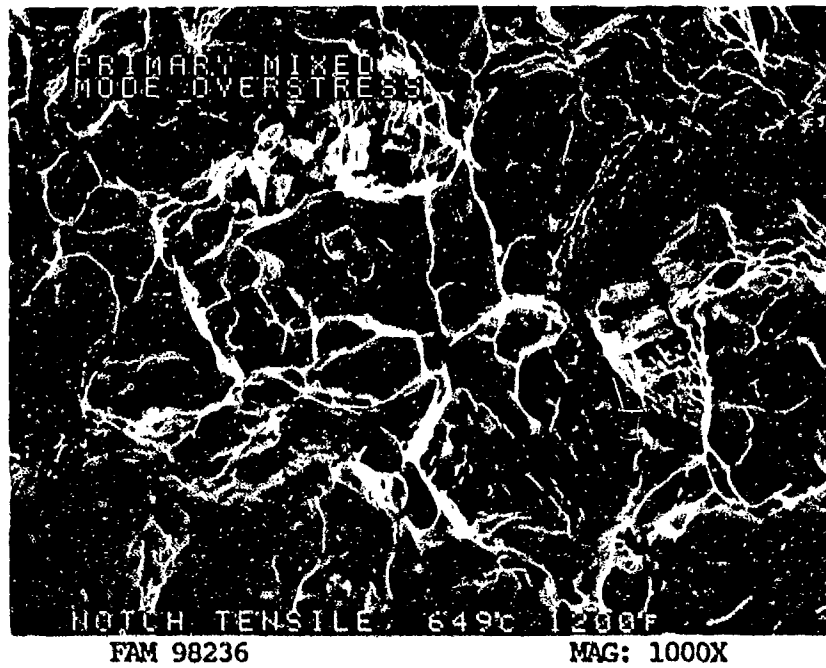


FIGURE 7-25: Mixed mode overstress in the primary overstress area. The fracture exhibits both intergranular overstress (arrow) and transgranular dimpled overstress.

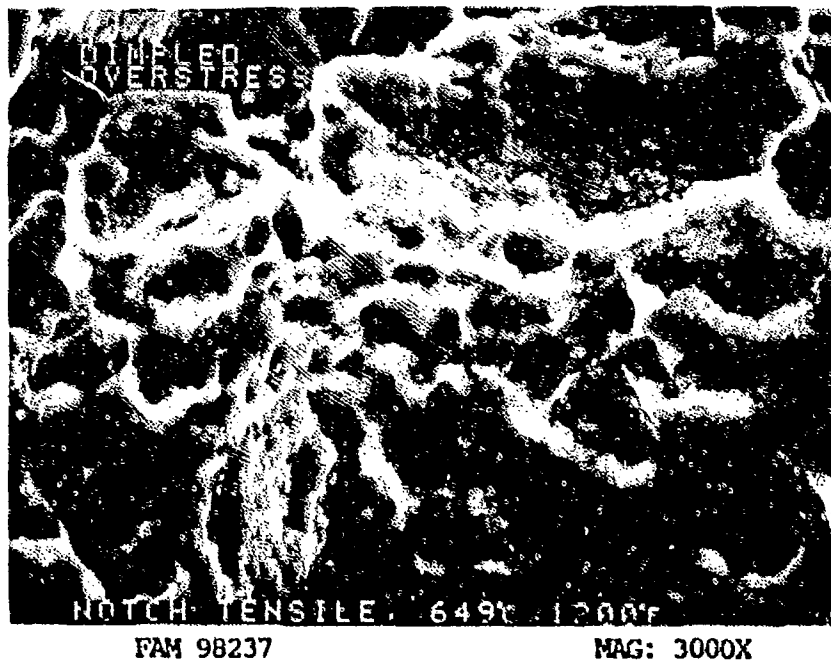


FIGURE 7-26: Moderately oxidized, transgranular dimpled overstress.

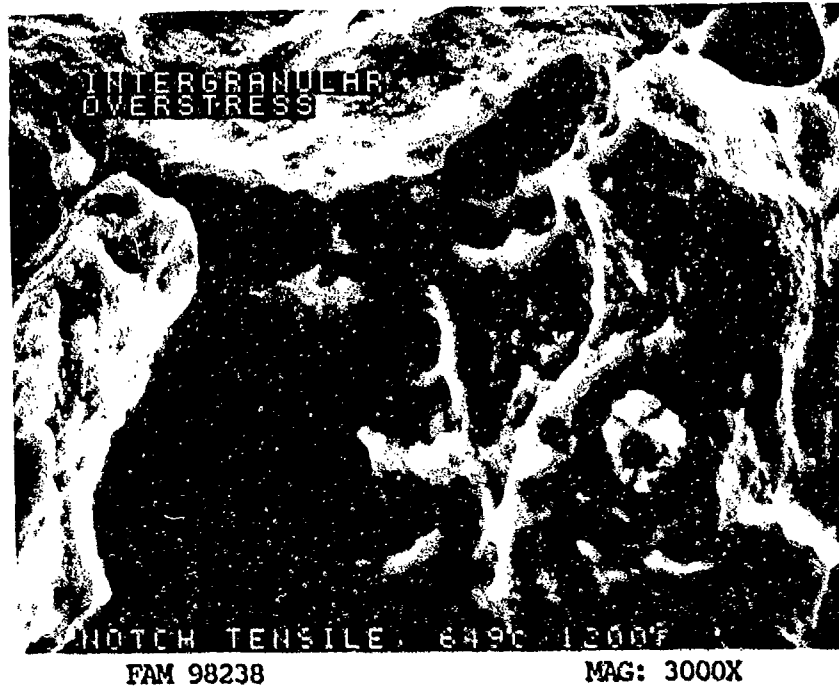


FIGURE 7-27: Oxidized, intergranular overstress.

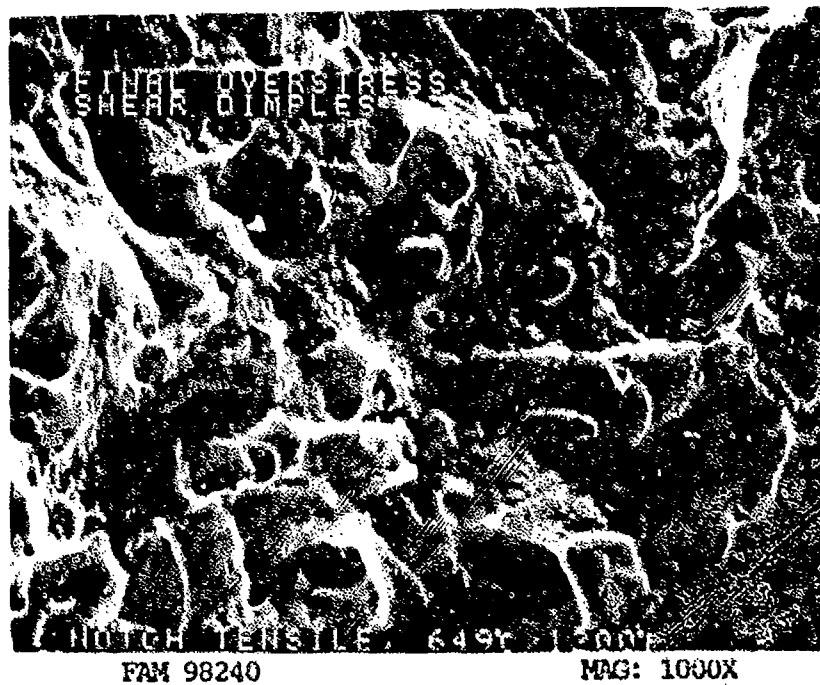


FIGURE 7-28: Oxidized shear dimples in the final overstress area (shear lip). The directions of relative motion are shown by arrows.

MATERIAL

Incoloy 909
PWA 1191 Bar

TEST DATA

TEST TYPE

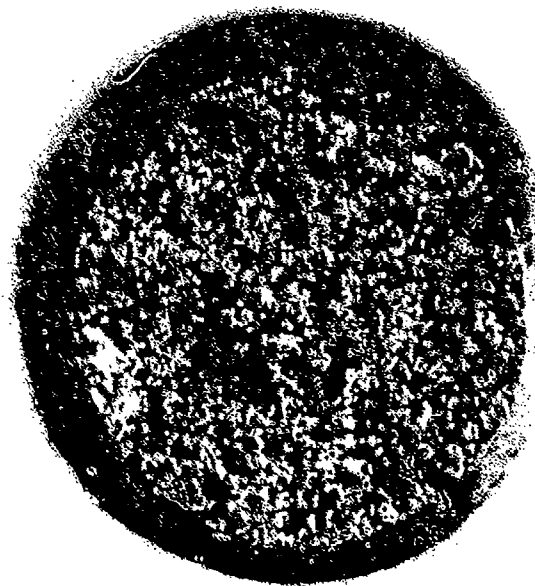
Stress Rupture

TEST CONDITIONS

Stress: 510.2 MPa (74.0 ksi)
Atmosphere: Air
Temperature: 649°C (1200°F)
Test Direction: Longitudinal

TEST RESULTS

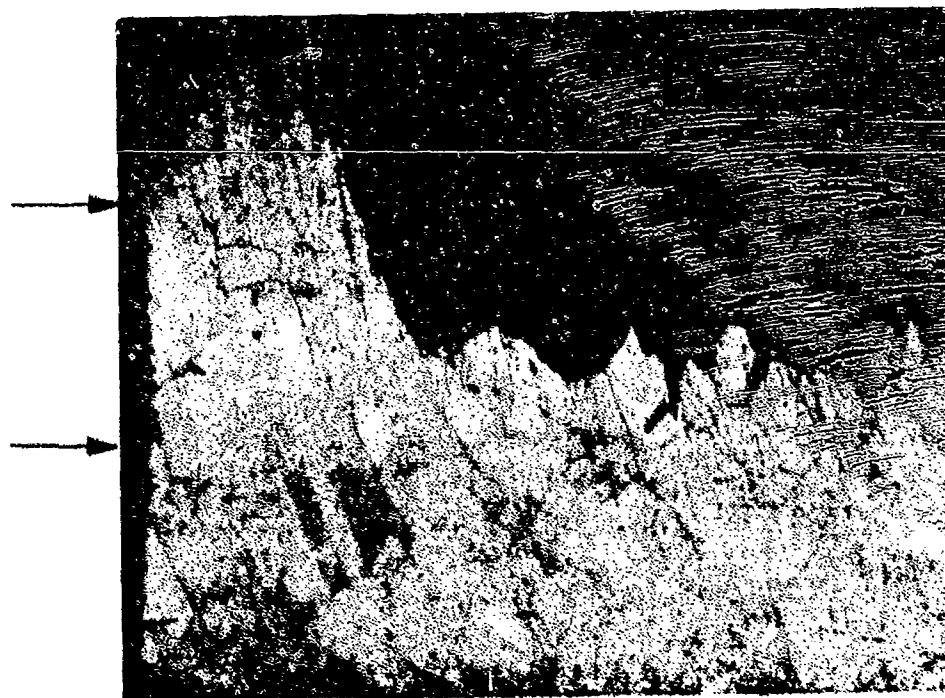
Time to Fracture: 77.8 hours
Percent Elongation: 7.97
Percent Reduction in Area: 7.07



FAL 92390

MAG: 10X

FIGURE 7-29: Test results and fractography of Incoloy 909 649°C (1200°F) stress rupture test. The fracture surface has a coarse intergranular appearance with no shear lip.

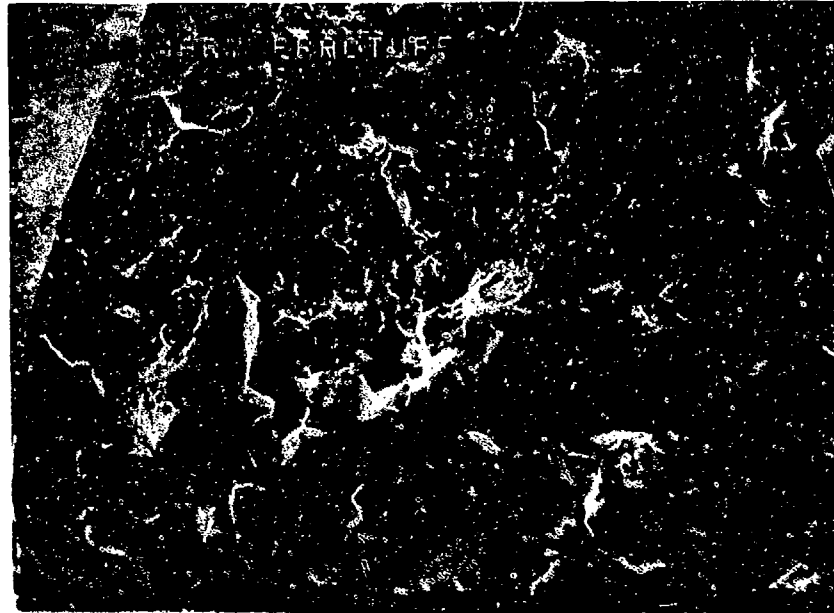


FAM 98985

MAG: 100X

FIGURE 7-30: Optical photomicrograph showing intergranular fracture path. An oxide can be seen covering the entire fracture surface and on the surface of the specimen (arrows). The grain size is significantly larger than the room temperature test specimens, indicating that grain growth occurred during testing.

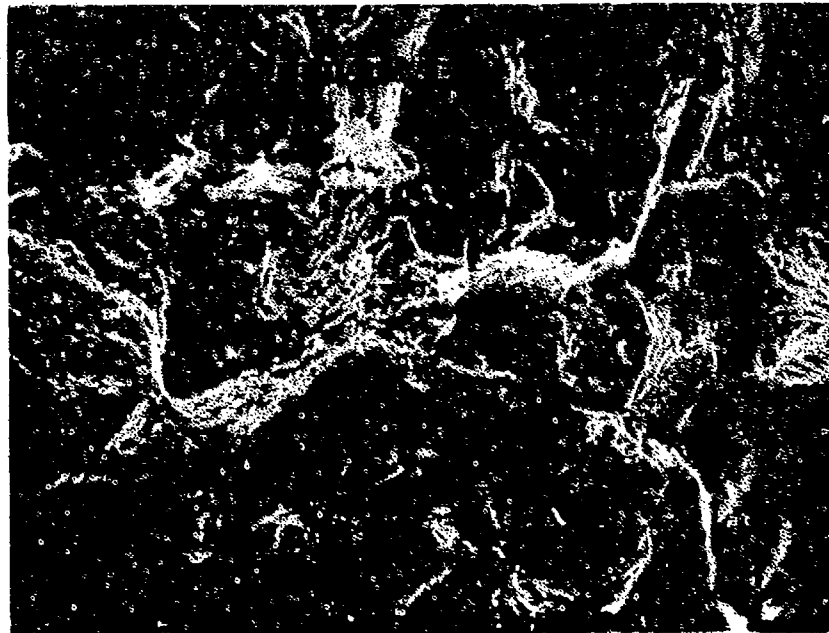
Etchant: Glyceregia



FAM 98260

MAG: 50X

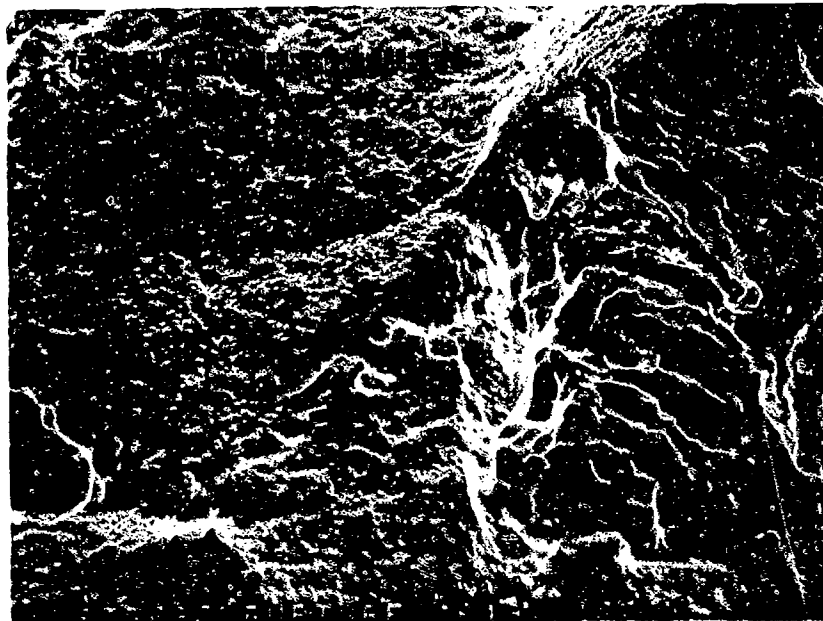
FIGURE 7-31: Low magnification view showing the primary fracture area (top), exhibiting moderate oxidation, and the final fracture area (bottom) that was very lightly oxidized.



FAM 98261

MAG: 200X

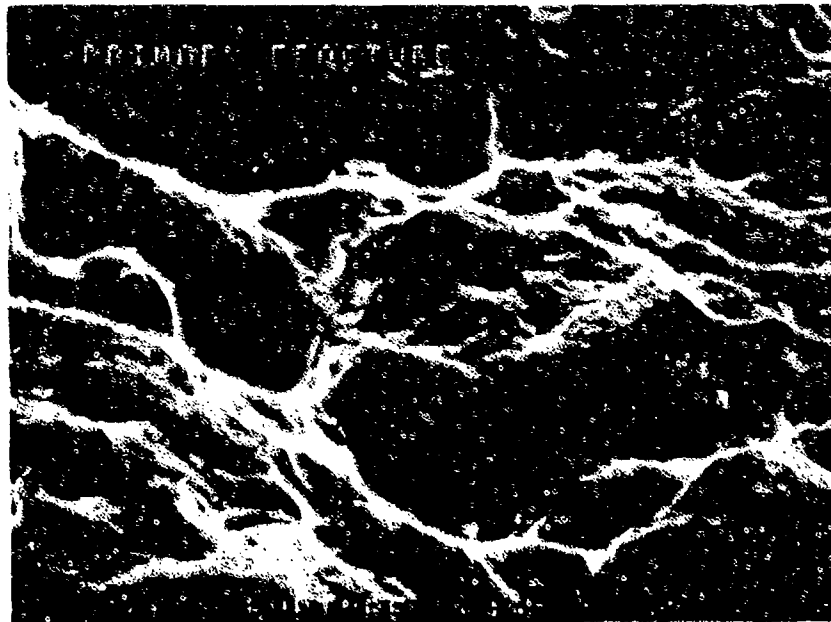
FIGURE 7-32: Primary fracture area exhibiting oxidized intergranular features.



FAM 98262

MAG: 1000X

FIGURE 7-33: Higher magnification view of an oxidized grain triple point in the primary fracture area (arrow). The presence of triple points is indicative of intergranular fracture.



FAM 98263

MAG: 3000X

FIGURE 7-34: Moderately oxidized primary fracture area.



FIGURE 7-35: Intergranular overstress with some grain boundary separation in the final fracture area. The fracture surface is only lightly oxidized.



FIGURE 7-36: Higher magnification photograph of a grain boundary quadruple point (arrow) in the final fracture area shown in Figure 7-35.

MATERIAL

Incoloy 909
FWA 1191 Bar

TEST DATA

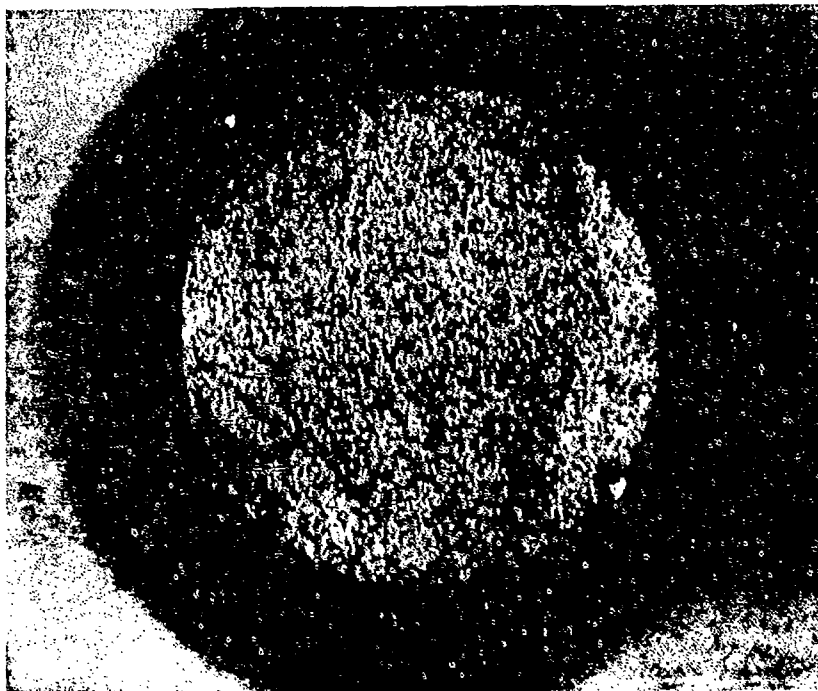
TEST TYPE
Smooth LCF

TEST CONDITIONS

Stress: 896.3 MPa (130.0 KSI)/44.8 MPa (6.5 KSI)
Stress Ratio: 0.05
Frequency: 10 cpm
Atmosphere: Air
Temperature: Room Temperature
Test Direction: Longitudinal

TEST RESULTS

Cycles to Fracture: 11,000



FAL 92384

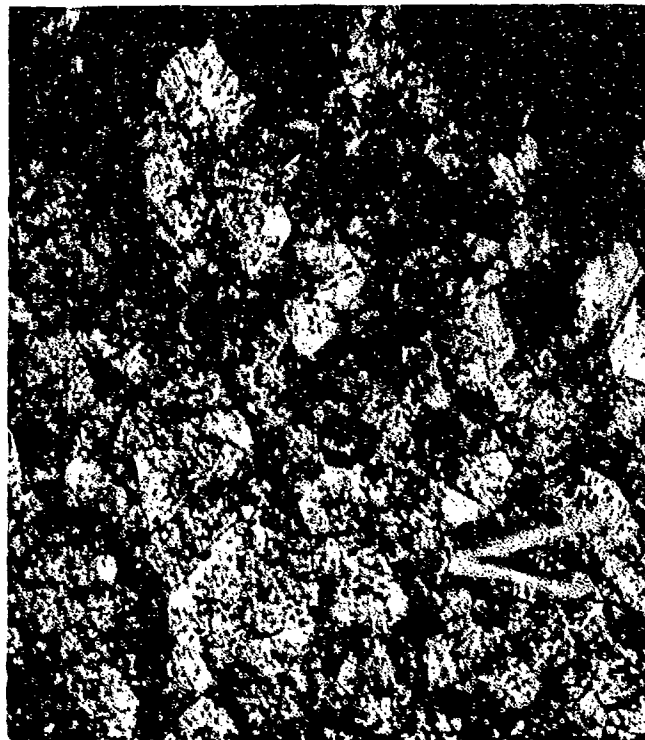
MAG: 10X

Figure 7-37: Test results and fractography of Incoloy 909 room temperature smooth LCF test. The fracture appears slightly intergranular with no obvious fatigue progression (thumbnails). The fatigue progression areas appear as lighter, granular areas (arrows).



FAM 99881

MAG: 200X



FAM 99882

MAG: 200X

FIGURE 7-38: Optical photomicrographs showing predominantly transgranular fracture path in the fatigue progression area near the origin (top) and intergranular fracture path in the final overstress area near the center of the specimen (bottom). A large quantity of structure is visible in the grains.

Etchant: Glyceregia

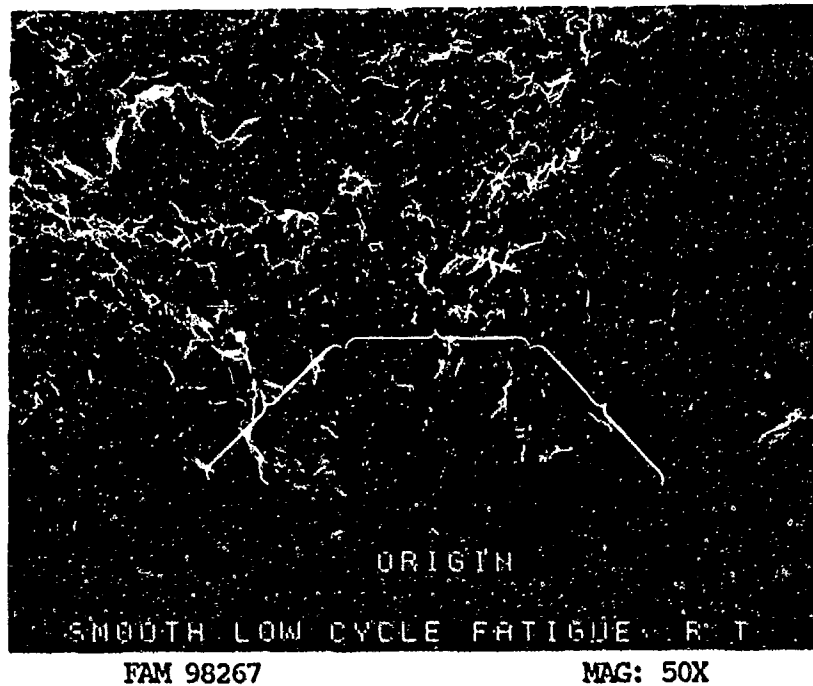


FIGURE 7-39: Low magnification view showing a fatigue origin. Fatigue propagation occurred in small patches near the surface of the specimen. The remainder of the fracture surface is a mixture of transgranular and intergranular overstress (mixed mode). Brackets show the extent of the fatigue.



FIGURE 7-40: Fracture origin shown in Figure 7-39, exhibiting smooth cleavage facets (Stage I fatigue).

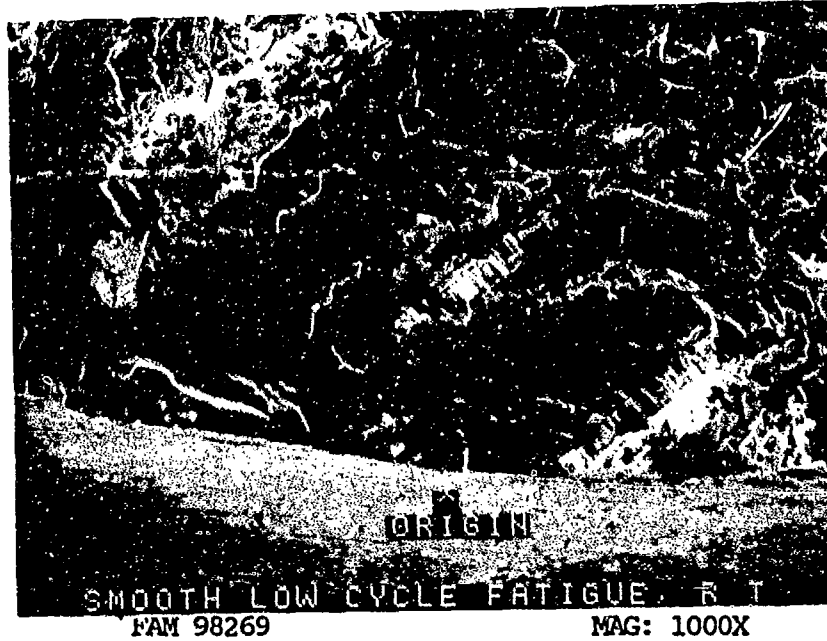


FIGURE 7-41: Higher magnification photograph of the origin area (Stage I fatigue facet) shown in Figure 7-40. The origin exhibits cleavage with bands of cyclic features (arrows).

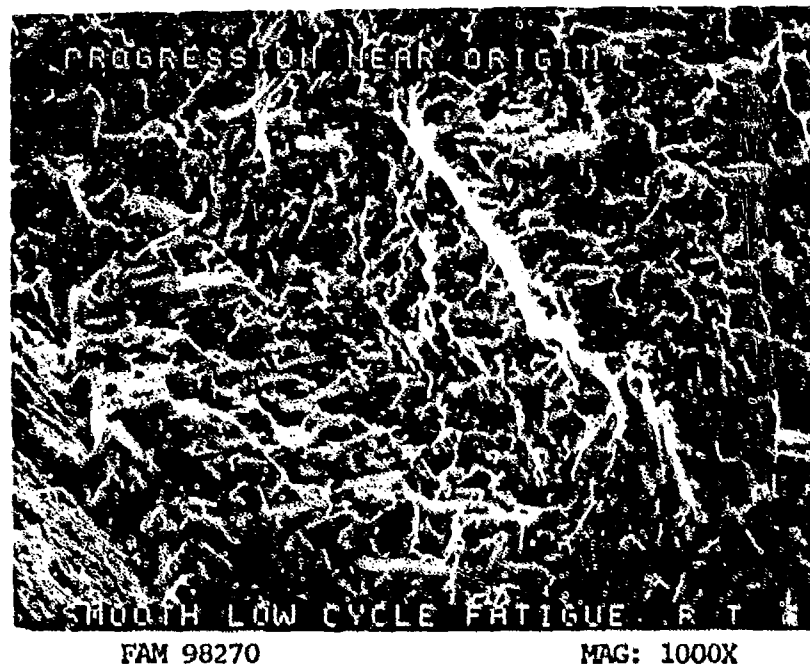


FIGURE 7-42: Fatigue progression near the origin.

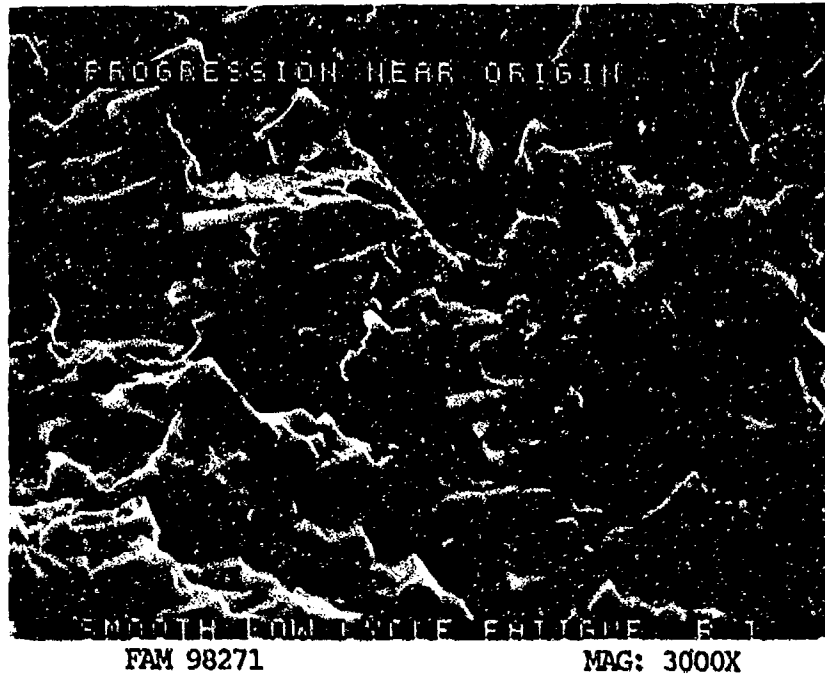


FIGURE 7-43: Fatigue progression near the origin exhibits parallel features (remnant striations) perpendicular to the direction of propagation. The direction of propagation is shown by an arrow.

MATERIAL

Incoloy 909
FWA 1191 Bar

TEST DATA

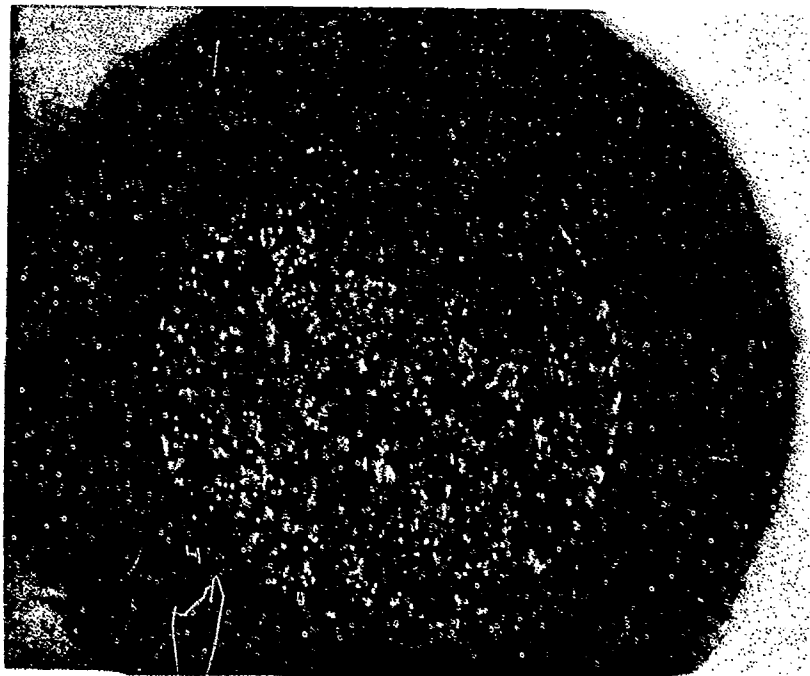
TEST TYPE
Smooth LCF

TEST CONDITIONS

Stress: 827.4 MPa (120 KSI)/41.37 MPa (6.0 KSI)
Stress Ratio: 0.05
Frequency: 10 cpm
Atmosphere: Air
Temperature: 204°C (400°F)
Test Direction: Longitudinal

TEST RESULTS

Cycles to Fracture: 11,000



FAL 92382

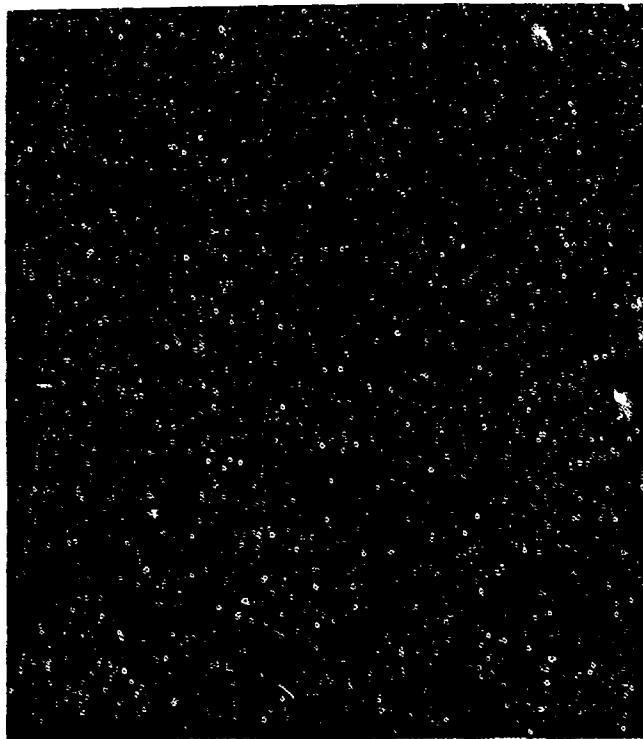
MAG: 10X

FIGURE 7-44: Test results and fractography of Incoloy 909 204°C (400°F) smooth LCF test. The entire fracture surface has a granular appearance. The fatigue progression area is reflective and has more clearly defined facets (arrow).



FAM 99877

MAG: 200X



FAM 99878

MAG: 100X

FIGURE 7-45: Optical photomicrograph showing intergranular fracture path in the fatigue progression area near the origin (top) and in the final overstress area near the center (bottom). Less structure is visible in the grains than in the room temperature specimen. See Figure 7-38.

Etchant: Glyceregia

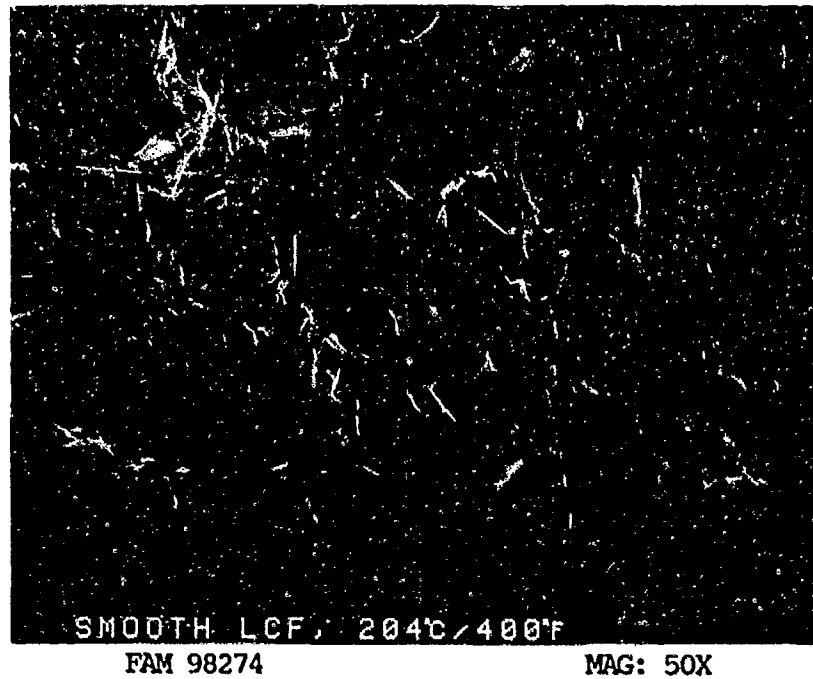


FIGURE 7-46: Low magnification view showing Stage I fatigue facets at an origin area (arrow).

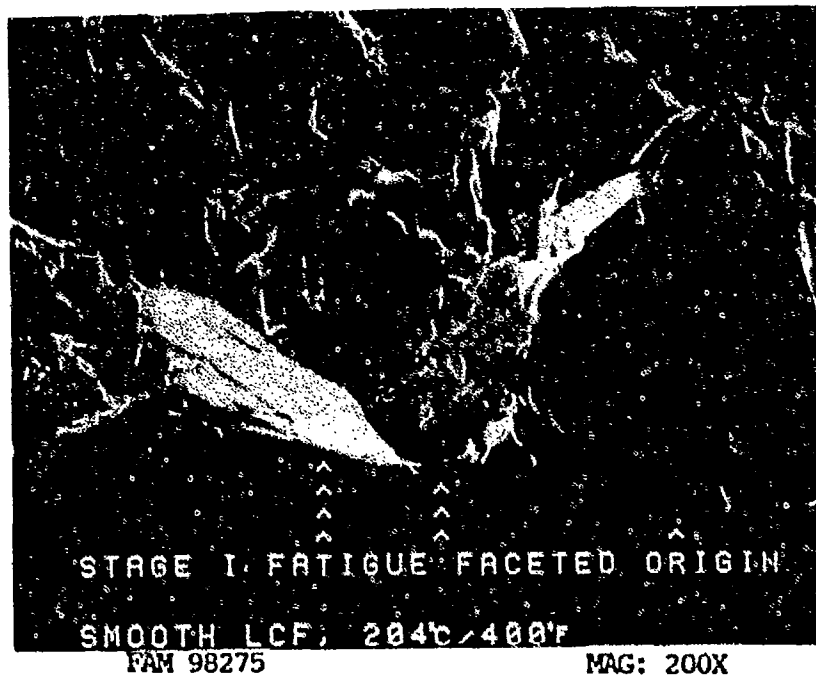


FIGURE 7-47: Smooth facets indicative of Stage I fatigue at an origin area.



FIGURE 7-48: High magnification view of the origin area. No fatigue features are visible on the Stage I facet.

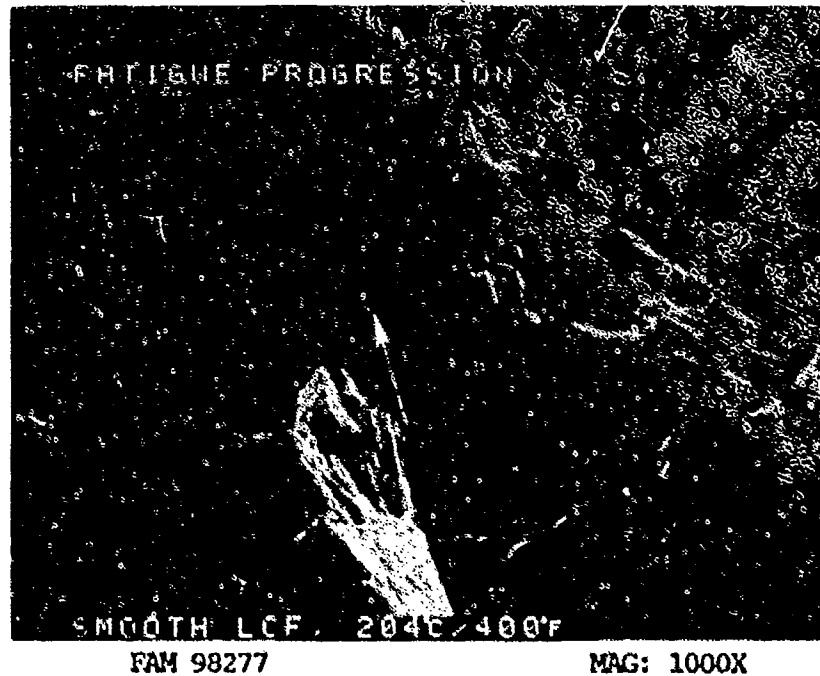


FIGURE 7-49: Fatigue progression near the origin area. Fatigue striations are visible on some of the Stage I facets (arrow).

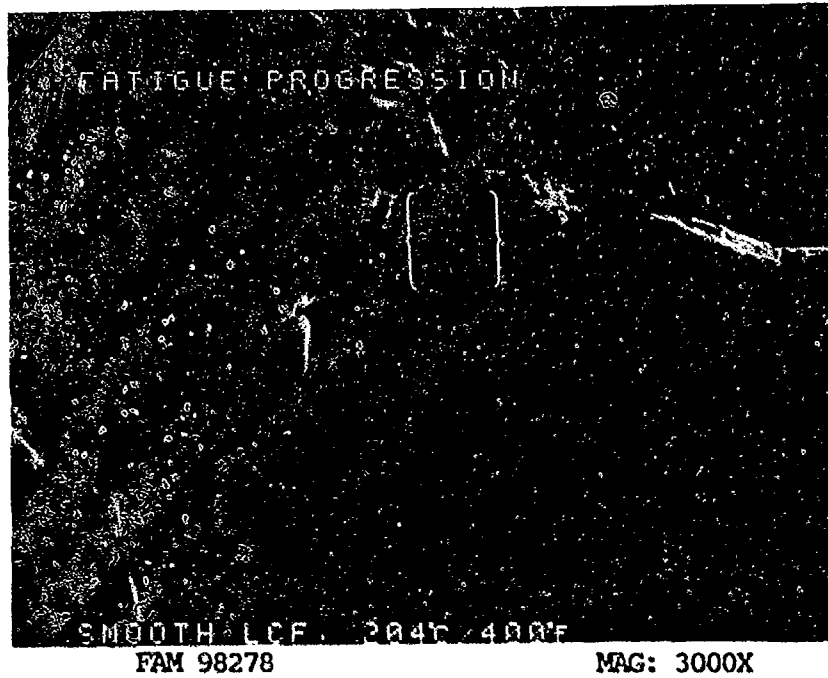


FIGURE 7-50: Fatigue striations in the fatigue progression area (brackets).

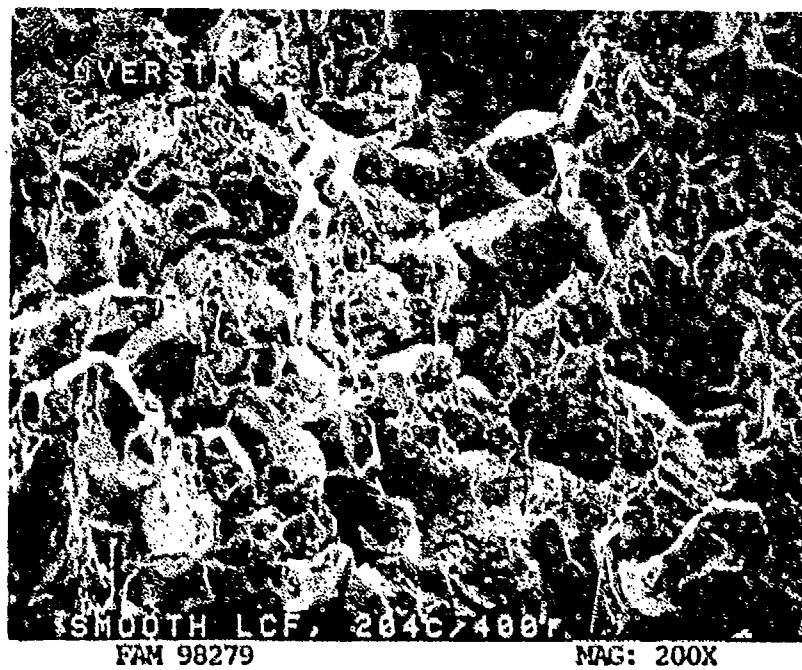


FIGURE 7-51: Intergranular overstress with grain boundary separation in the final overstress area.

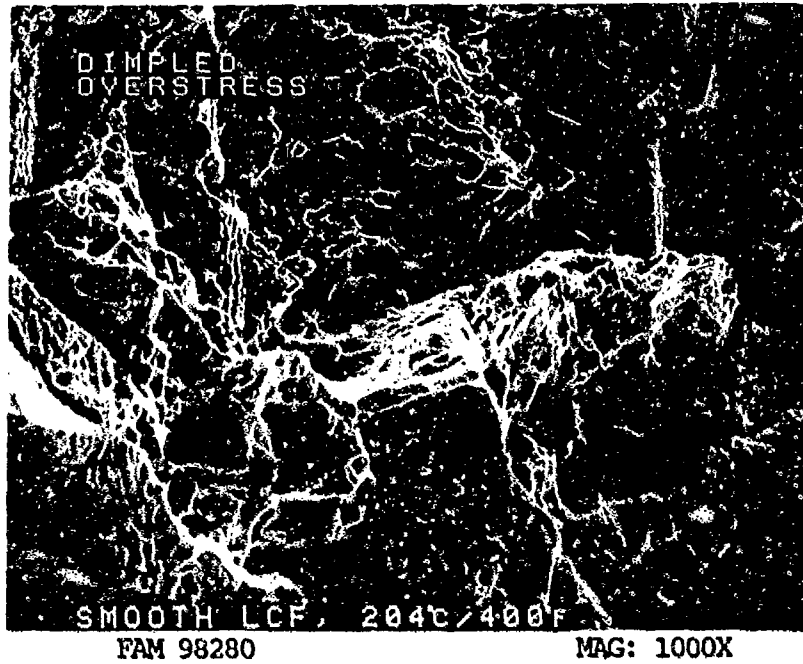


FIGURE 7-52: Dimpled intergranular overstress in the final overstress area. Grain faces are covered with randomly shaped dimples.

MATERIAL

Incoloy 909
FWA 1191 Bar

TEST DATA

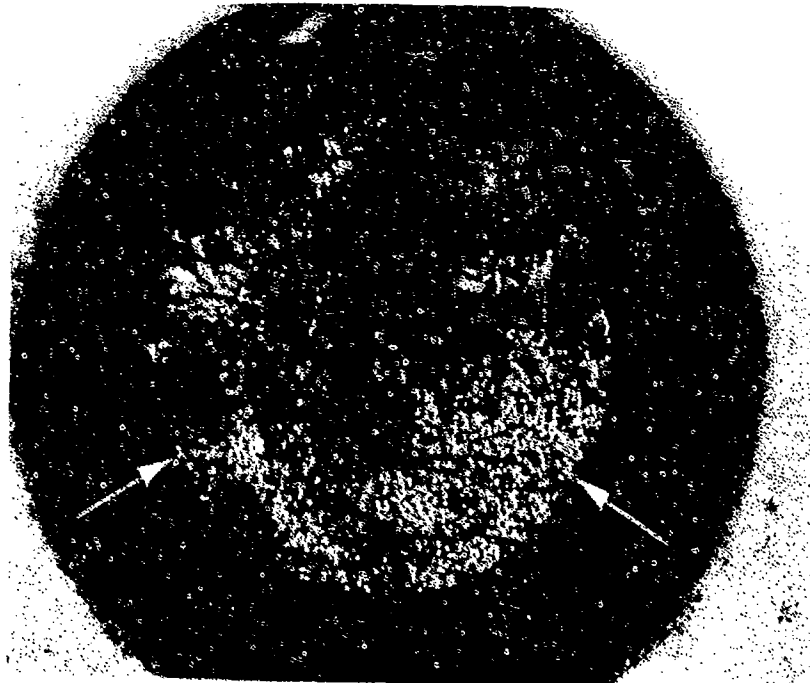
TEST TYPE
Smooth LCF

TEST CONDITIONS

Stress: 689.5 MPa (100.0 ksi)/34.5 MPa (5.0 ksi)
Stress Ratio: 0.05
Frequency: 10 cpm
Atmosphere: Air
Temperature: 649°C (1200°F)
Test Direction: Longitudinal

TEST RESULTS

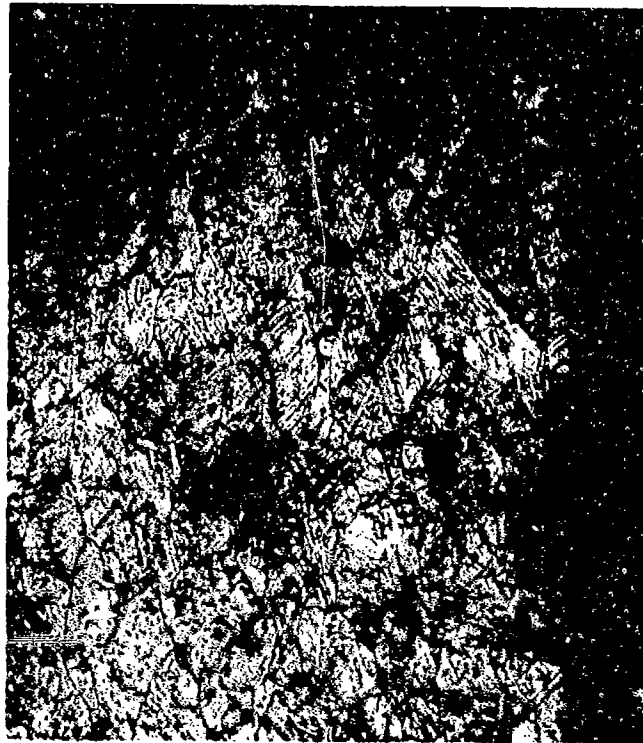
Cycles to Fracture: 11,750



FAL 92383

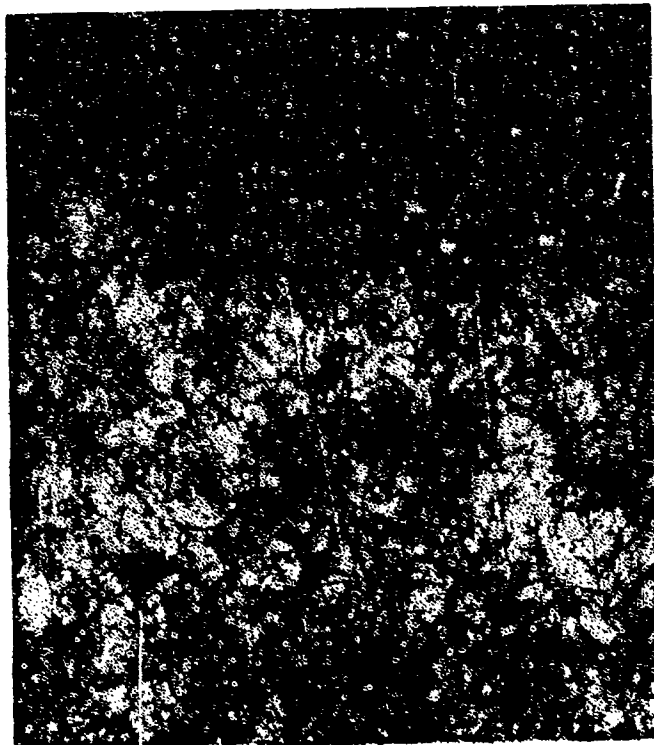
MAG: 10X

FIGURE 7-53: Test results and fractography of Incoloy 909 649°C (1200°F) smooth LCF test. Several fatigue progression thumbnails appear as shiny faceted areas (arrows). The remainder of the fracture surface has a dull granular appearance.



FAM 99782

MAG: 200X



FAM 99783

MAG: 200X

FIGURE 7-54: Optical photomicrographs showing predominantly transgranular fracture path in the fatigue progression area near the origin (top) and in the final overstress area near the center of the specimen (bottom).

Etchant: Glyceregia

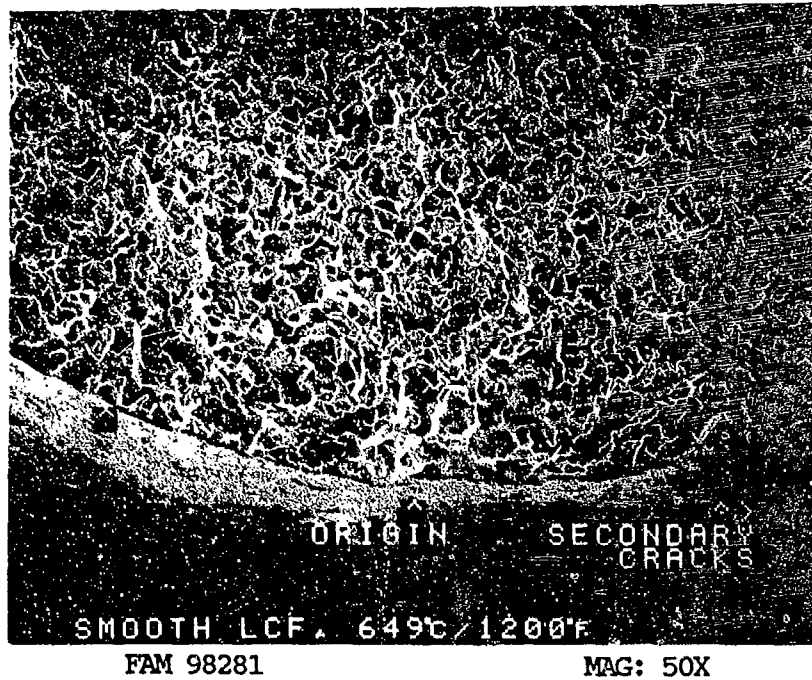


FIGURE 7-55: Low magnification view showing several fatigue origins and secondary cracking on the outside surface of the specimen. The fracture surface appears to be oxidized.

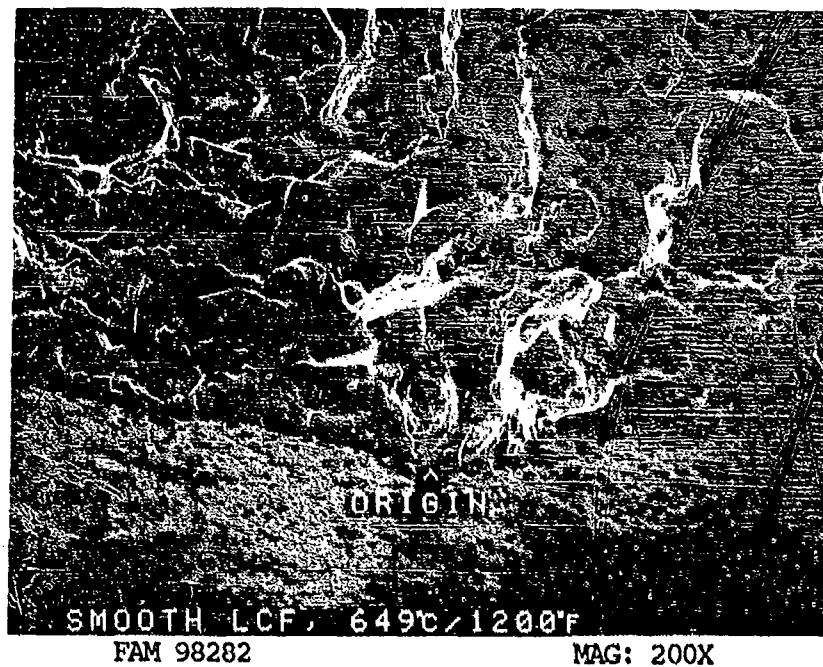
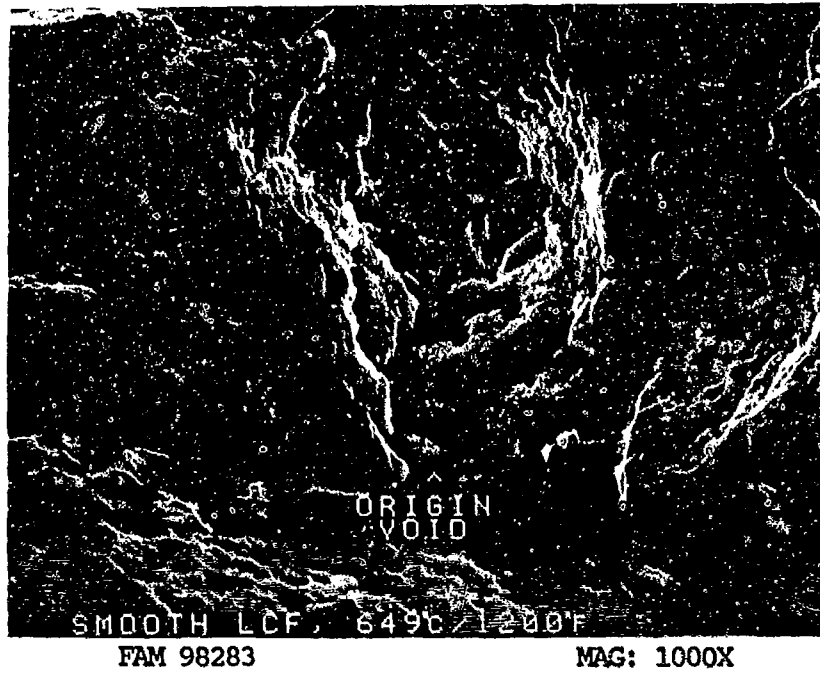


FIGURE 7-56: Oxidized fatigue origin shown in Figure 7-55.



FAM 98283

MAG: 1000X

FIGURE 7-57: High magnification photograph reveals that the fatigue originated at a slightly subsurface void. The void produced a stress concentration.



FAM 98284

MAG: 1000X

FIGURE 7-58: Heavily oxidized fatigue progression area. No fatigue features are discernible.

MATERIAL

Incoloy 909
FWA 1191 Bar

TEST DATA

TEST TYPE

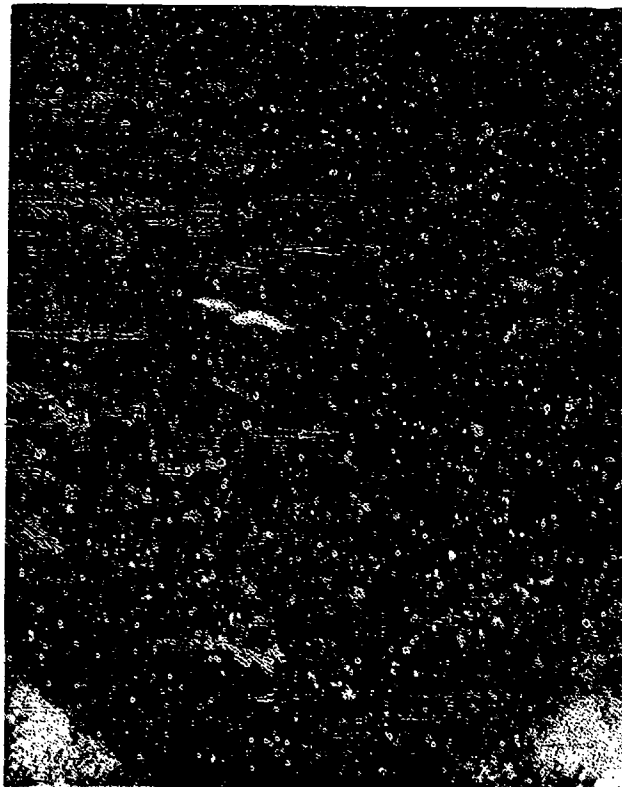
In-phase TMF

TEST CONDITIONS

Stress: 510.2 MPa (74.0 ksi)/-455.1 MPa (-66.0 ksi)
Stress Ratio: -1.12
Frequency: 1 cpm
Atmosphere: Air
Temperature: 260°C (500°F)/704°C (1300°F)
Test Direction: Longitudinal

TEST RESULTS

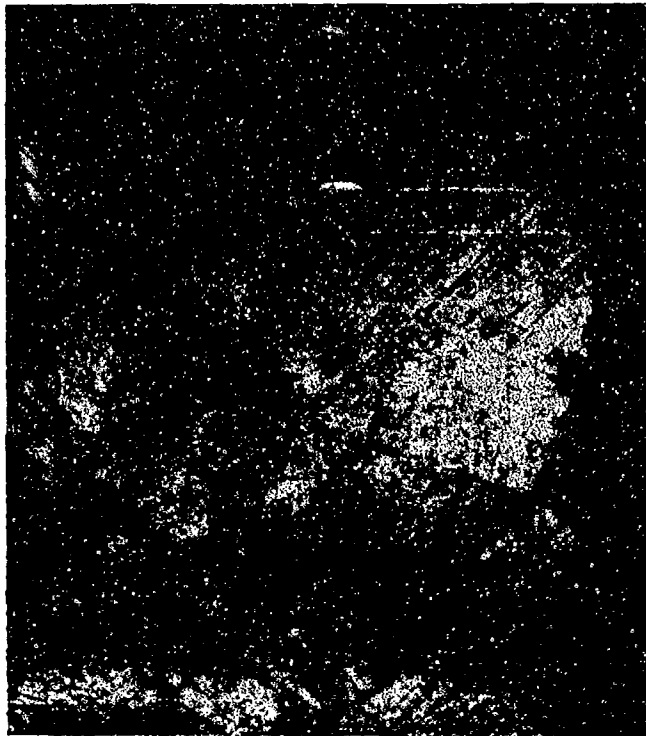
Cycles to Fracture: 1483



FAL 92924

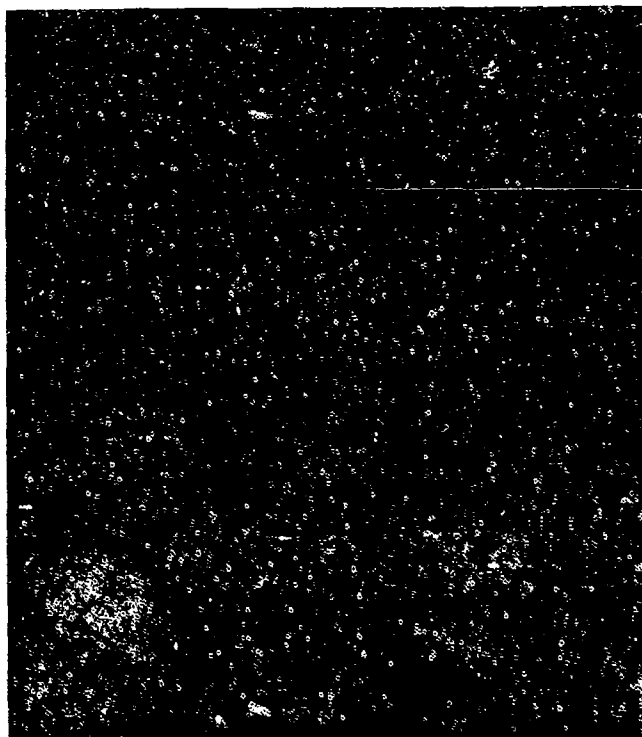
MAG: 10X

Figure 7-59: Test results and fractography of Incoloy 909 in-phase TMF test. The fracture exhibits multiple origins on both the I.D. and O.D. surfaces of the specimen.



FAM 99804

MAG: 200X



FAM 99805

MAG: 200X

FIGURE 7-60: Optical photomicrographs showing heavily oxidized transgranular fracture path with numerous secondary cracks in the specimen surface (arrows). The cracks exhibit the typical oxide-filled "V" shape.

Etchant: Glyceregia

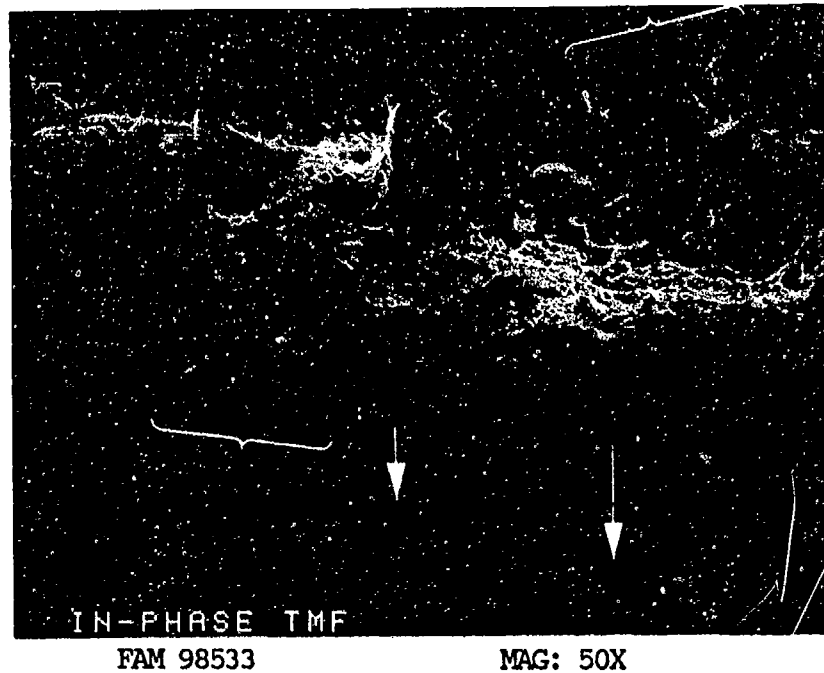


FIGURE 7-61: Low magnification photograph showing TMF origins (brackets) on both the I.D. and O.D. surfaces of the specimen, and secondary cracking on the O.D. surface (arrows). The origin areas appear to be faceted.

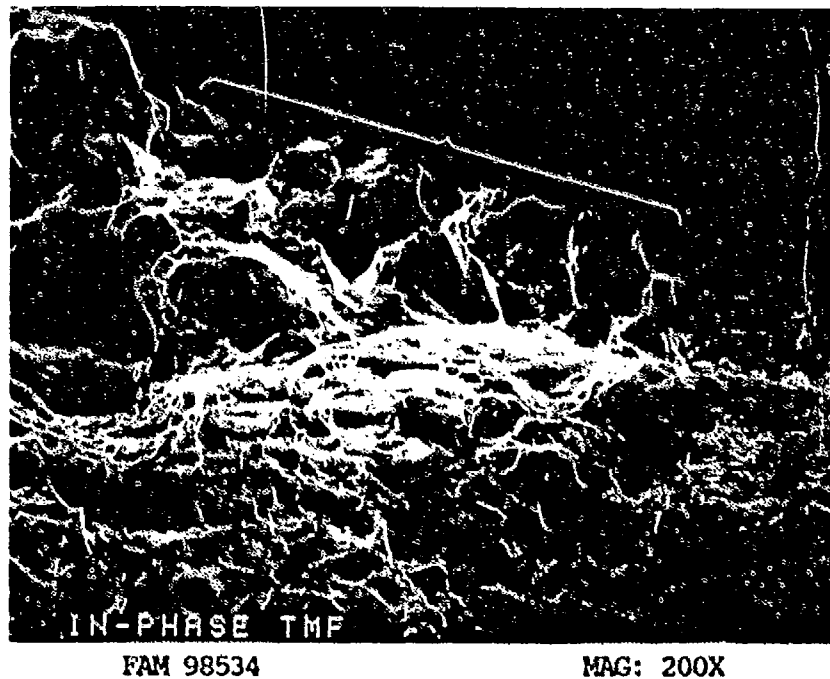


FIGURE 7-62: Faceted fatigue area at the I.D. surface of the specimen (brackets) and dimpled overstress near the center of the fracture surface.

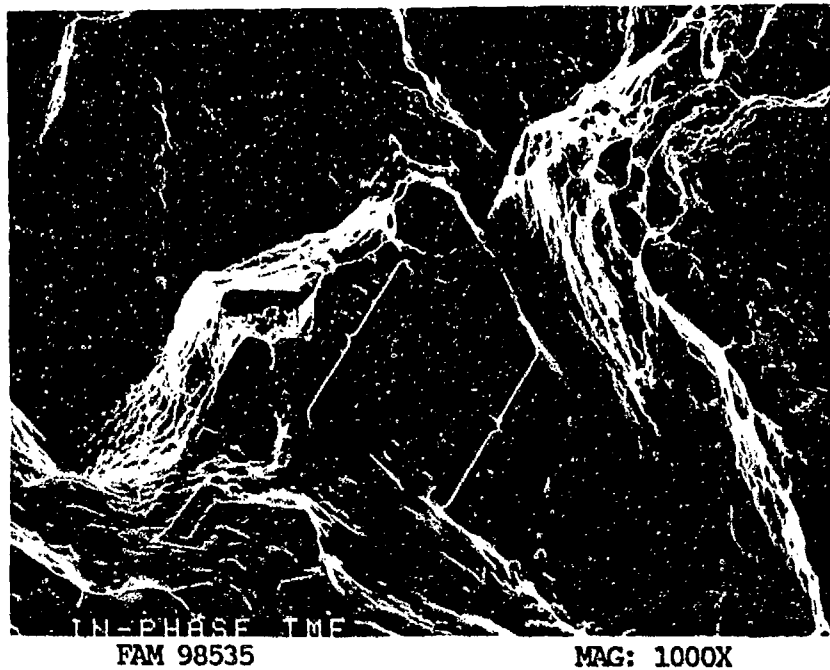


FIGURE 7-63: Oxidized fatigue striations near the I.D. surface of the specimen (brackets).

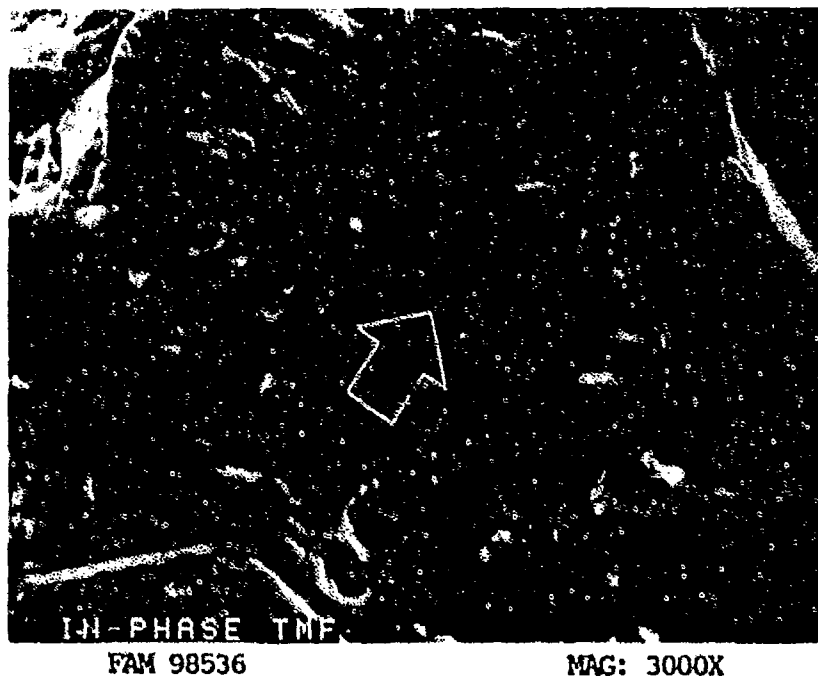


FIGURE 7-64: High magnification photograph showing oxidized fatigue striations (Figure 7-63). Arrow shows the direction of propagation.

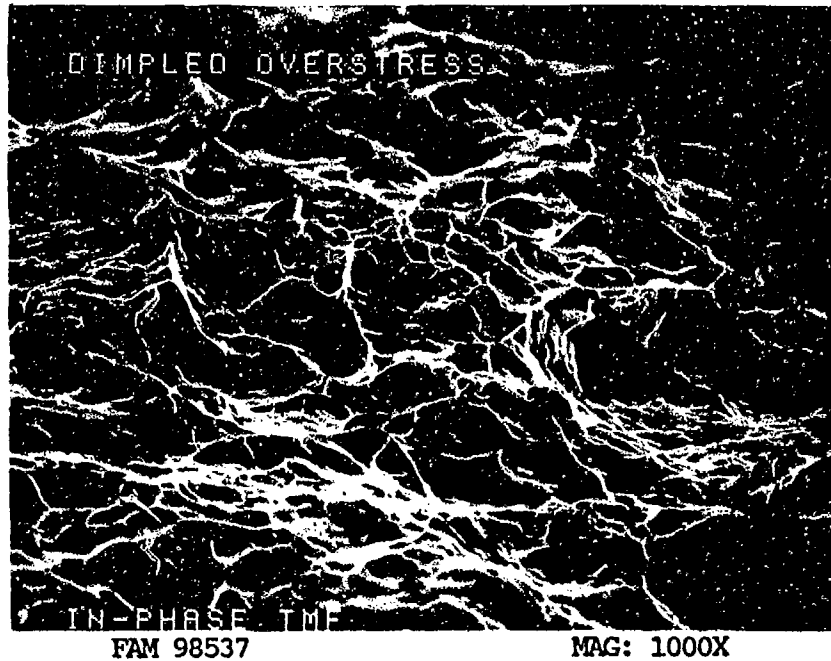


FIGURE 7-65: Dimpled overstress near the center of the fracture surface.

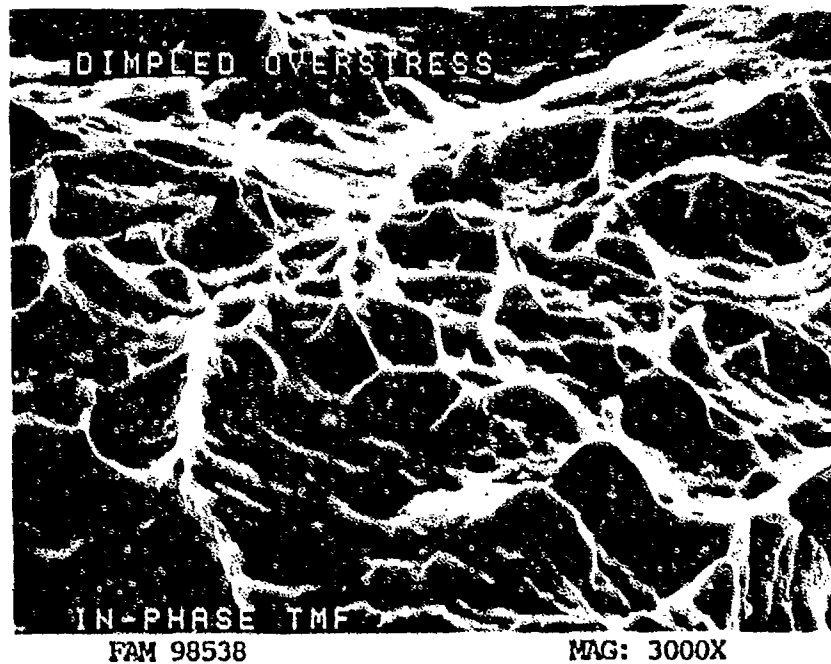
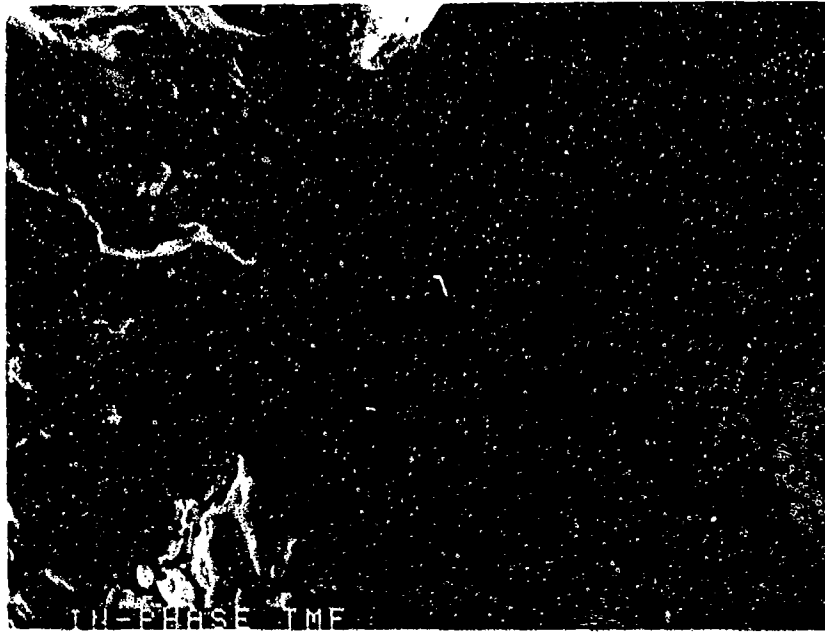


FIGURE 7-66: Higher magnification photograph of the area in Figure 7-65, showing oxidized dimpled overstress near the center of the fracture surface.



FAM 98539

MAG: 1000X

FIGURE 7-67: Mud cracking of heavy oxide in the fatigue area near an origin. This type of oxide cracking is characteristic of TMF.

MATERIAL

Incoloy 909
PWA 1191 Bar

TEST DATA

TEST TYPE

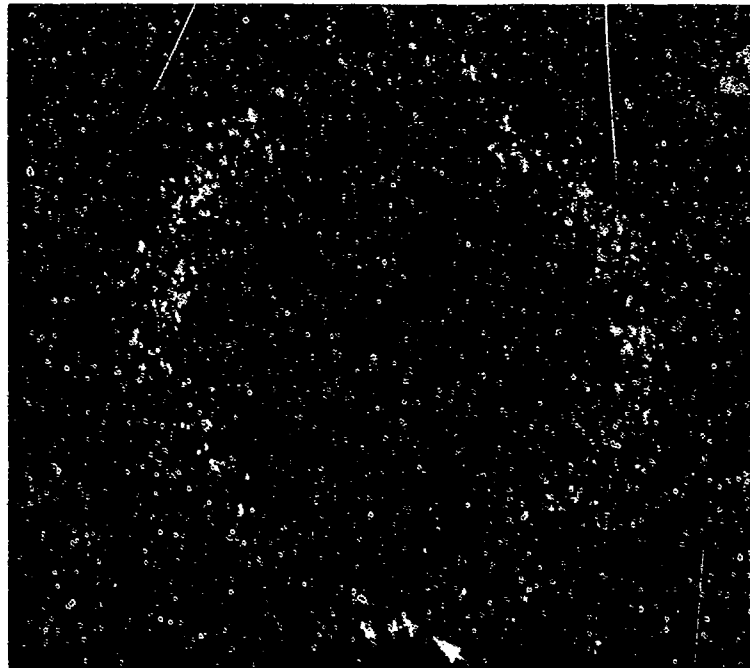
Out-of-phase TMF

TEST CONDITIONS

Stress: 510.2 MPa (74.0 ksi)/-455.1 MPa (-66.0 ksi)
Stress Ratio: -1.12
Frequency: 1 cpm
Atmosphere: Air
Temperature: 260°C (500°F)/649°C (1200°F)
Test Direction: Longitudinal

TEST RESULTS

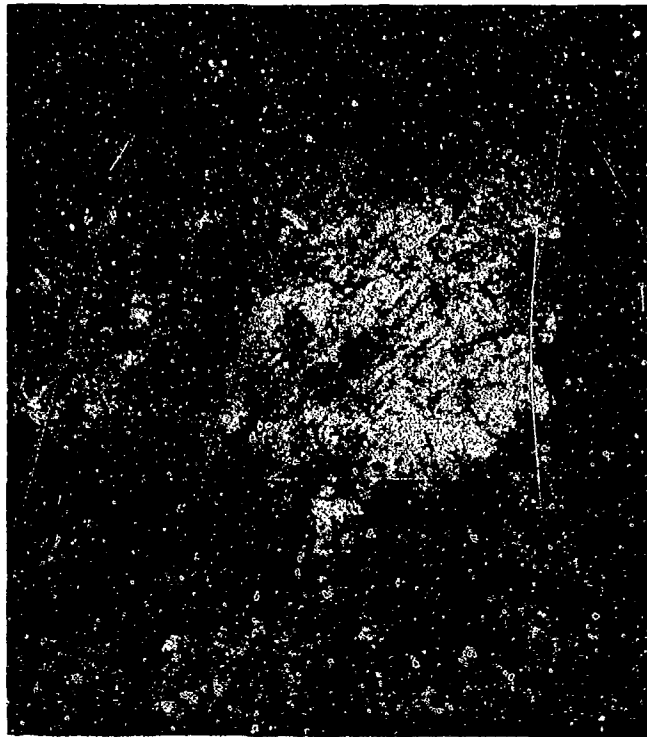
Cycles to Fracture: 1609



FAL 92925

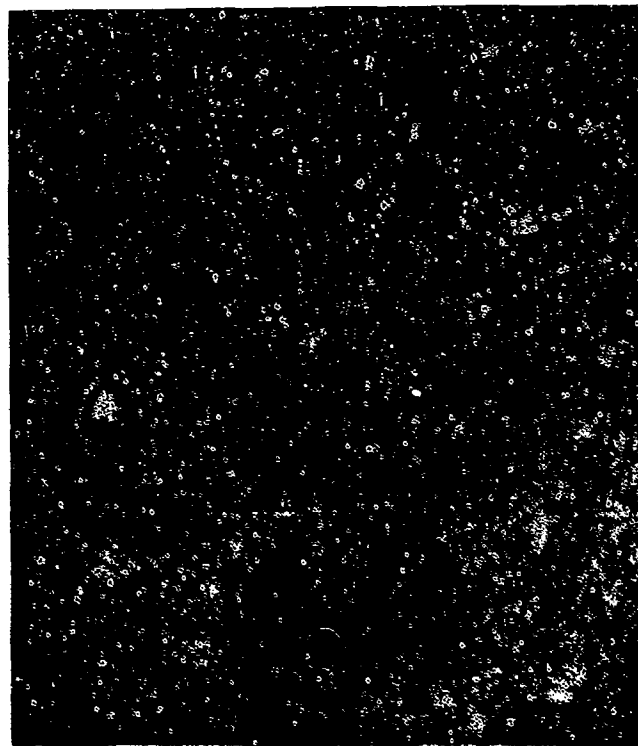
MAG: 10X

Figure 7-68: Test results and fractography of Incoloy 909 out-of-phase TMF test. A fatigue progression area (thumbnail) is visible at the bottom of the photograph (arrow).



FAM 99806

MAG: 200X



FAM 99807

MAG: 200X

FIGURE 7-69: Optical photomicrographs showing heavily oxidized predominantly transgranular fatigue path (bracket, top). The specimen surface exhibits secondary cracks and grain boundary separation. The center of the specimen (bottom) exhibits non-oxidized final overstress. Some intergranular overstress is visible (arrow).

Etchant: Glyceregia

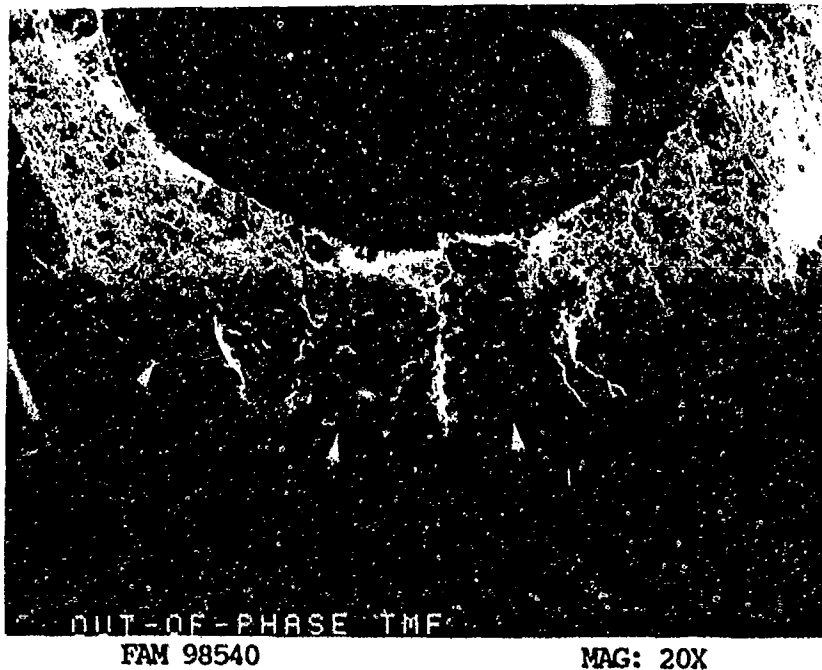


FIGURE 7-70: Low magnification view showing several fatigue origins on the O.D. surface of the specimen (arrows).

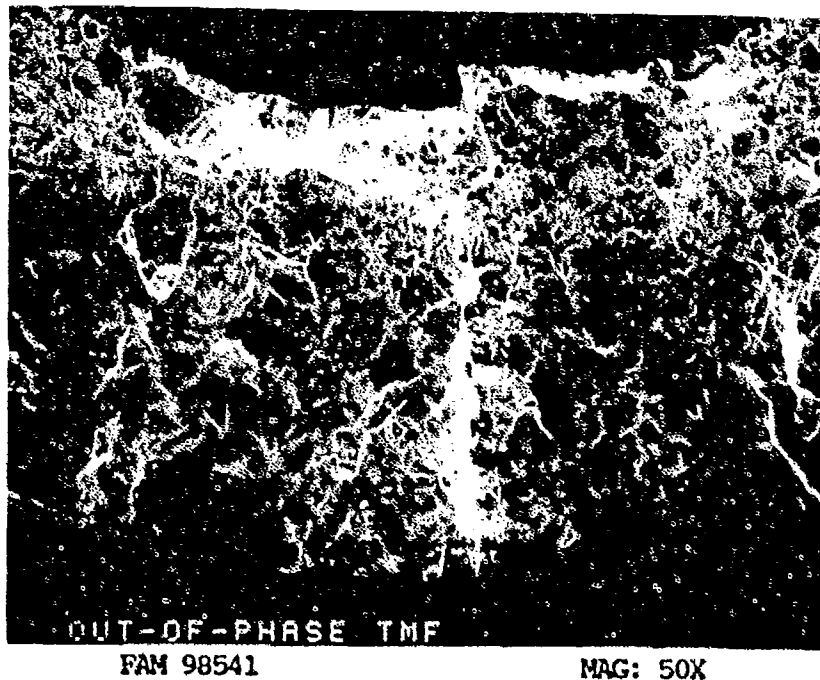


FIGURE 7-71: TMF origin on the O.D. surface of the specimen. The fatigue progression area appears smooth and oxidized.

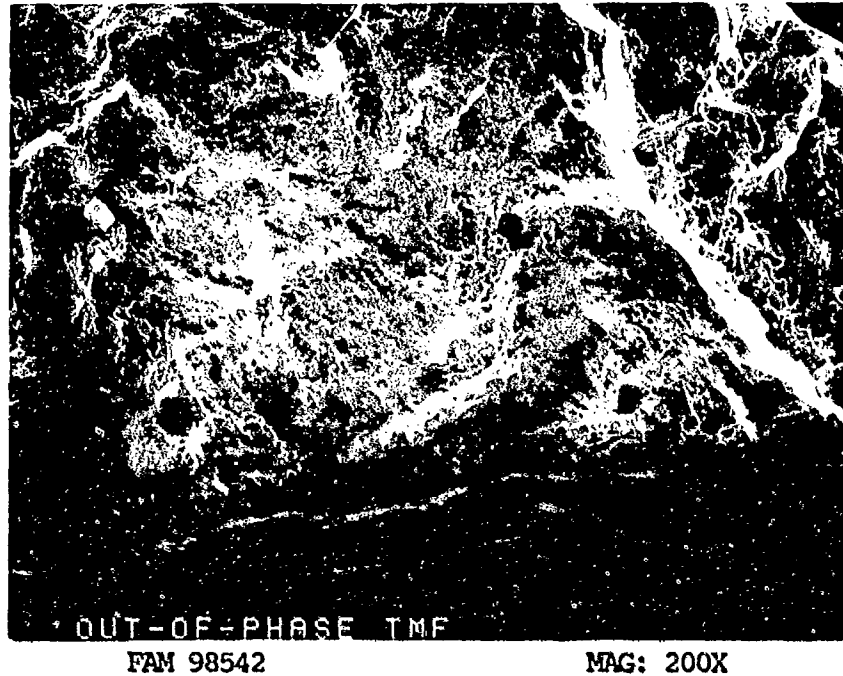


FIGURE 7-72: Fatigue area near an origin. The fracture surface is relatively flat and oxidized.

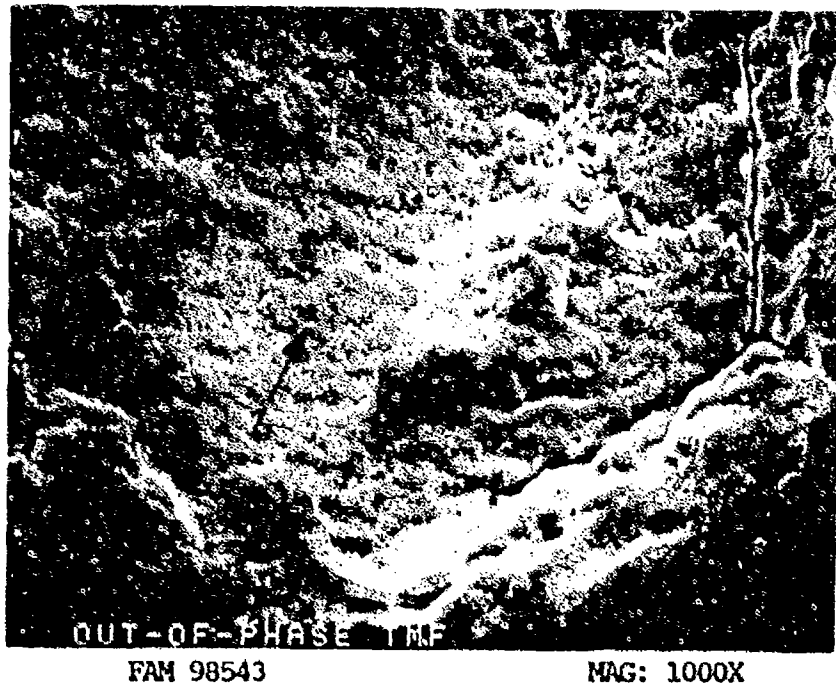


FIGURE 7-73: Possible remnant striations in the fatigue zone. An arrow shows the direction of propagation.

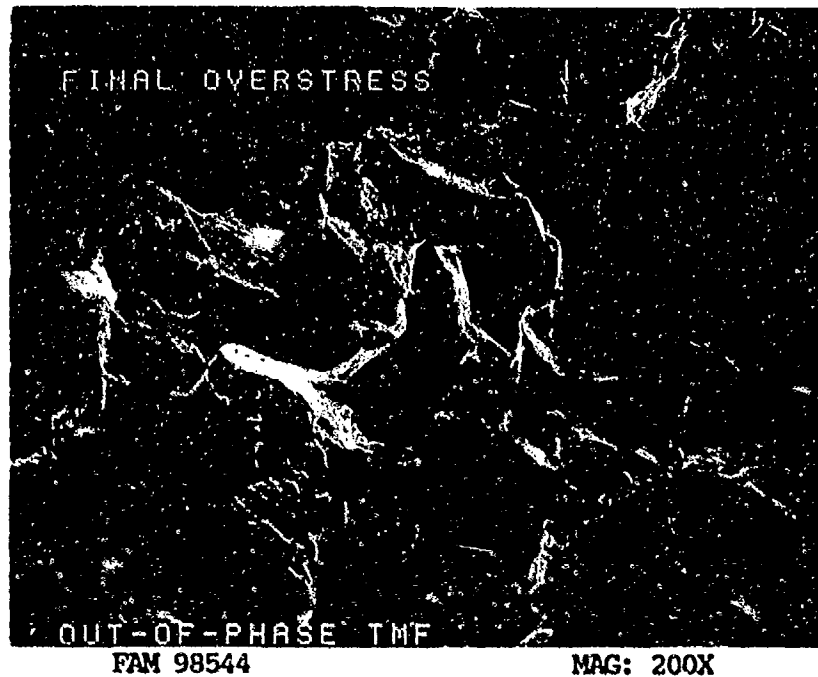


FIGURE 7-74: Final overstress area exhibits a mixture of transgranular and intergranular overstress (mixed mode).

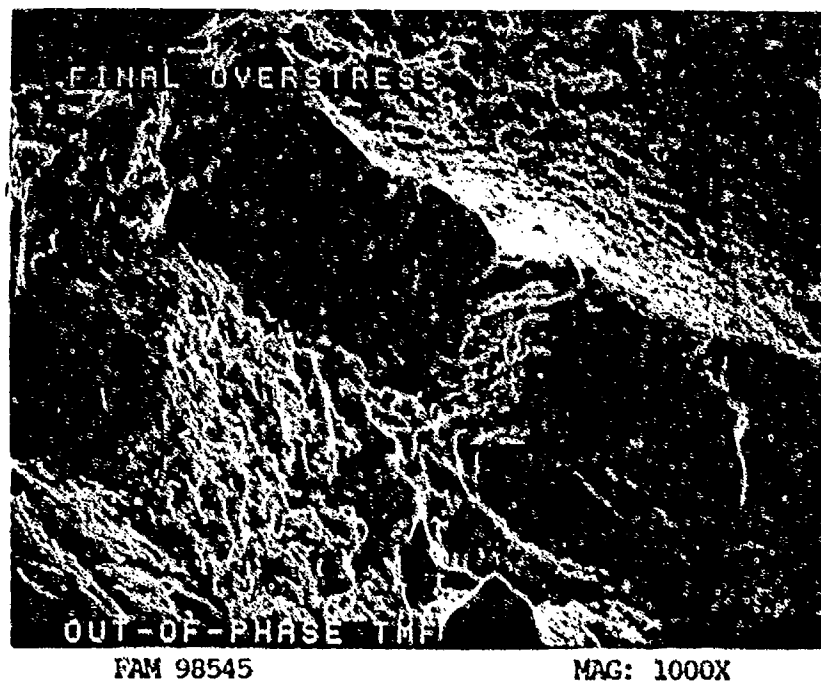


FIGURE 7-75: Higher magnification photograph of the area shown in Figure 7-74, showing a mixture of transgranular and intergranular overstress.

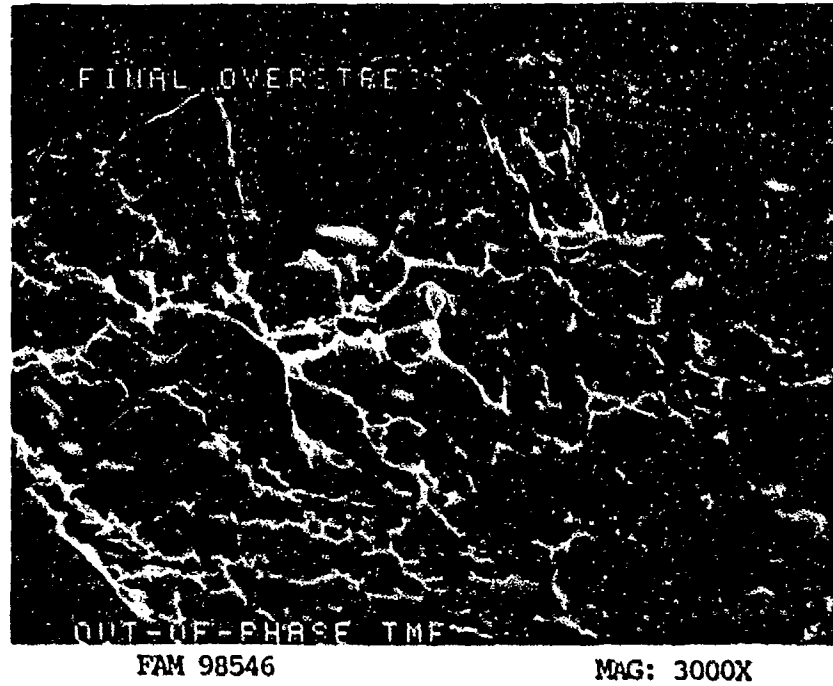


FIGURE 7-76: Very fine dimples in the final overstress area.

SERVICE FAILURE

FRACTURE MODE Thermal-Mechanical Fatigue (TMF)

PART NAME Second Stage Turbine Duct Segment (Tip Shroud) Support Ring

OPERATION DATA Operated under standard gas turbine engine operating condition in an accelerated mission test (AMT). The segments were subjected to moderate steady and cyclic stresses at high temperatures.

PART TIME 929 hours (4000 operational cycles)

	<u>REQUIRED</u>	<u>ACTUAL</u>
MAT'L		
BASE	<u>Incoloy 909</u>	<u>Confirmed</u>
OTHER	<u>Aluminide Coating</u>	<u>Confirmed</u>
HARDNESS	<u>HRC 36 minimum (HB conv.)</u>	<u>HRC 21-35 *</u>
GRAIN SIZE	<u>ASTM 2 or finer, occas. 1</u>	<u>ASTM 2-3</u>
DIMENSIONAL	<u>-</u>	<u>-</u>

* Diamond pyramid hardness (DPH) conversions.

SUMMARY: The cracking associated with the duct segment attachment window was the result of TMF. Distressed areas between the tip shroud segments also appeared to be thermally induced, with evidence of local hot spots exceeding 1350^oF (maximum metal temperature). Erosion by hot gases also contributed to the problem. The variation in the hardness readings was attributed to local hot spots. No contributing material or microstructural defects were found.



FAL 87682

MAG: 4X

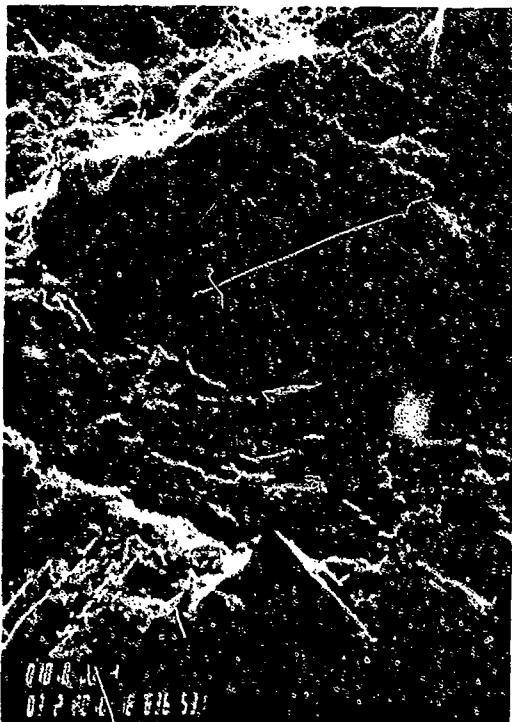


FAL 93460

MAG: 10X

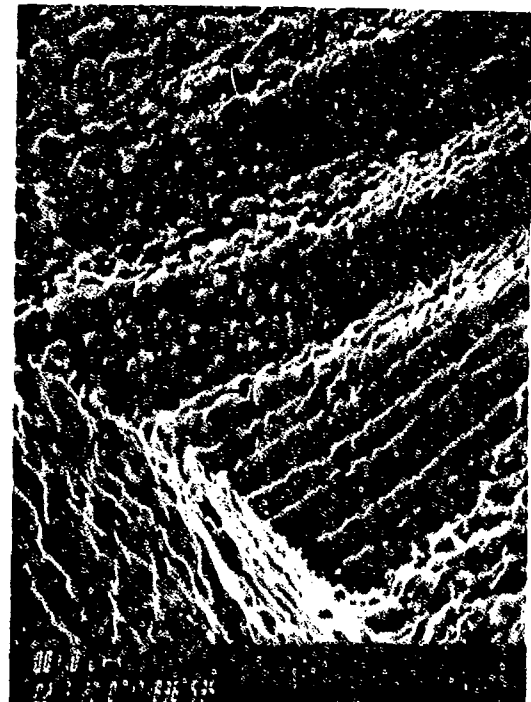
FIGURE 7-77: Close-up view of the duct segment attachment window exhibiting cracking (arrows).

FIGURE 7-78: Overall photograph of an opened crack surface.



FAL 93457

MAG: 300X

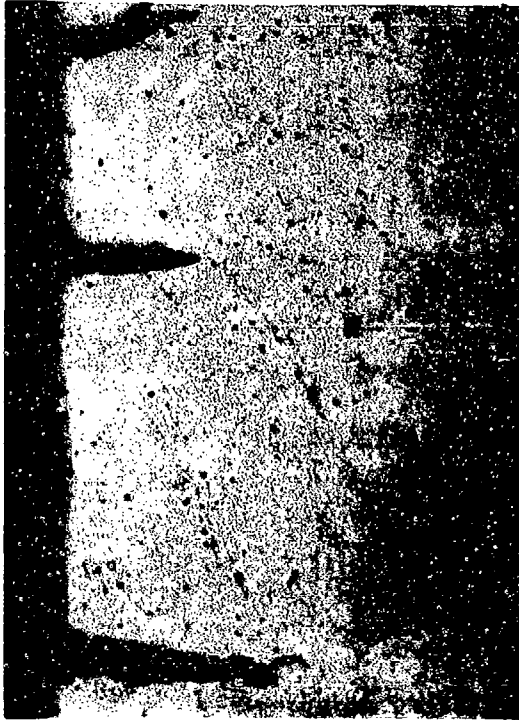


FAL 93458

MAG: 2000X

FIGURE 7-79: Relatively flat oxidized features on the opened crack surface.

FIGURE 7-80: High magnification SEM photograph showing the oxide structure.



FAL 93461

MAG: 20X



FAL 93462

MAG: 160X

FIGURE 7-81: Pair of optical photomicrographs of a metallographic cross section through several cracks. The cracks exhibit the oxidized wedge shape characteristic of IMF.

Etchant: Glyceregia

Inconel 600

Material Description

Inconel 600 is a corrosion and oxidation resistant non-age-hardenable nickel-chromium alloy. Inconel 600 is easily welded and is available as sheet, strip, plate, bar, wire, tubing and castings. The strength at elevated temperatures is similar to 18-8 stainless steel and it is oxidation resistant to 2000 F, but is useful only when stresses are low.

The material used in this study was heat treated to AMS 5665 (bar) with a required hardness of BHN 229-311 for cold drawn stock up to 1.0 inch and BHN 134-241 when hot finished up to 0.5 inch thick. The typical room temperature mechanical properties for AMS 5665 (bar) are as follows:

Ultimate Tensile Strength:	85 ksi
0.2% Yield Strength:	35 ksi
Percent Elongation:	30%
ASTM Grain Size:	<u>Required</u> _____ <u>Measured</u>
	No Requirement 14
Measured Hardness:	BHN 164-171 (DPH conversions)

Fractography Overview

The room temperature smooth and notched tensile specimens exhibited dimpled overstress with some grain boundary separation. The smooth specimen had a large 0.05 inch shear lip containing shear dimples and other shear features. The notched specimen had no shear lip and a more intergranular appearance than the room temperature specimen. Some of the grain faces and cleavage facets had slip lines visible. Both elevated temperature specimens exhibited primarily transgranular dimpled overstress. Neither specimen had a shear lip. The dimples on the smooth specimen were deep and coarse. The notched specimen had shallower dimples with areas of void coalescence. Many of the larger dimples had ripples on their walls. The stress rupture specimen was heavily oxidized dimpled rupture with numerous deep voids. The fracture occurred at an angle to the stress axis. All the fine features were obscured by the oxide.

Each of the three HCF specimens exhibited one localized origin area and fatigue progression that covered greater than 90% of the cross section before final overstress occurred. The room temperature and 800 F specimens had several individual origins within the single local origin area. The 1300 F specimen propagated from a single origin. The two lower temperature specimens had similar origin appearances, having several Stage I facets at the surface. The fatigue propagation areas (stage II) exhibited fine fatigue striations on plateaus separated by fatigue steps and, in some cases, broader tearing features. The striations were significantly finer on the 800 F specimen due to the lower applied stress. The final overstress areas were a mixture of dimpled overstress and quasi-cleavage

features occurring in a narrow crescent shape. The 1300^oF specimen had no facets in the stage I area, having only feathery cleavage features with no striations directly adjacent to the origin and plateaus containing fine fatigue striations separated by steps. Individual striations were not resolvable adjacent to the origin because they were fine and were covered by a uniform oxide. The striations became significantly coarser in the fatigue progression. The final overstress area was heavily oxidized with no discernible features.

The three notched HCF specimens exhibited similar trends with temperature as the smooth specimens. The major difference was that the notched specimens propagated from multiple origins spread over as much as 120^o of the surface. The local origins were separated by small steps (ratchet marks). The 1300^oF specimen had feathery cleavage and patches of oxidized striations in the origin areas. All three specimens had plateaus with very fine striations. The two elevated temperature specimens exhibited more increase in striation spacing as the crack progressed than the room temperature specimen. The final overstress areas on all three specimens had a mixture of dimpled overstress and quasi-cleavage.

Two LCF specimens were run, one at 800^oF and one at 1300^oF. The 800^oF specimen had a small oxidized thumbnail with fatigue propagating from two origins separated by a step. Both origins had a small stage I facet at the surface with feathery cleavage and some fine striations. The fatigue propagated beyond the thumbnail, exhibiting coarser striations and crack-like striations. The 1300^oF specimen exhibited multiple origins along a 120^o area on the surface. The fatigue crack thumbnail progressed across 40% of the specimen before final overstress occurred. Heavily oxidized striations and crack-like striations were visible near the origin, with remnant striations and secondary cracks perpendicular to the direction of propagation in the fatigue progression area. The final overstress areas on both specimens had a mixture of dimpled overstress and quasi-cleavage, with a lower percentage of quasi-cleavage features on the high temperature fracture.

MATERIAL

Inconel 600
AMS 5665 Bar

TEST DATA

TEST TYPE

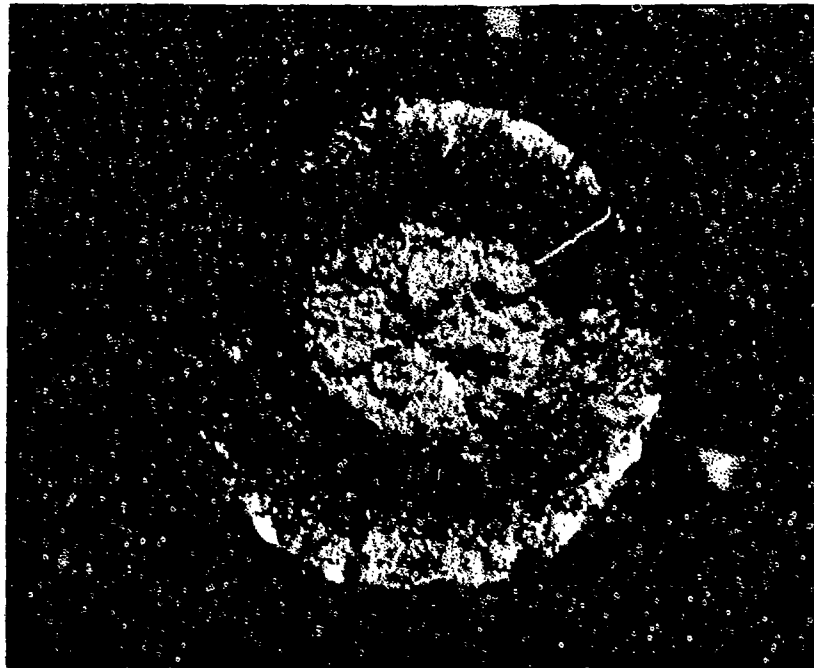
Smooth Tensile

TEST CONDITIONS

Strain Rate: 0.005 mm/mm/min (0.005 in/in/min)
Atmosphere: Air
Temperature: Room Temperature
Test Direction: Longitudinal

TEST RESULTS

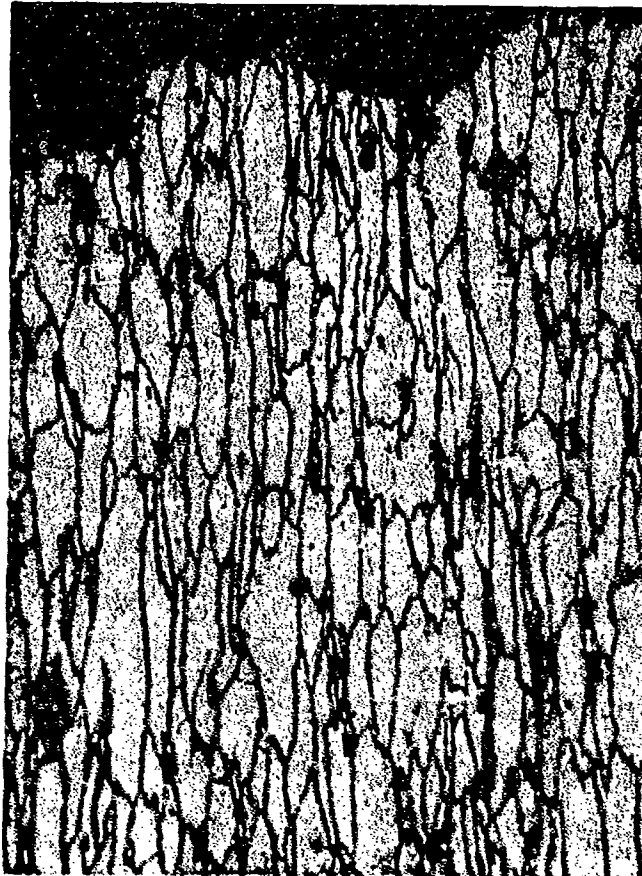
0.2% Yield Strength:	286.8 MPa (41,600 PSI)
Ultimate Strength:	684.0 MPa (99,200 PSI)
Percent Elongation:	48.5
Percent Reduction of Area:	60.6



FAL 92441

MAG: 15X

FIGURE 8-1: Test results and fractography of Inconel 600 room temperature smooth tensile test. The fracture surface is dominated by a very large shear lip (bracket). Compare with the 1300 F smooth tensile specimen (Figure 8-9) that has no shear lip.



FAM 99839

MAG: 200X

FIGURE 8-2: Optical photomicrograph showing elongated grain structure near the center of the sample indicating plastic deformation prior to the final fracture. Elongated voids are visible (arrows). These voids are also visible on the fracture surface near the center of the specimen (Figures 8-3 and 8-5).

Etchant: 5% Nital electrolytic

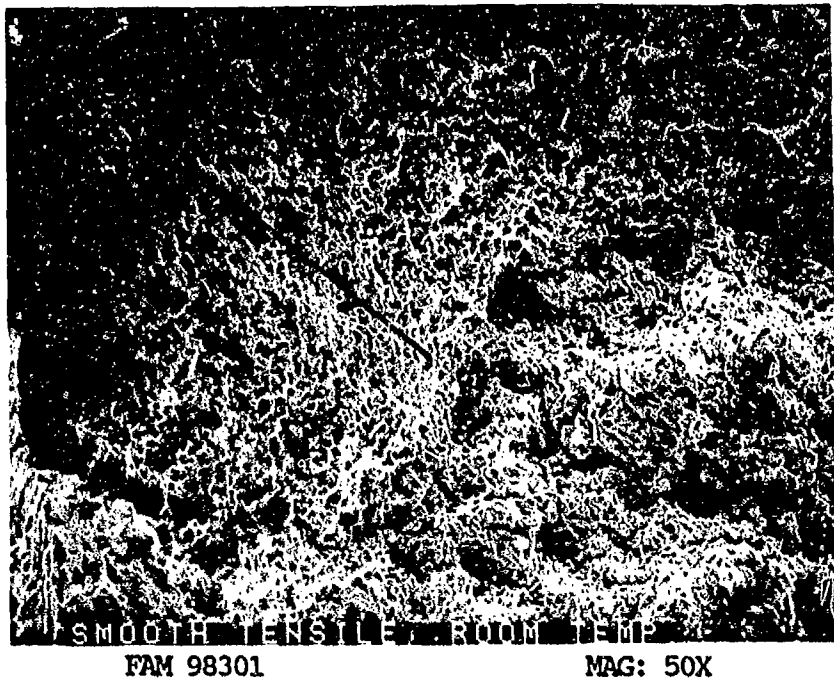


FIGURE 8-3: Low magnification view showing the large shear lip (bracket).

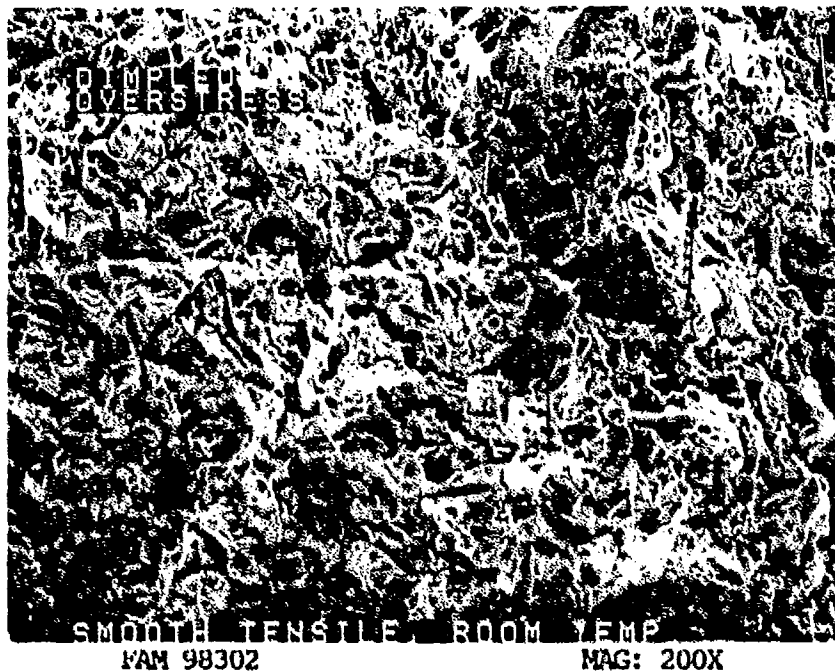


FIGURE 8-4: Dimpled overstress with some grain boundary separation (arrows) in the primary fracture area. At least two elongated voids are visible (arrow A). These are also visible in the metallographic cross section (Figure 8-2).

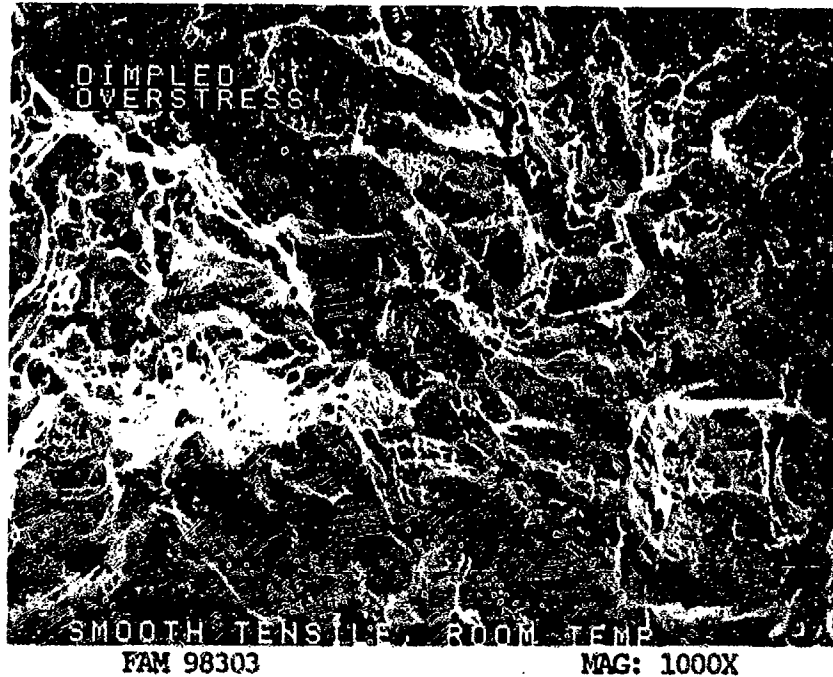


FIGURE 3-5: Dimpled overstress with grain boundary separation. An arrow shows a triple point between three grains.

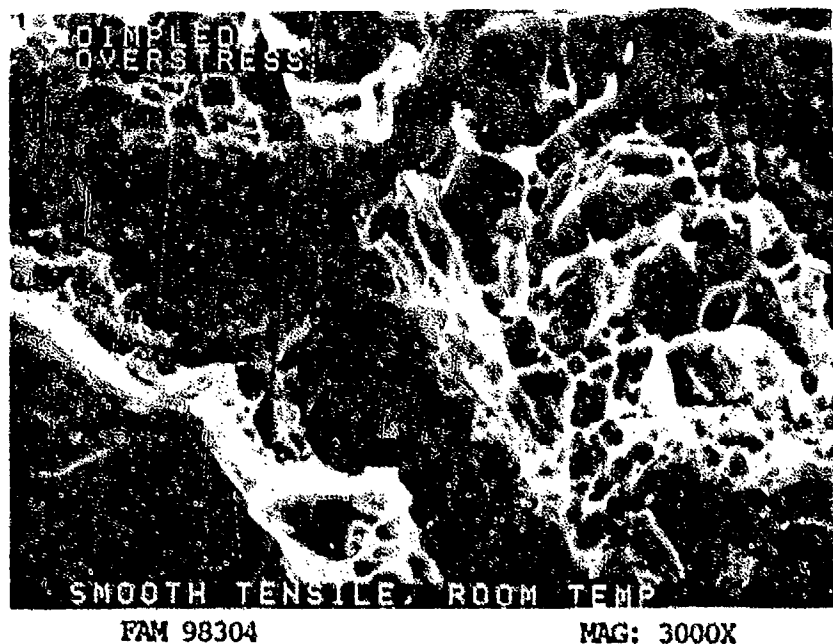


FIGURE 8-6: Grain boundary separation at a triple point. An elongated tubular void is visible near the center of the photograph (arrow).

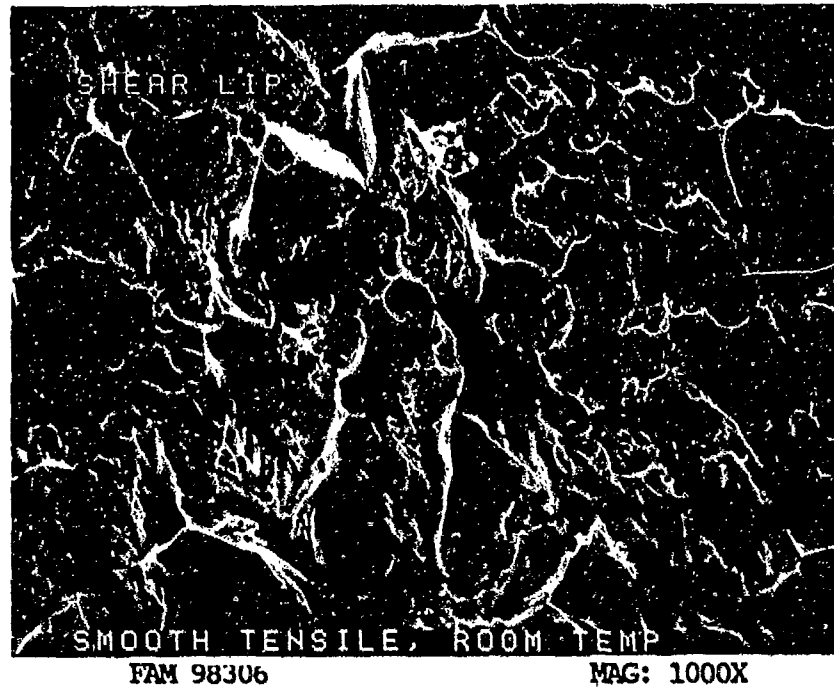


FIGURE 8-7: Shear features in final overstress area. The directions of relative motion are shown by arrows. Areas of smear are separated by patches of fine shear dimples.

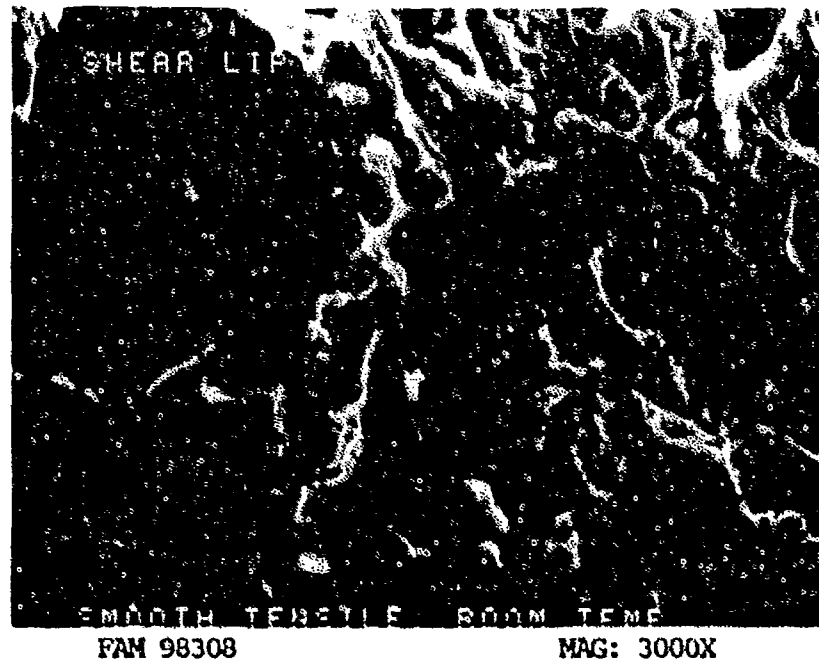


FIGURE 8-8: Shear dimples and other shear features in the final overstress area.

MATERIAL

Inconel 600
AMS 5665 Bar

TEST DATA

TEST TYPE

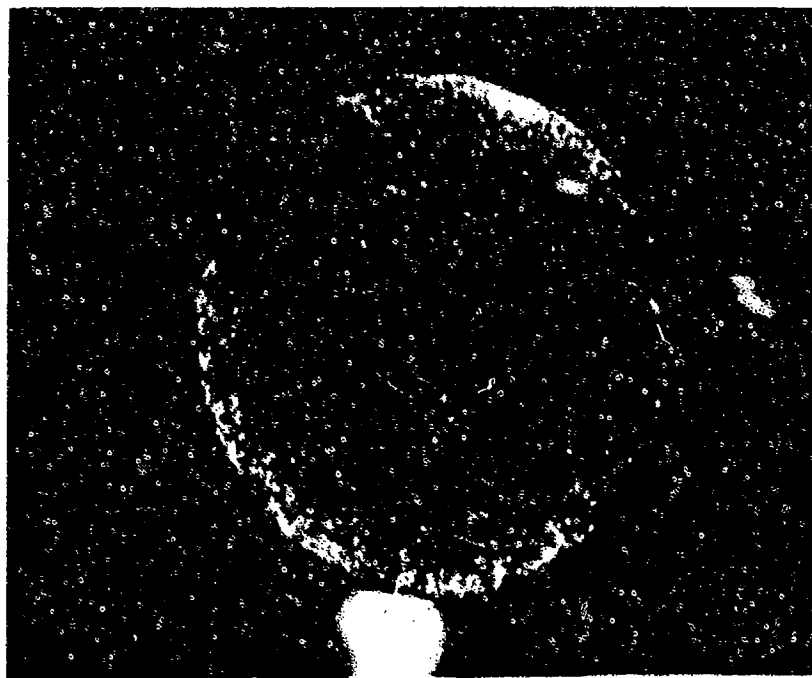
Smooth Tensile

TEST CONDITIONS

Strain Rate: 0.005 mm/mm/min (0.005 in/in/min)
Atmosphere: Air
Temperature: 704°C (1300°F)
Test Direction: Longitudinal

TEST RESULTS

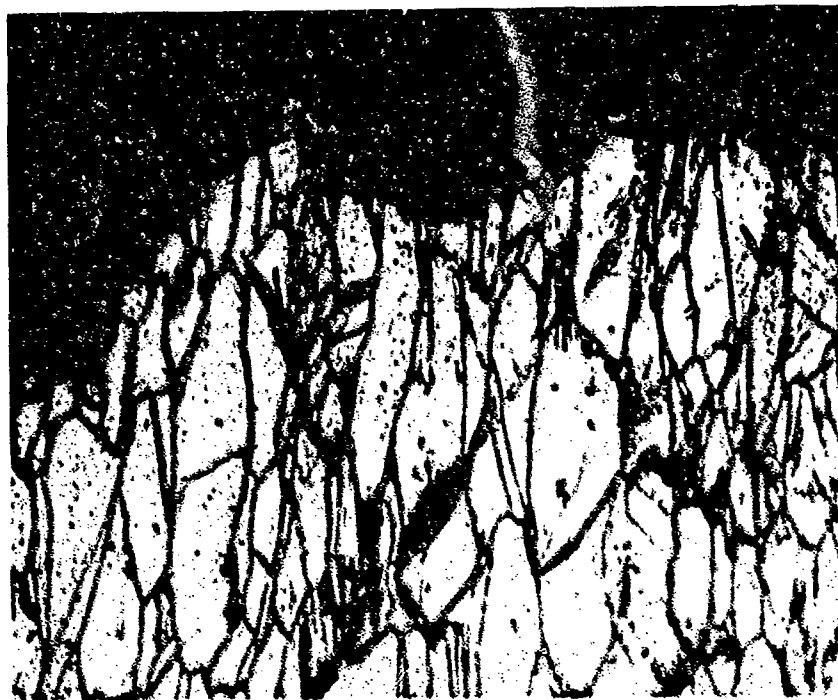
0.2% Yield Strength:	168.2 MPa (24,400 PSI)
Ultimate Strength:	459.9 MPa (66,700 PSI)
Percent Elongation:	49.5
Percent Reduction of Area:	55.3



FAL 92442

MAG: 15X

FIGURE 8-9: Test results and fractography of Inconel 600 704°C (1300°F) smooth tensile test. The fracture surface is generally perpendicular to the stress axis. No shear lip is visible. The percent elongation and reduction of area values are similar to the room temperature specimen values.



FAM 100466

MAG: 200X

FIGURE 8-10: Optical photomicrograph showing grain elongation and secondary cracking adjacent to the fracture.

Etchant: 5% Nital electrolytic

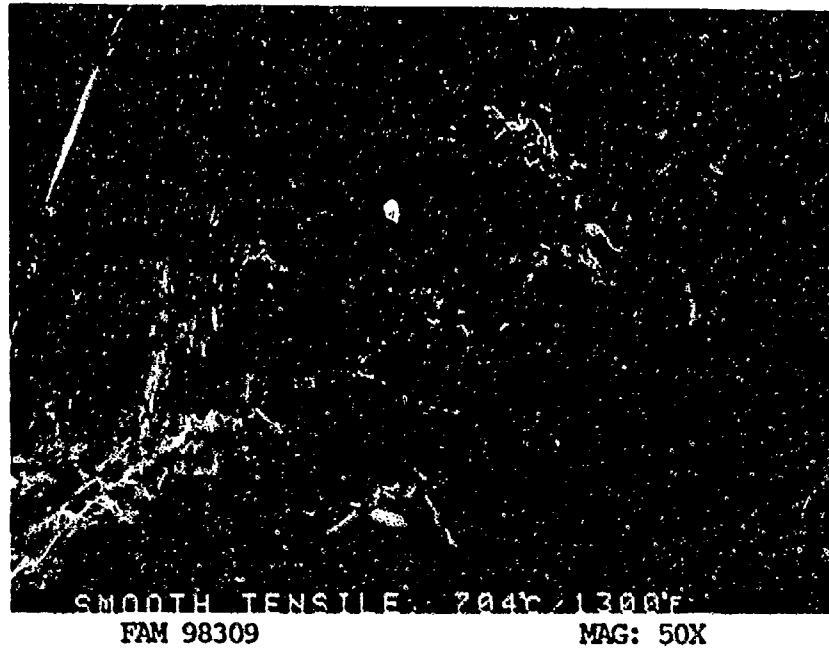


FIGURE 8-11: Dimpled overstress with secondary cracking. No shear lip is visible. Tensile dimples extend all the way to the edge of the specimen.

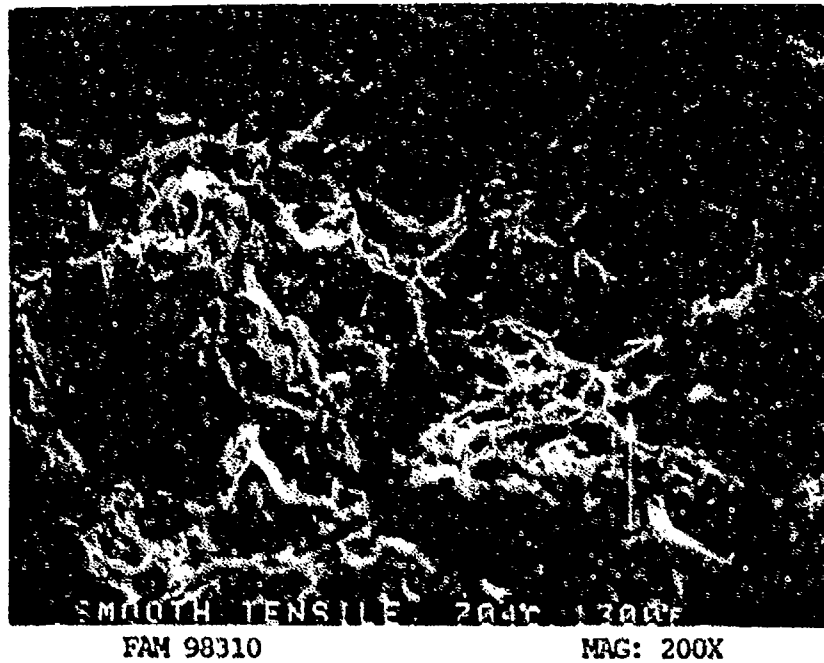


FIGURE 8-12: Dimpled overstress with coarse features. The dimple size varies from large (white arrows) to very small (black arrows).

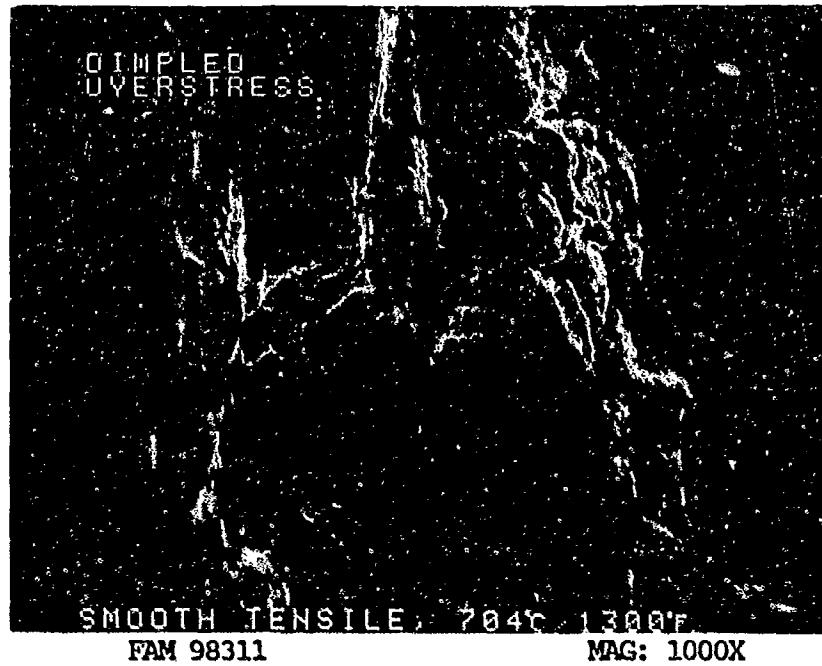


FIGURE 8-13: Mixture of coarse and fine dimpled overstress. A light oxide is now visible on the fracture surface.

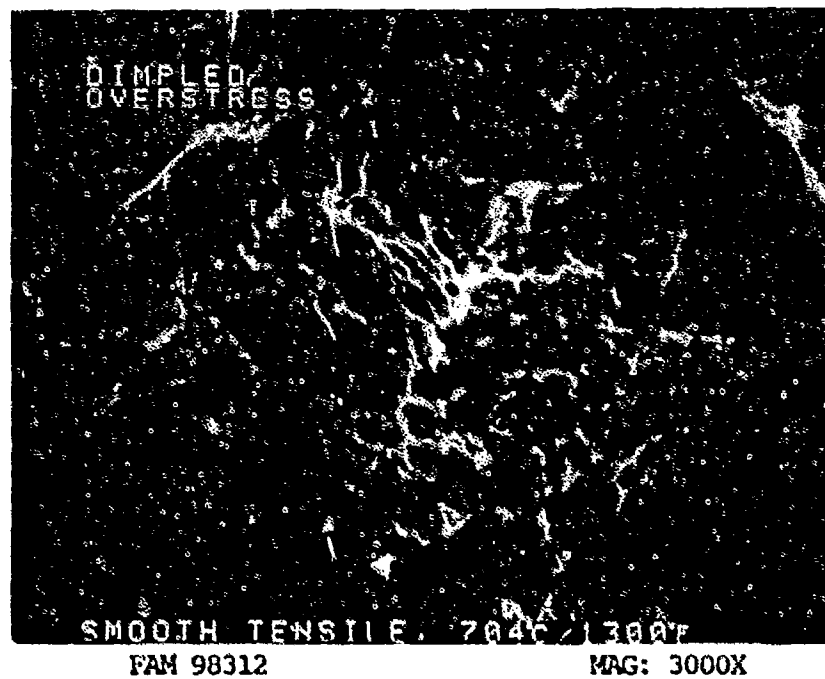


FIGURE 8-14: Fine oxidized dimples on coarse ductile features.

MATERIAL

Inconel 600
AMS 5665 Bar

TEST DATA

TEST TYPE

Notched Tensile

TEST CONDITIONS

Crosshead Speed: 1.27 mm/min (0.05 in/min)

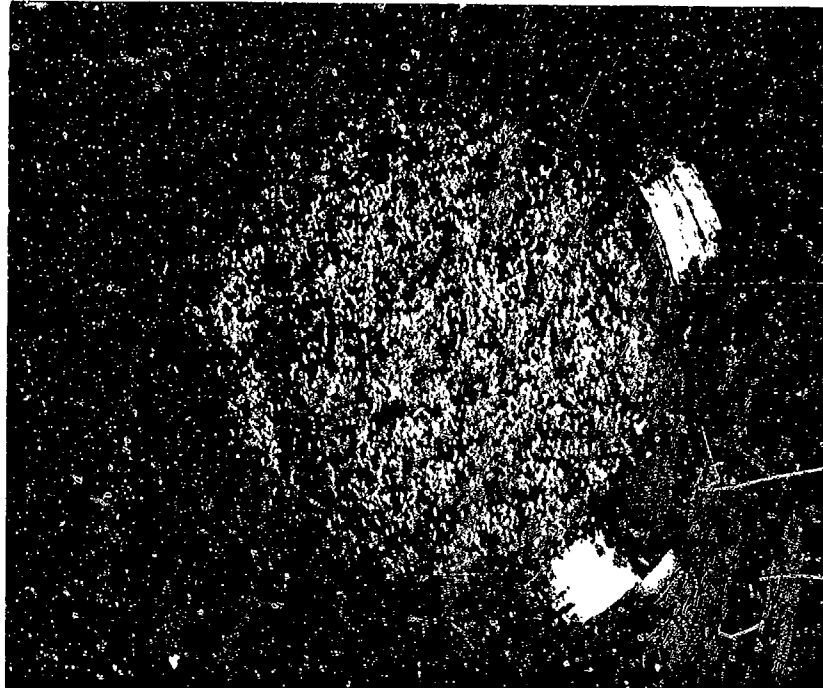
Atmosphere: Air

Temperature: Room Temperature

Test Direction: Longitudinal

TEST RESULTS

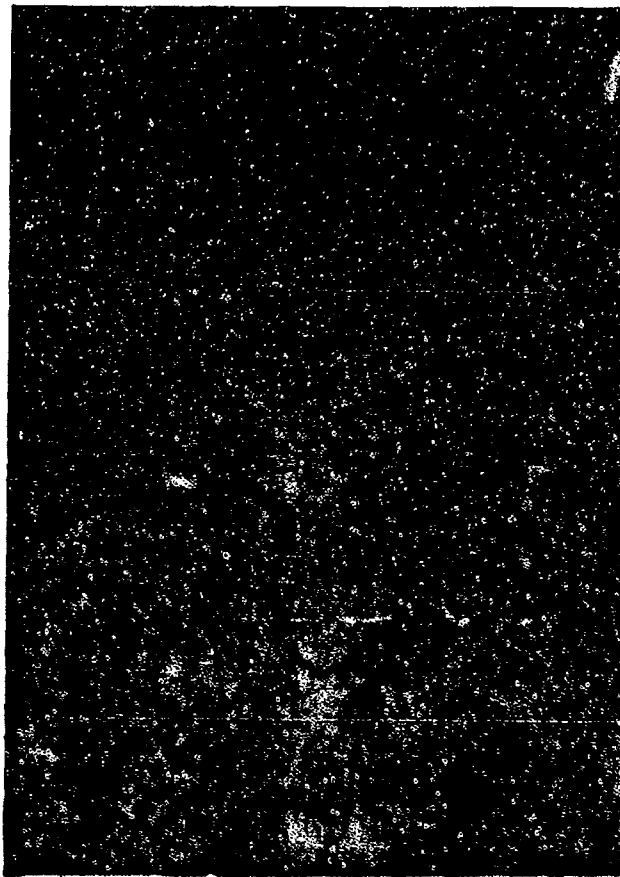
Ultimate Strength: 1332.1 MPa (193,200 PSI)



FAL 92443

MAG: 10X

FIGURE 8-15: Test results and fractography of Inconel 600 room temperature notched tensile test. The entire fracture surface is shiny (free of oxide) and has a granular appearance. No shear lip is visible.



FAM 99851

MAG: 200X

FIGURE 8-16: Optical photomicrograph of a metallographic cross section through the fracture surface. The fracture appears at least partially intergranular.

Etchant: 5% Nital electrolytic

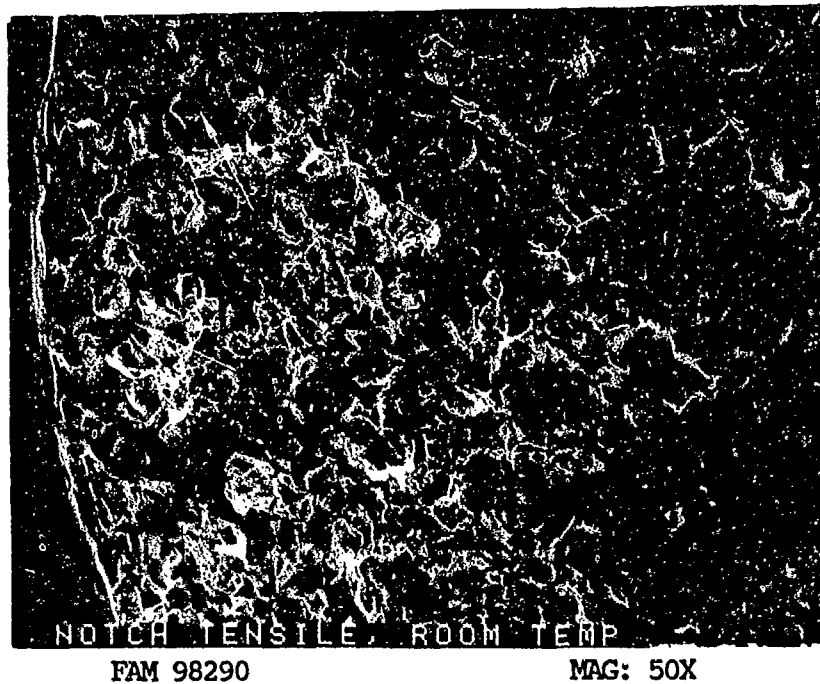


FIGURE 8-17: Low magnification view showing a mixture of intergranular (white arrows) and transgranular (black arrows) overstress features.

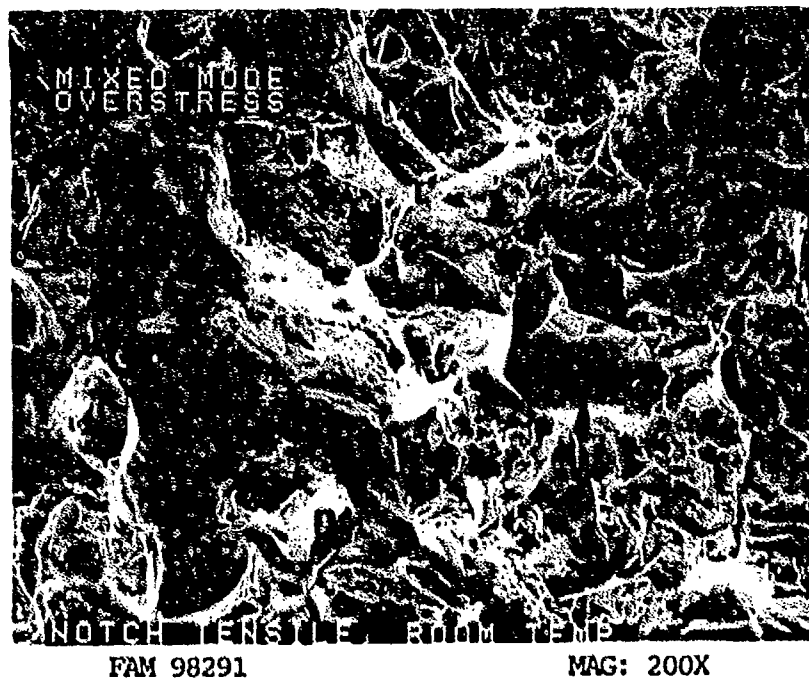


FIGURE 8-18: Mixed mode overstress exhibiting areas of transgranular dimpled overstress (arrow A) cleavage (arrows B) and intergranular overstress (arrow C).

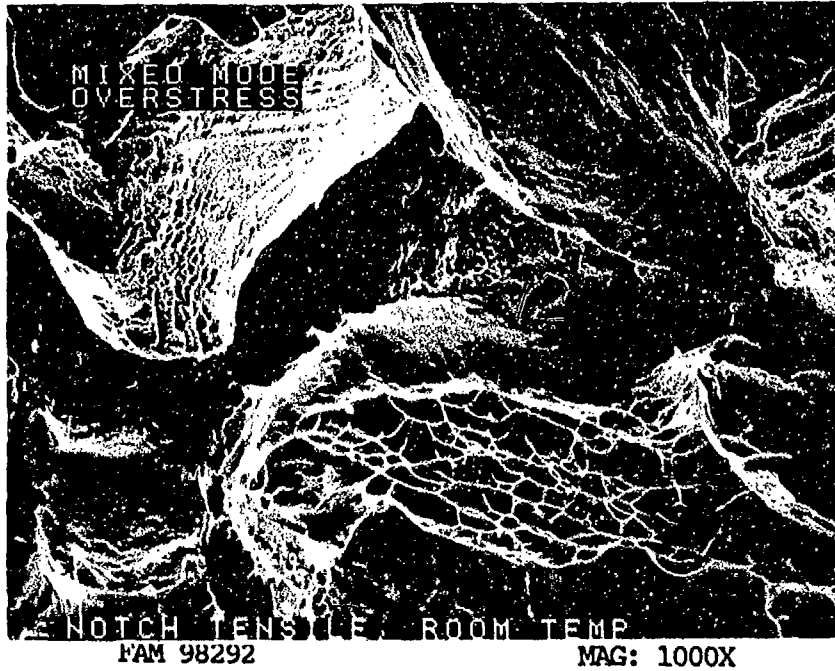


FIGURE 8-19: Mixed mode overstress. Slip lines are visible on several cleavage facets (arrows). These should not be confused with fatigue striations.

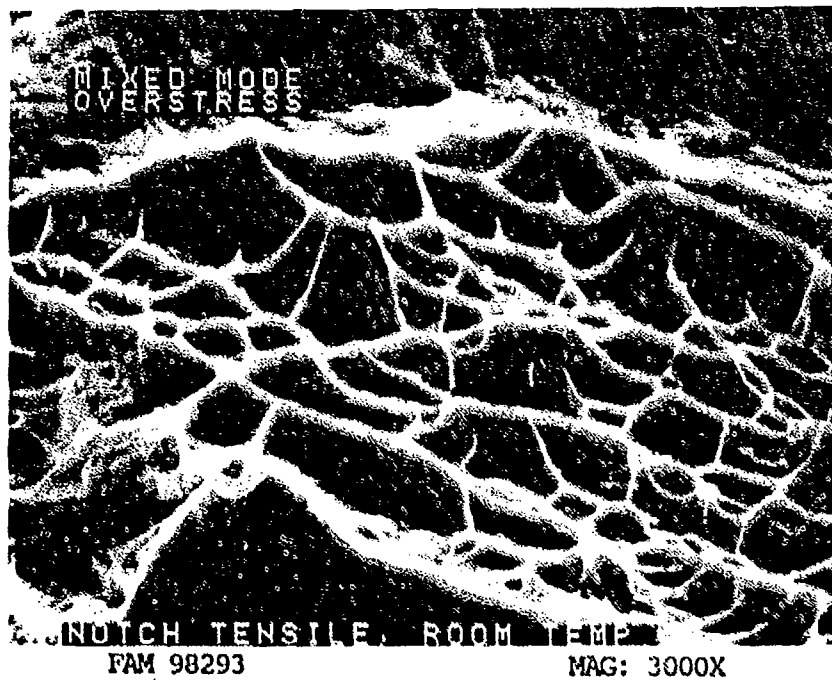


FIGURE 8-20: Shallow equiaxed tensile dimples between intergranular and transgranular cleavage.

MATERIAL

Inconel 600
AMS 5665 Bar

TEST DATA

TEST TYPE

Notched Tensile

TEST CONDITIONS

Crosshead Speed: 1.27 mm/min (0.05 in/min)

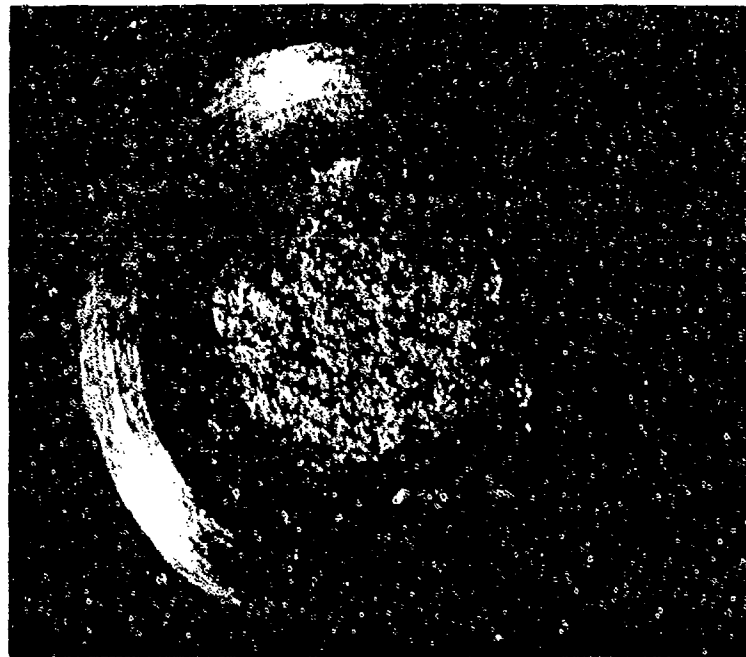
Atmosphere: Air

Temperature: 704°C (1300°F)

Test Direction: Longitudinal

TEST RESULTS

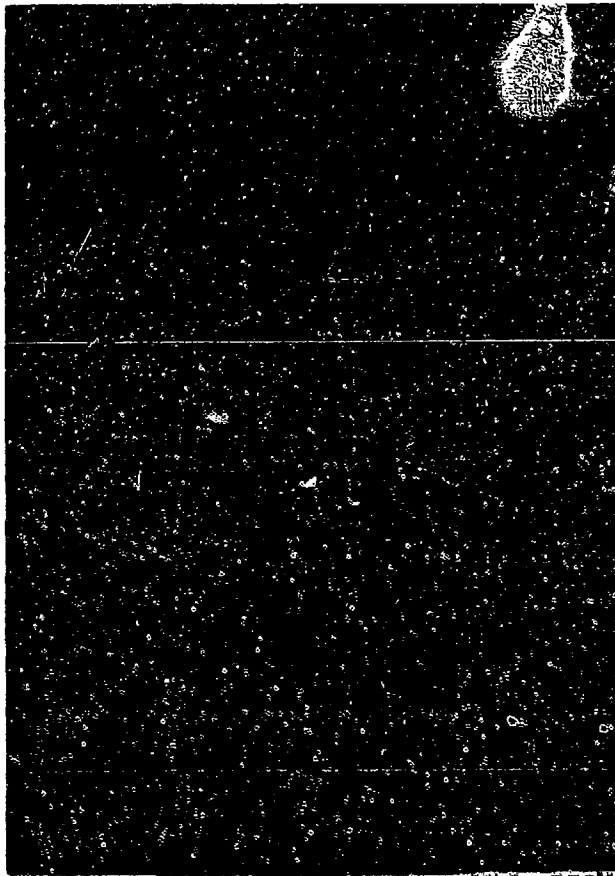
Ultimate Strength: 621.9 MPa (90,200 PSI)



FAL 92444

MAG: 10X

FIGURE 8-21: Test results and fractography of Inconel 600 704°C (1300°F) notched tensile test. The fracture exhibits oxidation and deeper features than the room temperature specimen (Figure 8-15). The center of the specimen is relatively flat compared to the edges.



FAM 99896

MAG: 200X

FIGURE 8-22: Optical photomicrograph taken near the center of the specimen. The grain structure is equiaxed exhibiting no visible plastic deformation. Compare this structure with the smooth specimens (Figures 8-2 and 8-10).

Etchant: 5% Nital electrolytic

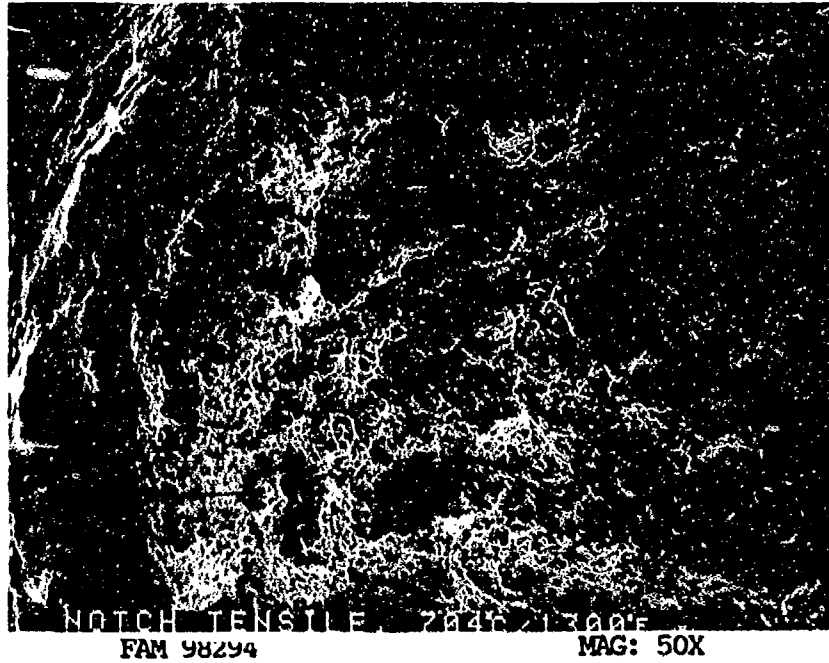


FIGURE 8-23: Low magnification view showing deep features near the edge (arrows). The center of the specimen is relatively flat (dimpled overstress).

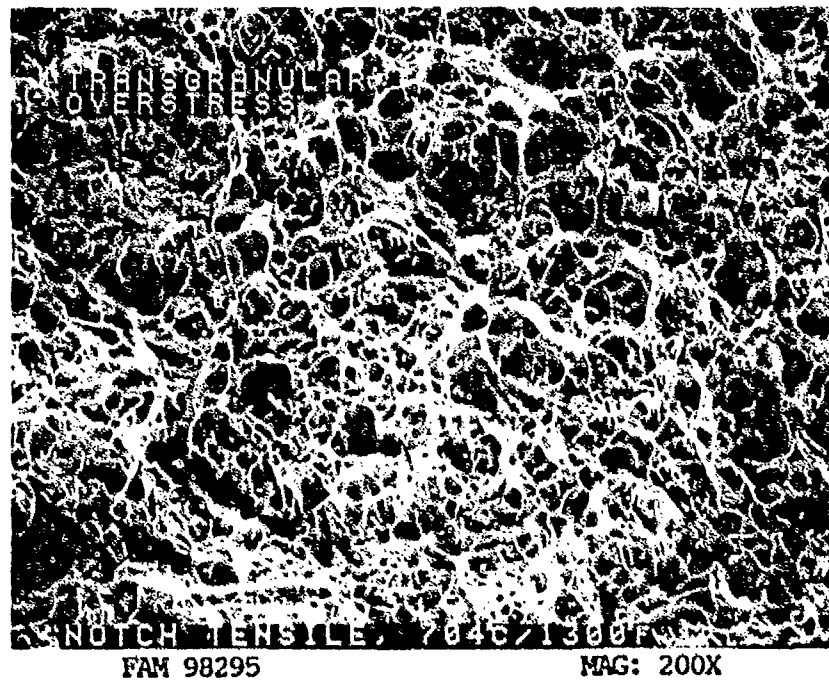


FIGURE 8-24: Primarily transgranular dimpled overstress with some void coalescence (arrows) in the center of the specimen. These voids are visible in the metallographic cross section (Figure 8-22).

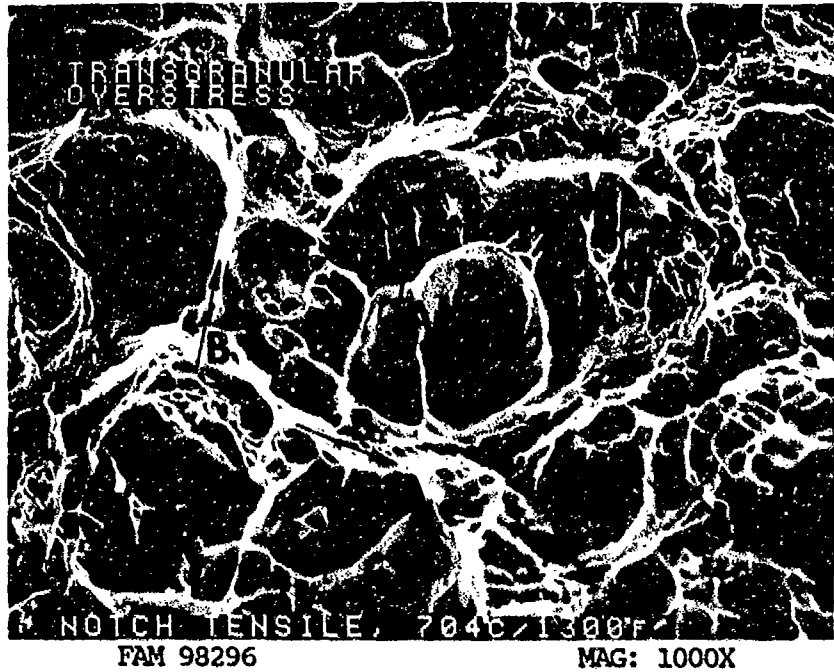


FIGURE 8-25: Transgranular cleavage overstress with some fine dimples. Slip lines are visible on some of the cleavage facets (arrows A). Tear ridges separate the areas of cleavage (arrows B).

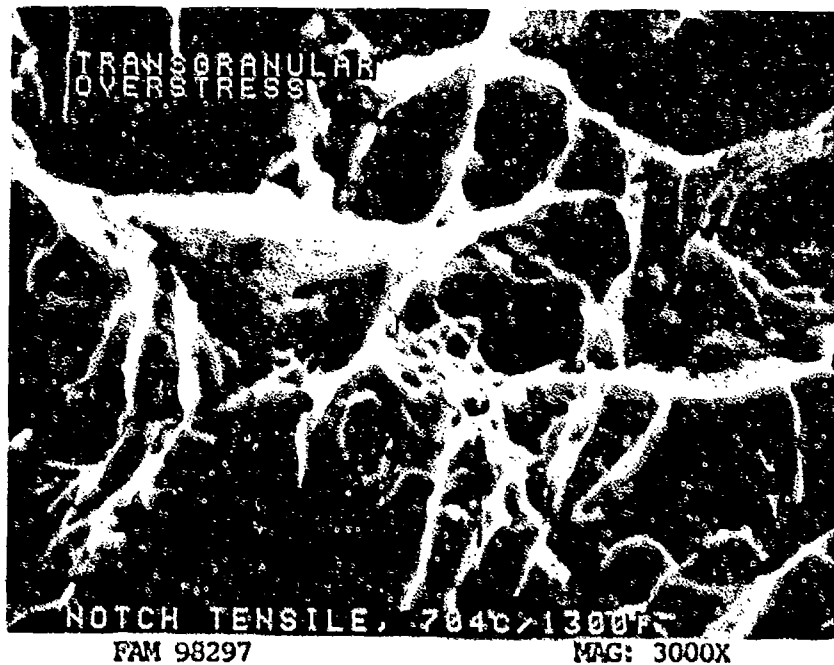


FIGURE 8-26: Transgranular cleavage facets with a few fine dimples in between (arrow).

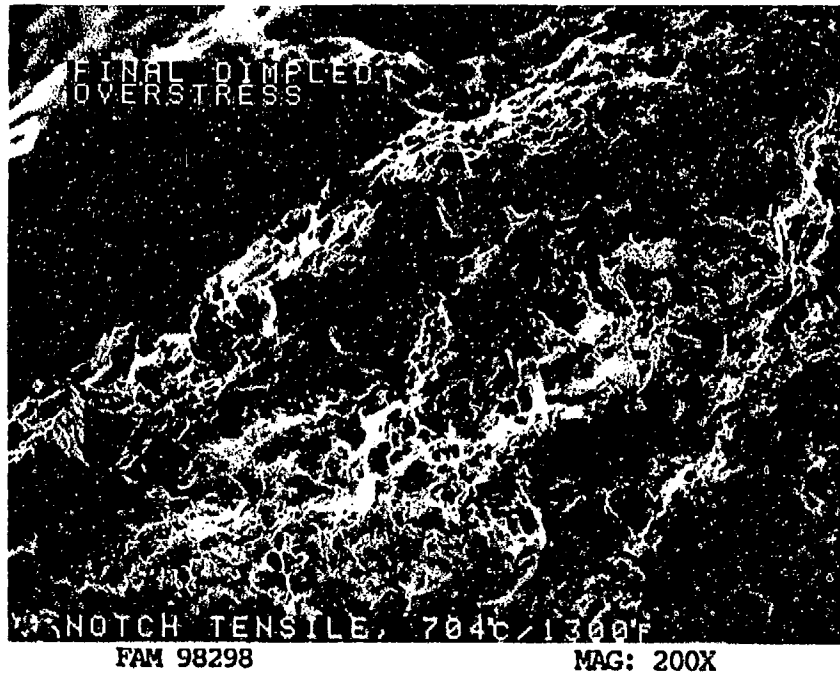


FIGURE 8-27: Mixture of dimpled overstress and fine cleavage in the final overstress area.

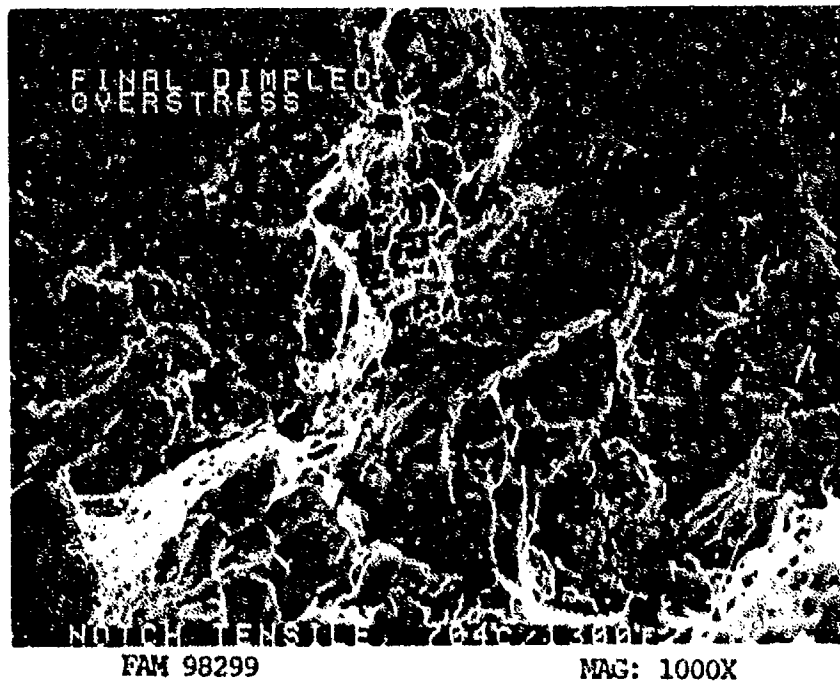


FIGURE 8-28: Higher magnification photograph of the area shown in Figure 8-27 showing fine randomly shaped dimples and fine cleavage (arrow). A light oxide is visible.

MATERIAL

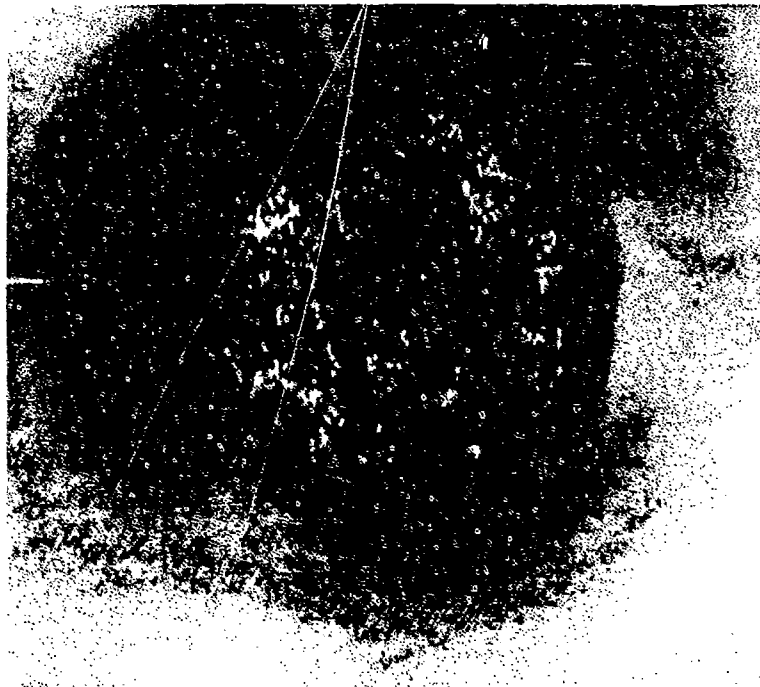
Inconel 600
AMS 5665 Bar

TEST DATA

TEST TYPE
Stress Rupture

TEST CONDITIONS
Stress: 103.4 MPa (15.0 ksi)
Atmosphere: Air
Temperature: 704°C (1300°F)
Test Direction: Longitudinal

TEST RESULTS
Time to Rupture: 407.5 hours
Percent Elongation: 48.4
Percent Reduction of Area: 74.0



FAL 92385

MAG: 15X

Figure 8-29: Test results and fractography of Inconel 600 stress rupture test. The fracture appears heavily oxidized and is oriented at an angle to the stress axis.



FAM 99841

MAG: 200X

FIGURE 8-30: Optical photomicrograph taken near the center of the specimen. The grains are larger than in the tensile specimens and, like the smooth tensile specimens, exhibit plastic deformation. In addition, secondary grain boundary separation is visible.

Etchant: 5% Nital electrolytic

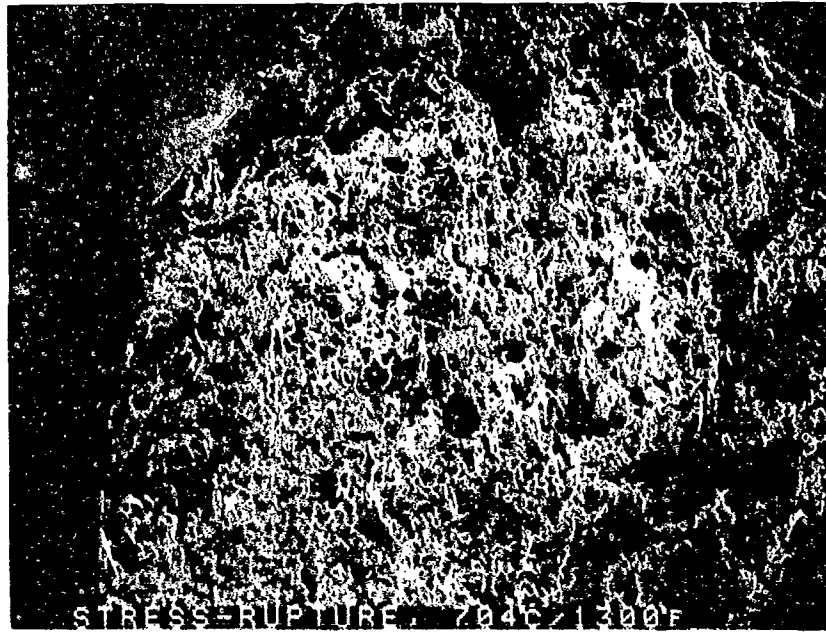


FIGURE 8-31: Low magnification view showing heavily oxidized deep dimples and voids. The oxide charges under the electron beam giving the fracture a bright appearance.

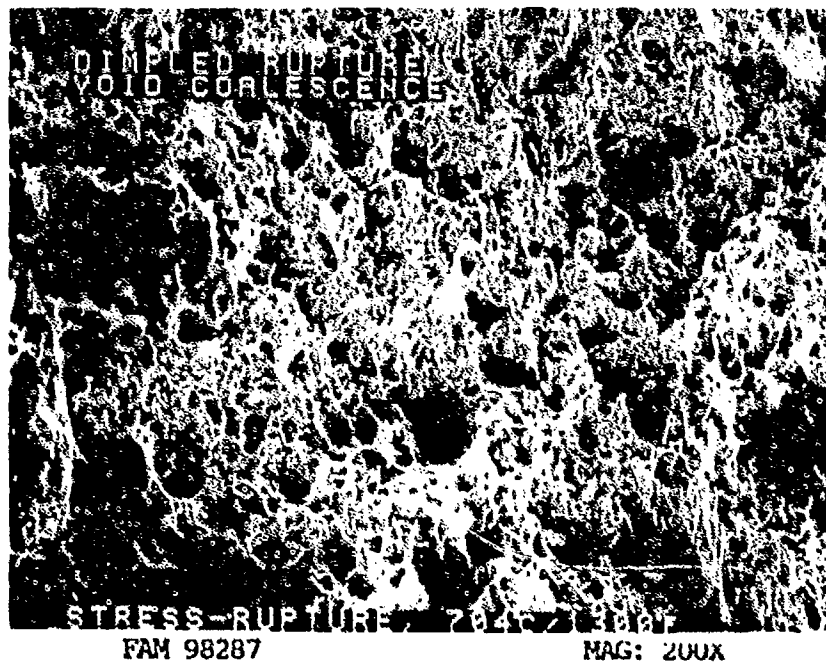


FIGURE 8-32: Dimpled rupture with void coalescence.

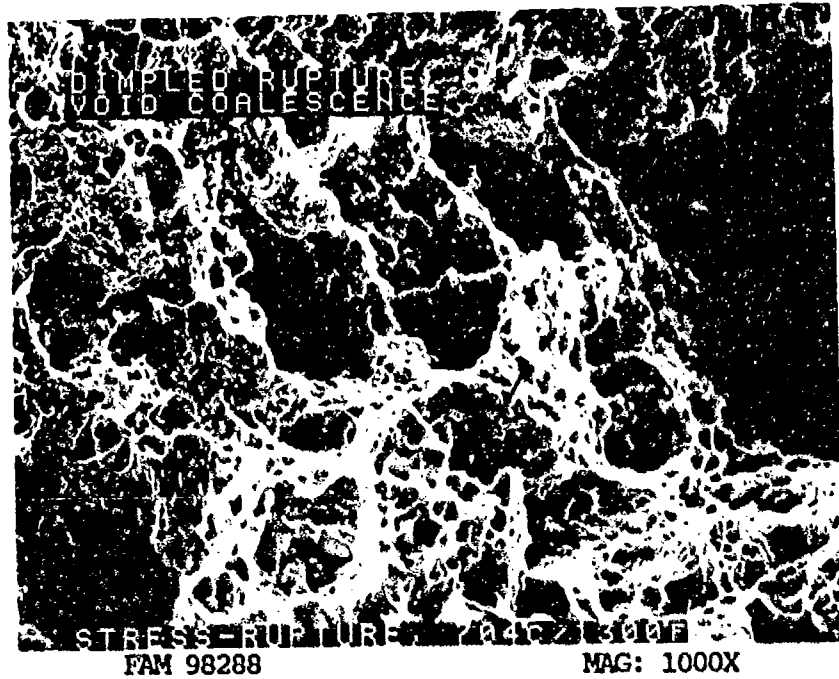


FIGURE 8-33: Oxidized dimpled rupture (black arrow). A void is visible on the right side of the photograph.

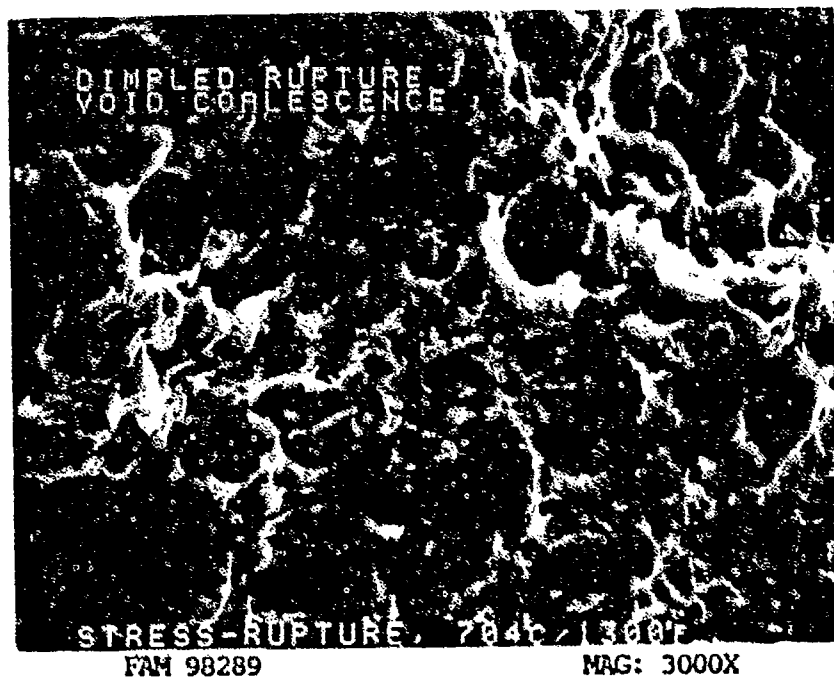


FIGURE 8-34: Oxidized dimpled rupture.

MATERIAL

Inconel 600
AMS 5665 Bar

TEST DATA

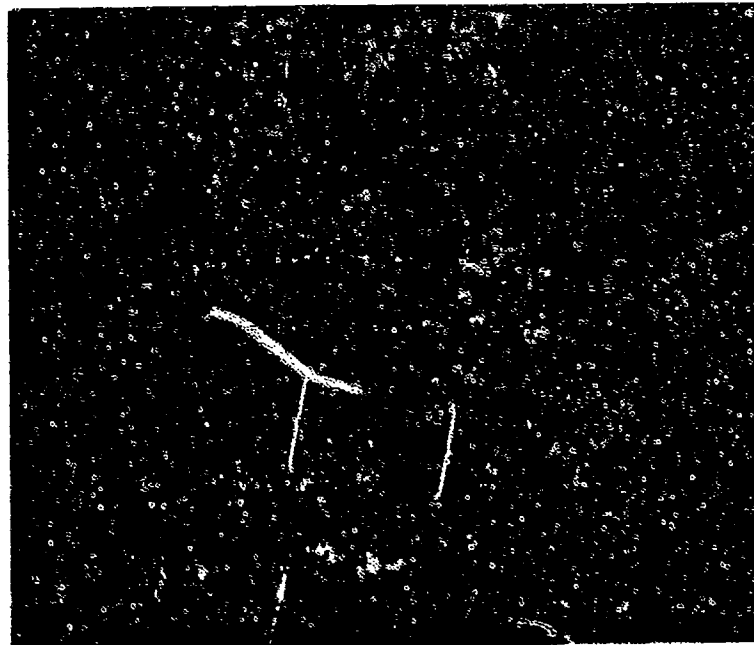
TEST TYPE
Smooth HCF

TEST CONDITIONS

Stress: 344.7 MPa (50.0 ksi)/-344.7 MPa (-50.0 ksi)
Stress Ratio: -1
Frequency: 1800 cpm
Atmosphere: Air
Temperature: Room Temperature
Test Direction: Longitudinal

TEST RESULTS

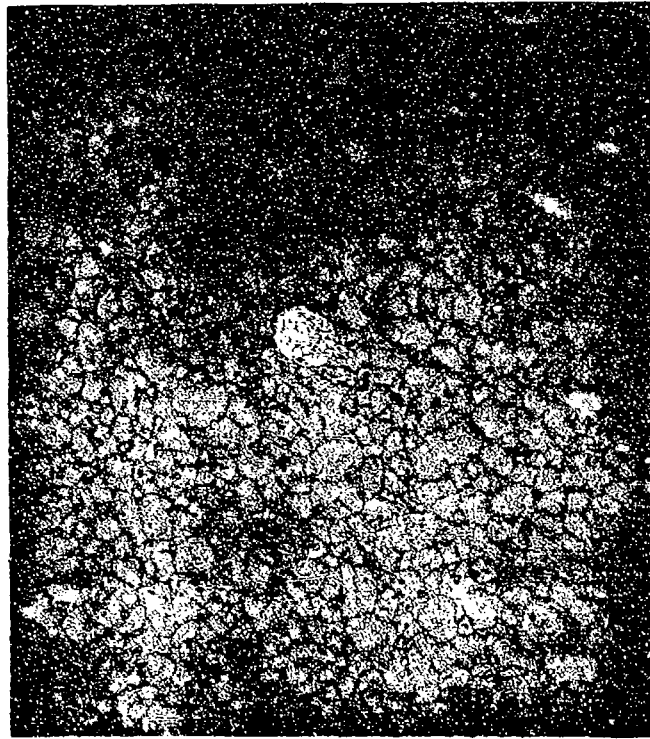
Cycles to Fracture: 343,000



FAL 93956

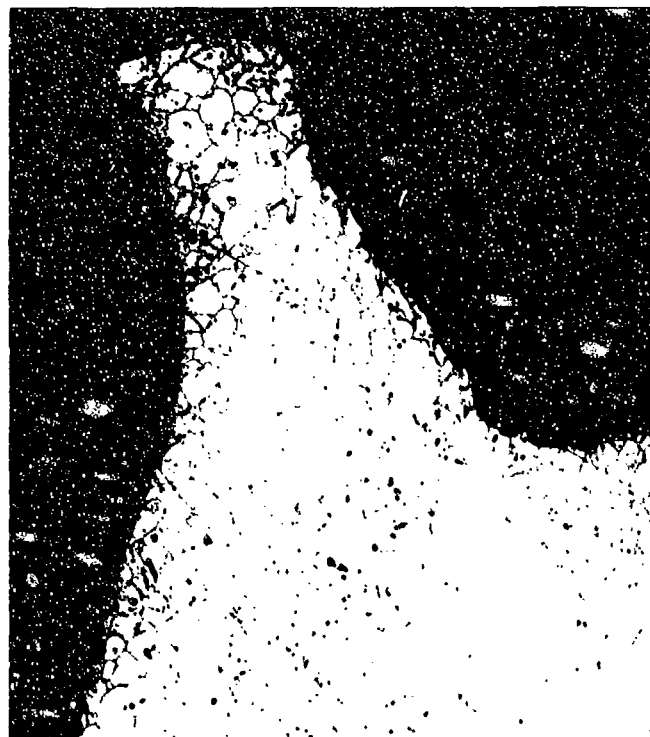
MAG: 15X

FIGURE 8-35: Test results and fractography of Inconel 600 room temperature smooth HCF test. The fracture exhibits fatigue progression over 90 percent of the fracture. Some arrest marks (brackets) are visible near the end of the progression. The final overstress area appears as a small thumbnail (arrow).



FAM 100240

MAG: 100X

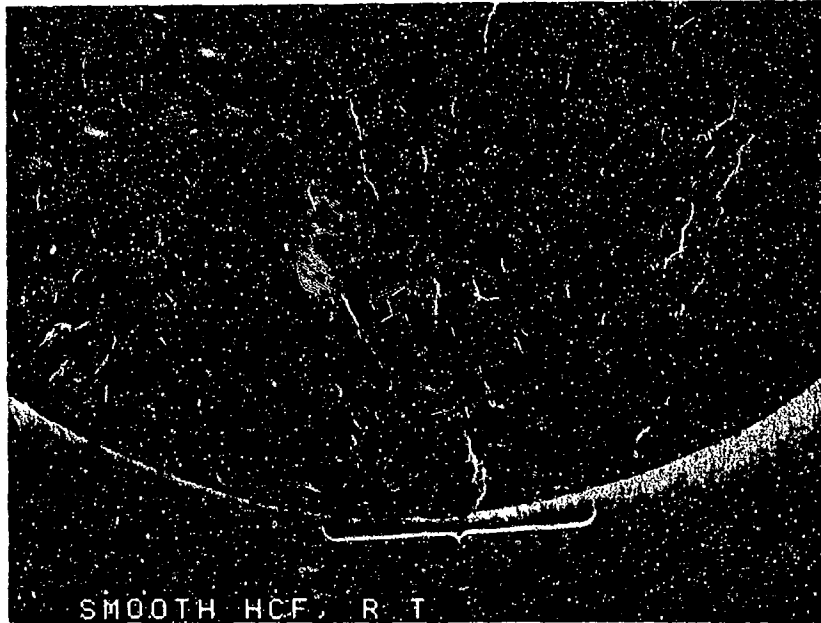


FAM 100241

MAG: 100X

FIGURE 8-36: Optical photomicrographs showing the fatigue progression (top) and final overstress area (bottom). The fatigue progression is transgranular and propagates on a plane perpendicular to the stress axis.

Etchant: 5% Nital electrolytic



SMOOTH HCF, R T

FAM 99297

MAG: 50X

FIGURE 8-37: Overall photograph of the origin area and initial fatigue progression zone. The fracture propagated from a relatively localized origin area but not from a point origin. Features are visible radiating from the area (bracket).



SMOOTH HCF, R T

FAM 99298

MAG: 200X

FIGURE 8-38: Higher magnification photograph of the localized origin area exhibiting feathery cleavage.

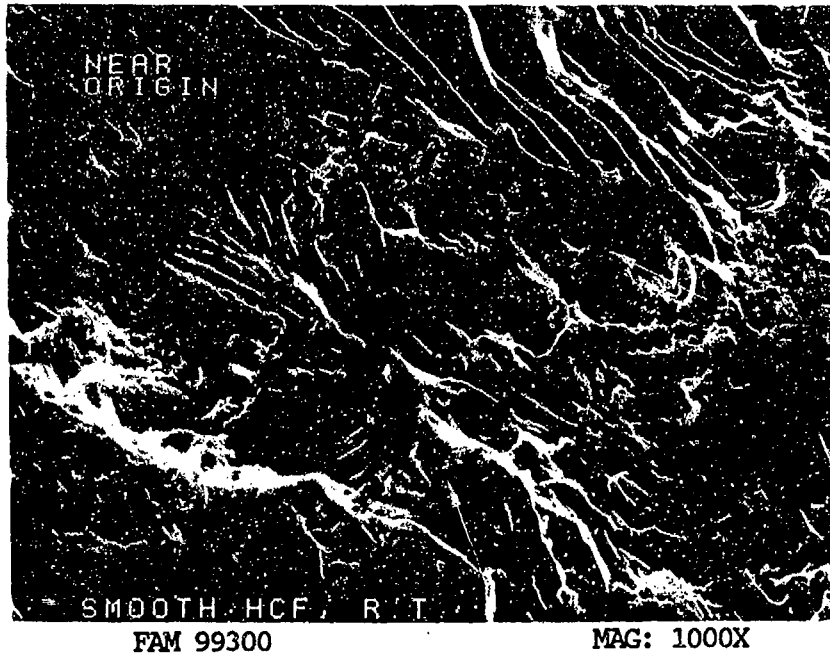


FIGURE 8-39: Fatigue progression near the origin. Fine striations are barely resolvable on fatigue plateaus (arrows).

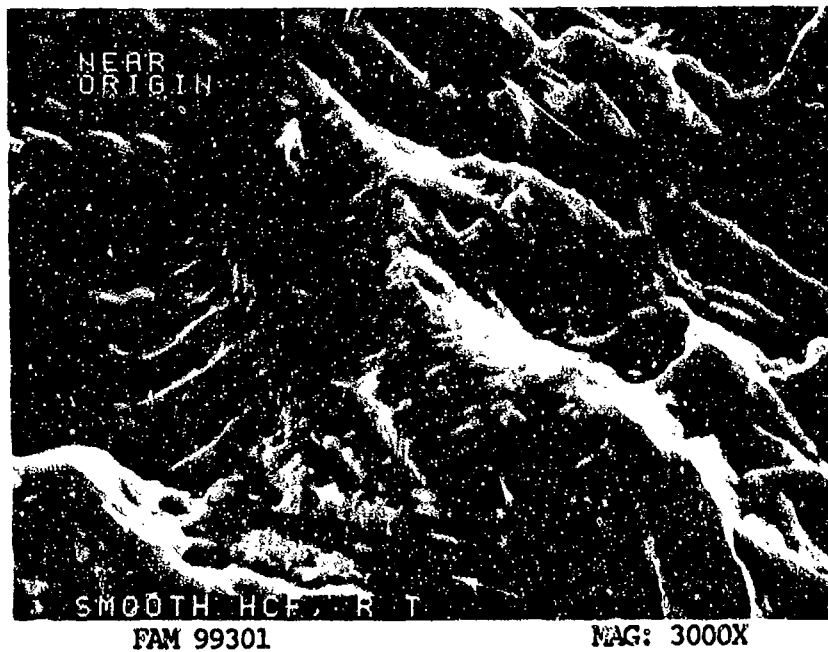


FIGURE 8-40: Higher magnification photograph of the area shown in Figure 8-39. Striations are clearly visible with very fine striations present on adjacent plateaus (arrows). Striations are visible with several orientations, indicating local propagation in several directions.

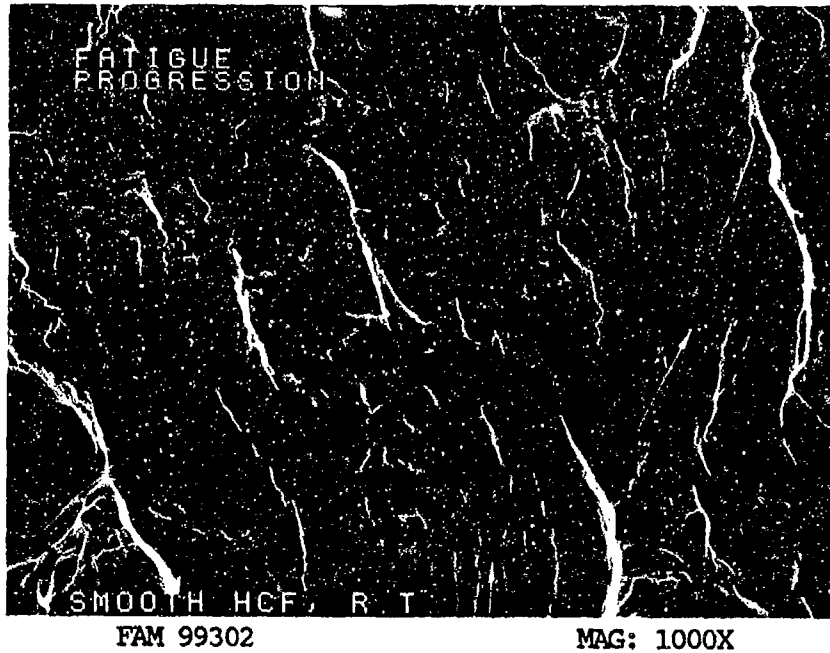


FIGURE 8-41: Fatigue progression zone exhibiting many changes of progression plane (plateaus). Arrows indicate directions of local progression.

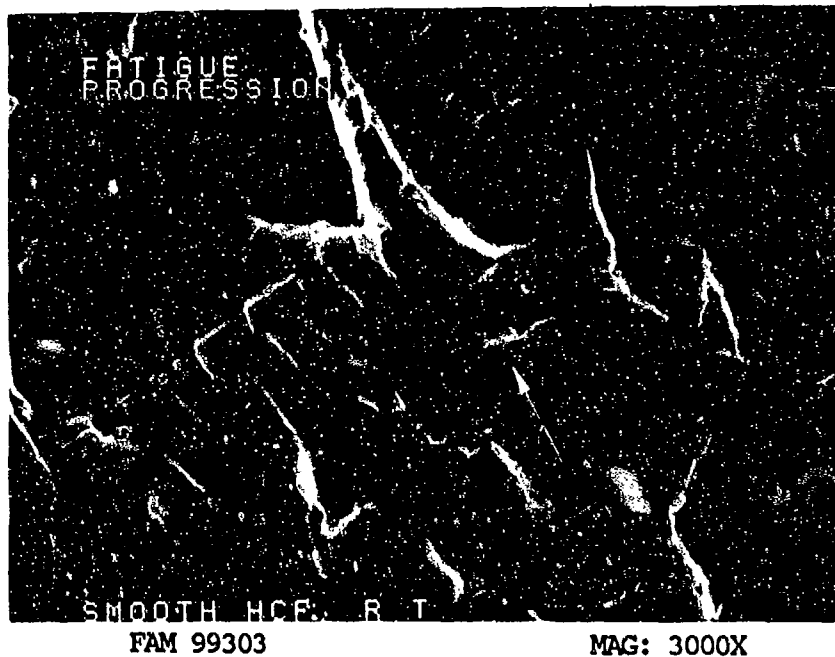


FIGURE 8-42: Mixture of coarser crack-like striations and very fine striations in the fatigue progression zone. The direction of propagation is shown by an arrow.

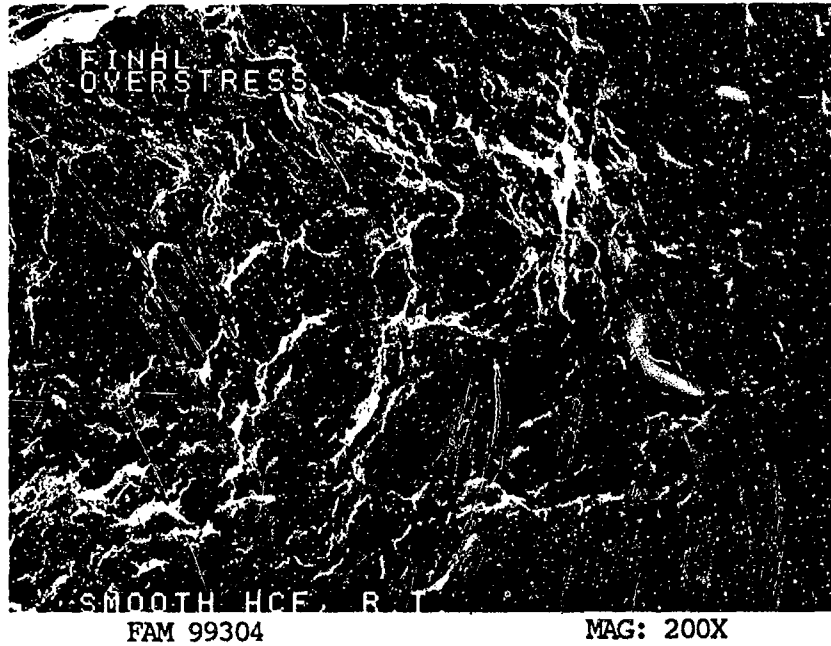


FIGURE 8-43: Final overstress area. No shear lip is present.

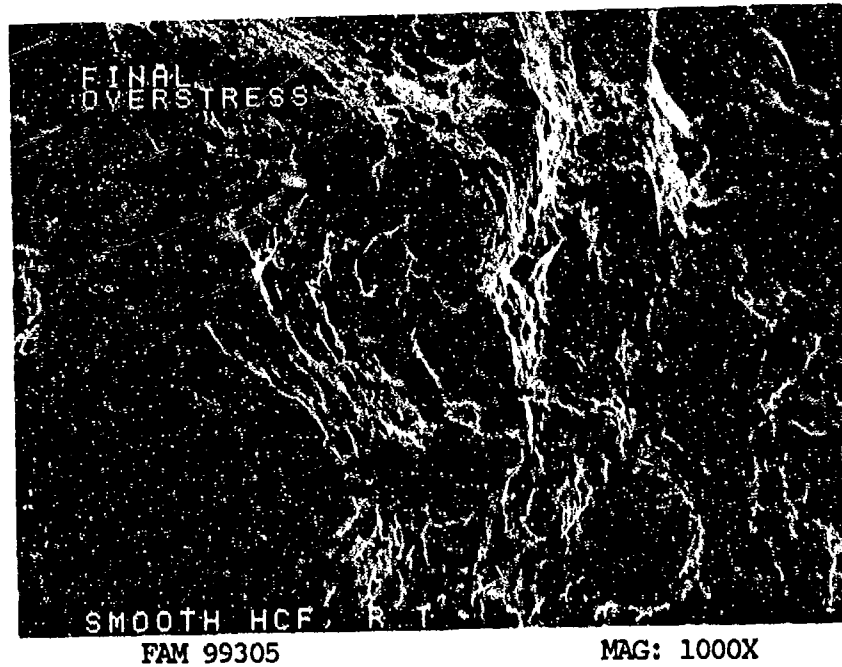


FIGURE 8-44: Dimpled overstress in the final overstress area shown in Figure 8-43. Fine dimples are visible.

MATERIAL

Inconel 600
AMS 5665 Bar

TEST DATA

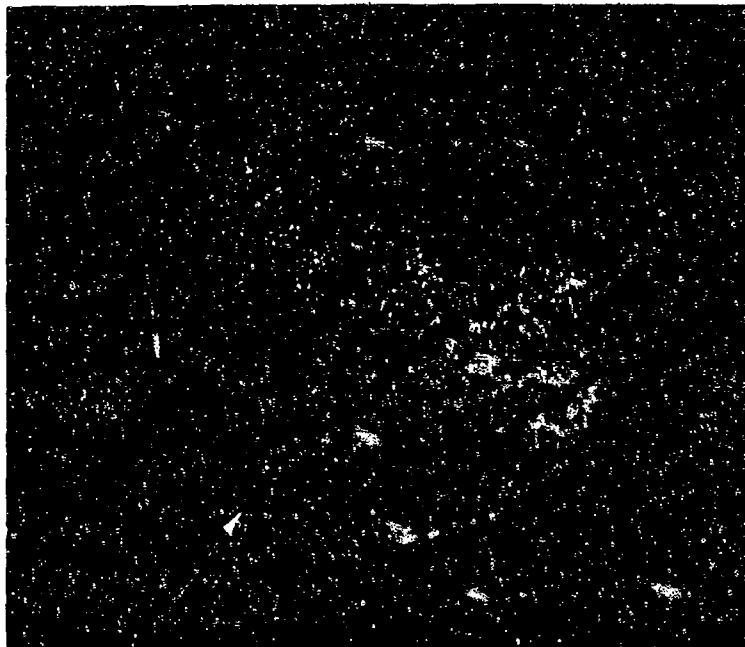
TEST TYPE
Smooth HCF

TEST CONDITIONS

Stress: 344.7 MPa (50.0 ksi)/-344.7 MPa (-50.0 ksi)
Stress Ratio: -1
Frequency: 1800 cpm
Atmosphere: Air
Temperature: 427°C (800°F)
Test Direction: Longitudinal

TEST RESULTS

Cycles to Fracture: 1,300,000



FAL 93955

MAG: 15X

FIGURE 8-45: Test results and fractography of Inconel 600 427°C (800°F) smooth HCF test. The fracture exhibits fatigue progression over 90 percent of the fracture. The fracture surface is not as flat as the room temperature specimen. The final overstress area appears as a small thumbnail (arrow).

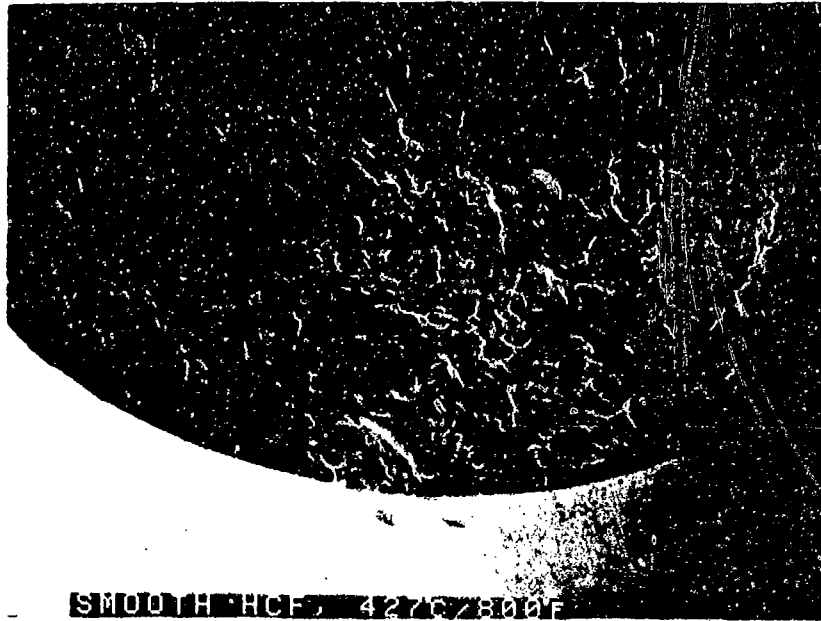


FAM 99850

MAG: 200X

FIGURE 8-46: Optical photomicrograph showing transgranular fracture paths in the origin and initial progression areas. No discernible plastic deformation has occurred.

Etchant: 5% Nital electrolytic



FAM 99315

MAG: 50X

FIGURE 8-47: Overall photograph of the origin area and initial progression zone. The fracture propagated from a relatively localized origin area but not from a point origin, much like the room temperature specimen.



FAM 99316

MAG: 200X

FIGURE 8-48: Higher magnification photograph of the localized origin area. Several stage I fatigue facets are visible at the surface (arrows).

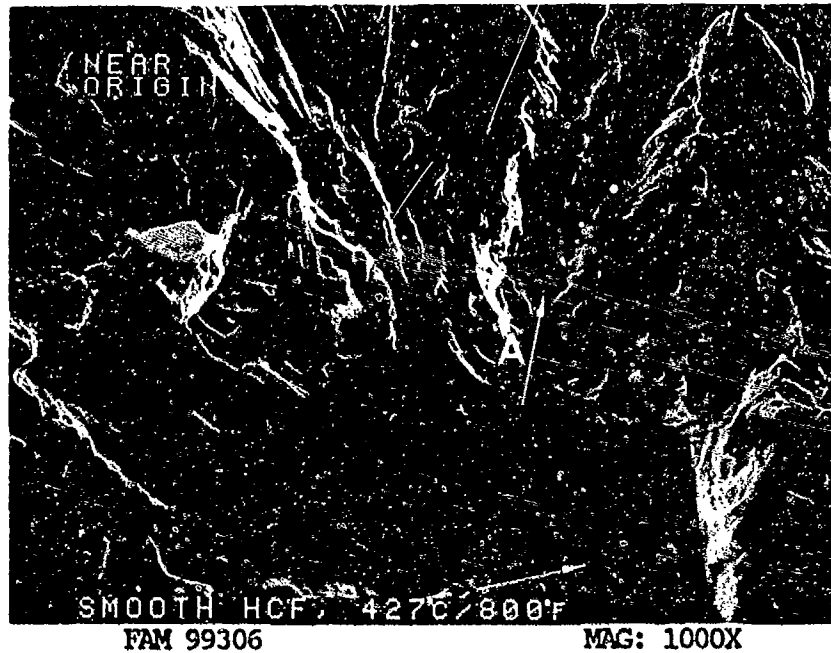


FIGURE 8-49: Fatigue progression near the origin. Fine striations are barely resolvable on fatigue plateaus (arrow A). A stage I fatigue facet is visible at the bottom of the photograph (arrow). No striations are visible on this facet.

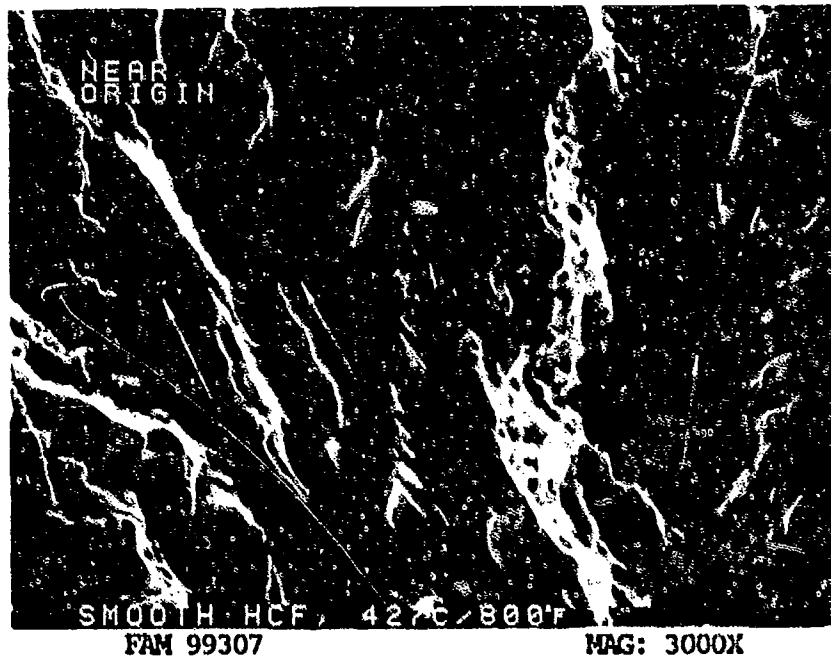


FIGURE 8-50: Higher magnification photograph of the area shown in Figure 8-49. Striations are clearly visible on planes (plateaus) propagating from the stage I facet. The directions of propagation on the various plateaus are shown by arrows.

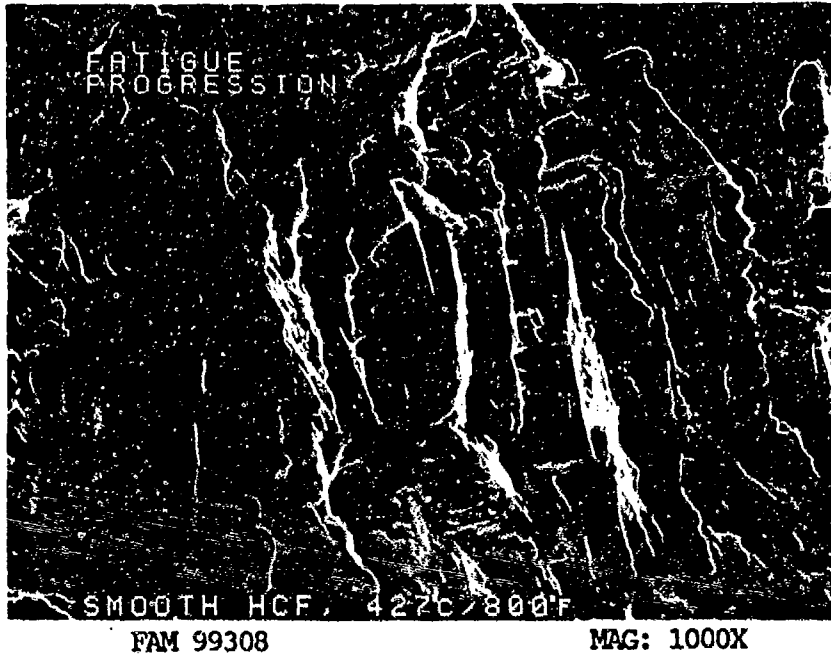


FIGURE 8-51: Fatigue progression zone exhibiting many changes of progression planes (plateaus). Fine striations are not resolvable.

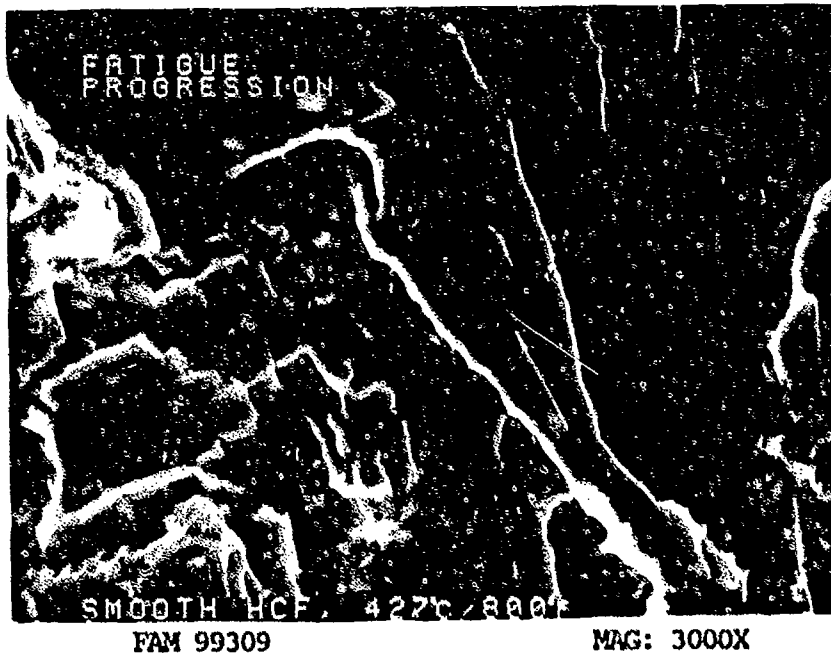


FIGURE 8-52: Fine striations in the fatigue progression zone. The direction of propagation is shown by an arrow.

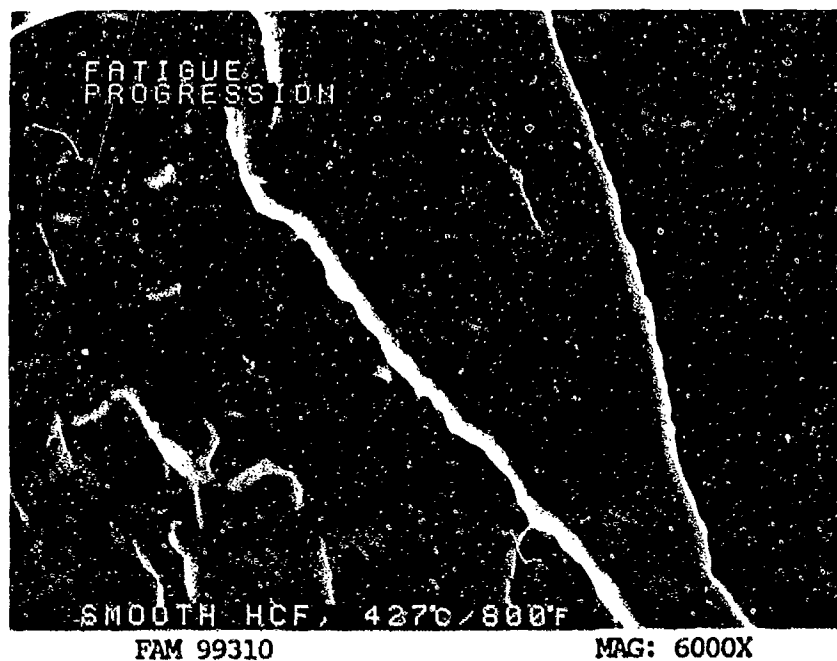


FIGURE 8-53: Higher magnification photograph of the area shown in Figure 8-52. Individual striations are not resolvable.

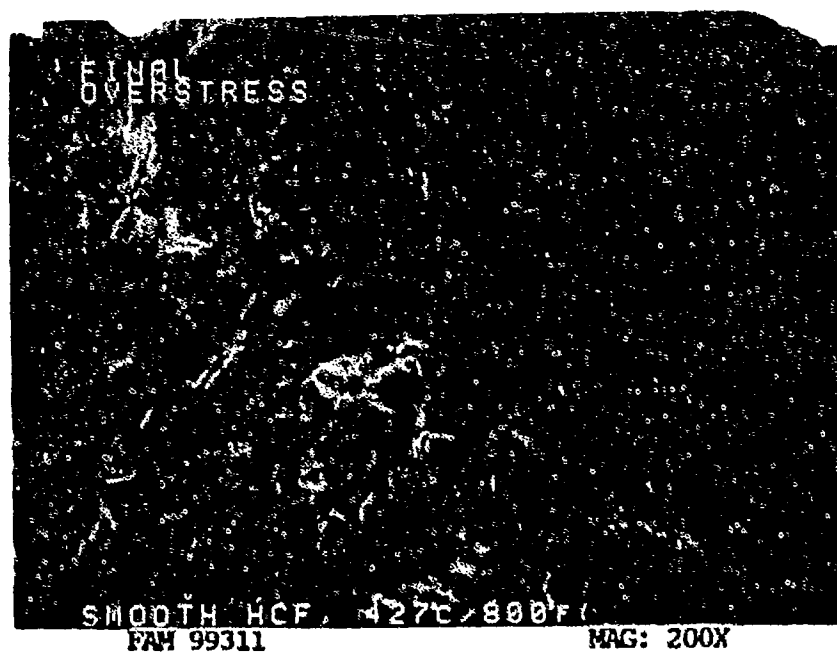


FIGURE 8-54: Final overstress area. No shear lip is present.

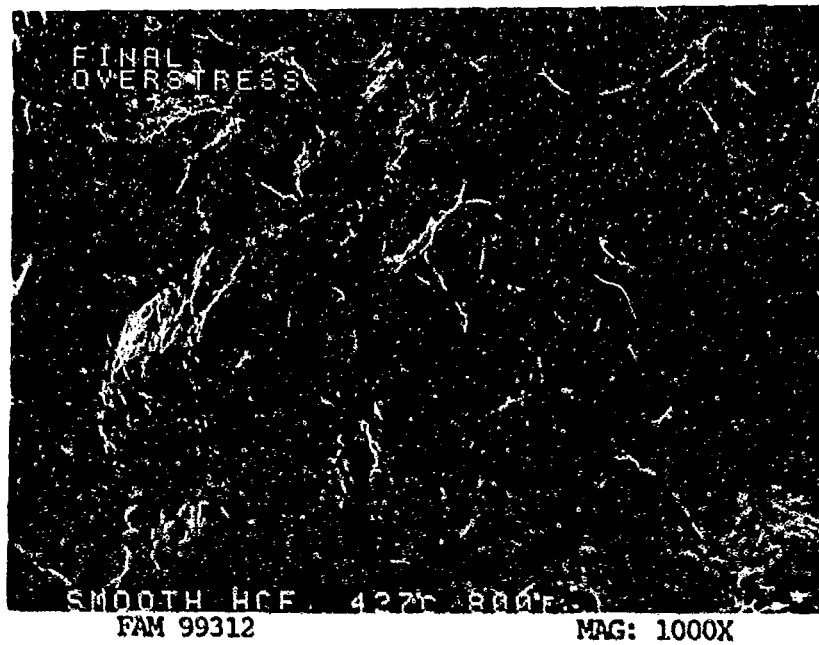


FIGURE 8-55: Mixture of dimpled overstress and cleavage in the final overstress area shown in Figure 8-54. Fine dimples are visible.

MATERIAL

Inconel 600
AMS 5665 Bar

TEST DATA

TEST TYPE
Smooth HCF

TEST CONDITIONS

Stress: 206.8 MPa (30.0 ksi)/-206.8 MPa (-30.0 ksi) DNF*
275.8 MPa (40.0 ksi)/-275.8 MPa (-40.0 ksi)
Stress Ratio: -1
Frequency: 1800 cpm
Atmosphere: Air
Temperature: 704°C (1300°F)
Test Direction: Longitudinal

TEST RESULTS

Cycles to Fracture: 1,900,000 (DNF), 30,500

* Did Not Fracture

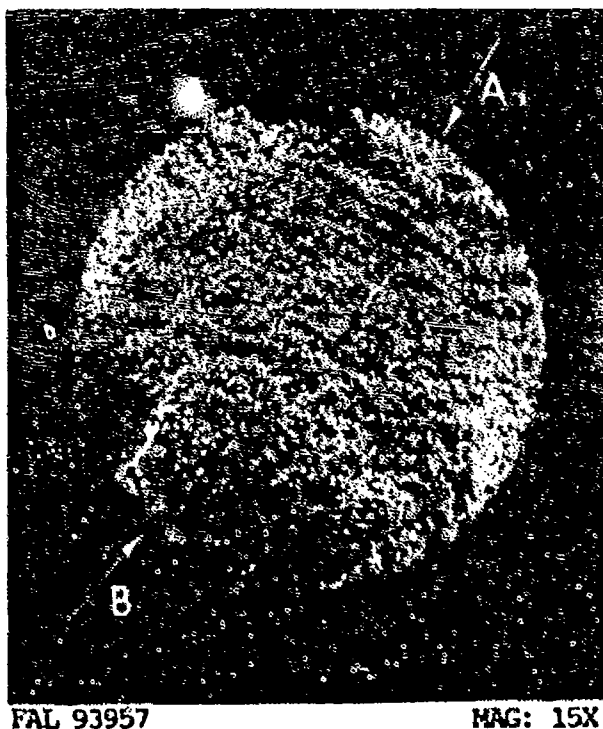
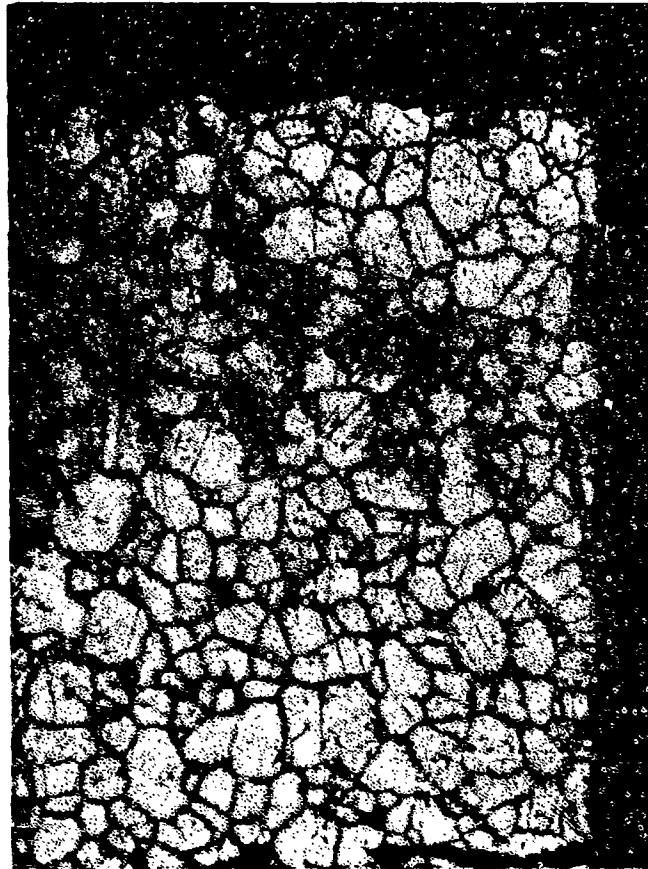


FIGURE 8-56: Test results and fractography of Inconel 600 704°C (1300°F) smooth HCF test. The specimen exhibits fatigue progression over 90 percent of the fracture. Arrest marks are clearly visible over the final third of the progression. The origin is shown by arrow B. The final overstress area appears as a small thumbnail (arrow A).



FAM 99848

MAG: 200X

FIGURE 8-57: Optical photomicrograph showing the origin and initial fatigue progression areas. The fracture propagated transgranularly. Numerous secondary cracks are visible adjacent to the primary fracture (arrows).

Etchant: 5% Nital electrolytic

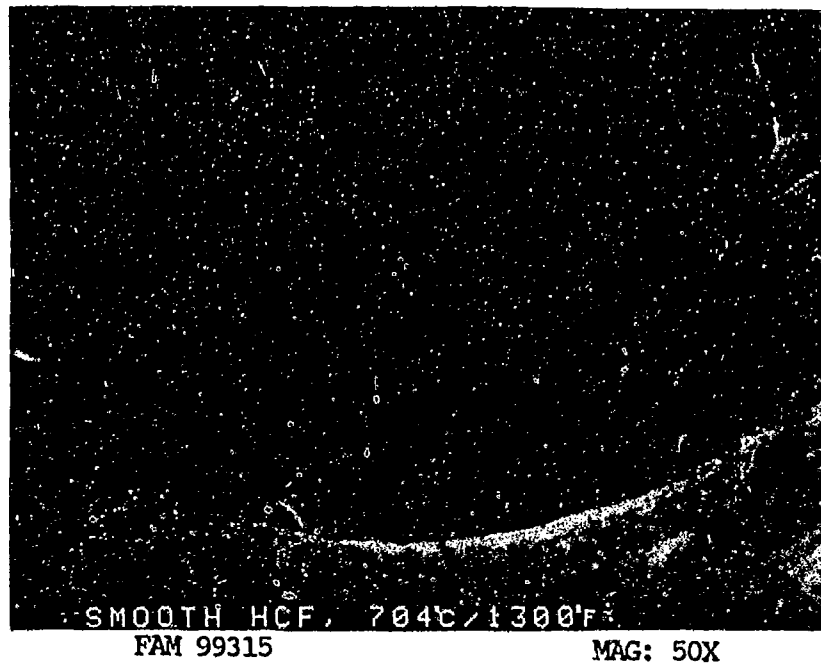


FIGURE 8-58: Overall photograph of the origin area and initial progression zone. The fracture propagated from a point origin (arrow). Features can be seen radiating from the origin.

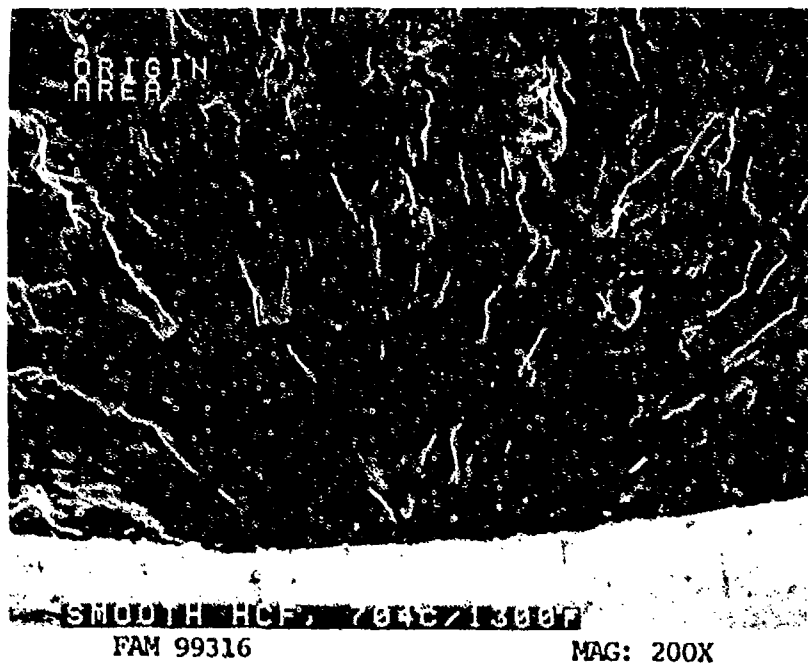


FIGURE 8-59: Higher magnification photograph of the localized origin area. The fracture appears relatively flat near the origin. Compare the appearance of this single origin with the diffuse origins on the room temperature and 800°F specimens (Figures 8-37 and 8-47).

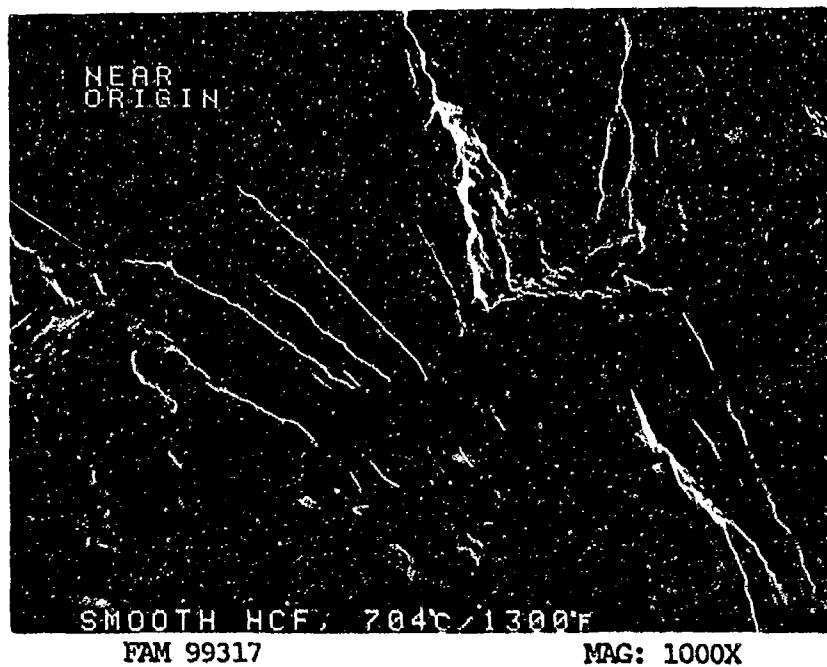


FIGURE 8-60: Fatigue progression near the origin. Fine striations are barely resolvable on fatigue plateaus separated by steps (arrow).

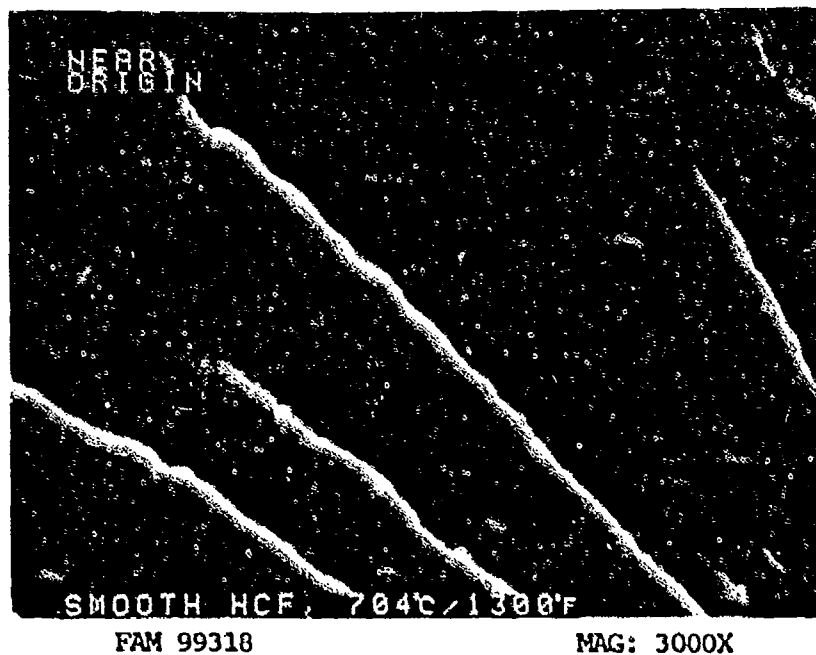


FIGURE 8-61: Higher magnification photograph of the area shown in Figure 8-60. Striations are clearly visible although not individually resolvable. The direction of propagation is shown by an arrow.

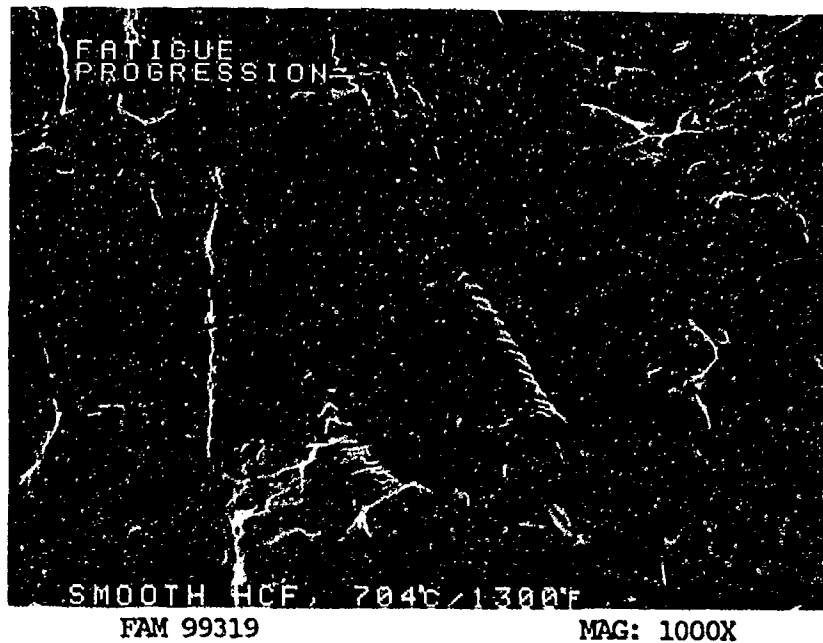


FIGURE 8-62: Fatigue progression zone exhibiting coarser oxidized fatigue striations.

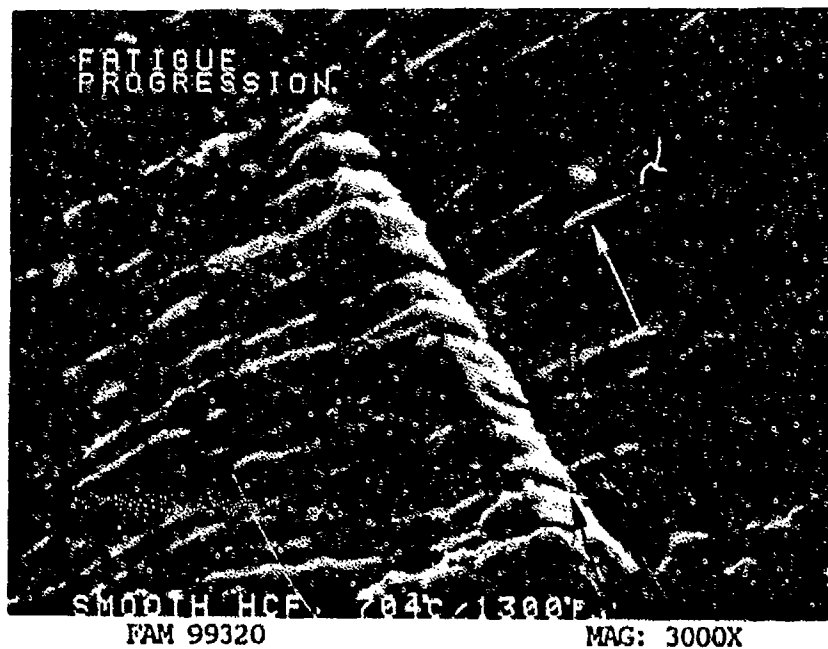


FIGURE 8-63: Higher magnification view of the area shown in Figure 8-62 showing coarser oxidized striations. The direction of propagation is shown by a white arrow. Note that striations progress over a step (black arrow) joining active fatigue progression planes.

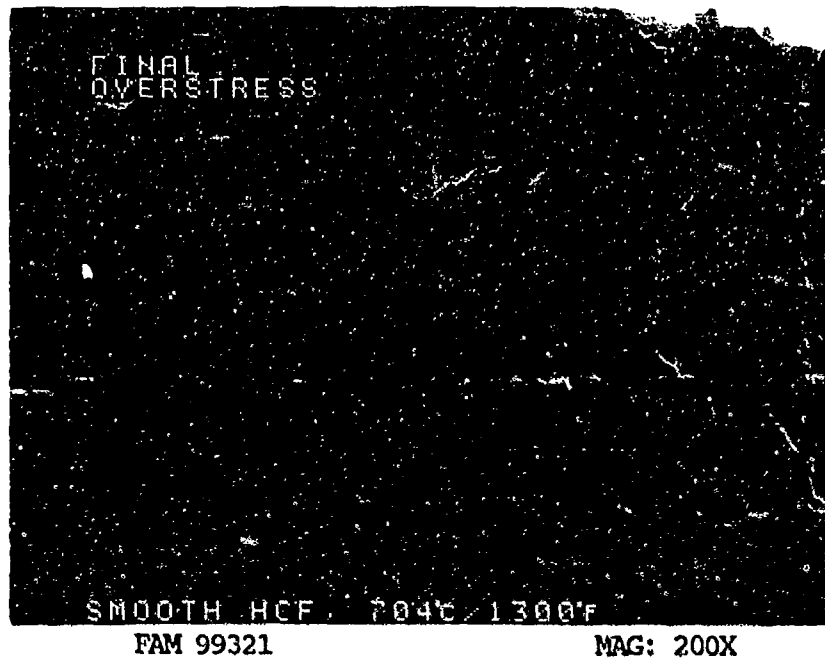


FIGURE 8-64: Oxidized final overstress area.

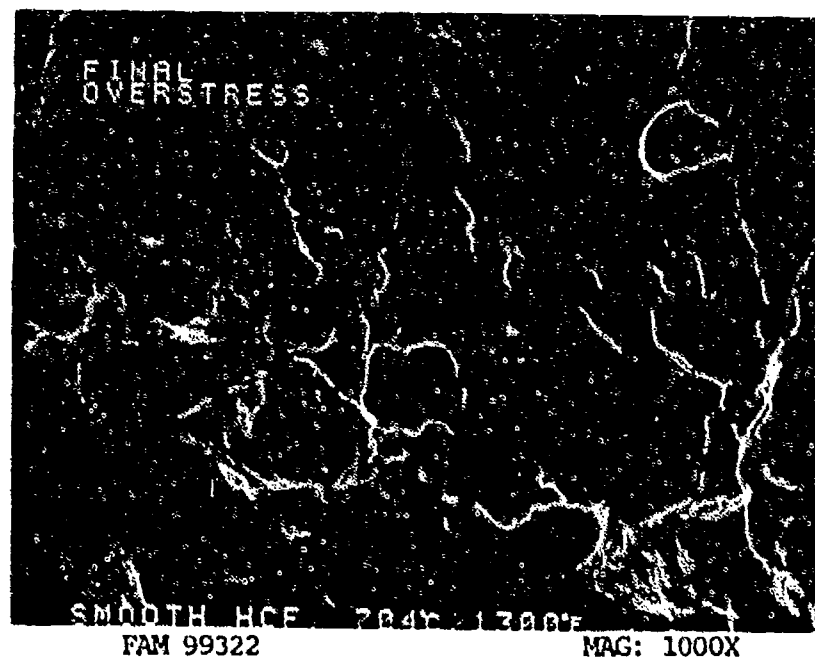


FIGURE 8-65: Oxidized overstress with no interpretable features.

MATERIAL

Inconel 600
AMS 5665 Bar

TEST DATA

TEST TYPE

Notched HCF

TEST CONDITIONS

Stress: 241.3 MPa (35.0 ksi)/-241.3 MPa (-35.0 ksi)
Stress Ratio: -1
Frequency: 1800 cpm
Atmosphere: Air
Temperature: Room Temperature
Test Direction: Longitudinal

TEST RESULTS

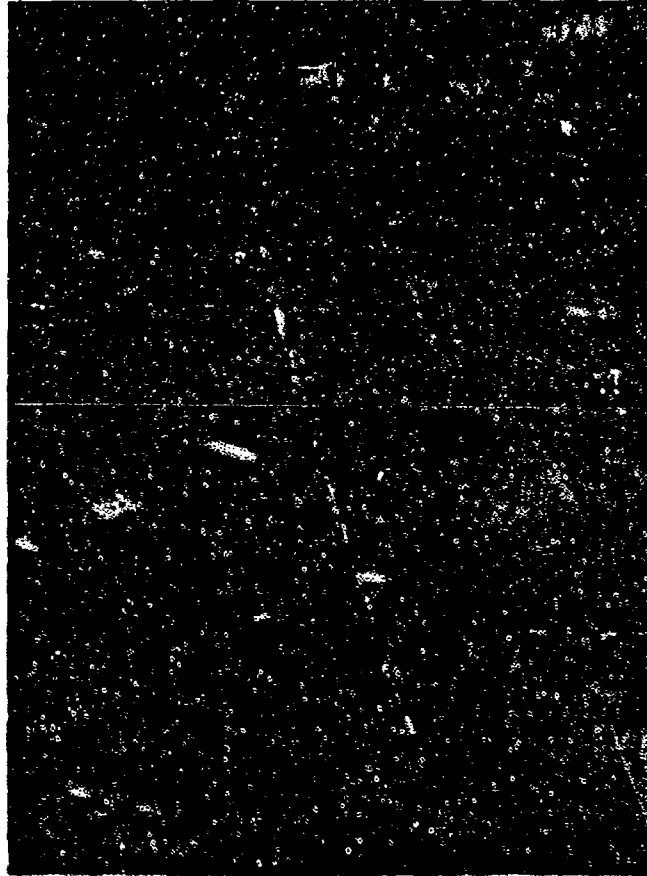
Cycles to Fracture: 179,000



FAL 93954

MAG: 10X

FIGURE 8-66: Test results and fractography of Inconel 600 room temperature notched HCF test. The specimen exhibits fatigue progression over 90 percent of the fracture. Fatigue steps are visible at the surface of the specimen indicating propagation from multiple origins (white arrows). The final overstress area appears as a small thumbnail (black arrow).



FAM 99894

MAG: 200X

FIGURE 8-67: Optical photomicrograph showing transgranular fracture path propagation near the center of the fracture.

Etchant: 5% Nital electrolytic

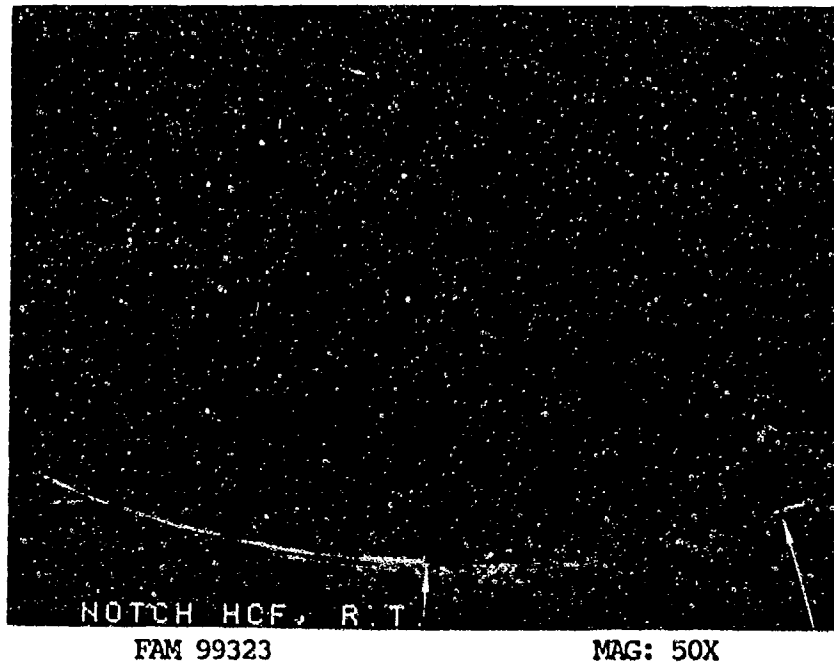


FIGURE 8-68: Overall photograph of the edge of the specimen and initial progression zone. The fracture propagated from multiple origins separated by steps (arrows).

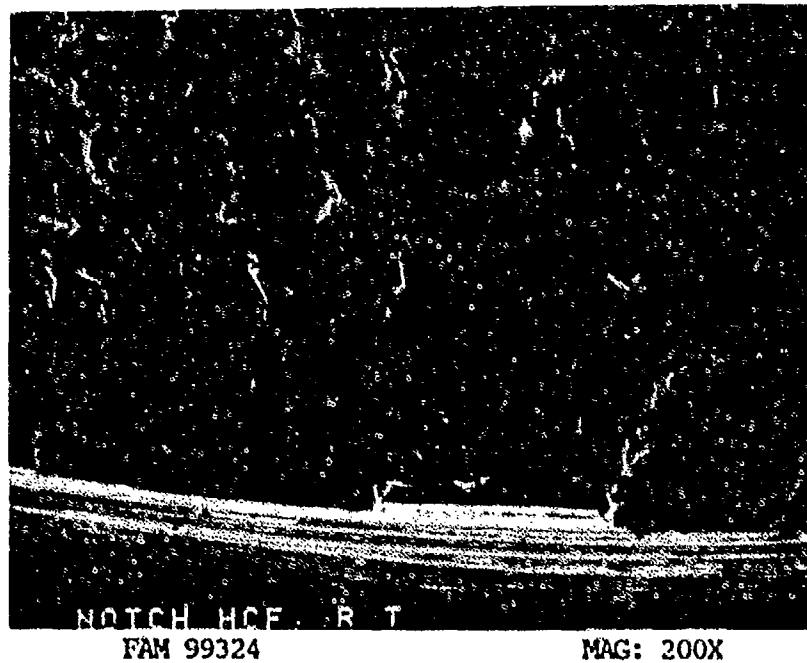


FIGURE 8-69: Higher magnification photograph of one localized origin area (bracket).

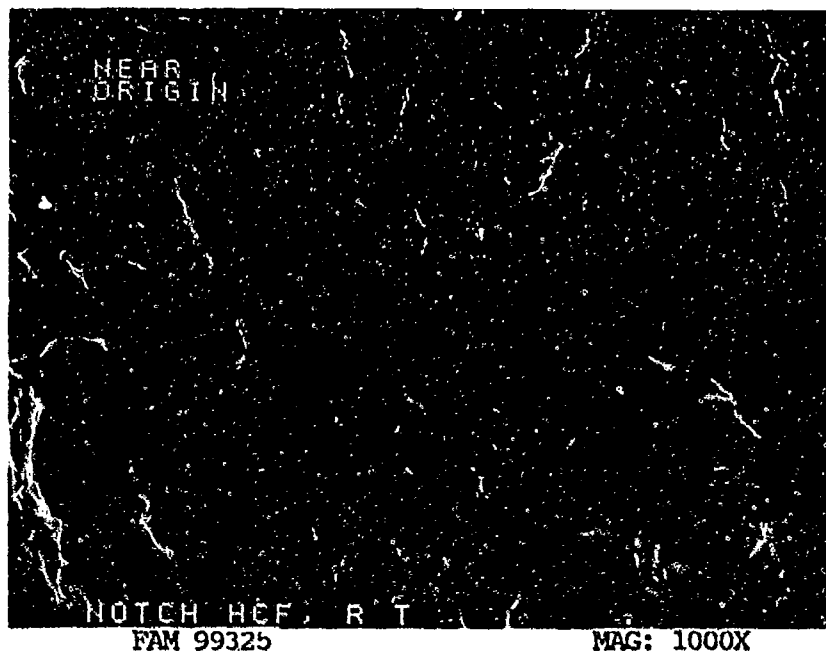


FIGURE 8-70: Fatigue progression near the origin. No striations are resolvable.

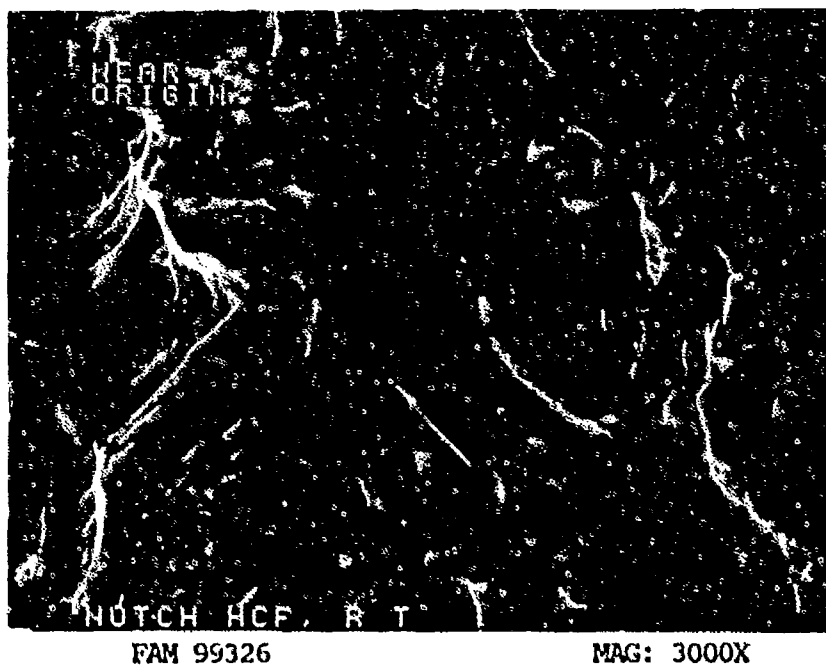


FIGURE 8-71: Higher magnification photograph of the area shown in Figure 8-70. Striations are visible on several plateaus. The direction of propagation is shown by an arrow.

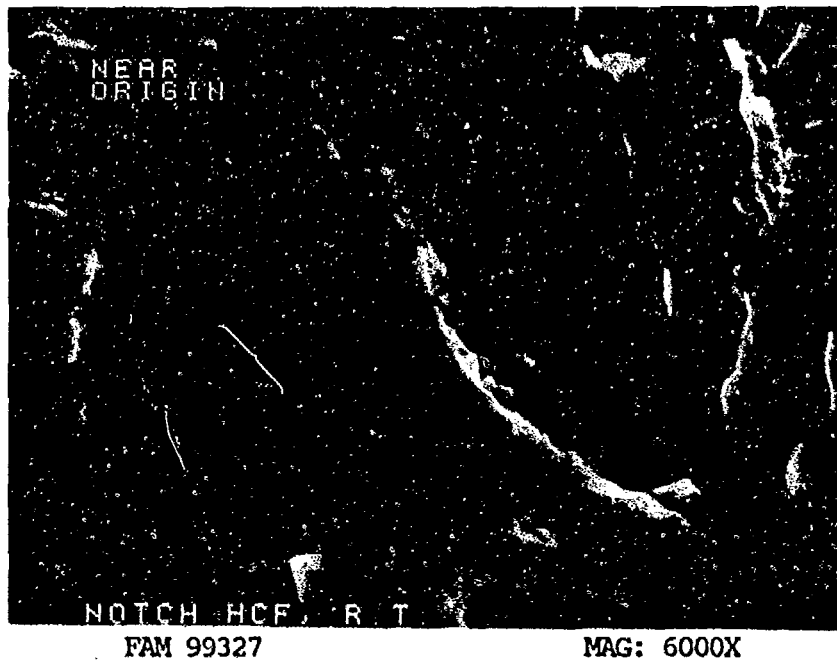


FIGURE 8-72: Higher magnification photograph showing fine striations in the area shown in Figure 8-71. Individual striations are barely resolvable. Bracket contains 10 striations.

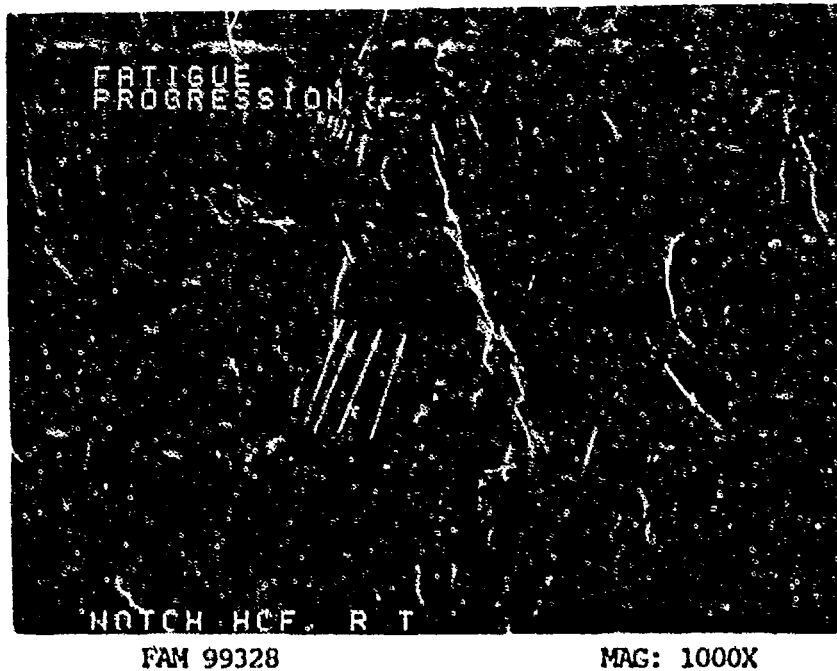


FIGURE 8-73: Small parallel fatigue plateaus in the fatigue progression zone (arrows).

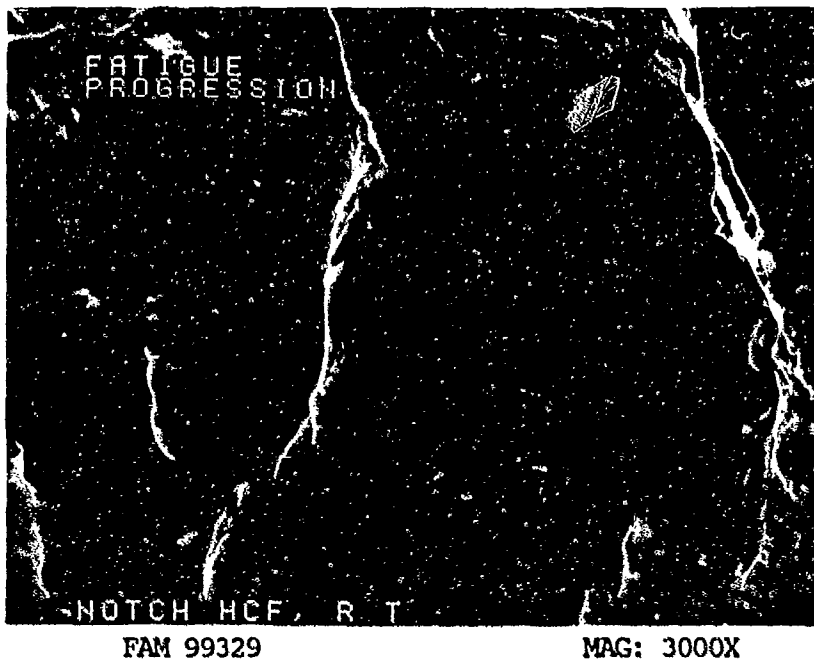


FIGURE 8-74: Higher magnification photograph of the area shown in Figure 8-73. Fine fatigue striations are visible on the plateaus. The direction of propagation is from bottom to top of the photograph.

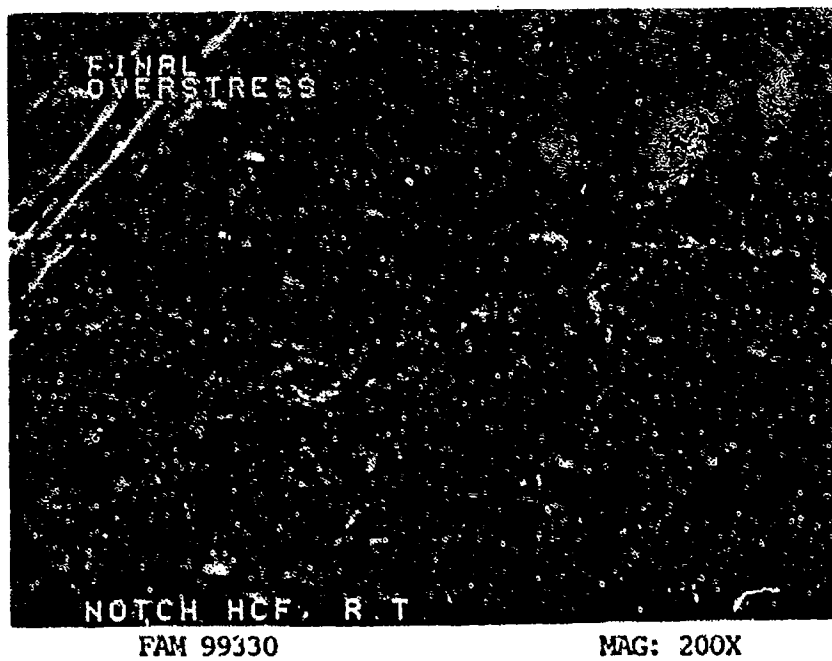


FIGURE 8-75: Final overstress area. No shear lip is present.

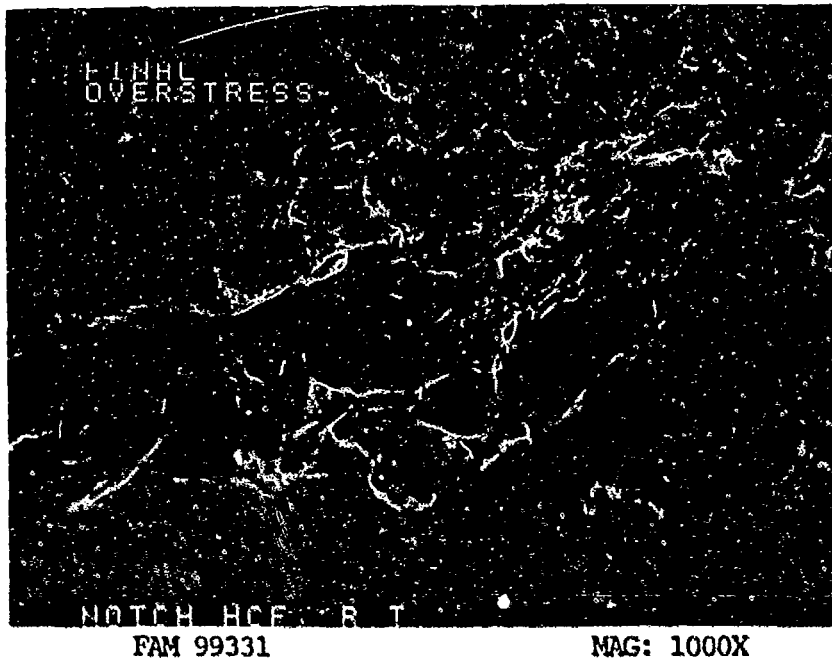


FIGURE 8-76: Oxidized final overstress area exhibiting dimpled overstress with small patches of cleavage.

MATERIAL

Inconel 600
AMS 5665 Bar

TEST DATA

TEST TYPE

Notched HCF

TEST CONDITIONS

Stress: 241.3 MPa (35.0 ksi)/-241.3 MPa (-35.0 ksi)
Stress Ratio: -1
Frequency: 1800 cpm
Atmosphere: Air
Temperature: 427°C (800°F)
Test Direction: Longitudinal

TEST RESULTS

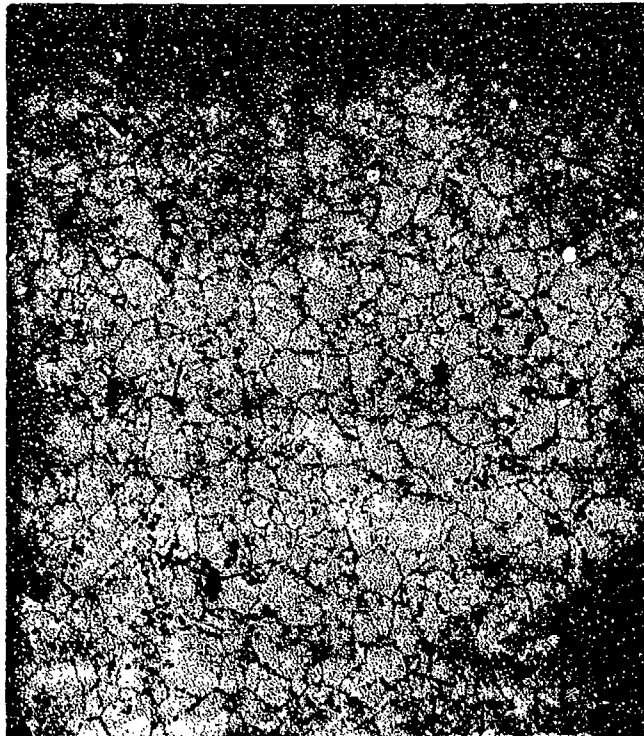
Cycles to Fracture: 95,000



FAL 94245

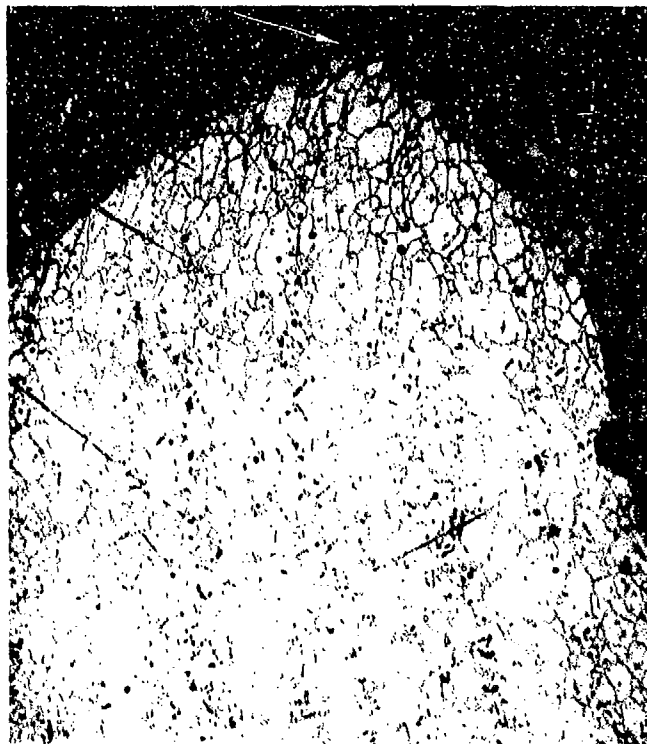
MAG: 10X

FIGURE 8-77: Test results and fractography of Inconel 600 427°C (800°F) notched HCF test. The specimen exhibits fatigue progression over 80 percent of the fracture. Fatigue steps are visible at the surface of the specimen indicating propagation from multiple origins. The final overstress area is indicated by arrows.



FAM 100237

MAG: 200X



FAM 100235

MAG: 100X

FIGURE 8-78: Optical photomicrographs showing transgranular fatigue progression area (top) and final overstress area (bottom). Significant grain elongation is visible in the final overstress area (arrow).

Etchant: 5% Nital electrolytic

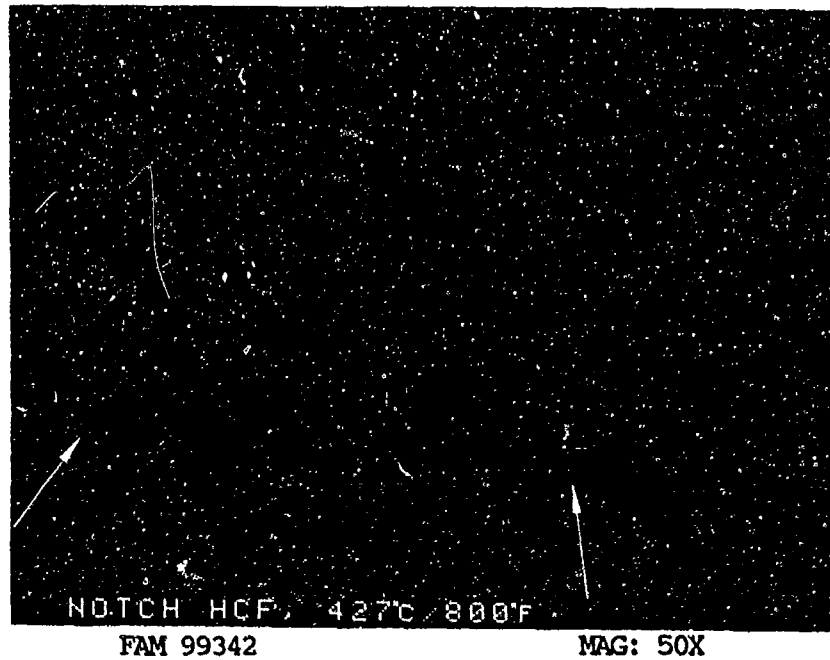


FIGURE 8-79: Overall photograph of the edge of the specimen and initial fatigue progression zone. The fracture propagated from multiple origins separated by small steps (arrows).

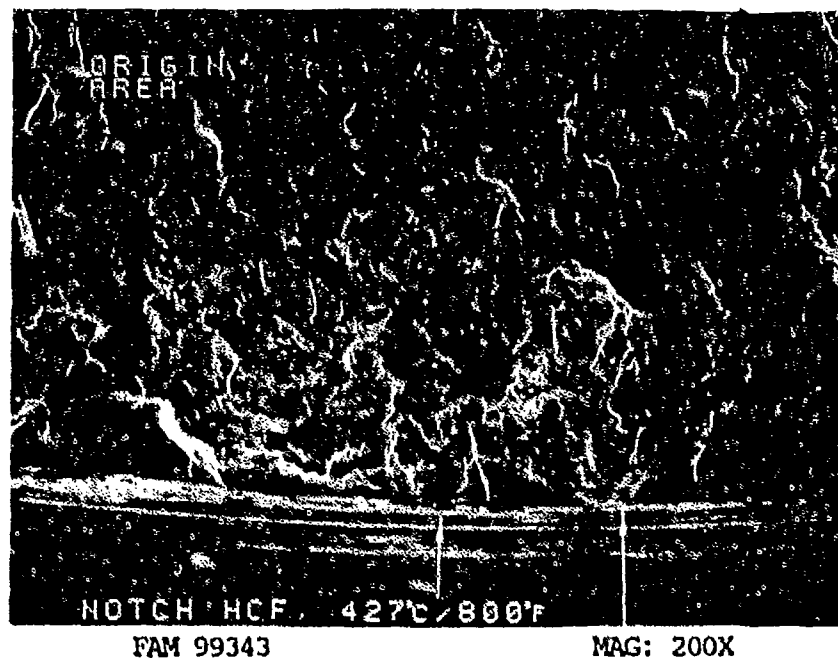


FIGURE 8-80: Higher magnification photograph of one localized origin area. Two stage I fatigue facets are visible at the surface (arrows).

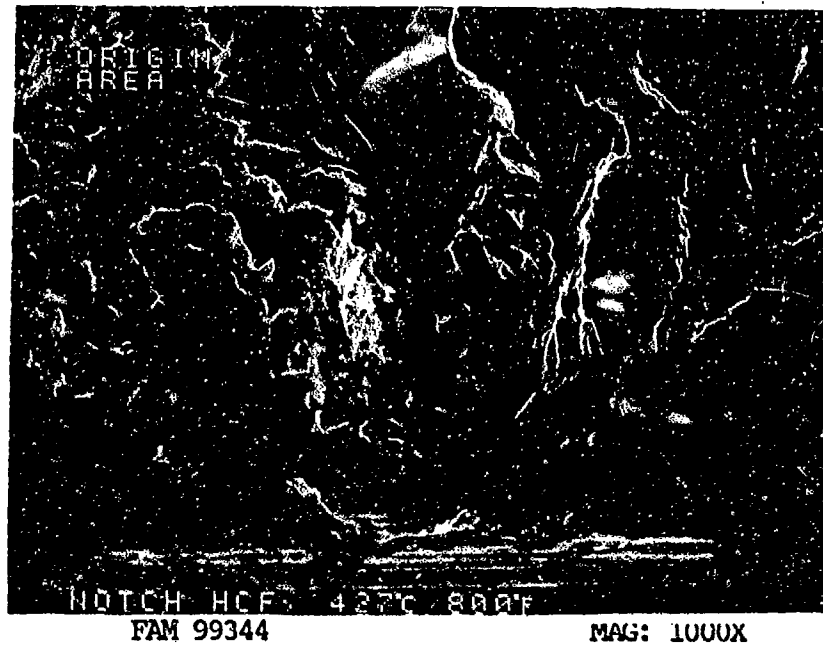


FIGURE 8-81: Higher magnification photograph of a localized origin. A stage I facet and initial progression near the origin are visible. No striations are visible on the stage I fatigue facet.

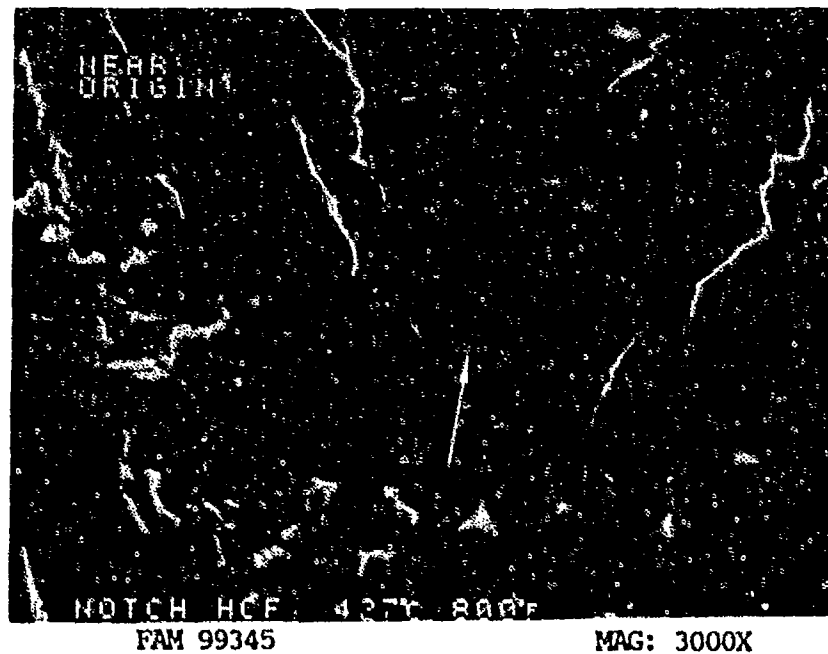


FIGURE 8-82: Higher magnification photograph of the area shown in Figure 8-81. Striations are visible on several plateaus. The direction of propagation is shown by an arrow.

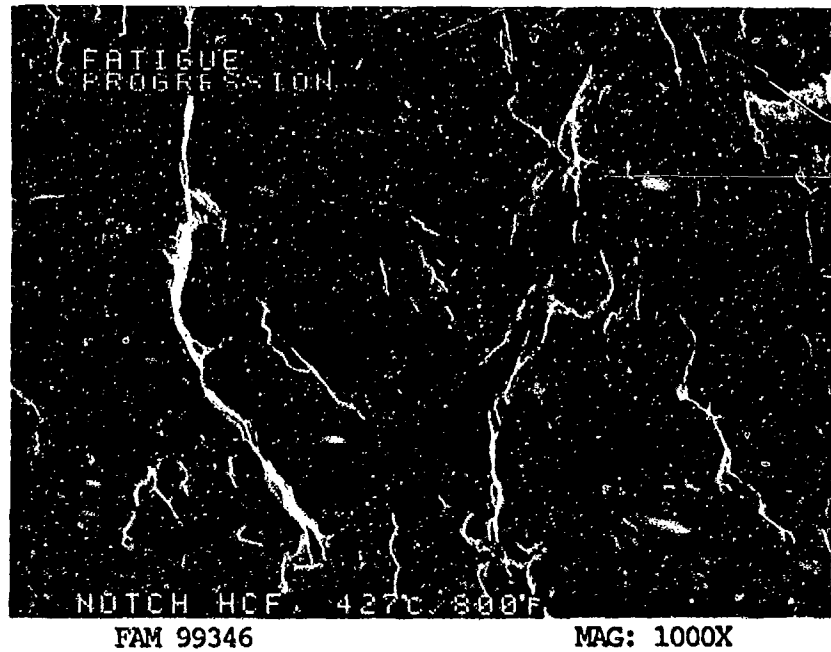


FIGURE 8-83: Fatigue progression exhibiting striations on several plateaus. The general direction of propagation is from bottom to top of the photograph.

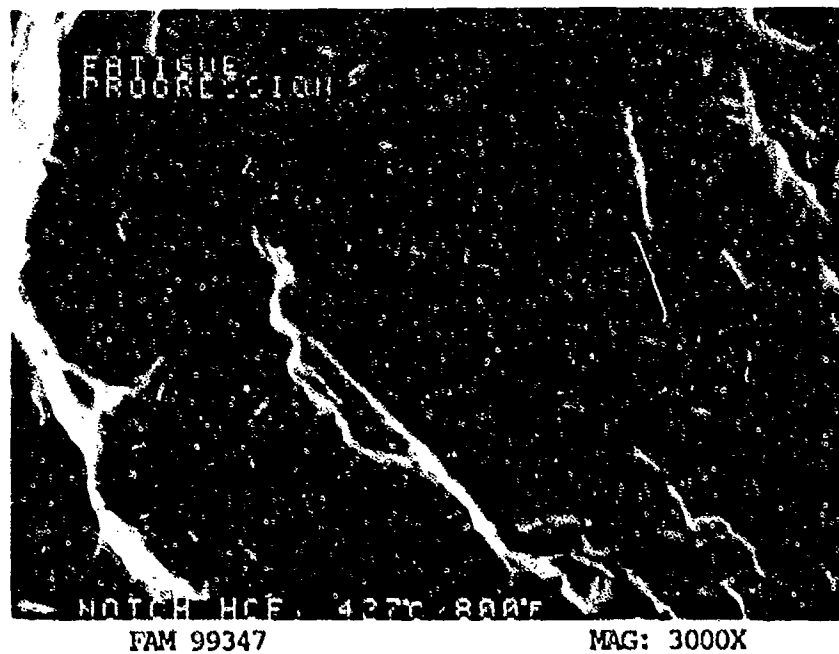


FIGURE 8-84: Higher magnification photograph of the fatigue striations in the progression zone (Figure 8-83). Brackets contain ten striations.

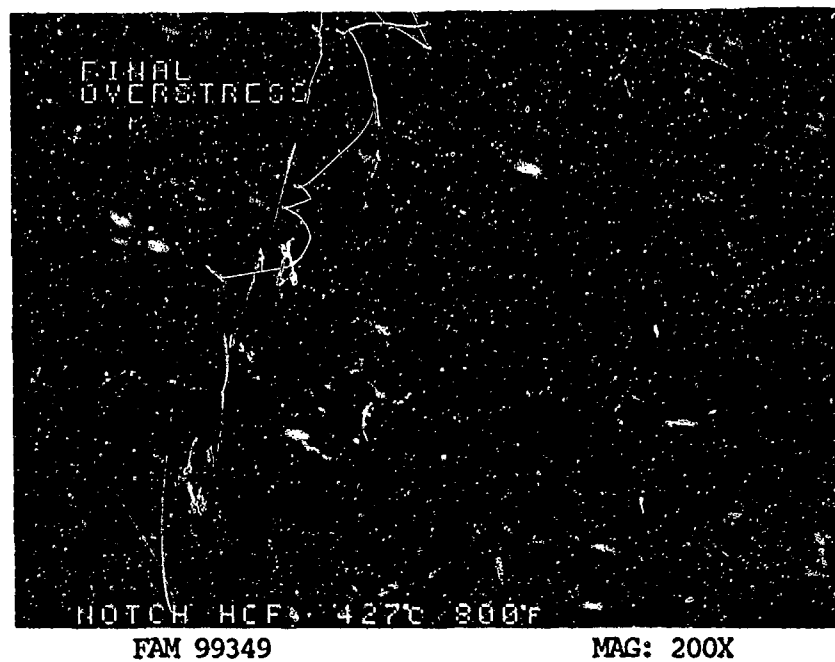


FIGURE 8-85: Final overstress area.

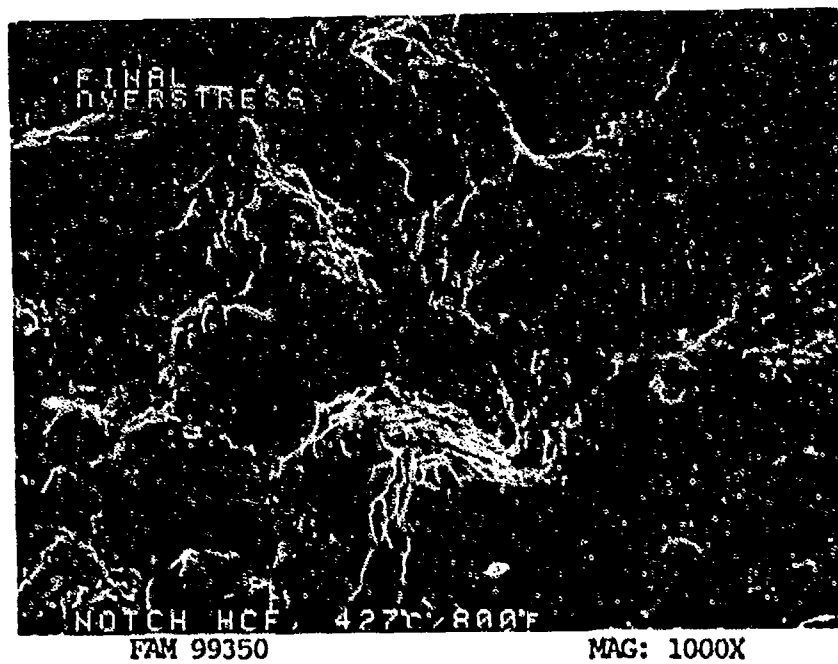


FIGURE 8-86: Final overstress area exhibiting a mixture of dimpled overstress and cleavage features.

MATERIAL

Inconel 600
AMS 5665 Bar

TEST DATA

TEST TYPE
Notched HCF

TEST CONDITIONS

Stress: 137.9 MPa (20.0 ksi)/-137.9 MPa (-20.0 ksi) DNF*
206.8 MPa (30.0 ksi)/-206.8 MPa (-30.0 ksi)
Stress Ratio: -1
Frequency: 1800 cpm
Atmosphere: Air
Temperature: 704°C (1300°F)
Test Direction: Longitudinal

TEST RESULTS

Cycles to Fracture: 2,060,000 (DNF), 30,000

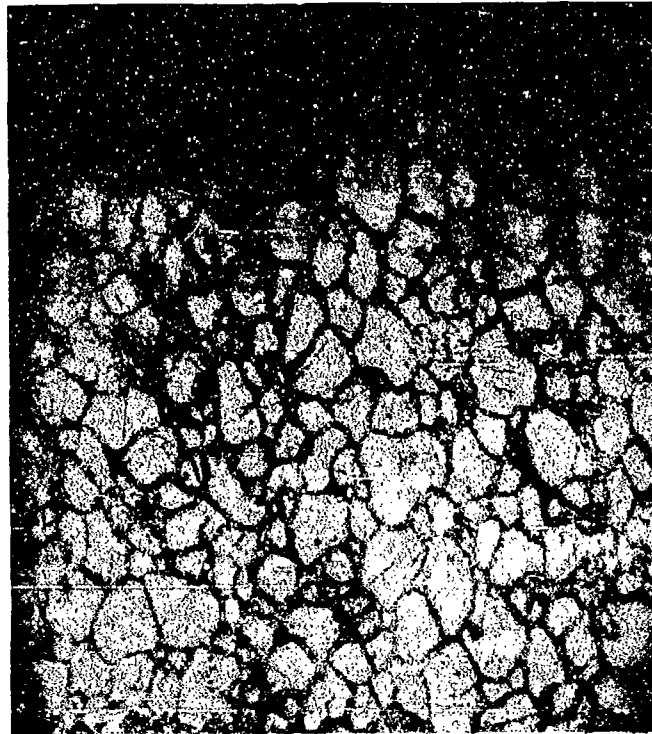
* Did Not Fracture



FAL 94244

MAG: 10X

FIGURE 8-87: Test results and fractography of Inconel 600 704°C (1300°F) notched HCF test. The specimen exhibits fatigue progression over 85 percent of the fracture. Three large fatigue steps are visible at the surface of the specimen indicating propagation from multiple origins. The final overstress area is indicated by arrows.



FAM 100238

MAG: 200X



FAM 100239

MAG: 200X

FIGURE 88: Optical photomicrographs showing fatigue progression area (top) and final overstress area (bottom). Compare the appearance of the grain boundaries with those in Figure 8-78, tested at 800° F.

Etchant: 5% Nital electrolytic

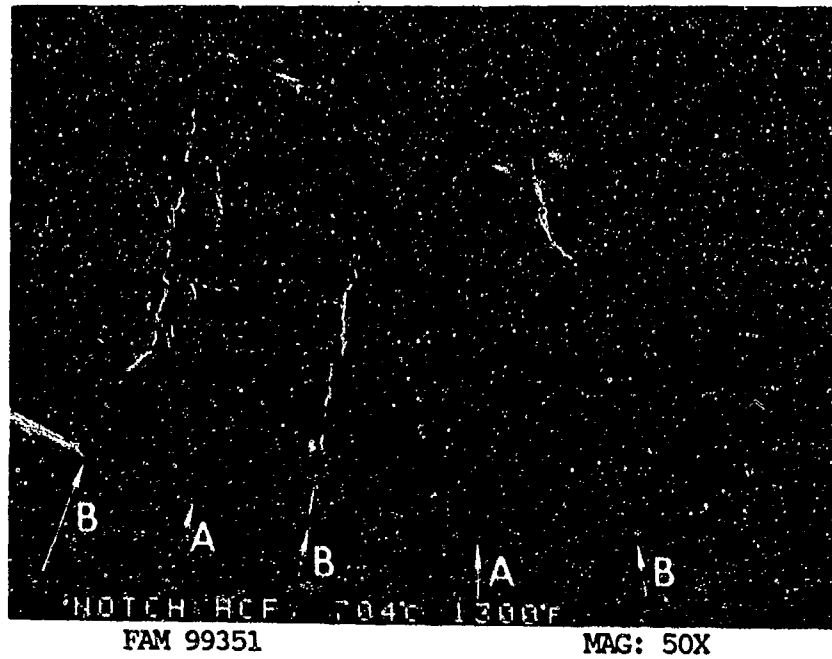


FIGURE 8-89: Overall photograph of the edge of the specimen and initial fatigue progression zone. The fracture propagated from multiple origins (arrows A) separated by large steps (arrows B). Features can be seen radiating from the origins.

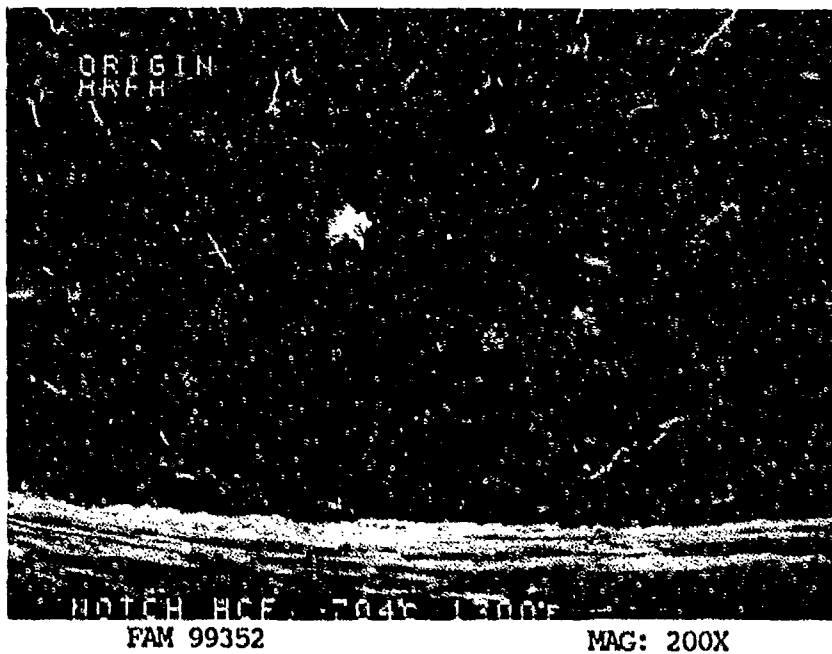


FIGURE 8-90: Higher magnification photograph of one localized origin area.

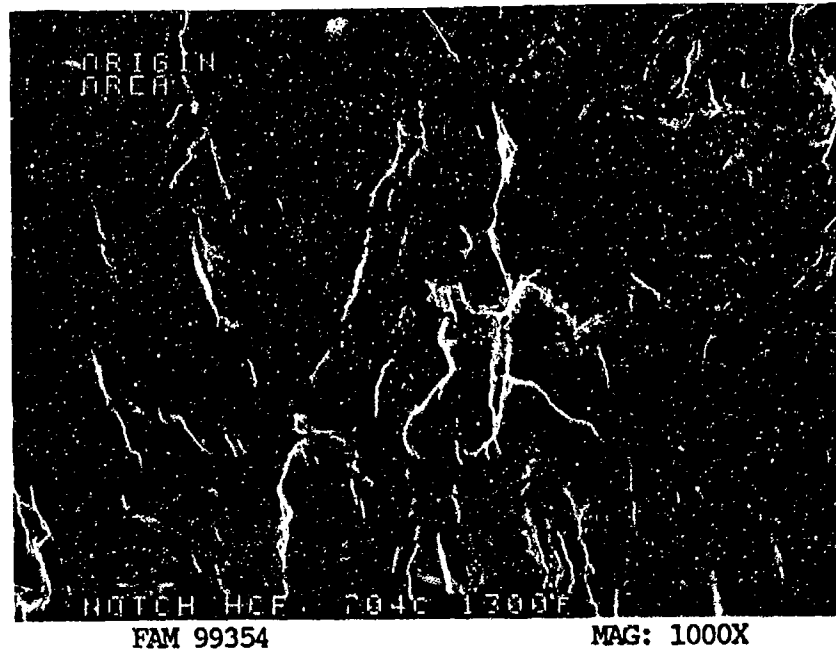


FIGURE 8-91: Oxidized features in the origin area. Remnant features indicative of fatigue are visible.

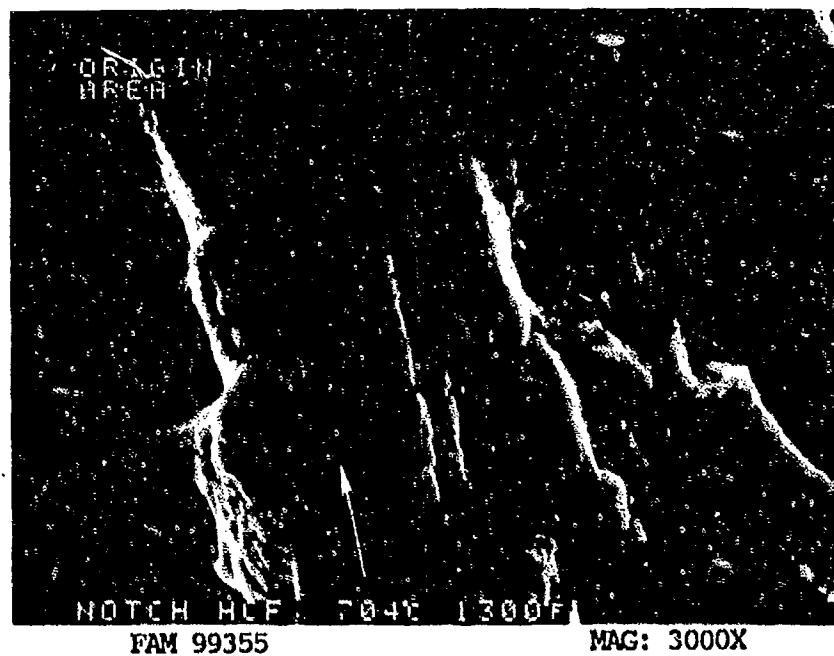


FIGURE 8-92: Higher magnification photograph of the area shown in Figure 8-91. Remnant striations are visible on several plateaus. The direction of propagation is shown by an arrow.

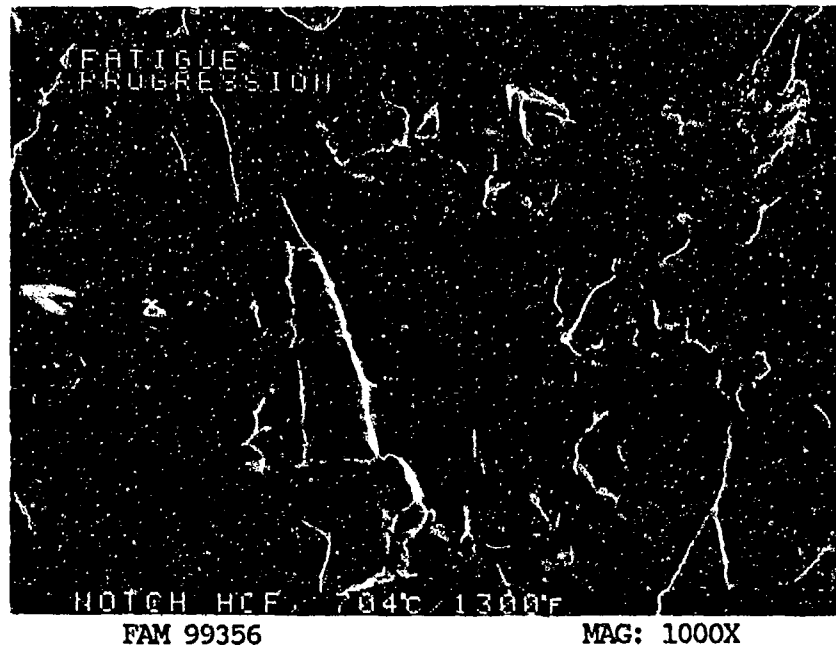


FIGURE 8-93: Fatigue progression exhibiting oxidized striations on several plateaus. The general direction of propagation is from bottom to top of the photograph.

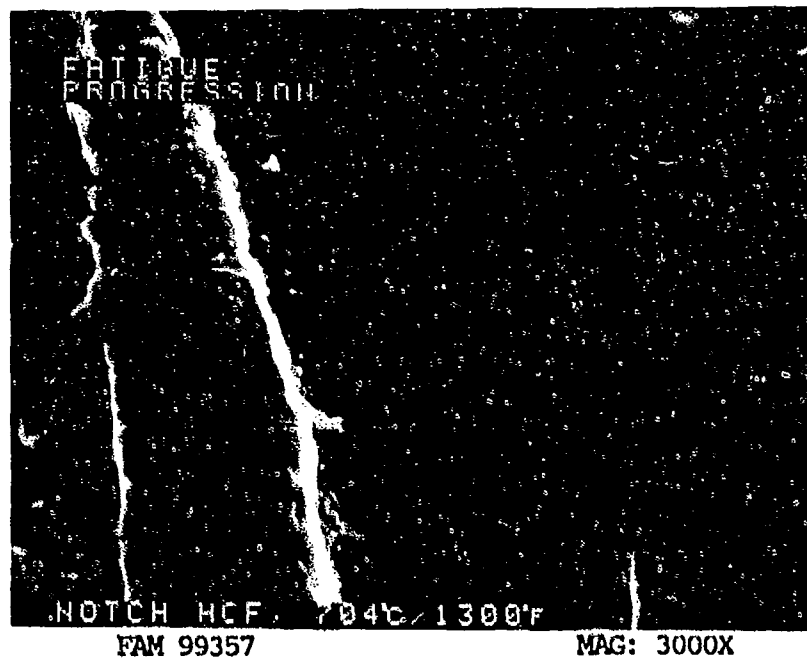


FIGURE 8-94: Higher magnification photograph of the area shown in Figure 8-93. Well developed oxidized fatigue striations are visible in the progression zone.

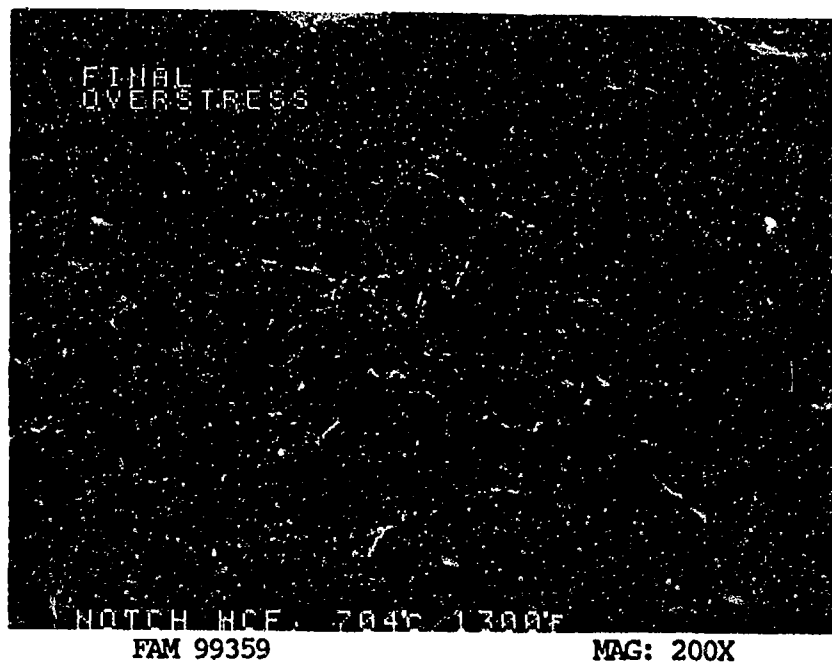


FIGURE 8-95: Final overstress area exhibiting no shear lip.

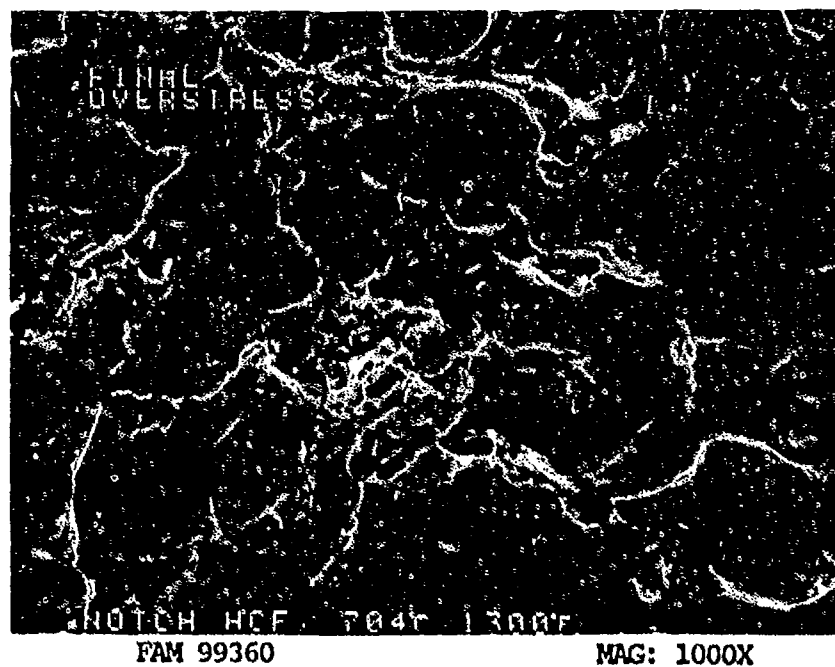


FIGURE 8-96: Final overstress area exhibiting a mixture of oxidized dimpled overstress and cleavage features.

MATERIAL

Inconel 600
AMS 5665 Bar

TEST DATA

TEST TYPE
Smooth LCF

TEST CONDITIONS

Stress: 448 MPa (65 ksi)/- 448 MPa (-65 ksi)
Stress Ratio: -1
Frequency: 10 cpm
Atmosphere: Air
Temperature: 427°C (800°F)
Test Direction: Longitudinal

TEST RESULTS

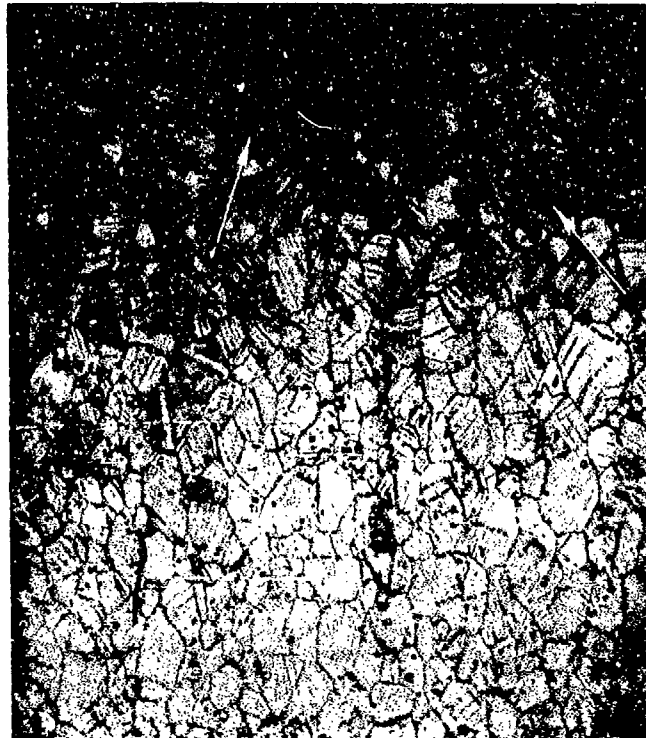
Cycles to Fracture: 1395



FAL 94241

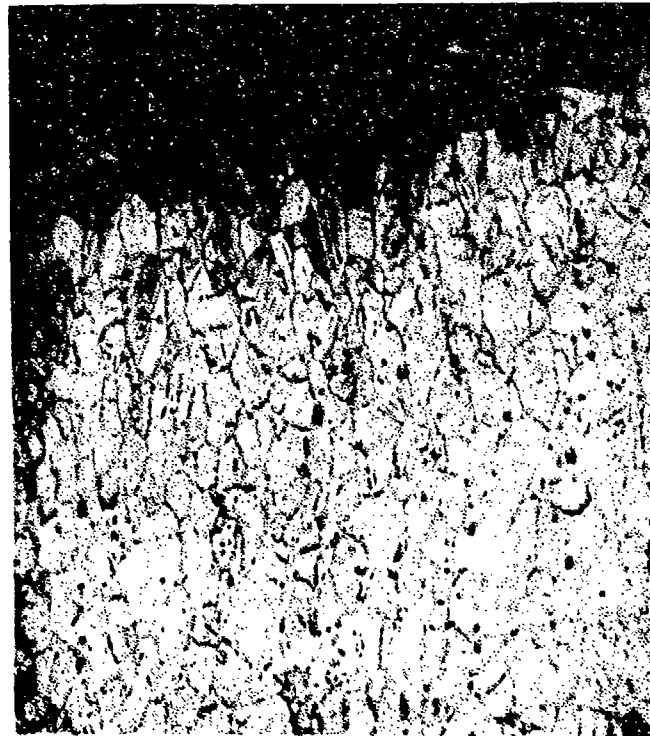
MAG: 13X

FIGURE 8-97: Test results and fractography of Inconel 600 427°C (800°F) smooth LCF test. The fracture propagated on several planes (plateaus). A small thumbnail perpendicular to the stress axis is visible at the origin (arrow).



FAM 100245

MAG: 100X



FAM 100247

MAG: 100X

FIGURE 8-98: Optical photomicrographs showing the fatigue progression area (top) and the final overstress area (bottom). Heavy strain lines are visible in the fatigue area (arrows) with fewer strain lines present in the overstress. These are produced by slip as the stress is cycled above and below the yield point. Figure 8-46 exhibits no strain lines because HCF loading does not surpass the yield point.

Etchant: 5% Nital electrolytic

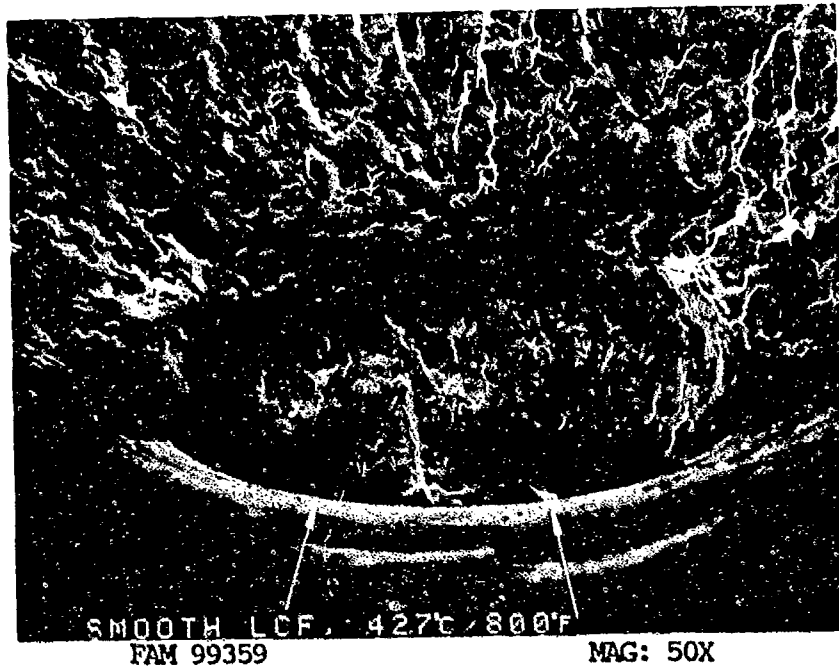


FIGURE 8-99: Overall photograph of the origin area exhibiting a thumbnail. Two local origins are visible (arrows) with features radiating from them.

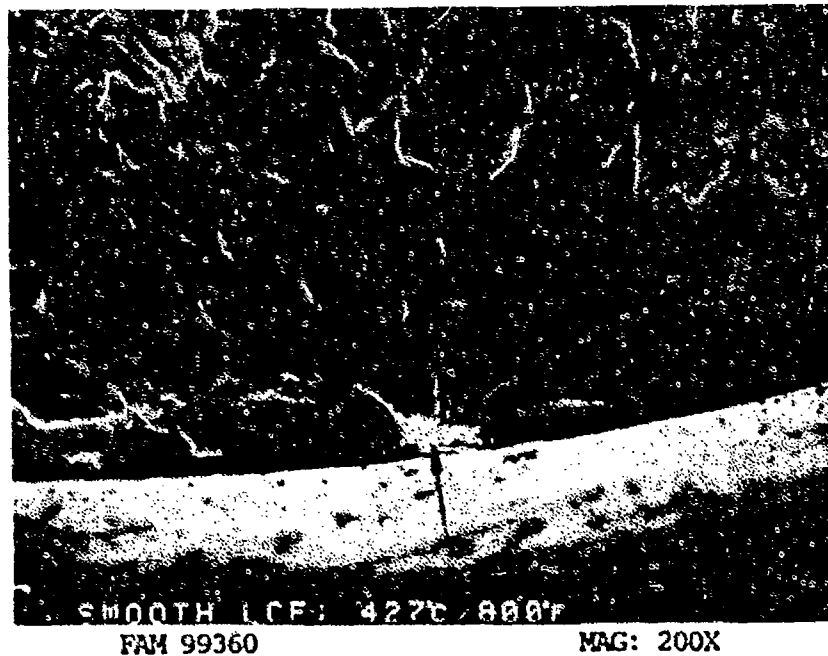


FIGURE 8-100: Higher magnification photograph of one local origin area. A stage I fatigue facet is visible at the surface (arrow). Feathery cleavage features radiate from the origin.



FIGURE 8-101: Higher magnification photograph of the origin area exhibiting a stage I fatigue facet at the surface. Striations and patches of feathery cleavage are visible adjacent to the stage I facet. No striations are visible on the facet.

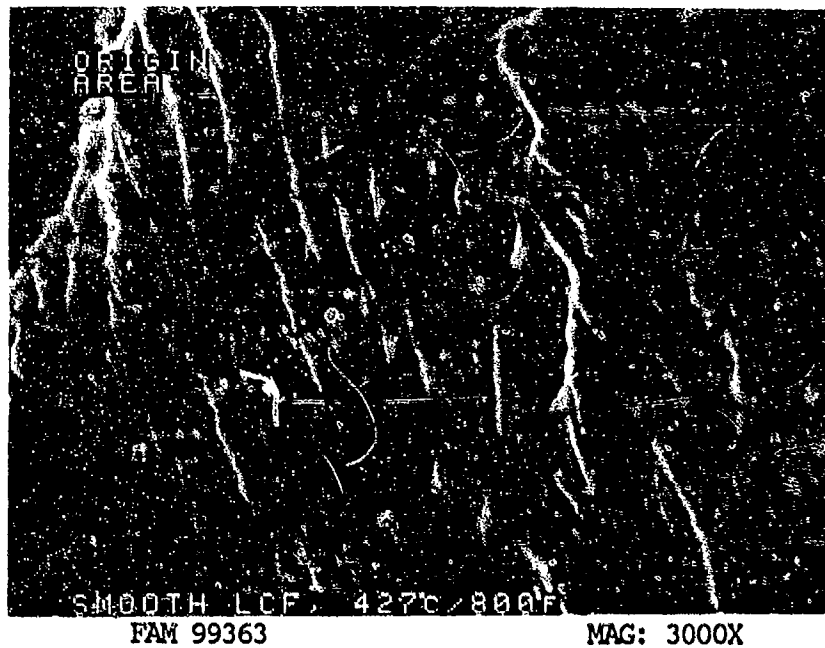


FIGURE 8-102: Higher magnification photograph of the area shown in Figure 8-101. Coarse striations are visible superimposed on fine feathery cleavage.

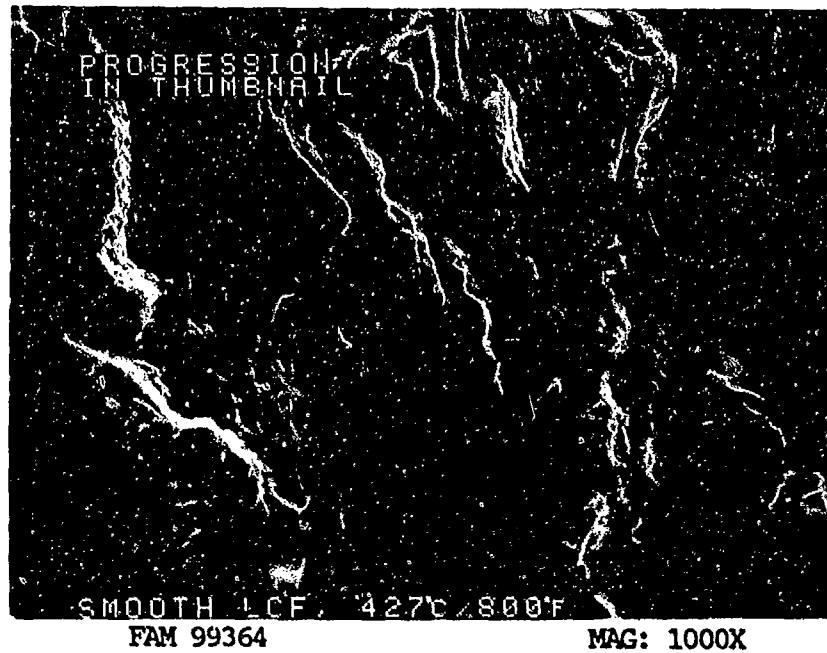


FIGURE 8-103: Fatigue progression zone in the thumbnail area exhibiting many changes of progression planes (plateaus) and feathery type cleavage.

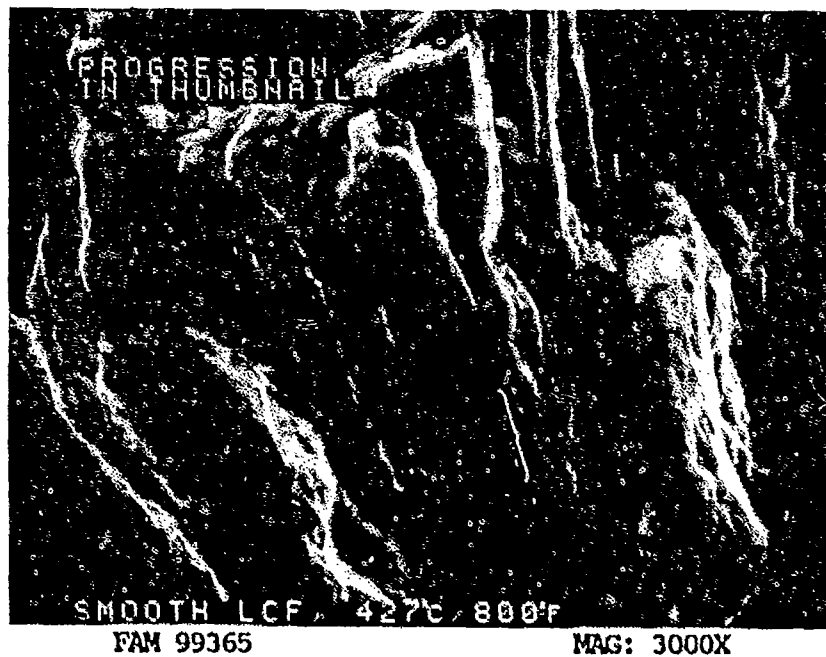


FIGURE 8-104: Fatigue striations in the area shown in Figure 8-103. Individual striations are barely resolvable. Bracket contains ten striations.

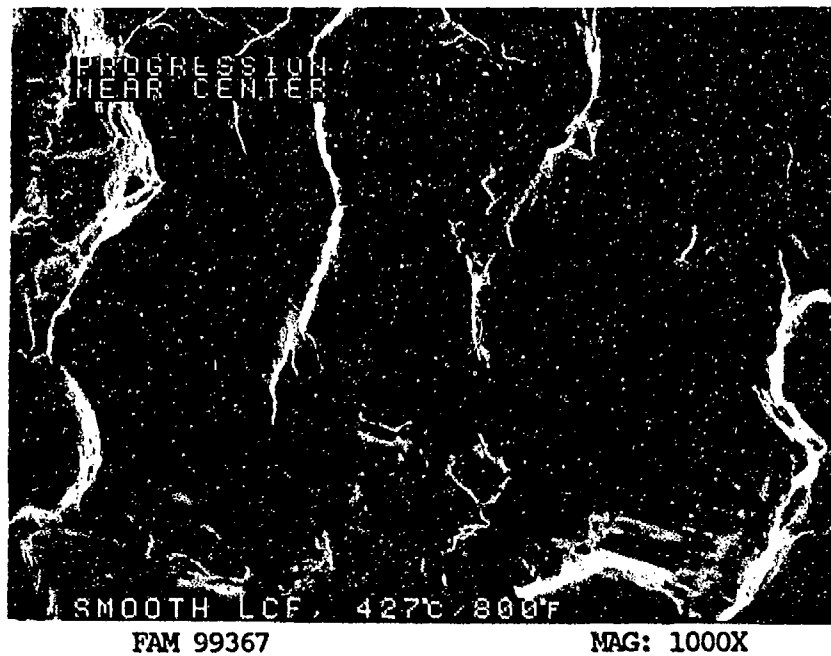


FIGURE 8-105: Fatigue progression near the center of the specimen. The features are coarser than those in the thumbnail area.

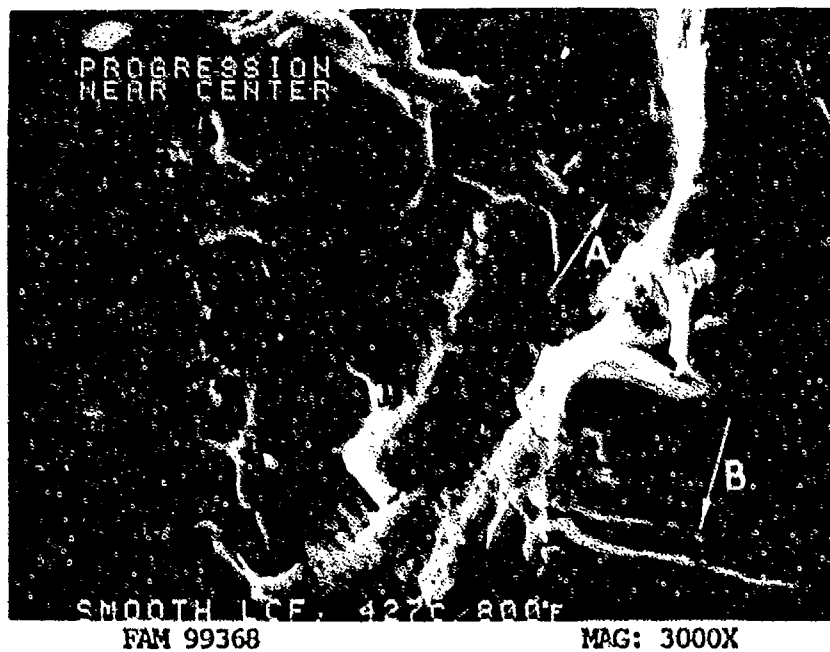


FIGURE 8-106: Higher magnification photograph of the area shown in Figure 8-105 showing remnant striations (arrow A) and crack-like striations (arrow B).

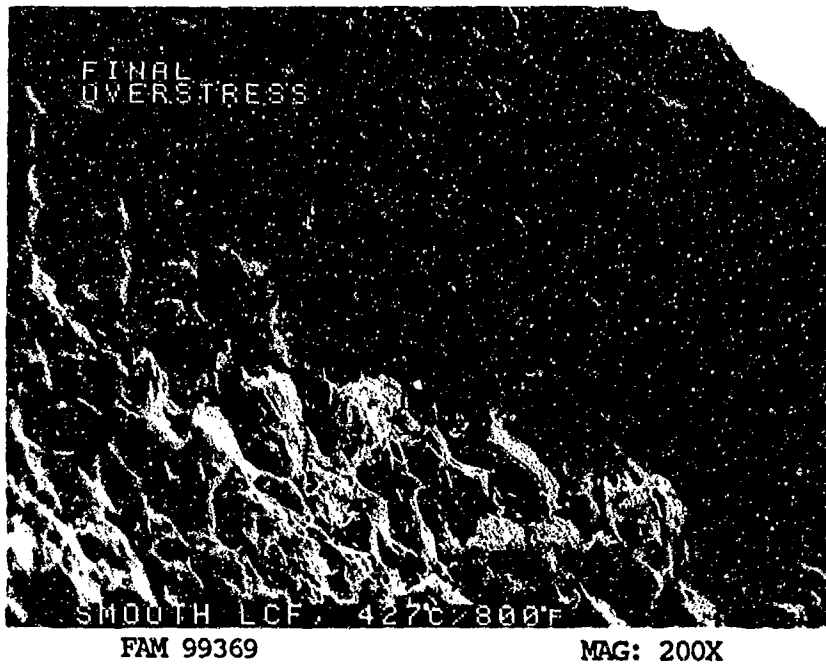


FIGURE 8-107: Final overstress area.

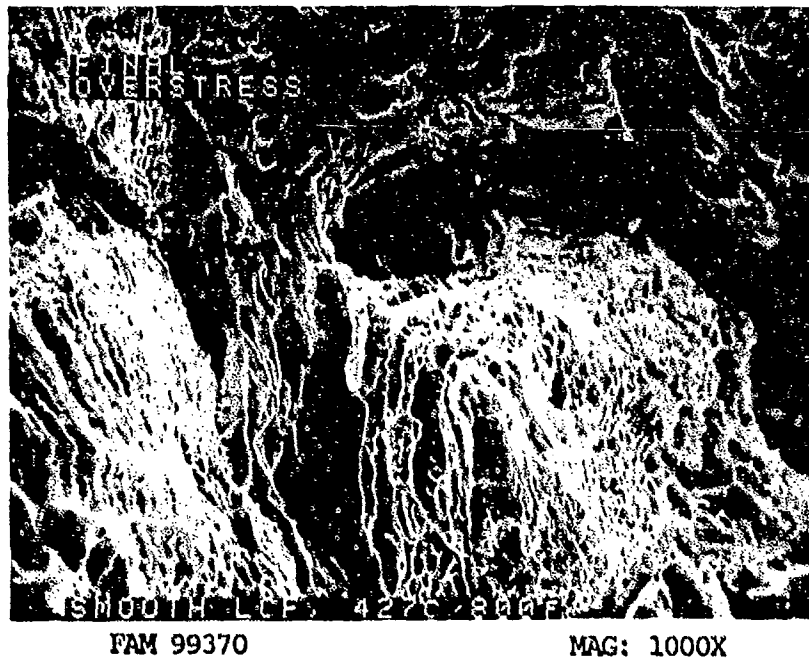


FIGURE 8-108: Mixture of dimpled overstress and cleavage in the final overstress area shown in Figure 8-107. Fine dimples are visible.

MATERIAL

Inconel 600
AMS 5665 Bar

TEST DATA

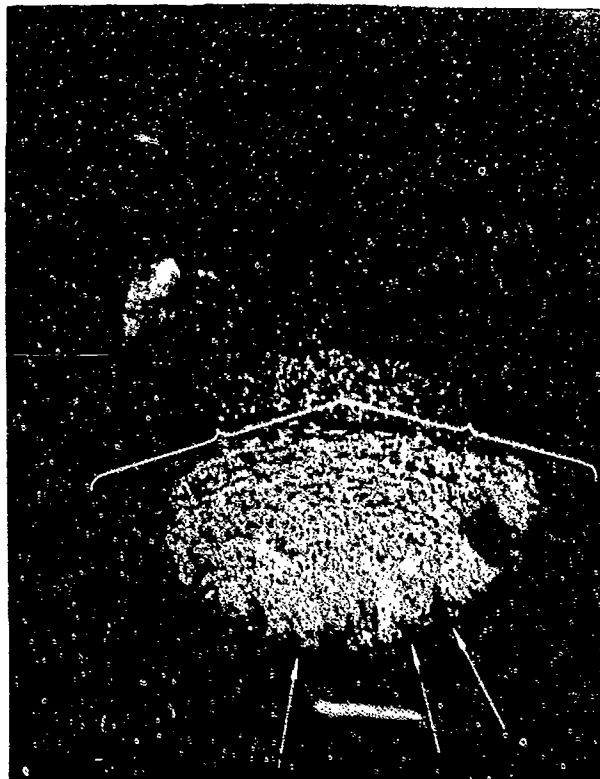
TEST TYPE
Smooth LCF

TEST CONDITIONS

Stress: 345 MPa (50 ksi)/- 345 MPa (- 50 ksi)
Stress Ratio: -1
Frequency: 10 cpm
Atmosphere: Air
Temperature: 704°C (1300°F)
Test Direction: Longitudinal

TEST RESULTS

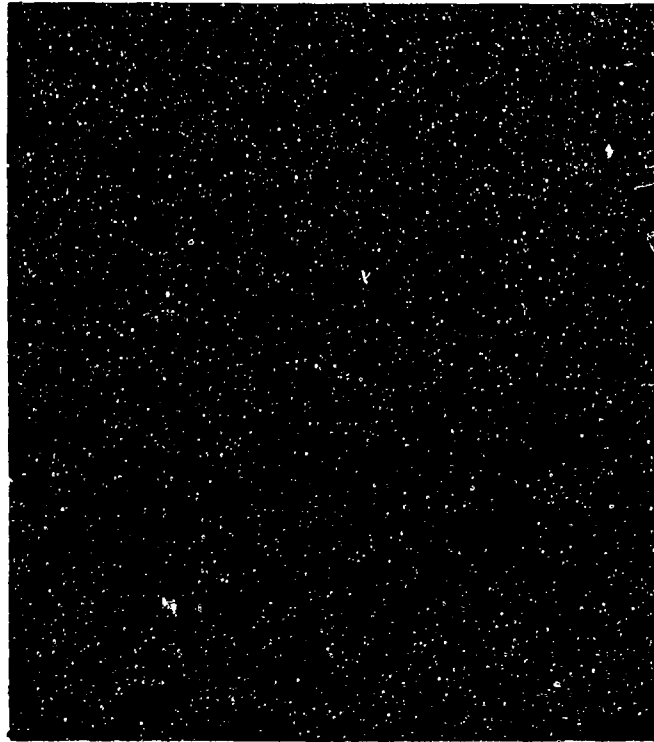
Cycles to Fracture: 648



FAL 94243

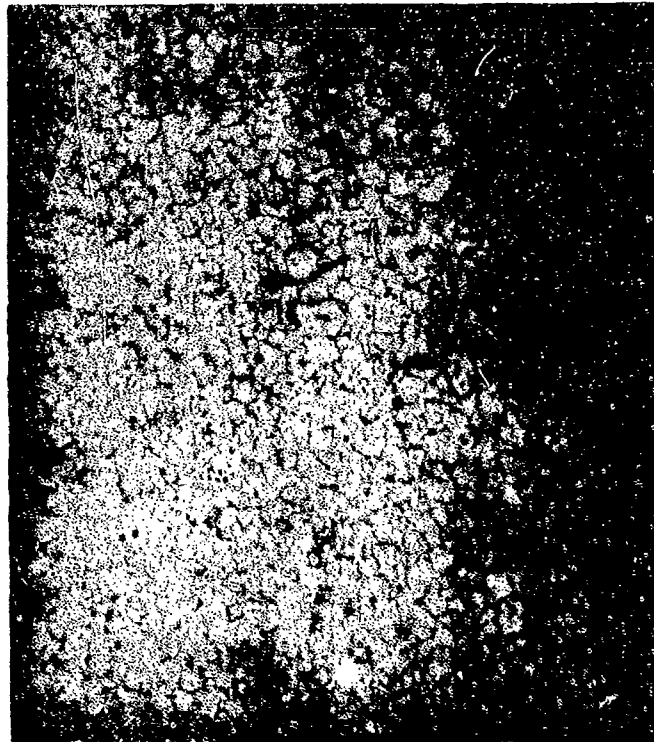
MAG: 10X

FIGURE 8-109: Test results and fractography of Inconel 600 704°C (1300°F) smooth LCF test. The fracture propagated on several planes. The fatigue progressed from multiple surface origins separated by steps (arrows). The extent of the fatigue is shown by brackets.



FAM 100242

MAG: 100X



FAM 100243

MAG: 100X

FIGURE 8-110: Optical photomicrographs showing the primary fracture surface (top) and several secondary cracks along the gage section (arrows, bottom). The fracture path appears to be more intergranular than the lower temperature fracture (Figure 8-98).

Etchant: 5% Nital electrolytic



FIGURE 8-111: Overall photograph of the origin area and initial fatigue propagation zone. Several localized origins separated by steps are visible. The origins are indicated by arrows.

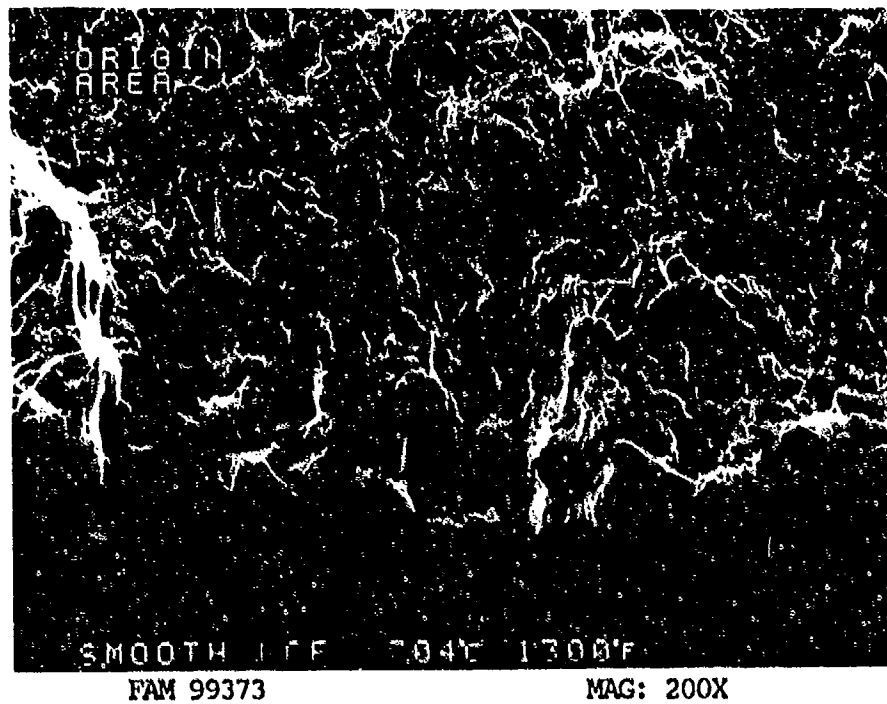


FIGURE 8-112: Higher magnification photograph of one localized origin area.

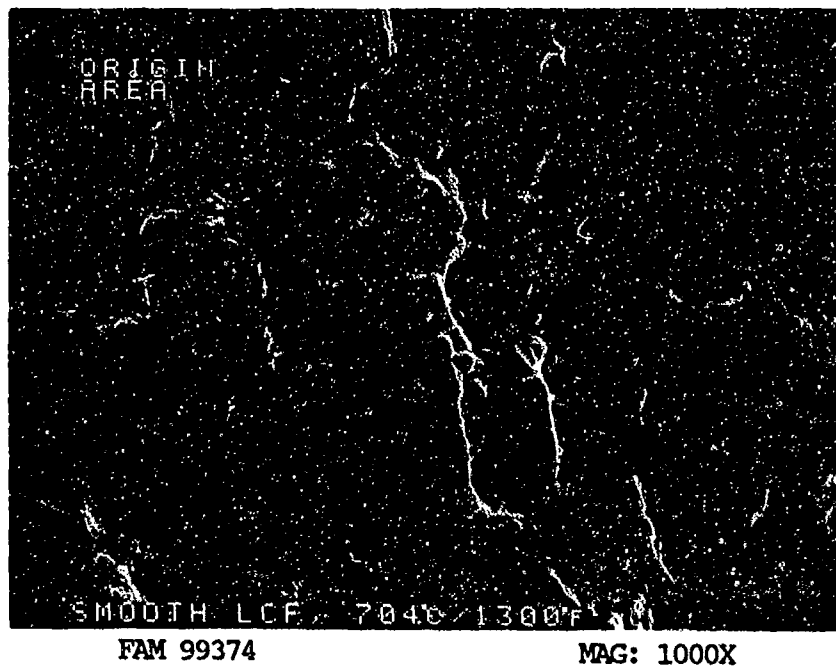


FIGURE 8-113: Oxidized fatigue features near the origin. Remnant striations are visible indicating propagation from bottom to top of photograph.

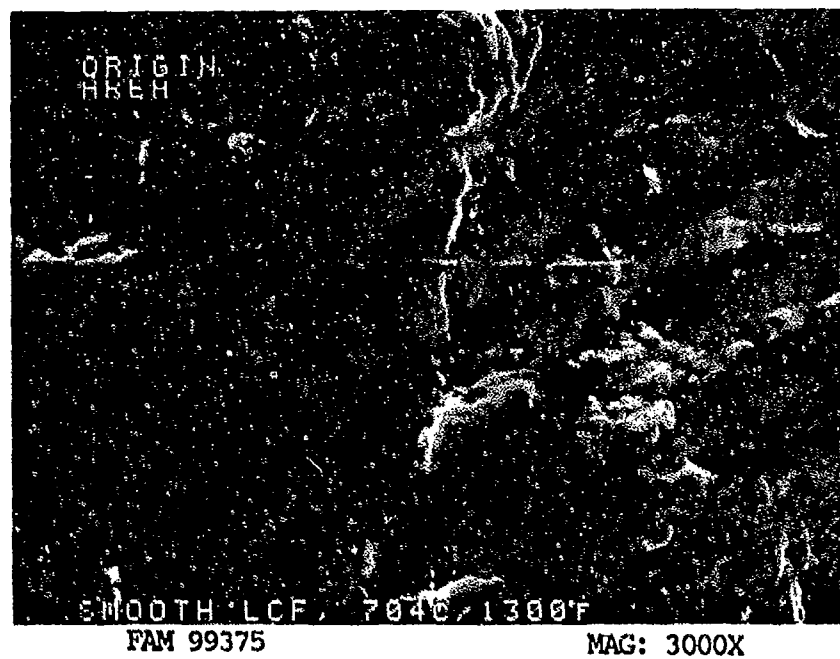


FIGURE 8-114: Higher magnification photograph of the area shown in Figure 8-113. Coarse oxidized striations are visible.

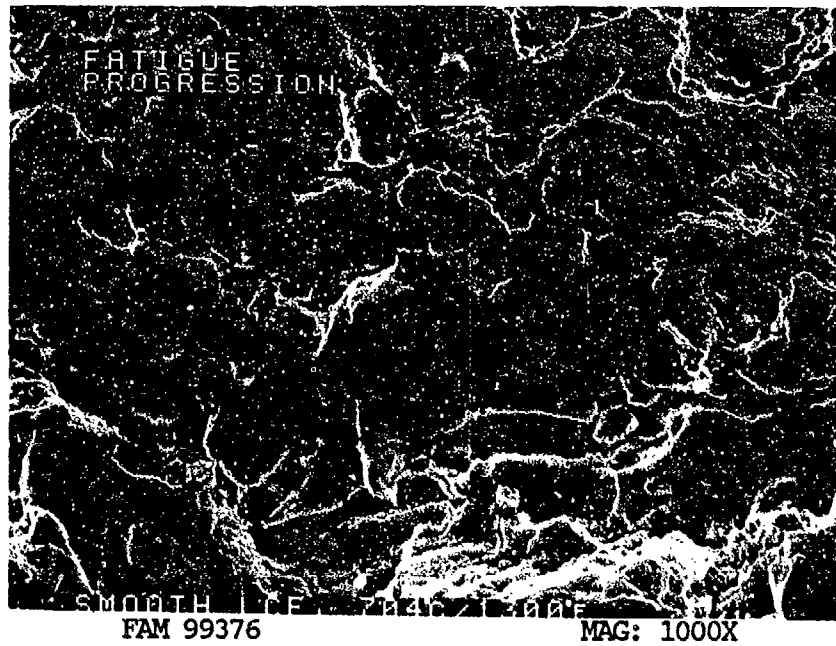


FIGURE 8-115: Fatigue progression zone exhibiting oxidized remnant fatigue the features (arrows).

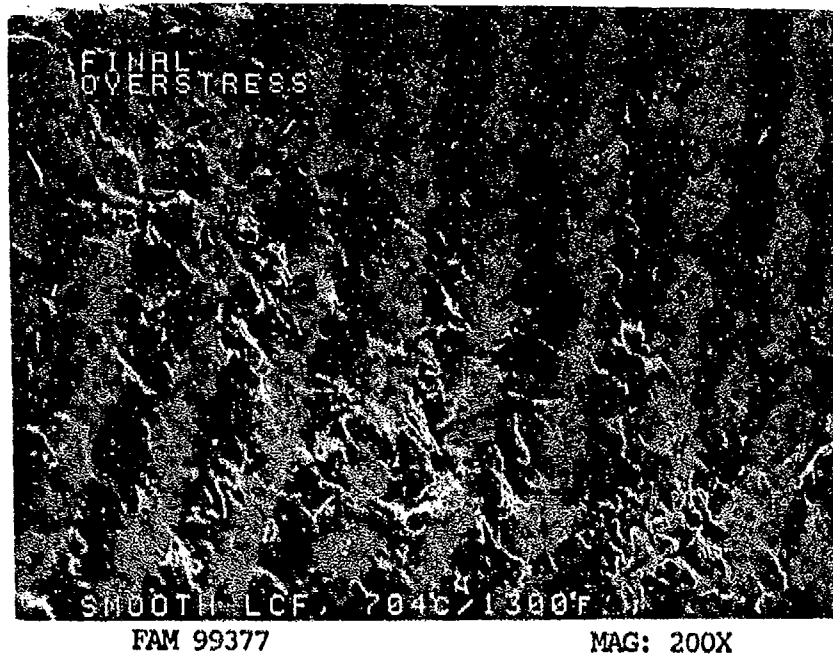


FIGURE 8-116: Final overstress area exhibiting no shear lip.

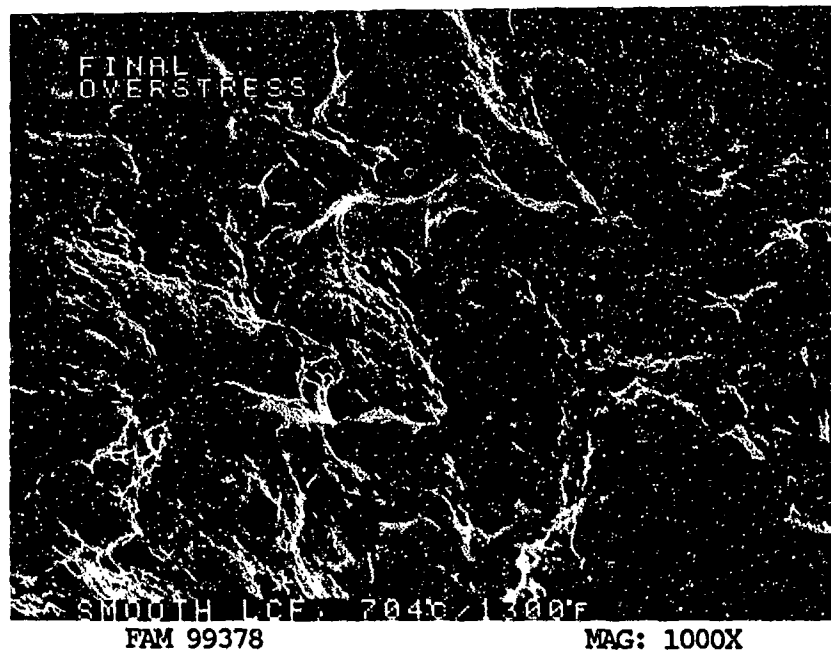


FIGURE 8-117: Dimpled overstress in the final overstress area.

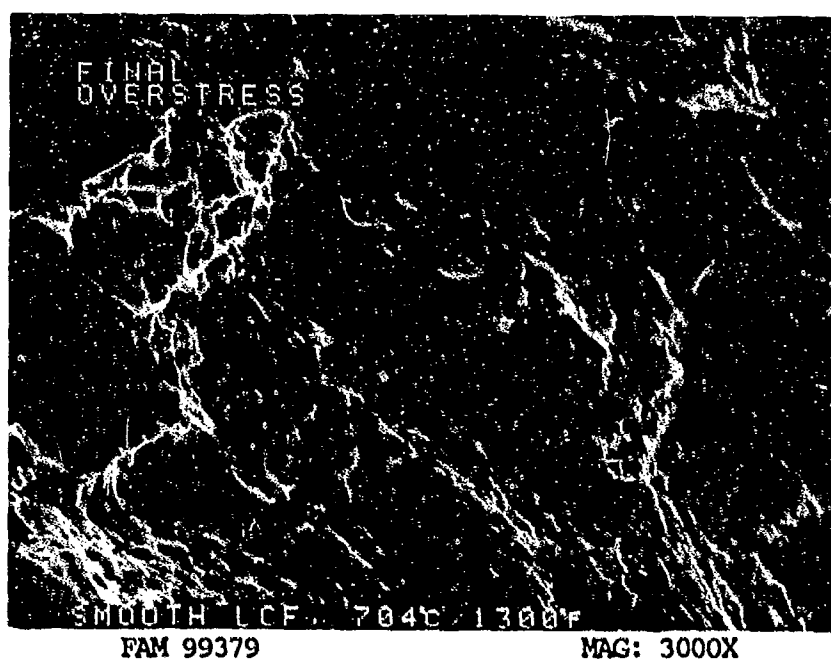


FIGURE 8-118: Higher magnification photograph of the area shown in Figure 8-117 showing fine oxidized dimpled overstress.

MATERIAL

Inconel 600
AMS 5665 Bar

TEST DATA

TEST TYPE

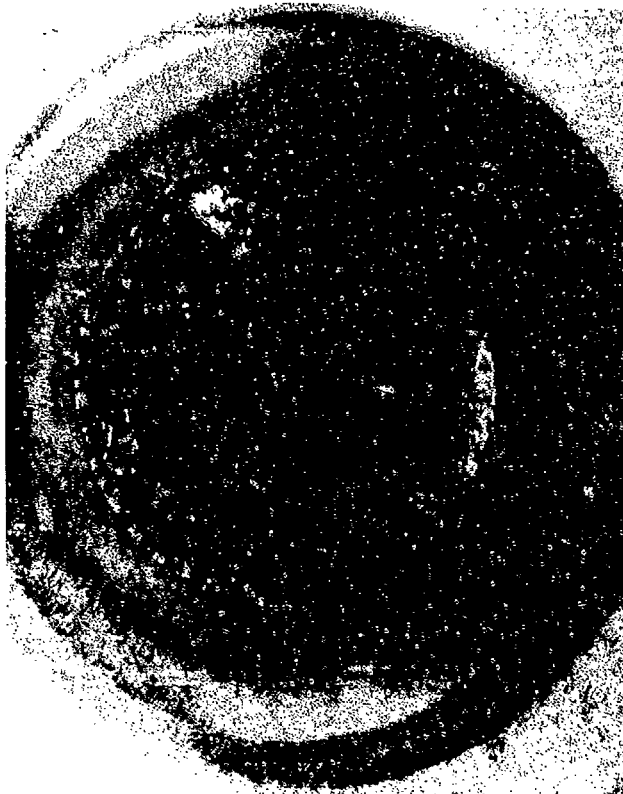
In-Phase/Out-of-Phase TMF

TEST CONDITIONS

Stress: 345 MPa (50 ksi)/- 345 MPa (- 50 ksi)
Stress Ratio: -1
Frequency: 10 cpm
Atmosphere: Air
Temperature: 704°C (1300°F)
Test Direction: Longitudinal

TEST RESULTS

Cycles to Fracture: 648



FAL 97148

MAG: 9X

FIGURE 8-119: Test results and fractography of Inconel 600 704°C (1300°F) In-phase TMF test. The fracture occurred by overstress after the stress was increased. No TMF fracture surface was produced for the out-of-phase specimen either.



FAM 100244

MAG: 200X

FIGURE 8-120: Optical photomicrograph showing the microstructure adjacent to the fracture.

Etchant: 5% Nital electrolytic

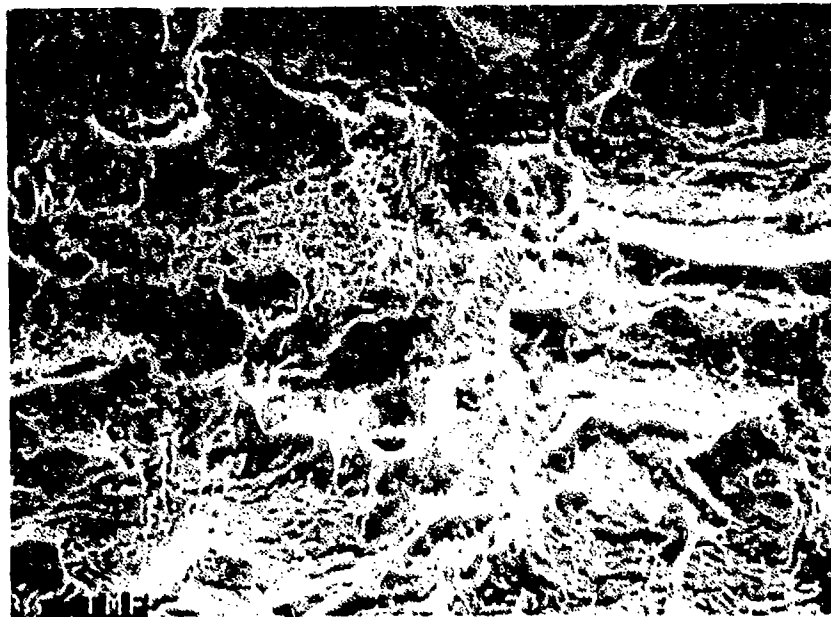


TME

FAM 100448

MAG: 50X

FIGURE 8-121: Overall photograph of the fracture surface showing tensile overstress features with no fatigue present.



TME

FAM 100449

MAG: 1000X

FIGURE 8-122: Higher magnification photograph showing dimpled overstress and quasi-cleavage features.

SERVICE FAILURE

FRACTURE MODE Liquid Metal Embrittlement

PART NAME Number One Oil Pressure Tube Assembly

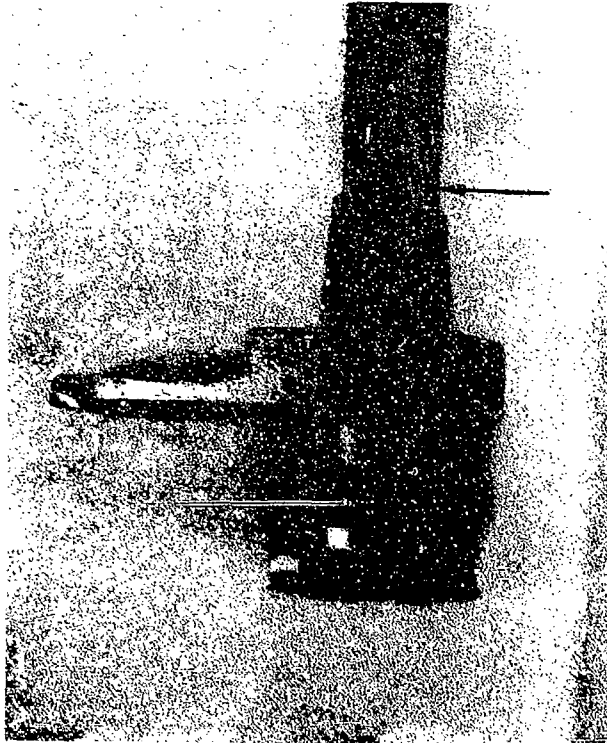
OPERATION DATA The tube operated in a field engine under standard conditions in which it is subjected to moderate loads at low temperatures.

PART TIME 49.1 hours

	<u>REQUIRED</u>	<u>ACTUAL</u>
MAT'L	BASE <u>Inconel 600</u>	<u>Confirmed</u>
	OTHER <u>Braze: AMS 4765 (silver-base)</u>	<u>Confirmed</u>
HARDNESS	<u>No Requirement</u>	<u>HRB 82-91 *</u>
GRAIN SIZE	<u>No Requirement</u>	<u>ASTM 4-6</u>
DIMENSIONAL	<u>Wall thickness: 0.025-0.030 inch</u>	<u>0.030-0.031 inch</u>

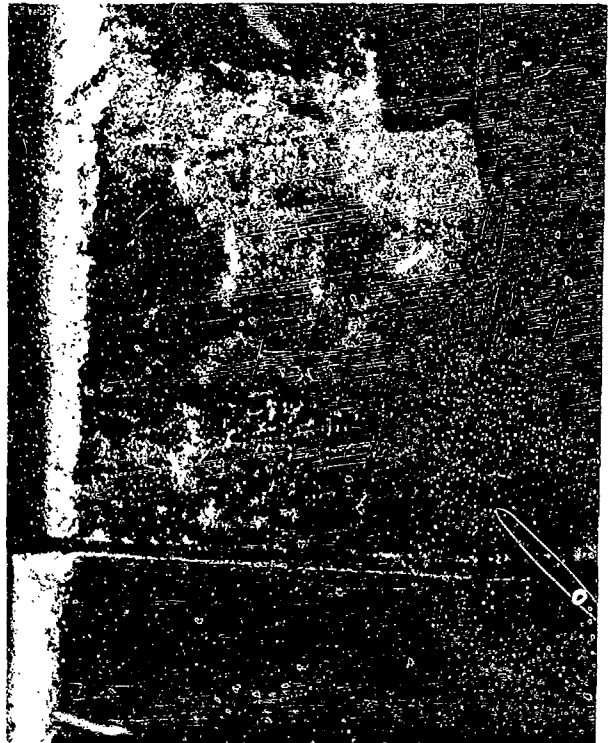
* Diamond pyramid hardness (DPH) conversions.

SUMMARY: Transverse cracking of the number one bearing oil pressure tube was the result of liquid metal embrittlement by silver braze. The embrittlement probably occurred during manufacture when the braze joint was overheated, allowing the braze metal to penetrate the grain boundaries and reduce their strength. The part should not see the temperatures required for braze melting to occur in service. No other material or microstructural anomalies were found in the base metal.



FAL 80846

MAG: 2 1/2X



FAL 80849

MAG: 8X

FIGURE 8-123: Overall view of the end pressure tube containing the crack (arrow). The tube has been sectioned for examination.

FIGURE 8-124: Close-up of the of crack adjacent to a braze joint. Residual silver braze is visible surrounding the crack.



FAL 93465

MAG: 10X

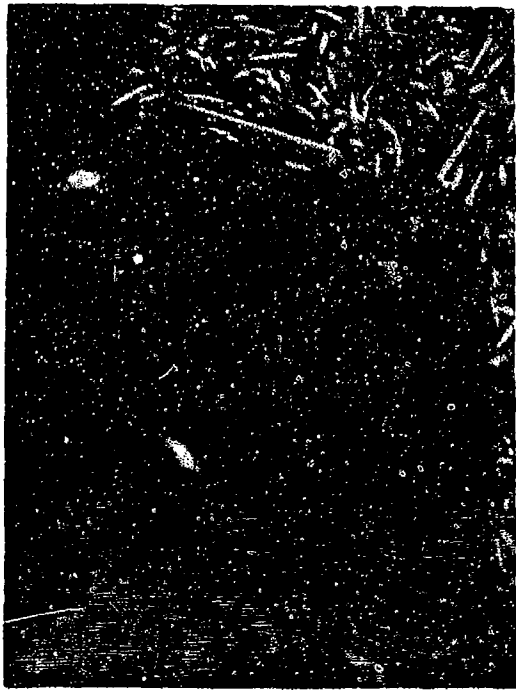


FAL 93463

MAG: 500X

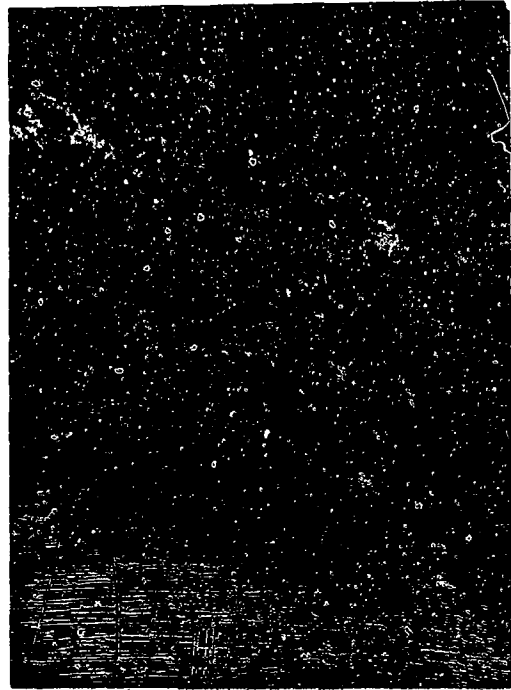
FIGURE 8-125: Overall photograph of the opened crack surface (arrows).

FIGURE 8-126: Ductile overstress dimples. The fracture generally appeared to be intergranular.



FAL 93467

MAG: 80X



FAL 93468

MAG: 80X

FIGURE 8-127: SEM photograph and associated XES elemental map showing the concentration of silver on the opened crack surface and penetrating into the other grain boundaries. The light areas on the X-ray map indicate concentrations of silver.

SERVICE FAILURE

FRACTURE MODE Intergranular Overstress (liquid metal embrittlement)

PART NAME Exhaust Duct Pressure Probe Rake

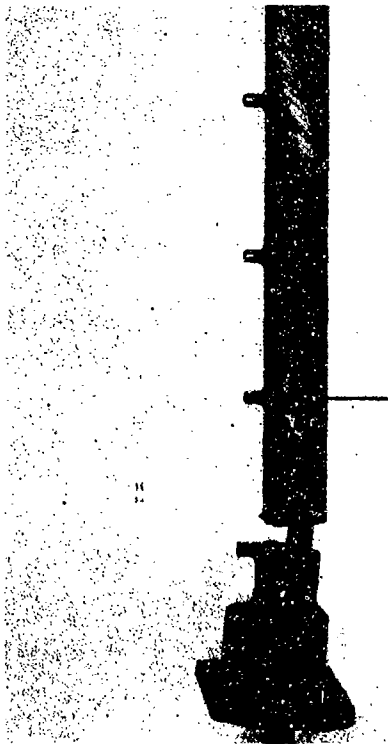
OPERATION DATA The part operates as a pressure probe inserted into the turbine exhaust path. It is subjected to static as well as cyclic loading.

PART TIME 37 hours

	<u>REQUIRED</u>	<u>ACTUAL</u>
MAT'L	BASE <u>Inconel 600</u>	<u>confirmed</u>
	OTHER <u>Braze: 54Ag-40Cu-5Zn-1Ni</u>	<u>confirmed</u>
HARDNESS	<u>Base: HB 134-241</u>	<u>HB 161-194 *</u>
GRAIN SIZE	<u>No Requirement</u>	<u>ASTM 3-4</u>
DIMENSIONAL	<u>Shell thickness: 0.025-0.035 inch</u>	<u>0.031-0.036 inch</u>

* Diamond pyramid hardness (DPH) conversions.

SUMMARY: The fracture adjacent to the first (outboard) hypo-tube and the crack adjacent to the second hypo-tube were the result of liquid metal embrittlement (stress alloying). This resulted when the silver base braze used to join the hypo-tubes to the shell melted. The liquid silver alloy penetrated along the grain boundaries of the Inconel 600 causing them to become weak and crack. It could not be determined whether the embrittlement occurred during manufacturing or was due to engine operation. The estimated gas path temperature in this area was determined to approach the temperature required to remelt the braze.



FAL 89206

MAG: 3/4X



FAL 89209

MAG: 4X

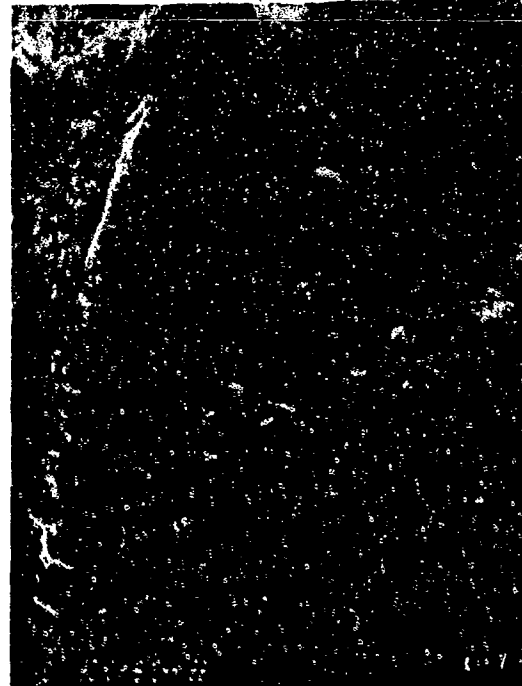
FIGURE 8-128: Overall photograph of the pressure probe rake showing the fracture adjacent to the first hypo-tube and a crack at the second hypo-tube (arrow).

FIGURE 8-129: Close-up photograph of the fracture surface. The extent of the oxidation indicates that the fracture started at the forward side (arrow).



FAL 93331

MAG: 20X

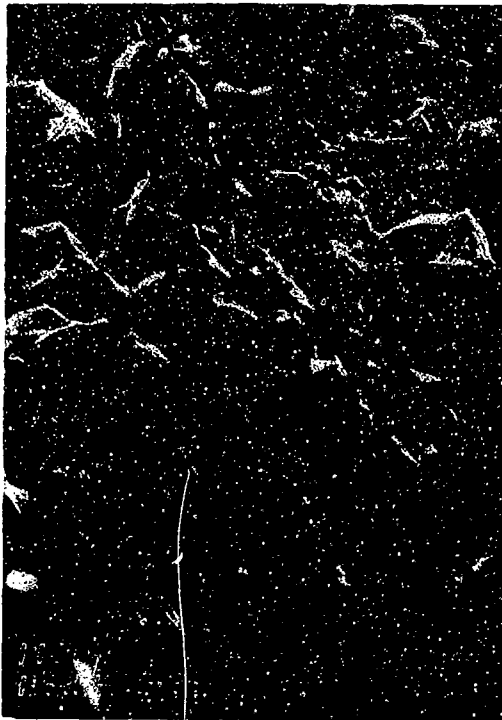


FAL 93330

MAG: 100X

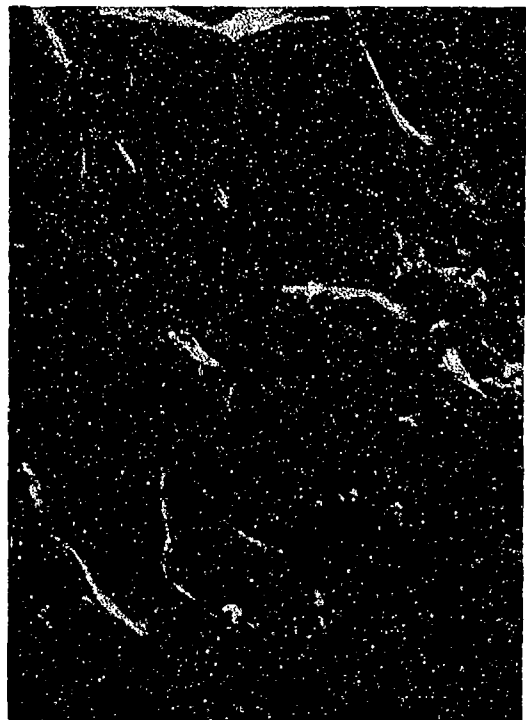
FIGURE 8-130: SEM photograph of the opened crack surface adjacent to the second hypo-tube.

FIGURE 8-131: Higher magnification photograph showing the intergranular nature of the crack.



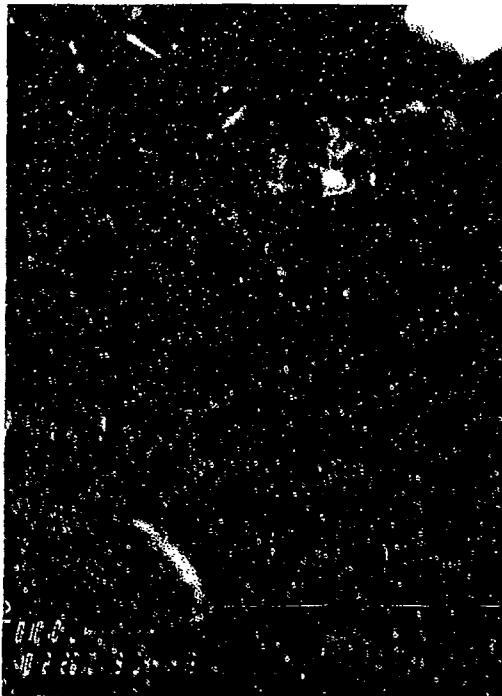
FAL 93333 MAG: 300X

FIGURE 8-132: Intergranular fracture with residual silver-rich braze on the fracture surface (arrow).



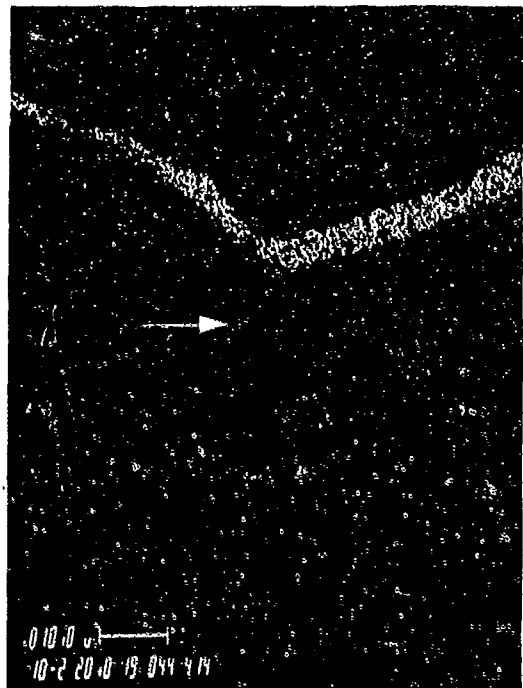
FAL 93332 MAG: 1000X

FIGURE 8-133: Intergranular fracture with grain boundary separation.



FAL 93334 MAG: 1000X

FIGURE 8-134: SEM photograph of a metallographic section through the opened crack surface showing a layer of silver at the grain boundaries.



FAL 93335 MAG: 1000X

FIGURE 8-135: SEM/XES elemental map showing silver braze on the crack surface and penetrating the grain boundaries (arrow).

Inconel X-750

Material Description

Inconel X-750 is a precipitation hardenable corrosion and heat resistant nickel-chromium alloy. The alloy is strengthened by precipitation of a nickel-aluminum-titanium phase $Ni_3(Ti, Al)$. The alloy is primarily used in parts requiring high strength at temperatures up to 1100 F such as bolts and turbine rotors. Although most of the effect of precipitation hardening is lost above 1300 F the alloy maintains usable strength and oxidation resistance to 1800 F.

The material used in this study was heat treated to AMS 5667 with a required hardness of BHN 302-363. The typical room temperature mechanical properties for AMS 5667 are as follows:

Ultimate Tensile Strength (min):	165 ksi
0.2% Yield Strength (min):	105 ksi
Percent Elongation (min):	20%
Percent Reduction in Area (min):	15%

	<u>Required</u>	<u>Measured</u>
ASTM Grain Size:	-	15.5
Measured Hardness:	BHN 305-344 (HRC conversion)	

Fractography Overview

All four Inconel X-750 tensile specimens exhibited similar features in the primary fracture areas. They were all primarily dimpled overstress with slightly different degrees of intergranular and quasi-cleavage features. The smooth specimens had a more ductile appearance, with the 1100 F specimen exhibiting the lowest percentage of quasi-cleavage features. This specimen also had the largest shear lip, 0.045 inch, compared to 0.037 inch for the smooth room temperature specimen and 0.004 and 0.006 inch for the room temperature and 1100 F notched specimens, respectively. Fine shear dimples were present on the smooth specimen shear lips. The stress rupture specimen exhibited oxidized coarse dimpled rupture with a moderate 0.023 inch shear lip. No intergranular or cleavage features were observed.

Six HCF specimens were tested: three each notched and smooth at room temperature, 800 F and 1100 F. The smooth room temperature specimen exhibited a single local origin with a Stage I facet at the specimen surface. The features adjacent to the origin were a mixture of fine feathery cleavage and larger plateaus containing striations. The 800 F and 1100 F specimens propagated from multiple origins located along a small arc along the surface. Multiple Stage I facets at the surface were followed by cleavage and feathery cleavage along with plateaus containing striations near the origin. Both of these specimens had a larger percentage of cleavage features than the room temperature specimen. The room temperature

specimen exhibited well developed striations in the Stage II fatigue propagation area. Neither the 800 F nor the 1000 F specimens had clearly resolvable striations. Both exhibited a mixture of quasi-cleavage with smooth patches of what appeared to be cleavage. These patches may contain striations that are not resolvable in the SEM. Macroscopically the room temperature specimen had a clearly defined fatigue progression extending over 75% of the specimen cross section. Neither of the elevated temperature specimens had visible fatigue progression. Final overstress in all three specimens exhibited dimpled overstress and quasi-cleavage.

Macroscopically, the three notched specimens appeared similar. The only clear difference was that the room temperature and 1100 F specimens propagated from multiple surface origins separated by steps, while the 800 F specimen had a single localized origin area. All three specimens had fatigue progression through greater than 75% of the cross section with shear lips visible in the overstress areas. The origin areas on the room temperature and 800 F specimens exhibited several Stage I facets in a very localized area at the surface, followed by an area containing multiple cleavage facets at various angles to the stress axis. As the fatigue crack progressed patches of fine striations separated by quasi-cleavage and then coarser well developed striations covering the entire field of view were observed. The 1100 F specimen had smoother origins exhibiting feathery cleavage. Clear striations covered the surface very close to the origins with coarser poorly defined striations and crack-like striations near the center of the specimen.

The two LCF specimens (800 F and 1100 F) exhibited markedly different appearances both macroscopically and microscopically. The 800 F specimen had a single surface origin at a titanium-rich inclusion. The fatigue origin area exhibited a faceted appearance with no striations visible. The fatigue propagated on a plane perpendicular to the stress axis with well developed striations towards the end of the Stage II area. Final overstress occurred on an angle to the stress axis. The 1100 F specimen had two oxidized fatigue progression thumbnails 180° apart. Both areas had single surface origins and an oxidized intergranular appearance. Oxidized fatigue striations were visible at high magnification on transgranular patches near the origin. Only remnant fatigue features were observed near the ends of the thumbnails. Final overstress occurred at an angle to the stress axis.

Both in-phase and out-of-phase TMF specimens propagated from multiple surface origins. The in-phase specimen had both O.D. and I.D. origins while the out-of-phase specimen had only I.D. origins. The appearance of the in-phase specimen was very similar to the 1100 F LCF specimen, having an oxidized intergranular appearance. No striations were observed. The out-of-phase specimen propagated from an almost continuous series of I.D. surface origins separated by small steps. The areas directly adjacent to the surface were smooth and heavily oxidized. As the fatigue progressed, heavily oxidized well developed striations covered the fracture. Fine equiaxed dimples were observed in the final overstress area.

MATERIAL

Inconel X-750
AMS 5667 Bar

TEST DATA

TEST TYPE

Smooth Tensile

TEST CONDITIONS

Strain Rate: 0.005 mm/mm/min (0.005 in/in/min)
Atmosphere: Air
Temperature: Room Temperature
Test Direction: Longitudinal

TEST RESULTS

0.2% Yield Strength:	898.4 MPa (130,300 PSI)
Ultimate Strength:	1265.9 MPa (183,600 PSI)
Percent Elongation:	25.5
Percent Reduction of Area:	46.1



FAL 92553

MAG: 12X

Figure 9-1: Test results and fractography of Inconel X-750 room temperature smooth tensile test. The final overstress area (shear lip) appears shiny due to smearing. The center of the specimen has a granular appearance.



FAM 99833

MAG: 200X

FIGURE 9-2: Optical photomicrograph showing the primary fracture area exhibiting a mixed transgranular and intergranular fracture path. Carbides are visible dispersed throughout the microstructure.

Etchant: Glyceregia

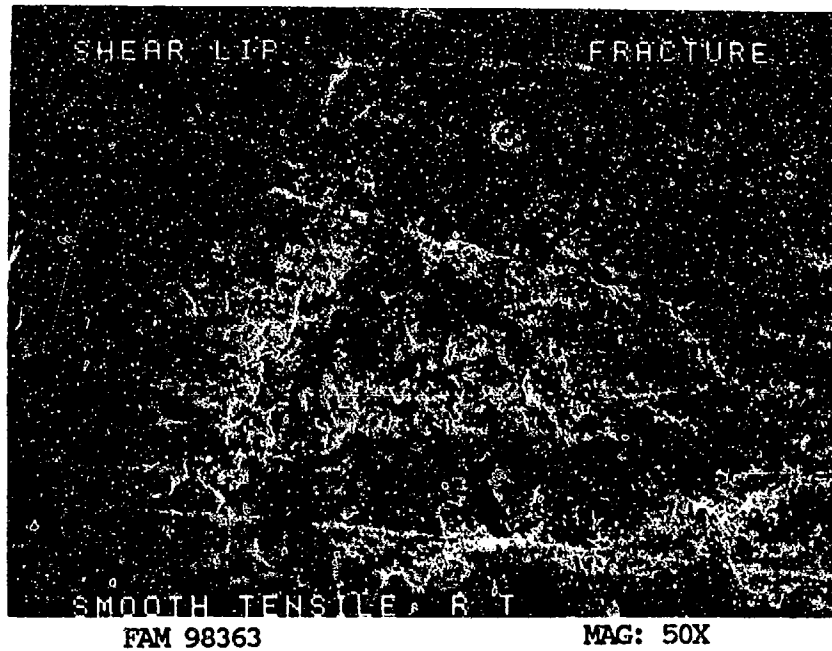


FIGURE 9-3: Low magnification view showing the primary fracture area near the center of the specimen and the final fracture (shear lip) along the edge of the specimen.

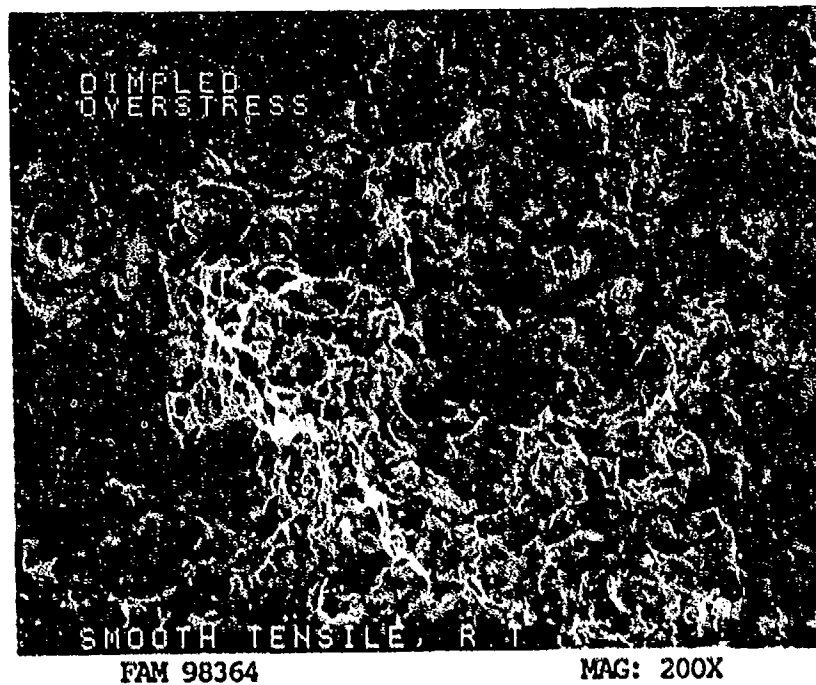


FIGURE 9-4: Primary fracture area exhibiting dimpled overstress with slight intergranular character.

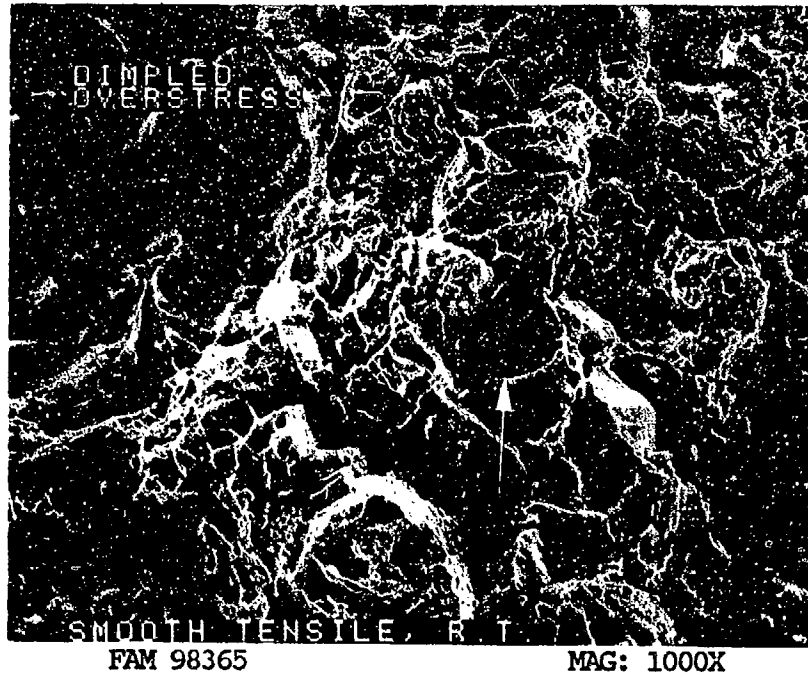


FIGURE 9-5: Fine equiaxed dimples with slight intergranular appearance. Fractured carbides are visible in some areas (arrow).

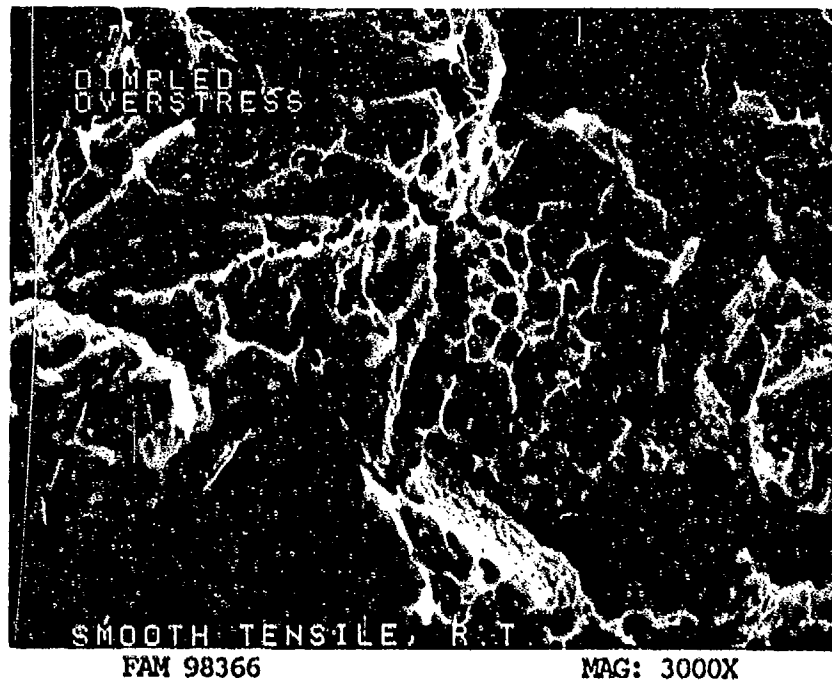


FIGURE 9-6: Higher magnification photograph of the area shown in Figure 9-4 showing fine equiaxed dimples and fractured carbides.

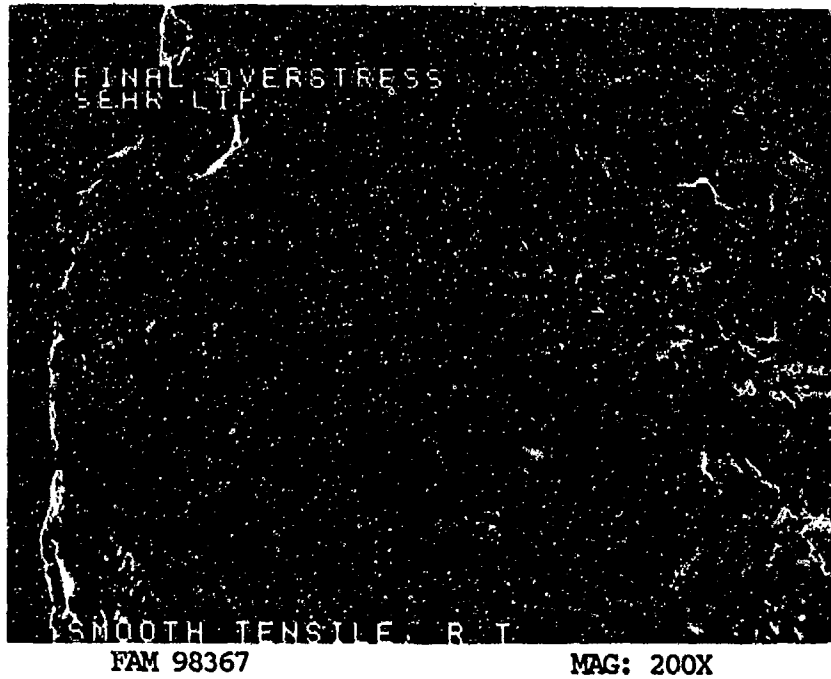


FIGURE 9-7: Final overstress area (shear lip).

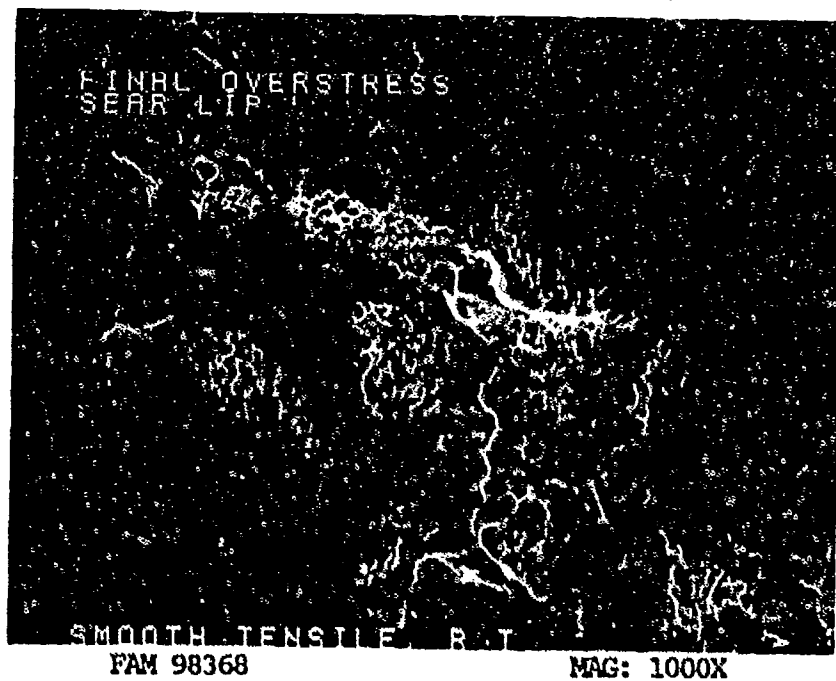


FIGURE 9-8: Higher magnification view of the final overstress area (shear lip) showing fine smeared shear dimples. The directions of relative motion is shown by arrows.

MATERIAL

Inconel X-750
AMS 5667 Bar

TEST DATA

TEST TYPE

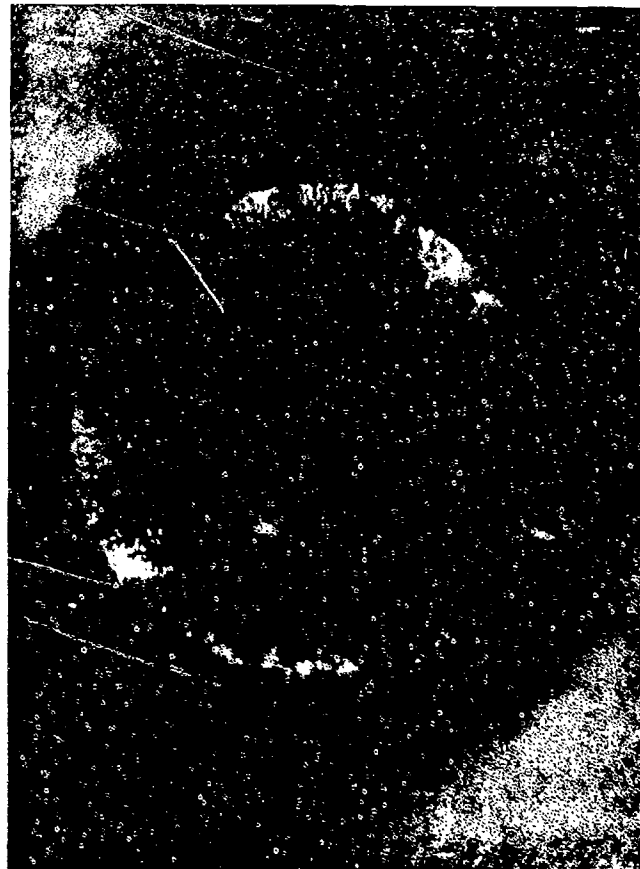
Smooth Tensile

TEST CONDITIONS

Strain Rate: 0.005 mm/mm/min (0.005 in/in/min)
Atmosphere: Air
Temperature: 593°C (1100°F)
Test Direction: Longitudinal

TEST RESULTS

0.2% Yield Strength:	768.1 MPa (111,400 PSI)
Ultimate Strength:	1125.9 MPa (163,300 PSI)
Percent Elongation:	20.0
Percent Reduction of Area:	37.1



FAL 92552

MAG: 10X

FIGURE 9-9: Test results and fractography of Inconel X-750 593°C (1100°F) smooth tensile test. The shear lip (bracket) is larger but not as clearly defined as on the room temperature specimen (Figure 9-1).

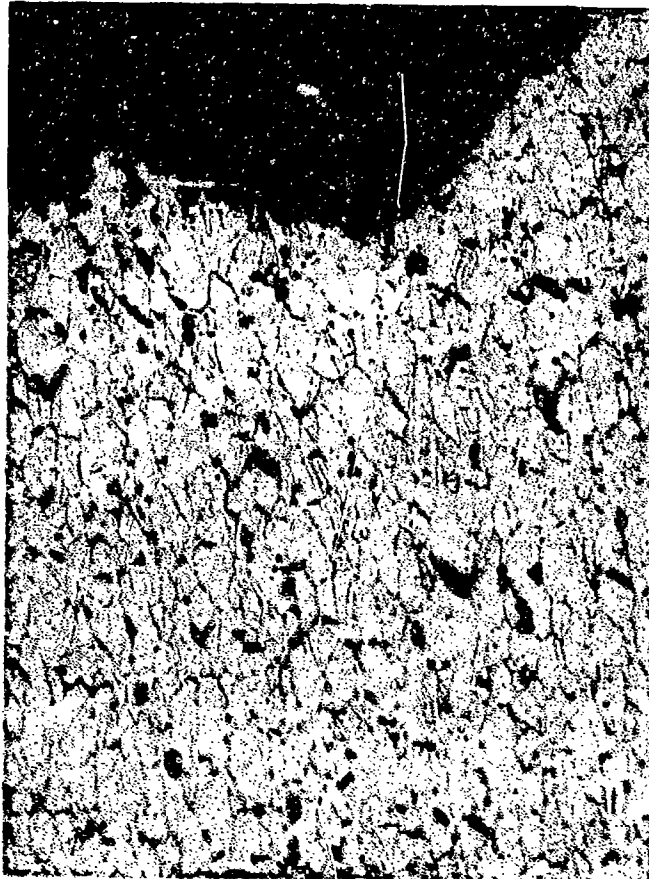


FIGURE 9-10: Optical photomicrograph showing the primary fracture area, exhibiting a predominantly transgranular fracture path. Carbides and voids are visible in the microstructure.

Etchant: Glyceregia

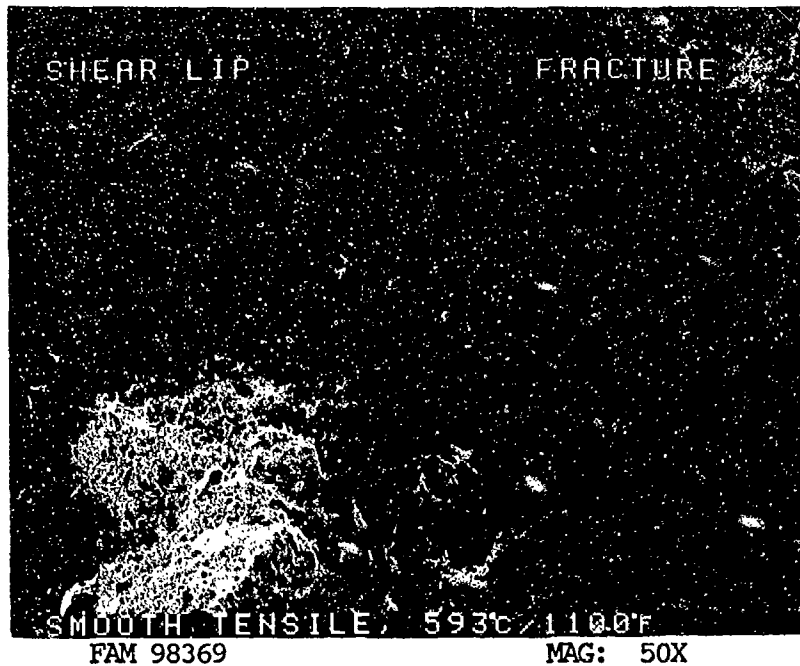


FIGURE 9-11: Overall view showing the primary fracture in the center of the specimen and a small area of final overstress (shear lip) along the edge of the specimen.

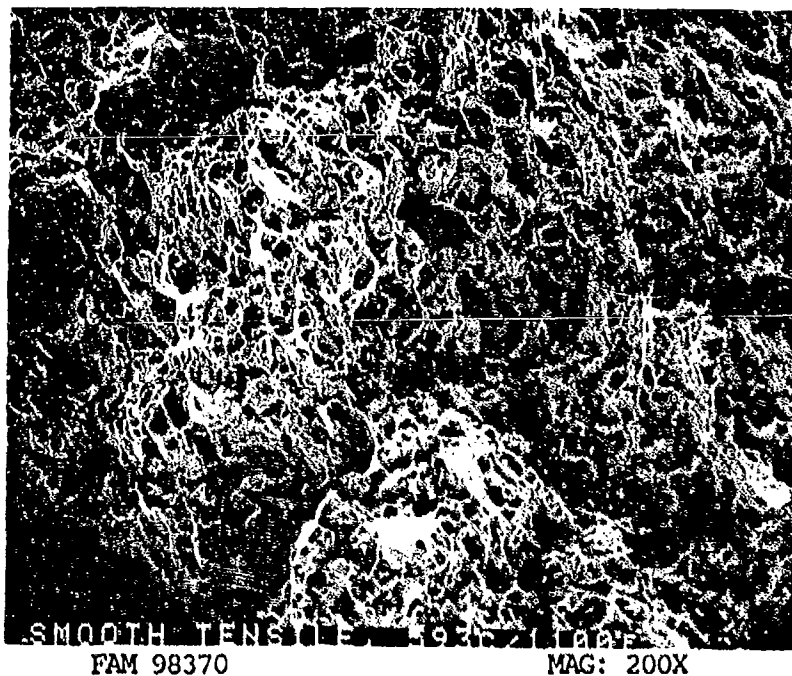


FIGURE 9-12: Dimpled overstress in the primary fracture area.

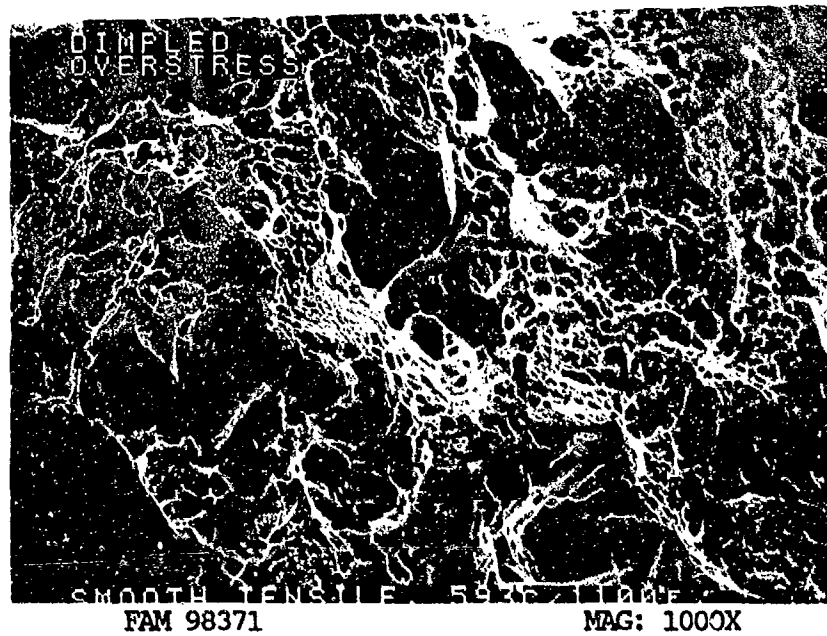


FIGURE 9-13: Fine equiaxed dimples in the primary fracture area. A fractured carbide is visible (arrow).

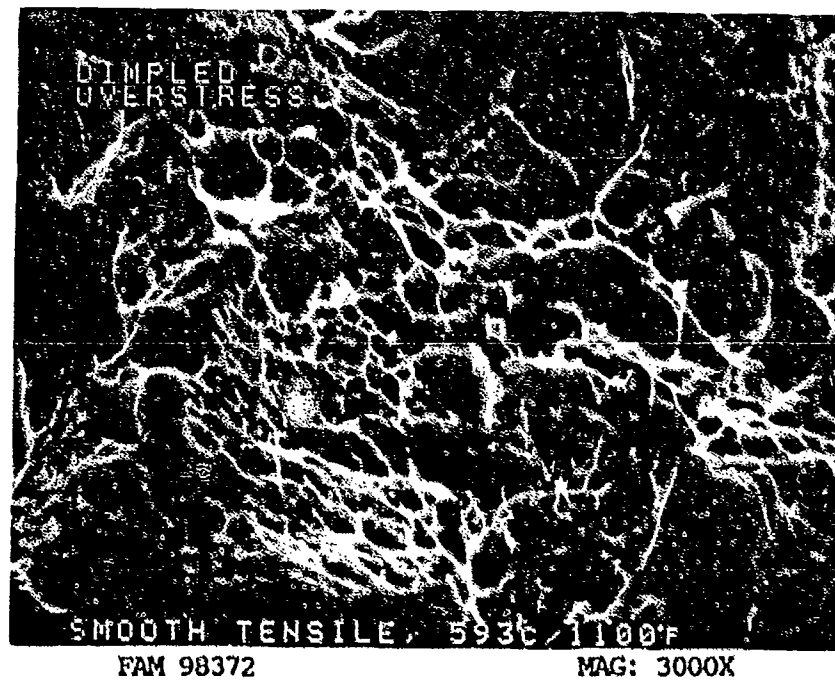


FIGURE 9-14: Higher magnification photograph of the area shown in Figure 9-13, showing fine equiaxed dimples in the primary fracture area.

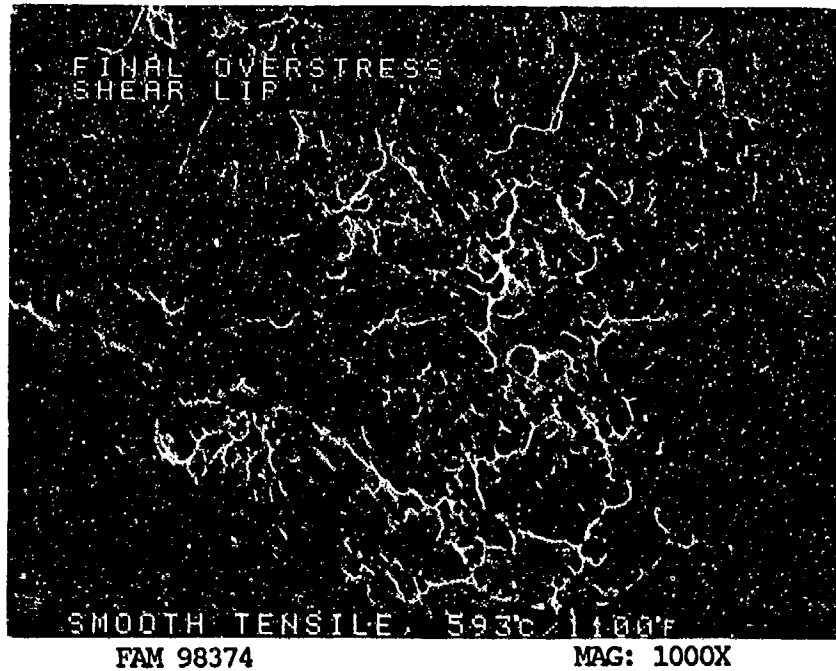


FIGURE 9-15: Fine smeared shear dimples in the final overstress (shear lip) area.

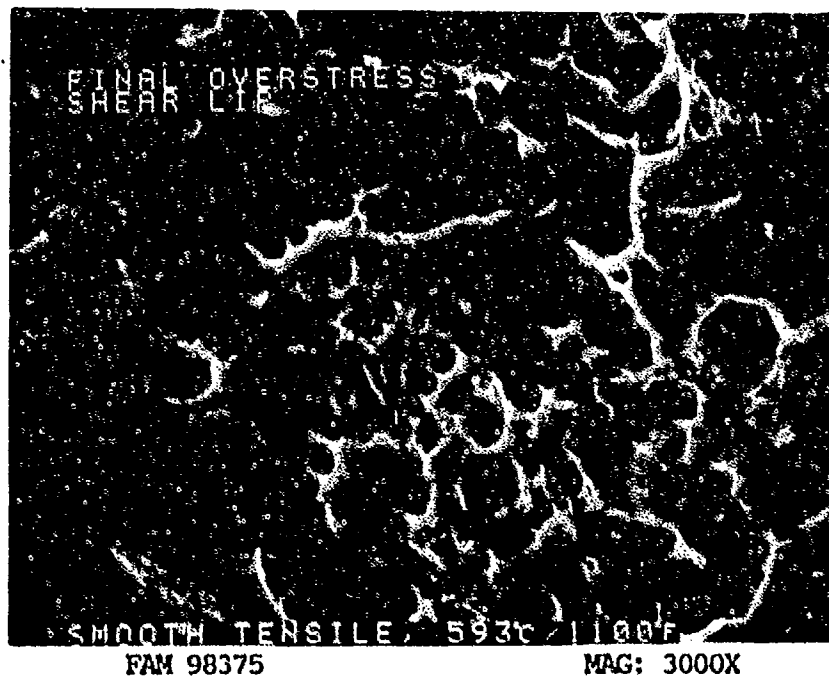


FIGURE 9-16: Higher magnification photograph of the area shown in Figure 9-15, showing fine shear dimples.

MATERIAL

Inconel X-750
AMS 5667 Bar

TEST DATA

TEST TYPE

Notched Tensile

TEST CONDITIONS

Crosshead Speed: 1.27 mm/min (0.05 in/min)

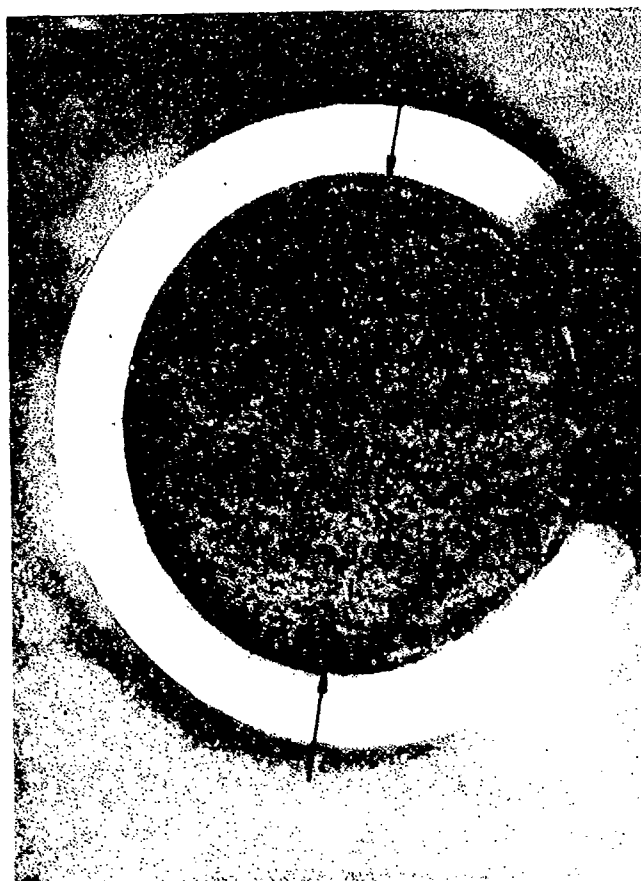
Atmosphere: Air

Temperature: Room Temperature

Test Direction: Longitudinal

TEST RESULTS

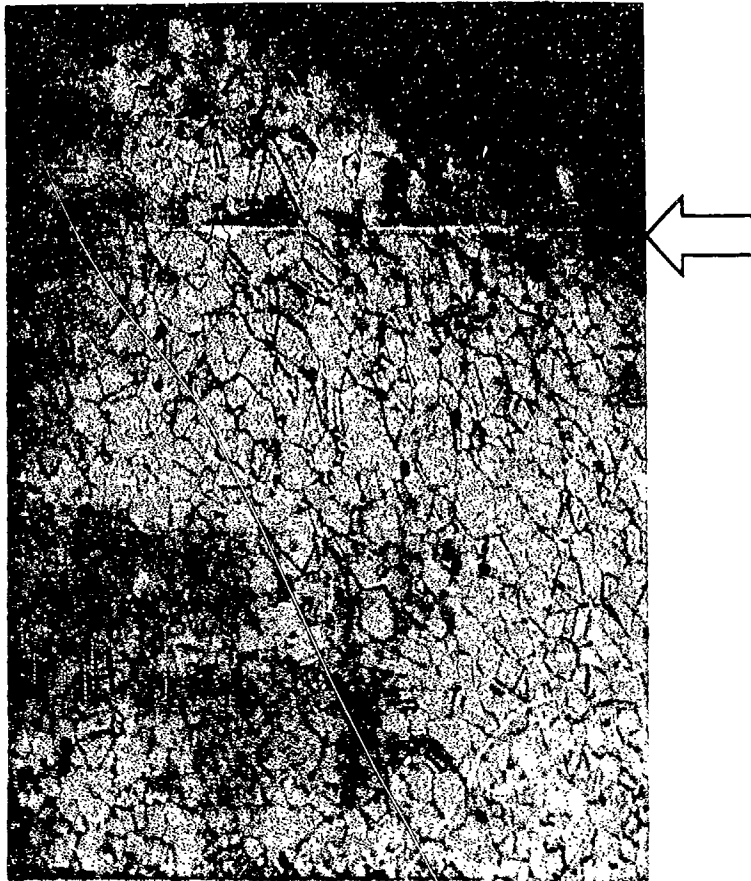
Ultimate Strength: 1605.1 MPa (232,800 PSI)



FAL 92551

MAG: 10X

FIGURE 9-17: Test results and fractography of Inconel X-750 room temperature notched tensile test. A very small discontinuous shear lip is visible (arrows) along the edge of the specimen.



FAM 99830

MAG: 200X

FIGURE 9-18: Optical photomicrograph showing the primary fracture area on the left side of the photograph and the final overstress area at the base of the notch on the right side of the photograph (arrow). The fracture propagated in both transgranular and intergranular modes. The grains in the final overstress area exhibit some plastic deformation.

Etchant: Glyceregia

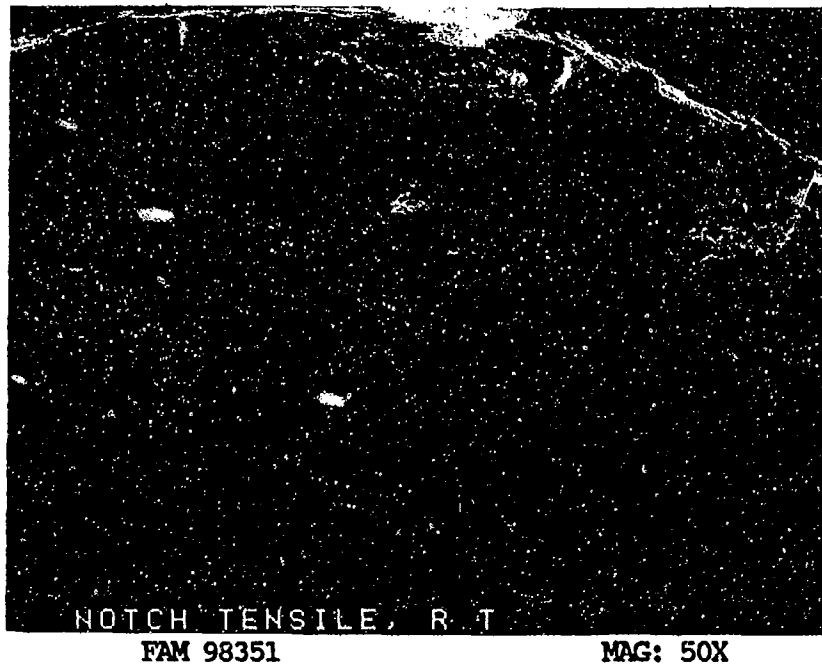


FIGURE 9-19: Low magnification view showing a very small final overstress area (shear lip). The extent of the shear lip is shown by brackets. The remainder of the fracture exhibits a mixture of transgranular and intergranular features.

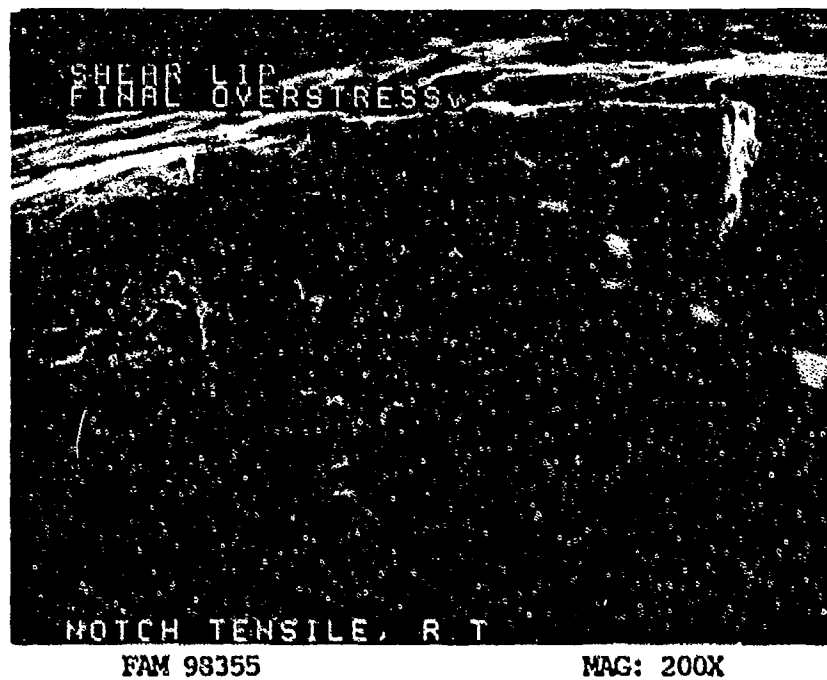


FIGURE 9-20: Higher magnification photograph including the shear lip area. The primary fracture has a slightly intergranular appearance.



FIGURE 9-21: Dimpled overstress in the primary fracture area. The fracture has a mixed intergranular/transgranular appearance. Fractured carbides are visible (arrows).

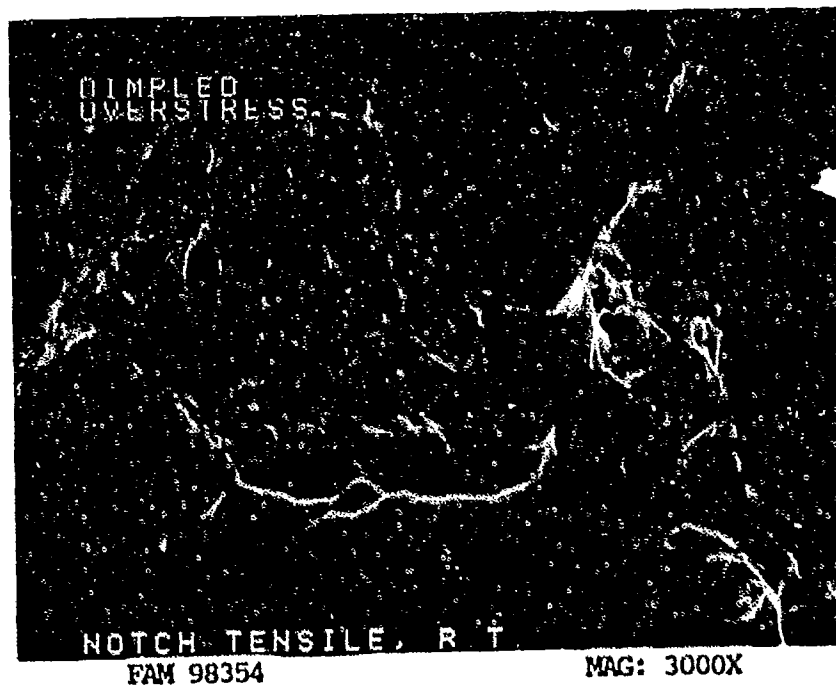


FIGURE 9-22: Higher magnification photograph of the area shown in Figure 9-21, showing equiaxed dimples in the primary fracture area.

MATERIAL

Inconel X-750
AMS 5667 Bar

TEST DATA

TEST TYPE

Notched Tensile

TEST CONDITIONS

Crosshead Speed: 1.27 mm/min (0.05 in/min)

Atmosphere: Air

Temperature: 593°C (1100°F)

Test Direction: Longitudinal

TEST RESULTS

Ultimate Strength: 1378.9 MPa (200,000 PSI)



FAL 92550

MAG: 10X

FIGURE 9-23: Test results and fractography of Inconel X-750 593°C (1100°F) notched tensile test. A discontinuous narrow shear lip is visible along the surface (arrows). The specimen appears oxidized.

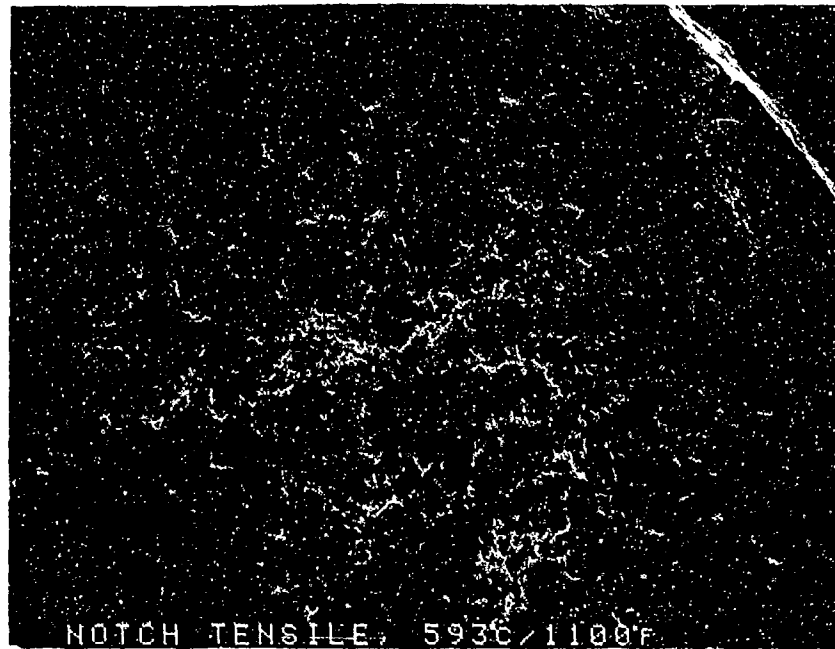


FAM 99828

MAG: 200X

FIGURE 9-24: Optical photomicrograph showing the primary fracture area on the left side of the photograph and the final overstress area (shear lip) at the base of the notch (arrow) on the right side of the photograph. The fracture propagated predominantly in an intergranular mode. The grains in the final overstress area exhibit some plastic deformation.

Etchant: Glyceregia



FAM 98357

MAG: 50X

FIGURE 9-25: Low magnification view showing primary overstress area and a very small final overstress area (shear lip) along the outside surface of the specimen (bracket).



FAM 98361

MAG: 200X

FIGURE 9-26: Small final overstress area (shear lip) along the outside surface. The shear lip was not present in all areas but its size varied.

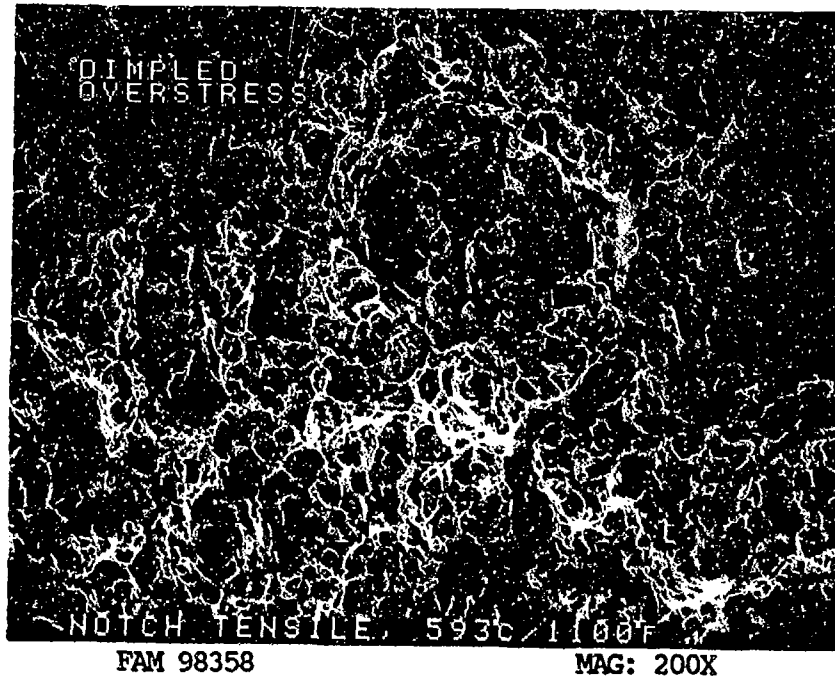


FIGURE 9-27: Equiaxed dimpled overstress in the primary fracture area. The fracture has a slightly intergranular appearance.

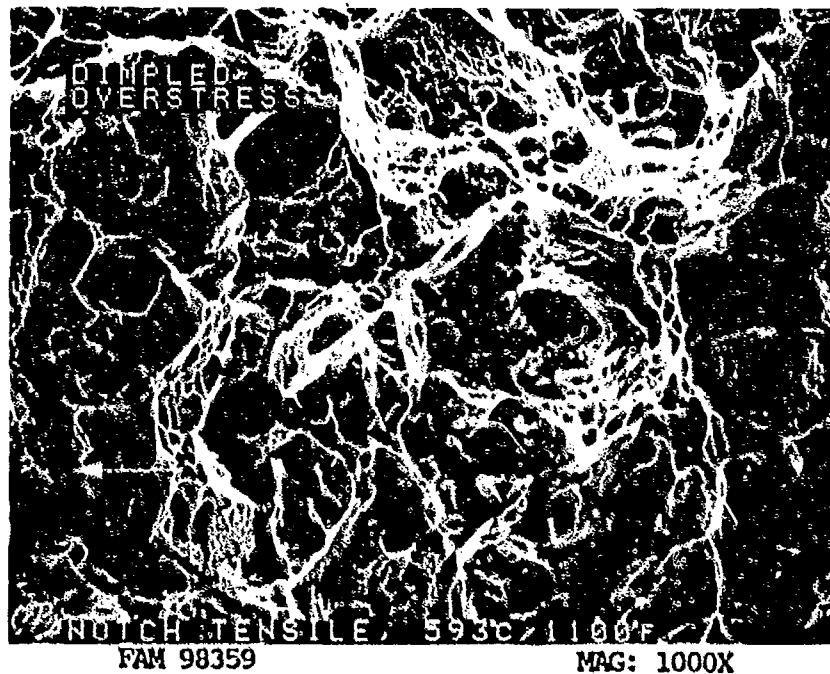


FIGURE 9-28: Mixed mode overstress exhibiting equiaxed dimpled overstress and small cleavage features in the primary fracture area. Secondary grain boundary separation is visible (arrow).

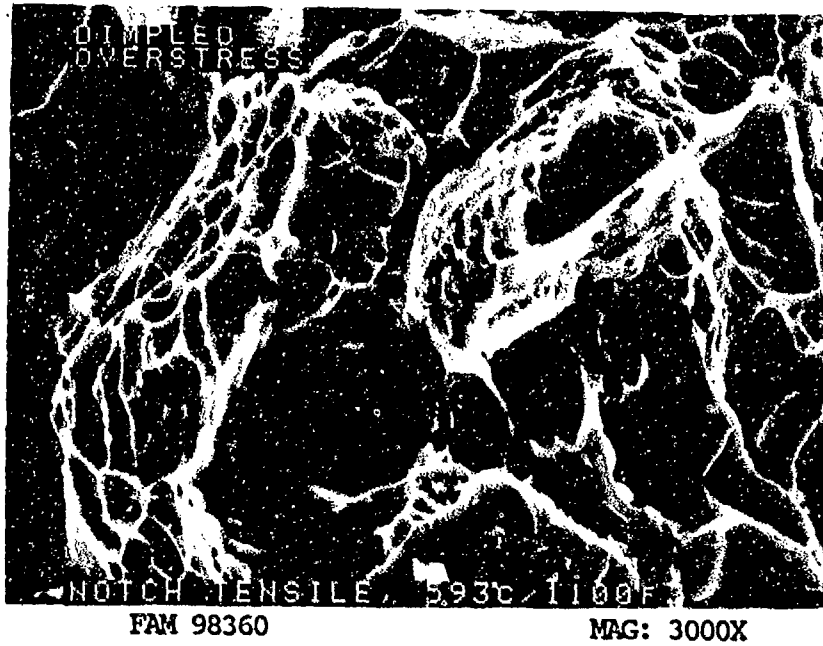


FIGURE 9-29: High magnification photograph showing dimples and fine cleavage features near the center of the specimen.

MATERIAL

Inconel X-750
AMS 5667 Bar

TEST DATA

TEST TYPE

Stress Rupture

TEST CONDITIONS

Stress: 723.9 MPa (105.0 ksi)

Atmosphere: Air

Temperature: 593°C (1100°F)

Test Direction: Longitudinal

TEST RESULTS

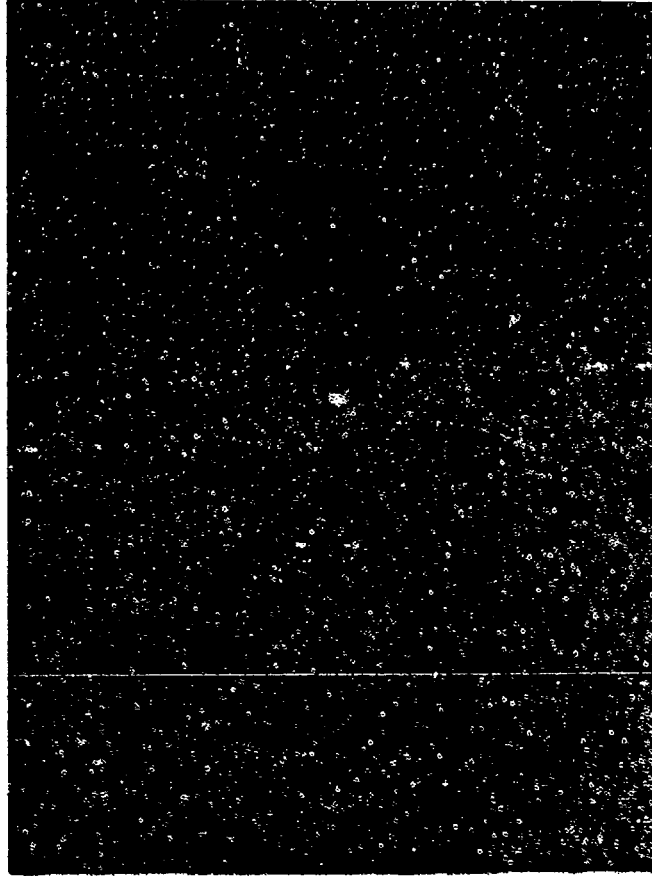
Time to Fracture: 3.9 hours



FAL 93826

MAG: 13X

FIGURE 9-30: Test results and fractography of Inconel X-750 593°C (1100°F) stress rupture test. The fracture exhibits a shear lip (arrows) with coarse oxidized features in the center of the specimen.



FAM 99861

MAG: 200X

FIGURE 9-31: Optical photomicrograph showing the primary fracture area near the center of the specimen. Substantial grain boundary separation has occurred throughout the matrix (arrows).

Etchant: Glyceregia

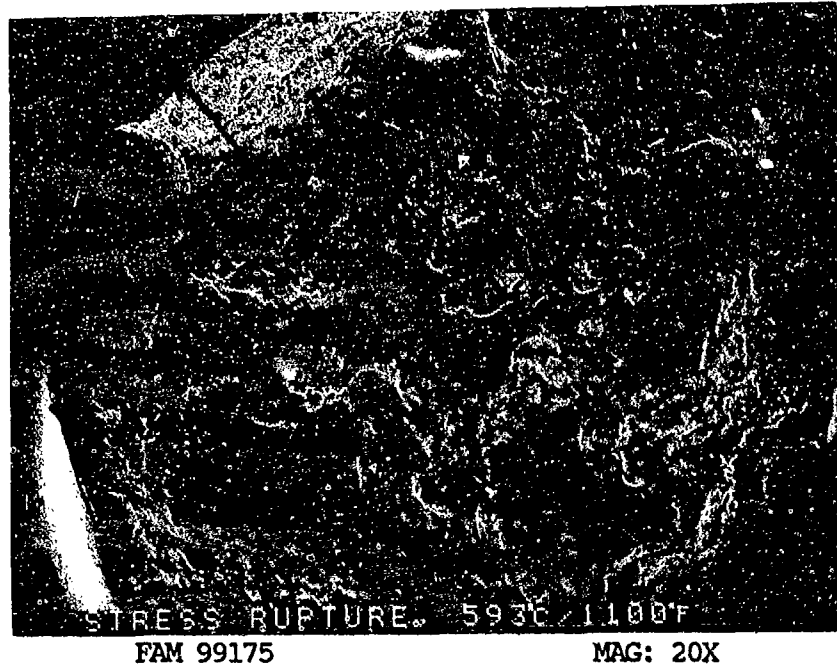


FIGURE 9-32: Low magnification view showing deep features in the primary rupture area and a large final overstress area (shear lip) along the outside surface of the specimen (brackets).

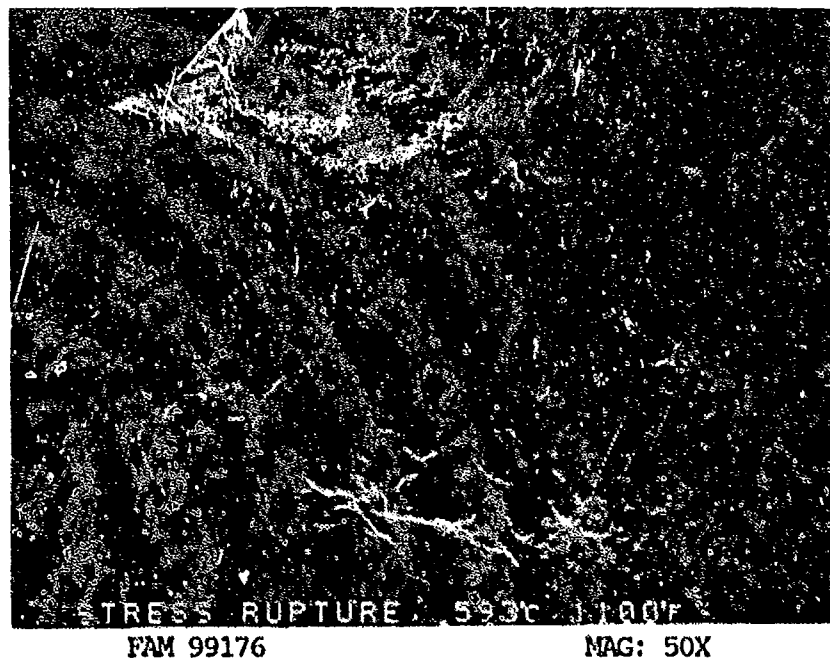


FIGURE 9-33: Large final overstress area (shear lip) along the outside surface. The shear lip was present in all areas but size and direction (up or down) varied.

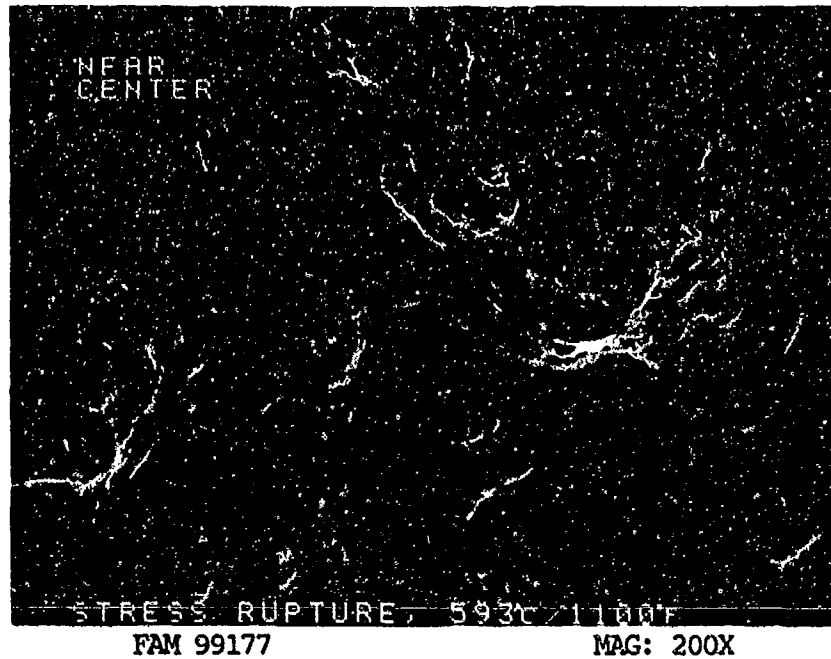


FIGURE 9-34: Oxidized dimpled rupture with void coalescence in the primary fracture area.

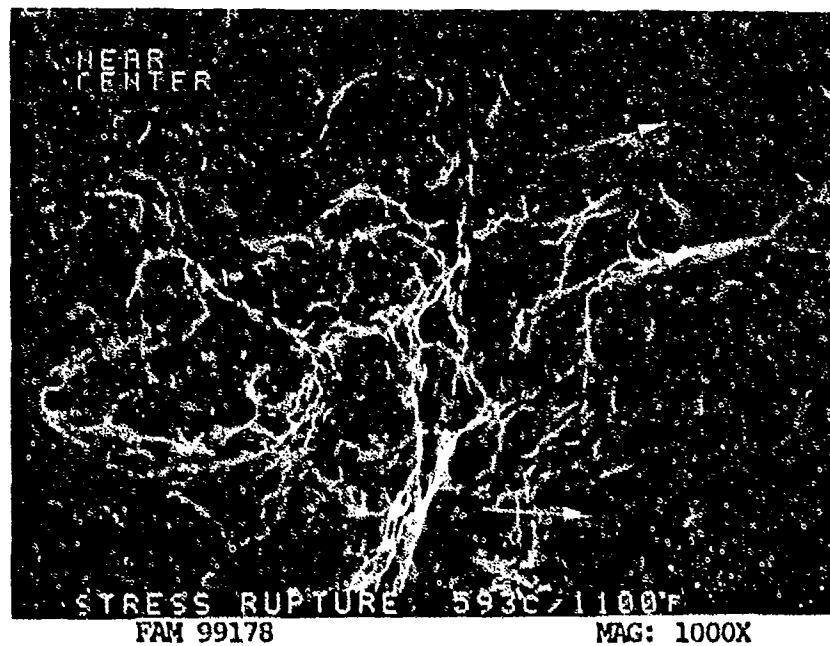


FIGURE 9-35: Higher magnification photograph of the area in Figure 9-34, showing coarse dimpled rupture with areas of void coalescence. The entire fracture surface is covered by a light oxide. Deep voids are shown by arrows.

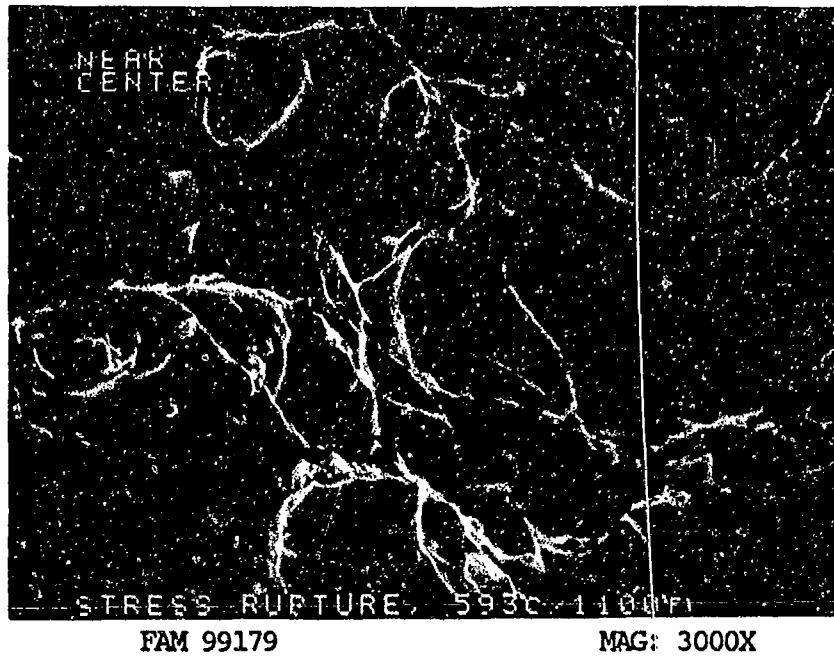


FIGURE 9-36: High magnification photograph showing coarse oxidized dimples with some finer dimples in between.

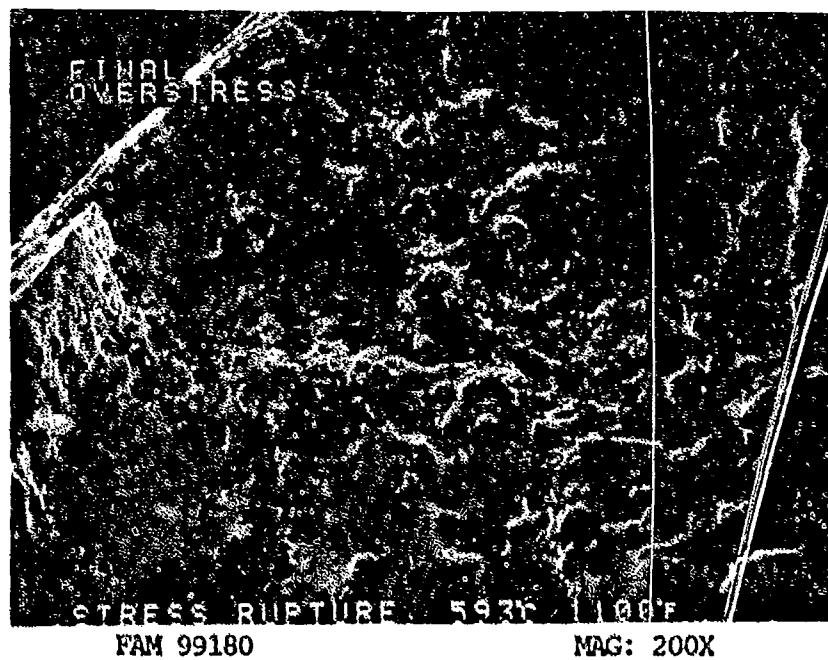
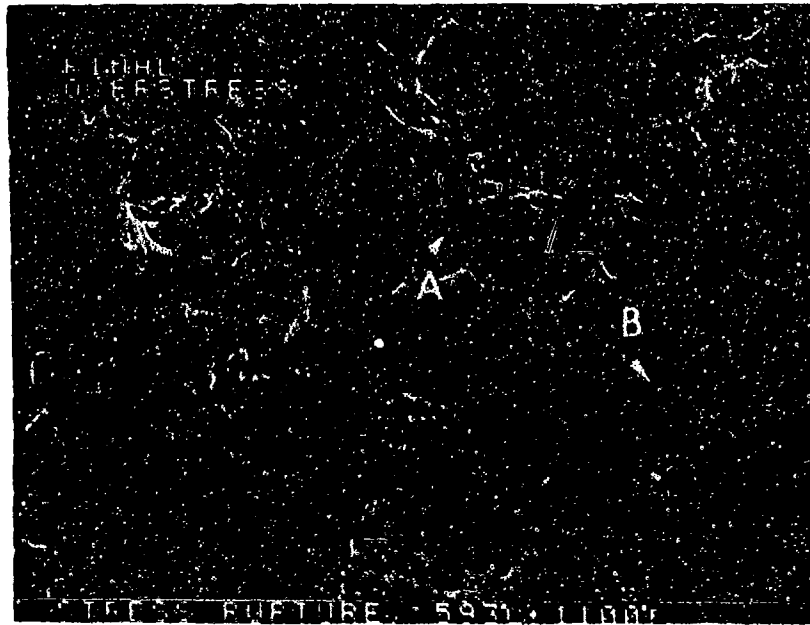


FIGURE 9-37: Final overstress area along the edge of the specimen.



FAM 99181

MAG: 1000X

FIGURE 9-38: Mixture of fine equiaxed dimples (arrow A) and shear dimples (arrow B) in the final overstress area.

MATERIAL

Inconel X-750
AMS 5667 Bar

TEST DATA

TEST TYPE
Smooth HCF

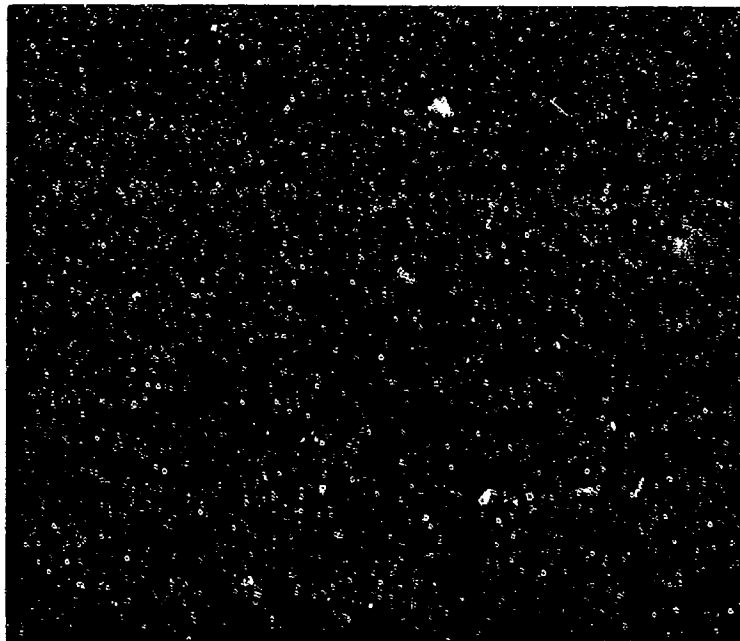
TEST CONDITIONS

Stress: 413.7 MPa (60.0 ksi)/ -413.7 MPa (-60.0 ksi) DNF*
482.6 MPa (70.0 ksi)/ -482.6 MPa (-70.0 ksi) DNF
551.6 MPa (80.0 ksi)/ -551.6 MPa (-80.0 ksi)
Stress Ratio: -1
Frequency: 1800 cpm
Atmosphere: Air
Temperature: Room Temperature
Test Direction: Longitudinal

TEST RESULTS

Cycles to Fracture: 1.84×10^6 (DNF); 5.5×10^5 (DNF); 2.3×10^5

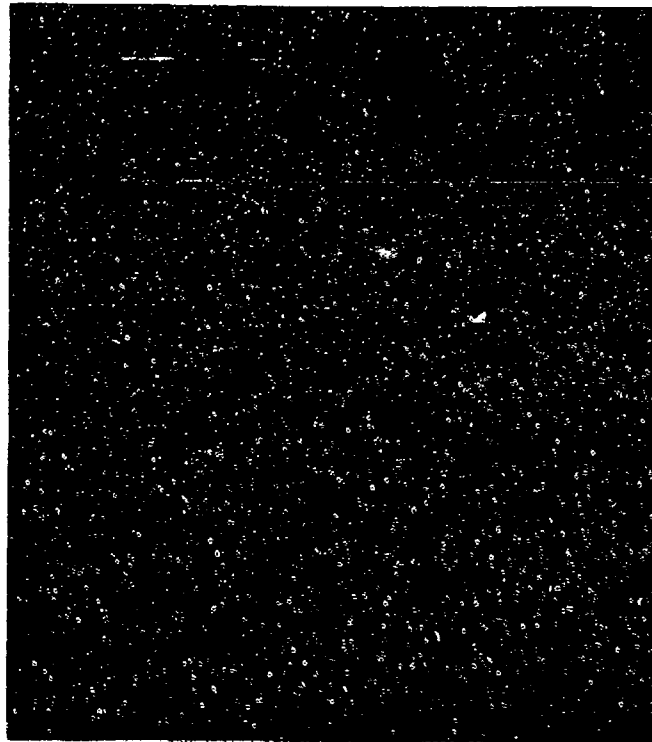
* Did Not Fracture



FAL 93832

MAG: 15X

FIGURE 9-39: Test results and fractography of Inconel X-750 room temperature smooth HCF test. The fatigue progression area extends over 75% of the specimen from an origin area near the bottom of the photograph (arrow). The final overstress area appears as a thumbnail at the top of the photograph.



FAM 100205

MAG: 100X

FIGURE 9-40: Optical photomicrograph showing a close-up of the fatigue progression area. No grain deformation is visible adjacent to the fracture. Fracture path is transgranular.

Etchant: Glyceresia

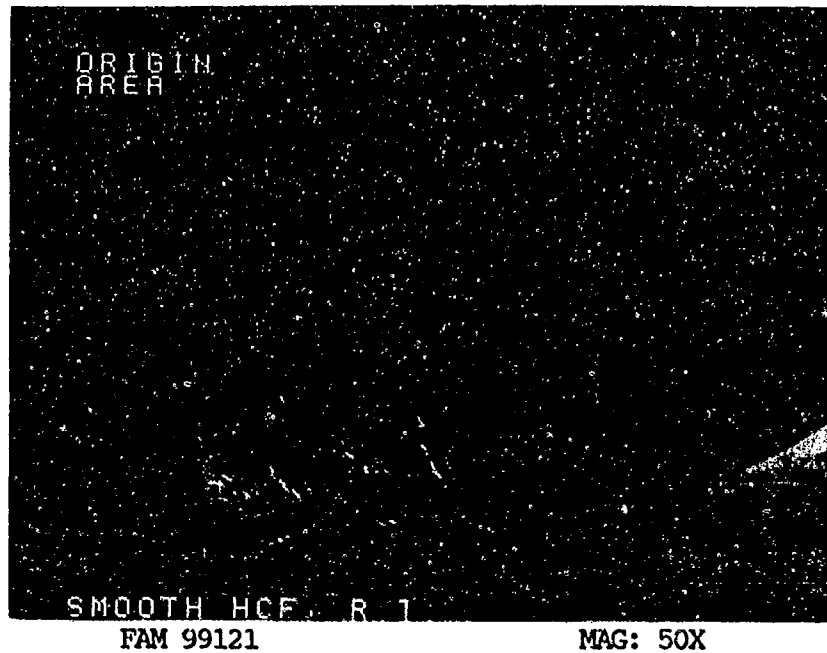


FIGURE 9-41: Overall photograph showing the origin area (arrow) and fatigue progression on a plane approximately perpendicular to the stress axis.

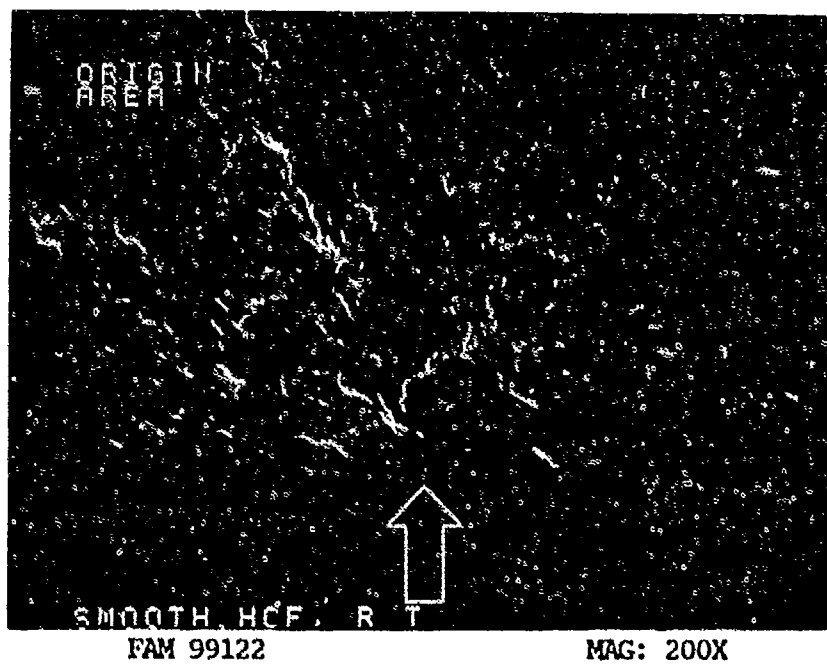


FIGURE 9-42: Higher magnification photograph of the origin area shown in Figure 9-41. A stage I fatigue facet is visible at the localized origin (arrow).

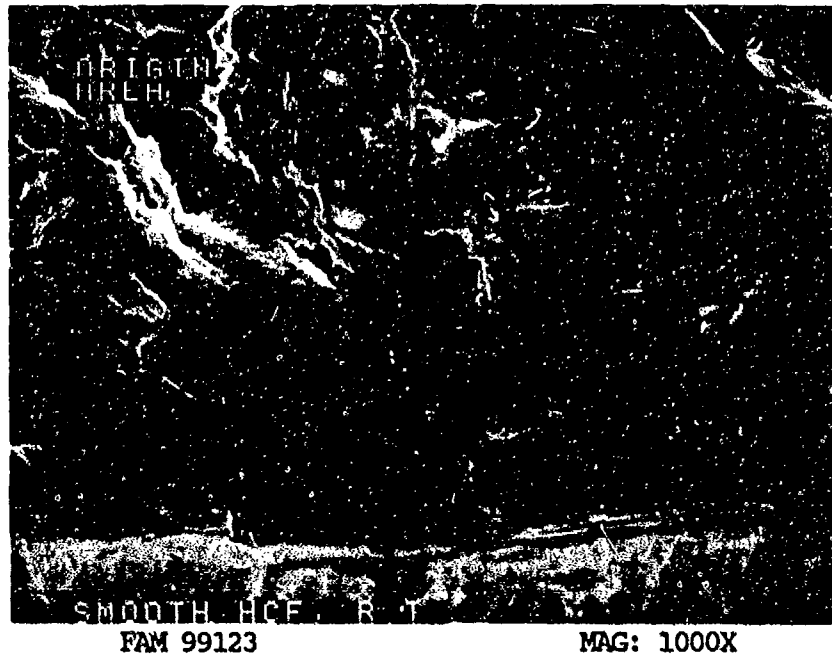


FIGURE 9-43: Stage I fatigue facet at the localized origin (see Figure 9-42). No defects are visible.

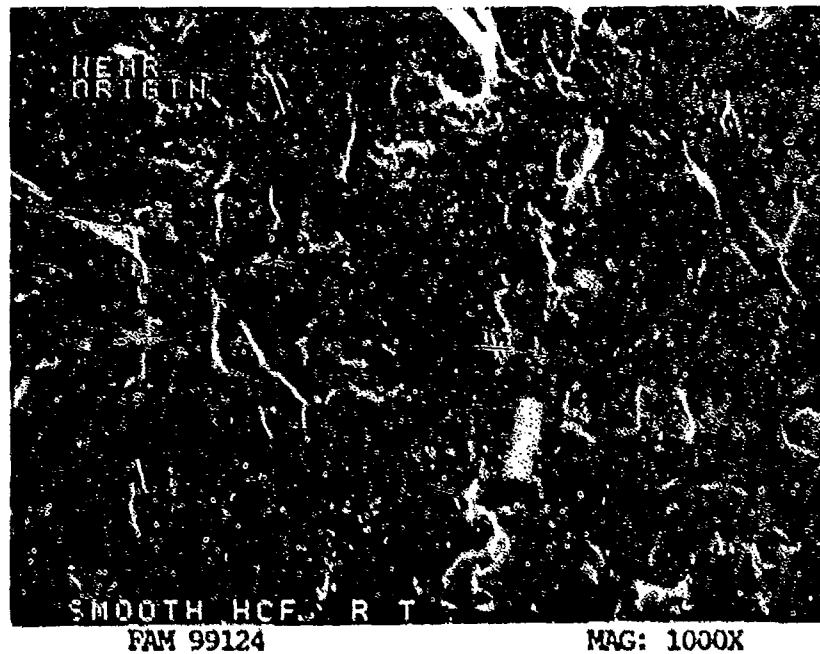


FIGURE 9-44: Photograph showing cleavage features near the origin. No striations are visible.

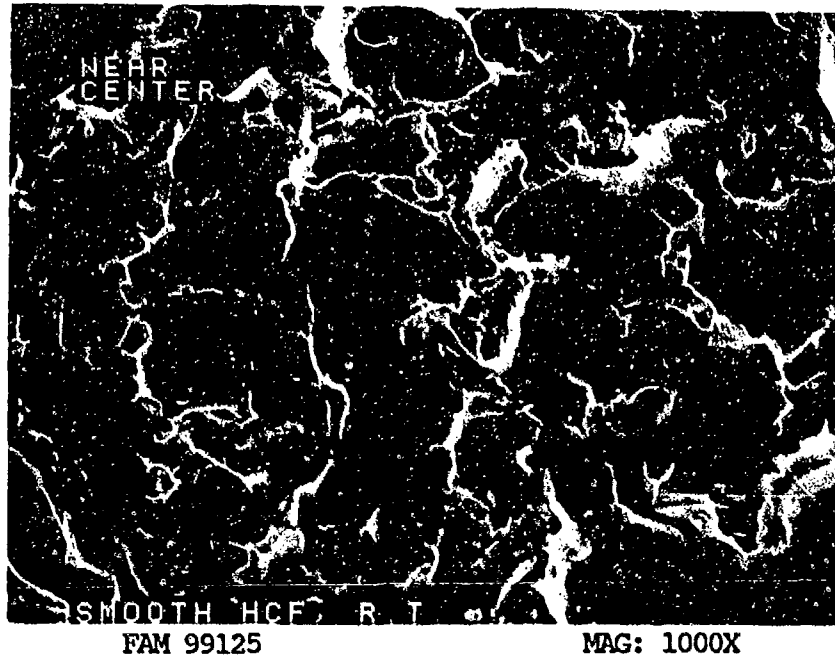


FIGURE 9-45: Fatigue striations near the end of the fatigue progression area. The direction of propagation is from bottom to top of the photograph.

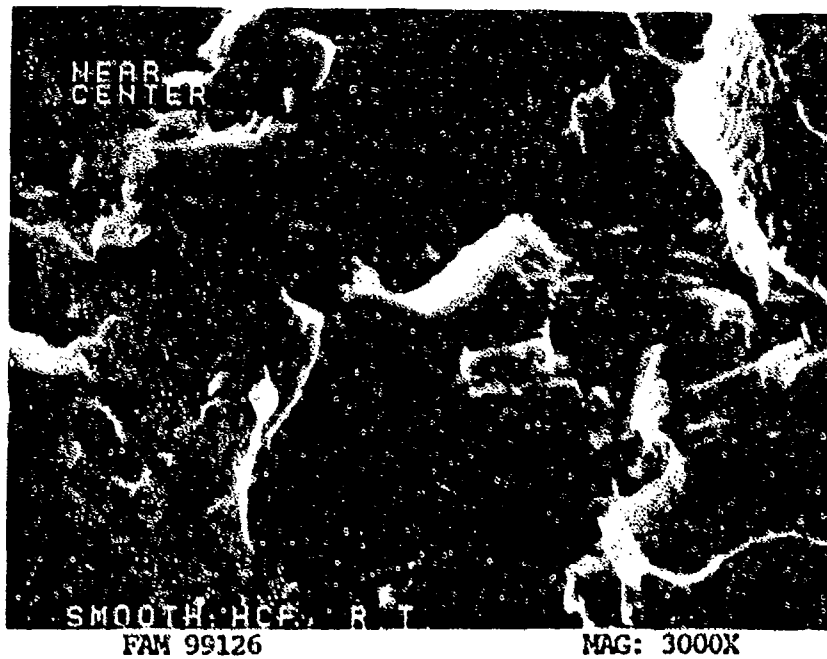
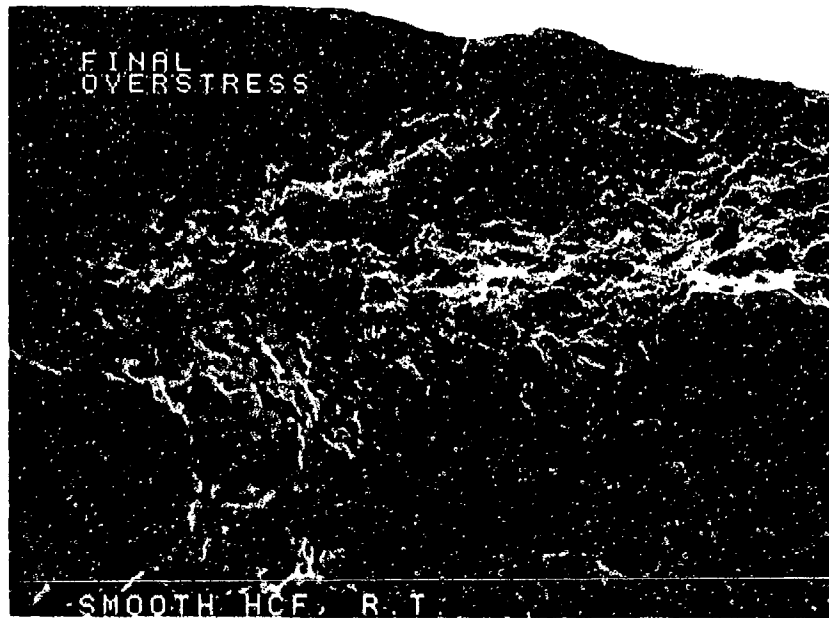


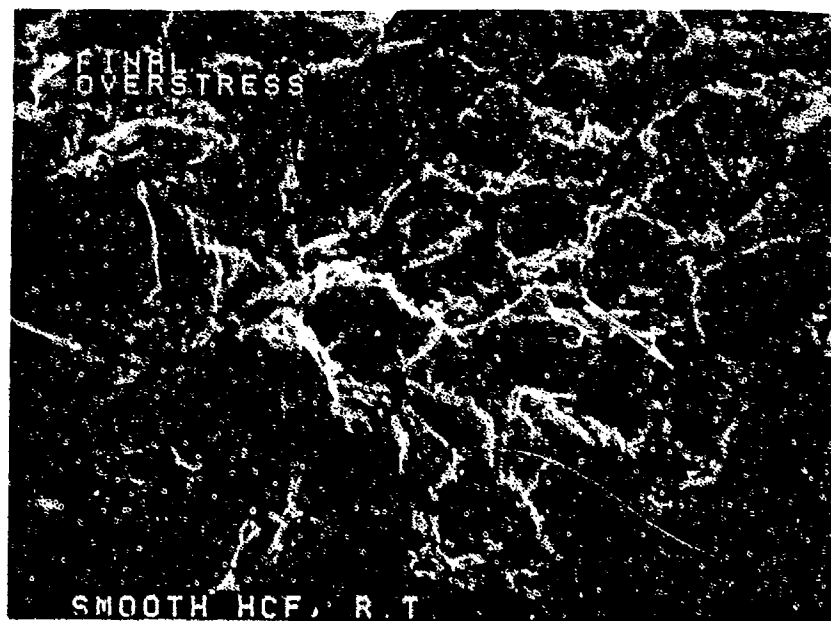
FIGURE 9-46: Higher magnification photograph of the area shown in Figure 9-45, showing fatigue striations near the center of the specimen in the fatigue progression area.



FAM 99127

MAG: 200X

FIGURE 9-47: Dimpled overstress in the final fracture area.



FAM 99128

MAG: 1000X

FIGURE 9-48: Fine dimpled overstress with coarse features in the final fracture area. Cracked carbides are visible in several locations (arrow).

MATERIAL

Inconel X-750
AMS 5667 Bar

TEST DATA

TEST TYPE

Smooth HCF

TEST CONDITIONS

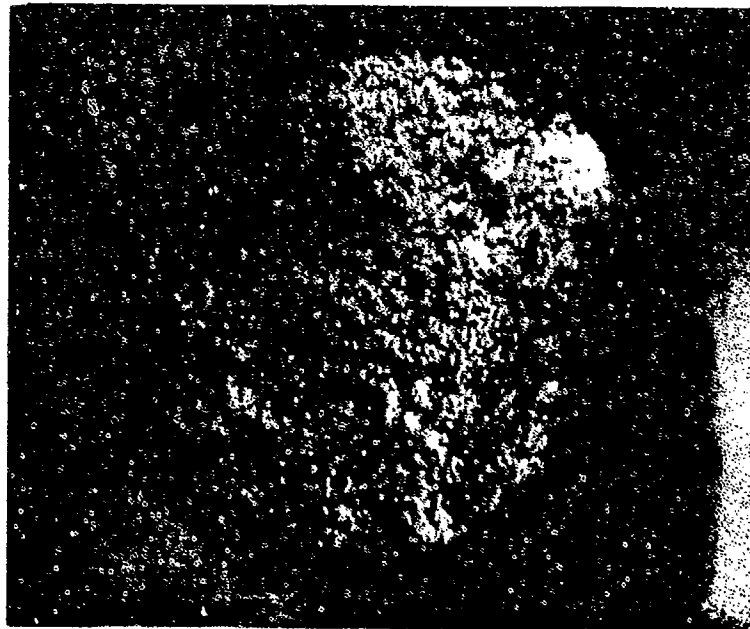
Stress: 517.1 MPa (75.0 ksi)/ -517.1 MPa (-75.0 ksi) DNF*
586.1 MPa (85.0 ksi)/ -586.1 MPa (-85.0 ksi) DNF
655.0 MPa (95.0 ksi)/ -655.0 MPa (-95.0 ksi)

Stress Ratio: -1
Frequency: 1800 cpm
Atmosphere: Air
Temperature: 427°C (800°F)
Test Direction: Longitudinal

TEST RESULTS

Cycles to Fracture: 4.2X10⁵ (DNF); 2.3X10⁵ (DNF); 4.05X10⁴

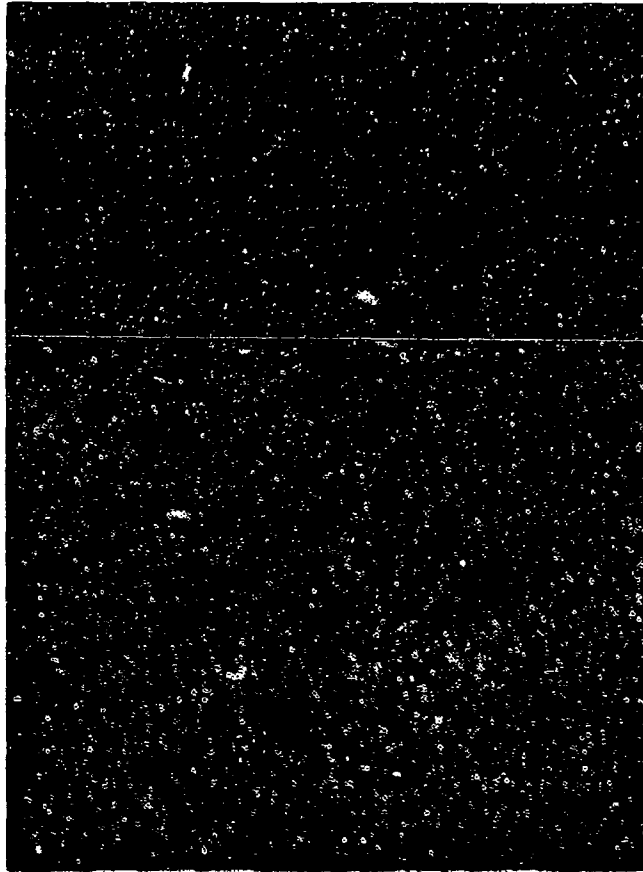
* Did Not Fracture



FAL 93823

MAG: 15X

FIGURE 9-49: Test results and fractography of Inconel X-750 427°C (800°F) smooth HCF test. No obvious origin or final overstress areas are discernible. Compare with the room temperature specimen (Figure 9-39).



FAM 100199

MAG: 100X

FIGURE 9-50: Optical photomicrograph showing the fatigue progression area. This specimen exhibits more variation in elevation than the room temperature specimen (Figure 9-40).

Etchant: Glyceregia

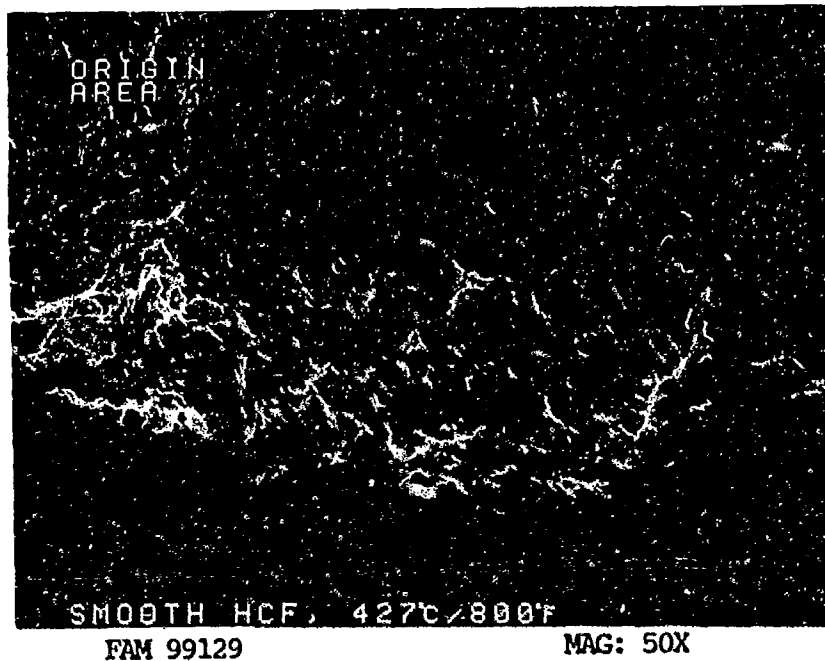


FIGURE 9-51: Overall photograph showing the general origin area and fatigue progression area. The fatigue propagated from multiple surface origins.

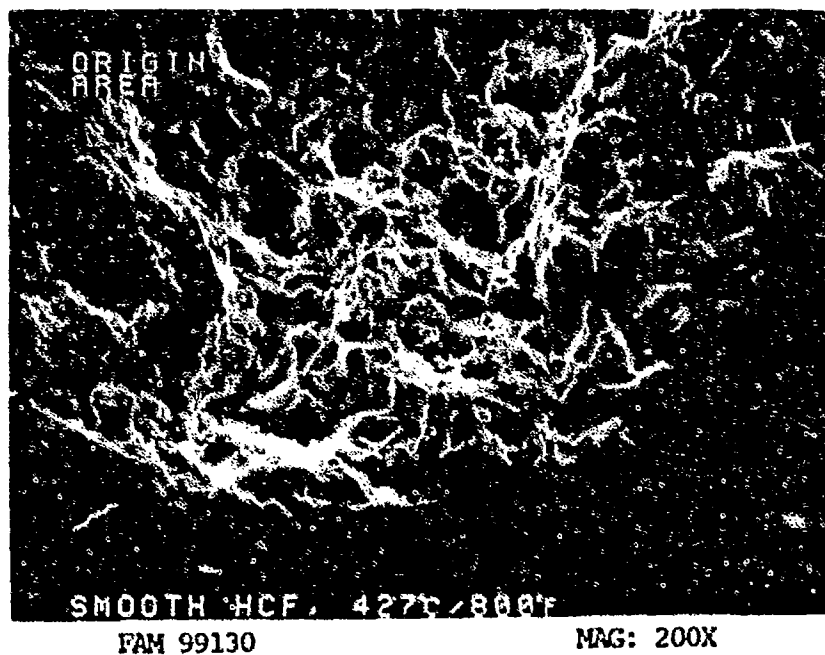


FIGURE 9-52: Higher magnification photograph of the origin area shown in Figure 9-51. Several Stage I fatigue facets are visible at the specimen surface (arrows).

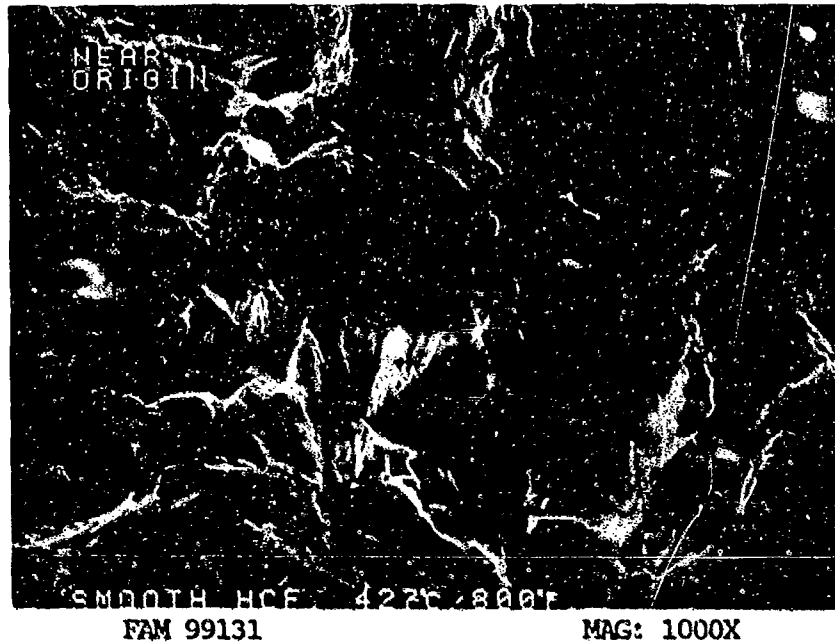


FIGURE 9-53: Mixture of cleavage and feathery cleavage near the origins.

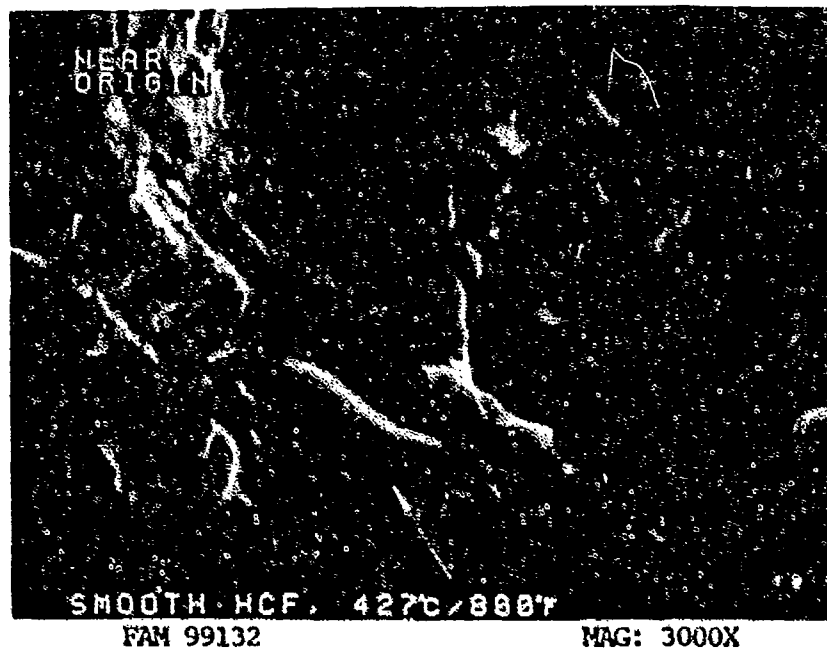
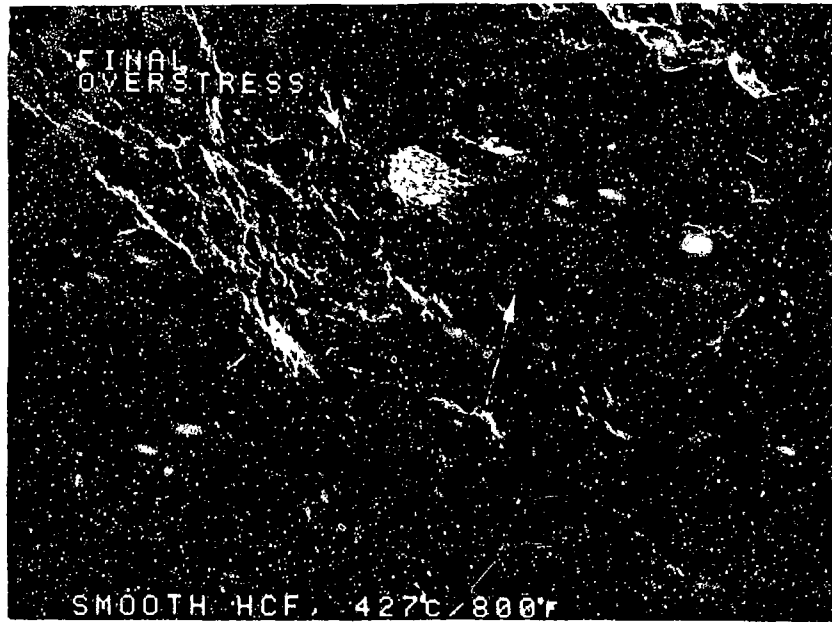


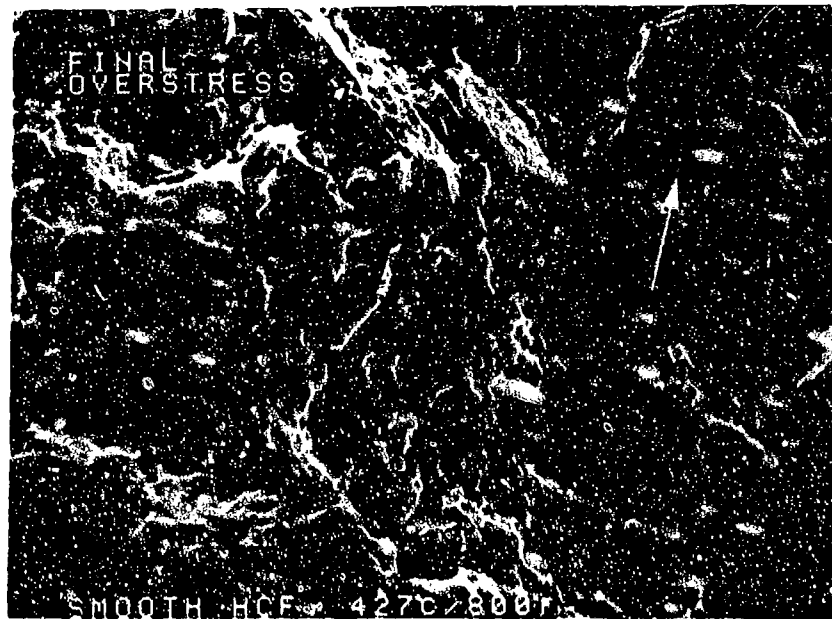
FIGURE 9-54: Higher magnification photograph of the area shown in Figure 9-53), showing cleavage features with small patches of fatigue features (arrows) near the origin.



FAM 99135

MAG: 200X

FIGURE 9-55: Mixture of overstress and smear features in the final overstress area. A patch of smeared material is indicated by an arrow.



FAM 99136

MAG: 1000X

FIGURE 9-56: Fine dimpled overstress with patches that have the appearance of fine fatigue features (arrow) in the final overstress area.

MATERIAL

Inconel X-750
AMS 5667 Bar

TEST DATA

TEST TYPE

Smooth HCF

TEST CONDITIONS

Stress: 620.5 MPa (90.0 ksi)/ -620.5 MPa (-90.0 ksi)
Stress Ratio: -1
Frequency: 1800 cpm
Atmosphere: Air
Temperature: 593°C (1100°F)
Test Direction: Longitudinal

TEST RESULTS

Cycles to Fracture: 205,000



FAL 93827

MAG: 15X

FIGURE 9-57: Test results and fractography of Inconel X-750 593°C (1100°F) smooth HCF test. The fatigue progression area appears generally darker (more oxidized) than the final overstress area. An arrow indicates the origin area. No clear boundary exists between fatigue and final overstress areas.



FAM 100301

MAG: 100X

FIGURE 9-58: Optical photomicrograph showing a close-up of the fatigue progression area. This specimen exhibits more variation in elevation than either the room temperature or the 800° F specimens (Figures 9-40 and 9-50). The grain boundaries are less distinct and a light oxide is visible on the fracture surface (arrows).

Etchant: Glyceregia

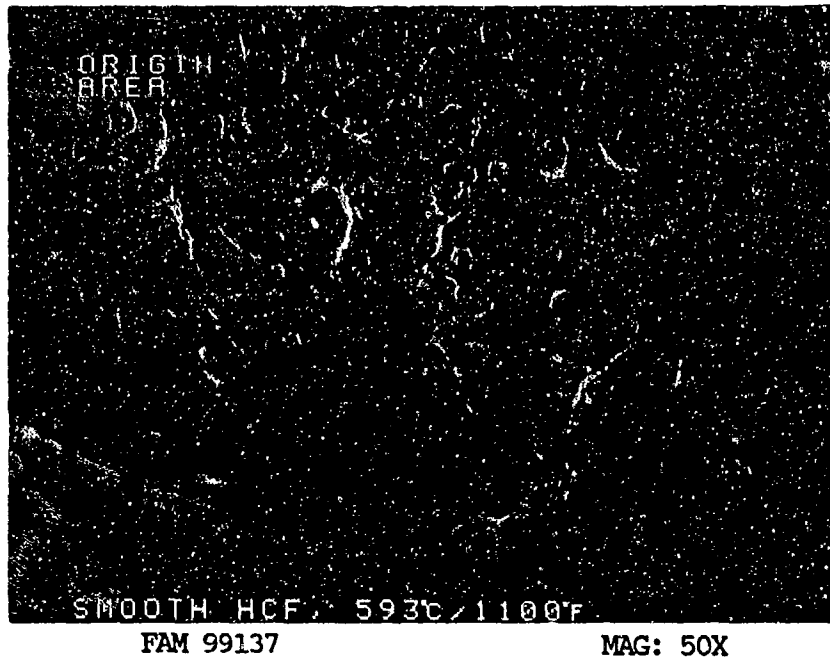


FIGURE 9-59: Overall photograph showing the origin area and the fatigue progression area. A series of Stage I fatigue facets are visible at the surface (arrows).

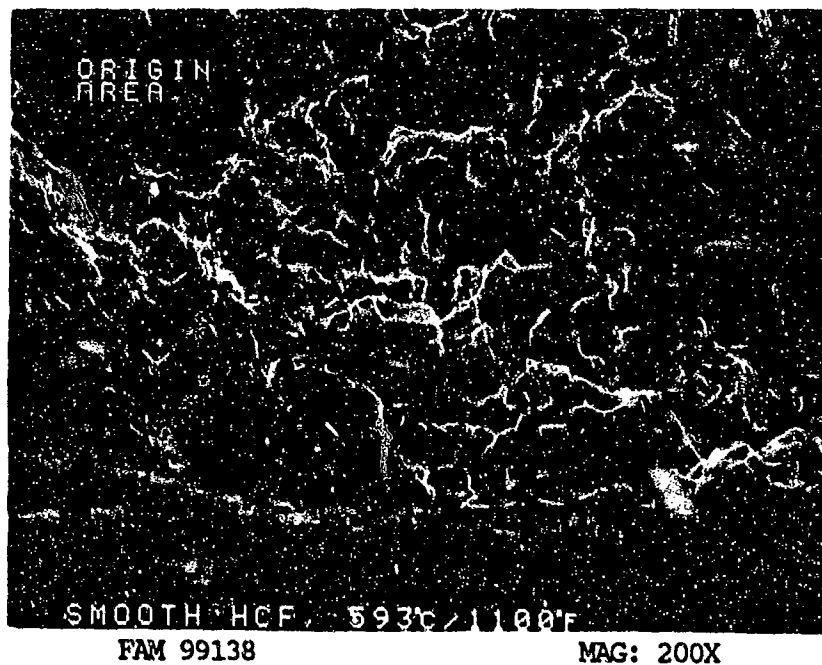


FIGURE 9-60: Higher magnification photograph of the origin area shown in Figure 9-59. Several Stage I facets are visible at the localized origins (arrows).

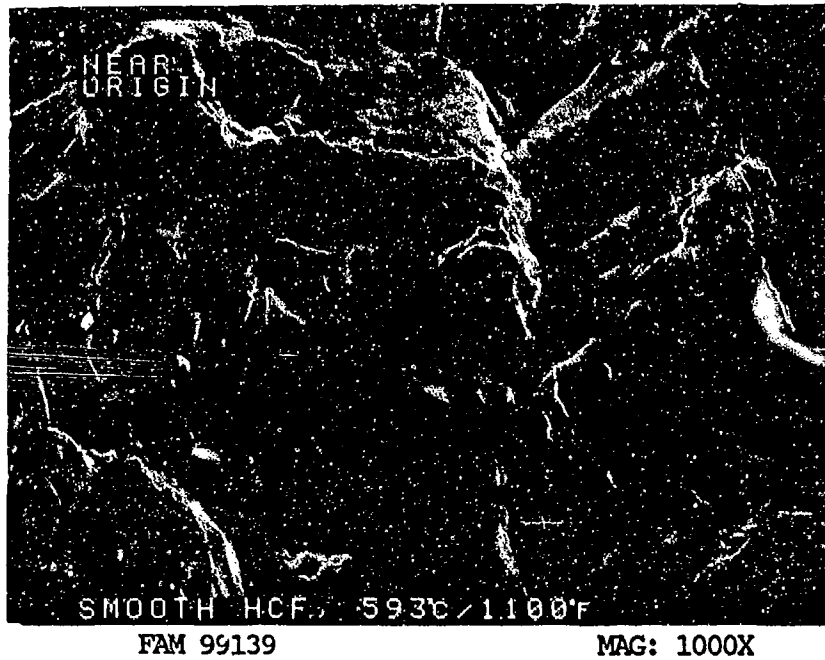


FIGURE 9-61: Fatigue facets near the origin area. No fatigue striations are visible even at high magnifications.

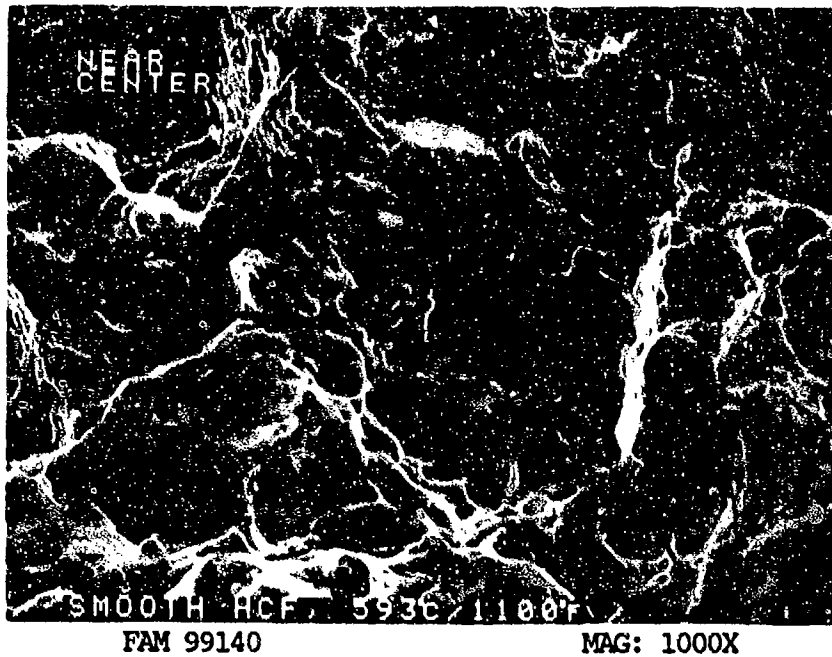


FIGURE 9-62: Mixture of smooth facets and overstress features near the center of the specimen. No fatigue striations are visible.

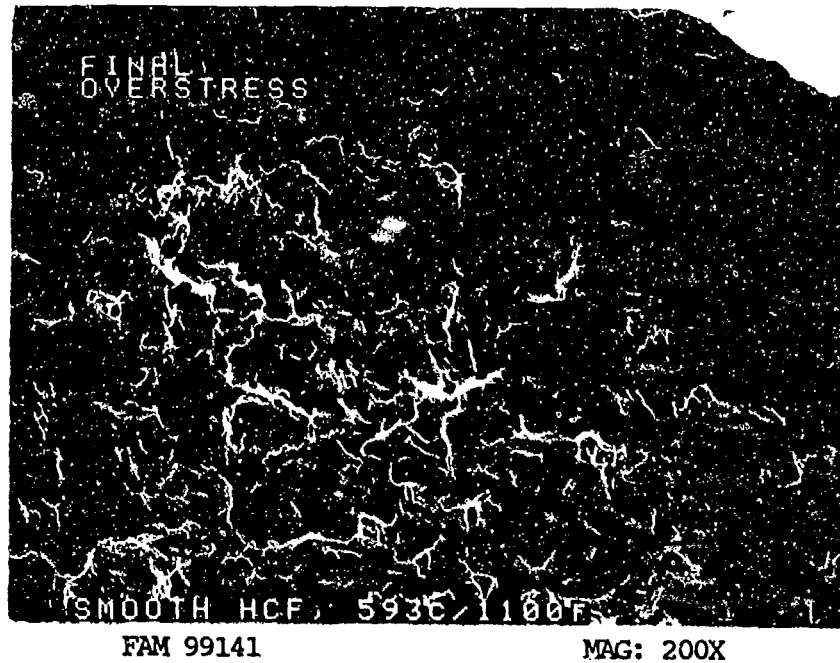


FIGURE 9-63: Mixed mode overstress in the final fracture area exhibiting both cleavage and dimpled overstress.

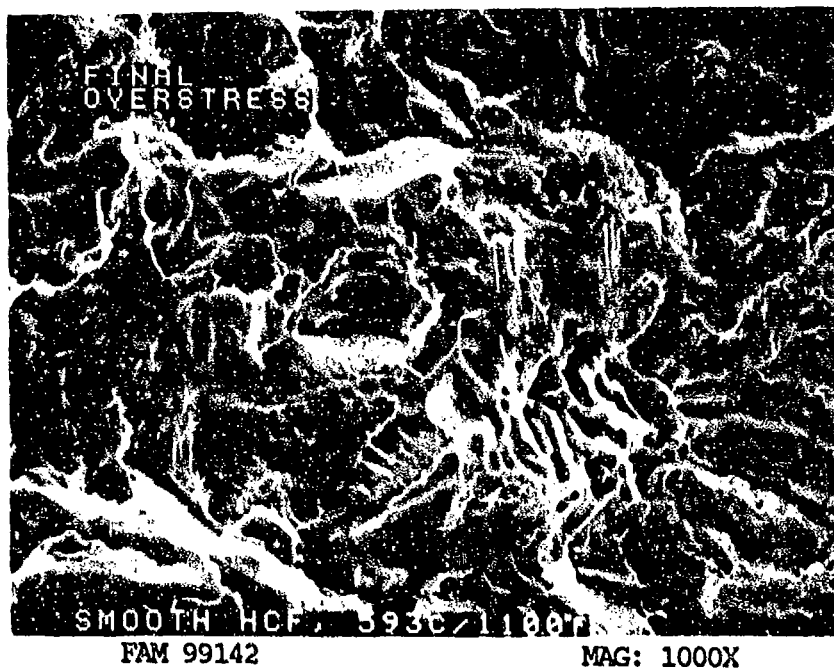


FIGURE 9-64: Higher magnification photograph of the area shown in Figure 9-63, showing a mixture of cleavage features and ductile overstress features in the final fracture area.

MATERIAL

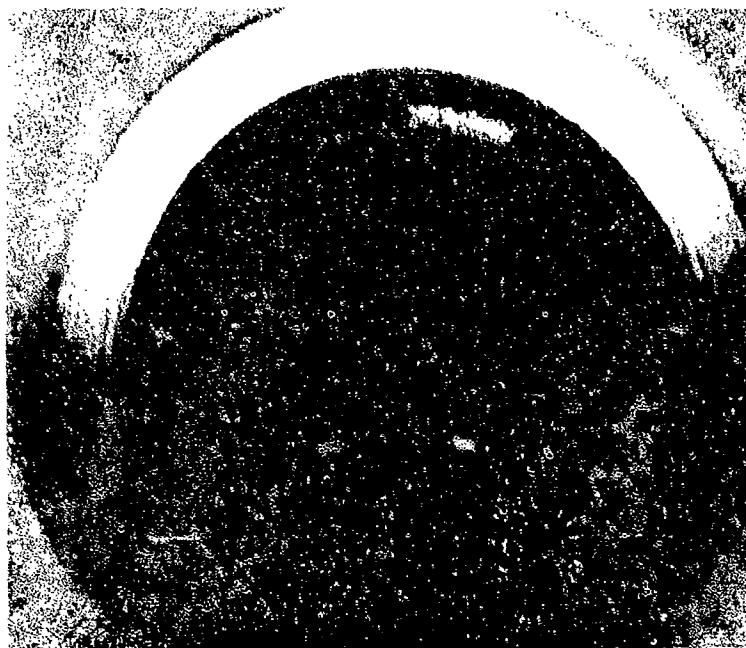
Inconel X-750
AMS 5667 Bar

TEST DATA

TEST TYPE
Notched HCF

TEST CONDITIONS
Stress: 413.7 MPa (60.0 ksi)/ -413.7 MPa (-60.0 ksi)
Stress Ratio: -1
Frequency: 1800 cpm
Atmosphere: Air
Temperature: Room Temperature
Test Direction: Longitudinal

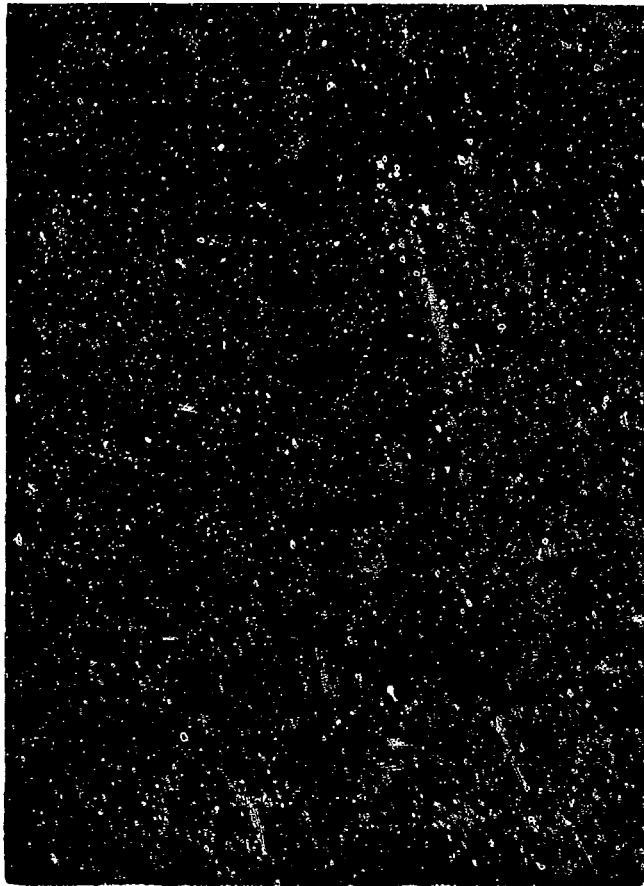
TEST RESULTS
Cycles to Fracture: 111,000



FAL 93821

MAG: 11X

FIGURE 9-65: Test results and fractography of Inconel X-750 room temperature notched HCF test. The fatigue propagated from multiple surface origins shown at the bottom of the photograph. Local origins are separated by fatigue steps (ratchet marks). The extent of the fatigue is shown by a bracket.



FAM 100232

MAG: 200X

FIGURE 9-66: Optical photomicrograph showing a close-up of the fatigue progression area. The fracture is relatively flat (predominantly transgranular) and occurred on a plane perpendicular to the stress axis. No grain deformation is visible adjacent to the fracture.

Etchant: Glyceregia

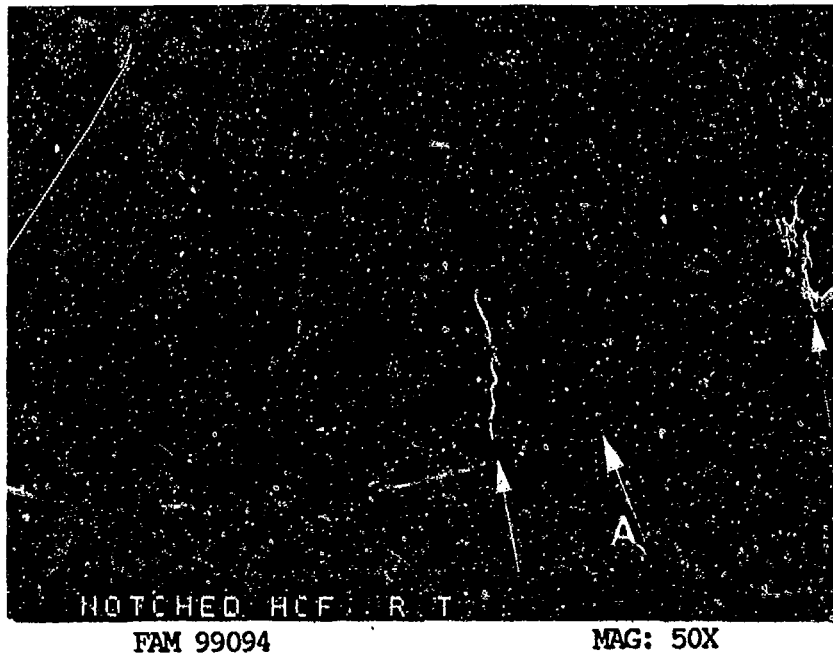


FIGURE 9-67: Overall photograph showing the general origin area and fatigue progression area. The fatigue propagated from multiple surface origins. Steps can be seen separating the origins (arrows). One origin is indicated by arrow A.

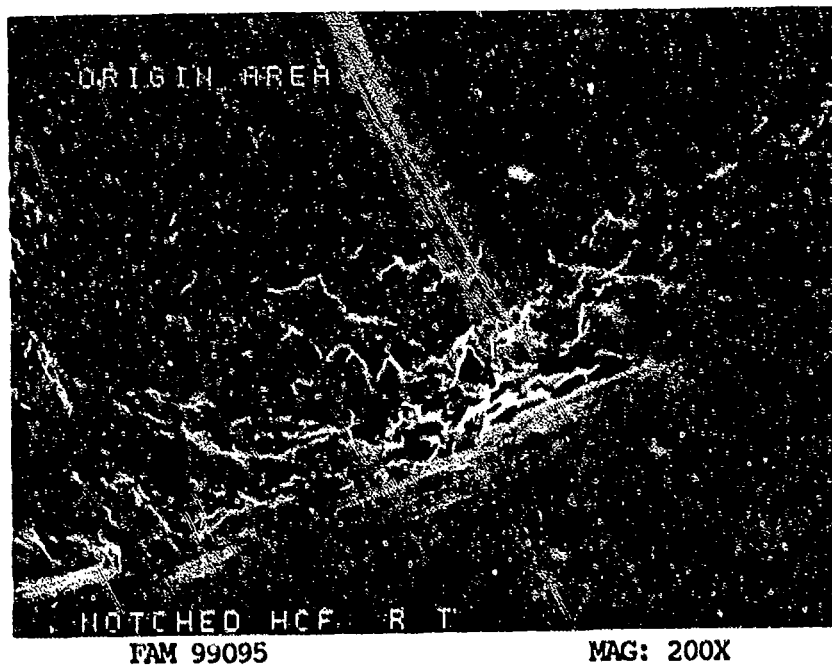


FIGURE 9-68: Higher magnification photograph of a local origin area (Area A, Figure 9-67). No defects are visible at the origin. Machining marks can be seen on the specimen surface.

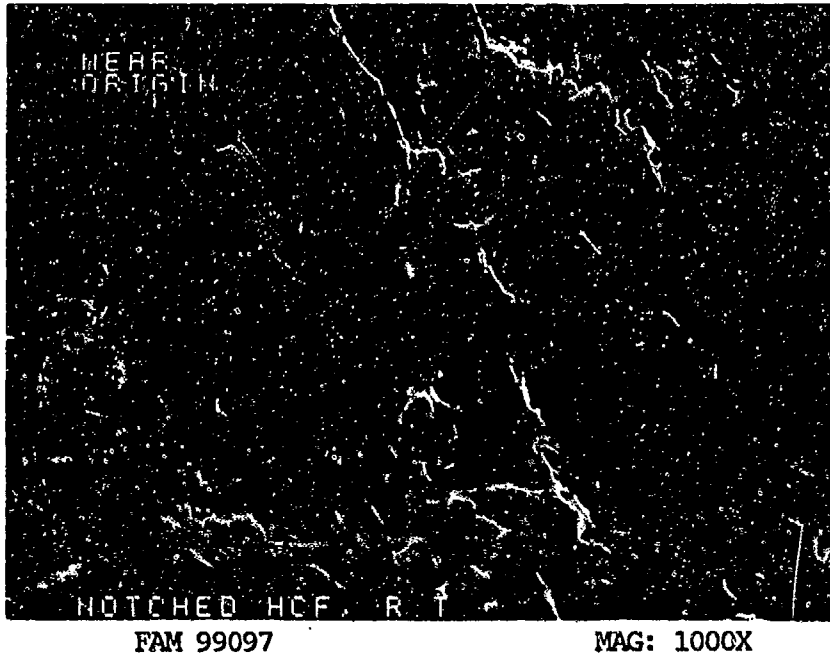


FIGURE 9-69: Mixture of cleavage and feathery cleavage near the origins. Fine cleavage steps are visible on the facets.

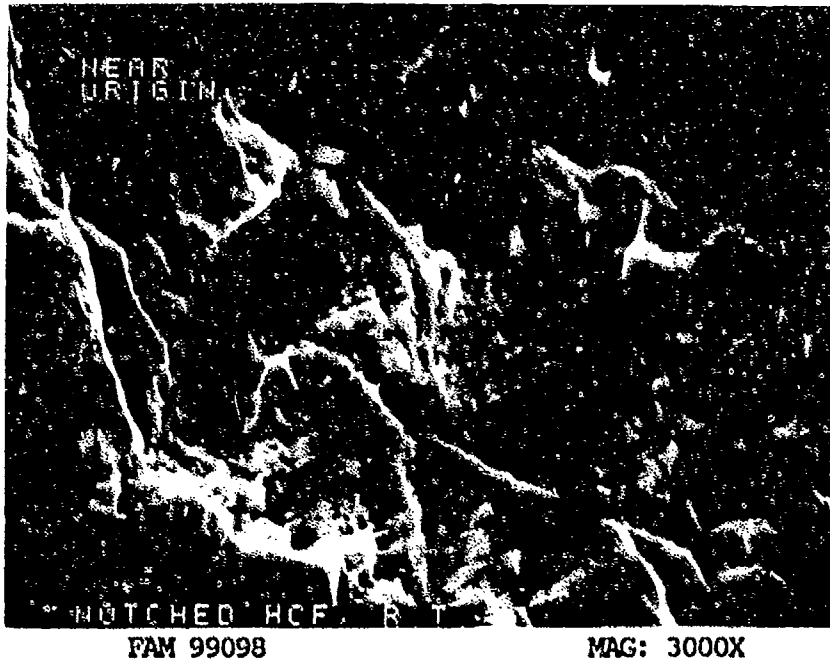


FIGURE 9-70: Higher magnification photograph showing fine cleavage steps on a facet. These steps are straight rather than curved like fatigue striations.

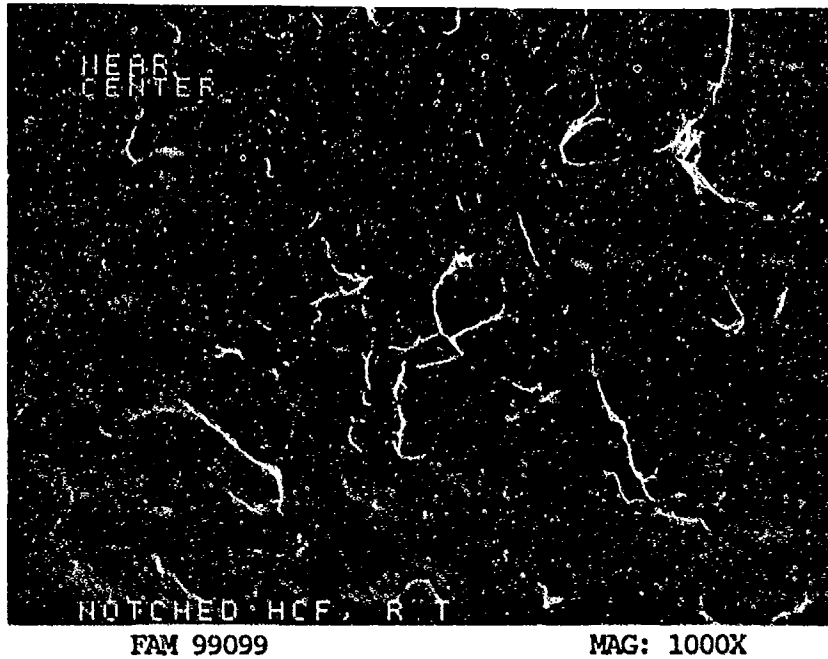


FIGURE 9-71: Fatigue striations near the center of the specimen in the fatigue progression area. The fatigue propagated from bottom to top of the photograph.



FIGURE 9-72: Higher magnification view of the fatigue striations shown in Figure 9-71. Bracket contains ten striations.

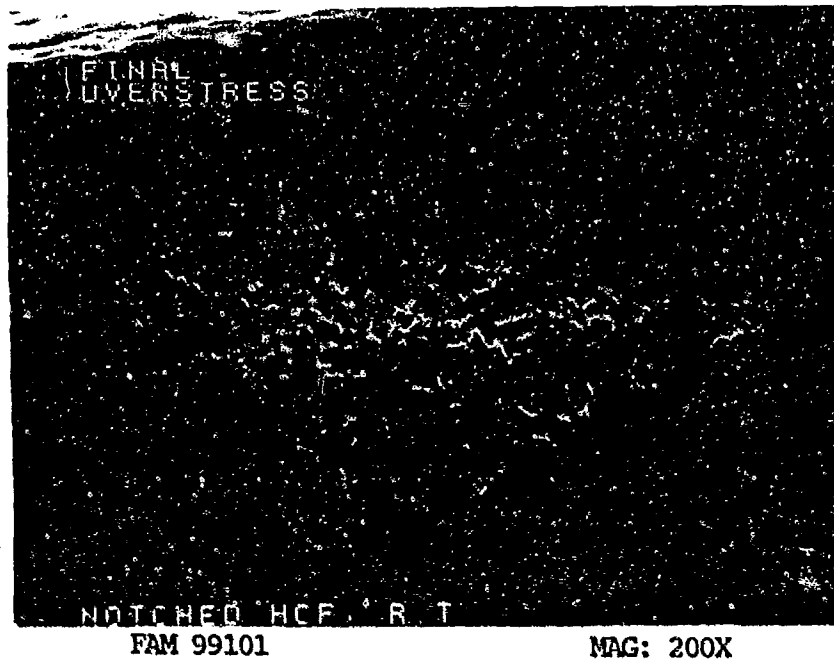


FIGURE 9-73: Mixture of smear and overstress features in the final fracture area.

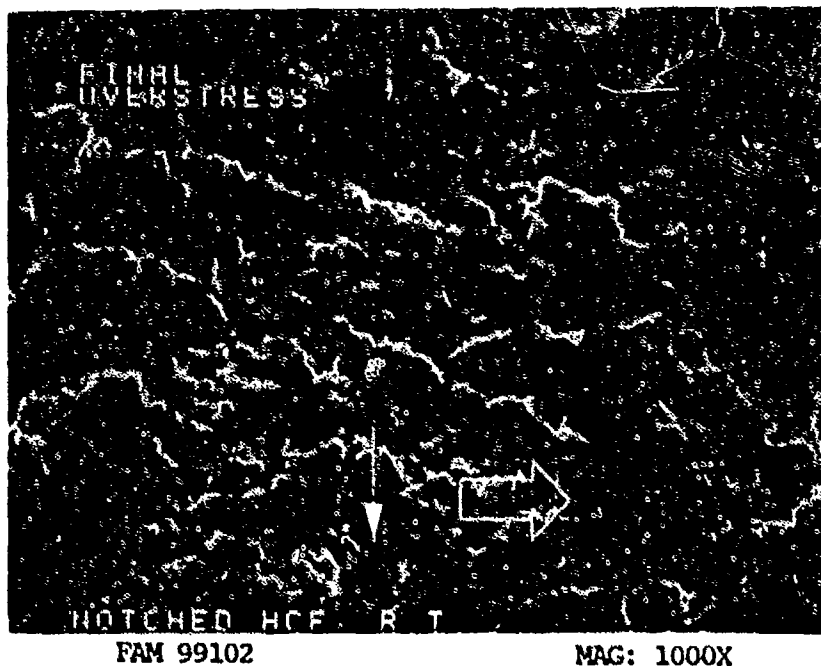


FIGURE 9-74: Mixture of smear and overstress features. The smear features (arrow, bottom right) should not be confused with fatigue striations. A carbide is visible at the bottom center of the photograph (arrow).

MATERIAL

Inconel X-750
AMS 5667 Bar

TEST DATA

TEST TYPE

Notched HCF

TEST CONDITIONS

Stress: 413.7 MPa (60.0 ksi)/ -413.7 MPa (-60.0 ksi)
Stress Ratio: -1
Frequency: 1800 cpm
Atmosphere: Air
Temperature: 427°C (800°F)
Test Direction: Longitudinal

TEST RESULTS

Cycles to Fracture: 140,000

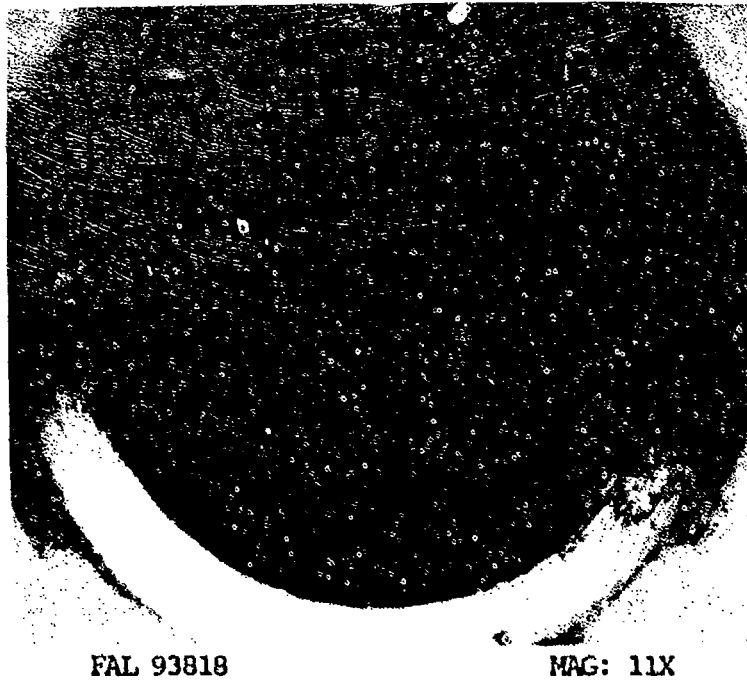
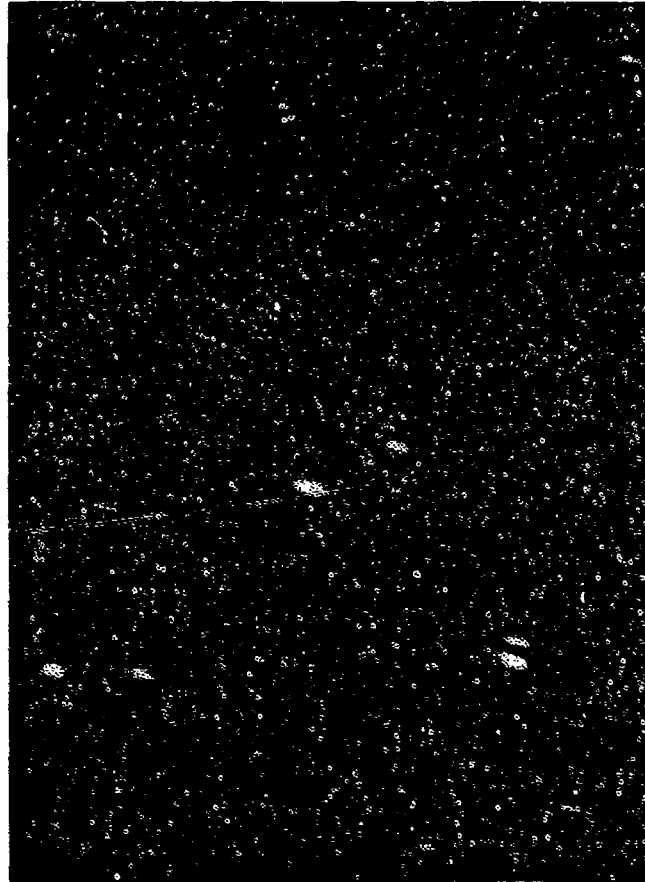


FIGURE 9-75: Test results and fractography of Inconel X-750 427°C (800°F) notched HCF test. The extent of the fatigue is shown by a bracket.



FAM 100200

MAG: 200X

FIGURE 9-76: Optical photomicrograph showing a close-up view of the fatigue progression area. The fracture is relatively flat (predominantly transgranular) and occurred on a plane perpendicular to the stress axis. No grain deformation is visible adjacent to the fracture. This fracture appears very similar to the room temperature specimen (Figure 9-66).

Etchant: Glyceregia

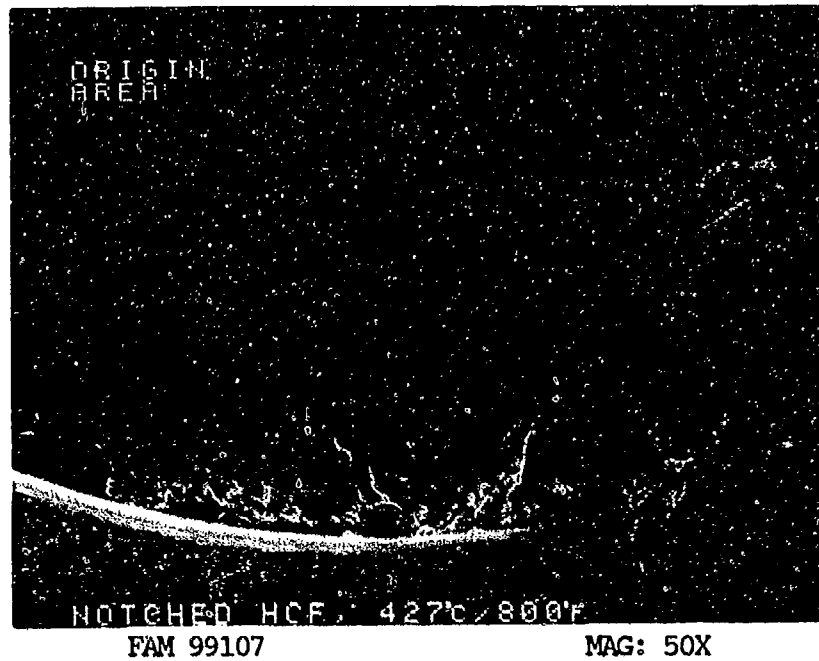


FIGURE 9-77: Overall photograph showing the origin area and initial fatigue progression area. Features can be seen radiating from the origin area (arrows).

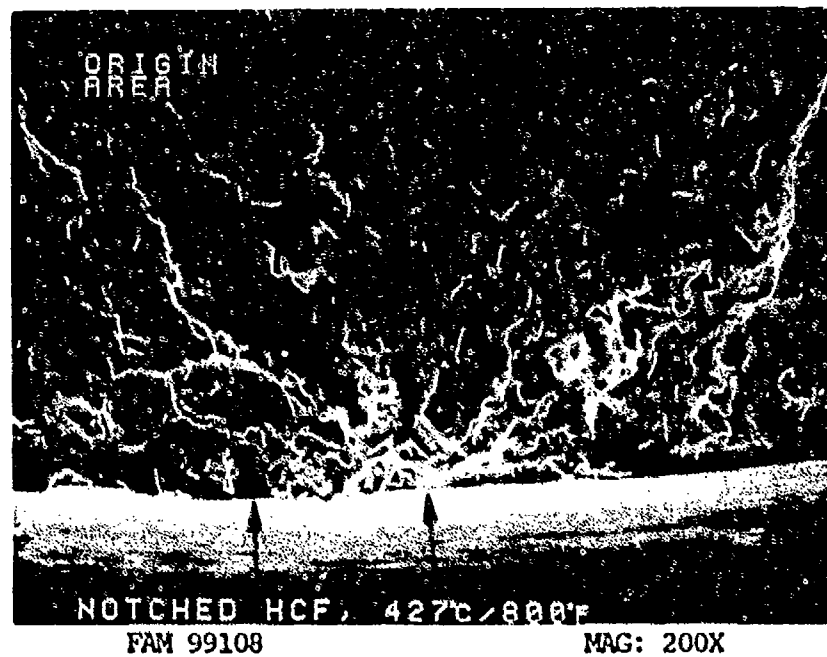


FIGURE 9-78: Higher magnification photograph of the origin area. Several Stage I fatigue facets (arrows) are visible in the localized origin area. Features radiate from the individual origins.



FAM 99109

MAG: 1000X

FIGURE 9-79: Stage I facet at the origin. No fatigue striations are visible on the facet in the Stage I area even at high magnifications.



FAM 99110

MAG: 1000X

FIGURE 9-80: Patches of fine fatigue striations (arrows) near the origin in the fatigue progression zone. The fatigue propagated from the bottom to the top of the photograph. The localized direction of propagation varies.

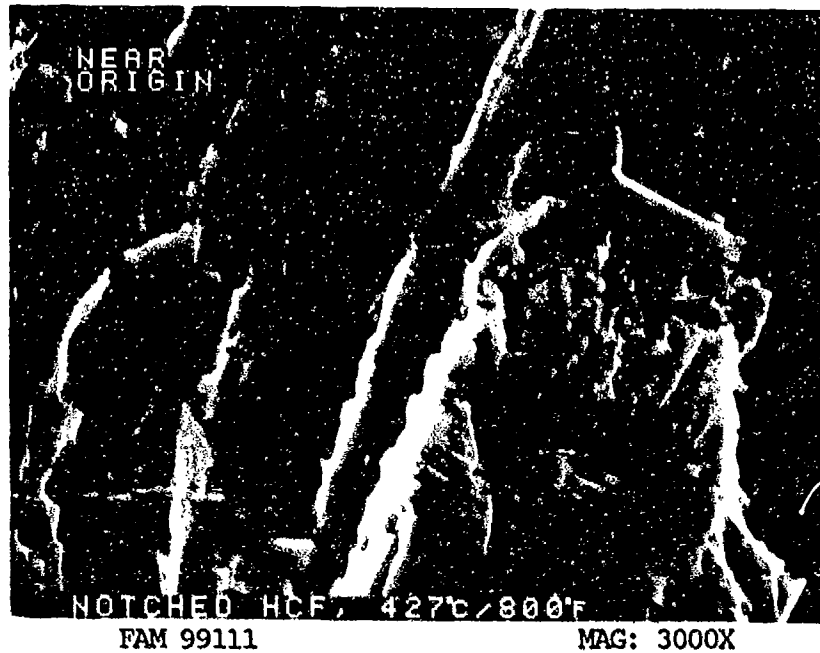


FIGURE 9-81: Higher magnification view of the patches of striations shown in Figure 9-80. Individual striations are barely resolvable.

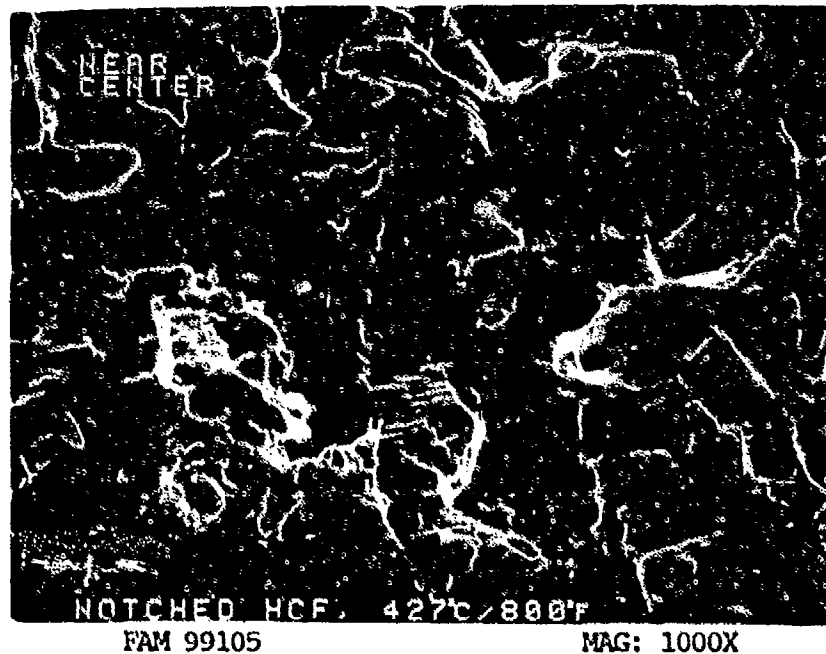


FIGURE 9-82: Coarser fatigue striations near the center of the specimen. The effective cross section of the specimen was reduced as the crack propagated, so the nominal stress increased. Bracket contains 5 striations.

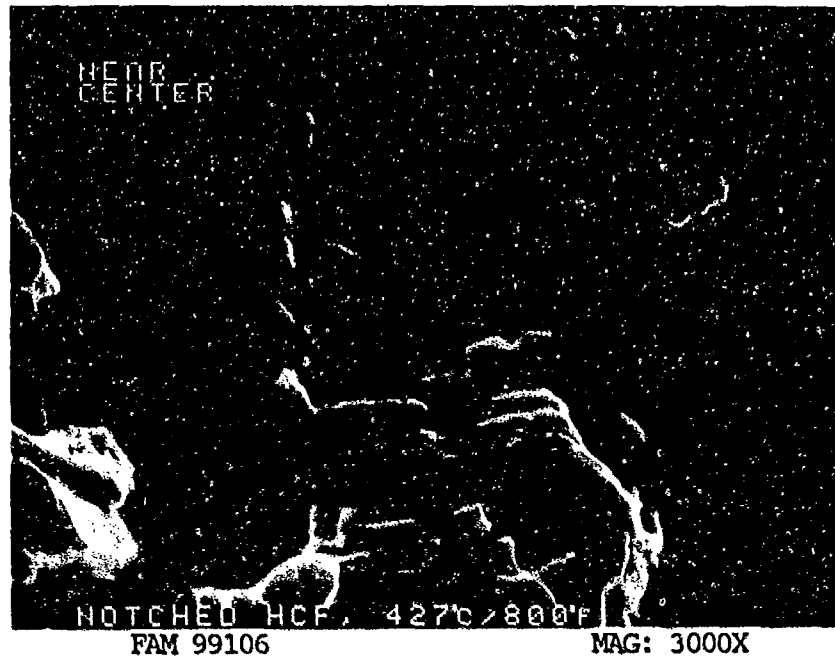


FIGURE 9-83: Higher magnification view of the striations shown in Figure 9-82.

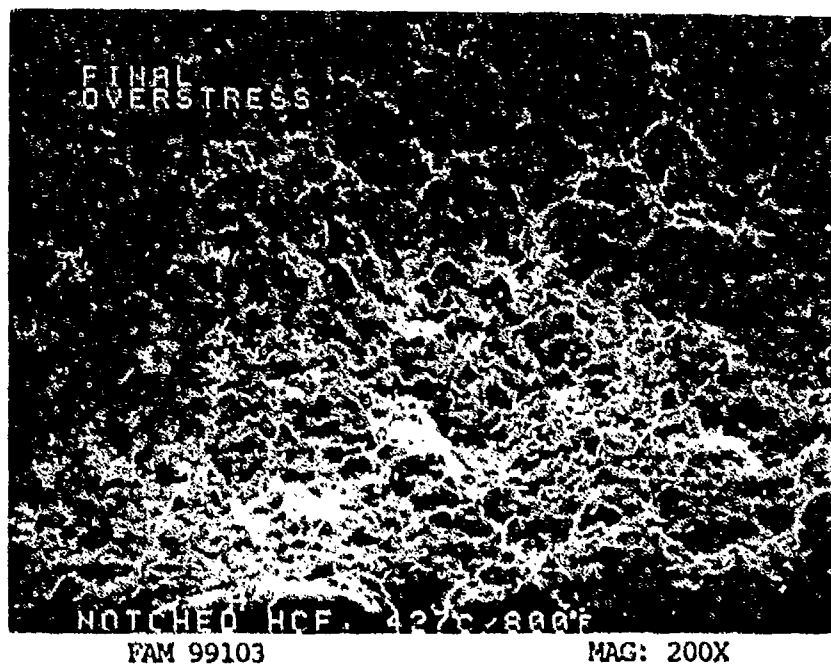


FIGURE 9-84: Final overstress area.

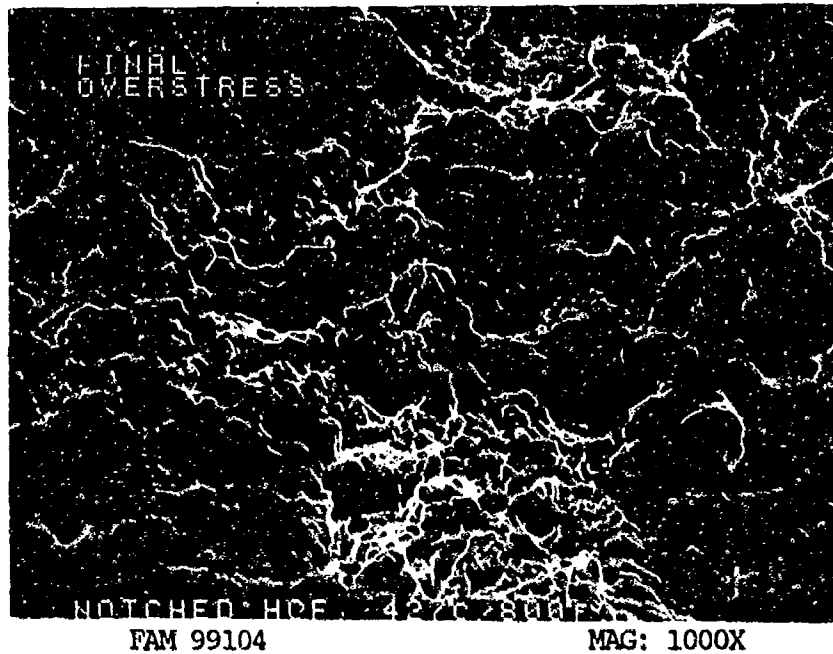


FIGURE 9-85: Higher magnification view of the final overstress area, exhibiting oxidized overstress features.

MATERIAL

Inconel X-750
AMS 5667 Bar

TEST DATA

TEST TYPE
Notched HCF

TEST CONDITIONS

Stress: 413.7 MPa (60.0 ksi)/ -413.7 MPa (-60.0 ksi)
Stress Ratio: -1
Frequency: 1800 cpm
Atmosphere: Air
Temperature: 593°C (1100°F)
Test Direction: Longitudinal

TEST RESULTS

Cycles to Fracture: 21,600

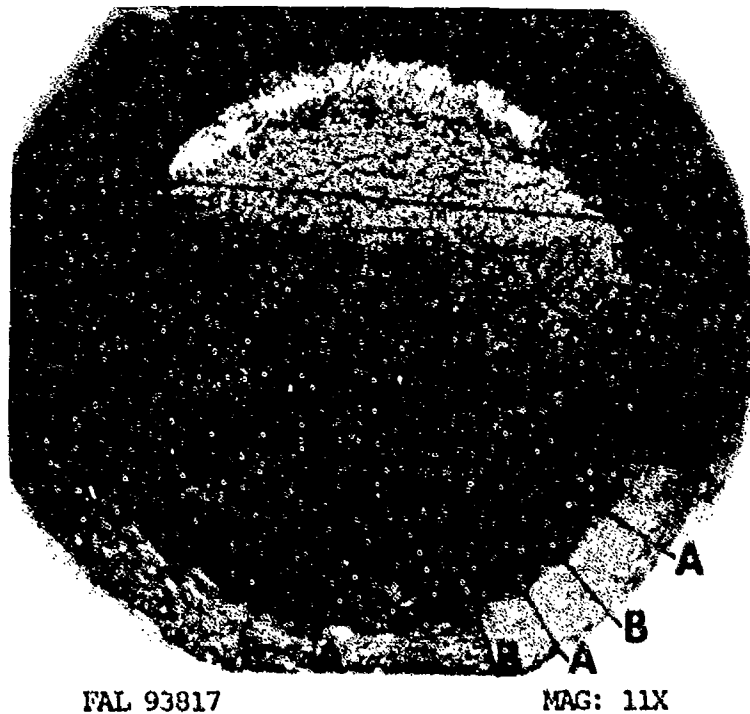


FIGURE 9-86: Test results and fractography of Inconel X-750 593°C (1100°F) notched HCF test. Several origins (arrows A) are separated by fatigue steps (arrows B). The extent of the fatigue is shown by a bracket.



FAM 100258

MAG: 200X



FAM 100259

MAG: 200X

FIGURE 9-87: Optical photomicrographs showing a close-up of the fatigue progression area (top) and the final overstress area (bottom). The fatigue progression is relatively flat (predominantly transgranular) and occurred on a plane perpendicular to the stress axis. No grain deformation is visible adjacent to the fracture. The final overstress area exhibits a more intergranular appearance.

Etchant: Glycoeregia



FIGURE 9-88: One of several fatigue origins separated by fatigue steps. Features can be seen radiating from a small localized (point) origin (arrow).

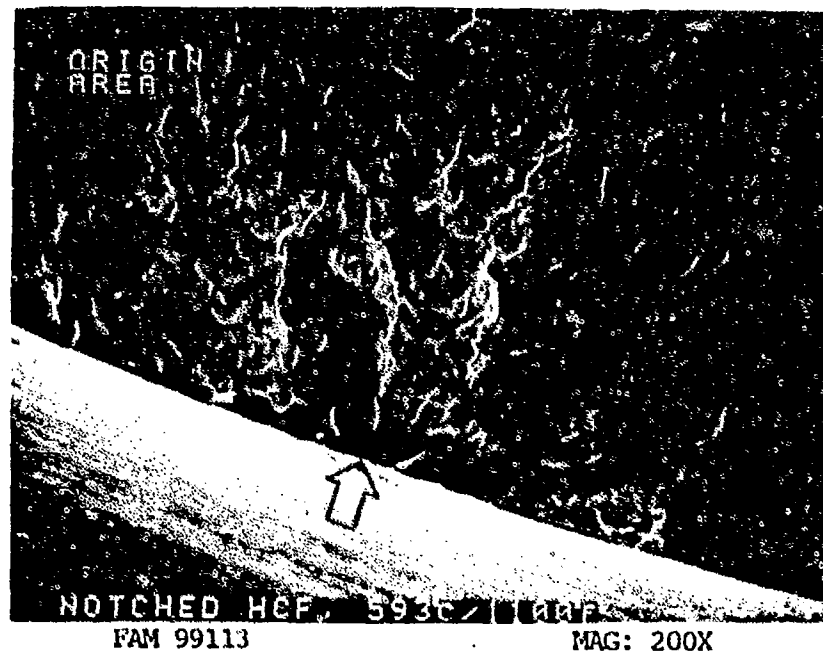


FIGURE 9-89: Higher magnification photograph of the localized origin area shown in Figure 9-88. No defects are visible at the origin (arrow).

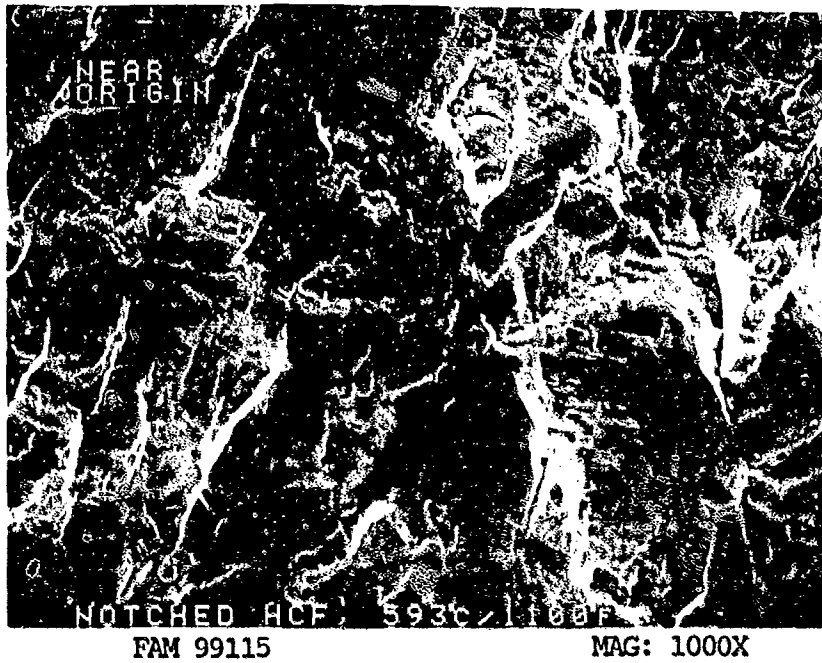


FIGURE 9-90: Fatigue striations near the origin area.

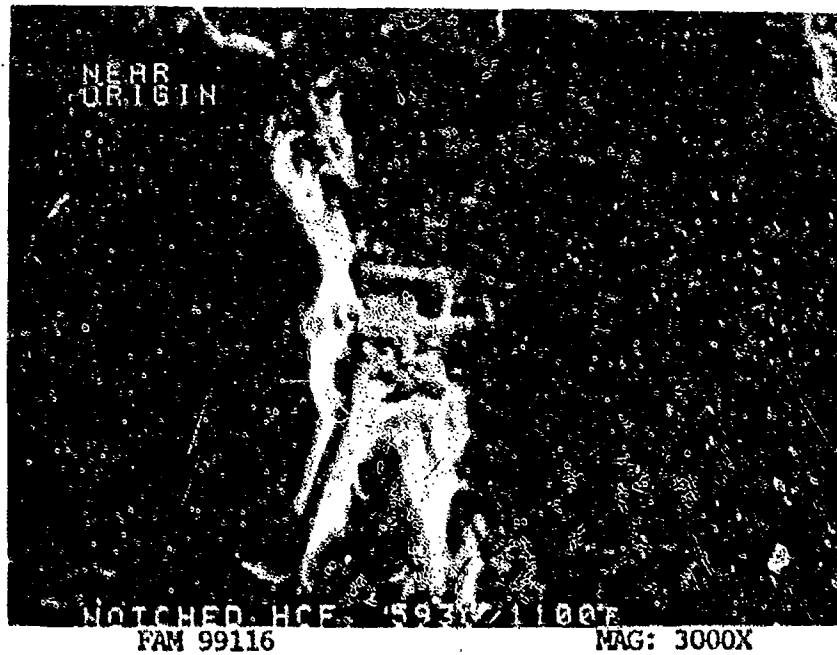


FIGURE 9-91: Higher magnification photograph of the area in Figure 9-90, showing fine oxidized fatigue striations. The direction of propagation is from bottom to top of the photograph.

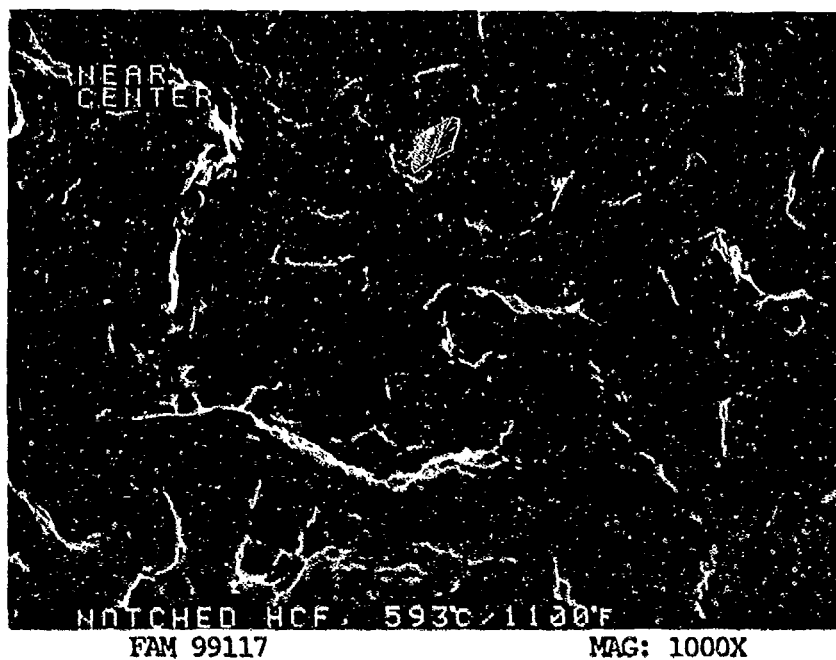


FIGURE 9-92: Coarser fatigue striations near the center of the specimen in the fatigue progression area. The fatigue propagated from bottom to top of the photograph.

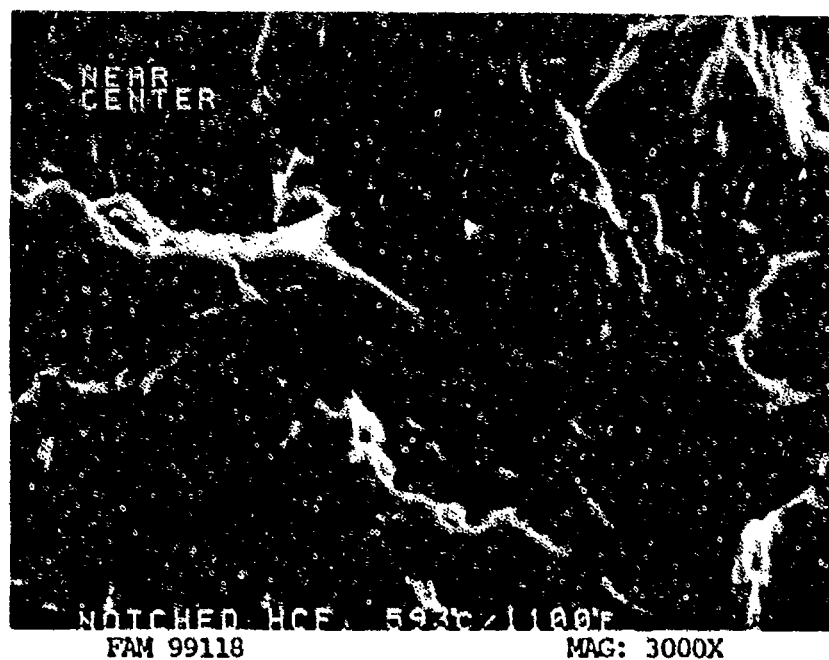


FIGURE 9-93: Higher magnification view of the fatigue striations shown in Figure 9-92.

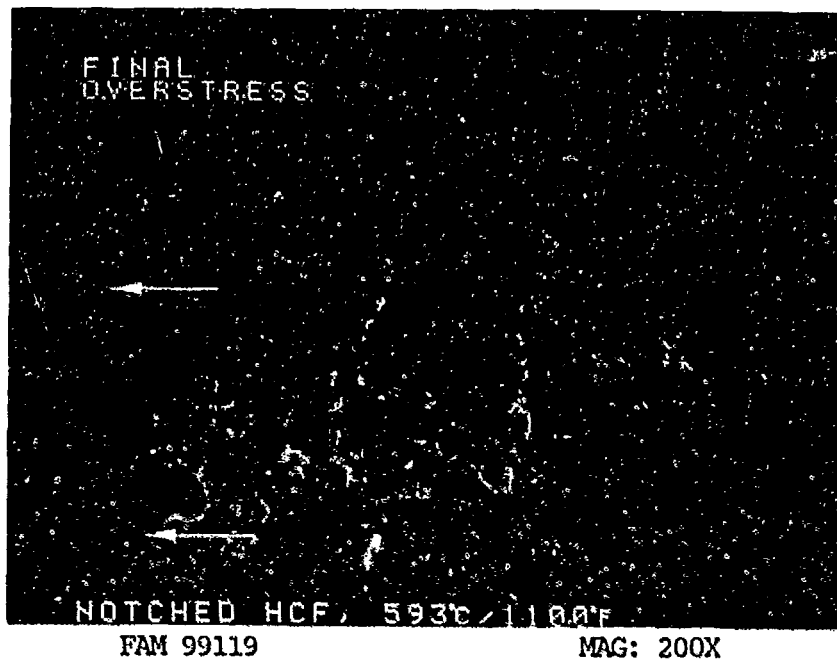


FIGURE 9-94: Mixture of smear (arrows) and oxidized overstress features in the final fracture area.

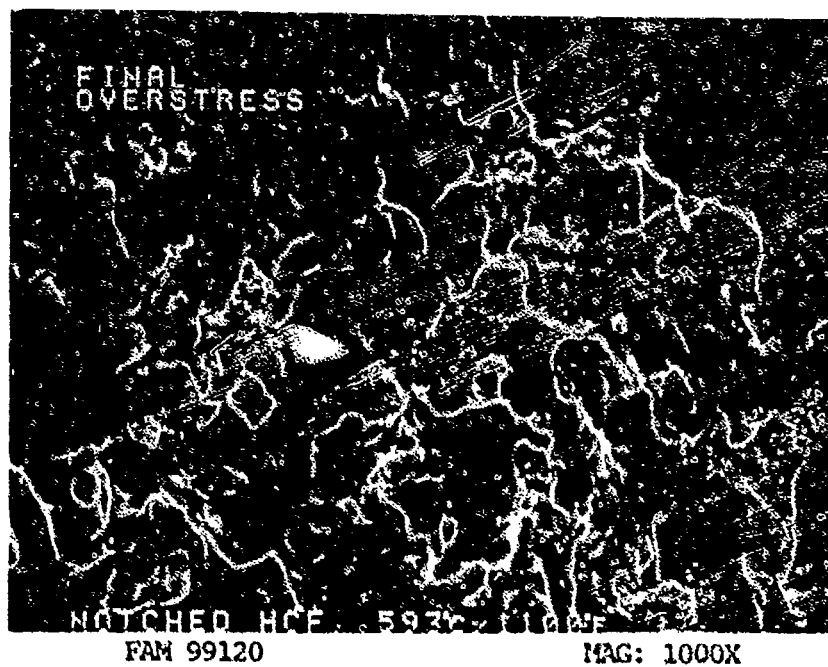


FIGURE 9-95: Higher magnification photograph of the area in Figure 9-94, showing a mixture of oxidized smear and dimpled overstress features.

MATERIAL

Inconel X-750
AMS 5667 Bar

TEST DATA

TEST TYPE
Smooth LCF

TEST CONDITIONS

Stress: 965.3 MPa (140 ksi)/ 48.3 MPa (7.0 ksi)
Stress Ratio: 0.05
Frequency: 10 cpm
Atmosphere: Air
Temperature: 260°C (500°F)
Test Direction: Longitudinal

TEST RESULTS

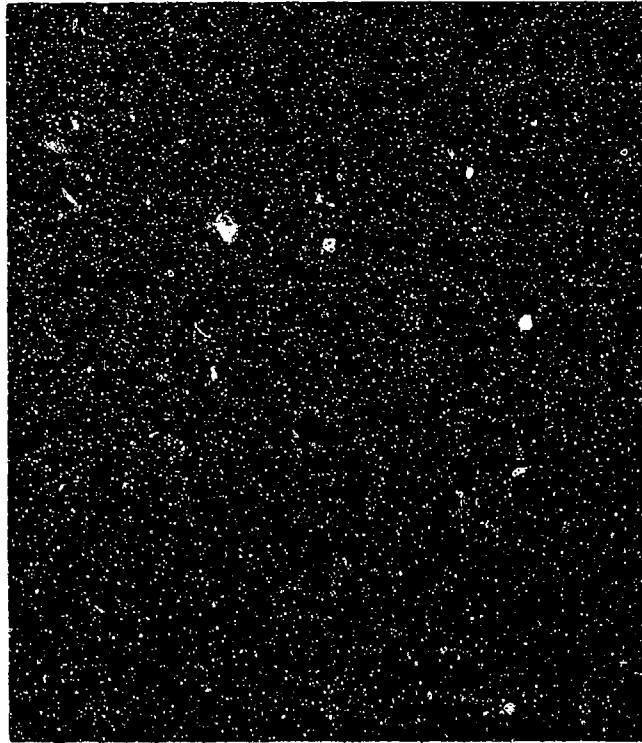
Cycles to Fracture: 58,810



FAL 93234

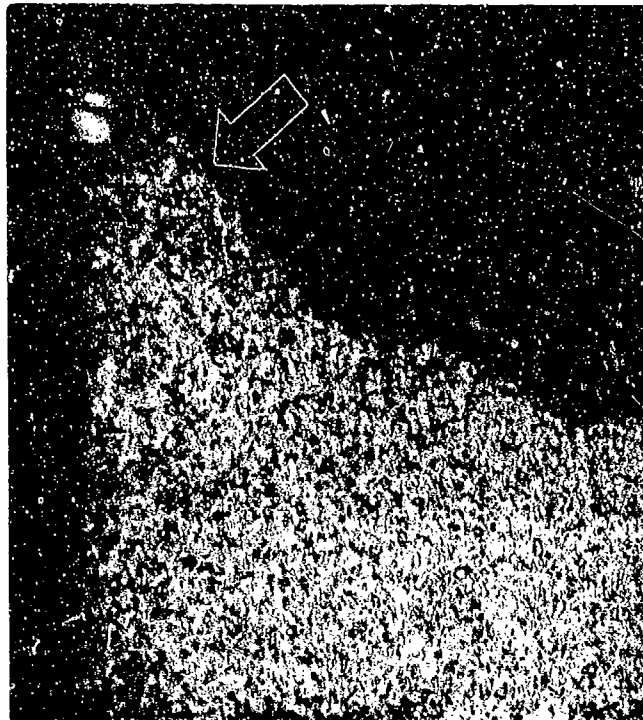
MAG: 10X

FIGURE 9-96: Test results and fractography of Inconel X-750 260°C (500°F) smooth LCF test. The origin and fatigue progression (arrow) occurred on a plane perpendicular to the stress axis. The remainder of the fracture occurred on a plane approximately 45° to the stress axis.



FAM 100203

MAG: 100X

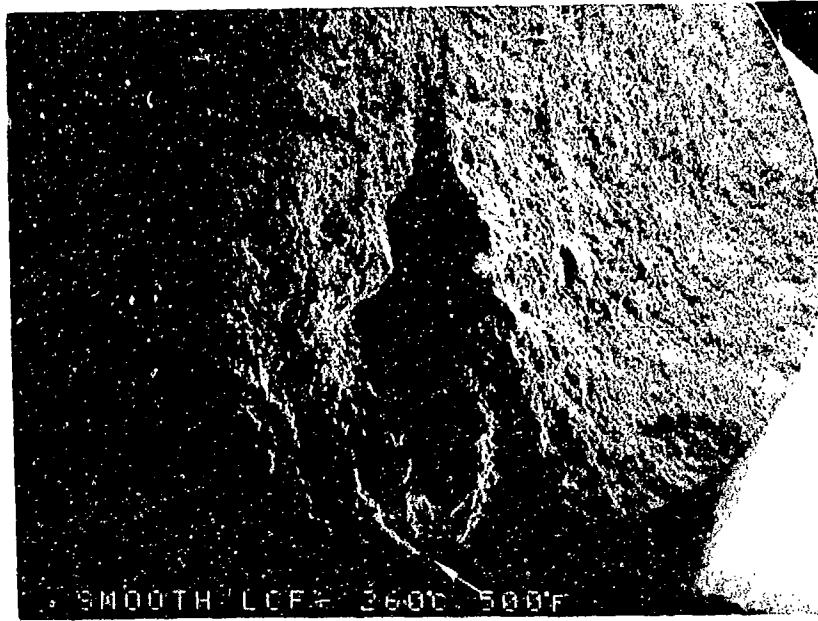


FAM 100204

MAG: 50X

FIGURE 9-97: Optical photomicrographs showing the fatigue progression area (top) and the final overstress area (bottom). The fatigue progression exhibits more variation in elevation than on the HCF specimens (Figures 9-50 and 9-53), but remains roughly perpendicular to the stress axis. A shear lip is visible in the final overstress area (arrow).

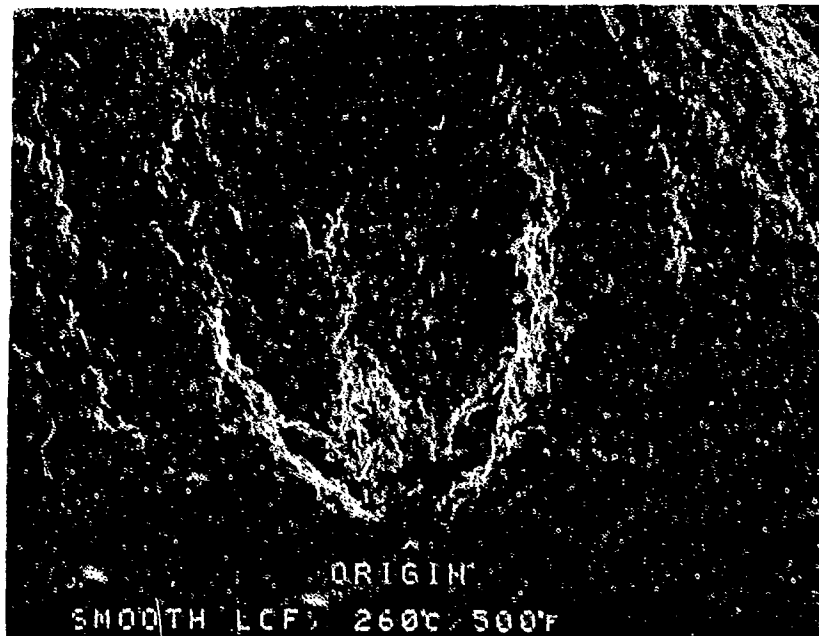
Etchant: Glyceregia



FAM 98709

MAG: 20X

FIGURE 9-98: Overall photograph showing the origin area (arrow) and the fatigue progression area on a plane approximately perpendicular to the stress axis. The remainder of the fracture is at a 45° angle to the stress axis.



FAM 78710

MAG: 50X

FIGURE 9-99: Higher magnification photograph of the origin area. The fatigue thumbnail is faintly visible (brackets).

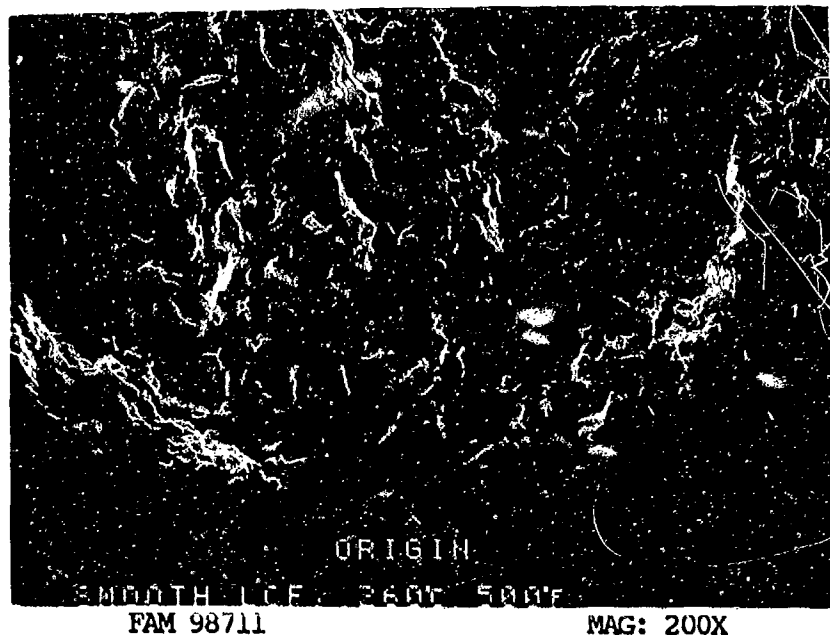


FIGURE 9-100: A small inclusion is visible at the origin. Fracture features radiate from this point. The inclusion appears darker than the background in the secondary electron image mode, indicating that it is of lower atomic number than the base material.

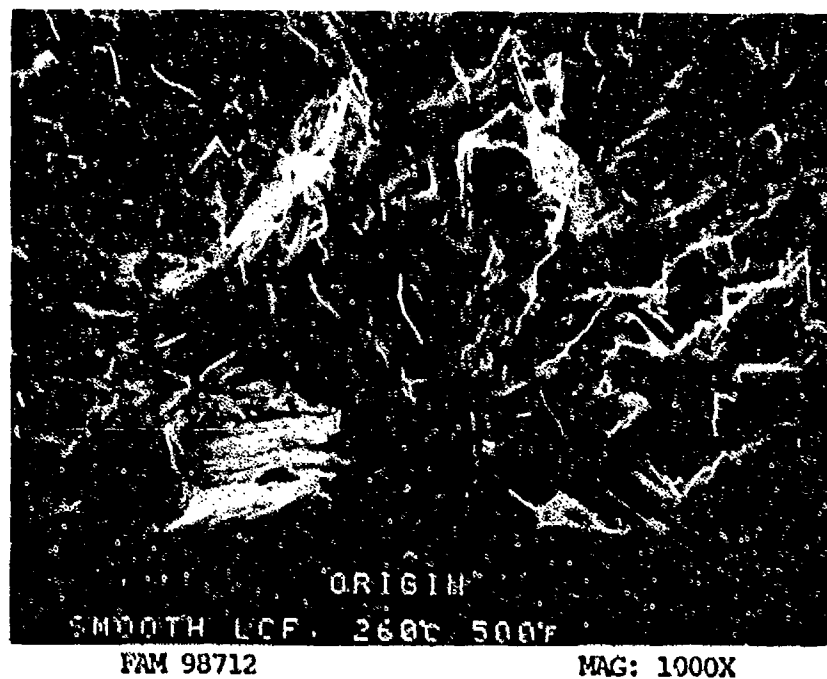
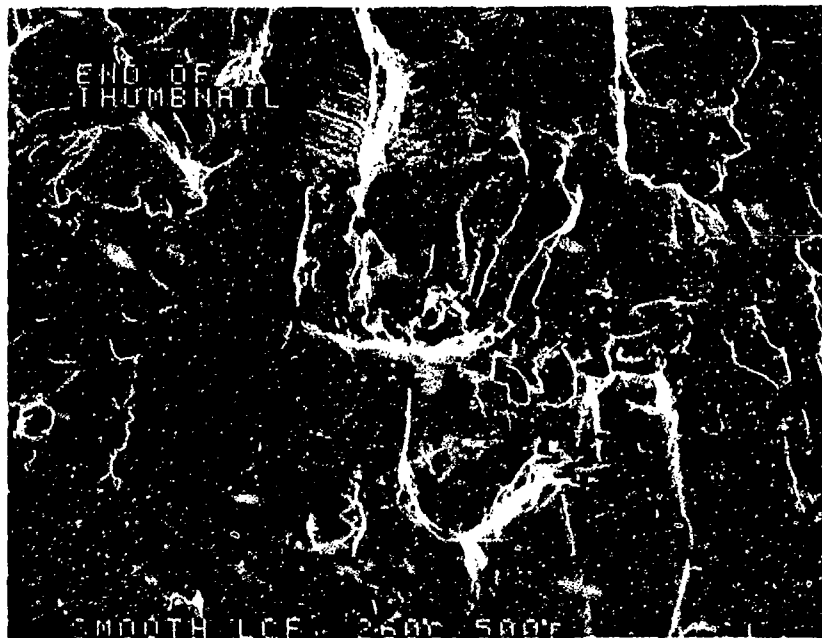


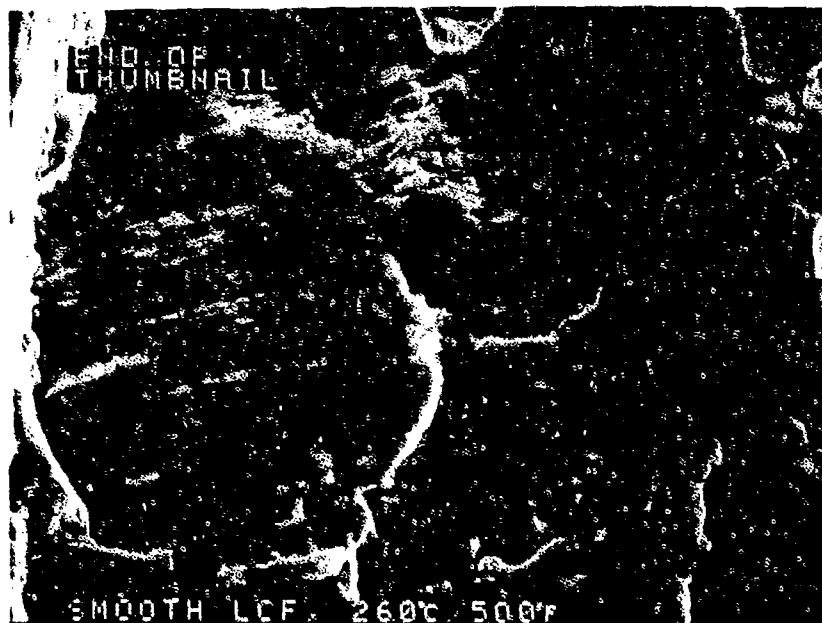
FIGURE 9-101: Higher magnification photograph of titanium-rich inclusion that acted as the origin. Scanning electron microscope/X-ray energy spectroscopy (SEM/XES) analysis determined the composition.



FAM 98716

MAG: 1000X

FIGURE 9-102: Fatigue striations near the end of the thumbnail. The direction of propagation is from bottom to top of the photograph. The direction of local propagation varies slightly on different plateaus.



FAM 98717

MAG: 3000X

FIGURE 9-103: Higher magnification photograph of the upper right corner area of Figure 9-102, showing well developed fatigue striations at the end of the thumbnail. Bracket contains ten striations.

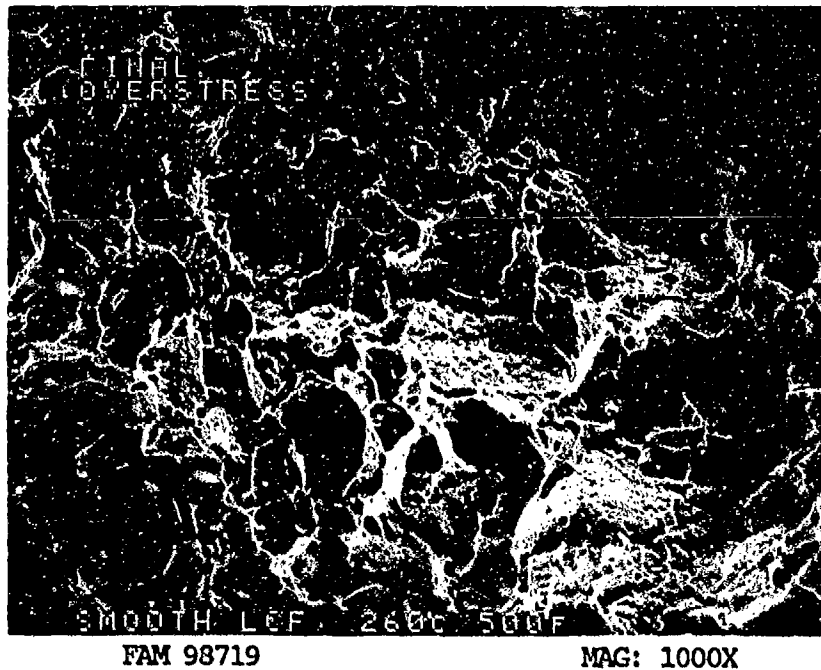


FIGURE 9-104: Dimpled overstress in the final fracture area.

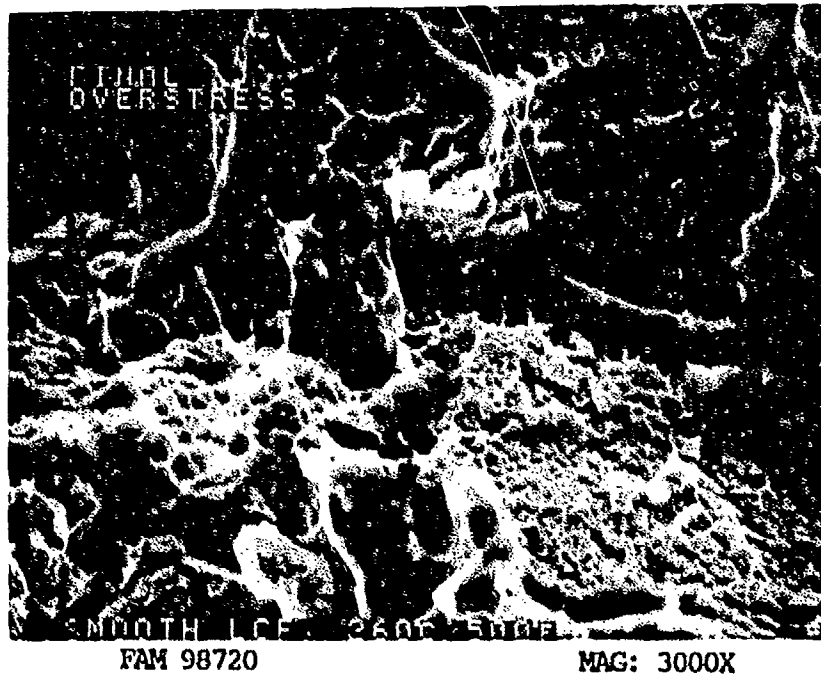


FIGURE 9-105: Fine dimpled overstress in the final fracture area. Cracked carbides are visible in several locations (arrows).

MATERIAL

Inconel X-750
AMS 5667 Bar

TEST DATA

TEST TYPE
Smooth LCF

TEST CONDITIONS

Stress: 965.3 MPa (140 ksi)/ 48.3 MPa (7.0 ksi)
Stress Ratio: 0.05
Frequency: 10 cpm
Atmosphere: Air
Temperature: 593°C (1100°F)
Test Direction: Longitudinal

TEST RESULTS

Cycles to Fracture: 9,499



FAL 93214

MAG: 9X

FIGURE 9-106: Test results and fractography of Inconel X-750 593°C (1100°F) smooth LCF test. Two thumbnails are visible on opposite sides of the specimen (arrows). These thumbnails are roughly perpendicular to the stress axis. The remainder of the fracture occurred at an angle to the stress axis.



FAM 100302

MAG: 200X



FAM 100303

MAG: 500X

FIGURE 9-107: Optical photomicrographs showing the primary fatigue progression area (top) and grain boundary oxidation along the test specimen gage area (bottom). The grain boundaries are less distinct than in the lower temperature specimens (Figure 9-98) and exposed grain boundaries along the gage area have been oxidized (arrows, bottom).

Etchant: Glyceregia

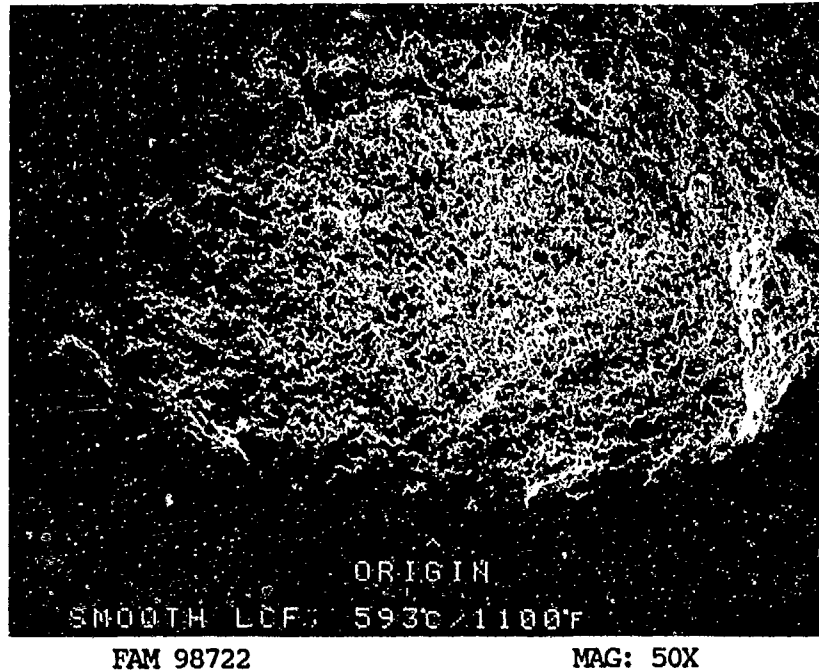


FIGURE 9-108: Low magnification photograph of the larger thumbnail. The localized origin area is indicated by an arrow.

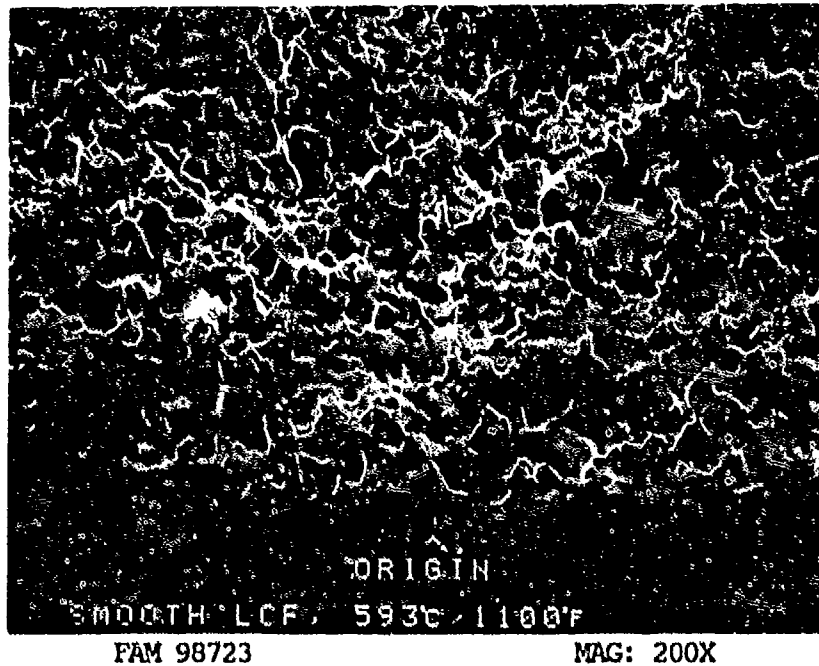


FIGURE 9-109: Higher magnification view of the origin area shown in Figure 9-108. The fracture surface within the thumbnail has a granular appearance.

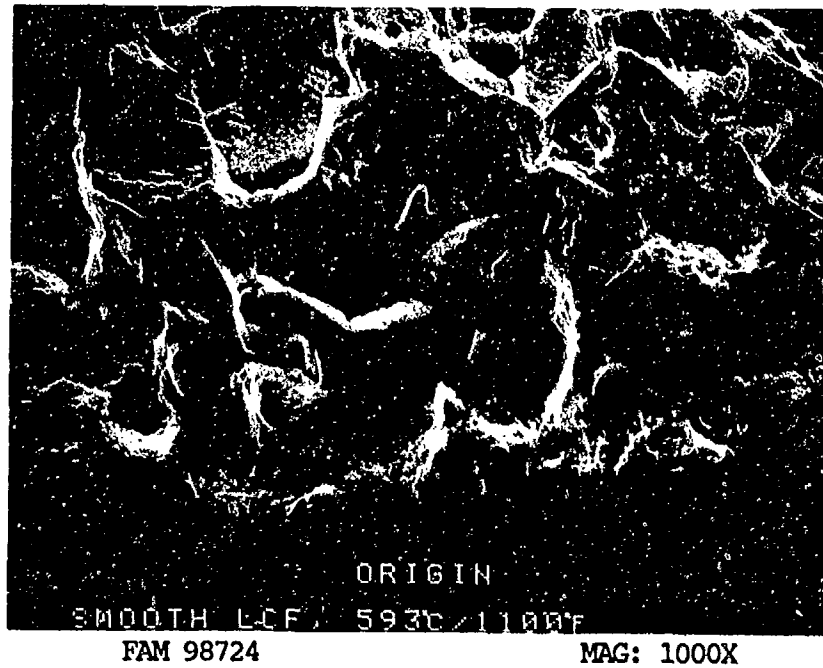


FIGURE 9-110: Higher magnification photograph of the origin area. The fracture appears to be intergranular within the thumbnail and is moderately oxidized. No striations are visible in the immediate origin area.

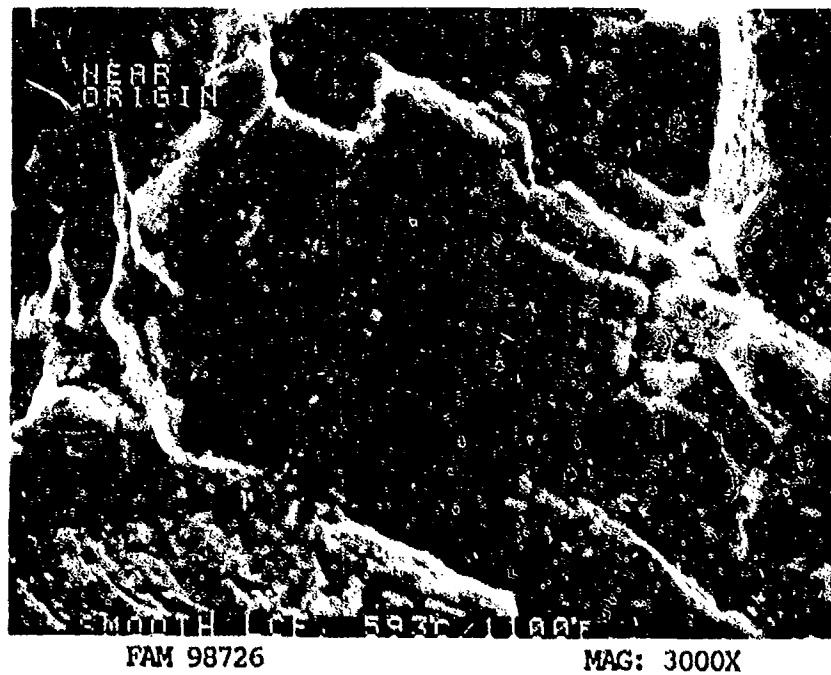


FIGURE 9-111: Oxidized fatigue striations near the origin. The direction of propagation is shown by an arrow.

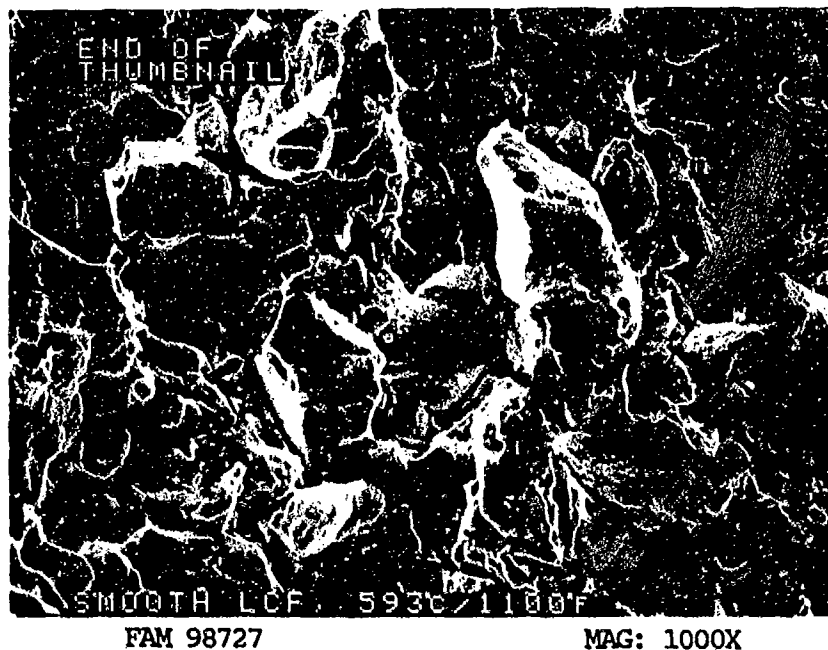


FIGURE 9-112: Grain boundary separation near the end of the thumbnail. Some remnant fatigue features are visible (arrows A). Grain boundary separation has occurred in several areas (arrows B).



FIGURE 9-113: Higher magnification photograph of the area shown in Figure 9-112, showing remnant fatigue features.

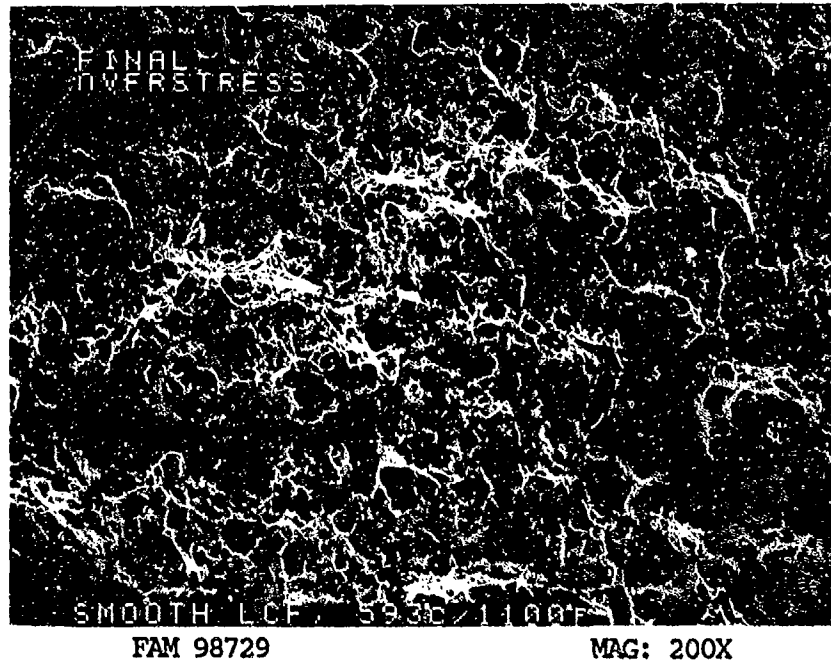


FIGURE 9-114: Transgranular dimpled overstress in the final fracture area.

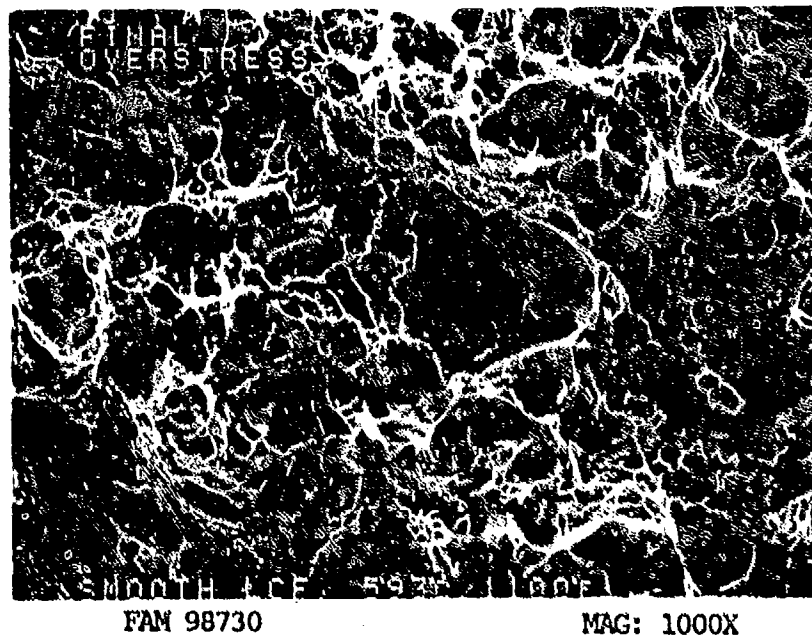


FIGURE 9-115: Higher magnification photograph of the area shown in Figure 9-114, showing transgranular dimpled overstress. The surface contains both very fine and coarser dimples.

MATERIAL

Inconel X-750
AMS 5667 Bar

TEST DATA

TEST TYPE

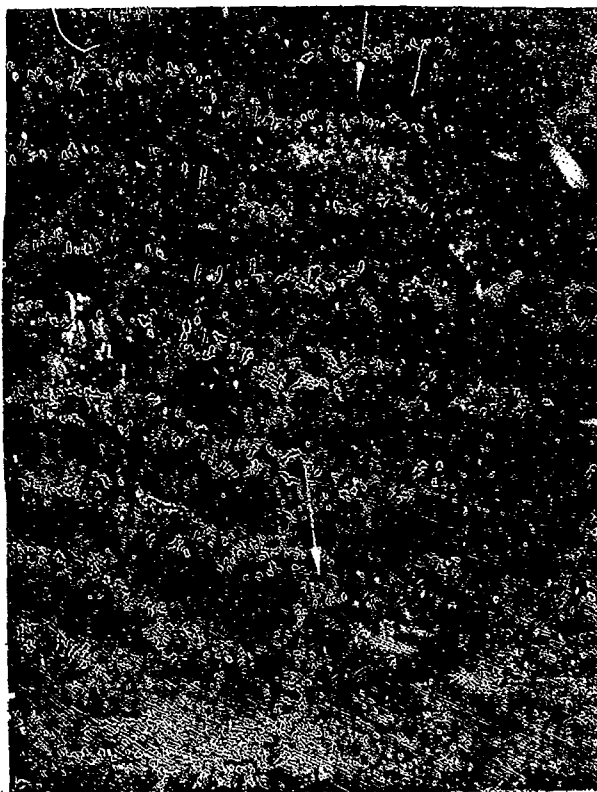
TMF, In-Phase

TEST CONDITIONS

Stress: 723.9 MPa (105.0 ksi)/-758.4 MPa (-110.0 ksi)
Stress Ratio: -1.05
Frequency: 1 cpm
Atmosphere: Air
Temperature: 593°C (1100°F)/260°C (500°F)
Test Direction: Longitudinal

TEST RESULTS

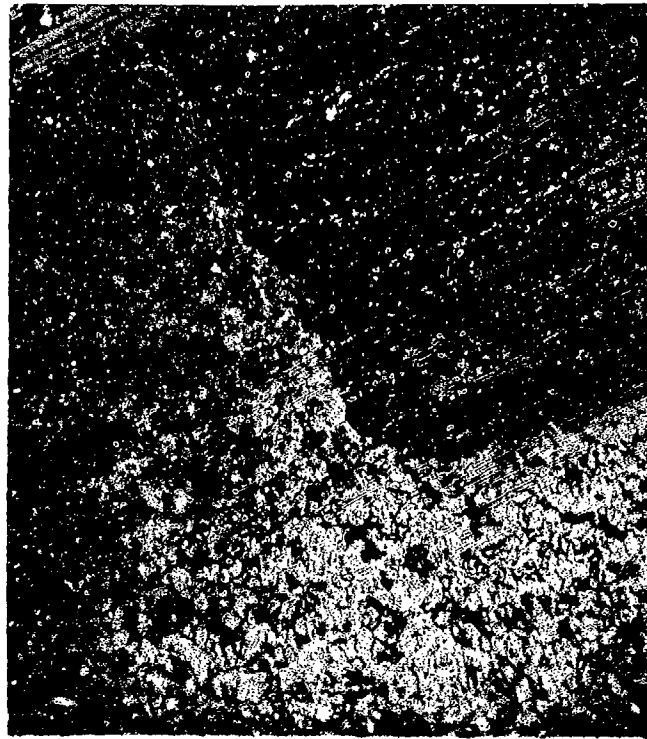
Cycles to Fracture: 704



FAL 94286

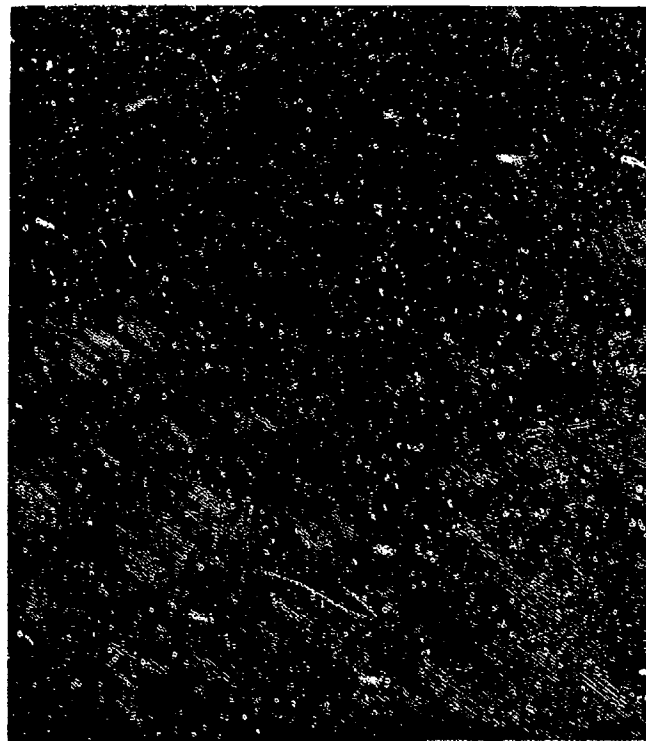
MAG: 10X

FIGURE 9-116: Test results and fractography of Inco X-750 In-Phase TMF test. Oxidized (dark) fatigue progression zones are visible on both the O.D. and I.D. surfaces. The origin areas are indicated by arrows.



FAM 100201

MAG: 200X

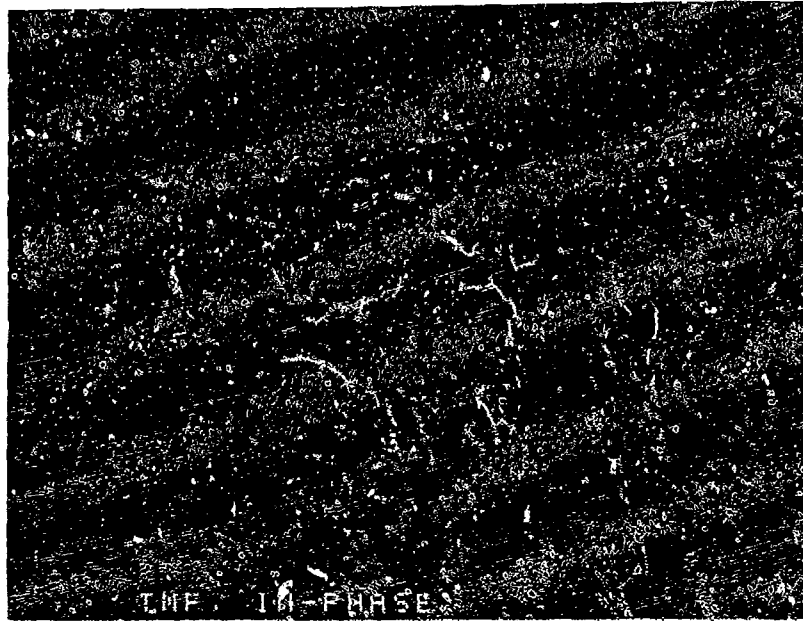


FAM 100202

MAG: 200X

FIGURE 9-117: Optical photomicrographs showing the primary fracture (top) and the microstructure away from the fracture (bottom). Extensive grain boundary separation and grain deformation is visible adjacent to the fracture. This is typical of high temperature/high stress fractures. Note that the specimen fractured after only 704 cycles.

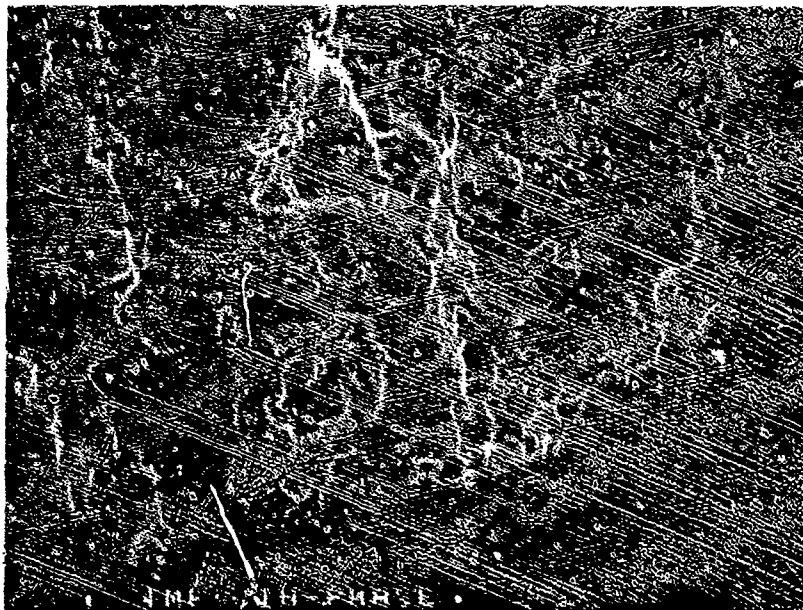
Etchant: Glyceregia



FAM 99456

MAG: 50X

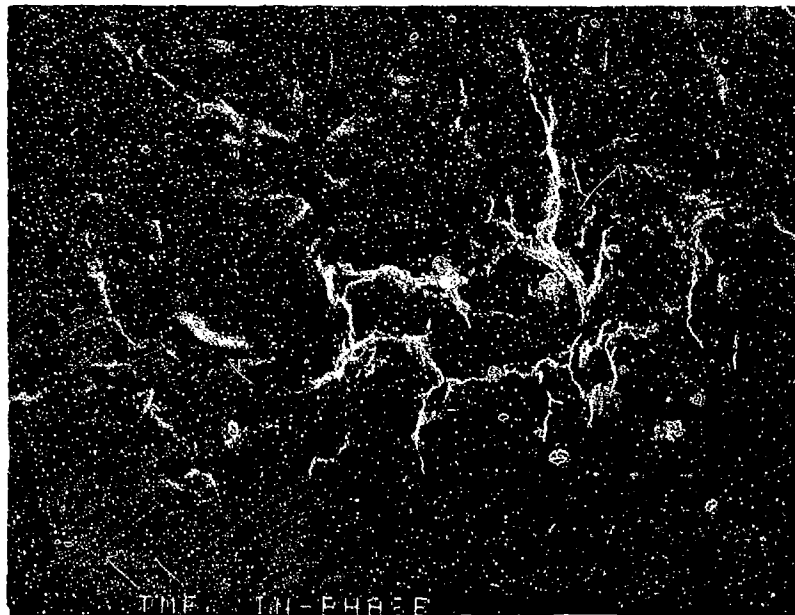
FIGURE 9-118: Low magnification photograph of the larger thumbnail. No localized origin can be identified. A shear lip is visible on the inside surface (top).



FAM 99457

MAG: 200X

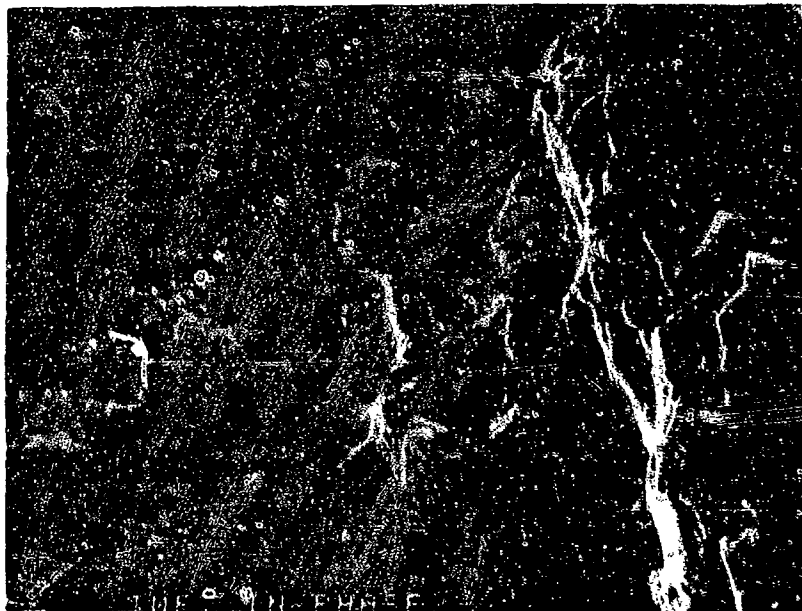
FIGURE 9-119: Higher magnification view of the fatigue progression zone shown in Figure 9-118. The fracture has oxidized areas and is intergranular in appearance.



FAM 99458

MAG: 1000X

FIGURE 9-120: High magnification photograph of the origin area. The fracture is heavily oxidized and intergranular within the thumbnail.



FAM 99459

MAG: 3000X

FIGURE 9-121: Heavily oxidized fatigue progression zone. No features are discernible.

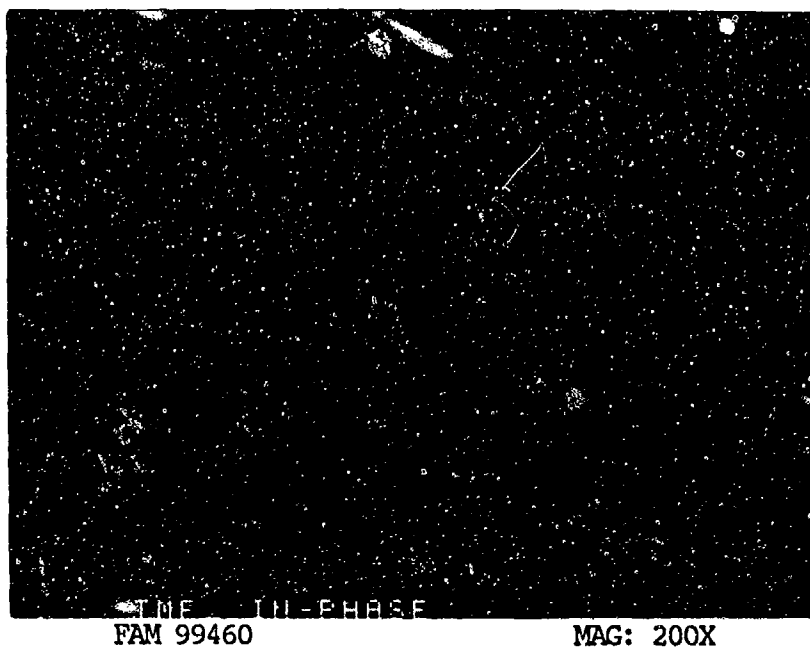


FIGURE 9-122: Final overstress area exhibiting oxidized dimpled overstress.

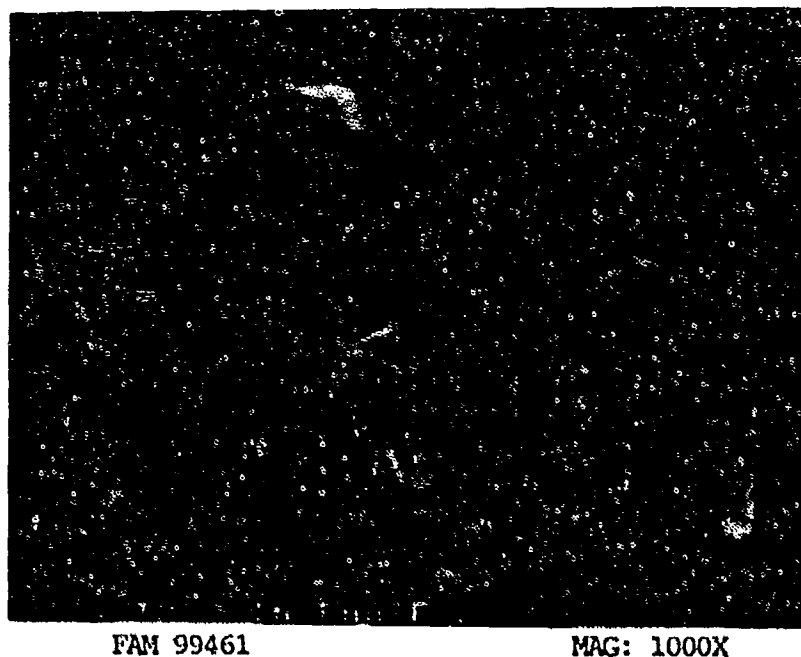


FIGURE 9-123: Oxidized dimpled overstress. The oxidation is not as severe as in the fatigue progression zone because the fatigue area was exposed to the air for a longer time.

MATERIAL

Inconel X-750
AMS 5667 Bar

TEST DATA

TEST TYPE

TMF, Out-of-Phase

TEST CONDITIONS

Stress: 758.4 MPa (110.0 ksi)/723.9 MPa (105.0 ksi)

Stress Ratio: -0.95

Frequency: 1 cpm

Atmosphere: Air

Temperature: 593°C (1100°F)/260°C (500°F)

Test Direction: Longitudinal

TEST RESULTS

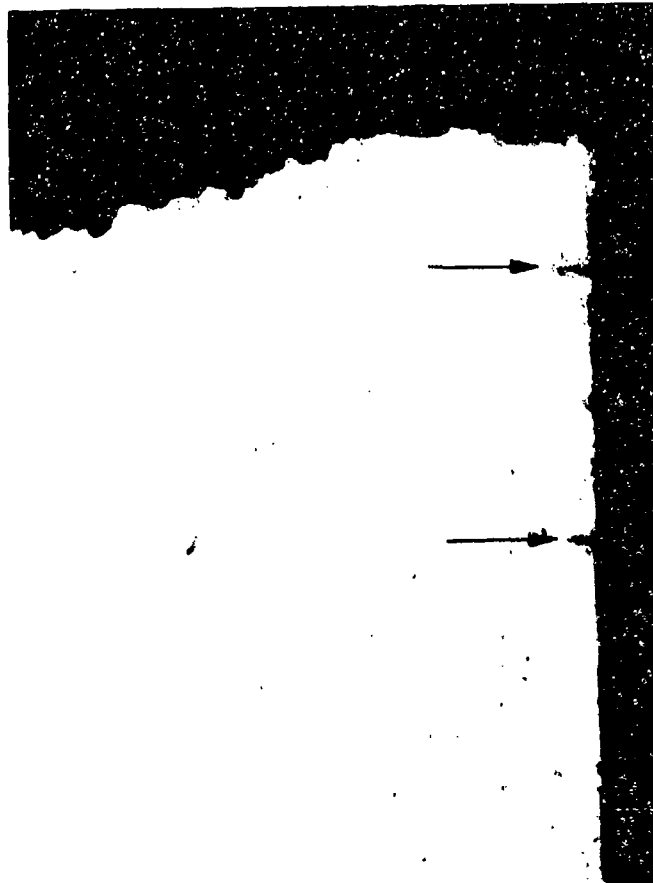
Cycles to Fracture: 2209



FAL 94287

MAG: 10X

FIGURE 9-124: Test results and fractography of Inco X-750 Out-of-Phase TMF test. Two oxidized fatigue progression zones (thumbnails) are visible at the I.D. surface of the specimen (arrows). Arrest marks can be seen within the thumbnails.

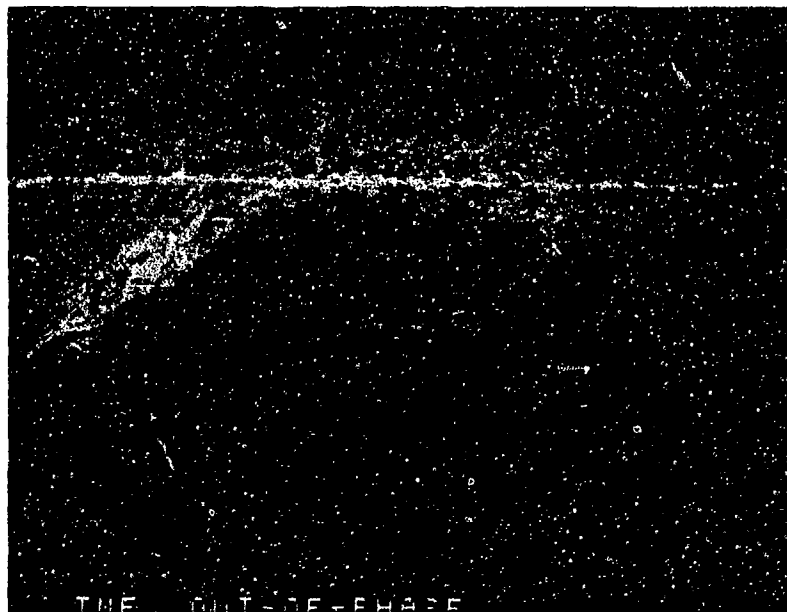


FAM 100283

MAG: 640X

FIGURE 9-125: Optical photomicrograph showing the primary fracture and V-shaped secondary cracks (arrows) along the specimen gage area. These oxidized secondary cracks are indicative of TMF.

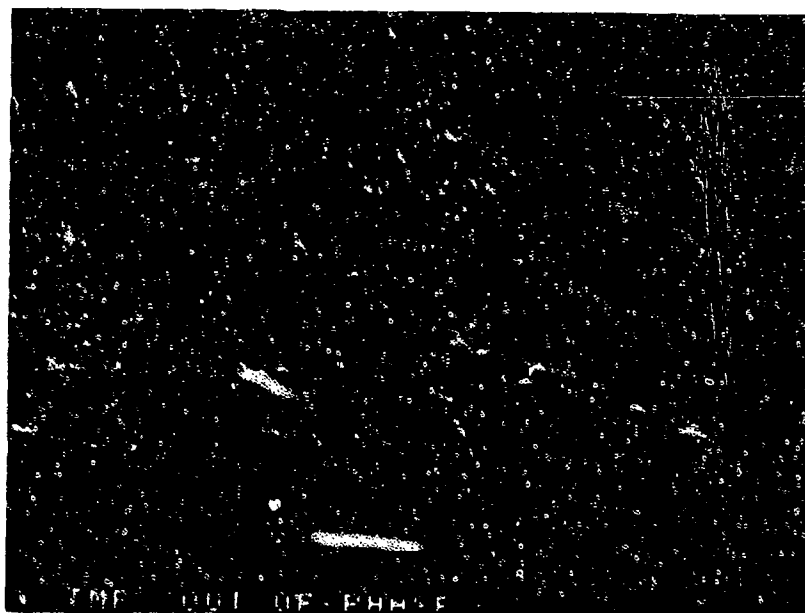
Etchant: Glyceregia



FAM 99447

MAG: 50X

FIGURE 9-126: Low magnification photograph of the larger thumbnail. The fatigue appears to propagate from multiple I.D. origins.



FAM 99448

MAG: 200X

FIGURE 9-127: Higher magnification view of the origin area and fatigue progression zone shown in Figure 9-126. A series of origins (arrows) are visible along the I.D. surface.

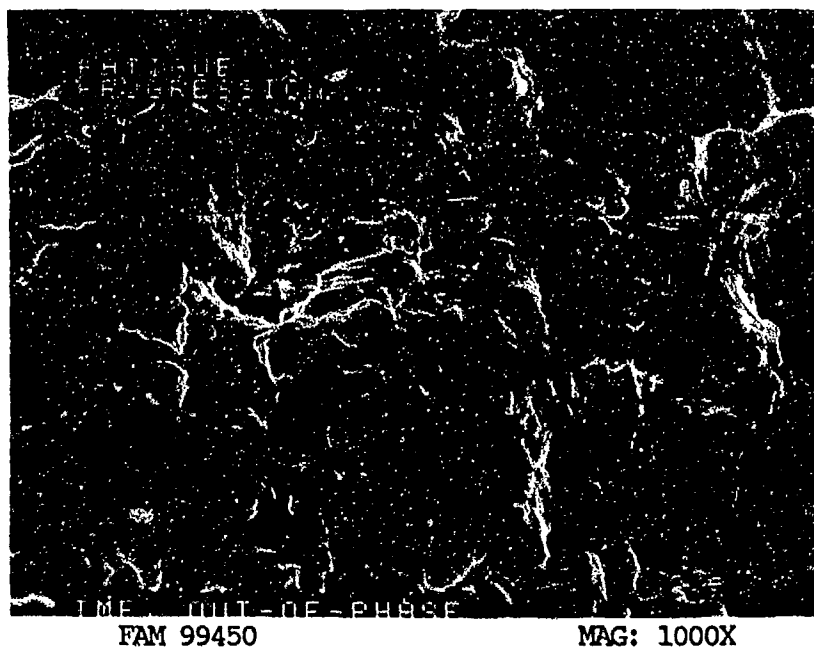


FIGURE 9-128: Coarse oxidized striations in the fatigue progression zone. The propagation is from bottom to top of the photograph.

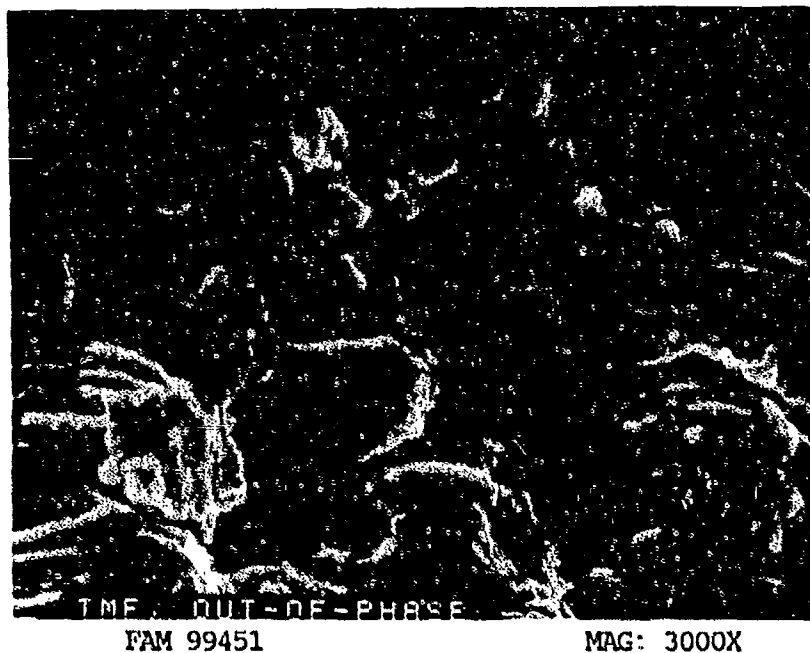


FIGURE 9-129: Higher magnification photograph of the area shown in Figure 9-128, showing both oxidized striations and crack-like striations.

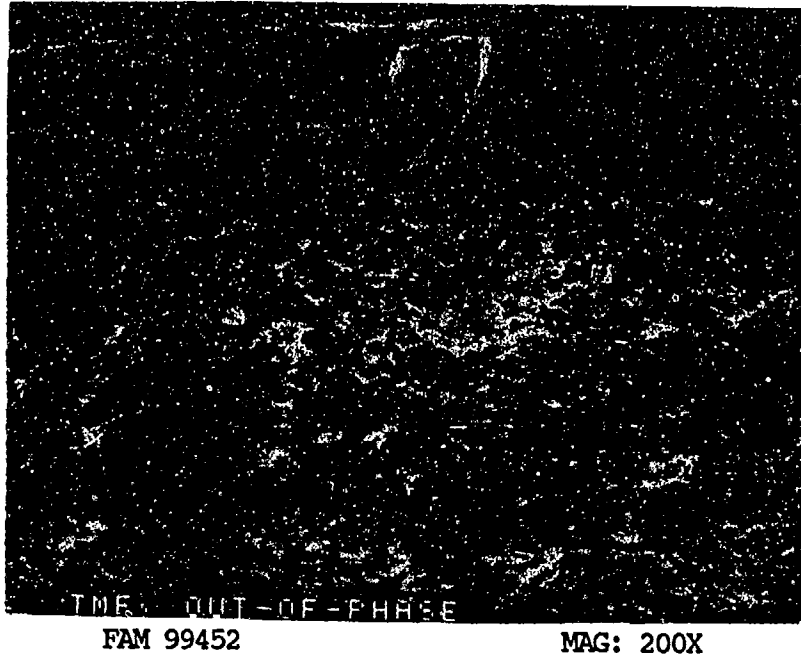


FIGURE 9-130: Final overstress area exhibiting oxidized dimpled overstress.

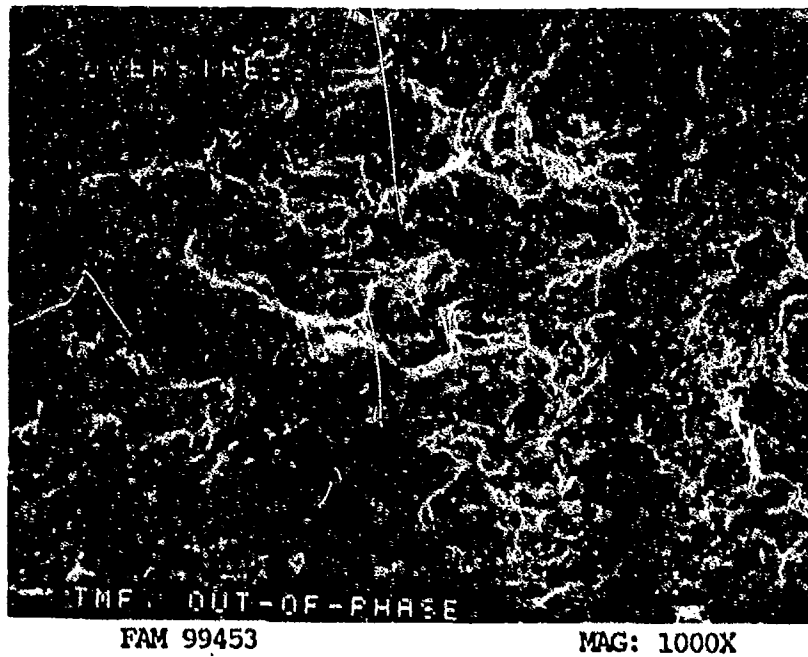
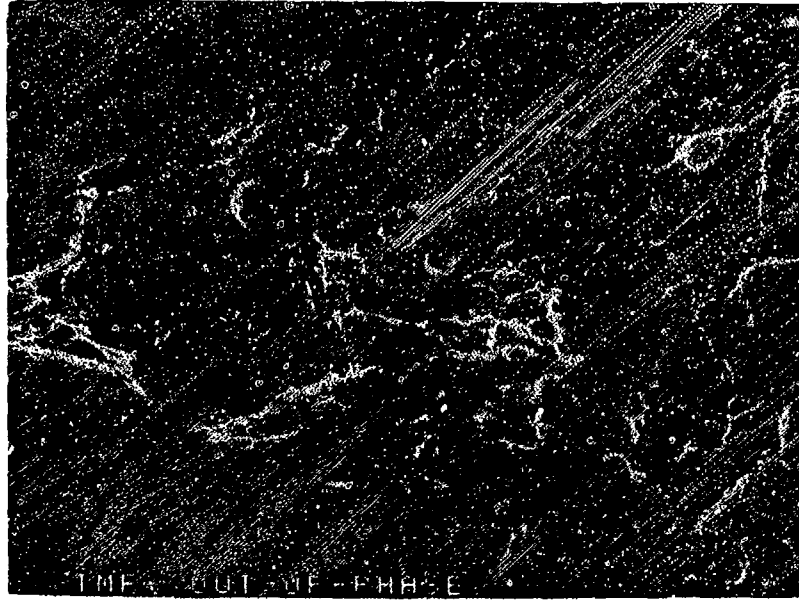


FIGURE 9-131: Fine oxidized dimpled overstress in the area shown in Figure 9-130.



FAM 99454

MAG: 3000X

FIGURE 9-132: Fine equiaxed dimpled overstress in the final overstress area.

SERVICE FAILURE

FRACTURE MODE Fatigue (probable high cycle fatigue)

PART NAME Quick Fill Bellows Assembly

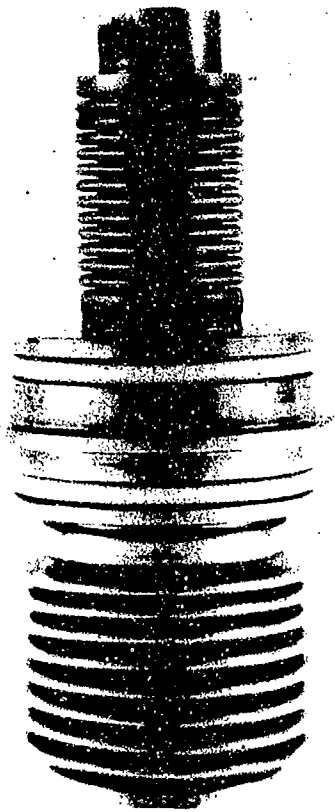
OPERATION DATA The bellows operated in a standard gas turbine engine environment and may have been subjected to both low cycle and vibratory loads.

PART TIME 5343 hours

	<u>REQUIRED</u>	<u>ACTUAL</u>
MAT'L		
BASE	<u>Inconel X-750</u>	<u>confirmed</u>
OTHER	<u>-</u>	<u>-</u>
HARDNESS	<u>No requirement</u>	<u>HRC 36-44 *</u>
GRAIN SIZE	<u>No requirement</u>	<u>ASTM 6-9</u>
DIMENSIONAL	<u>Wall thickness: 0.004-0.005 inch</u>	<u>0.0039 inch</u>

* Diamond pyramid hardness (DPH) conversions.

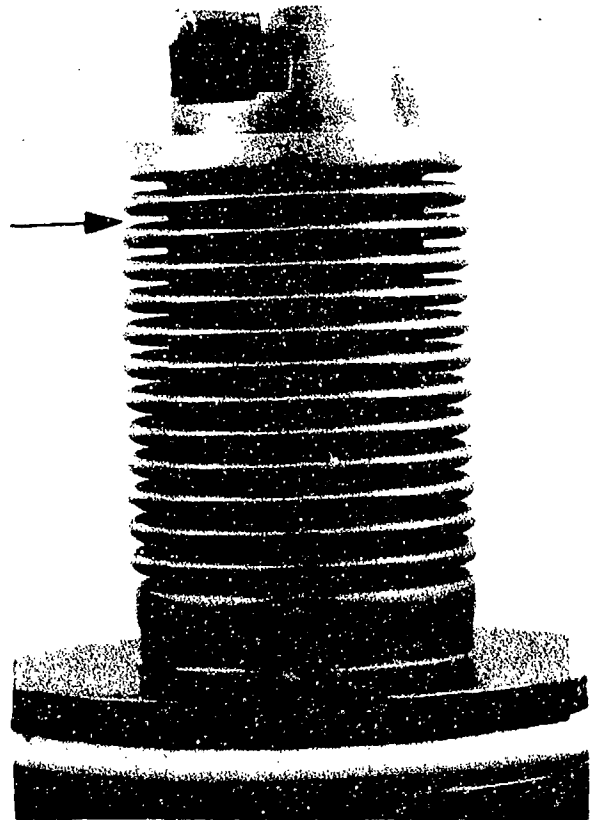
SUMMARY: The crack in the second convolution of the small bellows of the quick fill bellows assembly was the result of fatigue (probable HCF) progressing from multiple origins on the O.D. surface. The crack extended 0.45 inch in length and was predominantly transgranular. No material defects were found. The hardness was HRC 36-39 in the flat sections of the bellows and HRC 40-44 in the bends. This variation in hardness was attributed to work hardening that probably occurred during manufacturing.



FAL 88632

MAG: 1 1/2X

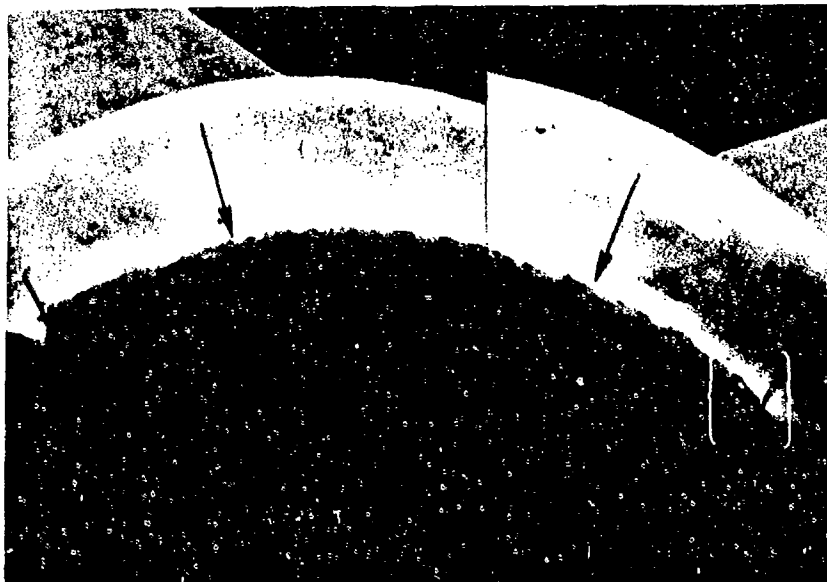
FIGURE 9-133: Overall photograph of the quick fill bellows assembly. The crack is in the small bellows (top).



FAL 88633

MAG: 3X

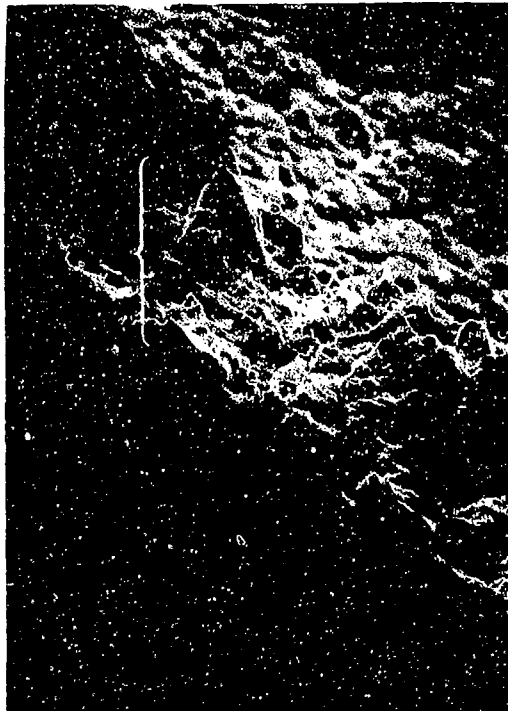
FIGURE 9-134: Close-up of the small bellows. Arrow indicate the location of the crack in the second convolution.



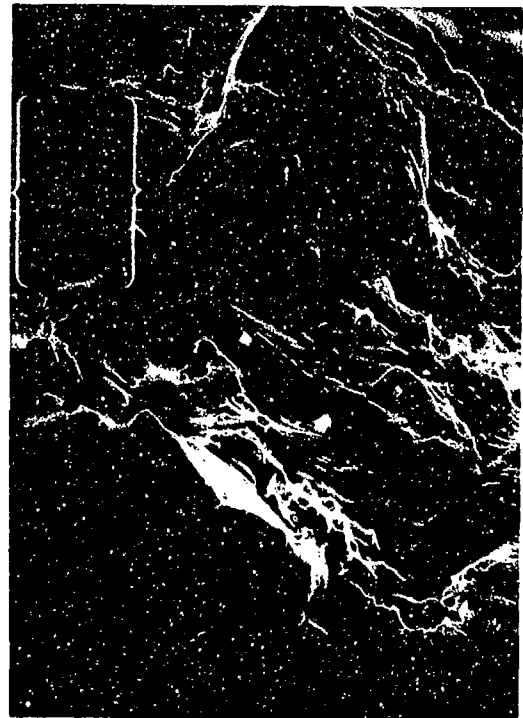
FAL 93341

MAG: 10X

FIGURE 9-135: Composite SEM photograph of the opened crack surface. The extent of the fatigue is shown by black brackets. Fatigue origins were on the O.D. surface (arrows).



FAL 93345 MAG: 300X



FAL 93346 MAG: 1000X

FIGURE 9-136: SEM photograph of the opened crack surface. The location of photograph 122 is shown by a bracket.

FIGURE 9-137: Photograph 122 relatively fine fatigue striations indicating propagation from the O.D. surface.



FAL 93344 MAG: 4000X



FAL 93347 MAG: 10,000X

FIGURE 9-138: Higher magnification photograph of the fatigue striations. The curvature of the striations with their concave side up indicates propagation from top to bottom of the photograph.

FIGURE 9-139: High magnification SEM photograph showing very fine fatigue striations (brackets).

PWA 1480 (Cast Ni-Based Single Crystal)

Material Description

PWA 1480 is a nickel-base vacuum melted, investment cast, single crystal alloy used in turbine airfoils at temperatures up to 1900 F. The alloy was tested in two orientations, [001] and [111]. The material used in this study was heat treated to PWA 1480 with a typical hardness of HRC 35-45. Measured hardness was HRC 40-43.

Fractography Overview

Four smooth tensile test specimens were examined, two each at 800° F and 1800 F. The difference between the specimens was the specimen orientation, with the stress axis aligned with the [001] crystal orientation for two specimens and the [111] orientation for the other two. Both the [001] and [111] orientated 800 F specimens had large facets covering almost the entire fracture surface with fracture occurring along preferred crystallographic planes in the lattice. These planes were at an angle to the stress axis. The [001] specimen had small patches of dimpled overstress and generally more change in fracture path than the [111] specimen. The cleavage planes on both specimens exhibited slip lines and the blocky microstructure constituent gamma prime. This gave the fractures a scaly appearance at high magnification. The two 1800 F specimens had more ductile appearances. Both had higher percent elongation and larger reduction of area than the 800 F specimens. The [001] specimen exhibited oxidized overstress features with areas of void coalescence. The [111] specimen had deep tearing features that appeared to be very large elongated and ruptured voids.

A single stress rupture specimen was examined in the [111] orientation. The macroscopic appearance was similar to the 1800 F tensile specimens. At higher magnifications the fracture exhibited round islands of lightly oxidized cleavage type fracture surrounded and separated by oxidized overstress features.

Three LCF specimens were examined; [001] orientation 800° F, [001] orientation 1800 F and [111] orientation 1800 F. The lower temperature specimen was coated with an aluminide diffusion coating. The fracture features were unlike any others observed. The fracture propagated from multiple origins along a plane roughly perpendicular to the stress axis. Between 0.010 and 0.020 inch subsurface, the fracture path changed directions to a series of planes forming roughly a 45° angle to the stress axis. This transition formed a saw tooth pattern with an axial secondary crack where the change of fracture path occurred. The planes at an angle to the stress axis exhibited unusual arrest marks radiating from the origin area. These marks appeared as a series of bands of smear features perpendicular to the direction of propagation. Between these bands the

fracture was cleavage associated with gamma prime precipitates in the microstructure. The bands of smeared features may be arrest marks that were smeared as the fracture propagated.

The [001] orientation 1800 F specimen ran only 718 cycles. No striations were visible in the fatigue area which was covered primarily with oxide and smear features. There was a clear difference between the fatigue and final overstress areas. The final overstress exhibited heavy oxide on a fracture associated with the gamma prime precipitates. The [111] orientation 1800 F specimen had a clear oxidized thumbnail fatigue progression. The fracture originated at a small subsurface void and was heavily oxidized and nearly featureless near the origin. At the end of the thumbnail, near the center of the specimen, heavily oxidized remnant striations were visible. The final overstress area exhibited oxidized cleavage features with discrete patches of feathery or fan-shaped cleavage.

One [001] orientation out-of-phase TMF specimen was examined. The fracture exhibited an oxidized fatigue progression area that originated at a heavily oxidized surface connected void. The area adjacent to the origin was flat and featureless. As the fatigue progressed the fracture exhibited a series of steps separated by oxidized regions. These steps occurred in an area where the fracture was changing direction and may be associated with the change in the relationship between the crystallographic orientation of the crack tip and the stress axis. Crack-like striations were also observed in the thumbnail area. Final overstress occurred by dimpled overstress associated with the gamma prime precipitates. Discrete patches of feathery or fan-shaped cleavage were also present.

MATERIAL

PWA 1480
[001] Orientation

TEST DATA

TEST TYPE
Smooth Tensile

TEST CONDITIONS
Strain Rate: 0.005 mm/mm/min (0.005 in/in/min)
Atmosphere: Air
Temperature: 427°C (800°F)
Test Direction: Longitudinal

TEST RESULTS
0.2% Yield Strength: 965.3 MPa (140.0 ksi)
Ultimate Strength: 1196.3 MPa (173.5 ksi)
% Elongation 5.0
% Reduction of Area: 7.1



FAL 92927

MAG: 10X

FIGURE 10-1: Test results and fractography of PWA 1480/[001] 427°C (800°F) smooth tensile test. The fracture has a faceted appearance because fracture occurred along crystallographic planes.



FAM 99826

MAG: 200X

FIGURE 10-2: Optical photomicrograph of a metallographic cross section through the fractured specimen. Eutectic phase formed islands in the microstructure and fine cuboidal Gamma Prime phase is dispersed throughout the microstructure. The fracture exhibits little discernible plastic deformation.

Etchant: AG-21

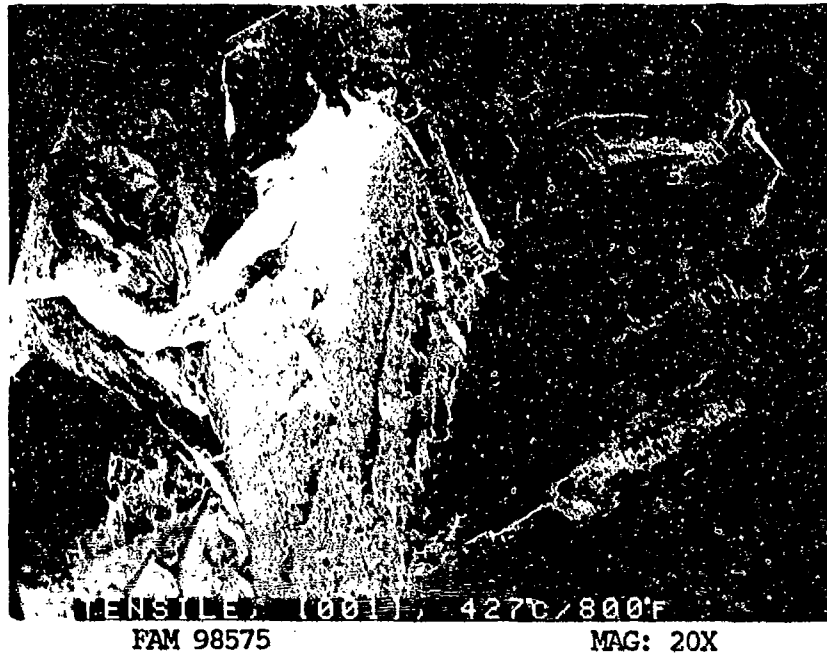


FIGURE 10-3: Low magnification photograph showing the faceted appearance of the fracture. This is the result of fracture along close-packed crystallographic planes.



FIGURE 10-4: Higher magnification photograph of the area shown in Figure 10-3, showing abrupt changes in fracture path (arrows) associated with fracture along close-packed planes.

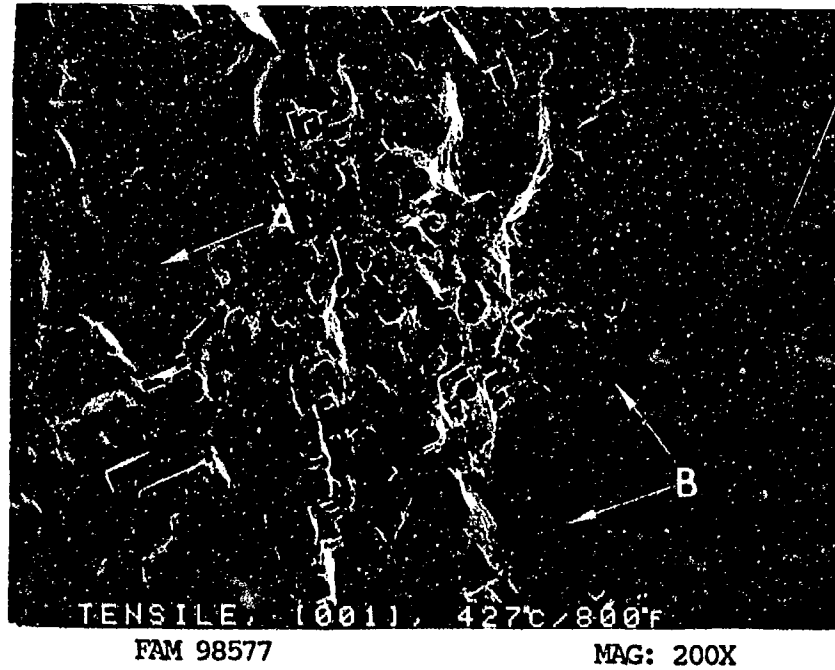


FIGURE 10-5: Higher magnification photograph showing cleavage fracture (arrow A) with patches of dimpled overstress (arrows B).

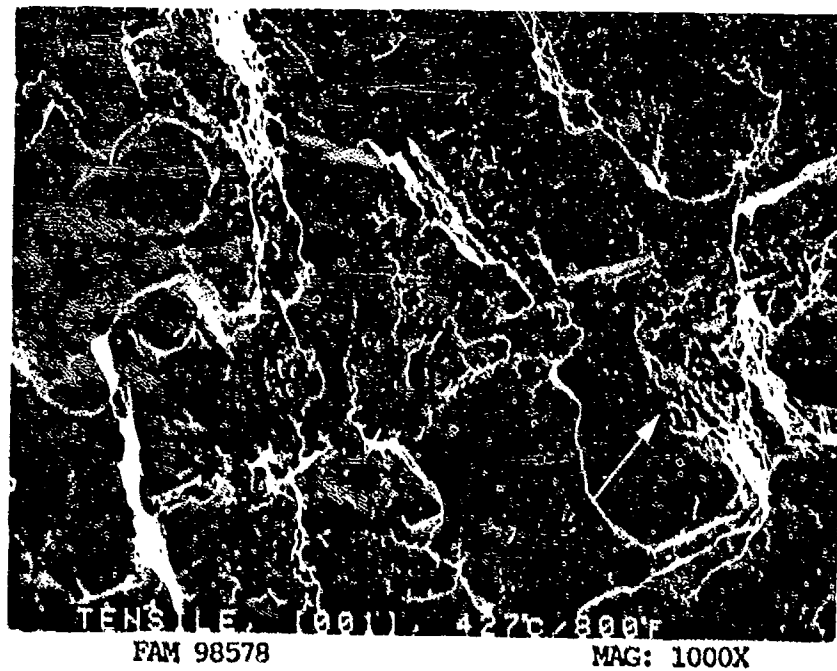


FIGURE 10-6: Higher magnification photograph of the area shown in Figure 10-5, showing dimpled overstress (arrow) between areas of cleavage.

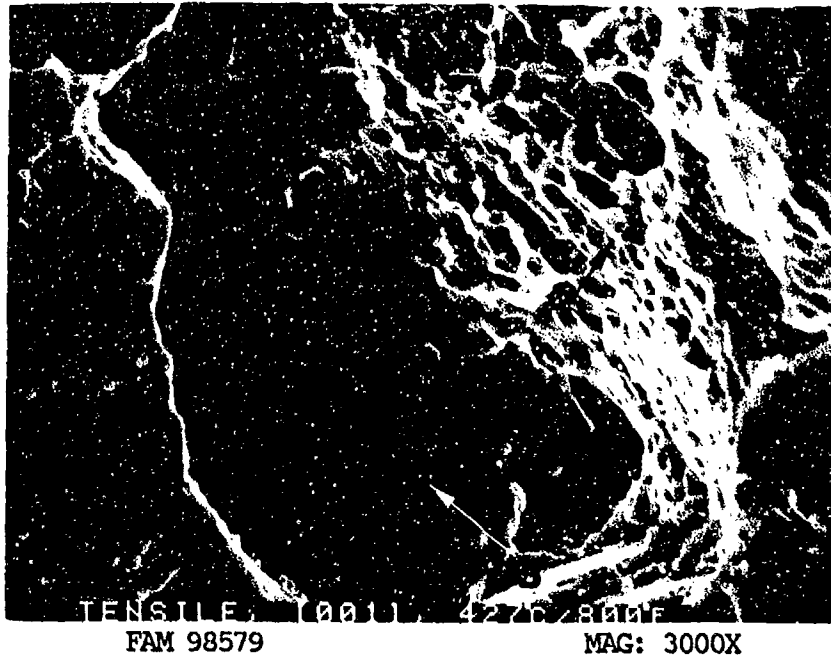


FIGURE 10-7: Mixture of dimpled overstress (arrow A) and cleavage (arrow B) features. The microstructural constituent gamma prime is visible on the cleavage facets, appearing as small squares on the surface (blocky appearance).

MATERIAL

PWA 1480
[001] Orientation

TEST DATA

TEST TYPE

Smooth Tensile

TEST CONDITIONS

Strain Rate: 0.005 mm/mm/min (0.005 in/in/min)
Atmosphere: Air
Temperature: 982°C (1800°F)
Test Direction: Longitudinal

TEST RESULTS

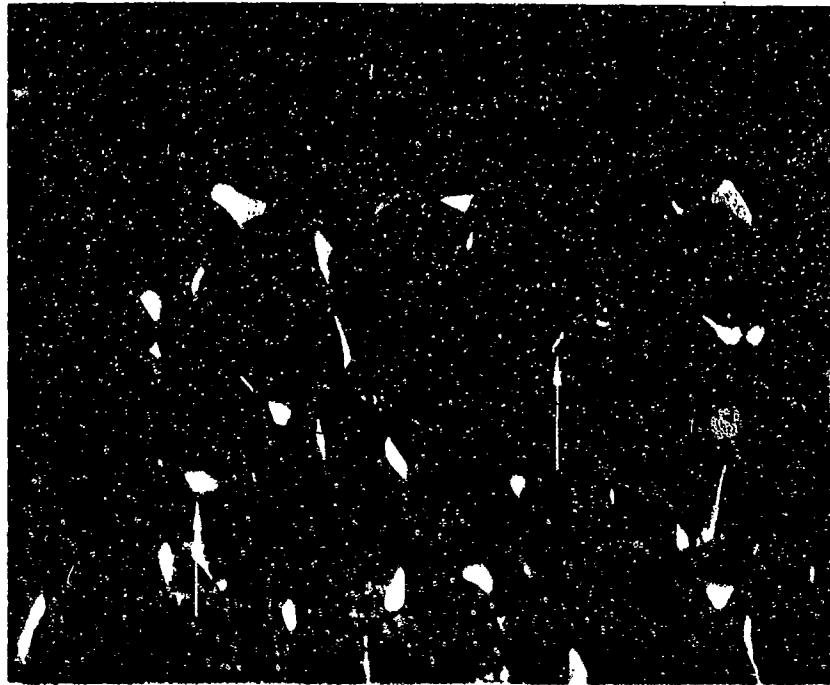
0.2% Yield Strength: 483.3 MPa (71.0 ksi)
Ultimate Strength: 648.1 MPa (94.0 ksi)
% Elongation 15.0
% Reduction of Area: 24.7



FAL 92928

MAG: 10X

FIGURE 10-8: Test results and fractography of PWA 1480/[001] 982°C (1800°F) smooth tensile test. The fracture exhibits less cleavage and more dimpled overstress.



FAM 98813

MAG: 100X

FIGURE 10-9: Optical photomicrograph of a metallographic cross section through the fractured specimen. Eutectic phase formed islands in the matrix of finely dispersed cuboidal gamma prime. The specimen exhibits secondary cracking originating at eutectic islands (arrows).

Etchant: AG-21

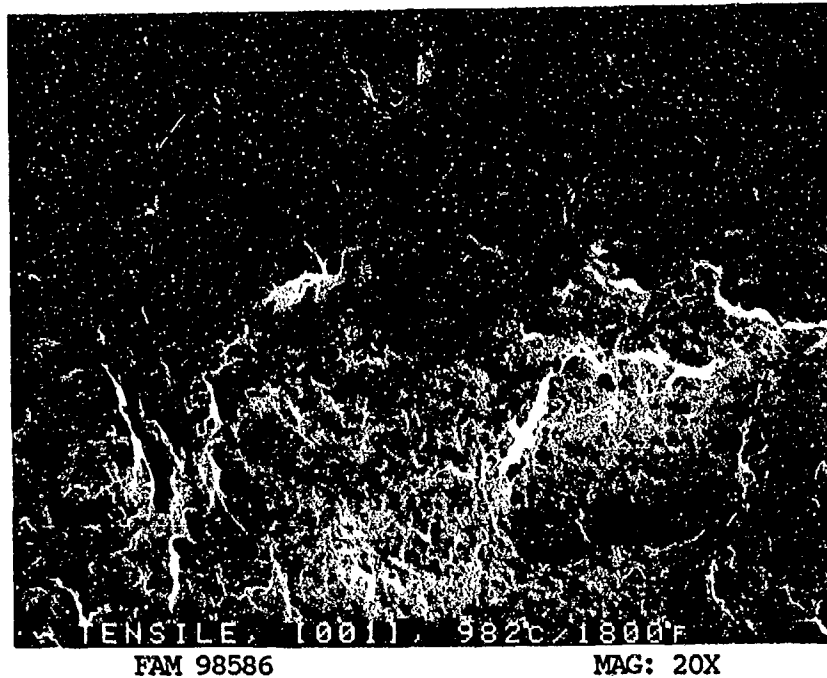


FIGURE 10-10: Low magnification photograph showing the non-crystallographic nature of the fracture. Compare with the 800°F specimen, Figures 10-3 through 10-5.

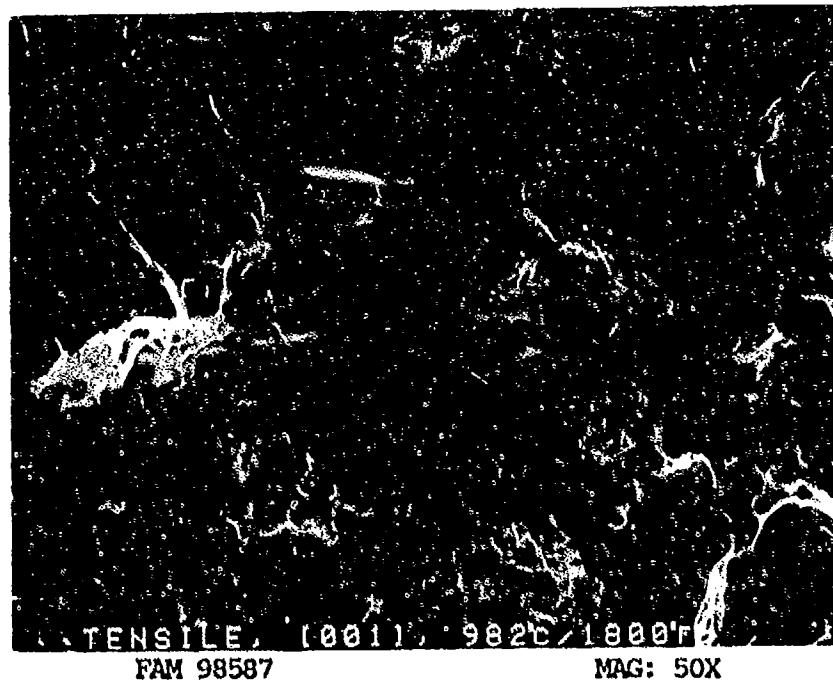


FIGURE 10-11: Oxidized non-crystallographic fracture with dimpled overstress and void coalescence.

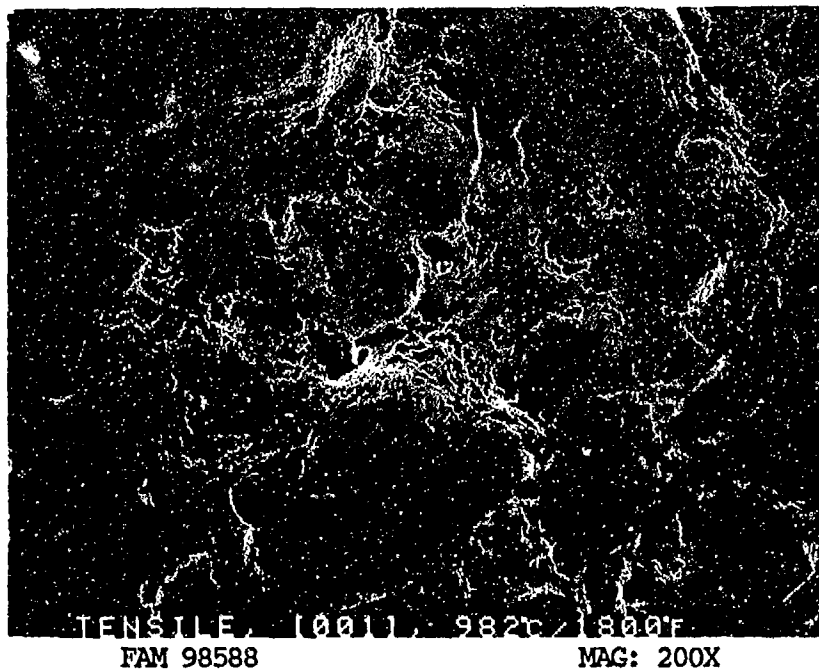


FIGURE 10-12: Higher magnification photograph of a portion of the area shown in Figure 10-11, showing oxidized overstress features.

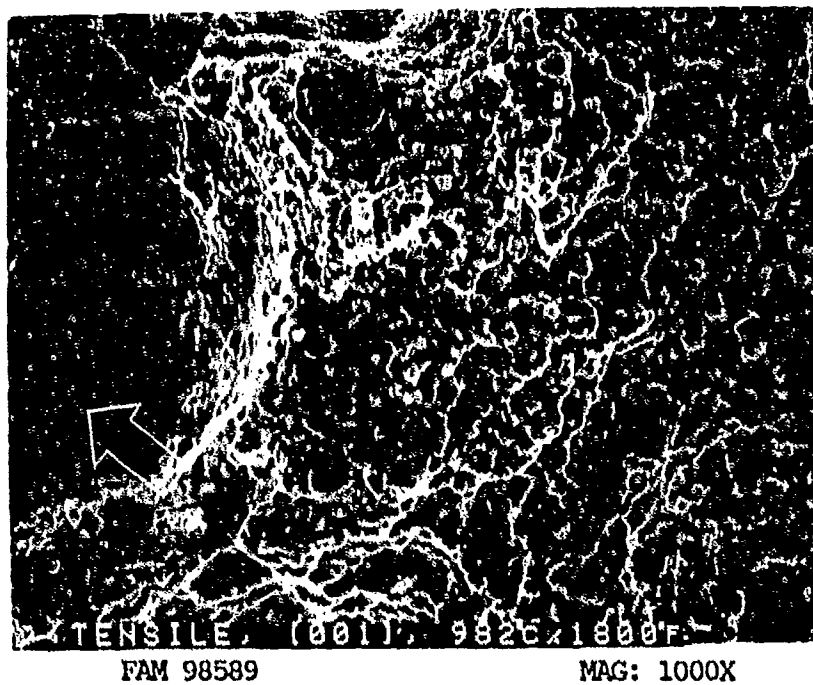


FIGURE 10-13: Oxidized overstress features with some void coalescence (arrow).

MATERIAL

FWA 1480
[111] Orientation

TEST DATA

TEST TYPE
Smooth Tensile

TEST CONDITIONS
Strain Rate: 0.005 mm/mm/min (0.005 in/in/min)
Atmosphere: Air
Temperature: 427°C (800°F)
Test Direction: Longitudinal

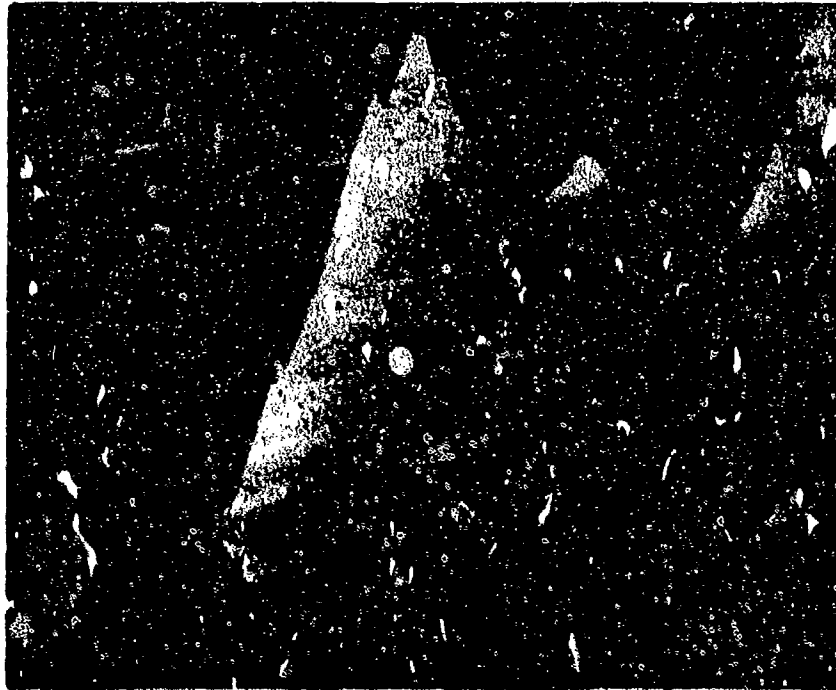
TEST RESULTS
0.2% Yield Strength: 821.2 MPa (119.1 ksi)
Ultimate Strength: 1390.0 MPa (201.6 ksi)
% Elongation 19.5
% Reduction of Area: 18.5



FAL 92929

MAG: 12X

FIGURE 10-14: Test results and fractography of FWA 1480/[111] 427°C (800°F) smooth tensile test. This fracture exhibits more facets than the [001] orientation fracture (Figure 10-1).



FAM 98771

MAG: 100X

FIGURE 10-15: Optical photomicrograph of a metallographic cross section through the fractured specimen. Eutectic phase formed islands in the matrix of finely dispersed cuboidal gamma prime. The fracture occurred on close-packed planes resulting in a jagged appearance.

Etchant: AG-21

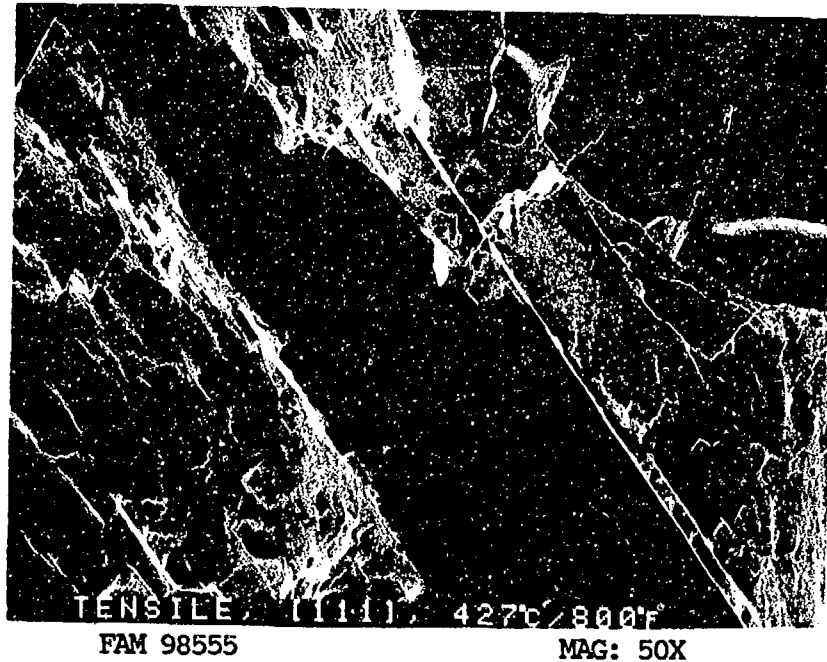


FIGURE 10-16: Low magnification photograph showing faceted crystallographic nature of the fracture surface. The faceting occurs when a specimen fractures along crystallographic planes oriented for maximum resolved shear stress.

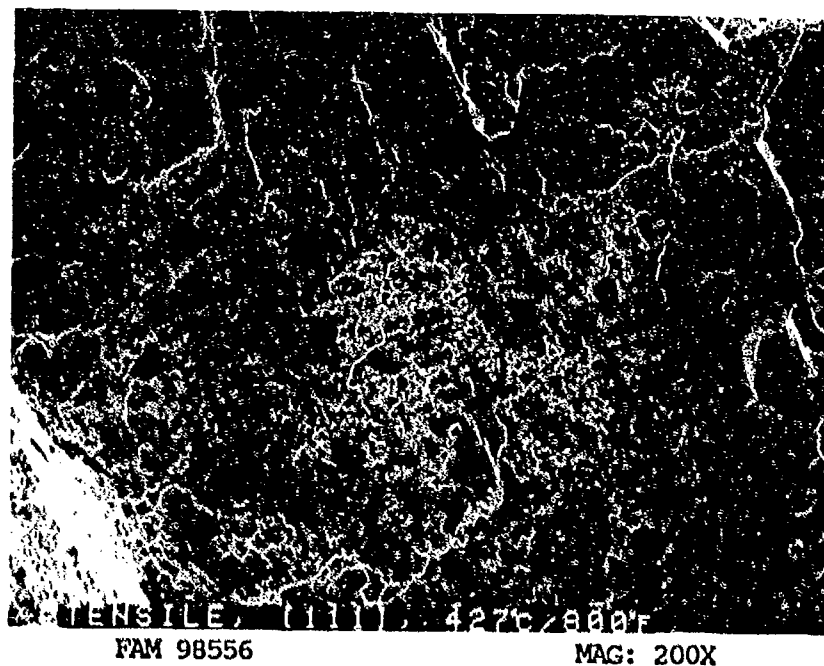


FIGURE 10-17: Cleavage fracture along crystallographic planes.

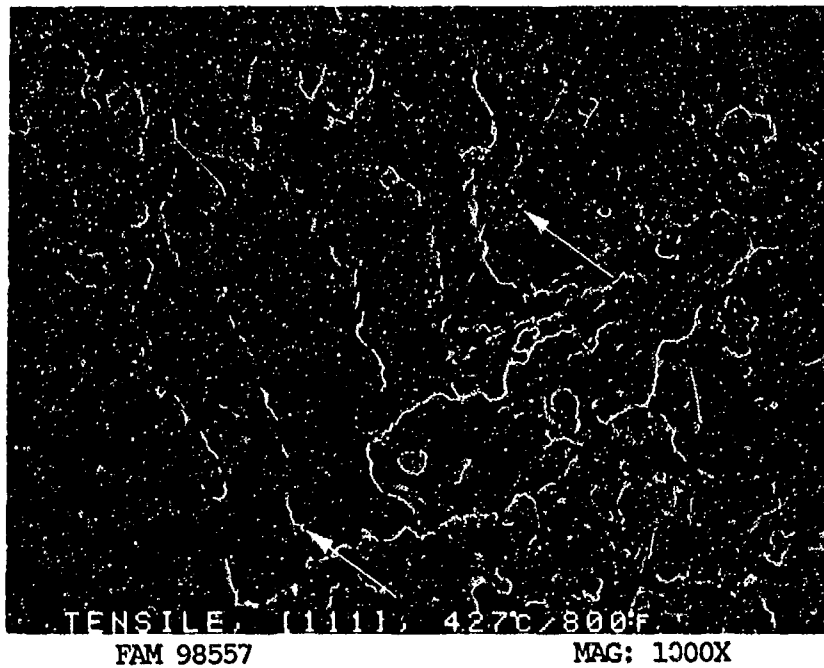


FIGURE 10-18: Higher magnification photograph showing cleavage fracture. Slip lines are visible (arrows).

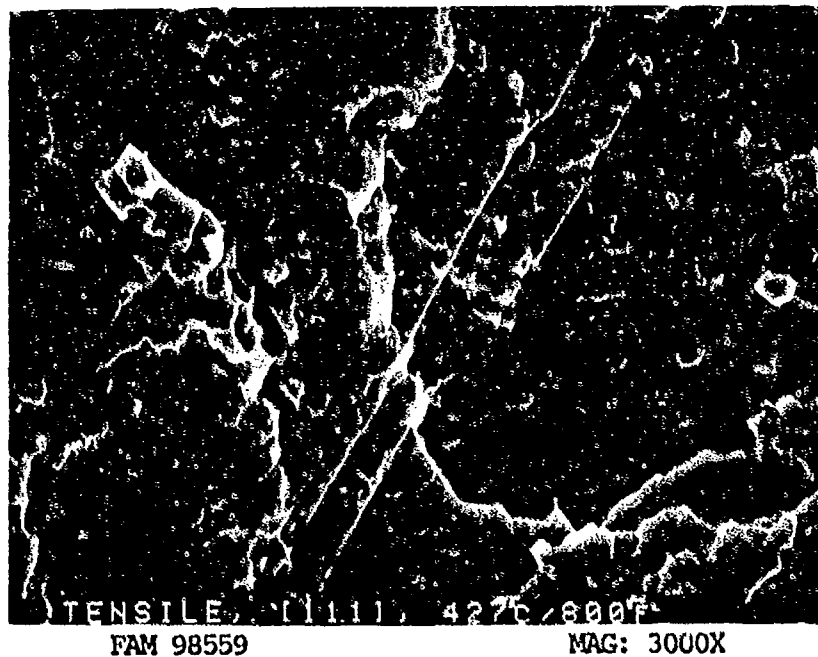


FIGURE 10-19: Cleavage fracture associated with gamma prime precipitates. These precipitates produce a blocky appearance on the fracture surface.

MATERIAL

PWA 1480
[111] Orientation

TEST DATA

TEST TYPE

Smooth Tensile

TEST CONDITIONS

Strain Rate: 0.005 mm/mm/min (0.005 in/in/min)
Atmosphere: Air
Temperature: 982°C (1800°F)
Test Direction: Longitudinal

TEST RESULTS

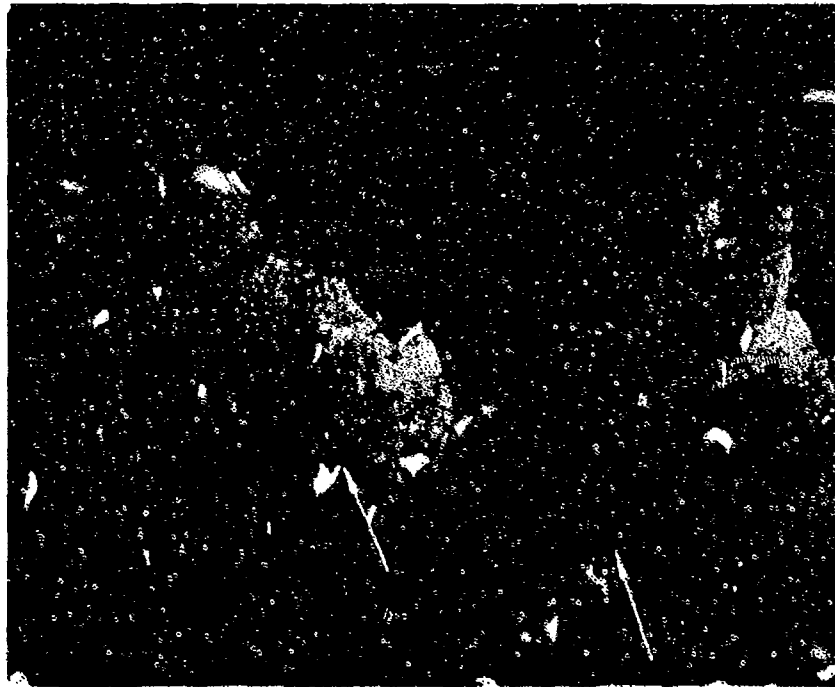
0.2% Yield Strength: 422.6 MPa (64.2 ksi)
Ultimate Strength: 573.7 MPa (83.2 ksi)
% Elongation 20.0
% Reduction of Area: 25.2



FAL 92923

MAG: 12X

FIGURE 10-20: Test results and fractography of PWA 1480/[111] 982°C (1800°F) smooth tensile test. This higher temperature fracture surface does not have the faceted appearance of the 800°F specimen (Figure 10-14).



FAM 98765

MAG: 100X

FIGURE 10-21: Optical photomicrograph of a metallographic cross section through the fractured specimen. Eutectic phase formed islands in the matrix of finely dispersed cuboidal gamma prime. The fracture occurred on close-packed planes resulting in a jagged appearance. Secondary cracks can be seen nucleating at the eutectic phase islands (arrows).

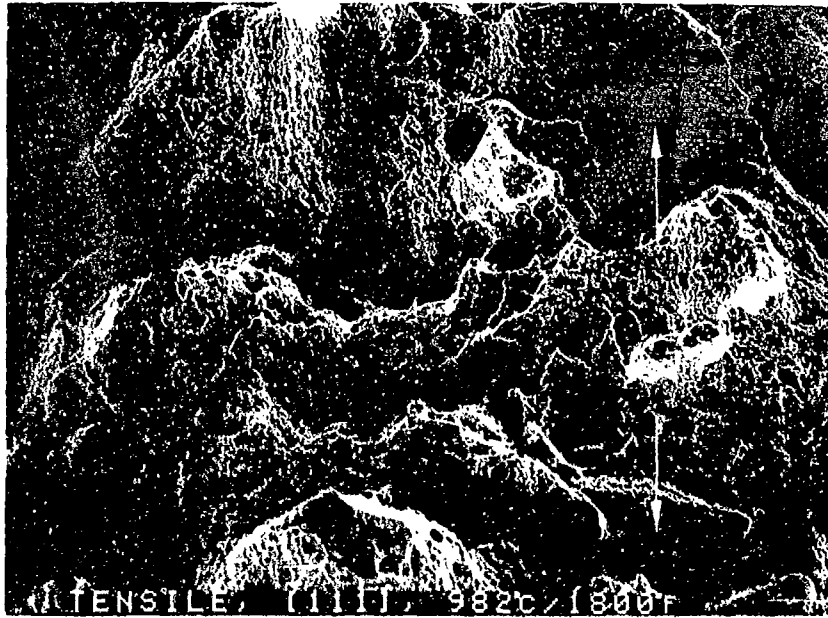
Etchant: AG-21



FIGURE 10-22: Low magnification photograph showing jagged appearance of the fracture.



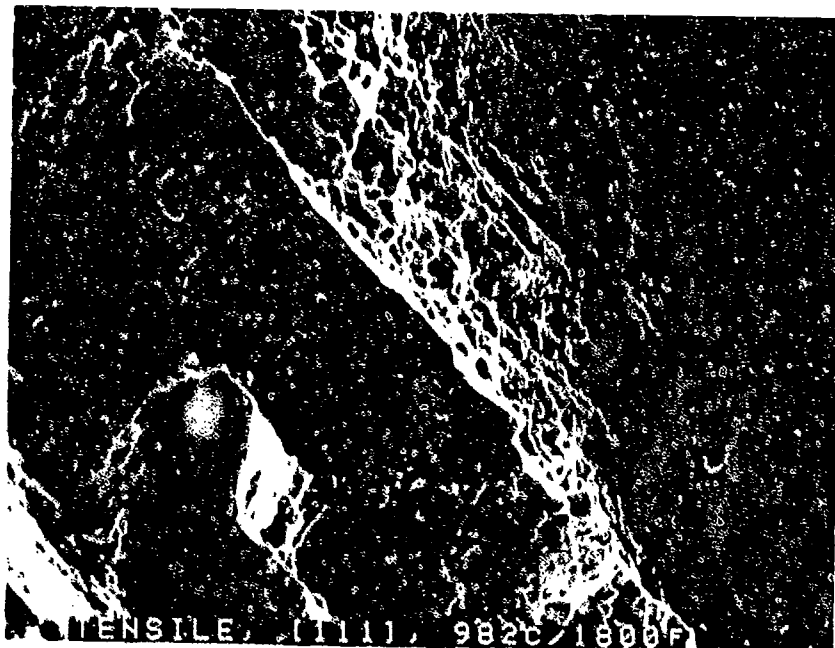
FIGURE 10-23: Oxidized fracture surface with deep jagged appearance resulting from localized cleavage along crystallographic planes. Compare this appearance with the 800°F specimen (Figures 10-16 through 10-19).



FAM 98571

MAG: 200X

FIGURE 10-24: Higher magnification photograph of the area shown in Figure 10-23, showing oxidized overstress features. At this magnification cleavage is visible (arrows).



FAM 98574

MAG: 1000X

FIGURE 10-25: Oxidized cleavage features.

MATERIAL

PWA 1480
[111] Orientation

TEST DATA

TEST TYPE

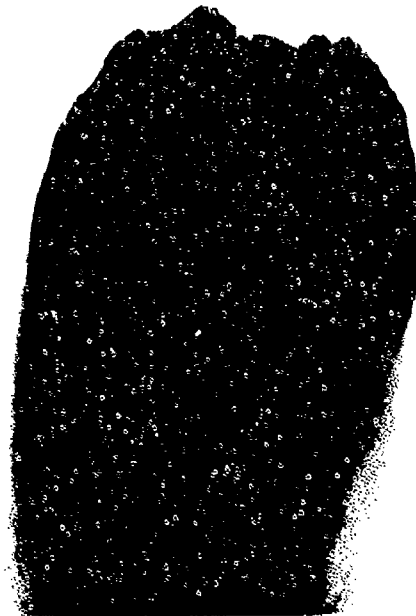
Stress Rupture

TEST CONDITIONS

Stress: 172.4 MPa (25.0 ksi)
Atmosphere: Air
Temperature: 982°C (1800°F)
Test Direction: Longitudinal

TEST RESULTS

Time to Fracture: 409.7 hours
% Elongation 17.8



FAL 94098

MAG: 14X

FIGURE 10-26: Test results and fractography of PWA 1480 982°C (1800°F) stress rupture test. The fracture surface appears heavily oxidized with no faceting.



FAM 100257

MAG: 50X



FAM 100257B

MAG: 200X

FIGURE 10-27: Optical photomicrographs showing void formation at islands of eutectic (arrows). The fracture had a jagged appearance.

Etchant: AG-21

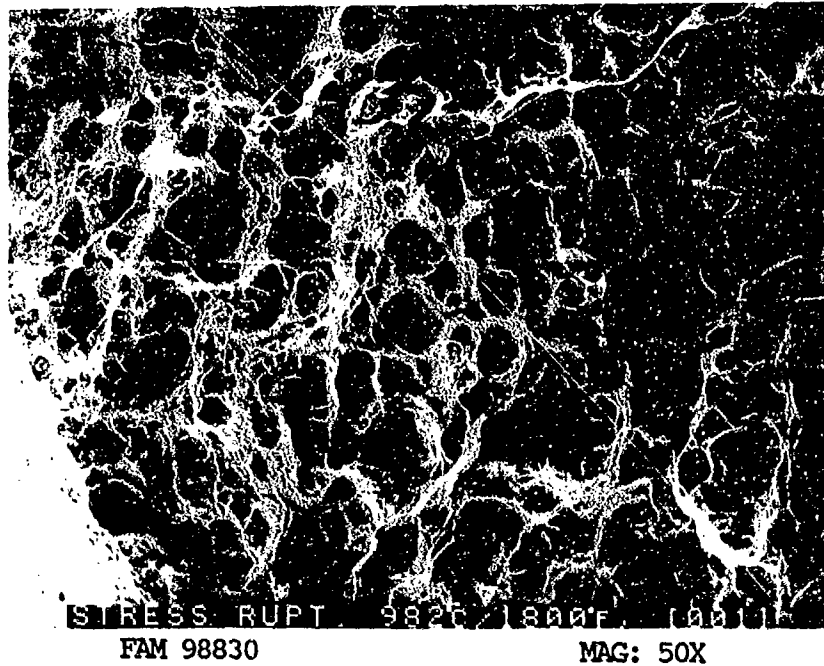


FIGURE 10-28: Low magnification photograph showing granular appearance.

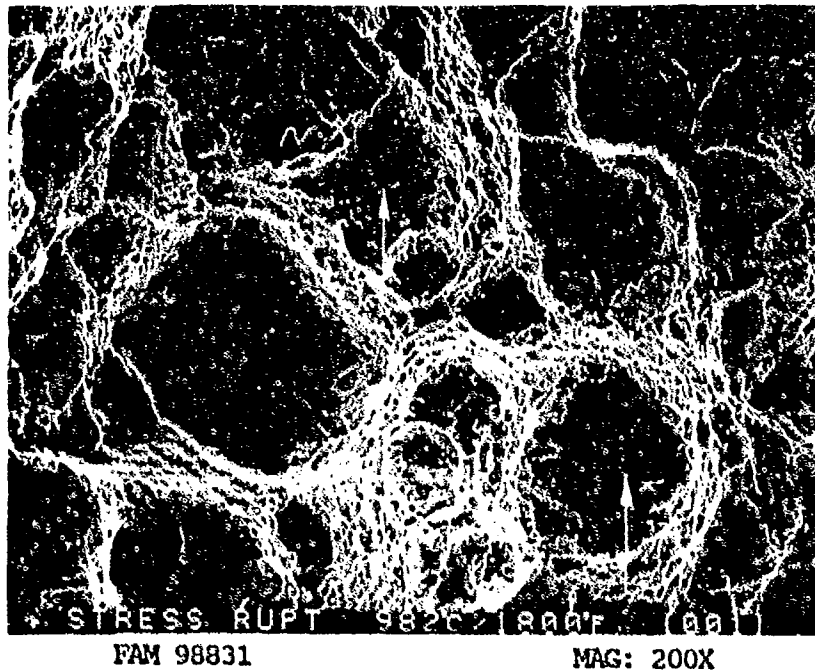
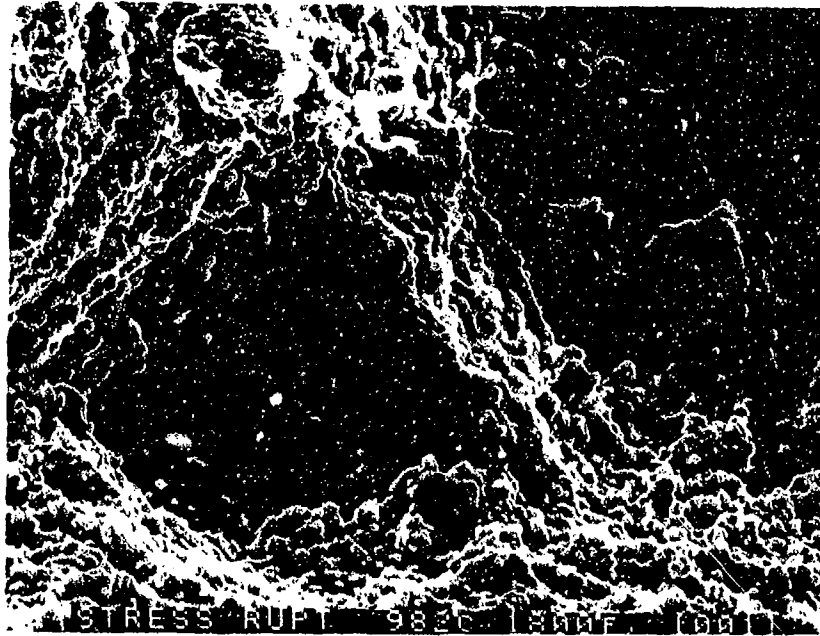


FIGURE 10-29: Higher magnification photograph showing islands of lightly oxidized fracture surrounded by heavily oxidized overstress features. Many of the islands have voids at their centers (arrows)



FAM 98833

MAG: 1000X

FIGURE 10-30: Higher magnification photograph showing oxidized overstress features between smoother, evenly oxidized islands with voids at their centers. These voids are visible in the metallographic cross section (Figure 10-27).

MATERIAL

FWA 1480
[001] Orientation
Coated FWA 275 (Aluminide Coating)

TEST DATA

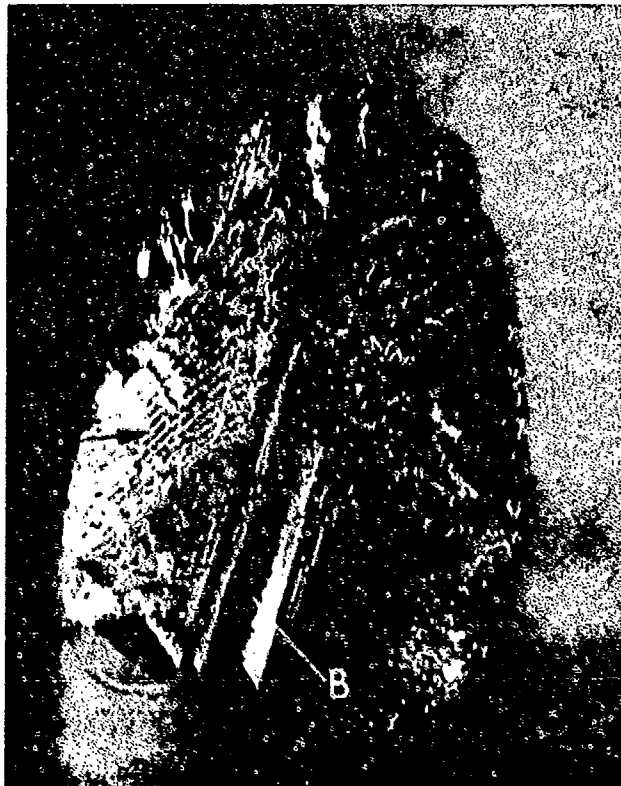
TEST TYPE
Smooth LCF

TEST CONDITIONS

Stress: 595.8 MPa (86.4 ksi)/-595.8 MPa (-86.4 ksi)
Stress Ratio: -1
Atmosphere: Air
Temperature: 427°C (800°F)
Test Direction: Longitudinal

TEST RESULTS

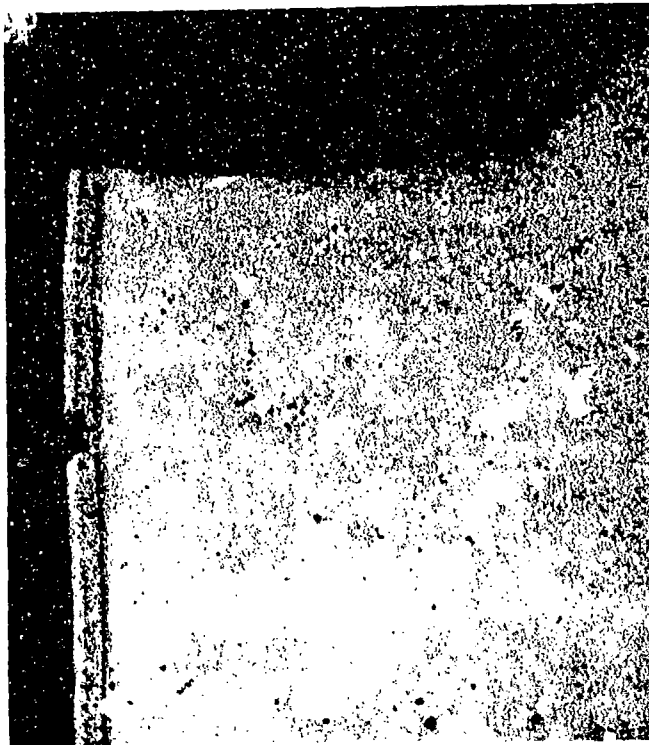
Cycles to Fracture: 3012



FAL 93403

MAG: 12X

FIGURE 10-31: Test results and fractography of FWA 1480/[001] 427°C (800°F) smooth LCF test. Arrest marks are clearly visible on the fracture surface (arrow A). The propagation changes planes across the specimen, resulting in steps on the surface (arrow B).



FAM 100255

MAG: 100X



FAM 100256

MAG: 100X

FIGURE 10-32: Optical photomicrographs showing stage I fatigue propagation area on a plane perpendicular to the stress axis (top) and final overstress (bottom). The fatigue fracture path is flat while the overstress is more jagged.

Etchant: AG-21

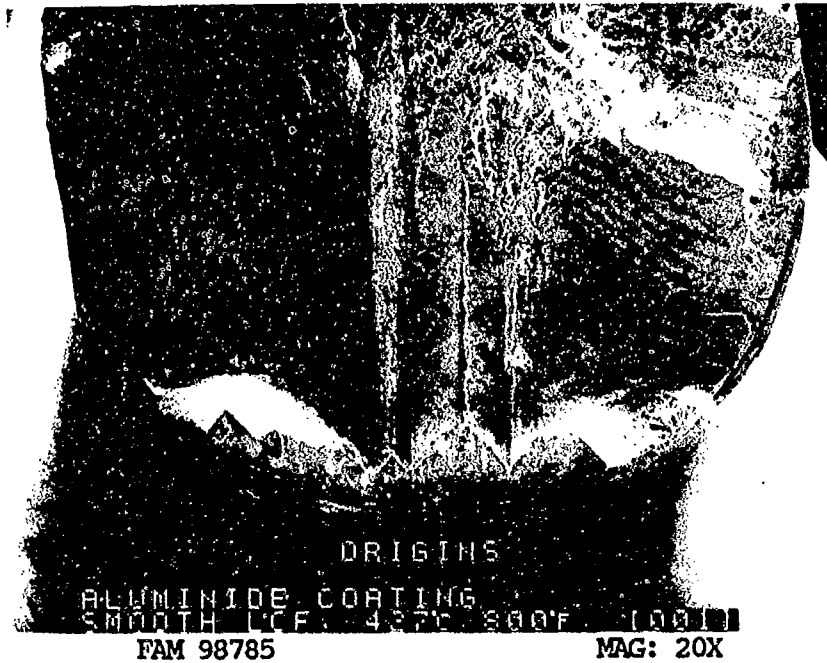


FIGURE 10-33: Low magnification photograph showing arrest marks (arrows A) indicating fatigue propagation from several origins near the bottom of the photograph (arrows B).



FIGURE 10-34: Higher magnification photograph showing three fatigue origins near the surface of the specimen (arrows).

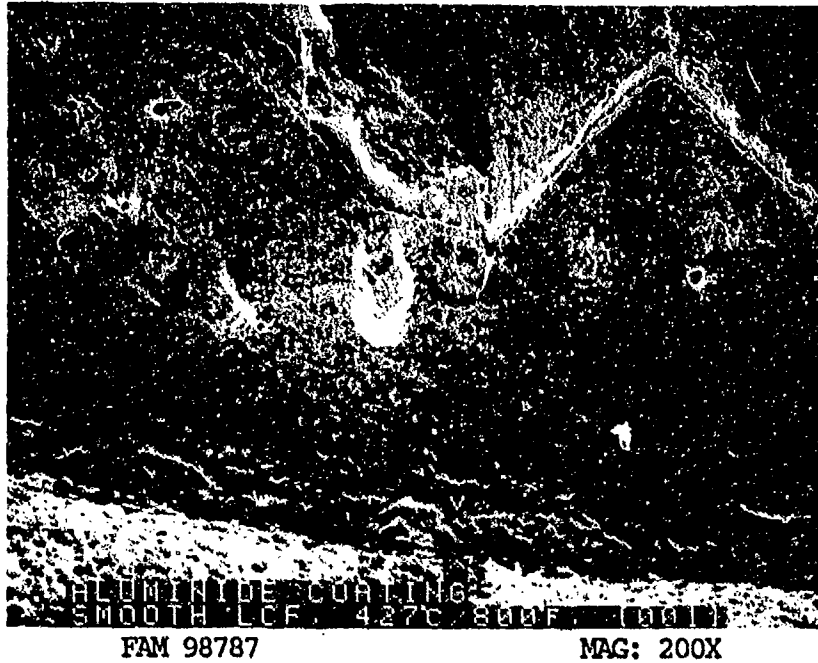


FIGURE 10-35: Close-up photograph of the origin area shown in Figure 10-34. The extent of the coating is shown by arrows.

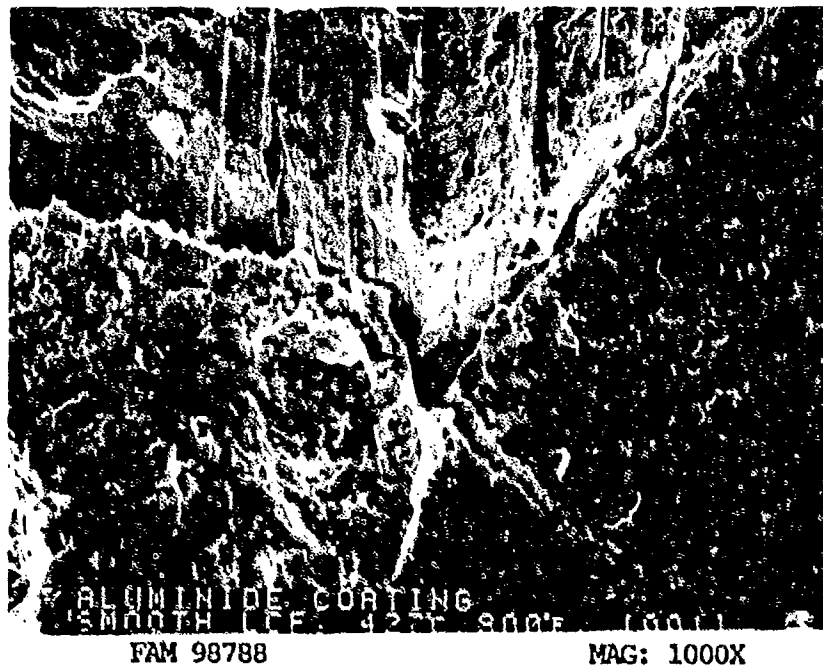


FIGURE 10-36: Higher magnification photograph showing oxidized fatigue features near the origin area. Three remnant fatigue striations are contained in a bracket.

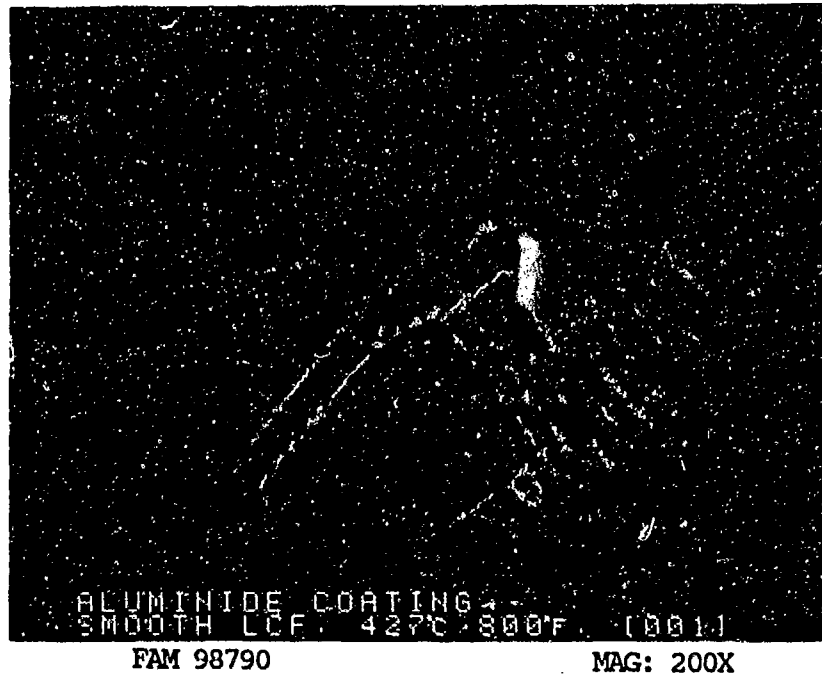


FIGURE 10-37: Coarse fatigue striations propagating from the bottom left corner of the photograph. The striation spacing increases as the crack front moves away from the origin area. This is more indicative of low cycle fatigue.



FIGURE 10-38: The fatigue striations consist of lines of smeared features with cleavage in between. The direction of propagation is shown by an arrow.

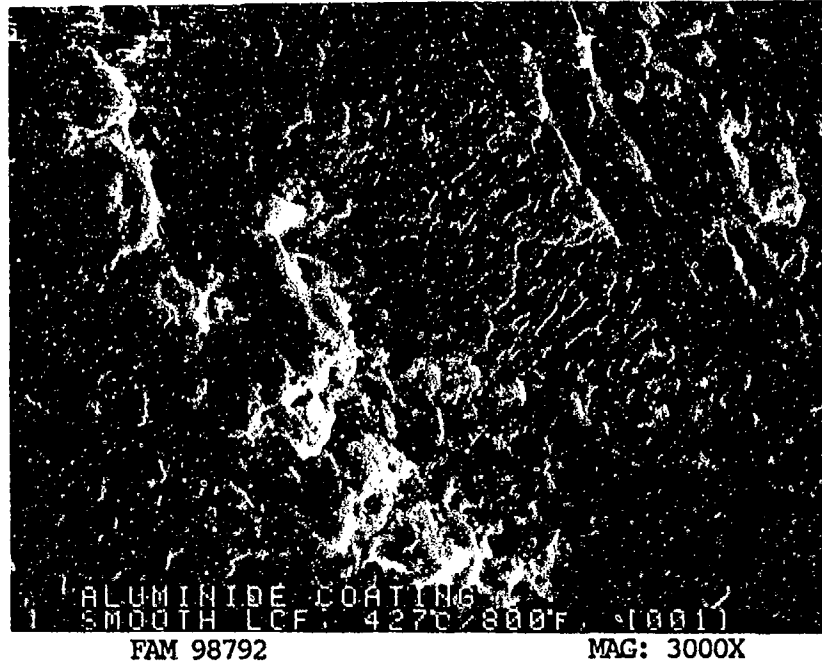


FIGURE 10-39: High magnification photograph showing the smeared striations from Figure 10-38.

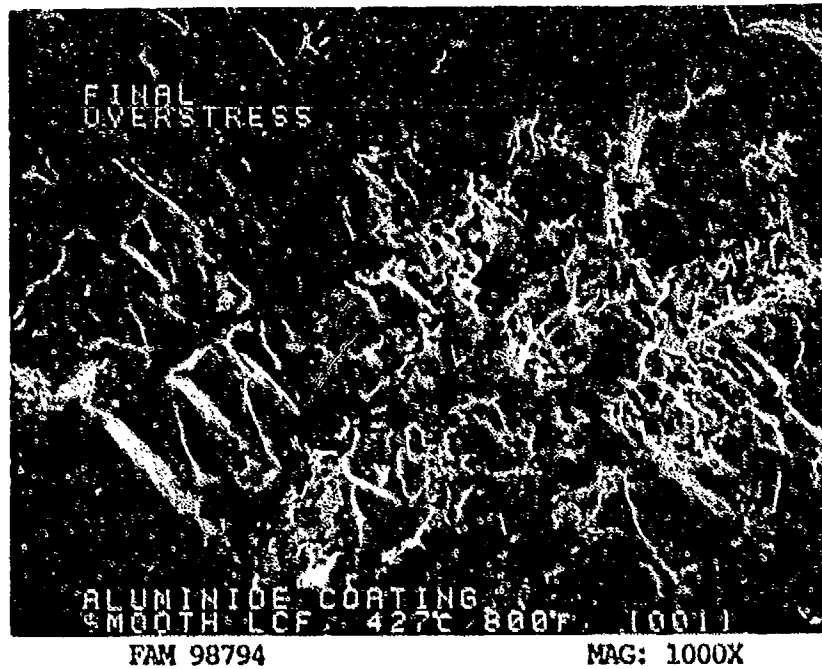


FIGURE 10-40: Final overstress area consisting of cleavage facets.

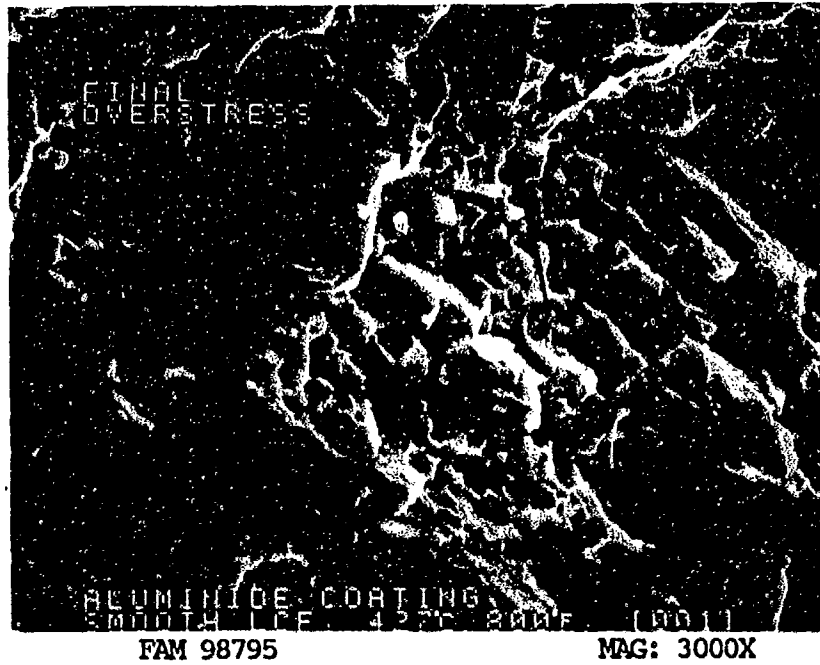


FIGURE 10-41: Final overstress area exhibiting gamma prime microstructural constituent on the fracture surface (arrows).

MATERIAL

PWA 1480
[001] Orientation

TEST DATA

TEST TYPE
Smooth LCF

TEST CONDITIONS

Stress: 1145.9 MPa (166.2 ksi)/-1145.9 MPa (-166.2 ksi)
Stress Ratio: -1
Atmosphere: Air
Temperature: 982°C (1800°F)
Test Direction: Longitudinal

TEST RESULTS

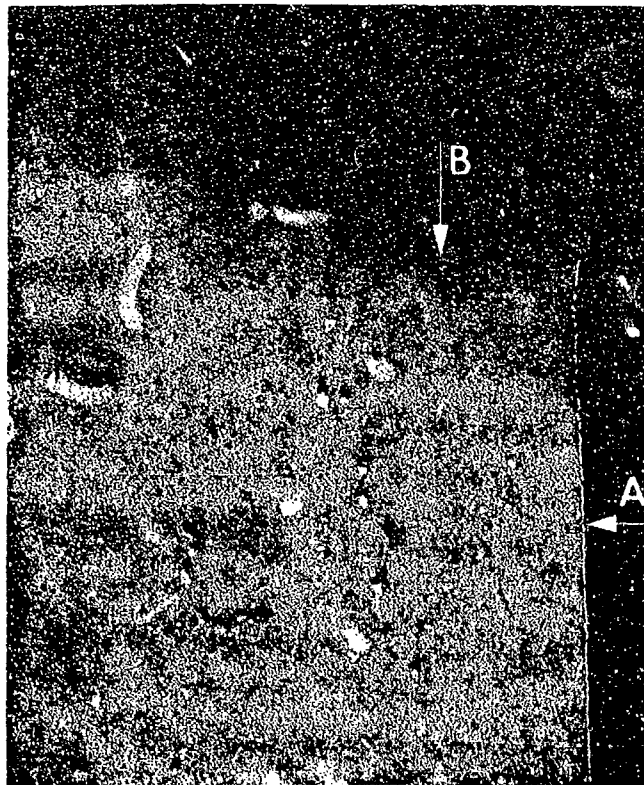
Cycles to Fracture: 718



FAL 93400

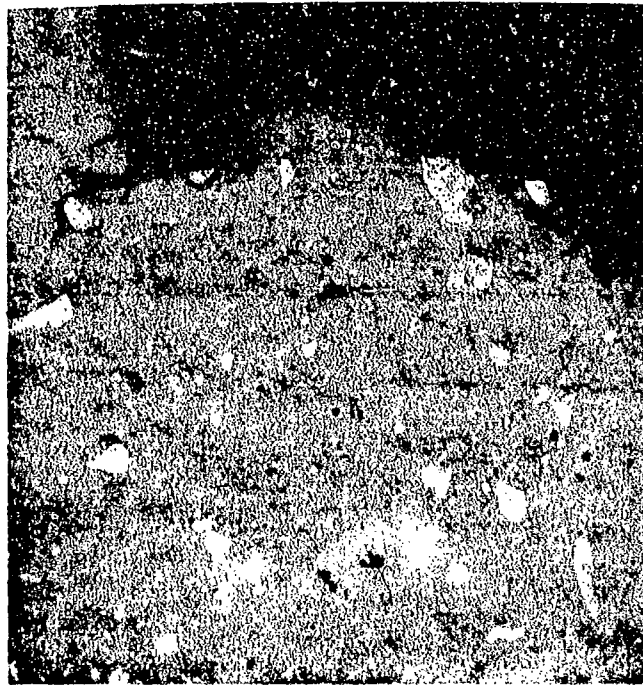
MAG: 11X

FIGURE 10-42: Test results and fractography of PWA 1480/[001] 982°C (1800°F) smooth LCF test. No fatigue propagation is discernible. This fracture surface appears less faceted than the 800°F specimen (Figure 10-31).



FAM 100248

MAG: 200X

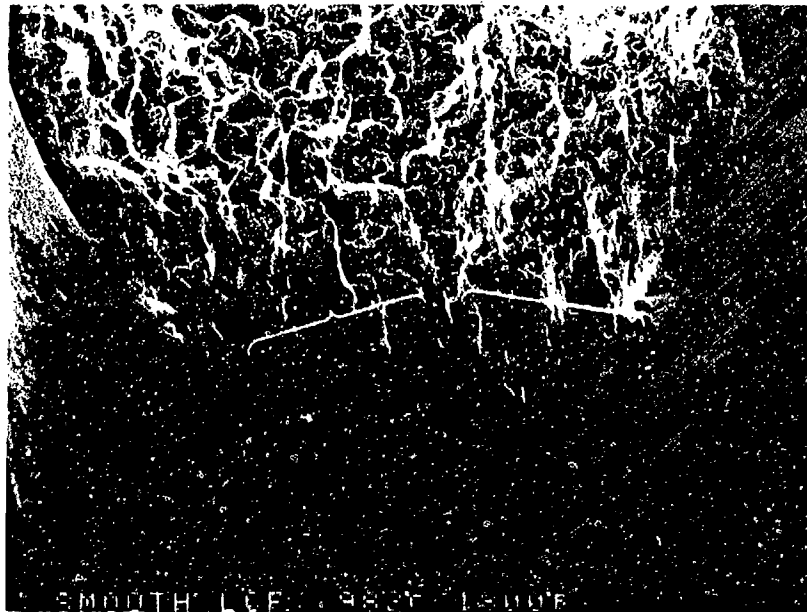


FAM 100250

MAG: 200X

FIGURE 10-43: Optical photomicrographs showing fatigue propagation area (top) and final overstress area (bottom). The fatigue progression is flatter while the overstress is more jagged. A thin alloy depleted layer is visible on the exposed gage section (arrow A) and on the fatigue progression area (arrow B). The fatigue area was exposed to the high temperature oxidizing environment (hot air) during propagation.

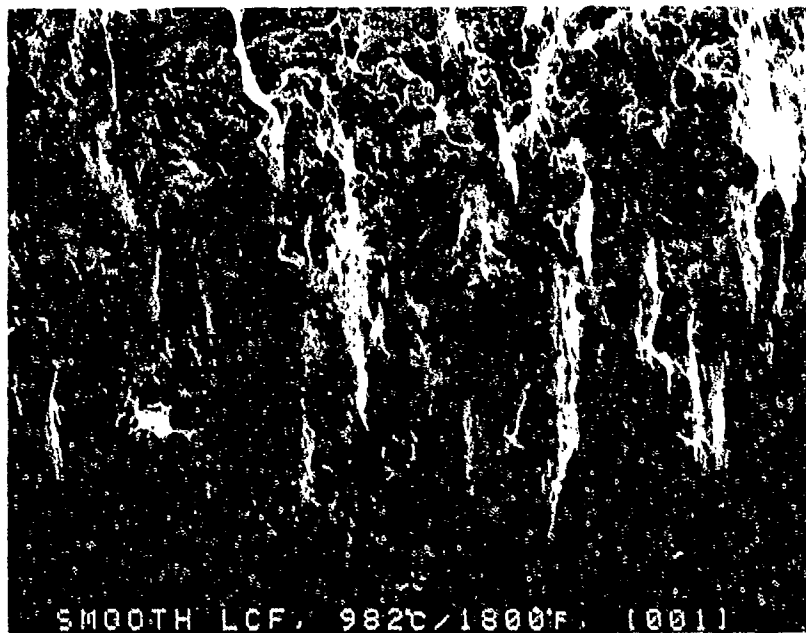
Etchant: AG-21



FAM 98803

MAG: 20X

FIGURE 10-44: Low magnification photograph showing smooth fatigue progression near the bottom of the photograph (brackets).



SMOOTH LCF, 982°C/1800°F. [001]

FAM 98804

MAG: 50X

FIGURE 10-45: Close-up photograph of the fatigue thumbnail area. The diffuse origin area is located at the bottom of the photograph.

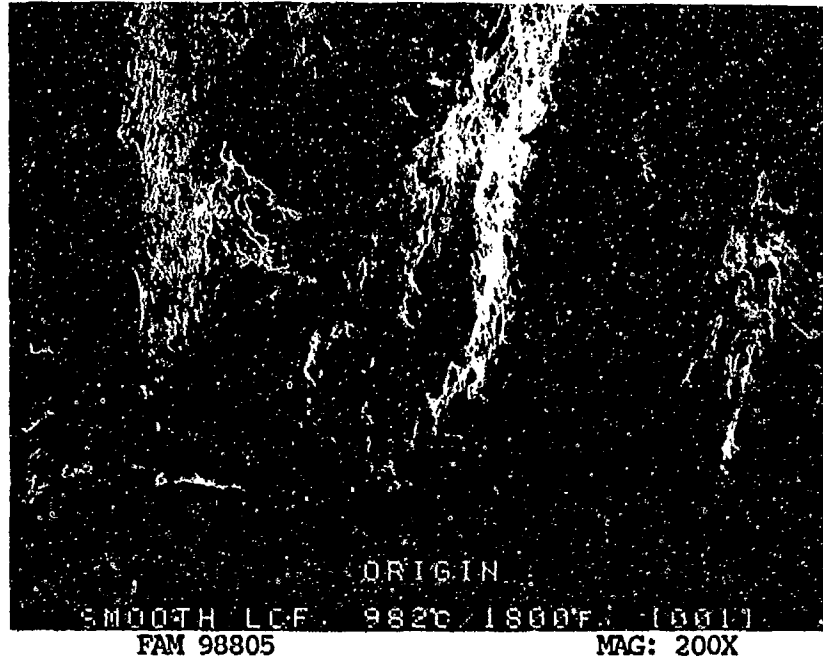


FIGURE 10-46: Close-up photograph of the origin area shown in Figure 10-45, showing no discernible features.

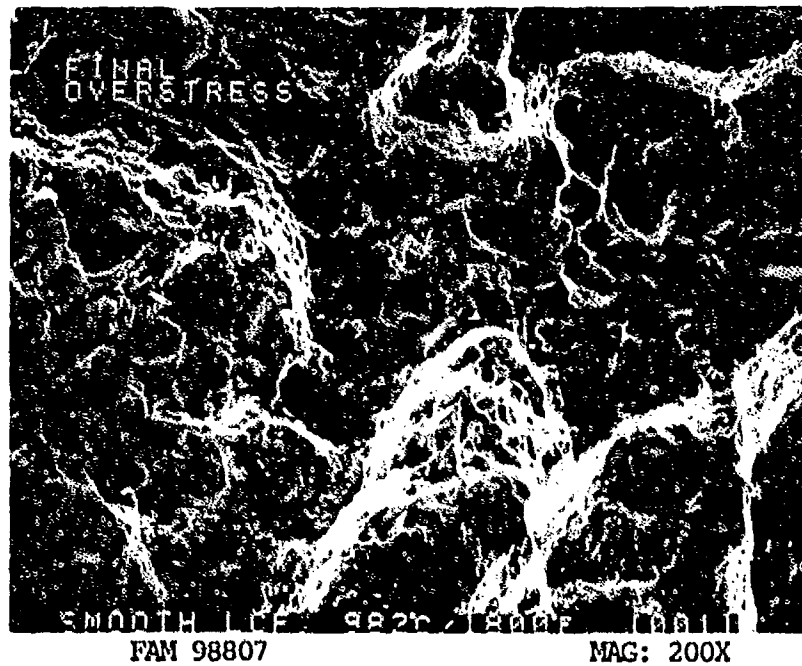
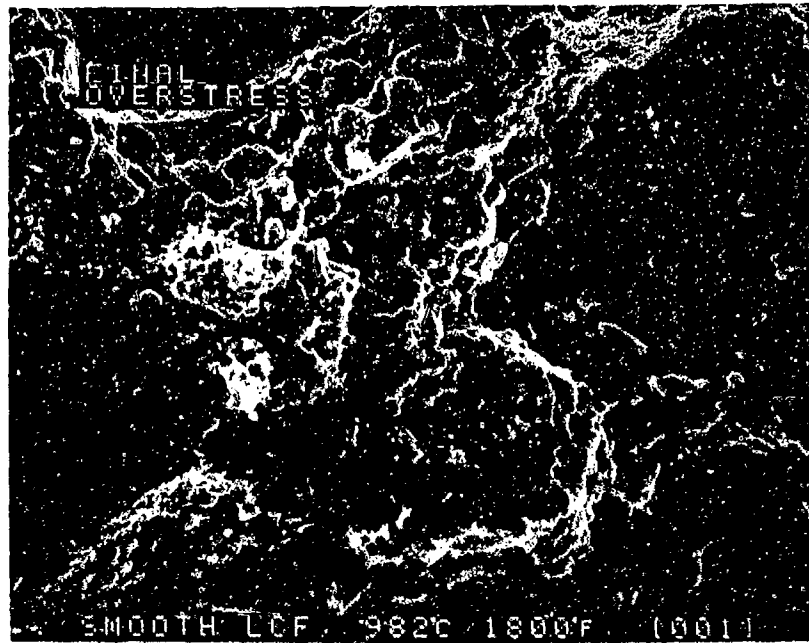


FIGURE 10-47: Oxidized final overstress area.



FAM 98808

MAG: 1000X

FIGURE 10-48: Oxidized final overstress area.

MATERIAL

FWA 1480
[111] Orientation

TEST DATA

TEST TYPE

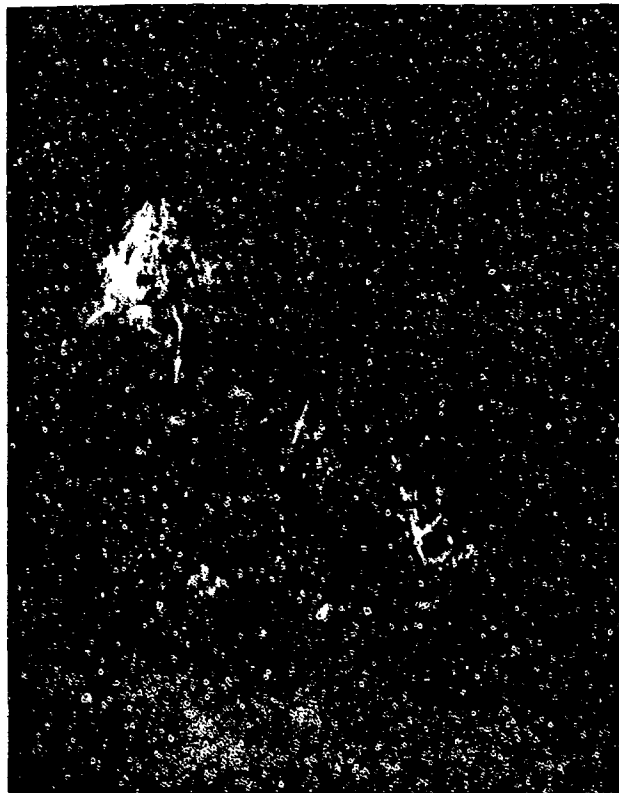
Smooth LCF

TEST CONDITIONS

Stress: 941.3 MPa (136.5 ksi)/-941.3 MPa (-136.5 ksi)
Stress Ratio: -1
Atmosphere: Air
Temperature: 982°C (1800°F)
Test Direction: Longitudinal

TEST RESULTS

Cycles to Fracture: 2307



FAL 93402

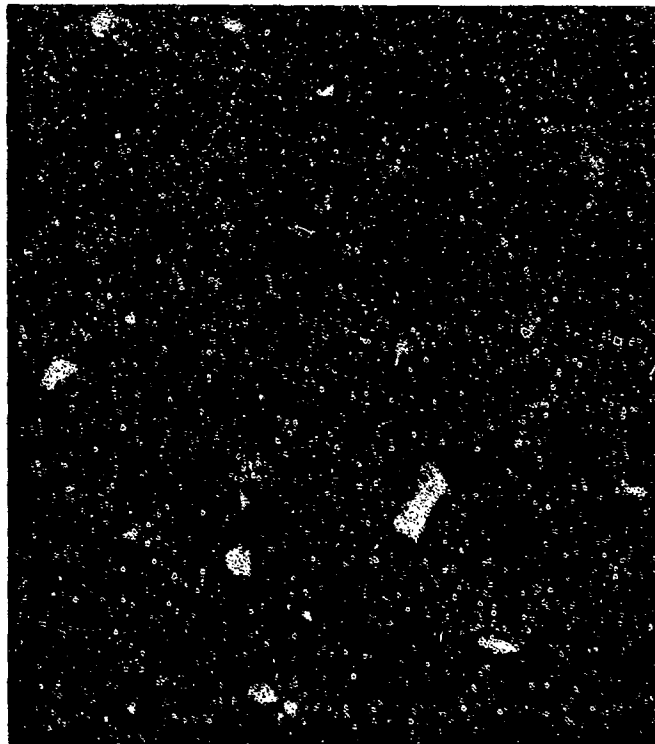
MAG: 12X

FIGURE 10-49: Test results and fractography of FWA 1480/[111] 982°C (1800°F) smooth LCF test. The fatigue progression area appears as a more oxidized area near the bottom of the photograph. The extent of the fatigue is shown by arrows.



FAM 100254

MAG: 500X



FAM 100253

MAG: 200X

FIGURE 10-50: Optical photomicrographs showing the primary fatigue progression area (top) and secondary cracks along the specimen gage (bottom). Both the cracks and the fatigue portion of the fracture surface exhibit thin alloy depleted layers that appear as white-etched areas along the exposed surfaces (arrows). Dark gray colored oxides are visible on top of the alloy depletion layers .

Etchant: AG-21

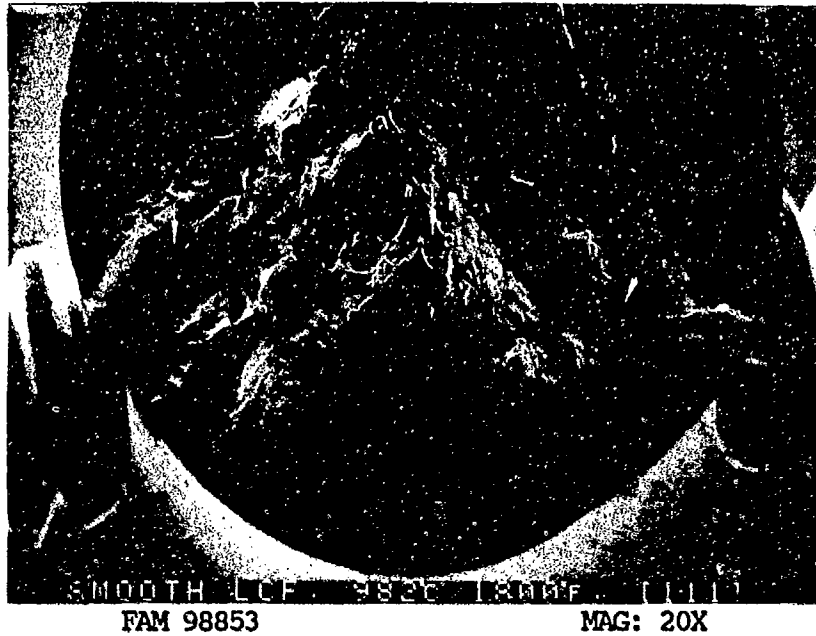


FIGURE 10-51: Low magnification photograph showing smooth fatigue area located near the bottom of the photograph. Arrows indicate the extent of the fatigue. The fracture propagated from multiple origins.



FIGURE 10-52: Close-up photograph showing a typical origin area. A localized origin is indicated by an arrow.

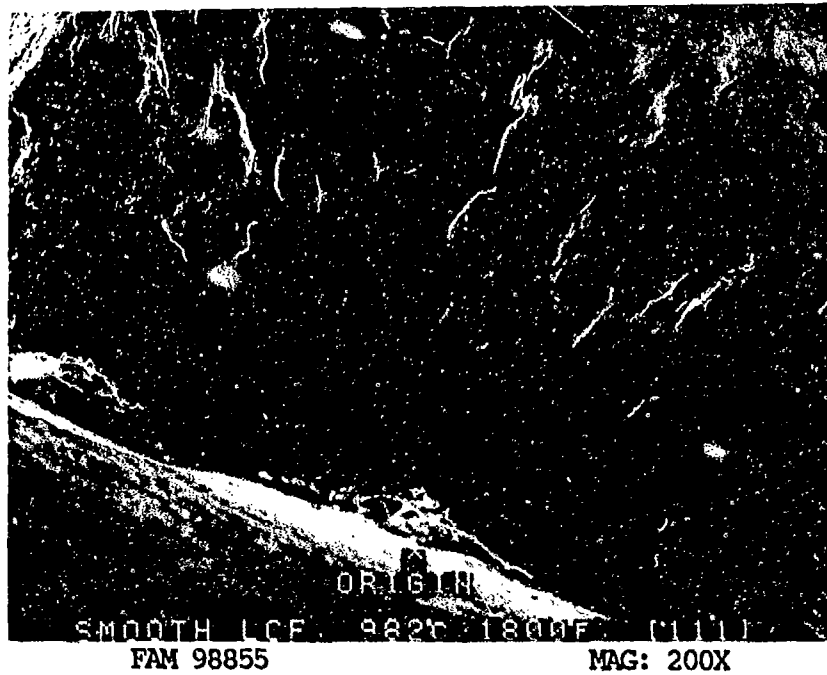


FIGURE 10-53: Higher magnification photograph of the area shown in Figure 10-52, showing a small void at the origin. No striations are visible in the origin area.

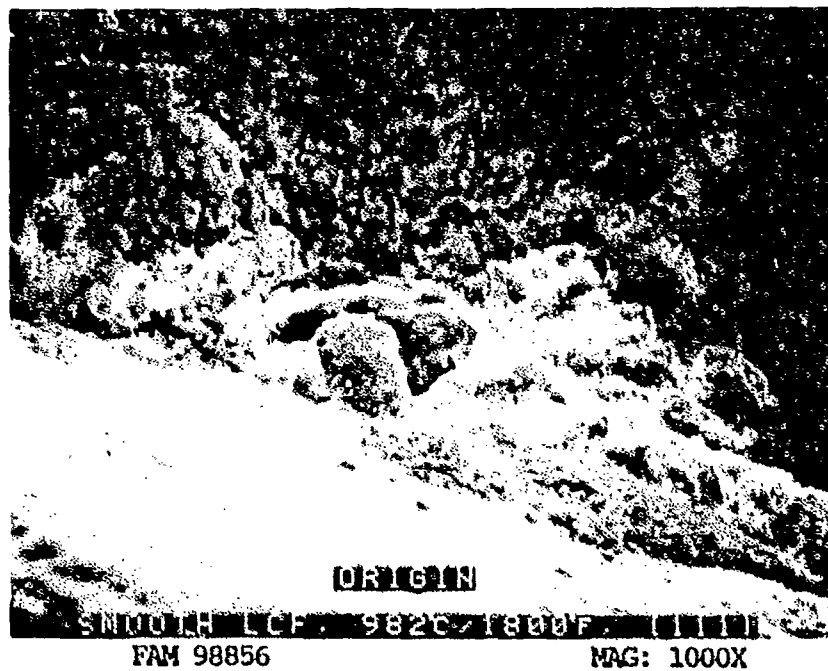
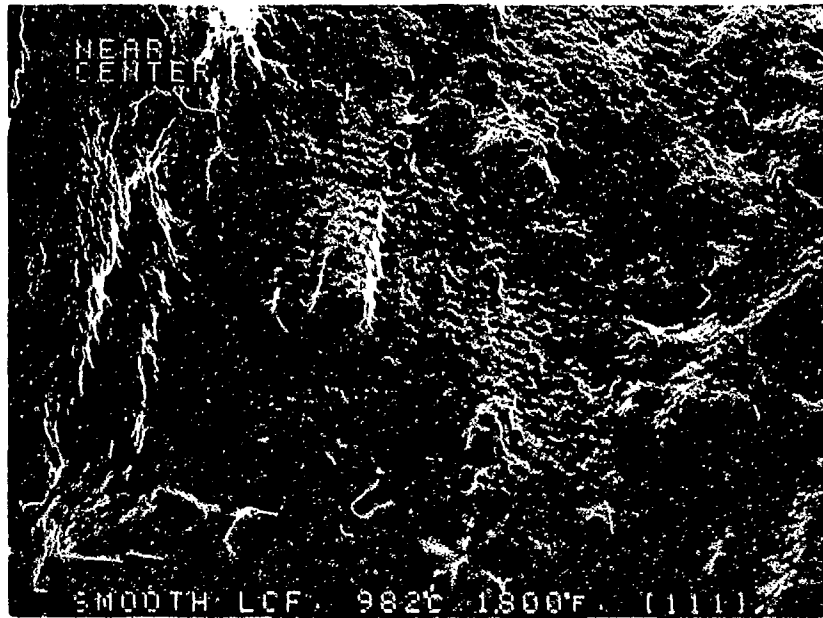


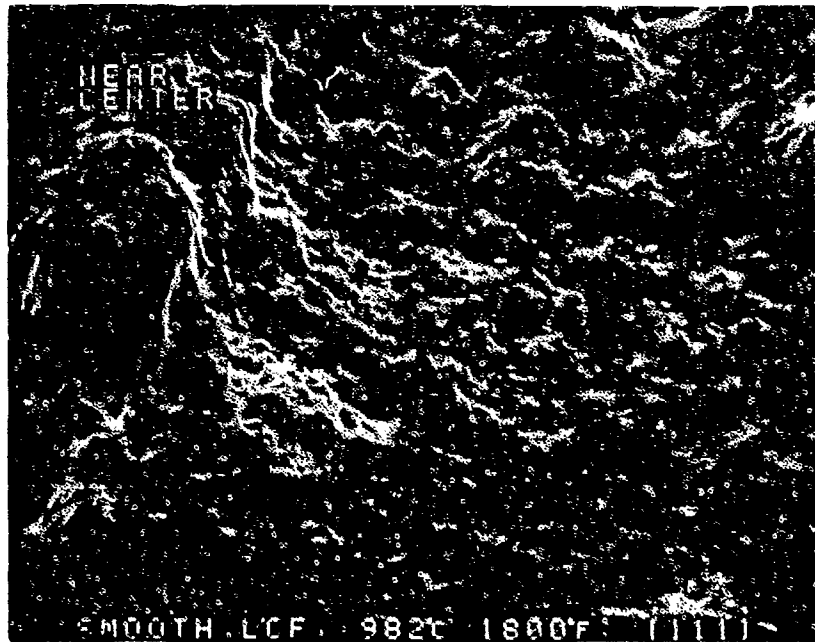
FIGURE 10-54: Small oxidized void at the origin.



FAM 98859

MAG: 200X

FIGURE 10-55: Fatigue progression near the center of the fracture surface. Coarse striations are visible. The direction of propagation is shown by an arrow.



FAM 98860

MAG: 1000X

FIGURE 10-56: Higher magnification photograph of the coarse oxidized striations shown in Figure 10-55.

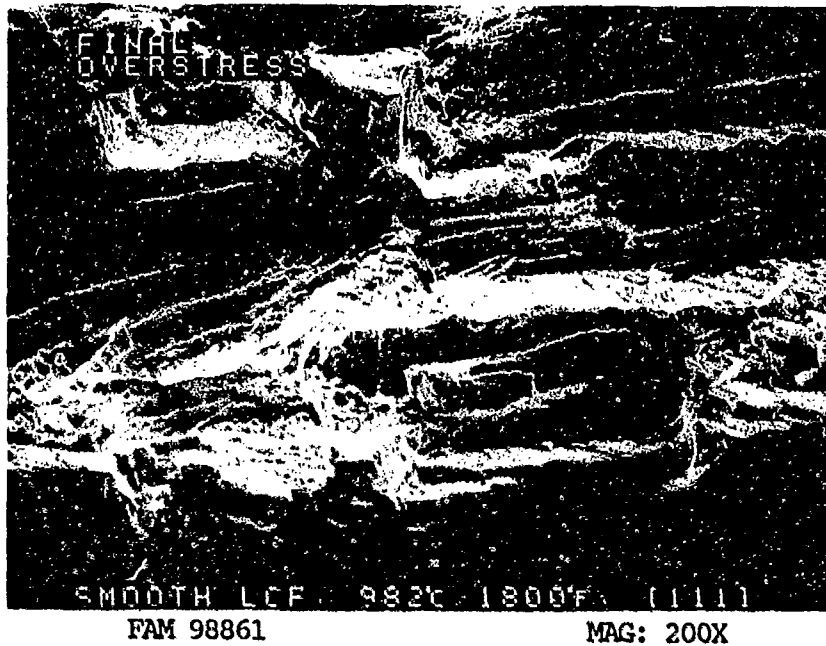


FIGURE 10-57: Cleavage features in the final overstress area.

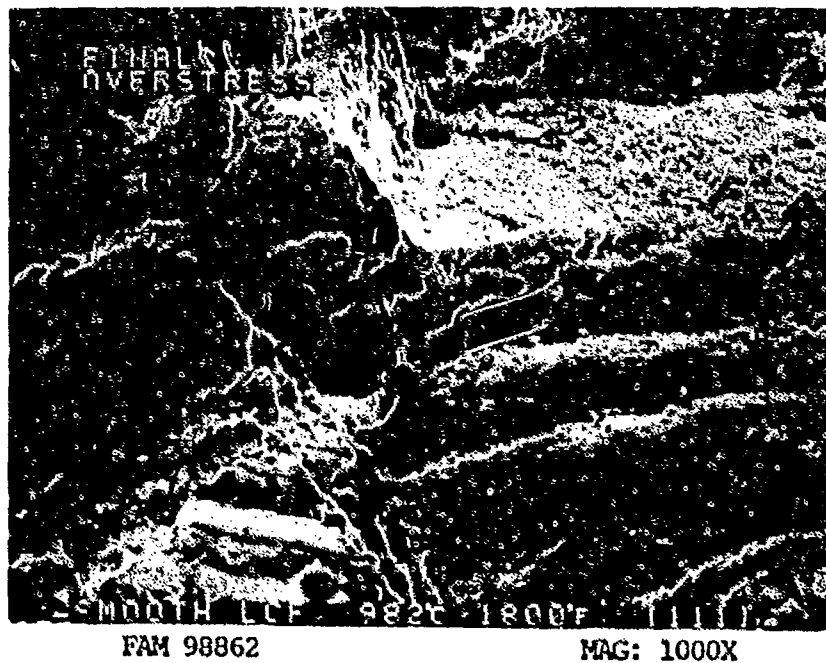


FIGURE 10-58: Higher magnification photograph of the area shown in Figure 10-57, showing oxidized cleavage features. Two small patches of fan-shaped cleavage are indicated by arrows.

MATERIAL

FWA 1480
[001] Orientation

TEST DATA

TEST TYPE

TMF, Out-of-Phase

TEST CONDITIONS

Stress Range: 903 MPa (131 ksi)
Mean Stress: 59 MPa (8.5 ksi)
Atmosphere: Air
Frequency: 1 cpm
Temperature: 982^oC (1800^oF)/427^oC (800^oF)
Test Direction: Longitudinal

TEST RESULTS

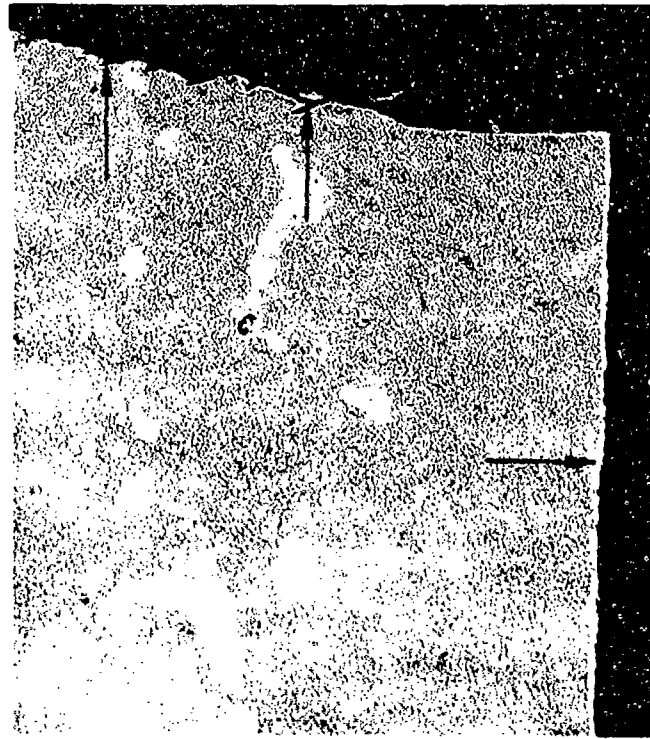
Cycles to Fracture: 3655



FAL 93404

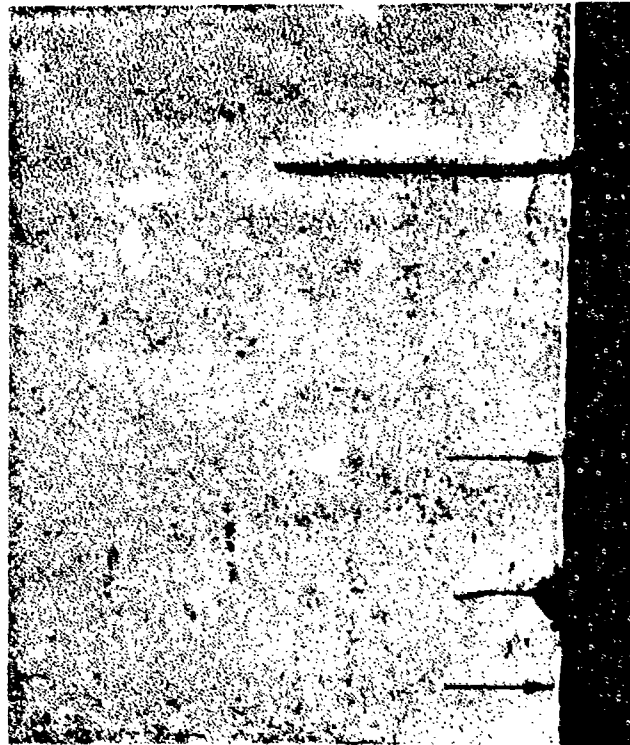
MAG: 12X

FIGURE 10-59: Test results and fractography of FWA 1480/[001] Out-of-Phase TMF test. An oxidized (dark) fatigue progression zone is visible at the bottom of the photograph. Arrows indicate the extent of the fatigue.



FAM 100251

MAG: 200X

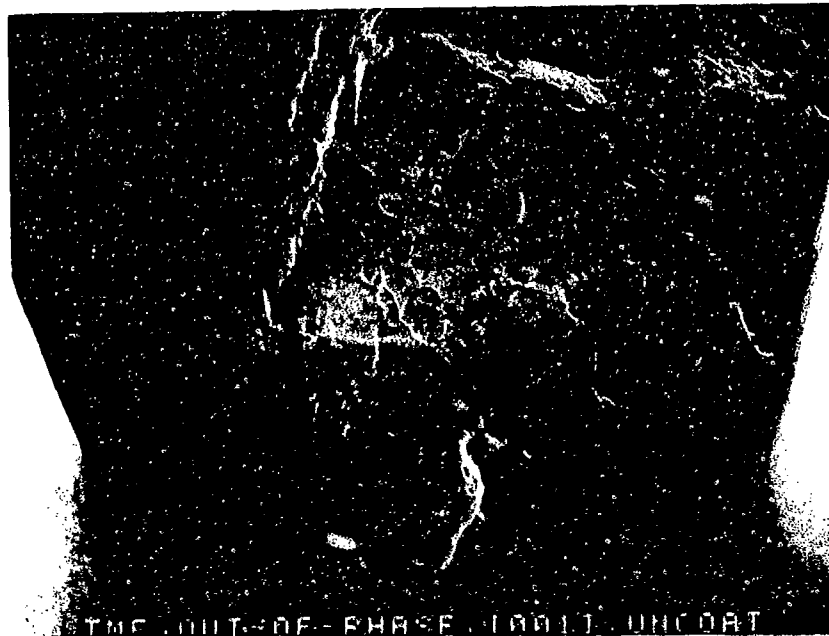


FAM 100252

MAG: 200X

FIGURE 10-60: Optical photomicrographs showing the primary fatigue progression area (top) and secondary cracks along the specimen gage section (bottom). Both the cracks and the fracture exhibit shallow alloy depleted layers that appear as white-etched layers along the exposed surfaces (arrows). Dark gray colored oxides are visible on top of the alloy depleted layers along the primary fracture surface. This appearance is similar to the high temperature LCF fracture (Figure 10-50).

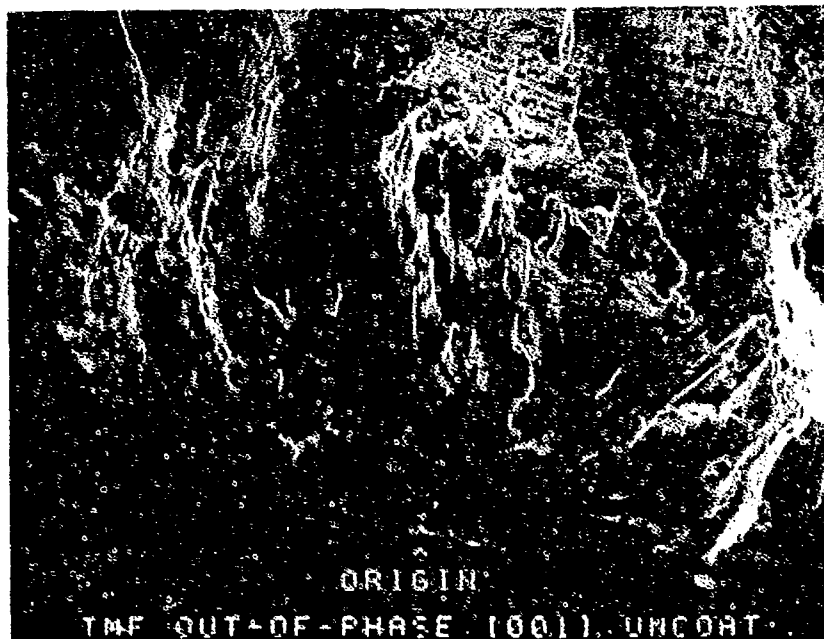
Etchant: AG-21



FAM 98838

MAG: 20X

FIGURE 10-61: Low magnification photograph showing fatigue progression area located at the bottom of the photograph. The extent of the fatigue is shown by arrow heads.



FAM 98839

MAG: 50X

FIGURE 10-62: Higher magnification photograph of the origin area. A void open to the surface is the local origin site (arrow).

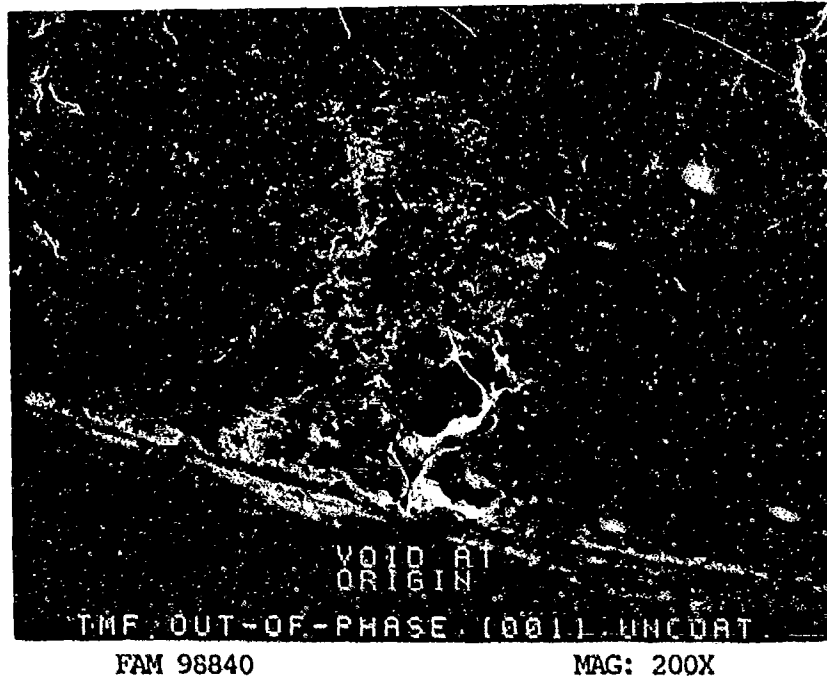


FIGURE 10-63: Close-up photograph of the surface connected void at the origin shown in Figure 10-62. No fatigue striations are visible adjacent to the void.

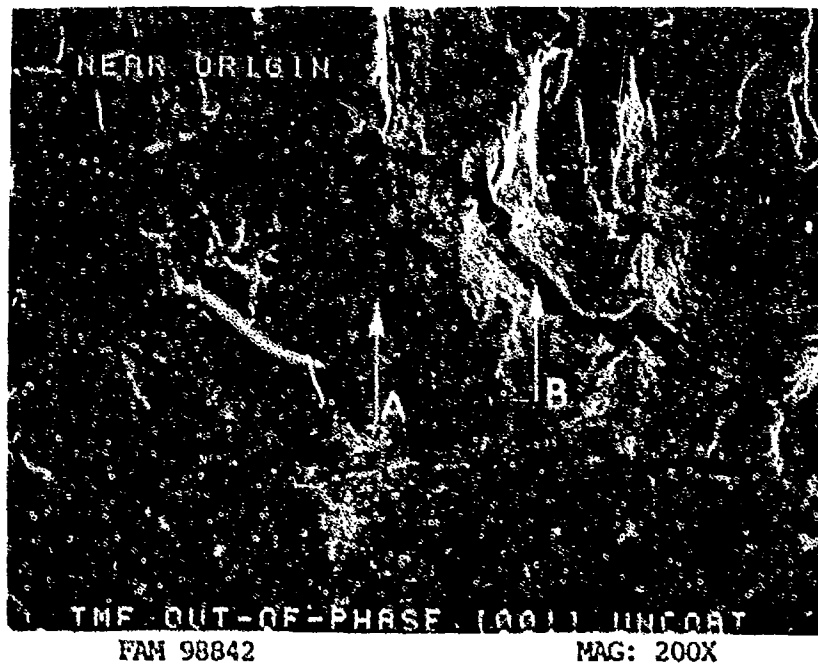


FIGURE 10-64: Remnant fatigue features near the origin. The direction of propagation is shown by arrow A. Arrow B shows a large secondary crack perpendicular to the direction of propagation.

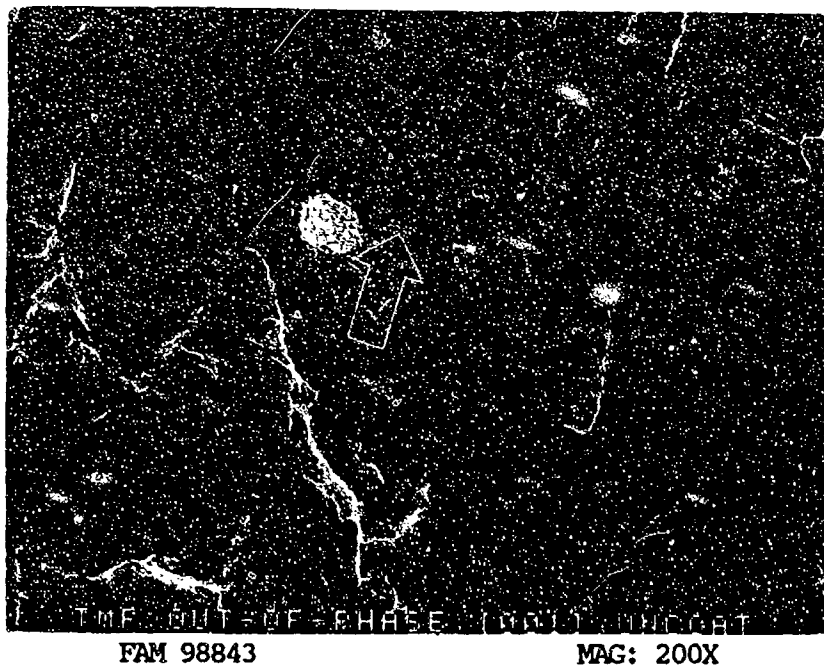


FIGURE 10-65: Fatigue features in the thumbnail area. The direction of propagation is shown by an arrow.

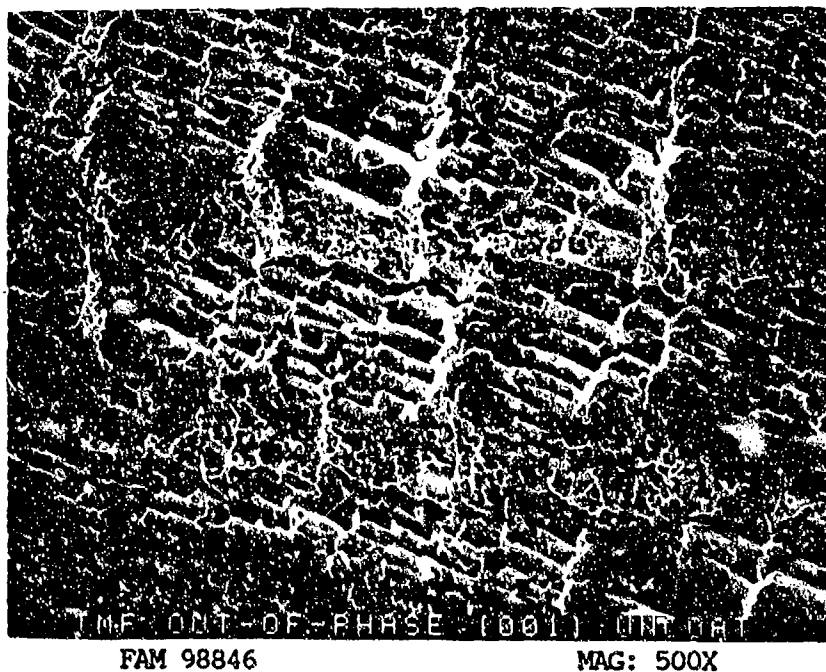


FIGURE 10-66: Higher magnification photograph of the fatigue features shown in Figure 10-65. Note presence of terrace steps separated by smoother, oxidized regions.

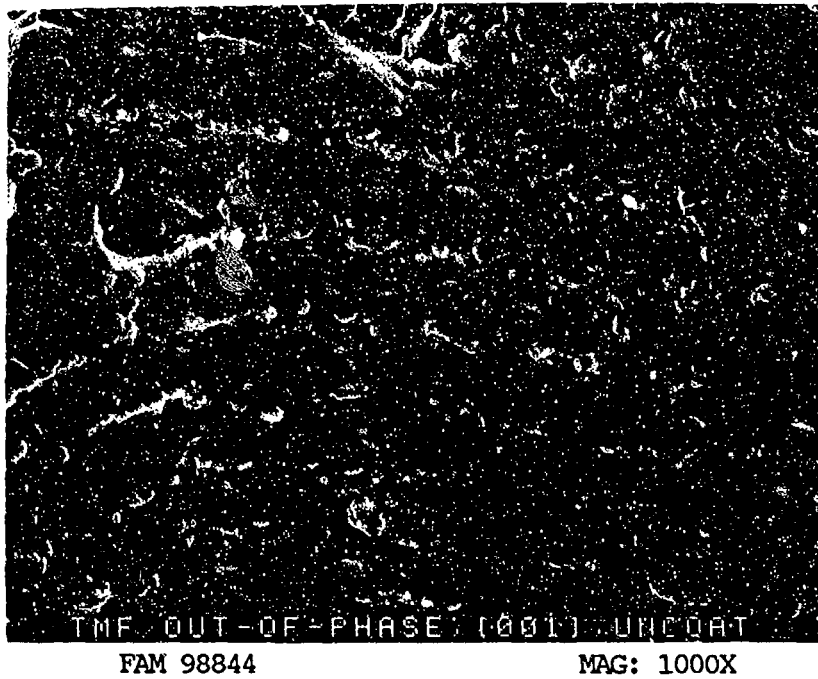


FIGURE 10-67: Oxidized crack-like striations in the thumbnail area. The direction of propagation is from bottom to top of the photograph.

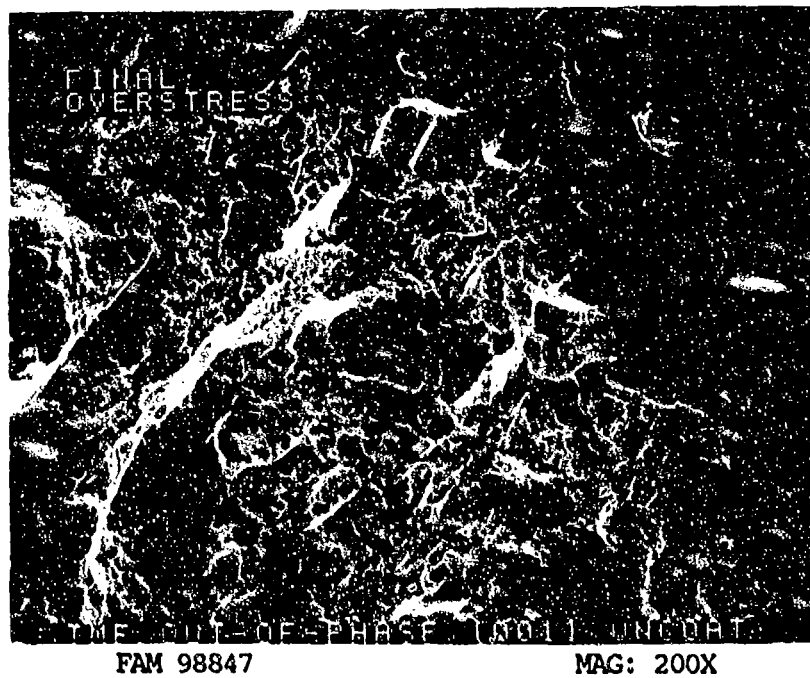


FIGURE 10-68: Final overstress area.

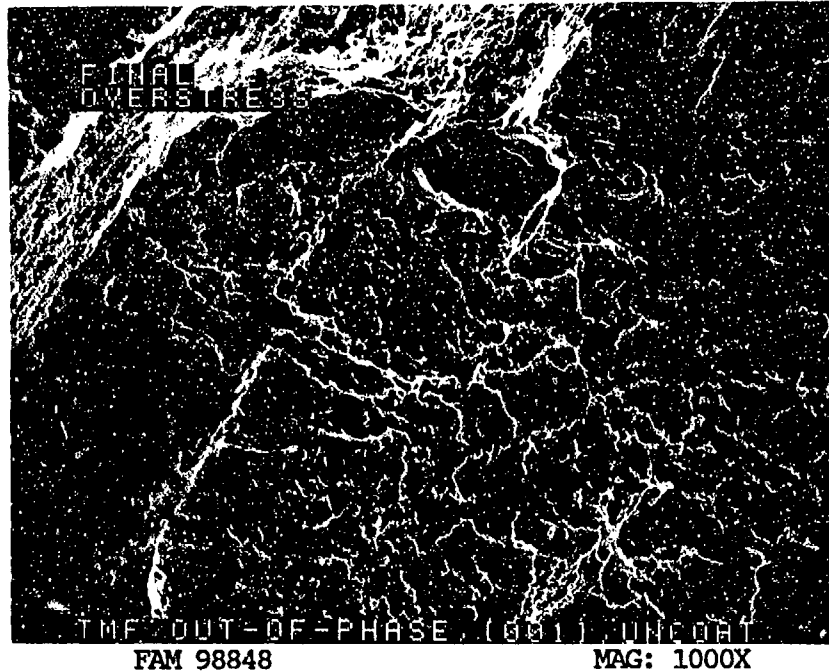


FIGURE 10-69: Higher magnification photograph of the area shown in Figure 10-68, exhibiting fine dimpled overstress associated with Gamma Prime phase and patches of feathery cleavage (arrows).

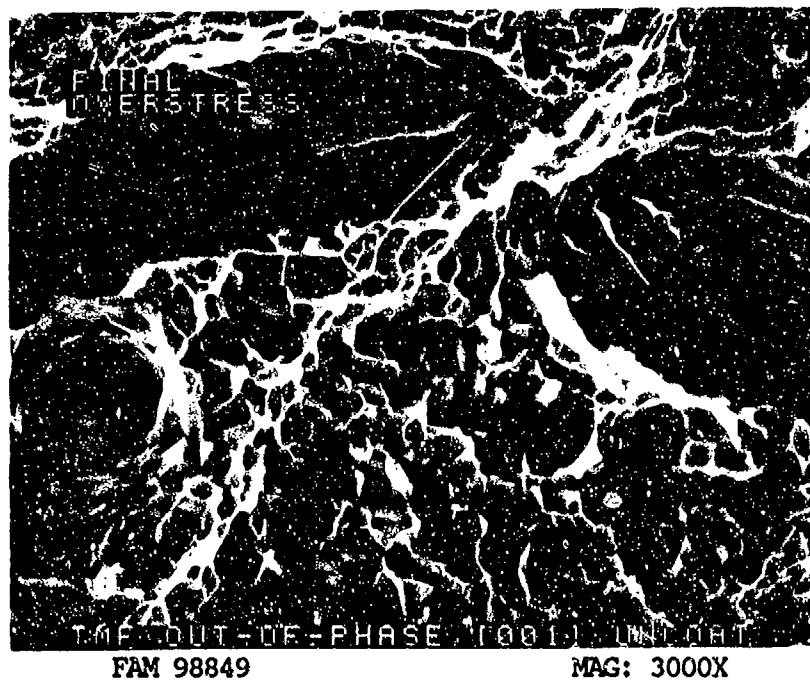


FIGURE 10-70: Very fine dimpled overstress between patches of feathery cleavage. The Gamma Prime phase in the microstructure is visible in the dimpled areas.

SERVICE FAILURE

FRACTURE MODE Fatigue (TMF and probable LCF)

PART NAME First and Second Stage Turbine Stator Vanes

OPERATION DATA Vaness operated in typical turbine environment under thermal stresses as well as cyclic and static mechanical stresses.

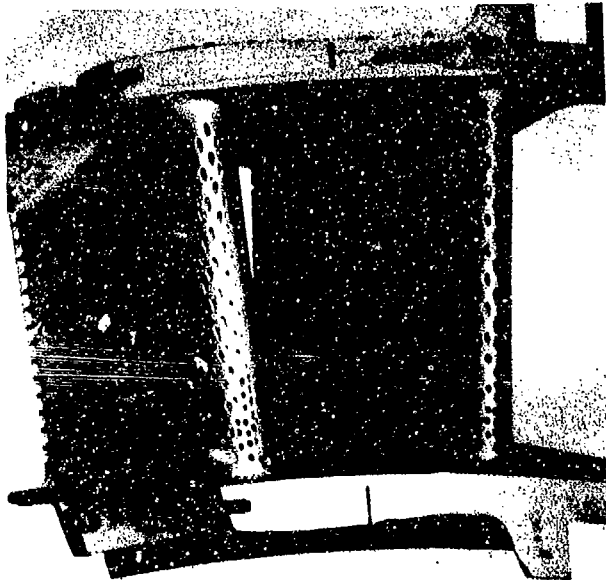
PART TIME 450.7 hours (2081.5 operational cycles)

	<u>REQUIRED</u>	<u>ACTUAL</u>
MAT'L		
BASE	<u>PWA 1480 (Single Crystal)</u>	<u>confirmed</u>
OTHER	<u>-</u>	<u>-</u>
HARDNESS	<u>No Requirement</u>	<u>HRC 41-48 *</u>
GRAIN SIZE	<u>N/A</u>	<u>N/A</u>
DIMENSIONAL	<u>-</u>	<u>-</u>

* Diamond pyramid hardness (DPH) conversions.

SUMMARY: First stage turbine vane exhibited microcracks in the laser drilled cooling holes on the airfoil surface. The opened crack surfaces were shallow and heavily oxidized. The only fracture features visible were mud-cracks commonly associated with TMF. The second stage turbine vane had tight cracks running roughly axially in the airfoil/platform fillet. The opened crack surfaces were oxidized but exhibited several very clear sets of arrest lines (beach marks).

Outboard

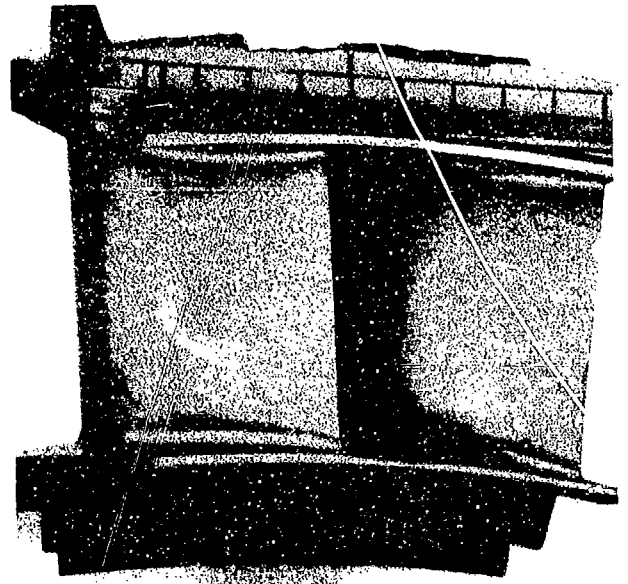


FAL 88111

MAG: 3/4X

FIGURE 10-71: Overall photograph of the first stage turbine vane, forward looking aft. Microcracks propagated from the corners of the cooling holes.

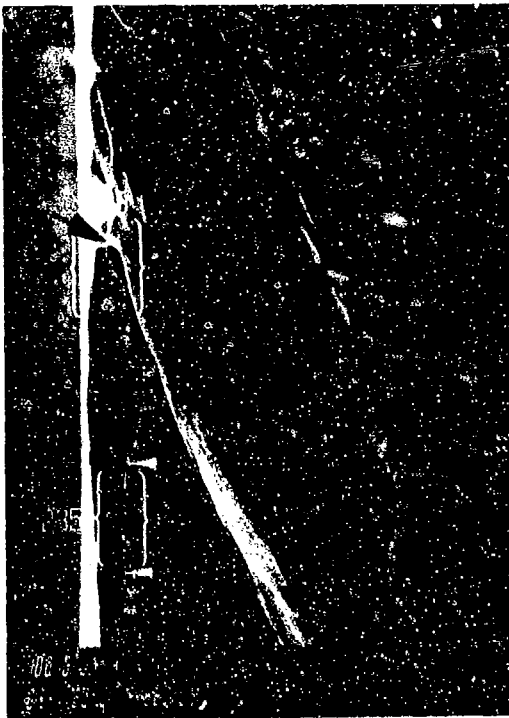
Outboard



FAL 88112

MAG: 3/4X

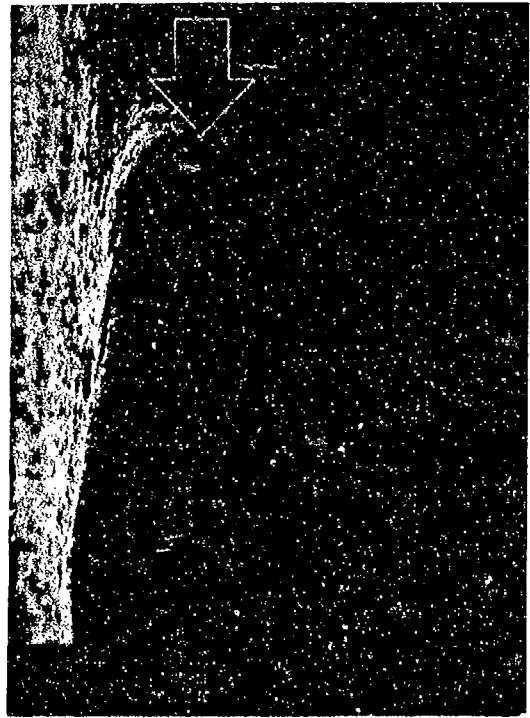
FIGURE 10-72: Aft view of the first turbine vane.



FAL 93448

MAG: 30X

FIGURE 10-73: Photograph showing shallow TMF crack surface originating in the corner of cooling hole (black arrow). The crack then propagated from multiple origins on the outside surface (left).

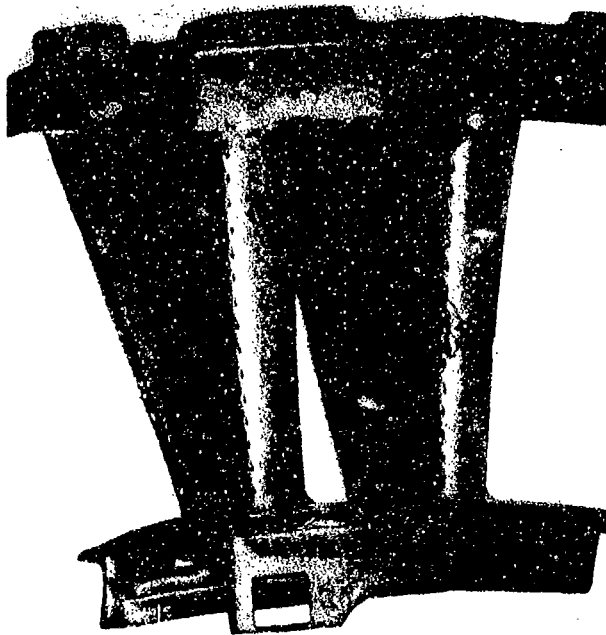


FAL 93449

MAG: 300X

FIGURE 10-74: Close-up of the primary origin area exhibiting only heavy oxidation.

Outboard

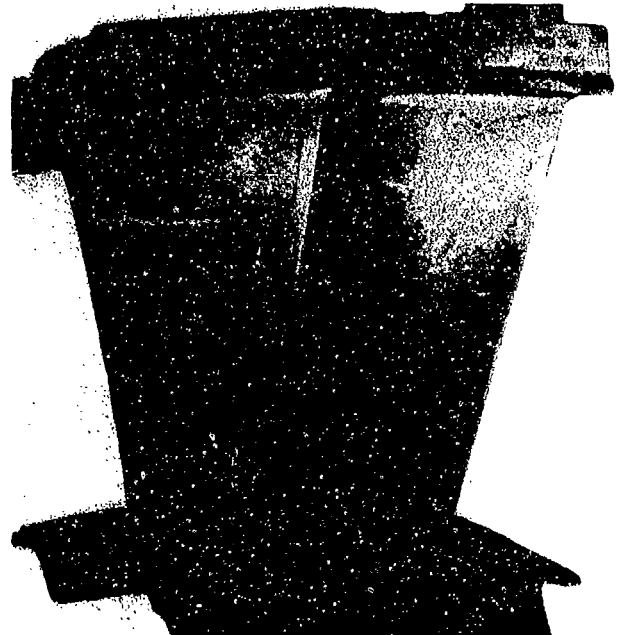


FAL 88115

MAG: 7/8X

FIGURE 10-75: Overall photograph of the second stage vane, forward looking aft.

Outboard



FAL 88116

MAG: 7/8X

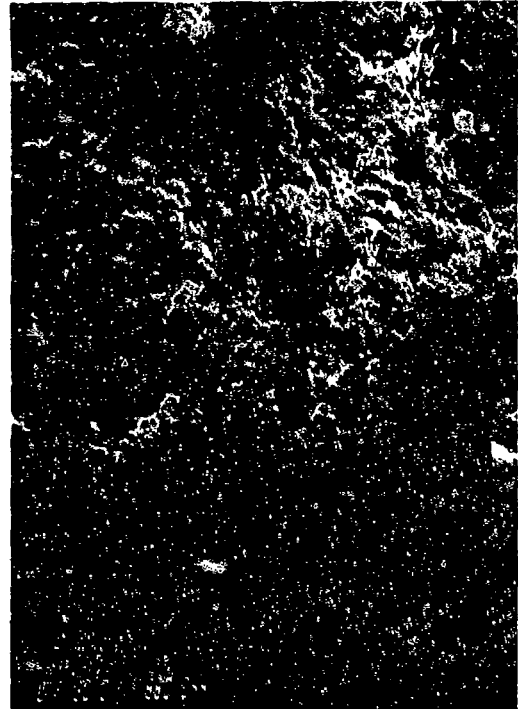
FIGURE 10-76: Aft view of the second stage turbine vane. Thermal distress is visible in several areas.



FAL 93452

MAG: 10X

FIGURE 10-77: Overall photograph of an opened airfoil/O.D. platform fillet crack. The origin area is indicated by an arrow.



FAL 93453

MAG: 100X

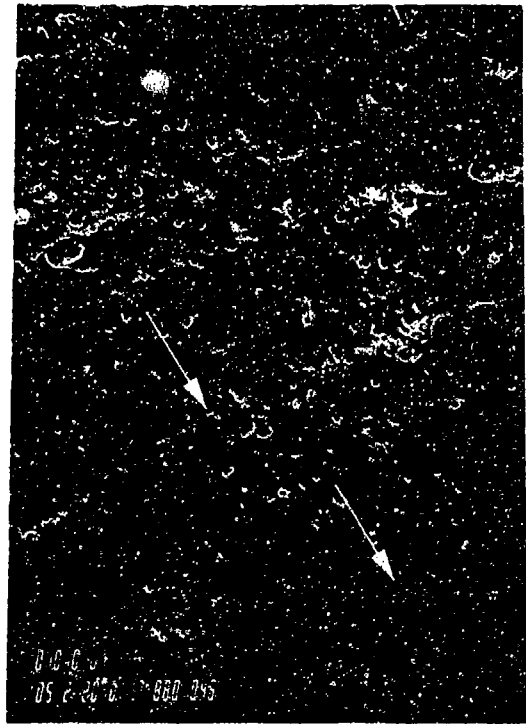
FIGURE 10-78: Higher magnification photograph showing arrest marks in the origin area.



FAL 93454

MAG: 120X

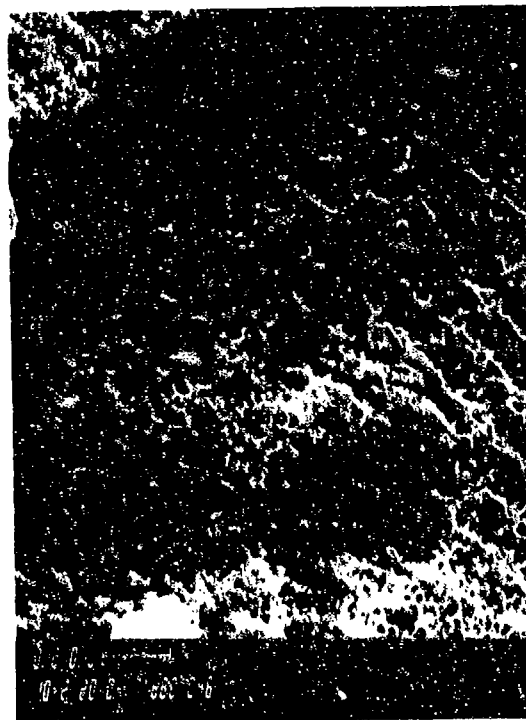
FIGURE 10-79: Banded striations indicating LCF. Brackets separate different striation spacings.



FAL 93455

MAG: 500X

FIGURE 10-80: Higher magnification photograph of the banded striations. Fine striations are separated by coarse striations (arrows).



FAL 93456

MAG: 1000X

FIGURE 10-81: Oxidized fatigue striations.

MP-159 (Cobalt-Based Alloy)

Material Description

MP-159 is a cobalt-nickel-chromium alloy that has very high strength up to 1100° F. It also has excellent resistance to corrosion, stress corrosion cracking and creep. It is generally processed by vacuum induction plus vacuum consumable electrode melting, solution treating, work hardening and precipitation hardening.

The material used in this study was heat treated to AMS 5843 with a required hardness of HRC 44 min. The typical room temperature mechanical properties for AMS 5843 (bar) are as follows:

Ultimate Tensile Strength (min):	260 ksi	
0.2% Yield Strength (min):	250 ksi	
Percent Elongation (min):	6%	
Percent Reduction in Area (min):	22%	
	<u>Required</u>	<u>Measured</u>
ASTM Grain Size:	4 or finer occas. 2	10.5
Measured Hardness:	HRC 42-47	

Fractography Overview

Notched and smooth tensile tests were run at 1100° F. The smooth specimen fractured on a 45° angle to the stress axis and exhibited shallow shear dimples over the entire fracture. The notched specimen exhibited coarse deep equiaxed dimples in the center of the specimen and shallow equiaxed and shear dimples in the final overstress area. Particles were visible associated with some of the dimples in both areas. The stress rupture specimen exhibited deep features macroscopically but shallow dimpled rupture on a microscopic scale. Deep voids and second phase particles were visible in the fracture composed of very shallow equiaxed dimples in the primary rupture area and shear dimples near the edge of the specimen.

Smooth HCF specimens were run at room temperature 800° F and 1100° F. The two lower temperature fractures were quite similar exhibiting cleavage in the Stage I fatigue area, followed by very fine striations on plateaus separated by steps and feathery cleavage. Towards the end of the fatigue progression the striations covered a higher percentage of the fracture and were substantially coarser particularly on the 800° F specimen. The 800° F specimen also had deep voids in this area. Final overstress on both specimens occurred by coarse shear dimpled overstress. Many of the dimples had ripples on their walls. The 1100° F specimen had a single origin near the center of the specimen. Features were visible radiating outward from the origin. No defects were found at the origin (Stage I) which exhibited cleavage features similar to the lower temperature specimen. The final overstress area exhibited poorly defined dimples and deep voids. No shear lip was found.

Two notched LCF specimens and one smooth LCF specimen were examined. The smooth LCF specimen fractured in 20 cycles and exhibited a cup-and-cone tensile fracture with a very large shear lip. Both notched specimens exhibited fatigue propagation from multiple origins in the base of the notch. The room temperature specimen had fatigue propagation in a crescent extending 270° around the specimen. The final overstress occurred in a circular shaped region exhibiting coarser features. No local origins could be identified on either specimen. Coarse striations with some voids were visible from near the base of the notch until final overstress occurred by equiaxed dimpled overstress. The 1100 F specimen exhibited similar features except the striations were coarser and more well defined, and the fatigue propagated from multiple origins 360° around the specimen.

Two TMF specimens were run: one in-phase and one out-of-phase. The in-phase specimen had seven thumbnail areas indicating propagation from origins on the O.D. surface. The origin areas exhibited Stage I fatigue facets with fatigue striations visible adjacent to the origins. Coarse striations and crack-like striations dominated the fatigue propagation area, Stage II. The out-of-phase specimen had a single O.D. origin thumbnail. The fatigue origin area had several localized surface origins. The progression area (Stage II) both near the origin and away from the origin exhibited oxidized striations and crack-like striations. Final overstress on both specimen occurred by a mixture of equiaxed tensile and shear dimpled overstress.

MATERIAL

MP-159
AMS 5843

TEST DATA

TEST TYPE

Smooth Tensile

TEST CONDITIONS

Strain Rate: 0.005 mm/mm/min (0.005 in/in/min)
Atmosphere: Air
Temperature: 593°C (1100°F)
Test Direction: Longitudinal

TEST RESULTS

0.2% Yield Strength: 1323.8 MPa (192 ksi)
Ultimate Strength: 1392.7 MPa (202 ksi)



FAL 94242

MAG: 10X

FIGURE 11-1: Test results and fractography of MP-159 593°C (1100°F) smooth tensile test. The fracture surface was oriented at an angle of approximately 45° to the stress axis.



FAM 100288

MAG: 100X

FIGURE 11-2: Optical photomicrograph showing grain deformation along the fracture surface which is oriented at an angle to the primary stress axis. The fracture was predominantly transgranular.

Etchant: HCl and H₂O₂ electrolytic

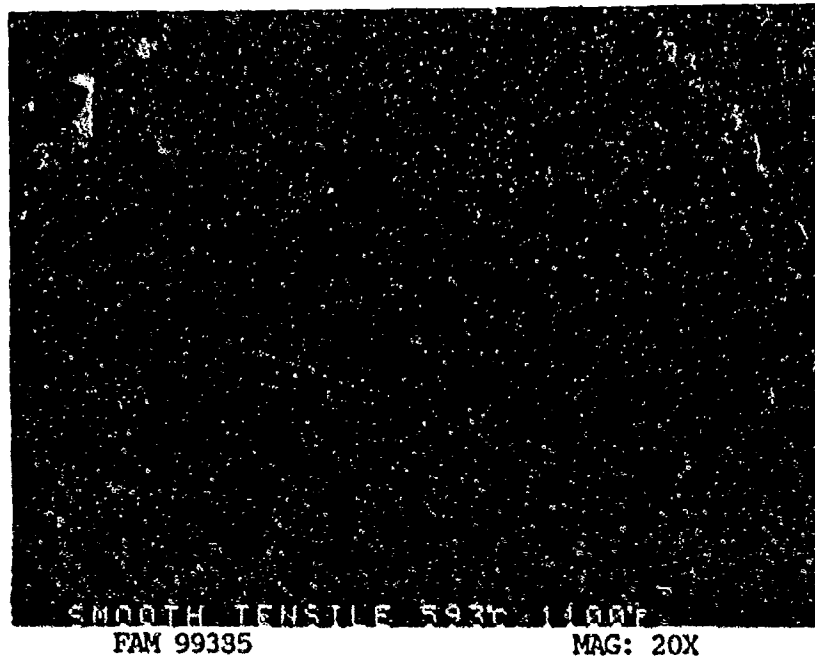


FIGURE 11-3: Low magnification photograph showing relatively flat fracture that occurred at an angle to the stress axis.

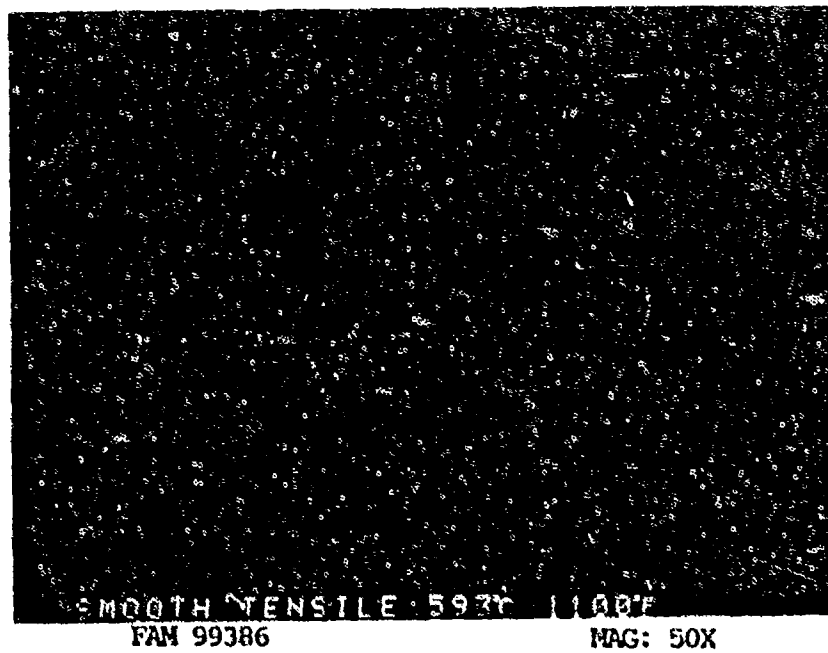


FIGURE 11-4: Higher magnification photograph of the center of the fracture surface, showing shear dimples.

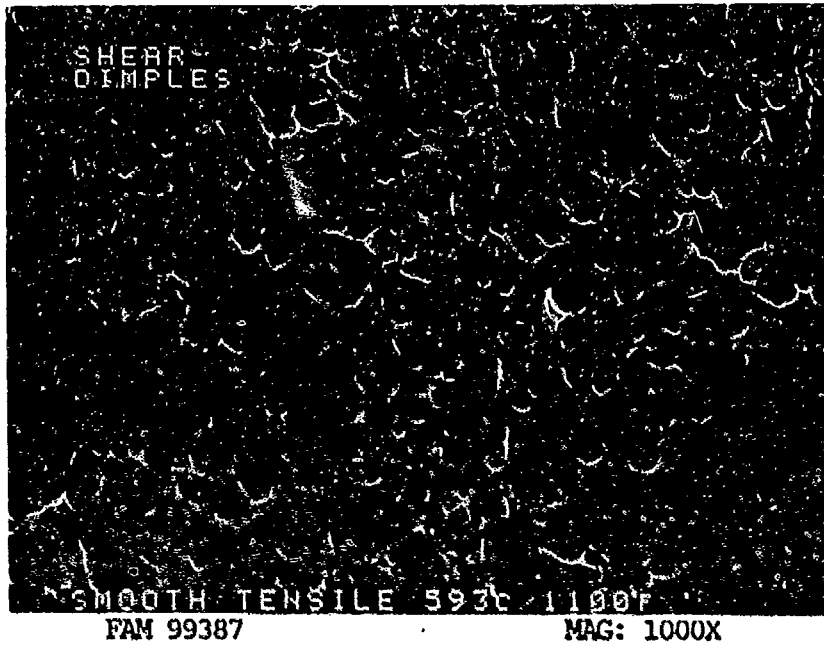


FIGURE 11-5: Shear dimpled overstress.

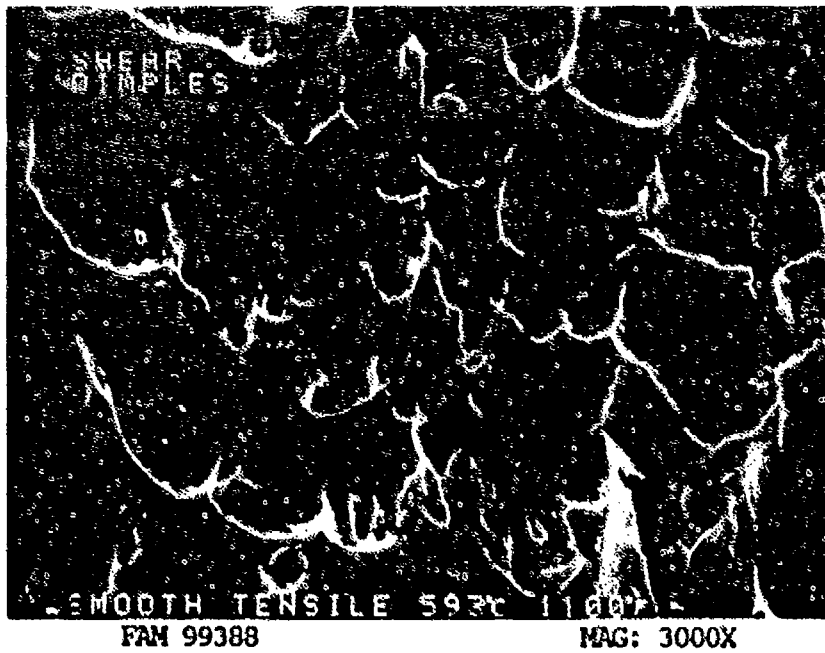


FIGURE 11-6: Higher magnification photograph of shallow shear dimpled overstress that covered the entire fracture surface.

MATERIAL

MP-159
AMS 5843

TEST DATA

TEST TYPE

Notched Tensile

TEST CONDITIONS

Crosshead Speed: 1.27 mm/min (0.05 in/min)

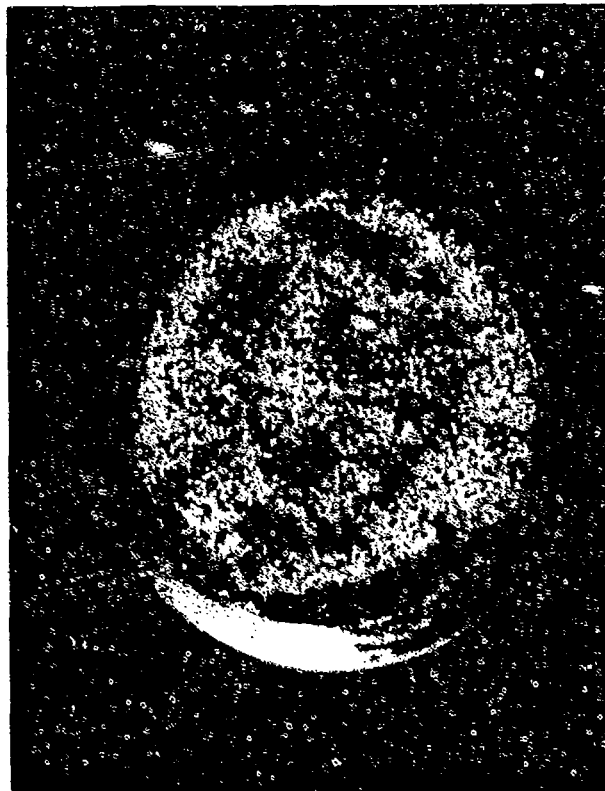
Atmosphere: Air

Temperature: 593°C (1100°F)

Test Direction: Longitudinal

TEST RESULTS

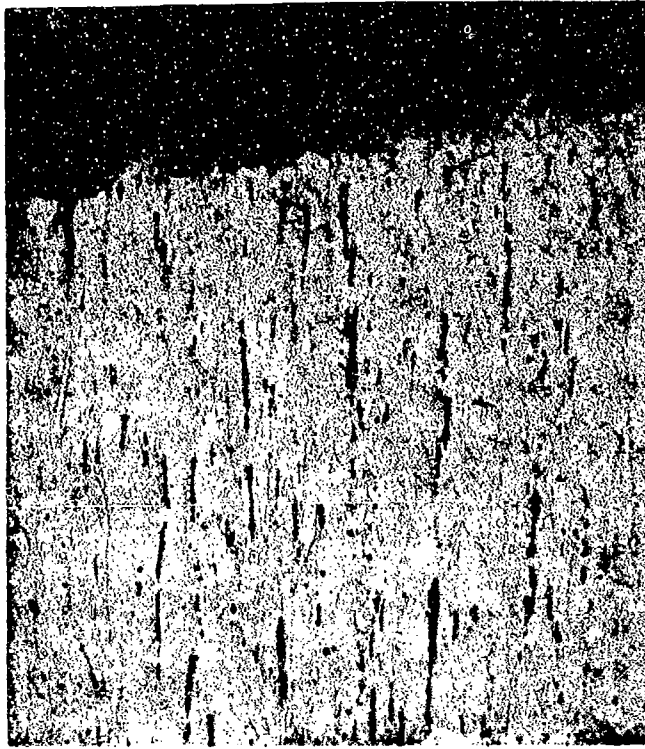
Data not available.



FAL 94238

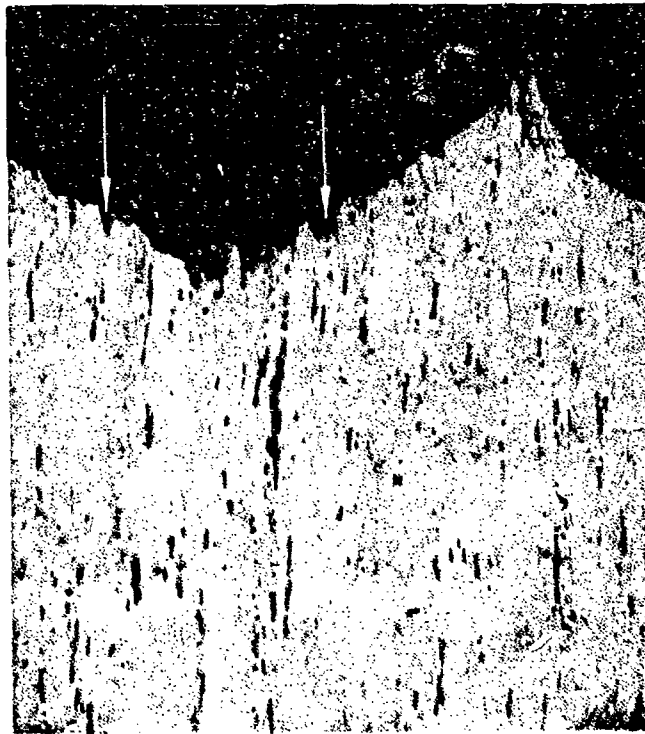
MAG: 14X

FIGURE 11-7: Test results and fractography of MP-159 593°C (1100°F) notched tensile test. The fracture surface has a granular appearance.



FAM 100184

MAG: 100X



FAM 100183

MAG: 100X

FIGURE 11-8: Optical photomicrographs showing the center (top) and edge (bottom) of the fracture. The fracture path is transgranular with dimples visible (arrows).

Etchant: HCl and H₂O₂ electrolytic

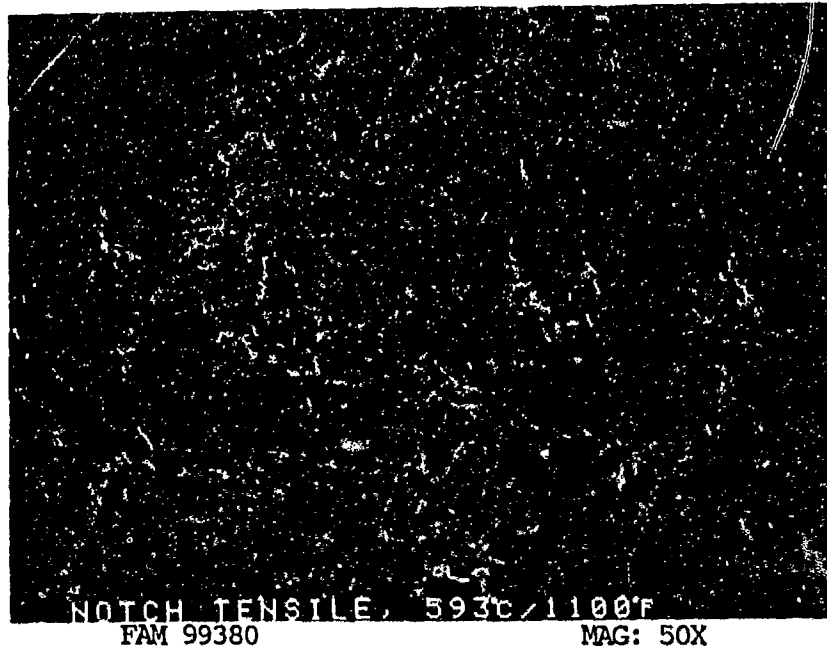


FIGURE 11-9: Low magnification photograph showing fracture surface to be relatively flat. Even at low magnification, equiaxed dimples are visible.

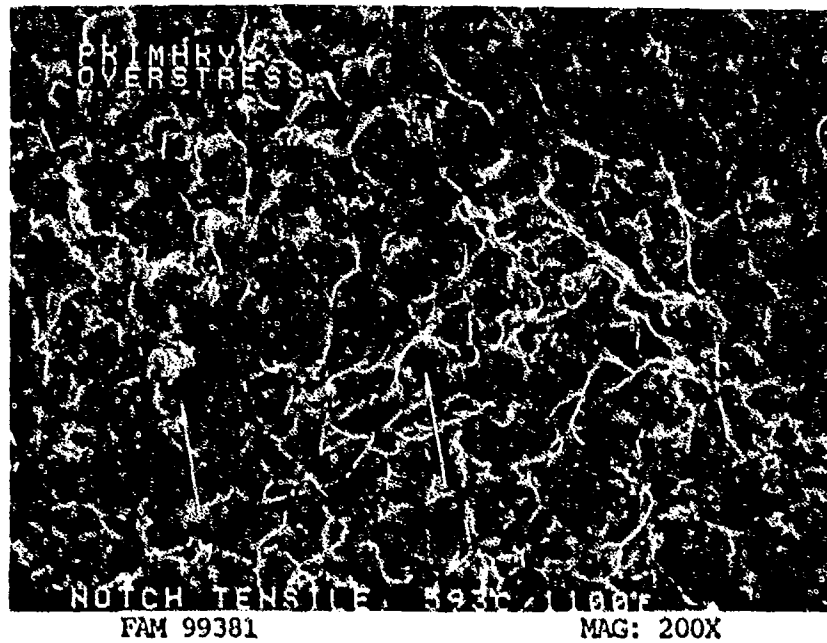


FIGURE 11-10: Coarse dimpled overstress with voids at the bases of dimples (arrows).

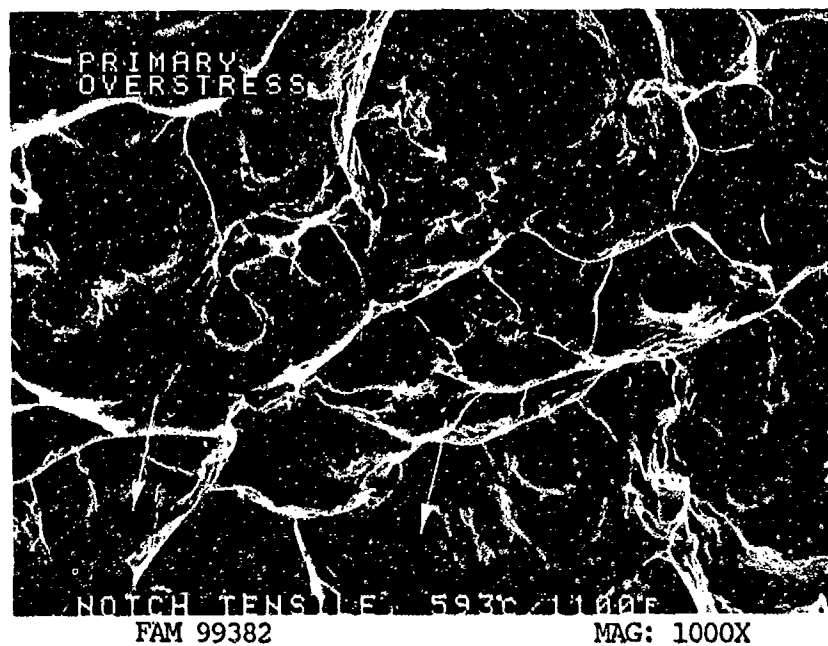


FIGURE 11-11: Higher magnification photograph of the area shown in Figure 11-10, exhibiting a mixture of large shallow dimples and deep voids. Second phase particles (carbides) are visible in several locations (arrows). The entire fracture surface is covered by a light oxide.

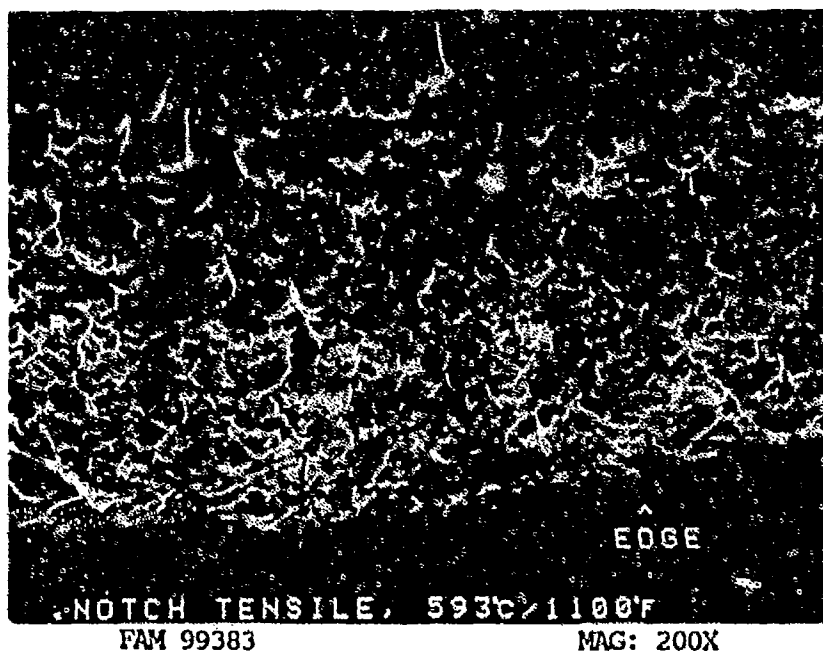


FIGURE 11-12: Shallow dimples in the final overstress area near the edge of the specimen.

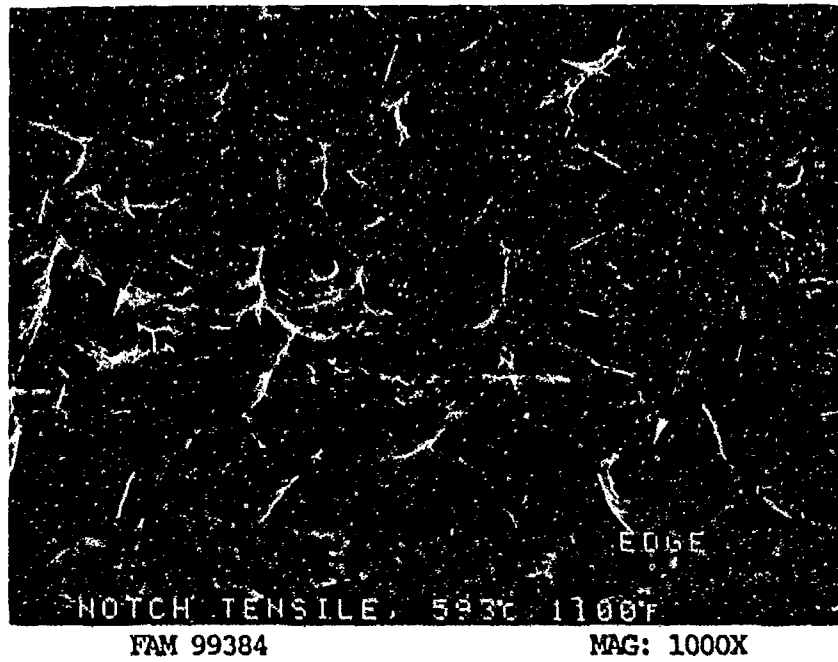


FIGURE 11-13: Shallow dimples in the final overstress area. Deep voids are visible in several locations (arrows).

MATERIAL

MP-159
AMS 5843

TEST DATA

TEST TYPE

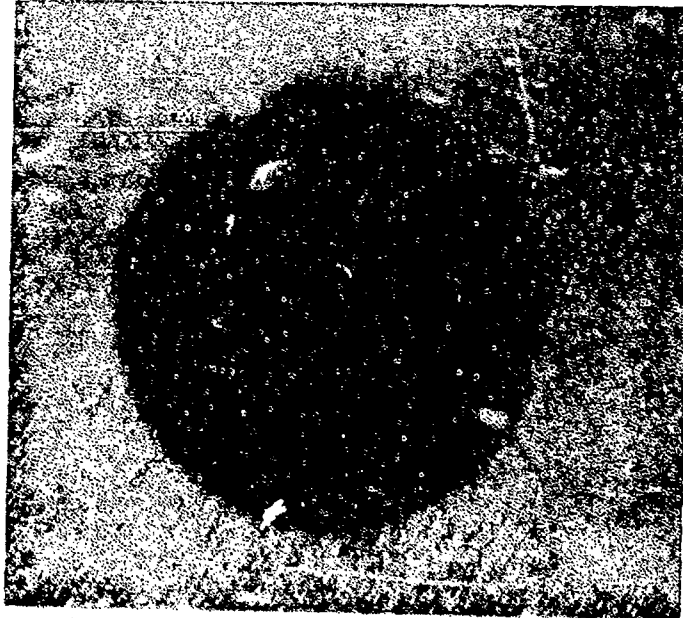
Stress Rupture

TEST CONDITIONS

Stress: 1103.2 MPa (160 ksi)
Atmosphere: Air
Temperature: 649°C (1200°F)
Test Direction: Longitudinal

TEST RESULTS

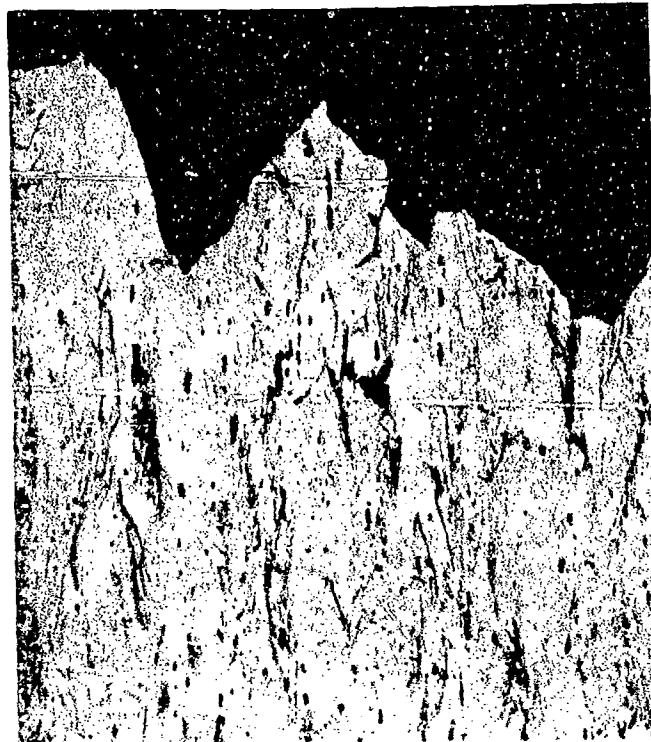
Time to Rupture: 22.9 hours
% Elongation: 16.8
% Reduction of Area: 50.5



FAL 93236

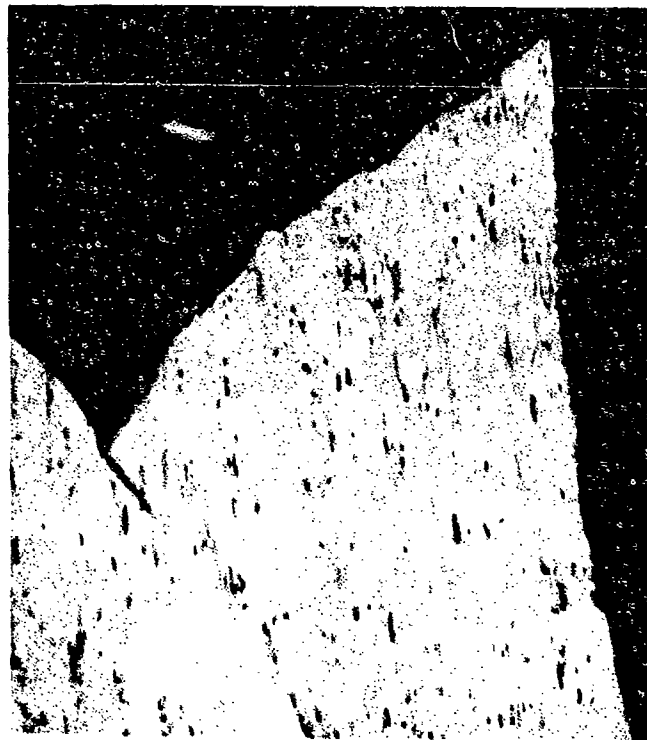
MAG: 10X

FIGURE 11-14: Test results and fractography of MP-159 649°C (1200°F) stress rupture test. The fracture surface appears oxidized and has deep fractures.



FAM 100180

MAG: 100X



FAM 100186

MAG: 100X

FIGURE 11-15: Optical photomicrographs of the center (top) and an edge (bottom) of the specimen, exhibiting intergranular dimpled overstress in the center and a large, well defined shear lip at the edge.

Etchant: HCl and H₂O₂ electrolytic

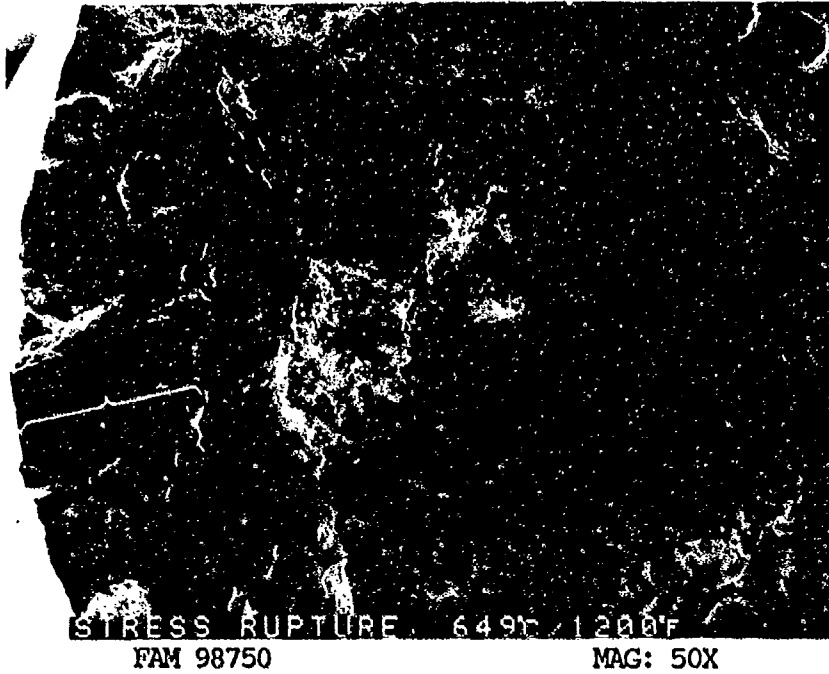


FIGURE 11-16: Low magnification photograph showing void coalescence near the center of the specimen and a large shear lip at the edge of the specimen. A bracket shows the extent of the shear lip.

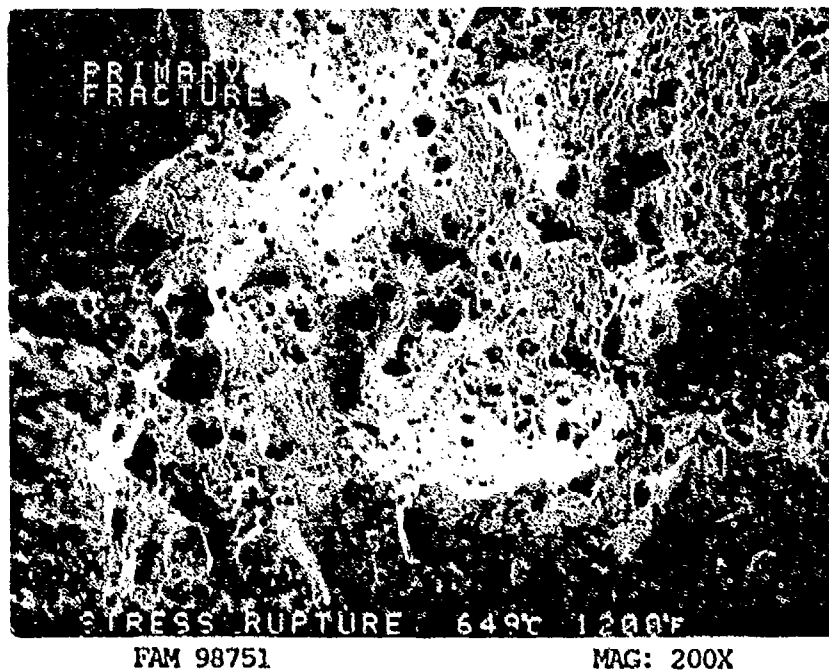


FIGURE 11-17: Higher magnification view of the primary fracture area in the center of the specimen. Dimpled overstress and void coalescence is clearly visible.

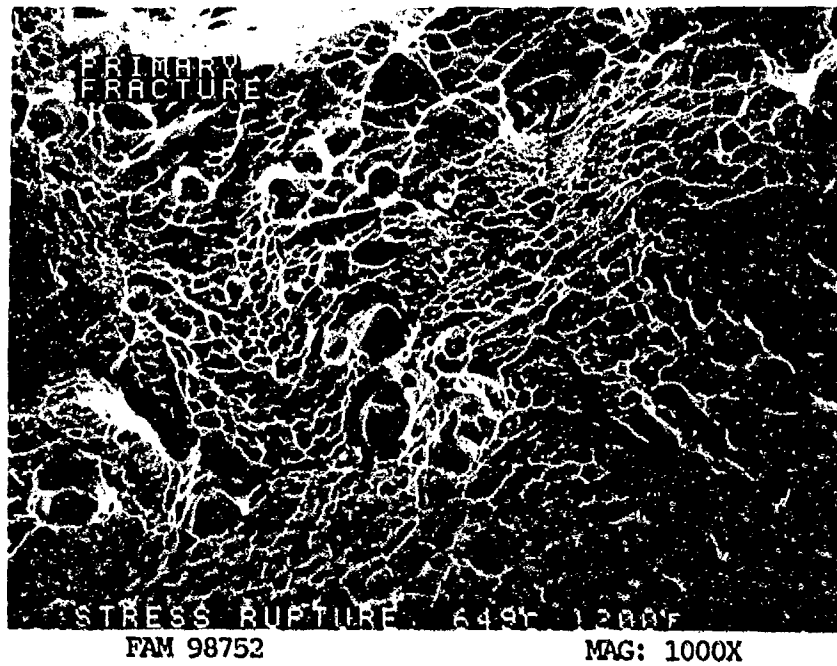


FIGURE 11-18: Shallow dimpled overstress with void coalescence (arrows A) near the center of the specimen in the primary fracture area. Several carbides are visible (arrows B).

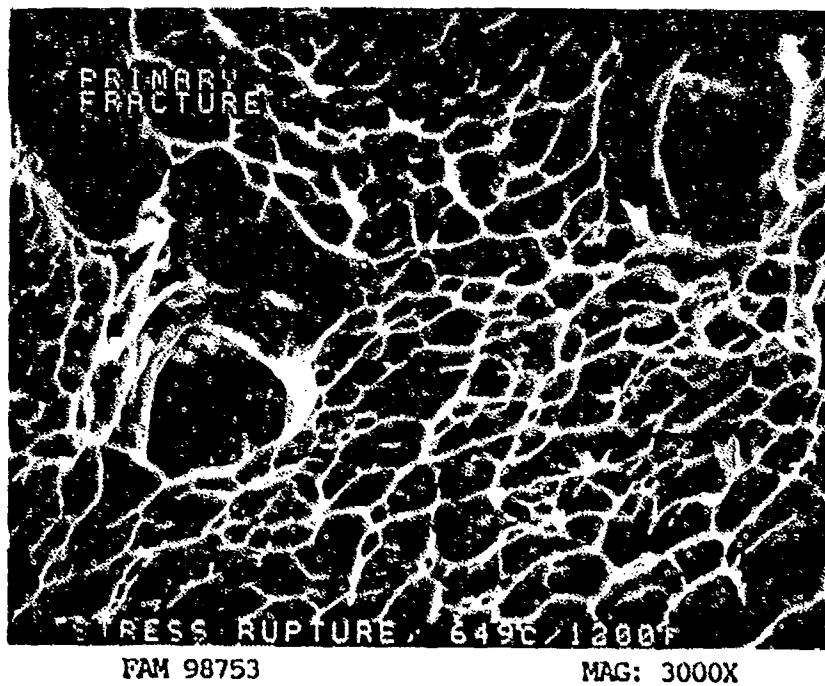


FIGURE 11-19: Higher magnification photograph of the area shown in Figure 11-18, showing overstress dimples and coalesced voids.

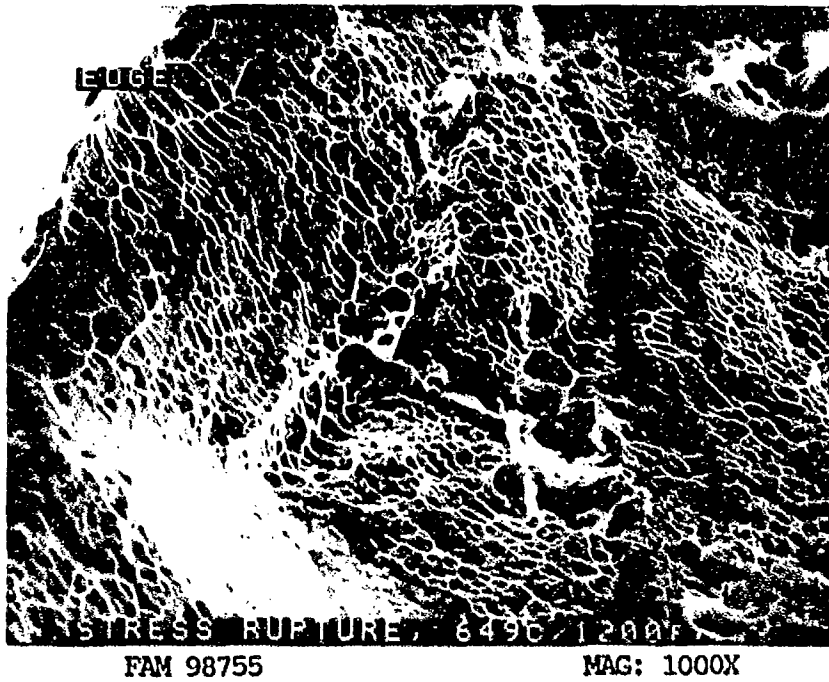


FIGURE 11-20: Final fracture area near the edge of the specimen, exhibiting shallow dimples.

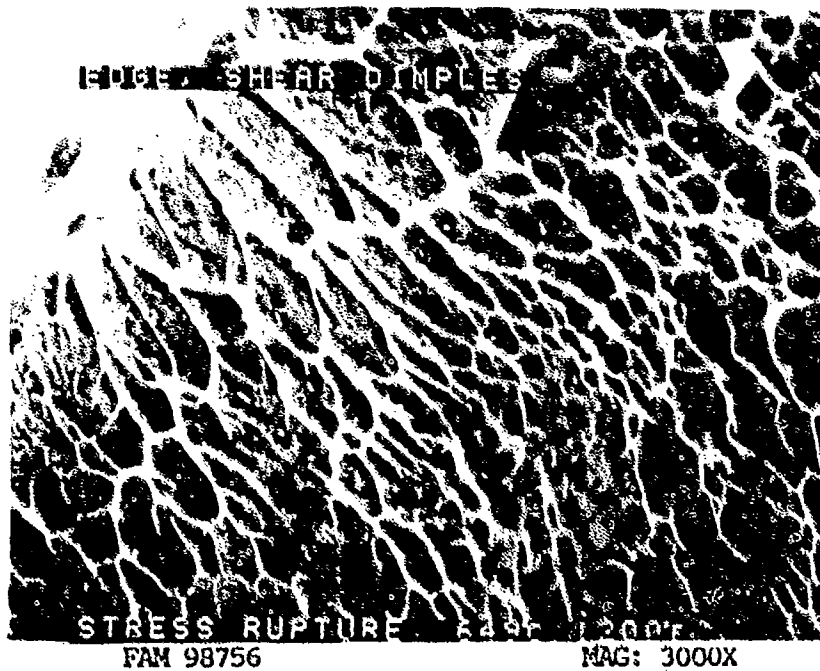


FIGURE 11-21: Higher magnification photograph of the specimen edge, Figure 11-20, showing shallow shear dimples.

MATERIAL

MP-159
AMS 5843

TEST DATA

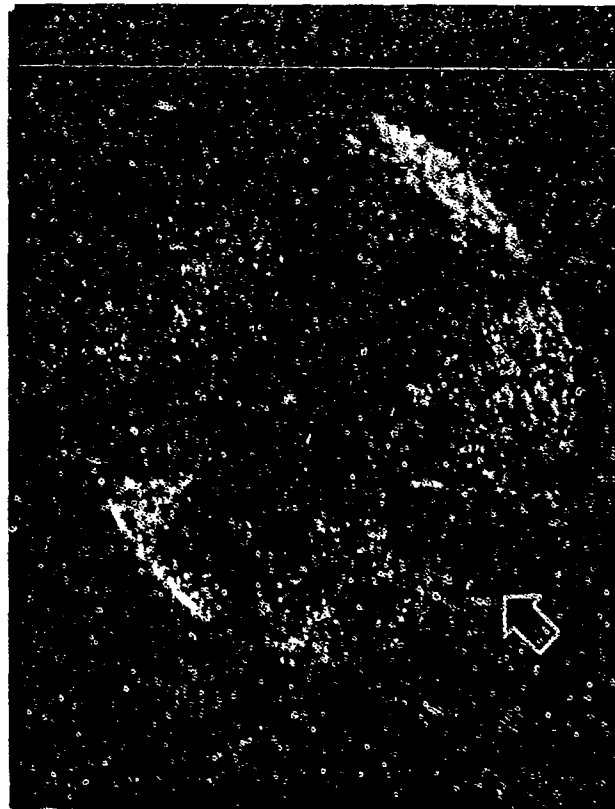
TEST TYPE
Smooth HCF

TEST CONDITIONS

Stress: 999.7 MPa (145 ksi)/99.9 MPa (14.5 ksi)
Stress Ratio: 0.10
Frequency: 1800 cpm
Atmosphere: Air
Temperature: Room Temperature
Test Direction: Longitudinal

TEST RESULTS

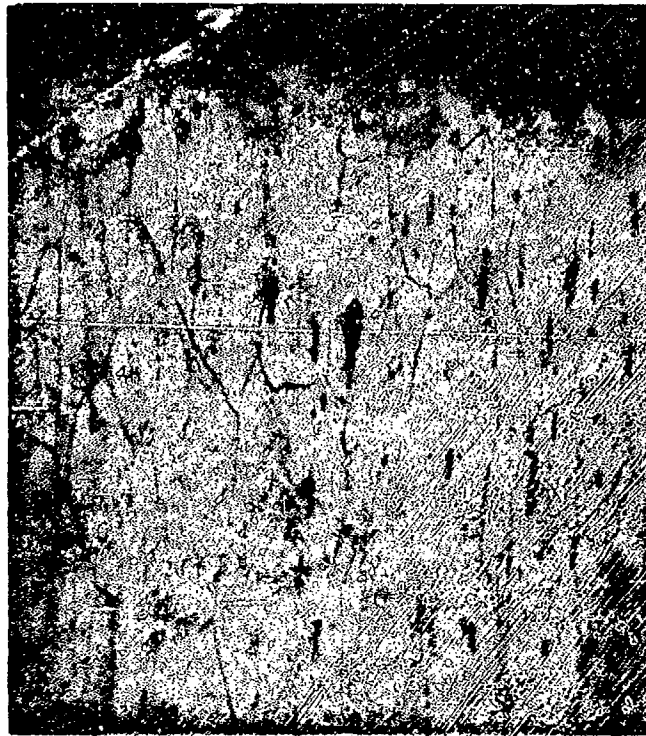
Cycles to Fracture: 238,500



FAL 94374

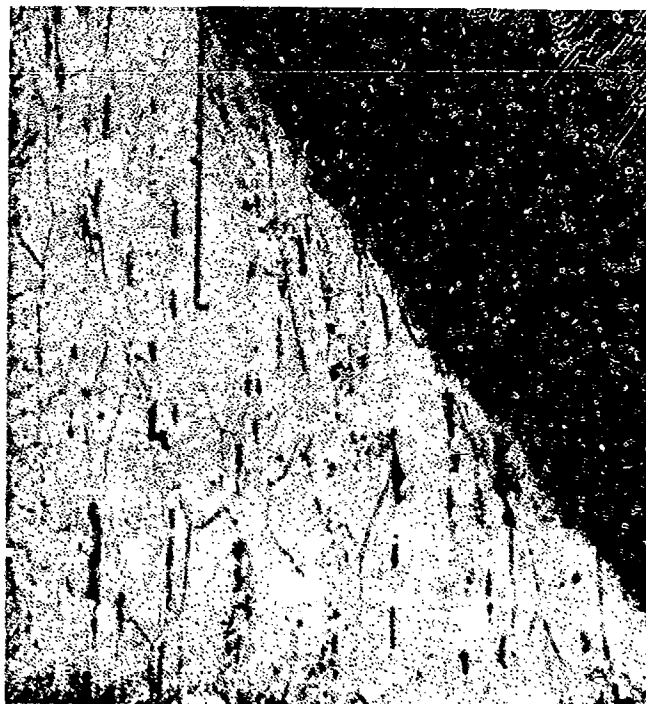
MAG: 15X

FIGURE 11-22: Test results and fractography of MP-159 room temperature smooth HCF test. The fatigue origin area (arrow) and propagation plane are not clearly discernible.



FAM 100281

MAG: 200X

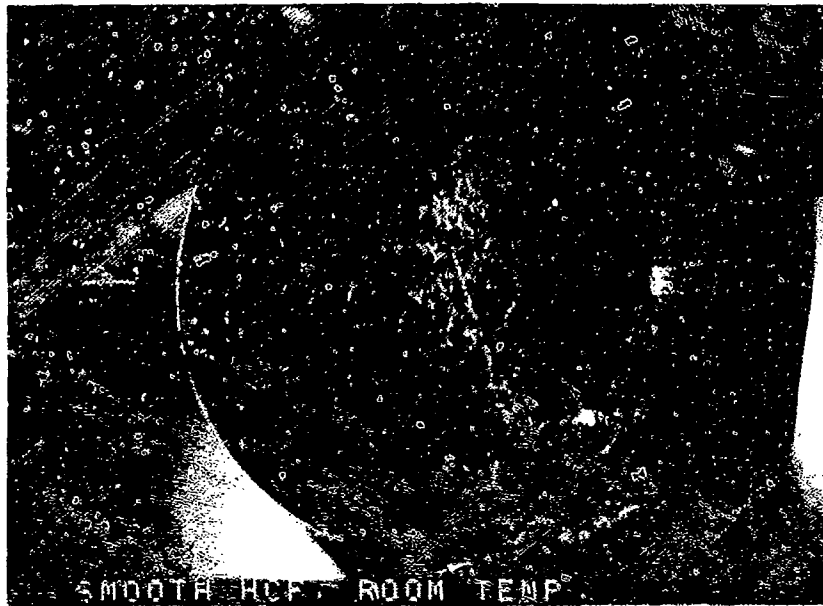


FAM 100282

MAG: 200X

FIGURE 11-23: Optical photomicrographs showing the fatigue progression area (top) and the final overstress area (bottom). The fatigue progressed on a plane perpendicular to the stress axis with little grain deformation in the grains adjacent to the fracture. The fracture path is predominantly transgranular. Final overstress occurred at an angle to the primary stress axis and was accompanied by grain elongation (bracket, bottom).

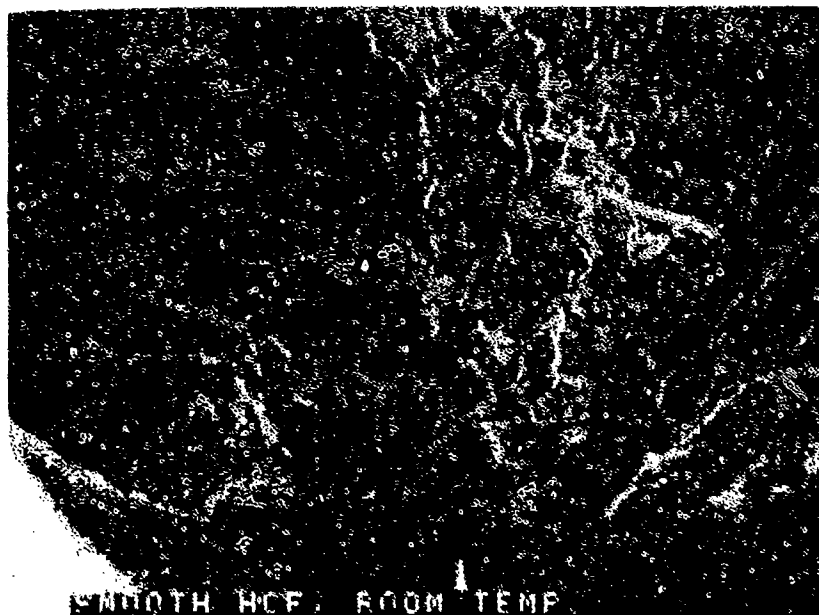
Etchant: HCl and H₂O₂ electrolytic



FAM 99544

MAG: 20X

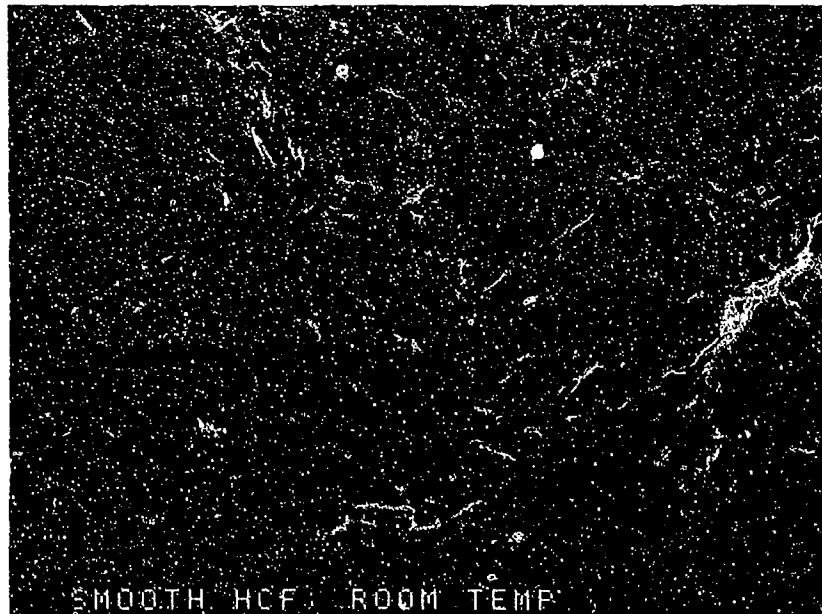
FIGURE 11-24: Low magnification photograph showing fatigue initiation (arrow) and progression on a plane approximately perpendicular to the stress axis. The fatigue progression area appears to be more granular than the surrounding overstress area. The final overstress fracture occurred at an angle. Features can be seen radiating from the origin area.



FAM 99545

MAG: 50X

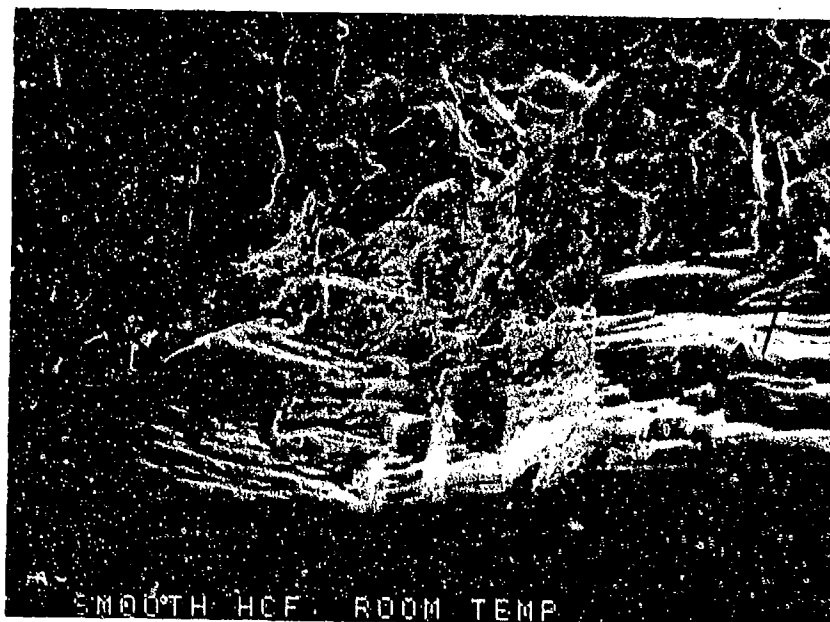
FIGURE 11-25: Higher magnification view of the origin area. The features are radiating from a diffuse origin area (arrow).



FAM 99546

MAG: 200X

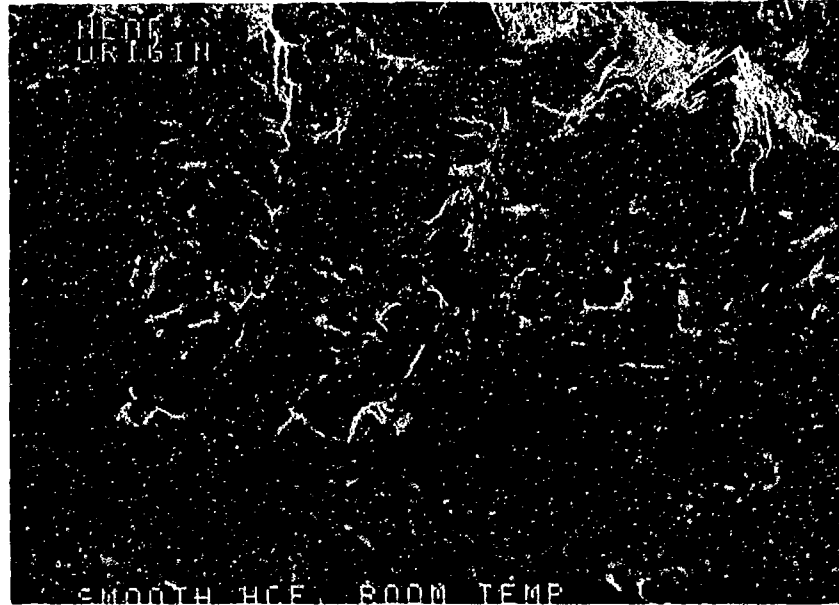
FIGURE 11-26: Fatigue steps and feathery cleavage in the origin area.



FAM 99547

MAG: 1000X

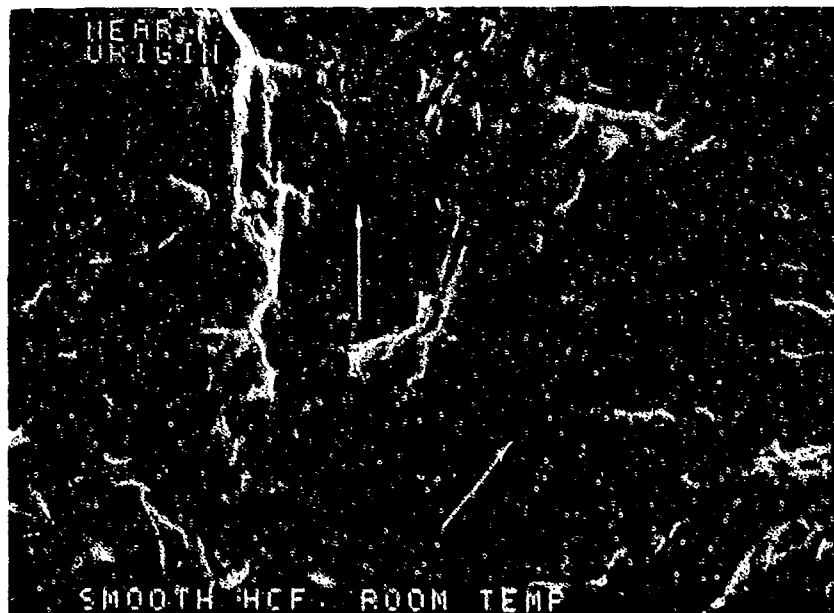
FIGURE 11-27: Higher magnification view of the origin area shown in Figure 11-26, exhibiting a faceted appearance. A void is visible (arrow, right) but it does not appear to have contributed to fatigue initiation.



FAM 99548

MAG: 1000X

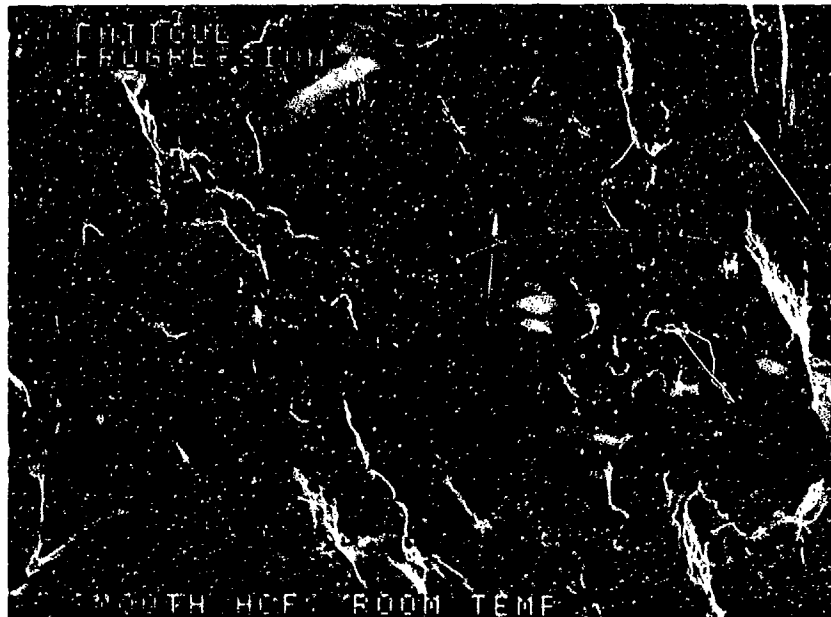
FIGURE 11-28: Fatigue progression near the origin area. The general direction of propagation is from bottom to top of the photograph.



FAM 99549

MAG: 3000X

FIGURE 11-29: Higher magnification view of the fatigue progression near the origin area showing fine fatigue striations on numerous plateaus (arrows). Individual striations are not resolvable.



FAM 99551

MAG: 1000X

FIGURE 11-30: Fatigue progression area away from the origin showing coarser striations and crack-like striations, indicating localized propagation in several directions (arrows).



FAM 99552

MAG: 3000X

FIGURE 11-31: Higher magnification view of the area shown in Figure 11-30, showing fatigue striations and crack-like striations.

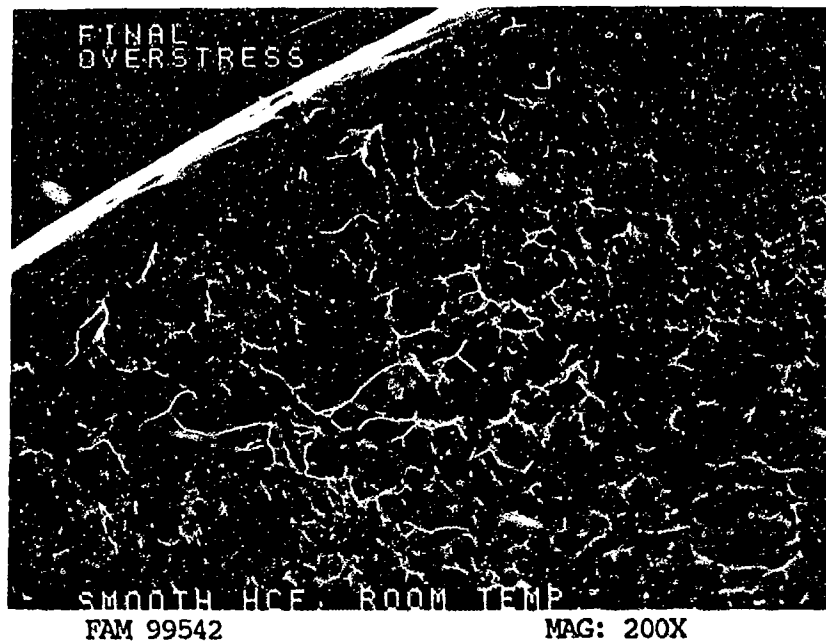


FIGURE 11-32: Final overstress area showing a mixture of equiaxed and shear dimples.

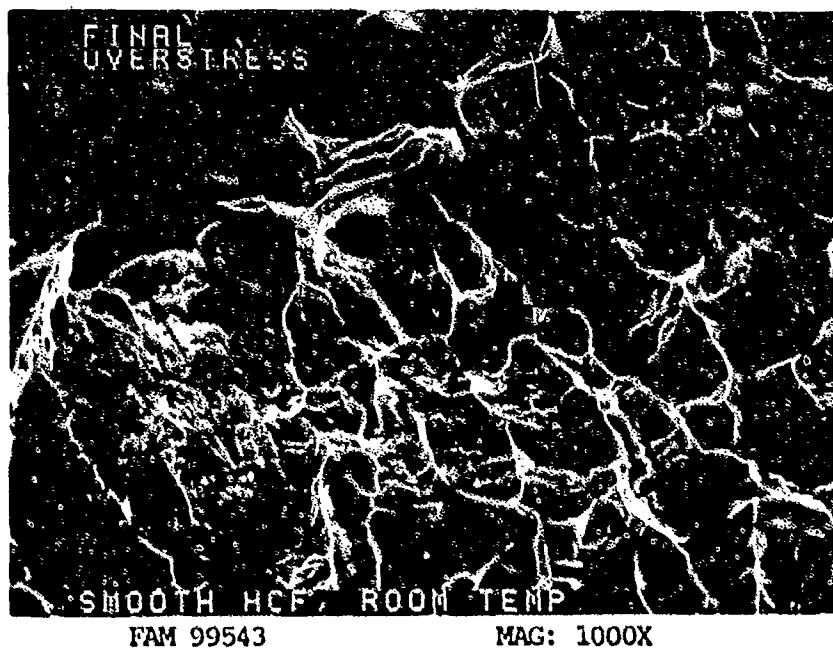


FIGURE 11-33: Higher magnification view of the area shown in Figure 11-28 showing remnant shear dimples and voids (arrow A). Serpentine glide ripples are visible in the dimples (arrow B).

MATERIAL

MP-159
AMS 5843

TEST DATA

TEST TYPE

Smooth HCF

TEST CONDITIONS

Stress: 965.3 MPa (140 ksi)/96.5 MPa (14.0 ksi)
Stress Ratio: 0.10
Frequency: 1800 cpm
Atmosphere: Air
Temperature: 427°C (800°F)
Test Direction: Longitudinal

TEST RESULTS

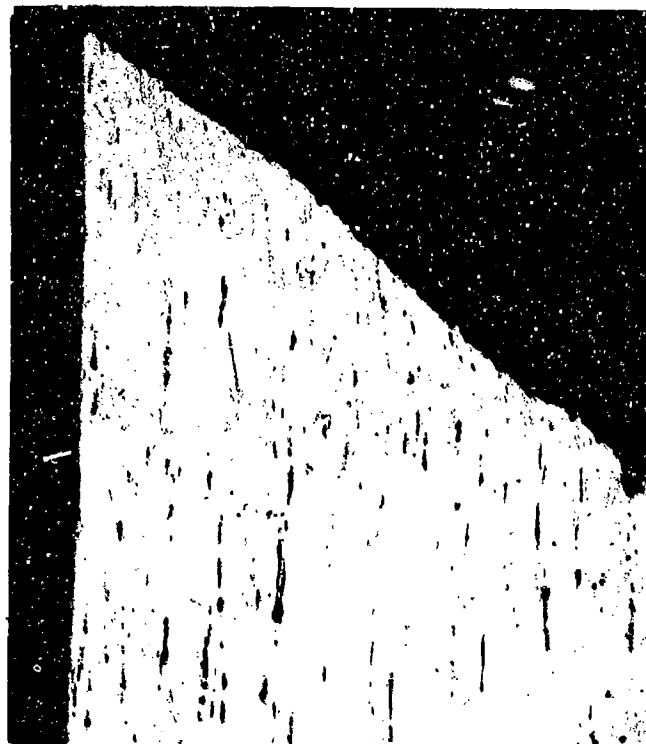
Cycles to Fracture: 692,000



FAL 94378

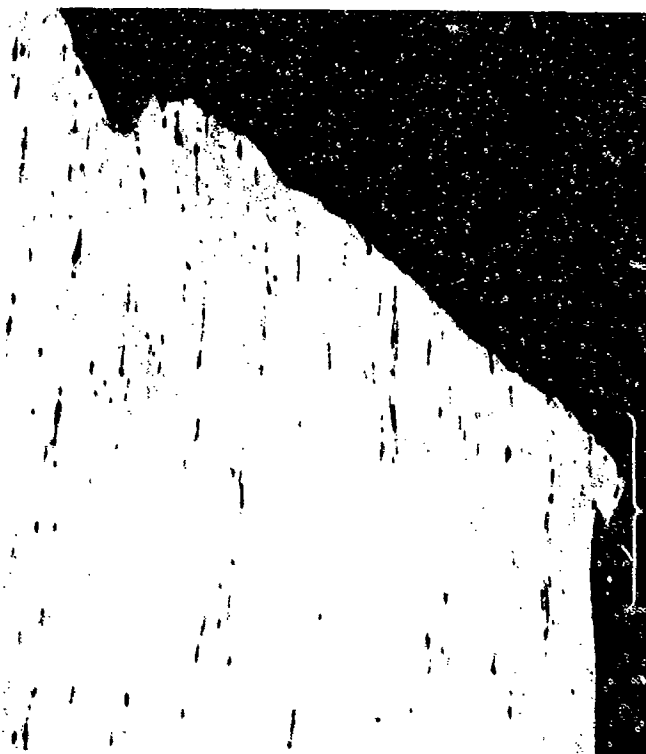
MAG: 15X

FIGURE 11-34: Test results and fractography of MP-159 427°C (800°F) smooth HCF test. The origin and fatigue progression area are not clearly discernible.



FAM 100182

MAG: 100X



FAM 100181

MAG: 100X

FIGURE 11-35: Optical photomicrographs showing the fatigue progression area (top) and the final overstress area (bottom). The fatigue progressed with little grain deformation in the grains adjacent to the fracture. Final overstress was accompanied by grain elongation (bracket, bottom).

Etchant: HCl and H₂O₂ electrolytic

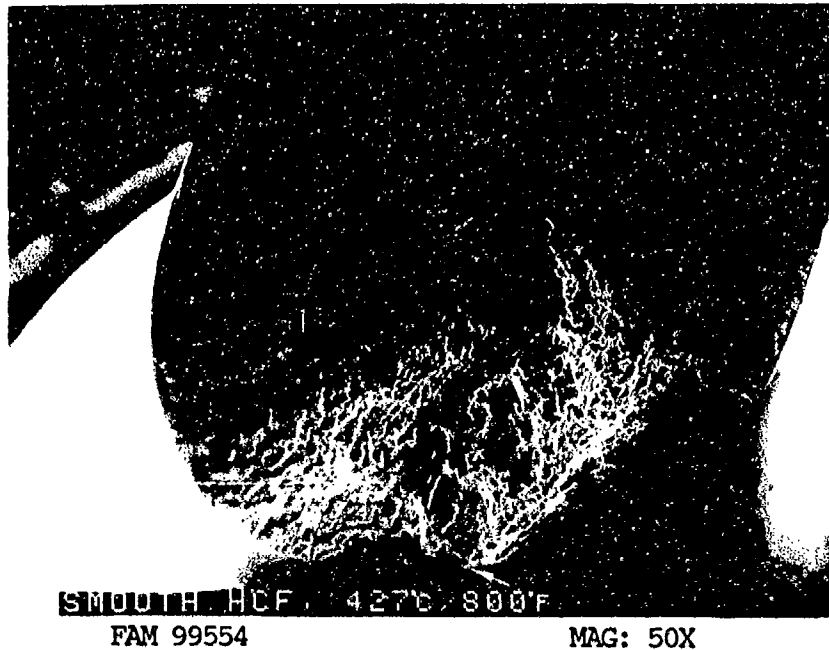


FIGURE 11-36: Low magnification photograph showing fatigue initiation and progression on a plane approximately perpendicular to the stress axis. The fatigue progression area appears to be more granular than the surrounding overstress area. The final overstress occurred at an angle to the stress axis. An arrow indicates the origin area.

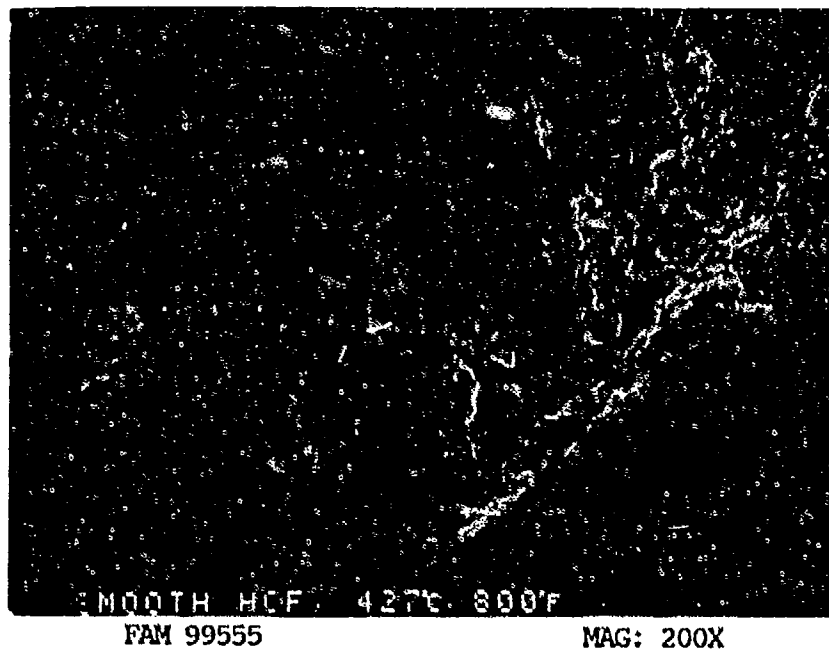


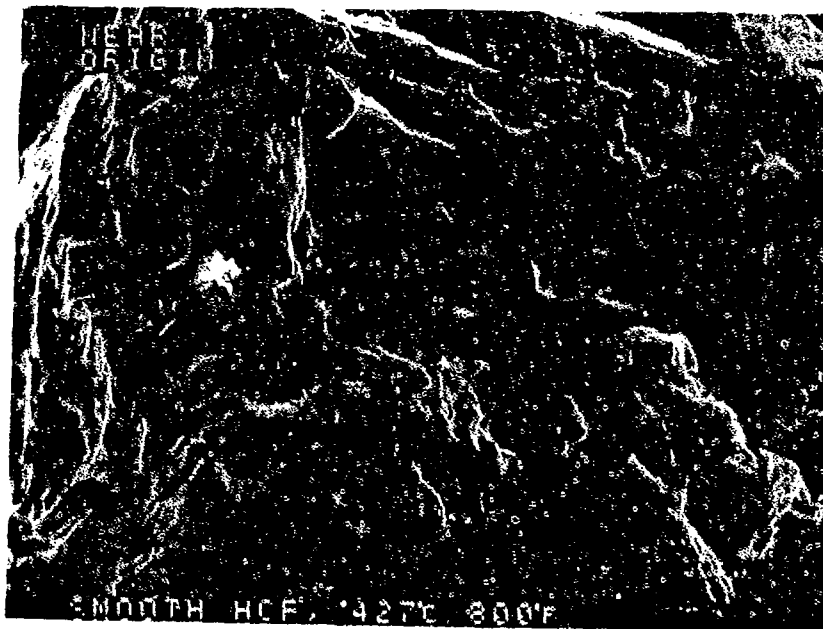
FIGURE 11-37: Higher magnification view of the origin area, showing no discernible features.



FAM 99557

MAG: 1000X

FIGURE 11-38: High magnification view of the origin area shown in Figure 11-37.



FAM 99558

MAG: 1000X

FIGURE 11-39: Area adjacent to the origin area exhibiting very fine striations on several plateaus.

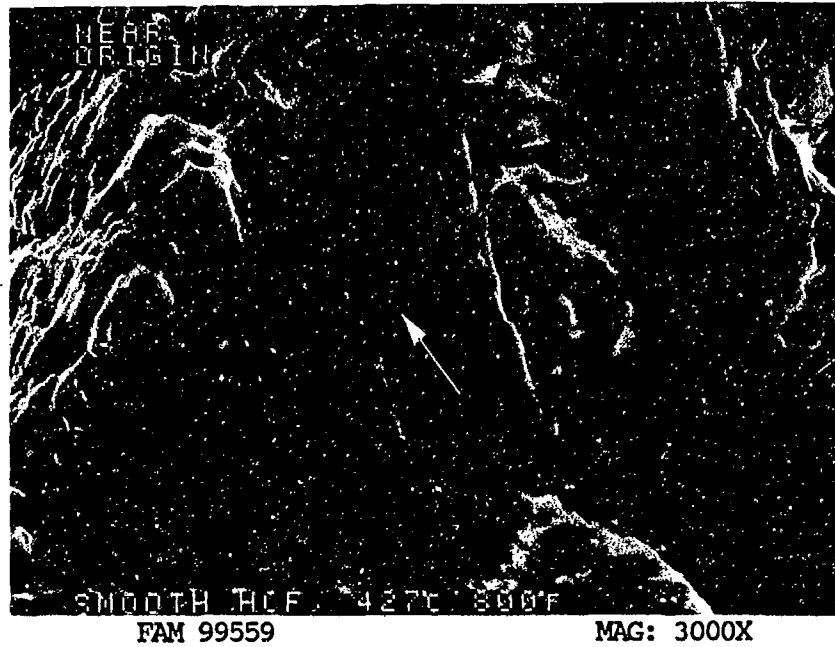


FIGURE 11-40: Higher magnification view of the area shown in Figure 11-39. Fine fatigue striations are visible on several plateaus separated by fatigue steps. The direction of propagation is shown by an arrow.

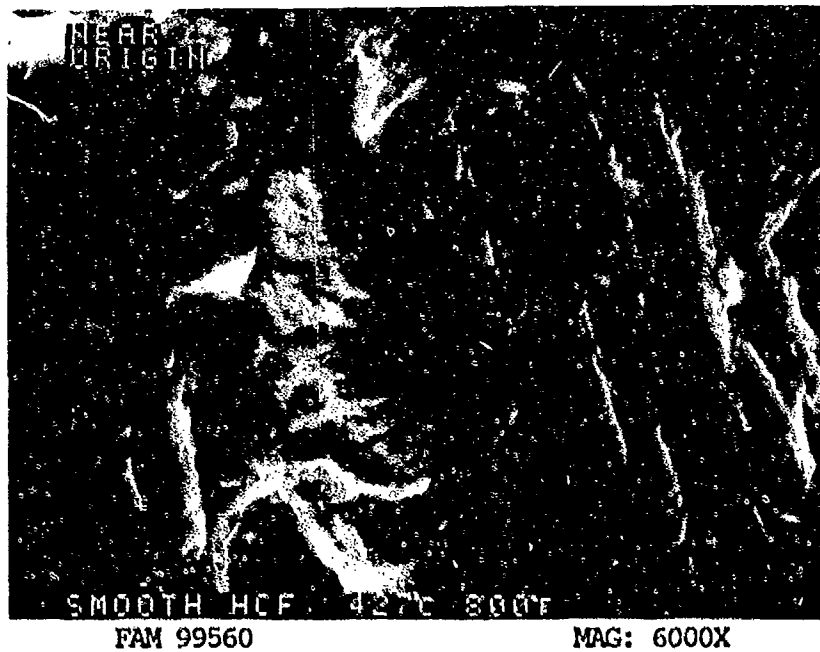


FIGURE 11-41: Higher magnification view of the area shown in Figure 11-40.

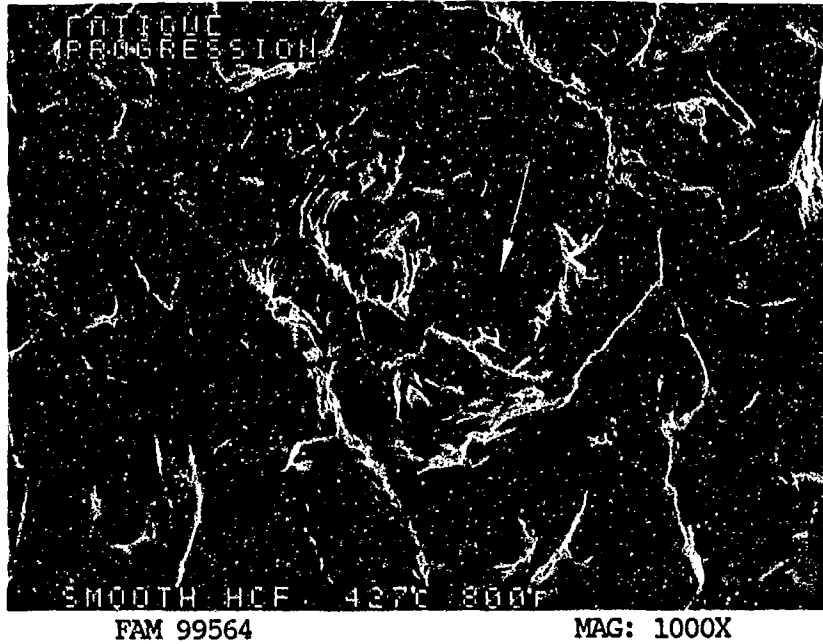


FIGURE 11-42: Relatively coarse striations in the fatigue progression zone away from the origin area (compare to Figure 11-39). Some void coalescence is also visible (arrow).

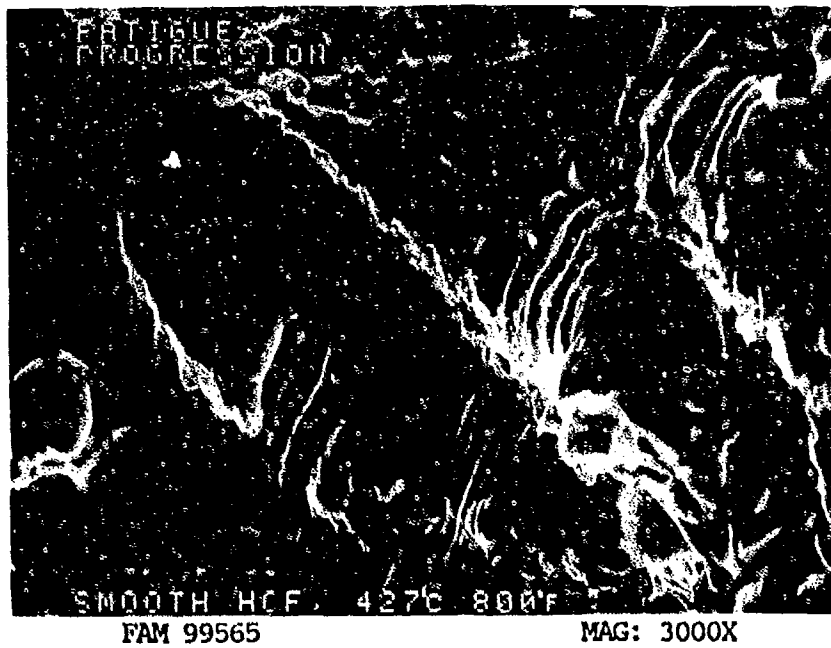


FIGURE 11-43: Higher magnification photograph of the fatigue striations shown in Figure 11-42.

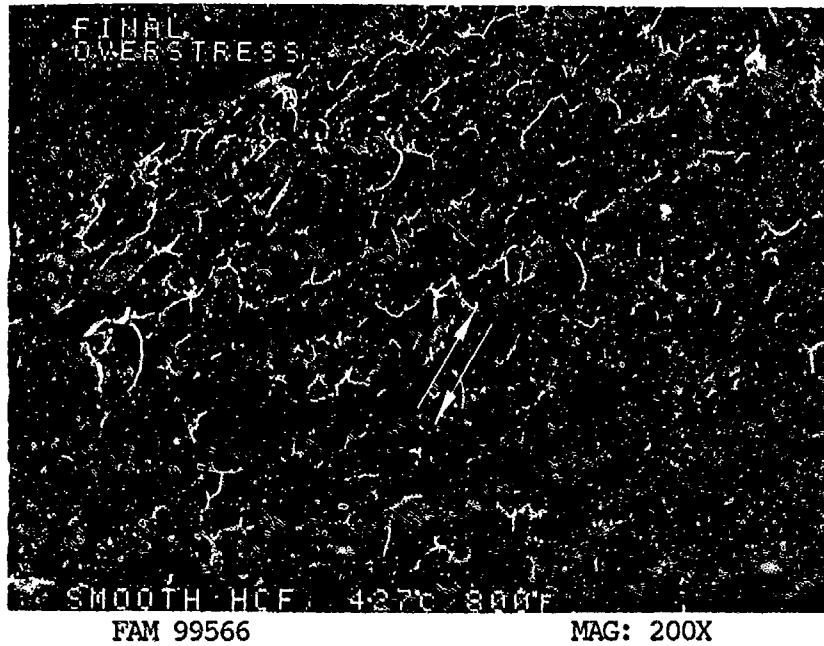


FIGURE 11-44: Shear dimples in the final overstress area. The directions of relative motion is shown by arrows.

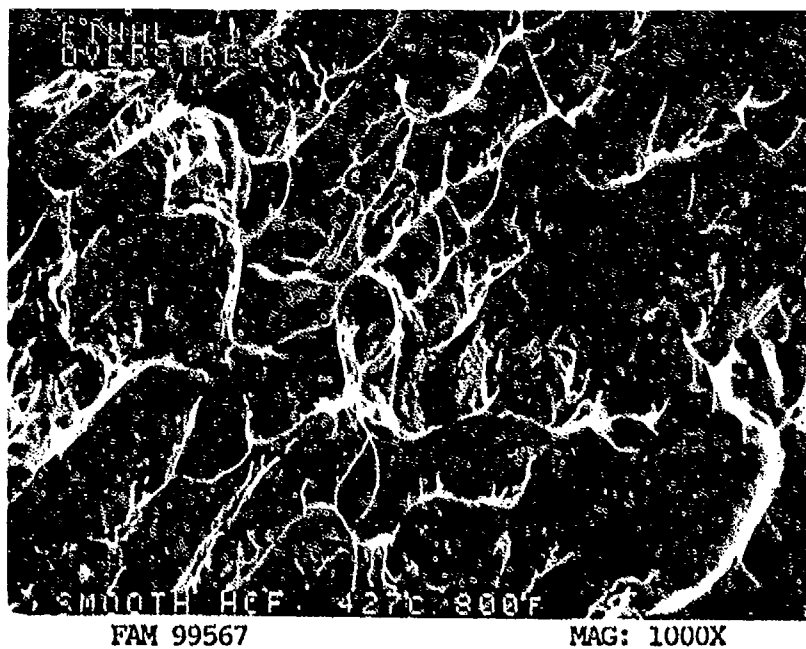


FIGURE 11-45: Higher magnification photograph of the final overstress area shown in Figure 11-44, again showing shear dimples.

MATERIAL

MP-159
AMS 5843

TEST DATA

TEST TYPE
Smooth HCF

TEST CONDITIONS

Stress: 896.3 MPa (130.0 ksi)/89.6 MPa (13.0 ksi)
Stress Ratio: 0.10
Frequency: 1800 cpm
Atmosphere: Air
Temperature: 593°C (1100°F)
Test Direction: Longitudinal

TEST RESULTS

Cycles to Fracture: 1,050,000



FAL 94376

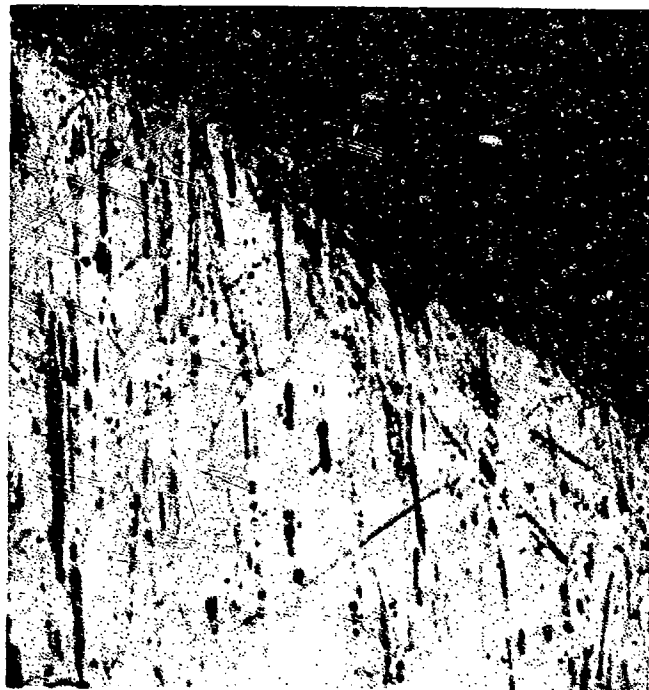
MAG: 15X

FIGURE 11-46: Test results and fractography of MP-159 593°C (1100°F) smooth HCF test. Fatigue initiated from an internal origin (arrow).



FAM 100284

MAG: 100X

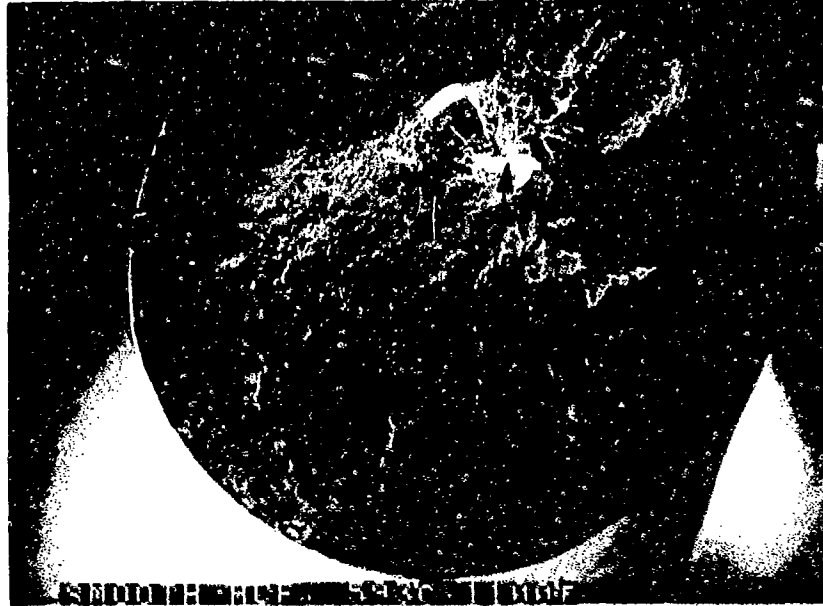


FAM 100285

MAG: 200X

FIGURE 11-47: Optical photomicrographs showing the fatigue progression area (top) and the final overstress area (bottom). The fatigue progressed on a plane perpendicular to the stress axis with little grain deformation in the grains adjacent to the fracture. Final overstress occurred at an angle to the primary stress axis and was accompanied by grain elongation (brackets, bottom). Oxidation is visible on the fracture surface and on the gage section (compare with Figures 11-23 through 11-35). The fracture was predominantly transgranular.

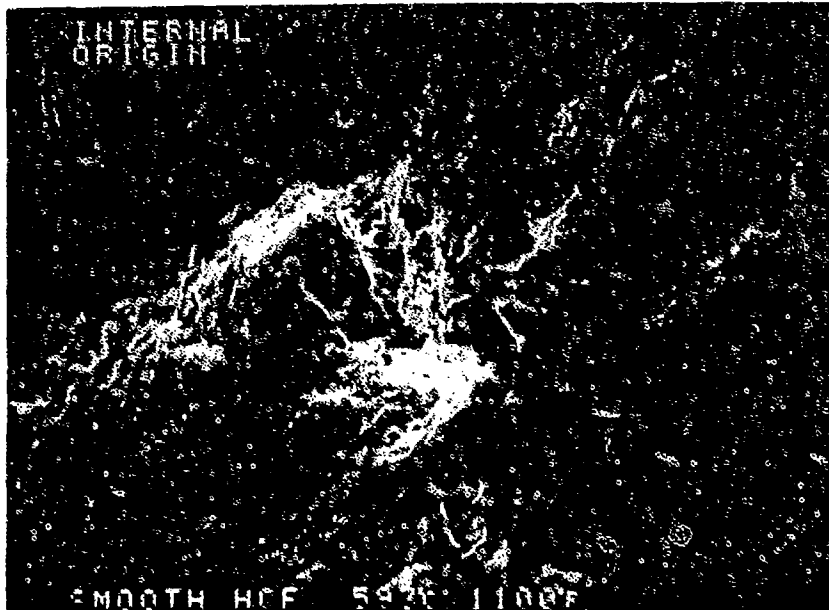
Etchant: HCl and H₂O₂ electrolytic



FAM 99568

MAG: 20X

FIGURE 11-48: Low magnification photograph showing fatigue initiation at an internal origin (arrow). Features can be seen radiating from the origin.



FAM 99569

MAG: 50X

FIGURE 11-49: Higher magnification view of the origin area near the center of the fracture surface. No material defects were found associated with the origin.

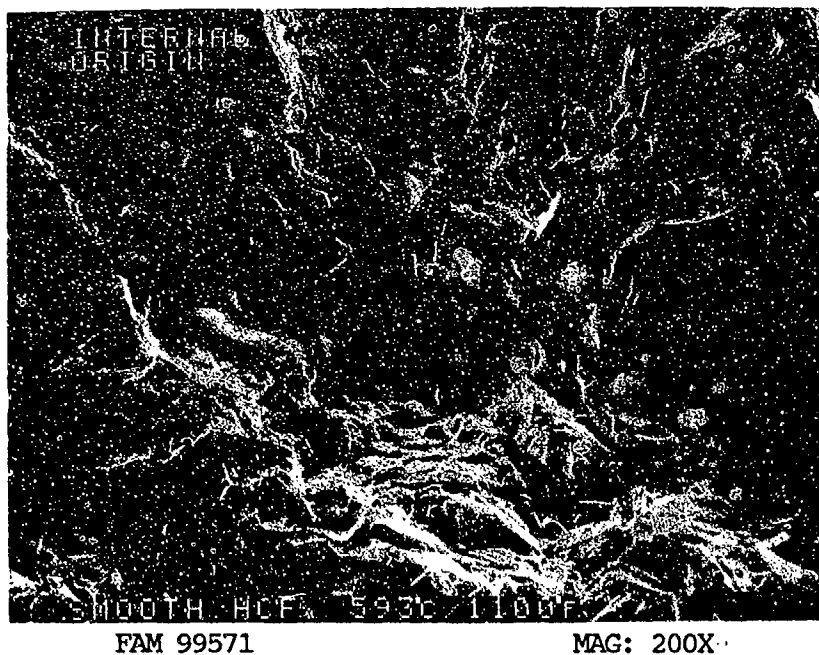


FIGURE 11-50: Higher magnification view of the origin shown in Figure 11-49. No defects are visible.

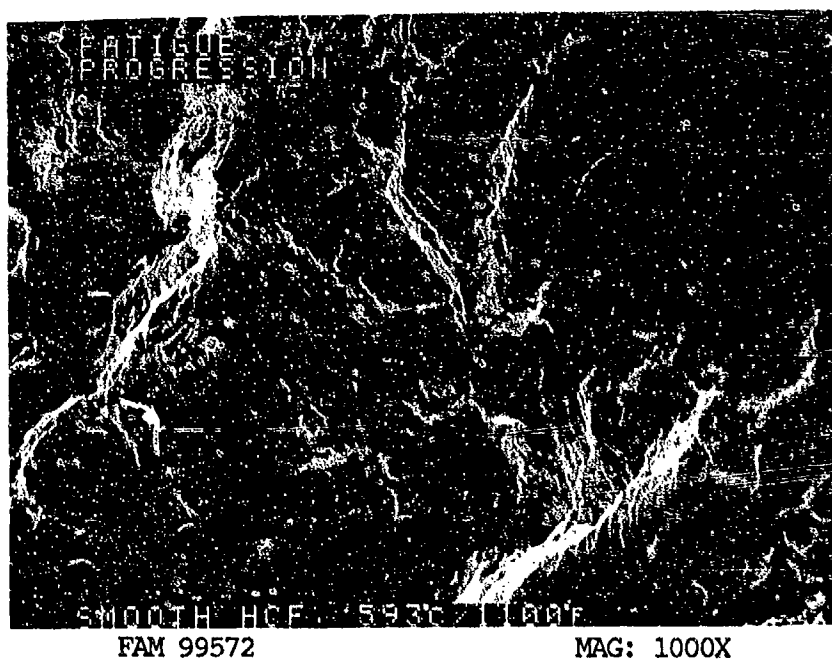


FIGURE 11-51: Remnant fatigue striations in the fatigue progression area. The direction of propagation is shown by an arrow.

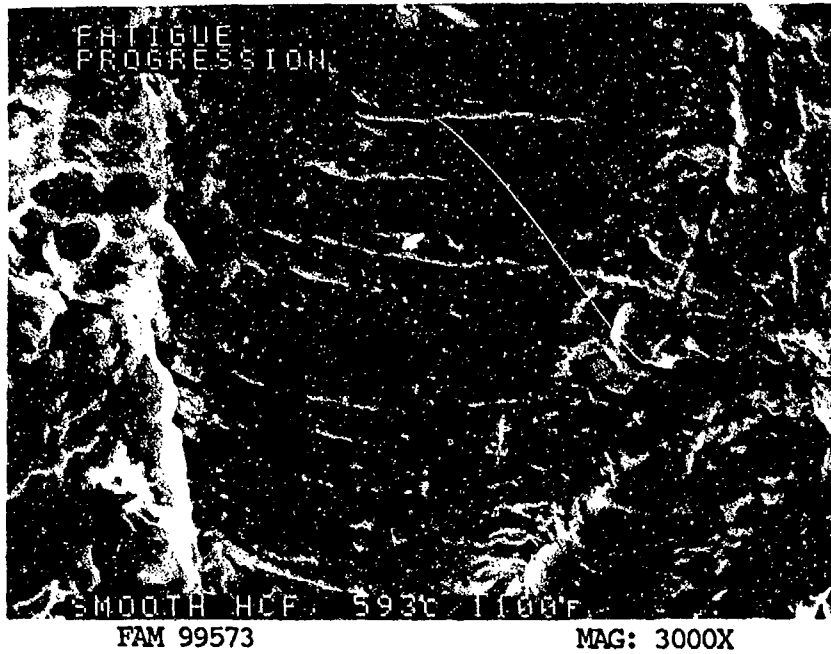


FIGURE 11-52: Higher magnification view of the area shown in Figure 11-51. Remnant fatigue striations are visible. The direction of propagation is shown by an arrow.

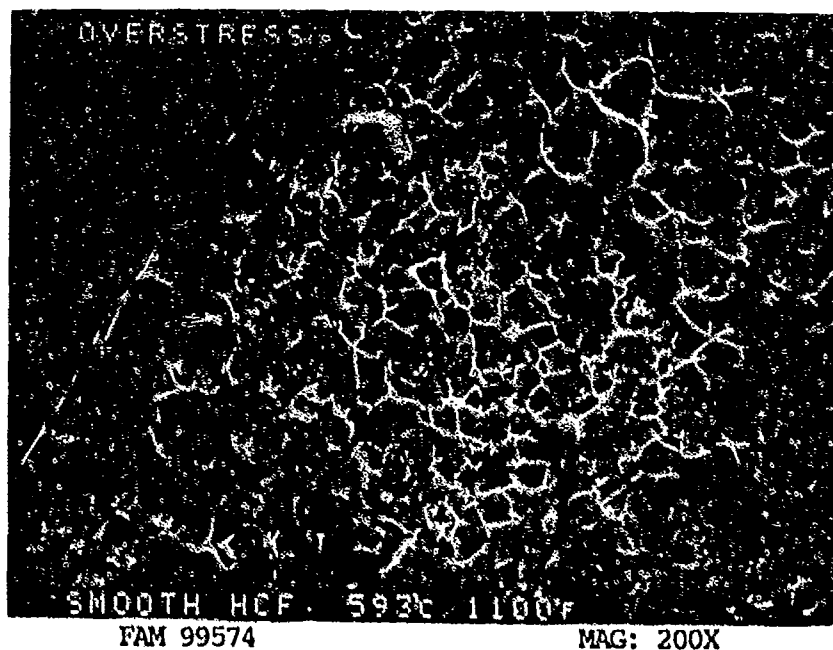


FIGURE 11-53: Final overstress area near the edge of the specimen. No shear lip is visible.

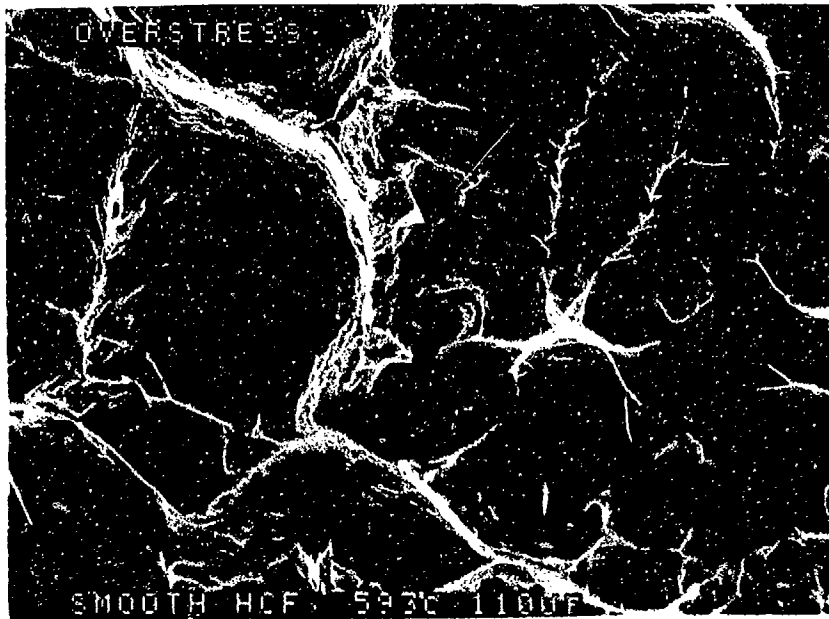


FIGURE 11-54: Coarse dimpled overstress with poorly defined dimples in the final overstress area.

MATERIAL

MP-159
AMS 5843

TEST DATA

TEST TYPE

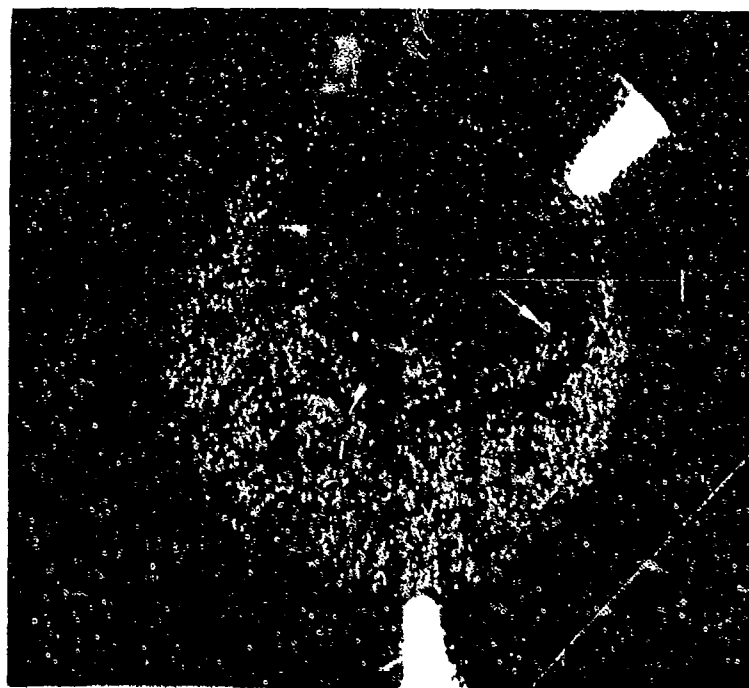
Notched LCF

TEST CONDITIONS

Stress: 1551.3 MPa (225.0 ksi)/77.6 MPa (11.3 ksi)
Stress Ratio: 0.05
Frequency: 1800 cpm
Atmosphere: Air
Temperature: Room Temperature
Test Direction: Longitudinal

TEST RESULTS

Cycles to Fracture: 9700



FAL 94379

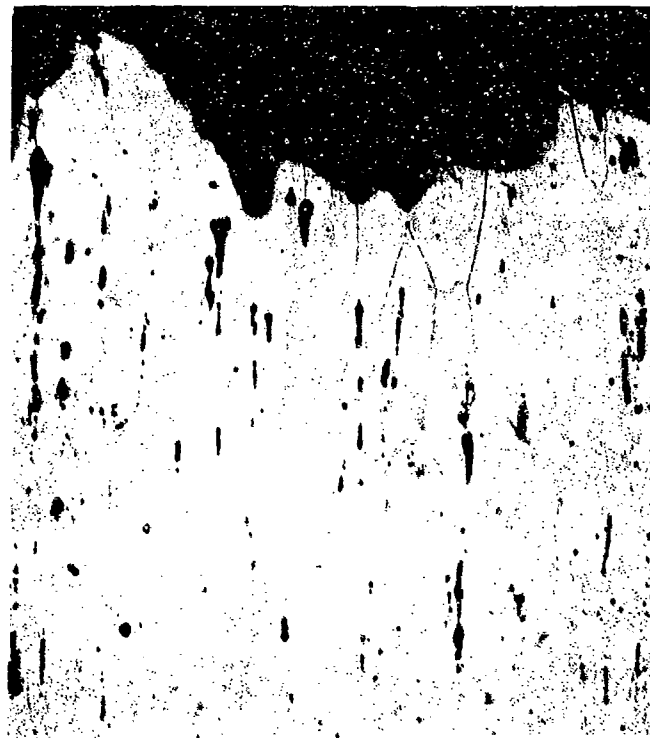
MAG: 14X

FIGURE 11-55: Test results and fractography of MP-159 room temperature notched LCF test. The fatigue propagated from along the surface in a crescent extending 75% of the way around the specimen. The final overstress area is a circular shaped region exhibiting coarser features. The extent of the fatigue is shown by arrows.



FAM 100286

MAG: 200X



FAM 100287

MAG: 200X

FIGURE 11-56: Optical photomicrographs showing the fatigue progression area (top) and the final overstress area (bottom). The fatigue progressed with little grain deformation in the grains adjacent to the fracture. Final overstress area exhibits grain deformation and dimpled overstress features. The fatigue progression is predominantly transgranular.

Etchant: HCl and H₂O₂ electrolytic

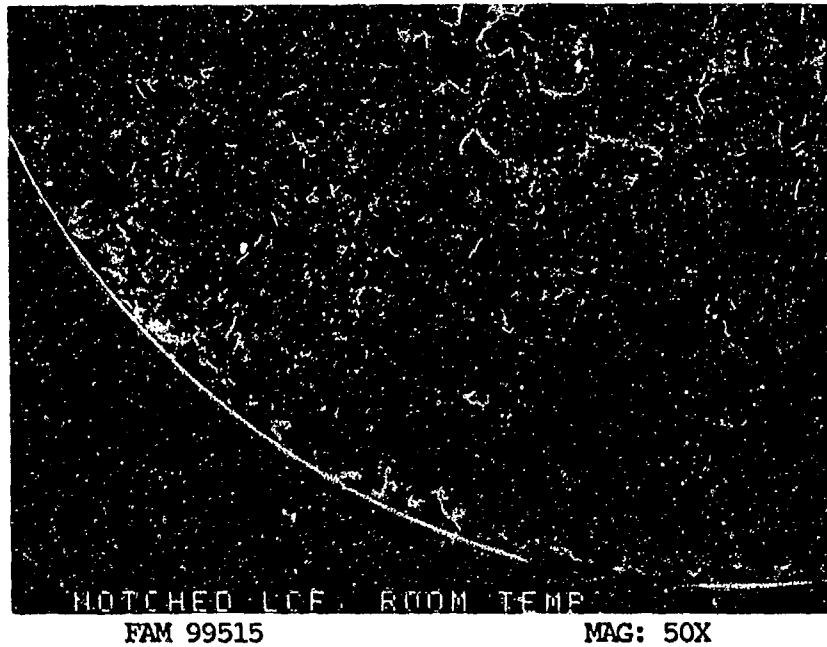


FIGURE 11-57: Low magnification photograph showing fatigue initiation and progression on a plane perpendicular to the stress axis. The fatigue progression appears smoother than the final overstress area.

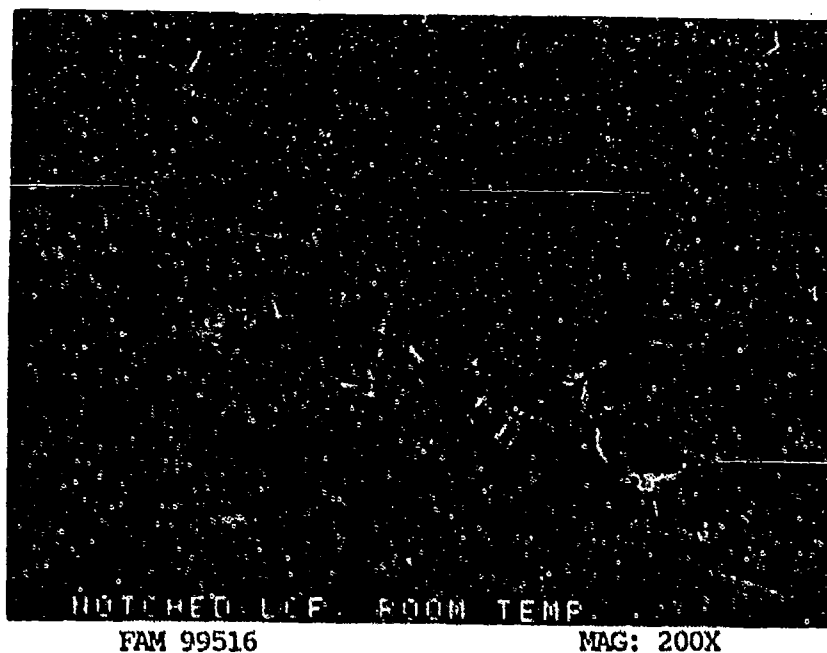


FIGURE 11-58: Higher magnification view of the surface of the specimen. No localized origin area is visible.

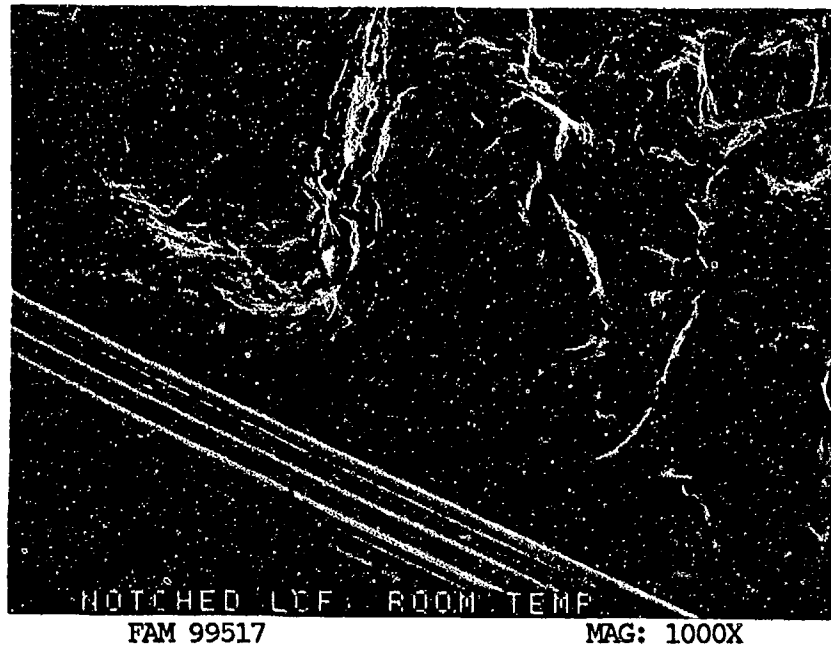


FIGURE 11-59: Fatigue origin area at the surface of the specimen at the base of the notch. Machining lines are visible adjacent to the fracture. Remnant fatigue features are visible just inboard of the notch surface (arrow). No localized origin can be identified.

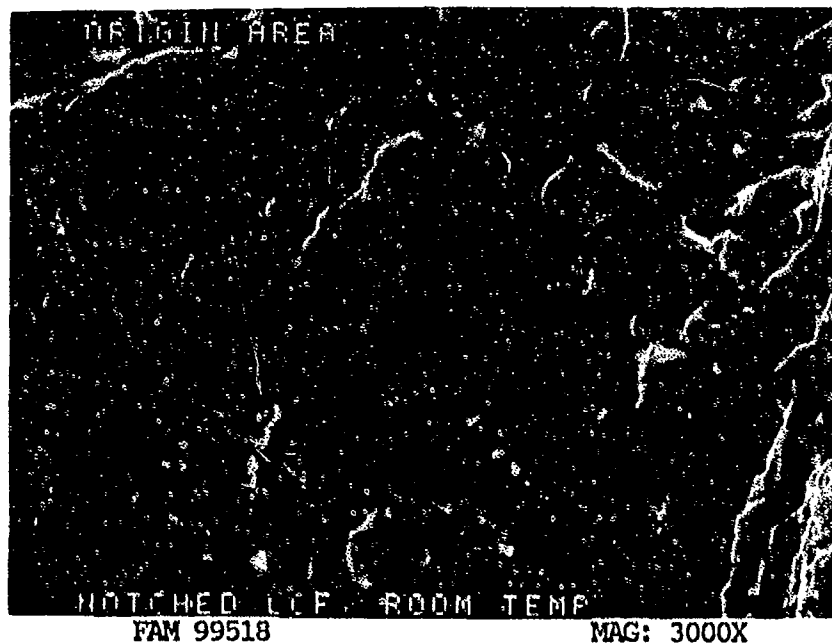


FIGURE 11-60: Higher magnification view of the remnant striations shown in Figure 11-59. The direction of propagation is shown by an arrow.

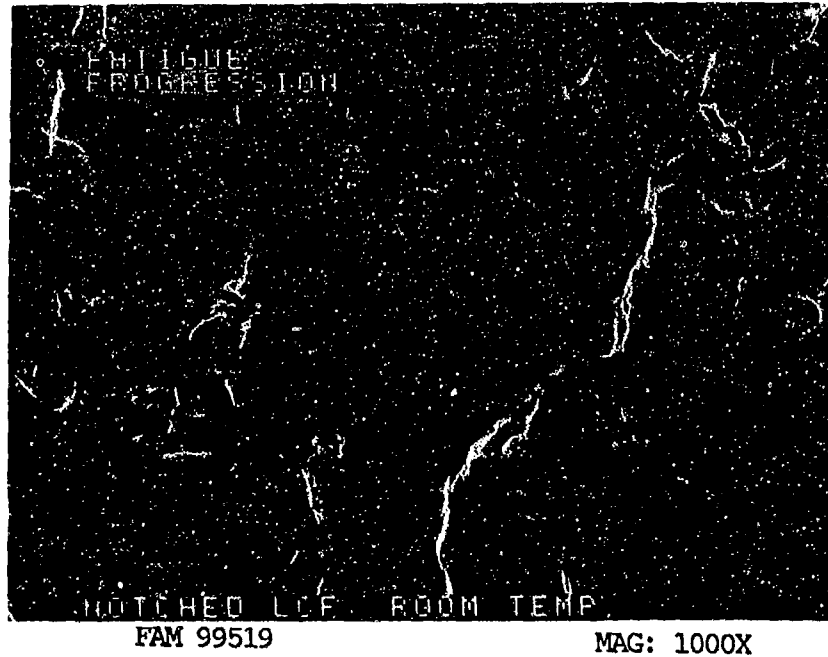


FIGURE 11-61: Fatigue propagation area exhibiting remnant striations and crack-like striations. The direction of propagation is from bottom to top of the photograph.

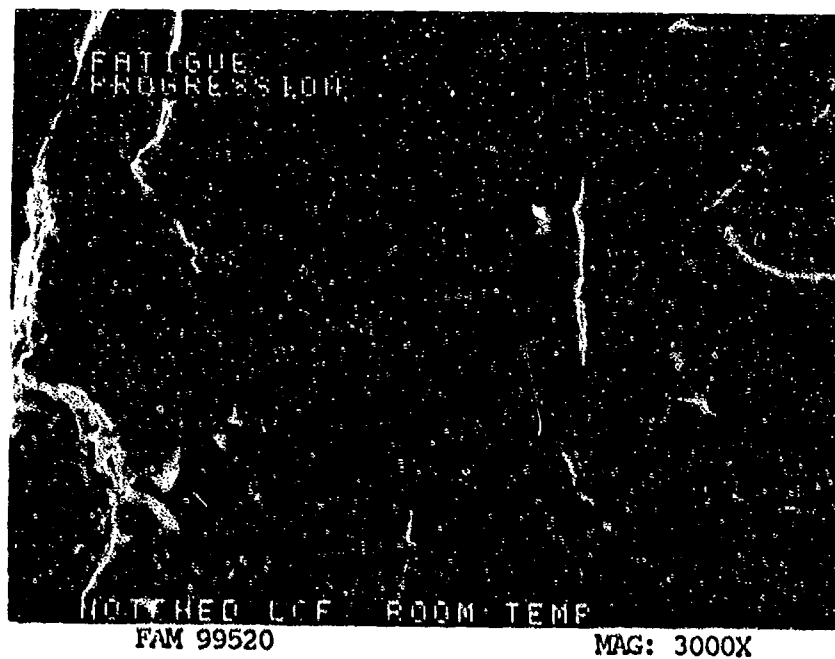
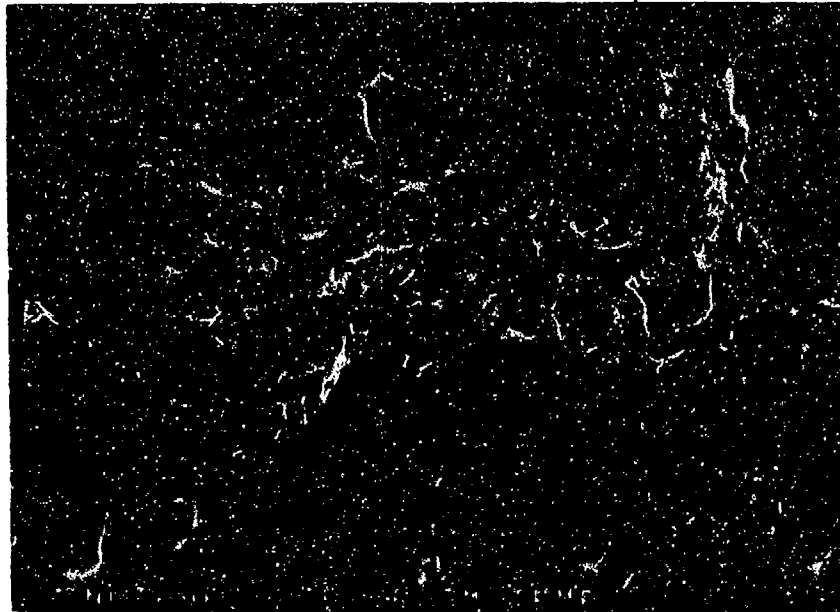


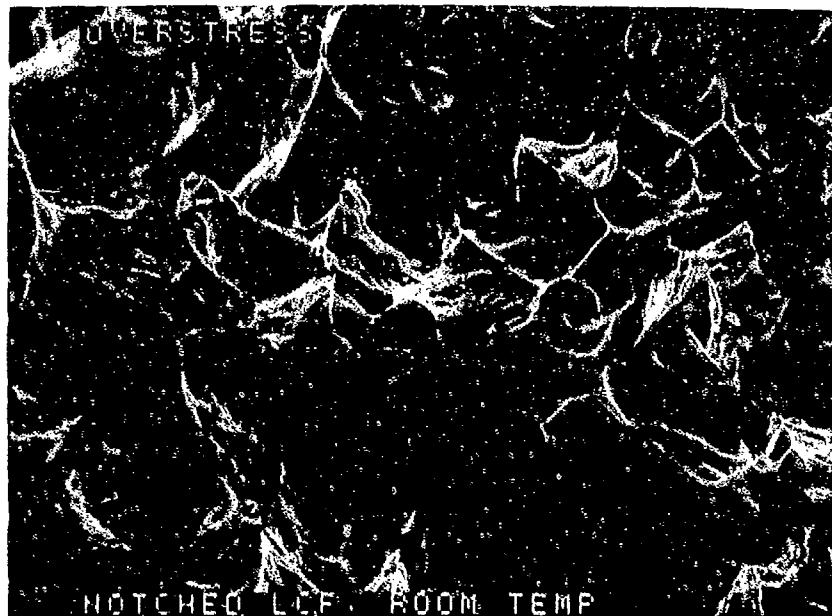
FIGURE 11-62: Higher magnification view of the area shown in Figure 11-61.



FAM 99521

MAG: 200X

FIGURE 11-63: Dimpled overstress in the final fracture area.



FAM 99522

MAG: 3000X

FIGURE 11-64: Higher magnification view of the area shown in Figure 11-63.

MATERIAL

MP-159
AMS 5843

TEST DATA

TEST TYPE
Notched LCF

TEST CONDITIONS

Stress: 896.3 MPa (130 ksi)/89.6 MPa (13 ksi)
Stress Ratio: 0.10
Frequency: 30 cpm
Atmosphere: Air
Temperature: 593°C (1100°F)
Test Direction: Longitudinal

TEST RESULTS

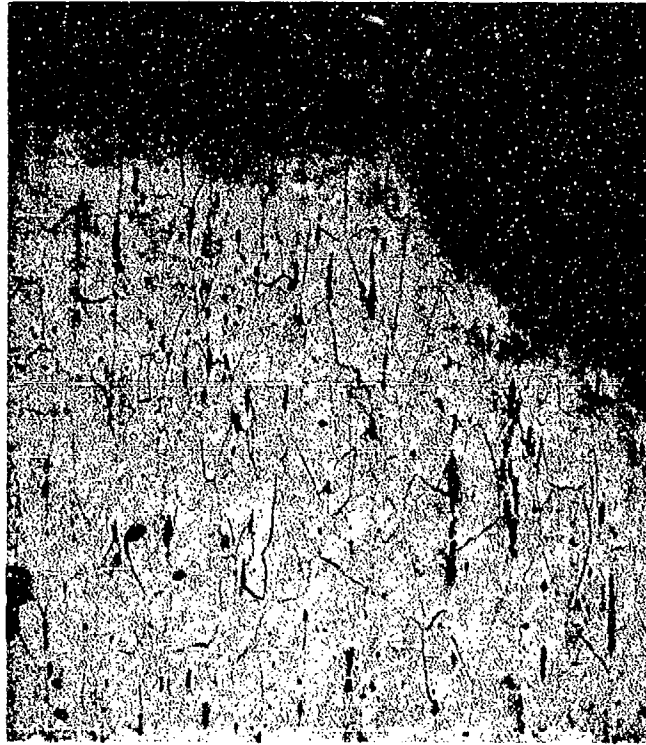
Cycles to Fracture: 3100



FAL 94380

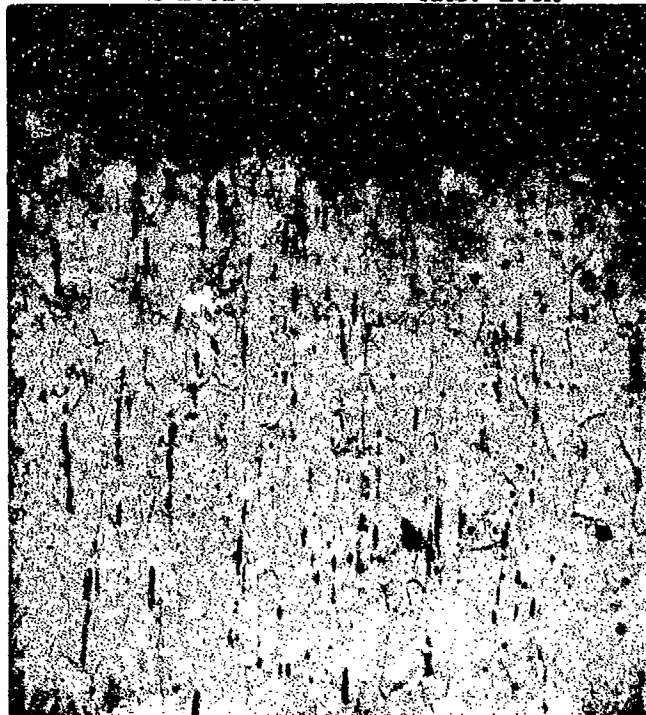
MAG: 14X

FIGURE 11-65: Test results and fractography of MP-159 593°C (1100°F) notched LCF test. The fatigue propagated from along the base of the notch 360° around the specimen. Arrowheads indicated the extent of the fatigue. The final overstress occurred roughly near the center of the specimen, exhibiting coarser features.



FAM 100289

MAG: 100X



FAM 100290

MAG: 100X

FIGURE 11-66: Optical photomicrographs showing the fatigue progression area (top) and the final overstress area (bottom). The fatigue progressed with little grain deformation in the grains adjacent to the fracture. The final overstress area exhibits grain deformation and dimpled overstress features. The appearance of the fracture path is transgranular, very similar to the room temperature specimen (Figure 11-56).

Etchant: HCl and H₂O₂ electrolytic

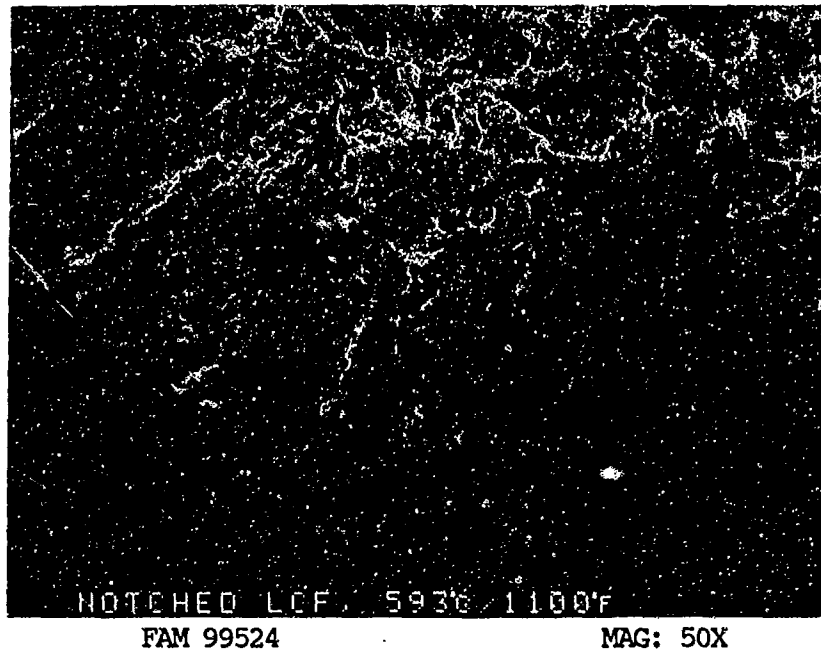


FIGURE 11-67: Low magnification photograph showing fatigue initiation and progression that appears to be relatively flat. The features become progressively coarser at locations away from the surface of the specimen.

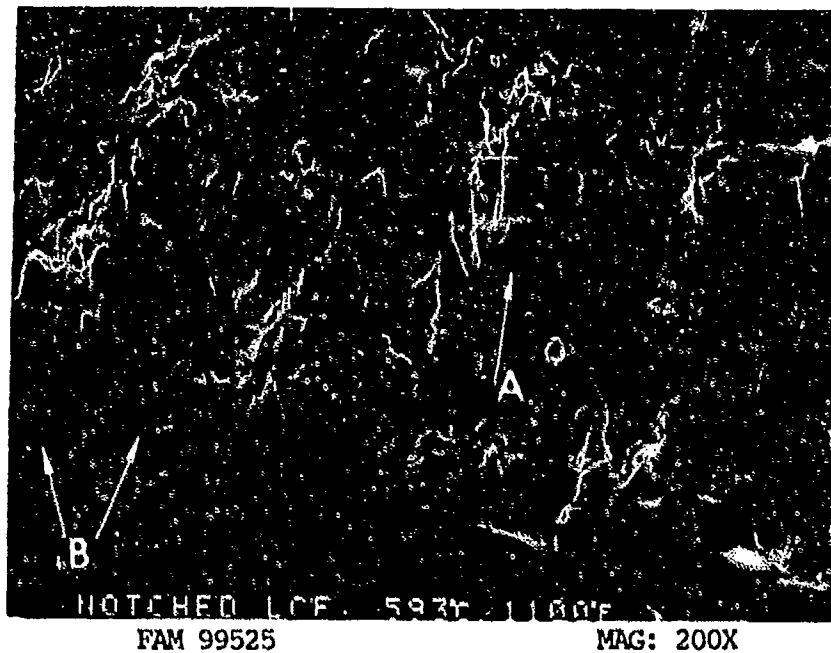


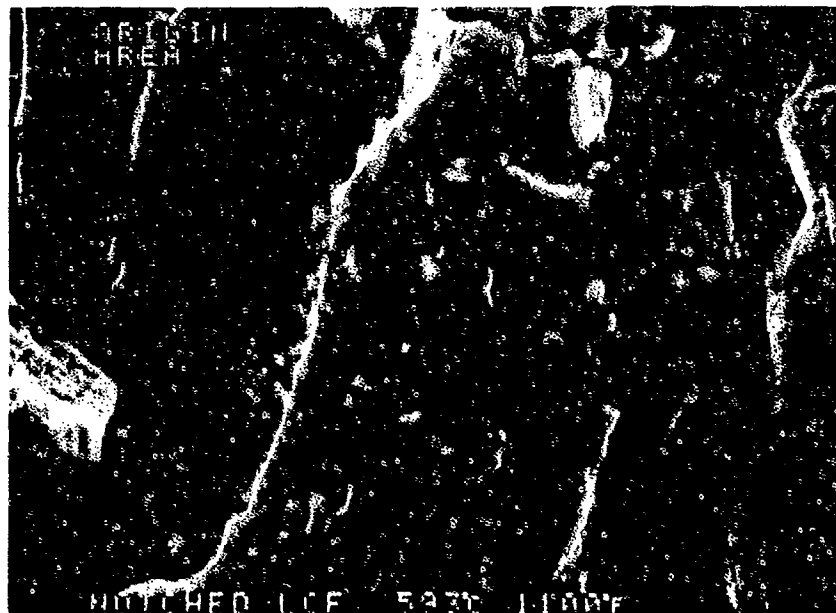
FIGURE 11-68: Higher magnification view of the origin area at the base of the notch. Fatigue striations are visible even at this low magnification (arrow A). Machining lines are visible adjacent to the fracture (arrows B).



FAM 99526

MAG: 1000X

FIGURE 11-69: High magnification photograph showing fatigue striations near the origin. The direction of propagation is from bottom to top of the photograph.



FAM 99527

MAG: 3000X

FIGURE 11-70: Higher magnification photograph of the area shown in Figure 11-69. Oxidized striations can be seen propagating on several plateaus separated by steps.

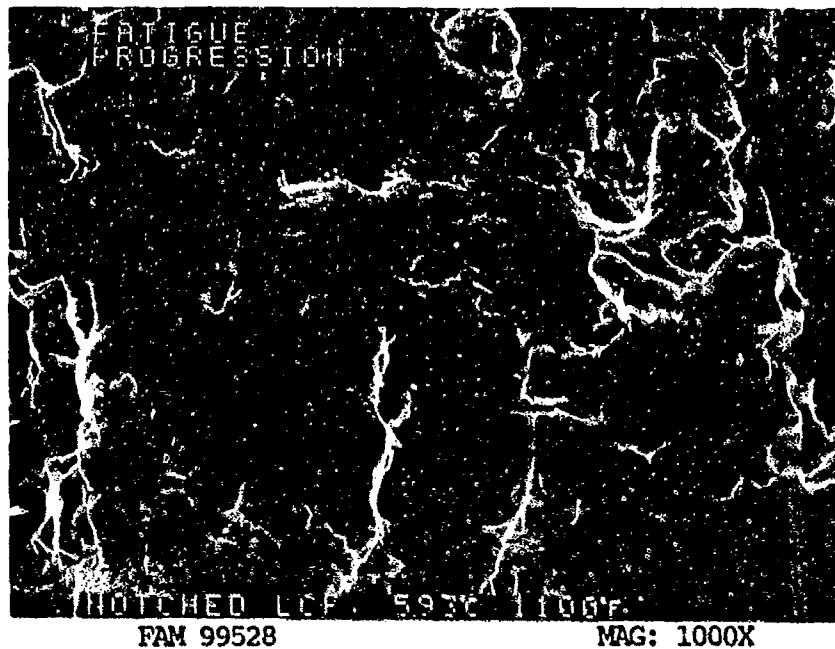


FIGURE 11-71: Well defined striations in the fatigue propagation area. The direction of propagation is from bottom to top of the photograph.

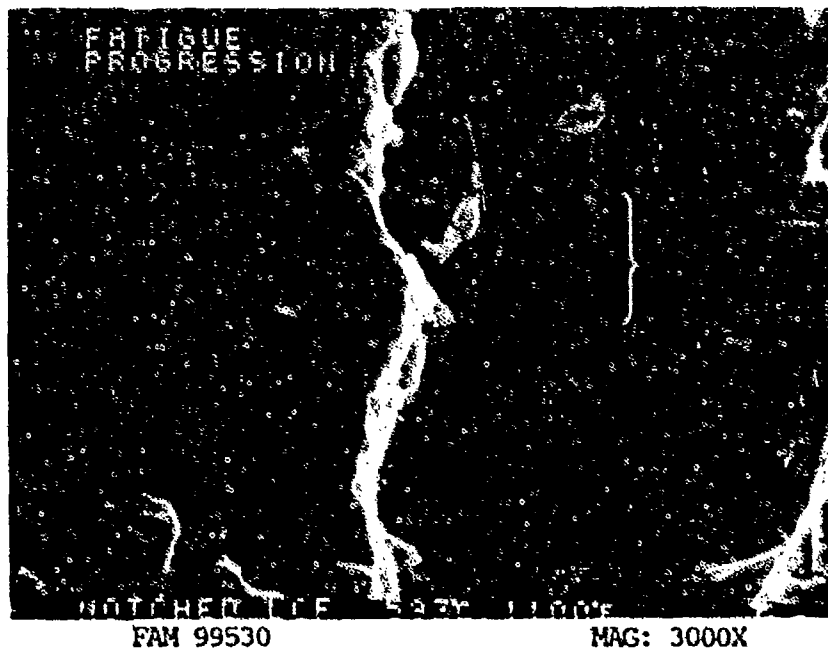
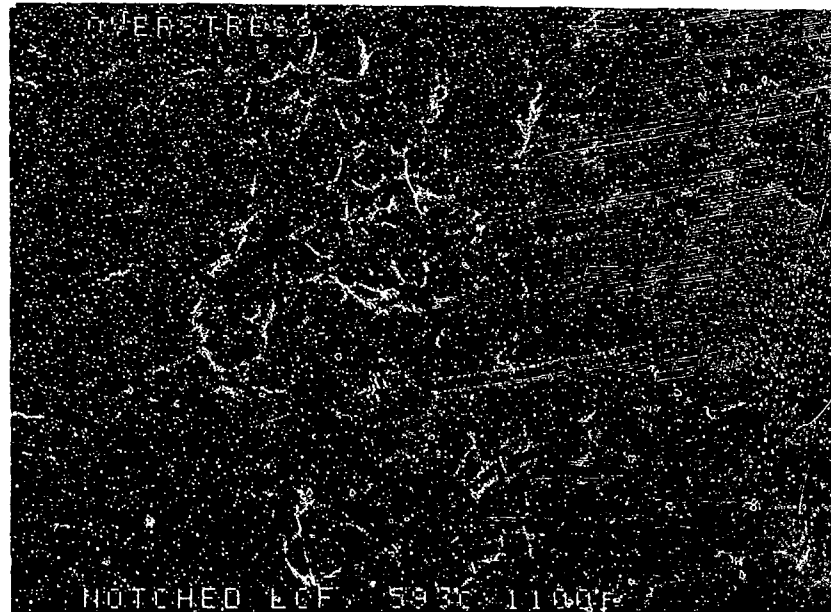


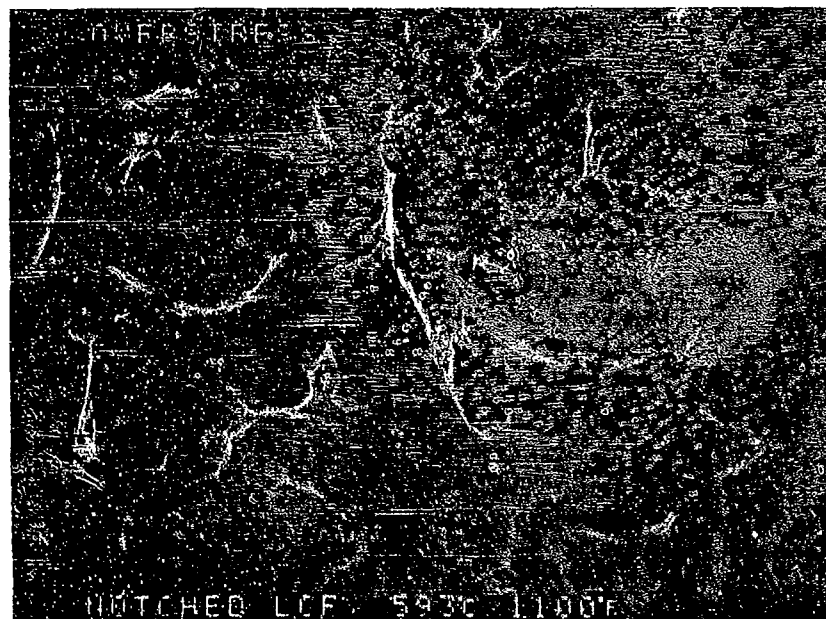
FIGURE 11-72: Higher magnification view of the area shown in Figure 11-71. Well developed striations can be seen propagating on adjacent plateaus separated by a step. Bracket contains ten striations.



FAM 99531

MAG: 200X

FIGURE 11-73: Conical equiaxed dimples and voids in the final overstress area.



FAM 99532

MAG: 1000X

FIGURE 11-74: Higher magnification photograph of the final overstress area revealing shallow dimples (arrows A) and deep conical voids (arrows B).

MATERIAL

MP-159
AMS 5843

TEST DATA

TEST TYPE
Smooth LCF

TEST CONDITIONS

Stress: 1551.3 MPa (225 ksi)/77.5 MPa (11.3 ksi)
Stress Ratio: 0.05
Frequency: 353 cpm
Atmosphere: Air
Temperature: Room Temperature
Test Direction: Longitudinal

TEST RESULTS

Cycles to Fracture: 20



FAL 94377

MAG: 15X

FIGURE 11-75: Test results and fractography of MP-159 room temperature smooth LCF test. No evidence of fatigue is visible. A central area of primary overstress and a large shear lip dominate the fracture.



FAM 100291

MAG: 100X

FIGURE 11-76: Optical photomicrograph showing dimpled overstress features in the final overstress area.

Etchant: HCl and H₂O₂ electrolytic

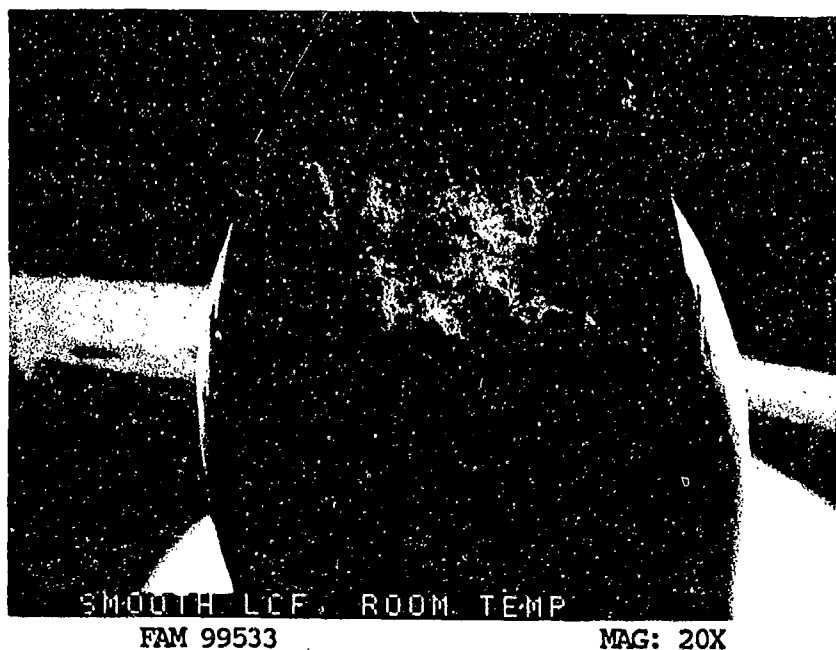


FIGURE 11-77: Low magnification photograph showing a central primary overstress area and a large final overstress area (shear lip). No evidence of fatigue is visible.

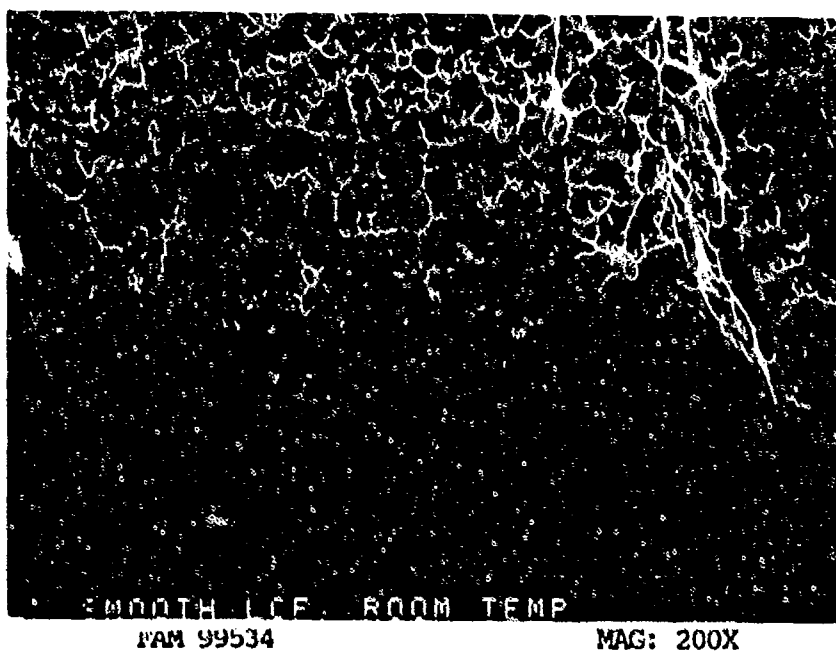


FIGURE 11-78: Shear dimples in the final overstress area.

MATERIAL

MP-159
AMS 5843

TEST DATA

TEST TYPE

TMF, In-Phase

TEST CONDITIONS

Stress: 1169 MPa (162 ksi)/-1507.8 MPa (-218.7 ksi)

Stress Ratio: -1.35

Frequency: 2 cpm

Atmosphere: Air

Temperature: 260°C (500°F)/593°C (1100°F)

Test Direction: Longitudinal

TEST RESULTS

Cycles to Fracture: 3390



FAL 94629

MAG: 8X

FIGURE 11-79: Test results and fractography of MP-159 in-phase TMF test. Seven thumbnails are visible propagating from origins (arrows) along the outside surface of the specimen. The thumbnails appear to be heavily oxidized.



FAM 100279

MAG: 200X

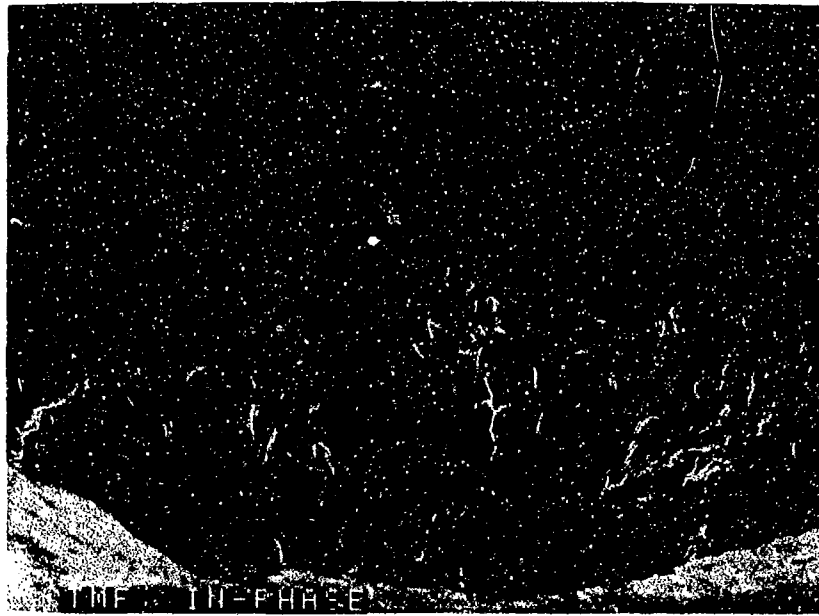


FAM 100280

MAG: 200X

FIGURE 11-80: Optical photomicrographs showing a primary thermal-mechanical fatigue progression area (top) and a secondary crack in the gage section (bottom). Strain lines are visible in both photographs (arrows). The primary progression surface exhibits oxidation (white arrows, top).

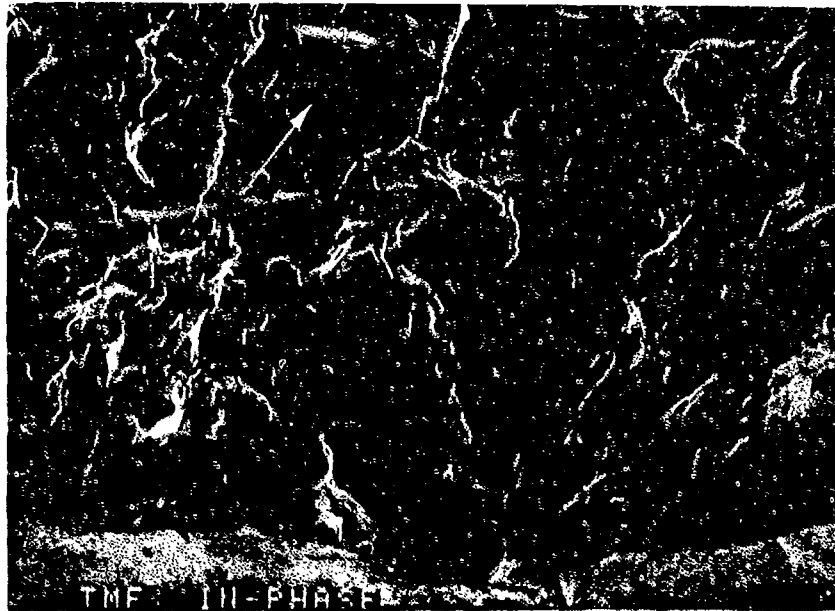
Etchant: HCl and H₂O₂ electrolytic



FAM 99701

MAG: 50X

FIGURE 11-81: Low magnification photograph of one fatigue thumbnail. The fatigue progression area exhibits a more granular appearance than the surrounding overstress area.



FAM 99702

MAG: 200X

FIGURE 11-82: Stage I fatigue facet at one of several origins in the thumbnail (arrow A). Features indicative of fatigue are visible (arrow B).

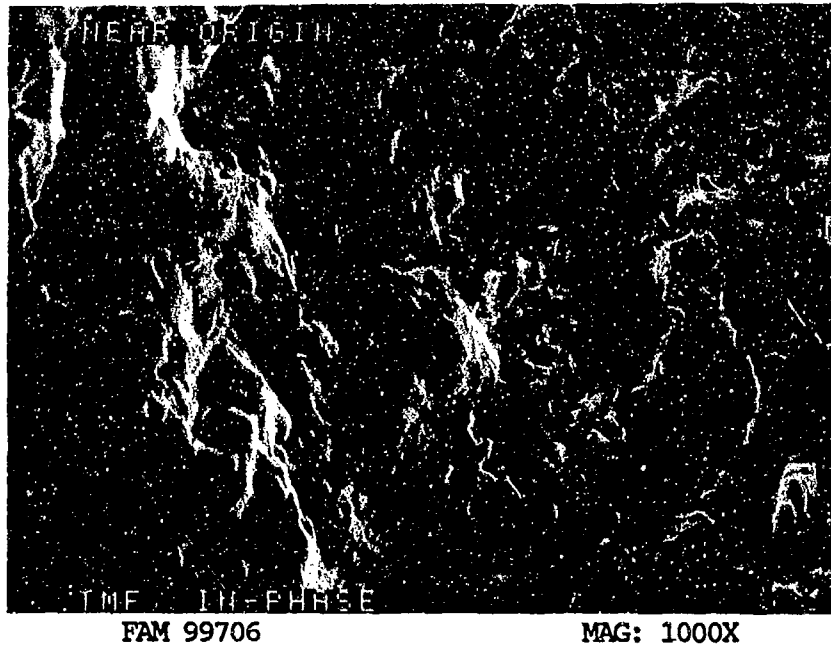


FIGURE 11-83: Higher magnification photograph of an area near the origin. Fatigue striations are visible indicating divergent directions of propagation.

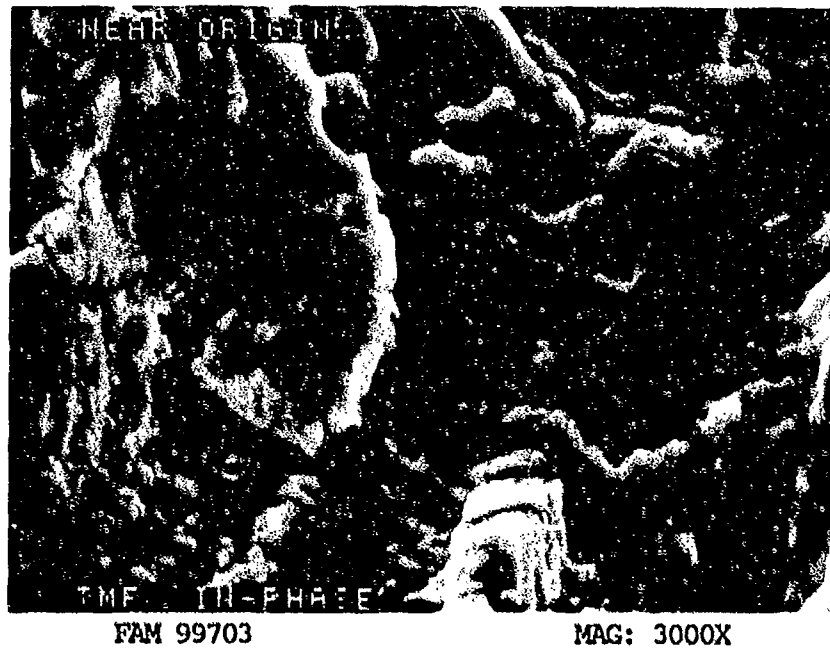


FIGURE 11-84: Higher magnification view of the fatigue striations shown in Figure 11-83. The direction of propagation is shown by an arrow.

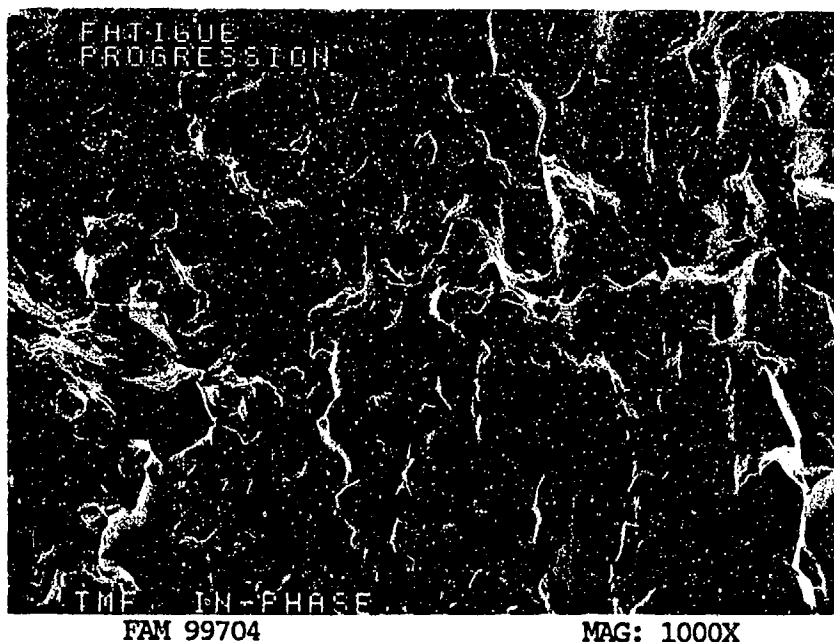


FIGURE 11-85: Fatigue propagation area exhibiting striations and crack-like striations. The direction of propagation is from bottom to top of the photograph.

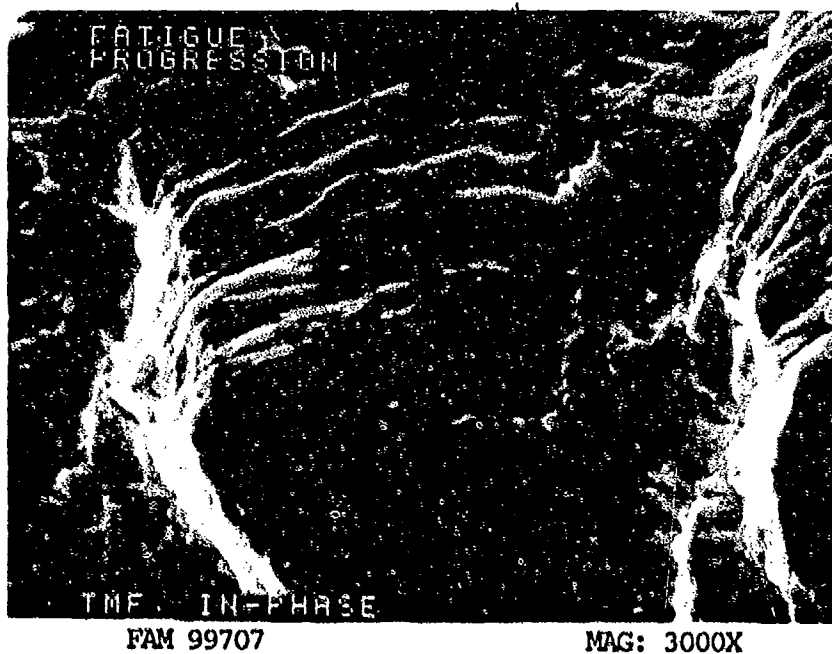
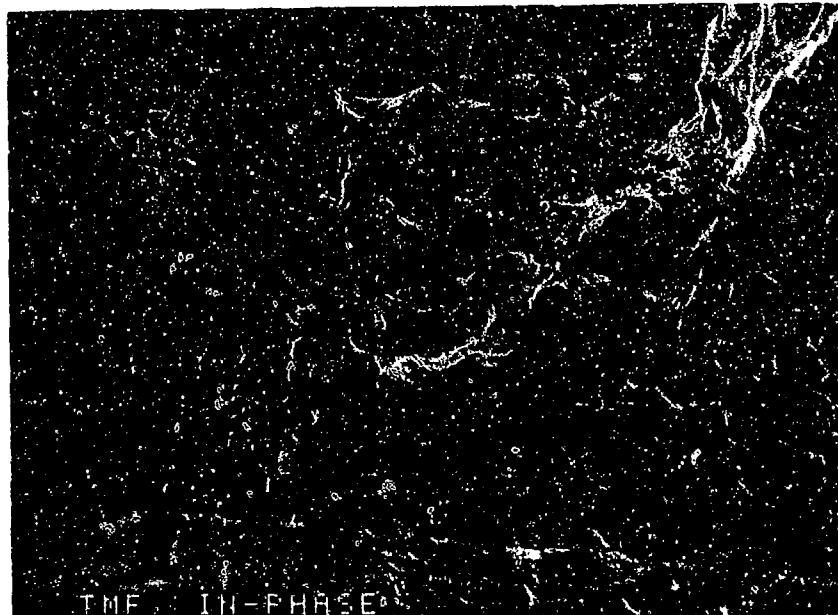


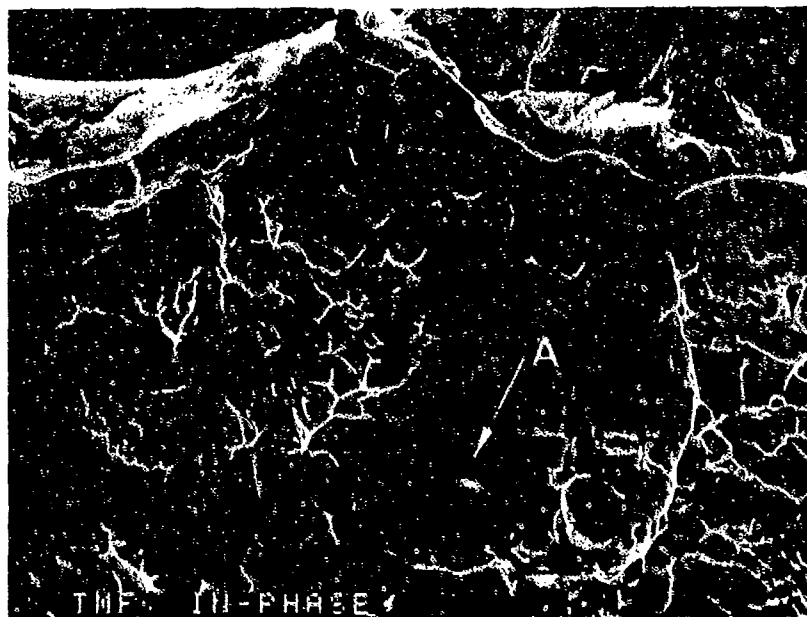
FIGURE 11-86: Higher magnification view of the area shown in Figure 11-85 exhibiting striations and crack-like striations.



FAM 99708

MAG: 200X

FIGURE 11-87: Mixture of shear and equiaxed dimpled overstress in the final fracture area.



FAM 99709

MAG: 1000X

FIGURE 11-88: Higher magnification view of the final overstress area exhibiting a mixture of shear (arrow A) and equiaxed (arrow B) dimples.

MATERIAL

MP-159
AMS 5843

TEST DATA

TEST TYPE

TMF, Out-of Phase

TEST CONDITIONS

Stress: 1344.5 MPa (195 ksi)/-1167 MPa (169.7 ksi)
Stress Ratio: -0.87
Frequency: 2 cpm
Atmosphere: Air
Temperature: 260^oF (500^oF)/593^oC (1100^oF)
Test Direction: Longitudinal

TEST RESULTS

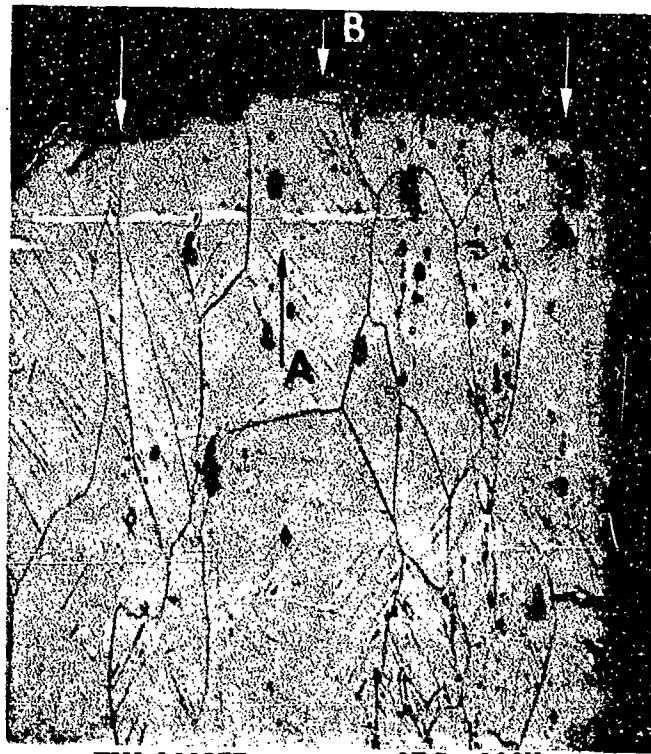
Cycles to Fracture: 2779



FAL 94628

MAG: 8X

FIGURE 11-89: Test results and fractography of MP-159 out-of-phase TMF test. An oxidized thumbnail indicates propagation from the outside surface (arrow) of the specimen.



FAM 100277

MAG: 200X

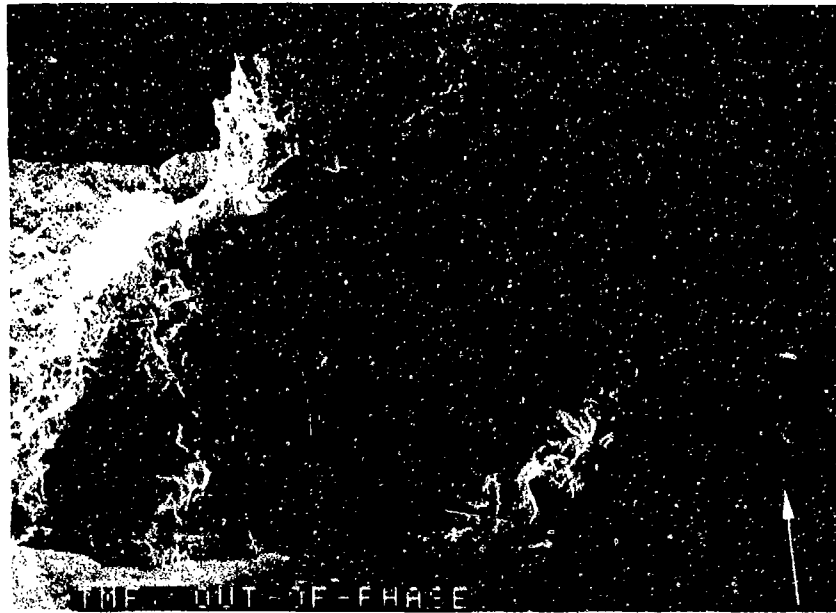


FAM 100278

MAG: 100X

FIGURE 11-90: Optical photomicrographs showing the primary thermal-mechanical fatigue progression area and a secondary crack in the gage section (top) and the final overstress area oriented at an angle to the stress axis (bottom). Strain lines are visible in both photographs (arrows A). The primary progression surface exhibits oxidation (arrows B).

Etchant: HCl and H₂O₂ electrolytic



FAM 99710

MAG: 50X

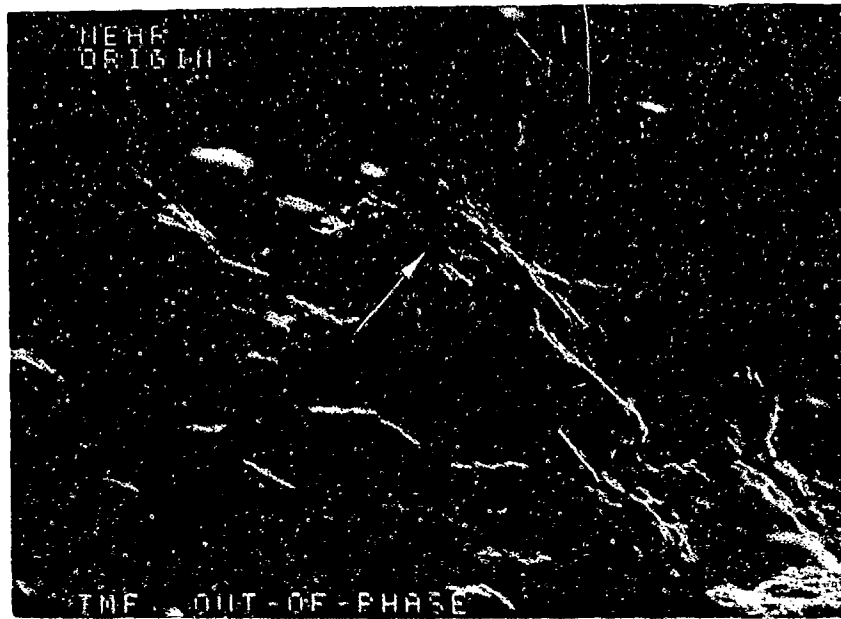
FIGURE 11-91: Low magnification photograph showing fatigue initiation and progression (thumbnail). A secondary crack is visible on the specimen surface (arrow).



FAM 99711

MAG: 200X

FIGURE 11-92: Higher magnification view of the origin area. No fatigue striations are visible at this magnification (compare to Figure 11-82).



FAM 99712

MAG: 1000X

FIGURE 11-93: Remnant fatigue striations and crack-like striations near the origin. The direction of propagation is shown by an arrow.



FAM 99713

MAG: 3000X

FIGURE 11-94: Higher magnification photograph of the area shown in Figure 11-93. Remnant crack-like striations are visible. The direction of propagation is shown by an arrow.

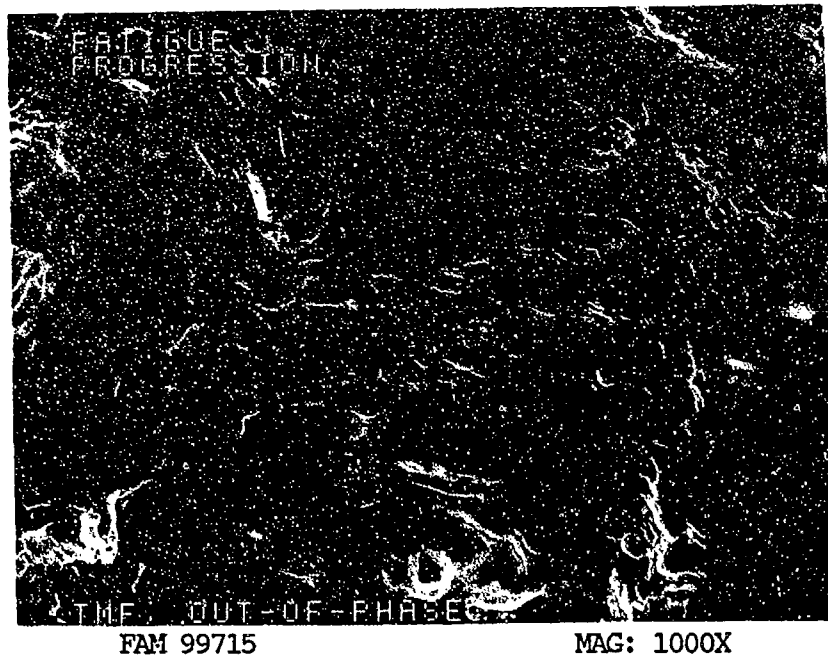


FIGURE 11-95: Fatigue progression near the end of the thumbnail exhibiting clearly defined fatigue striations (compare to Figure 11-93).

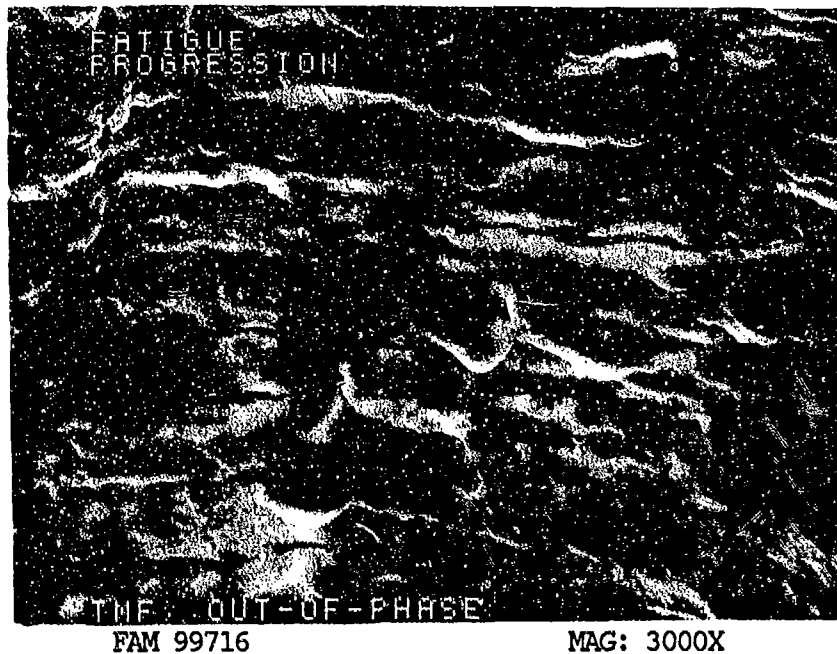
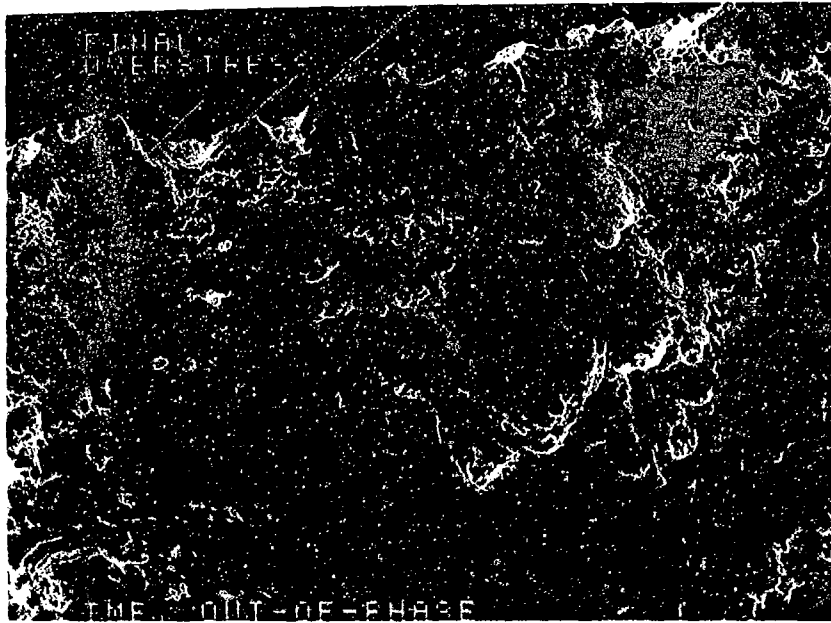


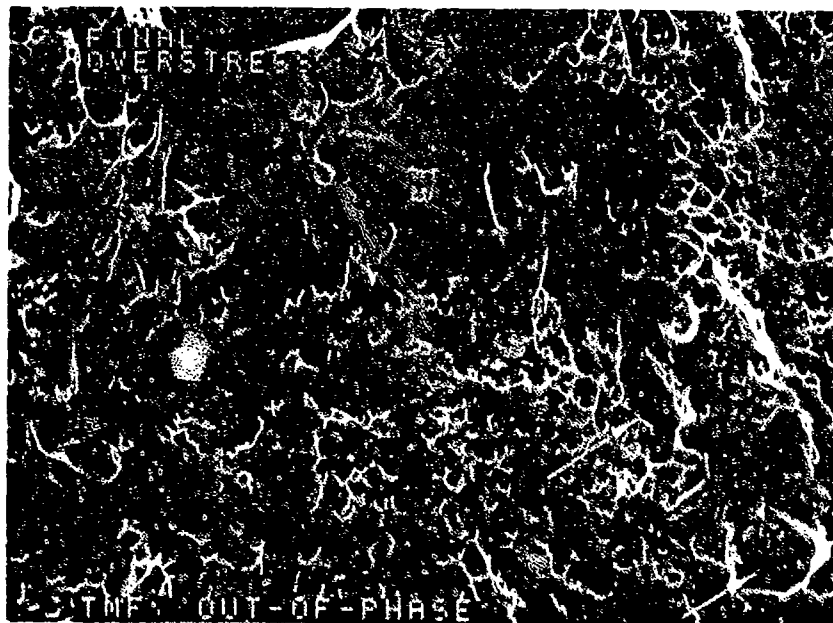
FIGURE 11-96: Higher magnification view of a portion of the area shown in Figure 11-95, showing crack-like striations.



FAM 99717

MAG: 200X

FIGURE 11-97: Final overstress area exhibiting shear dimpled overstress.



FAM 99718

MAG: 1000X

FIGURE 11-98: Higher magnification photograph of the final overstress area (Figure 11-97) exhibiting shallow dimples and deep voids (arrows).

SERVICE FAILURE

FRACTURE MODE Fatigue (Probable HCF)

PART NAME First Stage Turbine Stator Vane Feather Seal

OPERATION DATA Feather seals were subjected to cyclic loading.

PART TIME 71.7 hours

	<u>REQUIRED</u>	<u>ACTUAL</u>
MAT'L		
BASE	<u>Haynes 188 (Co-base alloy)</u>	<u>confirmed</u>
OTHER	<u>-</u>	<u>-</u>
HARDNESS	<u>No Requirement</u>	<u>HRC 22-26 *</u>
GRAIN SIZE	<u>ASTM average 4 or finer</u>	<u>ASTM 7-8</u>
DIMENSIONAL	<u>Thickness: 0.009-0.011 inch</u>	<u>0.010-0.012 inch</u>

* Diamond pyramid hardness (DPH) conversions.

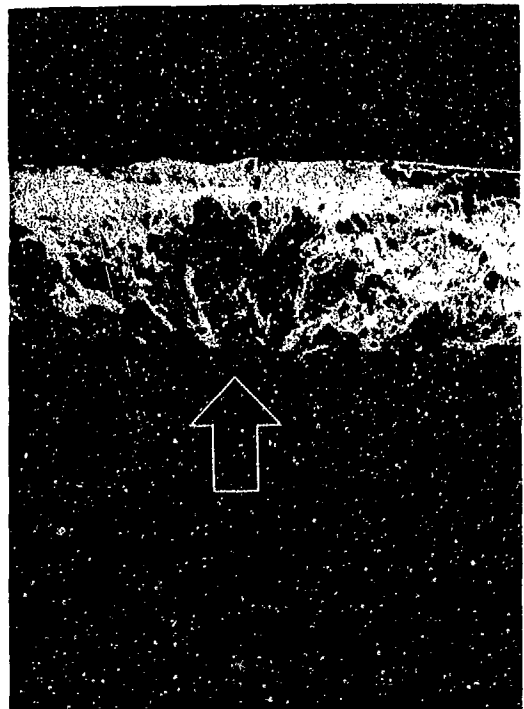
SUMMARY: Several feather seals in the set were found to be cracked when the engine was disassembled following a low turbine incident. The fracture exhibited relatively fine fatigue striations (probable HCF) propagating from multiple origins. No material or microstructural defects were found.



FAL 93418

MAG: 10X

FIGURE 11-99: Overall photograph of the fractured feather seal.



FAL 93352

MAG: 100X

FIGURE 11-100: One of several possible origin areas (arrow).



FAL 93417

MAG: 1000X

FIGURE 11-101: Remnant striations indicative of fatigue.



FAL 93416

MAG: 3000X

FIGURE 11-102: Fine remnant fatigue striations (brackets).

Ti-6Al-2Sn-4Zr-2Mo

Material Description

Ti-6Al-2Sn-4Zr-2Mo is an alpha-beta processed titanium-base alloy used primarily for parts operating at temperatures up to 1000 F, such as engine compressor parts and airframe components, where good LCF characteristics are required. The alloy generally receives two or three heat treatment cycles. The first cycle is the solution anneal and consists of 2 hours or less at 50 F below the beta transus. The second cycle is a stabilization anneal and is followed by precipitation, typically at 1100 F, with the time period varying depending on the form.

The material used in this study was heat treated to FWA 1224 (bar) with a typical hardness of HRC 33-40. The typical room and elevated temperature mechanical properties for FWA 1224 are as follows:

	<u>Room Temperature</u>	<u>900° F</u>
Ultimate Tensile Strength (min):	140 ksi	95 ksi
0.2% Yield Strength (min):	125 ksi	72 ksi
Percent Elongation (min):	10%	13%
Percent Reduction in Area (min):	17%	26%
Measured Hardness:	HRC 34-36 (DPH conversions)	

Fractography Overview

Four Ti-6-2-4-2 specimens were examined. The room temperature smooth tensile specimen had a well defined shear lip 0.035 inch wide and a sugary appearance in the primary overstress area in the center of the specimen. The 1000 F smooth specimen had a very large shear lip (0.045 inch) with respect to the final cross section, which was smaller than the room temperature specimen. The primary overstress area had deeper features than the room temperature specimen. High magnification examination of the primary fracture areas revealed equiaxed and randomly shaped dimples with some quasi-cleavage type features. The 1000 F specimen had shallow equiaxed dimples covered by a light oxide. Both specimens had shear dimples in the final overstress area, but the dimple appearance was more ductile for the 1000 F specimen. The notched tensile specimens followed the same trends as the smooth specimens. Neither notched specimen had a shear lip but the dimples in the centers of the specimens exhibited a brittle character for the room temperature specimen and had a more ductile appearance at 1000 F.

The stress rupture specimen was run at 950° F and fractured in 451.1 hours. It had a shear lip (0.025 inch) in the final rupture area but it was not as large or well defined as the smooth tensile specimens. The dimples in the center of the specimen were deeper than the tensile specimens and were covered by a light oxide. The final rupture area exhibited ductile shear dimples.

Three smooth and three notched HCF specimens were examined, one each at room temperature, 500 F and 1000 F. Macroscopically, the smooth HCF specimens appeared very similar. The fatigue propagated from a single general origin area exhibiting a smooth appearance until the crack covered approximately 50-60% of the cross section, at which point final overstress occurred. High magnification examination revealed a single stage I facet at the origin of the room temperature specimen, with feathery features near the origin. The origin areas on the two elevated temperature specimens became more diffuse with increasing temperature. The elevated temperature specimens had more smear in the origin area so no features could be identified. All three specimens exhibited only remnant striations near the origins. The Stage II fatigue areas near the centers of the specimens exhibited crack-like striations with more well defined striations as test temperature increased. The final overstress areas exhibited a mixture of dimpled overstress and quasi-cleavage for the room temperature and 500 F specimens, and dimpled overstress for the 1000 F specimen. All these notched specimens propagated from multiple surface origins separated by steps. The room temperature specimen exhibited fatigue through 90% of its cross section, finally fracturing in shear overstress with no tensile overstress region. Both elevated temperature specimens exhibited fatigue over 80% of their cross sections, with a small tensile overstress region and finally a shear lip. Higher magnification examination of the origin area on all three specimens revealed features radiating from local surface origins on the room temperature and 1000 F specimen, and no discernible local origin on the 500 F specimen. Fine fatigue striations were visible near the origin on all three specimens. Well defined striations and crack-like striations were visible near the centers of the specimens.

Two LCF specimens were examined, one at 500 F and one at 1000 F. Both specimens initiated at a single surface origin that did not exhibit a Stage I fatigue facet. Feathery features radiated from the origin with no striations visible adjacent to the origin. Remnant striations and crack-like striations were visible in the fatigue progression area on the 500 F specimen. The 1000 F specimen showed crack-like striations but had some secondary cracking in the progression area.

In-phase and out-of-phase TMF specimens were examined. The in-phase TMF specimen had multiple origins and thumbnail areas on both the I.D. and O.D. surfaces. Multiple diffuse origins were found on each thumbnail. Fatigue striations near the origin area became coarser and less well defined as the fatigue progressed. Final fracture occurred by dimpled overstress. The out-of-phase TMF specimen had a large I.D. origin fatigue thumbnail. The fatigue propagated from several local origins that had feathery cleavage features radiating from them. Patches of striations and crack-like striations were observed in the Stage II area. The striations became coarser and had a high percentage of crack-like striations near the end of the thumbnail. Final fracture occurred by dimpled overstress.

MATERIAL

Ti-6Al-2Sn-4Zr-2Mo
FWA 1224 Bar

TEST DATA

TEST TYPE

Smooth Tensile

TEST CONDITIONS

Strain Rate: 0.005 mm/mm/min (0.005 in/in/min)

Atmosphere: Air

Temperature: Room Temperature

Test Direction: Longitudinal

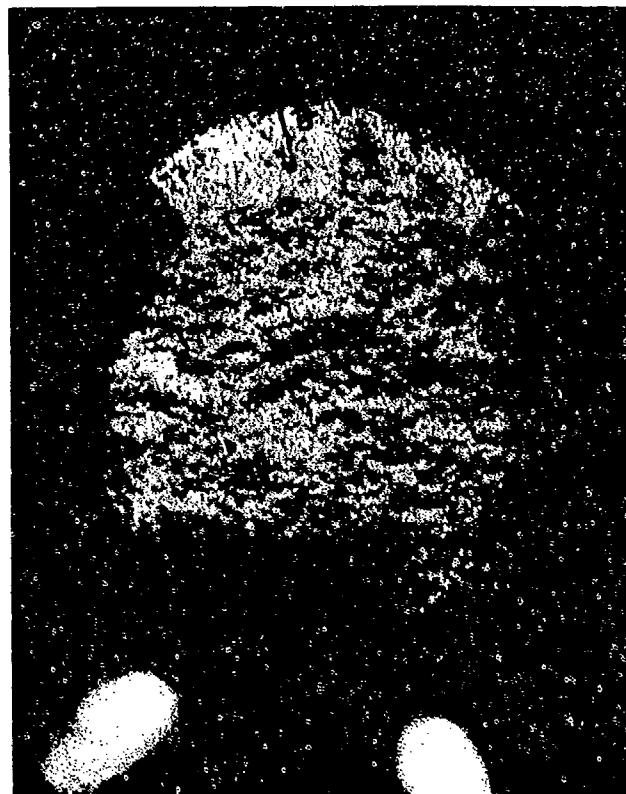
TEST RESULTS

0.2% Yield Strength: 921.1 MPa (133.6 ksi)

Ultimate Strength: 993.5 MPa (144.1 ksi)

Percent Elongation: 17.5

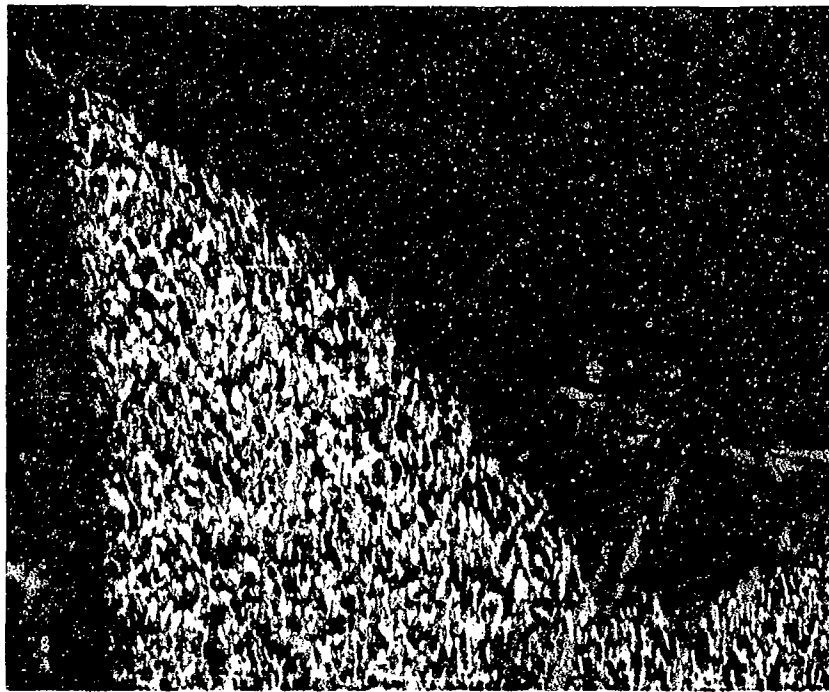
Percent Reduction of Area: 39.3



FAL 92935

MAG: 13X

FIGURE 12-1: Test results and fractography of Ti-6-2-4-2 smooth tensile test. The fracture exhibits a distinct shear lip (bracket). The size of the shear lip varies with location around the specimen.



FAM 98908

MAG: 100X



FAM 99769

MAG: 200X

FIGURE 12-2: Optical photomicrographs showing the final overstress area (shear lip) (top) and the primary fracture area (bottom). Both areas exhibit elongated grains indicating plastic deformation.

Etchant: Kroll's Reagent

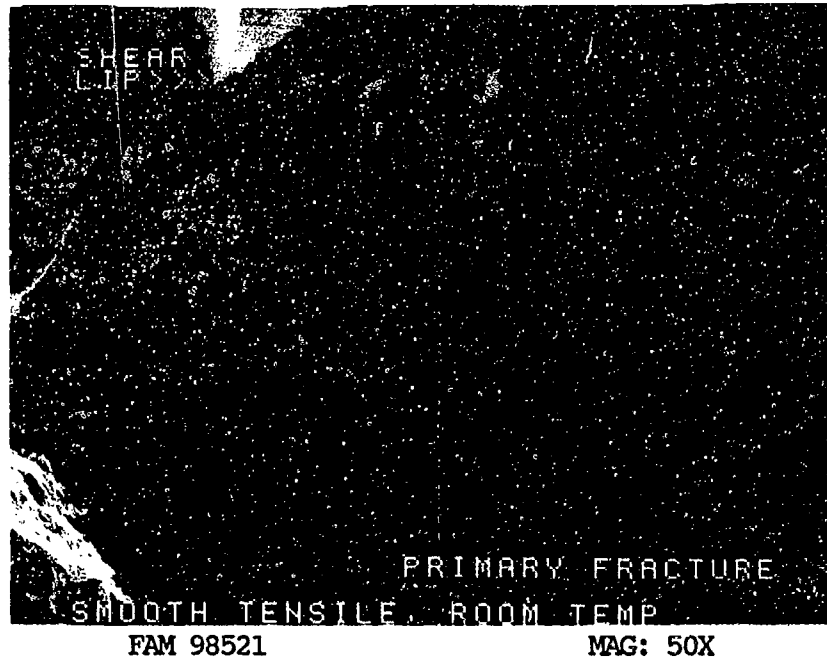


FIGURE 12-3: Low magnification photograph showing primary fracture area and large shear lip.

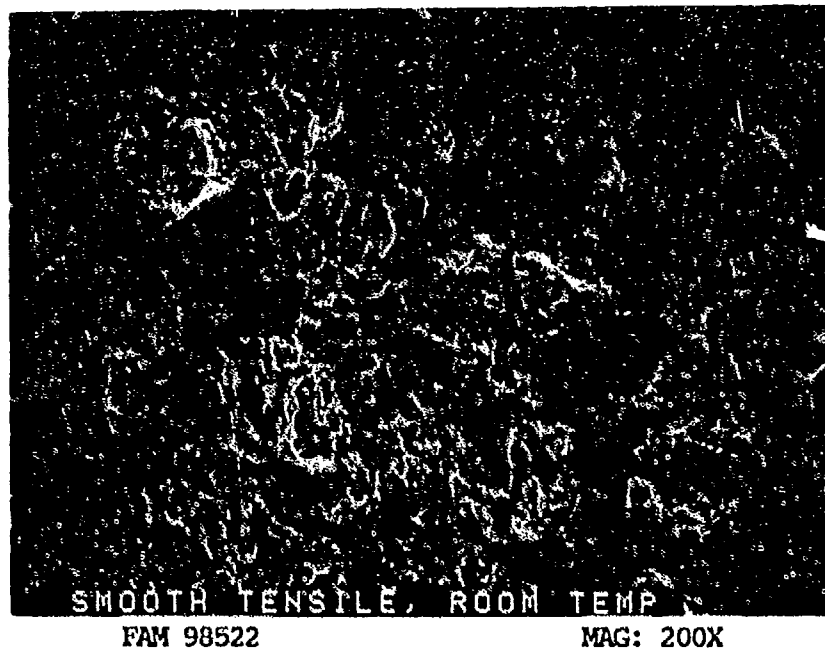


FIGURE 12-4: Dimpled overstress in the primary fracture area.

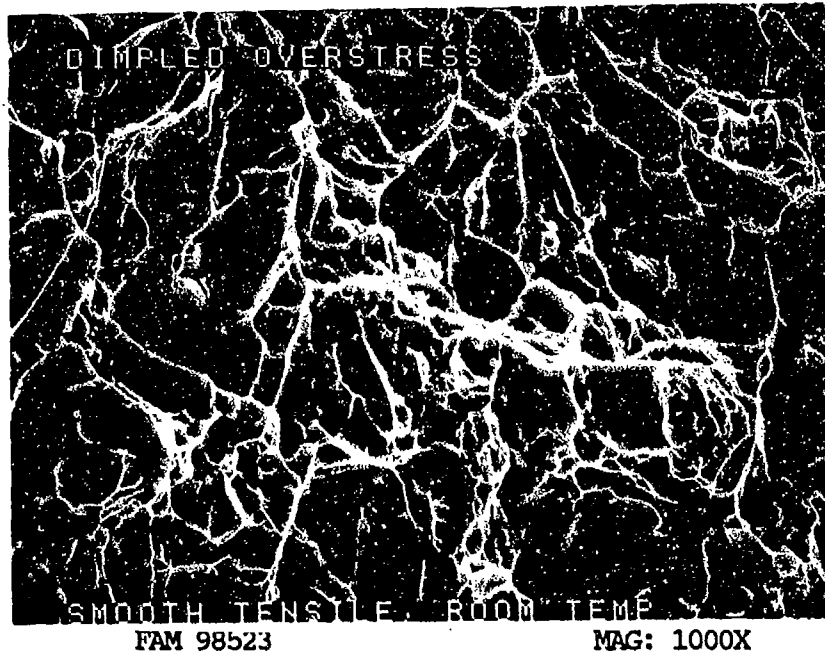


FIGURE 12-5: Higher magnification photograph of the area shown in Figure 12-4, showing dimpled overstress in the primary fracture area.

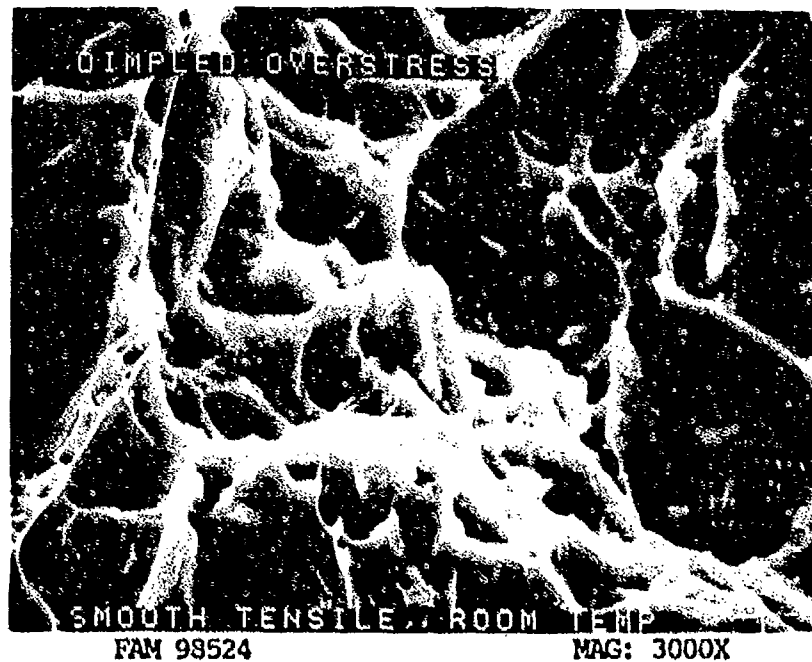


FIGURE 12-6: Dimpled overstress in the primary fracture area, exhibiting variation in dimple size.

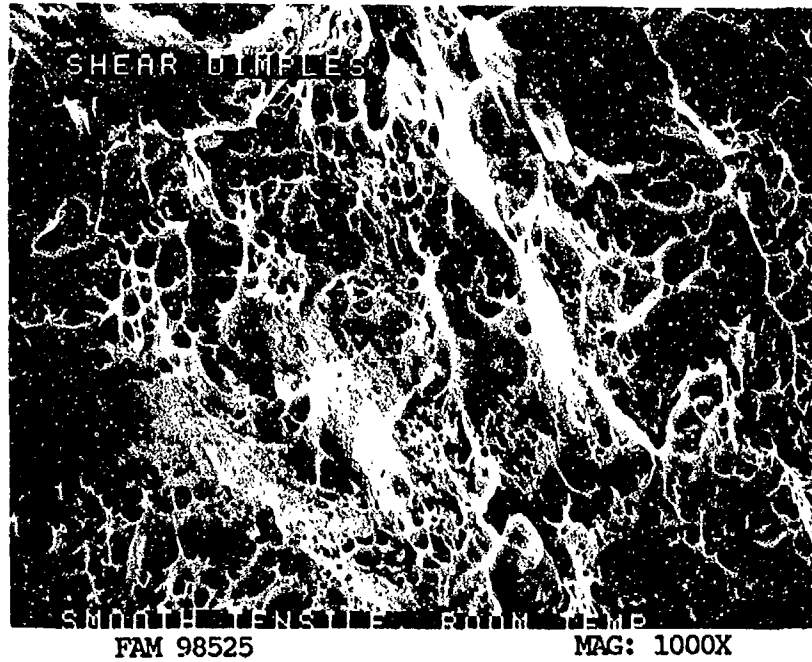


FIGURE 12-7: Shear dimpled overstress in the final fracture area (shear lip).

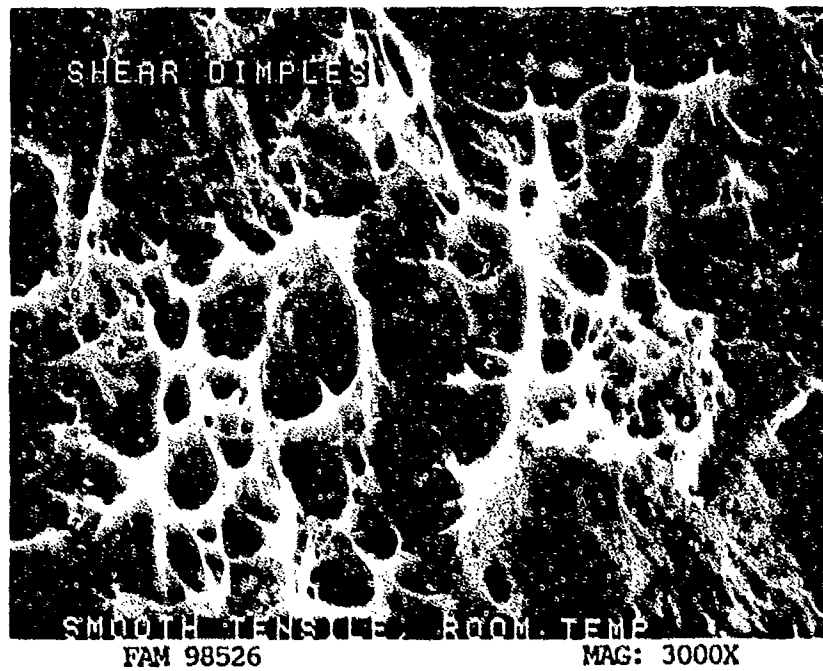


FIGURE 12-8: Shear dimpled overstress in the final fracture area. The directions of relative motion are shown by arrows.

MATERIAL

Ti-6Al-2Sn-4Zr-2Mo
FWA 1224 Bar

TEST DATA

TEST TYPE

Smooth Tensile

TEST CONDITIONS

Strain Rate: 0.005 mm/mm/min (0.005 in/in/min)
Atmosphere: Air
Temperature: 538°C (1000°F)
Test Direction: Longitudinal

TEST RESULTS

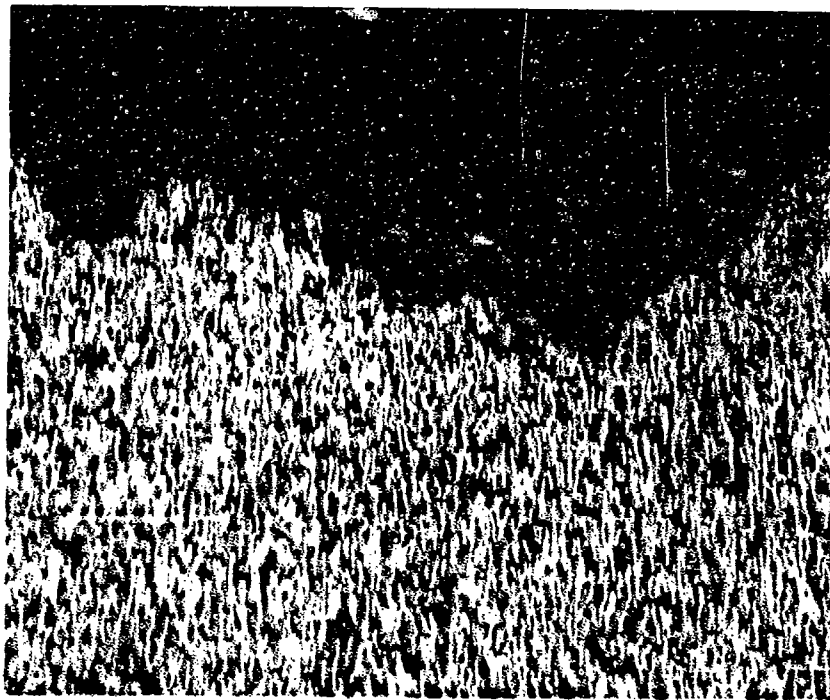
0.2% Yield Strength:	501.9 MPa (72.8 ksi)
Ultimate Strength:	675.7 MPa (98.0 ksi)
Percent Elongation:	24.0
Percent Reduction of Area:	64.7



FAL 92934

MAG: 15X

FIGURE 12-9: Test results and fractography of Ti-6-2-4-2 538°C (1000°F) smooth tensile test. The fracture surface is dominated by a large shear lip. Compare elongation and reduction of area with the room temperature specimen (Figure 12-1). The higher values at 1000°F indicate greater plastic deformation.



FAM 98904

MAG: 100X

FIGURE 12-10: Optical photomicrograph showing the primary overstress area. The entire fracture exhibits elongated grains indicating plastic deformation. The deformation is significantly greater than for the room temperature specimen (Figure 12-2).

Etchant: Kroll's Reagent

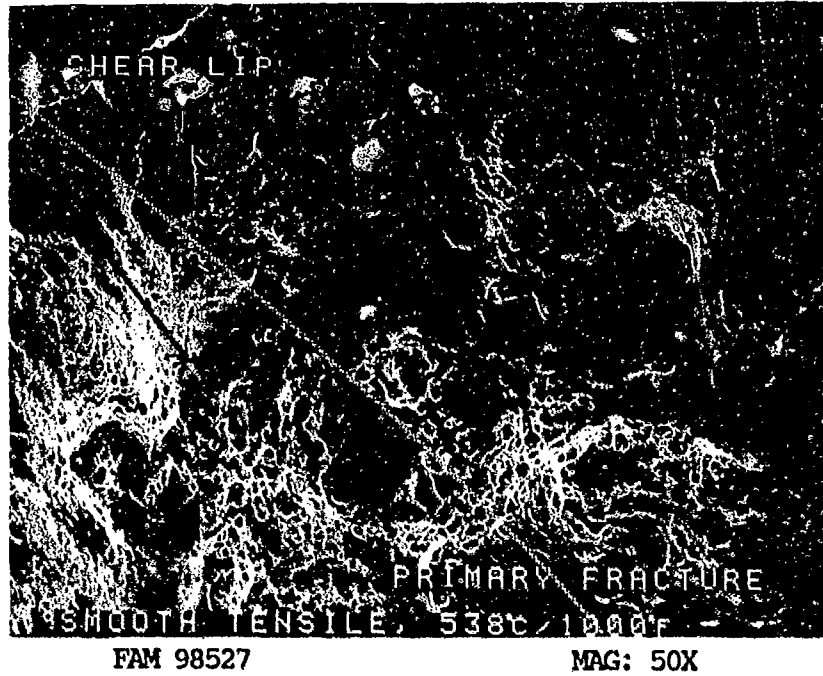


FIGURE 12-11: Low magnification photograph showing primary fracture area and large shear lip. A bracket indicates the extent of the shear lip.

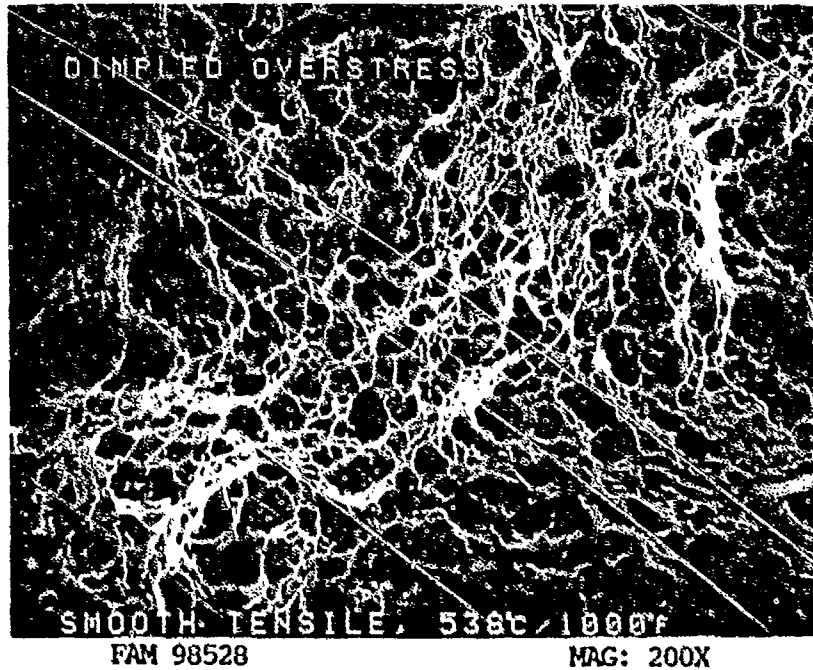


FIGURE 12-12: Equiaxed dimpled overstress in the primary fracture area.

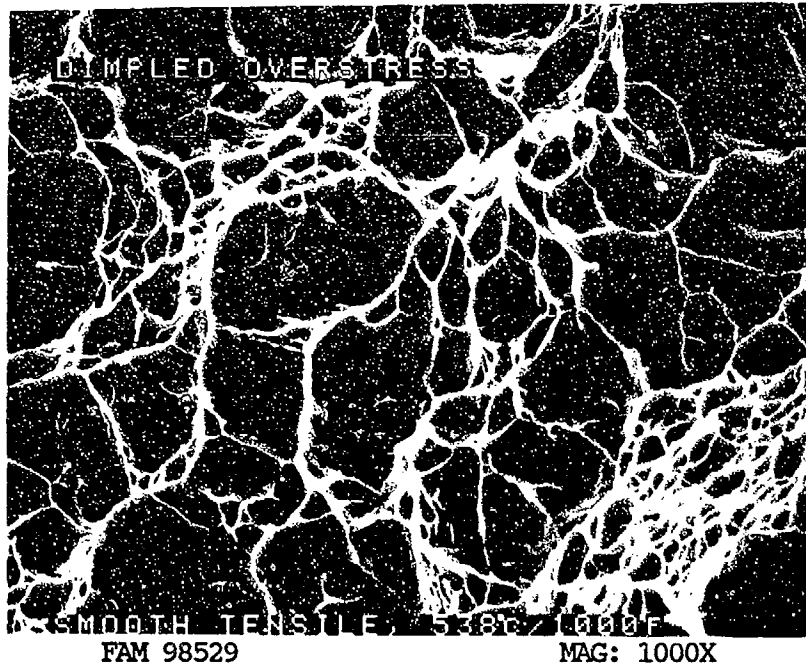


FIGURE 12-13: Higher magnification photograph of the area shown in Figure 12-12, showing oxidized equiaxed dimpled overstress in the primary fracture area.

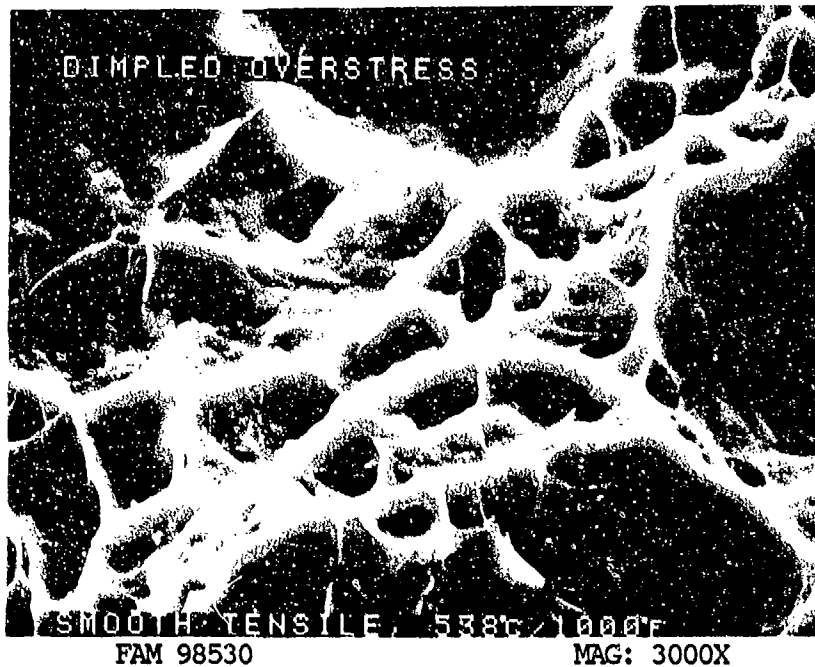


FIGURE 12-14: Shallow oxidized equiaxed dimpled overstress in the primary fracture area.

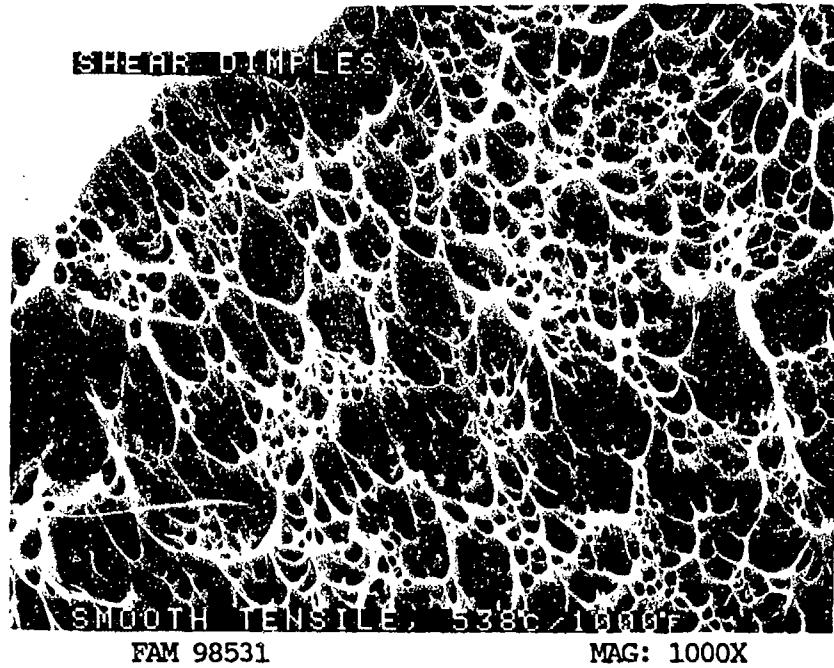


FIGURE 12-15: Shear dimpled overstress in the final fracture area (shear lip).

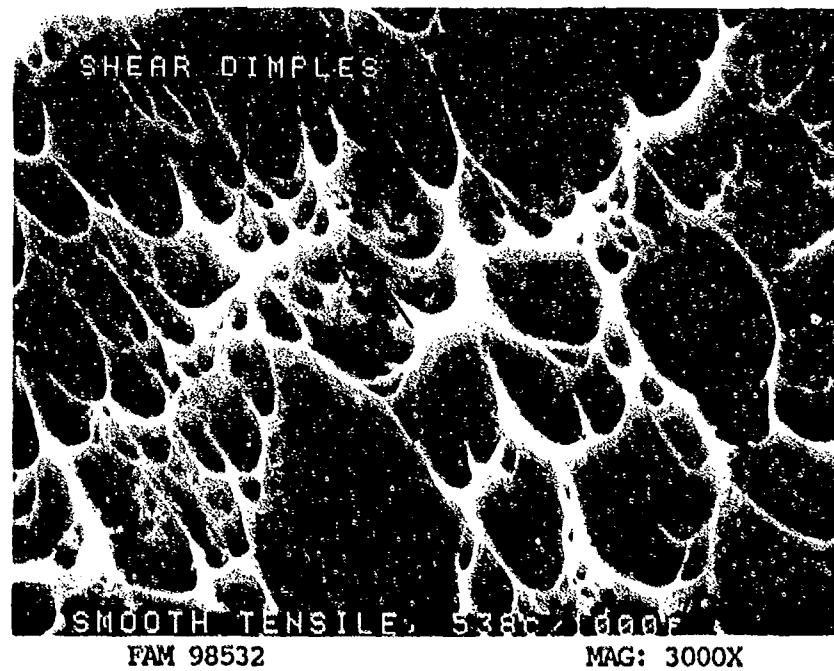


FIGURE 12-16: Shear dimpled overstress in the final fracture area. The directions of relative motion are shown by arrows.

MATERIAL

Ti-6Al-2Sn-4Zr-2Mo
PWA 1224 Bar

TEST DATA

TEST TYPE

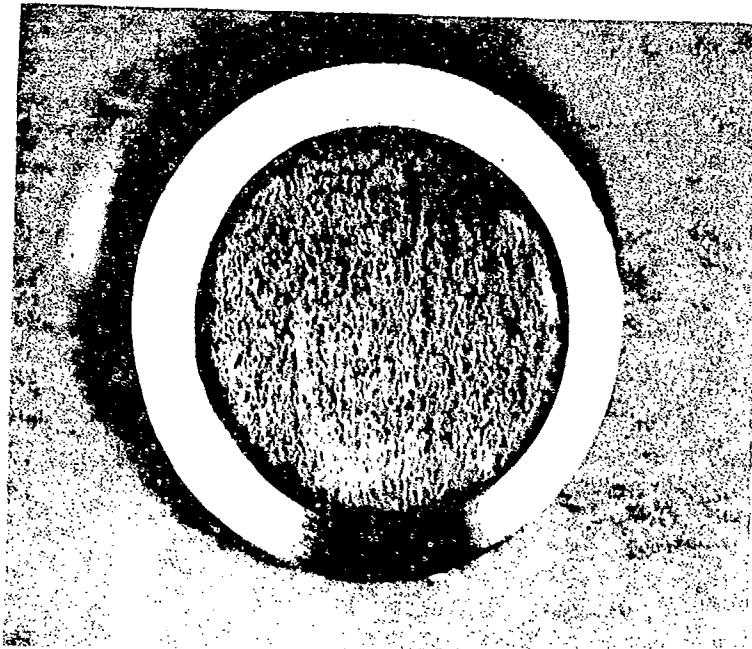
Notched Tensile

TEST CONDITIONS

Crosshead Speed: 1.27 mm/min (0.05 in/min)
Atmosphere: Air
Temperature: Room Temperature
Test Direction: Longitudinal

TEST RESULTS

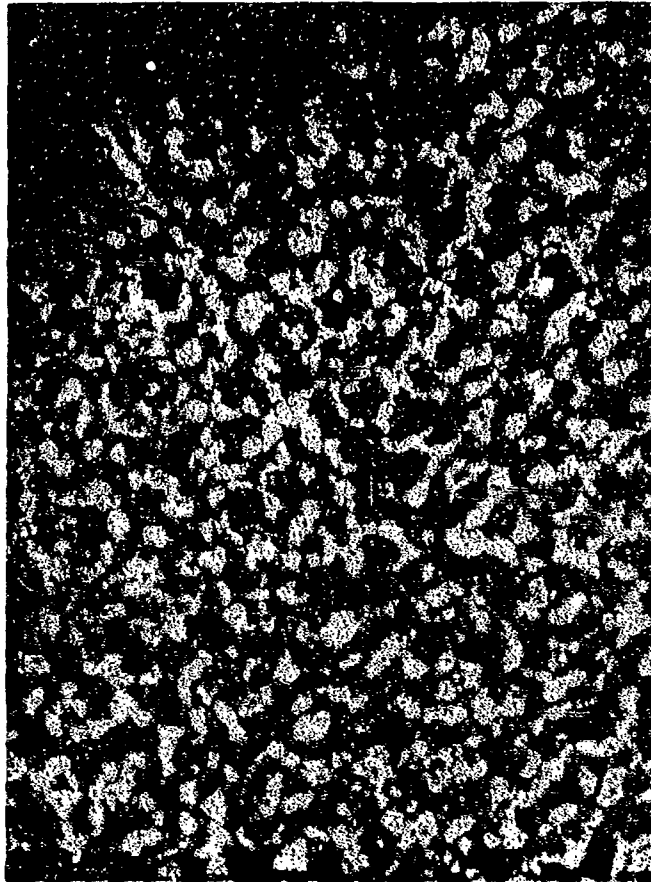
Ultimate Strength: 1483.1 MPa (215,100 PSI)



FAL 92494

MAG: 10X

FIGURE 12-17: Test results and fractography of Ti-6-2-4-2 notched tensile test. No shear lip is visible.



FAM 99767

MAG: 200X

FIGURE 12-18: Optical photomicrograph showing the primary overstress area. The grains remain equiaxed adjacent to the fracture indicating that little or no plastic deformation accompanied the fracture.

Etchant: Kroll's Reagent

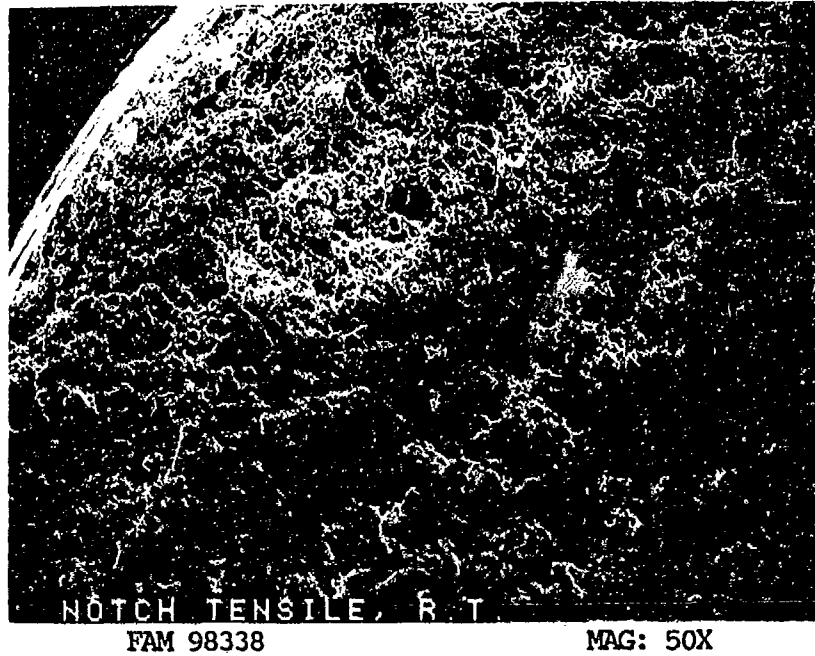


FIGURE 12-19: Low magnification photograph showing no apparent shear lip. The base of the notch is visible (top left).

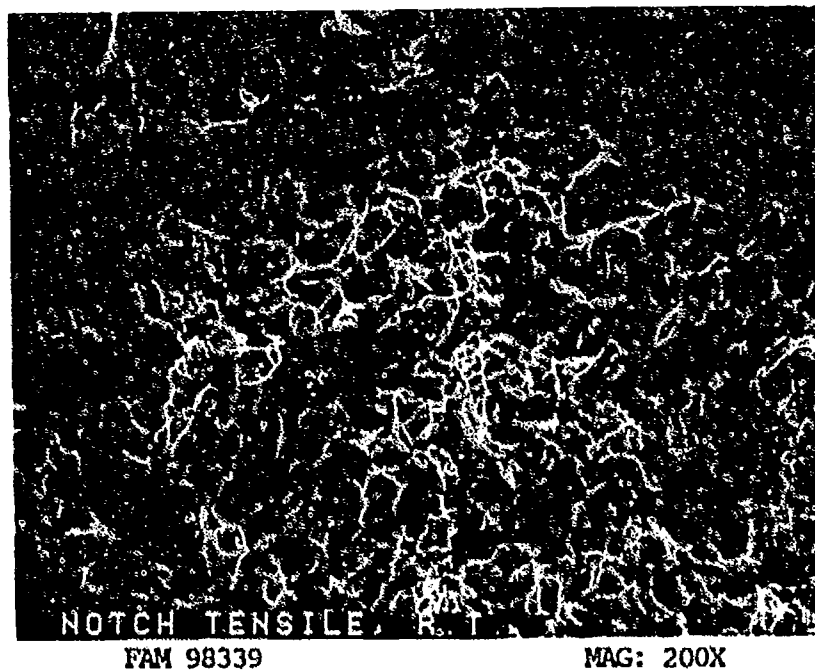
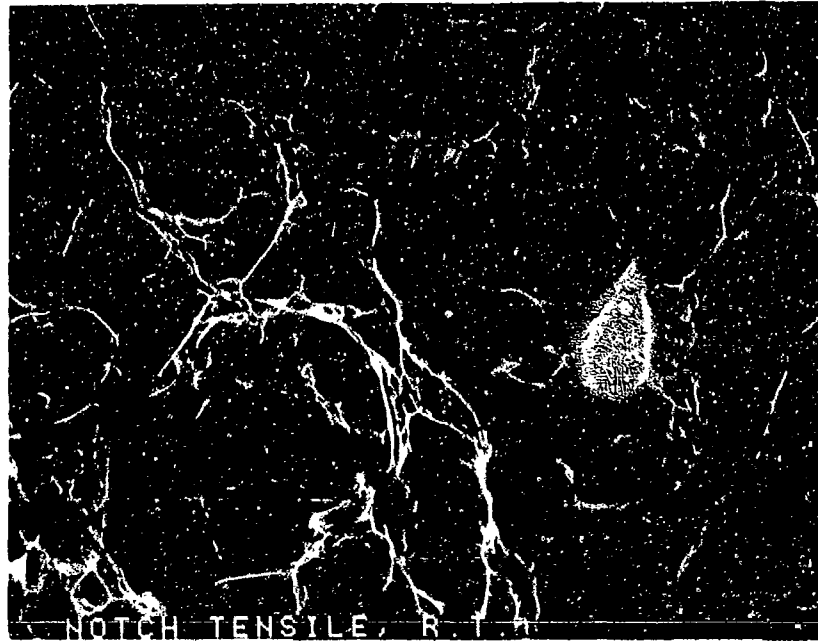


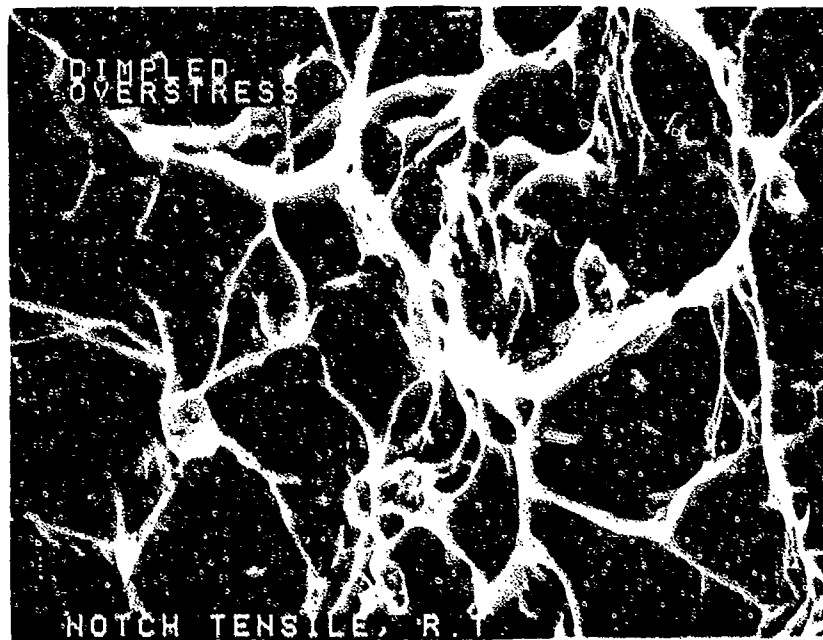
FIGURE 12-20: Dimpled overstress in the center of the specimen.



FAM 98342

MAG: 1000X

FIGURE 12-21: Higher magnification photograph of the area shown in Figure 12-20, showing dimpled overstress.



FAM 98341

MAG: 3000X

FIGURE 12-22: Dimpled overstress with various sized dimples.

MATERIAL

Ti-6Al-2Sn-4Zr-2Mo
FWA 1224 Bar

TEST DATA

TEST TYPE

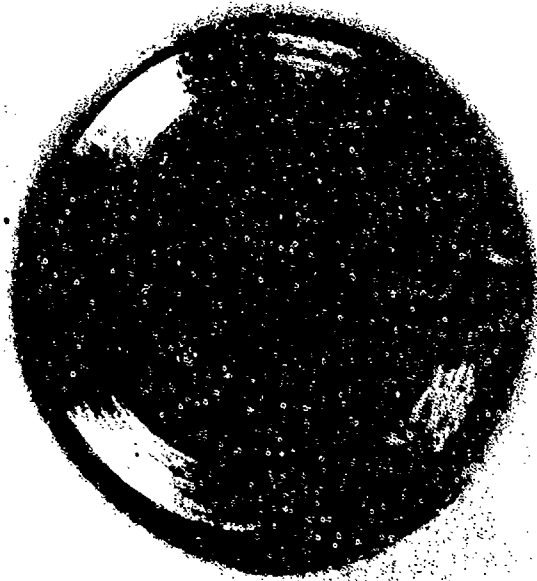
Notched Tensile

TEST CONDITIONS

Crosshead Speed: 1.27 mm/min (0.05 in/min)
Atmosphere: Air
Temperature: 538°C (1000°F)
Test Direction: Longitudinal

TEST RESULTS

Ultimate Strength: 661.8 MPa (139,500 PSI)



FAL 92495

MAG: 13X

FIGURE 12-23: Test results and fractography of Ti-6-2-4-2 538°C (1000°F) notched tensile test. The fracture appears oxidized with no shear lip visible.



FAM 99788

MAG: 200X

FIGURE 12-24: Optical photomicrograph of the base of the notch (arrow). The final overstress area is the only region exhibiting elongated grains. Just inboard of the notch, the grains are equiaxed. The grains remain equiaxed adjacent to the fracture surface, indicating that little or no plastic deformation accompanied the fracture.

Etchant: Kroil's Reagent

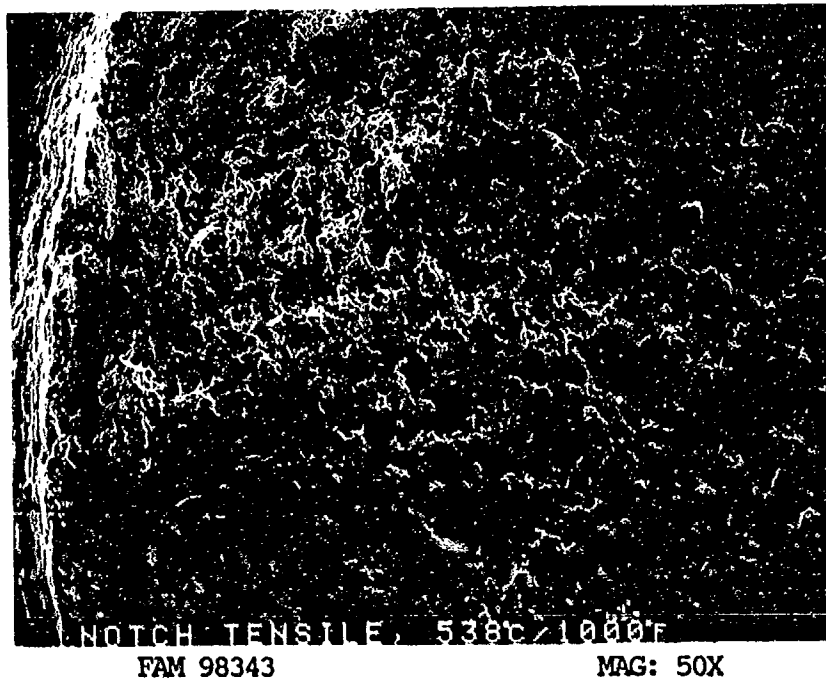


FIGURE 12-25: Low magnification photograph showing no apparent shear lip. The base of the notch is visible on the left side of the photograph.

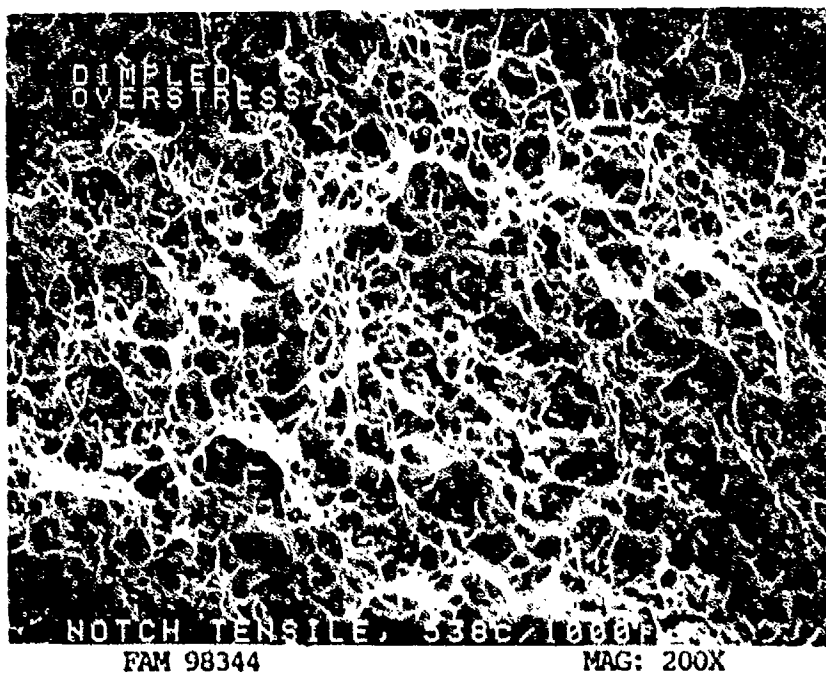


FIGURE 12-26: Equiaxed dimpled overstress in the center of the specimen.

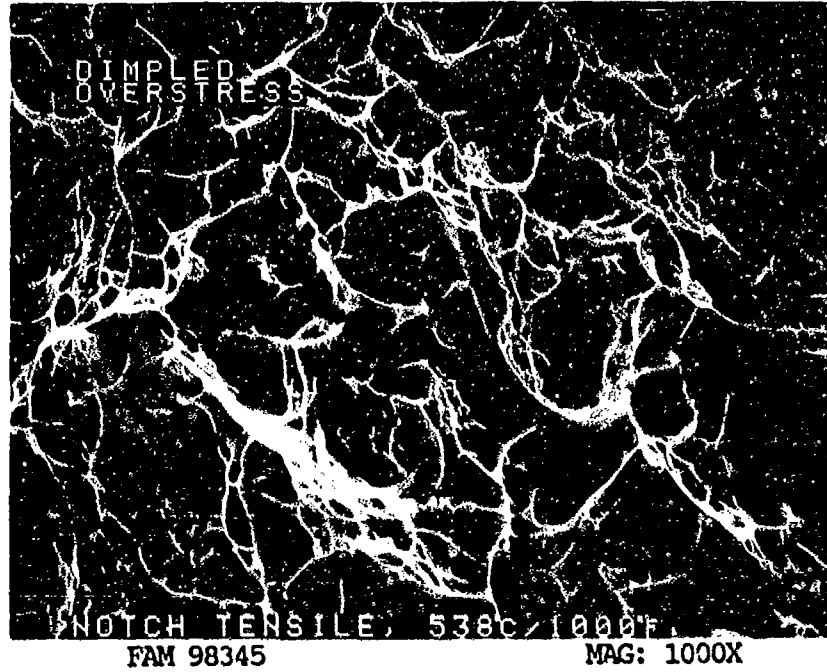


FIGURE 12-27: Higher magnification photograph of the center of the fracture surface, showing equiaxed dimpled overstress.

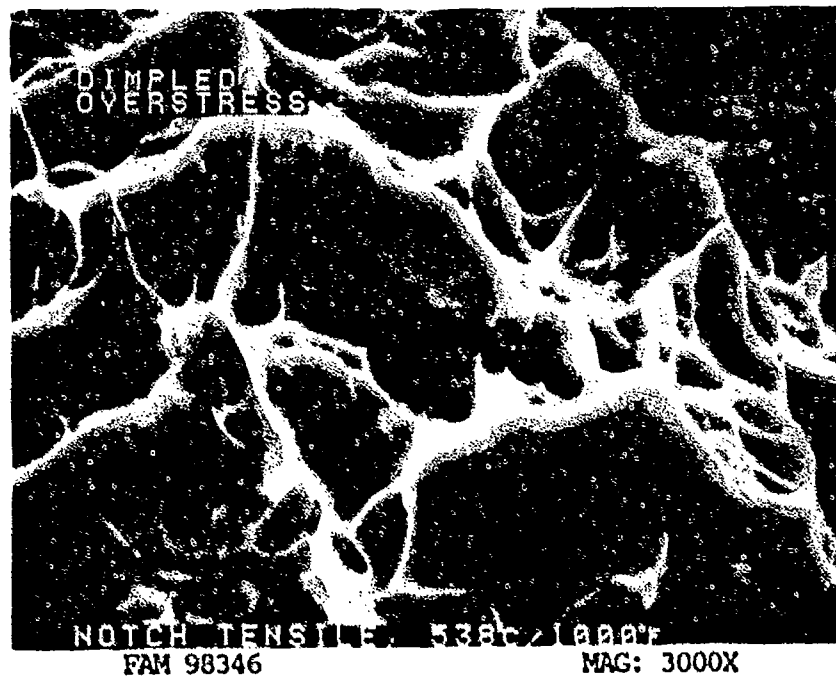


FIGURE 12-28: Equiaxed dimpled overstress with various sized dimples.

MATERIAL

Ti-6Al-2Sn-4Zr-2Mo
PWA 1224 Bar

TEST DATA

TEST TYPE

Stress Rupture

TEST CONDITIONS

Stress: 406.8 MPa (59.0 ksi) (DNF)
448.2 MPa (65.0 ksi)

Atmosphere: Air

Temperature: 510°C (950°F)

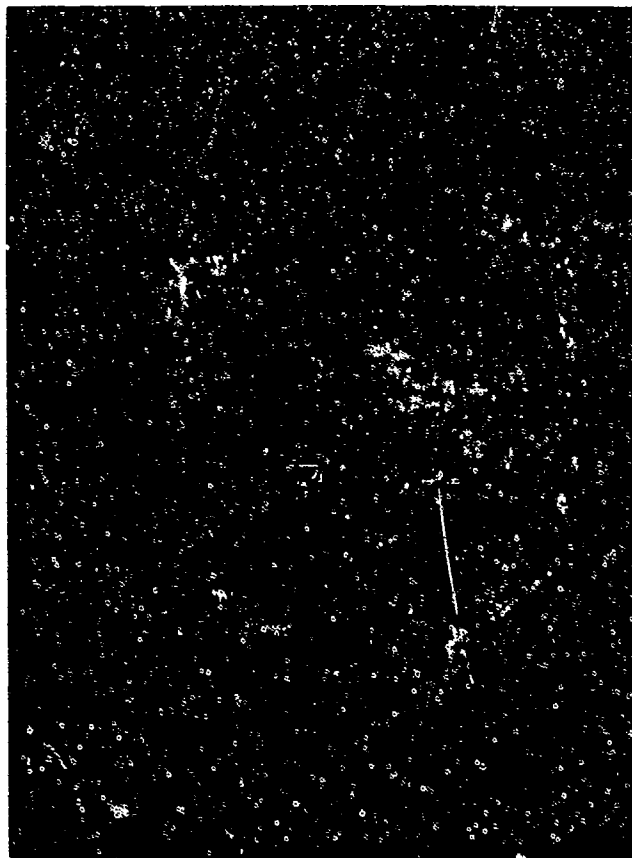
Test Direction: Longitudinal

TEST RESULTS

Time to Rupture: 544.6 hours (DNF)/ 451.1 hours

% Elongation: 24.0

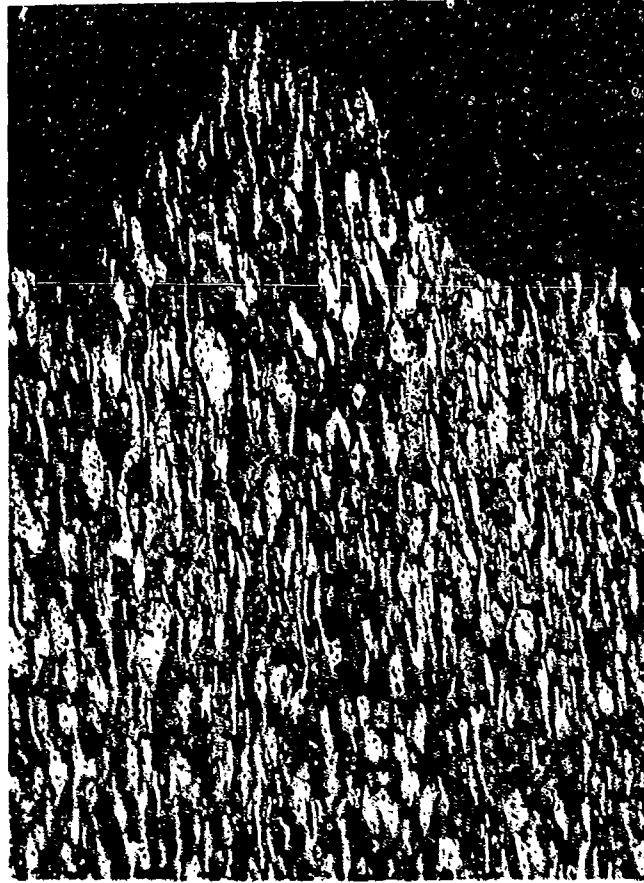
% Reduction of Area: 51.3



FAL 97221

MAG: 10X

FIGURE 12-29: Test results and fractography of Ti-6-2-4-2 510°C (950°F) stress rupture test. The fracture surface appears to be oxidized and has deeper features than the tensile test specimens.



FAM 99759

MAG: 200X

FIGURE 12-30: Optical photomicrograph showing severely elongated grains near the center of the specimen. The fracture is predominantly transgranular.

Etchant: Kroll's Reagent

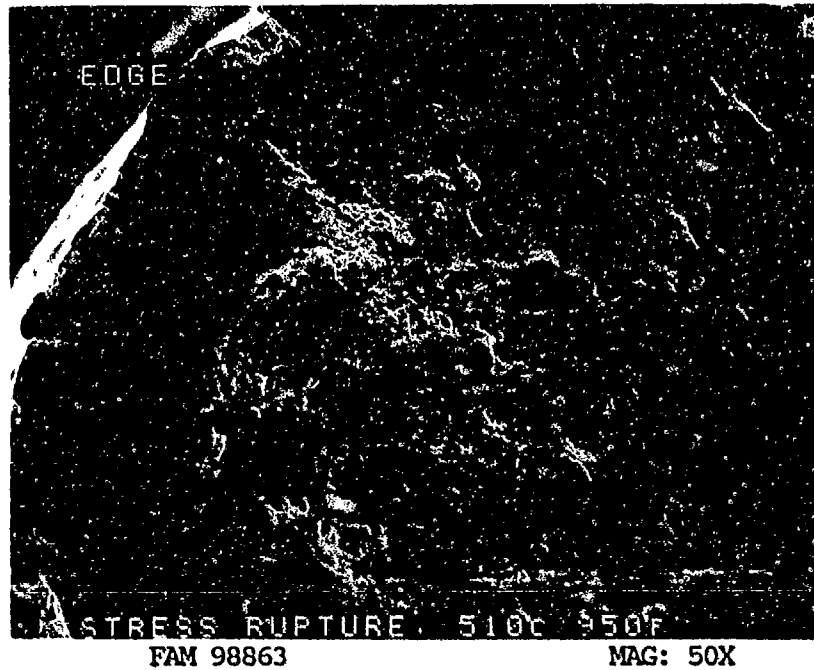


FIGURE 12-31: Low magnification photograph showing primary overstress area near the center of the specimen and a shear lip near the edge.

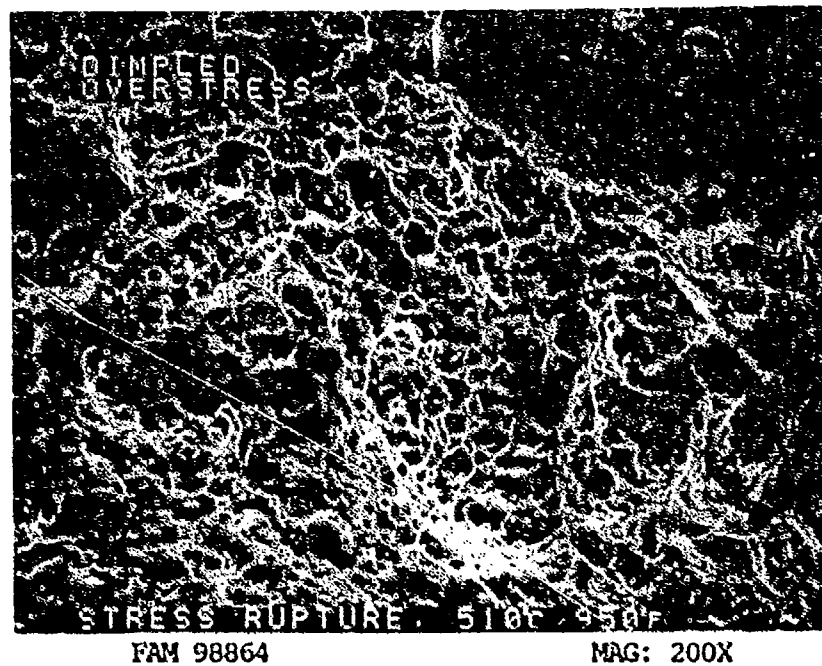
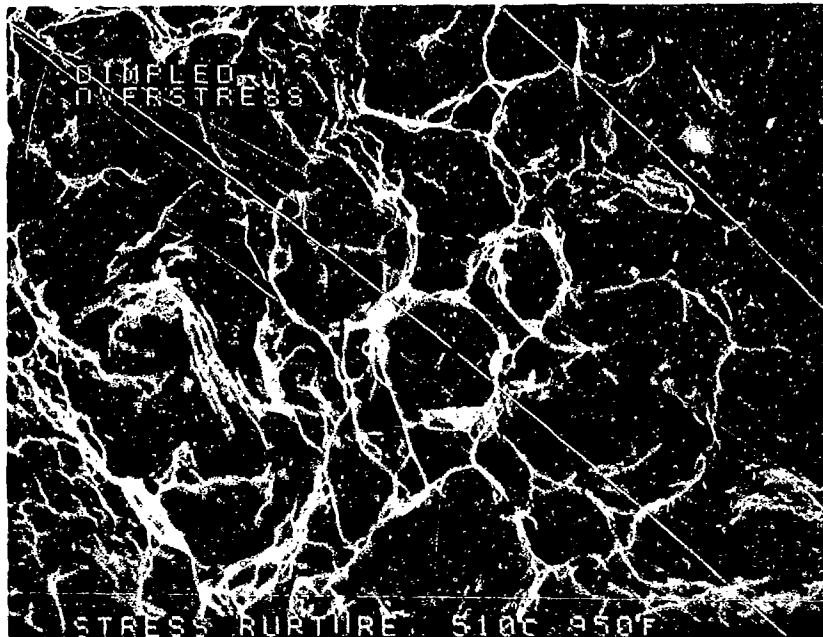


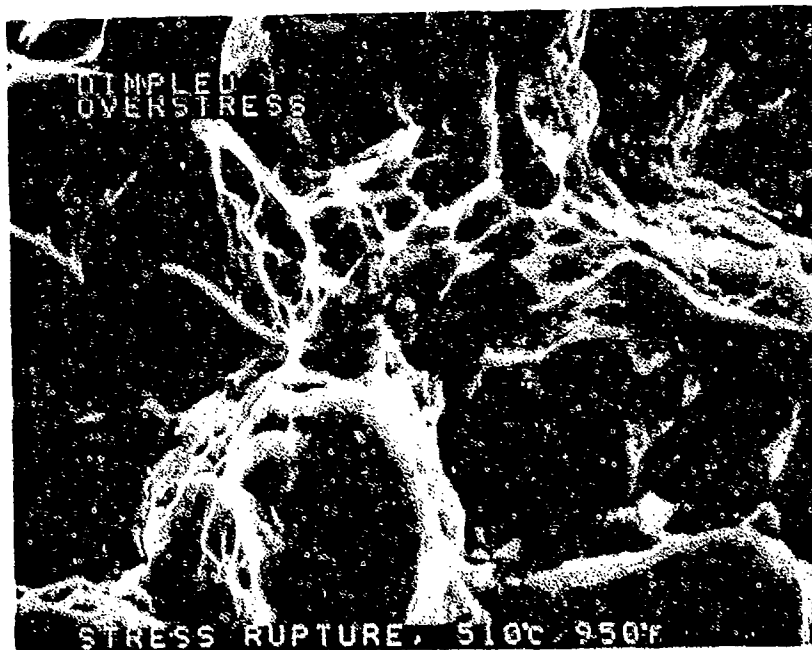
FIGURE 12-32: Equiaxed dimpled overstress in the primary fracture area. Small areas of void coalescence are visible near the center of the specimen (arrows).



FAM 98865

MAG: 1000X

FIGURE 12-33: Lightly oxidized equiaxed dimpled overstress with small areas of void coalescence (arrows).



FAM 98866

MAG: 3000X

FIGURE 12-34: Higher magnification photograph of the area shown in Figure 12-33, showing fine equiaxed dimples between areas of void coalescence.

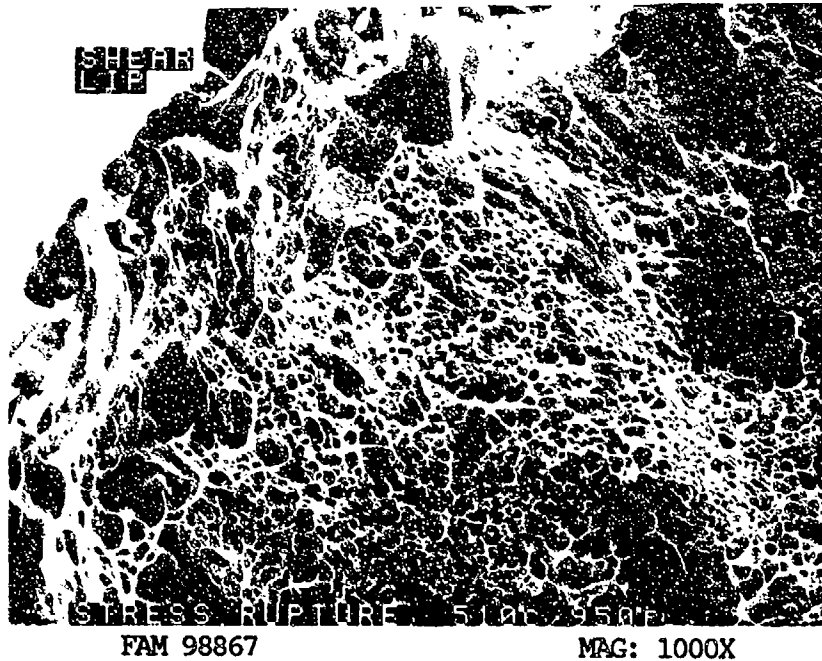


FIGURE 12-35: Shear dimples in the final fracture area.

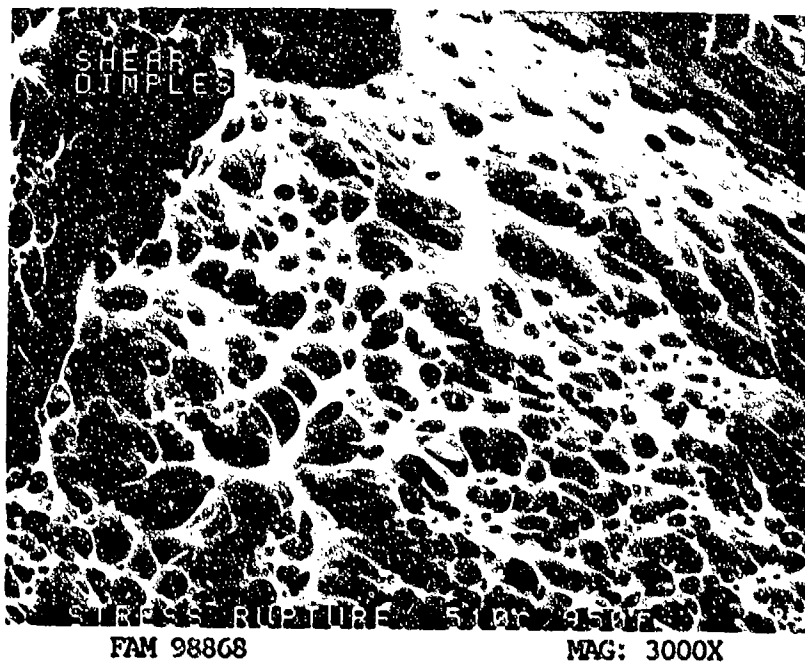


FIGURE 12-36: Fine shear dimples in the final overstress area. Arrows show the directions of relative motion.

MATERIAL

Ti-6Al-2Sn-4Zr-2Mo
PWA 1224 Bar

TEST DATA

TEST TYPE

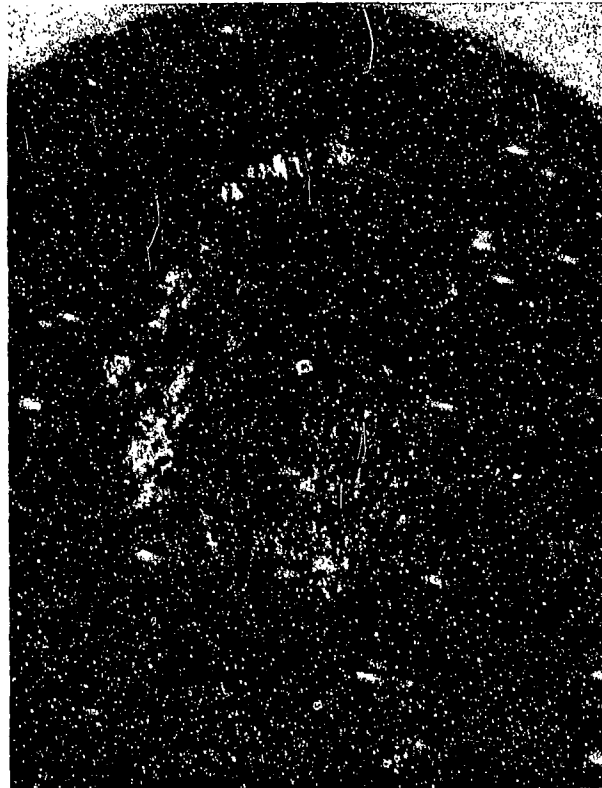
Smooth HCF

TEST CONDITIONS

Stress: 482.6 MPa (70.0 ksi)/-482.6 MPa (-70.0 ksi)
Stress Ratio: -1
Frequency: 1800 cpm
Atmosphere: Air
Temperature: Room Temperature
Test Direction: Longitudinal

TEST RESULTS

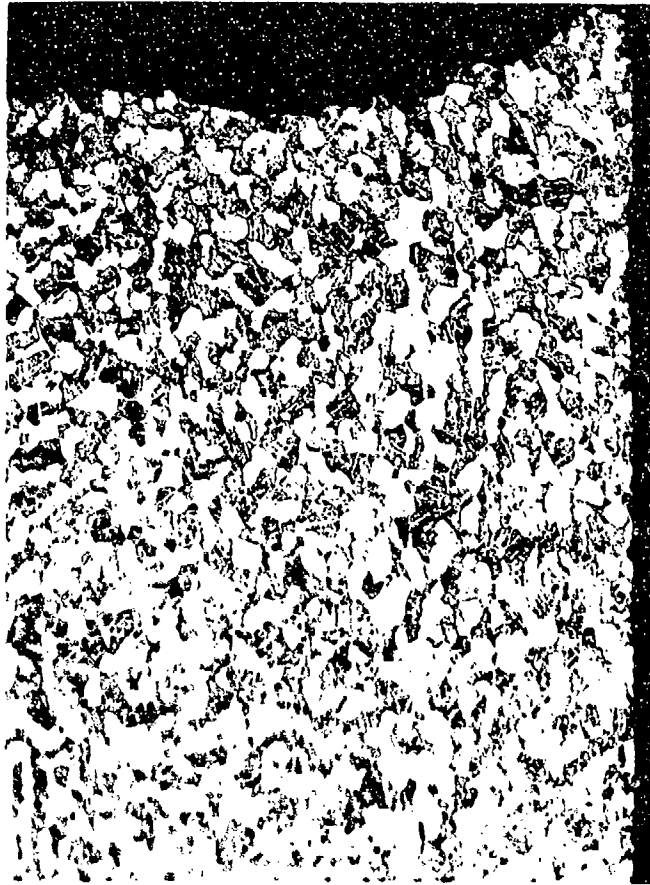
Cycles to Fracture: 52,800



FAL 93830

MAG: 15X

FIGURE 12-37: Test results and fractography of Ti-6-2-4-2 room temperature smooth HCF test. Features appear to radiate from a general origin area (arrow A). The extent of fatigue is shown by arrow heads.



FAM 99782

MAG: 200X

FIGURE 12-38: Optical photomicrograph showing the fatigue progression zone, exhibiting a relatively flat transgranular fracture path.

Etchant: Kroll's Reagent

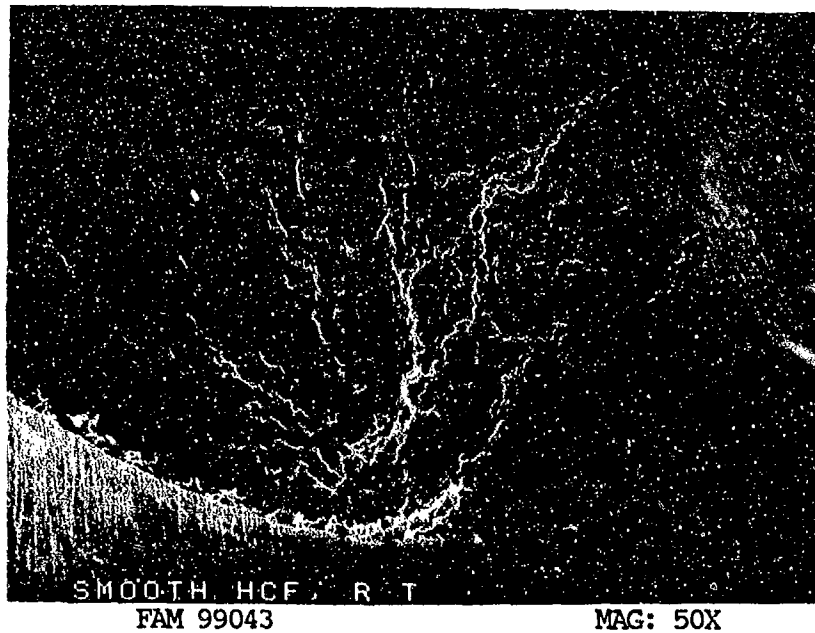


FIGURE 12-39: Low magnification view of the origin area. The specimen exhibited a single surface origin (arrow).

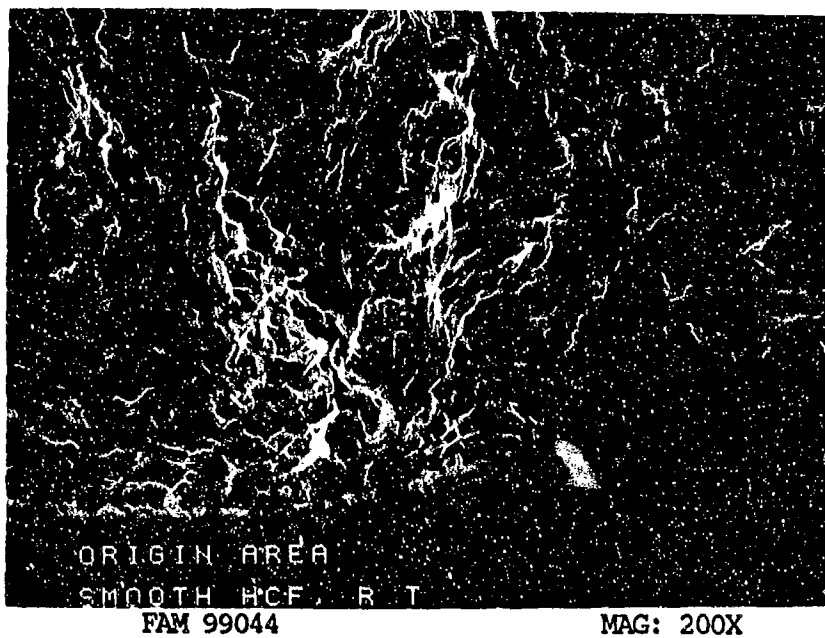


FIGURE 12-40: Higher magnification view of the origin area shown in Figure 12-39. A Stage I fatigue facet is visible at the origin (arrow). Features can be seen radiating from the facet.

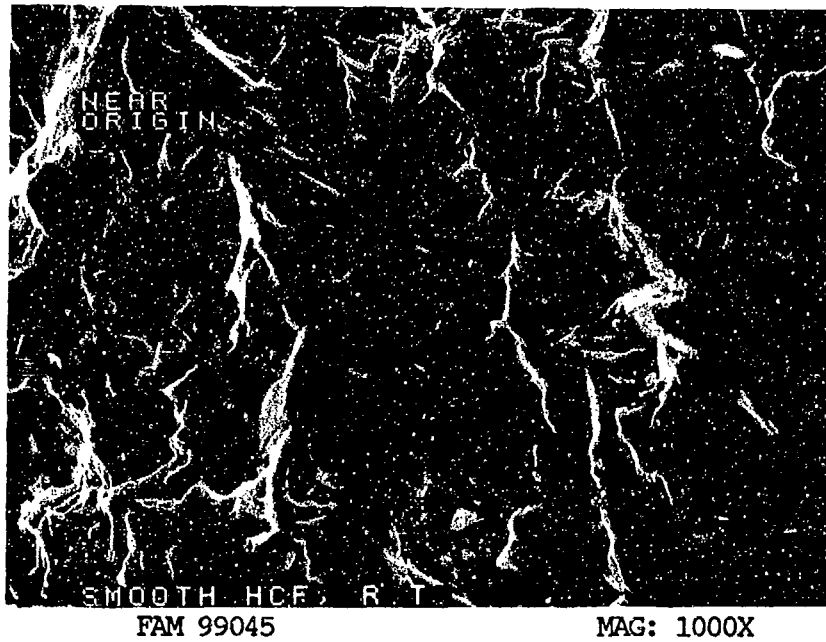


FIGURE 12-41: Feathery cleavage near the origin area. The direction of propagation is from bottom to top of the photograph.

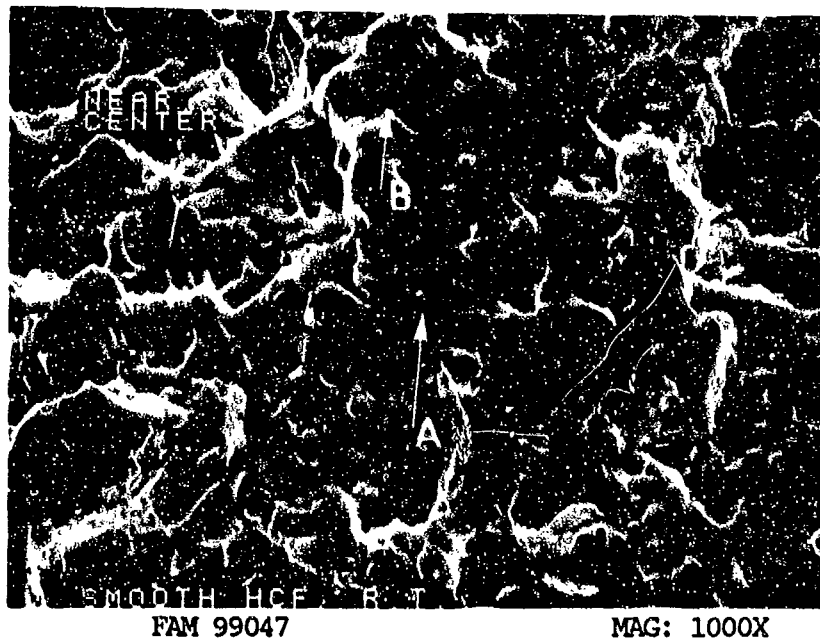


FIGURE 12-42: Fatigue progression near the center of the specimen. The fracture surface is characterized by remnant fatigue striations (arrow A) and secondary cracking (remnant crack-like striations) (arrow B) perpendicular to the direction of propagation.

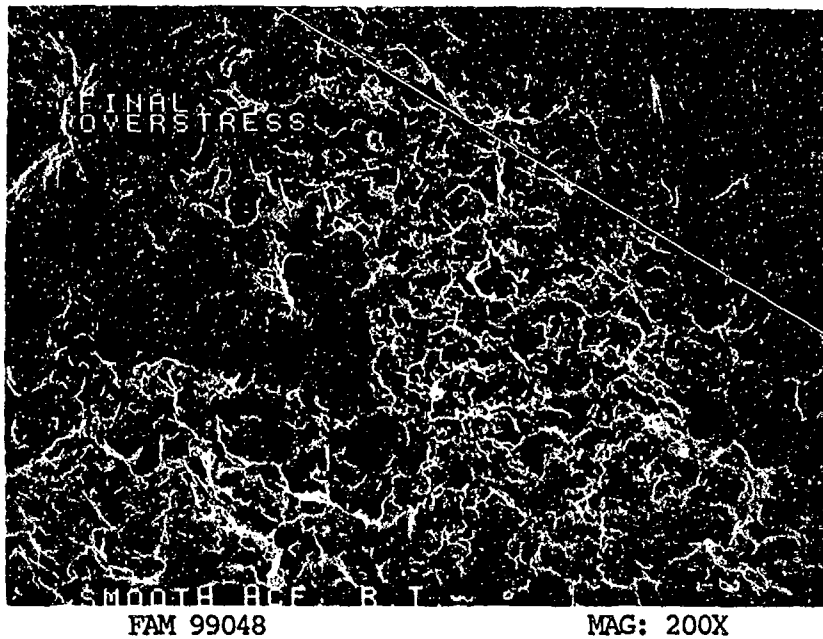


FIGURE 12-43: Partially smeared overstress features in the final overstress area. Arrows indicate areas of smear.

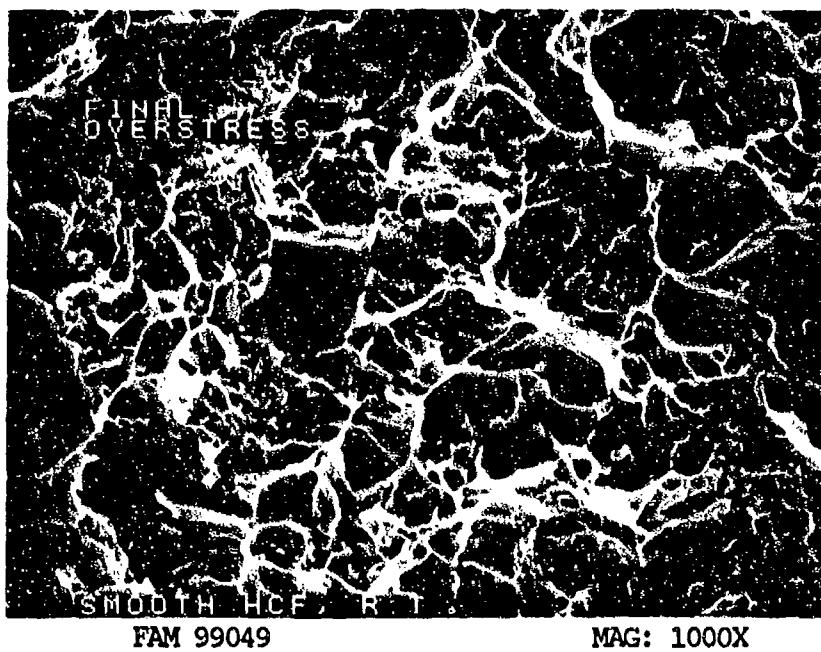


FIGURE 12-44: Higher magnification photograph of the final overstress area. Fine dimples (arrow A) are separated by patches of cleavage.

MATERIAL

Ti-6Al-2Sn-4Zr-2Mo
PWA 1224 Bar

TEST DATA

TEST TYPE

Smooth HCF

TEST CONDITIONS

Stress: 482.6 MPa (70.0 ksi)/-482.6 MPa (-70.0 ksi)

Stress Ratio: -1

Frequency: 1800 cpm

Atmosphere: Air

Temperature: 260°C (500°F)

Test Direction: Longitudinal

TEST RESULTS

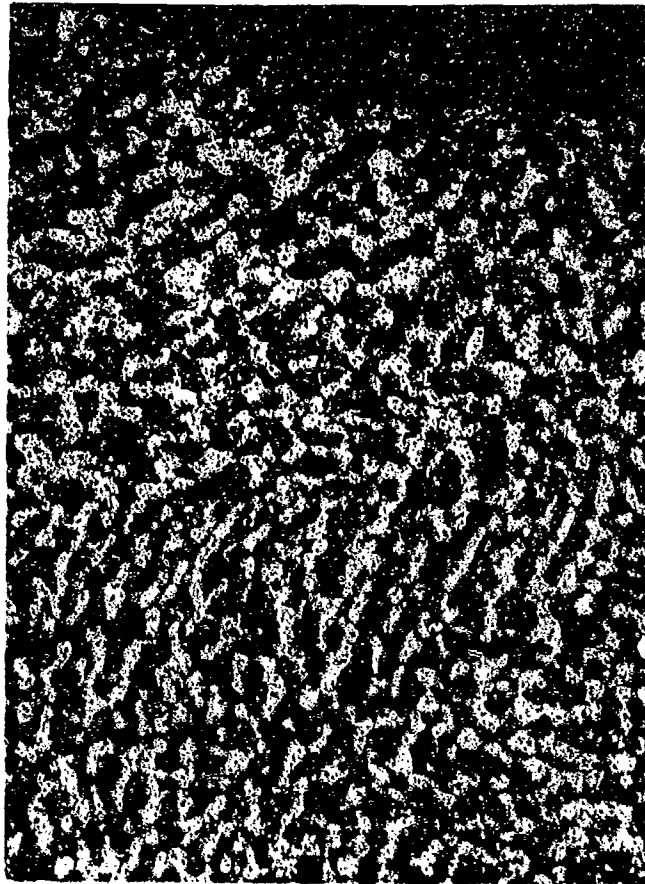
Cycles to Fracture: 53,300



FAL 93815

MAG: 13X

FIGURE 12-45: Test results and fractography of Ti-6-2-4-2 260°C (500°F) smooth HCF test. No clear origin or progression zone is visible.



FAM 99761

MAG: 200X

FIGURE 12-46: Optical photomicrograph showing the fatigue progression zone exhibiting a relatively flat, transgranular fracture path similar to the room temperature specimen.

Etchant: Kroll's Reagent

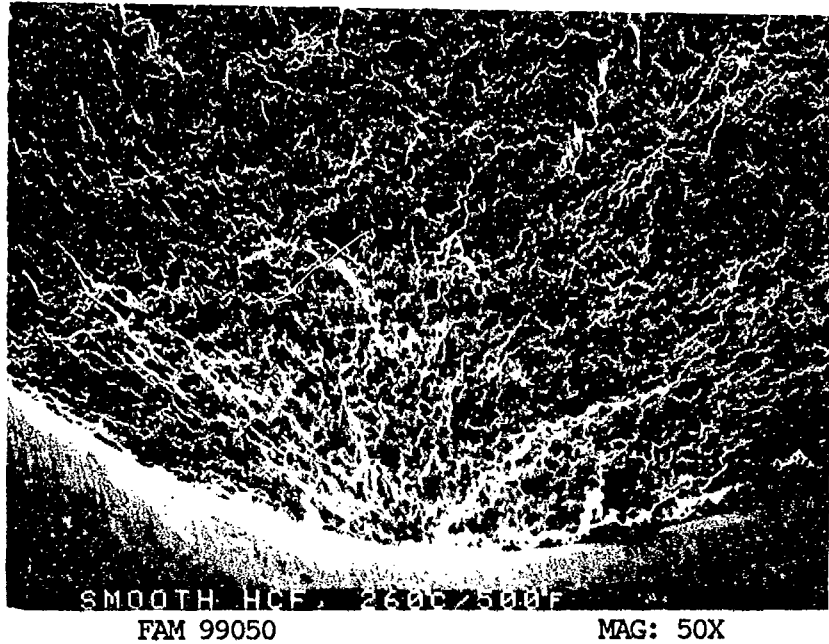


FIGURE 12-47: Low magnification view of the origin area and initial fatigue progression area. Features can be seen radiating from the origin.

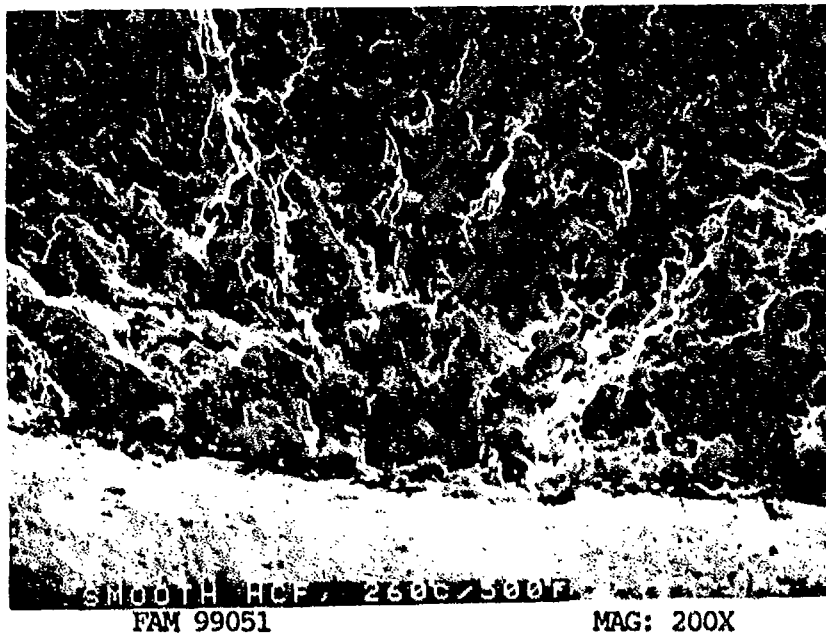


FIGURE 12-48: Higher magnification view of the origin area. The features are relatively flat with no localized origin discernible.

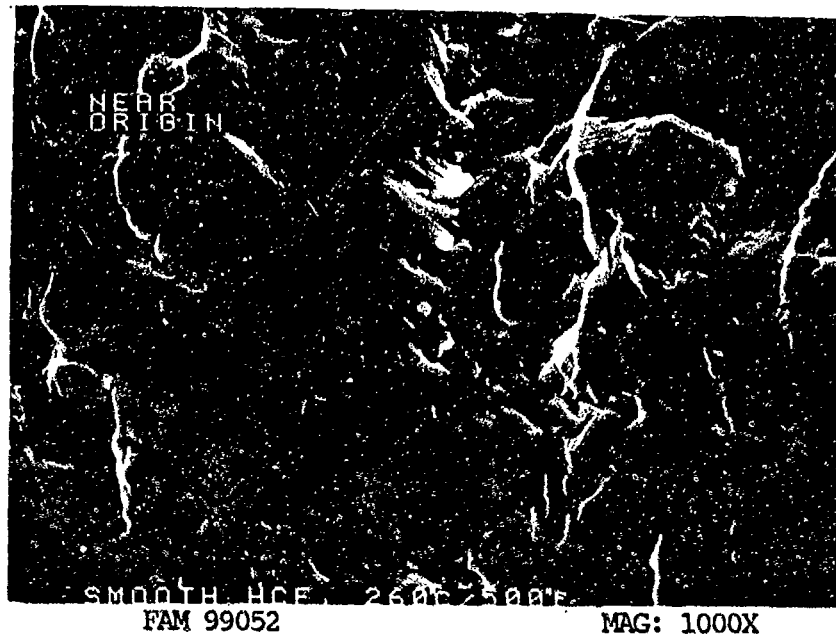


FIGURE 12-49: Combination of remnant fatigue features (arrow A) and smear (arrow B) near the origin area. The fracture propagated from bottom to top of the photograph.

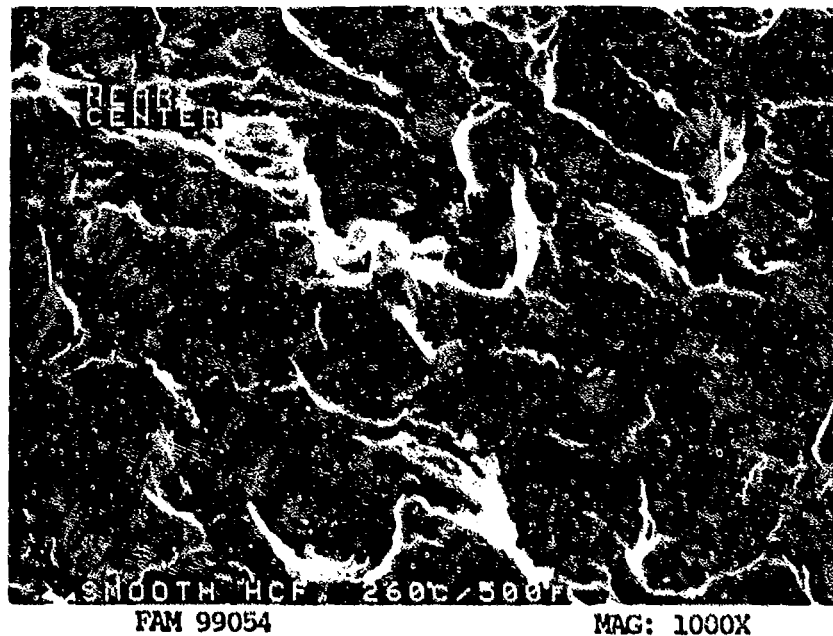


FIGURE 12-50: Crack-like striations near the center of the specimen (end of fatigue thumbnail). The direction of propagation is from bottom to top of the photograph.

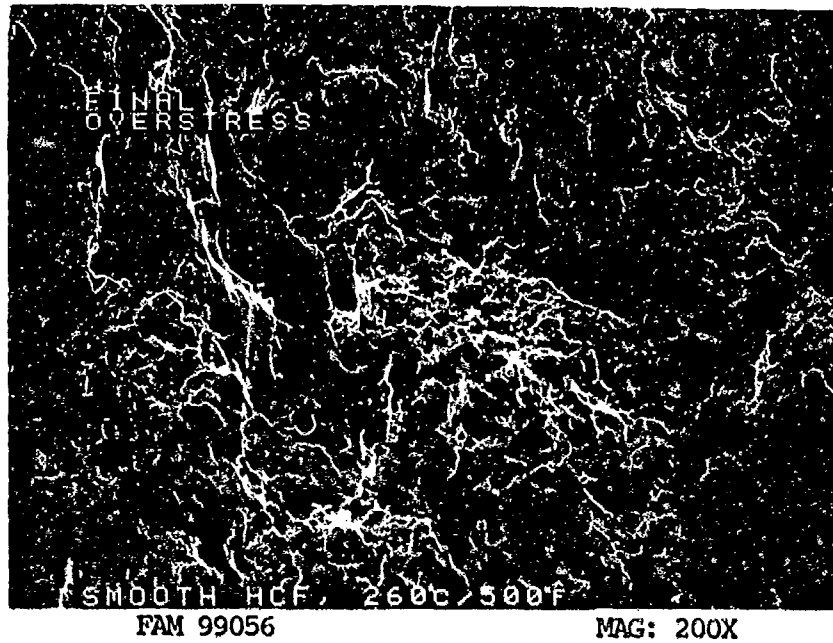


FIGURE 12-51: Mixture of overstress and smear features (arrows) in the final overstress area.

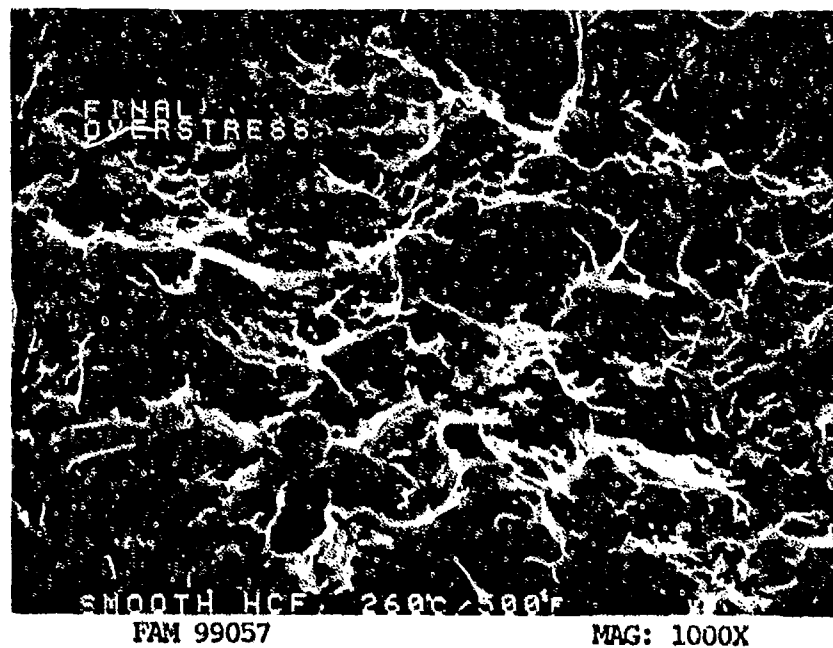


FIGURE 12-52: Higher magnification photograph of the area shown in Figure 12-51, showing fine dimples and smear features in the final overstress area.

MATERIAL

Ti-6Al-2Sn-4Zr-2Mo
FWA 1224 Bar

TEST DATA

TEST TYPE

Smooth HCF

TEST CONDITIONS

Stress: 379.2 MPa (55.0 ksi)/-379.2 MPa (-55.0 ksi) DNF*
413.7 MPa (60.0 ksi)/-413.7 MPa (-60.0 ksi) DNF
448.2 MPa (65.0 ksi)/-448.2 MPa (-65.0 ksi) DNF
482.6 MPa (70.0 ksi)/-482.6 MPa (-70.0 ksi)
Stress Ratio: -1
Frequency: 1800 cpm
Atmosphere: Air
Temperature: 538°C (1000°F)
Test Direction: Longitudinal

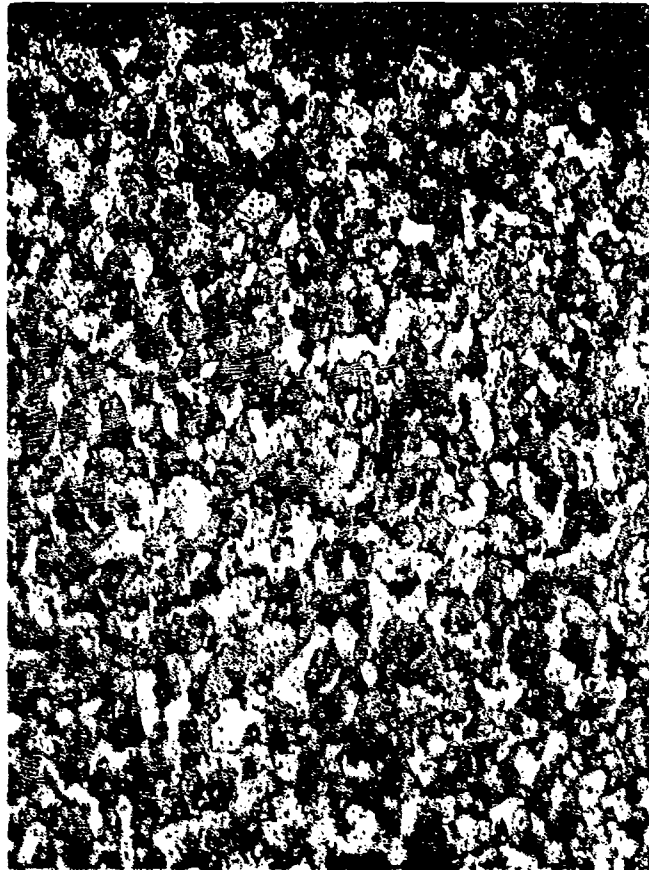
TEST RESULTS

Cycles to Fracture: 1.0×10^7 (DNF), 1.0×10^6 (DNF), 1.0×10^6 (DNF),
14,700

* Did Not Fracture



FIGURE 12-53: Test results and fractography of Ti-6-2-4-2 538°C (1000°F) smooth HCF test. The fatigue progression appears as a relatively flat area covering 70% of the fracture surface. The origin area is shown by an arrow.



FAM 99765

MAG: 200X

FIGURE 12-54: Optical photomicrograph showing the fatigue progression zone, exhibiting a mixture of transgranular and intergranular fracture.

Etchant: Kroll's Reagent

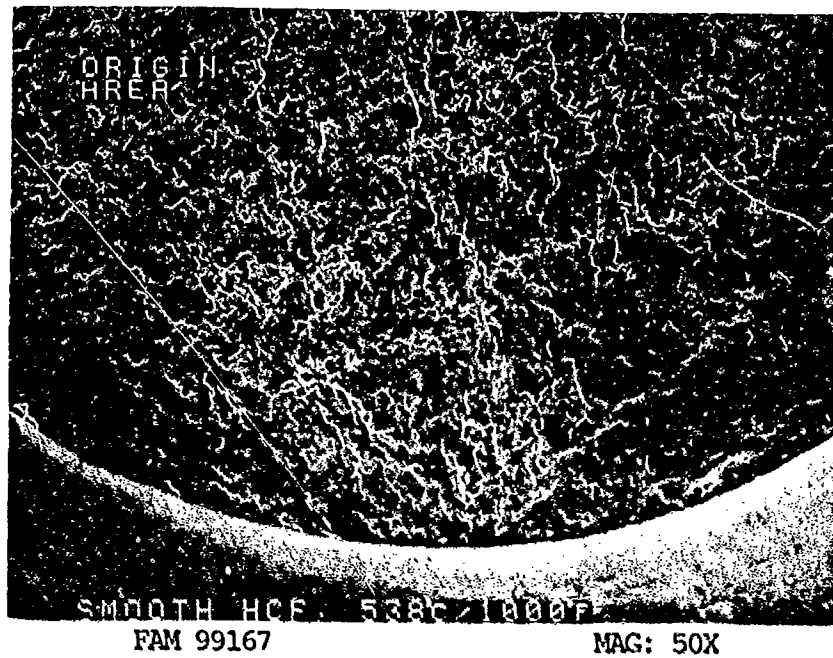


FIGURE 12-55: Low magnification view of the origin area and initial fatigue progression area.

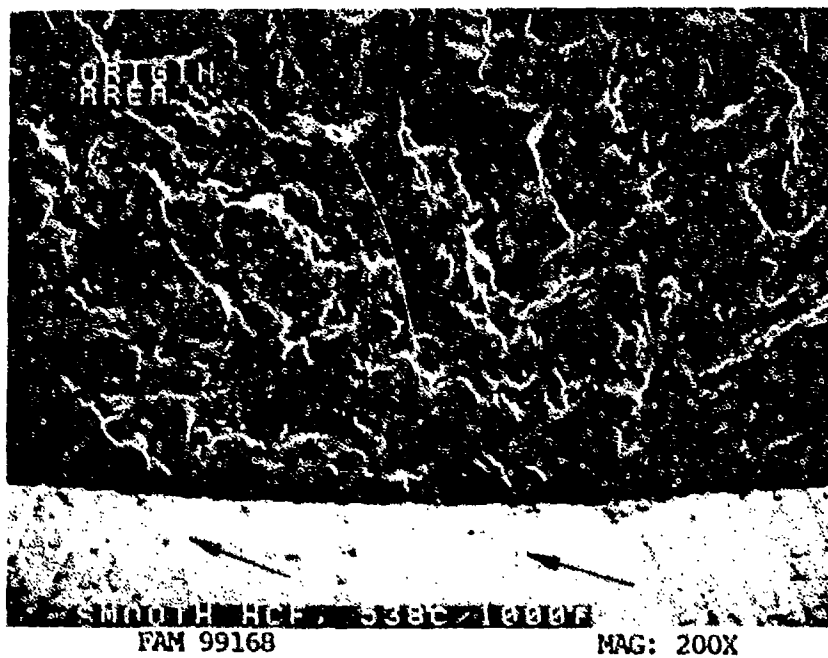


FIGURE 12-56: Higher magnification view of the origin area. The features are relatively flat with no localized origin discernible. Machining/polishing marks (arrows) are visible on the specimen surface, adjacent to the origin. These probably did not contribute to the fracture.

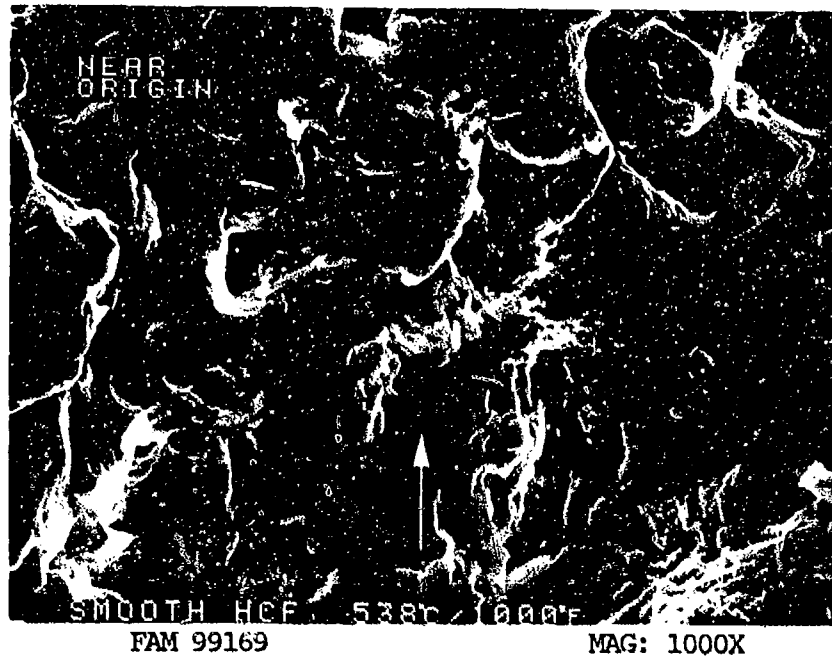


FIGURE 12-57: Combination of remnant fatigue features and smear near the origin. The fracture propagated from bottom to top of the photograph. Arrow indicates a patch of remnant striations.



FIGURE 12-58: High magnification view of the remnant striations pointed out in Figure 12-57.

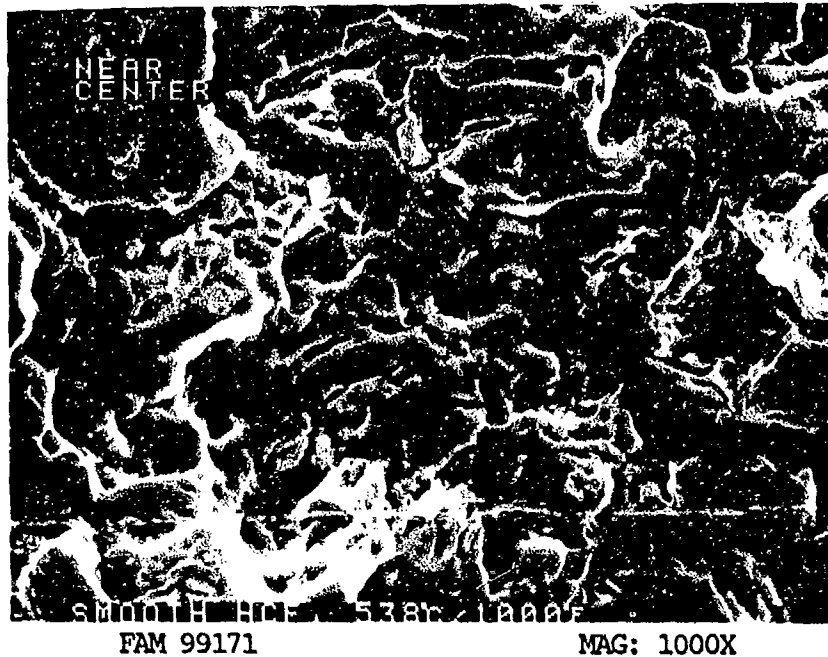


FIGURE 12-59: Oxidized crack-like fatigue striations near the center of the specimen (end of fatigue thumbnail). The direction of propagation is from the bottom to the top of the photograph. Compare these striations with those near the origin (Figure 12-58).



FIGURE 12-60: Higher magnification view of the oxidized crack-like striations shown in Figure 12-59.

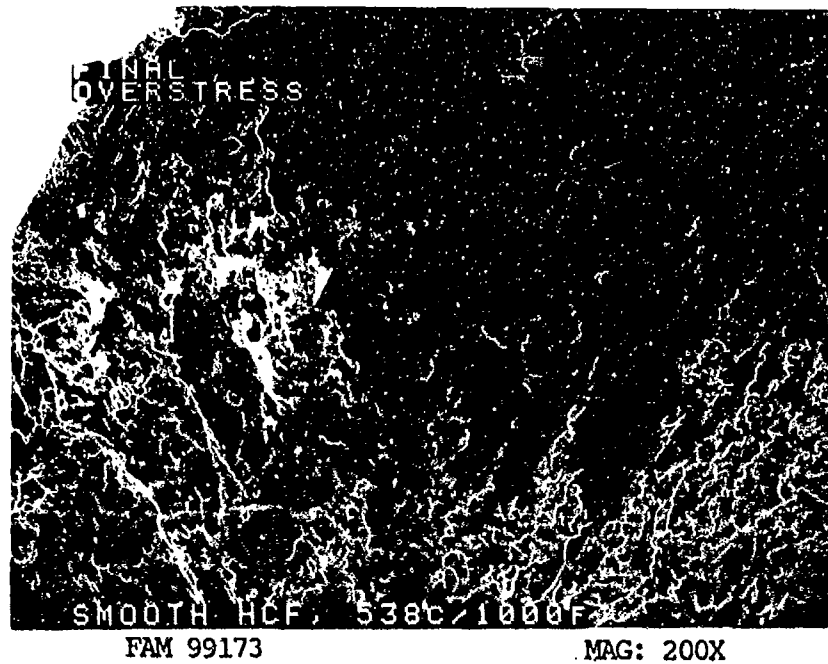


FIGURE 12-61: Mixture of overstress and smear features in the final overstress area.

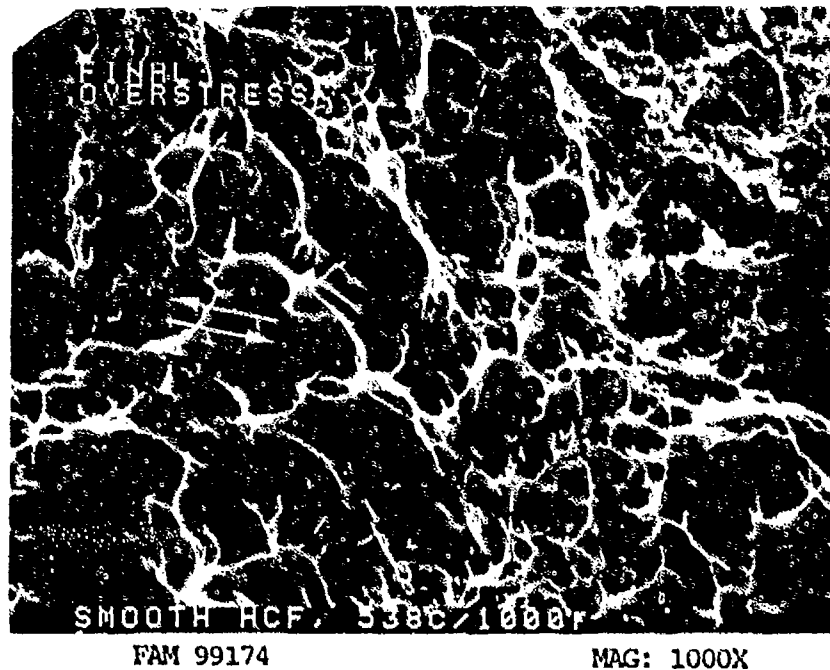


FIGURE 12-62: Higher magnification photograph of the area shown in Figure 12-61, showing shear dimples in the final overstress area. Arrows indicate the directions of relative motion.

MATERIAL

Ti-6Al-2Sn-4Zr-2Mo
PWA 1224 Bar

TEST DATA

TEST TYPE

Notched HCF

TEST CONDITIONS

Stress: 413.7 MPa (60.0 ksi)/-413.7 MPa (-60.0 ksi)
Stress Ratio: -1
Frequency: 1800 cpm
Atmosphere: Air
Temperature: Room Temperature
Test Direction: Longitudinal

TEST RESULTS

Cycles to Fracture: 28,400



FAL 93822

MAG: 11X

FIGURE 12-63: Test results and fractography of Ti-6-2-4-2 room temperature notched HCF test. The fatigue progression area extends over 85% of the fracture surface. The fatigue propagated from multiple surface origins (bottom of the photograph). The extent of the fatigue is shown by arrowheads.



FAM 100190

MAG: 100X



FAM 100191

MAG: 100X

FIGURE 12-64: Optical photomicrographs showing the fatigue progression zone, exhibiting a transgranular fracture path perpendicular to the stress axis (top). The bottom photograph shows a well defined shear lip in the final overstress area.

Etchant: Kroll's Reagent

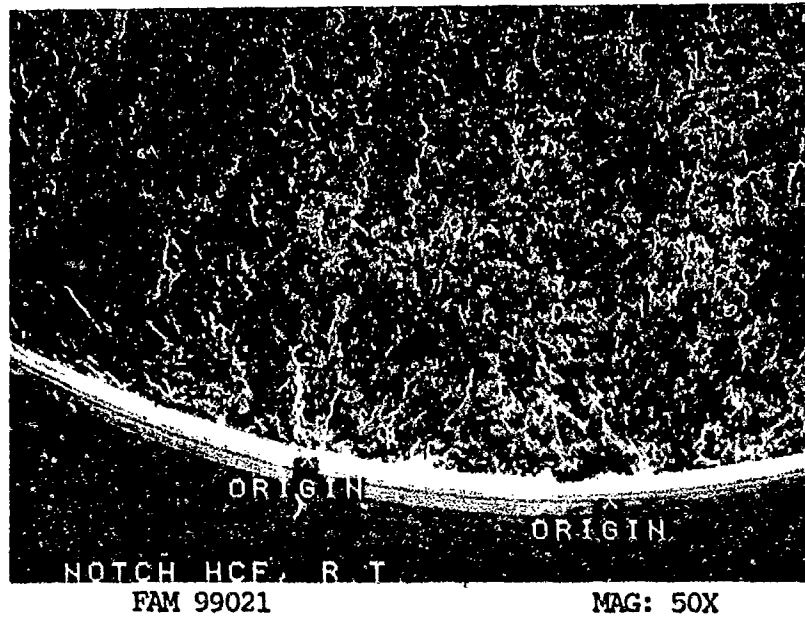


FIGURE 12-65: Low magnification view of the origin area. The specimen exhibited two surface origins. Features can be seen radiating from each origin.

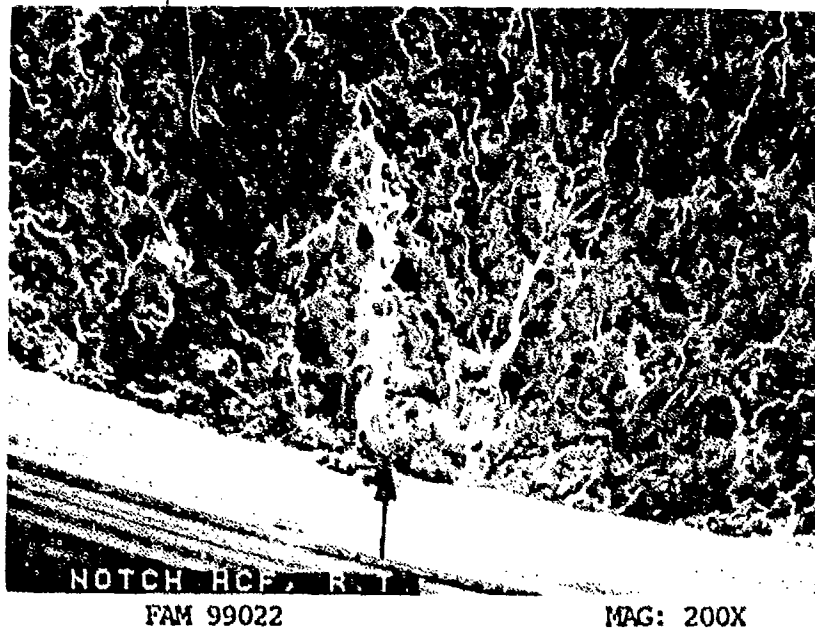


FIGURE 12-66: Higher magnification view of one of the origins (arrow). Machining marks are visible adjacent to the origin. Features can be seen radiating from the origin.

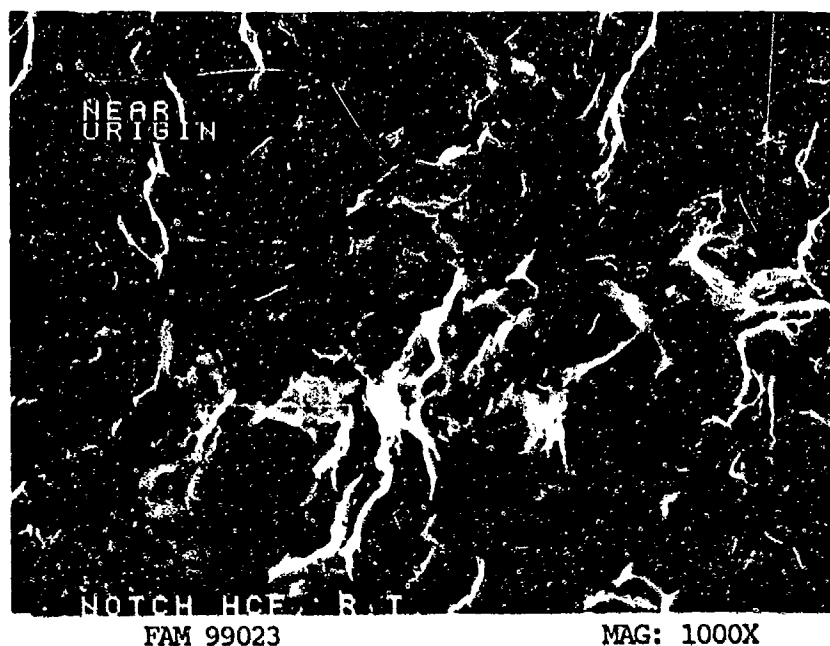


FIGURE 12-67: Remnant fatigue striations near the origin.

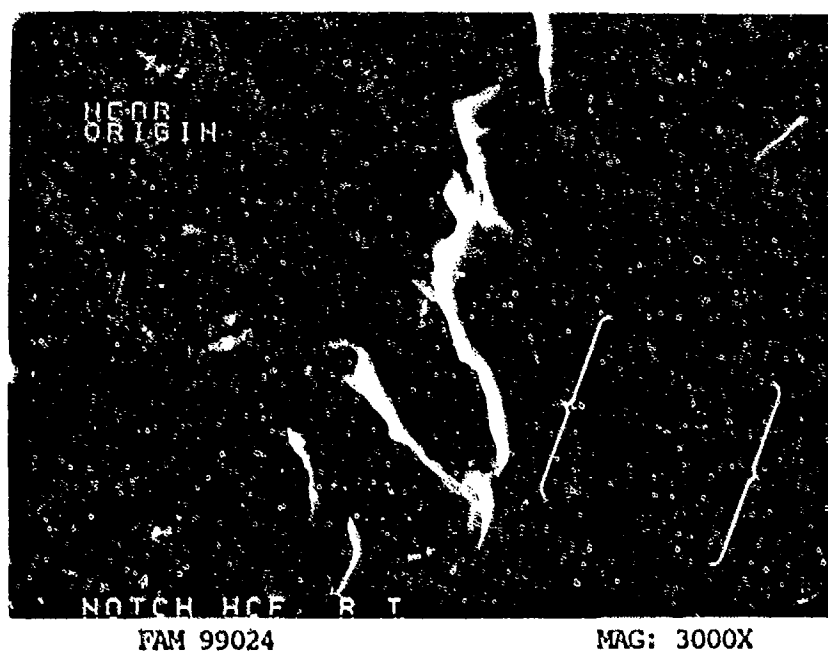


FIGURE 12-68: Higher magnification view of Figure 12-67, showing remnant fatigue striations (brackets, right) and smear features (left).

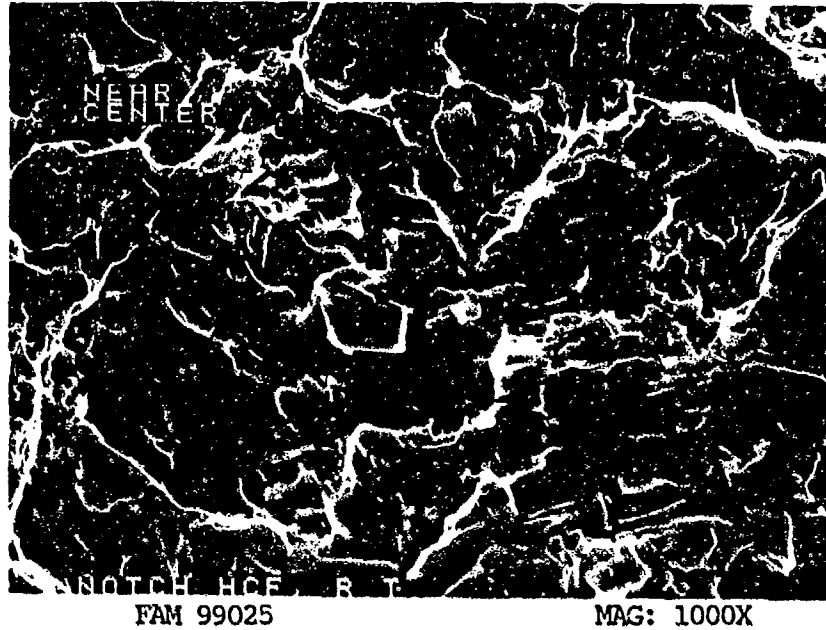


FIGURE 12-69: Mixture of fatigue striations and crack-like striations near the center of the specimen in the fatigue progression area. The fatigue is propagating from bottom to top of the photograph.

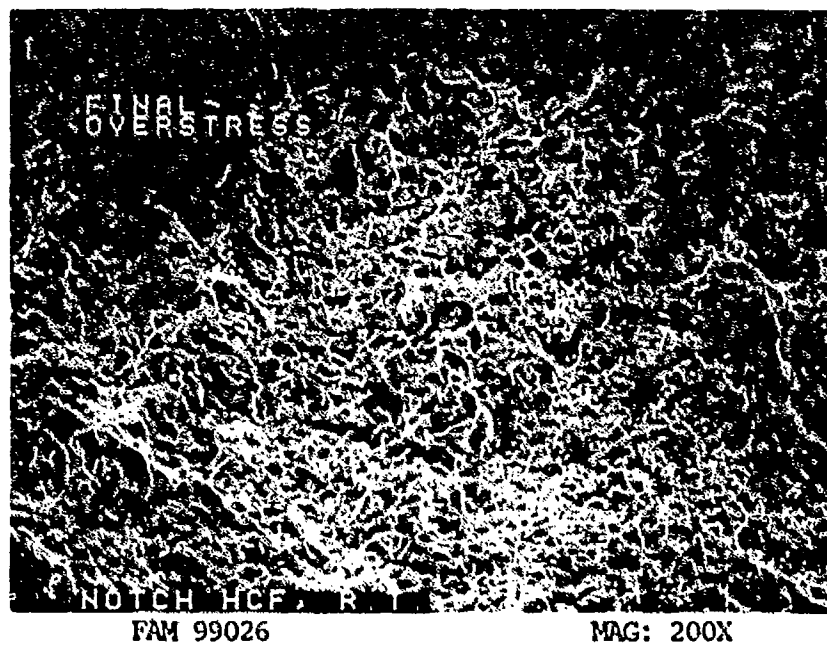


FIGURE 12-70: Final overstress area exhibiting dimpled overstress.

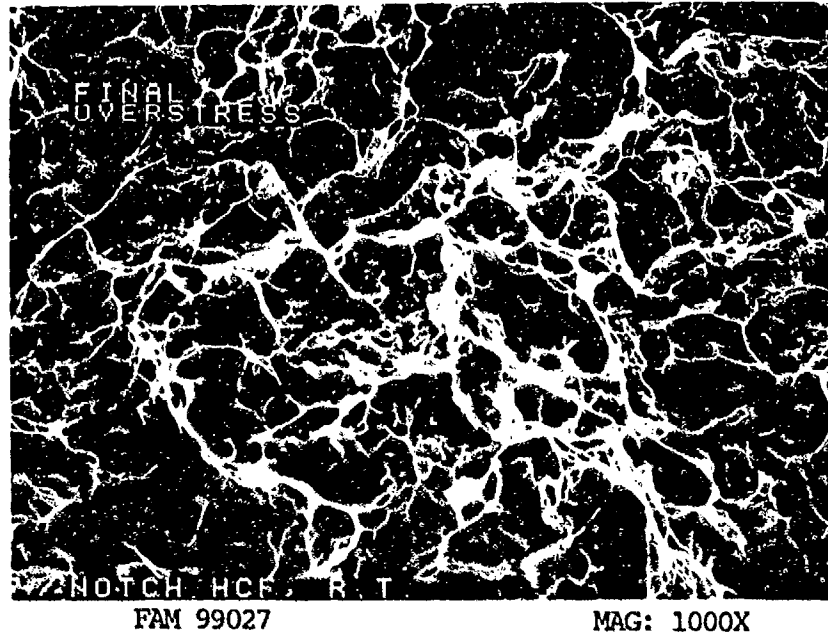


FIGURE 12-71: Higher magnification photograph of the final overstress area shown in Figure 12-70 exhibiting dimpled overstress.

MATERIAL

Ti-6Al-2Sn-4Zr-2Mo
PWA 1224 Bar

TEST DATA

TEST TYPE

Notched HCF

TEST CONDITIONS

Stress: 344.7 MPa (50.0 ksi)/-344.7 MPa (-50.0 ksi)
Stress Ratio: -1
Frequency: 1800 cpm
Atmosphere: Air
Temperature: 260°C (500°F)
Test Direction: Longitudinal

TEST RESULTS

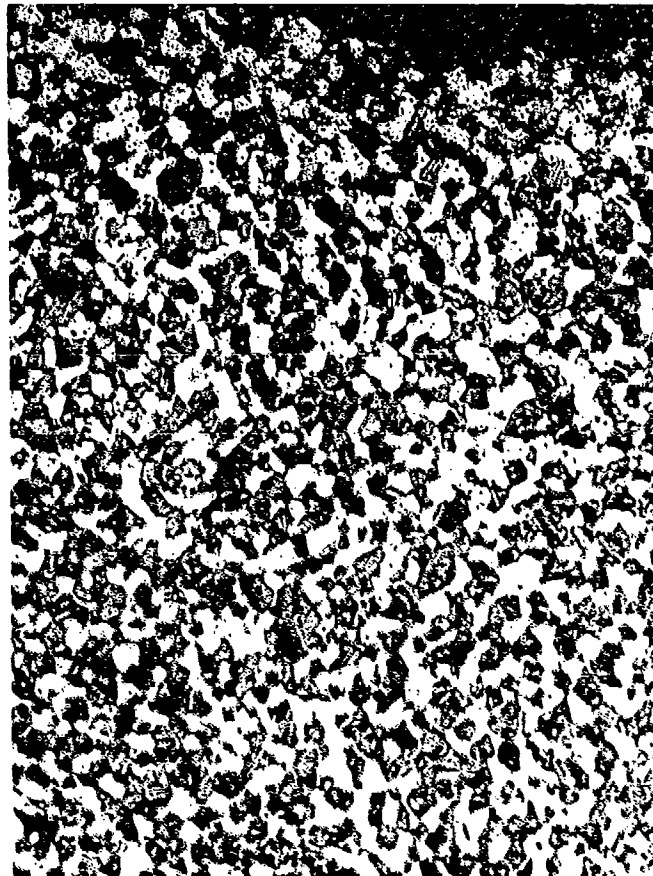
Cycles to Fracture: 19,400



FAL 93820

MAG: 11X

FIGURE 12-72: Test results and fractography of Ti-6-2-4-2 260°C (500°F) notched HCF test. The extent of the fatigue is delineated by a bracket. A shear lip is visible in the final fracture area.



FAM 99776

MAG: 200X

FIGURE 12-73: Optical photomicrograph showing the fatigue progression zone, exhibiting a mixture of transgranular and intergranular fracture.

Etchant: Kroll's Reagent

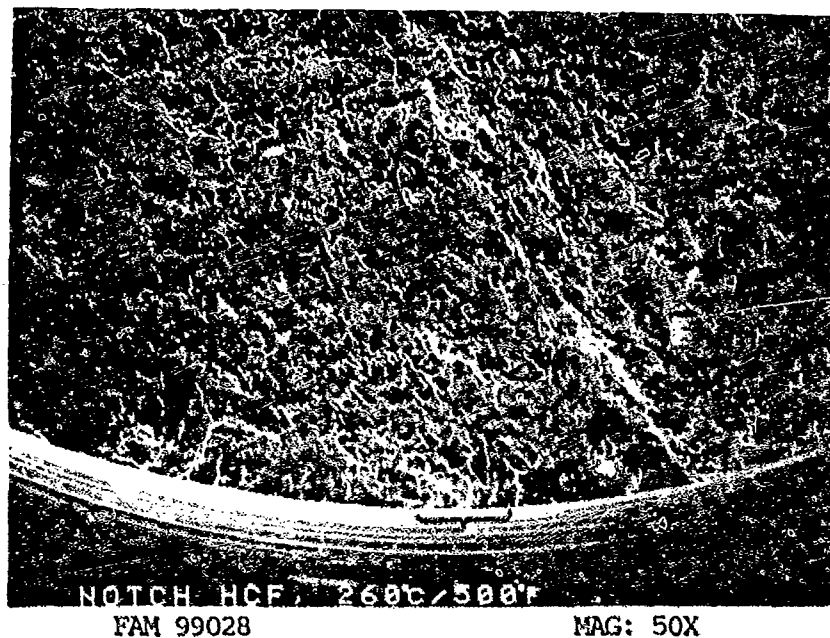


FIGURE 12-74: Low magnification view of the origin area and initial fatigue progression area. The diffuse origin area is shown by a bracket.

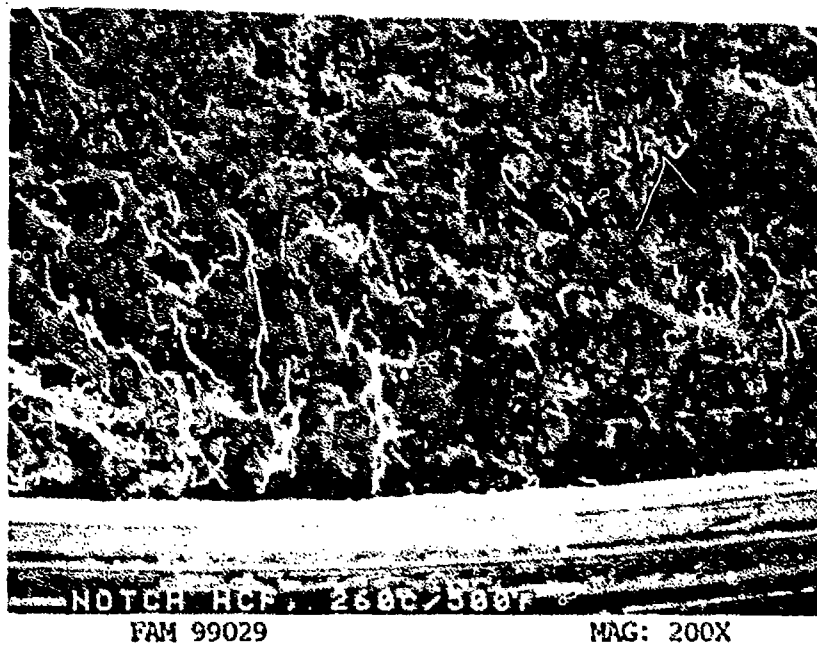


FIGURE 12-75: Higher magnification view of the origin area shown in Figure 12-74. The features are relatively flat with no localized origin discernible. Machining marks are visible adjacent to the origin area (bottom).

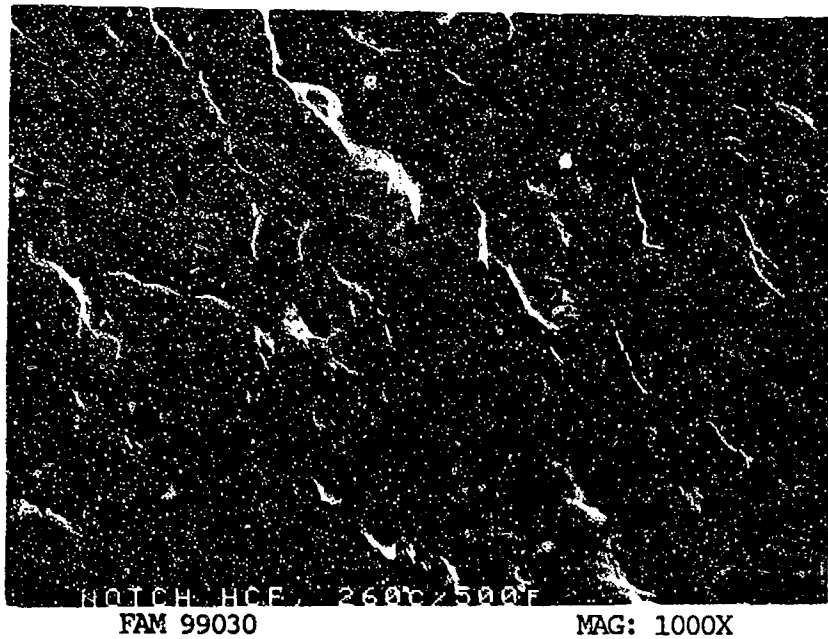


FIGURE 12-76: Remnant fatigue features near the origin area. The fracture propagated from bottom to top of the photograph.



FIGURE 12-77: Higher magnification photograph of the area shown in Figure 12-76, showing remnant fatigue striations near the origin area. The direction of propagation is from bottom to top of the photograph.

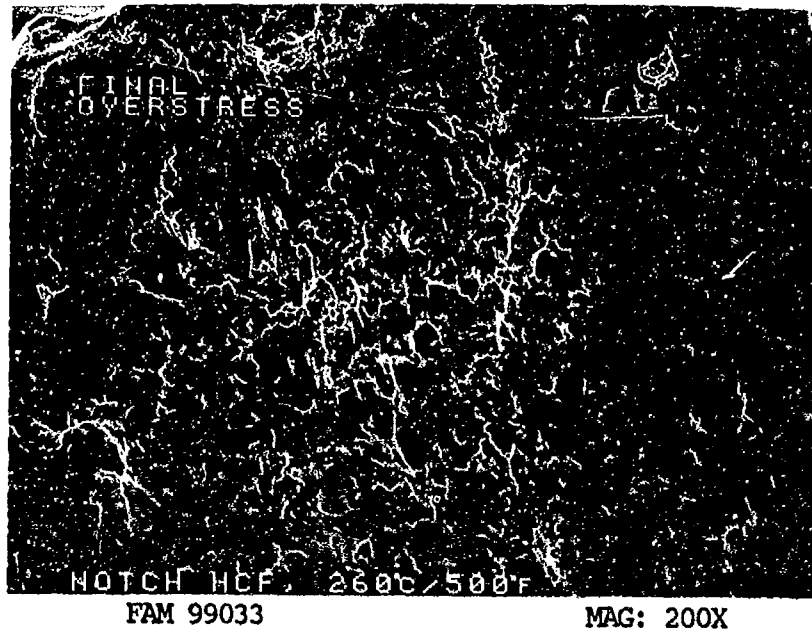


FIGURE 12-78: Mixture of overstress and smear features in the final overstress area.

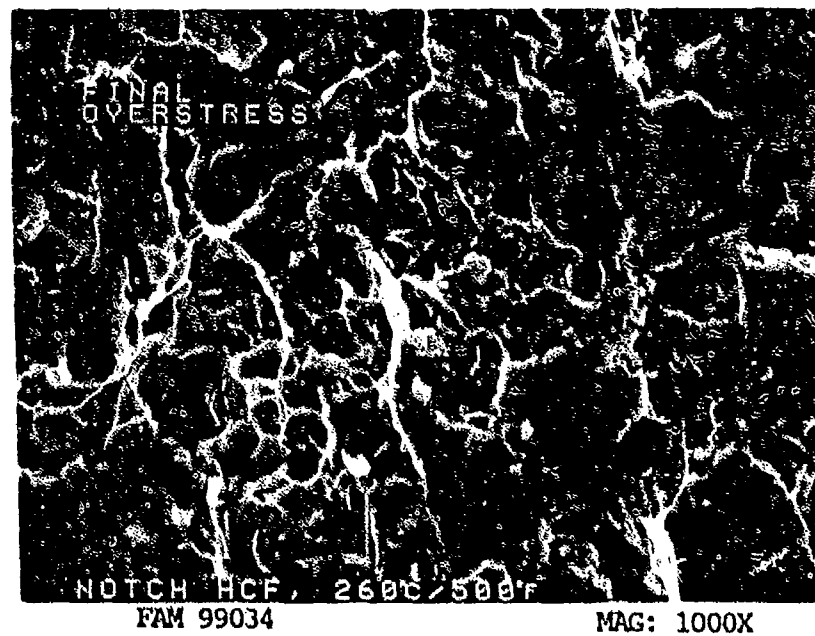


FIGURE 12-79: Higher magnification photograph showing equiaxed dimples and smear features in the final overstress area (Figure 12-78).

MATERIAL

Ti-6Al-2Sn-4Zr-2Mo
PWA 1224 Bar

TEST DATA

TEST TYPE

Notched HCF

TEST CONDITIONS

Stress: 275.8 MPa (40.0 ksi)/-275.8 MPa (-40.0 ksi)
Stress Ratio: -1
Frequency: 1800 cpm
Atmosphere: Air
Temperature: 538°C (1000°F)
Test Direction: Longitudinal

TEST RESULTS

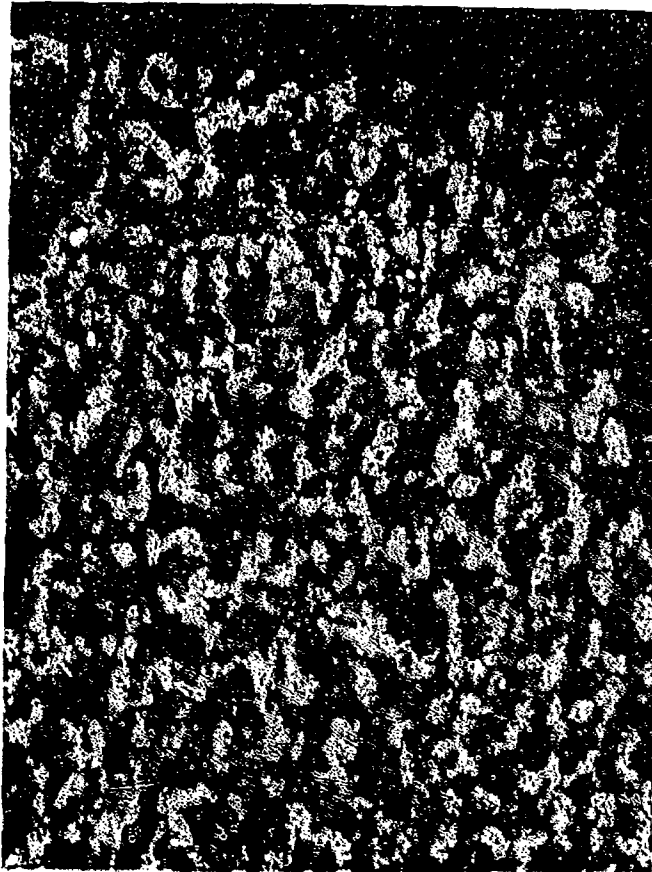
Cycles to Fracture: 14,000



FAL 93819

MAG: 11X

FIGURE 12-80: Test results and fractography of Ti-6-2-4-2 538°C (1000°F) notched HCF test. The extent of the fatigue is shown by a bracket. A fatigue step (arrow) separates two origins.



FAM 99762

MAG: 200X

FIGURE 12-81: Optical photomicrograph showing the fatigue progression zone exhibiting predominantly transgranular fracture path. No grain deformation is visible.

Etchant: Kroll's Reagent

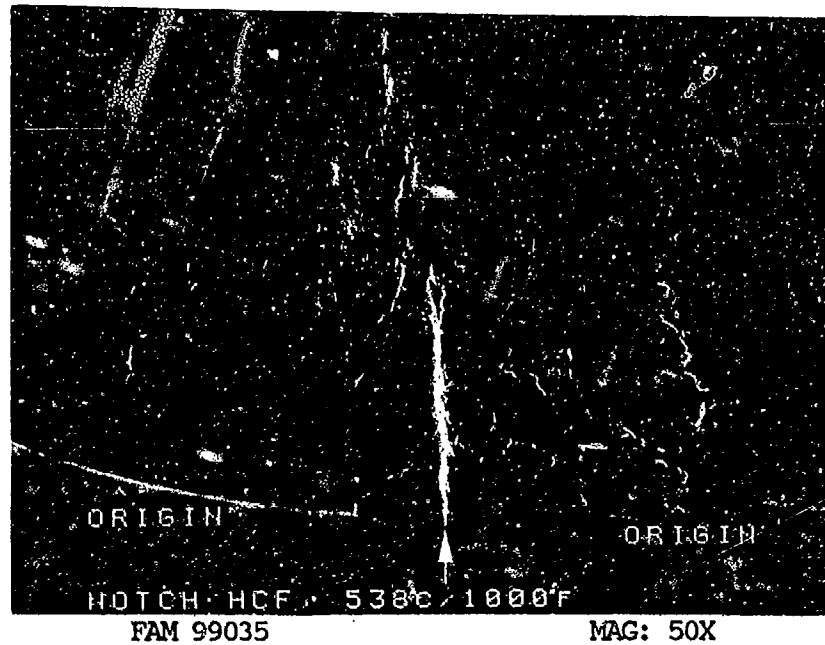


FIGURE 12-82: Low magnification view of the origin area and initial fatigue progression area. Two origins are clearly visible separated by a fatigue step (arrow).

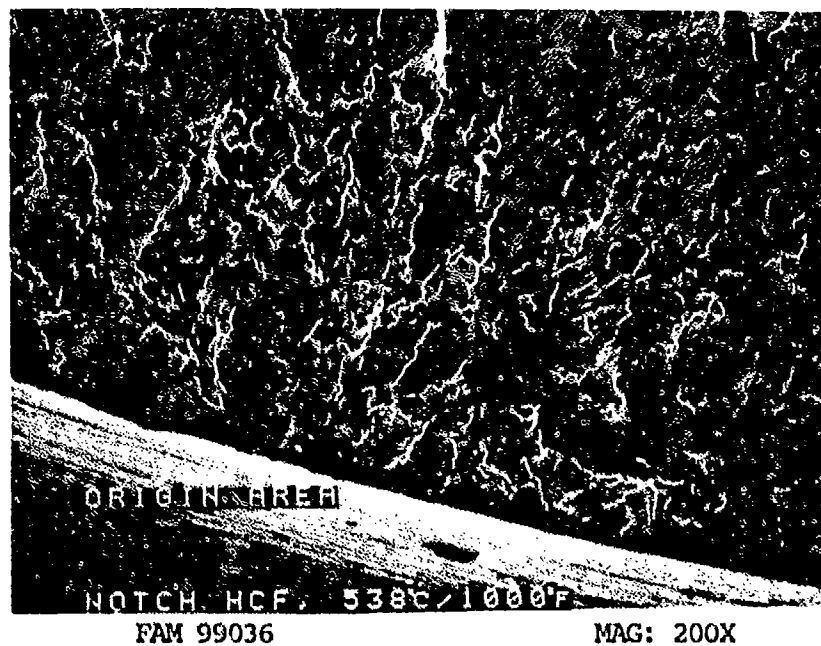


FIGURE 12-83: Higher magnification view of one origin area. Fatigue features can be seen radiating from the origin. Machining marks are visible on the specimen surface adjacent to the origin. These probably did not contribute to the fracture.

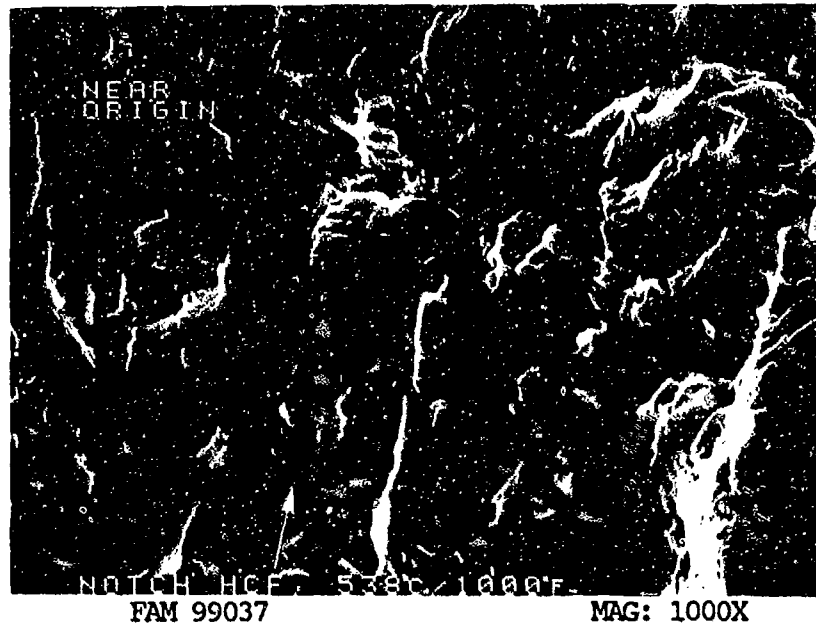


FIGURE 12-84: Fine fatigue striations near the origin. The fracture propagated from bottom to top of the photograph. Arrow indicates a patch of remnant striations.

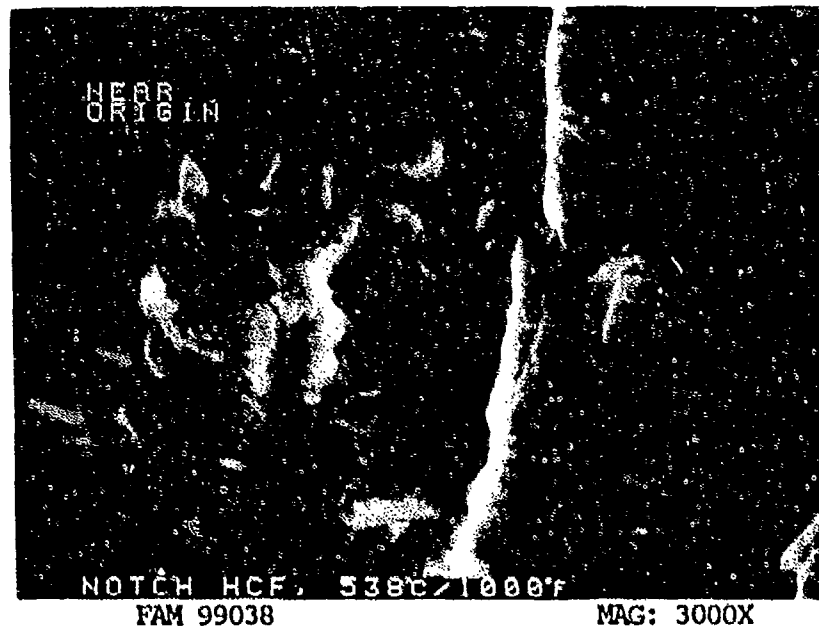


FIGURE 12-85: High magnification view of the fine striations shown in Figure 12-84. Individual striations are barely resolvable. Bracket contains five striations.

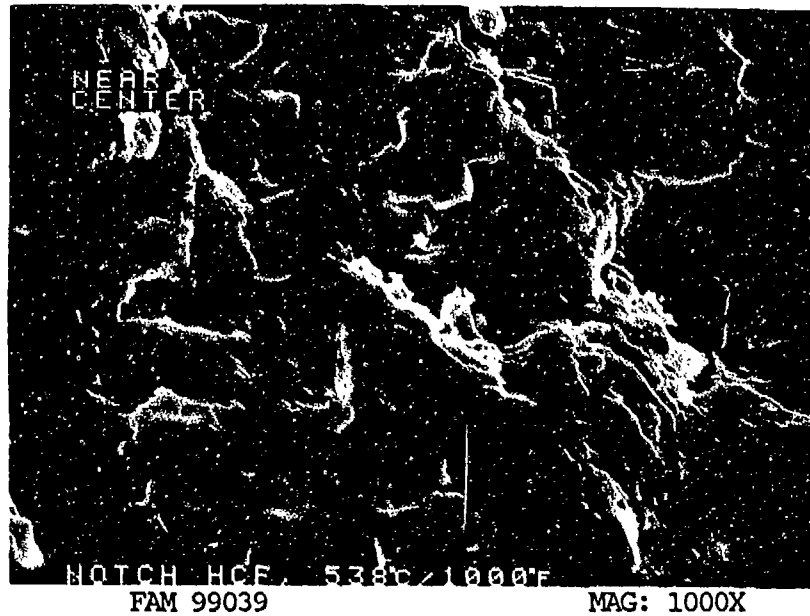


FIGURE 12-86: Oxidized striations near the center of the specimen (end of thumbnail). The striations are slightly coarser than near the origin. The direction of propagation is from the bottom to top of the photograph.

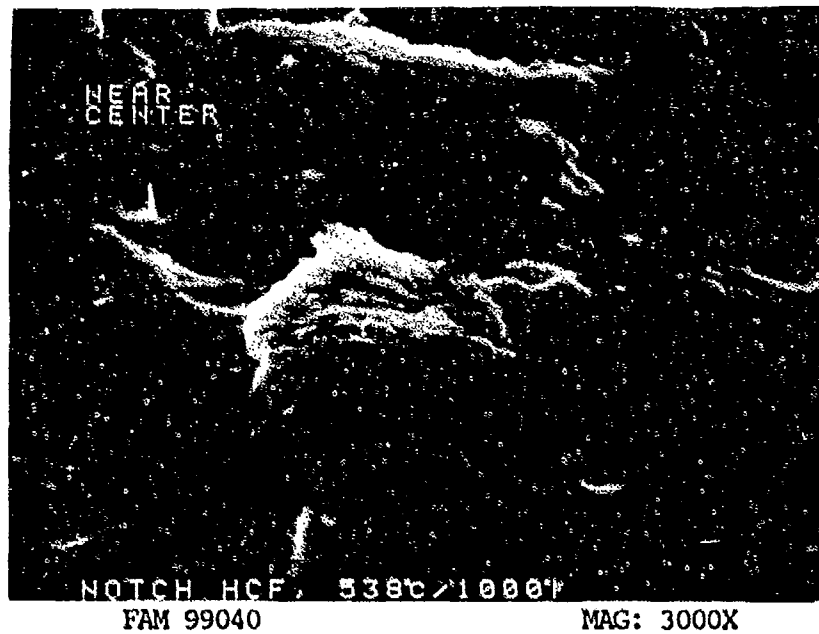


FIGURE 12-87: Higher magnification view of the oxidized striations shown in Figure 12-84.

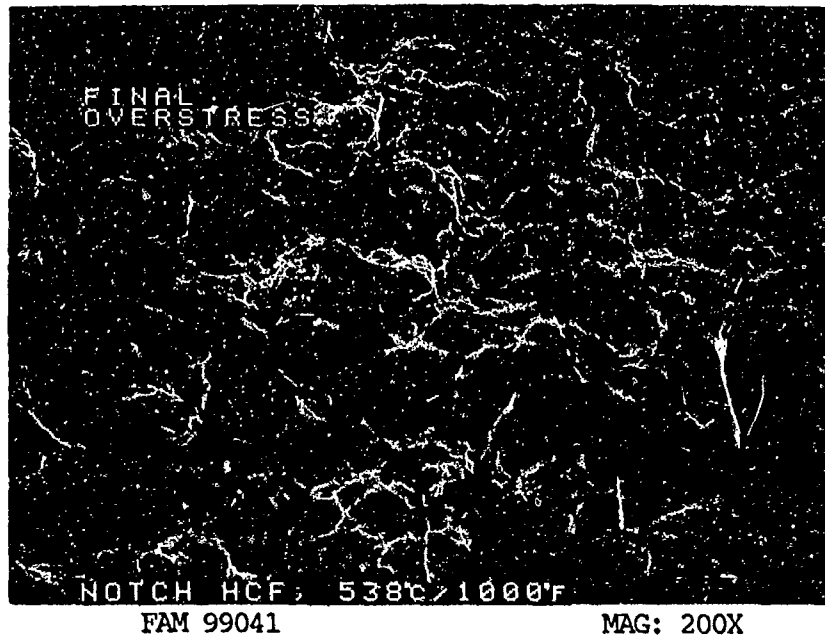


FIGURE 12-88: Dimpled overstress features in the final overstress area.

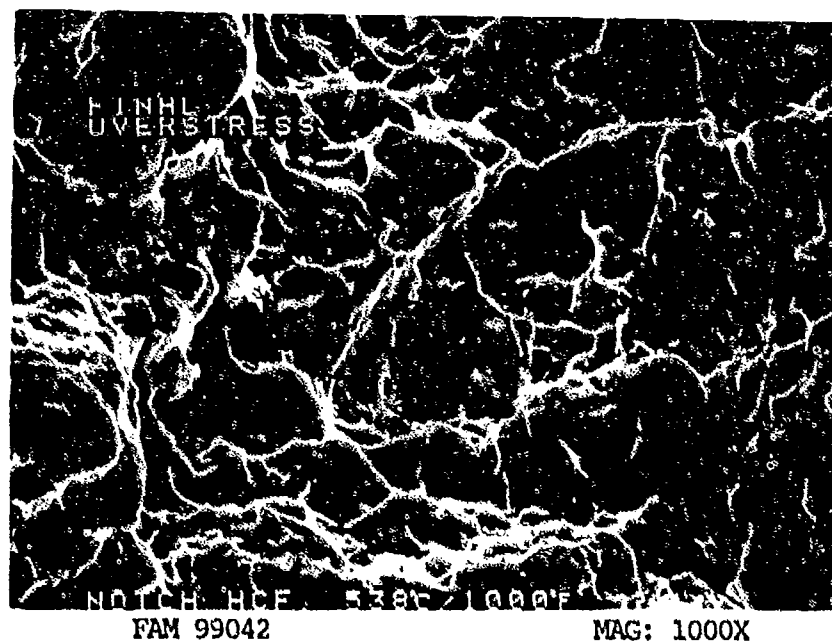


FIGURE 12-89: Higher magnification photograph of a portion of Figure 12-86, showing dimples and other ductile features in the final overstress area.

MATERIAL

Ti-6Al-2Sn-4Zr-2Mo
FWA 1224 Bar

TEST DATA

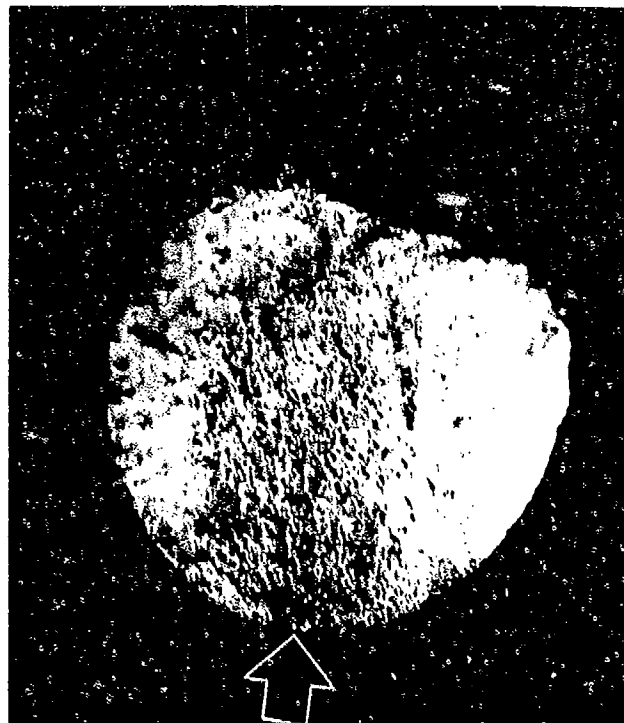
TEST TYPE
Smooth LCF

TEST CONDITIONS

Stress: 655 MPa (95.0 ksi)/ 32.4 MPa (4.8 ksi)
Stress Ratio: 0.05
Frequency: 10 cpm
Atmosphere: Air
Temperature: 260°C (500°F)
Test Direction: Longitudinal

TEST RESULTS

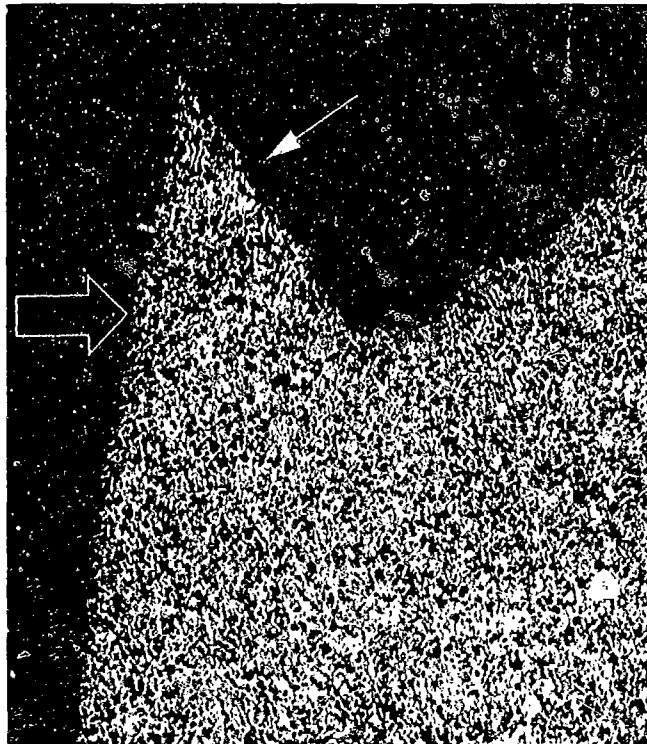
Cycles to Fracture: 36,886



FAL 93235

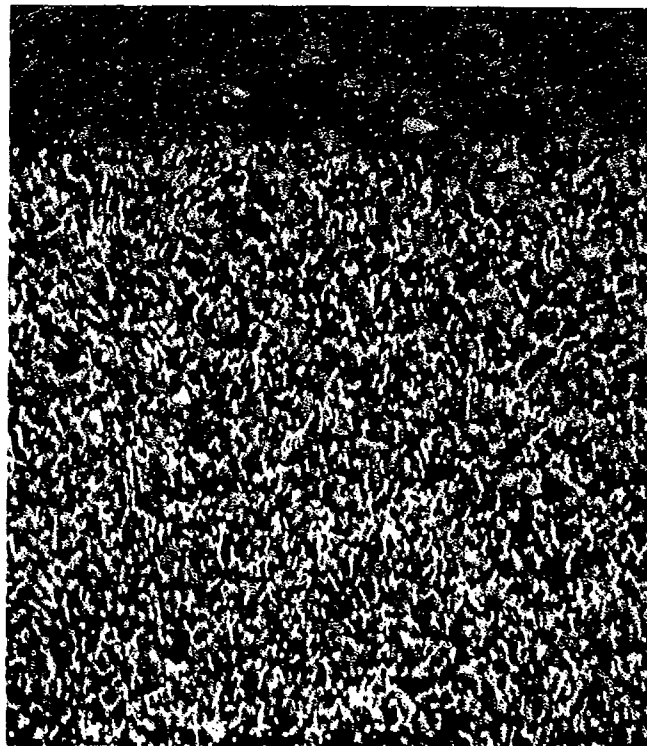
MAG: 9X

FIGURE 12-90: Test results and fractography of Ti-6-2-4-2 260°C (500°F) smooth LCF test. The origin area is indicated by an arrow. The fatigue progression area covers less than 30% of the fracture surface.



FAM 100197

MAG: 50X



FAM 100196

MAG: 100X

FIGURE 12-91: Optical photomicrographs showing necking (hollow arrow) and a well defined shear lip (arrow) in the final overstress area (top) and the fatigue progression area (bottom). No grain deformation is visible in the fatigue progression area.

Etchant: Kroll's Reagent

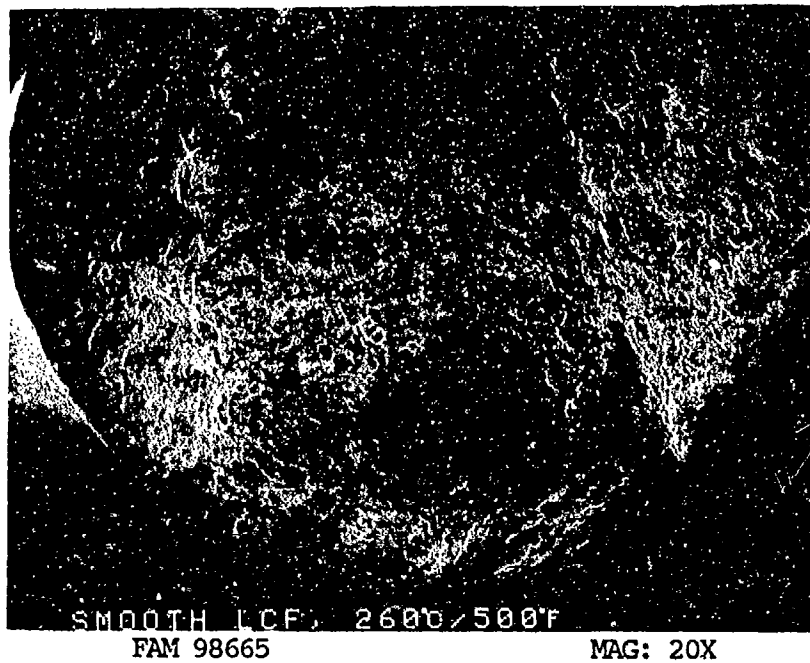


FIGURE 12-92: Overall photograph showing fatigue area on a plane perpendicular to the stress axis.

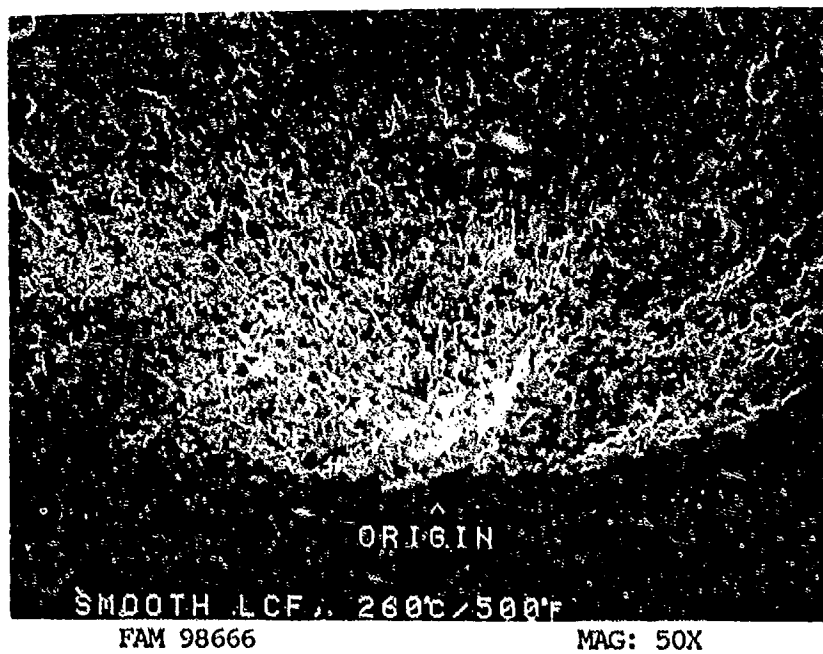


FIGURE 12-93: Fracture features can be seen radiating from the fatigue origin.

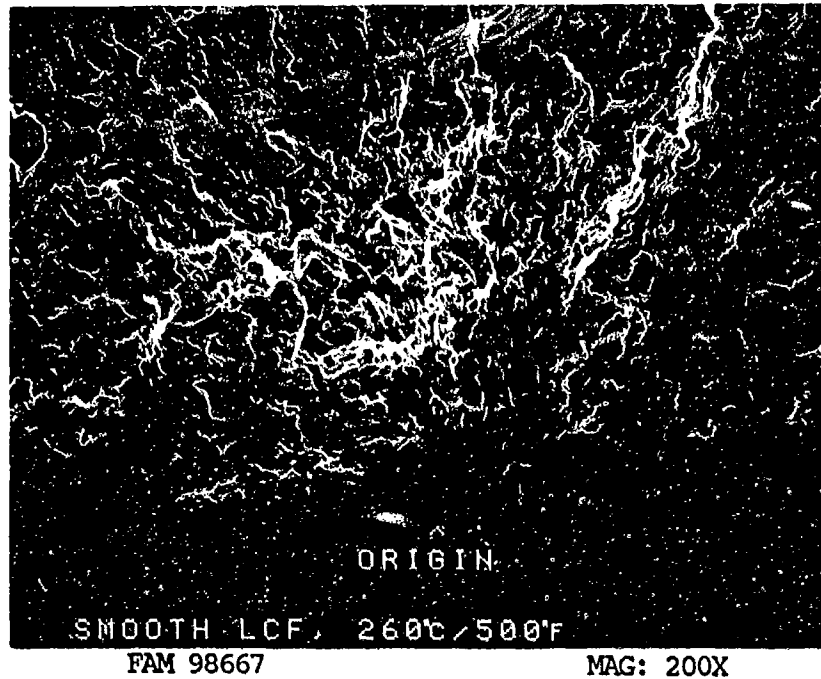


FIGURE 12-94: Higher magnification photograph of the origin area shown in Figure 12-92. Features can be seen radiating from the origin.



FIGURE 12-95: Remnant fatigue striations in the fatigue thumbnail region. An arrow indicates one patch. The direction of local propagation varies from one patch to another.

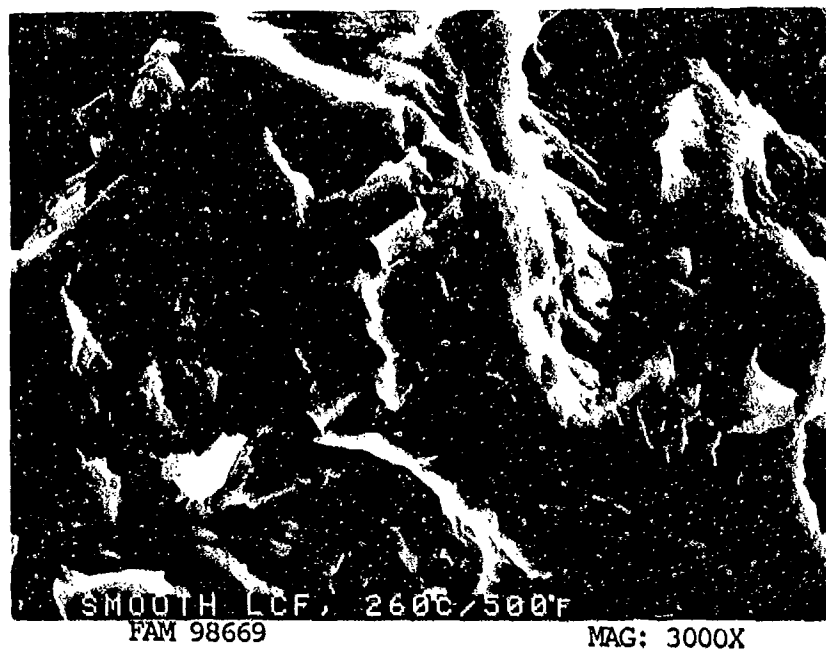


FIGURE 12-96: Higher magnification photograph of the area shown in Figure 12-94, showing remnant fatigue features.



FIGURE 12-97: High magnification photograph showing remnant fatigue striations. The direction of propagation is shown by an arrow.

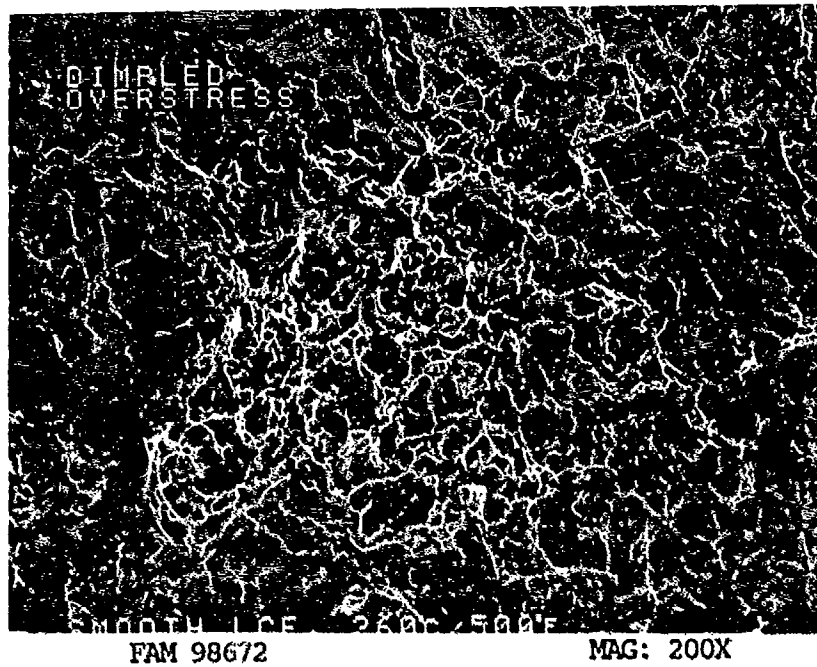


FIGURE 12-98: Equiaxed dimpled overstress in the final overstress area.

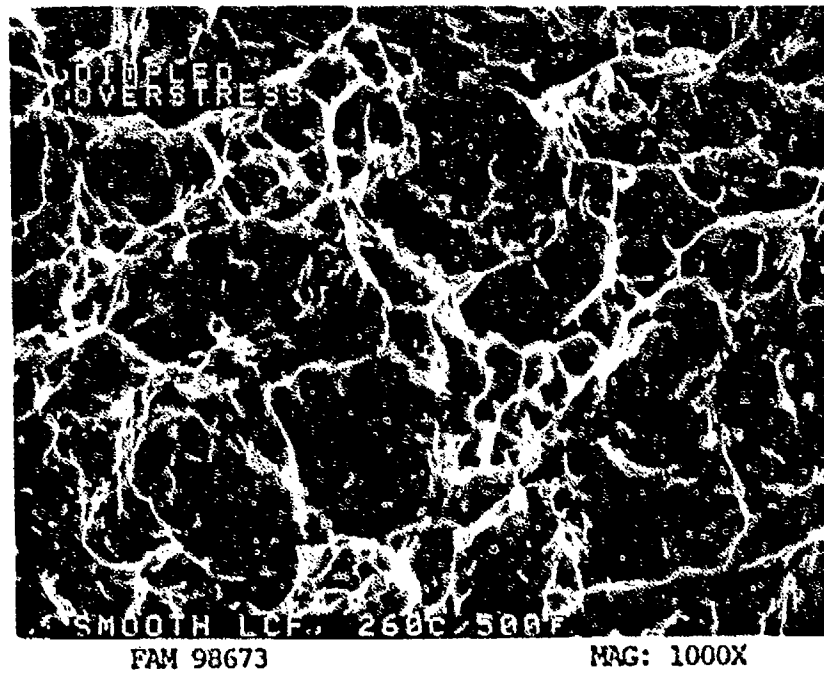


FIGURE 12-99: Higher magnification photograph showing equiaxed dimpled overstress in the final overstress area.

MATERIAL

Ti-6Al-2Sn-4Zr-2Mo
FWA 1224 Bar

TEST DATA

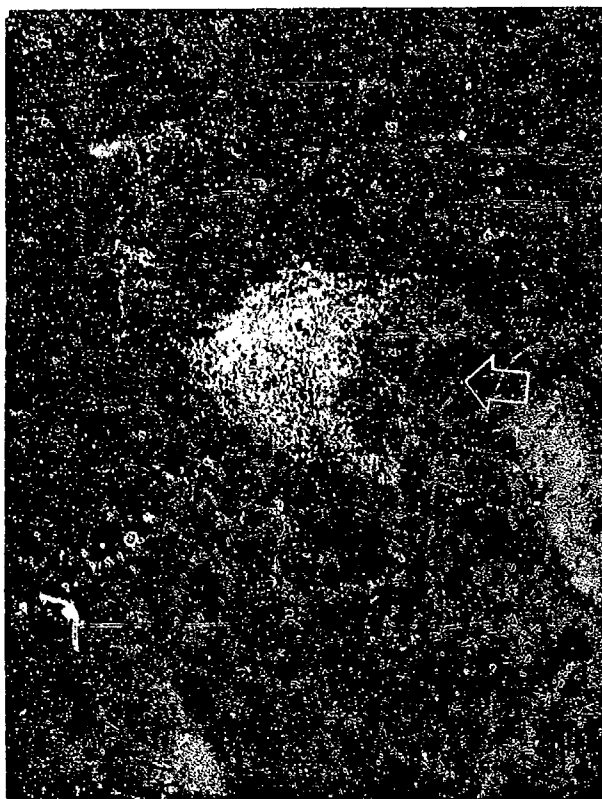
TEST TYPE
Smooth LCF

TEST CONDITIONS

Stress: 517.1 MPa (75.0 ksi)/ 25.5 MPa (3.7 ksi)
Stress Ratio: 0.05
Frequency: 10 cpm
Atmosphere: Air
Temperature: 538°C (1000°F)
Test Direction: Longitudinal

TEST RESULTS

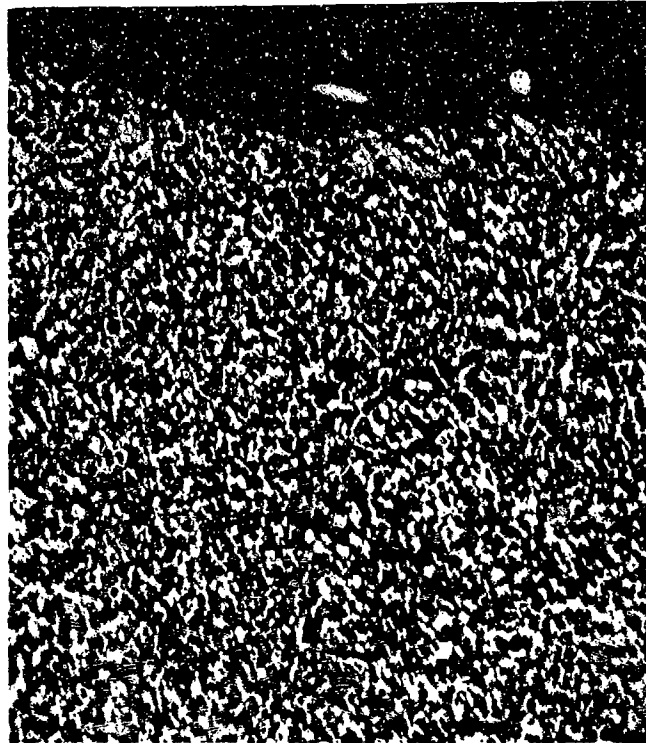
Cycles to Fracture: 37,000



FAL 93213

MAG: 9X

FIGURE 12-100: Test results and fractography of Ti-6-2-4-2 538°C (1000°F) smooth LCF test. The origin and fracture progression areas (arrow) are on a plane perpendicular to the stress axis. The fatigue progression area accounts for less than 30% of the fracture surface.



FAM 100194

MAG: 100X



FAM 100195

MAG: 100X

FIGURE 12-101: Optical photomicrographs showing the fatigue progression area (top) and the shear lip in the final overstress area (bottom). Grain deformation is visible in the final overstress area (arrow).

Etchant: Kroll's Reagent

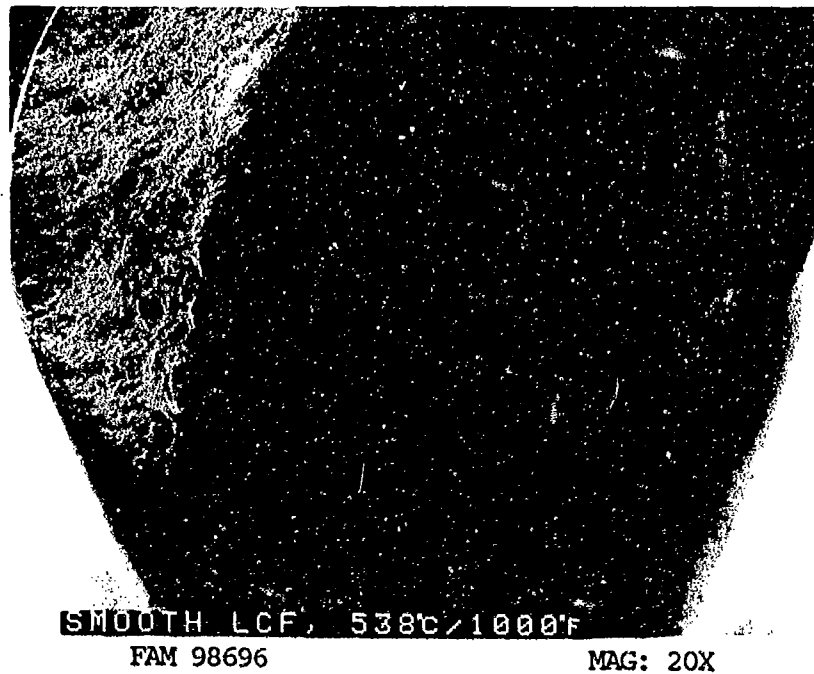


FIGURE 12-102: Overall photograph showing the origin area and fatigue thumbnail (brackets). The fatigue progression area is on a plane perpendicular to the stress axis.

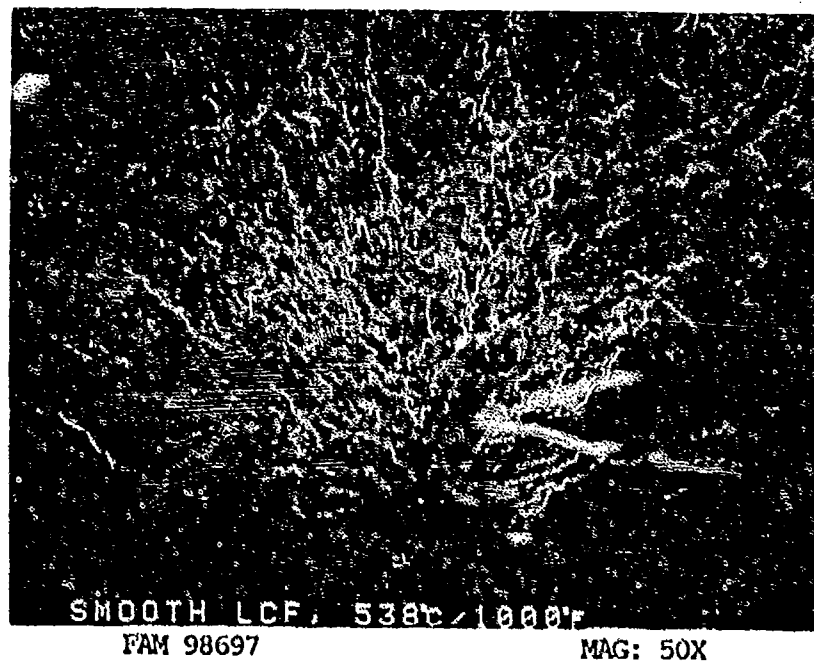


FIGURE 12-103: Fracture features can be seen radiating from the origin (arrow).

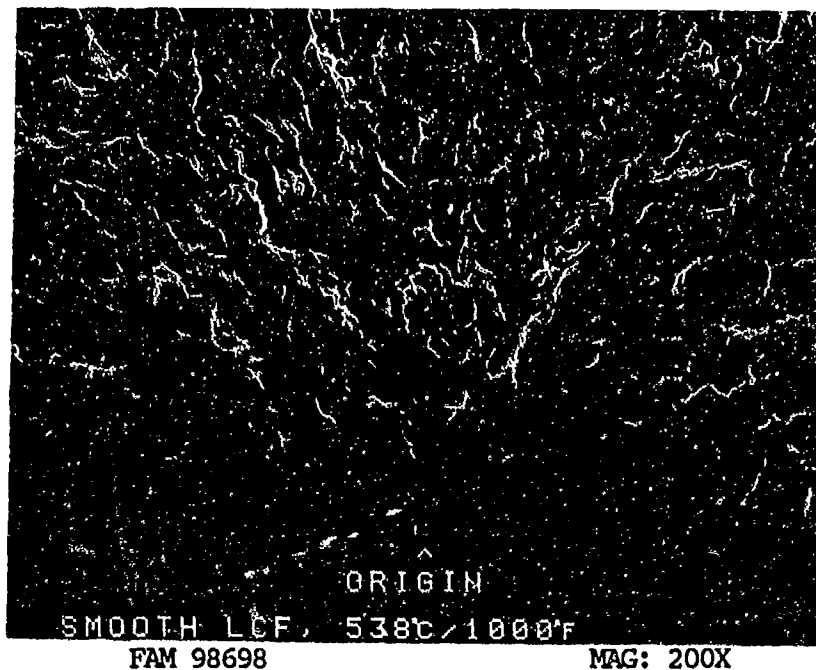


FIGURE 12-104: Close-up photograph of the origin (arrow). Features radiate from the localized origin.

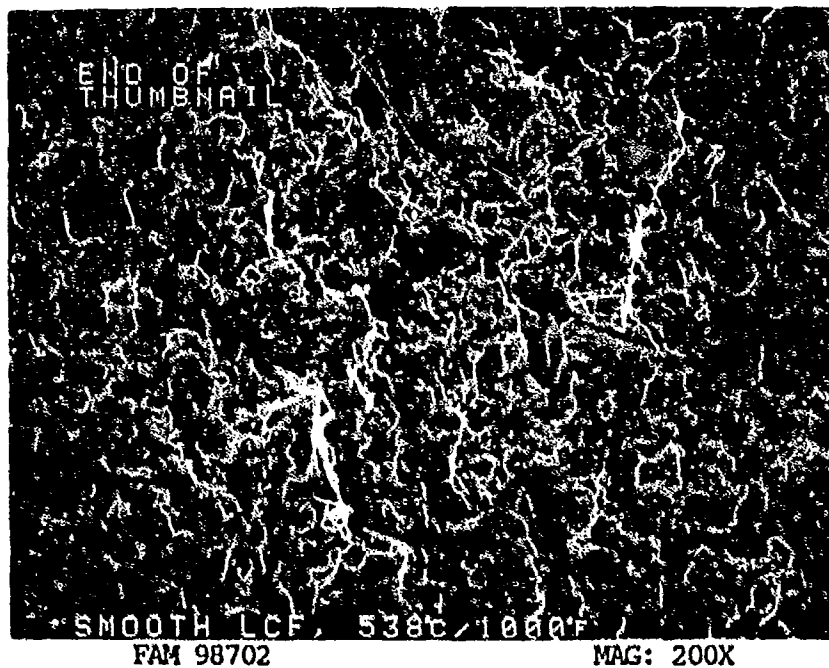


FIGURE 12-105: End of the fatigue thumbnail exhibits striations and crack-like striations.

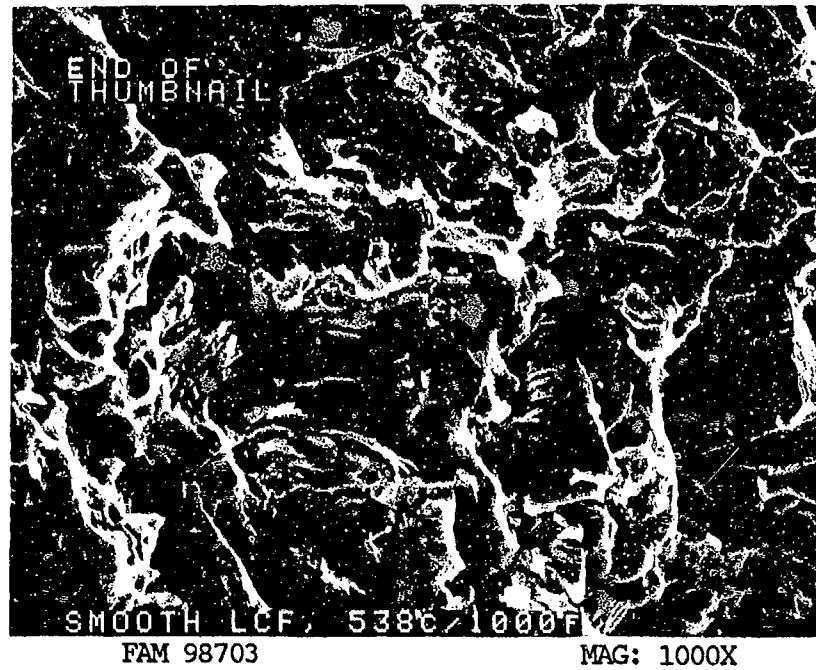


FIGURE 12-106: Crack-like striations near the end of the fatigue thumbnail. The direction of propagation is from bottom to top of the photograph.

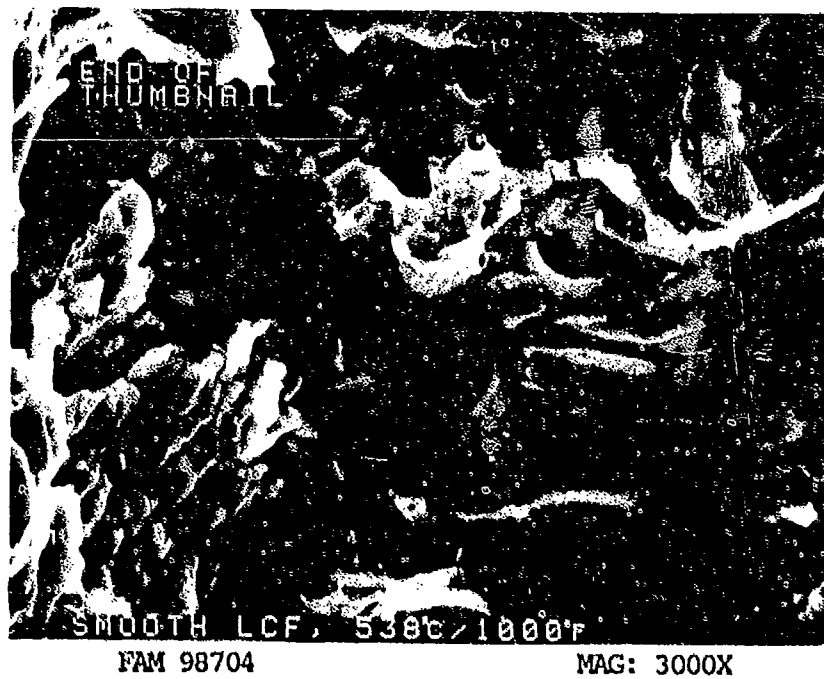


FIGURE 12-107: Higher magnification photograph of the area shown in Figure 12-106, showing crack-like striations with some secondary cracking.

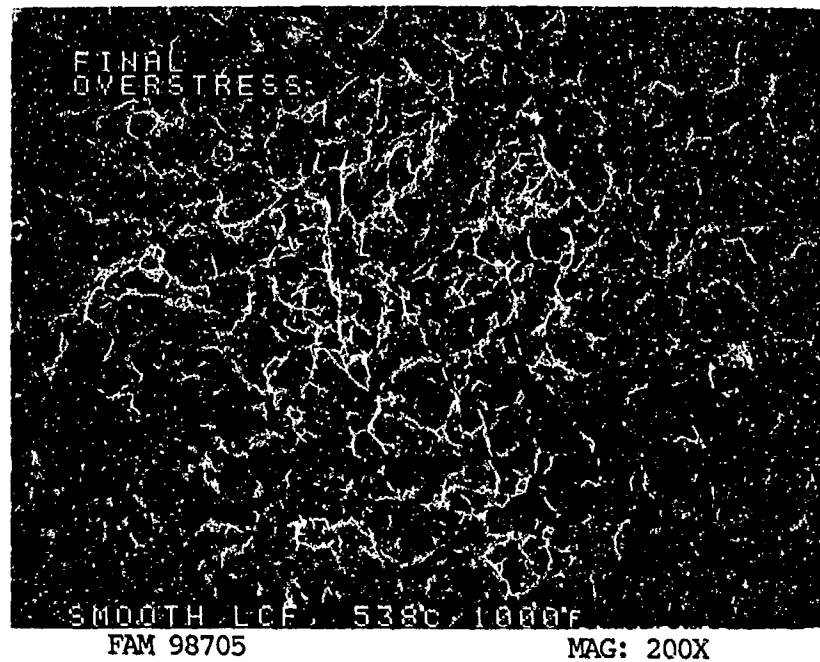


FIGURE 12-108: Equiaxed dimpled overstress in the final fracture area.

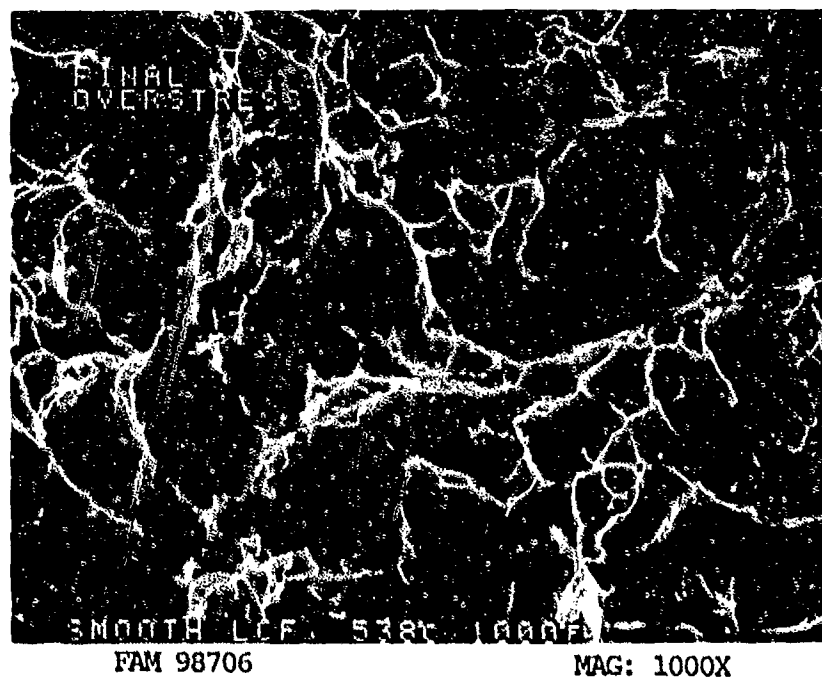


FIGURE 12-109: Higher magnification photograph showing equiaxed dimpled overstress in the final fracture area (Figure 12-108).

MATERIAL

Ti-6Al-2Sn-4Zr-2Mo
PWA 1224 Bar

TEST DATA

TEST TYPE

TMF, In-Phase

TEST CONDITIONS

Stress: 461.9 MPa (67 ksi)/537.8 MPa (-78 ksi)

Stress Ratio: -1.16

Frequency: 2 cpm

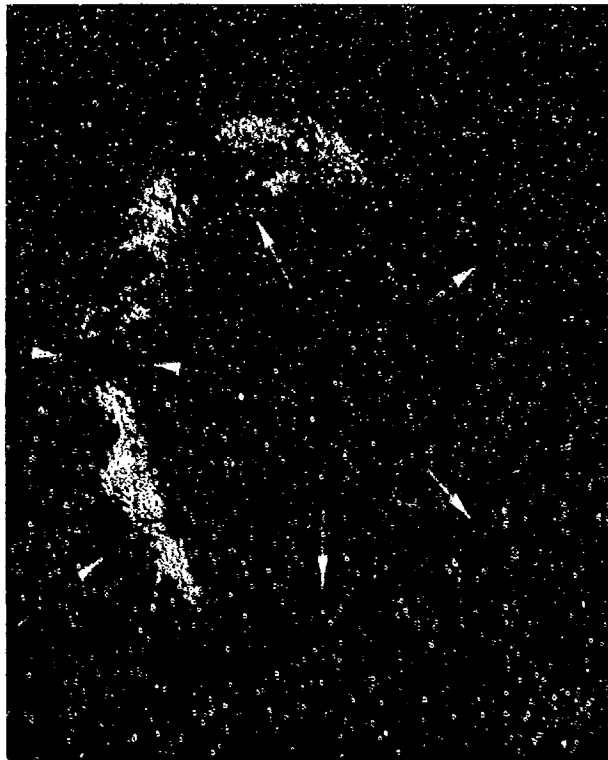
Atmosphere: Air

Temperature: 260°C (500°F)/538°C (1000°F)

Test Direction: Longitudinal

TEST RESULTS

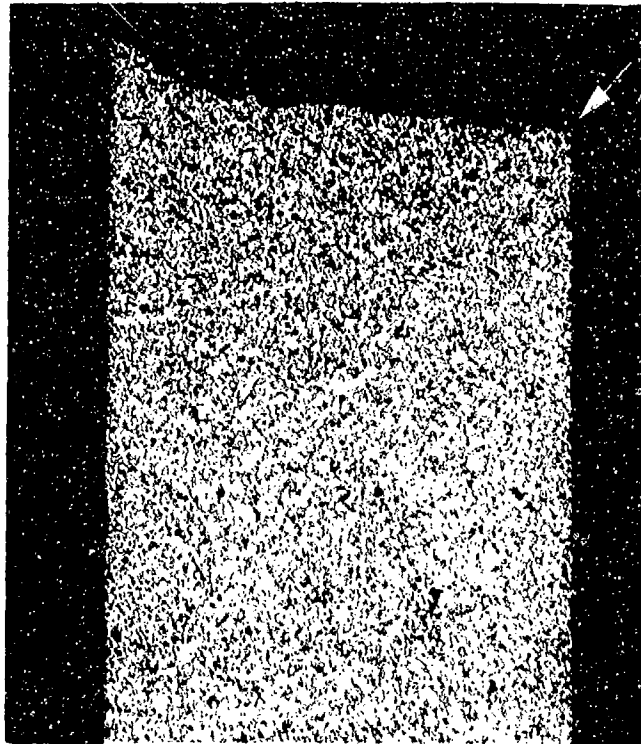
Cycles to Fracture: 8013



FAL 94529

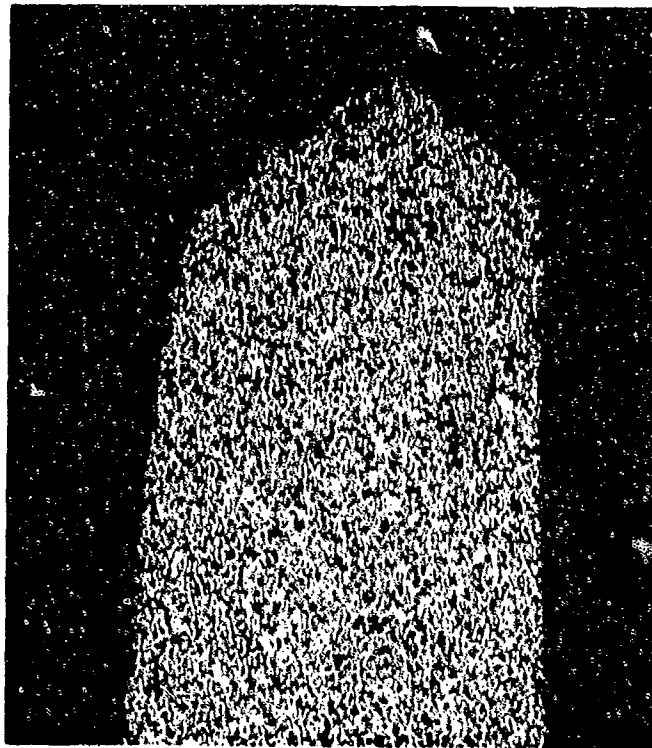
MAG: 10X

FIGURE 12-110: Test results and fractography of Ti-6-2-4-2 in-phase TMF test. Fatigue propagated from multiple origins on both the inside and outside surfaces of the specimen (arrows). The final overstress area appears to be unoxidized.



FAM 100192

MAG: 50X

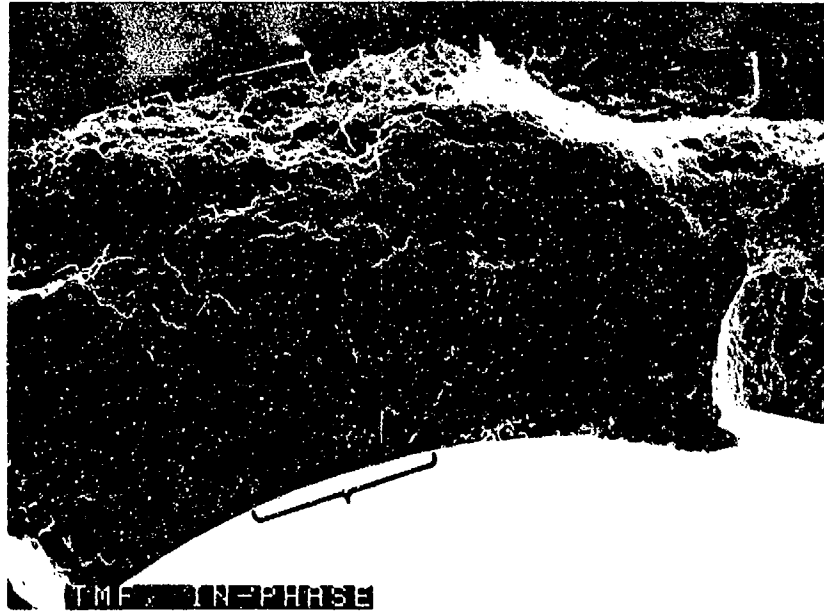


FAM 100193

MAG: 50X

FIGURE 12-111: Pair of optical photomicrographs of a longitudinal metallographic cross section through the two walls of the tubular specimen. The fatigue progressed from the inside surface (arrow) of the top photograph. The bottom photograph shows necking associated with final overstress on the side of the specimen opposite the fatigue.

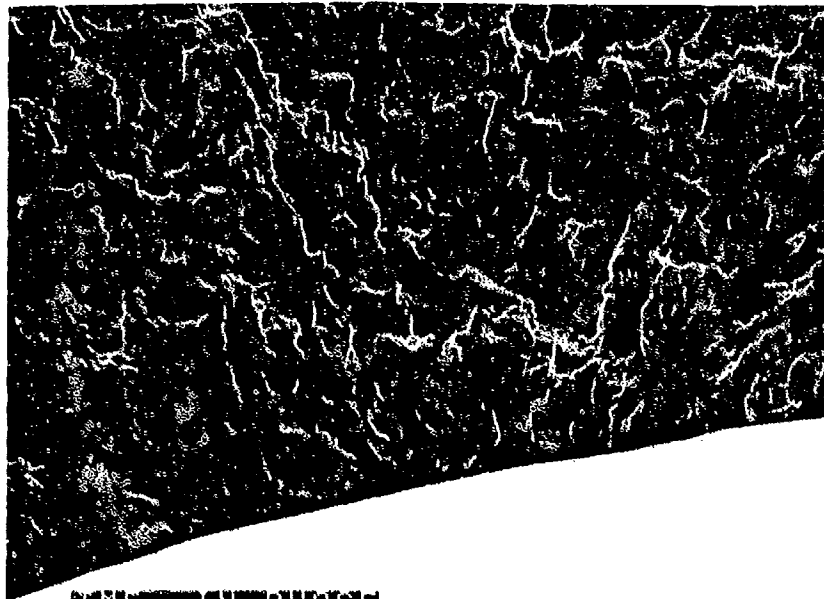
Etchant: Kroll's Reagent



FAM 99620

MAG: 50X

FIGURE 12-112: Low magnification photograph showing an origin area on the inside surface of the specimen (bracket) and the associated fatigue thumbnail.



FAM 99621

MAG: 200X

FIGURE 12-113: No localized origin can be identified in the origin area.

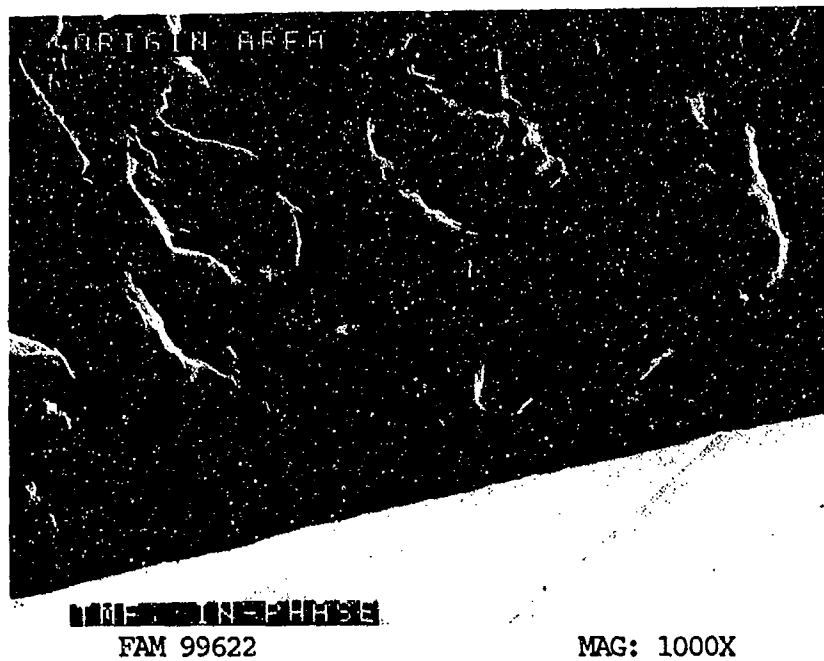


FIGURE 12-114: Close-up photograph of the origin area shown in Figure 12-113.

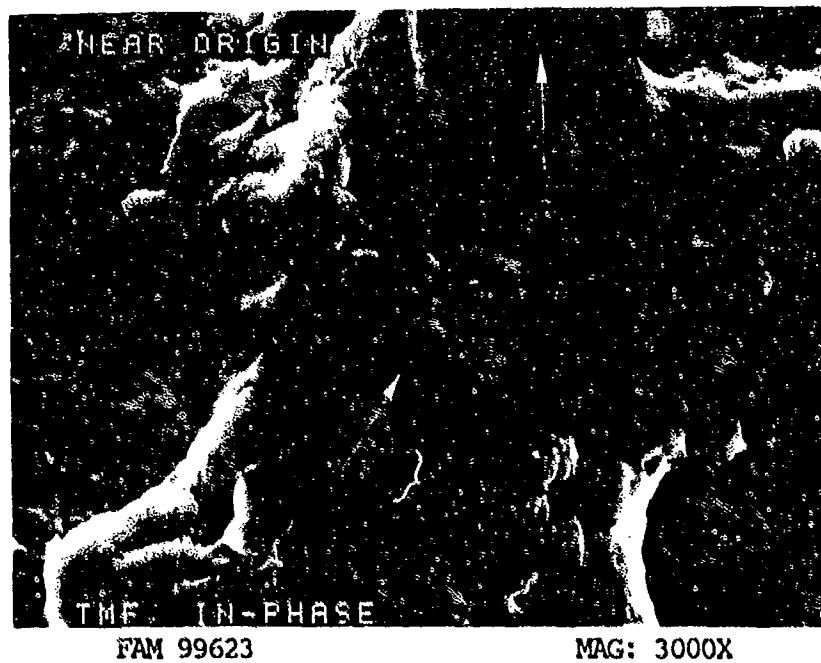


FIGURE 12-115: Fatigue striations near the origin area. The direction of propagation is shown by an arrow. Bracket contains five striations.

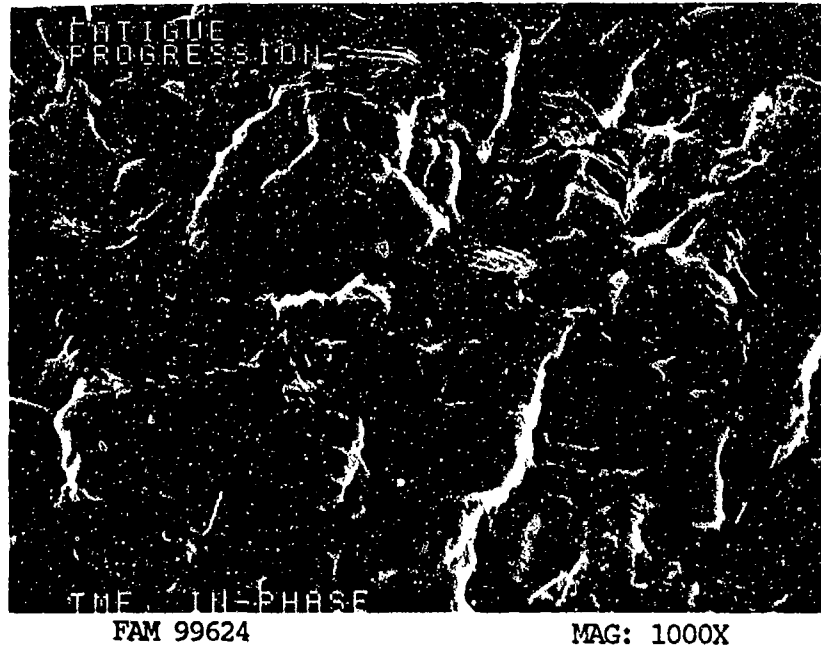


FIGURE 12-116: Oxidized striations in the fatigue progression zone. Compare these with the striations in Figure 12-115.

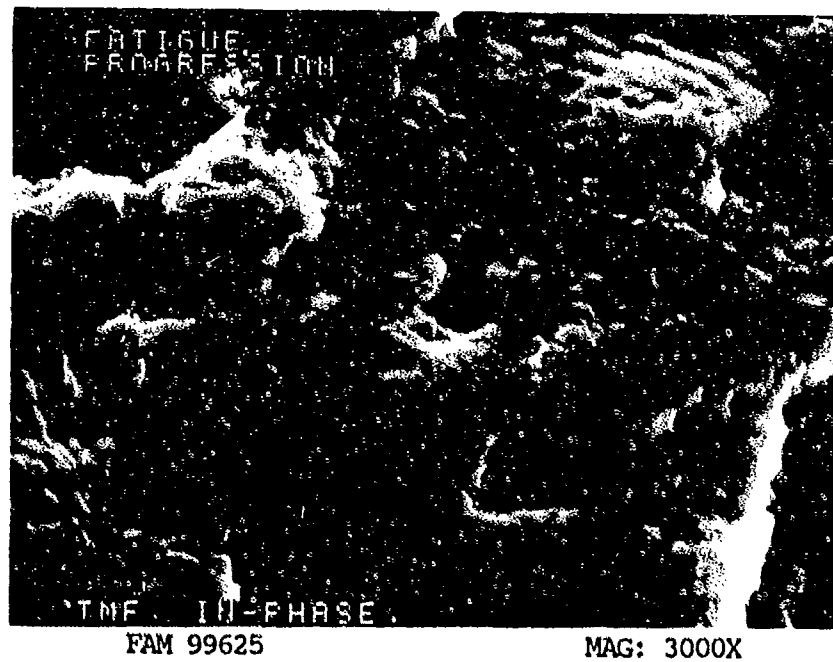


FIGURE 12-117: Higher magnification photograph of a portion of the area shown in Figure 12-116, showing fatigue striations with some secondary cracking.

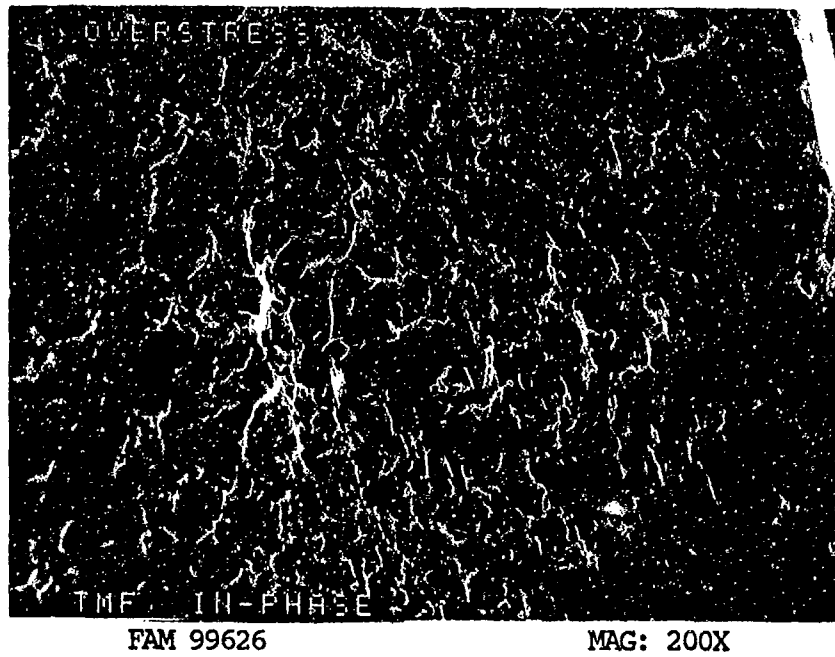


FIGURE 12-118: Dimpled overstress in the final fracture area.

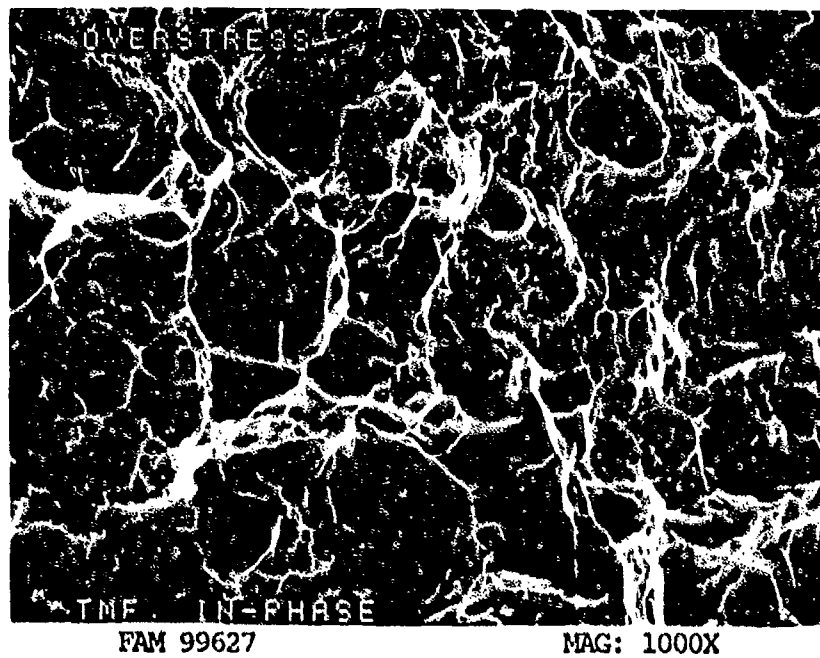


FIGURE 12-119: Higher magnification photograph showing dimpled overstress in the final fracture area. Fine dimples are contained within large ductile dimples.

MATERIAL

Ti-6Al-2Sn-4Zr-2Mo
PWA 1224 Bar

TEST DATA

TEST TYPE

TMF, Out-of-Phase

TEST CONDITIONS

Stress: 4275 MPa (62 ksi)/365.4 MPa (-53 ksi)
Stress Ratio: 0.85
Frequency: 1 cpm
Atmosphere: Air
Temperature: 260°C (500°F)/538°C (1000°F)
Test Direction: Longitudinal

TEST RESULTS

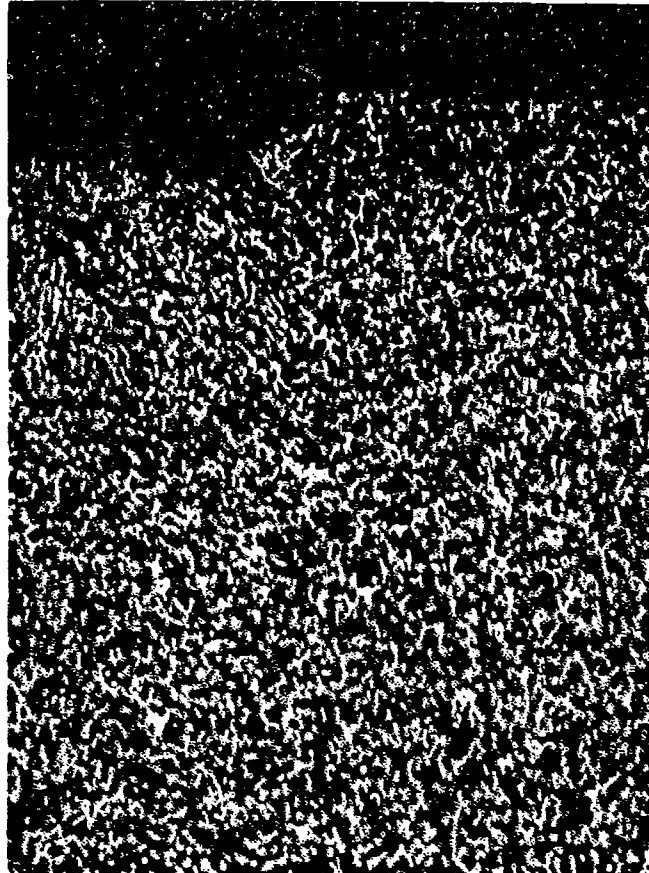
Cycles to Fracture: 8002



FAL 94530

MAG: 10X

FIGURE 12-120: Test results and fractography of Ti-6-2-4-2 out-of-phase TMF test. Fatigue propagated from a diffuse origin area on the inside surface of the specimen (bracket).

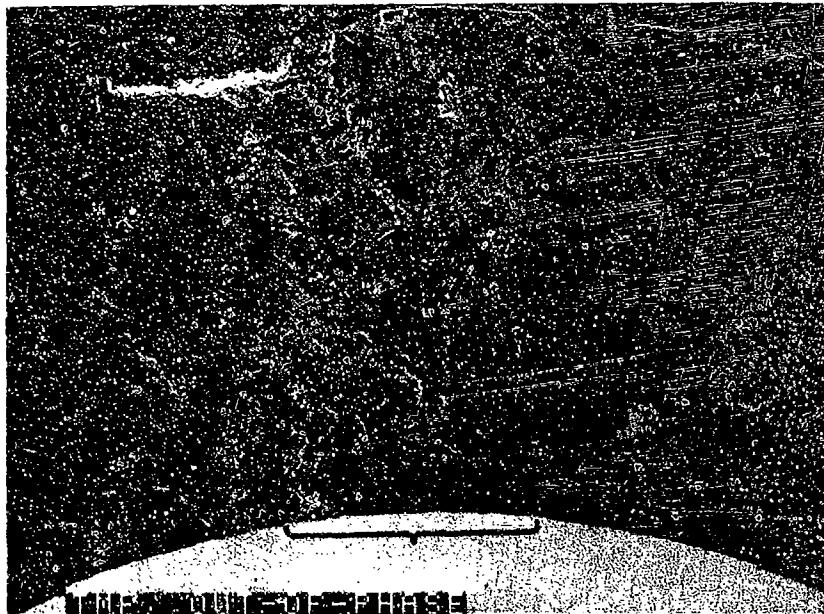


FAM 100198

MAG: 100X

FIGURE 12-121: Optical photomicrograph showing the fatigue progression area. No grain deformation is visible. The fracture is predominantly transgranular

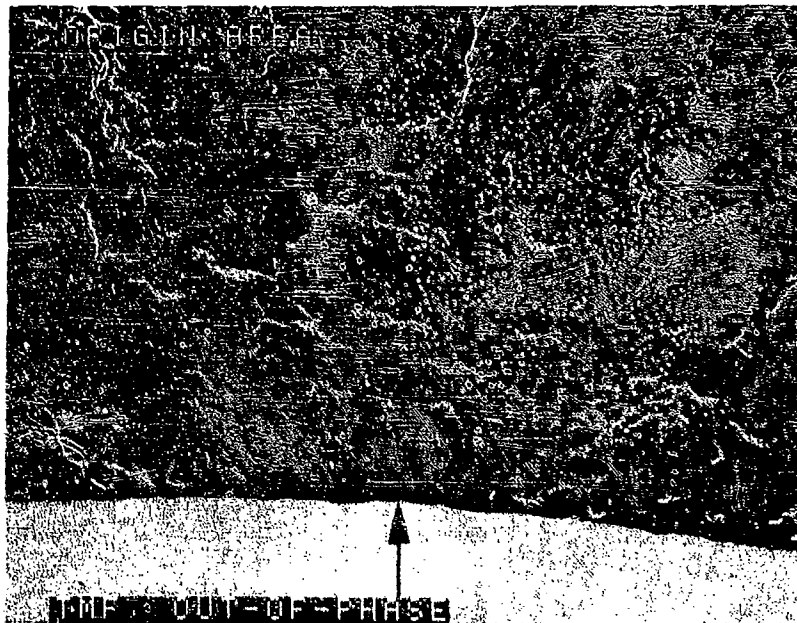
Etchant: Kroll's Reagent



FAM 99629

MAG: 50X

FIGURE 12-122: Low magnification photograph showing the origin area on the inside surface of the specimen (bracket) and the associated fatigue progression area.



FAM 99630

MAG: 200X

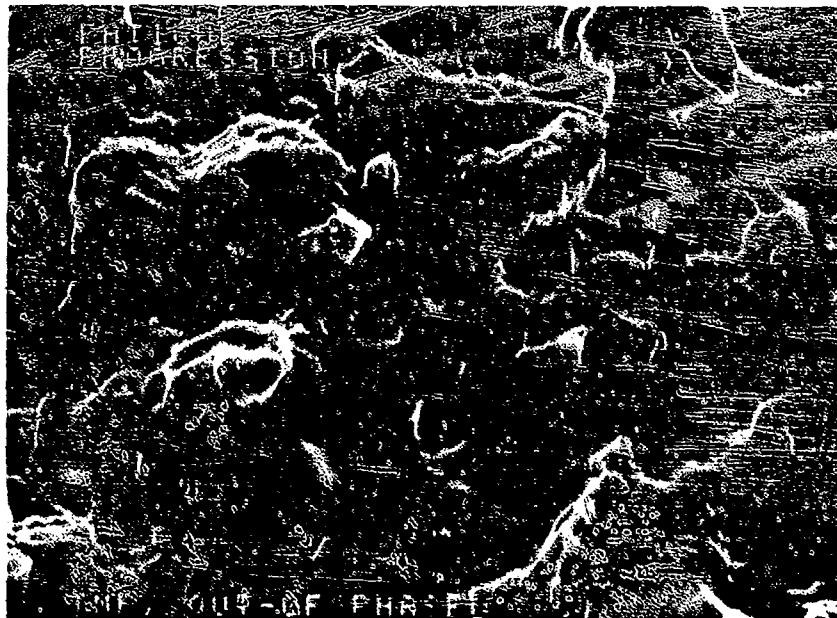
FIGURE 12-123: One of several localized origins is shown by an arrow. Machining lines are faintly visible on the inside surface adjacent to the origin.



FAM 99631

MAG: 1000X

FIGURE 12-124: Close-up photograph of one localized origin area shown in Figure 12-123. Features can be seen radiating from a small fatigue facet (arrow).



FAM 99633

MAG: 1000X

FIGURE 12-125: Fatigue striations and crack-like striations in the fatigue progression area near the I.D. surface of the specimen. Bracket contains ten striations.



FAM 99634

MAG: 3000X

FIGURE 12-126: Higher magnification photograph of a portion of the area shown in Figure 12-125, showing oxidized fatigue striations.



FAM 99635

MAG: 1000X

FIGURE 12-127: Striations and crack-like striations in the fatigue progression area near the O.D. of the specimen. The striation spacing has increased significantly as the crack has progressed (Figure 12-125).

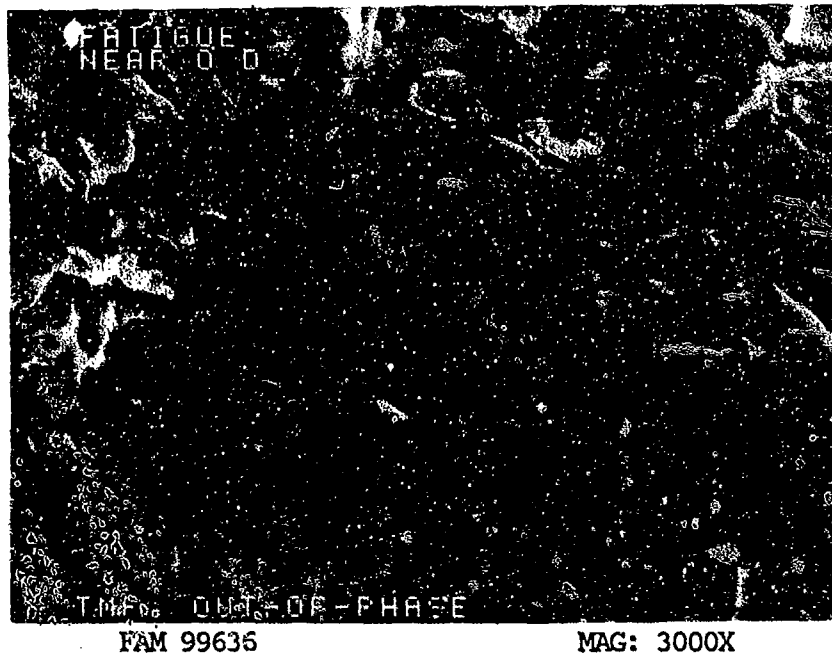


FIGURE 12-128: Higher magnification photograph of a portion of the area shown in Figure 12-127, showing striations and crack-like striations near the O.D. surface of the specimen.

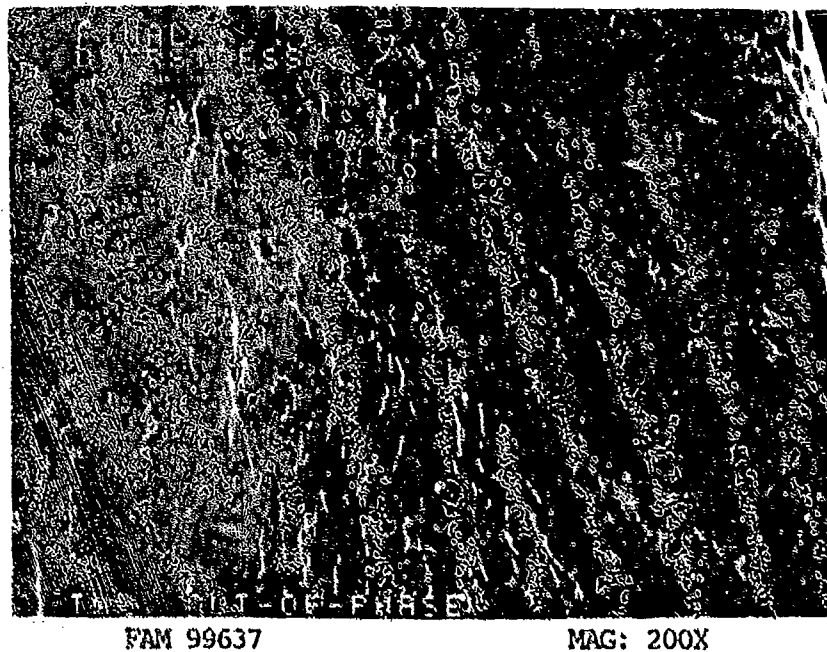


FIGURE 12-129: Dimpled overstress in the final fracture area.

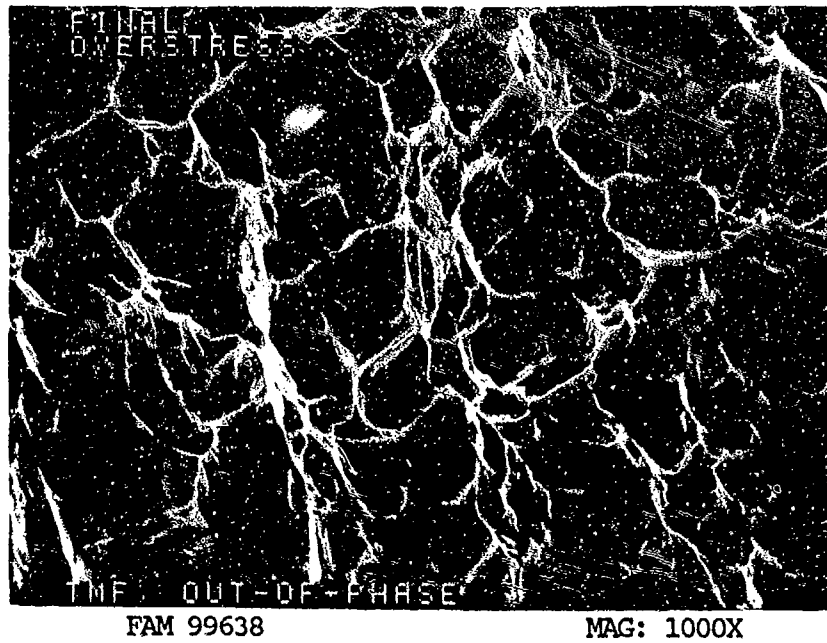


FIGURE 12-130: Higher magnification photograph showing dimpled overstress in the final fracture area.

Ti-6Al-4V

Material Description

Ti-6Al-4V is the most widely used of the alpha-beta processed titanium-base alloys. It maintains its strength up to 750 F when the part is used in the annealed condition. Very high strengths are reported at cryogenic temperatures although the alloy is susceptible to hydrogen embrittlement. The alloy is generally solution heat treated within 50-150 F below the beta transus and annealed between 1300 F and 1450 F for greater than 1 hour. Ti-6-4 is available as bar, wire, forgings and flash welded rings.

The material used in this study was heat treated to AMS 4928 (bar) with a typical hardness of HRC 35. The typical room temperature mechanical properties for AMS 4928 are as follows:

Ultimate Tensile Strength (min):	130 ksi
0.2% Yield Strength (min):	120 ksi
Percent Elongation (min):	10%
Percent Reduction in Area (min):	20%
Measured Hardness:	HRC 31-33

Fractography Overview

The only specimen examined was room temperature hydrogen embrittlement. The specimen exhibited equiaxed dimpled overstress with no evidence of "fluting." Some secondary cracking was observed in the base of the notch. The outermost surface of the fracture was smooth and featureless.

MATERIAL

Ti-6Al-4V
PWA 1215 Bar

TEST DATA

TEST TYPE

Hydrogen Embrittlement

TEST CONDITIONS

Stress: 985.9 MPa (143 ksi) DNF*
1116.9 MPa (162 ksi) DNF
1247.9 MPa (181 ksi)

Atmosphere: Air

Temperature: Room Temperature

Test Direction: Longitudinal

Specimen Charging: The specimen was initially charged for 12 hours in gaseous H₂ at 5000 psi. Cathodically, charged for 2 hours in 1% aqueous HCl, 15 VDC anode platinum.

TEST RESULTS

Time to Fracture: 285.1 hours (DNF), 99.4 hours (DNF),
24.9 hours

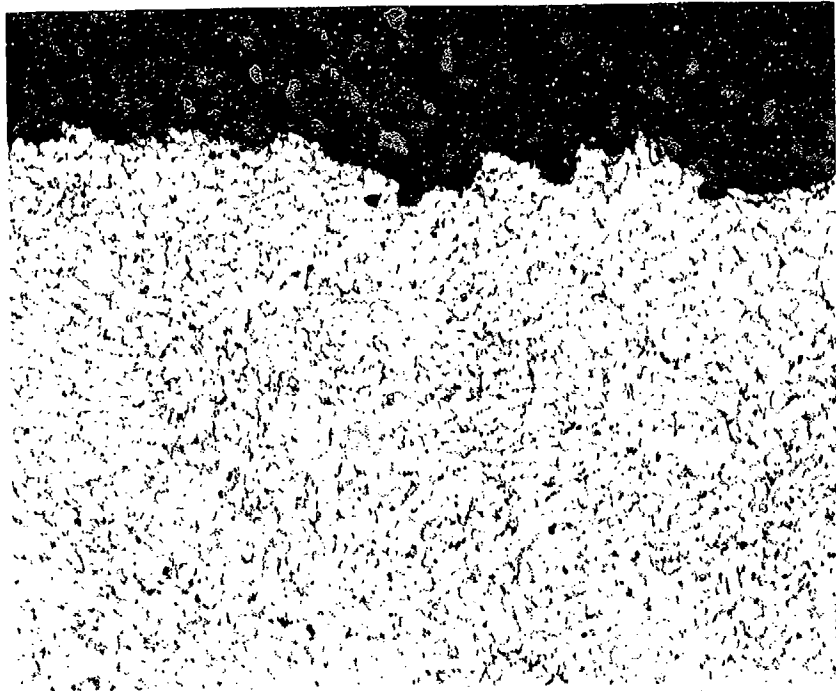
* Did Not Fracture



FAL 93949

MAG: 10X

FIGURE 13-1: Test results and fractography of Ti-6Al-4V room temperature hydrogen embrittlement test.



FAM 100189

MAG: 200X

FIGURE 13-2: Optical photomicrograph showing the dimpled overstress area near the center of the specimen fracture. The specimen exhibits a mixture of transgranular and intergranular fracture.

Etchant: Kroll's Reagent

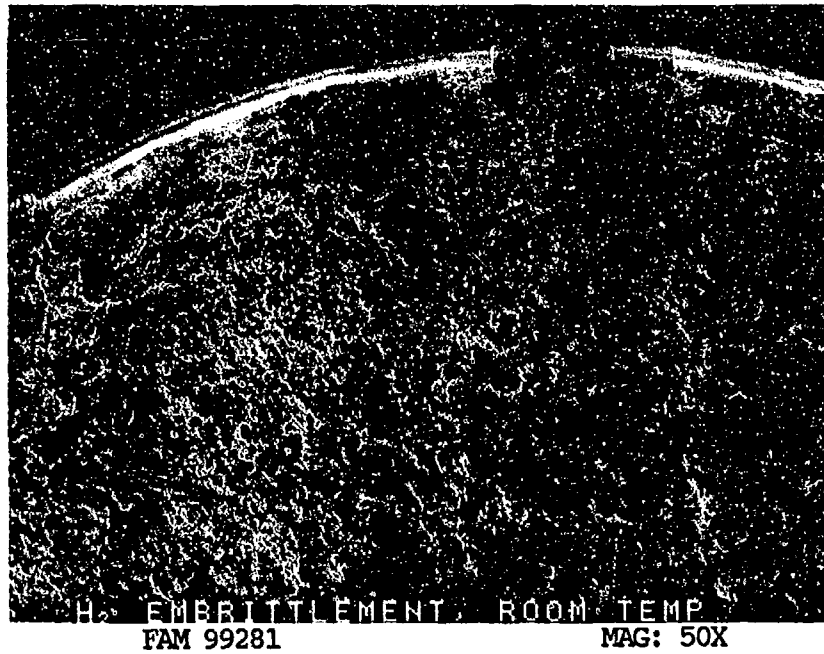


FIGURE 13-3: Low magnification photograph showing overstress features on the fracture surface.

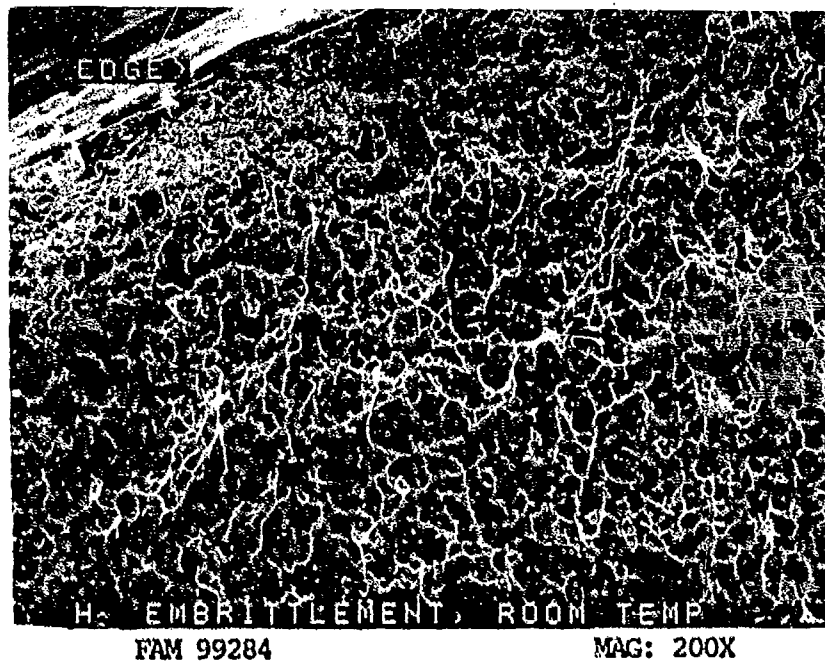


FIGURE 13-4: Higher magnification photograph of the edge of the specimen. The edge appears flat with no clear shear lip.

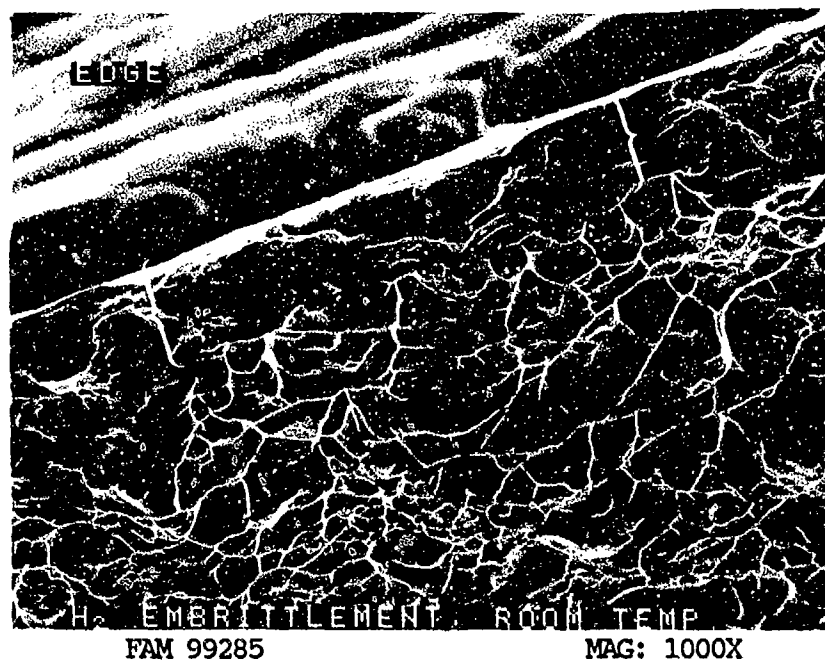


FIGURE 13-5: Tensile dimples near the edge of the specimen. The outermost fracture surface is relatively smooth and featureless (brackets).

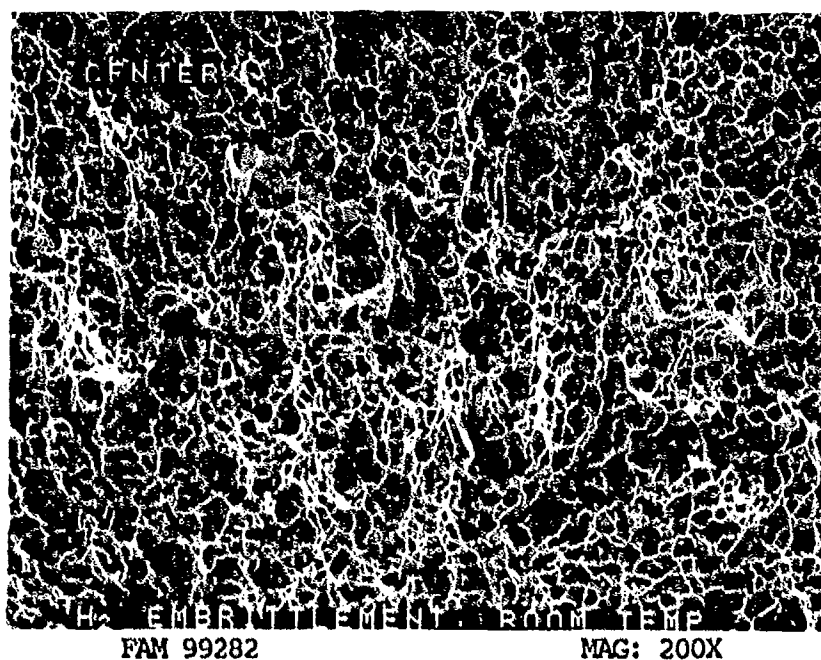


FIGURE 13-6: Equiaxed dimpled overstress near the center of the fracture surface.

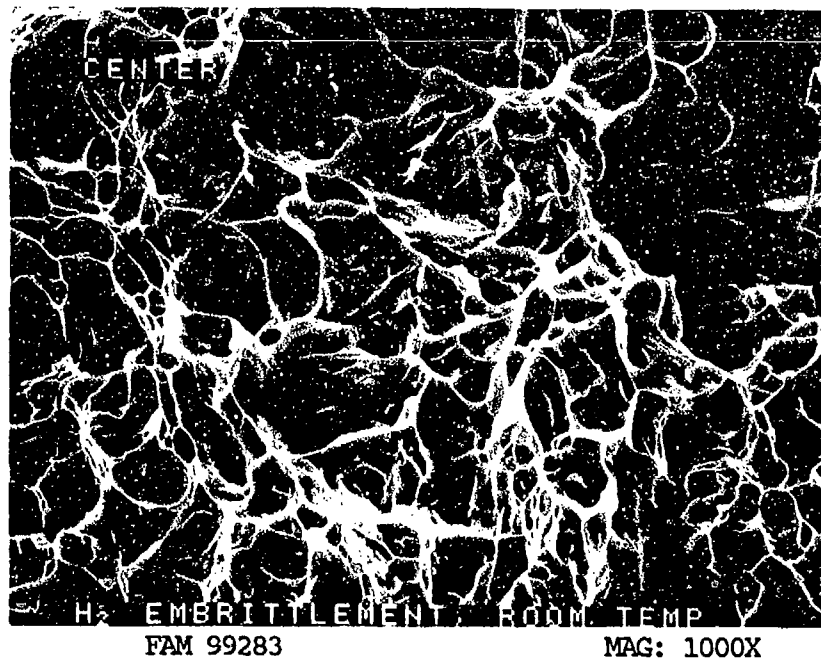


FIGURE 13-7: Dimpled overstress in the center of the fracture surface.

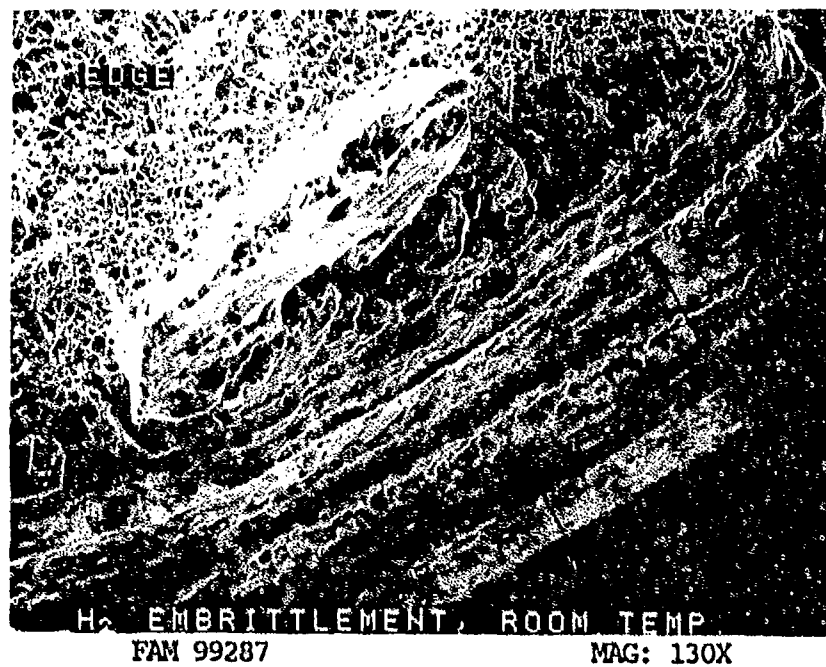


FIGURE 13-8: Secondary cracking in the notch adjacent to the primary fracture surface (arrows).

SERVICE FAILURE

FRACTURE MODE Fatigue (probable HCF)

PART NAME Loop Clamp Bracket

OPERATION DATA Bracket secures a cushioned loop clamp to the case.
It is subjected to high vibratory stresses.

PART TIME 599.3 hours (2473.0 operational cycles)

	<u>REQUIRED</u>	<u>ACTUAL</u>
MAT'L		
BASE	<u>Ti-6Al-4V</u>	<u>confirmed</u>
OTHER	<u>-</u>	<u>-</u>
HARDNESS	<u>No Requirement</u>	<u>HRC 32-34 *</u>
GRAIN SIZE	<u>No Requirement</u>	<u>-</u>
DIMENSIONAL	<u>Thickness: 0.045-0.055 inch</u>	<u>0.047-0.048 inch</u>

* Diamond pyramid hardness (DPH) conversions

SUMMARY: The bracket fractured by fatigue (probable HCF) progressing from an origin adjacent to the bolt hole at the bolt head contact circle (fretting). The fatigue progressed approximately 0.45 inch before the final fracture occurred by overstress. This thumbnail was clearly visible. No material or microstructural defects were found.



FAL 88737

MAG: 1 1/2X

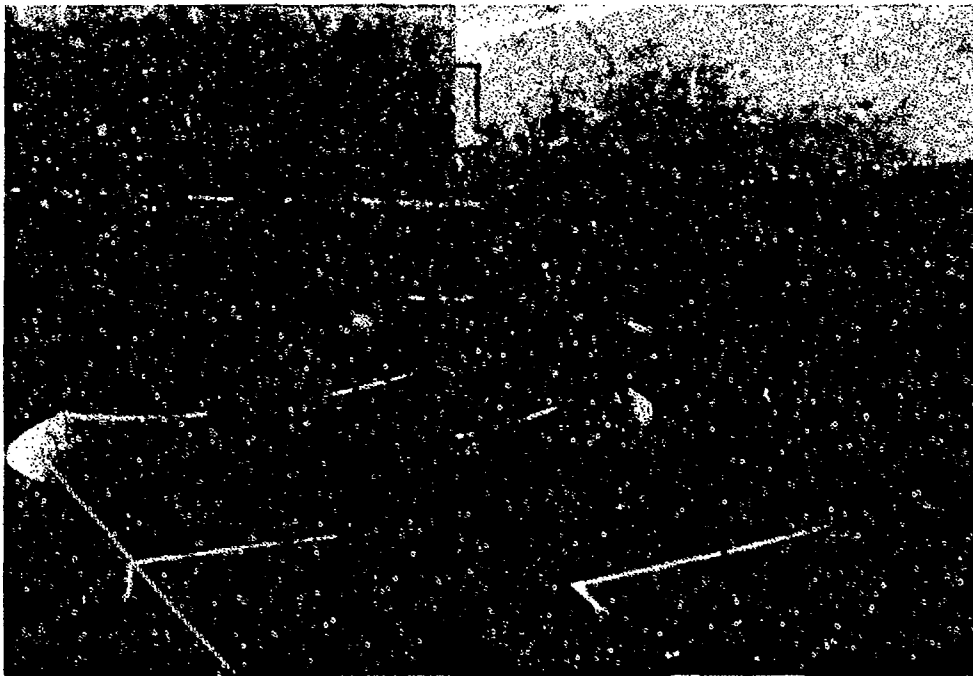


FAL 88738

MAG: 4X

FIGURE 13-9: Overall photograph of the reassembled loop clamp bracket. The origin area is shown by an arrow at attachment bolt head contact circle.

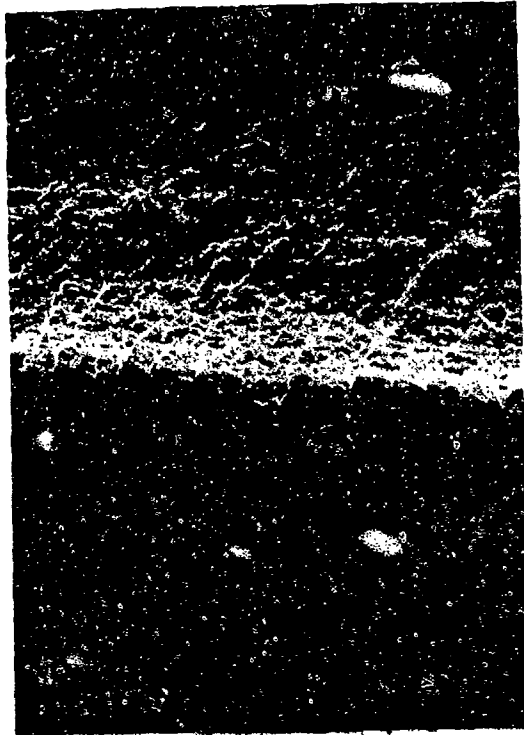
FIGURE 13-10: Overall photograph of the fracture surface. The thumbnail is clearly visible indicating propagation from origins in the bolt head contact circle.



FAL 93469-93470

MAG: 10X

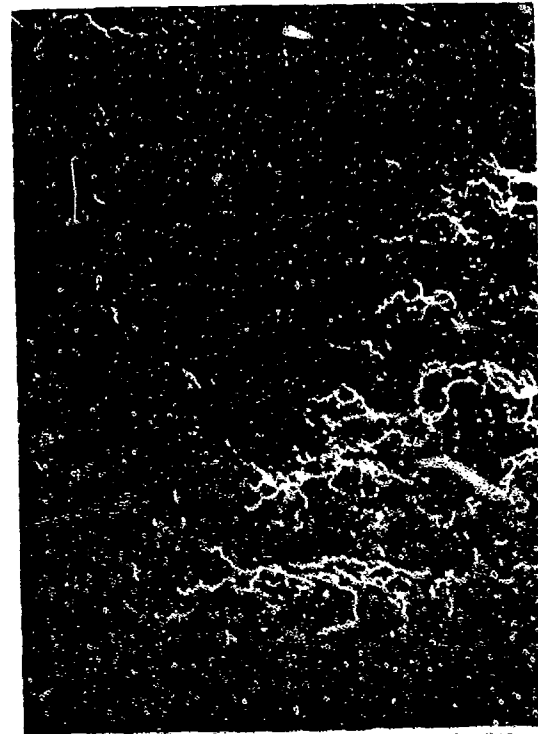
FIGURE 13-11: Composite SEM photograph of the thumbnail region. The origin is at an area of fretting associated with the attachment bolt head contact circle (arrow and bracket).



FAL 93475

MAG: 100X

FIGURE 13-12: Remnant features indicating fatigue at the boundary between the thumbnail (top) and the overstress (bottom).



FAL 93471

MAG: 300X

FIGURE 13-13: Boundary between fatigue progression (left) and overstress (right).

SERVICE FAILURE

FRACTURE MODE High Cycle Fatigue

PART NAME Augmentor Divergent Section Mode Strut Bracket

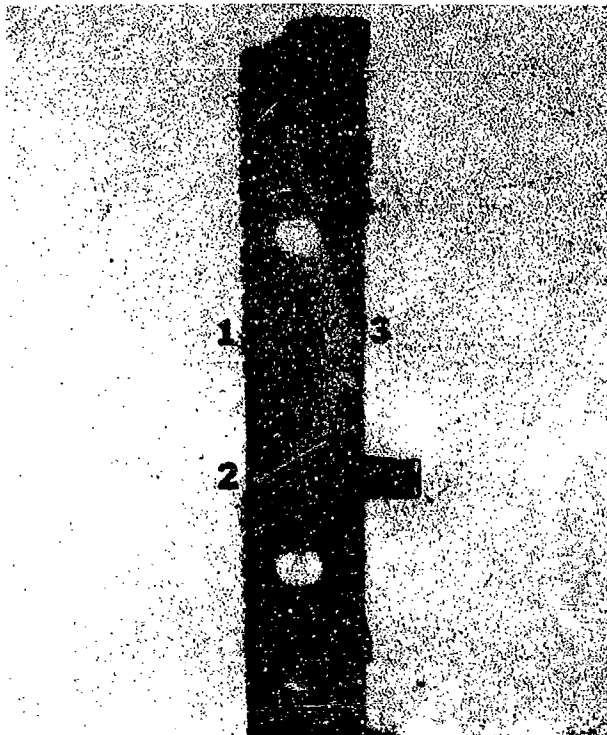
OPERATION DATA The bracket operated on a test engine in an accelerated mission test (AMT). The bracket is subjected to both static and cyclic loading.

PART TIME 709.4 hours (3062.75 operational cycles)

	<u>REQUIRED</u>	<u>ACTUAL</u>
MAT'L		
BASE	<u>Ti-6Al-4V</u>	<u>confirmed</u>
OTHER	<u>Plating: Ni-Ti-B</u>	<u>confirmed</u>
HARDNESS	<u>No Requirement</u>	<u>HRC 31-40 *</u>
GRAIN SIZE	<u>No Requirement</u>	<u>ASTM 0-2</u>
DIMENSIONAL	<u>Plating Thickness: 0.001-0.0015 inch</u>	<u>0.0011-0.0014 inch</u>

* Diamond pyramid hardness (DPH) conversions.

SUMMARY: Bracket fractured through the mode strut attachment due to high cycle fatigue (HCF). Transmission electron microscope (TEM) examination estimated the number of striations on fracture 2 bracket position E, to be 75,000. The smaller cross section (inboard sides) cracked first, with origins on the inside surface at the interface of the base metal and the plating. Aluminum-rich particles, probably aluminum oxide embedded during grit blasting prior to plating were found at the interface. These may have acted as origin sites. The fatigue progressed through the entire cross section of the smaller sides and through over 75% of the larger outboard sides. The most probable order of fracture is indicated in Figure 13-14.



FAL 88822

MAG: 7/8X

FIGURE 13-14: Overall photograph of the mode strut bracket aft looking forward. The probable order of fracture is indicated by numbers.



FAL 88827

MAG: 3X

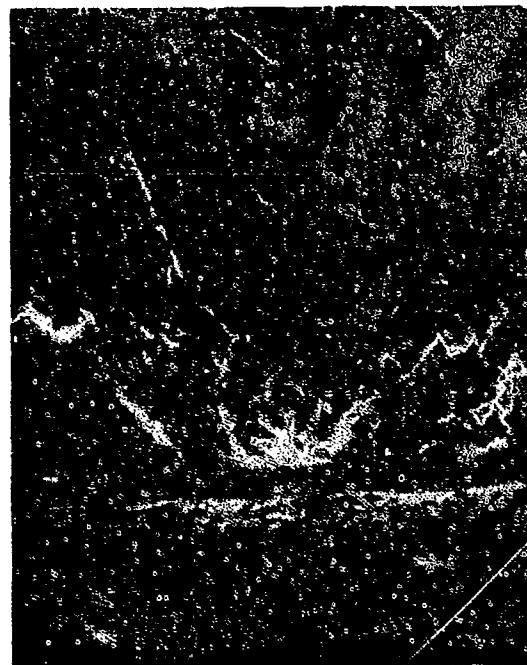
FIGURE 13-15: Side view of the fractured bracket channels.



FAL 88825

MAG: 12X

FIGURE 13-16: Overall photograph of fracture number 3. The origin area is indicated by a bracket.



FAL 93392

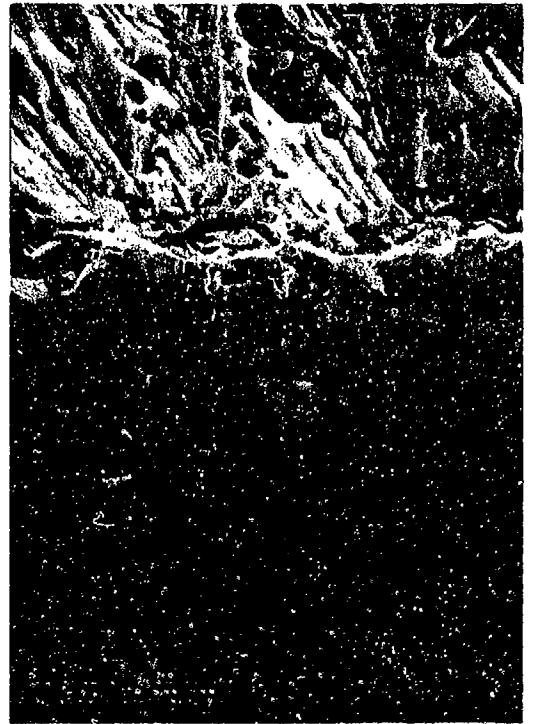
MAG: 100X

FIGURE 13-17: SEM photograph of the origin area on fracture number 3. Feathery cleavage facets indicate multiple origins at the plating/base metal interface (arrow).



FAL 93391

MAG: 300X



FAL 93394

MAG: 1000X

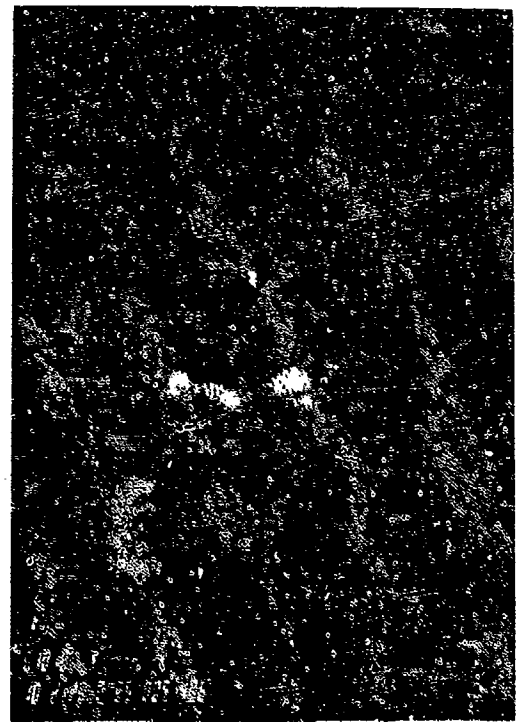
FIGURE 13-18: Feathery cleavage facets can be seen propagating in both directions from the plating base metal interface (arrows).

FIGURE 13-19: Higher magnification view of the origin area.



FAL 93397

MAG: 1000X



FAL 93398

MAG: 1000X

FIGURE 13-20: SEM photograph of a metallographic cross section through plating/base metal interface in the origin area (arrow).

FIGURE 13-21: SEM/XES elemental map showing the concentration of Al at the interface (light areas indicate elevated Al concentration).

SERVICE FAILURE

FRACTURE MODE Tensile Overstress

PART NAME Augmentor Pump Mounting Bolt

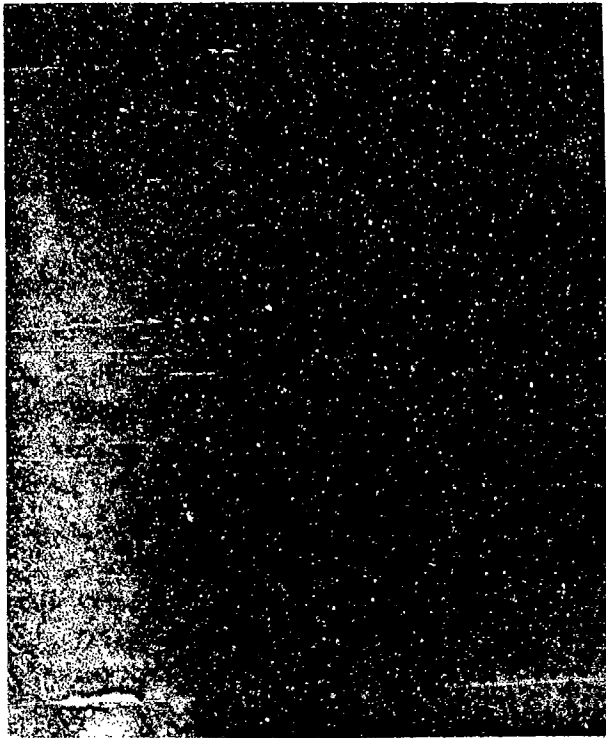
OPERATION DATA Part operated in a field engine for an unknown period.
It is subjected to moderate temperatures and stresses.

PART TIME Unknown

	<u>REQUIRED</u>	<u>ACTUAL</u>
MAT'L		
BASE	<u>Ti-6Al-4V</u>	<u>Confirmed</u>
OTHER	<u>-</u>	<u>-</u>
HARDNESS	<u>No Requirement</u>	<u>HRC 32-34 *</u>
GRAIN SIZE	<u>No Requirement</u>	<u>-</u>
DIMENSIONAL	<u>Diameter: 0.120-0.160 inch</u>	<u>0.137 inch</u>

* Diamond pyramid hardness (DPH) conversions.

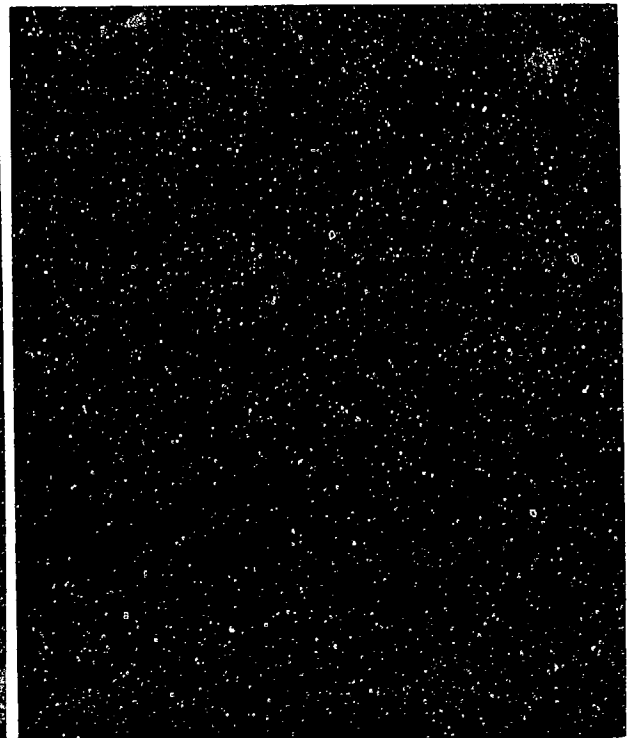
SUMMARY: Bolt fractured in tensile material overstress through the neck adjacent to a change in section. No evidence of a torsional component was found, indicating that the bolt was not cracked during assembly or fractured during disassembly. No material or microstructural defects were found.



FAL 49057

MAG: 2X

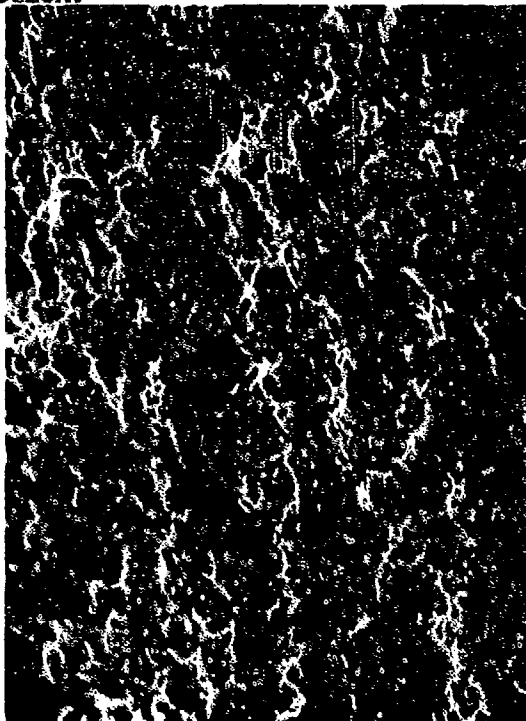
FIGURE 13-22: Overall photograph of the fractured bolt. An arrow indicates the location of the fracture at a change in section.



FAL 49058

MAG: 10X

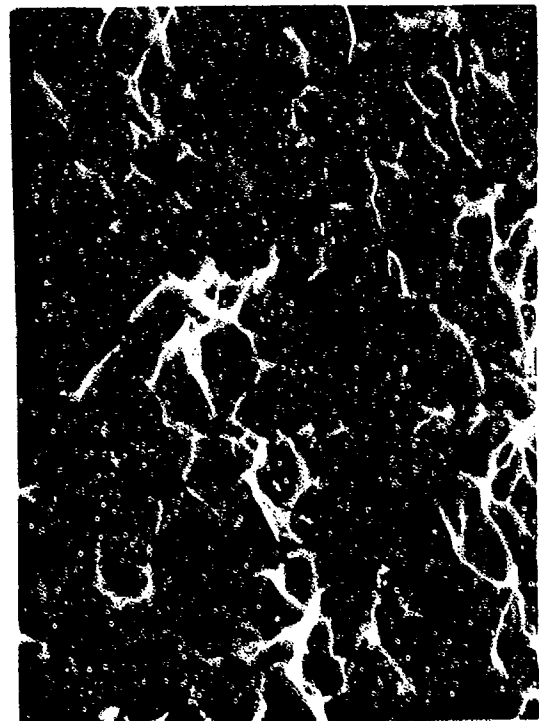
FIGURE 13-23: Overall photograph of the fracture surface.



FAL 93477

MAG: 500X

FIGURE 13-24: SEM photograph of the fracture surface showing fine equiaxed dimples.



FAL 93479

MAG: 2000X

FIGURE 13-25: Fine equiaxed dimples.

V - REFERENCE SECTION

INTRODUCTION

A general literature survey of books, periodicals, and reports pertaining to failure analysis and fractography was used to create an annotated reference section for the failure analyst. This reference section is a cross referenced source of information where data on specific subjects of interest to the analyst may be obtained. These sources include text, computer information services, various organizations and professional societies.

A literature search was performed through the United Technologies Corporation Library System (UTCLS) for books, reports and periodicals in the system, and through the DIALOG computer-based search service. Through the DIALOG system, the following two data bases were accessed and searched: 1) Metadex, produced by the American Society for Metals and 2) Aerospace Abstracts. Key words "failure analysis," "fractography," "fracture surface(s)" and "fractograph(s)" yielded over two hundred potential references. Publications locally available were also reviewed. Fifty-one references have been selected and included below. Those references considered to be more generally useful are discussed in more detail, others more briefly mentioned. They are organized into subject categories.

Failure Analysis Handbooks

The American Society for Metals, now ASM International, has produced two very useful failure analysis handbooks, primarily for metals. Also, the Air Force has produced an extensive failure analysis handbook for composite materials. These publications are summarized below in chronological order:

- 1) American Society for Metals, "Failure Analysis and Prevention," Metals Handbook, 8th Ed., Vol. 10, Metals Park, Ohio, 1975, 604 pp.

The 1975 ASM Failure Analysis Handbook is an excellent reference source for both beginning and experienced failure analysts. The book is divided into four principal sections, all of which are illustrated with drawings and photographs:

"Engineering Aspects of Failure and Failure Analysis"

This section discusses fundamental sources of failures, then describes general practice and techniques to be used in failure analysis.

"Failures from Various Mechanisms and Related Environmental Factors"

This second section emphasizes identification and characteristics of

various types of failure modes, including those induced by stress, temperature and environmental factors.

"Analysis and Prevention of Service Failures: Products of Principal Metalworking Processes"

This third section describes types and causes of failures of metal products, including those produced by cold forming, forging, casting, welding and brazing.

"Analysis and Prevention of Service Failures: Manufactured Components and Assemblies"

The final section of the book is a very useful compilation of service failures of various types of components, such as shafts, bearings, mechanical fasteners, springs, dies, gears and pressure vessels.

- 2) American Society for Metals, "Failure Analysis and Prevention," Metals Handbook, 9th Ed., Vol. 11, Metals Park, Ohio, 1986, 843 pp.

The 1986 ASM Failure Analysis Handbook, an updated and expanded version of the 1975 ASM Failure Analysis Handbook, again is an excellent reference source for both beginning and experienced failure analysts. The book is divided into five principal sections, all of which are illustrated with drawings and photographs:

"Engineering Aspects of Failure and Failure Analysis"

This section includes a glossary of terms and describes general practice and techniques to be used in failure analysis.

"Failure Mechanisms and Related Environmental Factors"

This second section emphasizes identification and characteristics of various types of failure modes, including those induced by stress, temperature and environmental factors.

"Products of Principal Metalworking Processes"

This third section describes types and causes of failure of metal products, including those produced by cold forming, forging, casting, welding and brazing.

"Manufactured Components and Assemblies"

The fourth section is a very useful compilation of service failures of various types of components, such as shafts, bearings, mechanical fasteners, springs, tools and dies, gears and pressure vessels.

"Engineered and Electronic Materials"

The final section of the book introduces the failure analysis of continuous fiber reinforced composites, ceramics, polymers and integrated circuits.

3) B. W. Smith, R. A. Grove and T. E. Munns, Failure Analysis of Composite Structural Materials, Interim Report AFWAL-TR-86-4033, May 1986, 225 pp.

R. A. Grove and B. W. Smith, Compendium of Post-Failure Analysis Techniques for Composite Materials, Interim Report AFWAL-TR-86-4137, January 1987, 399 pp.

B. W. Smith and R. A. Grove, Failure Analysis of Composite Structural Materials, Final Report AFWAL-TR-87-4001, May 1987, 172 pp.

These reports present work done at Boeing Military Airplane Company, Seattle, Washington. The work was supported by the Materials Laboratory, (now Wright Research and Development Center - WRDC), Air Force Wright Aeronautical Laboratory, Air Force Systems Command, Wright-Patterson Air Force Base, Ohio.

Interim Report TR-86-4033 summarizes a literature search, specimen production and testing, and evolution of diagnostic techniques. Interim Report TR-86-4137 combines the above and other information into a compendium of failure analysis techniques for composite materials. Final Report TR-87-4011 summarizes the results published in more detail in the above reports, and demonstrates the use of selected failure analysis techniques for actual service failures.

Fractographic Handbooks

Both the Air Force and the American Society for Metals (ASM International) have produced very useful fractography handbooks for both transmission electron microscope (TEM) fractographs and scanning electron microscope (SEM) fractographs. Other authors' publications are also noteworthy. A general limitation of all fractography handbooks, however, is that not all specific alloys of interest or test/operating conditions can be included. In most cases, the quality of reproduced fractographs could be improved. These publications are summarized below in chronological order:

4) A. Phillips, V. Kerlins and B. V. Whiteson, Electron Fractography Handbook, Technical Report ML-TDR-64-416, Air Force Materials Laboratory, Research and Technology Division, Air Force Systems Command, Wright-Patterson Air Force Base, Ohio, January 31, 1965, 879 pp, 137 references. and

A. Phillips, V. Kerlins, R. A. Rowe and B. V. Whiteson, Electron Fractography Handbook - Specific Applications of Electron Fractography, Technical Report AFML-TR-64-416, Supplement II, Air Force Materials Laboratory, Air Force Systems Command, Wright-Patterson Air Force Base, Ohio, March, 1968, 275 pp, 172 references (including previous 137). Note: Supplement I (December 1966) emphasized special techniques rather than fractographs.

The Electron Fractography Handbook (MCIC-HB-08, June 1976) contains an extensive atlas of TEM fractographs for forty-five aerospace alloys, including specimens of smooth and notched tensile, shear, torsion and impact overload (overstress), high and low cycle fatigue, corrosion fatigue and thermal fatigue, at low, ambient and high test temperatures. Alloys and types of test specimens are listed in Tables V-1 and V-2. The atlas contains TEM fractographs (usually at 6500X) and overall photographs (1X - 18X). Sections on replication techniques, typical fracture modes and environmental effects are also included. This handbook is very useful, the significant limitation being that only TEM fractographs are included.

- 5) J. L. Harmon and C. T. Torrey, Fractographic Handbook, AEC Research and Development Report KAPL-3355, Knolls Atomic Power Laboratory, Schenectady, New York, September 19, 1968, 85 pp.

The Fractographic Handbook contains an atlas of TEM fractographs for reactor materials, including zirconium, hafnium, niobium and nickel alloy test specimens. This publication was given only limited distribution.

- 6) D. A. Ryder, The Elements of Fractography, North Atlantic Treaty Organization Advisory Group for Aerospace Research and Development, AGARDograph No. 155, 1971, 190 pp.

This publication discusses and illustrates the use of transmission electron microscopy in fractography and failure analysis. Divided into twelve chapters, instrumentation techniques and various fracture modes are included.

- 7) American Society for Metals, "Fractography and Atlas of Fractographs," Metals Handbook, 8th Ed., Vol. 9, Metals Park, Ohio, 1974, 499 pp., references on techniques.

The 1974 ASM Fractography Handbook contains an extensive atlas of fractographs for nineteen types of industrial and aerospace alloys, with well over a hundred individual alloys. Light microscope, SEM, TEM and comparison SEM/TEM fractographs are presented. Both parts and test specimens are included, primarily exhibiting tension overload, bending, impact, fatigue and stress corrosion cracking, with some shear and torsion overload, stress-rupture and hydrogen embrittlement. Sections on the history of fractography, the care, handling and preparation of specimens, photography, scanning electron microscopy and transmission electron microscopy are also included. This handbook is very useful, the primary limitation being that no attempt was made to show the effects of variables, such as stress conditions and temperature, on fracture features.

TABLE V-1.
 CROSS REFERENCE INDEX FOR ATLAS OF ELECTRON FRACTOGRAPHS, ELECTRON FRACTOGRAPHY
 HANDBOOK —
 OVERLOAD TEST CONDITIONS

Alloy	Strength Level or Heat Treatment	Test Type and Test Temperature												
		Unnotched Tension		Notched Tension		Shear		Torsion		Impact				
		Low	Ambient	High	Low	Ambient	High	Low	Ambient	High	Low	Ambient	High	Ambient
Aluminum Alloys														
1100	As Fabricated	X	X	X	X	X								X
2014	Fusion Weld													
2014	T6		X		X									
2024	T851													
6061	T6													
7075	T6 Spot Weld													
7075	T6		X		X									X
7075	T651													
7075	T7351													
7079	T651													
Fe-Iron Alloys														
Armco Iron	Annealed		X		X									
AISI 1018	Cold Rolled													
AISI 4340	Annealed		X		X									X
AISI 4340	125 145 ksi													
AISI 4340	180 200 ksi													
AISI 4340	260 280 ksi		X		X									X
AISI 52100	R _c 50													
AISI 4620	Carburized		X		X									X
17-4PH S.S.	180 200 ksi													
AISI 302 S.S.	Annealed		X		X									X
AISI 403 S.S.	180 ksi min													
A-286	140 ksi min		X		X									
Alnico	As Cast													X
Ti Titanium Alloys														
75A	Annealed		X		X									X
6Al-4V	Annealed													
6Al-4V	150 ksi		X		X									X

TABLE V-1.
 CROSS REFERENCE INDEX FOR ATLAS OF ELECTRON FRACTOGRAPHS, ELECTRON FRACTOGRAPHY
HANDBOOK —
 OVERLOAD TEST CONDITIONS (CONTINUED)

Alloy	Strength Level or Heat Treatment	Test Type and Test Temperature													
		Unnotched Tension		Notched Tension		Shear		Torsion		Impact					
		Low	High	Low	High	Low	High	Low	High	Low	High				
Ni-Nickel Alloys															
Rene 41	180 ksi		X		X										
TD-Nickel	Annealed		X		X										X
Hastelloy X															
713C	Annealed		X		X										
IN-100															
Inconel 718	Annealed		X		X										
	180/200 ksi		X		X										
Waspaloy															
	160/180 ksi		X		X										
Udimet 700															
	180/200 ksi		X		X										
Mg-Magnesium Alloys															
AZ-31B	As Extruded		X		X										X
Be-Beryllium Alloy															
Unalloyed Beryllium	Annealed														
Mo-Molybdenum Alloy															
T2M	Stress Relieved		X		X										
Cb-Columbium Alloy															
B-66	Annealed														X
W-Tungsten															
CMI Pure Tungsten	Stress Relieved		X		X										
Co-Cobalt Alloy															
L 605	125 ksi min		X		X										X
Cu-Copper Alloy															
Cu-2% Be	150/175 ksi		X		X										X

708C

TABLE V-2.
 CROSS REFERENCE INDEX FOR ATLAS OF ELECTRON FRACTOGRAPHS, ELECTRON
FRACTOGRAPHY HANDBOOK — FATIGUE TEST CONDITIONS

Alloy	Strength Level or Heat Treatment	Test Type and Test Temperature						Thermal Fatigue	
		High Cycle Fatigue			Low Cycle Fatigue				Corrosion Fatigue
		Low	Ambient	High	Low	Ambient	High		
Al- Aluminum Alloy									
2014	Fusion Weld								
2014	T6	X				X			
2024	T4								
2024	T4 (Air Quench)		X				X		
2024	T851								
6061	Fusion Weld	X	X						
6061	T6								
7075	T6-Spot Weld		X			X			
7075	T6								
7075	T651		X			X	X		
7079	T6								
7079	T651		X				X		
356	T6		X						
Fe- Iron Alloy									
AISI 1018	Cold Rolled			X	X			X	
AISI 4340	180/200 ksi								
AISI 4340	260/280 ksi								
HY-TUF	240 ksi	X	X			X		X	
AISI H-11	220/240 ksi								
AISI H-11	270/290 ksi		X			X		X	
T-1	Fusion Weld								
AISI 52100	R _c 60		X			X			
AISI 431 S.S.	180/200 ksi								
17-4PH S.S.	170/200 ksi		X			X			
PH14-8Mo S.S.	SRH 950								
AM 350 S.S.	SCT 850		X					X	
AISI 301 S.S.	1/4 Hard								
AISI 302 S.S.	Annealed	X	X	X					
AISI 403 S.S.	180 ksi min								
A-288	140 ksi min		X	X					
18Ni-9Co-6Mo	300 ksi	X	X					X	

TABLE V-2.
 CROSS REFERENCE INDEX FOR ATLAS OF ELECTRON FRACTOGRAPHS, ELECTRON FRACTOGRAPHY HANDBOOK — FATIGUE TEST CONDITIONS (CONTINUED)

Alloy	Strength Level or Heat Treatment	Test Type and Test Temperature						Corrosion		Thermal Fatigue
		High Cycle Fatigue			Low Cycle Fatigue			Fatigue		
		Low	Ambient	High	Low	Ambient	High	Ambient	High	
Ti-Titanium Alloy										
5Al-2.5Sn	Annealed			X						
8Al-1Mo-1V	Annealed			X					X	
6Al-4V	Annealed			X	X	X	X	X		
13V-11Cr-3Al	Aged			X	X	X	X	X		
Ni-Nickel Alloys										
Rene 41	180 ksi			X	X					
TD-Nickel	Annealed			X	X					
713C	Annealed			X	X					
Inconel 718	180/200 ksi			X	X					X
Waspaloy	160/180 ksi			X	X					
Udimet 700	180/200 ksi			X	X					
Mg-Magnesium										
AZ-81	T4			X					X	
AZ-31B	As Extruded			X					X	
Be-Beryllium Alloy										
Unalloyed Beryllium	Annealed				X					
Mo-Molybdenum										
TZM	Stress Relieved			X						
Ta-Tantalum Alloy										
90Ta-10W	Stress Relieved			X						
Co-Cobalt Alloy										
L 605	125 ksi min			X	X					
Cu-Copper Alloy										
Cu-2% Be	150/175 ksi				X		X			

V58C

- 8) T. E. Tallian, G. H. Baile, H. Dalal and O. G. Gustafson, Rolling Bearing Damage - A Morphological Atlas, SKF Industries, Inc., King of Prussia, Pennsylvania, 1974, 351 pp.

This book, divided into twenty-three chapters, is a very good collection of illustrations of various kinds of bearing damage and failures. Overall photographs, optical and scanning electron microscope photographs, and optical photomicrographs are included.

- 9) G. F. Pittinato, V. Kerlins, A. Phillips and M. A. Russo, SEM/TEM Fractography Handbook, compiled by McDonnell-Douglas Astronautics Company, Huntington Beach, California, published by Metals and Ceramics Information Center, Battelle Columbus Laboratories, Columbus, Ohio, and sponsored by the Air Force Materials Laboratory, Air Force Wright Aeronautical Laboratories, Air Force Systems Command, Wright-Patterson AFB, Ohio, December, 1975, 691 pp, 34 references.

The SEM/TEM Fractography Handbook (MCIC-HB-06) contains an extensive atlas of fractographs for twenty-six aerospace alloys, including specimens of smooth and notched tensile overload (overstress), smooth and notched high cycle fatigue, low cycle fatigue, stress rupture, thermal fatigue and stress corrosion. Alloys and types of test specimens are listed in Table V-3. Although the atlas predominantly contains SEM and TEM fractographs at appropriate magnifications, overall photographs (usually at 8X) and optical photomicrographs of metallographic sections (usually in the 100X-400X range) are included. Chapters on the care, handling and preparation of samples, and on typical fracture modes, are also included. This handbook is very useful, the only limitation being that no attempt was made to show the effects of variables, such as stress conditions and temperature, on fracture features.

- 10) S. Bhattacharyya, V. E. Johnson, S. Agarwal and M.A.H. Howes (Ed.), IITRI Fracture Handbook - Failure Analysis of Metallic Materials by Scanning Electron Microscopy, Metals Research Division, IIT Research Institute, Chicago, Illinois, January, 1979, 570 pp., 20 references.

The IITRI Fracture Handbook contains an extensive atlas of fractographs for thirty-four industrial and aerospace alloys, including specimens of tensile, torsion and notch bend overstress, low and high cycle fatigue in axial, bending, rotating beam and rolling contact modes, Charpy V-notch impact and stress rupture. Although the atlas predominantly contains SEM fractographs at appropriate magnifications, overall photographs and optical photomicrographs of metallographic sections are included. Specimen surface conditions are also documented by SEM photographs. A brief introductory section summarizes the care, handling and preparation of samples, and describes some typical fracture modes. This handbook is very useful,

TABLE V-3.
INDEX OF ATLAS OF FRACTOGRAPHS, SEM/TEM FRACTOGRAPHY HANDBOOK

Material and Heat Treatment	Tensile		Fatigue			Stress Rupture	Thermal Fatigue	Stress Corrosion
	Overload		High Cycle		Low			
	Smooth	Notched	Smooth	Notched	Cycle Smooth			
2124 T851	X	X	X	X	X			X
2219 T87	X	X	X	X	X			X
7075 T76511	X	X	X	X	X			X
7175 T736	X	X	X	X	X			X
7050 T736	X	X	X	X	X			X
7049 T73	X	X	X	X	X			X
Ti-8Al-1Mo-1V Ann.	X	X	X	X	X			
Ti-6Al-6V-2Sn Ann.	X	X	X	X	X			
Ti-6Al-2Sn-4Zr-6Mo Ann.	X	X	X	X	X			
Ti-17 STA	X	X	X	X	X			
MP35N WSA	X	X	X	X	X			
HY-180-10Ni QA	X	X	X	X	X			
300M QT	X	X	X	X	X			X
PH 13-8Mo H-1000	X	X	X	X	X			
440C Rc55 min.	X	X	X	X	X			X
9Ni-4Co-3C QT	X	X	X	X	X			
9Ni-4Co-2C QT	X	X	X	X	X			
D6AC QT	X	X	X	X	X			
IN100 STA	X	X	X	X	X	X	X	
Incoloy 901 STA	X	X	X	X	X	X	X	
Inconel 625 ST	X	X	X	X	X	X	X	
Haynes 188 Ann.	X	X	X	X	X	X	X	
MAR-M-200+Hf STA	X	X	X	X	X	X	X	
Rene 95 STA	X	X	X	X	X	X	X	
TD Ni-20Cr Ann.	X	X	X	X	X	X	X	
Rene 120 STA	X	X	X	X	X	X	X	

7088C

the major limitation being that environmental modes (such as stress corrosion cracking and hydrogen embrittlement) were not emphasized.

- 11) G. Henry and D. Horstmann, "Fractography and Microfractography," De Ferri Metallographia, Vol. 5, Verlag Stahleisen m.b.H., Dusseldorf, 1979, 445 pp.

Fractography and Microfractography contains an atlas of SEM and TEM fractographs and some photomicrographs for plain carbon steels, low alloy steels, cast irons and some stainless steels. Both specimen and service fractures are included, as are various rupture (fracture) mechanisms, such as ductile dimples, cleavage, fatigue, intergranular and creep. An introductory chapter discusses experimental techniques, scanning and transmission electron microscopy. This handbook is of limited utility for aerospace alloys since it is limited to ferrous alloys.

- 12) L. Engel and S. Murray, An Atlas of Metal Damage, Translated by S. Murray, Prentice-Hall, Inc., Englewood Cliffs, New Jersey, 1981, 271 pp.

The Atlas of Metal Damage, as the title implies, is organized according to various damage mechanisms and their appearances. The general categories are internal metallurgical defects, mechanical fracture, mechanical loading and chemical attack, thermal stress fracture and surface damage. Included within mechanical fracture are ductile rupture at room and elevated temperatures, transcrystalline and intercrystalline brittle fractures, fatigue fractures, stress corrosion cracking, corrosion fatigue and hydrogen-induced fracture. Although not conducive to locating fractographs for a particular alloy, the quality of diagrams and SEM fractographs at appropriate magnifications is excellent, making this a useful reference book for fractography features. Also included are brief introductions to the structure of metals and methods of examination, including scanning electron microscopy, X-ray microanalysis and Auger electron spectroscopy.

- 13) S. P. Abeln, B. A. Cowles and E. I. Veil, Fractography of PWA 1073/1074 Gatorized IN100 Nickel-Base Powder Metallurgy Superalloy, Report FR-15704, prepared for Air Force Wright Aeronautical Laboratory, Wright Patterson AFB, Dayton, Ohio, YZFS/ASD, Air Force Contract F33657-81-C-0001, United Technologies/Pratt & Whitney Aircraft, October 30, 1981, 78 pp.

The IN100 Fractography Report contains an extensive atlas of SEM and TEM fractographs taken from test specimens, including tensile, stress rupture, high cycle fatigue and low cycle fatigue specimens, tested at various temperatures. Overall photographs are also included. The main limitation is that this report is not widely available.

- 14) P. L. Stumpff and J. A. Snide, Fractography of Composites, Interim Technical Report AFWAL-TR-86-4044, Materials Laboratory, Air Force Wright Aeronautical Laboratories, Air Force Systems Command, Wright-Patterson Air Force Base, Ohio, October 1986, 113 pp.

Fractography of Composites is the first step in the development of a comprehensive fractography handbook for composite materials. This publication predominantly included specimens of graphite/epoxy material in tension, compression, flexure, fatigue and interlaminar shear in orientations of 0, 90 and 45 degrees at room temperature.

- 15) ASM International (formerly American Society for Metals), "Fractography," Metals Handbook, 9th Ed., Vol. 12, Metals Park, Ohio, 1987, 517 pp., references on techniques.

The 1987 ASM Fractography Handbook contains an extensive atlas of fractographs for twenty-five types of industrial and aerospace alloys, plus composite, ceramic and polymer materials. Although light microscope, SEM and TEM fractographs are presented, the latter received much less emphasis in this edition than in the previous 1974 edition. Both parts and test specimens are included, primarily exhibiting dimple rupture, cleavage, decohesive rupture and fatigue features. Sections on the history of fractography, the care, handling and preparation of specimens, photography, scanning electron microscopy and transmission electron microscopy are also included. This handbook is very useful, the primary limitation again being that no attempt was made to show the effects of variables, such as stress conditions and temperature, on fracture features.

Failure Analysis Books and Articles

In addition to failure analysis handbooks, a number of failure analysis books and articles have been published. Some of these are good introductory sources of information, while others deal with more specific topics. Selected publications are summarized below in chronological order:

- 16) D. J. Wulpi, "How Components Fail," Metal Progress Book Shelf, American Society for Metals, Metals Park, Ohio, 1966, 56 pp.

This publication presents a practical introductory treatment of failure analysis. It is divided into ten chapters, including types of loading, modes of fracture, fatigue, failures of shafts and gears. Although no longer in print, many copies still exist.

- 17) C. Lipson, "Basic Course in Failure Analysis," reprint of articles published in Machine Design, October 16, 1969 - January 22, 1970, Penton Education Division, Cleveland, Ohio, 1970, 40 pp.

As the title implies, this is a good basic course on failure analysis. The course is divided into eight lessons, including types of failures, failure modes, wear, pitting and corrosion.

- 18) V. J. Colangelo and F. A. Heiser, Analysis of Metallurgical Failures, John Wiley and Sons, Inc., 1974, 357 pp.

The authors present a coordinated approach to failure analysis. The book is divided into thirteen chapters, including investigative procedures, testing methods, fractography, and various failure modes.

- 19) S. Kocanda, Fatigue Failure of Metals, translated by E. Lepa, Wydawnictwa Naukowo-Techniczne, Warsaw, Poland, 1978, 368 pp.

Chapter 5 of this book, p. 269, discusses and illustrates many of the characteristic features of fatigue fractures, both macrostructurally and microstructurally. A model for the formation of fatigue striations is discussed.

- 20) A. Madeyski, "A Systematic Approach to Failure Analysis" - Parts I, II and III, Metal Progress, May, June and July 1984, pp. 57-61, 37-43 and 33-36.

Part I "presents a recipe for conducting typical metallurgical failure analyses," including the gathering of preliminary evidence, protection of fracture surfaces, non-destructive examination and measurements, preparing specimens and identifying fracture origins, and the use of low power light microscopy.

Part II discusses and illustrates the use of scanning electron microscopy in failure analysis. Methods of removing surface oxides are also discussed, as are various fracture modes in steel.

Part III discusses other analytical methods that may be used in failure analysis, such as transmission electron microscopy of replicas and thin foils, and more advanced techniques. Conventional metallography, both with optical and electron microscopes, should not be neglected.

- 21) C. M. Jackson and R. D. Buchheit, "Failure Analysis of Industrial Equipment and Products," Mechanical Engineering, July 1984, pp. 33-37.

In addition to discussing why and how to perform failure analyses, the authors also distinguish between how something fails and why it fails. The ultimate goal is to determine the root-cause of the failure.

- 22) D. J. Wulpi, Understanding How Components Fail, American Society for Metals, Metals Park, Ohio, 1985, 262 pp.

This book is more than just an expanded version of Wulpi's previous publication. It is divided into fourteen chapters, including failure analysis techniques, types of failures, modes of fracture, mechanical aspects of fracture, and a good chapter on residual stresses.

- 23) L. E. Alban, Systematic Analysis of Gear Failures, American Society for Metals, Metals Park, Ohio, 1985, 227 pp.

The author offers a systematic approach to the analysis of gear failures. The book is divided into seven chapters, including design and characteristics of gears, operating environments, methods of examination, modes and causes of failure, analysis and report writing.

- 24) G. A. Lange (Ed.), Systematic Analysis of Technical Failures, Deutsche Gesellschaft für Metallkunde, Germany, 1986, 401 pp.

This book is divided into fifteen sections, including working procedures, causes and characteristics of fractures, and various modes of failure. Also presented are sections on fractography of fractures, including a good section on fractographic features of fatigue.

- 25) L. E. Murr, What Every Engineer Should Know About Material and Component Failure, Failure Analysis, and Litigation, Marcel Dekker, Inc., 1987, 160 pp.

The author emphasizes some of the legal aspects of failure analysis, in addition to introductory chapters on the structure, characterization and testing of materials. Case examples are included.

Failure Analysis Source Books and Case Histories

Several failure analysis source books and case histories have been compiled, again with the American Society for Metals (ASM International) being a prominent contributor. These publications are summarized below in chronological order:

- 26) American Society for Metals, Source Book in Failure Analysis, Metals Park, Ohio, 1974, 406 pp.

This source book is a collection of articles and case histories from the periodical literature. It is divided into three sections: Analysis and Interpretation, Case Histories, and Techniques and Tests. Over fifty case histories are presented, primarily industrial, with some aerospace failures included.

- 27) American Society for Metals, Case Histories in Failure Analysis, Metals Park, Ohio, 1979, 427 pp.

These case histories were originally published in German and English in Praktische Metallographie by Dr. Riederer - Verlag GmbH, Stuttgart, West Germany, 1968-1977. Included in this book are 112 case histories organized into four sections: design/processing, service, materials and environment-related failures. Examples of many failure modes are included, such as fatigue, hydrogen damage, corrosion, etc. Most of the histories are industrial (non-aerospace) in nature. A major limitation is that mostly optical photographs and photomicrographs were included, with only a few scanning electron fractographs.

- 28) F. R. Hutchings and P. M. Unterweiser, Failure Analysis : The British Engine Technical Reports, American Society for Metals, Metals Park, Ohio, 1981, 496 pp.

The contents of this book were originally presented in Volumes I through XIII of Technical Reports published by British Engine Insurance Ltd. It is predominantly a compilation of case histories, with failures organized as to being environment, design/processing, materials or service related. Most of the histories are industrial (non-aerospace) in nature and some tend to be dated. A major limitation is that only optical photographs and photomicrographs were included, with no scanning or transmission electron fractographs.

- 29) American Society for Metals, Tool and Die Failures - Source Book, compiled and edited by S. Kalpakjian, Metals Park, Ohio, 1982, 430 pp.

This source book is a collection of forty articles from the technical literature. It is a good reference source for this narrow field, and is divided into six sections: Tool and Die Steels, Carbide and Ceramic Tools and Dies, Die Casting Dies, Fracture Toughness - Tool and Die Steels, Fracture Toughness - Carbides, and Properties of Tool and Die Steels.

- 30) F. K. Naumann, Failure Analysis - Case Histories and Methodology, translated from the German version by C. G. Goetzel and L. K. Goetzel, Dr. Riederer - Verlag GmbH, Stuttgart, West Germany, and American Society for Metals, Metals Park, Ohio, 1983, 483 pp.

Most of the investigations described in this book were conducted at the Max-Planck-Institut für Eisenforschung, Dusseldorf, West Germany. The case histories are organized into chapters covering various root causes of failures, such as planning errors, faulty material selection, processing errors, etc. A major limitation is that the histories are limited to iron and steel parts.

Special Publications

Many special publications are collections of technical papers presented at conferences and symposiums. The American Society for Testing and Materials (ASIM) and the American Society for Metals (ASM International) are prominent sponsors. These technical papers are often of specific interest to a few rather than of general interest to many failure analysts. Selected publications are briefly summarized below in chronological order, along with mention of some included papers that may be of more general interest:

- 31) American Society for Testing and Materials, Electron Fractography, a symposium, ASIM Special Technical Publication (STP) 436, July 1968, 230 pp.

This book is a collection of technical papers presented at the Seventieth Annual Meeting of the American Society for Testing and Materials in 1967. It is a good early reference source of transmission electron microscope fractography techniques, including a paper by Beachem and Meyn.

- 32) American Society for Testing and Materials, Electron Microfractography, a symposium, ASIM Special Technical Publication (STP) 453, October 1969, 235 pp.

This book is a collection of technical papers presented at the Seventy-first Annual Meeting of the American Society for Testing and Materials in 1968. It includes a good paper by Williams, Boyer and Blackburn on the influence of microstructure on the fracture topography of titanium alloys.

- 33) American Society for Testing and Materials, Fractography - Microscopic Cracking Processes, a symposium, ASIM Special Technical Publication (STP) 600, edited by C. D. Beachem and W. R. Warke, June 1976, 261 pp.

This book is a collection of technical papers presented at the Seventy-eighth Annual Meeting of the American Society for Testing and Materials in 1975. It includes a good paper by Chesnutt, Rhodes and Williams relating mechanical properties, microstructure and fracture surface topography in alpha plus beta titanium alloys.

- 34) American Society for Testing and Materials, Fractography in Failure Analysis, a symposium, ASIM Special Technical Publication (STP) 645, May 1978, 387 pp.

This book is a collection of technical papers presented at a symposium during the May Committee Week of the American Society for Testing and Materials in 1977. It includes a paper by Meyn illustrating fractographic analysis techniques through several case histories.

- 35) Metallography in Failure Analysis, a symposium, edited by J. L. McCall and P. M. French, Plenum Press, New York, 1978, 301 pp.

Proceedings of a symposium sponsored by the American Society for Metals and the International Metallographic Society held in Houston, Texas, July 1977. This book presents several good review sections on failure mechanisms, macroscopic examinations, SEM examinations, origin areas in fatigue, along with included case histories.

- 36) American Institute of Mining, Metallurgical and Petroleum Engineers, Hydrogen Effects in Metals, a conference, edited by I. M. Bernstein and A. W. Thompson, The Metallurgical Society of AIME, 1980, 1059 pp.

This book is a collection of technical papers presented at the Third International Conference on Effects of Hydrogen on Behavior of Metals, sponsored by the Physical Metallurgy and Mechanical Metallurgy Committees of The Metallurgical Society of AIME, the National Science Foundation, and the U.S. Air Force Office of Scientific Research, Moran, Wyoming, August 1980.

Included is a paper by Walter, Frandsen and Jewett on the fractography of alloys tested in high pressure hydrogen. Specimens of Inconel 718 (wrought and cast), Waspaloy, Incoloy 903, Mar-M-246 and Haynes 188 were tested and examined. Examination showed that the hydrogen environment produced a brittle fracture mode, either transgranular or intergranular, in all alloys examined except for Incoloy 903 and cast Inconel 718, which were basically ductile.

- 37) Engineering Applications of Fracture Analysis, a conference, edited by G. G. Garrett and D. L. Marriott, Pergamon Press, 1980, 440 pp.

This book is a collection of technical papers presented at the First National Conference on Fracture held in Johannesburg, South Africa, in 1979, including a review by Luyckx on fractography as a tool for failure analysis.

- 38) American Society for Testing and Materials, Fractography and Material Science, a symposium, ASTM Special Technical Publication (STP) 733, edited by L. N. Gilbertson and R. D. Zipp, May 1981, 447 pp.

This book is a collection of technical papers presented at a symposium sponsored by ASTM Committee E-24 on Fracture Testing and Subcommittee E24.02 on Fractography and Associated Microstructures in Williamsburg, Virginia, November 1979. Included is a good paper by Meyn and Brooks on the microstructural origin of flutes on fracture surfaces of titanium alloys, and how these distinguish stress corrosion cracking from striationless fatigue cleavage.

Another paper included, by Au and Ke, correlates fatigue crack growth rate and striation spacing in AISI 9310 (AMS 6265) steel. Fatigue fractographs are given for both carburized and non-carburized specimens.

- 39) International Metallographic Society, "Proceedings of the Thirteenth Annual Technical Meeting," Microstructural Science, Vol. 9, edited by G. Petzow, R. Paris, E. D. Albrecht and J. L. McCall, Elsevier North Holland, Inc., New York, 1981, 446 pp.

Included is a technical paper by Caskey that discusses and illustrates the fractography of hydrogen embrittled iron-chromium-nickel alloys.

- 40) American Society for Metals, Fracture and Failure: Analyses, Mechanisms and Applications, edited by P. P. Tung, S. P. Agrawal, A. Kumar and M. Katcher, Metals Park, Ohio, 1981, 183 pp.

This book is a collection of technical papers presented at American Society for Metals Fracture and Failure Sessions, at the 1980 Western Metal and Tool Exposition and Conference (WESTEC), Los Angeles, California, March 1980.

- 41) Atomistics of Fracture, a conference, edited by R. M. Latanision and J. R. Pickens, NATO Conference Series VI (Materials Science), Vol. 5, Plenum Press, New York and London, 1983, 1071 pp.

This book is a collection of technical papers presented at NATO Advanced Institute on Atomistics of Fracture held at Calcatoggio, France, in 1981. It includes a good introductory discussion of fractography and how it is used to identify fracture modes, by Pelloux. Also included is a somewhat theoretical review of hydrogen related fracture of metals, by Birnbaum.

- 42) American Society for Testing and Materials, Fractography of Ceramic and Metal Failures, a symposium, ASIM Special Technical Publication (STP) 827, edited by J. J. Mecholsky, Jr., and S. R. Powell, Jr., 1984, 416 pp.

This book is a collection of technical papers presented as a symposium sponsored by ASIM Committee E-24 on Fracture Testing in Philadelphia, Pennsylvania, April 1982. Included is a paper by Vecchio and Hartzberg on cleaning techniques for post-failure analysis, and examination of the effectiveness of Alconox in cleaning corroded fracture surfaces of bridge steel.

- 43) Time-Dependent Fracture, "Proceedings of the Eleventh Canadian Fracture Conference," edited by A. S. Krausz, Martinus Nijhoff Publishers, 1985, 298 pp.

This book is a collection of technical papers presented during the conference at Ottawa, Canada, June 1984. Included is a paper by Dickson and Bailon that discusses and illustrates some of the fractographic features associated with environmentally assisted cracking.

- 44) International Metallographic Society, "Proceedings of the Eighteenth Annual Technical Meeting," Microstructural Science, Vol. 14, edited by M. R. Louthan, Jr., I. LeMay and G. F. Vander Voort, American Society for Metals, 1987, 598 pp.

Included is a technical paper by Cialone and Holbrook that discusses and illustrates some microstructural and fractographic features of hydrogen accelerated fatigue crack growth in steels.

- 45) American Society for Testing and Materials, Fractography of Modern Engineering Materials: Composites and Metals, a symposium, ASTM Special Technical Publication (STP) 948, edited by J. E. Masters and J. J. Au, 1987, 460 pp.

This book is a collection of technical papers presented at a symposium sponsored by ASTM Committees E-24 on Fracture Testing and D-30 on High Modulus Fibers and Their Composites in Nashville, Tennessee, November 1985. Included is a paper by Ibidunni on enhancing corroded high strength low alloy (HSLA) and stainless steel fracture surfaces by chemical cleaning. Another included paper by Venkataraman, Nicholas and Ashbaugh discusses the fractography of Inconel 718 that had been fatigue tested under combined major/minor cycle loading.

Logic Networks, Fault Trees and Other Approaches to Failure Analysis

- 46) C. W. George, "Investigation of Failures of Aircraft Components," Journal of the Birmingham Metallurgical Society, 1947, pp. 308-336.

George developed a chart in which he divided and subdivided various causes of failure of metallic components. Failure categories included fracture and non-fracture, temperature, mechanical (stress) and corrosion (environment), and defects in design, manufacturing and assembly.

- 47) J. A. Collins, B. T. Hagan and H. M. Bratt, "The Failure- Experience Matrix - A Useful Design Tool," Transactions of the ASME - Journal of Engineering for Industry, Vol. 98, August 1976, pp. 1074-1079.

Collins, Hagan and Bratt described a method they called the "failure-experience matrix." This matrix was a three dimensional array of cells, with failure modes along one axis, component mechanical function along a second axis and corrective actions taken

along the third axis. The matrix was used to help categorize failure analysis data for a large number of failed helicopter components. Even so, the matrix was sparsely populated. If more data were available, a designer could enter the matrix with a component of particular function and easily find out the known failure modes and possible corrective actions.

- 48) M. R. Louthan, Jr., "Fault Tree Technique and Failure Analysis," Metallography, Vol. 11, 1978, pp. 33-42.

Louthan applied Fault Tree techniques to the failure analysis of high strength low alloy (HSLA) steels, emphasizing stress corrosion cracking and hydrogen embrittlement. He defined a fault tree to be "a graphical technique that provides a systematic description of the combinations of possible occurrences in a system which can result in a fault or undesired event," in this case, a failure.

- 49) C. M. Jackson, R. A. Wood, D. N. Williams, J. H. Payer, W. E. Berry and J. P. Dimmer, "The Application of Kepner-Tregoe Methodology to the Root-Cause Failure Analysis of Boiler Tubes," Failures and Inspection of Fossil-Fired Boiler Tubes: 1983 Conference and Workshop (Proceedings), EPRI Report CS-3272, December 1983, pp. 3-1 to 3-17.

Jackson et al. applied Kepner-Tregoe methodology to the failure analysis of boiler tubes. They used Kepner-Tregoe, a systematic problem-solving methodology, to help identify the root cause of failure, in addition to identifying the mode.

- 50) A. C. Raghuran and A. R. Shamal, "Failure Analysis - Present Concepts and Future Perspectives," Advances in Fracture Research (Fracture 84), Vol. 6, Pergamon Press, 1986, pp. 3903-3917.

Raghuran and Shamala reviewed the fault tree technique and the failure experience matrix as applied to failure analysis. Again, the emphasis was to go beyond determining the mode of fracture, to the root cause of the failure, then using this information effectively to help prevent future failures.

- 51) B. W. Smith and R. A. Grove, Failure Analysis of Composite Structural Materials, Final Report AFWAL/TR-87-4001, Air Force Wright Aeronautical Laboratory, Air Force Systems Command, Wright-Patterson Air Force Base, Ohio, May 1987, pp. 129-134.

Smith and Grove applied failure analysis logic networks (FALN) to the failure analysis of composite materials. Logic networks are related to fault trees and flow charts, in that they can help guide failure analysts through the various non-destructive and destructive analysis techniques and procedures that are available.

Computerized Data Bases

A number of computerized data bases exist. Both titles and abstracts are available, and searches can be limited by the use of key words. Probably the best way to access and search these data bases is with the help of a technical library, since these libraries are equipped

and staffed to do this. The systems are usually interactive in nature and, if desired, real time searches can be made in the presence of the failure analyst. Selected potentially useful data bases that are available through the Dialog system are briefly summarized below in alphabetical order:

AEROSPACE DATABASE

File 108

Coverage: 1962 to the present
File Size: 1,500,000 records
Provider: American Institute of Aeronautics and
Astronautics/Technical Information Service

The AEROSPACE DATABASE provides references, abstracts, and controlled-vocabulary indexing of key scientific and technical documents, as well as books, reports, and conferences, covering aerospace research and development in over 40 countries including Japan and Communist-bloc nations. The AEROSPACE DATABASE combines in one database two publications: Scientific and Technical Aerospace Reports (STAR), produced by the National Aeronautics and Space Administration (NASA), and International Aerospace Abstracts (IAA), produced by AIAA under contract to NASA.

COMPENDEX

File 8

Coverage: 1970 to the present
File Size: 1,616,000 records
Provider: Engineering Information, Inc., New York, NY

The COMPENDEX database is the machine-readable version of the Engineering Index (monthly/annual), which provides abstracted information from the world's significant engineering and technological literature. The COMPENDEX database provides worldwide coverage of approximately 4,500 journals and selected government reports and books.

Coverage: 1966 to the present (Alloys Index, 1974-present; Steels Supplement, 1983-present)
 File Size: 658,000 records
 Provider: American Society for Metals (Now ASM International), Metals Park, OH, and The Metals Society, London, England

The METADEX database, produced by ASM International and the Metals Society (London), provides the most comprehensive coverage of international literature on the science and practice of metallurgy. Included in this database are Review of Metal Literature (1966-67), Metals Abstract (1968 to present), and Alloys Index (1974 to present). The Steels Supplement to Metals Abstracts was added in 1983.

WORLD ALUMINUM ABSTRACTS

File 33

Coverage: 1968 to the present
 File Size: 120,000 records
 Provider: ASM International, Metals Park, OH

WORLD ALUMINUM ABSTRACTS provides coverage of the world's technical literature on aluminum, ranging from ore processing (exclusive of mining) through end uses. The WORLD ALUMINUM ABSTRACTS database includes information abstracted from approximately 1,600 scientific and technical patents, government reports, conference proceedings, dissertations, books and journals.

Journals and Abstracts

Technical journals and abstracts are a continuing source of information that can be applied to failure analysis activities. The technical papers contained in these journals, however, are often of specific interest to a few rather than of general interest to many failure analysts. Selected technical journals and abstracts are listed below in alphabetical order:

ACTA METALLURGICA: an international journal for the science of materials. (Text in English, French, German) 1953, Pergamon Press, Inc., Journals Division, Maxwell House, Fairview Park, Elmsford, NY, 10523.

ADVANCED MATERIALS & PROCESSES: (American Society for Metals) 1985. ASM International Materials Information, Metals Park, OH, 44073. Incorporating (1930-1985): Metal Progress.

ALLOYS INDEX; (Auxiliary publication to Metals Abstracts and Metals Abstracts Index) 1974, International Materials Information, Metals Park, OH, 44073. (Co-sponsor: Institute of Metals, London)

CORROSION ABSTRACTS; abstracts of the world's literature on corrosion and corrosion mitigation, 1962. National Association of Corrosion Engineers, Box 218340, Houston, TX, 77218.

CORROSION; scientific articles on corrosion and its control, 1945. National Association of Corrosion Engineers, Box 218340, Houston, TX, 77218.

MATERIALS PERFORMANCE; articles on corrosion science and engineering solutions for corrosion problems. 1962. National Association of Corrosion Engineers, Box 218340, Houston, TX, 77218. Former titles: Materials Protection & Performance; Materials Protection.

METALLOGRAPHY; an international journal on materials structure and behavior, 1968. (International Metallographic Society, Inc.) Elsevier Science Publishing Co., Inc. (New York), 52 Vanderbilt Ave., New York, NY, 10017.

METALS ABSTRACTS; (American Society for Metals) 1968. ASM International, Materials Information, Metals Park, OH, 44073.

METALS ABSTRACTS INDEX; (American Society for Metals) 1968. ASM International, Materials Information, Metals Park, OH, 44073.

METALLURGICAL TRANSACTIONS A - PHYSICAL METALLURGY AND MATERIALS SCIENCE; 1970. (American Society for Metals, Materials Information) ASM International, Metals Park, OH, 44073. (Co-sponsor: American Institute of Mining Metallurgical and Petroleum Engineers, Inc.). Supersedes in part: Metallurgical Transactions which was formed by the merger of: American Society for Metals, Transactions Quarterly & T M S Transactions.

SCRIPTA METALLURGICA; 1967. Pergamon Press, Inc., Journals Division, Maxwell House, Fairview Park, Elmsford, NY, 10523. (And Headington Hill Hall, Oxford OX3 0BW, England).

Technical Societies and Institutes

Technical societies and institutes foster advances in failure analysis and fractography through published journals, by sponsoring technical conferences and symposiums, and by publishing collections of technical papers presented at conferences and symposiums. The American Society for Testing and Materials (ASTM) and The American Society for Metals (ASM International) are prominent among these. Selected technical societies and institutes are described below in alphabetical order:

AMERICAN INSTITUTE OF MINING, METALLURGICAL AND PETROLEUM ENGINEERS (AIME)

345 E. 47th St., 14th Fl., New York, NY, 10017.
(212) 705-7695

Founded: 1871. Members: 99,000. Student Groups: 157.
Sections: 176.

Professionals in the fields of mining, metallurgical and petroleum engineering. Objectives are: to promote the advancement of knowledge to the arts and sciences involved in the production and use of minerals, metals, energy sources, and materials; to record and disseminate developments in these areas of technology for the benefit of mankind. Bestows awards. Reorganized in 1957 into three constituent societies: Society of Mining Engineers; The Metallurgical Society; and the Society of Petroleum Engineers. Established fourth constituent society, the Iron and Steel Society, in 1974. Publications: 1) Iron and Steelmaker, monthly; 2) Journal of Metals, monthly, 3) Journal of Petroleum Technology, monthly; 4) Metallurgical Transactions, monthly; 5) Mining Engineering, monthly. Formerly: (1957) American Institute of Mining and Metallurgical Engineers.

AMERICAN SOCIETY FOR METALS (ASM) (NOW ASM INTERNATIONAL)

Metals Park, OH 44073
(216) 338-5151

Founded: 1913. Members: 53,000. Staff: 115. Local Groups: 256. Metallurgists, materials engineers, executives in metals producing and consuming industries; teachers and students. Disseminates educational information about the manufacture, use, and treatment of metals and engineering materials. Offers in-plant, home study, and intensive courses through Metals Engineering Institute; conducts conferences, seminars, and lectures on metals; presents awards to teachers of metallurgy and science awards to junior and senior high school students and teachers; grants, scholarships and fellowships. Conducts career development program. Established ASM Foundation for Education and Research. Maintains library of 9000 volumes on metallurgy.

Sponsors annual Western Metal and Tool Exposition and Conference (WESTEC); Orange County Manufacturing and Metalworking Conference and Exposition (Orcal Expo); Materials Week; Heat Treating Conference/Workshop. Computerized Services: Information services. Divisions: Electronic Materials and Processing; Energy; Heat Treating; Joining; Materials Science: Materials Systems and Design: Materials Testing and Quality Control; Mechanical Working and Forming; Primary Metalworking; Society of Carbide and Tool Engineers; Specialty Materials; Surface Treating and Coating. Publications: 1) Advanced Materials and Processes, monthly; 2) ASM Newsletter, monthly; 3) Metal Abstracts, monthly, 4) Metal Progress (now Advanced Materials and Processes), monthly; 5) Metallurgical Transactions A, monthly; 6) Metals Abstracts Index, monthly; 7) Bulletin of Alloy Phase Diagrams, bimonthly; 8) Journal of Materials for Energy Systems, quarterly; 9) Metallurgical Transactions B, quarterly; 10) Journal of Applied Metalworking, semiannual; 11) Journal of Heat Treating, semiannual; 12) Data Book, annual; 13) Heat Treating Buyers Guide and Directory, annual; 14) Testing and Inspection Buyers Guide and Directory, annual; also publishes Metals Handbook and over 120 texts on metals and materials. Formed by merger of: Steel Treaters Club (founded 1913) and American Steel Treaters Society (founded 1918). Formerly: (1920) American Society for Steel Treaters.

ASTM

1916 Race St., Philadelphia, PA 19103
(215) 299-5400

Founded: 1898. Members: 30,500. Staff: 200. Engineers, scientists, managers, professionals, academicians, consumers, and skilled technicians holding membership as individuals in or representatives of business firms, government agencies, educational institutions, and laboratories. Establishes voluntary consensus standards for materials, products, systems, and services. Has 140 technical committees (each having five to 50 subcommittees). New committees are organized each year to keep pace with technological advances. Sponsors more than 40 symposia each year; issues various awards for significant contributions in research. Has developed more than 7300 standard test methods, specifications, classifications, definitions, and recommended practices now in use. Publications: 1) Standardization News, monthly; 2) Journal of Testing and Evaluation, bimonthly; 3) Composites Technology and Research, quarterly; 4) Geotechnical Testing Journal, quarterly; 5) Cement, Concrete, and Aggregates Journal, semiannual; 6) Book of ASTM

Standards, annual; also publishes numerous technical papers and reports. Formerly: (1902) American Section, International Association for Testing Materials; (1982) American Society for Testing and Materials.

BATELLE MEMORIAL INSTITUTE (Research) (BMI)
505 King Ave., Columbus, OH 43201
(614) 424-6424

Founded: 1929. Staff: 7400. Nonprofit, public purpose organization. Conducts scientific research on a contract basis for industrial firms and government agencies in chemistry, biochemistry, metallurgy, physics, energy, computer technology, electronics, nucleonics, ceramics, transportation, education and training, environmental quality, medical engineering, urban problems, mechanical engineering, and other fields. Maintains research centers in Geneva, Switzerland; Frankfurt/Main, West Germany; Richland, WA; and Columbus, OH. Columbus, OH laboratories maintain library of over 150,000 volumes; other research centers also have library facilities. Conducts educational programs including seminars and fellowships. Subsidiary corporation works to stimulate use of technological discoveries in industry. Publications: 1) Batelle Today, 5/Year; 2) Annual Report; 3) Published Papers and Articles, annual; also publishes original research papers, articles, and abstracts.

INTERNATIONAL METALLOGRAPHIC SOCIETY (Metallurgy) (IMS)
P.O. Box 2489, Columbus, OH 43216
(614) 860-3535

Founded: 1967. Members: 600. Persons and firms engaged in optical, electron, and X-ray metallography, ceramography, petrography, micrography (including plastics, chemicals, petroleum, aerosols), and their allied sciences. Serves as a means of international communication among scientists in these fields. Makes available on loan a metallographic exhibit with award-winning photomicrographs. Bestows Sorby Award annually to an internationally recognized contributor to the field of metallography. Publications: 1) Metallography (international journal), quarterly, 2) Sliplines, quarterly; 3) Directory, annual; 4) Proceedings, annual. Also known as: International Microstructural Analysis Society.

NATIONAL ASSOCIATION OF CORROSION ENGINEERS

P.O. Box 218340, Houston, TX 77218

(713) 492-0535

Founded: 1943. Members: 15,000. Staff: 50. Regional Groups; 6. Local Groups: 67. Technical society of engineers and scientists concerned with corrosion and its prevention. Conducts research on corrosion control; sponsors short courses annually at colleges and universities, covering subjects such as coatings and linings, inspection, inhibitors, design and biological factors, surface treatment, and selection of materials. Sponsors technical seminars. Maintains accreditation program for engineers and technicians. Operates 5000 volume library; bestows awards. Computerized Services: Data base. Industrial Groups: Corrosion Coordinating Committee; Corrosion of Military Equipment; Corrosion in Oil and Gas Well Equipment; Corrosion Problems in the Process Industries; General; Pipe Line Corrosion; Protective Coatings; Refining Industry Corrosion; Utilities; also has 200 technical subgroups. Publications: 1) Corrosion, monthly; 2) Materials Performance, monthly, 3) Corrosion Abstracts, bimonthly; 4) Corrosion Abstracts Yearbook; also publishes monographs and technical books.